THE JOURNAL OF

PHYSICAL CHEMISTRY

Volume 71, Number 12 November 1967

HYPERFINE INTERACTIONS

edited by ARTHUR J. FREEMAN
RICHARD B. FRANKEL

This unique collection of papers covers the entire range of basic principles, current status and latest advances in the field of hyperfine interactions and associated relaxation phenomena. Nuclear Magnetic Resonance, Mössbauer Effect, Atomic Beams, Optical Hyperfine, Perturbed Angular Correlations, Electron Paramagnetic Resonance, Nuclear Specific Heats and other topics are treated with textbook thoroughness and with a view towards clarifying the general relationships between them. This presentation, based on the proceedings of a NATO Advanced Study Institute held at Aix-en-Provence, France, 1966, includes papers by such eminent authorities as A. Abragam, B. Bleaney, S. Geschwind, R. L. Mössbauer and A. Steudel.

1967, 758 pp., $16.00

A NEW SERIAL PUBLICATION

revised edition

THERMODYNAMIC PROPERTIES OF ORGANIC COMPOUNDS

ESTIMATION METHODS, PRINCIPLES AND PRACTICE
by GEORGE J. JANZ
Volume 6 of Physical Chemistry

Presents principles and methods for calculating thermodynamic properties of organic compounds and for predicting the feasibility of chemical stability and reactivity from the thermodynamic point of view. Exact and estimated data tables are included for the thermodynamic analysis of a wide variety of problems.

1967, 249 pp., $10.50

Volume 1

ADVANCES IN HIGH TEMPERATURE CHEMISTRY

edited by LEROY EYRING

Reviews advances in knowledge of the high temperature behavior of materials and the latest experimental techniques. Emphasis is placed on the complex and unfamiliar characteristics of matter at high temperature. The articles are contributed by established investigators.

Contents: P. GOLDFINGER, A Definition of High Temperature Chemistry. C. J. CHEETHAM and R. F. BARROW, The Spectroscopy of Diatomic Transition Element Molecules. K. D. CARLSON and C. R. CLAYDON, Electronic Structure of Molecules of High Temperature Interest. A. BUCHLER and J. B. BERKOWITZ-MATTUCK, Gaseous Ternary Compounds of the Alkali Metals. R. J. THORN and G. H. WINSLOW, Valence States in High Temperature Chemistry; Energic Structures in Transitional Elements. D. L. HILDENBRAND, Bond Energy Relationships in Polyvalent Metal Fluorides. J. B. EZELL, J. C. THOMPSON, J. L. MARGRAVE and P. L. TIMMS, The Chemical Reactions of High Temperature Species. E. F. WESTRUM, JR., High Temperature Adiabatic Calorimetry. T. B. REED, Plasmas for High Temperature Chemistry. Author Index. Subject Index.

1967, 334 pp., $14.50

FUNDAMENTALS OF GAS-SURFACE INTERACTIONS

edited by HOWARD SALTSBURG, JOE N. SMITH, JR. and MILTON ROGERS
Air Force Office of Scientific Research, Arlington, Virginia

An up-to-date survey of modern research in gas-surface interactions. Reports investigations of the properties of the surface itself—structure and forces between surfaces—and investigations of the gas-surface interaction using as a probe the properties of the gas phase-adsorption, chemical reaction on or with surfaces, molecular beam scattering and energy transfer in the gas-solid system.

1967, 555 pp., $14.50

ELECTRONIC ABSORPTION SPECTRA AND GEOMETRY OF ORGANIC MOLECULES

AN APPLICATION OF MOLECULAR ORBITAL THEORY
by HIROSHI SUZUKI

Describes aspects of the relation between electronic absorption spectra of organic compounds and geometry of molecules. In terms of molecular orbital theory, special detailed emphasis is placed on basic concepts, various useful methods within its framework, and composite-molecule methods, and their application to interpretation of electronic spectra.

1967, 569 pp., $24.00

AN INTRODUCTION TO THE LIQUID STATE

by P. A. EGELSTAFF

Developed from a series of lectures given at the University of Reading, this volume gives a general introduction to the liquid state. Equilibrium and transport properties and microscopic behavior of liquids are covered. The basic theory involving pair potentials and pair distribution functions is presented in the earlier part of the book, and the more complicated space and time dependent correlation functions follow. Monotomic liquids, such as rare-gas liquids and liquid metals, are discussed in detail and their properties compared.

1967, 236 pp., $10.00

ACADEMIC PRESS NEW YORK AND LONDON
111 FIFTH AVENUE, NEW YORK, N.Y. 10003

NOTES

COMMUNICATIONS TO THE EDITOR

THE JOURNAL OF
PHYSICAL CHEMISTRY

VOLUME 71, NUMBER 12 NOVEMBER 15, 1967

The Partial Specific Volume of Bovine Plasma Albumin in the Presence of Potassium Chloride[1]

by Margaret J. Hunter

Institute of Science and Technology, Biophysics Research Division, and Department of Biological Chemistry, Medical School, University of Michigan, Ann Arbor, Michigan *(Received June 12, 1967)*

The densities of various albumin–KCl solutions of known albumin and KCl concentration were determined by the use of a calibrated glass diver in the manner described in a previous communication.[2] Specific volume data were obtained from the density data, and the specific volume of the albumin was found to be independent of protein and KCl concentration. The partial specific volume of apotransferrin was also determined.

Introduction

In a previous communication[2] a method for the determination of protein-solution densities by means of a calibrated glass diver or float was described, and the partial specific volumes of three isoionic salt-free albumin preparations were determined from the density data. These studies have now been extended to an investigation of the effect of salt (KCl) on the partial specific volume of the protein. This information is of importance in the analysis of sedimentation data since most sedimentation velocity and sedimentation equilibrium analyses on proteins are performed in the presence of dilute salt or buffer solutions.

Although many partial specific volume measurements on proteins in the presence of salts or buffers have been reported,[3-7] no systematic investigation of the effect of salt on the partial specific volume has been undertaken. The more accurate specific volume studies (those of Dayhoff, *et al.*,[5] and Ulrich, *et al.*[6]) do not give parallel data in the absence of salt. The variability of the other published data is great enough that small salt effects would not be detectable.

Recently a study of the partial specific volume of ribonuclease in the presence of an uncharged solute, sucrose, has been undertaken by Kupke and his coworkers.[8] These workers have shown the partial specific volume of the ribonuclease to be independent of sucrose concentration.

(1) This work was supported by National Institutes of Health Grant No. GM-11842.

(2) M. J. Hunter, *J. Phys. Chem.*, **70**, 3285 (1966).

(3) P. A. Charlwood, *J. Am. Chem. Soc.*, **79**, 776 (1957).

(4) V. L. Koenig, *Arch. Biochem. Biophys.*, **25**, 241 (1950).

(5) M. O. Dayhoff, G. E. Perlmann, and D. A. MacInnes, *J. Am. Chem. Soc.*, **74**, 2515 (1952).

(6) D. V. Ulrich, D. W. Kupke, and J. W. Beams, *Proc. Natl. Acad. Sci. U. S.*, 52, 349 (1964).

(7) J. L. Oncley, G. Scatchard, and A. Brown, *J. Phys. Colloid Chem.*, 51, 184 (1947).

(8) D. W. Kupke, J. P. Senter, and P. F. Fahey, Jr., Abstracts, 11th Annual Meeting of the Biophysical Society, Houston, Texas, Feb 1967, p 118.

Experimental Section

Methods and Materials. The albumin used in these studies was crystalline bovine plasma albumin, Lot 2267, Armour Pharmaceutical Co. Stock 5% albumin solutions were dialyzed extensively against glass-distilled water at 2°. The dialyzed solutions were filtered through Whatman No. 1 filter paper, passed through a mixed-bed deionizing column,[9] and stored at 2°.

The human apotransferrin was a three times crystallized protein which had been prepared by Dr. E. Hazen from Cohn Fraction IV-7 of human plasma. The crystalline protein contained about 5% dimer. Apotransferrin monomer was prepared by Mr. P. Eggena by passage of the apotransferrin through a column of Sephadex G-200. Isoionic salt-free apotransferrin monomer solution was prepared by the method described above for the preparation of isoionic salt-free albumin. No inhomogeneity of the apotransferrin monomer was detectable by electrophoretic or ultracentrifugal analyses.

The equipment used in the solution-density and dry-weight determinations has been described in detail in a previous communication.[2] In brief, the apparatus for the density determinations consists of a test tube suspended in a constant temperature bath. The glass diver, a platinum stirrer, the solution whose density is to be determined, and a thermometer are placed in the test tube and the temperature of the bath varied until a temperature is reached at which the diver neither rises nor sinks. The temperature at which this equilibrium occurs will be referred to as the solution–diver isopycnic temperature (or simply isopycnic temperature). If the density–temperature profile of the diver has previously been determined by isopycnic-temperature determinations on solutions of known density, the density of a solution of unknown density can be determined from the solution–diver isopycnic temperature obtained with that solution.

The method employed in determining the isopycnic temperature has been modified in one particular since the previous paper was published. It has been observed on many occasions that, if the isopycnic temperature is approached rather rapidly, a false zero is obtained. The following procedure has therefore been adopted.

The temperature of the bath is adjusted rather rapidly until it is very close to that at which the diver neither sinks nor floats. The system is then allowed to equilibrate at this temperature for 20 min. The precise isopycnic temperature is then determined in the manner described previously.[2] On many occasions two determinations of the isopycnic temperature have been performed on the solution; in one case the isopycnic temperature has been approached from lower temperature values while in the other case it has been approached from the high side of the temperature scale. Duplicate results obtained in this manner have agreed to within 0.01°.

Calibration of Diver. The divers were calibrated by the use of KCl solutions of known concentration. Concentration, density, and temperature correlations on these KCl solutions were obtained by interpolation of the density data in the "International Critical Tables"[10] in the manner described in the previous communication.

Three glass divers were used in the density determinations. Their density–temperature correlations are given in the equations

$$\text{diver K:}\quad \rho = 1.000100 - 1.423 \times 10^{-5}t$$

$$\text{diver B:}\quad \rho = 1.002248 - 1.312 \times 10^{-5}t$$

$$\text{diver C:}\quad \rho = 1.010110 - 1.221 \times 10^{-5}t$$

where ρ = density and t = temperature (°C).

Determination of Density of Protein Solutions. Weight dilutions of the protein solutions were obtained by weighing aliquots of the stock isoionic salt-free protein solutions and glass-distilled water or standard KCl solutions into weighing bottles. The diluted protein solutions were mixed well and placed in the test tube with the diver, and the isopycnic temperature was determined. The density of the solution was obtained from the diver's density–temperature calibration curve.

Determination of Protein Concentration by Dry-Weight Measurements. All dry-weight measurements were made on the stock isoionic salt-free protein solutions. The samples were heated at 110° *in vacuo* to constant weight in the manner described in the previous communication.[2]

Investigations on the variation of albumin dry weights with the conditions used to dry the albumin samples have been continued. The consistency of the dry-weight data obtained *in vacuo* at all temperatures studied (75–115°) is better than one part in a thousand. The day to day variation in the dry weights obtained after drying in air at 110° is considerably greater than this value. The air-dried weights have varied from 1.000 to 1.005 times that obtained *in vacuo* at 75°. This variability combined with the discoloration of the

(9) W. L. Hughes and H. M. Dintzis, *J. Biol. Chem.*, **239**, 845 (1964).

(10) "International Critical Tables," McGraw-Hill Book Co., Inc., New York, N. Y., 1933.

air-dried protein, the relatively high dry-weight value, and the fibrous character of the protein on the addition of water to the dried sample has led to the conclusion that drying *in vacuo* is the method of choice in the determination of the dry weight of albumin.

Determination of Partial Specific Volume. The specific volumes of the proteins were calculated by the use of the relationship

$$\phi = \frac{1}{n}\left(\frac{1}{\rho_t} - \frac{1-n}{\rho_{o,t}}\right)$$

where ϕ is the apparent specific volume. In the absence of concentration dependence of the specific volume, ϕ is equal to the partial-specific volume, $\bar{v}$. n is the weight fraction of the protein (g/g of solution), ρ_t is the density of the solution at temperature t, and $\rho_{o,t}$ is the density of the solvent at temperature t. In the case of the protein–KCl solutions the solvent is composed of the nonprotein species present in the solution, *i.e.*, KCl and water. The concentration units of the KCl are g/100 g of water. Since $\rho_{o,t}$ can be expressed as $\rho_{H_2O,t} + \rho_{KCl,t}$, its value can be calculated from the tabulated water and KCl increment density data. The specific volume of bovine plasma albumin in the presence and absence of KCl was determined using each of the three divers. The individual datum points are shown in Figure 1. Mean data are presented in Table I. Eight density measurements were performed on isoionic salt-free albumin using diver K. A least-squares best-fit analysis of these data related the specific volume and the temperature in the following manner

$$\bar{v} = 0.72596 + 0.00035t$$

The $\bar{v}_{25}°$ value given in row 1 of Table I was obtained from the least-squares analysis. Apart from the data in row 1 of Table I, the mean data were obtained in the following manner. Since replicates were prepared by a weight-dilution procedure, the preparation of exact replicates was not possible. However the replicate samples were prepared at approximately the same protein concentration and, in the case of the protein–KCl solutions, the same KCl concentration. A mean temperature was chosen for the quasi replicates and the individual specific-volume values were converted to this temperature by use of a temperature coefficient of 0.000366 ml/g deg. This value had been obtained previously in the studies with isoionic salt-free albumin. The specific-volume data listed in column 6 of Table I are thus an average of the various individual specific-volume values, each of which had been corrected to the mean temperature given in column 5 of Table I. The number of data points used to obtain the average values are listed in brackets in column 2 of the Table. Average protein and KCl concentrations are given in columns 3 and 4. The $\bar{v}_{25}°$ data tabulated in column 7 were obtained by standardizing the data in column 6 to 25° by use of a temperature coefficient of 0.000366 ml/g deg.

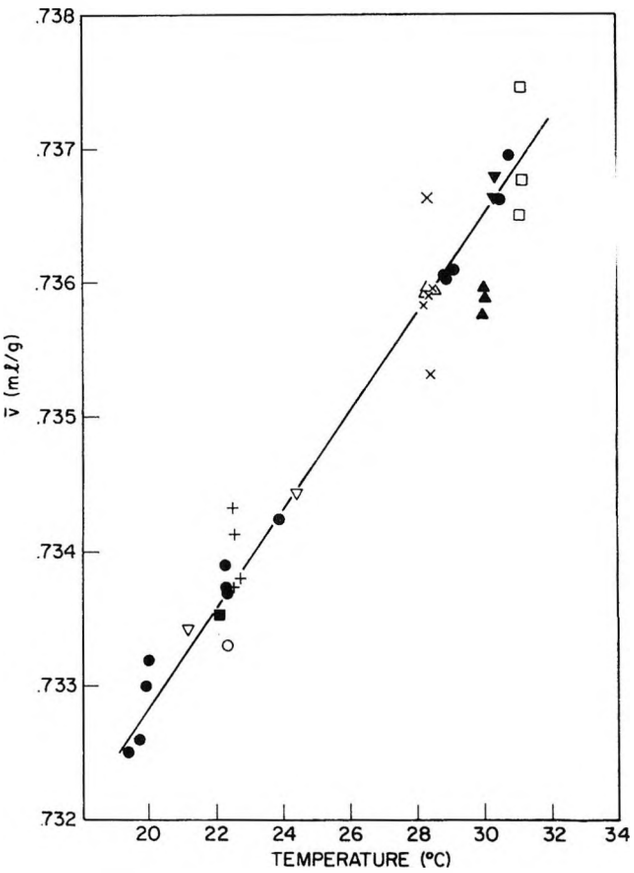

Figure 1. Partial specific volume of bovine plasma albumin at various protein and KCl concentrations: ●, albumin in H_2O; ○, 0.20% KCl and 4.0% albumin; ▲, 0.56% KCl and 1.0% albumin; □, 0.79% KCl and 0.58% albumin; ▽, 1.65% KCl and 0.67% albumin; +, 0.19% KCl and 0.34% albumin; △, 0.26% KCl and 1.5% albumin; ×, 0.76% KCl and 0.34% albumin; ■, 0.81% KCl and 2.6% albumin; and ▼, 1.67% KCl and 1.4% albumin.

The values in the first three rows of column 7 indicate that no significant variation in the specific volume with concentration occurs. Specific volumes may therefore properly be equated with the partial specific volume. The lack of variation in the $\bar{v}_{25}°$ values in column 7 clearly demonstrates that the presence of KCl does not affect the protein partial specific volume. The temperature coefficient, $d\bar{v}/dt$, in the presence of a relatively high KCl concentration can be obtained from the data in rows 11 and 12 of Table I. A value of 0.000367 ml/g deg is obtained from these data.

Table I: Partial Specific Volume of Bovine Plasma Albumin at Various Protein and KCl Concentrations

No.	Diver	Protein concn, g/100 g of soln	KCl concn, g/100 g of H_2O	Temp, t, °C	$\bar{v}_t$, ml/g	$\bar{v}_{25°}$, ml/g
1	K(8)	0.5–1.4	0	19.39–28.96	...	0.73468
2	B(3)	2.3	0	30.00	0.73651	0.73468
3	C(2)	4.5	0	22.33	0.73372	0.73470
4	K(4)	0.34	0.19	22.50	0.73398	0.73490
5	C(1)	4.0	0.20	22.37	0.73330	0.73426
6	B(3)	1.5	0.26	28.35	0.73593	0.73470
7	B(3)	1.0	0.56	30.00	0.73586	0.73403
8	B(5)	0.34	0.77	28.35	0.73592	0.73469
9	B(3)	0.58	0.80	31.10	0.73690	0.73467
10	C(1)	2.6	0.82	22.11	0.73353	0.73459
11	C(2)	0.67	1.68	22.50	0.73382	0.73474
12	C(2)	1.4	1.70	30.35	0.73670	0.73474

Six density determinations were performed on human apotransferrin. The resultant partial specific volumes are shown in Table II. A least-squares best-fit analysis

Table II: Partial Specific Volume of Human Apotransferrin

Diver	Protein concn, g/100 g of soln	KCl concn, g/100 g of H_2O	Temp, t, °C	$\bar{v}_t$, ml/g	$\bar{v}_{25°}$, ml/g
B	1.4282	0	21.36	0.72019	0.72135
B	1.4009	0	20.99	0.72000	0.72130
B	1.9225	0	27.19	0.72210	0.72139
B	1.9558	0	27.545	0.72212	0.72129
C	1.5610	1.2419	22.545	0.72046	0.72126
C	1.5751	1.2311	22.41	0.72064	0.72148

of the four values obtained with the isoionic salt-free protein gave the following partial specific volume–temperature correlation

$$\bar{v} = 0.71321 + 0.00033t$$

The partial specific volume data in column 5 of Table II were converted to 25° by use of the temperature coefficient obtained by the least-squares analysis of the salt-free data (*i.e.*, $d\bar{v}/dt = 0.00033$ ml/g deg). As can be seen from the data in column 6 of Table II, the presence of KCl does not alter the partial specific volume of the protein.

Discussion

Of the many protein specific-volume determinations that have been published only one has shown a dependency of the partial specific volume on protein concentration. McMeekin and co-workers studied the partial specific volume of casein at pH 6.4 and pH 3.1.[11] While the data at pH 6.4 showed no variation of the volume with casein concentration, the values at pH 3.1 showed a rather large dependency of the volume on concentration.

The accuracy of most of the published specific-volume data, however, is not great enough to permit the detection of small specific-volume changes (±0.002). Accurate specific-volume data for two proteins in water (bovine serum albumin and ovalbumin) have been reported by Dayhoff, Perlmann, and MacInnes.[5] These authors found no variation in the specific volume with protein concentration in the concentration range of 0.2–0.8 g/100 g of solution. The method of density determination employed in the present studies is not really suited to specific-volume–concentration correlations since, for a particular diver, only one concentration of solute will give a particular density at a particular temperature. The use of three divers of differing density, however, does permit the determination of the specific volume at three protein concentrations at the same temperature. Measurements conducted in this manner showed no significant variation in specific volume with concentration (rows 1, 2, and 3, Table I) in agreement with the findings of Dayhoff, *et al.*[5]

The accuracy of the partial specific volume data at low protein concentrations is greatly decreased since ρ_t approaches $\rho_{o,t}$; for example, an error of 0.01° in the determination of the isopycnic temperature would result in an error of 0.0007 in $\bar{v}$ at a protein concentration of 0.34 g/100 g of solution.

The value obtained for the partial specific volume of apotransferrin is in good agreement with literature

(11) T. L. McMeekin, M. L. Groves, and N. J. Hipp, *J. Am. Chem. Soc.*, 71, 3298 (1949).

values of 0.725 (37°),[7] 0.716 (presumably 20°),[12] and 0.72 (from amino acid analysis).[13]

Prior to undertaking these experiments, it had been thought that changes in the ionic environment of the protein might cause small variations in the volume of the protein. No such effect has been observed either with albumin or apotransferrin. The protein–salt density determinations were all conducted on solutions which had been prepared by adding known weights of standard protein solution to known weights of standard KCl solutions. The KCl and water were assumed to have the same density characteristics as they would have had in the absence of protein. The density of the KCl and water fractions of the protein solution could thus be calculated from the KCl and water density tables. The albumin partial specific volume obtained in the presence of salt, when calculated in this manner, was the same as that obtained in the absence of salt. Therefore, no measurable change in the volume of the protein or of the salt ions must have occurred on mixing the protein and salt solutions (unless of course the volume of one solute increased while that of the other decreased in a compensatory manner; however, this occurrence is regarded as most unlikely). Furthermore, it is known that chloride ions are bound by both albumin[14] and transferrin.[15] It therefore follows that chloride binding by the protein is not accompanied *per se* by any measurable change in the volume of the protein or of the bound chloride ions. Changes in electrostriction or excluded volumes must also be very small.

The lack of variation of the protein specific volume with protein and salt concentration simplifies investigation of the specific volume of the protein component. Studies on albumin–KCl systems with and without the concomitant addition of HCl or KOH, dialyzed and undialyzed, are being undertaken to obtain more exact information on the nature and volume of the protein species which obtains in sedimentation experiments.

Acknowledgments. The author wishes to acknowledge the help of Miss Nancy Myerson, who performed many of the density determinations.

(12) H. E. Schultze, R. Schmidtberger, and H. Haupt, *Biochem. Z.*, **329**, 490 (1958).

(13) A. Bezkorovainy, M. E. Rafelson, Jr., and V. Likhite, *Arch. Biochem. Biophys.*, **103**, 371 (1963).

(14) G. Scatchard, Y. V. Wu, and A. L. Shen, *J. Am. Chem. Soc.*, **81**, 6104 (1959).

(15) J. K. Inman, Ph.D. Thesis, Harvard University, Cambridge, Mass., 1956.

The Role of Hydrogen Peroxide in Oxygen Reduction at Rhodium Electrodes

by M. A. Genshaw, A. Damjanovic, and J. O'M. Bockris

The Electrochemistry Laboratory, The University of Pennsylvania, Philadelphia, Pennsylvania 19104
(Received December 15, 1966)

The role of hydrogen peroxide in oxygen reduction at rhodium electrodes in acid and alkaline solution has been analyzed using the rotating disk electrode with the concentric ring. If hydrogen peroxide is formed at the rhodium disk electrode, it may diffuse away from it and be carried by forced convection to the ring electrode where it is detected. In purified 0.1 *N* H_2SO_4 solutions, no H_2O_2 formation is detected. In insufficiently purified solutions, hydrogen peroxide is a reaction intermediate in a path parallel to that in which oxygen is reduced to water without peroxide intermediates. In 0.1 *N* KOH solution, hydrogen peroxide is a reaction intermediate which partially reduces to water. Mechanisms for oxygen reduction at prereduced and preoxidized rhodium electrodes are suggested.

Introduction

The use of the rotating disk electrode with a concentric ring[1,2] in the determination of the mechanisms of oxygen reduction and, in particular, in finding the role of hydrogen peroxide in the reduction has recently been discussed.[3-8] With this electrode assembly it was possible to discriminate between H_2O_2 formed as an intermediate or as a product in a parallel reaction path.[9] Thus, at Pt electrodes in H_2SO_4 solution, it was shown that H_2O_2 is formed in a reaction path parallel to that in which oxygen is reduced to water without H_2O_2 as an intermediate.[10] If, however, the solution is sufficiently purified to remove residual organic impurities, *no* H_2O_2 is formed either as an intermediate or in a parallel reaction path providing the electrode potential is anodic to 0.15 v *vs.* hydrogen electrode. In "insufficiently purified" acid solutions the rate of the further reduction of H_2O_2 to water is lower than the rate by which H_2O_2 is formed at the same electrode. In alkaline solution at Pt electrodes, hydrogen peroxide is also an intermediate in a parallel path but it reduces at least partially further to water.[11]

To understand more fully the mechanism of oxygen reduction at a variety of electrode materials and the role of hydrogen peroxide in the reduction, oxygen reduction at rhodium electrodes was studied in acid and in alkaline solutions. For this study, the rotating disk electrode with a concentric ring is used along with some standard electrochemical techniques.

Analysis of the Parallel Reaction Paths

The application of the rotating disk electrode with a concentric ring in an analysis of parallel reaction paths was recently discussed[9] and this electrode assembly was used to determine the role of hydrogen peroxide in oxygen reduction at platinum electrodes.[10-12]

If hydrogen peroxide is formed in oxygen reduction at the disk electrode kept at a given potential, it may diffuse away from the disk and be carried by forced convection to a ring electrode which is coplanar with the

(1) A. N. Frumkin and L. N. Nekrassov, *Dokl. Akad. Nauk SSSR*, 126, 115 (1959).

(2) V. G. Levich, "Physicochemical Hydrodynamics," Prentice-Hall, Inc., Englewood Cliffs, N. J., 1962, p 327.

(3) L. Müller and L. N. Nekrassov, *Electrochim. Acta*, 9, 1015 (1964).

(4) L. Müller and L. N. Nekrassov, *Dokl. Akad. Nauk SSSR*, 154, 437 (1964).

(5) A. N. Frumkin, L. N. Nekrassov, V. G. Levich, and Yu. B. Ivanov, *J. Electroanal. Chem.*, 1, 84 (1959).

(6) L. Müller and L. N. Nekrassov, *ibid.*, 9, 282 (1965).

(7) L. Müller and V. V. Sobol, *Elektrokhimiya*, 1, 111 (1965).

(8) E. Yeager, "The Oxygen Electrode in Aqueous Fuel Cells," in Bransleceller, IVA Meddelande NR 134, Stockholm, 1963.

(9) A. Damjanovic, M. A. Genshaw, and J. O'M. Bockris, *J. Chem. Phys.*, 45, 4057 (1966).

(10) A. Damjanovic, M. A. Genshaw, and J. O'M. Bockris, *J. Electrochem. Soc.*, 114, 466 (1967).

(11) A. Damjanovic, M. A. Genshaw, and J. O'M. Bockris, *J. Electrochem. Soc.*, in press.

(12) A. Damjanovic, M. A. Genshaw, and J. O'M. Bockris, *J. Phys. Chem.*, 70, 3761 (1966).

disk electrode. The potential of the ring electrode is kept high enough so that practically all H_2O_2 which is transported to it is oxidized while oxygen evolution does not yet occur with any significant rate.

Hydrogen peroxide can form in a reaction path parallel to that in which O_2 is reduced to water without hydrogen peroxide as an intermediate. This is schematically represented by eq 1 and 2. Hydrogen peroxide,

$$O_2 \xrightarrow{I_1} H_2O \qquad (1)$$

$$O_2 \xrightarrow{I_2} H_2O_2 \xrightarrow{I_3} H_2O \qquad (2)$$

$$\downarrow I_4$$

to solution and ring electrode

formed as a reaction intermediate in path 2, is partially reduced further at the same disk electrode to water and partially carried away from the disk electrodes to the solution and ring electrode by convective diffusion. I_1, I_2, and I_3 are the respective currents. I_4 represents the rate in current by which H_2O_2 diffuses away from the disk electrode.

With the rotating disk electrode with the concentric ring it is possible to distinguish between reaction intermediates and products in a parallel reaction path. For this distinction the diagnostic equation[9]

$$\frac{I_d}{I_r} = \frac{x+1}{N} + \frac{1.61(x+2)D^{2/3}\nu^{1/6}k_3}{N\omega^{1/2}} \qquad (3)$$

is used. I_d and I_r are the currents which are detected at the disk and ring electrode, respectively, k_3 is the rate constant for the further reduction of H_2O_2 at the disk electrode, and ω is the rate of disk rotation. N is a geometric factor, which is calculable from the dimensions of the electrodes.[2,13] D is the diffusion coefficient for reaction intermediates and ν is kinematic viscosity. In the equation, x is defined as

$$x = I_1/I_2 \qquad (4)$$

From the intercepts of I_d/I_r *vs.* $\omega^{-1/2}$ plots with the I_d/I_r axis, x can be determined and, hence, conclusions can be made concerning the presence of parallel reaction paths.

Since current at the disk electrode is given by

$$I_d = I_1 + I_2 + I_3 \qquad (5)$$

and at the ring electrode by[2]

$$I_r = NI_4 \qquad (6)$$

and since

$$I_2 = I_3 + I_4 \qquad (7)$$

it follows that

$$I_d = I_1 + 2I_2 - (I_r/N) \qquad (8)$$

With known x, and from eq 4 and 8, the current at the disk electrode due to the reaction path which does not involve the formation of hydrogen peroxide, I_1, and the current due to the reduction of O_2 to hydrogen peroxide, I_2, can be calculated.

Experimental Section

The rotating disk apparatus consists of a rhodium electrode in the form of a rod (diameter 0.234 cm) which is pressed fit into a thin Teflon cylinder. The ring electrode is a hollow platinum cylinder (i.d. 0.29 cm, o.d. 0.35 cm) which is concentric with the rhodium rod from which it is electrically isolated by the thin Teflon cylinder. Only the bases of the rhodium rod and platinum cylinder are exposed to the solution. These bases are coplanar. Details of the electrode assembly are much the same as given in a previous paper.[10] The area of the rhodium electrode (disk) is 0.17 cm^2. The ring electrode is lightly platinized.

The cell consists of a spherical compartment (main cell) with a water-sealed connection to the mechanical assembly for the disk and ring electrodes. A hydrogen electrode compartment is isolated from the main cell by a water-sealed stopcock. An auxiliary vessel, which served for electrochemical purification of the solution, is also attached to the main cell. In Figures 1 and 2, the cell and the auxiliary vessel are shown.[10] Between experiments, the cell was soaked in a HNO_3–H_2SO_4 mixture. Before an experiment it was thoroughly washed with conductivity water.

Sulfuric acid solution (0.1 N) was prepared from H_2O_2-treated[14] Baker Analyzed reagent H_2SO_4 and conductivity water. In some experiments, this solution was further electrochemically purified. The solution under nitrogen pressure was circulated from the main cell to the auxiliary vessel for purification. In the auxiliary vessel a large platinized platinum gauze was potentiostated at 0.3 v.[15] At this potential, the residual impurities from the solution adsorb at Pt and a high purity of the solution is achieved. The electrochemically purified solution will be referred to here as "pure," in contrast to H_2O_2-treated acid which will be called "insufficiently purified." KOH solutions (0.1 N) were prepared from Baker Analyzed reagent grade KOH diluted with conductivity water. Gases used in the work are purified in a standard way.

(13) W. J. Albery and S. Bruckenstein, *Trans. Faraday Soc.*, **62**, 1920 (1966).

(14) W. Visscher and M. A. V. Devanathan, *J. Electroanal. Chem.*, **8**, 127 (1964).

(15) All potentials in this paper are referred to the reversible hydrogen electrode in the same solution.

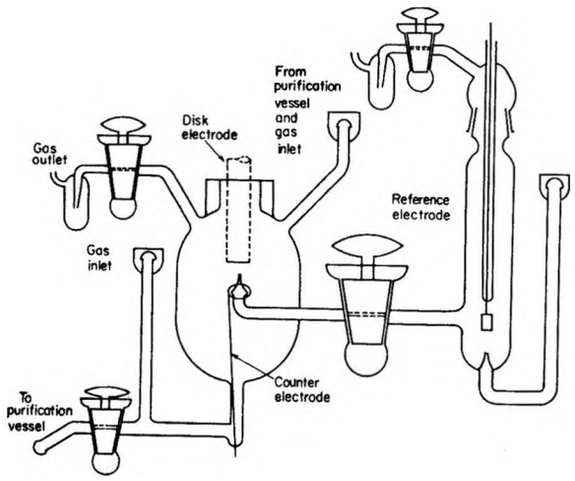

Figure 1. The cell. Position of the disk electrode is indicated.

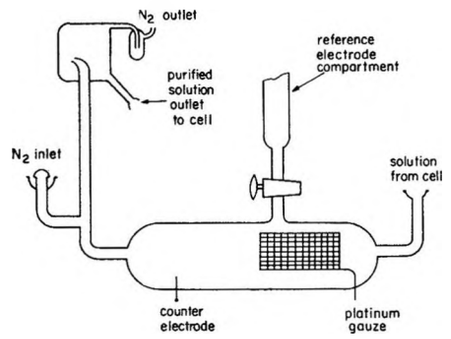

Figure 2. Auxiliary vessel for solution purification. The vessel is attached to the cell.

Oxygen reduction at 1 atm pressure of O_2 is followed at the disk electrode. The potential of the disk electrode was controlled by a potentiostat (Wenking 61R). The ring electrode potential was kept[10] at +1.4 v. At this high anodic potential, essentially all H_2O_2 which reaches the ring electrode is detected. The oxygen evolution current at this potential is still negligible. The currents at the disk and ring electrode were measured using electrometers (Keithley 600 A). The rate of disk rotation was determined by comparing on an oscilloscope the signal produced by a coil placed near a magnet in the shaft of the disk electrode assembly with a standard frequency produced by an audio oscillator.

The rhodium disk electrode was washed with acetone, conductivity water, 10% HCl, concentrated H_2SO_4, and conductivity water. For measurements in alkaline solution, this washing sequence was followed by soaking the electrode for a few minutes in KOH solution of the same concentration as used in experiments. Once in the test solution, the disk electrode was treated in one

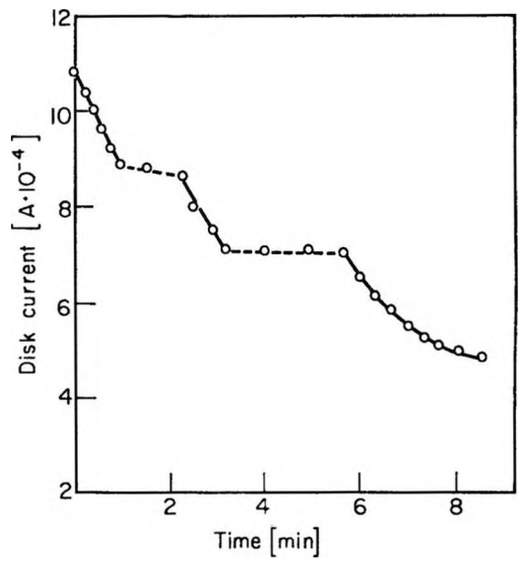

Figure 3. Time dependence of disk current at 0.40 v: ———, 60 rps; – – – –, stationary electrode. Insufficiently purified acid solution.

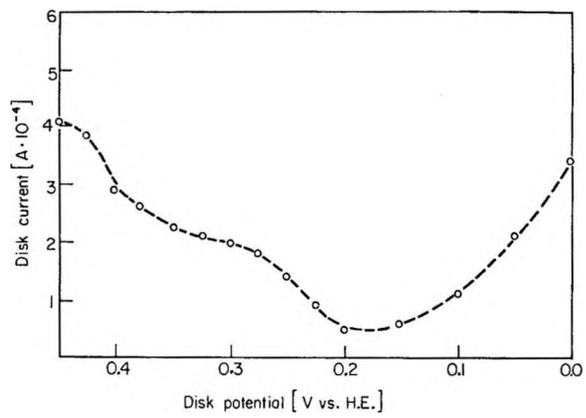

Figure 4. Steady-state disk current as a function of disk potential. The area of the disk electrode is 0.17 cm².

of the two following ways: (1) it was potentiostated at 0.05 v for 1 min and measurements were then taken starting from the most cathodic potential and (2) the electrode was potentiostated anodic to 1 v for 1 min and the measurements were then taken starting from the most anodic potential. To the first electrode it will be referred here as "prereduced" and to the second as "preoxidized."

Results

Prereduced Electrode in Sulfuric Acid Solution. At a prereduced electrode in "insufficiently purified" acid solution, the current at the disk electrode for a potential cathodic to about 0.5 v is very much time dependent

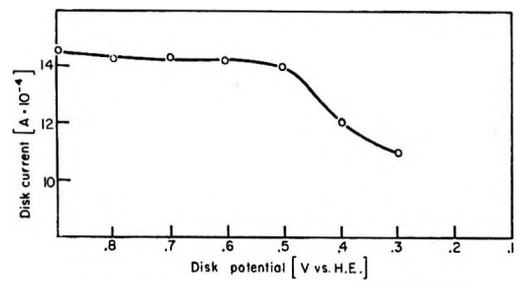

Figure 5. Initial disk current at 0.10 v after the disk electrode was kept at a given potential for 1 min.

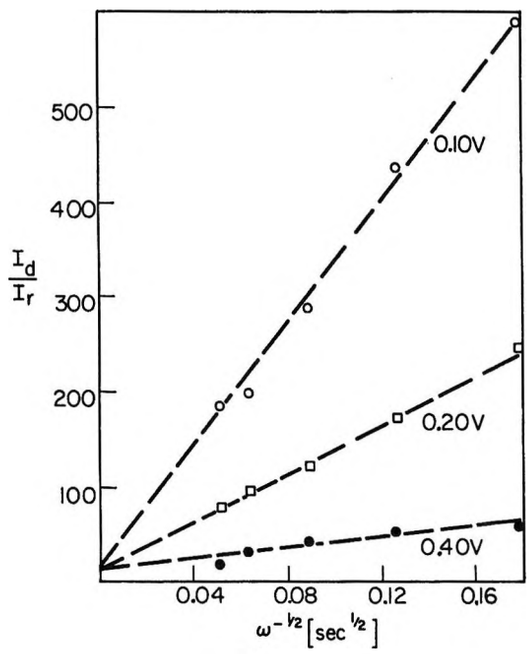

Figure 6. Plot of I_d/I_r *vs.* $\omega^{-1/2}$ for the prereduced rhodium electrode in acid solution. Potentials of the electrode are given in the figure.

(*cf.* Figure 3). When an electrode is brought from 0.05 to, say, 0.2 v, current initially decreases with time while the yield of hydrogen peroxide, as detected at the ring electrode, gradually increases. The time for establishing the steady state depends for a given solution on the rate of disk rotation (see below). The steady-state disk current for a given rate of disk rotation is shown in Figure 4. In the region 0.20–0.45 v the disk current increases with increasing potential.

The initial activity of the electrode can be restored, however, or the electrode can even be made more "active" than it had been after the reduction at 0.05 v, if it is brought to a higher potential for a short (order of minutes) time. In a series of measurements the lower limit of the potential is determined which is required to

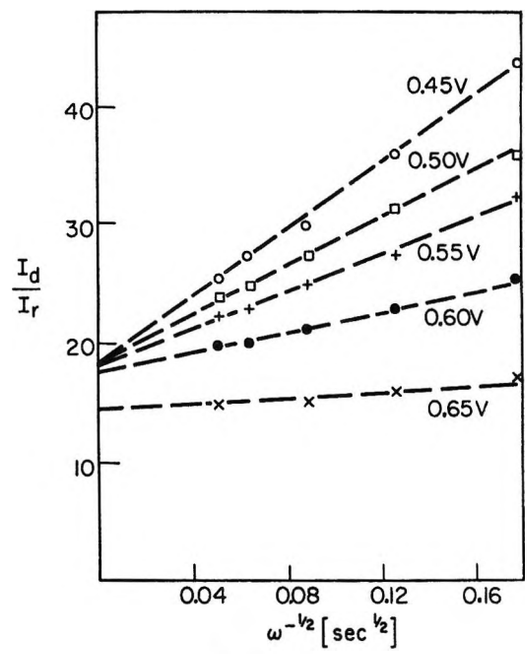

Figure 7. Plot of I_d/I_r *vs.* $\omega^{-1/2}$ ($sec^{1/2}$) for the prereduced rhodium electrode in acid solution.

restore the initial "activity" of the disk electrode. The current at the disk electrode was first allowed to decrease at 0.10 v to its minimum, steady-state value for this potential. After this, the electrode was brought to a more anodic potential for 1 min. The electrode potential was then changed again to 0.10 v and the *initial* current was measured. In Figure 5 this initial current is plotted against the potential at which the electrode was kept for 1 min in order to be "activated." An essentially complete restoration of the "activity" occurs when the potential of the electrode is made anodic to 0.50 v for 1 min.

For a given potential of the disk electrode, the ratio I_d/I_r of the *steady-state current* at the disk, I_d, to that at the ring electrode, I_r, is linearly dependent on $\omega^{-1/2}$ (Figures 6 and 7). The I_d/I_r lines are dependent on the disk potential. The slope of the lines increases as the potential decreases. The intercepts of the lines with the I_d/I_r axis are all clustered around the value of 18. When experiments were repeated in newly prepared solutions, similar results are obtained, though the magnitude of I_d/I_r for a given ω and electrode potential may change, particularly at low potentials. These differences are attributed to different purities of solutions (see below).

The observed time effect for the prereduced rhodium electrode in acid solution resembles that reported[10] for Pt electrodes under similar experimental conditions and is evidently caused, as in the case of Pt, by adsorption

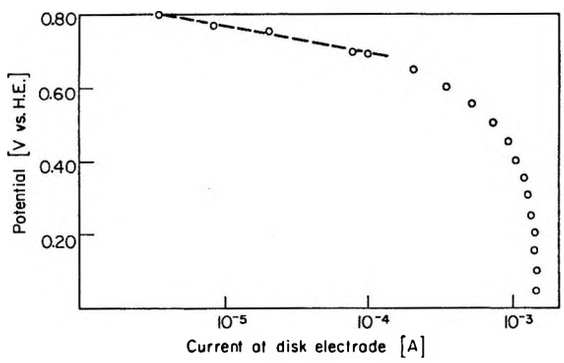

Figure 8. Current–potential relationship for the prereduced rhodium electrodes in acid solution. The area of the disk electrode is 0.17 cm².

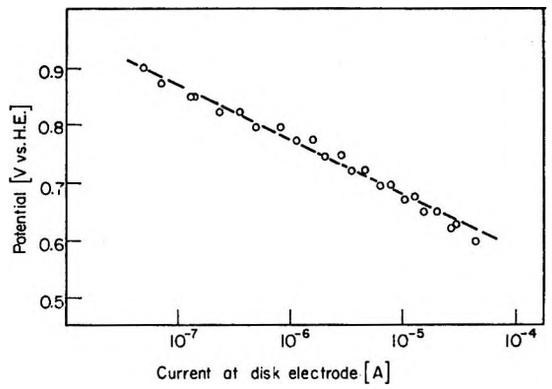

Figure 9. Current–potential relationship for the preoxidized rhodium electrode in acid solution. The area of the electrode is 0.17 cm².

of residual impurities from the solution. This is based on the following observations. (i) The initial change in the disk current is strongly dependent on the rate of disk rotation; when the electrode is made stationary this change is much less (Figure 3). (ii) The electrode can be "activated" if brought to a potential anodic to 0.50 v (presumably a desorption or oxidation of the adsorbed organic impurities). (iii) The electrochemical purification of the solution results in a great decrease in the time effects and eventually practically no time effect is observed.

With electrochemical purification of the solution, not only the time effects diminish but also the behavior of the electrode changes. Thus, *in "pure" solutions only traces of H_2O_2 are detected* at the ring electrode. Hence, no I_d/I_r *vs.* $\omega^{-1/2}$ plot could be made ($I_r \approx 0$).

The current–potential relationship for the prereduced electrode in "pure" solutions is given in Figure 8. No minimum in the current at low electrode potentials is observed here, but only well-defined limiting current close to 10^{-3} amp (compare Figures 4 and 8). Tafel behavior is observed between 0.70 and 0.8 v with a slope close to the ideal $-RT/F$. These results are in agreement with those previously reported for prereduced rhodium electrodes.[16] Both in "pure" and in "insufficiently purified" solutions, potential–current relationships for the prereduced electrodes are almost identical at potentials anodic to about 0.60 v.

"Peroxidized" Electrode in Sulfuric Acid Solution. At rhodium electrodes initially potentiostated anodic to 1 v, the Tafel slope for oxygen reduction is close to −0.100 v (Figure 9). This is in a marked contrast to the prereduced electrodes for which $\partial V/\partial \ln i \approx -RT/F$. The average value of the slope from six independent measurements is 0.105 v. This is in agreement with a previously reported value.[16a] At these preoxidized electrodes, the reproducibility is not as high as

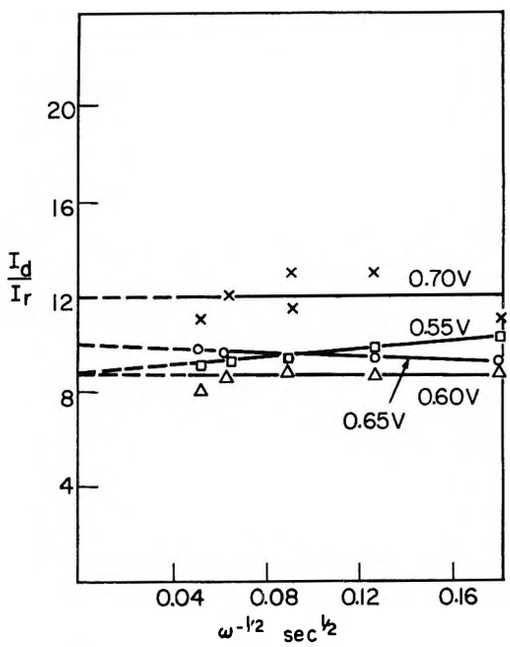

Figure 10. Plot of I_d/I_r *vs.* $\omega^{-1/2}$ for the preoxidized rhodium electrode in acid solution. Potentials of the electrode are given in the figure.

at the prereduced electrodes. If the potential of the electrode was brought below about 0.60 v, the same Tafel behavior could not be retraced.

At potentials anodic to 0.55 v, the diagnostic plots of I_d/I_r *vs.* $\omega^{-1/2}$ both in "pure" and in "insufficiently purified" solutions are nearly the same. Data of such an experiment are shown in Figure 10 for 0.55 v and more anodic potentials. Below 0.50 v in "insufficiently

(16) (a) A. Damjanovic, A. Dey, and J. O'M. Bockris, *J. Electrochem. Soc.*, **113**, 739 (1966); (b) V. Brusić in "Reversible Oxygen Electrodes," Report No. 11, U. S. Army Electronics Laboratories, Fort Monmouth, N. J., 1964.

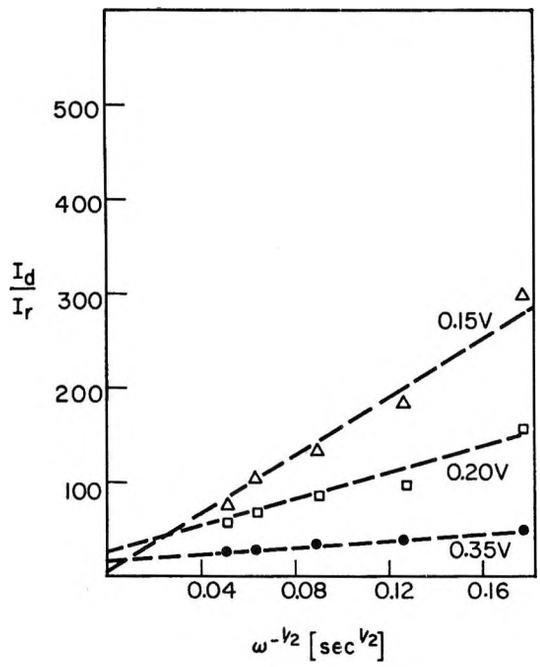

Figure 11. Plot of I_d/I_r *vs.* $\omega^{-1/2}$ for the preoxidized electrodes in acid solution. Potentials of the electrode are given in the figure.

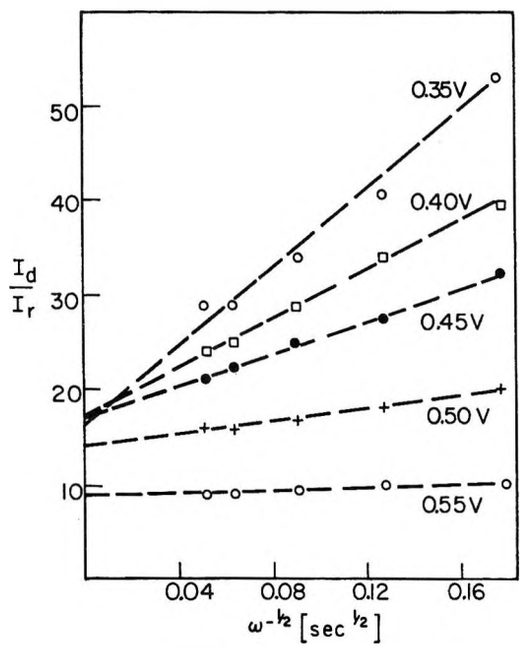

Figure 12. Plot of I_d/I_r *vs.* $\omega^{-1/2}$ for the preoxidized rhodium electrode in acid solution.

purified" solution, I_d/I_r lines (Figures 11 and 12) resembled those for the prereduced electrodes. The intercepts of the lines with the I_d/I_r axis cluster around 20 (about the same value as for the prereduced electrodes). In "pure" solutions, no I_d/I_r plot was possible below about 0.6 v ($I_r \approx 0$).

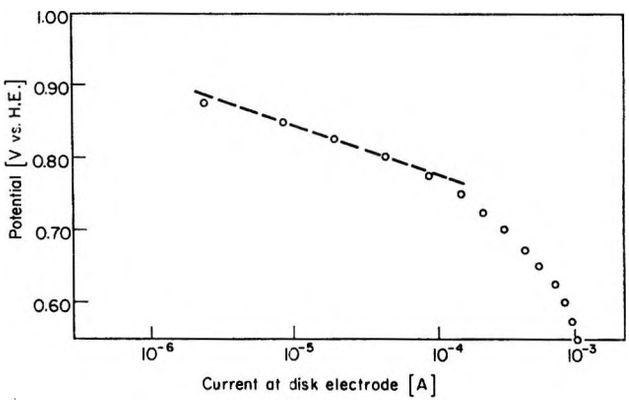

Figure 13. Current–potential relationship for the prereduced rhodium electrodes in alkaline solution. The area of the electrode is 0.17 cm².

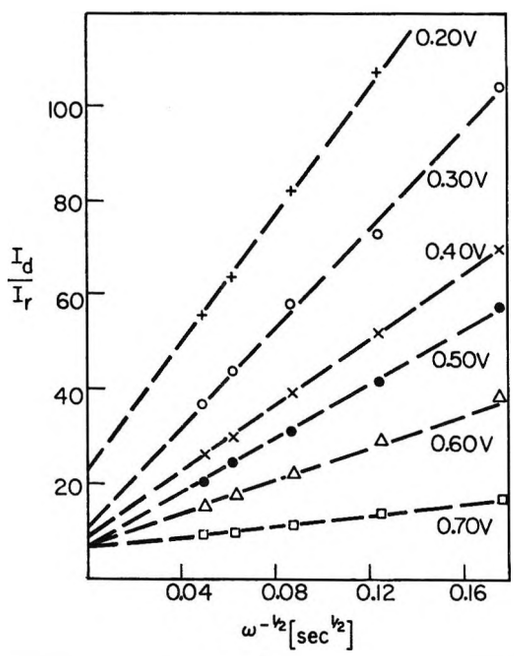

Figure 14. Plot of I_d/I_r *vs.* $\omega^{-1/2}$ for the prereduced electrode in alkaline solution. Potentials of the electrode are given in the figure.

Reduction in Alkaline Solution. A short Tafel region with a slope close to −60 mv is observed for the prereduced rhodium electrodes at potentials anodic to about 0.8 v (Figure 13). The dependence of I_d/I_r on $\omega^{-1/2}$ at various electrode potentials is shown in Figure 14. The intercept of the lines with the I_d/I_r axis ranges from 5 to 12. The slopes of the lines decrease as the potential is made more anodic. At the preoxidized electrode (Figure 15) less satisfactory reproduciblity of the results

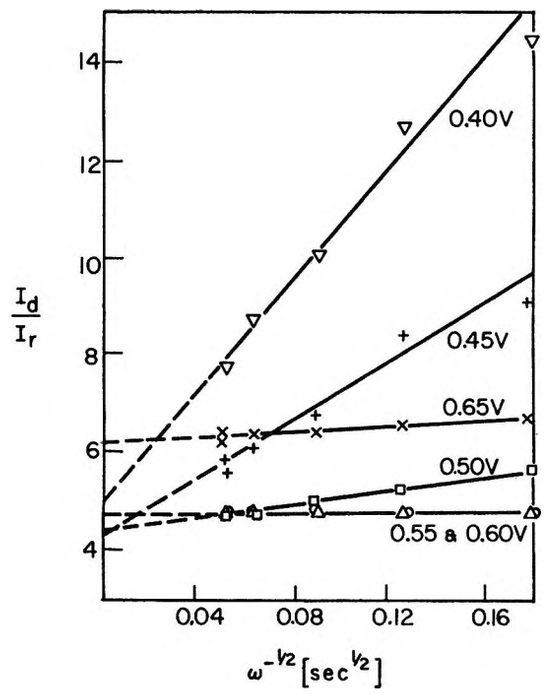

Figure 15. Plot of I_d/I_r *vs.* $\omega^{-1/2}$ for the preoxidized electrode in alkaline solution.

was obtained. I_d/I_r plots *vs.* $\omega^{-1/2}$ have intercepts between 4 and 6. The slope of the I_d/I_r lines changes with potential.

Discussion

Hydrogen Peroxide in Oxygen Reduction in Acid Solution. In the diagnostic plot of I_d/I_r *vs.* $\omega^{-1/2}$ for the prereduced electrodes in "insufficiently purified" acid solution, the intercepts are clustered between 15 and 20. From eq 3, the intercept is given by

$$\text{intercept} = (x + 1)/N \qquad (9)$$

and with $N = 0.3$,[13,17] as calculated from the dimensions of the disk and ring electrodes, and with an average value for the intercept of 18, $x = 4.5$. Since x is the ratio of current I_1 and I_2 (*cf.* eq 4), *oxygen reduction at the prereduced rhodium electrodes in "insufficiently" purified acid solution proceeds along two parallel paths.* Hydrogen peroxide is formed in the path parallel to that in which O_2 is reduced to water without hydrogen peroxide as an intermediate. The major reaction is the reduction to H_2O without peroxide intermediate.

At the potentials cathodic to 0.60 v, slopes in the plots of I_d/I_r against $\omega^{-1/2}$ are positive. It follows that the rate constant k_3 in eq 3 is not zero and that hydrogen peroxide is at least partially reduced further to water. At potentials anodic to about 0.60 v, $k_3 = 0$ and hence the reduction of hydrogen peroxide is slow in comparison to its formation at the same electrode. In this respect rhodium resembles a platinum electrode. On the latter electrode, too, in "insufficiently purified" solutions the rate of further reduction of hydrogen peroxide is negligible in comparison to the rate by which it is produced.

After the sulfuric acid is purified, only traces of hydrogen peroxide are detected to form. *In this "pure" acid solution oxygen reduction at the prereduced rhodium electrodes proceeds along a single path which does not involve hydrogen peroxide formation.*

The basically similar I_d/I_r *vs.* $\omega^{-1/2}$ dependence to those at the prereduced electrodes, which are obtained at the preoxidixed electrodes for potentials cathodic to 0.5 v, indicate that in either case the electrode surfaces are the same. This behavior is possibly due to gradual reduction of oxides initially present at the surface of the preoxidized electrodes. Once these oxides are reduced, at least over the most of the electrode surface,[18] the electrode behaves as if it is prereduced (see below). Above 0.55 v, I_d/I_r lines are not as reproducible as those for more cathodic potentials. The slopes of I_d/I_r lines appear to be close to zero and the intercepts are less than in the case of the prereduced electrodes. Hence, two parallel reactions are present at the preoxidized electrodes.

Hydrogen Peroxide in Alkaline Solution. For alkaline solution, the I_d/I_r *vs* $\omega^{-1/2}$ plots are similar to those in "insufficiently purified" acid solution. The yield of hydrogen peroxide in alkaline solution is, however, greater than in acid solution. With the intercept of 5, $x \approx 0.5$. Hence, *at the prereduced rhodium electrodes in alkaline solution, the main path for oxygen reduction is that in which oxygen is reduced to hydrogen peroxide.* Hydrogen peroxide then reduces further to water. Were the intercept equal to 3.3, the only reaction path would be that in which hydrogen peroxide is an intermediate.

Prereduced and Preoxidized Electrodes. At platinum electrodes, it is known[19,20] that oxides form rapidly at potential anodic to about 1 v. Below this potential, oxides gradually reduce. A similar situation is expected for rhodium electrodes, except that probably oxides begin to form at lower potentials.[18,19] If the rate of oxide formation or of their reduction is slow enough, it is possible to examine the kinetics of oxygen

(17) S. Bruckenstein, private communication.

(18) Below about 0.5 v, oxides become unstable and are reduced; F. G. Will and C. A. Knorr, *Z. Elektrochem.*, **64**, 270 (1960).

(19) W. M. Latimer, "Oxidation Potentials," Prentice-Hall, Inc., Englewood Cliffs, N. J., 1964, p 198.

(20) A. K. N. Reddy, M. A. Genshaw, and J. O'M. Bockris, *J. Electroanal. Chem.*, **8**, 406 (1964).

reduction in a certain range of potential either on a predominantly oxide-free or an oxide-covered electrode surface. This was previously illustrated for the case of platinum in acid solution,[21] where, in the potential range of 0.8–1 v, oxygen reduction occurs either at predominantly oxide-covered or oxide-free electrode surfaces. The mechanisms of the reduction are different on these two types of surfaces as shown by different values of $\partial V/\partial \ln i$ on these surfaces. Here, for the reduction at rhodium electrodes, two reaction mechanisms are evident, too, at least for the reduction in acid solutions. At the prereduced, oxide-free surface, the slope ($\partial V/\partial \ln i \approx -RT/F$) is different from that at the preoxidized, and presumably oxide-covered, electrode surfaces ($\partial V/\partial \ln i \approx -2RT/F$).

Reduction at the Prereduced Electrodes in Acid Solution. The Tafel slope is close to the ideal $-RT/F$. In "pure" solution, a plot of $1/I_d$ *vs.* $\omega^{-1/2}$ gives straight lines (Figure 16), thus indicating[22] that the reaction is first order with respect to oxygen. Though the path of oxygen reduction cannot be determined with this information only, a number of paths can be eliminated.

Since the reaction is first order in oxygen, dissociation of the oxygen occurs in or after the rate-controlling step. Thus, any intermediates which would form before the rate-controlling step must contain two oxygen atoms. Since no hydrogen peroxide is detected as an intermediate in the reduction path in "pure" solution, species like HO_2^- and H_2O_2 are not expected to form. Intermediates like O_2^- and HO_2 are possible. The rate-controlling step may either be the formation of these intermediates or a step in which they dissociate.

The similarity of the kinetics at this electrode with that at a prereduced Pt electrode in "pure" H_2SO_4 solution may indicate basically the same mechanism for the reduction of oxygen to hold for both electrodes. If so, then the rate-controlling step is the first discharge step under Temkin conditions of adsorption.[10,23] The pH dependence of the reaction is required for a further analysis of the mechanism.

Reduction to Water at Preoxidized Electrodes in Acid Solution. In Figure 17, the values of I_d/I_r at ω = 380 sec^{-1}, which reflect the value of the intercept since the slopes of the lines are low (*cf.* Figure 10), are plotted as a function of potential from three independent experiments. A variation with the potential is evident: the higher the potential, the lower is the relative yield in hydrogen peroxide. Hence, at the potentials at which Tafel relationship is observed, the major reaction at the preoxidized electrodes in acid solutions is the reduction to water.

The results of the present work are not sufficient to allow an analysis of this path. In a recent analysis of

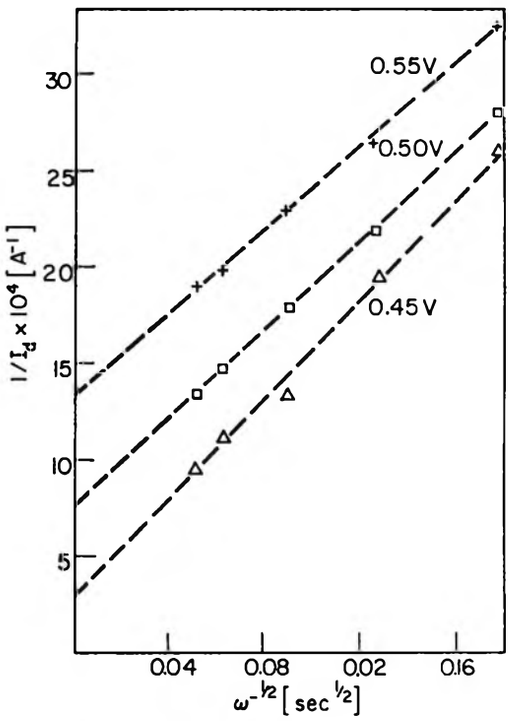

Figure 16. Plot of $1/I_d$ *vs.* $\omega^{-1/2}$. Prereduced rhodium electrodes in acid solution.

oxygen evolution and reduction at preoxidized Rh electrodes,[16a] it was suggested that in perchloric acid the following two paths are possible (S = substrate metal or oxide)

$$S + H_2O \rightleftarrows SOH + H^+ + e^- \quad (10)$$

$$SOH + H_2O \rightleftarrows SOHOH^- + H^+ \quad (11)$$

$$SOHOH^- \rightleftarrows SOHOH + e^- \quad (12)$$

$$SOHOH \rightleftarrows SO + H_2O \quad (13)$$

$$2SO \rightleftarrows 2S + O_2 \quad (14)$$

and

$$S + H_2O \rightleftarrows SOH + H^+ + e^- \quad (10)$$

$$SOH \rightleftarrows SO^- + H^+ \quad (15)$$

$$SO^- \rightleftarrows SO + e^- \quad (16)$$

$$2SO \rightleftarrows O_2 + 2S \quad (17)$$

In the first path, step 11 is rate controlling at low overpotentials with a change to step 10 as the rate-control-

(21) A. Damjanovic and J. O'M. Bockris, *Electrochim. Acta*, 11, 376 (1966).

(22) A. C. Riddiford, *Advan. Electrochem. Electrochem. Eng.*, 4, 96 (1966).

(23) A. Damjanovic and V. Brusić, *Electrochem. Acta*, in press.

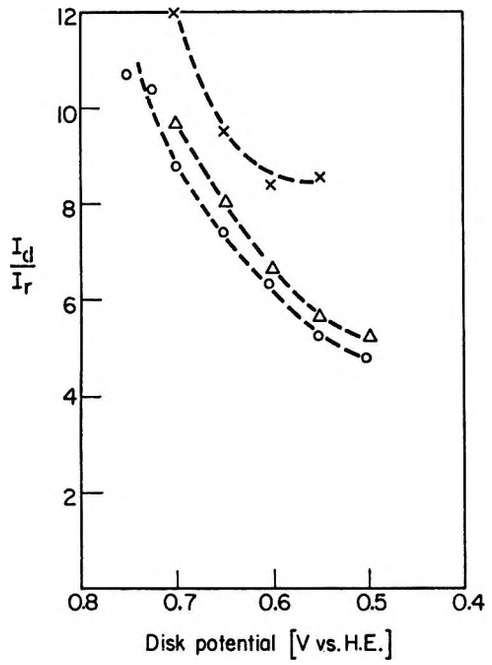

Figure 17. Three independent measurements of the plot of I_d/I_r *vs.* electrode potential; $\omega = 380$ sec^{-1}.

ling one at higher anodic overpotentials; step 12 is rate controlling at higher cathodic overpotentials. In the second path, step 15 is rate controlling at low overpotentials with steps 10 and 16 becoming the rate-controlling ones at higher anodic and cathodic overpotentials, respectively. These proposed mechanisms are consistent with the experimental results reported here. Neither mechanism has a hydrogen peroxide intermediate.

If in the potential region where I_d/I_r *vs.* $\omega^{-1/2}$ is not changing appreciably with potential (*cf.* Figures 10, 11, and 12), the partial current due to the reduction of oxygen to water is nearly a constant fraction of the total current, then the Tafel slope for this partial current should be the ideal $-2RT/F$ slope. With this the probable mechanism is then

$$O_2 + H^+ + e^- \longrightarrow HO_2 \quad (18)$$

$$HO_2 + H^+ + e^- \rightleftharpoons H_2O_2 \quad (19)$$

or

$$O_2 + e^- \longrightarrow O_2^- \quad (20)$$

$$O_2^- + 2H^+ + e^- \rightleftharpoons H_2O_2 \quad (21)$$

Other mechanisms would either require dissociation of the O_2 or do not have a single electron transfer in the rate-controlling step.

The Mechanism of Oxygen Reduction in Alkaline Solution. Insufficient data exist for a more complete discussion of the mechanism of reduction in alkaline solution. In the potential range where the path in which oxygen is reduced to hydrogen peroxide is the major one, the slope of $-RT/F$ indicates that a chemical step which follows a charge-transfer step is the rate-controlling one

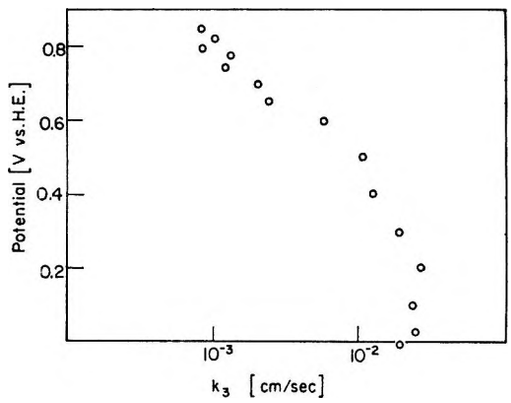

Figure 18. Dependence of rate constant k_3 for hydrogen reduction in alkaline solution.

$$O_2 + e^- \rightleftharpoons O_2^- \quad (22)$$

$$O_2^- + H_2O \longrightarrow HO_2^- + OH \quad (23)$$

$$OH + e^- \rightleftharpoons OH^- \quad (24)$$

Further reduction of hydrogen peroxide appears to be little dependent on the electrode potential. Thus, the constant k_3 in eq 3 as calculated from slopes of the I_d/I_r *vs.* $\omega^{-1/2}$ lines changes by less than two orders of magnitude for an 0.8-v change in potential (Figure 18). This indicates a chemical rate-controlling step as in the path

$$H_2O_2 \longrightarrow 2OH \quad (25)$$

$$2OH + 2e^- \rightleftharpoons 2OH^- \quad (26)$$

A similar situation was previously reported[11] for Pt electrodes in alkaline solution.

Summary of the Conclusions

At prereduced rhodium electrodes in purified acid solutions, no hydrogen peroxide is formed either as a reaction intermediate or as a product in a path parallel to that in which oxygen is reduced to water. At this electrode in insufficiently purified solution, oxygen reduction proceeds along two parallel paths. Hydrogen peroxide is formed in a path parallel to that in which oxygen is reduced to water without hydrogen peroxide

as an intermediate. The major reaction is the reduction to water.

At the prereduced rhodium electrodes in alkaline solution, the main path for oxygen reduction is that in which oxygen is reduced to hydrogen peroxide. Hydrogen peroxide reduces further to water. Reduction to water without hydrogen peroxide is a minor reaction.

The mechanism of oxygen reduction at the preoxidized rhodium electrodes in acid solution ($\partial V/\partial \ln i \approx -2RT/F$) is different from that at the prereduced electrodes ($\partial V/\partial \ln i \approx -RT/F$).

Acknowledgments. We wish to thank the U. S. Army Electronics Research and Development Laboratory, Fort Monmouth, N. J., for financial support (Contract No. DA-36-039-SC88921) and Dr. H. F. Hunger and Mr. J. Wynn for discussions. We also thank Mr. O. Shannon for machining the rotating disk apparatus and Dr. E. Yeager for the design.

Adsorption of Polar Organic Molecules on Chromium

by B. J. Bornong and P. Martin, Jr.

Rock Island Arsenal, Laboratory Branch, Rock Island, Illinois 61201 *(Received January 30, 1967)*

Ellipsometric and surface potential (ΔV) data were obtained, at 25° and 40% relative humidity, on retracted monolayers of the homologous series of amines, amides, acids, and alcohols on chromium. Curves of ΔV *vs.* N, where N is the number of carbon atoms per adsorbed molecule, reached an asymptotic maximum at $N \geq 14$ for the amines and at $N \geq 18$ for the acids and alcohols. ΔV was constant for the amides up to $N = 18$. Surface dipole moments (μ_D) were calculated from the Helmholtz equation using ΔV and surface coverage data.

Introduction

Studies have been made using ellipsometry[1-4] and surface potential techniques[5-10] to measure the adsorption of certain polar organic compounds on metals. A recent work[11] combined the two methods to perform parallel experiments on the growth of oxide films on metals. The work reported here, using these methods, was intended to improve our understanding of molecular packing and dipole orientation in adsorbed films and to develop specific models for the systems studied.

Experimental Section

Materials. The following reagent grade or White Label compounds were used in this investigation: acetic acid (Du Pont); formic, palmitic, and stearic acids, 1-octanol, butylamine (Fisher Scientific Co.); octanoic, decanoic, lauric, and myristic acids, butyl, decyl, and dodecyl alcohols, 1-tetradecanol, 1-octadecanol, hexylamine, stearamide (Eastman Kodak). Compounds of other purity designations were: docosanoic acid 99%, cerotic acid of undesignated purity (Eastern Chemical Corp.); acetamide, butyramide, hexanamide, octanamide, lauramide, myristamide, pal-

(1) J. R. Miller and J. E. Berger, *J. Phys. Chem.*, **70**, 3070 (1966).
(2) L. S. Bartell and J. F. Betts, *ibid.*, **64**, 1075 (1960).
(3) W. T. Pimbley and H. R. MacQueen, *ibid.*, **68**, 1101 (1964).
(4) R. R. Stromberg, E. Passaglia, and D. J. Tutas, *J. Res. Natl. Bur. Std.*, **A67**, 431 (1963).
(5) K. W. Bewig and W. A. Zisman, *J. Phys. Chem.*, **67**, 130 (1963).
(6) C. O. Timmons and W. A. Zisman, *ibid.*, **69**, 984 (1965).
(7) M. H. Gottlieb, *ibid.*, **64**, 427 (1960).
(8) F. M. Fowkes, *ibid.*, **64**, 726 (1960).
(9) B. J. Intorre, T. K. Kwei and C. M. Peterson, *ibid.*, **67**, 55 (1963).
(10) D. A. Haydon, *Kolloid Z.*, **188**, 141 (1963).
(11) J. E. Boggio and R. C. Plumb, *J. Chem. Phys.*, **44**, 1081 (1966).

mitamide, and stearamide, 95–99% (K & K Laboratories, Inc.); 1-hexadecanol, Fisher N.F. grade, and a commercial sample from Archer Daniels Midland Co. Hexyl alcohol, 1-eicosanol, octylamine, decylamine, dodecylamine, tetradecylamine, hexadecylamine, and octadecylamine were practical or technical grade (Eastman Kodak).

All the alcohols, liquid acids, docosanoic, and cerotic acids were percolated through alumina or silica gel columns while molten or in their normal liquid state to remove more adsorbable impurities. The amides, except the White Label sample which was used as received, were recrystallized from ethanol after treatment with activated carbon. The remaining compounds were used as received. Amines used probably contained carbon dioxide because they melted over wide temperature ranges. Other compounds used had melting points within 1–2° of their literature values.

Thickness Measurements. Ellipsometer measurements were made with a Rudolph Model 436/200 E with photoelectric attachments. Procedures for use of the ellipsometer have been described.[12-14] The instrument was calibrated for this study with Langmuir–Blodgett barium stearate films deposited on chromium (ferrotype plate) surfaces.[15,16] Polarizer and compensator were placed before reflection. A mercury light source giving the 5461-A line was used. The change in Δ, the phase difference caused by reflection, in going from film-free to film-coated surface was taken to be proportional to film thickness in the thickness range measured here.[17] Each thickness was obtained by a difference measurement on every chromium specimen; the calibration factor of 6.32 A/deg change in Δ was used. It was assumed that refractive indexes of calibration films and measured films were the same. Comparison of the calibration procedure with the Drude linear approximation[18,19] gave the same film thickness when a film refractive index of 1.52 was substituted into the approximate equation. The angle of incidence was 70°.

Surface Potential Measurements. The vibrating condenser method as originally described by Zisman[20] was used to make surface potential measurements. A diagram of the apparatus is shown in Figure 1. The reference electrode of platinum (1 cm diameter) was above the test electrode and vibrated at 500 cps by a permanent magnet speaker cone energized by a General Radio audio oscillator, Type 1311-A. The metal to be measured was placed on a metal platform. A bakelite holder for the platform could be made parallel to the upper electrode by three leveling screws. In addition, the entire leveling device holding the lower electrode could be raised or lowered by means of a large screw at the bottom of the chamber. The entire assembly

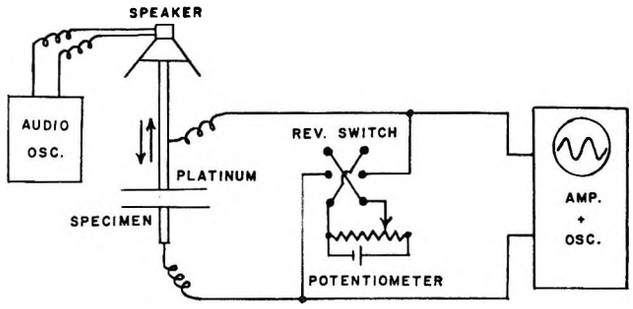

Figure 1. Diagram of the vibrating condenser apparatus.

was housed in a heavy metal chamber to minimize any electrical interference.

The signal generated by the vibrating condenser was fed into a Keithley decade isolation amplifier, Model 102-B, followed by a General Radio amplifier and null detector, Type 1232A, which filtered out all frequencies except 500 cps. The amplified and filtered signal was registered on the null detector or observed on a Dumont oscilloscope 304H as a sine wave.

To measure a potential, the metal specimen studied was placed on the platform directly under the platinum electrode. The specimen was raised to within approximately 0.5 mm of the reference electrode. The sensitivity of the condenser could be improved by decreasing the distance between the electrodes without affecting the potential.

The magnitude of the potential was obtained by applying an opposing voltage across the two electrodes by using a 1.5-v battery and a ten-turn potentiometer. When the null detector indicated zero or the sine wave on the oscilloscope disappeared, the potential was measured with a Precision Scientific titrometer, Model 8860. Measurements could be made within 2 mv. A reversing switch was used to indicate the presence of any additional electrical fields. Using this switch, the polarity of the potential would be reversed but its magnitude would not.

In this work, the surface potential (ΔV) represented the change from the initial to the final potential which is

(12) A. B. Winterbottom, "Optical Studies of Metal Surfaces," The Royal Norwegian Scientific Society, Report No. 1, F. Bruns, Trondheim, Norway, 1955, Chapter 3.

(13) A. Rothen, *Rev. Sci. Instr.*, **28**, 283 (1957).

(14) F. L. McCrackin, E. Passaglia, R. R. Stromberg, and H. L. Steinberg, *J. Res. Natl. Bur. Std.*, **A67**, 363 (1963).

(15) K. B. Blodgett, *J. Am. Chem. Soc.*, **57**, 1007 (1935).

(16) K. B. Blodgett and I. Langmuir, *Phys. Rev.*, **51**, 964 (1937).

(17) See ref 12, p 42.

(18) P. Drude, *Ann. Physik*, **36** (3), 865 (1889).

(19) A. C. Hall, *J. Phys. Chem.*, **69**, 1654 (1965).

(20) W. A. Zisman, *Rev. Sci. Instr.*, **3**, 367 (1932).

produced when a film is adsorbed on an initially clean surface. Electrical interference was minimized by using shielded cables throughout, enclosing the loudspeaker and potentiometer in metal boxes, and connecting the entire shielding system to a common ground. The aged platinum reference electrode was checked periodically with a second platinum specimen. The potential difference did not change by more than 10 mv over a period of several weeks. The aged platinum was considered suitable since it did not vary during the time for a measurement.

Procedures. Commercial ferrotype plates, chromium plated steel (Apollo Metal Works), were sheared into 20 × 25 mm pieces. Residual organic films were removed from the chromium surface by dipping the metal pieces in chromic acid and flaming, as previously described.[14] This procedure probably produces a chromium–chromium oxide surface. Ellipsometer readings were taken on each surface immediately after flaming. The average Δ value for these film-free surfaces was 133.69° and was reproducible to within 0.48°. For a given chromium specimen, Δ could be reproduced to within 0.1°. Potential measurements were made within 6–8 min after flaming; the average potential value was 265 mv and was reproducible to within 5 mv. The organic film was applied immediately after these measurements were made. Retraction from the melt was the usual method of application of a film.[21] The chromium specimen was placed on the heating stage of a melting point apparatus; the retraction temperature was 5–10° above the melting point of the compound. Liquids were applied at room temperature. Homologs with less than six carbons did not retract; these compounds were placed on the chromium and allowed to evaporate for 3–5 min. Final potential and ellipsometer readings were taken immediately after application of the films. Additional retracted films of octadecylamine and stearic acid were applied at higher temperatures to determine the effect of retraction temperature on film thickness and surface potential. All potential and ellipsometric measurements were made at 25 ± 1° and 40 ± 10% relative humidity.

Results and Discussion

All the experimental and calculated data for the adsorbed organic films on chromium are shown in Table I. Surface potential data from Table I are shown in Figure 2, plotted against N, the number of carbon atoms for the homologous series of fatty acids, alcohols, amines, and amides. Markers on the graph represent the arithmetical mean for each compound. The curves rise to an asymptotic maximum at $N \geq 18$ for the acids and alcohols and at $N \geq 14$ for the amines. The amides

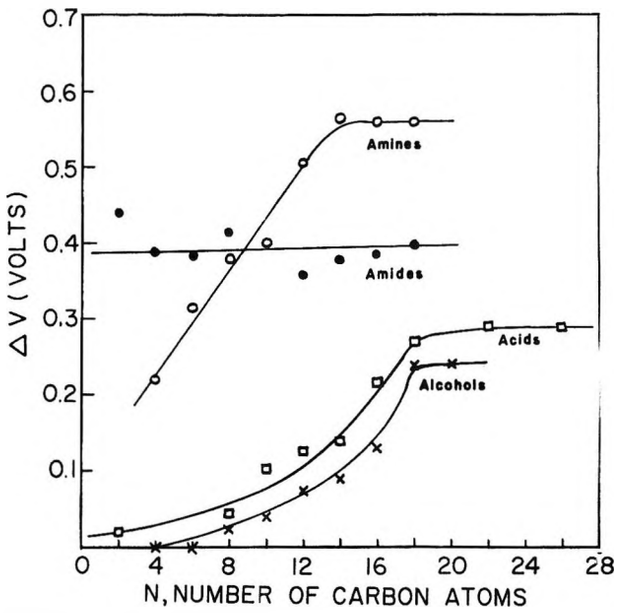

Figure 2. Surface potentials for homologs adsorbed on chromium.

gave a horizontal line indicating surface potential independent of chain length.

The behavior of amines on platinum as reported by Bewig and Zisman[5] is analogous to that obtained here. ΔV for stearic acid adsorbed on chromium agrees with that obtained by Timmons and Zisman.[6] However, they obtained an asymptote at $N \geq 14$ for the adsorption of acids on Pt and NiO. This difference may be caused by the dissimilar metals, different surface preparations, and dipole orientation.

Ellipsometric data from Table I on the homologous series of compounds are plotted in Figure 3. Data for the acids and amines are joined by the longest curve, the alcohols by the lower curve, and the amides by the dotted line. The curves show thicknesses somewhat lower than expected for close-packed monolayers. For example, stearic acid has a measured thickness of 18.4 A, which is less than the expected value of 24.4 A.[15,16] Thinning of the monolayers is taken to indicate that the films are not close packed. The ellipsometer, then, measures the average thickness of partially depleted films. Previous work has shown that film thicknesses of monolayers measured ellipsometrically are proportional to the number of adsorbed molecules.[1,2]

That the monolayers studied here are not close packed is in part caused by their method of application. Figure 4 shows the effect of the retraction temperature

(21) W. A. Zisman, Advances in Chemistry Series, No. 43, R. F. Gould, Ed., American Chemical Society, Washington, D. C., 1964, pp 8–11.

Table I: Properties of Adsorbed Films on Chromium

No. of carbon atoms	No. of measurements	ΔV (av dev),[a] mv	No. of measurements	Film thickness (av dev),[a] A	Surface coverage, θ	Av dipole moments, lit. values,[b] μ, D.	Surface dipole moment, μ_p, D.
				Amines			
4	1	220	1	4.7	0.69	1.4	0.17
6	6	316 (±5)	6	4.6 (±1.8)	0.57	1.3–1.6	0.29
8	4	380 (±20)	6	6.5 (±0.9)	0.60	1.4	0.34
10	2	400 (±25)	2	8.4 (±1.6)	0.62	1.3	0.34
12	3	505 (±30)	4	11.4 (±1.1)	0.70		0.38
14	4	565 (±30)	4	13.7 (±0.5)	0.72		0.42
16	4	560 (±20)	4	14.2 (±1.7)	0.66		0.45
18	4	560 (±30)	6	18.5 (±0.8)	0.76		0.39
				Amides			
2	1	450				3.6	
4	1	390				3.5	
6	2	385 (±5)	2	4.5 (±0.9)	0.56		0.36
8	4	415 (±35)	4	6.5 (±0.3)	0.60		0.37
12	8	359 (±40)	8	11.8 (±1.5)	0.72		0.26
14	12	377 (±40)	12	12.1 (±1.1)	0.64		0.31
16	11	385 (±30)	11	13.2 (±0.7)	0.61		0.33
18	21	398 (±10)	23	14.6 (±0.9)	0.60		0.35
				Acids			
2	3	20 (±10)	3	2.3 (±1.8)	0.85	1–1.5	0.012
8	3	47 (±7)	3	5.9 (±0.9)	0.55	1.2	0.045
10	2	105 (±5)	2	8.6 (±1.5)	0.63		0.088
12	5	125 (±20)	8	9.6 (±1.0)	0.59	0.8	0.11
14	2	140 (±10)	6	13.1 (±0.9)	0.69		0.11
16	2	217 (±7)	5	16.0 (±0.6)	0.74		0.16
18	14	270 (±10)	18	18.4 (±1.5)	0.75		0.19
22	2	292 (±8)	18	23.5 (±1.4)	0.79		0.20
26	6	290 (±10)	15	28.4 (±1.9)	0.80		0.19
				Alcohols			
4	2	0 (±5)	3	4.0 (±1.2)	0.74	1.7	0
6	2	0 (±10)	3	2.8 (±1.1)	0.35	1.65	0
8	2	25	4	4.4 (±1.1)	0.41	1.7	0.032
10	5	40 (±10)	7	5.7 (±0.9)	0.42	1.65	0.050
12	4	75 (±5)	4	8.1 (±0.6)	0.50	1.5	0.080
14	6	90 (±10)	7	11.1 (±1.5)	0.58		0.082
16	2	130 (±10)	2	15.1 (±0.1)	0.70		0.098
18	3	240 (±10)	4	19.1 (±2.6)	0.78		0.16
20	3	240 (±10)	6	21.6 (±3.0)	0.80		0.16

[a] Average deviation from the mean shown. [b] A. L. McClellan, "Tables of Experimental Dipole Moments," W. H. Freeman and Co., San Francisco, Calif., 1963.

on ellipsometric film thickness for stearic acid and octadecylamine. The rapid initial drop in thickness shows that close-packed monolayers could not be obtained when films were applied at 5–10° above the melting points of the compounds. That the curves shown level out at higher temperatures suggests a strong adsorption under these conditions, probably chemisorption, on the chromium–chromium oxide substrate. Incomplete desorption has also been reported for stearic acid on NiO.[6]

Estimates of surface coverage (θ) in Table I were made by taking the thickness (24.4 A) to correspond to a close-packed film of vertically oriented molecules for the 18-carbon compounds. It is assumed that thicknesses for close-packed monolayers of lower and higher straight chain homologs fall on a line from the origin

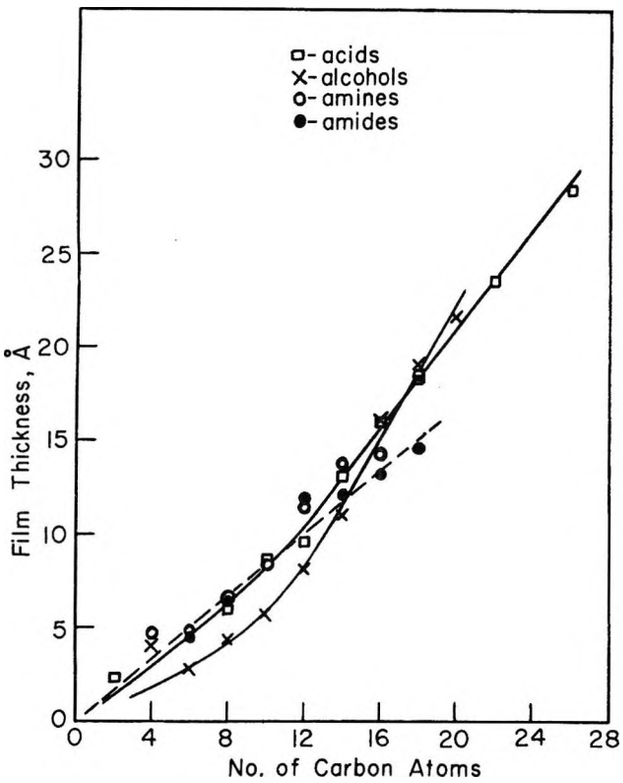

Figure 3. Ellipsometric film thicknesses of homologs adsorbed on chromium.

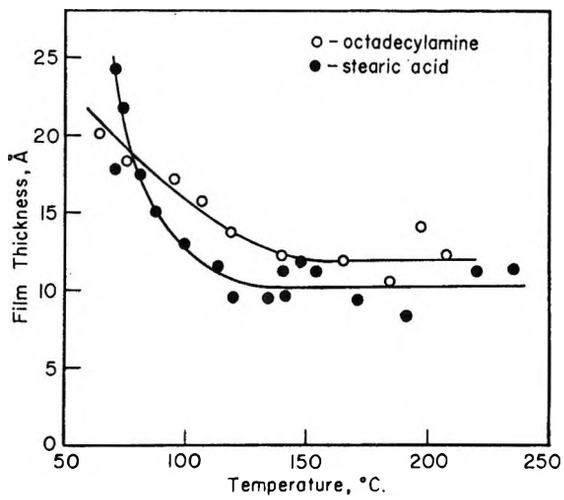

Figure 4. Effect of retraction temperature on adsorbed monolayers of stearic acid and octadecylamine.

through the 24.4-A thickness value. The stearic acid film, then, contains about 75% of the number of molecules of a close-packed monolayer.

The Helmholtz relation can be used to correlate the data shown in Table I. This relation is

$$\Delta V = 4\pi n\mu_p$$

where n is the number of molecules per unit area and μ_p is the total perpendicular component or surface dipole moment. Changes in ΔV from one member of the series to another should reflect differences in molecular packing and dipole orientation. ΔV increases with chain length for the amines, acids, and alcohols. This increase indicates an increase in the number of molecules adsorbed and an increase in dipole orientation. The constant ΔV for the higher homologs is indicated by both constant coverage and maximum orientation. For the amides, both the surface coverage and ΔV are constant; therefore, these homologs have the same packing and orientation.

The last column in Table I shows the experimental surface dipole moments calculated by the Helmholtz equation using n equal to θ/A, where A is the molecular area. The molecular area for a close-packed molecule was assumed to be 20 A^2. The moments obtained were less than the known values available for the compounds in the gaseous state. This is probably due to the induced polarization caused by the metal and other adsorbed molecules.[22] Since μ_p is derived from ΔV and θ, relationships between it and chain length can also be explained by molecular packing and orientation.

It can be seen in Table I that μ_p for the amides and amines at about 60% coverage is three times larger than μ_p for the acids and alcohols at the same coverage. For the amides, these large differences can be explained by the average dipole moments (μ) being about three times higher than for the acids and alcohols. However, this explanation does not satisfy the μ_p values shown for the amines. An alternative is that the relatively large differences may be associated with the more basic property (the electron-donating capacity) of the NH_2 group as compared to the OH group. Therefore, interactions of these groups with the metal–metal oxide surface appears to be more important in determining ΔV than does surface coverage for the compounds studied.

The variation of μ_p with chain length, as shown in Table I, requires some discussion. The surface dipole moment is composed of the following dipole vector terms: those of the head group in its adsorbed state, those of adsorbed atmospheric gases, and that of the methyl group. The increase in μ_p observed for the amines, acids, and alcohols from the lower to higher homologs was about 0.15 D. This increase may be attributed to changes in the vertical components of the three dipole vector terms. Variations in these vectors can be brought about by changes in the angle of tilt, rearrange-

(22) C. O. Timmons and W. A. Zisman, *J. Phys. Chem.*, **68**, 1336 (1964).

ments of dipoles in the substrate surface layer, changes in bonding of the adsorbed head group to substrate, and changes in lateral interactions between adsorbed molecules. Each of these terms can be expected to vary when the chain length and surface coverage change.

The apparently constant orientation of the amides, reflected by their constant ΔV, can perhaps be interpreted as follows. Stuart–Briegleb models show that the aliphatic carbon chain can exist in a spiral vertical form which occupies about one-third greater surface area than the straight chain model. If the amide films were in this configuration, they would be nearly "close packed" at 60% coverage as calculated from a straight-chain model. At other surface coverages, the amides would be expected to behave like the other homologous series studied.

The results of this study show that ellipsometric and surface potential measurements can be used to obtain reproducible surface dipole moments. More work is needed to separate the various dipole vector terms involved before the data can be analyzed further.

Acknowledgment. The authors thank Dr. L. G. Wiedenmann for helpful discussions on molecular structure.

Photodecomposition of α-Lead Azide in the Solid State

by V. R. Pai Verneker[1] and A. C. Forsyth

Explosives Laboratory, Picatinny Arsenal, Dover, New Jersey *(Received March 6, 1967)*

The kinetics of nitrogen evolution from α-lead azide during irradiation with ultraviolet light from a low-pressure mercury lamp has been investigated as a function of the intensity, temperature, and time of the irradiation, the method of preparation, and the age of the sample. The data clearly demonstrate the dependence of the initial photolytic decomposition rate on the method of preparation. It is further concluded that, during the aging process, the defects (resulting from the incorporation of impurities) which participate in the photodecomposition disappear irreversibly. The efficiency of the photolytic process is seen to be greater at $+10°$ than at $+25°$. This is discussed in the light of possible electron traps and intermediate free radicals.

Photodecomposition of Lead Azide in the Solid State

The thermal decomposition of α-lead azide under vacuum and in air has been extensively studied.[2] The mechanism, which assumes that the final product of decomposition, lead, catalyzes the reaction, has been shown to be valid by the experiments by Reitzner, *et al.*[3a] Acceleration of the thermal decomposition of α-PbN_6 as a result of prior irradiation has also been demonstrated experimentally.[3b] Recently Jacobs, *et al.*,[4] have shown how the photodecomposition of BaN_6 is affected by its prior partial thermal decomposition. On the other hand, no work on the photolysis of PbN_6 is reported in the literature.

Experimental Section

PbN_6 was contained in a small boat so as to keep constant the surface area exposed to the light source.

(1) Research Institute for Advanced Studies, Baltimore, Md. 21227.

(2) W. E. Garner and A. S. Gomm, *J. Chem. Soc.*, 2123 (1931); W. E. Garner, A. S. Gomm, and N. R. Hailes, *ibid.*, 1393 (1933); W. E. Garner, *Proc. Roy. Soc.* (London), **A246**, 203 (1958); W. E. Garner, "Chemistry of the Solid State," Butterworth and Co. Ltd., London, 1955, Chapters 7 and 9; G. Todd, *Chem. Ind.* (London), 1005 (1958); M. Stammler, J. E. Abel, and J. V. R. Kaufman, *Nature*, **185**, 456 (1960); B. Reitzner, *J. Phys. Chem.*, **65**, 948 (1961).

(3) (a) B. Reitzner, J. V. R. Kaufman, and E. F. Bartell, *ibid.*, **66**, 421 (1962); (b) J. V. R. Kaufman, *Proc. Roy. Soc.* (London), **A246**, 219 (1958); W. Groocock, *ibid.*, **A246**, 225 (1958); J. Jach, *J. Phys. Chem. Solids*, **24**, 63 (1963).

The boat was in turn placed in a transparent silica cell with a flat window connected *via* a B-24 standard joint to a vacuum line. This consisted, in sequence, of a trap immersed in liquid nitrogen, a standard volume, a Pirani gauge, a McLeod gauge, a cutoff, a second trap, a diffusion pump, and a backing pump. The temperature of the azide was measured with a calibrated copper–constantan thermocouple in the sample. The intensity of the light (λ ~2537 A) was changed whenever desired by changing its distance from the sample. The PbN_6 used throughout the course of the work, except when the effect of different preparations was being studied, was prepared as follows. PbO as supplied by Messrs. Johnson and Matthey, United Kingdom, was converted to lead nitrite by bubbling nitrous oxide through an aqueous suspension of PbO. Gaseous HN_3 prepared from a Reitzner generator[5] was collected in alcohol and the alcoholic solution of HN_3 was added to the solution of lead nitrite to obtain PbN_6. X-Ray and chemical analyses revealed the product to be α-PbN_6. Three other preparations, as follows, were also investigated. Instead of using spectroscopic grade PbO, reagent grade PbO was used as the starting material. A solution of lead acetate was allowed to react with a solution of NaN_3. PbN_6 as supplied by Du Pont [prepared from $Pb(NO_3)_2$] is also used. Fresh PbN_6, prepared as described above, was stored in the dark in a vacuum desiccator (pressure 10^{-2} mm). Before the start of any photolysis experiment, the pressure was always less than 1×10^{-6} mm. The low-pressure mercury lamp was allowed to warm up for a minimum of 20 min before a run. The nitrogen gas evolved was measured with a Pirani gauge.

Results

The rate of nitrogen evolution from a freshly prepared sample of α-PbN_6 plotted against the time of irradiation is shown in Figure 1. The rate decreases and then attains a constant value. Figure 1 also shows how different preparations behave when photolyzed. Except for the Du Pont material, the samples show approximately the same final, constant rate although the initial rates vary. If the light is switched off after the photolytic rate has attained a constant value, gas continues to be evolved. The rate of this reaction (termed hereafter the dark rate) falls off gradually and ultimately becomes zero, as shown in Figure 2. The total gas collected after the light is switched off is directly proportional to the total time of irradiation, as can be seen in Figure 3. If the sample is reirradiated after the postirradiation gas evolution stops, *i.e.*, the dark rate becomes zero, the rate starts at a lower value. This rate is lower than the constant rate in the initial

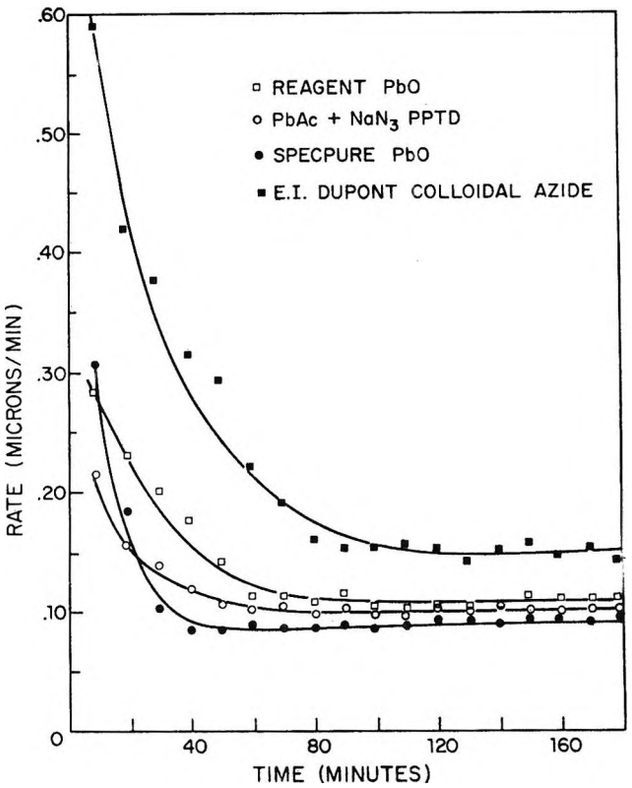

Figure 1. Decomposition rate *vs.* time of irradiation (λ ~2537 A) for various preparative methods of α-PbN_6.

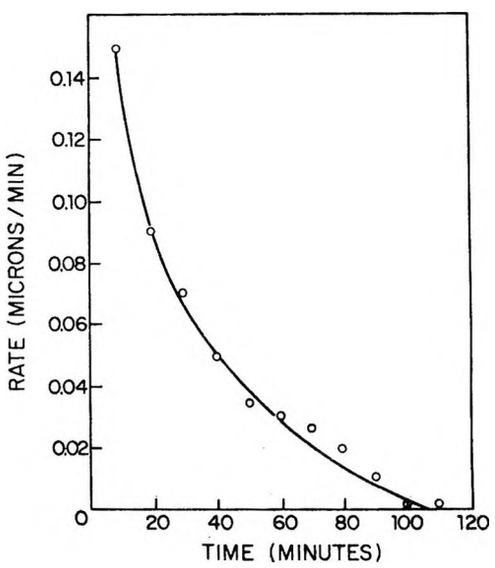

Figure 2. Dark rate *vs.* time.

(4) P. W. M. Jacobs, F. C. Tompkins, and V. R. Pai Verneker, *J. Phys. Chem.*, 66, 1113 (1962).

(5) B. Reitzner and R. Manno, *Nature*, 198, 991 (1963).

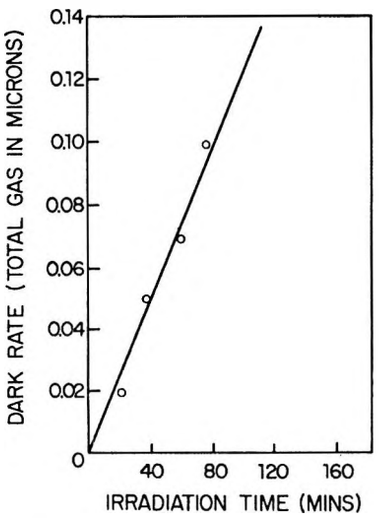

Figure 3. Dark rate as a function of irradiation time.

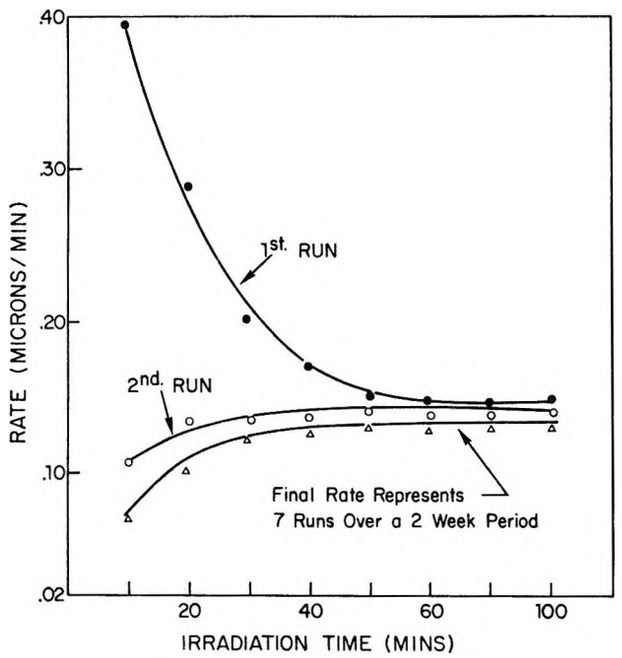

Figure 4. Subsequent rate–time plots on the same sample of α-PbN_6.

run and increases to attain approximately the same value as that of the constant rate in the initial run. Figure 4 presents plots of these curves. The starting point of the Nth run depends on the time that has elapsed between the Nth and the $(N - 1)$th runs. If the initial rate is R_1 and the final constant rate R_2, then $(R_2 - R_1)$ is dependent on the time elapsed between the two runs if the time is of the order of 10 min. This is shown in Figure 5. From Figure 6 it can be

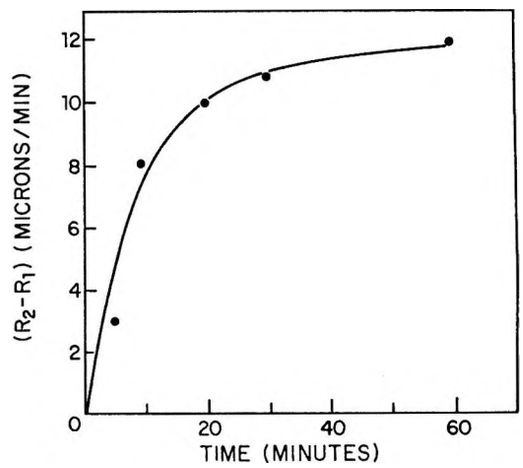

Figure 5. Plot of final rate minus the subsequent starting rate $(R_2 - R_1)$ *vs.* time.

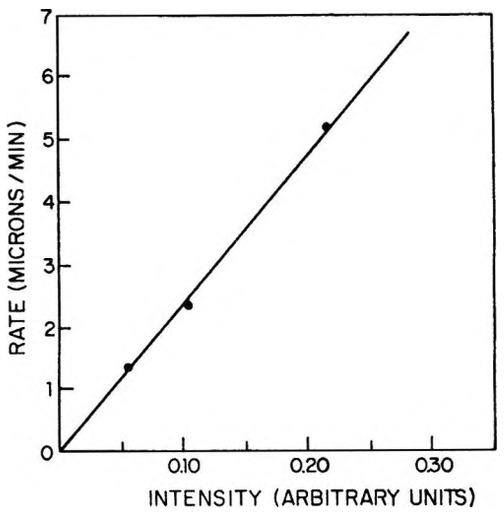

Figure 6. Final constant rate *vs.* light intensity.

seen that the constant rate is directly proportional to the intensity of the light. Finally, the activation energy for the process is found to be negligible between 30 and 80°.

If 2% of the sample is thermally decomposed prior to photolysis, the behavior of the sample does not change, *i.e.*, the photolytic rates are the same as those of an untreated sample, shown in Figure 1. The total decomposition caused by photolysis amounts to less than 10^{-5} %.

During the first photolytic run the sample turns brown. If a few millimeters of oxygen is then admitted into the system and kept in contact with the sample for about 24 hr the sample turns white and, on reirradiation, behaves as if it were a fresh sample (Figure 7).

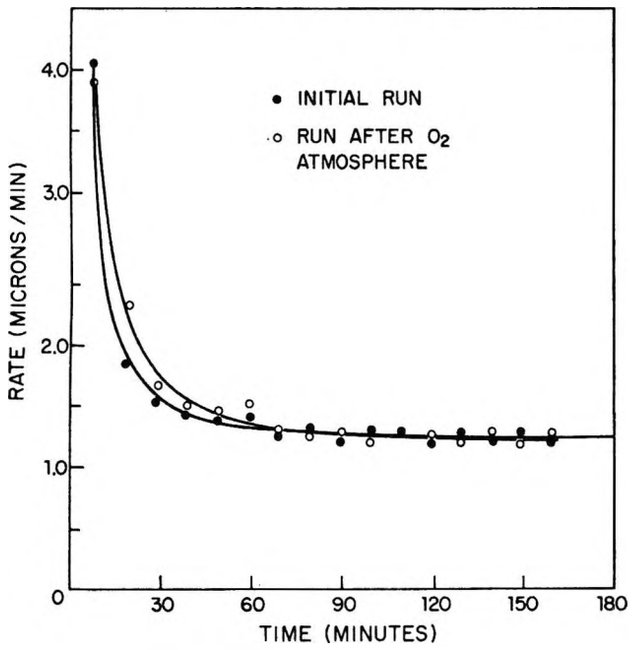

Figure 7. Rate–time plot: ●, fresh sample of α-PbN_6; ○, the same photolyzed sample of α-PbN_6 on exposure to oxygen.

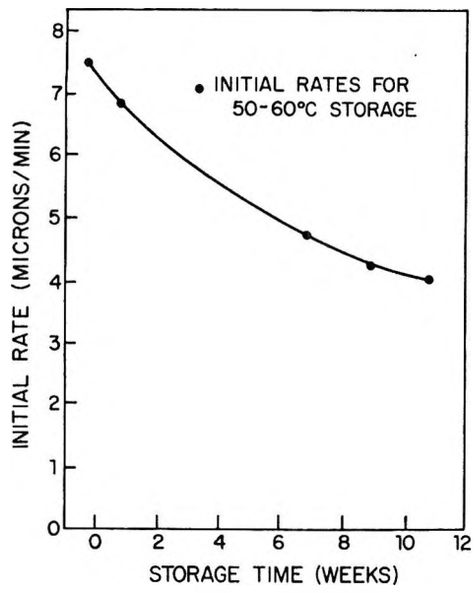

Figure 8. Effect of long-term storage at 50–60° on the photolytic decomposition of α-PbN_6.

Figure 8 shows how samples not exposed to any light and preserved *in vacuo* behave when photolyzed after different storage times. Storage at different temperatures (−196 to +55°) does not seem to have an appreciable effect. When kept at −196° the aging process (the falling off of the initial photolytic rate with storage time) seems to slow down slightly, particularly

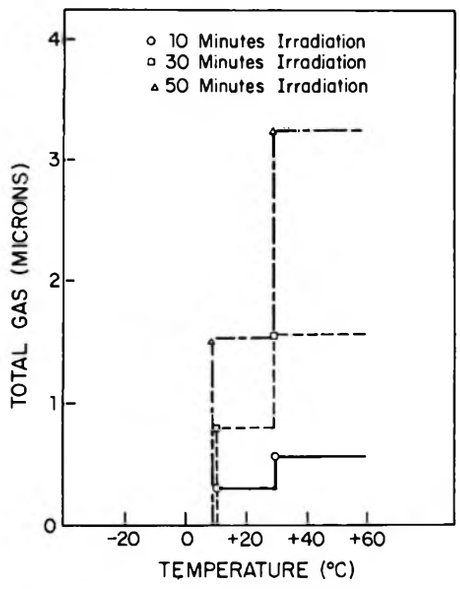

Figure 9. Irradiation of α-PbN_6 at −30° and subsequent gas evolution on warm-up at higher temperatures.

during the first week. A sample which has aged for several months does not show any change in behavior even when exposed to oxygen (compared with Figure 7). Photolysis of PbN_6 in the temperature range −40 to 0° does not produce any gas during irradiation but, if the irradiation is stopped and the sample warmed up, a burst of gas is given off at +10°. On further warming another burst is observed at +25° (Figure 9). The total gas collected at +10° is double that collected at +25°.

Irradiation of a sample at a constant lamp intensity and for a constant time at both +10° and also at +25° shows a marked difference. Irradiation at +10° produces a certain quantity of gas, but on warming to +25° more gas is evolved. The total gas thus collected is about 15% greater than the volume of gas evolved when the irradiation is done only at +25°. Figure 10 is a plot of the gas collected on warm-up *vs.* the time of irradiation at −40°. It can be seen that for short irradiations the gas evolved depends on the time of irradiation but for long irradiations the gas volume is independent of the time of irradiation and is constant. Furthermore, during the initial part of the curve in Figure 10, the rate of gas evolution is proportional to the intensity of the light.

Discussion

In all azides studies thus far,[6] the photolytic rate (rate of gas evolution) decreases and then attains a

(6) V. R. Pai Verneker, submitted for publication.

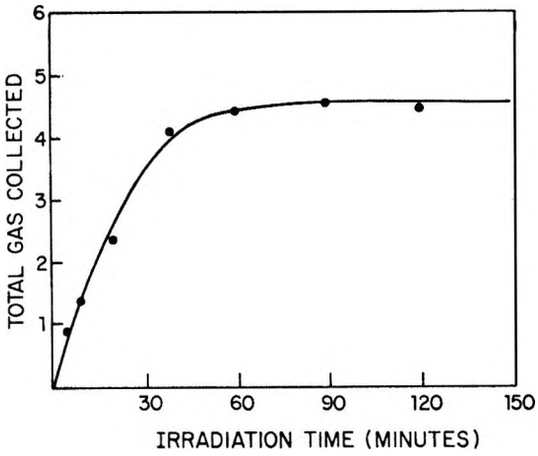

Figure 10. Total gas collected on warming to room temperature as a function of irradiation time at −40°.

constant value. The behavior of α-PbN_6 is in conformity with the other azides. There are certain defects, *e.g.*, negative ion vacancies, impurity ions acting as electron traps, etc., present in a crystal of PbN_6 and these defects are assumed to be consumed in the process of photolysis; hence, the original rate decreases. Metal, present in the form of nuclei or small specks and produced during the photolysis presumably initiates a new process. The photolytic reactions in sequence are

$$N_3^- + h\nu \xrightarrow[A]{\text{trap}} (AN_3^-)^* \quad \text{exciton trapped} \quad (1)$$

$$(AN_3^-)^* + N_3^- \longrightarrow 3N_2 + (eAe) + 2 \text{ vacancies} \quad (2)$$

$$Pb^{2+} + (eAe) \longrightarrow Pb^0 + \text{aggregate of traps} \quad (3)$$

Repetition of eq 1, 2, and 3 will produce Pb_n having a metallic character.

$$Pb_n + h\nu \longrightarrow Pb_n^+ + e \quad (4)$$

$$Pb_n^+ + N_3^- \longrightarrow Pb_n + N_3 \quad (5)$$

$$N_3 + N_3^- \longrightarrow 3N_2 + e + \text{vacancies} \quad (6)$$

As photolysis proceeds more metallic specks are produced and the constant rate might be expected to increase steadily. However, the small specks aggregate and thus have proportionately fewer neighboring azide ions to ionize. Thus, on one hand metallic lead of requisite size is formed and on the other hand its influence is destroyed as larger aggregates develop. The constant rate can, therefore, be considered as the steady-state rate resulting from these opposing reactions. The mechanism described above requires the photolytic rate to be proportional to the intensity. This is indeed the case (Figure 6). Details of the rate–intensity relationship are discussed by Jacobs, *et al.*[4]

Different preparations incorporate different impurities into the lead azide crystals and the variation in the initial rates is, therefore, not surprising. The mechanism of the dark rate, however, is difficult to envisage. It is possible that at the end of a photolytic run there are inside the crystal charged lead specks which continue reaction 5 after the light is switched off. Jacobs, *et al.*,[4] have explained the postirradiation gas evolution in BaN_6 in this way. It is also found that irradiated samples hold within the crystals a considerable amount of gas which can be liberated by dissolution.[7] It is possible that during the aggregation of small metallic specks some of this gas is released. This process would also show an exponential decay. The fact that the dark rate increases with the fraction of the salt decomposed, however, would favor the mechanism put forth by Jacobs, *et al.*[4]

Although the subsequent runs show the same constant photolytic rate, the initial rate of photolysis of the Nth run depends on the time elapsed between the Nth and $(N - 1)$th runs. This can also be understood on the basis of the aggregation of metallic specks. If the time elapsed between the runs is more than 10 min the initial rate is relatively independent of the elapsed time. This indicates that the aggregation is a fast process.

Experiments on the aging of lead azide samples point out that the defects which are present are steadily destroyed in an irreversible manner. Cunningham and Tompkins[8] have reported a decrease in the F center concentration in KN_3 after aging. A fresh sample of PbN_6 which has been irradiated and then subjected to oxygen suggests that the defects which were destroyed during the photolysis may be regenerated. However, an aged sample, even on exposure to oxygen, does not regenerate these defects. In the first case, during photolysis metallic lead is produced and it is possible that oxygen reacts with the lead and, in so doing, recreates the original defects (perhaps negative ion vacancies). In the second case no metallic lead is produced and hence the oxygen has nothing with which to react.

The low-temperature experiments also revealed some interesting findings which are subject to several speculative interpretations. It is possible that intermediates like N_4^- and N_2^-, which have been found in other azides,[9] are formed. The stability of these intermediates varies from azide to azide. The decomposition of N_4^- to give N_2 at +10° and of N_2^- to give N_2 at +25° would

(7) V. R. Pai Verneker, submitted for publication.

(8) J. Cunningham and F. C. Tompkins, *Proc. Roy. Soc.* (London), **A251**, 27 (1959).

(9) A. J. Shuskas, C. G. Young, O. R. Gilliam, and P. W. Levy, *J. Chem. Phys.*, **33**, 622 (1960); G. J. King, B. S. Miller, F. F. Carlson, and R. C. McMillan, *ibid.*, **35**, 1442 (1961).

explain the present results. However, it is possible to have different types of traps characterized by different trapping stabilities. If the starting reaction is represented as

$$h\nu + N_3^- \xrightarrow{\text{trap A}} (AN_3^-)^* \quad (7)$$

$$h\nu + N_3^- \xrightarrow{\text{trap B}} (BN_3^-)^* \quad (8)$$

and if one of the traps, say A, empties rapidly above +10°, then the efficiency of the backward reaction would be greater at higher temperatures. This is a possible reason why there is a 15% difference in the total gas evolution when experiments are done at +10 and +25°. The possibility that the two bursts are due to one state and caused by the method of heating cannot be ruled out. Finally, experiments carried out at −40° show that either (1) the traps are limited in number or (2) the crystal has a finite capacity to accommodate the intermediates produced. In either case one would observe a saturation effect, as observed in these experiments.

Self-Association of Alcohols in Nonpolar Solvents

by Aaron N. Fletcher and Carl A. Heller

Chemistry Division, Research Department, Naval Weapons Center, China Lake, California 93555 *(Received March 10, 1967)*

Studies were made of solutions of 1-octanol and 1-butanol in *n*-decane using the infrared absorption of the first overtone of the O–H stretch vibrations of the monomer and self-association polymers. Evaluation was made on 1-octanol solutions from 5 to 100°, *without making use of a priori self-association models*. Evaluations were performed by three methods involving comparisons of: (I) the monomer absorbance and the total alcohol concention, (II) the monomer absorbance and the polymer absorbance, and (III) a combination of I and II. The following new assignments were made: (1) the end O–H of linear self-association polymers do not contribute significant absorbance at the monomer peak in the first overtone region; (2) the monomer molar absorptivity is constant with temperature; (3) the usual "dimer" peak at 1.528 μ *cannot* be due to a O–H $\cdots$ O–H dimer as its absorbance varies directly proportionally to that of the monomer (it is tentatively assigned to an alcohol–solvent interaction); (4) the remainder of the polymer absorption is assigned solely to tetramers; and (5) the tetramers give partially overlapping peaks which are due to O–H bonds in two different tetramers. Thermodynamic values indicate a linear and a cyclic tetramer. The linear with three bonds has a ΔH of -16.5 kcal/mole and the cyclic with four bonds has a ΔH of -20.3 kcal/mole. Thus within the limits of error, all O–H first overtone absorption is explained by assigning a monomer in equilibrium with two tetramers. This holds from 10^{-4} M to neat 1-octanol over a 95° temperature range. Data from other workers for other alcohols in CCl_4 are evaluated and found to be consistent with the present assignments. Much more self-association of alcohols was observed in *n*-decane than was observed in CCl_4. In particular, kinetic data involving alcohols are explained by the physical model described.

Introduction

The literature on the self-association of alcohols in nonpolar solvents does not present a uniform picture.[1-3] In general, alcohols are considered to associate into a series of *n*-mers.[3] There have been many attempts at classifying the *n*-mers and at evaluating the equilibrium constants between the monomer and each *n*-mer. Ultrasonics,[4] dielectric,[5] spectrophotometric,[2,3] vapor pressure,[6] equation of state,[7] methyl radical abstraction,[8] and nmr[9] have been used with ambiguous results.

Infrared spectra show a monomer O–H stretch peak at low concentrations and polymer peaks which grow with concentration. Quantitative measurements have been made of the association of the monomer as shown by the monomer peak height. Assignments of polymer absorbances to dimer, trimer, and higher *n*-mers have been made. Both linear (acyclic) and cyclic *n*-mers have been postulated. At the present time there is no agreed physical picture, much less quantitative constants, which can be used to describe an alcohol solution.

(1) F. Franks and D. J. G. Ives, *Quart. Rev.* (London), **20**, 1 (1966).

(2) D. Hadzi, "Hydrogen Bonding," Pergamon Press, New York, N. Y., 1959.

(3) G. C. Pimentel and A. L. McClellan, "The Hydrogen Bond," W. H. Freeman and Co., San Francisco, Calif., 1960.

(4) R. S. Musa and M. Eisner, *J. Chem. Phys.*, **30**, 227 (1959).

(5) J. Malecki, *ibid.*, **43**, 1351 (1965).

(6) E. Steurer and K. C. Wolf, *Z. Physik. Chem.* (Leipzig), **B39**, 101 (1938).

(7) N. S. Berman and J. J. McKetta, *J. Phys. Chem.*, **66**, 1444 (1962).

(8) I. V. Berezin, K. Vatsek, and N. F. Kazanskaya, *Dokl. Akad. Nauk SSSR*, **144**, 139 (1962).

(9) V. S. Griffiths and G. Socrates, *J. Mol. Spectry.*, **21**, 302 (1966).

Our interest arose through studies of an alcohol-catalyzed autoxidation of tetrakis(dimethylamino)-ethylene[10] in *n*-decane. The oxidation rate was found to be fourth order in alcohol monomer over four orders of magnitude of the rate constant and first order at the lower concentrations. We monitored the monomer by the absorbance at 1.405 μ. We interpreted these results as indicating that the tetramer was the major alcohol polymer in the solution. Alcohol dimers and trimers should also have shown a catalytic effect, yet we found negligible evidence of their existence.

A preliminary spectrophotometric evaluation[11] of a tetramer equilibrium constant for 1-octanol was made at 30° on the basis that only monomers and tetramers were present. The equilibrium constant was used to evaluate Stern–Volmer fluorescence quenching constants.[12] From the kinetic study[10,11] we found that the tetramer had a much larger catalytic effect for the autoxidation than did the monomer. In the present work a detailed examination has been given to the self-association of alcohols *where we start with no a priori assumption with respect to the combination of n-mers.* In particular, 1-octanol has been studied since it was used in the autoxidation kinetic work. Through examination of the near-infrared absorption of the monomeric *and polymeric species* we now find evidence for only the monomer and two tetramers. This is in sharp contrast with a number of recent papers[13-16] where experimental evidence is attributed to the presence of O–H···O–H dimers. We hope that our experimental evidence will correct the widespread concept that the self-association O–H···O–H dimer is present in appreciable quantities in nonpolar solutions. It has become rather common practice to *assume* the presence of a dimer at the start of alcohol self-association studies. Without a measurable dimer, these evaluations have no meaning.

We have evaluated the extent of self-association of 1-octanol over a wide range of concentrations and temperatures. Through a short study of the self-association of 1-butanol in *n*-decane and the reevaluation of self-association data of other alcohols in carbon tetrachloride, we believe that the results of the present study can be extended to give approximate equilibrium quotients for alcohols in hydrocarbon or carbon tetrachloride systems.

Experimental Approach

Because of its chemical reactivity, we could not use carbon tetrachloride as a solvent in our autoxidation studies.[10] Instead, we used *n*-decane because of its high boiling point and its chemical inertness. Since *n*-decane absorbs heavily in the fundamental

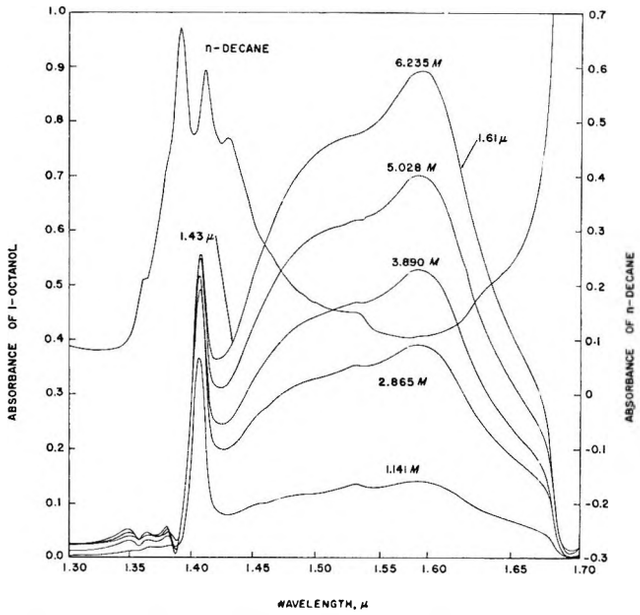

Figure 1. Varying concentrations of 1-octanol in *n*-decane at 45° with *n*-decane in the reference beam, 1-cm cells. The *n*-decane absorbance measurements were made with CCl_4 in the reference beam.

O–H stretch region, we were forced to use the region of the first overtone from 1.4 to 1.65 μ for spectrophotometric examination. As can be seen in Figure 1, *n*-decane also absorbs in this region. However, the hydrocarbon functional groups which cause the absorption by *n*-decane also exist in *n*-aliphatic alcohols. Thus it is possible to physically replace one for the other, as shown in Figure 1 by the near-isosbestic point at 1.39 μ for varying concentrations of *n*-decane and 1-octanol. By using a double-beam technique with *n*-decane in the reference, we cancel almost all of the absorbance due to the CH_2 groups of the hydrocarbon solvent. Complete cancellation is not necessary as we do not measure peak heights from the zero absorbance line but rather perform measurements from selected base points in the absorption spectra. Some type of cancellation is necessary in order to evaluate alcohol polymerization in the overtone

(10) A. N. Fletcher and C. A. Heller, *J. Catalysis*, **6**, 263 (1966).

(11) A. N. Fletcher and C. A. Heller, presented at the Symposium on Chemiluminescence, March 31–April 2, 1965, at Durham, N. C.

(12) A. N. Fletcher and C. A. Heller, *Photochem. Photobiol.*, **4**, 1041 (1965).

(13) L. J. Bellamy and R. J. Pace, *Spectrochim. Acta*, **22**, 525 (1966).

(14) A. B. Littlewood and F. W. Willmott, *Trans. Faraday Soc.*, **62**, 3287 (1966).

(15) D. A. Ibbitson and L. F. Moore, *J. Chem. Soc.*, 76 (1967).

(16) (a) S. Singh and C. N. R. Rao, *J. Phys. Chem.*, **71**, 1074 (1967); (b) A. Kivinen and J. Murto, *Suomen Kemistilehti*, **B40**, 6 (1967).

region. The results of Ens and Murray,[17] for example, who looked at a number of alcohols in carbon tetrachloride in this region, are invalid at higher concentrations since they did not correct for the effect of the CH_2 groups of their alcohol polymers.

Most of the attempts to evaluate quantitative equilibrium constants for alcohol self-association using spectrophotometric techniques make use of the variation of the monomer concentration, A_1, with respect to the formal (added) alcohol concentration, A_0, in order to determine the extent of polymerization. The majority of the workers, however, use concentrations of alcohol only up to a few tenths formal. Most of the previous infrared papers covered the fundamental region where the large molar absorptivity of the species requires very small path lengths and where the polymer has a higher absorbance relative to the monomer[18,19] (and consequent possible interference with monomer-absorbance measurements) than it does in the overtone region. By working in the overtone region and by using a Beckman DK-2 spectrophotometer with full scale ranges from 90 to 100% transmission up to 1–2 in absorbance, it was possible to use only a single 1-cm path length for a range of concentrations of 10^{-3} M up to above 6 M for pure 1-octanol or above 10 M for 1-butanol.

Measurement of Absorbances. We make the hypothesis that the absorbance peak at 1.405 μ is due solely to the monomer. We measure the 1.405-μ peak from the solution absorbance at 1.39 μ. The CH_2 absorption at 1.39 μ is almost an isosbestic point below 50° for solutions of 1-butanol and 1-octanol in *n*-decane. Mecke[20] has shown an approximate 1–1 relationship between the 1.405-μ overtone absorbance and the 2.76-μ fundamental absorbance associated with the monomer. We measure the absorbance of a polymeric species at 1.43 μ from the 1.39-μ base point since 1.43 μ also corresponds to a large amount of *n*-decane absorption. For regions that have a low *n*-decane absorption such as at 1.61 μ, we use the minimum solution absorption near 1.30 μ where *n*-decane has another area of low absorption.

The problem of considering whether polymeric species absorb at the same region as the monomer is very vital to the mathematical evaluation. Pimentel and McClellan[3] conclude that the absorbance associated with the monomer cannot be directly related to the concentration of the monomer if linear polymeric species are present. This conclusion is based upon the assumption that an O–H group with a hydrogen-bonded oxygen will absorb at or near the wavelength of the monomer. There is, indeed, a large absorbance at wavelengths only slightly higher than the 1.405-μ peak. However, none of the polymer absorbance is observed to extend lower than the 1.405-μ peak as shown in Figure 1 for even neat alcohol, and the monomer peak remains at essentially the same wavelength.

Figure 2 shows the variation of the absorbance of neat 1-octanol with temperature. It is obvious that the relative shape of curves in the polymer region (1.42–1.65 μ) vary considerably with temperature changes. Yet when the concentration changes for any specific temperature, the relative proportions of the curves change similarly to that found in Figure 1. Since the relative shapes (Figure 2) do not change from 1.61 to 1.65 μ, we have concluded that absorbance in this region is due only to one species while we shall test whether the absorbance at 1.43 μ is due only to a second species.

By using the above working hypothesis, we shall evaluate monomer and polymer absorbances. The mathematical consistency of the results will be used to test the stated working hypothesis and to assist in the assignment of the absorption bands.

Experimental Details

Apparatus. A Beckman DK-2 spectrophotometer was used to determine the absorption spectra. A Beckman No. 92527 temperature-regulated cell holder was used to control the temperature of the sample and reference solutions to within ±1° above 45°. The solutions were controlled to ±0.10° at 30°, and to ±0.5° at the remaining temperatures by circulating a tempering solution to the cell holder from a thermistor-controlled external source. The temperature of the solutions were measured in their cells by means of a Digitec digital thermometer.

Chemicals. The 1-octanol was reagent grade obtained from J. T. Baker Chemical Co. It was dried by Linde molecular sieve 4A and distilled under an atmosphere of purified helium. The *n*-decane was 95 mole % obtained from the Phillips Petroleum Co. It was digested with 30% fuming sulfuric acid, washed with concentrated sulfuric acid, water, and sodium hydroxide solution, and dried with activated alumina. It was then distilled from sodium under an atmosphere of purified helium. The 1-butanol was A.C.S. grade obtained from Allied Chemical Co. Methanol and toluene were Spectroquality reagent

(17) A. Ens and F. E. Murray, *Can. J. Chem.*, 35, 170 (1957).

(18) F. A. Smith and E. C. Creitz, *J. Res. Natl. Bur. Std.*, 46, 145 (1951).

(19) S. C. Stanford and W. Gordy, *J. Am. Chem. Soc.*, 62, 1247 (1940).

(20) R. Mecke, *Discussions Faraday Soc.*, 9, 161 (1950).

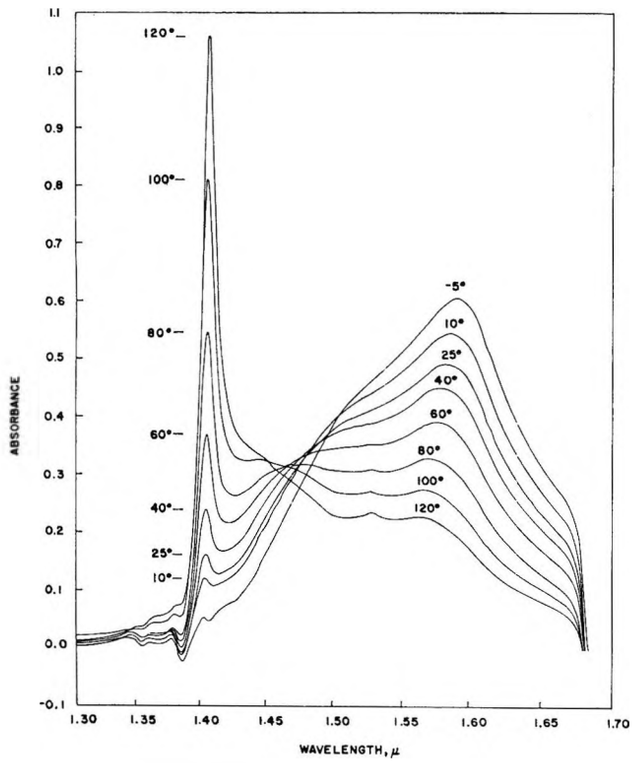

Figure 2. Neat 1-octanol in the sample beam and *n*-decane in the reference beam at various approximate temperatures in 0.5-cm cells.

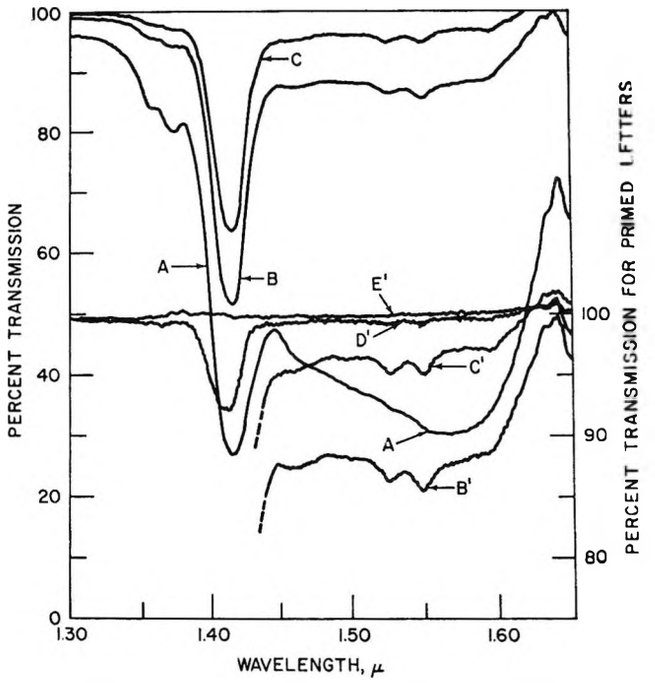

Figure 3. Methanol in toluene solutions at about 30°. Concentrations are: A, 2.5 *F*; B, 0.5 *F*; C, 0.25 *F*; D, 0.1 *F*; and E, 0.0 *F*. A prime is used for spectra of the solution when it is examined using the 75–125% transmission mode.

grade from Matheson Coleman and Bell. The last three chemicals were used without further purification.

Results

The absorbances assigned to distinct species are calculated by the differences

$$a_1 = a'_{1.405} - a'_{1.39} \quad (1)$$

$$a_{1.43} = a'_{1.43} - a'_{1.39} \quad (2)$$

$$a_{1.61} = a'_{1.61} + a'_{1.30} \quad (3)$$

where primed values indicate values measured from the zero absorbance line. The absorbance a_1 is considered as representing the monomer at concentration A_1, where the formal (added) alcohol concentration is A_0. Tables of our data are available elsewhere.[21] Figure 3 shows the spectra of solutions of methanol in toluene at about 30°. Here an example of the scale expansion of the Beckman DK-2 can be seen.

Calculations

Method I—Graphical. A molar absorptivity, ϵ_1, can be calculated for the alcohol monomer from the relationship, $\epsilon_1 A_0 = a_1$ since a plot[21] of a_1/A_0 *vs.* A_0 gives a constant value as $A_0 \rightarrow 0$. For 30° we found ϵ_1 to be 1.65 as reported earlier.[10-12] Using this ϵ_1 we can calculate the monomer concentration, A_1, in any sample from the relationship $A_1 = a_1/\epsilon_1$. The total polymer will be $(A_0 - A_1)$ formal. The concentration of each *n*-mer, A_n, will be given by the thermodynamic equilibrium constant

$$K_{1,n} = \frac{A_n}{(A_1)^n} \quad (4)$$

If any one *n*-mer is predominant it will show on a log plot of $(A_0 - A_1)$ *vs.* A_1. When such a plot is made[21] we find a fourth-order relationship between A_1 and $(A_0 - A_1)$ for concentrations down to the region where A_1 approaches the value of A_0, making the value of $(A_0 - A_1)$ inaccurate. Since this method does not yield easily accessible information concerning small amounts of other *n*-mers, we tested our data further in the following section.

Method I— Computer Fit. One can also express the

(21) Tables containing data supplementary to this article have been deposited as Document No. 9555 with the ADI Auxiliary Publications Project, Photoduplication Service, Library of Congress, Washington, D. C. 20540. A copy may be secured by citing the document number and by remitting $2.50 for photoprints or $1.75 for 35-mm microfilm. Advance payment is required. Make checks or money orders payable to Chief, Photoduplication Service, Library of Congress.

Table I: Variation of the Coefficients[a] of the Regression Equation With Some Terms Set to Zero for 30°

$$A_0 = C_1a_1 + C_2a_1^2 \cdots + C_na_1^n$$

C_6	C_5	C_4	C_3	C_2	C_1	σ[b]
0.25×10^4	-0.22×10^4	0.90×10^3	-0.62×10^2	0.23×10^1	0.5866	0.0482
-0.32×10^4	0.0	0.32×10^3	-0.15×10^2	0.81×10^{-1}	0.6055	0.0492
0.0	-0.29×10^4	0.40×10^3	-0.12×10^2	0.51	0.6017	0.0490
0.0	-0.18×10^3	0.34×10^3	0.0	−0.14	0.6085	0.0492
-0.30×10^4	0.0	0.31×10^3	0.0	−0.12	0.6065	0.0493
0.0	0.0	0.24×10^3	0.16×10^2	−0.91	0.6156	0.0500
0.0	0.0	0.26×10^2	0.59×10^1	0.0	0.6022	0.0509[c]
0.0	0.0	0.27×10^3	0.0	0.43	0.5981	0.0521
0.0	0.0	0.28×10^3	0.0	0.0	0.6127	0.0545
0.0	0.0	0.0	0.11×10^3	-0.83×10^1	0.7079	0.1013

[a] $C_i = iK_{1,i}/\epsilon_1^i$. [b] Average relative standard deviation. [c] Best fit with no negative coefficients.

Table II: Best-Fit Equations with No Negative Coefficients from 5 to 100° for 1-Octanol

$$A_0 = C_1a_1 + C_2a_1^2 \cdots + C_na_1^n$$

Temp, °C	C_4	C_3	C_2	C_1	σ[a]	j[b]
100	0.84	0.0	0.26	0.6176	0.0463	30
75	0.53×10^1	0.0	0.21	0.6227	0.0578	25
45	0.62×10^2	0.0	0.34	0.5908	0.0611	31
30	0.26×10^3	0.59×10^1	0.0	0.6022	0.0509	38
15	0.12×10^4	0.11×10^2	0.0	0.6811	0.1298	20
5	0.30×10^4	0.13×10^3	0.0	0.5381	0.1079	23

[a] Average relative standard deviation. [b] j = number of paired values of added alcohol concentration, A_0, and monomer absorbance, a_1.

relationship between A_0 and the monomer absorbance, a_1, in an algebraic equation. First we write

$$A_0 = A_1 + 2A_2 + 3A_3 + \cdots + nA_n \qquad (5)$$

where A_n is the molar concentration of the n-mer or the sum of several subforms of the n-mer. Then by making use of eq 4 between the monomer and each n-mer, it is possible to rewrite eq 5 as

$$A_0 = A_1 + 2K_{1,2}A_1^2 \cdots + nK_{1,n}A_1^n \qquad (6)$$

Substituting the absorbance and molar absorptivity for the concentration of the monomer, we obtain

$$A_0 = a_1/\epsilon_1 + 2K_{1,2}a_1^2/(\epsilon_1)^2 + \cdots + nK_{1,n}a_1^n/(\epsilon_1)^n \qquad (7)$$

The coefficients, C_i, of the power series in a_1 were obtained by fitting a regression line to the data in which the square of the relative difference between the summation of j observed and calculated values of the added alcohol

$$\sum_1^j([A_0(\text{obsd}) - A_0(\text{calcd})]/A_0(\text{obsd}))^2$$

was minimized. The program was written so that it was possible to set any coefficient equal to zero or to some other fixed value. This made it possible to eliminate results which yielded negative coefficients, and also to evaluate results from different temperatures using the same molar absorptivity for the monomer.

We searched for the mathematical best fit of eq 7, using an IBM 7094 computer, using the chemical criterion that no coefficient could be negative. Of the valid (no negative coefficients) solutions, we used the one with the smallest average relative standard derivation

$$\sigma = \left(\sum_1^j[(Y_{\text{obsd}} - Y_{\text{calcd}})/Y_{\text{obsd}}]^2/j)\right)^{1/2} \qquad (8)$$

as the closest approach to the correct polymer picture. This search was done at each temperature for which we had data, using as high as sixth-order terms. Table I shows an example of how the coefficients varied at one temperature as we searched for a best solution. Table II shows the coefficients for the valid best-fit equations for each temperature. The predominance of the fourth power is evident from this table.

Table III: Equilibrium Quotients for 5–100° Polymerization of 1-Octanol Using $1/\epsilon_1$ Equal to 0.6065. Only All Positive Combinations of K's Are Shown

$K_{1,4}$	$K_{1,3}$	$K_{1,2}$	σ^a
	100°		
1.887	0.0	0.0	0.0776
0.968	0.940	0.0	0.0618
1.523	0.0	0.408	0.0478
0.0	0.188×10^1	0.0	0.0784
0.0	0.0	0.149×10^1	0.2093
	75°		
1.064×10^1	0.0	0.0	0.0743
0.801×10^1	0.165×10^1	0.0	0.0638
0.966×10^1	0.0	0.396	0.0597
0.0	0.622×10^1	0.0	0.1276
0.0	0.0	0.236×10^1	0.3153
	45°		
1.179×10^2	0.0	0.0	0.0643
1.106×10^2	0.241×10^1	0.0	0.0628
1.157×10^2	0.0	0.234	0.0629
1.106×10^2	0.237×10^1	0.416×10^{-2}	0.0628
0.0	0.331×10^2	0.0	0.2028
0.0	0.0	$0\ 464 \times 10^1$	0.4087
	30°		
0.518×10^3	0.0	0 0	0.0550
0.480×10^3	0.774×10^1	0 0	0.0511
0.507×10^3	0.0	0 397	0.0526
0.0	0.843×10^2	0.0	0.2340
0.0	0.0	0.608×10^1	0.4257
	15°		
0.241×10^4	0.0	0.0	0.1444
0.209×10^4	0.459×10^2	0.0	0.1352
0.229×10^4	0.0	0.226×10^1	0.1360
0.0	0.280×10^3	0.0	0.3220
0.0	0.0	0.1821×10^2	0.5680
	5°		
0.701×10^4	0.0	0.0	0.1323
0.611×10^4	0.994×10^2	0.0	0.1224
0.692×10^4	0.0	0.875	0.1315
0.0	0.590×10^3	0.0	0.3145
0.0	0.0	0.167×10^2	0.5709

[a] Average relative standard deviation.

We next looked at the values of $1/\epsilon_1$ ($=C_1$). The values of Table II indicate no specific drift with temperature, so we decided to use one value at all temperatures. To do this we used j-weighted averages of the values of $1/\epsilon_1$ in Table II and obtained an average of 0.6065. This value compares closely with the 30° value of 0.60606 we obtained by measurement of the 30° molar absorptivities at low alcohol concentrations.[10-12] Fixing this coefficient we again solved for the valid combination of eq 7. Table III shows the calculated value of $K_{1,n}$ obtained in this fashion, making use of a constant value of 0.6065 for $1/\epsilon_1$ at all temperatures.

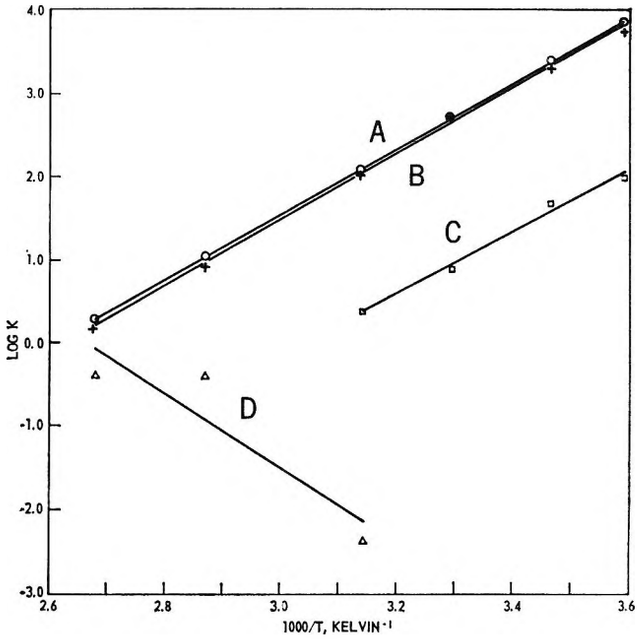

Figure 4. van't Hoff plot of method I equilibrium quotients of 1-octanol. Curve A represents the least-squares line for the monomer–tetramer equilibrium quotient, $K_{1,4}$, calculated by considering the tetramer as being the only polymer while curve B represents $K_{1,4}$ from the best-fit data where other polymers are allowed. Curves C and D represent the monomer–trimer and the monomer–dimer equilibrium quotients, respectively, from best-fit equations.

The mathematical fit of the data in Table III can be given an additional chemical restraint by a comparison of the various chemically valid equilibrium quotients with changing temperatures. Figure 4 shows a van't Hoff plot of the equilibrium constants for the best-fit data of Table III. The dimer values are obviously scattered and yield a positive ΔH. The trimer line looks good but the slope is almost the same as that of the tetramer and probably represents just errors from the tetramer line.

General Evaluation of ΔH Values Determined from Method I Type Calculations. Values of ΔH from method I type calculations have been used to support a particular equilibrium model if the ΔH/bond value falls near values found in other studies. We started to use this approach by dividing ΔH by either n or $n-1$. Surprisingly, we found that the ΔH/bond values varied from -4 to -6 kcal for almost *all* of the alcohol self-association models which gave positive equilibrium quotients from our data.

In order to test the validity of this type of evaluation, we took the absorbance values from our 5, 45, and

100° data, and used the $K_{1,4}$ equilibrium quotients for the monomer–tetramer(only) model from Table III to calculate synthetic formal 1-octanol concentrations to 10 significant digits. These values would thus correspond closely to the actual concentrations and yet would represent a precise tetramer(only)–monomer equilibrium with the same number of data points and absorbance values as the real data. We then fit second- through sixth-order equations where we evaluated only the constant of the highest order terms and the monomer terms from the synthetic data. Sixth-order equations evaluating all terms were calculated which gave very good checks on the computer. At 100°, for example, we obtained

$$A_0 = -0.28 \times 10^{-9}a_1^6 + 0.24 \times 10^{-8}a_1^5 + 0.1021 \times 10^{1}a_1^4 + 0.14 \times 10^{-8}a_1^3 - 0.15 \times 10^{-10}a_1^2 + 0.6064999983a_1 \quad (9)$$

where only tetramer and monomer values are significant.

The average relative standard deviation values for these calculations were on the order of 10^{-8}% for the tetramer(only) model and varied from 8% up to 55% for the wrong-order models. This is, of course, to be expected. The equilibrium quotients from these data were then used to determine ΔH/bond as shown in Table IV. Here we again find very reasonable values

Table IV: ΔH/Bond Values Calculated From Synthetic Tetramer(Only)–Monomer Values

Model	$-\Delta H$/bond,[a] kcal mole^{-1}	
	Cyclic	Linear
Hexamer–monomer	4.44 ± 0.01	5.32 ± 0.02
Pentamer–monomer	4.47 ± 0.02	5.87 ± 0.02
Tetramer–monomer	4.46 ± 0.02	5.94 ± 0.02
Trimer–monomer	4.13 ± 0.004	6.19 ± 0.006
Dimer–monomer	2.89 ± 0.07	5.76 ± 0.14

[a] Total ΔH divided by n for cyclic n-mer and by $n - 1$ for linear n-mer.

calculated from *any* of the models, just as we had observed from our real data (where we also tested tetramer–trimer–monomer and tetramer–dimer–monomer models). *It would appear that one can fit data to polynomials of the wrong-order models, even though there may be a very poor goodness-of-fit, and yet obtain very reasonable ΔH/bond results.* One must consequently look with skepticism upon conclusions based upon ΔH values obtained from equilibrium quotients which in turn required an *a priori* decision in the establishment of a mathematical relationship for their determination. An example of this type of situation can be seen in the work of Liddel and Becker[22] where they argue for a cyclic dimer.

Data and Calculations for 1-Butanol. Our data[21] for the system consist of 11 points at 30° in n-decane. The results of our calculations are shown in Table V.

Table V: 1-Butanol Self-Association at 30°

$A_0 = C_1a_1 + C_2a_1^2 \cdots + C_6a_1^6$				
C_4[a]	C_3	C_2	C_1	σ[b]
0.238×10^3	0.0	0.0	0.6095	0.1185
0.218×10^3	0.0	0.259×10^1	0.5125	0.0985
0.155×10^3	0.298×10^2	0.0	0.5542	0.0803
0.720×10^2	0.758×10^2	-0.561×10^1	0.6794	0.0642
0.107×10^2	0.558×10^2	-0.294×10^1	0.6061[c]	0.0691

[a] Average relative standard deviation. [b] Sixth- and fifth-order coefficients were negative when reduced in the manner for 1-octanol. [c] Fixed in order to calculate using the same molar absorptivity as that of 1-octanol.

With these few points at one temperature we cannot show that the tetramer(only) model is valid as we did for 1-octanol. However, the results are not too much different from a single temperature evaluation of 1-octanol, and it is possible to assume the tetramer(only) model and calculate the equilibrium constant $K_{1,4}$ for 1-butanol.

The butanol values fall on the same line as 1-octanol for a graphical method I plot. The computer value for $K_{1,4}$ is 432, which is close to the 530 value for 1-octanol.

Method I Values from Other Studies. We have also tried our method I computer technique on the alcohol self-association data of other workers. Unfortunately, the amount of data reported in the literature is rather limited. We examined the results for carbon tetrachloride solutions of ethanol,[23] 2-propanol,[24] and phenol[25] where the monomer absorbance had been measured by the fundamental O–H stretch peak. The results of these calculations are shown in Table VI.

None of the calculations showed the strong evidence for the lack of fifth- and sixth-order valid equilibrium quotients as we found for 1-octanol. The results often indicated negative tetramer equilibrium quotients for many of the 5- and 6-mer self-association models. To

(22) U. Liddel and E. D. Becker, *Spectrochim. Acta*, 10, 70 (1957).
(23) W. C. Coburn, Jr., and E. Grunwald, *J. Am. Chem. Soc.*, 80, 1318 (1958).
(24) H. Dunken and H. Fritzsche, *Spectrochim. Acta*, 20, 785 (1964).
(25) N. D. Coggeshall and E. L. Saier, *J. Am. Chem. Soc.*, 73, 5414 (1951).

Table VI: Self-Association of Other Alcohols in Carbon Tetrachloride Measured by the O–H Fundamental Absorption Peak. Calculation by Method I—Computer

$K_{1,4}$	$K_{1,3}$	$K_{1,2}$	σ[a]
	Ethanol[b] at 25°		
14.3[c]	0.0	0.64[c]	...
42.7	0.0	0.14	0.0538
41.0	0.97	0.0	0.0545
44.6	0.0	0.0	0.0552
	2-Propanol[d] at 20°		
65.7	2.24	0.88	0.0167
71.7	0.0	1.01	0.0172
42.7	11.4	0.0	0.0247
87.9	0.0	0.0	0.0648
	Phenol[e] at Room Temperature		
45.9	0.0	1.87	0.0155
5.9	17.2	0.0	0.0452
69.8	0.0	0.0	0.1038

[a] Average relative standard deviation. [b] From the data of Coburn and Grunwald.[23] Seven different concentrations, including their 1.03 M data, were used for these calculations. $1/\epsilon_1$ equal to 0.026676 was used for all of these results except for Coburn and Grunwald's own calculations where they used 0.02645. Other σ values for higher valid n-mer models were: 0.041 (6/4/2), 0.054 (6/4), and 0.045 (5/3/2). Some higher n-mer models result in negative tetramer terms. The notation $(x/y/z)$ indicates a model which includes only x-, y-, and z-mers in addition to the monomer. [c] Results reported by Coburn and Grunwald where they omitted their datum for 1.03 M. [d] From the data of Dunken and Fritzche.[24] Five different concentrations up to and including 1.0 M, were used. Also valid was the 6/4/2 n-mer with a σ of 0.017. Most higher n-mer models result in negative tetramer terms. [e] From the data of Coggeshall and Saier.[25] Seven concentrations were used for these computations. Maximum concentration was 0.67 F. Other valid higher n-mer models resulted in the following σ values: 0.0079 (6/4/3/2), 0.0096 (6/4/6), and 0.0102 (5/4/2). Some of the higher n-mer models resulted in negative tetramer terms. A $1/\epsilon_1$ value of 0.462 was used for all of these calculations.

some extent this is due to the lower values of A_0 used for these calculations, but other factors also have a strong bearing as will be discussed later. If the models are restricted to the tetramer and lower n-mers, however, the σ values for ethanol again indicate that the tetramer(only)–monomer model gives about as good a fit as the tetramer–trimer–monomer and the tetramer–dimer–monomer models. The preference for the tetramer is not as evident from the σ values for 2-propanol and phenol. This may be due either to the fewer data points or else to the fact that the monomer peak for the latter alcohols were not corrected for the neighboring absorption of the "dimer" as Coburn and Grunwald did for ethanol.[23]

We had anticipated the reduction of the data of others to show a more distinct fourth order. However, we now feel that there is in the data of other workers an inherent problem in the choice of the region of the fundamental to measure O–H monomer absorbance values and the almost universal choice of carbon tetrachloride as a solvent. This shall be discussed later.

Method II. A Comparison of Monomer and Polymer Absorbances. The results of method I indicated that all of the polymer absorbance might be due to just the tetramer. This means that the absorbance in the polymer region should not change shape with concentration at a fixed temperature. Measurements every 0.02 μ for the 100° results[21] showed this to be essentially correct. In Figure 1 this can also be seen to be true except for the small peak near 1.528 μ. This will be considered below but neglected here as only a small portion of the total area.

If the base point corrected absorbances at 1.61 and 1.43 μ are divided by the fourth power of the monomer absorbance, we have absorbance equilibrium quotients even though we do not make use of, nor yet know the molar absorptivity of, the species involved. In Figure 5 we have tested this ratio for the $1.61/(1.405)^4$ absorbance quotient and in Figure 6 for the $1.43/(1.405)^4$ absorbance quotient for all six temperatures.

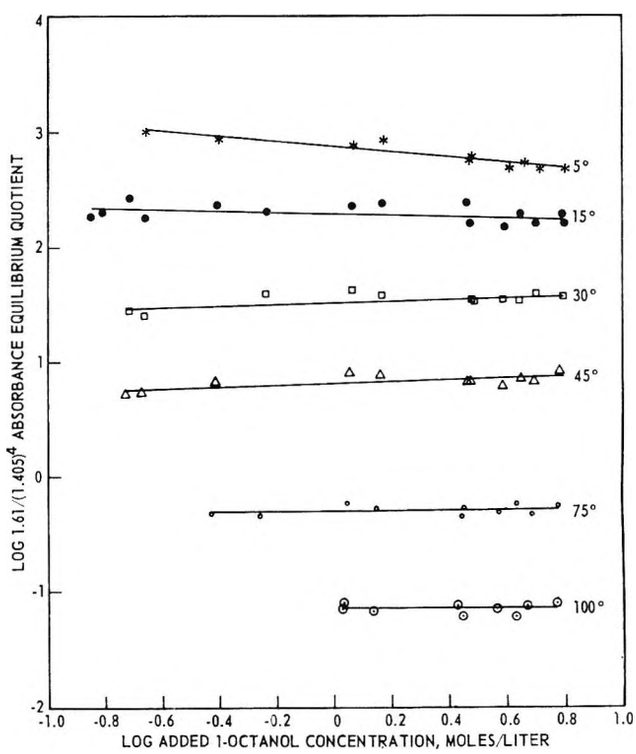

Figure 5. Test for tetramer at 1.61 μ at varying temperatures and concentrations of 1-octanol. Lines are least-squares plots.

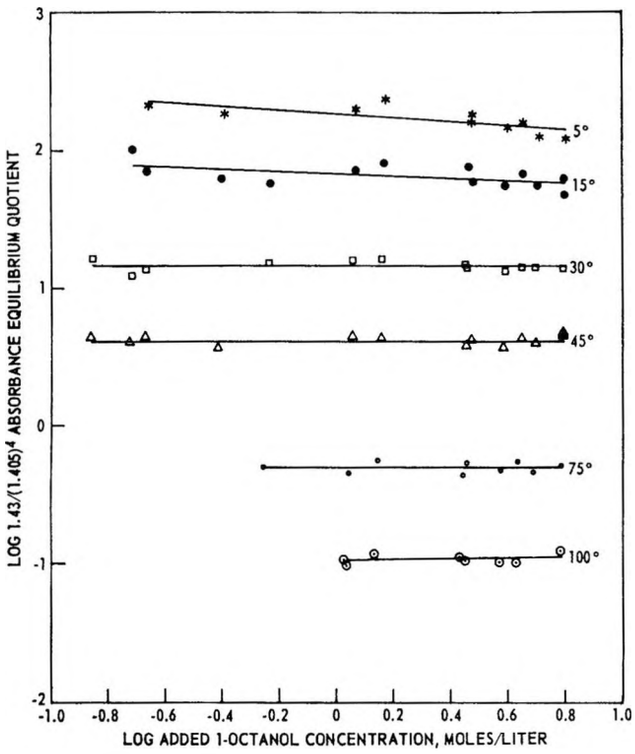

Figure 6. Test for tetramer at 1.43 μ at varying temperatures and concentrations of 1-octanol. Lines are least-squares plots.

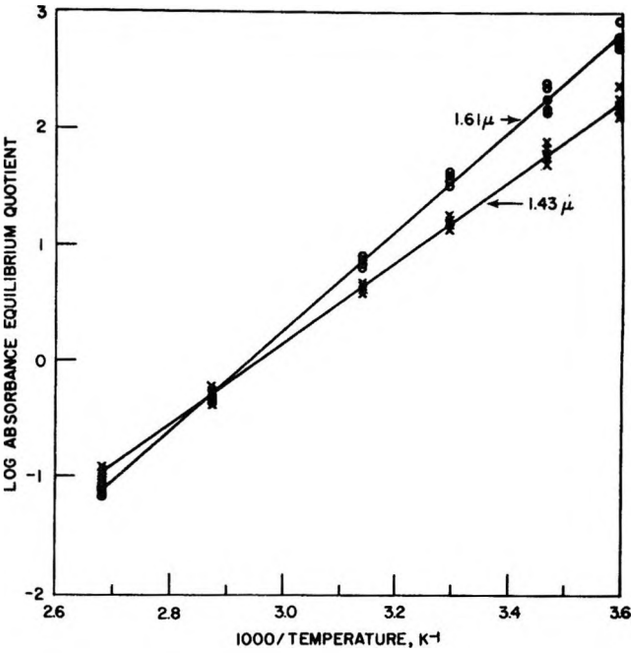

Figure 7. van't Hoff plot of absorbance equilibrium quotients of method II.

These results show that the polymer absorbance at two widely separated wavelengths are fourth order with respect to the monomer. The fourth-order absorbance relationships not only confirm the existence of the tetramer as an important species, but they give very strong support to the working hypothesis presented in the *Experimental Approach* section. The variation in the absorbance quotients at 5° is probably due to the errors in measurement associated with the small monomer peak. Any errors after being raised to the fourth power are, of course, quite magnified.

Next we considered the effect of temperature on the polymer absorbance region. From Figure 2 it is obvious that the shapes of the absorption curves change. Since the absorbance of the polymer region is fourth order with respect to the monomer, a temperature dependence indicates two forms of tetramer. The two absorbances at 1.43 and 1.61 μ were chosen in the hope that they could be shown independent and each represent a measure of only one structural isomer of the tetramer.

The first test was a van't Hoff plot of $a_{1.43}/a_1^4$ and $a_{1.61}/a_1^4$ as shown in Figure 7. The enthalpies were calculated by least squares to be -16.48 ± 0.11 kcal mole^{-1} for the 1.43-μ quotient, and -20.32 ± 0.13 kcal mole^{-1} for the 1.61-μ quotient. The linear correlation coefficients[26] were 0.9989 and 0.9990, respectively. *The magnitude of these enthalpies justifies assigning a linear structure to the tetramer at 1.43 μ and a cyclic structure to that at 1.61 μ since the average bond enthalpy for the linear tetramer is -5.5 kcal mole for three bonds and -5.1 kcal mole for four bonds for the cyclic tetramer.*

Method II. Minor Peak at 1.528 μ. The small peak at 1.528 μ appears to have less than a fourth-order dependence on the monomer. It is considered[3] as being the dimer peak since it is the first noticeable new absorbance peak observed as the concentration is raised (it corresponds to the 2.86-μ peak in the fundamental region). We measure this peak from an almost flat polymer absorbance base line when the polymer absorbance is low as in curves B′ and C′ of Figure 3. Measurements can be made at low temperatures only within a small range of concentrations before the tetramer peak interferes. In Figure 8 we have plotted the 1.528-μ peak as a function of the 1.405-μ peak. As can be seen, *the 1.528-μ peak varies linearly with respect to the monomer peak, independent of temperature.* The 100° results, at high concentrations, are somewhat off the line but in the wrong direction to show a dimer. These 100° high absorbance values were included to show the trend when measurements were made on top of signifi-

(26) P. G. Hoel, "Introduction to Mathematical Statistics," 2nd ed, John Wiley and Sons, Inc., New York, N. Y., 1954, p 117.

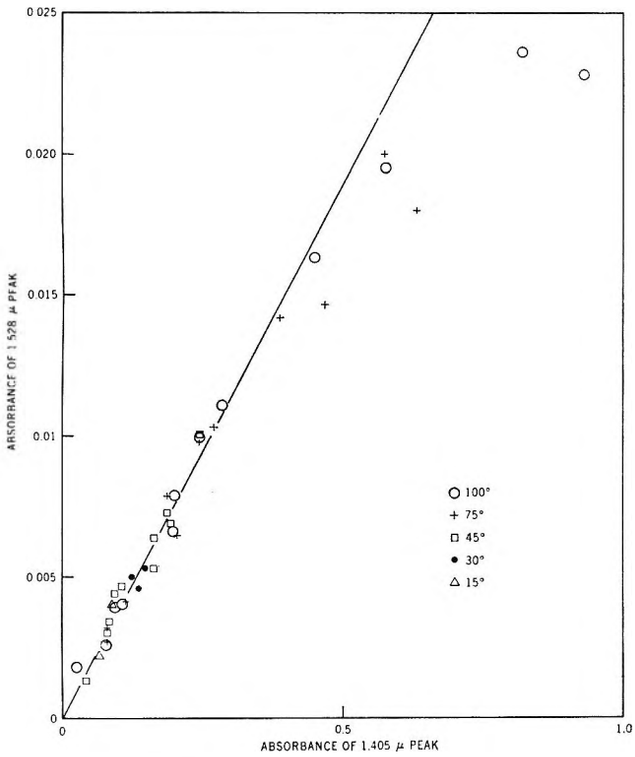

Figure 8. Variation in 1-octanol 1.528-μ peak with the 1.405-μ monomer peak from 15 to 100°.

cant tetramer absorbance. *These results indicate that the "dimer" peak is unequivocally not due to an O–H···O–H dimer*, but is due to some species whose concentration is directly proportional to the concentration of the monomer, possibly an alcohol–hydrocarbon complex.

The temperature independence shows a very small ΔH of formation for an alcohol–hydrocarbon complex.

Method III. By using all the data we can now calculate the actual amount of each tetramer. This will depend upon the fact that only the monomer and two tetramers need be considered. The results of methods I and II permit this assumption within a few per cent. We can consider the base-point corrected absorbance at 1.43 μ as being due to the linear tetramer (a_{4l}) and that at 1.61 μ as being due to the cyclic tetramer (a_{4c}). Mathematically we can write

$$A_0 - A_1 = 4A_4 = 4(A_{4l} + A_{4c}) \qquad (10)$$

where A's are concentrations of added alcohol, monomer, total tetramer, linear tetramer, and cyclic tetramer, respectively. This can be expressed in terms of absorbances of a_{4l} and a_{4c}.

$$\frac{A_0 - A_1}{4} = \frac{a_{4l}}{\epsilon_{4l}} + \frac{a_{4c}}{\epsilon_{4c}} \qquad (11)$$

Rearranging this, we get

$$\frac{a_{4c}}{(A_0 - A_1)} = \epsilon_{4c}/4 - \frac{\epsilon_{4c}}{\epsilon_{4l}} \frac{a_{4l}}{(A_0 - A_1)} \qquad (12)$$

By plotting $a_{4c}/(A_0 - A_1)$ *vs.* $a_{4l}/(A_0 - A_1)$ we can get the molar absorptivities. It may be noted that these terms are the apparent formal absorptivities which, in the limits (when all the tetramer is either all linear or all cyclic), become the formal absorptivities. Figure 9 shows the data plotted. The least-square calculation has a linear correlation coefficient[26] of 0.967. Thus there is a slight curvature which is probably due to errors in measurements plus a breakdown in some of our assumptions. In general, however, the linearity of this method of plotting data that depends on so many of our parameters on one graph lends validity to the general picture. *It should be noted that this type of plot does not include an a priori assumption of a tetramer in that no fourth-order terms are used.*

From the slope and intercept of Figure 9 we get $\epsilon_{4l} = 0.6786$ and $\epsilon_{4c} = 0.7476$ at 1.43 and 1.61 μ, respectively, where there is an *a priori* assumption of two tetramers (as we use the value 4 in eq 12). These can be used with the temperature data of a_{4l}/a_1^4 and a_{4c}/a_1^4 to calculate values of $K_{1,4l}$ and $K_{1,4c}$ which are shown in Table VII. A comparison of the results of methods I and III is also given in Table VII. Thermodynamic calculations from the data of Table VII are given in Table VIII after conversion of the data to mole fractions.

Table VII: Equilibrium Quotients for Linear and Cyclic Tetramers of 1-Octanol

Temp, °C	$K_{1,4l}$ (M^{-3})	$K_{1,4c}$ (M^{-3})	% rel diff methods I and III[a]
100	1.17	7.36×10^{-1}	−1.1%
75	5.46	4.89	2.8
45	4.72×10	7.02×10	0.5
30	1.63×10^2	3.24×10^2	6.5
15	6.41×10^2	1.75×10^3	0.7
5	1.73×10^3	5.98×10^3	−9.1
		Sum	0.3%

[a] Using $K_{1,4}$ values by method I for monomer–tetramer(only) model listed in Table III, % rel diff = $100[K_{1,4} - (K_{1,4l} + K_{1,4c})]/(K_{1,4l} + K_{1,4c})$.

Discussion and Conclusions

By starting with a general sixth-order equation, we find that our method I computer technique reduced to polymer models of a tetramer and either a dimer or a

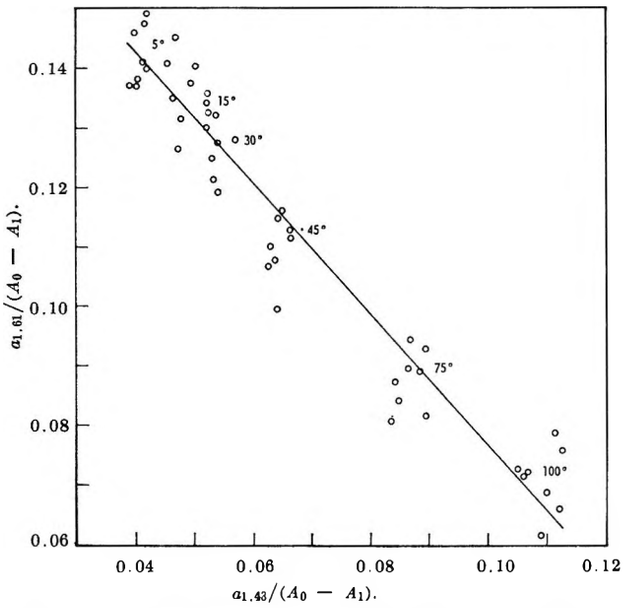

Figure 9. Determination of formal absorptivities by plotting the apparent formal absorptivities at 1.61 and 1.43 μ.

Table VIII: Thermodynamic Values for 1-Octanol Self-Association

Reaction	$-\Delta G°_{298}$, kcal/mole	$-\Delta H°_{298}$, kcal/mole	$-\Delta S°_{298}$, cal/mole deg
$4A_1 \rightleftarrows A_{4l}$	5.91	16.5	35.6
$4A_1 \rightleftarrows A_{4c}$	6.37	20.3	46.8
$A_{4l} \rightleftarrows A_{4c}$	0.46	3.8	11.2

trimer for 1-octanol–*n*-decane solutions. Only at 45° was it found possible to obtain values for both dimers and trimers along with the tetramer. In all other cases either the dimer or the trimer yielded the chemically impossible negative equilibrium quotient. However, whenever a tetramer–dimer–monomer model is determined as having the lowest error, *only a slight increase in the error function can be fit to a different model*, the tetramer–trimer–monomer and *vice versa*. Furthermore, the best-fit models indicate that these $K_{1,2}$ and $K_{1,3}$ values do not yield chemically significant results when evaluated by van't Hoff plots to get ΔH.

When *a priori* decisions are made as to a specific polymer model, Dunken and Fritzsche[24] have also shown that a number of other models can be fit to the same data. Thus it must be concluded that the evidence for dimers and trimers found by other workers who had to determine coefficients in a two-parameter polynomial expression (for fewer points, and usually over a smaller concentration range) cannot be accepted as proof or evidence of these species. In addition, ΔH/bond evidence from the polynomial expressions is also invalid as we have demonstrated in Table IV by obtaining almost identical ΔH/bond values for a number of linear or cyclic models fit to synthetic tetramer(only) data.

The "Dimer" Peak. Most workers who have determined dimer equilibrium constants have made *a priori* decisions that the dimers existed and then set up their mathematics to determine the constant. Their major justification for the presence of the dimer has been that a polymer peak at 2.86 μ or its overtone at 1.528 μ disappears after the major 2.96-μ polymer peak upon dilution of the alcohol. Since we find a 1–1 relationship independent of temperature between the monomer peak and the 1.528-μ "dimer" peak in *n*-decane, the formation of either linear or cyclic dimers through the formation of O–H···O–H bonds does not appear to be the cause of the "dimer" peak.

We at first pictured the 1.528-μ peak as being due to another vibrational mode related to the O–H in alcohols. However, Van Theil, Becker, and Pimentel[27] find a variation in the intensity of the "dimer" peak with respect to the monomer peak by the matrix isolation technique. Since we do not observe this, we conclude that the "dimer" band in *n*-decane is due to the interaction of the O–H with the solvent but can be an interaction with the hydrocarbon "tail" of the alcohol in the matrix isolation technique. Thus the alcohol–hydrocarbon complex will be pseudo first order in a 1-octanol–*n*-decane solution since the concentration of the CH_2 and CH_3 groups will be constant. In an N_2 matrix, this complex will be between two alcohols and the "dimer" peak will be second order with respect to the monomer absorbance. We do not know the nature of this interaction; however, hydrogen bonding is a likely suspect.[28]

It should be noted that our equilibrium quotients have been calculated using a concentration of the monomer which also includes any solvated monomer. Thus our values for K_4 should be multiplied by $(1 + K_{1,1s})^4$ where $K_{1,1s}$ is the equilibrium quotient between the monomer and the solvated monomer. Our data were not sufficiently accurate nor amenable to the calculation of $K_{1,1s}$. Since the size of the 1.528-μ peak is so small, we treat our data as if $K_{1,1s}$ were negligible.

Molar Absorptivity of the Monomer. Other workers[3,16b,22] have reported that the molar absorptivity of the monomer in carbon tetrachloride solutions changes

(27) M. Van Thiel, E. D. Becker, and G. C. Pimentel, *J. Chem. Phys.*, **27**, 95 (1957).

(28) D. J. Sutor, *J. Chem. Soc.*, 1105 (1963).

with the temperature. Using either method I—graphical or method I—computer, we find the same molar absorptivity for the monomer in *n*-decane independent of the temperature.

If the variation of the molar absorptivity of the monomer with temperature is due to an interaction of the alcohol monomer with carbon tetrachloride as was suggested by Liddel and Becker,[22] then we must conclude that this interaction in *n*-decane is not seen in the region of the first overtone or else that the degree of solvent interaction is *less* (or both).

Polymer Absorbance at Wavelength of Monomer. Bellamy and Pace[13] have recently used a double-beam cancelling technique to look at the polymer peaks in the region of the fundamental O–H stretching mode. They use a dilute solution in the reference beam to cancel the monomer absorption while leaving most of the polymer absorption. They find a polymer peak which is close to and overlaps that of the monomer. They assign this peak as being due to the "free" O–H at the end of the linear dimer.

If such a peak were significant for the 1-octanol system in the overtone region, we should not have obtained the clean relationships by methods II and III, as we would not have had a good measure of the monomer concentration. Their technique, if compensation were exact, should have shown no "dimer" peak if the 1.528 μ peak is due to a monomer–solvent interaction as we have postulated.

We were thus forced to examine closely the paper of Bellamy and Pace. A comparison of their results in carbon tetrachloride with the spectra for methanol[29] and other alcohols[18,20,23] indicated that *at the concentrations used by Bellamy and Pace, there was present an appreciable amount of n-mers larger than the dimer.* This can be seen by the presence of absorption bands of the higher polymers at concentrations where Bellamy and Pace consider only the dimer to be present. We further checked the overtone region with solutions of methanol in toluene as shown in Figure 3.

There are several important observations to be made from Figure 3. First, a comparison of the 0.25 *F* spectra with the spectrum of the same solution shown by Bellamy and Pace shows the reduced intensity of the polymer in the overtone region as compared to the monomer. Second, the reduced intensity of the polymer allows us to see that the "dimer" peak is split to form peaks at 1.523 and 1.546 μ for methanol in toluene. We attribute this to interaction of the O–H with both the methyl and the π electrons of the aromatic ring of toluene if the "dimer" peak is due to a monomer–solvent complex. Third, by examination of the 2.5 *F* methanol spectrum or the 1-octanol spectra in Figures 1 and 2, the higher polymer absorption can be seen to be still present in the 0.25 *F* solutions. We interpret Bellamy and Pace's "associated O–H of the dimer" in our Figure 3 and in their Figure 1 as representing minor monomer–solvent peaks on top of the linear tetramer and cyclic tetramer peaks for the 0.25 and 0.5 *F* methanol solutions. We feel that the free O–H band of the "dimer" as assigned by Bellamy and Pace is really due to the linear tetramer which can be seen in Figure 3 at 1.45 μ.

Assignment of O–H Polymer Absorbance Areas in the First Overtone Region. If one considers that the electronic nature of the O–H group is distorted whenever the oxygen is hydrogen bonded, it can be seen that the linear tetramer contains three different hydrogen bonds and four different O–H groups

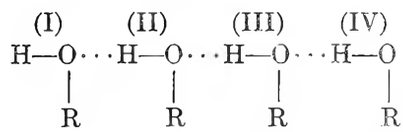

The O–H (IV) group corresponds to what has been called[13] "associated" while O–H (I) has been called "free." Groups (II) and (III) are not identical since, for both, the H and the O are hydrogen bonded to slightly different species. For the cyclic tetramer, however, all four O–H groups and hydrogen bonds are equivalent.

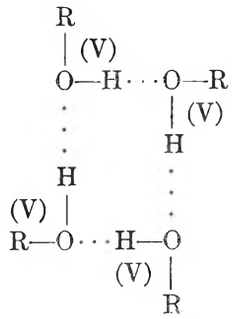

The O–H groups of the cyclic tetramer can be considered as being type (V) since the hydrogen bonds are formed between groups different from those joining O–H (II) and (III) of the linear tetramer.

Now, although these O–H groups can be geometrically identified as being different, the question arises as to whether they are physically and chemically different. There is little question that O–H (I) differs from O–H (IV), but what about the difference between O–H (II–IV) and O–H (V)? We believe that the uniformity of the curve shape between 1.61 and 1.65 μ

(29) M. S. Smith, P. A. D. de Maine, and M. M. de Maine, *J. Miss. Acad. Sci.*, 8, 244 (1962).

as found in Figure 2 is an indication that O–H (V) is distinct from the other O–H groups. The O–H (II–IV) groups appear to absorb at slightly shorter wavelengths and thus involve weaker hydrogen bonds.[18]

Since O–H (I) of the linear tetramer is the only group without its H being involved in a hydrogen bond, it is more distinct from the others and is more like the monomer. It can be seen at 1.45 μ for methanol in toluene (Figure 3). For 1-octanol, 1.43 μ appears to be a good place to measure the O–H (I) bond free from the monomer and the other O–H groups. The remaining four groups of the linear and cyclic tetramer absorb at higher wavelengths in the order of the increase in their designation numbers, (II–V) with the type V of the linear tetramer being distinct at 1.61 μ and higher.

The ability to obtain similar ΔH/bond values at 1.43 and 1.61 μ supports the argument above. It should be noted that we do not place significance on the relative magnitude of these values since we do not feel the accuracy of our results warrants this comparison. Also, since the bonds are different, one would not expect the values to be exactly the same.

The gradual shift with increasing temperature of the maximum of the polymer near 1.6 μ can now be explained on the basis of the increased proportion of the linear tetramers type (II–IV) O–H groups in respect to the type (V) of the cyclic tetramer.

Comparison of Results from the Three Methods. Method II independently confirms the tetramer(only) self-association model which had been suggested by the results of method I. The temperature data from method II have been incorporated into the values of Table VII so that major comparison is between the constants of method I and method III. These can be compared on the basis that

$$K_{1,4} = K_{1,4l} + K_{1,4c} \qquad (13)$$

Table VII shows the small per cent relative difference in the $K_{1,4}$ values calculated by method I with the values computed by eq 13.

It is interesting to note that although we obtained a linear van't Hoff plot of log $K_{1,4}$ (only) in Figure 4, the line should have shown a slight curvature since two species with different ΔH were involved.

Method II plots of the polymer absorbance divided by the fourth power of the monomer absorbance had lower concentration limits of about 0.2–0.5 F due to the limited absorbance of the polymer. Our autoxidation studies[10] led to fourth-order plots from 0.02 to 0.5 F and first order down to 10^{-4} F. Thus we have examined the concentration range 10^{-4} to 6 F (neat 1-octanol) without finding evidence of significant amounts of dimeric species.

Carbon Tetrachloride as a Solvent for the Study of Alcohol Polymerization. Since so much work has been performed in carbon tetrachloride, we believe a special evaluation should be made concerning the use of this solvent for the study of alcohol polymerization.

In the fundamental region, not only has the monomer's molar absorptivity in CCl_4 been observed to change with temperature,[22] but the polymer is found to absorb at almost the same wavelength as the monomer.[13] In the region of the first overtone of O–H, the CH_2 groups of the polymer also add to the absorbance of the monomer and interfere in its measurement.

There is an additional problem for those who use other than aliphatic hydrocarbons as solvents. As indicated by our Figure 3, methanol is almost pure monomer in toluene at 0.1 F. In decane, however, the concentration would have to be much lower (0.02 F) before no polymer is observed. Even in carbon tetrachloride the extent of polymerization of 1-octanol[30] is found to be less than that found in n-decane. This can also be seen in the smaller equilibrium quotients of Table VI as compared to those of Table III (at a comparable temperature). When one performs a method I log plot of $(A_0 - A_1)$ *vs.* A_1, two different lines with the same fourth-order slope are found for low concentrations of 1-octanol in the two solvents. However, as the concentration of the alcohol is increased, the solution finally must revert to neat alcohol. *Thus a method I graphical log plot using carbon tetrachloride or some other nonhydrocarbon as the solvent will bend at high alcohol concentrations*[30] *in order to intersect the linear relationship found in the hydrocarbon solvent* (which was valid up to neat alcohol) even when one has a good measure of the monomer concentration. Consequently, the values of the equilibrium quotients will change at the higher concentrations. For this reason we limited our computer fit of data to concentrations not greater than 1 F in the analysis of the 2-propanol self-association given in Table VI.

It is thus not too surprising that so many workers have fit so many polymer models to data obtained using carbon tetrachloride.

Alcohols as Reactants. Alcohols as reactants return us to our original interest. Some important mechanistic conclusions have been based on the change in order for alcohol at increasing concentrations.[31,32] We agree with the conclusions[33–39] that the changing order with

(30) A. N. Fletcher, unpublished work.

(31) C. G. Swain and E. E. Pegues, *J. Am. Chem. Soc.*, **80**, 812 (1958).

(32) S. W. Benson, "The Foundations of Chemical Kinetics," McGraw-Hill Book Co., Inc., New York, N. Y., 1960, p 551.

concentration is due to polymers. Earlier workers plotted rate *vs.* added alcohol (formal concentration). This gives an S-shaped curve with a third-order portion on a log plot. The correct plot is rate *vs.* monomer concentrations which leads to a fourth-order relationship.[10] The monomer concentration of an alcohol solution either may be determined experimentally or else it may be calculated from known equilibrium constants.[10] In the latter case, we prepare log plots of A_0 *vs.* A_1 which are calculated from eq 6 using arbitrary monomer values.

The question was raised[34] as to why a polymer should be a better catalyst than a monomer. The difference can be quite strikingly a factor of 100–1000. The linear and cyclic tetramer equilibrium we have found shows there can be an available proton on one of the two tetramers. The higher rates are probably due to this being a more acidic proton.[13] This also explains why no dimers and trimers are found. These lower linear *n*-mers rapidly combine with monomers.

Assocation Model. The picture of alcohols existing mainly as tetramers in pure alcohols and concentrated solutions demands some explanation. A thermodynamic picture would be better if we could actually measure dimer and trimer so as to obtain $K_{1,2}$ and $K_{1,3}$ and related thermodynamic properties. All we have is the difference between the two tetramers which shows only a slightly larger stability for the cyclic form.

A kinetic explanation can give an idea of why the tetramer is present in such large concentrations. In such a picture, dimers, trimers, and pentamers must all disappear with higher rate constants than for their formation. The tetramers must be formed in reactions involving large rate constants (or alternatively disappear in slow reactions).

A higher acidity of the terminal hydrogen on all polymers provides a strong driving force toward higher polymers. This would normally lead to pentamers and higher polymers. Even a cyclizing reaction of the tetramer does not provide a satisfactory answer by itself. However, if the pentamer can react to give cyclic tetramer plus monomer, the observed model is explained by the assignment of reasonable rate constants. The suggested reaction scheme is shown below.

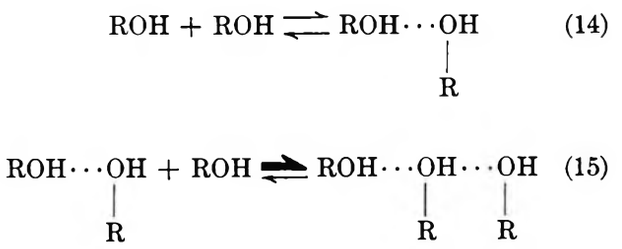

(14)

(15)

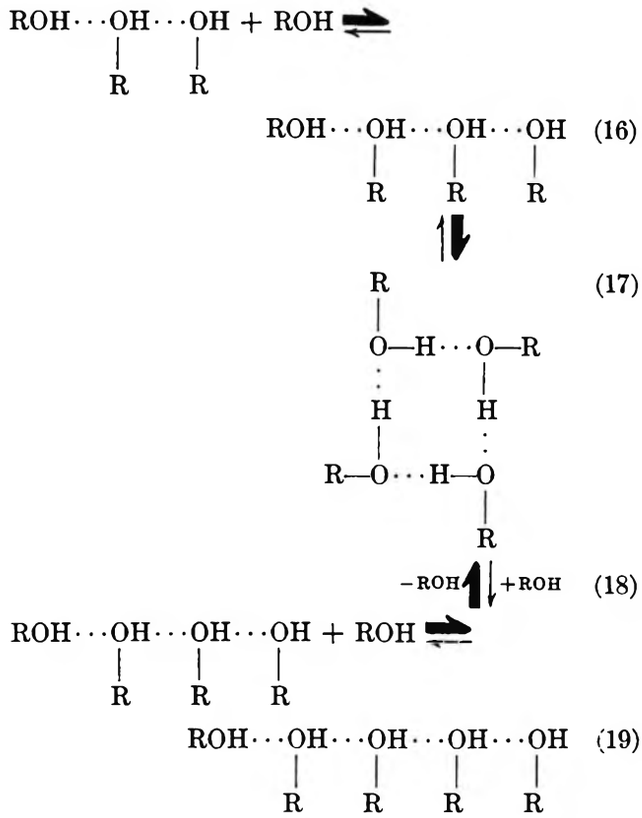

(16)

(17)

(18)

(19)

Here the broad arrows represent reactions with large rate constants. Thus each linear *n*-mer adds another monomer rapidly. Losing a monomer is a slower reaction since there will be an activation energy at least equal to the enthalpy.

The reaction of the linear pentamer to lose a monomer and form the cyclic tetramer must be rapid. Since a bond is formed at the same time one is broken, the enthalpy change should be small. The difference in rate constants is therefore ascribed to an entropy change for the reaction intermediate.

We know of no kinetic measurements which may have any bearing on this mechanism. It does explain the observed results.

Summation

Although dimeric and trimeric species must occur in the self-association of alcohols, we can find no evidence

(33) R. F. Hudson and B. Saville, *J. Chem. Soc.*, 4130 (1955).

(34) E. D. Hughes, C. K. Ingold, S. F. Mok, and Y. Pocker, *ibid.*, 1238 (1957).

(35) R. F. Hudson, *ibid.*, 761 (1966).

(36) R. F. Hudson and G. W. Loveday, *ibid.*, 766 (1966).

(37) R. F. Hudson, G. W. Loveday, S. Fliszár, and G. Salvadori, *ibid.*, 769 (1966).

(38) S. K. De and S. R. Palit, *J. Indian Chem. Soc.*, **43**, 679 (1966).

(39) S. K. De and S. R. Palit, *J. Phys. Chem.*, **71**, 444 (1967).

of their existence in sufficient quantity to be considered in the material balance equations. We can find evidence for only monomer, a possible monomer–solvent species, and linear and cyclic tetramers. Our limited results indicate that the equilibrium quotient for total tetramer, $K_{1,4}$, probably does not vary to a very great extent for similar nonsterically hindered alcohols in the same solvent. Our 30° values of 490 for 1-octanol and 430 for 1-butanol compare well with the value of 312 obtained by Musa and Eisner[4] for the slightly hindered *t*-butyl alcohol in cyclohexane using an ultrasonic technique. Sterically hindered alcohols would of course have lower self-association constants.[18] In carbon tetrachloride, the self-association is found to be significantly lower than in *n*-decane, yet again does not appear to change to any great extent for the three different alcohols which were evaluated. Although the more acidic phenol shows a higher degree of self-association ($K_{1,4}$ = 70) than ethanol ($K_{1,4}$ = 45), the equilibrium quotients are still within a factor of 2 while the change in solvent involves a factor of 10 change.[40]

Acknowledgments. We wish to express appreciation to Dr. Arnold T. Nielsen for the encouragement that he has given this work. Conversations with Dr. Lester Kuhn were quite helpful. Professor W. H. Urry has suggested many useful ideas. In particular, he suggested the ring-closing reactions of pentamers. Mr. James Nichols adapted his curve-fitting program to our needs, and Dr. Howard Shomate gave us his linear data-fitting program. Mrs. Edith Kirk performed much of the experimental work.

This research was supported by the Bureau of Naval Weapons and the Army Munitions Command.

(40) NOTE ADDED IN PROOF. The recent paper by Van Ness, *et al.* (H. C. Van Ness, J. Van Winkle, H. H. Richtol, and H. B. Hollinger, *J. Phys. Chem.*, 71, 1483 (1967)) gives valuable support to our work even though we are in disagreement with many of their initial hypotheses and conclusions. Their heat of mixing for ethanol in *n*-heptane of 5.2 kcal/mole of bonds is intermediate to our values of 5.6 and 5.1 for the two tetramers. Their evidence for an appreciable solvation energy gives support to our alcohol–hydrocarbon interaction species. Their spectrophotometric results and their conclusions that toluene (and carbon tetrachloride) interacts with the monomer and thus reduces further polymerization are in agreement with our observations.

A Nuclear Magnetic Resonance Investigation of Molecular Motion in Urea-d_4–*n*-Hydrocarbon and Urea-d_4–Fatty Acid Adducts

by Kimiko Umemoto and Steven S. Danyluk[1]

Department of Chemistry, University of Toronto, Toronto, Canada (*Received March 10, 1967*)

The wide-line proton magnetic resonance spectra have been measured for urea-d_4 adducts of even-numbered straight-chain hydrocarbons from $C_{12}H_{26}$ to $C_{18}H_{38}$ and for urea-d_4 adducts of stearic and palmitic acids from 80 to 300°K. For the *n*-hydrocarbon adducts, marked decreases are noted for the line widths and second moments over relatively narrow temperature ranges at low temperatures. The transition temperatures for these changes increase in a regular manner with increasing chain length of the *n*-hydrocarbon. For the fatty acid adducts, three distinct regions are noted in both the line-width and second-moment curves. In the temperature range 80–200°K the parameters decrease at a moderate rate; in the range 200–240°K the changes are much more marked, and, finally, above 240°K the changes are again gradual. The line-width and second-moment changes for the adducts have been attributed to the onset of specific motional processes of the enclathrated molecules. From a comparison of observed and calculated second moment values it is concluded that the methyl groups of *n*-$C_{12}H_{26}$, *n*-$C_{14}H_{30}$, stearic acid, and palmitic acid are rotating freely, based upon the nmr time scale, about the threefold axis at 95°K. Under the same conditions the motion of a significant fraction of the methyl groups in the *n*-$C_{16}H_{34}$ and *n*-$C_{18}H_{38}$ adducts is more restricted. It is also concluded that the large second-moment transitions observed at low temperatures for the *n*-hydrocarbon adducts, and at higher temperatures for the fatty acid adducts, result in each case from the onset of rotational motion of the long-chain derivatives about their longitudinal axes. The much higher transition temperatures of the fatty acid adducts have been attributed to the hindering effect of intermolecular hydrogen-bonding interactions.

Introduction

The structural stabilities and motional properties of urea adducts of *n*-hydrocarbon derivatives have been studied by a variety of techniques.[2-13] From wide-line proton magnetic resonance measurements of *n*-$C_{13}H_{28}$ and *n*-$C_{14}H_{34}$–urea-d_4 adducts Gilson and McDowell[9] concluded that the hydrocarbon molecules were able to rotate more or less freely about their longitudinal axis at temperatures well below the decomposition points of the adducts. The onset of rotational motion is further confirmed by recent calorimetric studies[11,12] which show the presence of an anomalously high heat absorption for urea adducts of straight-chain hydrocarbons at temperatures roughly corresponding to the regions in which second-moment transitions are observed in the nmr spectra. In contrast, no anomalous heat absorption was noted in the heat capacity curves for adducts of isomeric branched-chain hydrocarbons.[12] Both the nmr and heat capacity measure-

(1) Address all correspondence to this author at Argonne National Laboratory, Argonne, Ill.

(2) (a) R. J. Meakins, *Trans. Faraday Soc.*, **51**, 953 (1955); (b) A. A. V. Stuart, *Rec. Trav. Chim.*, **75**, 906 (1956).

(3) G. Caroti and B. Casu, *Riv. Combust.*, **12**, 451 (1958).

(4) G. B. Barlow and P. J. Corish, *J. Chem. Soc.*, 1706 (1959).

(5) R. Mecke and W. Kutzelnigg, *Z. Anal. Chem.*, **170**, 114 (1959).

(6) P. H. H. Fischer and C. A. McDowell, *Can. J. Chem.*, **38**, 187 (1960).

(7) G. Geiseler and P. Richter, *Chem. Ber.*, **93**, 2511 (1960).

(8) R. A. Durie and R. J. Harrisson, *Spectrochim. Acta*, **18**, 1505 (1962).

(9) D. F. R. Gilson and C. A. McDowell, *Mol. Phys.*, **4**, 125 (1961).

(10) H. G. McAdie, *Can. J. Chem.*, **40**, 2195 (1962).

ments also indicate that the onset of rotational motion of the straight-chain hydrocarbon molecules occurs at much lower temperatures in the adducts than in the corresponding solid hydrocarbons. This suggests that the intermolecular forces between hydrocarbon molecules and the urea lattice and between hydrocarbon molecules in different channels are much weaker than in the hydrocarbon alone.

Although fewer comparable data are available for urea adducts of straight-chain hydrocarbon derivatives with polar groups such as OH or COOH, it might be expected that the rotational motion of these molecules would be hindered because of intermolecular hydrogen bonding with urea molecules and with hydrogen-bonding groups on adjacent molecules in the urea channel. An indication that this is the case is provided by recent epr measurements[13] of urea–decanoic acid and urea–sebacic acid adducts which show a much smaller rotational amplitude for the β protons of the acid radicals than for corresponding protons of ester radicals.

In view of the continuing interest in the theoretical and practical aspects of urea adducts,[14] additional information pertaining to the motional properties of the enclosed molecules would be desirable. In this connection we have measured the proton resonance spectra for urea-d_4 adducts of the even-numbered straight-chain hydrocarbons from n-$C_{12}H_{26}$ to n-$C_{18}H_{38}$ and for the adducts of stearic and palmitic acids, over a wide range of temperature. The line-width changes and second-moment curves for these adducts are discussed in terms of the various modes of motion possible.

Experimental Section

Materials. The n-hydrocarbons were of high purity (99%) and were used in the adduct preparation without further treatment. Palmitic and stearic acids were of reagent grade and were also used without further purification. Urea-d_4, CH_3OD, and $(CH_3)_2CHOD$ were prepared according to procedures described elsewhere.[15]

Preparation of Adducts. The urea-d_4–n-hydrocarbon and urea-d_4–fatty acid adducts were prepared following procedures described in the literature.[10,15] All of the preparative steps and handling procedures were carried out in a drybox and the adducts were stored at low temperature in stoppered tubes in a desiccator until use.

Measurement of Spectra. The proton spectra of powdered samples, packed into 8-mm nmr tubes, were measured with a Varian DP 60 spectrometer equipped with a variable-temperature dewar assembly.[16] All of the spectra were recorded in both forward and reverse directions at least four times and an average derivative signal, corrected for a small contribution (<5%) from residual proton impurities of the probe and insert, was obtained. The line widths were measured as the separation between maximum and minimum points of the derivative curves and second moments were evaluated numerically. Modulation amplitudes ranged from 0.60 to 1.7 gauss and appropriate corrections[17] were applied to the experimental second moments. The measured line widths and second moments are accurate to ± 0.20 gauss and ± 0.50 gauss^2, respectively, while the temperatures are accurate to ± 2°K.

Results

Urea-d_4–n-Hydrocarbon Adducts. Observed Line Widths and Second Moments. The line-shape changes with temperature follow essentially the same pattern for the four urea-d_4–n-hydrocarbon adducts over the temperature range investigated. Typical derivative spectra are illustrated in Figure 1 for the n-octadecane adduct at a number of representative temperatures. At low temperatures (<100°K) the spectra for all of the adducts consist of two components, a broad component with ΔH in the range 9–12 gauss, and a narrow component with ΔH ranging from 2.1 to 2.9 gauss. A progressive narrowing of the broad component is noted in the temperature range 100–160°K for all of the adducts. Above 160°K the broad components show only a slight additional narrowing with increasing temperature up to 298°K. The narrow components decrease only slightly in width over the entire temperature range (ΔH values for the narrow signals are uncertain in the range 110–150°K because of overlap with the broad component).

A sharp line, with $\Delta H < 0.10$ gauss, is observed to form in all of the adducts except urea-d_4–n-$C_{12}H_{26}$, at approximately 160°K. This signal cannot be attributed to residual host or n-hydrocarbon protons and is most probably due to small amounts of occluded CH_3OD molecules. A graphical representation of the line-width variation with temperature for all of the adducts is given in Figure 2.

Figure 3 shows the second-moment variation with temperature for the n-hydrocarbon adducts. At 95°K

(11) R. C. Pemberton and N. G. Parsonage, *Trans. Faraday Soc.*, **61**, 2112 (1965).

(12) R. C. Pemberton and N. G. Parsonage, *ibid.*, **62**, 553 (1966).

(13) O. H. Griffith, *J. Chem. Phys.*, **41**, 1093 (1964).

(14) L. Mandelcorn, Ed., "Non-Stoichiometric Compounds," Academic Press, New York, N. Y., 1964, Chapters 8 and 10.

(15) K. Takahashi, Ph.D. Thesis, University of Toronto, 1965.

(16) W. G. Schneider, H. J. Bernstein, and J. A. Pople, *J. Chem. Phys.*, **28**, 601 (1958).

(17) E. R. Andrew, *Phys. Rev.*, **91**, 425 (1953).

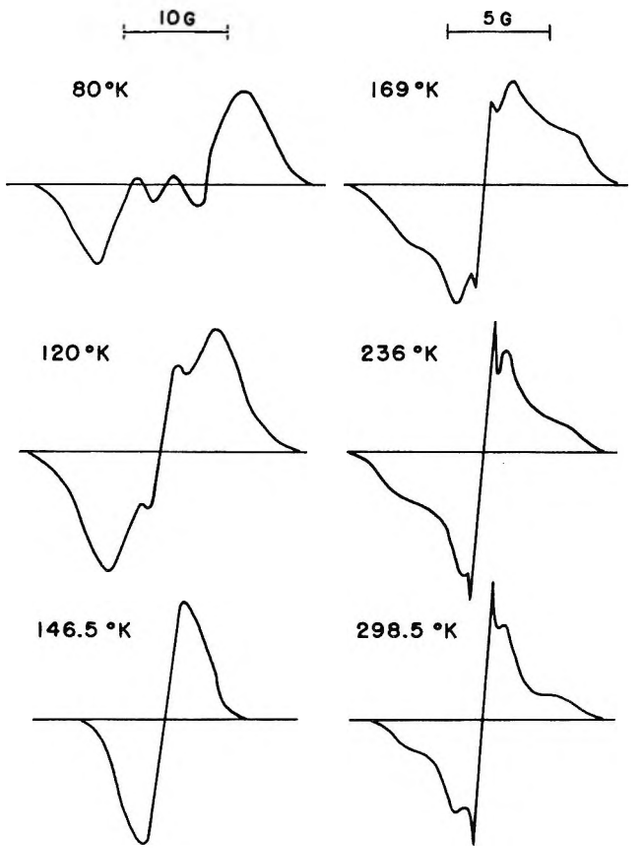

Figure 1. Wide-line proton magnetic resonance spectra for the urea-d_4–n-$C_{18}H_{38}$ adduct at a number of temperatures.

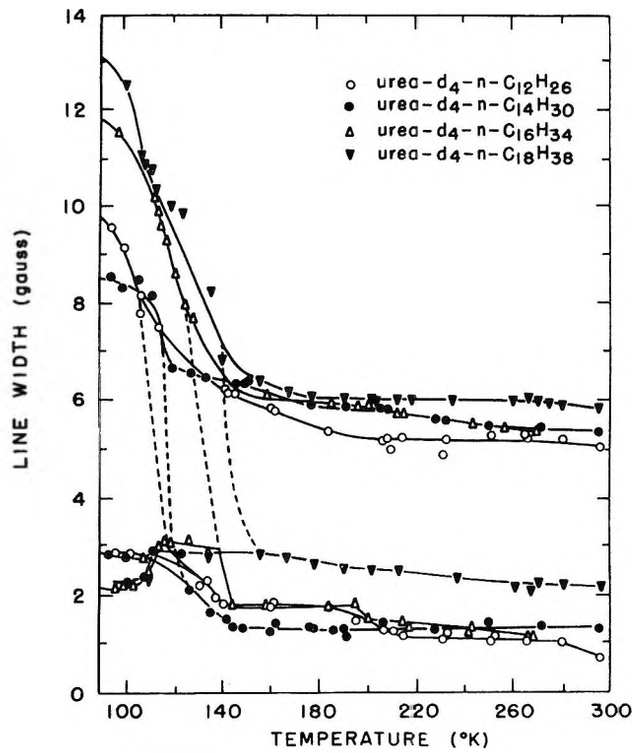

Figure 2. Line-width variation with temperature for derivative spectra of urea-d_4–n-hydrocarbon adducts.

the magnitudes of the second moments vary in the order n-$C_{12}H_{26} \simeq n$-$C_{14}H_{30} < n$-$C_{16}H_{34} < n$-$C_{18}H_{38}$. As the temperature is increased the second moments for all of the adducts decrease markedly with the curves for the individual adducts being displaced to higher temperatures in a regular manner with increasing chain length. A leveling-off of the curves is noted at 130–150°K, depending upon n. Small inflections in the curves for the n-$C_{16}H_{34}$ and n-$C_{18}H_{38}$ adducts are observed at 115 and 122°K, respectively; no inflections are present in the curves for the other adducts. Further small, but measurable, discontinuities are observed in the second-moment curves for all of the adducts at temperatures ranging from 184 to 236°K, Figure 3. Above these temperatures, the second moments decrease gradually, with no further abrupt changes up to the highest temperature studied, 298°K.

Calculated Second Moments. Intra- and intermolecular contributions to the rigid lattice second moments of the four urea-d_4–n-hydrocarbon adducts have been calculated on the assumption that the crystal structure and internuclear distances are the same as in the corresponding fully protonated adducts.[18–20] The C–C and C–H bond lengths were taken as 1.54[21] and 1.094 A,[22] respectively, and an angle of 109° 28′ was assumed between the carbon atoms. A summary of the calculated values is given in Table I along with the experimental values observed at a number of temperatures. The largest errors in the calculated moments are due to uncertainties in bond angles and bond lengths for the hydrocarbons and are of the order of ± 0.40 and ± 0.20 gauss^2 for intramolecular and intermolecular contributions, respectively. Since the urea is better than 96% deuterated, the intermolecular contribution from this source is estimated to be less than 0.10 gauss^2.

The reductions in inter- and intramolecular second moments resulting from a reorientation of the methyl groups (with the rest of the chain fixed) have been calculated by the method of Gutowsky and Pake,[23] and the S_2 values are summarized in Table I. Also in-

(18) A. E. Smith, *J. Chem. Soc.*, 2416 (1951).

(19) A. E. Smith, *Acta Cryst.*, **5**, 224 (1952).

(20) H. V. Lenne, *ibid.*, **7**, 1 (1954).

(21) A. Müller, *Proc. Roy. Soc.* (London), **A120**, 437 (1928); **A127**, 477 (1930).

(22) G. Herzberg, "Infrared and Raman Spectra of Poly-Atomic Molecules," D. Van Nostrand Co., Inc., New York, N. Y., 1945, p 45.

(23) H. S. Gutowsky and G. E. Pake, *J. Chem. Phys.*, **18**, 162 (1950).

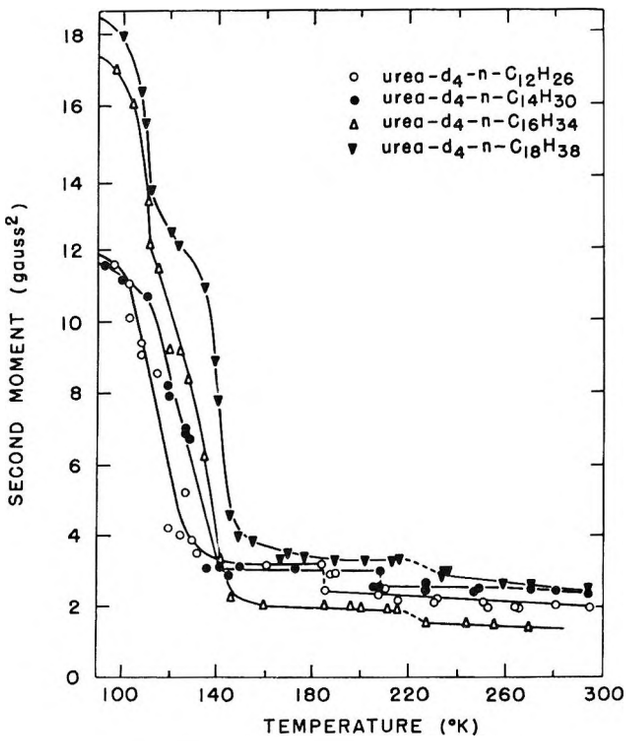

Figure 3. Variation of second moments with temperature for the spectra of urea-d_4–n-hydrocarbon adducts.

Table I: Calculated and Observed Second Moments[a] for Urea-d_4–n-Hydrocarbon Adducts

	n-$C_{12}H_{26}$	n-$C_{14}H_{30}$	n-$C_{16}H_{34}$	n-$C_{18}H_{38}$
Calculated Second Moments				
Rigid lattice				
Intramolecular	20.21	20.02	19.88	19.77
Intermolecular	0.97	0.97	0.97	0.97
Total second moment	21.18	20.99	20.85	20.74
Methyl group rotation				
Intramolecular	14.84	15.37	15.78	16.10
Intermolecular	0.24	0.24	0.24	0.24
Total second moment	15.08	15.61	16.02	16.34
Rotational oscillation				
Amplitude 30°	10.92	11.40	11.77	11.99
60°	5.49	5.77	5.98	6.16
Observed Second Moments				
95°K	12.0	11.6	17.5	18.5
150°K	3.2	3.0	2.2	4.0
200°K	2.4	3.0	2.0	3.3
240°K	2.2	2.5	1.5	2.9

[a] In gauss^2.

cluded in Table I are the S_2 values calculated for the case of rotational oscillation of the n-hydrocarbon chain about its longitudinal axis. The reduction in second moment caused by such reorientations was calculated following the procedure of Andrew.[24]

Urea-d_4–Fatty Acid Adducts. Observed Line Widths and Second Moments. Figure 4 illustrates spectra observed for the urea-d_4–palmitic acid adduct at a number of temperatures. Similar spectra were obtained for the urea-d_4–stearic acid adduct. In both adducts two superimposed components with different line widths were resolved in the derivative spectra over the entire temperature range, 80–298°K. At 80°K, the broad components have line widths of 12.8 and 12.3 gauss for the palmitic acid and stearic acid adducts, respectively, while the narrow components have line widths of 2.3 and 2.6 gauss. The line widths of the broad components decrease steadily with increasing temperature until approximately 190°K, where the rate of decrease increases sharply. Above 220°K, the broad components for both adducts appear to level off at 6.5–7.0 gauss while the narrow components decrease gradually to ~0.5 gauss at 298°K. The line

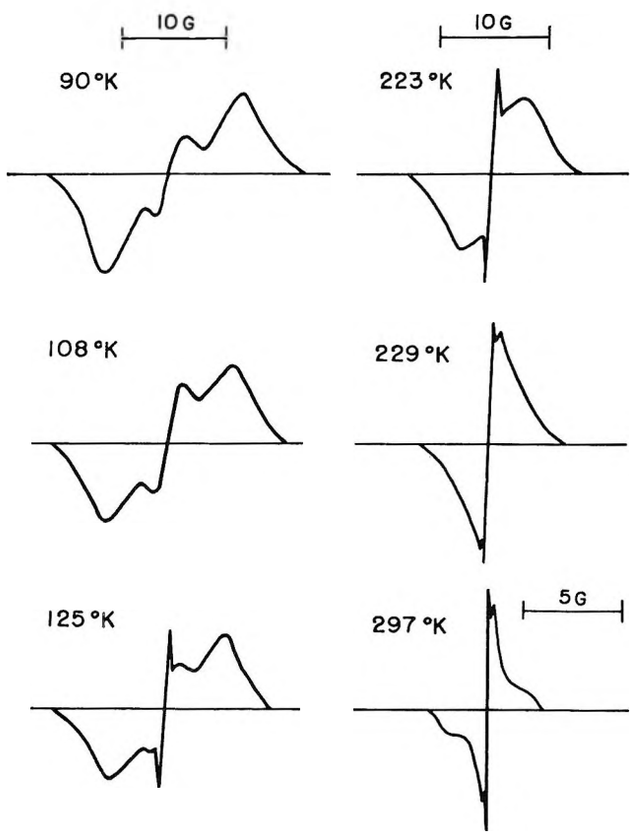

Figure 4. Wide-line derivative spectra for the urea-d_4–palmitic acid adduct at a number of temperatures.

(24) E. R. Andrew, *J. Chem. Phys.*, 18, 607 (1950).

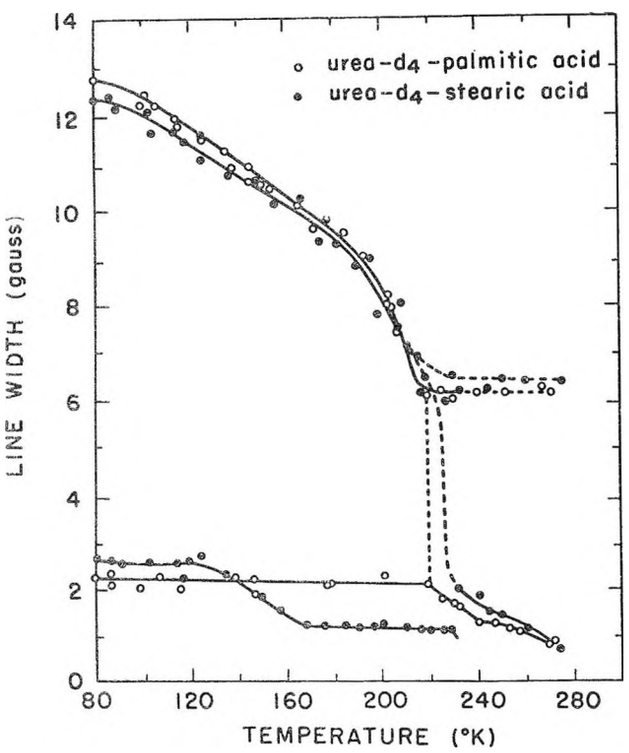

Figure 5. Line-width variation with temperature for urea-d_4 adducts of palmitic acid and stearic acid.

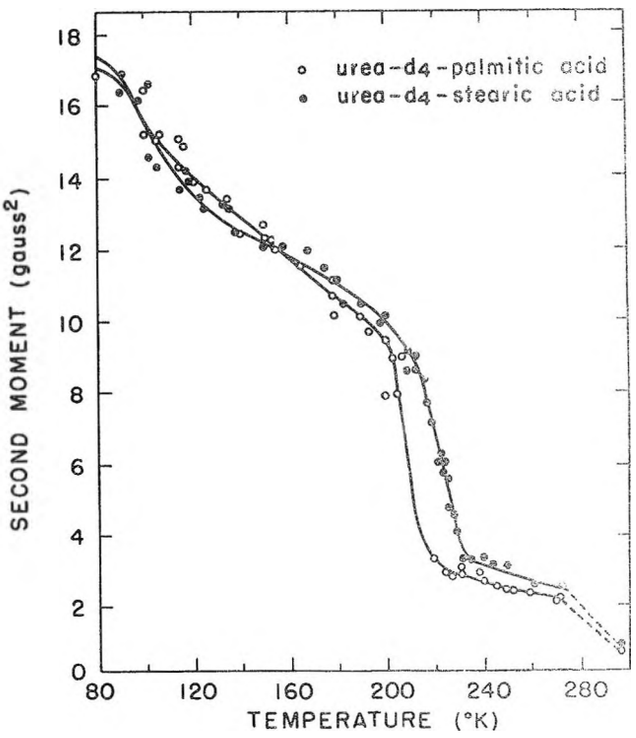

Figure 6. Second-moment variation with temperature for the urea-d_4 adducts of palmitic acid and stearic acid.

width–temperature dependence for both adducts is summarized in Figure 5.

Figure 6 illustrates the second-moment variation with temperature for the adducts. At 80°K, the experimental second moments are 17.0 and 17.3 gauss² for the palmitic acid and stearic acid adducts, respectively. As the temperature is increased, the second moments for both adducts decrease uniformly until approximately 200°K, where the rate of decrease increases sharply. In the region 200–220°K, S_2 decreases from 9.3 to 3.1 gauss² for urea-d_4–palmitic acid while S_2 for the stearic acid adduct changes from 10.0 to 3.4 gauss² in the range 200–235°K. The second-moment curve for the stearic acid adduct is displaced in the transition region by approximately 15° to higher temperature relative to the curve for the palmitic acid adduct. At temperatures above the sharp transition region, the second moments show a more gradual decrease with increasing temperature up to 298°K, with small inflections noted in both curves at 270°K. The second moments at 298°K are 0.3 and 0.4 gauss² for the palmitic and stearic acid adducts, respectively.

Calculated Second Moments. Rigid-lattice second-moment values for the acid adducts have been calculated on the assumption that (i) the crystal structure and internuclear distances are the same as for the corresponding urea–*n*-hydrocarbon adducts; (ii) the acid molecules are aligned in the urea channel in a head-to-head arrangement, *i.e.*, with the carboxyl groups adjacent to each other; (iii) the methylene groups are arranged in a planar zigzag configuration. Assumption (i) is reasonable since X-ray diffraction studies have shown that the crystal structure and dimensions of the urea channels do not differ significantly for a wide range of adducts from straight-chain hydrocarbons to paraffin derivatives with polar groups such as esters (a small distortion of the urea channel is noted, however, in adducts containing a short branch chain).[18,19,25,26]

A head-to-head arrangement of the acid molecules has been indicated by heat of reaction studies[27] and X-ray measurements[28] for a number of urea–di- and monocarboxylic acid adducts, and a similar arrangement is most likely in the present systems. Previous X-ray studies have also shown that the planar arrangement of the methylene groups is the most favored configura-

(25) W. Schlenk, Jr., *Ann.*, 565, 204 (1949).

(26) A. E. Smith, *J. Chem. Phys.*, 18, 150 (1950).

(27) L. C. Fetterly, Ph.D. Thesis, University of Washington, 1950.

(28) L. C. Fetterly, "Non-Stoichiometric Compounds," L. Mandelkern, Ed., Academic Press Inc., New York, N. Y., 1964, Chapter 8, ref 28.

tion in a wide variety of urea–paraffin adducts at room temperature.[18,19,25,26] The bond lengths used in the calculations were C–C bond,[21] 1.54 A, C–H bond, 1.094 A,[22] and all bond angles about the carbon atoms were assumed to be 109° 28′. A summary of the calculated rigid lattice second moments is given in Table II along with the experimental second-moment values obtained at a number of temperatures. The errors in the theoretical second moments are estimated to be ±0.40 gauss^2.

Table II also includes second moments calculated for the cases of methyl group rotation[23] and rotational oscillation of the methylene chain[24] of the acid molecules. The second-moment reductions for these types of motion were calculated by the same methods as for the hydrocarbon adducts.

Table II: Observed and Calculated Second Moments[a] for Urea-d_4–Fatty Acid Adducts

	Palmitic acid	Stearic acid
Calculated Second Moments		
Rigid lattice		
Intramolecular	18.83	18.92
Intermolecular	1.01	1.01
Total second moment	19.84	19.93
Methyl group rotation		
Intramolecular	16.12	16.41
Intermolecular	0.25	0.25
Total second moment	16.37	16.66
Rotational oscillation		
Amplitude 30°	12.01	12.23
60°	6.18	6.36
Observed Second Moments		
95°K	16.4	16.4
150°K	12.2	12.0
200°K	9.4	10.0
240°K	2.6	3.6

[a] In gauss^2.

Discussion

Urea-d_4–n-Hydrocarbon Adducts. The general features of the spectra for the hydrocarbon adducts are similar to those observed previously[9] for the n-$C_{18}H_{28}$ and n-$C_{16}H_{34}$ adducts and for shorter chain n-hydrocarbons at low temperatures.[29] Slight differences between the present results for the n-$C_{16}H_{34}$ adduct and the earlier data of Gilson and McDowell[9] can be attributed to an overlap of the narrow and broad components in the ranges 120–140 and 220–290°K.

Comparison of the line-width variation with temperature for each of the n-hydrocarbon adducts with the line-width behavior for the corresponding pure n-hydrocarbons[24,29] shows that marked line-narrowing transitions occur at much lower temperatures for hydrocarbon molecules in the adducts. In the pure n-hydrocarbons the main line-width transitions occur typically within a few degrees of the melting points, while in the adducts the transitions are approximately 250° below the decomposition temperatures. Accordingly, the onset of extensive motional freedom associated with the transition occurs more readily in urea channels than in the hydrocarbon phase. An indication of the nature of the motional processes is provided by a comparison of observed and calculated second-moment values.

For urea–n-hydrocarbon adducts the various motional processes possible include (i) rotation of the terminal methyl groups about their threefold axis, (ii) rotational oscillation of the main paraffin chain about the longitudinal axis (the methylene groups are assumed to be rigidly oriented in their planar zigzag form), (iii) translational motion of the chains along the channel, (iv) flexing and twisting of the hydrocarbon chain (giving rise to out-of-plane motion for the methylene groups), and (v) intra- and interchannel diffusion. Qualitatively, it is reasonable to expect the motional processes to occur in sequence (i) to (v) with increasing temperature. Processes (iv) and (v) presumably involve some rearrangement of the host molecules and are unlikely to be of importance much below (<10–20°) the decomposition temperatures. Accordingly, the second-moment reductions have been calculated for (i) and (ii) only, Table I. The intramolecular second moments calculated for methyl group rotation are 3.6–5.4 gauss^2 lower than the corresponding rigid lattice values and are in good agreement with the values reported recently by Anderson and Slichter,[29] $S_2 = 18.5 - 46.3/(n + 1)$. Satisfactory agreement is also noted between the total second moment for the n-$C_{16}H_{34}$ adduct, 16.0 gauss^2, and the value given by Gilson and McDowell,[9] 15.8 gauss^2. With respect to motion of type (ii) the total second moments calculated for a rotational oscillation of amplitude 60° for the hydrocarbon chain (*i.e.*, freely reorienting chains) range from 5.5 gauss^2 for the n-$C_{12}H_{26}$ adduct to 6.2 gauss^2 for the n-$C_{19}H_{38}$ adduct. These values are comparable to the intramolecular second moments calculated by Andrew,[24] $S_2 = 6.8 - 11.6/(n + 1)$ for free rotation of the pure n-hydrocarbons.

(29) J. E. Anderson and W. P. Slichter, *J. Phys. Chem.*, **69**, 3099 (1965).

From Table I it is evident that the hydrocarbon molecules are not immobile in the urea channels even at the lowest temperature studied. For the n-$C_{12}H_{26}$ and n-$C_{14}H_{30}$ adducts it seems likely that the methyl groups are reorienting freely (on the nmr time scale) at 95°K while for the n-$C_{16}H_{34}$ and n-$C_{18}H_{38}$ adducts the methyl group reorientation is apparently more hindered. There is also a strong indication that hydrocarbon molecules are undergoing at least a partial rotational oscillation (ii) in the C_{12} and C_{14} adducts at 95°K. No motion of this type is indicated for the higher hydrocarbons.

The sharp decrease in second moment observed for the adducts at higher temperatures can be explained most readily by the onset of rotational oscillation of the hydrocarbon chains in the urea channels. However, the second moment values at temperatures immediately above the transition regions (~150°K) are from 2 to 3 gauss[2] smaller than the values calculated for free rotational oscillation (Table I). It is possible that these differences arise because of limitations in the model adopted for the calculations.[24] Alternatively, the observed S_2 values may indicate the presence of additional modes of motion such as (iii) and (iv). A calculation of the second-moment reduction due to (iii) and (iv) is precluded, however, by the complexity of the present systems. Of the various possibilities the most reasonable, at the temperatures involved, would apear to be a small translational motion of the hydrocarbon molecules along the channels.

It is interesting to note that the main second-moment transitions occur over roughly the same temperature ranges and vary with increasing chain length in the same manner as the anomalous transitions in the heat capacity curves[11,12] for the adducts (Table III). It is reasonable to conclude that the same motional process, namely, rotation of the hydrocarbon molecule in the channel, is responsible for the changes in both cases.

Urea-d_4–Fatty Acids. The line-width and second-moment curves for the fatty acid adducts differ markedly from the curves for the corresponding n-hydrocarbon adducts. In particular, the second-moment curves for the acid adducts show a steady decrease from 80 to 200°K and the main S_2 transitions at 200–230°K occur approximately 100° higher than for the hydrocarbons. These differences can be attributed in part to the effects of hydrogen-bonding interactions in the acid adducts. Such interactions could take the form of head-to-head hydrogen bonds between adjacent carboxyl groups within a channel (to form in effect a dimer with twice the chain length of the monomer) and/or hydrogen bonds between carboxyl groups and the urea molecules. In either case the motion of the acid molecules would be more hindered than for corresponding hydrocarbon molecules, and a shift of the main line-width and second-moment transitions to higher temperatures would be expected. Some support for such interactions is provided by recent epr results[13] for urea adducts of several fatty acid and ester free radicals which showed that at room temperature the amplitude of the motional process averaging the β-proton coupling constant is significantly less for acid radicals than for ester radicals.

As in the case of the hydrocarbon adducts a qualitative indication of the motional processes can be obtained from a comparison of observed and calculated second moments. In the temperature range covered the two types of motion most likely are (i) rotation of the methyl groups and (ii) rotational oscillation of the molecule about the longitudinal axis; S_2 values calculated for these cases are given in Table II. At 95°K the close agreement (Table II) between observed S_2 values and those calculated for motion of type (i) strongly indicates that the methyl groups are rotating freely in the adducts at this temperature. This can be contrasted with the results for acid salts,[30,31] where the methyl groups were found to be rigidly oriented under the same conditions.

The steady decrease in second moment with increasing temperature from 95 to ~200°K can be attributed to the onset of rotational oscillation of the acid molecules. However, the sharp drop in S_2 values above 200°K cannot be explained solely in terms of freely rotating molecules since the observed moments are more than 3 gauss[2] lower than values calculated for free rotational oscillation. This difference is greater

Table III: Transition Temperatures for Urea–n-Hydrocarbon Adducts from Second Moment and Heat Capacity Measurements

Urea–n-Hydrocarbon	T_t (C curves)[11-12]	T_t[a] (S_2 curves)
n-$C_{10}H_{22}$	110.9	...
n-$C_{12}H_{26}$	123.2	114
n-$C_{14}H_{30}$	136[b]	126
n-$C_{15}H_{32}$	158.4	...
n-$C_{16}H_{34}$	151.8	132
n-$C_{18}H_{38}$	166[b]	144
n-$C_{20}H_{42}$	189.3	...

[a] Errors in the second moment transition temperatures are estimated to be ±4°. [b] Estimated from Figure 4 in ref 12.

(30) R. F. Grant and B. A. Dunell, *Can. J. Chem.*, 38, 1951 (1960).
(31) R. F. Grant and B. A. Dunell, *ibid.*, 38, 2395 (1960).

than any experimental or computational errors involved and another motional process must be invoked to explain the decrease. Of the various possibilities the one which would appear to be the most reasonable is a rotation of the methylene groups about the C–C bonds. A calculation of the decrease expected from such a motional process superimposed upon a rotation of the main chain has not been attempted, however.

Comparison of the present adduct spectra with proton spectra for a number of fatty acids[30-33] shows a number of distinct differences. Previous studies had shown that the line widths and second moments for anhydrous sodium and potassium stearates[30,31] vary only slightly with temperture until approximately 390 and 330°K, respectively, where sharp decreases are observed for both. These decreases, which can be associated with the onset of extensive oscillating motion of the molecules, occur at much higher temperatures (~120° higher) than in the urea-d_4–stearic acid adduct, Figures 2 and 3. As in the case of the hydrocarbon adducts, the shifts of the transition to lower temperature indicates that intermolecular forces hindering motion in the urea channels are considerably weaker in the adducts than in the pure acids.

Acknowledgments. The authors are greatly indebted to Dr. H. G. McAdie of the Ontario Research Foundation for providing the pure *n*-hydrocarbons and for numerous helpful comments and suggestions. Grateful acknowledgment is also made to the Ontario Research Foundation for a grant in support of this work. Parts of this work were completed at Argonne National Laboratory with support of the U. S. Atomic Energy Commission.

(32) W. R. Janzen and B. A. Dunell, *Trans. Faraday Soc.*, 59, 1260 (1963).

(33) K. L. Lawson and T. J. Flautt, *J. Phys. Chem.*, 69, 4256 (1965).

The Asymmetry Potential Effect across Nonuniform Ion Selective Membranes

by A. M. Liquori

Centro Nazionale di Chimica della Macromolecole, Sezione III, Laboratorio di Chimica Fisica, Istituto Chimico, Università di Roma, Roma, Italy

and C. Botré

Istituto di Chimica Farmaceutica, Università di Roma, Roma, Italy

Accepted and Transmitted by The Faraday Society (March 13, 1967)

The unusual electrochemical behavior of previously described asymmetric membranes is explained using a model system as reference. It is concluded that these membranes act as microcells made of elements with different permselectivity coefficients separated by highly swollen gels of polystyrenesulfonate. Asymmetric membranes made of two films of collodion polystyrenesulfonic acid with different charge densities sandwiching a film of polystyrenesulfonic acid show, after sodium exchange, an electrochemical behavior very close to that of the previously described asymmetric membranes. The asymmetry potential between two identical electrolyte solutions separated by such a membrane is theoretically explained according to the thermodynamics of irreversible processes.

Asymmetric Membranes

In a previous paper[1] the electrochemical behavior of collodion polystyrenesulfonic acid membranes (CPS) characterized by different concentrations of polystyrenesulfonate in the two external layers, si and so, was described. A peculiar effect was observed when such membranes were put in contact with two solutions, i and o, of a uni-univalent electrolyte having identical composition. In fact, an electrical potential difference could be measured between the two identical solutions separated by the asymmetric membrane. Such an "asymmetry potential" was found to increase with increasing the difference of fixed charge densities between the two external layers si and so. When the asymmetric membrane was put in contact with two solutions of a uni-univalent electrolyte at different mean activities, the observed membrane potential was found to depend on the orientation of the membrane with respect to the two solutions. Such a behavior is shown in Figure 1. Although in the previous paper[1] an attempt was made to interpret this peculiar electrochemical behavior on the basis of an extention of Meyer–Teorell theory, it will be shown here that a simple straightforward explanation can be given if the following model system is considered. Let si and so be two ion selective membranes having different charge densities in contact with two uni-univalent electrolyte solutions (*e.g.*, NaCl) i and o separated by a middle compartment containing a solution of the same uni-univalent electrolyte, solution "m."

When there is no current flow across the system, an electrical potential difference is established between the solutions i and o given by

$$\Delta\psi = \psi^{i} - \psi^{o} = (\psi^{i} - \psi^{m}) - (\psi^{o} - \psi^{m}) \quad (1)$$

where

$$\psi^{i} - \psi^{m} = -\alpha^{si}\frac{RT}{F}\ln\frac{a_{\pm}^{\,i}}{a_{\pm}^{\,m}} \quad (2)$$

and

$$\psi^{o} - \psi^{m} = -\alpha^{so}\frac{RT}{F}\ln\frac{a_{\pm}^{\,o}}{a_{\pm}^{\,m}} \quad (3)$$

where α^{si} and α^{so} are the selectivity coefficients of the

(1) A. M. Liquori and C. Botré, *Ric. Sci.*, 6, 71 (1964).

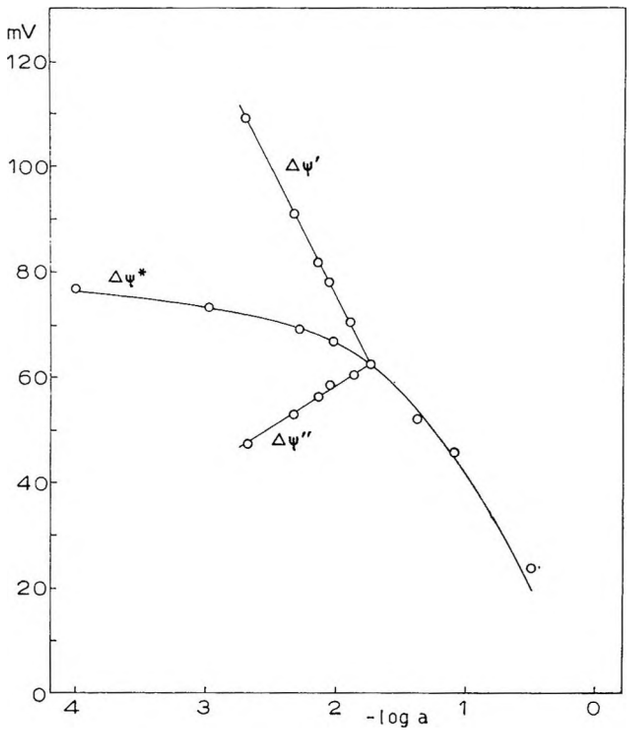

Figure 1. Asymmetry potential $\Delta\psi^*$ across an asymmetric membrane of the previously described type[1] as a function of the log $a_\pm$ of the two identical electrolyte (NaCl) solutions in contact with the membrane. The membrane potentials $\Delta\psi'$ and $\Delta\psi''$ observed for two opposite orientations of the asymmetric membrane with respect to the two bathing electrolyte solutions of NaCl. The mean activity $a_\pm$ in one electrolyte solution is fixed at 1.7×10^{-2} whereas the mean activity of the other electrolyte solution is varied.

two membranes si and so having different charge densities. If the two electrolyte solutions i and o have identical composition, $a_\pm^{\,i} = a_\pm^{\,o} = a_\pm$, the electrical potential difference (eq 1) becomes

$$\Delta\psi^* = -\frac{RT}{F}(\alpha^{si} - \alpha^{so}) \ln \frac{a_\pm}{a_\pm^{\,m}} \qquad (4)$$

An electrical potential difference between the two identical electrolyte solutions i and o must, therefore, be observed which is due to the asymmetry of the system which imposes the condition that $\alpha^{si} \neq \alpha^{so}$. It is in fact interesting to observe that if

$$\bar{\mu}_j^{\,o} = \mu_j^{\,o} + z_j F \psi_j$$

and

$$\bar{\mu}_j^{\,i} = \mu_j^{\,i} + z_j F \psi_j \qquad (5)$$

are the electrochemical potentials of an ion in the two solutions i and o when these have identical composition

$$\mu_j^{\,i} = \mu_j^{\,o} \qquad (6)$$

and

$$\bar{\mu}_j^{\,i} - \bar{\mu}_j^{\,o} = \Delta\bar{\mu}_j^* = z_j F \Delta\psi^* = -\frac{RT}{F}(\alpha^{si} - \alpha^{so}) \ln \frac{a_\pm}{a_\pm^{\,m}} \qquad (7)$$

Therefore, the asymmetry potential corresponds to the electrochemical potential difference of the jth ion between the two solutions, which at the steady state is generated by the different ionic activities of the salt in the compartments i, o if the system is asymmetric ($\alpha^{si} \neq \alpha^{so}$). When the two electrolyte solutions i and o have different mean activities, eq 2, 3, and 7 may be combined to give the membrane potentials

$$\Delta\psi' = \frac{RT}{F}\alpha^{so} \ln \frac{a_\pm^{\,i}}{a_\pm^{\,o}} + \frac{\Delta\mu^*}{F} \qquad (8)$$

and

$$\Delta\psi'' = -\frac{RT}{F}\alpha^{si} \ln \frac{a_\pm^{\,i}}{a_\pm^{\,o}} + \frac{\Delta\mu^*}{F} \qquad (9)$$

corresponding to the two opposite orientations of the

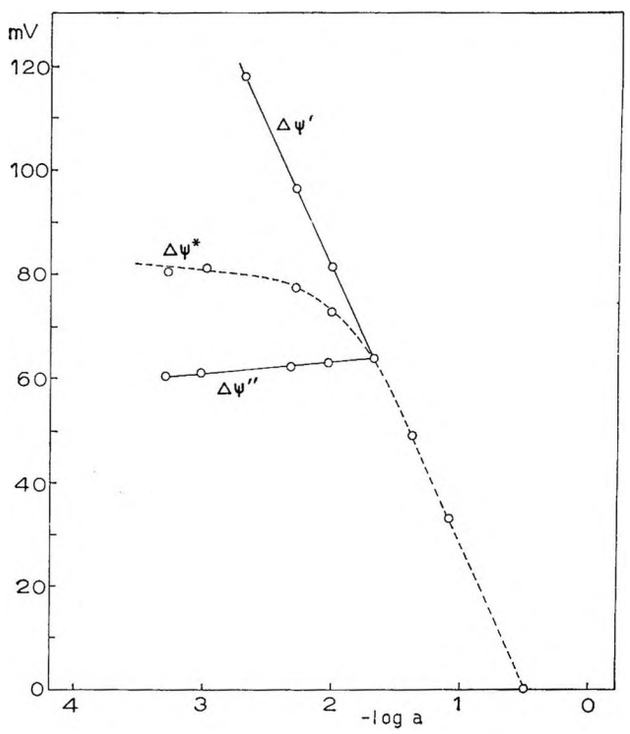

Figure 2. Asymmetry potential $\Delta\psi^*$ between two NaCl solutions i and o in contact with two membranes si and so separated by a middle compartment containing NaCl solution having a mean activity of 3.37×10^{-1}. Membrane potentials $\Delta\psi'$ and $\Delta\psi''$ between two solutions i and o separated by the same system, with opposite orientations. The mean activity of one solution is kept at 1.7×10^{-2} whereas that in the other solution is varied.

system, namely, with the membrane si in contact with the solution i or o, respectively. The behavior of $\Delta\psi^*$, $\Delta\psi'$, and $\Delta\psi''$ is illustrated in Figure 2 for the system $a_{\pm}^{m} = 3.37 \times 10^{-1}$, $d_{si} = s \times 10^{-4}$ mequiv of SO_4/g, $d_{so} = 5 \times 10^{-1}$ mequiv of SO_4/g, $\alpha^{si} = 0.04$, $\alpha^{so} = 1.0$. The very close analogy between the behavior of asymmetric membranes and the asymmetric model system considered above is clearly apparent from a comparison of Figure 2 and Figure 1. Such an analogy readily suggests that electrolyte is present in the regions of contact between the elements of an asymmetric membrane having different charge densities. This hypothesis is confirmed by a microscopic examination of the asymmetric membranes prepared as described in the previous paper. In fact, in the membrane elements with higher charge density the presence of very small granules of polystyrenesulfonic acid may be observed which is in excess with respect to that homogeneously dispersed in the collodion matrix. This is very likely the result of the very high concentration of the polyelectrolyte in the collodion solutions from which the high charge density layer was cast. It may, therefore, be concluded that when such granules of the sodium exchanged polyelectrolyte, highly swollen by water, happen to be in contact between two membranes with different charge densities, a system of asymmetric microcells is formed which is analogous to the model system described above.

A confirmation of the above conclusion stems from the behavior of asymmetric membranes made by sandwiching a thin layer of polystyrenesulfonic acid between two layers, si and so, of CPS having the same charge densities as the external layers of the previously described asymmetric membranes. After exchange with a 0.5 N solution of NaCl, the asymmetric potential $\Delta\psi^*$ and the membrane potentials $\Delta\psi'$ and $\Delta\psi''$ were measured. The results are shown in Figure 3. The similarity between the behavior of this type of asymmetric membranes and the previously described ones is striking. Applying eq 8 and 9, the electrical potentials differences $\Delta\psi'$ and $\Delta\psi''$ should be obtained from the asymmetry potential $\Delta\psi^*$ and the activity ratios $a_{\pm}^{i}/a_{\pm}^{o}$ inserting the best values of α^{si} and α^{so}. When this is done for the curves of Figures 1, 2, and 3, values of α^{si} and α^{so} are obtained as given in Table I. The permselectivity coefficients of the previously described asymmetric membranes and the new type appear to compare rather satisfactorily.

Experimental Section

Uniform Membranes. Uniform membranes of polystyrenesulfonic acid embedded in a collodion matrix were made according to Gregor and Sollner.[2] The polystyrenesulfonic acid obtained according to Neihof[3] had an average molecular weight of about 9×10^4. After purification, its acid value was 4.80 mequiv/g, as compared with a theoretical value of 5.43 mequiv/g calculated assuming one sulfonic acid group per benzene ring. Membranes were cast from solutions of 4% collodion in a 1:2 mixture of alcohol and ether containing 4 mg/ml or 4×10^{-3} mg/ml of polystyrenesulfonic acid. The charge densities of the membranes thus obtained were 5×10^{-1} mequiv of SO_4/g and 5×10^{-4}/mequiv of SO_4/g, respectively. Total ex-

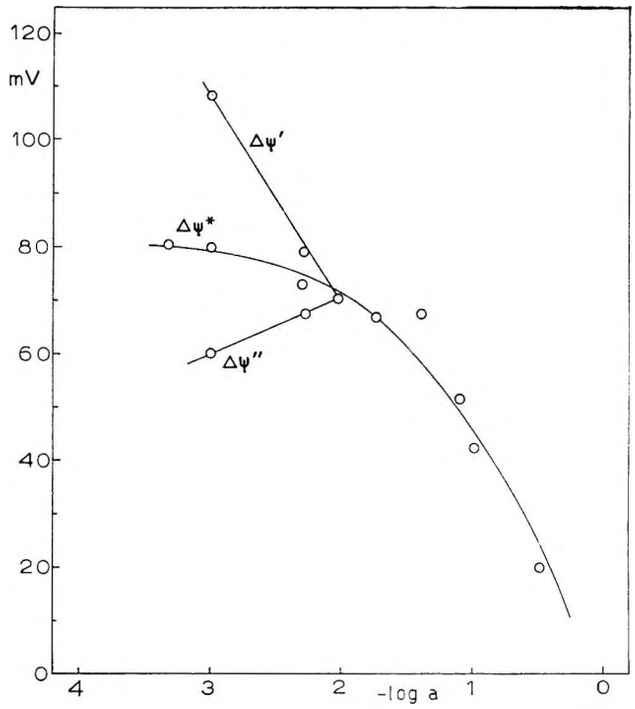

Figure 3. Asymmetry potential $\Delta\psi^*$ and membrane potentials $\Delta\psi'$ and $\Delta\psi''$ a Na^+ exchanged asymmetric membranes made of two layers si and so of CPS sandwiching a film of polystyrenesulfonic acid. The other conditions are the same as in Figure 1, but the fixed mean activity is 1×10^{-2} for the membrane potentials $\Delta\psi'$ and $\Delta\psi''$.

Table I

	α^{so}	α^{si}
Model system	1.00	0.04
Previous asymmetric membrane	0.80	0.25
New asymmetric membrane	0.81	0.17

(2) H. P. Gregor and K. Sollner, *J. Phys. Chem.*, 58, 409 (1954).
(3) R. Neihof, *ibid.*, 58, 916 (1954).

change of the hydrogen ions was achieved by equilibrating the membranes with a 0.5 N NaCl solution.

Asymmetric Membranes. The previously described asymmetric membranes were prepared according to the previous paper. The new asymmetric membranes were obtained by casting a thin membrane of CPS with a charge density of 5×10^{-4} mequiv of SO_4/g and then evaporating over it a water solution of polystyrenesulfonic acid having a concentration of 4 mg/ml. Finally a thin membrane of CPS with a charge density of 5×10^{-1} mequiv of SO_4/g was cast over the film of polystyrenesulfonic acid. Total exchange of the hydrogen ions with sodium was achieved as for the uniform membranes.

Apparatus. (*a*) *Electrical Potentials in the Model System.* A three-compartment cell made of Pyrex glass was used for this experiment. The membranes si and so were clamped between two flanges. Saturated calomel electrodes were immersed through agar bridges in the solutions i and o, and the potential differences were recorded with a Pye precision potentiometer equipped with a Multiflex Lange galvanometer with an internal resistance of 1200 ohms and a sensitivity of 4×10^{-9} amp/mm.

(*b*) *Electrical Potential across Asymmetric Membranes.* The potential differences across asymmetric membranes were recorded with calomel electrodes in a standard cell similar to that previously described.[1]

The Kinetics of the Reaction between Neptunium(III) and Iron(III) in Aqueous Perchlorate Solutions[1]

by T. W. Newton and N. A. Daugherty

University of California, Los Alamos Scientific Laboratory, Los Alamos, New Mexico *(Received March 13, 1967)*

Rates of the reaction $Np^{3+} + Fe^{3+} = Np^{4+} + Fe^{2+}$ in aqueous perchlorate solutions are given by $d[Np(IV)]/dt = [Np^{3+}][Fe^{3+}](k_0 + k_{-1}[H^+]^{-1})$ for acid concentrations ranging from 0.05 to 2.0 M at constant ionic strength. The effect of temperature was determined from 0.5 to 36.7°; k_{-1} is from about 4 to 30 times larger than k_0 in this range. The temperature coefficient of k_{-1} was used to determine the activation parameters for the predominant net activation process $Np^{3+} + Fe^{3+} + H_2O = [(Np)(OH)(Fe^{5+})]^* + H^+$, $\Delta F^* = 13.66$ kcal/mole ($k_{-1} = 600$ sec^{-1} at 25°), $\Delta H^* = 14.55 \pm 0.1$ kcal/mole, and $\Delta S^* = 3.0 \pm 0.3$ cal/mole deg. The results for this reaction are compared with those for the similar Pu(IV)–Fe(II) and Np(IV)–Cr(II) reactions.

Introduction

A number of apparently simple oxidation–reduction reactions have been studied in which the net change is in the charge on the ions involved. Reactions of this type among aqua ions are usually inhibited by H^+, showing that various hydrolyzed species are reactive intermediates. The Np(III)–Fe(III) reaction belongs in this class and its kinetics were studied for comparison with analogous reactions in order to obtain a better understanding of the factors which influence these rates. Recent success in the application of parts of Marcus' theory[2] to inner-sphere reactions[3] suggests the examina-

(1) Work done under the auspices of the U. S. Atomic Energy Commission; presented in part at the 153rd National Meeting of the American Chemical Society, Miami, Fla., April 1967.

tion of sets of similar reactions from this point of view even though the general structure of the activated complexes involved is not known.

Experimental Section

Reagents. Neptunium solutions were prepared from a sample of NpO_2 for which spectrographic analysis showed the transition metals to be less than 0.1 ppm and the rare earths to be less than 0.5 ppm. Radioassay showed the presence of about 200 ppm Pu-238.[4] The oxide was dissolved in concentrated perchloric acid which contained a trace of fluoride and taken to copious fumes, then diluted to give a Np(VI) perchlorate solution. A sample of this stock was reduced to Np(V) with a slight excess of H_2O_2 and the free acid was determined by titration with standard NaOH to the congo red end point. Solutions of Np(III) were prepared from this stock solution by reduction with zinc amalgam. The total neptunium content of these completely reduced solutions was determined by a spectrophotometric titration using standard Ce(IV). Excess Ce(IV) was detected at about 3700 A after oxidation of the neptunium to the VI state was complete. Purification of the neptunium solutions using a cation-exchange resin was found not to influence the observed reaction rates.

Iron(III) perchlorate was prepared from the nitrate (Mallinckrodt) which was strongly fumed with perchloric acid and cooled to give crude crystals. These were crystallized twice from water and dissolved to make a stock solution. Total iron was determined with standard Ce(IV) after complete reduction with zinc amalgam. Total perchlorate was determined by the use of Dowex 50 in the hydrogen ion form. Free acid was estimated by difference. The distilled water and solutions of $HClO_4$, $LiClO_4$, and $NaClO_4$ were prepared and analyzed as before.[5] The concentration units used in this paper are moles per liter, M, at 23°.

Procedure. One of the reactants and appropriate amounts of salt and acid were brought to the required temperature in a stirred absorption cell in a small thermostat in the light beam of a Cary recording spectrophotometer, Model 14.[5] The reaction was started by injecting the final reactant, also at the required temperature, from a calibrated hypodermic syringe with a Teflon needle. Timing was by means of the recorder chart drive. The reaction was followed at 7230 A where Np(IV) is the predominant absorbing species. All stock solutions were deaerated with purified argon and the reaction mixtures were protected from air by means of an argon blanket. The spectrophotometric titration mentioned above was used to determine total reducing agent after representative runs in order to check the calculated initial Np(III) concentrations.

Results. Data from individual rate runs were found to satisfy the usual integrated form of the second-order rate law, first order in each of the reactants, Np(III) and Fe(III). Results of a typical run are shown in Table I, where observed and calculated absorbance values are given as a function of time. The apparent second-order rate constant for this reaction is defined by $k' = (\mathrm{d}[\mathrm{Np(IV)}]/\mathrm{d}t)/[\mathrm{Fe(III)}]\,[\mathrm{Np(III)}])$. Values were calculated from the absorbance data using a nonlinear least-squares program which minimizes $\Sigma(A_{\mathrm{obsd}} - A_{\mathrm{calcd}})^2$.[5]

Table I: Typical Rate Run[a]

Time, sec	Absorbance	
	Obsd	Calcd
0	0.100	(0.100)
2.5	0.228	0.229
3.0	0.242	0.241
4.0	0.261	0.261
5.0	0.277	0.276
6.0	0.288	0.288
7.0	0.300	0.301
9.0	0.311	0.311
10.0	0.316	0.316
12.5	0.325	0.326
15.0	0.332	0.333
17.5	0.338	0.337
20.0	0.341	0.341
∞	...	0.351

[a] Conditions: 25°, μ = 2.0 M ($LiClO_4$), 0.40 M $HClO_4$, 1.58×10^{-4} M Np(III), 2.24×10^{-4} M Fe(III).

Initial concentrations of Fe(III) and Np(III) were varied by factors of about 8 without significantly affecting the apparent second-order rate constants. This is shown by the data in Table II. The products of reaction, Np(IV) and Fe(II), were also shown to be without significant effect at 4.4×10^{-4} M.

The effect of ionic strength was determined in a series of rate measurements at 0.8° in 0.100 M $HClO_4$. The data from both $LiClO_4$ and $NaClO_4$ solutions were found to be represented satisfactorily by the extended form of the Debye–Hückel equation. The results of these measurements are given in Table III. The data show that substituting 1.9 M $LiClO_4$ for 1.9 M $NaClO_4$ increases the rate about 16%. Similar experiments at 25° showed a 13% increase for 1.8 M salts in 0.2 M $HClO_4$.

(2) R. A. Marcus, *J. Phys. Chem.*, **67**, 853 (1963).

(3) A. Haim and N. Sutin, *J. Am. Chem. Soc.*, **88**, 434 (1966).

(4) These results were provided by the Analytical Chemistry Group of this laboratory.

(5) T. W. Newton and F. B. Baker, *J. Phys. Chem.*, **67**, 1425 (1963).

Table II: Effect of Initial Reactant Concentrations on the Apparent Second-Order Rate Constant[a]

Fe(III), $M \times 10^4$	Np(III), $M \times 10^4$	k', M^{-1} sec^{-1}
2.99	3.56	51.2
2.99	10.67	50.7
2.99	17.8	50.5
2.99	28.4	50.0
5.01	2.96	49.6
12.5	2.96	49.0
25.0	2.96	49.9

[a] Conditions: 0.8°, 1.99 M $HClO_4$.

Table III: Effect of Ionic Strength[a]

Ionic strength, μ, M	k' in $LiClO_4$ solution, M^{-1} sec^{-1} Obsd	Calcd[b]	k' in $NaClO_4$ solution, M^{-1} sec^{-1} Obsd	Calcd[c]
0.103	177	179	173	173
0.293	275	273	258	258
0.483	332	335	324	312
0.673	386	384	350	353
1.054	466	465	412	419
1.434	542	535	466	473
1.624	570	568	489	498
2.004	636	633	561	545

[a] Conditions: 0.8° and 0.100 M $HClO_4$. [b] Calculated using $\log k' = \log 39.79 + [3.911\mu^{1/2}/(1 + 2.93\mu^{1/2})] + 0.0634\mu$. [c] Calculated using $\log k' = \log 39.79 + [3.911\mu^{1/2}/(1 + 3.04\mu^{1/2})] + 0.0472\mu$. The parameters in these expressions were calculated by least squares with the requirement that the first be the same for both sets of solutions.

The hydrogen ion and temperature dependences were studied in a series of runs in which the ionic strength was maintained at 2.0 M with $LiClO_4$. The results are summarized in Table IV.

Chloride ion was found to catalyze the reaction and to complicate it so that strict second-order behavior was not observed in the individual runs. A concentration of 0.1 M chloride in 2 M total acid at 0.8° was found to increase the initial rate by a factor of about 5.

Interpretation and Discussion

The reaction which was investigated

$$Np^{3+} + Fe^{3+} = Np^{4+} + Fe^{2+} \quad (1)$$

is completely quantitative; the oxidation potentials involved[6] indicate that the equilibrium quotient is about 10^{10}. However, for the possible continuing reaction

$$Np^{4+} + Fe^{3+} + 2H_2O = NpO_2^+ + Fe^{2+} + 4H^+ \quad (2)$$

Table IV: Effect of Hydrogen Ion Concentration and Temperature on the Apparent Second-Order Rate Constant (μ = 2.0 M ($LiClO_4$))

Temp, °C	$[HClO_4]$, M	No. of detn	Av k', M^{-1} sec^{-1}	Calcd k',[a] M^{-1} sec^{-1}
0.85	1.99	11	49.5	48.8
	1.50	9	58.1	59.5
	1.10	4	77.0	75.4
	0.737	1	104	103.2
	0.500	9	146	144.6
	0.379	3	188	185
	0.200	7	333	336
	0.100	3	633	654.7
	0.050	4	1288	1302
25.1	1.99	2	344	339
	1.30	3	529	501
	0.879	2	764	724
	0.750	2	870	842
	0.400	3	1650	1546
	0.200	4	3132	3043
12.3	1.99	2	117.5	121.8
	1.50	2	156	152
	1.10	2	203.5	201
	0.80	3	273	263
	0.520	3	396	392
	0.200	2	1014	988
	0.100	2	1958	1924
36.7	1.99	2	778	838
	1.80	2	878	922
	1.67	1	963	990
	1.41	1	1157	1163
	1.19	2	1319	1371
	0.885	2	1745	1823
	0.740	2	2152	2171
	0.500	2	3100	3180
	0.400	1	4154	3957

[a] Calculated using the parameters in line 1 of Table V.

the equilibrium quotient is about unity. Thus, the effect of reaction 2 must be considered, particularly in solutions low in acid concentration. Huizenga and Magnusson[7] report $-d[Np(IV)]/dt = 0.057[Np(IV)]\cdot[Fe(III)][H^+]^{-3}$ M sec^{-1} at 25° and μ = 1 M ($NaClO_4$); this gives an apparent second-order rate constant of 57 M^{-1} sec^{-1} in 0.1 M acid. Data in Tables III and IV show that the apparent second-order rate constant for reaction 1 is about 4100 M^{-1} sec^{-1} under similar conditions. It is concluded that, since the rate of reaction 2 is only about 0.014 as large as that of reaction 1 in the

(6) W. M. Latimer, "Oxidation Potentials," 2nd ed, Prentice-Hall, Inc., Englewood Cliffs, N. J., 1952.

(7) J. R. Huizenga and L. B. Magnusson, *J. Am. Chem. Soc.*, **73**, 3202 (1951).

Table V: Activation Parameters

No.	ΔS_h, cal/mole deg	ΔH_h, kcal/mole	ΔS_{-1}*, cal/mole deg	ΔH_1*, kcal/mole	ΔS_0*, cal/mole deg	ΔH_0*, kcal/mole	a_0	b	Rms,[a] % dev
1.	21.2884	10.2	2.64 ± 0.32[b]	14.45 ± 0.09	-35.8 ± 5.0	4.66 ± 1.37	...	...	4.44
2.	21.2884[c]	10.2	3.33 ± 0.35	14.64 ± 0.10	...	...	0.211 ± 0.008	0.031 ± 0.002	4.10
3.	46.2461[d]	17.85	2.67 ± 0.32	14.46 ± 0.09	-35.8 ± 4.9	4.67 ± 1.36	...	...	4.43

[a] Root-mean-square per cent deviation between observed and calculated values. [b] Standard deviation calculated by the least-squares program. [c] ΔS for the first hydrolysis of Fe(III) calculated from $K_h = 1.5 \times 10^{-3}$ at 25° and $\Delta H_h = 10.2$ kcal/mole.[9] [d] ΔS for the first hydrolysis of Fe(III) calculated from $K_h = 1.055 \times 10^{-3}$ at 25° and $\Delta H_h = 17.85$ kcal/mole. This K_h value was corrected to $\mu = 2$ using previously determined[9b] ionic strength dependence; and ΔH_h value is the average of the two reported.[10]

least favorable case, complications due to reaction 2 can be ignored.

The data show that reaction 1 is first power in each of Np(III) and Fe(III) and is predominantly inverse first power in the hydrogen ion concentration. Plots of either $k'([H^+] + K_h)$ or $\log k'([H^+] + K_h)$ *vs.* $[H^+]$ were essentially linear with slopes much smaller than the intercepts. The expression $[Fe^{3+}] = [Fe(III)]/([H^+] + K_h)$ was used to correct for the small amount of hydrolysis of Fe(III) which occurs. The hydrolysis of Np(III) may reasonably be assumed[8] to be much smaller than that for Fe(III) and has been neglected. These plots showed that the two rate laws

$$d[Np(IV)]/dt = [Np^{3+}][Fe^{3+}](k_0 + k_{-1}[H^+]^{-1}) \quad (3)$$

$$d[Np(IV)]/dt = [Np^{3+}][Fe^{3+}]k_{-1}[H^+]^{-1}e^{a[H^+]} \quad (4)$$

are equally satisfactory. Both indicate that the most important path for reaction involves the formation of an activated complex from Np^{3+} and Fe^{3+} with the prior loss of H^+ in an unspecified preequilibrium. The minor terms are best interpreted as an additional path for eq 3 and as a medium effect for eq 4.

The temperature-dependence data were treated according to both rate laws by making the assumption that the rate constants k_0 and k_{-1} are given by the Eyring equation, $k_i = (kT/h) \exp(\Delta S_i^*/R) \exp(-\Delta H_i^*/RT)$, and that the Harned parameter, a, is linear in temperature: $a = a_0 + bt$. The recent literature gives discrepant values for ΔH_h for the first hydrolysis of Fe(III) (10.2 kcal/mole according to Milburn[9] and 16.0 or 19.7 kcal/mole according to Schlyter).[10] Calculations were made using the first value and the average of the other two. The necessary ΔS_h values were chosen to give the appropriate K_h values at 25°. The calculations were by least squares in which the hydrogen ion and temperature data were used simultaneously to find values of ΔH_{-1}^*, ΔS_{-1}^*, ΔH_0^*, and ΔS_0^*, or a_0 and b which best reproduce the experimental data. The results are given in Table V.

It is seen that the activation parameters for the principal path depend only slightly on the assumptions made about the minor term in the rate law and about the hydrolysis correction. We conclude, therefore, that $\Delta F^* = 13.66$ kcal/mole, $\Delta H^* = 14.55 \pm 0.1$ kcal/mole, and $\Delta S^* = 3.0 \pm 0.3$ cal/mole deg for the principal net activation process

$$Np^{3+} + Fe^{3+} + H_2O = [(Np)(OH)(Fe)^{5+}]^* + H^+ \quad (5)$$

where the composition but not necessarily the structure of the activated complex is indicated. The rate constant for the net activation process is 600 sec^{-1} at 25°.

The present results are compared with those obtained for some formally similar reactions in Table VI. The net activation processes and activation parameters serve to summarize the kinetic results in terms which are independent of assumptions about the details of the mechanism. All of the reactions referred to in Table VI are similar in that the most important activation process involves the formation of a +5 activated complex from the initial reactants with the prior loss of one H^+. An understanding of the relative values of the activation parameters will require assumptions with respect to the mechanisms involved and the actual rate-determining reactions.

It is of interest to try to rationalize the observed relative rates on the basis of the plausible assumption that these reactions occur by a common mechanism in which the rate-determining step is the formal transfer of OH from the more highly hydrolyzed reactant to the other ion. This might occur directly by an inner-sphere transfer or by some sort of outer-sphere H-atom

(8) J. J. Katz and G. T. Seaborg, "The Chemistry of the Actinide Elements," Methuen and Co., Ltd., London, 1957 (also, John Wiley and Sons, Inc., New York, N. Y.), p 298.

(9) (a) R. M. Milburn, *J. Am. Chem. Soc.*, **79**, 537 (1957); (b) R. M. Milburn and W. C. Vosburgh, *ibid.*, **77**, 1352 (1955).

(10) K. Schlyter, *Trans. Roy. Inst. Technol. Stockholm*, No. 196 (1962).

Table VI: Activation Processes and Parameters[a]

Process	ΔF^*	ΔH^*	ΔS^*	S_{comp}^*	μ	Ref
$Np^{3+} + Fe^{3+} + H_2O = [*]^{5+} + H^+$	13.7	14.6	3.0 ± 0.3	−87	2	This work
$Np^{4+} + Fe^{2+} + H_2O = [*]^{5+} + H^+$	27.9	29.9	7			Reverse
$Pu^{4+} + Fe^{2+} + H_2O = [*]^{5+} + H^+$	15.1	19.1	13.3 ± 1.3	−82	2	*b*
$Np^{4+} + Cr^{2+} + H_2O = [*]^{5+} + H^+$	16.7	16.2	-1.6 ± 1.4	−93	1	*c*

[a] The units for ΔF^* and ΔH^* are kcal/mole; for the entropies, cal/mole deg; and for the ionic strength, M. [b] T. W. Newton and H. D. Cowan, *J. Phys. Chem.*, **64**, 244 (1960). [c] Values were computed from the data of R. C. Thompson and J. C. Sullivan, *J. Am. Chem. Soc.*, **89**, 1096 (1967). These authors showed that the $[H^+]$ independent term in their rate law is small, erratic, and not significant statistically, but chose to include it in their calculations of the other terms. We prefer, instead, to assume that this term is zero and find somewhat different values for ΔH^* and ΔS^* but essentially the same for ΔF^* for the major ($[H^+]^{-1}$) term.

Table VII: Some OH Transfer Reactions. Values[a,h–j] for 25° and $\mu = 1.0\ M$

No.	Reaction	ΔF^* (obsd)	ΔF°	ΔF^f	ΔF^* (calcd)[b]	Ref
12.	$Cr^{2+} + FeOH^{2+} = CrOH^{2+} + Fe^{2+}$	8.6	−25.8	6.7	5.5	*c*
14.	$Cr^{2+} + NpOH^{3+} = CrOH^{2+} + Np^{3+}$	13.6	−10.9	1.4–1.2	...	*d*
23.	$Fe^{2+} + PuOH^{3+} = FeOH^{2+} + Pu^{3+}$	13.6	−2.8	0.1	11.0	10
24.	$Np^{3+} + FeOH^{2+} = NpOH^{3+} + Fe^{2+}$	10.1	−14.9	3.2–2.6	...	This work
11.	$Cr^{2+} + CrOH^{2+} = CrOH^{2+} + Cr^{2+}$	17.4	0			*e*
22.	$Fe^{2+} + FeOH^{2+} = FeOH^{2+} + Fe^{2+}$	12.7	0			*f*
33.	$Pr^{3+} + PuOH^{3+} = PuOH^{3+} + Pu^{3+}$	11.9	0			*g*
44.	$Np^{3+} + NpOH^{3+} = NpOH^{3+} + Np^{3+}$	(10–14)	0			Estimate

[a] May be in error by at least 0.2 kcal/mole due to uncertainties in medium effects and hydrolysis constants. The free energies of hydrolysis for Fe^{3+}, Cr^{3+}, Np^{4+}, and Pu^{4+} were taken as 3.9, 5.5, 3.1, and 1.7 kcal/mole, respectively, based on the data in ref 8 and footnotes *h–j* of this table. [b] Calculated using eq 8. [c] G. Dulz and N. Sutin, *J. Am. Chem. Soc.*, **86**, 829 (1964). [d] See Table VI, footnote *c*. [e] A. Anderson and N. A. Bonner, *J. Am. Chem. Soc.*, **76**, 3826 (1954). [f] J. Silverman and R. W. Dodson, *J. Phys. Chem.*, **56**, 846 (1952). [g] T. K. Keenan, *ibid.*, **61**, 1117 (1957). [h] C. Postmus and E. L. King, *ibid.*, **59**, 1208 (1955). [i] J. C. Hindman, J. C. Sullivan, and D. Cohen, *J. Am. Chem. Soc.*, **81**, 2316 (1959). [j] S. W. Rabideau, *ibid.*, **79**, 3675 (1957).

transfer. These reactions are considered in this way in Table VII. The related Cr(II)–Fe(III) reaction and the possibly pertinent electron-exchange reactions are included also.

Rates of similar reactions often indicate nearly linear relations between ΔF^* and ΔF°. An examination of the data in Table VII shows that if such a relation applies here, the two reactions which involve the Cr(II)–Cr(III) couple are inherently slower than the two which involve the Fe(II)–Fe(III) couple. This suggests that some of the factors which make the chromium-exchange reaction slower than the iron one are important in the net reactions also.

Such effects are predicted for outer-sphere reactions by the Marcus expression[2]

$$k_{12} = (k_{11}k_{22}K_{12}f_{12})^{1/2} \quad (6)$$

where $\log f_{12} = (\log K_{12})^2/[4 \log (k_{11}k_{22}/Z^2)]$.

The form of this expression depends primarily on the assumptions that an approximately harmonic distortion of coordination and solvent spheres about an ion occurs prior to electron transfer under Franck–Condon conditions, the force constants for the distortions are essentially independent of the reaction partner, and that the work terms are small or cancel. Some of these assumptions may reasonably be expected to apply to inner-sphere reactions as well; therefore it is worthwhile to examine the activation free energies in Table VII in terms of eq 6 even though the nature of the various activated complexes is unknown.

In terms of free energies, Marcus' expression becomes[11]

$$\Delta G_{12}^* = {}^1/_2(\Delta G_{11}^* + \Delta G_{22}^* + \Delta G_{12}^\circ + \Delta G_{12}^f) \quad (7)$$

where $\Delta G_{12}^f = (\Delta G_{12}^\circ)^2/[4(\Delta G_{11}^* + \Delta G_{22}^* - w_{11} - w_{22})]$, w_{11} and w_{22} are the work terms as usually defined,[2] and it is assumed that $w_{11} + w_{22} \cong 2w_{12} \cong 2w_{21}$. The free energies in these expressions are indicated by ΔG^*

(11) N. Sutin, *Ann. Rev. Phys. Chem.*, **17**, 119 (1966).

rather than by ΔF^* to emphasize that activation free energies are usually defined, following Eyring, by the equation $k = (kT/h) \exp(-\Delta F^*/RT)$, while Marcus uses $k = Z \exp(-\Delta G^*/RT)$, where Z is the collision frequency of the hypothetically uncharged ions (10^{11} M^{-1} sec^{-1}). The effect of this difference in definition cancels in all terms in eq 7 except for ΔG_{12}^f, and eq 7 may be rewritten

$$\Delta F_{12}^* = {}^1/_2(\Delta F_{11}^* + \Delta F_{22}^* + \Delta F_{12}^\circ + \Delta F_{12}^f) \quad (8)$$

where $\Delta F_{12}^f = (\Delta F_{12}^\circ)^2/[4(\Delta F_{11} + \Delta F_{22}^* - w_{11} - w_{22} - 4.89)]$ kcal/mole at 25°.

A requirement for the application of eq 8 to a set of net reactions like those in Table VII is that the reactants in the appropriate pair of exchange reactions appear as the reactants and products in the net reaction. However, this condition makes the actual values chosen for the hydrolysis free energies quite unimportant. It may be shown that these quantities cancel exactly except in the small ΔF^f term where their influence is not large.

Application of eq 8 to the calculation of activation free energies requires estimates of the electrostatic work terms. These are probably small in solutions for which the ionic strength is 1 M and values of sufficient precision were estimated as described by Sutin[12] to be 0.24, 0.24, and 0.45 kcal/mole for w_{11}, w_{22}, and w_{33} respectively. (The subscripts here and below refer to the reactions in Table VII.) These values, together with others from Table VII give 5.5 and 11.0 for ΔF_{12}^* and ΔF_{23}^*. The observed values are higher than these by 2.85 ± 0.25 kcal/mole, corresponding to a factor greater than 100 in the rates at 25°. It is unlikely that uncertainties in the estimates for w are important; changing w_{22} by 1 kcal/mole changes ΔF_{12}^* by about 0.2 kcal/mole and ΔF_{23}^* by a negligible amount.

Although eq 8 gives only approximate values for ΔF_{12}^* and ΔF_{23}^*, the difference between these two quantities is accurate to within 0.5 kcal/mole. This is considered satisfactory in view of the uncertainties in the entries in Table VII. The analogous difference, $\Delta F_{14}^* - \Delta F_{24}^*$, can also be estimated since it depends only slightly on the unknown value of ΔF_{44}^*. Values ranging from 3.4 to 3.6 kcal/mole were found when ΔF_{44}^* was assumed to lie between 10 and 14 kcal/mole. Again, the calculated difference is in satisfactory agreement with the observed one (3.5 kcal/mole).

The results of these calculations are similar to those of Sutin[13] on some chloro-bridged reactions. Both calculations suggest that Marcus' expression, eq 8, may prove to be fairly satisfactory for estimating rate ratios for similar reactions of unknown mechanism even though the individual rates are poorly predicted.

Acknowledgments. We gratefully acknowledge many helpful discussions with Dr. Norman Sutin. We also thank Dr. J. C. Sullivan for his interest and for making the data in Table VI, footnote *c*, available to us prior to publication.

(12) N. Sutin, *Ann. Rev. Nucl. Sci.*, **12**, 2845 (1962); B. M. Gordon, L. L. Williams, and N. Sutin, *J. Am. Chem. Soc.*, **83**, 2061 (1961).

(13) N. Sutin, "Exchange Reactions," International Atomic Energy Agency, Vienna, 1965.

The Kinetics of Oxidation Induced in Solid Systems by Ultrasonic Radiation[1]

by F. A. H. Rice and L. A. Veguilla-Berdecia

Department of Chemistry, The American University, Washington, D. C. 20016
(Received March 13, 1967)

The oxidation of lauryl aldehyde to lauric acid by potassium chlorate under the influence of an ultrasonic field is found to follow the equation for a second-order reaction. The specific rate constant varies directly as the first power of the ultrasonic intensity. Any one intensity of radiation will only induce the oxidation of a small fraction of the aldehyde present. The rate of oxidation depends on the crystal size and increases with a decrease in the size of the crystal. Increasing the intensity of the radiation increases the total amount of aldehyde that can be oxidized. However, this amount asymptotically approaches an upper limit. The results can be interpreted on the basis that the reaction takes place at certain sites on the $KClO_3$ crystal surface and these sites vary in their sensitivity to the action of ultrasonic radiation. An increase in intensity therefore might be expected to increase the number of sensitive sites and hence the total quantity of aldehyde that can be oxidized. The upper limit is reached when the total number of surface sites has been oxidized. The rate would depend on the total number of sensitive sites and should increase as the crystal size decreases.

Introduction

Ultrasonic radiation, like electromagnetic radiation, is capable of initiating and sustaining a variety of chemical reactions. Oxidations may result from the irradiation of liquid systems (methanol to formaldehyde in aqueous solutions,[2a] liberation of free iodine from KI solutions,[2b] degradation of toluene to phenol and formaldehyde,[3] etc.). Molecular rearrangements, deflagration of solid explosives, depolymerizations, and other chemical reactions have been found to occur when systems are exposed to ultrasonic radiation.[4] The feasibility of initiating and sustaining a slow oxidative chemical reaction in a solid system by ultrasonic radiation has been demonstrated by one of the authors and a co-worker.[5]

In liquid systems the cavitation theory seems to explain the occurrence of chemical reactions in the ultrasonic field. The collapse of the cavities formed in the liquid medium produces intense hydraulic shocks leading to high local temperatures and consequent initiation of chemical reactions.[6,7] Other mechanisms are needed to explain the initiation of some chemical reactions in liquids in an ultrasonic field. These mechanisms also assume the formation of "bubbles" in the liquid medium.[8,9] It is unlikely that cavitation mechanisms are operative in solid systems, since there would not be an easily volatilized liquid or gas present. The hot-spot theory used by Eyring, *et al.*,[10] and by Bowden, *et al.*,[11] postulated to explain the detonation of explosives or the burning of propellants strongly suggests that oxidation should be induced by ultrasonic

(1) Supported in part by U. S. Public Health Service Research Career Program Award 3-K3-GM-19, 470-03.

(2) (a) M. A. Khenokh, *Zh. Obshch. Khim.*, **23**, 1464 (1953); (b) I. E. Elpiner and Kolesnikova, *Dokl. Akad. Nauk SSSR*, **75**, 837 (1950).

(3) M. A. Khenokh and E. M. Lapinskaya, *Zh. Obshch. Khim.*, **26**, 2439 (1956).

(4) I. E. Elpiner, "Ultrasound, Physical, Chemical and Biological Effects," Consultants Bureau, New York, N. Y., 1964.

(5) F. A. H. Rice and D. Levine, *Proc. Roy. Soc.* (London), **A246**, 180 (1958).

(6) B. E. Noltingh and E. A. Nippiras, *ibid.*, **B63**, 674 (1950).

(7) M. E Fitzgerald, V. Griffing. and J. Sullivan, *J. Chem. Phys.*, **25**, 926 (1956).

(8) Y. I. Frenkel, *Zh. Fiz. Khim.*, **14**, 305 (1940).

(9) T. L. Natanson, *Dokl. Akad. Nauk SSSR*, **59**, 83 (1948).

(10) H. Eyring, R. E. Powell, G. H. Duffey, and R. B. Parlin, *Chem. Rev.*, **45**, 69 (1949).

(11) F. P. Bowden and D. A. Yoffee, "The Initiation and Growth of Explosives in Liquids and Solids," Cambridge University Press, Cambridge, 1952.

irradiation of appropriate solid systems. The ultrasonic field should produce local stresses in the irradiated solid and these stresses should behave as thermal spikes leading to localized reaction regions. This was found to be true[5] in a system made of a solid oxidizable substance (lauryl aldehyde) and a crystalline oxidizing agent (potassium chlorate) randomly mixed, pressed in close contact under high pressure, and then ultrasonically irradiated. The resulting oxidation that occurred could be explained on the basis that hot spots developed at certain points of contact between the two substances and the chemical reaction was initiated at these hot spots.[5]

We wish to report a kinetic analysis of the data previously reported, together with additional data and analysis of the dependence of the degree of oxidation on crystal size.

Experimental Section

The experimental technique was previously described in detail[5] so it is only described briefly here. Accurately weighed equimolar samples of recrystallized $KClO_3$ and lauryl aldehyde (mp 54°) were mixed and made into pellets. The disks were placed between cellophane sheets, mounted, and placed in a water bath maintained at 25 ± 0.01°. The samples were irradiated for the desired length of time at 2 Mc and at intensities of 2.0, 3.0, 4.0, and 6.0 w/cm.^{2} After irradiation, the disks were placed in diethyl ether to dissolve the organic matter. The ether extract was evaporated to dryness under reduced pressure and further dried over P_2O_5 under high vacuum for over 16 hr. The resulting dried mixtures of lauric acid and lauryl aldehyde were accurately weighed and dissolved in 30 ml of a 1:1 (by volume) solution of ethanol and water. This solution was titrated under helium gas with 0.05 N sodium hydroxide, and the quantity of lauric acid that had formed was then calculated.

The inorganic salts ($KClO_2$ and $KClO_3$) were dried under high vacuum over P_2O_5 and weighed. $KClO_3$ was determined by the Furman method.[12] No measurable amount of chloride or hypochlorite was found so it could be presumed that only chlorite was formed. The values for the loss in chlorate were in close agreement with the quantity of lauric acid formed and the two values varied by only $\pm 2.5 \times 10^{-4}$.

"Small" crystals of potassium chlorate were prepared by slowly adding acetone to a solution of potassium chlorate saturated at room temperature. The "large" crystals were formed by quickly cooling to 0° a solution of potassium chlorate saturated at the temperature of the boiling water bath. The particle size distribution (Figure 4) for the samples of "large" and "small" crystals was obtained from a Micromerograph plot.[13] Since the Micromerograph provided stepwise data on the weight of particles less than a certain particle size, the data were plotted on arithmetic probability paper[14] to obtain the distribution of crystal sizes. When mixtures of potassium chlorate (0.6 g) and lauryl aldehyde (0.2 g) were heated together in an iron crucible for 15 min at temperatures ranging from 30 to 200°, no oxidation of the lauryl aldehyde was observed until a temperature of 180° was reached. At this temperature 3×10^{-3} mole for each mole of the aldehyde was oxidized. No measurable increase above this was found at 200°. The mixture ignited at 320–325°.

Results

Figure 1 shows the relationship between the time of irradiation and the oxidation of the aldehyde (mole of lauric acid formed/mole of lauryl aldehyde originally present). All oxidation experiments with randomly selected crystal sizes show this type of curve. There is an initial rapid oxidation which asymptotically tapers off to very low rates after irradiation times longer than about 10 min. Within experimental error, therefore, it would seem that, even on prolonged irradiation, only a certain fraction of the aldehyde is oxidizable by the chlorate under the influence of any one intensity of ultrasonic radiation.

Figure 2 shows the effect of the intensity of radiation at fixed times (t = 3 and 10 min) on the quantity of aldehyde oxidized. All of the samples had the same distribution of particle size. It will be noted that increasing the intensity of the ultrasonic radiation increases both the final degree of oxidation and the rate at which the final oxidation is reached. The two curves approach each other and the ratios of the experimentally determined points after 10 and 3 min of irradiaton decrease with increasing intensity as 1.5, 1.3, 1.2, and 1.1, thus suggesting that they have an extrapolated common asymptote between 10.5 and 11% oxidation. (This is more readily deduced from Figure 8, where the reciprocals of intensity and per cent oxidation are plotted.) This value of between 10.5 and 11% oxidation appears to be the maximum value for the per cent oxidation obtainable at the highest intensities of radiation. The initial rates of oxidation are greatly increased as the intensity is increased. The data at two fixed times depicted in Figure 2 were obtained from

(12) N. H. Furman, "Scott's Standard Methods of Chemical Analysis," 5th ed, D. Van Nostrand Co. Inc., New York, N. Y., 1939, p 274.

(13) The Sharples Micromerograph, manufactured by the Sharples Corp. Research Laboratories, Bridgeport, Pa.

(14) Manufactured by Codex Book Co., Inc., Norwood, Mass.

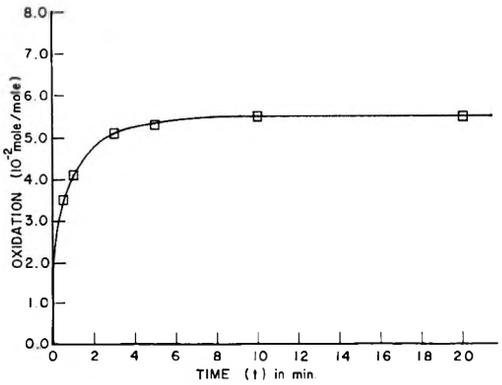

Figure 1. Oxidation of solid mixtures of lauryl aldehyde and potassium chlorate upon treatment with ultrasonic radiation at 2 Mc/sec.

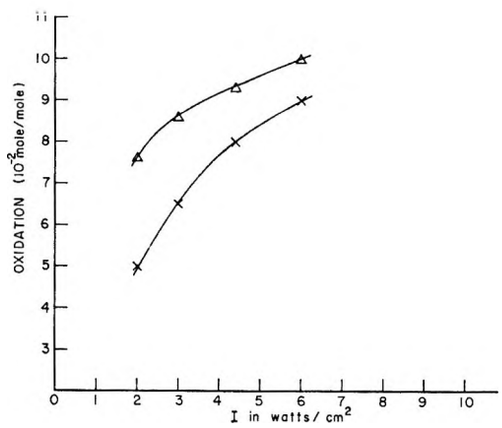

Figure 2. Oxidation of solid mixtures of lauryl aldehyde and potassium chlorate upon treatment with ultrasonic radiation for 3 min (×) and 10 min (Δ) at several intensities (I) of radiation.

a series of experiments carried out to yield data analogous to that shown in Figure 1. The intensity of the radiation was increased, however, to the various levels shown in Figure 2. Inspection of these curves (not shown), in which the per cent oxidation was plotted against time of irradiation at any one intensity of radiation, shows that increasing the intensity of radiation increases the initial rate of oxidation. In order to condense the presentation of the data, however, the times t = 3 and 10 min were chosen since t = 3 min represents a point on the curves during which rapid oxidation takes place and t = 10 min represents a point during which slow oxidation is taking place. As the intensity is increased, there is an increase in the early rate of oxidation; consequently, the quantity of aldehyde oxidized after 3-min irradiation approaches the quantity oxidized after 10-min irradiation which in turn approaches the total amount that it is possible to oxidize.

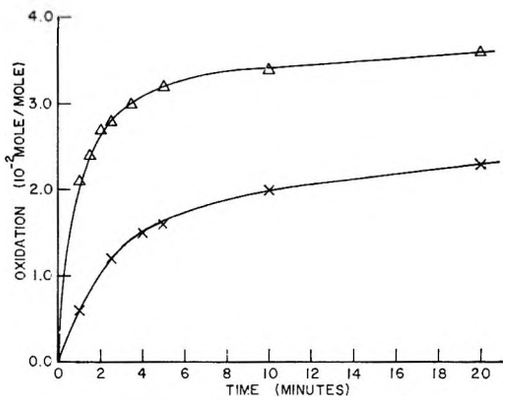

Figure 3. Effect of particle size on the oxidation induced by ultrasonic radiation. Δ represents "small" particles and × represents "large" particles.

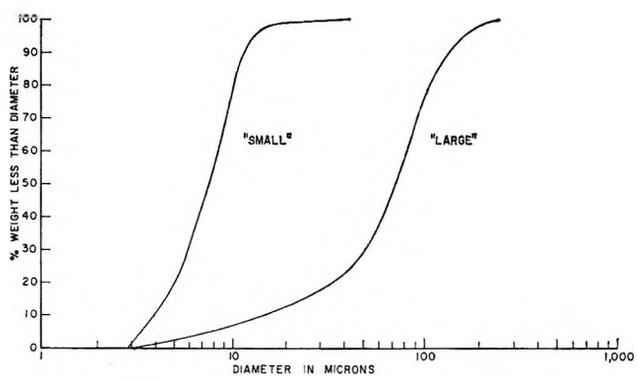

Figure 4. Particle size distribution analysis, "small" and "large" crystals as indicated.

Figure 3 shows the effect of particle size distribution on both the initial rate of oxidation and on the final per cent oxidation. Figure 4 depicts the particle size distribution for the same two samples shown in Figure 3 as obtained from a Micromerograph plot.[13] Figure 5 shows the data obtained from the Micromerograph plotted on arithmetic probability paper.[14] It will be seen that the distribution is almost if not exactly gaussian.

Discussion

The over-all reaction induced by the ultrasonic irradiation of solid mixtures of lauryl aldehyde and potassium chlorate is

$$ClO_3^- + RC(=O)H \longrightarrow ClO_2^- + RC(=O)OH \qquad (1)$$

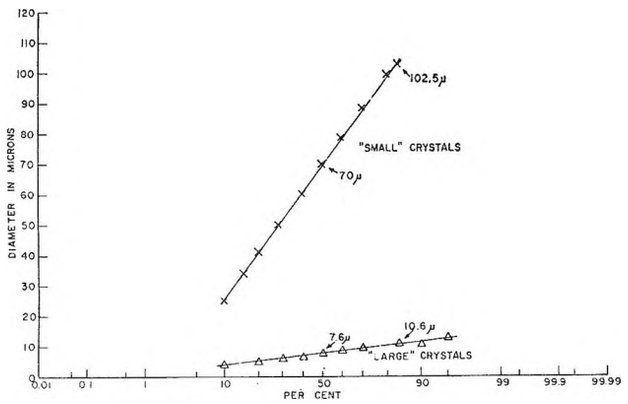

Figure 5. Arithmetic probability plot of data shown in Figure 4.

Since we are dealing with a solid mixture, we must concern ourselves with the kinetics of a heterogeneous reaction. We might expect the reaction to occur only at or near the surface of the $KClO_3$ grain, and therefore the number of molecules reacting per second should be proportional to the area of the interface. That is, we are dealing with a kind of surface concentration and not with bulk concentration. Furthermore, if, of the total available area, only some preferential sites are regions of high potential energy and only these sites become activated by the ultrasonic field, then the extent of the reaction is limited to but a fraction of the total available area.

The kinetic data shown in Figures 1 and 3 can be fitted to the second-order plot

$$\frac{1}{a - x} = kt + \frac{1}{a} \qquad (2)$$

The value of a in (2) is taken to be the maximum per cent oxidation for that particular curve. The plots are shown in Figures 6 and 7 for the "large" and "small" crystals of Figure 3. The linearity is remarkably good. Another linear graph is obtained if we plot the reciprocal of the intensity *vs.* the reciprocal of the per cent oxidation. Figure 8 shows this clearly. This linear plot implies that the specific rate constant k varies directly as the first power of the ultrasonic intensity. In this sense the ultrasonic radiation field shows the same behavior as the electromagnetic field in photochemically induced reactions where in many cases the same dependence is observed.[15]

It will be seen from Figure 5 that for "small" crystals the mean particle size was of the order of 7 μ and the distribution has a standard deviation of about 3 μ. The surface density (calculated from crystal data) for $KClO_3$ is about 5×10^{14} ClO_3^-/cm^2. For the distribution given above, a sample of $KClO_3$ of approximately 0.2 g (about the amount used in the experiments) would have a total area of about 700 cm^2, assuming an ensemble of perfect single crystals. (Incidentally, when the relative quantity of aldehyde to $KClO_3$ was increased tenfold, there was no measurable change in the moles of aldehyde oxidized per mole of $KClO_3$.) The number of possible surface oxidant molecules is therefore only about 0.04% of the total amount of $KClO_3$ present. This is about two orders of magnitude less than the maximum oxidation that can apparently be obtained with this sample of crystals. Similar calculations hold true for the "large" crystals. The calculations are based on the $KClO_3$ grains being

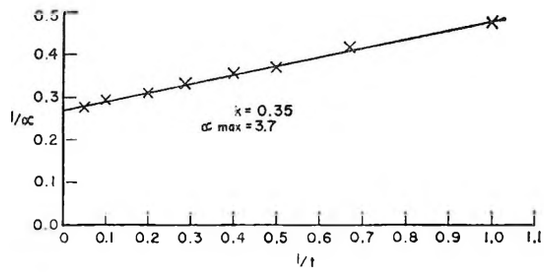

Figure 6. Kinetic data for "small" crystals plotted as $1/\alpha$ *vs.* $1/t$.

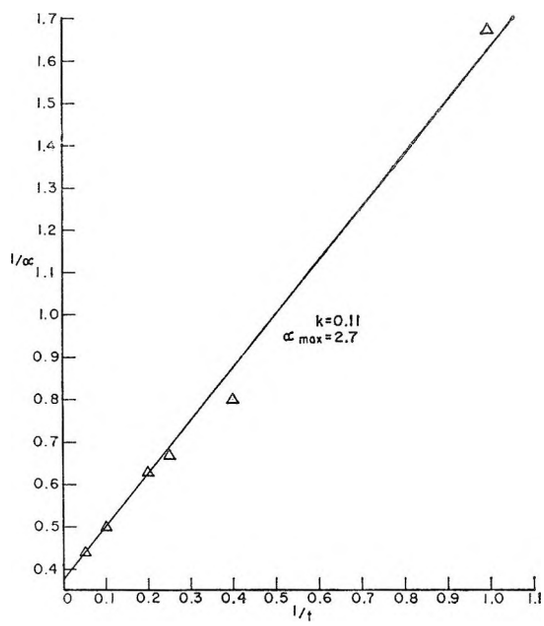

Figure 7. Kinetic data for "large" crystals plotted as $1/\alpha$ *vs.* $1/t$.

(15) E. A. Moelwyn-Hughes, "Physical Chemistry," 2nd ed, Pergamon Press Inc., New York, N. Y., 1961, p 1225.

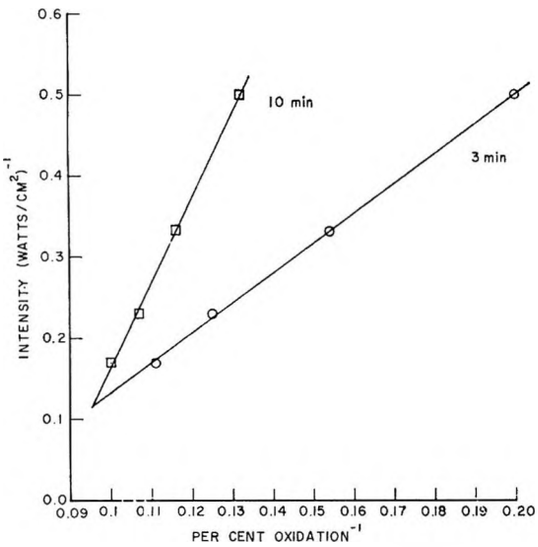

Figure 8. Plot of the reciprocal of the intensity (w/cm²) *vs.* the reciprocal of the per cent oxidation.

cubes (actually $KClO_3$ is monoclinic[16]). Since odd shapes with jagged edges, cracks, etc. will have only a slightly greater surface area than cubes of corresponding masses, we suggest that the total possible extent of oxidation in our system cannot possibly be determined by the total available surface ClO_3^- which is estimated to be, at the most, 0.1% of the total amount of $KClO_3$ present. That the surface itself is not a determining factor is also indicated by the fact that simple heating of the aldehyde–$KClO_3$ mixtures up to 180° does not lead to measurable oxidation.

We propose therefore that the ultrasonic wave activates certain sites on the crystal surface (probably nonbasal dislocations) and that these sites become spots where reaction occurs. It is of particular interest in this connection that nonbasal dislocations in graphite are the centers of enhanced reactivity when the solid is oxidized.[17] Also, the basal surfaces of molybdenum disulfide when oxidized by oxygen develop etch pits at the site of emergence of *c*-axis screw dislocations.[18] It is suggested that the ultrasonic wave raises the effective temperature of the ClO_3^- ions at nonbasal dislocation sites so that reaction takes place. The heat of reaction further helps to raise other reactant molecules at or near the site to sufficiently high energy, and consequently the reaction region may spread along and below the surface. At low intensities not all of the potential surface sites would be activated and hence only a small degree of oxidation would take place. As we increase the intensity, however, the probability of activating all of the sites would be increased until the maximum oxidation was obtained. It is pertinent that there is evidence that the extent of enhanced reactivity due to nonbasal dislocations may be proportional to the strength of the dislocation.[18]

It is conceivable that it is the aldehyde rather than the ClO_3^- that is activated. It is also possible that both species are activated simultaneously. In either case the chlorate grains cannot supply only their surface ions for the reaction.

The suggestion that increasing the intensity increases the number of activated sites is substantiated by the degree of oxidation as related to the particle size distribution. Specifically, let us consider the ratio of the rate constants for the two samples shown in Figure 3. Since the intensities for these oxidation curves were the same, the ratios of the specific rate constants are

$$\frac{k(\text{"large" particles})}{k(\text{"small" particles})} = 0.315 \tag{3}$$

If certain sites on the surface of the $KClO_3$ grains are responsible for the oxidative reaction induced by the ultrasonic radiation and the total number of sites is determined by the total surface area, the oxidation obtained with "large" and "small" $KClO_3$ particles should be proportional to the respective areas. If, for ease of computation, we assume the particles to be spherical, the areas can be calculated as follows. The gaussian distribution is given by

$$f(r) = \frac{N}{\sigma\sqrt{2\pi}} e^{-(1/2)((r-r_0)/\sigma)^2} \tag{4}$$

where N is the total number of particles, r_0 is the mean radius, and σ is the standard deviation. The area and weights of the samples are obtained by computing the second and third moments of (4), *viz.*

$$\text{area} = 4\pi \int_{-\infty}^{+\infty} r^2 f(r) dr \tag{5}$$

$$\text{weight} = \frac{4}{3}\pi\rho \int_{-\infty}^{+\infty} r^3 f(r) dr \tag{6}$$

with ρ the density of $KClO_3$. We recall that the weights of $KClO_3$ in the two samples are the same, so that the number of particles in the two samples are not the same. However, by equating the weights (relation 6) we can obtain the ratio of the areas in eq 7

(16) R. W. G. Wyckoff, "Crystal Structures," Vol. 2, 2nd ed, Interscience Publishers, Inc., New York, N. Y., 1964, p 383.

(17) C. Roscoe and J. M. Thomas, *Carbon*, **4**, 383 (1966); C. Roscoe and J. M. Thomas, *Proc. Roy. Soc.* (London), **A297**, 327 (1967).

(18) J. M. Thomas and E. L. Evans, *Nature*, **214**, 167 (1967).

$$\frac{\text{area ("large" particles)}}{\text{area ("small" particles)}} = \frac{(r_{0_2}^3 + 3r_{0_2}\sigma_2^2)(r_0 + \sigma_1^2)}{(r_{0_1}^3 + 3r_{0_1}\sigma_1^2)(r_{0_2}^2 + \sigma_2^2)} = 0.08 \quad (7)$$

where the subscripts 1 and 2 refer to the "large" particles and the "small" particles, respectively. It should be noted that the area ratio is calculated on the basis of spheres for ease of computation. A gaussian distribution of monoclinic, cubic, or odd-shaped crystals would not give a ratio too different from 0.08. This can be verified by performing the integration numerically from the Micromerograph data.

If we compare the ratio of the specific rate constants as observed in (3) with the calculated ratios of the corresponding areas in (7), we find that the ratio of the specific rate constants is only four times that of the calculated areas. Considering the many approximations made in calculating the ratio of the areas for these two samples, we believe that the results support our contention that certain specific sites, probably nonbasal dislocations, on the $KClO_3$ grains become activated by the ultrasonic field thus leading to reaction with neighboring aldehyde molecules.

A Nuclear Magnetic Resonance Study of Hydrogen Bonding in the Succinimide–Dimethyl Sulfoxide System

by David M. Porter and Wallace S. Brey, Jr.

Department of Chemistry, University of Florida, Gainesville, Florida 32601 *(Received March 17, 1967)*

The hydrogen bonding between succinimide and dimethyl sulfoxide has been studied by nuclear magnetic resonance. The concentration and temperature dependence of the chemical shift of the NH resonance of succinimide shows that the succinimide–dimethyl sulfoxide interaction is probably of the "n-donor" type. The experimental chemical shift data were interpreted in terms of an equilibrium between a succinimide–dimethyl sulfoxide complex and a succinimide dimer plus solvent molecules. The equilibrium constant for this equilibrium, written for the dissociation of the succinimide–dimethyl sulfoxide complex, was 0.096 at 33° and determinations of the equilibrium constant at four temperatures gave a ΔH of 5.0 ± 1.0 kcal/mole and a $\Delta S°_{306}$ of 12 ± 4 cal/mole deg. The chemical shifts for the hydrogen-bonded protons in the succinimide–dimethyl sulfoxide complex showed a regular trend to higher field with increasing temperature.

Introduction

Proton magnetic resonance measurements have shown that a significant chemical shift change accompanies the formation of a hydrogen bond.[1,2] The formation of hydrogen bonds displaces the magnetic resonance of the protons involved toward lower magnetic field, except in certain cases involving aromatic molecules.[3] If the primary function of the electron donor atom is to produce a strong electric field in the vicinity of the hydrogen-bonded proton, then a shift toward lower field is

(1) U. Liddell and N. F. Ramsey, *J. Chem. Phys.*, **19**, 1608 (1951); J. T. Arnold and M. E. Packard, *ibid.*, **19**, 1608 (1951).

(2) H. S. Gotowsky and A. Saika, *ibid.*, **21**, 1688 (1953); C. M. Huggins, G. C. Pimentel, and J. N. Shoolery, *ibid.*, **23**, 1244 (1955).

quite reasonable.[3] The electric field deforms the electron distribution about the proton in the hydrogen bond, decreasing the electron density in its vicinity and increasing its asymmetry; both of these effects decrease the proton shielding.[4]

In the case of an equilibrium between hydrogen-bonded and nonhydrogen-bonded species, if the lifetimes in the associated and unassociated states are short, the diamagnetic shielding is an average over the two states and the proton resonance will be observed at a frequency corresponding to the average shielding for the two states. Since both temperature and concentration affect the extent of association, the chemical shift of the proton varies with these conditions.

The purpose of the present investigation is to study the nature of the hydrogen bonding in the succinimide–dimethyl sulfoxide system. Of primary interest are the various chemical equilibria which may be present in solutions of succinimide in dimethyl sulfoxide and the calculation of the equilibrium constants and the changes in enthalpy and entropy for these equilibria from the nuclear magnetic resonance chemical shift data. Also of interest are the chemical shifts of the hydrogen-bonded protons present in the species involved in these equilibria.

Experimental Section

The spectra of the solutions of succinimide in dimethyl sulfoxide were obtained using a DP-60 Varian Associates nuclear magnetic resonance spectrometer operating at 60.0 Mc/sec. The spectrum of the saturated solution of succinimide in deuterated chloroform was obtained using a Model A-60A Varian Associates nuclear magnetic resonance spectrometer operating at 60.0 Mc/sec, with the aid of a Model C-1024 Varian Associates time-averaging computer.

The dimethyl sulfoxide used was obtained from the J. T. Baker Chemical Co. and was dried over Type 4A Fisher Molecular Sieve. The succinimide, from Eastman Organic Chemicals, was dissolved in the dimethyl sulfoxide immediately after opening without additional purification. The solutions of succinimide in dimethyl sulfoxide were made up by weight.

The chemical shift of the NH was determined by the usual side-band method with the audio frequency continuously monitored by a Model 523B Hewlett-Packard counter. The concentration dependence of the dimethyl sulfoxide peak was checked with respect to internal tetramethylsilane reference and found to be negligible. Small quantities of water added to various samples confirmed that the presence of moisture has no measurable effect on the NH chemical shift.

The chemical shift, Δ, is defined as the number of cycles per second downfield from the dimethyl sulfoxide peak. All chemical shifts are the average of five individual determinations and are considered to be accurate to within 1 cps or less. This apparently large maximum error is a consequence of the uncertainty in estimating the position of the center of the broad NH peak, especially for the very dilute solutions.

The temperature of the sample was regulated by the flow rate of dry nitrogen through a Varian V-4340 variable temperature probe assembly. A copper–constantan thermocouple positioned within the dewar insert was used to determine the temperature of the sample. The thermocouple was calibrated against a second thermocouple which was positioned in a sample tube in the spectrometer. All temperature measurements are considered to be accurate to within 1 deg. The experimental results are given in Table I.

Table I: Observed Chemical Shifts[a] of the NH of Succinimide in Dimethyl Sulfoxide

Mole fraction of succinimide	Temperature, °C			
	33	43	57	72
0.096	507.1	505.6	499.4	494.8
0.137	505.6	504.9	497.0	492.8
0.193	503.4	500.7	495.2	489.7
0.271	500.4	498.6	492.3	485.7
0.348	494.8	493.0	487.2	479.8
0.412	489.3	487.8	483.1	475.6

[a] Expressed in cycles per second downfield from dimethyl sulfoxide resonance.

Treatment of Data

A saturated solution of succinimide in deuterated chloroform, in which succinimide is very sparingly soluble, was investigated using the A-60A and the time-averaging computer in an attempt to estimate the chemical shift of the NH in the unassociated or self-associated succinimide, whichever the case may be. The chemical shift obtained provides a downfield limit for the chemical shift of the NH in the succinimide monomer and an upfield limit for the chemical shift of the NH in the succinimide dimer.

A study of the self-association of succinimide in an inert solvent would have aided this work considerably, but succinimide is not sufficiently soluble in inert sol-

(3) J. A. Pople, W. G. Schneider, and H. J. Bernstein, "High-Resolution Nuclear Magnetic Resonance," McGraw-Hill Book Co., Inc., New York, N. Y., 1959.

(4) H. S. Gutowsky, *Ann. N. Y. Acad. Sci.*, **70**, 786 (1958); P. J. Frank and H. S. Gutowsky, *Arch. Sci.*, **11**, 216 (1958).

vents such as carbon tetrachloride and cyclohexane for nuclear magnetic resonance investigation. In fact, dimethyl sulfoxide is the only solvent tried in which the NH peak of the succinimide was readily observable over a significantly large concentration range. Dimethyl sulfoxide is also a suitable choice in view of the work of Allerhand and Schleyer,[5] who concluded that in order to extend the spectral shift criterion to very weak proton donors, very strong proton acceptors must be used. They found that hydrogen bonding equilibria involving dimethyl sulfoxide are favorable and explained this phenomenon in terms of the availability of the two equivalent p-orbital bonding sites on the oxygen in dimethyl sulfoxide. They also reported that the infrared spectrum of dimethyl sulfoxide in carbon tetrachloride solution, up to 100% dimethyl sulfoxide, was not concentration dependent. This is evidence against self-association of the solvent.

Each solution of succinimide in dimethyl sulfoxide displayed only one proton resonance which could be attributed to the NH proton of succinimide. The $-CH_2CH_2-$ resonance was concealed by the solvent peak. The chemical shift of the NH resonance was strongly dependent upon concentration and temperature, moving to lower fields with increased concentration of dimethyl sulfoxide and to higher fields with increased temperature. This direction of change of the chemical shift is consistent with the results of similar studies of other hydrogen-bonding systems[1] in which "n-donor" association occurs. Dimethyl sulfoxide hydrogen bonds to proton donors by use of the lone pairs of electrons on the oxygen, as pointed out by Allerhand and Schleyer.[5]

An attempt was made to fit the experimental results with either of two equilibria

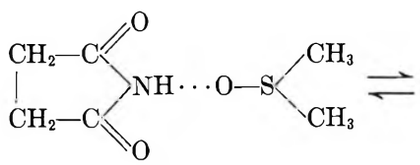

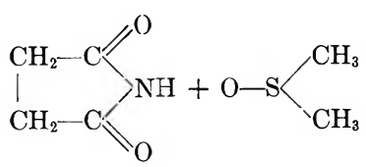

(1)

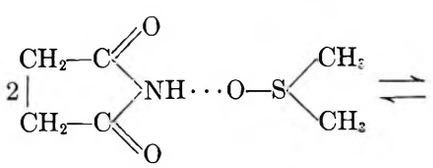

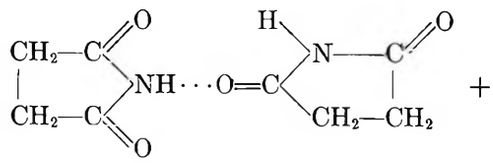

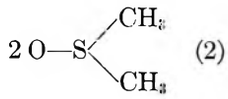

(2)

The equilibrium constant in mole fraction units for reaction 1 is given by

$$K_1 = \frac{(N - C)(S - C)}{C(N + S - C)} = \frac{M(S - C)}{C(M + S)} \tag{3}$$

where N = moles of total succinimide, S = moles of total dimethyl sulfoxide, C = moles of succinimide–dimethyl sulfoxide complex, and $M = N - C$ = moles of succinimide monomer. The observed chemical shift, Δ, for the NH in the system is expressed as a weighted average of the contributions of the two NH-containing species present and is given, for this case, by

$$\Delta = \frac{M}{N}\Delta_m + \frac{C}{N}\Delta_c = \frac{N - C}{N}\Delta_m + \frac{C}{N}\Delta_c \tag{4}$$

where Δ_m = chemical shift of the NH in the succinimide monomer and Δ_c = chemical shift of the NH in the succinimide–dimethyl sulfoxide complex. Solving eq 4 for C

$$C = \left(\frac{\Delta - \Delta_m}{\Delta_c - \Delta_m}\right)N \tag{5}$$

Solving eq 3 for C, the physically reasonable root obtained is

$$C = \frac{N + S - \sqrt{(N + S)^2 - 4NS/(1 + K_1)}}{2} \tag{6}$$

The equilibrium constant in mole fraction units for the other possible equilibrium, as shown in eq 2, is given by

$$K_2 = \frac{{}^1/_2(N - C)(S - C)^2}{C^2[{}^1/_2(N - C) + S]} = \frac{D(S - C)^2}{C^2(D + S)} \tag{7}$$

where $D = {}^1/_2(N - C)$ = moles of succinimide dimer. The observed chemical shift of the NH is given for this case by

$$\Delta = \frac{2D}{N}\Delta_d + \frac{C}{N}\Delta_c = \frac{N - C}{N}\Delta_d + \frac{C}{N}\Delta_c \tag{8}$$

(5) A. Allerhand and P. von R. Schleyer, *J. Am. Chem. Soc.*, **85**, 1715 (1963).

where Δ_d = chemical shift of the NH in the succinimide dimer. Solving eq 8 for C

$$C = \left(\frac{\Delta - \Delta_d}{\Delta_c - \Delta_d}\right)N \quad (9)$$

Solving eq 7 for C gives the third degree equation

$$(1 - K_2)C^3 - (1 - K_2)(N + 2S)C^2 + (S^2 + 2NS)C - NS^2 = 0 \quad (10)$$

Method of Calculation

An initial estimate of Δ_c is obtained by extrapolating a plot of Δ *vs.* mole fraction of succinimide to infinite dilution. A value is assumed for the other limiting chemical shift (Δ_m for reaction 1, Δ_d for reaction 2) and C is then calculated for reaction 1 from eq 5 or for reaction 2 from eq 9. The equilibrium constant is then calculated (K_1 from eq 3 or K_2 from eq 7) using the appropriate value of C. The limiting chemical shifts are varied over the chemically reasonable ranges for these shifts.

The values of the equilibrium constant for the various solutions are averaged and from this average equilibrium constant there is then calculated a value of C from eq 6 for reaction 1 or from eq 10 for reaction 2. The new approximation to the value of C is then used to calculate a predicted chemical shift from eq 4 for reaction 1 or from eq 8 for reaction 2. The values of Δ_c and Δ_m or Δ_d are varied over their chemically reasonable ranges until the best least-squares fit between the observed Δ and the predicted Δ is obtained. This best least-squares fit yields the values of Δ_c, Δ_m, and K_1 when considering reaction 1 and Δ_c, Δ_d, and K_2 when considering reaction 2, for one temperature. This process is then repeated for each individual temperature. The logarithm of the equilibrium constant is plotted against the reciprocal temperature and ΔH is estimated from this plot. ΔS is then calculated from ΔH and the equilibrium constant.

FORTRAN IV programs were written for these calculations and all calculations were carried out at the University of Florida Computing Center on an IBM 709 computer.

Results and Discussion

Reaction 1 did not fit the experimental results for reasonable values of the limiting chemical shifts Δ_c and Δ_m. The results of the calculations based on reaction 2 are listed in Table II and are shown in Figures 1 and 2. Table II lists the limiting chemical shifts and the equilibrium constant as functions of temperature based on reaction 2. Figure 1 shows the concentration dependence of the observed chemical shift of the NH in succinimide at the various temperatures. The solid curves show the predicted chemical shift of the NH as calculated for reaction 2. Figure 2 shows the variation of log K_2 with reciprocal temperature. The temperature dependence of the equilibrium constant gives a ΔH of 5.0 ± 1.0 kcal/mole and a $\Delta S°_{306}$ of 12 ± 4 cal/mole deg. The probable errors were estimated by standard methods.[6] These values fall within the normal range of ΔH and ΔS values for this type of interaction.[7]

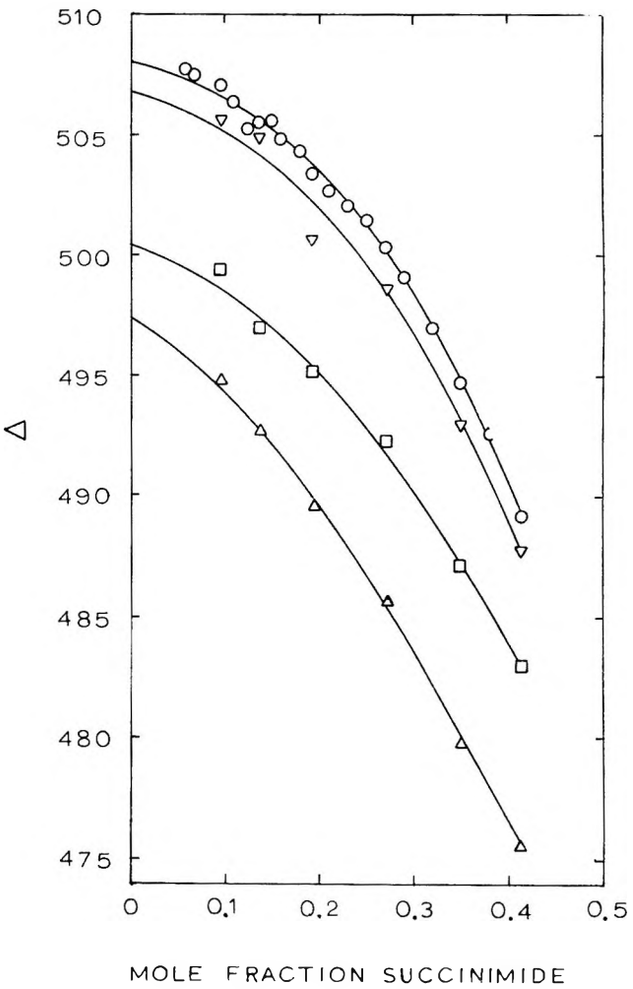

Figure 1. Variation of Δ with concentration at various temperatures: O, 33°; ▽, 43°; □, 57°; △, 72°. The solid curves are calculated for reaction 2.

The apparently random variation of the limiting chemical shift Δ_d does not lend itself to any simple explanation, although this parameter is not very sensitive to the experimental results. The temperature depen-

(6) F. Daniels, J. W. Williams, P. Bender, R. A. Alberty, and C. D. Cornwell, "Experimental Physical Chemistry," 6th ed, McGraw-Hill Book Co., Inc., New York, N. Y., 1962, pp 401, 402.

(7) G. C. Pimentel and A. L. McClellan, "The Hydrogen Bond," W. H. Freeman and Co., San Francisco, Calif., 1960.

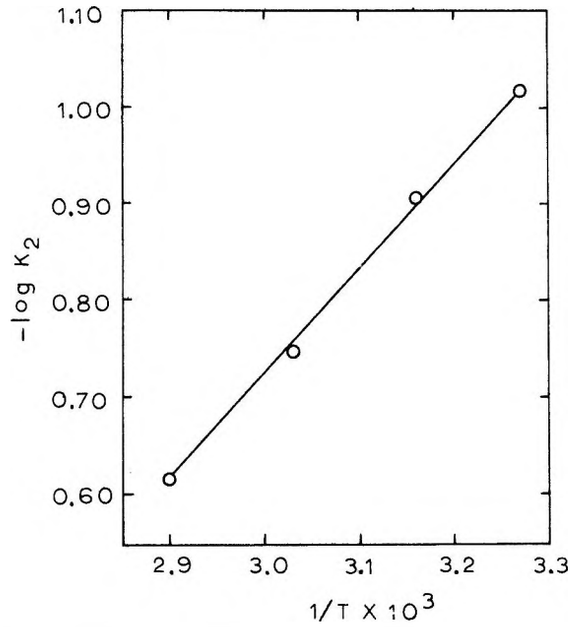

Figure 2. Variation of log K_2 with reciprocal temperature.

dence of the limiting chemical shift Δ_c is clearly real and could indeed correspond to a change in the chemical shift brought about by a change in molecular vibrations with temperature within the complex. This explanation is consistent with the findings of Muller and Reiter,[8] who have suggested that a part of the observed variations with temperature of the chemical shifts of protons involved in hydrogen bonds which has previously been attributed to shifts in association equilibria favoring a larger fraction of broken hydrogen bonds with increasing temperature may be due to another mechanism. The chemical shift for the associated species depends quite strongly on the degree of excitation of the hydrogen bond stretching vibrational mode. Because this is an unusually low-frequency motion, several excited states are significantly populated even at temperatures as low as 200°K. When an appropriate average over vibrational levels is used to evaluate the chemical shift, the results show a temperature dependence similar to those found experimentally even though it is assumed in the calculations that no dissociation of the hydrogen-bonded species occurs.[8]

Table II: Chemical Shifts[a] of Succinimide-Dimethyl Sulfoxide Complex and Succinimide Dimer and Equilibrium Constant as Functions of Temperature

Temp, °C	Δ_c, cps	Δ_d, cps	K_2
33	508.0	444.0	0.096
43	507.0	448.0	0.126
57	500.5	453.0	0.179
72	497.5	443.0	0.242

[a] Expressed in cycles per second downfield from dimethyl sulfoxide resonance.

The chemical shift of the NH in succinimide in deuterated chloroform was determined to be approximately 535 cps downfield from tetramethylsilane, which would be 382 cps downfield from dimethyl sulfoxide. This value is obviously an upfield limit for the limiting chemical shift of the NH in the succinimide dimer, Δ_d. Thus the value obtained for Δ_d at 33° of 444 cps is apparently very reasonable since in this very dilute solution of succinimide in deuterated chloroform there should be some succinimide monomer present.

Acknowledgment. This research was supported by Grant GM-09343 from the National Institutes of Health.

(8) N. Muller and R. C. Reiter, *J. Chem. Phys.*, **42**, 3265 (1965).

Diffusion Coefficients of Ag^+ and $Ag(SO_3)_2^{3-}$ by the Rotating Disk Method

by R. R. M. Johnston[1] and M. Spiro

Department of Chemistry, Imperial College of Science and Technology, London, S.W.7, England

Accepted and Transmitted by The Faraday Society (March 20, 1967)

The diffusion coefficients at 25° of Ag^+ in aqueous KNO_3 and $HClO_4$ solutions and of $Ag(SO_3)_2^{3-}$ in a Na_2SO_3–$NaNO_3$ solution were determined from the limiting currents at rotating silver disk cathodes. The effects of prolonged electrolysis, of dissolved oxygen, and of added gelatin have also been investigated.

Introduction

A simple way of determining the diffusion coefficient, D_i, of a single ion, i, in an excess of indifferent electrolyte is by means of the rotating disk electrode (rde). According to the Levich equation[2] as modified by Gregory and Riddiford,[3] the limiting diffusion current (in milliamperes) is given by

$$I_{lim} = 0.620nFAc_iD_i^{2/3}\nu^{-1/6}\omega^{1/2}/[1 + 0.354(D_i/\nu)^{0.36}] \quad (1)$$

where n is the number of electrons involved in the electrode process per mole of i, F is Faraday's constant, A the geometric electrode area (square centimeters), c_i the bulk concentration of i (moles per liter), ν the kinematic viscosity of the solution, and ω the angular velocity of the disk (radians per second). The diffusion coefficient can therefore be derived from the slope of a plot, against $\omega^{1/2}$, of I_{lim} or the corresponding current density i_{lim}.

Although the theory is now well known,[4,5] certain aspects of the experimental conditions are still uncertain. For example, in two previous publications[6a,7] on the reduction at solid cathodes of Ag^+ in nitrate solutions, the absence of oxygen and the presence of 0.01% gelatin were advocated without giving details. These and other factors have been investigated in the present work in which we have measured the diffusion coefficient of Ag(I) in noncomplexing (KNO_3, $HClO_4$) and complexing (Na_2SO_3) media by means of rotating silver disk cathodes.

Experimental Section

Apparatus. The various rotating disk electrode (rde) shapes and dimensions are shown in Figure 1. The working surface was "chemically pure" Johnson and Matthey (99.98%) silver. Disk D was made from silver rod and the others from 2 mm thick sheet soldered onto a brass former; the brass and the edge of the silver were protected by a layer of Araldite 985 brushed on and cured at 180°. The inert annulus on disks A, B, and D was made by forcing on a solid Teflon ring and machining it to shape. The rde was attached by nylon screws to the lower end of a hollow steel shaft (Figure 2) which was held in a bearing, B, and driven through a gear by a motor, M, at the upper end. Rotation speed was controlled by an M. C. 43 Servomex unit and could be varied continuously from 0 to 7000 rpm. The calibration of the Servomex was constantly checked by a series of stroboscopic disks which responded to the fluctuation of intensity (100 ± 0.1 cps) of the room light.

The vessel, V, was a lipless Pyrex beaker of diameter 16.5 cm, a value large enough for eq 1 to apply.[8] The perspex lid, P, was fitted with a rubber gasket and clamped as shown. A neoprene "oil seal," O, lubri-

(1) Central Research Laboratories, Broken Hill Proprietary Co. Ltd., Shortland, N.S.W., Australia.

(2) V. G. Levich, *Acta Physicochem. USSR*, **17**, 257 (1942).

(3) D. P. Gregory and A. C. Riddiford, *J. Chem. Soc.*, 3756 (1956); J. Newman *J. Phys. Chem.*, **70**, 1327 (1966).

(4) V. G. Levich, "Physicochemical Hydrodynamics," Prentice-Hall Inc., Englewood Cliffs, N. J., 1962.

(5) A. C. Riddiford, *Advan. Electrochem. Electrochem. Eng.*, **4**, 47 (1966).

(6) I. M. Kolthoff and J. J. Lingane, "Polarography," Vol. I, Interscience Publishers, New York, N. Y., 1952, (a) p 418, (b) pp 64–67, 151.

(7) M. B. Kraichman and E. A. Hogge, *J. Phys. Chem.*, **59**, 986 (1955).

(8) R. R. M. Johnston and M. Spiro, unpublished work.

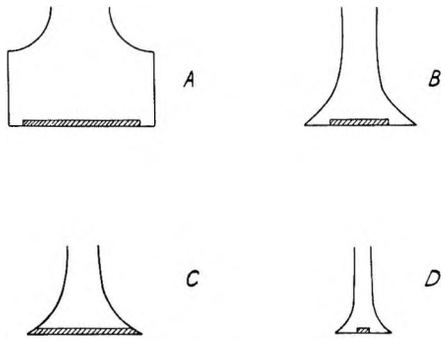

Figure 1. The rotating disk electrodes employed. The dimensions are as follows, with r_0 (cm) standing for the radius of the active (shaded) area and r_1 (cm) for the over-all radius at the bottom of disks A, B, C, and D, respectively: r_0, r_1 = 3.9, 4.3; 2.0, 4.0; 3.8, 3.8; 0.25, 1.26.

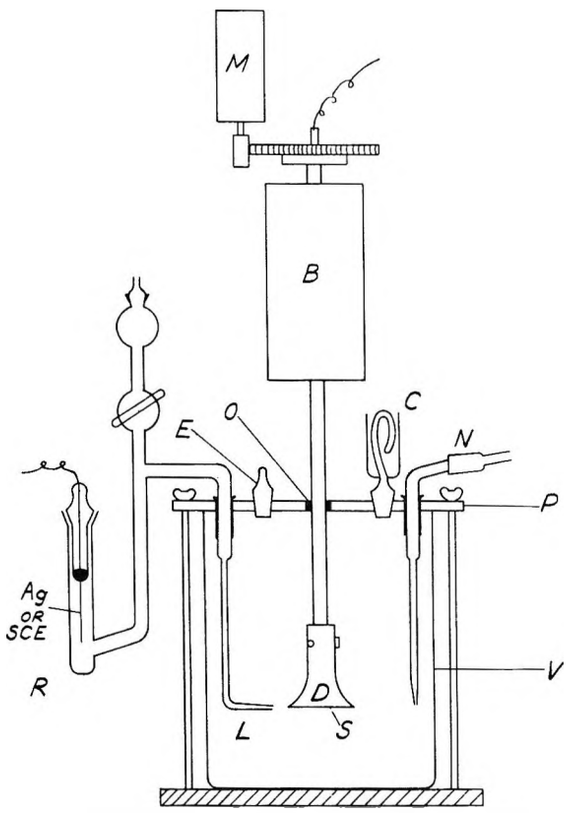

Figure 2. The rotating disk rig and the reaction vessel.

cated with a trace of Vaseline, sealed off the aperture through which the disk shaft was inserted. N was a delivery tube for presaturated oxygen-free nitrogen, excess pressure being relieved through the bubbling device C. The reference electrode was contained in a small Pyrex cell, R, connected to the main vessel by a salt bridge and Luggin capillary, L. For nitrate and perchlorate solutions the reference was a silver wire, the cell-bridge unit being filled with a solution of the same composition as that in the main vessel. For sulfite solutions the cell-bridge unit was filled with only the $NaNO_3$ background electrolyte and the silver wire was replaced by a Radiometer Type K 100 saturated calomel electrode. Potentials are expressed relative to the nhe.

Electrical contact with the rde was made by dipping a copper wire centrally into a Teflon cup of mercury rotating at the top of the main shaft. The cup was sealed to an insulated silver rod which ran down the hollow axis of the shaft and screwed into the back of the rde. This minimized splashing of the mercury and provided convenience in assembly. The rde was insulated from the shaft by a Tufnol sleeve.

The anode (except for SO_3^{2-} solutions) was a sheet of silver (99.98%) foil 10 cm wide and extending across the bottom of the vessel, its area (*ca.* 300 cm^2 total) being sufficient for it to remain relatively unpolarized during electrolysis. Disturbance of the foil by the swirling solution was prevented by anchoring it beneath a frame of thin glass rods. Contact to the external circuit was provided by fusing silver wire onto one corner of the foil and leading it out under the rubber gasket in the lid.

One or more 2-v accumulators acted as the source of potential and a Helipot Model LP10 rheostat of total resistance 10,000 ohms was used as a voltage divider. Current was determined by measuring, with a Cambridge Vernier potentiometer, the potential drop across a 1000-ohm standard resistor connected in series with the disk. Potentials between the reference electrode and the working electrode were measured to the nearest millivolt using a Radiometer 4 pH meter.

Reagents. Solutions were prepared from weighed amounts of reagents of AnalaR quality whenever available, dissolved in water redistilled from alkaline permanganate and having a conductivity of between 1.0 and 1.6 $\times$ 10^{-6} ohm^{-1} cm^{-1}.

The AnalaR KNO_3 used as supporting electrolyte contained sufficient impurity (*e.g.*, up to 0.0005 wt % Cl^-) to give an appreciable precipitate when $AgNO_3$ was added. This insoluble material was removed by allowing it to settle overnight and filtering through a number three porosity glass frit. The silver ion concentration was determined in the filtrate, after this had been made up to volume, by potentiometric titration with *ca.* 2 $\times$ 10^{-5} *M* potassium iodide. The reproducibility was better than $\pm 0.5\%$. Potential drift near the end point, due to various precipitation phenomena,[9] could be reduced by titrating slowly. The potassium iodide solution was standardized against a weighed amount of $AgNO_3$ dried at 115° for 1.5 hr.

The results of the potentiometric analysis agreed within experimental error with those of the spectrophotometric method of measuring the absorbance at 390 mμ of the pyrogallol red–silver ion complex.[10] The latter method, however, was less precise and suffered from the fact that the presence of KNO_3 caused the color to develop more rapidly in the test solutions than in the standardizing solutions containing silver nitrate only.

The silver ion–perchloric acid solutions were prepared by the addition, to a standard solution of AnalaR $HClO_4$, of an appropriate aliquot of $AgClO_4$ previously standardized by Volhard's titration. The sulfite solutions are discussed in the next section.

Procedure. Prior to each run the disk surface was cleaned by abrasion in running water with 600-mesh emery paper. The roughness so produced (maximum height of irregularities on the silver surface *ca.* 1 μ) represents only one-twentieth of the thickness of the transport boundary layer for silver ion at 1000 rpm and is negligible. The disk was finally rinsed with doubly distilled water, attached to the shaft, and immersed about 1 cm in the test solution contained in a water bath thermostated at 25 ± 0.02°. With the system sealed, air was removed by bubbling nitrogen for 3–4 hr prior to each run, the nitrogen being passed over the surface during measurements. Identical results were obtained when bubbling was prolonged for 8–9 hr. Concentration changes due to evaporation were shown to be negligible by analysis and by repeating I_{lim} measurements on the same batch of solution on successive days. The necessity for deoxygenation is discussed below.

In sulfite solution, silver ion undergoes a slow reduction which is catalyzed by silver metal.[11] In the present work the following procedure gave reproducible results. Solutions of supporting electrolyte were prepared afresh each day by dissolving an appropriate weight of Na_2SO_3 and $NaNO_3$ in 1 l. This solution was placed in the thermostat and flushed with nitrogen long enough to displace the air enclosed above it by the perspex lid. The removal of dissolved oxygen in these solutions was obviated by its destruction by SO_3^{2-} ion. A small aliquot (1–10 ml) of standard $AgNO_3$ was then run in through a stoppered hole in the lid and after a further 10 min the nitrogen tube was raised above the surface of the solution and measurements were started. Disk D (Figure 1) was used in conjunction with an anode measuring 2 × 2 cm so that the total area of silver in contact with the solution was less than 10 cm^2.

Results and Discussion

The Effect of Oxygen. Figure 3 shows current–voltage curves obtained for the reduction of silver ions in a

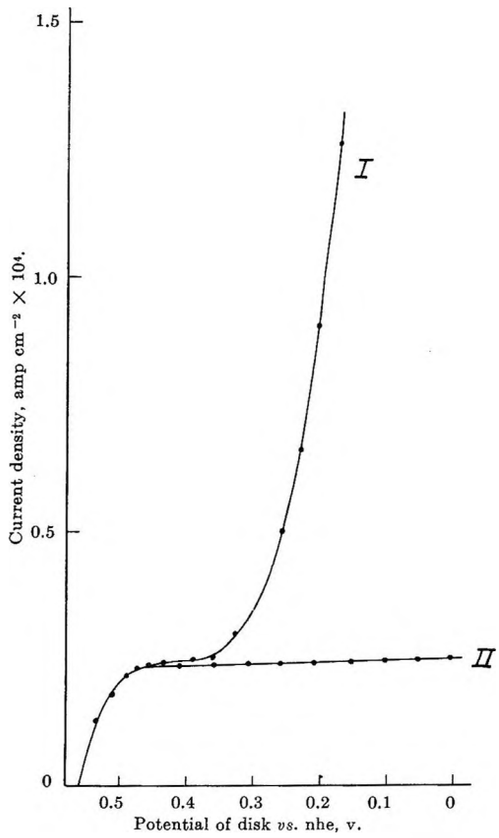

Figure 3. Current density–voltage curves at disk B for a solution 0.9 × 10^{-4} *M* in $AgNO_3$ and 0.2 *M* in KNO_3 left open to the air (curve I) and thoroughly flushed with nitrogen gas (curve II).

0.2 *M* KNO_3 solution left open to the air (curve I) and for a similar solution from which air had been removed (curve II) by flushing with nitrogen for 3–4 hr prior to the measurements. The difference in current density, Δi, between the two curves at any given potential V is clearly due to the reduction of dissolved oxygen and indeed a plot of log (Δi) against V was linear as would be expected from the Tafel equation

$$V^0 - V = b \log (\Delta i/i_0) \qquad (2)$$

Here V^0 is the equilibrium potential of the O_2–H_2O couple in the solution in question, b the cathodic Tafel slope, and i_0 the exchange current density. From the plot, b was found to be 0.12 and i_0, the intercept after a long extrapolation, was *ca.* 2 × 10^{-10} amp cm^{-2}. Although these values are not very accurate, they appear to be the only data available for the reduction of oxygen

(9) E. Lange and E. Schwartz, *Z. Elektrochem.*, **32**, 240 (1926); E. Lange and R. Berger, *ibid.*, **36**, 171, 980 (1930).

(10) R. M. Dagnall and T. S. West, *Talanta*, **8**, 711 (1961).

(11) T. H. James, *J. Am. Chem. Soc.*, **62**, 3411 (1940).

on silver under conditions (pH 5.5, continuous plating of silver) in which the presence of a surface oxide layer is unlikely. These figures may be compared with $b = 0.09$ and $i_0 = 2 \times 10^{-10}$ for oxygen reduction on bright platinum in dilute sulfuric acid solutions.[12]

Because of the long time necessary for proper deoxygenation of the solutions, an attempt was made to determine the limiting current density from curves of type I (in the presence of air) by keeping the disk potential more positive than +0.3 v. It was found, however, that such currents slowly increased with time, and analysis showed that this was due to a rise in the silver ion concentration in the solution. The reason is that even at 0.38 v the reduction of dissolved oxygen contributed approximately 10% to the observed current so that the cathodic current efficiency for silver deposition dropped to around 90%. Since the efficiency of anodic silver dissolution remained at 100%, the bulk silver ion concentration slowly increased. This effect is more marked with large disks for which the number of faradays passed across the electrodes during the time of the experiment is comparable with the number of equivalents present in the solution. Moreover, when i_{lim} values, obtained at instants of known silver ion concentration, were plotted against $\omega^{1/2}$, the resulting lines exhibited small but definite intercepts on the i_{lim} axis. These can be attributed to oxygen reduction for, following Pleskov,[13] when two electrode processes occur simultaneously at an rde

$$i = i_1 + i_2 = k\omega^{1/2} + i_2 \qquad (3)$$

where process 1 (reduction of silver) is diffusion controlled while process 2 (reduction of oxygen) is not. It was therefore considered advisable to deoxygenate all solutions.

The Effect of Silver Deposition. In the absence of dissolved oxygen in supporting electrolytes of nitrate, perchlorate, or sulfate (but not in sulfite or cyanide nor in the presence of gelatin as discussed below), it was found that limiting currents were constant for an initial period and then rose exponentially with time. It may be noted that if oxygen was not removed, this effect was superimposed on the slow steady rise mentioned above. A typical plot of current against time for disk A (7.8 cm diameter) is shown in Figure 4. Moreover, as the current rose, at constant applied voltage, the potential (*vs.* nhe) of the disk became less cathodic as is indicated by the millivolt readings in brackets. The broken line in the figure shows that rotation of the disk could be continued on open circuit without causing any further rise in the current when

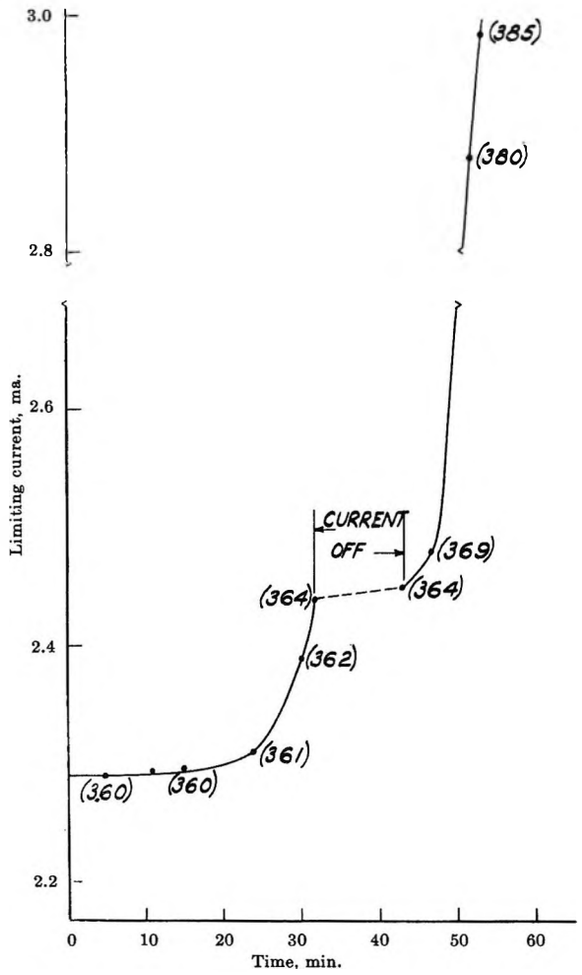

Figure 4. Increase of limiting current with time for disk A rotating at 400 rpm in a solution 1×10^{-4} *M* in $AgNO_3$ and 0.2 *M* in KNO_3, under nitrogen. Each bracketed number is the potential of the disk in millivolts *vs.* nhe.

the latter was resumed. The following additional observations were made.

(a) The initial stable period, which was somewhat irreproducible, appeared to be independent of disk diameter but to be shortened by an increase of rotation speed and by an increase in silver ion concentration, both factors which raise the current density.

(b) The rising current was not accompanied by any change in the deposition potential of Ag^+ (*i.e.*, +0.56 v for 10^{-4} *M* solution) or any increase in Ag^+ concentration.

(c) In a typical run (10^{-4} *M* Ag^+, 0.2 *M* KNO_3), the current at 400 rpm was allowed to rise to double

(12) J. O. Bockris and A. K. M. S. Huq, *Proc. Roy. Soc.* (London), **A237**, 277 (1956).

(13) Y. V. Pleskov, *Russ. J. Phys. Chem.*, **34**, 296 (1960).

its initial value and the current at other speeds was then quickly remeasured with the following results

rotation speed (rpm)	400	200	100	60
i_{lim} increase over initial value (%)	100	50	22	10

(d) Removal of the electrodeposit with emery paper restored the current to its initial value.

All these rising current phenomena can be explained as due to the roughening of the disk surface by the electrodeposit. However, the amount of silver that has been deposited at the onset of the exponential rise in Figure 4 is sufficient to form a uniform layer of only about 0.1 μ whereas the transport boundary layer at this rotation speed is about 25 μ thick. Hence the deposition must have occurred in the form of dendrites, well known for silver, growing perpendicularly to the working surface. Indeed, in a run with a more concentrated (10^{-3} M $AgClO_4$) solution, dendrites of silver 2–3 mm long were observed dangling from the periphery. Such growths would not cause any current rise until their size became comparable with the thickness of the boundary layer and hence the effect is much less at lower rotation speeds. As mentioned above, the presence of gelatin prevented this current rise. Wranglen[14] made a study of dendrites formed during electrocrystallization in unstirred solutions of a variety of metals including silver and reported, in confirmation of earlier work, that gelatin retarded their formation.

Phenomena similar to those described above have been experienced by other workers[15] during the reduction of cupric ions. Limiting currents which rise with time at fixed potential have also been observed[16] with platinum wire cathodes rotating in the presence of precipitated silver bromide particles. This effect was favored by a small excess of silver nitrate but was eliminated by introducing a little gelatin.

The Effect of Gelatin. When, following Kraichman and Hogge[7] and Kolthoff and Lingane,[6a] 0.01 wt % gelatin (B. D. H. powder) was added to a solution of 1×10^{-4} M $AgNO_3$ in 0.2 M KNO_3, the limiting currents were quite stable (*cf.* the preceding section) but were significantly lower than the initial currents obtained in the absence of gelatin. The plot of i_{lim} *vs.* $\omega^{1/2}$ showed a positive intercept on the i_{lim} axis. However, since the gelatin used had produced a faint turbidity in the silver solutions, further experiments were carried out with a higher grade material,[17] this time with a solution containing 1×10^{-4} M $AgNO_3$, 0.025 M Na_2SO_3, and 0.925 M $NaNO_3$. With 0.001 wt % gelatin present, the plot of i_{lim} *vs.* $\omega^{1/2}$ was a straight line through the origin, but its slope and the limiting current plateaux of the individual current–voltage curves were some 8% lower than those obtained without the addition of gelatin. The gelatin plateaux seemed to approach the nongelatin ones asymptotically with increasing cathodic polarization. When the gelatin concentration was raised to 0.01 wt %, the current (at a potential of the rde of +100 mv *vs.* nhe) was very much smaller than before (7 μa cm^{-2} at 200 rpm as compared with 40 μa cm^{-2}) and became independent of rotation speed above about 200 rpm. The rde had apparently become covered with a layer of adsorbed gelatin which hindered the discharge process at the electrode surface, and indeed there is much evidence in the literature[18] to show that gelatin and other addition reagents can greatly reduce the rates of electrode processes. One must conclude, therefore, that in rotating disk work it is unwise to add even small amounts of gelatin or similar materials until their effect has been investigated.

Treatment of Experimental Data. In the past it has been usual to take values of i_{lim} at one potential of the rde, chosen well up on the limiting plateau. However, Figure 5a shows that the limiting plateaux have definite positive slopes which increase at higher values of the rotation speed. These positive slopes largely arise from a residual current caused by impurities present in the solution and, in normal polarographic practice,[6b] this is subtracted from the limiting currents. In the present work, residual currents could not be measured directly because of the presence of the silver anode and corrected i_{lim} values were obtained by extrapolating the current–voltage plateaux back to the equilibrium potential of the solution as illustrated by the broken lines in Figure 5a. The effect on plots of i_{lim} *vs.* $\omega^{1/2}$ was to reduce the slope by about 4% (Figure 5b), a fact which indicates that the residual currents are functions of ω. This is confirmed by the observation that both plots pass through the origin.

Riddiford[5] considered that positive intercepts obtained for $i_{lim} - \omega^{1/2}$ plots are due to shortcomings in the shape of the disk former and the attendant effect on hydrodynamics. However, with the large disks used in the present work, shape has been found to be unimportant and, as has already been mentioned,

(14) G. Wranglen, *Electrochim. Acta*, 2, 130 (1960).

(15) E. A. Hogge and M. B. Kraichman, *J. Am. Chem. Soc.*, 76, 1431 (1954); A. C. Riddiford, private communication; N. Ibl and K. Schadegg, *J. Electrochem. Soc.*, 114, 54 (1967).

(16) I. M. Kolthoff and J. T. Stock, *Analyst*, 80, 860 (1955); J. T. Stock and W. R. Turner, *Chem. Ind.* (London), 1710 (1961).

(17) Pigskin gelatin supplied by Kodak Ltd. of Harrow, Middlesex. This had been acid processed and deashed by the Sheppard–Loeb process. The moisture content was given as 13% (by drying at 105°), the ash as 0.01%, and the isoelectric point as 9.0–9.3.

(18) *E.g.*, H. Fischer, *Z. Elektrochem.*, 49, 342, 376 (1943); P. Delahay and I. Trachtenberg, *J. Am. Chem. Soc.*, 80, 2094 (1958).

positive intercepts were obtained only in those runs that took place in the presence of dissolved oxygen and one type of gelatin. Positive intercepts were also found with solutions containing certain complex ions known to be unstable. Hence it does not seem unreasonable that nonzero intercepts arise wholly or partly from the onset of a second simultaneous electrode process.

Diffusion Coefficient of Ag^+ in Nitrate and Perchlorate Solutions. In nitrate and perchlorate media, current–voltage curves were determined with disks A, B, C, and D (Figure 1) over a range of 250 mv and from 60 to 700 rpm. Typical plots of the experimental data and of the Levich equation are shown in Figures 5a and b and the full results are given in Table I. All $i_{lim} - \omega^{1/2}$ plots passed through the origin and the fourth column of the table shows their slopes divided by the Ag^+ concentration. The mean deviation for the eight sets of runs in 0.2 M KNO_3 is ±1% and it is clear that the results are independent of the shape of the rde for these relatively large disks. The viscosity and density data needed to calculate the diffusion coefficients in the last column come from ref 19.

The nitrate results agree almost within experimental error with those obtained by v. Stackelberg, *et al.*,[20] by polarography and by the Cottrell linear diffusion method, *viz.*, 10^5D = 1.55, 1.56, and 1.57 cm^2 sec^{-1} in 0.1, 0.5, and 1.0 M KNO_3, respectively. Other groups of workers making use of the Cottrell method have reported figures that are either higher by *ca.* 14%[21] or lower by approximately 9%.[22] Rotating disk measurements by Kraichman and Hogge,[7] later recalculated by Gregory and Riddiford,[3] gave a diffusion coefficient of 1.48×10^{-5} cm^2 sec^{-1} in 0.2 N KNO_3. That this value is somewhat lower than ours is probably due to the fact that Kraichman and Hogge's solution contained 0.01% gelatin; we have already mentioned above that gelatin depresses the limiting current, and v. Stackelberg, *et al.*,[20] found in their own work that 0.01% gelatin decreased the diffusion coefficients by almost 1%.

The limiting silver ion diffusion coefficient can be calculated by the Nernst expression (eq 4)

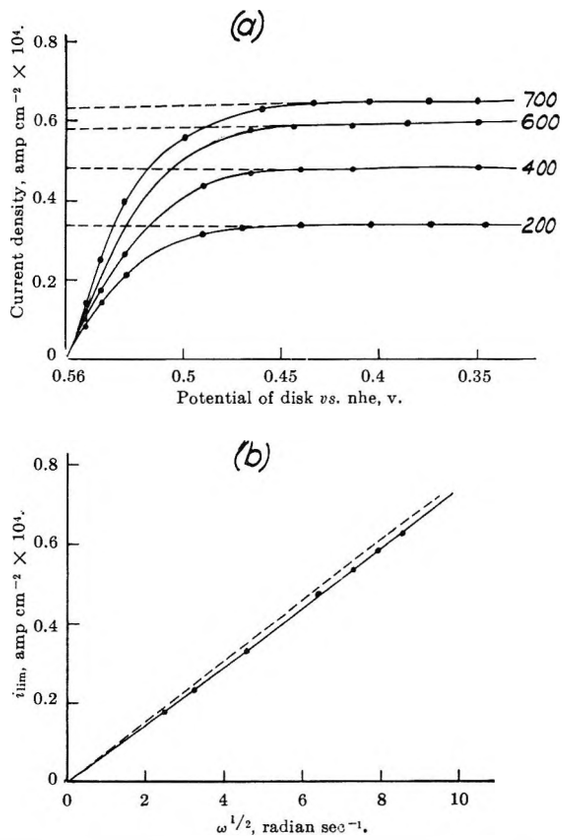

Figure 5. Treatment of experimental data for a solution 0.936×10^{-4} M in $AgNO_3$ and 0.2 M in KNO_3 at disk B. The numbers in (a) signify the rotation speeds in rpm and the dotted lines show the extrapolation of limiting current densities to the equilibrium potential. Diagram b tests the Levich equation, the dashed line representing limiting current densities taken at a fixed potential (0.36 v) and the solid line those extrapolated to the equilibrium potential.

Table I: Results of Experiments with Nitrate and Perchlorate Media at 25°

Supporting electrolyte	Disk (Figure 1)	10^4[Ag^+], mole/l.	$10^2 i_{lim}\omega^{-1/2}$/[$Ag^+$]	$10^5 D_{Ag^+}$, cm^2/sec
0.2 M KNO_3	A	0.936	7.81	
	A	0.936	7.85	
	C	0.936	7.88	
	C	0.919	7.94	
	B	0.919	7.99	
	B	0.936	7.82	
	B	0.678	7.68	
	B	0.678	7.88	
			Mean 7.86	1.53
1 M KNO_3	C	0.758	7.99	1.55
	B	0.758	7.92	1.53
0.1 M $HClO_4$	B	1.000	7.90	1.55
	D	1.000	8.12	1.62
1 M $HClO_4$	C	1.000	8.02	1.58

(19) "International Critical Tables," McGraw-Hill Book Co., Inc., New York, N. Y., 1929. The viscosities were corrected to the standard obtained by J. R. Coe and T. B. Godfrey, *J. Appl. Phys.*, 15, 625 (1944).

(20) M. v. Stackelberg, M. Pilgram, and V. Toome, *Z. Elektrochem.*, 57, 342 (1953).

(21) H. A. Laitinen and I. M. Kolthoff, *J. Am. Chem. Soc.*, 61, 3344 (1939).

(22) D. J. Macero and C. L. Rulfs, *ibid.*, 81, 2942 (1959).

$$D^0_{Ag^+} = RT\lambda^0_{Ag^+}/F^2z_{Ag^+} \quad (4)$$

where R is the gas constant, T the absolute temperature, λ^0 the limiting equivalent conductance, and z the charge number, to be 1.65×10^{-5} cm^2 sec^{-1}. Table I shows that the measured values are a few per cent lower, although in interpreting the variation with ionic strength the uncertainty of $\pm 1\%$ in the figures must be borne in mind. Bearman[23] has pointed out that the polarographic diffusion coefficient in excess supporting electrolyte, while not exactly equal to the tracer diffusion coefficient, is probably identical with it within the limits of validity of the limiting current equations. It is therefore interesting to find that trace ion diffusion coefficients of alkali cations and halide anions in alkali halide solutions exhibit a similar few per cent decrease as the ionic strength of the medium rises.[24]

Diffusion Coefficient of the $Ag(SO_3)_2^{3-}$ Ion. A sodium sulfite concentration of 0.025 M was chosen so as to make $Ag(SO_3)_2^{3-}$ the predominant species. For this medium we calculated from the literature stability constants[25] that $Ag(SO_3)_3^{5-}$:$Ag(SO_3)_2^{3-}$:$AgSO_3^-$:Ag^+ = 0.045:1:0.05:7 $\times 10^{-6}$. The ionic strength was made up to unity by the addition of 0.925 M sodium nitrate to eliminate migration effects.

As described in the Experimental Section, it was necessary to use the small disk D and a small counter-electrode to avoid silver catalysis of the slow Ag^+–SO_3^{2-} reaction. The plots of i_{lim} *vs.* $\omega^{1/2}$ were straight lines passing through the origin (Figure 6), and the results are summarized in Table II. In the calculation of the diffusion coefficient by eq 1, the kinematic viscosity was taken as that of a 0.925 M $NaNO_3$ solution because viscosity data for sulfites are not available.

Table II: Results of Experiments with 0.025 M Na_2SO_3 + 0.925 M $NaNO_3$ Solutions at 25° (Ionic Strength 1.00)

10^4[$AgNO_3$], moles/l.	$10^2 i_{lim}\omega^{-1/2}$/[$AgNO_3$]	10^6D, cm^2/sec
1.005	4.06	
2.000	4.03	
4.98	4.04	
	Mean 4.04	5.61

The value of D for $Ag(SO_3)_2^{3-}$ of 5.6×10^{-6} cm^2 sec^{-1} is approximately one-third of that obtained for the hydrated silver ion in perchlorate and nitrate solutions. According to the Nernst expression (eq 4), this means that the $Ag(SO_3)_2^{3-}$ ion has approximately the same equivalent conductance as the (hydrated) silver ion. From the Stokes–Einstein equation

$$D = kT/6\pi r\eta \quad (5)$$

derived for the movement of a large spherical ion of radius r in a continuum of viscosity η (k is Boltzmann's constant), which does of course not hold exactly for the movement of nonspherical ions in water, the effective hydrodynamic radius of the $Ag(SO_3)_2^{3-}$ ion is approximately three times that of the (hydrated) silver ion. This seems physically reasonable.

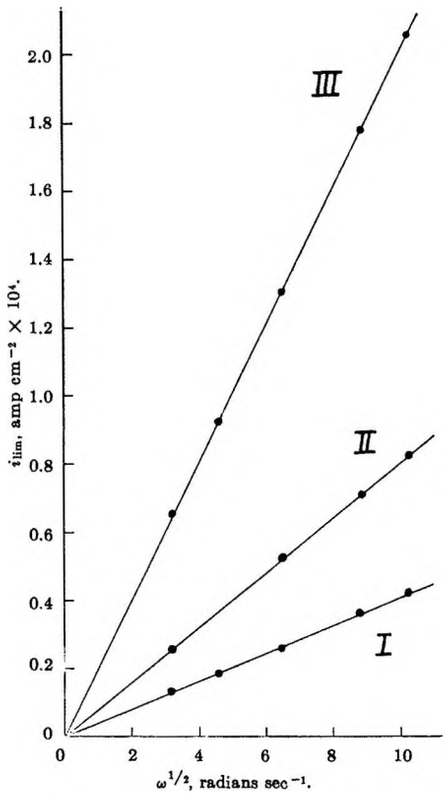

Figure 6. Levich equation plots for disk D in a solution 0.025 M in Na_2SO_3, 0.925 M in $NaNO_3$, and with $AgNO_3$ concentration of 1.005×10^{-4} M (line I), 2.00×10^{-4} M (line II), and 4.98×10^{-4} M (line III).

Acknowledgment. We are grateful to Kodak Ltd. for the award of a research grant to R. R. M. J.

(23) R. J. Bearman, *J. Phys. Chem.*, **66**, 2072 (1962).

(24) R. A. Robinson and R. H. Stokes, "Electrolyte Solutions," 2nd ed, Butterworth and Co. Ltd., London, 1959, p 317.

(25) L. G. Sillén and A. E. Martell, "Stability Constants of Metal-Ion Complexes," The Chemical Society, London, 1964, p 231.

Mass Spectrometric Investigation of Ion–Molecule Reactions in Cyclohexane[1a]

by Fred P. Abramson[1b] and Jean H. Futrell

Aerospace Research Laboratories, Chemistry Research Laboratory, Office of Aerospace Research, Wright-Patterson Air Force Base, Ohio 45433 (*Received March 27, 1967*)

The various ion–molecule reactions of fragment ions produced from cyclohexane have been investigated in conventional high-pressure mass spectrometers as well as in a tandem mass spectrometer. The results from the single-stage instruments showed that (i) all fragment ions with less than six carbon atoms react with cyclohexane, (ii) the major secondary ions are $C_6H_{11}^+$ and $C_6H_{10}^+$ with minor amounts of $C_4H_9^+$, (iii) $C_4H_8^+$ and $C_3H_6^+$ fragment ions react in a similar way to 1-butene and propylene parent ions, respectively, and (iv) there is a net charge exchange reaction of parent ions which will cause the ratio of isotopically substituted cyclohexane ions to differ considerably from the ratio of the neutral molecules in an isotopically mixed system. All fragment ions react *via* the hydride transfer reaction, $R^+ + C_6H_{12} \rightarrow RH + C_6H_{11}^+$, and $C_3H_6^+$ and $C_4H_8^+$ ions also abstract H_2^- to product $C_6H_{10}^+$.

Introduction

The radiolysis of cyclohexane has been investigated for many years, but there have been few quantitative studies of ionic reactions in the cyclohexane system. Milhaud and Durup[2] briefly studied ion–molecule reactions of cyclohexane in a mass spectrometer and reported that $C_6H_{10}^+$ and $C_6H_{11}^+$ were produced by secondary reactions involving H_2^- and H^- transfer from neutral cyclohexane molecules. Doepker and Ausloos[3] have also observed the H_2^- reaction in the radiolysis of cyclohexane vapor using mixtures of normal and deuterated cyclohexane. Ausloos and Lias[4] further observed reactions of $C_6H_{12}^+$ which involve the transfer of H_2 to unsaturated molecules. We have also examined[5] these reactions and have found an $H\cdot$ transfer reaction from cyclohexane ions in addition to H_2 transfer reactions. In the present study we have investigated the individual reactions of each fragment ion by impacting that ion onto cyclohexane in a tandem mass spectrometer. Additionally, we have obtained the over-all disappearance cross sections for many of the fragment ions from cyclohexane in conventional high-pressure mass spectrometric experiments. Finally, we have searched for possible structural effects in the reactions of $C_3H_6^+$ and $C_4H_8^+$ ions formed in the decomposition of cyclohexane by comparing the ratios of H_2^-/H^- transfer from these ions with the ratio for molecular ions formed from stable olefin and cyclane species.

Experimental Section

The ARL tandem mass spectrometer was used for studying the individual ion reactions. The instrument has been described previously[6] and the experimental techniques are also reported.[7] For all the experiments in this paper, the ion energy was 0.3 ± 0.3 ev and pulse counting was used in all cases. The measurements of reaction cross section were made using a specially modified Bendix Model 12-101 time-of-flight mass spectrometer which permits operation at source pres-

(1) (a) Presented at the 152nd National Meeting of the American Chemical Society, New York, N. Y., Sept 1966; (b) National Academy of Science–National Research Council Postdoctoral Research Associate, 1965–1966. To whom correspondence should be addressed at Consolidated Electrodynamics Corp., 1500 S. Shamrock Ave., Monrovia, Calif. 91017.

(2) J. Milhaud and J. Durup, *Compt. Rend.*, **260**, 6363 (1965).

(3) R. D. Doepker and P. Ausloos, presented at the 148th National Meeting of the American Chemical Society, Chicago, Ill., Aug–Sept 1964.

(4) P. Ausloos and S. G. Lias, *J. Chem. Phys.*, **43**, 127 (1965).

(5) F. P. Abramson and J. H. Futrell, *J. Phys. Chem.*, **71**, 1233 (1967).

(6) (a) J. H. Futrell and C. D. Miller, *Rev. Sci. Instr.*, **37**, 1521 (1966); (b) C. D. Miller, F. P. Abramson, and J. H. Futrell, *ibid.*, 1618 (1966).

(7) F. P. Abramson and J. H. Futrell, *J. Chem. Phys.*, **45**, 1925 (1966).

sures up to 1 torr.[8] Electrons (100 ev) were used at a very low (<0.1 μa) electron current and a repeller field of 10 v/cm. For some experiments where better resolution and sensitivity were required a C.E.C. Model 21-103C which has been modified to allow operation at elevated source pressures[9] was employed. The standard Bendix analog output system was used in conjunction with a C.E.C. Model 5-124 oscillograph to record peak intensities.[10]

The cyclohexane used was Matheson Coleman and Bell Chromatoquality while the C_6D_{12} was obtained from Merck Sharp and Dohme Ltd. of Canada. Other compounds used were Phillips Research grade. All were used as received except for degassing by standard techniques.

Results and Discussion

The results from the high-pressure experiments indicated that all fragment ions react with cyclohexane and that the only secondary species were $C_6H_{11}^+$, $C_6H_{10}^+$, and a very small amount of $C_4H_9^+$. The behavior of the system with respect to pressure is shown in Figures 1 and 2. It may be seen that masses 83 and 82 grow continuously with pressure while all the primary ions, except parent, m/e 84, decrease with increasing pressure. Experiments at pressures up to 600 μ indicate that the yield of m/e 84 becomes essentially constant at 0.25 ± 0.01. No ions with greater mass than parent are observed at ion source pressures up to 0.6 torr, showing that no condensation or proton-transfer reactions occur. Figure 3 clearly demonstrates the absence of proton-transfer reactions. These data, obtained on the C.E.C. instrument, show no measurable increase in the ratio of (molecular weight + 1)/molecular weight ions in cyclohexane above the isotopic contribution, while the corresponding ratio in methane is superimposed to show the growth of protonated methane. Such a comparison indicates that if any proton-transfer reactions exist in cyclohexane, they must have a rate constant which is several orders of magnitude less than that for methane (*i.e.*, $k < 10^{-13}$ cm^3/molecule sec).

By plotting the data in Figures 1 and 2 on a semilogarithmic scale, disappearance cross sections may be obtained from the slope of the line for each ion. Such a graph is shown in Figure 4 and the resulting cross sections are reported in Table I. The considerable uncertainty in the cross section for m/e 56 reflects the difficulty in measuring a cross section of this magnitude, as well as some peculiar scatter in the data. It is apparent, however, that the reactions of m/e 56 are slower than any other ion reported. No cross sections are reported

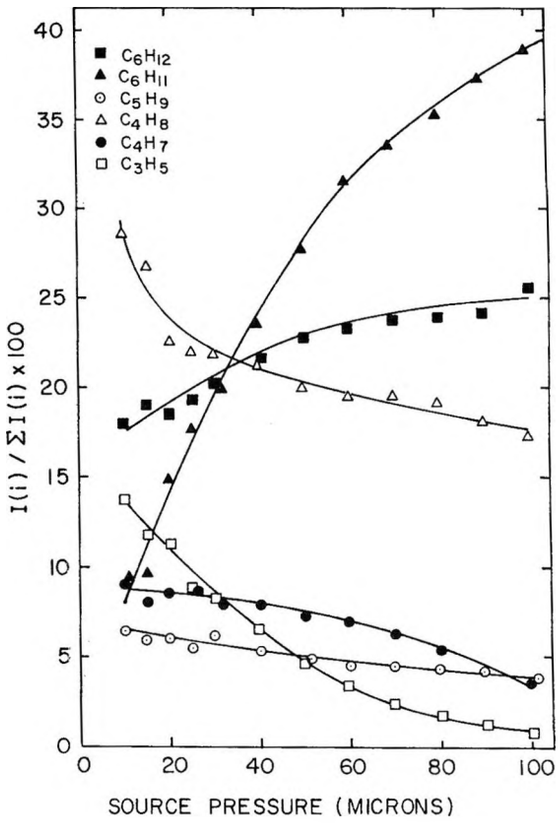

Figure 1. Pressure dependence of major ions in cyclohexane.

for m/e 39 or 55 because their disappearance kinetics do not yield straight lines.

A disappearance cross section for $C_2H_4^+$ ions was not measured in this experiment because of its low concentration and high reactivity. Other experiments

(8) J. H. Futrell, T. O. Tiernan, F. P. Abramson, and C. D. Miller, *Rev. Sci. Instr.*, in press.

(9) L. W. Sieck and J. H. Futrell, *J. Chem. Phys.*, 45, 540 (1966).

(10) It was suggested by a referee that "chemical effects" on multiplier gain might affect the reliability of our measurements in the single-stage mass spectrometer. The Bendix time-of-flight mass spectrometer requires the use of an electron multiplier for recording the mass spectrum. Hence the normal method of assessing mass-dependent gain effects, by comparing ion signals measured using the multiplier with an absolute measurement using an electrometer, cannot be employed here. Careful experiments in this laboratory on a differentially pumped electron multiplier show only small (±20%) mass-gain correction factors for diverse types of ions and an even smaller (±10%) effect for hydrocarbon ions. The somewhat larger mass-gain discrimination factors previously reported both from this laboratory and elsewhere are attributable to adsorbed gases on multiplier surfaces. In our Bendix instrument, the multiplier is differentially pumped and we assume that multiplier effects are small. Although significant relative gain effects would certainly alter the cross sections we report, this would occur through their influence on the $\Sigma(I)$ term; this has the effect of averaging out any deviation. The further observation that for some simple systems, *e.g.*, CH_4 and H_2, the disappearance cross section for a primary ion equals the appearance cross section for the corresponding product ion within experimental error suggests that chemical effects are not especially significant in the Bendix instrument.

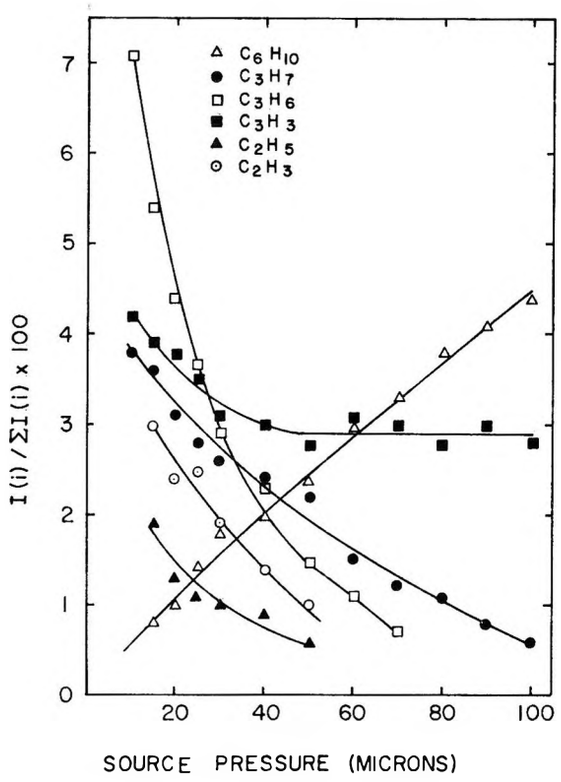

Figure 2. Pressure dependence of minor ions in cyclohexane.

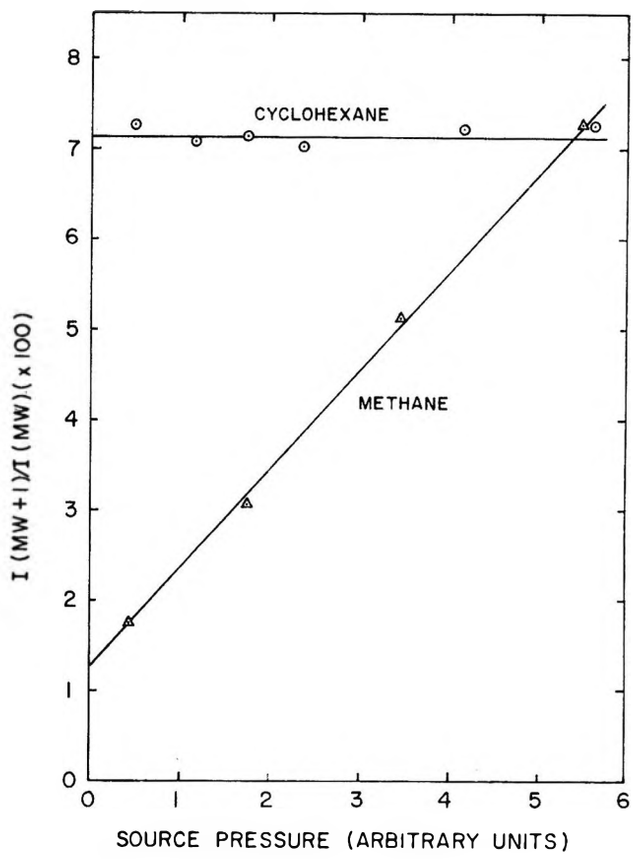

Figure 3. Comparison of proton-transfer reaction rates in cyclohexane and methane.

Table I: Total Cross Sections for Reactions in Cyclohexane at a Field Strength of 10 v/cm

m/e	*Q* (× 10^{16} cm²)
27 ($C_2H_3^+$)	60 ± 12
29 ($C_2H_5^+$)	62 ± 12
41 ($C_3H_5^+$)	60 ± 6
42 ($C_3H_6^+$)	73 ± 7
43 ($C_3H_7^+$)	37 ± 4
56 ($C_4H_8^+$)	3–10
69 ($C_5H_9^+$)	11 ± 3

using a source with enlarged ion exit and electron entrance holes showed that the cross section for the disappearance of *m/e* 28 was about 2 × 10^{-14} cm². The cross section for this reaction calculated from the elementary point charge–induced dipole model of Gioumousis and Stevenson[11] is 0.76 × 10^{-14} cm². Thus, the observed cross section exceeds the theoretical one by a factor of nearly 3. As will be shown subsequently, the major reaction pathway for $C_2H_4^+$ ions is charge transfer. The very large cross section for $C_2H_4^+$ disappearance may therefore readily be explained in terms of a significantly greater interaction length for charge exchange than for atom-transfer reactions.

Cross sections for the other ions reported in Table I show a great deal more variation than that predicted from theory,[11] there being a difference of only 15% between the predicted cross section for *m/e* 27 ions and that for *m/e* 69 with the predicted rate being greater for the heavier ion. For this system, chemical effects appear to be a more significant factor in determining the reaction cross section than the fundamental physical interaction itself. We infer that this is commonly the case for complex polyatomic molecules.

The results from the tandem mass spectrometer are presented in Table II. They are consistent with the high-pressure mass spectrometer experiments in the sense that these data also show that there are only (excluding production of parent) three secondary ions produced, $C_6H_{11}^+$, $C_6H_{10}^+$, and $C_4H_9^+$. Every ion studied reacts *via* hydride transfer to produce cyclohexyl ions, as illustrated in reaction 1. This represents

$$R^+ + c\text{-}C_6H_{12} \longrightarrow RH + C_6H_{11}^+ \qquad (1)$$

the only reaction channel for all of the fragment ions

(11) G. Gioumousis and D. P. Stevenson, *J. Chem. Phys.*, 29, 294 (1958).

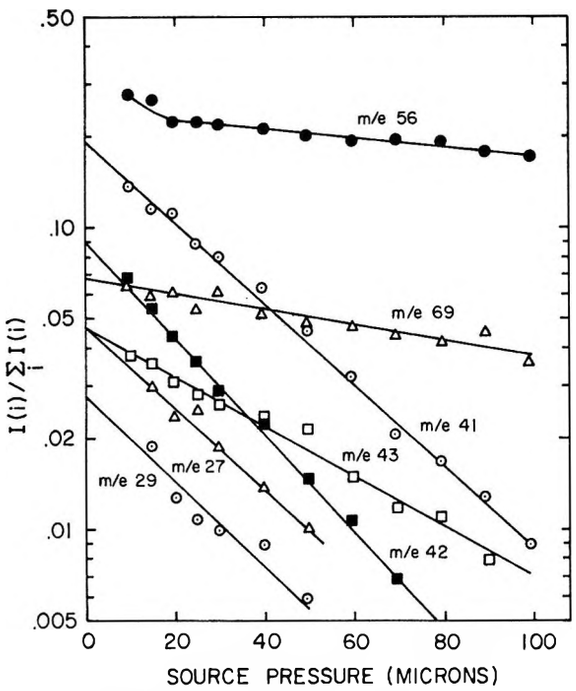

Figure 4. Disappearance cross-section plot for some ions in cyclohexane.

with an odd number of hydrogens, with the exception of the small amount of H_2 abstraction by the $C_4H_7^+$ ions to produce $C_4H_9^+$.

Reaction 2 involving H_2^- transfer is also observed for $C_4H_8^+$ and $C_3H_6^+$ ions. Such reactions have been

$$C_nH_{2n}^+ + c\text{-}C_4H_{12} \longrightarrow C_nH_{2n+2} + C_6N_{10}^+ \quad (2)$$

observed previously[9,12] in a mass spectrometer as well as in radiolysis systems.[13] Doepker and Ausloos[3] deduced from an analysis of the partially substituted butane and propane products resulting from the radiolysis of mixtures of C_6H_{12} and C_6D_{12} that stereospecific reactions of $C_4H_8^+$ and $C_3H_6^+$ occur. We were interested in seeing whether we could deduce similar effects for such fragment ions by comparing the ratio of H_2^-/H^- for these ions with the ratios for molecular ions of the same mass from the corresponding olefin or cyclane species. These experiments showed definite differences in the ratios of H_2^-/H^- depending on the source of the $C_nH_{2n}^+$ ions. Our conclusions agree with those of Doepker and Ausloos in that we find that the fragment $C_4H_8^+$ and $C_3H_6^+$ ions react most like ions produced from 1-butene and propylene. The H_2^-/H^- ratio for fragment $C_3H_6^+$ ions is 0.66 ± 0.07, which agrees more closely with propylene (1.0 ± 1) than cyclopropane (0.13 ± 0.01). The nature of the fragment $C_4H_8^+$ ions cannot be assessed as directly because both 1-butene ions (6.7 ± 0.7) and isobutene ions (5.5 ± 1) have H_2^-/H^- ratios which are near that for the cyclohexane fragment ions (5.1). *cis*-2-Butene yields a ratio of 0.4 + 0.2. Additionally, we note that the data in Figure 1 indicate an initially rapid reaction of *ca.* 25% of the *m/e* 56 ions with an increase in pressure followed by a less rapid decay of *m/e* 56 at higher pressure. A possible explanation of this phenomenon is the reactions of more than one isomeric species. The following relative cross sections for the sum of H_2^- and H^- from $C_4H_8^+$ ions produced from different sources were obtained on the tandem mass spectrometer with an estimated error of ±20%: C_6H_{12}, 1.0; 1-C_4H_8, 5.0; *i*-C_4H_8, 0.6; *cis*-2-C_4H_8, 0.08. This indicates that the most reactive $C_4H_8^+$ fragment ions might be possibly identified with 1-butene because no other isomer has an appropriately high reactivity. The discrepancy between the H_2^-/H^- ratio and reaction cross section for 1-$C_4H_8^+$ and fragment $C_4H_8^+$ ions may result from the perturbing influence of reactions of $C_4H_8^+$ ions with 2-butene and other isobutene structures. Hence, the linear portion of the $C_4H_8^+$ plot of Figure 4 yields the cross section for ions with structures other than those derived from butene-1.

As mentioned previously, the major reaction pathway for $C_2H_4^+$ ions from cyclohexane is charge exchange. The ionization potential[14] of cyclohexane is 9.88 ev and that for ethylene is 10.52 so that the charge-exchange reaction is exothermic by approximately 0.6 ev. Although the reaction for ground-state ethylene ions is exothermic, it also seemed desirable to compare reac-

Table II: Ionic Products from the Reaction of 0.3-ev Cyclohexane Fragment Ions with Cyclohexane

Impacting ion	Secondary reactions, %			
	$C_6H_{12}^+$	$C_6H_{11}^+$	$C_6H_{10}^+$	$C_4H_9^+$
$C_2H_3^+$		100		
$C_2H_4^+$	76	24		
$C_2H_5^+$		100		
$C_3H_3^+$		100		
$C_3H_5^+$		100		
$C_3H_6^+$	12	53	35	
$C_3H_7^+$		100		
$C_4H_7^+$		92		8
$C_4H_8^+$		14	72	13
$C_5H_9^+$		100		

(12) M. S. B. Munson, J. L. Franklin, and F. H. Field, *J. Phys. Chem.*, **68**, 3098 (1964).

(13) P. Ausloos, S. G. Lias, and A. Scala, Advances in Chemistry Series, No. 58, American Chemical Society, Washington, D. C., 1966, p 264.

(14) K. Watanabe, T. Nakayama, and J. Mottl, *J. Quant. Spectry. Radiative Transfer*, **2**, 369 (1962).

tions of $C_2H_4^+$ fragment ions from cyclohexane with $C_2H_4^+$ ions from other sources. We found that reactions of $C_2H_4^+$ ions from both ethylene and cyclobutane were identical within 10%. This observation suggests that the $C_2H_4^+$ fragment ions are either produced in quite similar distributions of excited states from all three molecules or that preference for charge exchange rather than H^- or H_2^- abstraction is a fundamental property of the $C_2H_4^+$–C_6H_{12} system. We are inclined toward the latter view.

We also observe some charge exchange between $C_3H_6^+$ and cyclohexane. The ionization potential of propylene is 9.73[14] so that in this case the reaction is endothermic for ground-state ions. In the center of mass system, the propylene ions have a kinetic energy spread between 0 and 0.2 ev. This could account for the observance of the endothermic charge-exchange reaction[15] although the presence of internal excitation in an ion has also been shown to be an effective means of promoting endothermic reactions.[16] We have also seen the charge-exchange reaction in the reverse direction[5] so that it is probable that in both cases the reactant ions contain some excitation.

We have noted a general relationship in the magnitude of the ratio H_2^-/H^- or $H_2/H\cdot$ between the H^-, H_2^- abstraction and the $H\cdot$, H_2 transfer types[5] of reactions. In comparing the reaction pairs $(C_6H_{12}$–$C_4H_8)^+$ and $(C_6H_{12}$–$C_3H_6)^+$ we see that there is a distinct preference for transfer of H_2 or H_2^- compared to $H\cdot$ or H^- for the former pair compared to the latter pair. The present results unfortunately do not suggest any explanation for this difference.

When parent ions from cyclohexane were impacted onto cyclohexane in the tandem instrument, a relatively strong secondary peak was observed one mass greater than parent. To evaluate whether this secondary ion was $C^{13}C_5H_{12}^+$ from a charge-exchange reaction or whether it was $C_6H_{13}^+$ from proton transfer or hydrogen abstraction, cyclohexane ions were impacted onto perdeuteriocyclohexane. The only reaction observed was a very large $C_6D_{12}^+$ signal resulting from charge exchange. In order to investigate this reaction more fully, we investigated an equimolar mixture of C_6H_{12} and C_6D_{12} in the C.E.C. mass spectrometer. We found that there is an ion–molecule interaction which produces $C_6H_{12}^+$ at the expense of $C_6D_{12}^+$. The ratio of $C_6H_{12}^+/C_6D_{12}^+$ rose steadily with increasing pressure from 1.04 to 1.39 at 1 v/cm repeller field and at the highest pressure decreased with increasing repeller potential from 1.39 to 1.02 at 25 v/cm. About the same increase with pressure (1.03 to 1.32) was observed with 10 ev ionizing electrons as with 50 ev electrons. This indicates that the net charge-exchange reaction

$$C_6D_{12}^+ + C_6H_{12} \longrightarrow C_6D_{12} + C_6H_{12}^+ \qquad (3)$$

is occurring in this system. In several recent photoionization studies[17] the ionization potentials of deuterated hydrocarbons were shown to be somewhat greater than those for their protonated analogs. Thus, for ground-state ions at thermal velocities, reaction 3 is slightly exothermic. For ions formed by electron impact presumably the exchange goes in both directions, but a net reaction favoring the formation of $C_6H_{12}^+$ is observed. This suggests the presence of a significant fraction of ground-state cyclohexane ions for which the reverse reaction is endothermic. This type of reaction should be a general one for nonreactive parent ions and is a possible explanation for some of the isotope effects observed in isotopically mixed radiolysis systems. The neutralization of those parent ions or a reaction of parent ions which is slower than reaction 3 may result in products which would not represent the concentration of neutral molecules in the mixture, but would be weighted in favor of the protonated species.

Another reaction which we have studied using the tandem mass spectrometer is proton transfer to cyclohexane. Here we have used CHO^+ ions from methanol as the proton-transfer agent. The results from this reaction are presented in Table III. The results are typical of a chemical ionization spectrum[18] inasmuch as the major ion is parent − 1. The other ions represent the simple type of fragmentation expected in such a system. We do see a small amount of protonated parent in this case, although in systems of acyclic hydrocarbons containing more than three carbons, such

Table III: Products from the Reaction of CHO^+ with c-C_6H_{12}

Ion	Percentage
$C_6H_{13}^+$	2
$C_6H_{12}^+$	7
$C_6H_{11}^+$	63
$C_4H_9^+$	4
$C_4H_7^+$	3
$C_3H_7^+$	21

(15) J. H. Futrell and F. P. Abramson, Advances in Chemistry Series, No. 58, American Chemical Society, Washington, D. C., 1936, p 107.

(16) F. P. Abramson and J. H. Futrell, *J. Chem. Phys.*, **46**, 3264 (1967).

(17) V. H. Dibeler, M. Krauss, R. M. Reese, and F. N. Harlee, *ibid.*, **42**, 3791 (1965); R. Botter, V. H. Dibeler, J. A. Walker, and H. M. Rosenstock, *ibid.*, **44**, 1271 (1966).

(18) F. H. Field, M. S. B. Munson, and D. A. Becker, Advances in Chemistry Series, No. 58, American Chemical Society, Washington, D. C., 1966, p 167.

ions have not previously been reported. Thus, the protonated cyclohexane parent ion is stable and, if produced, should have been observed as m/e 85 in the high-pressure investigations. This further affirms that proton transfer is unimportant in the pure cyclohexane system.

One important aspect of Figure 1 which has not been accounted for is the increase of m/e 84. We have noted that ethylene and propylene ions will produce m/e 84 by charge exchange, but their contributions can only constitute about 3% of total ionization.

Metastable dissociation reactions

$$C_6H_{12}^{+} * \longrightarrow C_4H_8^{+} + C_2H_4 \qquad (4a)$$

$$\longrightarrow C_5H_9^{+} + CH_3 \qquad (4b)$$

are known to exist[19] and are observed in the tandem instrument. The ARL tandem mass spectrometer is similar in concept to an instrument especially constructed for investigating metastable transitions which take place in the 10–100-μsec region.[20] In our spectrometer an ion of m/e 84 has a transit time from formation to impact of the order of 50 μsec. Any dissociation which takes place beyond the reacceleration lens will not be detected at an integral mass and any dissociation which occurs before the first mass resolving slit will not be detected at all. When tuned on m/e 84, we are able to detect $C_4H_8^{+}$ or $C_5H_9^{+}$ ions (*ca.* 0.1% of $C_6H_{12}^{+}$) at the detector of the second mass spectrometer with no gas in the reaction chamber.

Because these excited parent ions have such a long lifetime, they must have had only a small amount of excess energy. The $C_4H_8^{+}$ and $C_5H_9^{+}$ are the first fragments formed from the dissociation of cyclohexane ions[21] with increasing electron energy and a substantial fraction of the m/e 56 and 69 fragment ions must result from the lowest energy dissociation paths available. Therefore, the most easily quenched reaction of the cyclohexane cracking pattern ought to be reaction 4. Such stabilization has been predicted at atmospheric pressure by considerations of the quasi-equilibrium theory of mass spectra[22] and it is plausible that quenching should occur for pressures used in this experiment. It seems likely, therefore, that reaction 5 competes

$$C_6H_{12}^{+} * + C_6H_{12} \longrightarrow C_6H_{12}^{+} + C_6H_{12}^{*} \qquad (5)$$

with reaction 4 and could be responsible for the observed increase with pressure of the m/e 84 ions in the cyclohexane system.

(19) Catalog of Mass Spectral Data, American Petroleum Institute Research Project 44, No. 118.

(20) U. Von Zahn and H. Tatarczyk, *Phys. Letters*, **12**, 190 (1960).

(21) See data in F. H. Field and J. L. Franklin, "Electron Impact Phenomenon," Academic Press Inc., New York, N. Y., 1957.

(22) D. P. Stevenson, *Radiation Res.*, **10**, 610 (1959).

Liquid–Liquid Phase Separation in Alkali Metal–Ammonia Solutions. V. A Model for Two-Component Systems, with Calculations

by Paul D. Schettler, Jr., Patricia White Doumaux, and Andrew Patterson, Jr.

Sterling Chemistry Laboratory, Yale University, New Haven, Connecticut 06520

Accepted and Transmitted by The Faraday Society (March 29, 1967)

An ionic-lattice model with long-range forces is proposed for alkali metal–ammonia solutions to allow calculation of the chemical potentials of both components in both phases as functions of a rationalized concentration scale in which ammonia molecules are presumed strongly to solvate the metal. From the chemical potentials both phase diagrams and vapor pressures can be calculated. The effect of varying the solvation number y and the parameters $\overline{V}_1$, $\overline{V}_2$, and D is examined. Of these, the dielectric constant has the most profound influence.

In a series of papers[1-4] we have investigated some experimental aspects of the phenomenon of liquid–liquid phase separation in solutions of alkali metals in liquid ammonia. The electrical and quasi-metallic properties of these solutions are such as to indicate phase separation in them is not, in a number of ways, comparable to that in other systems, essentially nonelectrolytic in character, which have heretofore been studied and interpreted in some detail.[5-9] Several proposals have been made toward an understanding of phase separation in metal–ammonia solution,[10-12] though in no case has an entire phase diagram been calculated. In the present paper we undertake such a calculation. The results offer insight into our experimental measurements and assistance in planning further studies.

Phase Separation Model

We propose to use an expression of the following form to give the chemical potential of the solute alkali metal in a concentrated metal–ammonia solution

$$\mu_2/RT = \ln c' + A'\sqrt[3]{c} \qquad (1)$$

where c' represents moles of solute per effective volume, and A' is an appropriate Madelung constant. Its theoretical basis is the assumption, particularly appropriate to concentrated metal–ammonia solutions, of a quasi-crystalline ordered structure or ionic lattice; the Madelung constant is used to determine the electrical potential in place of the Debye–Hückel potential function, and a $c^{1/3}$ concentration dependence results from the assumption of a lattice structure. Robinson and Stokes[13] note that an expression of this type will adequately represent various thermodynamic data for concentrated aqueous solutions. The chemical potential is a well-defined quantity which can be related to activity values; a theoretical calculation of the Madelung constant can usually be avoided by algebraic manipulation of experimental activity data, which are often readily available. Equation 1 can be put in a

(1) P. D. Schettler and A. Patterson, *J. Phys. Chem.*, **68**, 2865 (1964).

(2) P. D. Schettler and A. Patterson, *ibid.*, **68**, 2870 (1964).

(3) P. W. Doumaux and A. Patterson, *ibid.*, **71**, 3535 (1967), paper III.

(4) P. W. Doumaux and A. Patterson, *ibid.*, **71**, 3540 (1967), paper IV.

(5) J. Houben and W. Fisher, *J. Prakt. Chem.*, **123**, 89 (1929).

(6) H. L. Friedman and H. Taube, *J. Am. Chem. Soc.*, **72**, 3362 (1950).

(7) H. L. Friedman, *ibid.*, **74**, 5 (1952).

(8) H. L. Friedman, *J. Phys. Chem.*, **66**, 1595 (1962).

(9) E. O. Eisen and J. Jaffe, *J. Chem. Eng. Data*, 11, 480 (1966).

(10) K. S. Pitzer, *J. Am. Chem. Soc.*, **80**, 5046 (1958).

(11) M. J. Sienko, "Solutions Métal-Ammoniac, Propriétés Physico-Chemiques, Colloque Weyl," M. J. Sienko and G. Lepoutre, Ed., W. A. Benjamin, New York, N. Y., 1964, pp 29–33.

(12) N. F. Mott, *Phil. Mag.*, **6** (62), 287 (1961).

(13) R. A. Robinson and R. H. Stokes, "Electrolytic Solutions," 2nd ed, revised, Butterworth and Co., Ltd., London, 1959, pp 225–226.

form more useful for the metal–ammonia case. As Blumberg and Das have suggested,[14] ammonia is strongly bound to sodium, so solvent molecules thus bound should be considered part of the solute, not the solvent. Expressed in mole fractions

$$c' = N_2'(V - N_2 b) \tag{2}$$

where b is the impenetrable volume of a molecule and hence $N_2 b$ is the excluded volume. Accordingly

$$c' = N_2'/(N_1'\overline{V}_1' + N_2'\overline{V}_2' - N_2'V_2') \tag{3}$$

The primed quantities thus represent a rationalized concentration scale defined as

$$N_2' = N_2/(N_2 + N_1 - yN_2) \tag{4}$$

$$N_1' = (N_1 - yN_2)/(N_2(1 - y) + N_1) \tag{5}$$

where y is the number of solvating ammonia molecules strongly bound to a metal atom. Combining these expressions and incorporating the dielectric constant, as Pitzer[10] has done, we obtain

$$(\mu_2 - \mu_2^0)/RT = \ln (N_2/N_1) + \frac{A}{DRT}\sqrt[3]{\frac{(N_2/N_1)}{\overline{V}_1\left(1 + \frac{\overline{V}_2 N_2}{\overline{V}_1 N_1}\right)}} - \ln\left((1 - y\frac{N_2}{N_1}\right) \tag{6}$$

The equation has not been arrived at by rigorous derivation from first principles and hence may be regarded as empirical. The use of the bulk solvent dielectric constant is here more acceptable than, for example, in the Debye–Hückel approach since it is believed the metal strongly binds ammonia[14] leaving the bulk ammonia unoriented and well described by the ordinary dielectric constant.

We have satisfied ourselves in some detail[15] that eq 6 expresses data for concentrated aqueous alkali–halide solutions satisfactorily. The principal concern is that the solvation number, y, should remain constant over the range of concentration to be considered.

If the equation is to be used to calculate phase-separation curves, its most important property is that it predict, for certain combinations of the parameters, that μ_2 is not single-valued. In Figure 1 μ_2 is plotted as a function of N_2'/N_1' at reduced temperature and dielectric constant. It is found that μ_2 is not single-valued, but that a range of μ_2 values is obtained such that three different concentrations have the same chemical potential. Further to determine the composition of the phases if a miscibility gap is predicted, one must involve the second component through the equality $\mu_1 = \mu_1'$. The chemical potential of the solvent can be calculated from the Gibbs–Duhem equation, which simply

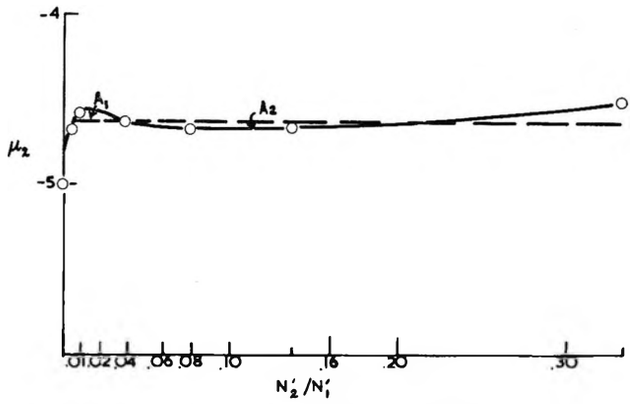

Figure 1. Plot of the chemical potential of a solute as function of concentration, expressed as mole ratio, calculated from eq 6 at reduced temperature and dielectric constant. The dashed line is drawn to emphasize the loop in the curve which defines three values of N_2'/N_1' at which μ_2 has the same value. The areas A_1 and A_2 are mentioned in the text in connection with eq 7.

represents the area plotted against the μ_2 axis in Figure 1. The equation reduces to

$$\int_{N_2/N_1}^{N_2'/N_1'} (N_2/N_1)\, d\mu_2 = 0 \tag{7}$$

where the primed quantities refer to the concentrated phase, the unprimed to the dilute phase. The only values of N_2'/N_1' and N_2/N_1 which can be chosen consistent with the restrictions of eq 7 are the two with $d\mu_2/d(N_2/N_1)$ positive such that the areas A_1 and A_2 in Figure 1 are equal and that the area under $\mu_2 - \mu_2^0$ between N_2/N_1 and N_2'/N_1' is zero.

It then becomes possible to calculate phase-separation curves, so long as the necessary parameters can be evaluated. For metal–ammonia solutions all the data of eq 6 are available, excepting a value of the Madelung constant. As earlier stated, one approach is to take experimental activity values and by manipulation of eq 6 to obtain y and A. In preference to this we have chosen to use the consolute data for phase separation for each metal as the only experimental datum to fix the phase-separation curve, since the only source of activity data is limited measurements of the vapor pressures of metal–ammonia solutions.

Reference to Figure 1 and consideration of eq 6 and 7 show that at the consolute point both the first and second derivatives of μ_2 with respect to N_2/N_2 are zero, as shown in eq 8 and 9.

(14) W. E. Blumberg and T. P. Das, *J. Chem. Phys.*, **30**, 251 (1959).

(15) P. D. Schettler, Dissertation, Yale University, New Haven, Conn., 1964; *Dissertation Abstr.*, **25**, 4432 (1965). Order No. 65-1949, University Microfilms, Inc., Ann Arbor, Mich.

$$(N_2/N_1)_{\text{consolute}} = \left(4y - 3\frac{\overline{V}_2}{\overline{V}_1}\right)^{-1} \quad (8)$$

$$(A/DRT)_{\text{consolute}} = -4^{4/3}\left(\overline{V}_1\left[y + \frac{\overline{V}_2}{\overline{V}_1}\right]\right)^{1/3} \quad (9)$$

By using, for each alkali metal studied, the experimental values of the consolute temperature and concentrations, one can evaluate the solvation number, y, and the Madelung constant, A, from eq 8 and 9. These experimentally derived values can then be used to calculate $\mu_2 - \mu_2^0$, and hence a complete liquid–liquid phase diagram for a particular metal. This has the effect of pinning the phase diagram computed with eq 6 at a single experimental point, the consolute point.

Calculations

To facilitate this procedure, and to make it easier to examine the effect on the phase-separation calculation of changing the parameters in the model, the equations have been programmed for machine computation.[16] The data for the calculations were arrived at through a careful reexamination of all existing data on phase separation of lithium, sodium, and potassium, including those of Kraus and Lucasse,[17] Loeffler,[18] Frappé,[19] Schettler and Patterson,[1] and Doumaux and Patterson.[4] Our best estimates of the consolute points for sodium are given in Table I; the data for sodium only are represented by the smooth curve E in Figure 2. The values of $\overline{V}_1$ and $\overline{V}_2$ were determined from density data on pure ammonia[20] and on sodium–ammonia solutions.[21] A plot of $\overline{V}_2$ for both sodium and potassium is slightly concave downward in the concentration region of the phase diagram; in initial calculations (see below) the value of the maximum was used. All values used in the calculation on sodium are shown in Table II. Since the results for the other metals are quite similar to those for sodium, only those for sodium will be discussed; lithium and potassium are fully covered in ref 16.

Table I: Consolute Temperature and Concentration—Two-Component Systems

	Investigator	$T_{\text{consolute}}$	$(N_2/N_1)_{\text{consolute}}$
Sodium	Kraus[17]	−41.6	0.0433
	Loeffler[18]	−41.6	0.0445
	This work	−41.55	0.0415

Calculations were made as follows.

I. The Madelung constant was calculated with eq 9, setting $y = 6$; these values were used to produce the phase diagram. Since $T_{\text{consolute}}$ was used, the consolute temperature has the correct value, but the temperature–concentration curve is found to be displaced toward a lower value of $N_2/N_1 = 0.0311$. Refer to curve I, Figure 2.

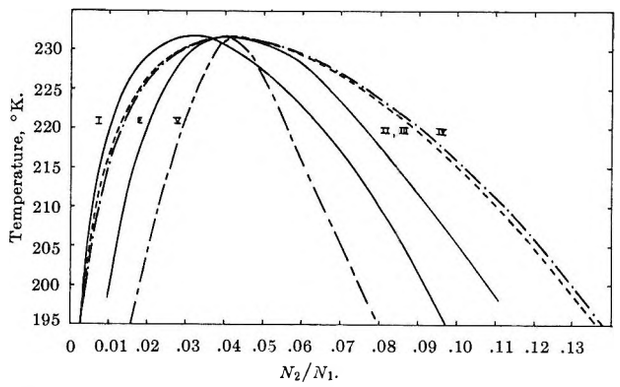

Figure 2. Phase-separation curves for sodium–ammonia solutions. The curve labeled E (solid line) is a plot, drawn as a smooth curve through a large number of points not shown, of data from a number of investigators.[1,4,17–19] The experimental points, which define the curve quite unambiguously, are omitted to avoid cluttering the graph. Curves marked I (solid line, toward left), II, III (– – – –), IV (— · —·), and V (— — —) represent various stages of the calculation using eq 6, 7, 8 and 9. The data used at each step of the calculation are discussed in the text and are listed in Tables I and II.

II. Both eq 8 and 9 were utilized, a solvation number of 3.99 was calculated, and the computation of the phase diagram repeated. See curve II. As a result of fixing the consolute point data the curve passes through this point correctly, but is, in comparison to curve I, expanded along the concentration axis, though the shape is like that of the experimental curve, E, with the same sharp rise on the dilute side and a gradual decrease on the concentrated side. Since A was the last of the parameters determined, it is sensitive to all other changes.

III. Next, a value of $\overline{V}_2$ was chosen at the consolute concentration rather than the maximum value mentioned above; refer to Table II for the values used.

(16) P. W. Doumaux, Dissertation, Yale University, New Haven, Conn., 1967.

(17) C. A. Kraus and W. W. Lucasse, *J. Am. Chem. Soc.*, **44**, 1949 (1922).

(18) D. E. Loeffler, Dissertation, Stamford University, Palo Alto, Calif., 1949.

(19) G. Frappé, Dissertation, Université Catholique de Lille, Lille, France, 1958.

(20) "International Critical Tables," E. W. Washburn, Ed., McGraw-Hill Book Co. Inc., New York, N. Y., 1928, Vol. III, p 23.

(21) C. A. Kraus, E. S. Carney, and W. C. Johnson, *J. Am. Chem. Soc.*, **49**, 2206 (1927).

Table II: Values of Parameters Used in Calculation—Two-Component Systems[a]

	Trial	A	$\bar{V}_1$	$\bar{V}_2$	y	D
Sodium	I	−39,360	0.02461	0.06679	6.00	22.5
	II	−39,060	0.02461	0.06679	3.99	22.5
	III	−36,050	0.02461	0.06595	4.01	22.5
	IV	−36,050	$\bar{V}_1(T)$	0.06595	4.01	22.5
	V	−36,050	$\bar{V}_1(T)$	0.06595	4.01	$D(T)$

[a] Units: A, (cal/mole)(l./mole)$^{1/3}$; $\bar{V}_1$, $\bar{V}_2$, l./mole.

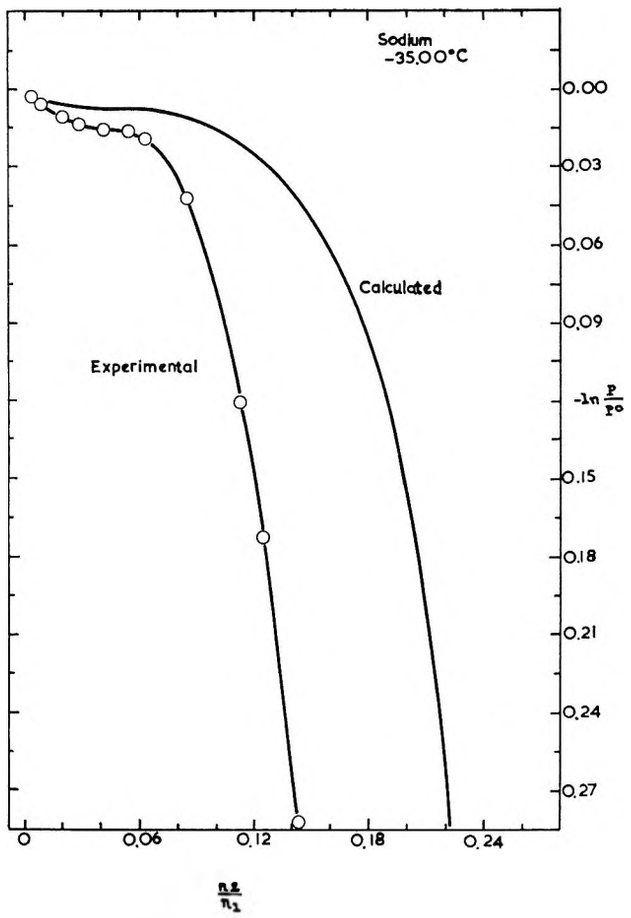

Figure 3. Plot of the vapor pressures of sodium–ammonia solutions at −35.00° shown as $\ln(p/p_0)$ *vs.* N_2/N_1. The experimental points are plotted in the curve to the left, and the calculated values derived from eq 6 are on the right. For a discussion of the lack of agreement between the two, refer to the text.

The effect is negligible, curves II and III being indistinguishable. They are not differentiated in Figure 3.

IV. The same values as employed in curve III are used, but $\bar{V}_1$ was permitted to vary as a function of temperature as specified in ref 20. The shape of the curve is retained, but there is a slight expansion along the concentration axis, curve IV.

V. Curve V was calculated in the same way as curve IV, but the dielectric constant was varied as a function of temperature in an arbitrary way. Burow and Lagowski[22] have determined the dielectric constant of ammonia at several temperatures and quote values reported earlier by others. If one plots these data and draws a "best" straight line through them, the function $D = 22.5 + 0.0970(231.6 - T)$ is obtained. This function was used to specify the variation of dielectric constant with temperature in the phase separation calculation. The result is curve V, which is so sharply contracted along the concentration axis as to fall well within the experimental curve. The asymmetry of the curve, mentioned earlier, is lost.

Discussion

It is evident from Figure 2 that the model adopted, when used with the consolute point fixed to experimental data for alkali metal–ammonia solutions, produced parabolic phase separation curves with close similarities to the experimental curve. The parameters in eq 6 affect the calculated results in varying degrees, D being the most significant, y less so, $\bar{V}_2$ appreciably less, and $\bar{V}_1$ least of all.

Because the calculation is so sensitive to variation of the dielectric constant, it would be very easy to cause curve IV (which was computed with the optimal values of the other parameters available from experimental sources) to coincide exactly with the experimental phase separation curve, simply by adjusting the dielectric constant. We have not done this because it did not seem proper, at this point, to manipulate an adjustable parameter while undertaking to justify a newly proposed model. It must be recalled that the dielectric constant values measured experimentally[22] are scattered and their temperature dependence is not yet precisely specified. At the same time, however, the changes which would be required in the dielectric constant are small, fall well within the experimental uncertainty

(22) D. F. Burow and J. J. Lagowski, "The Solvated Electron," Advances in Chemistry Series, No. 50, American Chemical Society, Washington, D. C., 1965.

of the quantity, and would be required to vary smoothly in just the way evidence from aqueous solutions suggest it does vary in the presence of different concentrations of solute. In aqueous solutions at 25°, Hasted, Ritson, and Collie[23] found that the dielectric constant of water fell as the concentration of electrolyte increased. If a similar effect of the magnitude of that found in water in the presence of 1–1 electrolytes existed in sodium–ammonia solution, the effect would be to shift curve V toward a better fit with the experimental curve, continuing to accept the variation of dielectric constant with temperature which we have arbitrarily used. In view of the present state of knowledge of the dielectric constant, it seemed to us unwise to do more than affirm its important bearing on the calculated results and to seek better data on it. At the same time, however, the prediction of the model is that D is the most interesting parameter to examine for its influence on phase separation.

As noted earlier, constancy of the solvation number over a range of concentration must obtain if eq 6 is to be used. In metal–ammonia solutions there is considerable evidence for strong and constant solvation even at concentrations approaching saturation. The values of y which result from the fitting of the consolute point data, $y_{Na} = 4.01$, $y_{Li} = 3.61$, and $y_K = 3.37$, do not follow the usual view that the smallest ion is the most solvated. In these solutions the metal which is solvated includes, beside the metal ion, the monomer of Blumberg and Das[14] and other species as well. Marshall has found a similar contradiction in studies of vapor-pressure lowering,[24] though with an order just the reverse: K, Li, Na. Unfortunately, the lowering of fugacity depends on concentration in such a way that the data for the several metals cross each other several times at different concentrations; it is not clear how an order should be specified. Also, the solvation numbers we obtain are for different temperatures, which may have an important bearing on their order.

Since μ_2 can be calculated, it is possible to calculate vapor-pressure curves.[16] Figure 3 is an example for sodium. As with the phase separation curves, these duplicate the trend of the experimental data but fall short of agreement in absolute magnitude; the values could, again, easily be arranged to agree by adjusting the dielectric constant. There would be interest in using vapor-pressure data, if of sufficient precision and detail, to obtain separate values of the parameters to be used in the phase-separation calculation.

Acknowledgment. This work was supported by the National Science Foundation. The computations were made possible by financial support from the Yale University Computer Center.

(23) J. B. Hasted, D. M. Ritson, and C. H. Collie, *J. Chem. Phys.*, **16**, 1 (1949).

(24) P. R. Marshall, *J. Chem. Eng. Data*, **7**, 399 (1962).

Transient Species Produced in the Photochemical Decomposition of Ceric Salts in Aqueous Solution. Reactivity of NO_3 and HSO_4 Free Radicals

by L. Dogliotti and E. Hayon

Pioneering Research Division, U. S. Army Natick Laboratories, Natick, Massachusetts *(Received April 3, 1967)*

The flash photolysis of ceric sulfate and ceric nitrate in aqueous solutions was studied. Ceric sulfate produced a transient species with an optical absorption maximum at 4550 A which decays bimolecularly with $k = 6.5 \pm 1.3 \times 10^8\ M^{-1}\ \text{sec}^{-1}$ and is assigned to the HSO_4 free radical. Ceric nitrate gave rise to an optical spectrum with maxima at 5950, 6400, and 6750 A. This intermediate was identified as the NO_3 radical by its characteristic absorption spectrum in the visible region. It was found to decay by a first-order process with $k = 9.5 \times 10^2\ \text{sec}^{-1}$. In addition, a new ultraviolet band with maxima at 3350 A is reported. The main primary photolytic process in *both* sulfate and nitrate salts is explained on the basis of a charge transfer from the hydration sphere to the Ce(IV) ion: $Ce(IV)\cdot H_2O \xrightarrow{h\nu} Ce(III) + OH + H^+$, followed by reactions $OH + HSO_4^- \rightarrow HSO_4 + OH^-$ and $OH + HNO_3 \rightarrow NO_3 + H_2O$. Evidence for this mechanism was derived from the extrapolation to "zero" time of the pseudo-first-order decay plots in presence of various additives. The decrease of the "initial" concentration of HSO_4 and NO_3 produced was found to be proportional to the $k(OH + S) \times C_s$ values of the solutes used. The rate constants for the reaction of HSO_4 and NO_3 with added solutes—formate, acetate, methanol, ethanol, 2-propanol, thallous ions, and cerous ions—were obtained. HSO_4 is found to be a stronger oxidizing agent than NO_3 although HSO_4 is not as strong as OH radicals.

Introduction

The action of ultraviolet light on ceric salts, particularly sulfate and perchlorate and also nitrate in aqueous solutions, has been studied considerably.[1-7] Weiss and Porret[1] interpreted the primary photochemical process due to the transfer of an electron from the hydration sphere to the excited ceric ion

$$Ce(IV)\cdot(H_2O) \xrightarrow{h\nu} Ce(III) + OH + H^+ \qquad (1)$$

or

$$Ce(IV)\cdot(H_2O) \xrightarrow{h\nu} Ce(III) + (H_2O)^+ \qquad (1')$$

followed by the back reaction (2) to account for the low net photochemical reduction of Ce(IV) ions in solutions free of impurities

$$Ce(III) + OH \longrightarrow Ce(IV) + OH^- \qquad (2)$$

This reaction scheme provided a satisfactory interpretation of the results obtained in the photolysis of ceric sulfate and perchlorate, and in the photolysis of ceric sulfate in the presence of OH-radical scavengers.[4] On photolysis of frozen aqueous solutions of 0.01 M ceric perchlorate in 6 M $HClO_4$, Moorthy and Weiss[6] have observed an esr absorption spectrum, which has been assigned to the positive "hole" $(H_2O)^+$, in accord with reaction 1'.

Indirect support for the over-all reaction mechanism was also provided from the study of the radiation chem-

(1) J. J. Weiss and D. Porret, *Nature*, **139**, 1019 (1937).

(2) E. Rabinovitch, *Rev. Mod. Phys.*, **14**, 112 (1942).

(3) L. J. Heidt and M. E. Smith, *J. Am. Chem. Soc.*, **70**, 2476 (1948); L. J. Heidt and A. F. McMillan, *Science*, **117**, 75 (1953).

(4) T. J. Sworski, *J. Am. Chem. Soc.*, **77**, 1074 (1955); **79**, 3655 (1957).

(5) T. W. Martin, A. Henshall, and R. C. Gross, *J. Am. Chem. Soc.*, **85**, 113 (1963); T. W. Martin, R. E. Rummel, and R. C. Gross, *ibid.*, **86**, 2595 (1964); T. W. Martin, J. M. Burk, and A. Henshall, *ibid.*, **88**, 1097 (1966).

(6) P. N. Moorthy and J. J. Weiss, *J. Chem. Phys.*, **42**, 3127 (1965).

(7) E. Hayon and E. Saito, *ibid.*, **43**, 4314 (1965).

istry of aqueous solutions of ceric salts.[8] There were indications, however, that at least in sulfuric acid solutions, OH radicals react with HSO_4^- to form HSO_4 radicals as intermediates

$$OH + HSO_4^- \longrightarrow HSO_4 + OH^- \qquad (3)$$

A similar indication was provided[7] for the reaction of OH radicals with HNO_3

$$OH + HNO_3 \longrightarrow NO_3 + H_2O \qquad (4)$$

Martin, *et al.*,[5] studied the flash photolysis and photochemistry of ceric nitrate, and have interpreted their observation of the optical spectrum of NO_3 radicals due to an intramolecular electron transfer from the nitrate to the ceric ion

$$Ce(IV)\cdot NO_3^- \xrightarrow{h\nu} Ce(III) + NO_3 \qquad (5)$$

This paper reports a study, using the technique of flash photolysis, of the transients produced in the photolysis of ceric sulfate, nitrate, and perchlorate. The effect of some added solutes has also been examined.

Experimental Section

The flash photolysis lamp, optical cells, optical detection system, and calculation of rate constants have been described.[9] Solutions were prepared using water purified by distillation, radiolysis, and photolysis.[9] Reagents supplied by G. F. Smith and Baker and Adamson were the best research grades available and were used without further purification. The ceric solutions, particularly potassium ceric nitrate, $K_2Ce(NO_3)_6$, were prepared daily and the addition of other solutes carried out just before photolysis. Particular attention was given to minimize exposure of the solutions to the monitoring light beam from the Osram XBO 450-w xenon lamp. The bimolecular rate constant values given here refer to $2k$.

Potassium ceric nitrate in aqueous solutions is acidic due to hydrolysis of the salt. The pH values of 10^{-1} M and 5×10^{-2} M $K_2Ce(NO_3)_6$ are 0.65 and 1.20, respectively. These solutions were photolyzed unbuffered at room temperature, 24 ± 1°. The nitrate, sulfate, and perchloric salts of ceric ions form various complexes in solution. The nature of these complexes is also known to depend on the hydrogen ion concentration and to a smaller extent on the ceric ion concentration. No attempt was made to characterize these complexes under the experimental conditions used in this work.

Results

The flash photolysis of ceric sulfate gave rise to a ransient species in the wavelength region 400–560 mμ,

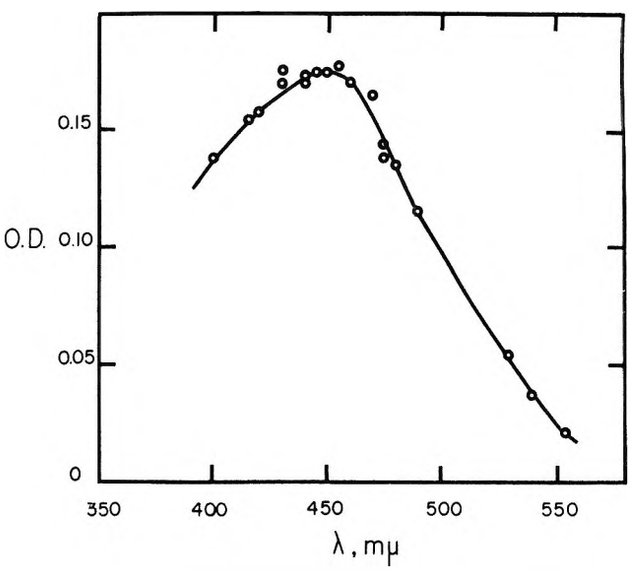

Figure 1. Absorption spectrum of HSO_4 transient produced on flash photolysis of aerated aqueous solutions of 10^{-4} M ceric sulfate in 1.0 M H_2SO_4. The optical density was measured at 40 μsec after the start of the flash. Identical spectrum was obtained in absence of O_2.

with a maximum at about 455 mμ (see Figure 1). The extent of formation of this intermediate was independent of the presence of oxygen, slightly dependent on the concentration of ceric sulfate in the range studied, 1–2.5 × 10^{-4} M, and very dependent on the concentration of sulfuric acid added. The amount of transient formed increased with increase in H_2SO_4 in the concentration range 10^{-2} to 1.0 M. This increase was considerably greater than the increase in the absorption coefficient of ceric ions with increase in H_2SO_4 concentration.[10] This transient decays bimolecularly, with a decay constant which is independent of O_2, Ce(IV), and H_2SO_4 concentration.

The optical absorption spectra and bimolecular decay constant for this transient are quite similar to those which have been observed on flash photolysis of persulfate ions[9] and sulfate ions,[11] and assigned to the SO_4^- radical anions. Since there appears to be essentially no difference in the absorption spectra and decay constants for SO_4^- and HSO_4, formed in acid solutions, there is no way of distinguishing between them or obtaining the pK value for this species (see Table I). It was not possible in this work to obtain the complete absorption spectra

(8) A. O. Allen, "The Radiation Chemistry of Water and Aqueous Solutions," D. Van Nostrand Company, Inc., Princeton, N. J., 1961, p 38.

(9) L. Dogliotti and E. Hayon, *J. Phys. Chem.*, **71**, 2511 (1967).

(10) C. M. Henderson and N. Miller, *Radiation Res.*, **13**, 641 (1960).

(11) E. Hayon and J. J. McGarvey, *J. Phys. Chem.*, **71**, 1472 (1967).

Table I: Bimolecular Decay of HSO_4 Radicals Formed on Flash Photolysis of Aerated Aqueous Solutions of 2.5×10^{-4} M Ceric Sulfate in 1.0 M H_2SO_4

λ, mμ	k/ϵ	ϵ used[a]	$k(HSO_4 + HSO_4)$, M^{-1} sec^{-1}	Published values, M^{-1} sec^{-1}
455	$1.55 \pm 0.4 \times 10^6$	460	$7.14 \pm 1.8 \times 10^8$	4.0×10^8 [9] at pH 4.8 3.6×10^8 [9] at pH 0.1 4.2×10^8 [11] at pH 5.5
475	$1.61 \pm 0.3 \times 10^6$	410	$6.60 \pm 1.2 \times 10^8$	
425	$1.36 \pm 0.3 \times 10^6$	415	$5.65 \pm 1.2 \times 10^8$	
400	$1.95 \pm 0.3 \times 10^6$	330	$6.45 \pm 1.0 \times 10^8$	
		Mean	$6.46 \pm 1.3 \times 10^8$	

[a] Molar extinction coefficient obtained from ref 9, assuming $\epsilon^{4550}_{SO_4^-} = \epsilon^{4550}_{HSO_4} = 460\ M^{-1}\ cm^{-1}$.

of HSO_4 down to 290 mμ, as was done in the flash photolysis studies of $S_2O_3^{2-}$ and SO_4^{2-}, due to the strong initial absorption of ceric sulfate itself in the wavelength range from 400 down to 290 mμ. Reduction in the ceric sulfate concentration below 10^{-4} M resulted in an appreciable decrease in the amount of transient observed.

The reactivity of HSO_4 radicals produced in the photolysis of ceric sulfate has been studied. A few selected organic and inorganic solutes were added initially, and changes in the decay of the transient species followed at 455 mμ. The HSO_4 radical was found to follow a pseudo-first-order decay in the presence of these additives. These first-order decay constants were plotted as a function of added solute concentration, and from the slope of this linear dependence the second-order rate constants for $k(HSO_4 + S)$ were obtained. These are given in Table II.

The flash photolysis of potassium ceric nitrate gave rise to one transient species having an optical absorption spectrum stretching from the far-ultraviolet to the far-visible region of the spectrum (see Figure 2). The three bands in the visible region with maxima at about 595, 640, and 675 mμ (in the liquid phase) are characteristic of the NO_3 free radical. Very similar spectra for this radical have been obtained in the gas phase,[12] on photolysis and radiolysis of HNO_3 ices,[7] on flash photolysis of ceric nitrate solutions,[5] and on pulse radiolysis of HNO_3 and NO_3^- ions.[13,14] In addition, a new absorption band has been observed in the ultraviolet region, $\lambda_{max} \simeq 335$ mμ (Figure 2), which has not been previously reported. This finding agrees with the esr observations[7] of the photolytic decomposition in the ultraviolet of NO_3 radicals trapped in HNO_3 ices.

The transient produced in the flash photolysis of ceric nitrate was found to be independent of the presence of oxygen, but the amount of transient formed was dependent on the concentration of $K_2Ce(NO_3)_6$, pH, and added HNO_3 or KNO_3. The effect of adding HNO_3 is to increase the extinction coefficient of $K_2Ce(NO_3)_6$ and to shift the over-all absorption spectrum to higher wavelengths. Consequently, all the work carried out here was done using 0.1 M $K_2Ce(NO_3)_6$ concentration.

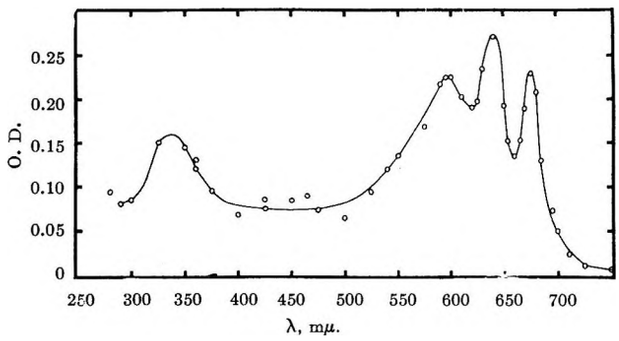

Figure 2. Absorption spectrum of NO_3 transient produced on flash photolysis of aerated aqueous solutions of 0.1 M potassium ceric nitrate. The optical density was measured at 200 μsec after the start of the flash. Identical spectrum was obtained in absence of O_2.

The NO_3 radical was found to decay by a first-order process, with a rate constant which is essentially independent of the presence of O_2, HNO_3, or KNO_3 concentrations in the concentration ranges studied, and is the same over the whole wavelength range 300–685 mμ, see Table III, indicating the presence of only one intermediate.

The reactivity of NO_3 radicals with a number of added organic and inorganic solutes was studied. In all cases, the plot of the pseudo-first-order decay constant in presence of additives *vs.* the concentration of additive

(12) D. Hussain and R. G. W. Norrish, *Proc. Roy. Soc.* (London), **A273**, 165 (1963); G. Schott and N. Davidson, *J. Am. Chem. Soc.*, **80**, 1841 (1958); E. J. Jones and T. R. Wulf, *J. Chem. Phys.*, **5**, 873 (1937).

(13) M. Daniels, *J. Phys. Chem.*, **70**, 3022 (1966).

(14) R. K. Broszkiewicz, *Intern. J. Radiation Isotopes*, **18**, 25 (1967).

Table II: Reactivity of HSO_4 Radicals with Added Solutes. Transient Formed on Flash Photolysis of Aerated Aqueous Solutions of 2.5×10^{-4} M Ceric Sulfate in 1.0 M H_2SO_4, and Monitored at 455 mμ

Solute	Concn range, M	$k(HSO_4 + S)$, M^{-1} sec^{-1}	Published values, M^{-1} sec^{-1} [b]
HCOOH	$0.4–5 \times 10^{-3}$	$1.35 \pm 0.2 \times 10^6$	...
CH_3COOH	$0.4–2 \times 10^{-2}$	$8.80 \pm 0.2 \times 10^4$	...
CH_3OH	$0.3–2 \times 10^{-3}$	$1.10 \pm 0.2 \times 10^7$	$2.5 \pm 0.6 \times 10^7$ [9] 2.0×10^7 [15]
CH_3CH_2OH	$0.6–5 \times 10^{-4}$	$3.44 \pm 0.3 \times 10^7$	$6.2 \pm 1.4 \times 10^7$ [9] 3.0×10^7 [15]
i-PrOH	$1–6 \times 10^{-4}$	$4.60 \pm 0.2 \times 10^7$	$9.1 \pm 2.8 \times 10^7$ [9]
Tl^{+a}	$0.5–2.5 \times 10^{-5}$	$1.70 \pm 0.2 \times 10^9$	...
$Ce(III)^a$	$0.5–2 \times 10^{-4}$	$1.43 \pm 0.3 \times 10^8$	...

[a] Sulfate salts. [b] The k values in ref 9 were obtained in neutral solutions.

Table III: First-Order Decay Constants for NO_3 Radicals Produced on Flash Photolysis of 0.1 M $K_2Ce(NO_3)_6$

Acid concn	Effect of O_2	λ monitored, mμ	k, sec^{-1}
Unbuffered, pH 0.65	Air-satd	600	$0.91 \pm 0.06 \times 10^3$
Unbuffered, pH 0.65	O_2 free	600	$0.95 \pm 0.05 \times 10^3$
Unbuffered, pH 0.65	Air-satd	300	$1.07 \pm 0.10 \times 10^3$
Unbuffered, pH 0.65	Air-satd	350	$1.08 \pm 0.10 \times 10^3$
Unbuffered, pH 0.65	Air-satd	450	$0.90 \pm 0.06 \times 10^3$
Unbuffered, pH 0.65	Air-satd	640	$0.99 \pm 0.10 \times 10^3$
Unbuffered, pH 0.65	Air-satd	685	$1.07 \pm 0.10 \times 10^3$
0.1 M HNO_3	Air-satd	600	$0.94 \pm 0.02 \times 10^3$
2 M HNO_3	Air-satd	600	$0.97 \pm 0.03 \times 10^3$
3 M HNO_3	Air-satd	600	$1.30 \pm 0.20 \times 10^3$
3 M HNO_3[a]	Air-satd	600	$0.91 \pm 0.10 \times 10^3$
6 M HNO_3[b]	Air-satd	600	$0.50 \pm 0.10 \times 10^3$

[a] In presence of 5×10^{-2} M $K_2Ce(NO_3)_6$. [b] In presence of 10^{-3} M $K_2Ce(NO_3)_6$.

was a straight line with an ordinate intercept equal to the first-order decay constant of the NO_3 radical itself in the absence of added solutes. From the slope of these plots the second-order rate constant for $k(NO_3 + S)$ was determined and the values are given in Table IV.

The flash photolysis of aerated aqueous solutions of 2.5×10^{-4} M ceric perchlorate in 0.6 M perchloric acid gave rise to a very weak absorption in the wavelength region 350–600 mμ. Due to this very weak absorption it was not possible to follow or study this transient.

Discussion

The photochemically induced charge-transfer reaction mechanism for the photolysis of ceric sulfate and ceric perchlorate in aqueous solution appears to explain adequately all the experimental facts known about these salts.

$$Ce(IV) \cdot H_2O \xrightarrow{h\nu} Ce(III) + (H_2O)^+ \qquad (1')$$

In aqueous solutions, $(H_2O)^+$ reacts very rapidly with water to give an OH radical

$$(H_2O)^+ + H_2O \longrightarrow OH + H_3O^+ \qquad (6)$$

so that the oxidizing species reacting in solution at room temperature is the OH radical. In ceric perchlorate–perchloric acid ices irradiated at 77°K an esr spectrum due to trapped $(H_2O)^+$ has, however, been reported.[6]

Table IV: Rate Constants of NO_3 Radicals with Added Solutes, Obtained from the Photolysis of Aerated Solutions of 0.1 M $K_2Ce(NO_3)_6$. NO_3 Transient Followed at 600 mμ

Solute	Concn range, M	$k(NO_3 + S)$, M^{-1} sec^{-1}
HCOOH	$10^{-3}–10^{-2}$	$2.06 \pm 0.1 \times 10^5$
CH_3COOH	$10^{-2}–4 \times 10^{-2}$	$4.6 \pm 0.4 \times 10^4$
CH_3OH	$2 \times 10^{-3}–10^{-2}$	$1.0 \pm 0.1 \times 10^6$
CH_3CH_2OH	$1.25 \times 10^{-4}–1.5 \times 10^{-3}$	$3.85 \pm 0.3 \times 10^6$
	$2.5 \times 10^{-4}–1.0 \times 10^{-3}$[b]	$3.90 \pm 0.4 \times 10^6$
i-PrOH	$10^{-4}–6 \times 10^{-4}$	$3.60 \pm 0.2 \times 10^6$
Tl^{+a}	$10^{-5}–8 \times 10^{-5}$	$3.46 \pm 0.1 \times 10^7$
$Ce(III)^a$	$2 \times 10^{-3}–2 \times 10^{-2}$	$3.70 \pm 0.1 \times 10^5$

[a] Nitrate salts. [b] In presence of 0.1 M and 0.01 M HNO_3.

Further support for this primary photolytic process comes from the observation that in flash photolysis of ceric sulfate, the formation of the HSO_4 transient is strongly dependent on the H_2SO_4 concentration. This is due to reaction 3 competing with reaction 2. The rate of reaction 3 is relatively low, with $k_3 = 8 \times 10^{-5}$ M^{-1} sec^{-1}.[15]

(15) E. Heckel, A. Henglein, and G. Beck, *Ber. Bunsengs. Physik. Chem.*, **70**, 149 (1966).

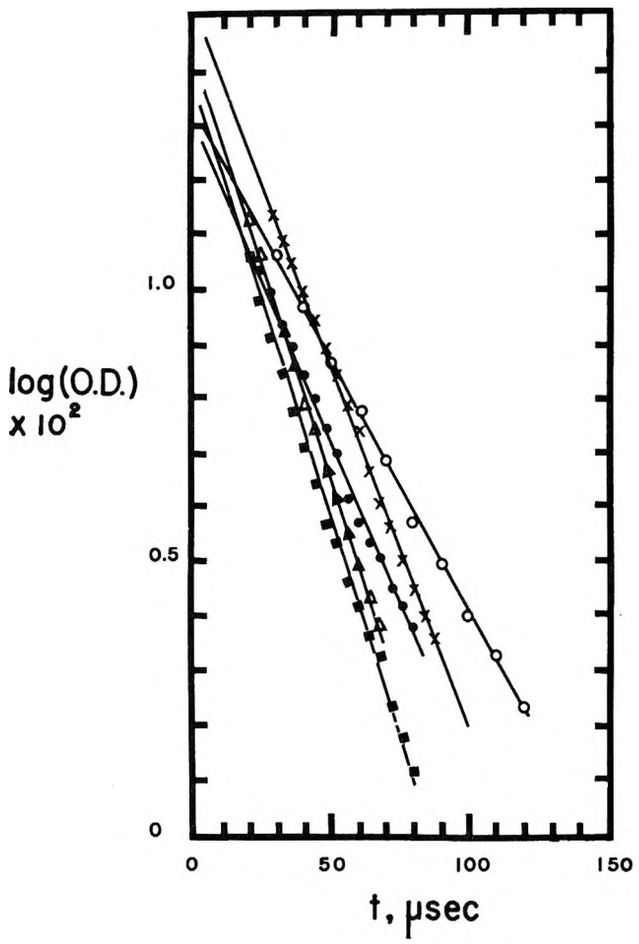

Figure 3. Pseudo-first-order decay plots of HSO_4 formed in the photolysis of 2.5×10^{-4} M ceric sulfate and 1.0 M H_2SO_4 in presence of additives. Transient monitored at 455 mμ. Values in parentheses are $k(OH + S) \times C_s$. ×, 2×10^{-4} M cerous sulfate (4.4×10^4 sec^{-1}); △, 2×10^{-5} M thallous sulfate (2×10^5 sec^{-1}); ■, 2.5×10^{-5} M thallous sulfate (2.5×10^5 sec^{-1}); ○, 3×10^{-4} M ethanol (3.3×10^5 sec^{-1}); ●, 5×10^{-4} M ethanol (5.5×10^5 sec^{-1}).

On addition of various organic and inorganic solutes to ceric sulfate solution previous to photolysis, it was possible to determine the reactivity of HSO_4 radicals with these solutes (see Table II). A plot of the pseudo-first-order decay in the presence of these additives is shown in Figure 3. On extrapolation of the pseudo-first-order plots to zero time (the maximum intensity of the flash, and hence the highest HSO_4 concentration, is at about 5 μsec), one can note that the straight lines do not extrapolate to a common point. Indeed, the log (OD) values are dependent on the solute used and its concentration. This dependence can be seen to follow the product of $k(OH + S) \times C_s$, and not $k(HSO_4 + S) \times C_s$ values for the different solutes examined. The $k(OH + S)$ values used are 2.2×10^8 M^{-1} sec^{-1},[4] 10^{10} M^{-1} sec^{-1},[4,16] and 1.1×10^9 M^{-1} sec^{-1} [17] for Ce(III), Tl^+, and ethanol, respectively. This observation shows that the solutes compete with HSO_4^- for the OH radicals produced in the primary photolytic process, in addition to their reaction with the formed HSO_4 radicals. This is in agreement with the results obtained in steady-state photolysis of ceric sulfate. Addition of OH radical scavengers like Tl^+ and Ce(III) was shown by Sworski[4] from competition kinetics measurements to compete with each other for the primary-produced OH radicals.

The flash photolysis of ceric nitrate solutions gives rise to the formation of NO_3 radicals. A new ultraviolet band has been observed for this radical, in addition to the characteristic three bands in the visible region of the spectrum (Figure 2). NO_3 decays by a first-order process, with a rate constant of about 9.5×10^2 sec^{-1} which is essentially independent of O_2 and nitric acid concentration (see Table III). That NO_3 does not decay by reaction with Ce(III) ions formed during the flash as a result of reduction of ceric ions was shown by adding cerous nitrate previous to irradiation. A plot of the pseudo-first-order rate constant as a function of [Ce(III)] extrapolates to a $k = 9.5 \times 10^2$ sec^{-1}, in agreement with the first-order k values for NO_3 itself.

Martin, *et al.*,[5] have reported that NO_3 decays bimolecularly on flash photolysis of 10^{-3} M $K_2Ce(NO_3)_6$ in 6.0 M HNO_3. The formation of NO_3 in the system was accounted as due to an intramolecular electron transfer from the nitrate to the ceric ion

$$Ce(IV) \cdot NO_3^- \xrightarrow{h\nu} Ce(III) + NO_3 \qquad (5)$$

We have repeated these conditions and find that NO_3 decays by a first-order process with $k = 5 \times 10^2$ sec^{-1} (see Table III). This value is lower than the rate constant obtained in ceric nitrate solutions containing up to 3.0 M HNO_3. In pulse radiolysis studies of HNO_3 and NO_3^- in aqueous solutions, Daniels[13] and Broszkiewicz[14] also find that NO_3 follows a first-order decay, with $k = 7.6 \times 10^3$ sec^{-1}.[14]

The formation of NO_3 is dependent partly upon the concentration of ceric nitrate and to a much larger extent on the hydrogen ion concentration. Increasing the pH of 0.1 M $K_2Ce(NO_3)_6$ above 0.65 decreases rapidly the amount of transient formed. Similarly, addition of HNO_3 increases considerably the concentration of NO_3. This observation plus the effect of added solutes known to be good OH-radical scavengers indicates that NO_3 is formed according to reaction 4.

(16) E. Hayon, *Trans. Faraday Soc.*, **61**, 723 (1965).

(17) G. E. Adams, J. W. Boag, and B. D. Michael, *ibid.*, **61**, 1417 (1965).

$$OH + HNO_3 \longrightarrow NO_3 + H_2O \qquad (4)$$

This dependence on hydrogen ion concentration (in the case of sulfuric acid and nitric acid) does not seem to be related to any change in the nature of the ceric complex with pH, since a very similar pH dependence for reactions 3 and 4 has been observed[13-14] in pulse radiolysis studies. The possibility still remains that in 6.0 *M* HNO_3 the ceric ion is present entirely as the hexanitratocerate ion, $Ce(NO_3)_6^{2-}$, while at low $[HNO_3]$, $Ce(OH)(NO_3)_3$ is also present, and one could explain the above results as follows

$$Ce(NO_3)^{2-}_6 \xrightarrow{h\nu} Ce(NO_3)^{2-}_5 + NO_3 \qquad (A)$$

$$Ce(OH)(NO_3)_3 \xrightarrow{h\nu} Ce(NO_3)_3 + OH \qquad (B)$$

However, though the results obtained above cannot entirely disprove reaction A in the photolysis of ceric nitrate in 6.0 *M* HNO_3 where the competition kinetics in the presence of added solutes cannot be followed, it can be excluded in solutions up to about 1 *M* HNO_3. In view of the results reported above, reactions A or B are considered unlikely and the work of Martin, *et al.*,[5] does not provide any evidence in its support.

The addition of solutes allows one to study the reactivity of NO_3 radicals in solution. A few organic and inorganic additives were examined and the rate constants $k(NO_3 + S)$ determined (see Table IV). The pseudo-first-order decays were plotted and are shown in Figure 4. Again one finds on extrapolation of these linear plots to zero time that the "initial" amount of transient formed is not constant, but decreases with increase in the concentration of the solutes present in solution. As in the case of the ceric sulfate photolysis, the decrease in $[NO_3]$ at "zero" time is proportional to the product $k(OH + S) \times C_s$ of the solutes added. From this one must conclude that the primary photolytic process in ceric nitrate solutions is the same as that in ceric sulfate, namely an electron transfer to the ceric ion with the subsequent formation of OH radicals.

On flash photolysis of 0.1 *M* ceric nitrate in the presence of 3.0 *M* (or 6.0 *M*) HNO_3, and the same additives, one finds that the first-order decay plots extrapolate at "zero" time to almost a common point. This provides strong support to the mechanism proposed, and indicates that in 3.0 *M* or in 6.0 *M* HNO_3 most of the OH radicals react *via* reaction 4 and that there is essentially no competition from reaction 7 for the OH radicals.

$$OH + S \longrightarrow \text{products} \qquad (7)$$

The OH radicals produced in 0.1 *M* ceric nitrate solutions (unbuffered pH of solutions is 0.65) react with HNO_3 present to form NO_3 radicals. A similar mechanism has been proposed to account for the formation of NO_3 in the esr study[7] of photolyzed HNO_3 and HNO_3 plus ceric nitrate glasses at 77°K, and in the pulse radiolysis of nitrate and nitric acid solutions.[14]

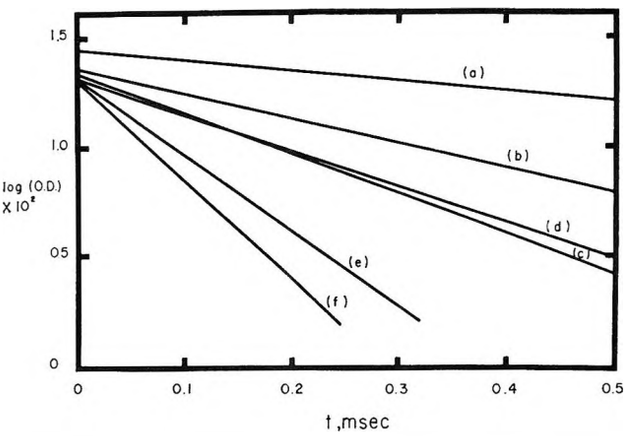

Figure 4. Pseudo-first-order decay plots of NO_3 formed in the photolysis of 0.1 *M* $K_2Ce(NO_3)_6$ in presence of additives. Transient monitored at 600 mμ. Values in parentheses are $k(OH + S) \times C_s$: (a) no additive; (b) 4×10^{-5} *M* Tl^+ (4×10^5 sec^{-1}); (c) 8×10^{-5} *M* Tl^+ (8×10^5 sec^{-1}); (d) 8×10^{-3} *M* Ce(III) (1.76×10^6 sec^{-1}); (e) 2×10^{-2} *M* Ce(III) (4.4×10^6 sec^{-1}); (f) 4×10^{-3} *M* ethanol (4.4×10^6 sec^{-1}). Experimental points have been left out.

The addition of solutes (except Ce(III) ions) and their reaction with HSO_4 or NO_3 leads to a final photoreduction of ceric ions in solution. This was observed in flash photolysis when events were followed at a wavelength where Ce(IV) ions absorb. The following reactions in addition to reaction 7 can explain the net Ce(IV) reduction: in the case of Tl^+

$$HSO_4 + Tl^+ \longrightarrow HSO_4^- + Tl^{2+}$$

$$Tl^{2+} + Ce(IV) \longrightarrow Tl^{3+} + Ce(III)$$

In the case of organic solutes

$$HSO_4 + CH_3CH_2OH \longrightarrow HSO_4^- + CH_3CHOH + H^+$$

$$CH_3CHOH + O_2 \longrightarrow CH_3CHO + HO_2$$

$$CH_3CHOH + Ce(IV) \longrightarrow CH_3CHO + Ce(III) + H^+$$

$$HO_2 + Ce(IV) \longrightarrow Ce(III) + H^+ + O_2$$

In the presence of Ce(III) ions, produced in the primary act or added previous to photolysis, the following reaction occurs

$$HSO_4 + Ce(III) \longrightarrow Ce(IV) + HSO_4^-$$

Similar reactions could explain the reduction of Ce(IV) ions in nitrate solutions.

The role and reactivity of the HSO_4, SO_4^-, and NO_3 free radicals have been largely ignored in explaining the

chemical kinetics of reactions taking place in photochemistry and radiation chemistry. These radicals can be formed by reaction of SO_4^{2-}, H_2SO_4, NO_3^-, or HNO_3 with OH radicals, or by direct photolytic or radiolytic decomposition of these molecules. In addition, these radicals once formed can react with other solutes present in solution. A comparison of k values in Tables II and IV shows that HSO_4 or SO_4^- is a much stronger oxidizing species than NO_3, though it is not as strong as hydroxyl radical.

Flash Photolysis Study of Mercury(II) Halide Complexes in Aqueous Solution. Rates of Reaction of X_2^- Radical Anions

by M. E. Langmuir and E. Hayon

Pioneering Research Division, U. S. Army Natick Laboratories, Natick, Massachusetts
(Received May 5, 1967)

The photochemistry of aqueous solutions of mercury(II) halide complexes has been studied. The optical spectra of the transient species formed have been observed using the technique of flash photolysis. The complexes $HgCl_2$, $HgCl_4^{2-}$, $HgBr_2$, $HgBr_4^{2-}$, and HgI_4^{2-} all give rise to the corresponding radical anions Cl_2^-, Br_2^-, and I_2^-. HgI_2 produced an intermediate with a maximum at 330 mμ. The decay kinetics of the transient species formed from the different polyhalide complexes have been examined in neutral and acid solutions. The rates of reaction of Cl_2^- and Br_2^- with added solutes (methanol, ethanol, isopropyl alcohol, oxalate, and H_2O_2) have also been determined in neutral and acid solutions. I_2^- radical anions are found to be relatively unreactive ($k_9 \leqslant 10^2\ M^{-1}\ sec^{-1}$ with alcohols). A comparison of the rates of reaction of the inorganic oxidizing radicals OH, SO_4^-, NO_3, Cl_2^-, Br_2^-, and I_2^- with some compounds indicates that the oxidizing power of these radicals follows the order $OH > SO_4^- > Cl_2^- > NO_3 > Br_2^- \gg I_2^-$.

A number of studies have dealt recently with the photochemistry of inorganic complexes in solution,[1] but only one investigation seems to have been made with the object of detecting the primary intermediates formed in the photochemical act. Penkett and Adamson[2] have briefly examined the flash photolysis of cobalt(III) acidopentaammine, $PtBr_6^{2-}$, and PtI_6^{2-} complexes in aqueous solutions. In this paper we report the results obtained on flash photolysis of aqueous solutions of the following mercury(II) halide complexes: $HgCl_2$, $HgCl_4^{2-}$, $HgBr_2$, $HgBr_4^{2-}$, HgI_2, and HgI_4^{2-}. The absorption spectra of the various short-lived intermediates produced on photolysis have been observed and their decay kinetics studied. Further, the reactivity of these species with some added solutes has been determined.

Experimental Section

The $HgCl_2$, $HgBr_2$, and HgI_2 (red powder) were all of reagent grade obtained from Baker and Adamson. The water used to prepare the solutions was purified as described elsewhere.[3] The concentrations of the solu-

(1) See, *e.g.*, Advances in Chemistry Series, No. 49, American Chemical Society, Washington, D. C., 1965.

(2) S. A. Penkett and A. W. Adamson, *J. Am. Chem. Soc.*, **87**, 2514 (1965).

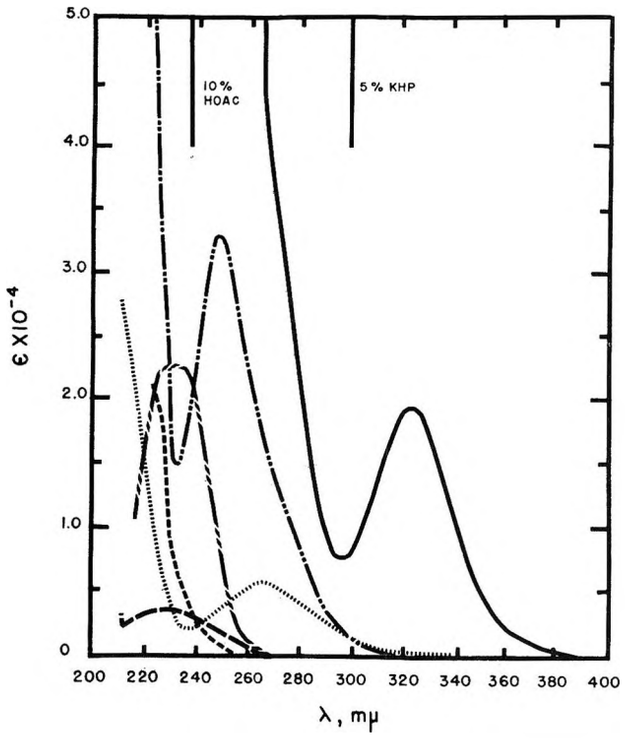

Figure 1. Absorption spectra and extinction coefficients of mercury(II) halide complexes: – – – –, $HgCl_2$ (× 10); —/ /—, $HgCl_4^{2-}$; — —, $HgBr_2$; —· · —, $HgBr_4^{2-}$; · · · · · ·, HgI_2; and ———, HgI_4^{2-}. Vertical lines show cutoff wavelength of liquid filters used.

tions were chosen to give the maximum amount of transient with minimum "inner-filtering" by the solute. A relatively high concentration of $HgCl_2$ (2×10^{-2} *M*) was necessary due to its low extinction coefficient (see Figure 1) and the low light output of the flash lamps at the required wavelength. At this concentration, hydrolysis[4] of $HgCl_2$ ($HgCl_2 + H_2O \rightarrow HgClOH + H^+ + Cl^-$) occurs to about 1% and the resulting solution has a pH ≃4. Hydrolysis in the $HgBr_2$ and HgI_2 solutions is negligible. In the case of HgI_2, a saturated solution was used. For the photolysis of the HgX_4^{2-} species, enough X^- ions were added to the HgX_2 to ensure 98% conversion to the HgX_4^{2-}, according to their formation constants.[5] Photolysis in the absence of oxygen was carried out using the syringe technique described elsewhere.[6]

The absorption spectra of the solutions taken with a Cary Model 11 spectrophotometer are shown in Figure 1 and the extinction coefficients of the various mercury complexes determined. Filter solutions were chosen to isolate the long wavelength band of the complexes and to eliminate absorption by uncomplexed halide ions. The acetic acid filter (10% by volume) has a cutoff at 237 mμ. Potassium acid phthalate (KHP), 5% by weight, has a cutoff at 300 mμ. The photolysis of $HgCl_4^{2-}$, $HgBr_2$, $HgBr_4^{2-}$, and HgI_2 was done using 10% acetic acid filter, $HgCl_2$ using 5% acetic acid, and HgI_4^{2-} using 5% KHP.

The flash apparatus has been previously described.[7,8] An 8-μsec (1/*e*th time) flash was produced at 1800 J (9 μf at 20 kv). Spectra of the transients so produced were taken by a point-by-point method at a given time *t* after flash and plotted as change in optical density, ΔOD *vs.* wavelength. Reaction rate constants were determined from oscilloscope traces (such as that shown in Figure 2) by least-squares approximation of first- or second-order reactions. The rate constants given in this paper have not been corrected for the effect of change in ionic strength on the rates of the reactions.

Results

An acetic acid or potassium hydrogen phthalate cutoff filter solution was always used to prevent the direct photolysis of uncomplexed halide ions present in some cases in solution. In all cases the nature of the optical absorption spectra of the transients formed on photolysis of HgX_2 and HgX_4^{2-} was the same in the presence or

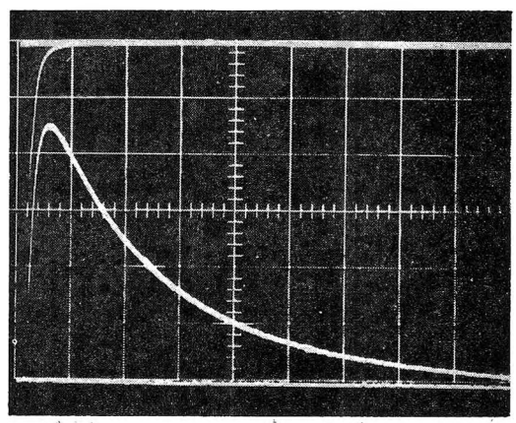

Figure 2. Oscilloscope trace of first-order decay curve of Cl_2^- produced on flash photolysis of 2×10^{-2} *M* $HgCl_2$ in 0.1 *M* $HClO_4$ (pH 1.1) (transient monitored at 344 mμ, time scale 50 μsec per large division, $k = 9.1 \times 10^3$ sec^{-1}). Top curve is stray light from the flash lamp under the same conditions.

(3) E. Hayon, *Trans. Faraday Soc.*, **60**, 1059 (1964).

(4) M. C. Sneed and R. C. Brasted, "Comprehensive Inorganic Chemistry," Vol. 4, D. Van Nostrand Co., New York, N. Y., 1955, p 99.

(5) "Handbook of Analytical Chemistry," McGraw-Hill Book Co., Inc., New York, N. Y., 1963, pp 1–37.

(6) J. K. Thomas, S. Gordon, and E. J. Hart, *J. Phys. Chem.*, **68**, 1524 (1964).

(7) L. Lindqvist, *Rev. Sci. Instr.*, **35**, 993 (1964).

(8) L. Dogliotti and E. Hayon, *J. Phys. Chem.*, **71**, 1472 (1967).

Table I: Decay Constants of Cl_2^- Radical Anions (λ_{max} = 350 mμ) Produced in the Flash Photolysis of Aqueous Solutions of NaCl, $HgCl_2$, and $HgCl_4^{2-}$

System	Concn, M	pH	Decay order	Decay rate[a]
NaCl	5×10^{-1}	6.0	Second order	$2k = 1.51 \pm 0.1 \times 10^{10}$
NaCl	5×10^{-1}	1.1	Second order	$2k = 1.38 \pm 0.2 \times 10^{10}$
$HgCl_2$	2×10^{-2}	4.0	First order	$k = 1.98 \pm 0.1 \times 10^{4}$
$HgCl_2$	2×10^{-2}	1.1	First order	$k = 1.03 \pm 0.1 \times 10^{4}$
$HgCl_4^{2-}$	2×10^{-4} $HgCl_2$ + 0.5 M NaCl	5.9	Second order	$2k = 1.25 \pm 0.1 \times 10^{10}$
$HgCl_4^{2-}$	2×10^{-4} $HgCl_2$ + 0.5 M NaCl	1.1	Second order	$2k = 1.50 \pm 0.1 \times 10^{10}$

[a] Decay rate: $2k$ given in M^{-1} sec^{-1}, calculated taking $\epsilon_{Cl_2^-}^{3500} = 1.25 \times 10^4$;[11] k, sec^{-1}.

absence of oxygen. The amount of transient formed varied slightly in the presence of oxygen, but the absorption maximum of the transient and the decay kinetics remained unchanged.

The flash photolysis of $HgCl_2$ at pH 4.0 (unbuffered) and 1.1 (acidified using perchloric acid) gave rise to a transient absorption spectrum (Figure 3a) with maximum at 350 mμ. This transient species decayed by a first-order process. The rate of decay increased by about a factor of 2 on going from pH 1.1 to 4.0 (Table I). Figure 2 shows a typical oscilloscope trace obtained on flash photolysis of 2×10^{-2} M $HgCl_2$ in 0.1 M $HClO_4$ with the transient monitored at 344 mμ. A similar spectrum was obtained on flashing $HgCl_4^{2-}$ (Figure 3a) at pH 5.9 and 1.1, but the transient decayed by a second-order process (See Table I). For comparison, NaCl solutions were photolyzed in order to compare the absorption spectrum and decay rates of the transients produced with those obtained with mercuric halide complexes (Table I). The same spectrum was obtained in all three cases and corresponded to the reported[9-11] absorption spectrum of Cl_2^- radical anion. The second-order decay rates shown in Table I were calculated using the molar extinction coefficient $\epsilon_{Cl_2^-}^{max} = 1.25 \times 10^4$ M^{-1} cm^{-1} derived from pulse radiolysis studies.[11] All the $2k$ values obtained in Table I are considered to be the same within experimental error.

The flash photolysis of aqueous solutions of 4×10^{-4} M $HgBr_2$ and 2×10^{-4} M $HgBr_4^{2-}$ at pH 6.0 and 1.1 gave an absorption spectrum with λ_{max} at 360 mμ, similar to that produced on flashing KBr solutions. This spectrum corresponds to that of Br_2^- radical anion previously reported to be formed in the flash photolysis[9,10] of Br^- ions and in the pulse radiolysis[12-14] of aqueous solutions containing Br^- ions. The molar extinction coefficient used to calculate second-order rate constants was $\epsilon_{Br_2^-}^{max} = 7.8 \pm 0.2 \times 10^3$ M^{-1} cm^{-1}.[14] $\epsilon_{Br_2^-}$ values of 8.2×10^3[12] and 9.6×10^3 M^{-1} cm^{-1}[13] have also been reported. These higher ϵ values nevertheless appear to give similar values for $2k$ ($Br_2^- + Br_2^-$) (see Table II, column 6). The Br_2^- transient from $HgBr_2$ decays by a first-order process at pH 1.1 but by a second-order process in neutral solution, while in $HgBr_4^{2-}$ it follows a second-order decay in both acid and neutral solution.

The flash photolysis of HgI_4^{2-} and I^- ions produced a transient species with λ_{max} = 385 mμ (Figure 3b) that is attributed to the I_2^- radical anion.[9,10,15] The $\epsilon_{I_2^-}^{max}$ used is 1.4×10^4 M^{-1} cm^{-1} [15] while the literature value[9] for $2k$ ($I_2^- + I_2^-$) was derived using $\epsilon = 1.56 \pm 0.3 \times 10^4$ M^{-1} cm^{-1} (see Table II). The photolysis of HgI_2, on the other hand, gave a transient with an absorption maximum at 330 mμ, which decayed by a first-order process.

The reactivity of Cl_2^- and Br_2^- radical anions with a number of added solutes has been studied and the rate constants for the reactions $k(X_2^- + S)$ are given in Tables III and IV. I_2^- appears to react more rapidly with itself than with the solutes studied, as no change in rate was observed on addition of O_2, H_2O_2, or ethanol.

Discussion

The photochemistry of the halide ions Cl^-, Br^-, and I^- has been thoroughly studied and the main photochemical

(9) L. I. Grossweiner and M. S. Matheson, *J. Phys. Chem.*, **61**, 1089 (1957).

(10) F. H. C. Edgecombe and R. G. W. Norrish, *Proc. Roy. Soc.* (London), **A253**, 154 (1959).

(11) M. Anbar and J. K. Thomas, *J. Phys. Chem.*, **68**, 3829 (1964).

(12) H. C. Sutton, G. E. Adams, J. W. Boag, and B. D. Michael, "Pulse Radiolysis," Ebert, Keene, Swallow, and Baxendale, Ed., Academic Press Inc., New York, N. Y., 1965, p 61.

(13) B. Cercek, M. Ebert, C. W. Gilbert, and A. J. Swallow, see ref 12, p 83.

(14) M. S. Matheson, W. A. Mulac, J. L. Weeks, and J. Rabani, *J. Phys. Chem.*, **70**, 2092 (1966).

(15) J. K. Thomas, *Trans. Faraday Soc.*, **61**, 702 (1965).

Table II: Decay Constants of Br_2^- (λ_{max} = 360 mμ) and I_2^- (λ_{max} = 385 mμ) Radical Anions Produced in the Flash Photolysis of Aqueous Solutions of NaX, HgX_2, and HgX_4^{2-}

Species	System	pH	Decay order	Decay rate[a]	Lit. value	Ref
Br_2^-	KBr, 2×10^{-2} *M*	6.0	Second order	$2k = 3.7 \pm 0.6 \times 10^9$	$2k = 3.3 \pm 1.0 \times 10^9$	14
Br_2^-	$HgBr_2$, 2–8 $\times 10^{-4}$ *M*	5.3	Second order	$2k = 5.2 \pm 0.6 \times 10^9$	$2k = 3.6 \times 10^9$	12, 13
Br_2^-	$HgBr_2$, 4×10^{-4} *M*	1.1	First order	$k = 2.0 \pm 0.1 \times 10^4$		
Br_2^-	$HgBr_4^{2-}$, 2×10^{-4} *M* $HgBr_2$ + 2×10^{-2} *M* KBr	6.0	Second order	$2k = 3.19 \pm 0.1 \times 10^9$		
I_2^-	KI, 10^{-3} *M*[b]	6.0	Second order	$2k = 1.17 \pm 0.2 \times 10^{10}$	$2k = 7.7 \pm 1.5 \times 10^9$	9
I_2^-	KI, 10^{-3} *M*[b]	1.1	Second order	$2k = 8.7 \pm 0.5 \times 10^9$		
λ_{max} = 330 mμ	HgI_2, 7.6×10^{-5} *M*	7.6	First order	$k = 1.0 \pm 0.05 \times 10^4$		
λ_{max} = 330 mμ	HgI_2, 7.6×10^{-5} *M*	1.1	First order	$k = 3.7 \pm 0.1 \times 10^4$		
I_2^-	HgI_4^{2-}, 10^{-4} *M* HgI_2 + 10^{-2} *M* KI	6.5	Second order	$2k = 6.7 \pm 0.6 \times 10^9$		

[a] $2k$ given in M^{-1} sec^{-1}; k given in sec^{-1}; $\epsilon_{Br_2^-}^{3600} = 7.8 \pm 0.2 \times 10^3$ [14] and $\epsilon_{I_2^-}^{3850} = 1.4 \times 10^4$.[15] [b] Solutions were saturated with N_2O.

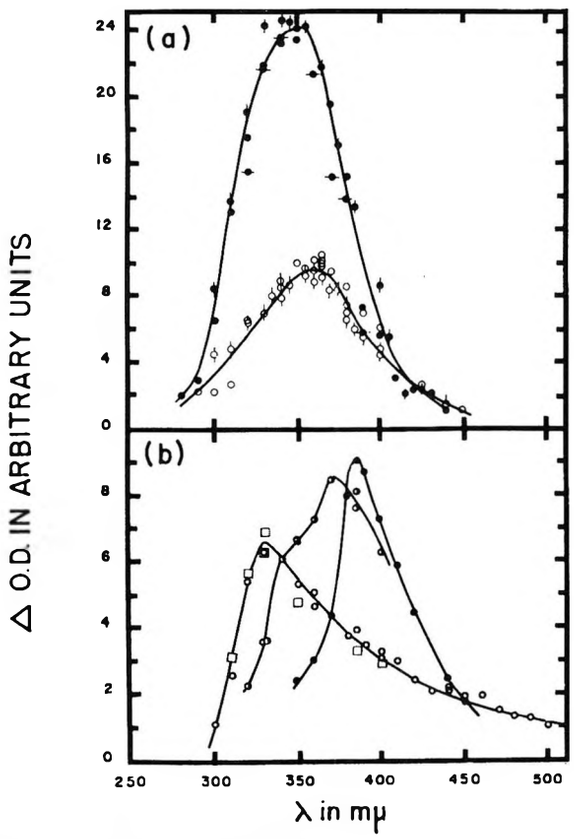

Figure 3. (a) Optical absorption spectra of transients produced in the flash photolysis of (i) 2×10^{-2} *M* $HgCl_2$ at pH 4.0 (-●-) and pH 1.1 (●); (ii) 2×10^{-4} *M* $HgCl_4^{2-}$ (in presence of 5×10^{-1} *M* NaCl) at pH 3.0 (●); (iii) 4×10^{-4} *M* $HgBr_2$ at pH 1.1 (ϕ); (iv) 4×10^{-4} *M* $HgBr_4^{2-}$ (in presence of 10^{-1} *M* KBr) at pH = 5.0 (○). (b) Optical spectra of transients produced in the flash photolysis of (i) 7×10^{-5} *M* HgI_2 at pH 6.0 (○) and pH 1.1 (□); (ii) 10^{-4} *M* HgI_4^{2-} (in presence of 10^{-2} *M* KI) at pH 7.6 (●); (iii) 9×10^{-6} *M* HgI_2 (in presence of 2×10^{-6} *M* KI) at pH 7.0 (◑). All spectra were measured at 40 μsec after the start of the flash.

Table III: Second-Order Rate Constants k_9 for the Reaction of Transient Cl_2^- Radical Anions with Added Solutes. Cl_2^- Produced in Flash Photolysis of Aerated 2×10^{-2} *M* $HgCl_2$ Solutions

Added solute	Concn range, *M*	pH	k_9, M^{-1} sec^{-1}
H_2O_2	$0.1–2.3 \times 10^{-4}$	4.0	$7.4 \pm 0.3 \times 10^7$
H_2O_2	$0.2–1.8 \times 10^{-4}$	1.1	$1.5 \pm 0.1 \times 10^8$
CH_3OH	$2–8 \times 10^{-4}$	4.0	$3.0 \pm 1.0 \times 10^7$
CH_3OH	$0.2–1 \times 10^{-3}$	1.1	$2.2 \pm 1.0 \times 10^7$
CH_3CH_2OH	$0.1–1 \times 10^{-3}$	4.0	$2.9 \pm 0.2 \times 10^7$
CH_3CH_2OH	$0.8–5 \times 10^{-4}$	1.1	$5.4 \pm 0.9 \times 10^7$
i-PrOH	$1.3–6.5 \times 10^{-4}$	4.0	$6.1 \pm 0.7 \times 10^7$
i-PrOH	$0.3–1.6 \times 10^{-4}$	1.1	$1.4 \pm 0.2 \times 10^8$
$C_2O_4^{2-}$	$0.6–3 \times 10^{-4}$	4.0	$9.4 \pm 1.4 \times 10^7$

Table IV: Second-Order Rate Constants k_9 for the Reaction of Transient Br_2^- Radical Anions with Added Solutes. Br_2^- Produced in Flash Photolysis of Aerated 4×10^{-4} $HgBr_2$ Solutions

Solute	Concn range, *M*	pH	k_9, M^{-1} sec^{-1}
H_2O_2	$0.9–2 \times 10^{-4}$	5.3	$3.9 \pm 0.2 \times 10^7$
H_2O_2	$4–9 \times 10^{-5}$	1.1	$1.50 \pm 0.05 \times 10^8$
CH_3OH	$0.1–2.5 \times 10^{-1}$	5.3	$1.5 \pm 0.2 \times 10^4$
CH_3OH	$0.05–5 \times 10^{-1}$	1.1	$2.8 \pm 0.4 \times 10^4$
CH_3CH_2OH	$0.4–3.4 \times 10^{-2}$	5.3	$1.4 \pm 0.2 \times 10^5$
CH_3CH_2OH	$0.01–1 \times 10^{-2}$	1.1	$4.5 \pm 0.2 \times 10^5$
i-PrOH	$0.2–3 \times 10^{-2}$	5.3	$3.0 \pm 0.5 \times 10^5$
i-PrOH	$0.3–2 \times 10^{-2}$	1.1	$9.0 \pm 1.0 \times 10^5$

process shown to result in the ejection of an electron from the halide ion

$$X^- \cdot H_2O \xrightarrow{h\nu} X + e_{aq}^- \qquad (1)$$

the halide atom formed then reacts with X^- to form X_2^- radical anions.

$$X + X^- \longrightarrow X_2^- \quad (2)$$

The transient absorption spectra of both X_2^- radical anions and solvated electrons has been observed.[9,10,16a] Most of the work done on the photochemistry of mercuric halides in aqueous solutions has been reviewed[16b] but no acceptable mechanism has been proposed for the light-induced reactions.

On flash photolysis of aqueous solutions of Cl^-, $HgCl_2$, $HgCl_4^{2-}$, Br^-, $HgBr_2$, $HgBr_4^{2-}$, I^-, and HgI_4^{2-}, the absorption spectra characteristic of the corresponding radical anions Cl_2^-, Br_2^-, and I_2^- have been observed in all cases, except in solutions of HgI_2. In the photochemistry of the three polyhalide complexes of mercury, the primary photochemical act leading to the formation of X_2^- radicals could be due to either (i) the transfer of an electron from a water molecule to give an OH radical

$$HgX_4^{2-} \cdot H_2O \xrightarrow{h\nu} [(HgX_4)^{2-}]^- + H^+ + OH \quad (3)$$

or

$$HgX_2 \cdot H_2O \xrightarrow{h\nu} [HgX_2]^- + H^+ + OH \quad (4)$$

(this OH radical reacts with X^- ions to form X_2^- *via* reactions 5 and 2)

$$OH + X^- \longrightarrow X + OH^- \quad (5)$$

and could possibly also react with the polyhalide complexes, (ii) the transfer of an electron from one of the ligands to the central ion of the complex, for example

$$HgX_4^{2-} \xrightarrow{h\nu} [Hg^+X_4^{3-}] \rightsquigarrow X_2^- + \text{products} \quad (6)$$

$$HgX_2 \xrightarrow{h\nu} [Hg^+Cl_2^-] \rightsquigarrow X_2^- + \text{products} \quad (7)$$

or (iii) the simple homolytic rupture of a mercury–halide bond.

To test which of these primary processes occur, use has been made of the fact that the rate constant of reaction 5 is pH dependent, particularly for Cl^- and also for Br^- ions. The formation of Cl_2^- by the reaction of OH radicals with Cl^- ions was found[11] to be first order in $[H^+]$ from pH 3 to pH 0. The flash photolysis of solutions of $HgCl_2$, $HgCl_4^{-2}$, $HgBr_2$, and $HgBr_4^{2-}$ in neutral and acid solutions was studied and the extent of formation of X_2^- radicals was determined. Though the rate constants for decay of the Cl_2^- and Br_2^- radicals were found to be pH dependent (see Table I and II), on extrapolation of the decay plots to "zero" time the initial concentration (OD) of the X_2^- transients formed was found to be independent of pH between 1.1 and 6.0. This observation, plus the fact that addition of OH radical scavengers (*e.g.*, alcohols) does not reduce the initial $[X_2^-]$, is interpreted to mean that the primary photolytic process is not the transfer of an electron from a water molecule to the complex (reactions 3 and 4).

Available data on the various polyhalide mercury complexes cannot distinguish categorically between processes (ii) and (iii). However, the absorption spectra of the HgX_4^{2-} complexes have been interpreted as electron-transfer spectra,[17] with the electron-transfer peak moving toward the visible, and the complex ion becomes less stable (see Figure 1). Thus the intraelectron-transfer mechanism, as indicated by reaction 6, is considered to be the most likely process to occur for HgX_4^{2-} complexes. No choice can be made at present between processes (ii) and (iii) to explain the primary chemical act in the photolysis of HgX_2 complexes. Since there is an excess of halide ions present in solution of these polyhalide complexes (except HgI_2), it is not unlikely that the X_2^- radical anions are produced by reaction of primarily formed X atoms with X^- ions (reaction 2).

The X_2^- radical anions formed in the photolysis of X^- and HgX_4^{2-} at pH 1.1 and at neutral pH decay by a second-order process, according to reactions

$$X_2^- + X_2^- \longrightarrow X_3^- + X^- \quad (8)$$

and

$$X_2^- + X_2^- \longrightarrow X_2 + 2X^- \quad (8')$$

The second-order decay constants for Br_2^- and I_2^- found in this work are in fairly good agreement with previously published values (see Table I and II). No published values are available for $2k(Cl_2^- + Cl_2^-)$.

The apparent first-order decay of X_2^- in the flash photolysis of $HgCl_2$ at pH 4.0 and 1.1 and of $HgBr_2$ at pH 1.1 is thought to be due to the reaction of X_2^- with HgX_2. A reduction in the initial concentrations of HgX_2 complexes to verify this pseudo-first-order decay was not feasible experimentally, since the concentration of X_2^- radicals produced under the flash photolysis conditions used was already quite low, $[X_2^-] \leqslant 10^{-6}\ M$. However, if $k(Cl_2^- + HgCl_2) \sim 10^6\ M^{-1}\ sec^{-1}$ and $k(Br_2^- + HgBr_2) \sim 10^8\ M^{-1}\ sec^{-1}$, this pseudo-first-order decay would be consistent with the ratios $[HgX_2]/[X_2^-]$ present after flashing. This means that HgX_2 at the concentration used competes effectively with reaction 8.

(16) (a) M. S. Matheson, W. A. Mulac, and J. Rabani. *J. Phys. Chem.*, **67**, 2613 (1963); (b) C. Ellis and A. A. Wells, "Chemical Action of UV Rays," Reinhold Publishing Corp., New York, N. Y., 1941, p 367.

(17) R. J. Marcus, *Solar Energy*, **4**, 20 (1960).

Table V: Comparison of the Rate Constants of Reaction of Inorganic Oxidizing Radicals with Some Simple Organic and Inorganic Compounds in Neutral Aqueous Solutions ($k(R_{Ox} + S)$, M^{-1} sec^{-1})

Compound	OH[a]	SO_4^- [b]	Cl_2^- [c]	NO_3[d]	Br_2^- [c]
CH_3OH	4.8×10^8	$2.5 \pm 0.4 \times 10^7$	$3.0 \pm 1.0 \times 10^7$	$1.0 \pm 0.1 \times 10^6$	$1.5 \pm 0.2 \times 10^4$
CH_3CH_2OH	1.1×10^9	$7.7 \pm 2.2 \times 10^7$	$2.9 \pm 0.2 \times 10^7$	$3.9 \pm 0.3 \times 10^6$	$1.4 \pm 0.2 \times 10^6$
i-PrOH	3.9×10^9	$8.3 \pm 3.0 \times 10^7$	$6.1 \pm 0.7 \times 10^7$	$3.6 \pm 0.2 \times 10^6$	$3.0 \pm 0.5 \times 10^5$
HCOOH	1.0×10^9 [e]	$1.4 \pm 0.2 \times 10^6$ [d]	...	$2.1 \pm 0.1 \times 10^5$	...
CH_3COOH	1.4×10^6 [h]	$8.8 \pm 0.2 \times 10^4$ [d]	...	$4.6 \pm 0.4 \times 10^4$	...
H_2O_2	4.5×10^7 [f]	...	$7.4 \pm 0.3 \times 10^7$	...	$3.9 \pm 0.2 \times 10^7$
Ce^{3+}	2.2×10^8 [g]	$1.4 \pm 0.3 \times 10^8$ [d]	...	$3.7 \pm 0.1 \times 10^5$	...
Tl^+	9.0×10^9 [g]	$1.7 \pm 0.2 \times 10^9$ [d]	...	$3.5 \pm 0.1 \times 10^7$	...
HCO_3^-	2.8×10^8	$9.1 \pm 0.4 \times 10^6$	...	...	...

[a] G. E. Adams, J. W. Boag, J. Currant, and B. D. Michael, *Trans. Faraday Soc.*, **61**, 1417 (1965). [b] See ref 8. [c] This work. [d] L. Dogliotti and E. Hayon, *J. Phys. Chem.*, **71**, 3802 (1967), pH 0.65. [e] M. Anbar and P. Neta, *Intern. J. Appl. Radiation Isotopes*, **16**, 227 (1965); in 1.0 M H_2SO_4. [f] H. Fricke and J. K. Thomas, *Radiation Res. Suppl.*, **4**, 35 (1964). [g] See footnote *a* of this table; pH 0.1. [h] pH 1.0.

In the photolysis of saturated (7.6×10^{-5} M) HgI_2 at pH 7.6 and 1.1, no I_2^- transient is observed. Instead, a new transient (present in presence or absence of O_2) is found, with $\lambda_{max} = 330$ mμ (Figure 3b). The absence of I_2^- radicals in this system is considered to be due to the very low ($<10^{-8}$ M) concentration of I^- ions present in solution. On addition of 2 μM I^-, both I_2^- and the species with $\lambda_{max} = 330$ mμ are observed (see Figure 3b). Thus it is suggested that the I atoms probably produced in the primary act can now react with I^- to form I_2^-. The unidentified species produced and observed in the absence of excess iodide ions is either the precursor of I_2^- or the partner of the I atom produced in the primary act. This unidentified species can also react with I^- ions since the formation of I_2^- is, at least in part, at the expense of this species. After flashing a solution of HgI_2 (in absence of added I^-), a red-brown precipitate was observed, due to Hg_2I_2.

Reaction of X_2^- Radical Anions with Added Solutes. In the pulse radiolysis of aqueous solutions, these radical anion species whenever observed are produced as a result of reaction of added halide ions with the OH radicals produced from the radiolysis of water. To study the reactivity of X_2^- radicals with added solutes gives rise to complex competition kinetics since a competition is likely to occur between the formation of X_2^- (reactions 5 and 2) and reactions 9 and 10.

$$X_2^- + S \longrightarrow \text{products} \quad (9)$$

$$OH + S \longrightarrow \text{products} \quad (10)$$

However, in flash photolysis the transient species are normally produced as a result of direct absorption of radiation by the solute and this provides a relatively simpler method for studing the chemical reactivities of these free radicals.

The free-radical chemistry of Cl_2^- and Br_2^- with H_2O_2, CH_3OH, CH_2CH_3OH, isopropyl alcohol, and oxalate ions has been studied. In all cases, the pseudo-first-order decay constant was plotted as a function of added solute concentration and the k_9 values calculated from the slope. The k_9 values were found to be greater for Cl_2^- than for Br_2^- and in almost all cases k_9 is greater at pH 1.1 than in neutral solutions. The reactivity of X_2^- is also greater on going from methanol to isopropyl alcohol.

The reaction of Cl_2^- with oxalate ions was studied as this formed the basis of an old actinometer used early this century and referred to as the Eder reaction. It is found that on photolysis of mercuric chloride at concentration of oxalate ions such that no change in the absorption spectrum of $HgCl_2$ occurred, the Cl_2^- radicals formed react relatively fast with $C_2O_4^{2-}$. However, at higher $[C_2O_4^{2-}]$ it complexes with $HgCl_2$, causing an increase in initial light absorption and resulting in a considerable increase in the concentration of Cl_2^- radicals and the precipitation of calomel.

The reactivity of I_2^- radical anions with the alcohols is extremely slow, $\leq 10^2$ M^{-1} sec^{-1}, with no change observed in the rate of disappearance of I_2^- on adding up to 3.4 M ethanol. Indeed, the I_2^- species has been observed in the flash photolysis of I^- ions in pure ethanol.[18] The reaction of I_2^- with H_2O_2 could not be studied because the concentration of H_2O_2 needed to compete with the recombination $I_2^- + I_2^-$ reaction was $\geq 5 \times 10^{-4}$ M and this resulted in the direct photolysis of H_2O_2 in addition to the photolysis of HgI_4^{2-}.

The rates of reaction of other simple inorganic oxidizing radicals have recently been studied. Thus the

(18) G. Dobson and L. I. Grossweiner, *Radiation Res.*, **23**, 290 (1964).

SO_4^- radical has been produced in the flash photolysis of persulfate ions[8] and ceric sulfate[19] and NO_3 radicals in the flash photolysis of ceric nitrate solutions.[19] A comparison of the reactivities of these oxidizing radicals and Cl_2^-, Br_2^-, and OH radicals with a few organic and inorganic compounds is presented in Table V. It can be seen that the decreasing power of oxidation of these radicals follows the order $OH > SO_4^- > Cl_2^- > NO_3 > Br_2^- \gg I_2^-$.

Finally, a preliminary investigation of the reported[20] mercury(0) photosensitized decomposition of liquid water was made using the technique of flash photolysis. No transient was observed down to 240 mμ in the presence or absence of oxygen. Addition of small amounts of Cl^- and Br^- ions, with care taken to use the appropriate light filter so as not to photolyze the X^- ions, gave rise to X_2^- transients. Furthermore, the absorption spectrum of the original unphotolyzed Hg solution increased with the time allowed for the Hg to dissolve in solution, the presence of O_2, and the temperature of the solution. These experiments suggest that the so-called "photosensitization" of water by mercury(0) could mainly be due instead to the photolysis of mercury(II) ion formed by autoxidation in air of the dissolved mercury, particularly at temperatures above room temperature.

(19) See footnote *d* of Table V.

(20) M. Z. Hoffman and A. Sher, *Nature*, 210, 1039 (1966).

Vibrational Spectra of Organophosphorus Compounds. III. Infrared and Raman Spectra of $(CH_3)_2PSCl$, $(CH_3)_2PSBr$, and $(CH_3)_2POCl$

by J. R. Durig, D. W. Wertz, B. R. Mitchell,[1]

Department of Chemistry, University of South Carolina, Columbia, South Carolina 29208

F. Block, and J. M. Greene

Defense Research Department, U. S. Army Edgewood Arsenal, Edgewood Arsenal, Maryland 21010
(Received April 3, 1967)

The infrared spectra of liquid $(CH_3)_2PSCl$ and $(CH_3)_2PSBr$ have been measured from 4000 to 33 cm^{-1}. The infrared spectrum of $(CH_3)_2POCl$ dissolved in various solvents has also been measured over the same frequency range. The Raman spectra of the sulfur-containing compounds in the liquid state have been recorded and depolarization values measured. The Raman spectrum of $(CH_3)_2POCl$ was measured both on the pure solid and as a solution in benzene. Assignment of the fundamental vibrations based on depolarization data and position of the absorption bands is given and discussed. An alternative explanation is presented for the origin of one of the two bands of the proposed doublet for the P=S stretching vibration.

Introduction

As part of our continued study of organophosphorus compounds,[2] the infrared and Raman spectra of dimethylphosphinoic chloride, dimethylphosphinothioic chloride, and dimethylphosphinothioic bromide have been recorded. Many conflicting assignments have appeared in the literature for the frequency of the stretching vibration of the P=S bond. Several alternative reasons have been put forth to explain the variations in the assigned frequencies for this normal mode. Recently, Chittenden and Thomas[3] tabulated the characteristic infrared absorption frequencies of the P=S, P—S—(C), P—S—(P), P—S—H, and P=Se bonds, and two characteristic bands of widely different frequencies have been assigned as the P=S stretching vibrations. The range for the higher band was given as 685–862 cm^{-1} and for the lower band 550–730 cm^{-1}. In some cases the difference in frequency between the two bands is quoted as 150–170 cm^{-1}. The most widely accepted suggestion for the origin of the two bands is that the bands correspond to different conformers of the molecule. However, the large variation in the frequency of these bands casts considerable doubt on this explanation. In order to shed more light on the subject, we have investigated the vibrational spectra of $(CH_3)_2POCl$, $(CH_3)_2PSCl$, and $(CH_3)_2PSBr$. This series of molecules cannot have different conformers, so if a second band is observed in the region of the P=S stretching mode, it must be assigned to a different motion in the molecule or a combination or overtone band. In order to be relatively certain as to the origin of the observed bands in the 550–860-cm^{-1} region it was necessary to make complete vibrational assignments for each of the molecules. A comparison of the frequencies of the normal modes for this series of molecules with those found for the CH_3POF_2 and CH_3PSCl_2 molecules was expected to help explain the problem of accidental degeneracy for the bending modes of the X—P=Y group when X and Y are very similar in mass.

(1) Taken in part from a thesis by B. R. Mitchell submitted to the Department of Chemistry in partial fulfillment for a Ph.D. degree.

(2) (a) J. R. Durig, F. Block, and I. W. Levin, *Spectrochim. Acta*, **21**, 1105 (1965); (b) J. R. Durig, B. R. Mitchell, J. S. DiYorio, and F. Block, *J. Phys. Chem.*, **70**, 3190 (1966).

(3) R. A. Chittenden and L. C. Thomas, *Spectrochim. Acta*, **20**, 1679 (1964).

Experimental Section

The infrared spectra were recorded from 4000 to 250 cm^{-1} with a Perkin-Elmer Model 521 spectrophotometer. The atmospheric water vapor was removed from the spectrometer housing by flushing with dry nitrogen. In the high-frequency region, the instrument was calibrated in the usual manner[4] while the lower region was calibrated by using atmospheric water vapor and the assignments of Randall, *et al.*[5] The $(CH_3)_2PSCl$ and $(CH_3)_2PSBr$ spectra were recorded as contact films between CsBr windows while the spectrum of $(CH_3)_2POCl$ was recorded as a CCl_4 solution contained in 0.1-mm CsBr liquid cells.

Infrared spectra of approximately 10 wt % solutions in benzene were recorded in polyethylene cells from 300 to 33 cm^{-1} with a Beckman Model IR-11 spectrophotometer. The instrument housing was purged with dry air and calibrated using water vapor and the assignments of Randall, *et al.*[5] All reported frequencies are expected to be accurate to better than ± 2 cm^{-1}.

The Raman spectra of the liquids were recorded on a Cary Model 81 Raman spectrophotometer which had a circulating filter solution of 125 ml of *o*-nitrotoluene and 1.75 g of ethyl violet in 3 l. of 2-propanol to isolate the 4358-A mercury excitation line. Depolarization values were measured by the method of Crawford and Horwitz.[6] The Raman spectrum of $(CH_3)_2PSBr$ was recorded using the normal 5-ml sample tube. A 0.6-ml sample tube was employed for the $(CH_3)_2PSCl$ compound. The Raman spectrum of $(CH_3)_2POCl$ was obtained in a benzene solution. Owing to the weakness of the resulting spectrum, the polarization data on this molecule are only qualitative; *i.e.*, the band was observed to be either polarized or depolarized only. The Raman effect on crystalline $(CH_3)_2POCl$ was observed with a Cary-81 Raman spectrometer equipped with an He–Ne laser source. The laser work was not done in this laboratory, and, unfortunately, no data were taken above 1500 cm^{-1}.

The samples were prepared *via* the method of Pollart and Harwood.[7,8]

Results and Discussion

All three molecules have at most a plane of symmetry which passes through the X—P=S or X—P=O bonds. Thus, they all belong to the point group C_s. Each molecule has 27 normal modes of vibration which can be broken down into 15 symmetric A′ modes giving rise to polarized lines in the Raman effect and 12 A″ modes involving motions antisymmetric to the plane. Nine of the normal modes are due to motions of the skeletal part of the molecule while the remaining 18 fundamental vibrations arise from movements of the methyl groups. As a result of the symmetry of the molecules being studied, all fundamentals of the methyl groups should give rise to both in-phase and out-of-phase vibrations of the two groups. However, because of the large mass of the phosphorus atom, the coupling is expected to be small and many of the vibrations are coincident in frequency.

Dimethylphosphinoic Chloride. Dimethylphosphinoic chloride, $(CH_3)_2POCl$, should exhibit six CH_3 stretching motions, three of which are in-phase motions and belong to the A′ symmetry species of the C_s point group whereas the other three vibrations are out of phase and belong to the A″ symmetry species. The three vibrations in each symmetry species can be directly correlated to the CH_3 motions in a methyl halide of C_{3v} symmetry. Thus, the four antisymmetric CH_3 stretching modes are assigned to the band at 2988 cm^{-1} in the infrared spectrum of $(CH_3)_2POCl$ (Figure 1). The lower frequency band, 2916 cm^{-1}, is then assigned to the two symmetric CH_3 stretching fundamentals. The infrared spectrum of the molecules also shows two peaks in the region of 1400 cm^{-1}, the expected frequency of the antisymmetric deformations, and two peaks in the 1300-cm^{-1} region, the frequency expected for the symmetric deformations. Thus, the bands at 1412 and 1400 cm^{-1} are ascribed to the four antisymmetric deformations which have been split either by lowering of the symmetry or a coupling of the methyl groups, but not both. The 1303- and 1292-cm^{-1} bands are then assigned to the symmetric deformations, one in phase and the other out of phase. The methyl modes of lowest frequency, excluding the torsions, are the CH_3 rocking fundamentals. If a comparison of polarization data obtained on the $(CH_3)_2PSCl$ molecule is made, there is little doubt that the 930- and 906-cm^{-1} bands are the in-phase CH_3 rockings. The out-of-phase CH_3 rocking modes evidently do not couple as strongly as do the in-phase motions, for only one band, at 865 cm^{-1}, is ascribable to both of these motions. The weak band at 836 cm^{-1} is too weak to be assigned to one of the rocking modes, and the only alternative is assignment as the $\nu_{11} + \nu_{25} = 855$ cm^{-1} combination band in Fermi resonance with the out-of-phase rocking modes.

The phosphoryl (P=O) stretching fundamental is assigned to the strong band at 1246 cm^{-1}. This band

(4) "Table of Wavelengths for the Calibration of Infrared Spectrometers," Butterworth Inc., Washington, D. C., 1961.

(5) H. M. Randall, D. M. Dennison, N. Ginsburg, and I. R. Weber, *Phys. Rev.*, **52**, 160 (1937).

(6) B. L. Crawford, Jr., and W. Horwitz, *J. Chem. Phys.*, **15**, 268 (1947).

(7) K. A. Pollart and H. J. Harwood, *J. Org. Chem.*, **27**, 4444 (1962).

(8) K. A. Pollart and H. J. Harwood, *ibid.*, **28**, 3430 (1963).

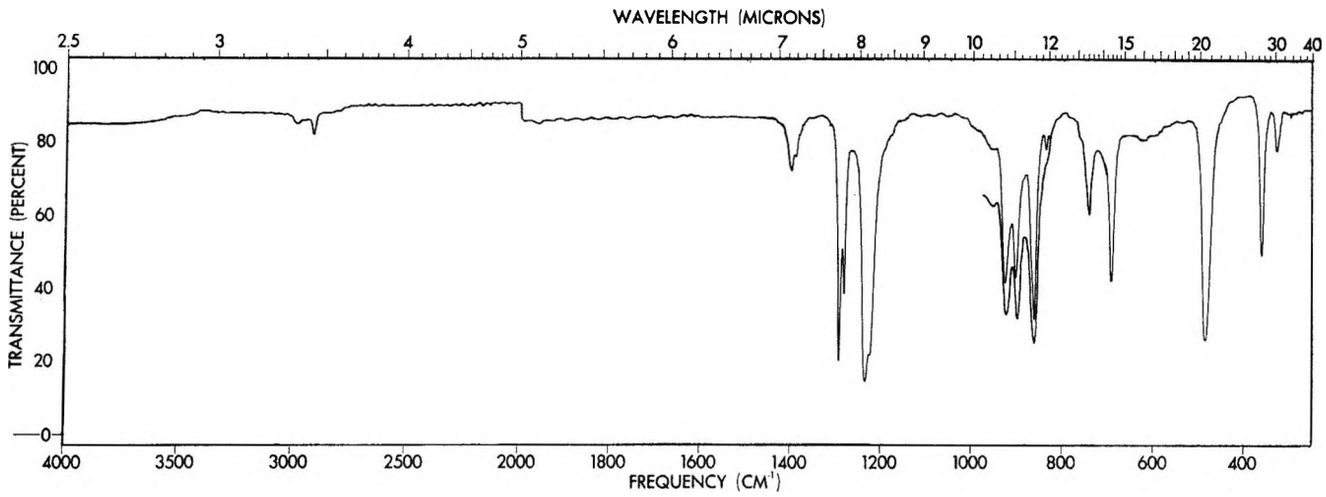

Figure 1. Infrared spectrum of a CCl_4 solution of $(CH_3)_2POCl$ in a 0.1-mm liquid cell equipped with CsBr plates. The regions of CCl_4 absorption were rerun in a benzene solution, and the inlay in the frequency range of 700–1000 cm^{-1} shows the result.

displays a very distinct shoulder at 1235 cm^{-1} in the infrared spectrum, a phenomenon common to phosphoryl stretching vibrations. The question of phosphoryl doublets has been discussed by many research workers, and it has been concluded that the doublet arises from two conformers with different phosphoryl vibrational frequencies[9–15] or that one component of the doublet has its origin in a molecular vibration not connected with the phosphoryl bond.[9,10,15] However, neither of these reasons is applicable to the dimethylphosphinoic chloride molecule because conformers cannot exist and there are no other fundamentals assignable to the region of 1250 cm^{-1}. We have, therefore, assigned the 1235-cm^{-1} band to the A′ combination band $\nu_9 + \nu_{12} = 1240$ cm^{-1} which has obtained considerable intensity from a Fermi resonance with the phosphoryl stretching mode. In the Raman effect of the benzene solution of $(CH_3)_2POCl$, only one strongly polarized line appears in this region at 1243 cm^{-1}. Our data are in good agreement with previous data on the effects of electronegativities on the phosphoryl stretching frequency. Thomas and Chittenden[16] give the empirical relationship $\nu_{P=O} = 930 + 40\ \Sigma\pi$, where the summation is of the electronegativities over all the substituents on the phosphorus. The π constants given yield an expected $\nu_{P=O}$ of 1234 cm^{-1} while the experimental value is slightly lower than 1246 cm^{-1}, but owing to the expected Fermi resonance, the exact frequency is not known. The Raman spectrum of crystalline $(CH_3)_2POCl$ has but one line in this frequency range at 1195 cm^{-1}. Thus, the frequency of the P=O stretching fundamental shifts about 50 cm^{-1} in the crystal which indicates that a considerable amount of association in the crystal must be through the phosphoryl oxygen.

The infrared spectrum of $(CH_3)_2POCl$ has two absorptions in the region expected for the PC_2 stretching modes: a medium-intensity band at 751 cm^{-1} and a strong band at 696 cm^{-1}. The Raman effect shows a strong, polarized line at 700 cm^{-1} and a weak depolarized line at 760 cm^{-1}. On this basis, we have assigned the higher frequency band to the antisymmetric PC_2 stretching mode and the 700-cm^{-1} band to the symmetric PC_2 stretching vibration. The three remaining fundamentals of the mid-infrared spectrum can readily be assigned to the P—Cl stretching and the in- and out-of-plane O=P—Cl bending modes. Durig, *et al.*,[2a] have shown that the P—Cl stretching mode is expected to lie in the region of 480 cm^{-1}. Therefore, the strongly polarized Raman line at 487 cm^{-1} is attributed to the P—Cl stretching motion. Polarization data on the two bands at 370 and 335 cm^{-1} indicate that the higher frequency band should be assigned to the out-of-plane O=P—Cl bending mode while the weakly polarized band at 335 cm^{-1} should be attributed to the A′ bending motion. The reversal of intensities occurring in the infrared and Raman spectra is strong support for these assignments; *i.e.*, the A′ bending mode is the

(9) F. S. Mortimer, *Spectrochim. Acta*, **9**, 270 (1957).

(10) J. V. Bell, J. Heisler, H. Tannenbaum, and J. Goldenson, *J. Am. Chem. Soc.*, **76**, 5185 (1954).

(11) R. C. Gore, *Discussions Faraday Soc.*, **9**, 138 (1950).

(12) L. J. Bellamy and L. Beecher, *J. Chem. Soc.*, 475 (1952).

(13) L. J. Bellamy and L. Beecher, *ibid.*, 1701 (1952).

(14) B. Holmstedt and L. Larsson, *Acta Chem. Scand.*, **5**, 1179 (1951).

(15) L. S. Maiants, E. M. Popov, and M. I. Kabachnik, *Opt. Spectry.* (USSR), **7**, 108 (1959).

(16) L. C. Thomas and R. A. Chittenden, *Spectrochim. Acta*, **20**, 467 (1964).

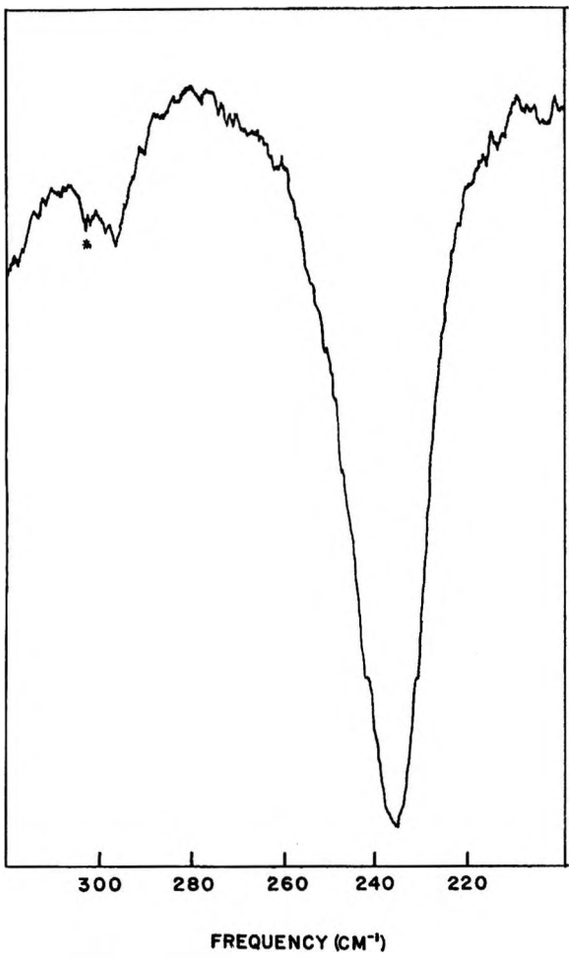

Figure 2. Region of absorption of $(CH_3)_2POCl$ in the far-infrared region. The spectrum was recorded in a benzene solution contained in 1-mm polyethylene liquid cells. The starred band at 303 cm^{-1} is the result of a weak absorption band in benzene.

stronger absorber in the Raman effect while the A'' bending motion is the more intense absorber in the infrared spectrum.

Examination of the far-infrared spectrum (below 300 cm^{-1}) was expected to produce the five fundamentals not already assigned, *i.e.*, the PC_2 twisting, wagging, and deformation, and the in-phase and out-of-phase methyl torsions. The region from 33 to 300 cm^{-1} produced only two additional bands (Figure 2): a very weak absorption at 298 cm^{-1} and a strong absorption at 237 cm^{-1}. These frequencies are much too high to be ascribed to the methyl torsions. The 298-cm^{-1} band is extremely weak, but it could not be attributed to a combination or difference band of any of the assigned fundamentals. Consequently, we have tentatively assigned the 298-cm^{-1} absorption to the PC_2 wagging which preserves the symmetry plane. The Raman effect of crystalline $(CH_3)_2POCl$ shows two bands in the region of 237 cm^{-1}: one at 258 cm^{-1} and the other at 221 cm^{-1}. It would appear then that in solution the PC_2 twisting and deformation are accidentally degenerate at 237 cm^{-1}, whereas in the solid the two bands are split by 17 cm^{-1}. The higher frequency band is ascribed to the twisting mode whereas the lower band is thought to be due to the PC_2 deformation. (See Table I for spectra of $(CH_3)_2POCl$.)

Dimethylphosphinothioic Chloride. The motions of the methyl groups of $(CH_3)_2PSCl$ are certainly expected to parallel those of the corresponding motions in the $(CH_3)_2POCl$ molecule disscussed above. The infrared and Raman spectra (Figures 3 and 4) show the obvious similarities; consequently, no discussion is given for the assignments of the methyl modes for the $(CH_3)_2PSCl$ molecule.

The spectrum of $(CH_3)_2PSCl$ has only three fundamental absorptions in the frequency region of 800–400 cm^{-1}, but four bands are expected: the symmetric and antisymmetric PC_2 stretching modes, the P=S stretching vibration, and the P—Cl stretching mode. The three bands are observed at 750, 608, and 455 cm^{-1} in the infrared spectrum. For CH_3PSCl_2, Durig, *et al.*,[2a] have shown that the P=S stretching mode absorbs at 672 cm^{-1}. The frequency of this mode in $(CH_3)_2PSCl$ is thus expected to lie lower than 672 cm^{-1}.[3] Thus, the 608-cm^{-1} band is assigned to the P=S stretching vibration. The 750-cm^{-1} absorption is ascribed to both PC_2 stretching modes. The apparent accidental degeneracy of the PC_2 stretching vibrations is believed to be the result of a mutual repulsion of the A' PC_2 and P=S stretching energy levels. The result is that the symmetric PC_2 stretching mode is pushed from its unperturbed frequency of about 700 cm^{-1} (696 cm^{-1} in $(CH_3)_2POCl$) to 750 cm^{-1}, the frequency of the antisymmetric PC_2 stretching fundamental. Such a perturbation would also lower the P=S stretching vibration which accounts for the rather low value of 608 cm^{-1} found for the P=S stretching motion is this molecule. The remaining band at 455 cm^{-1} is confidently assigned to the P—Cl stretching vibration.

The low region of the spectrum displays two bands in the infrared and three in the Raman. All the bands found are considerably higher than would be expected for the two methyl torsions. Thus, there are five modes which are expected to absorb energy in this region of the spectrum. The polarized band at 276 cm^{-1} in the Raman effect is assigned to the PC_2 wagging of symmetry species A'. The band at 217 cm^{-1} is depolarized and is assigned to the A'' fundamental described as a PC_2 twisting motion. The third absorption is found at 198 cm^{-1} and is polarized; it is attributed to the PC_2

Table I: Infrared and Raman Spectra of $(CH_3)_2POCl$

Infrared, CCl_4 soln, cm^{-1}	Intens[c]	Raman, benzene soln (cm^{-1})	Intens[b]	Depolarization[c]	Raman, crystal, cm^{-1}	Assignments
2988	vw	3000	30	dp		ν_1, ν_2, ν_{16}, ν_{17}, antisym CH_3 str
2916	w	2917	100	p		ν_3, ν_{18} sym CH_3 str
1412	m	1409	30	p		ν_4, ν_5, ν_{19}, ν_{20} antisym CH_3 def
1400	sh					
1303	s					ν_6, ν_{21} sym CH_3 def
1292	s					
1246	vs	1243	15	p	1195	ν_7 P=O str
1235	sh					$\nu_9 + \nu_{12} = 1240\ cm^{-1}$ in Fermi resonance with ν_7
930	s	934	14	p		ν_8 sym CH_3 rock (in-phase)
906	s					ν_9 antisym CH_3 rock (in-phase)
865	s					ν_{22}, ν_{23} sym and antisym CH_3 rock (out-of-phase)
836	w					$\nu_{11} + \nu_{25} = 855\ cm^{-1}$ in Fermi resonance with ν_{22} and ν_{23}
751	m	760	2	dp		ν_{24} antisym PC_2 str
696	s	700	20	p	710	ν_{10} sym PC_2 str
488	s	487	17	p	484	ν_{11} P—Cl str
367	s	370	4	dp	368	ν_{25} O=P—Cl bend
334	m	335	8	p	350	ν_{12} O=P—Cl bend
298[a]	m	297	5	p	308	ν_{13} PC_2 wag
237[a]	vw	234	7	dp	258	ν_{14} PC_2 twist
					221	ν_{26} PC_2 def
...		...		...	...	ν_{15}, ν_{27} CH_3 torsions

[a] Far-infrared spectrum was obtained in benzene solution. [b] Intensity measurements in this sample are very rough owing to noise and fluorescence. [c] Abbreviations used: s, m, w, v, p, dp, and sh denote strong, medium, weak, very, polarized, depolarized, and shoulder, respectively.

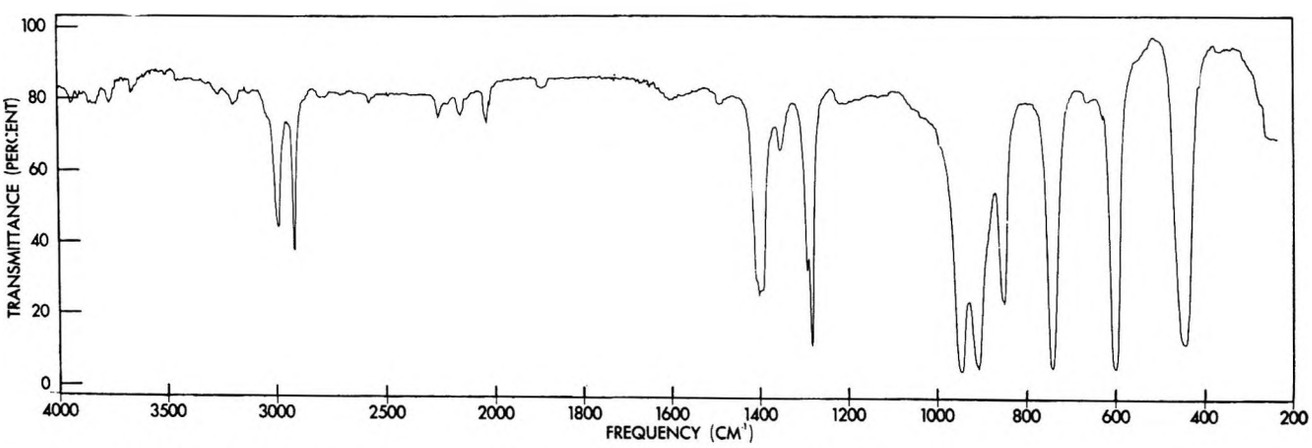

Figure 3. Infrared spectrum of $(CH_3)_2PSCl$ recorded as a contact film between CsBr plates.

deformation vibration. Thus, the Cl—P=S bending motions have not been assigned. The 276-cm^{-1} band, however, is considerably more intense in the spectrum of $(CH_3)_2PSCl$ than it is in the spectrum of $(CH_3)_2POCl$. It seems reasonable, therefore, to assume that this mode obtains a portion of its intensity from an accidentally degenerate in-plane Cl—P=S bending mode which is also expected to give rise to a polarized Raman line. It is believed that the out-of-plane Cl—P=S bending is not observed here owing to the similarity in the masses and bond lengths of the P—Cl and P=S bonds. Durig, *et al.*[2b], have shown that the bending modes for the molecules CH_3POF_2 and CH_3PSCl_2 behave as if the molecules had C_{3v} symmetry, and, consequently, only

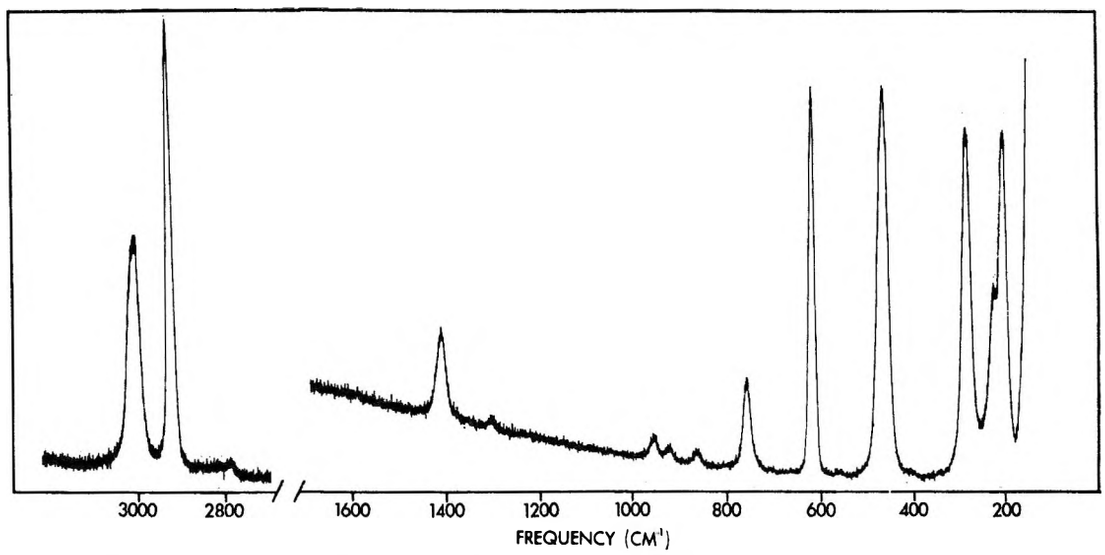

Figure 4. Raman spectrum of 0.6 ml of liquid $(CH_3)_2PSCl$.

Table II: Infrared and Raman Spectra of $(CH_3)_2PSCl$[a]

Infrared, liquid, cm^{-1}	Intens	Raman, liquid, cm^{-1}	Intens	Depolarization	Assignment
2990	s	2987	49	$^6/_7$ dp	ν_1, ν_2, ν_{16}, ν_{17} antisym CH_3 str
2915	s	2911	100	0.14 p	ν_3, ν_{18} sym CH_3 str
		2786	2	0.33 p	$2 \times (\nu_4, \nu_5, \nu_{19}, \text{or } \nu_{20}) = 2810\ cm^{-1}$
2255	w				$(\nu_4, \nu_5, \nu_{19}, \text{or } \nu_{20}) + (\nu_{22} \text{ or } \nu_{23}) = 2263\ cm^{-1}$
2215	vw				$(\nu_6 \text{ or } \nu_{21}) + \nu_7 = 2243\ cm^{-1}$
2155	w				$(\nu_4, \nu_5, \nu_{19}, \text{or } \nu_{20}) + \nu_{24} = 2155\ cm^{-1}$
2038	w				$(\nu_6 \text{ or } \nu_{21}) + \nu_{24} = 2039\ cm^{-1}$
1408	s	1405	21	$^6/_7$ dp	ν_4, ν_5, ν_{19}, ν_{20} antisym CH_3 def
1359	w				$\nu_{10} + \nu_{24} = 1358\ cm^{-1}$
1299	sh	1294	2	$^6/_7$ dp	ν_6, ν_{21} sym CH_3 def
1289	s				
1225	w				$\nu_7 + (\nu_{12} \text{ or } \nu_{13}) = 1226\ cm^{-1}$
954	s	950	6	0.26 p	ν_7 sym CH_3 rock (in-phase)
915	s	918	4	0.31 p	ν_8 antisym CH_3 rock (in-phase)
857	s	858	4	$^6/_7$ dp	ν_{22}, ν_{23} sym and antisym rock (out-of-phase)
750	s	750	21	$^6/_7$ dp	ν_9, ν_{24} sym and antisym PC_2 str
678	w				?
608	s	612	78	0.19 p	ν_{10} P=S str
		555	1	0.39 p	$2 \times (\nu_{12} \text{ or } \nu_{13}) = 556\ cm^{-1}$
455	s	457	93	0.23 p	ν_{11} P—Cl str
278	s	276	78	0.73 p	ν_{12}, ν_{13} PC_2 wag, Cl—P=S bend
		217	40	$^6/_7$ dp	ν_{25} PC_2 twist
196	s	198	74	0.76 p	ν_{14} PC_2 def
...		...			ν_{26} Cl—P=S bend
...		...			ν_{15}, ν_{27} CH_3 torsions

[a] Abbreviations used as in Table I.

three of the five bending modes are observed. Analogously, the $(CH_3)_2PSCl$ molecule would behave like a molecule with C_{2v} symmetry; the A'' Cl—P=S bending mode is transformed to the A_2 mode. An A_2 mode for a C_{2v} molecule is infrared inactive and is usually not observed in the Raman effect. An alternative explanation could be that the in- and out-of-plane Cl—P=S bending modes are degenerate since only a small split-

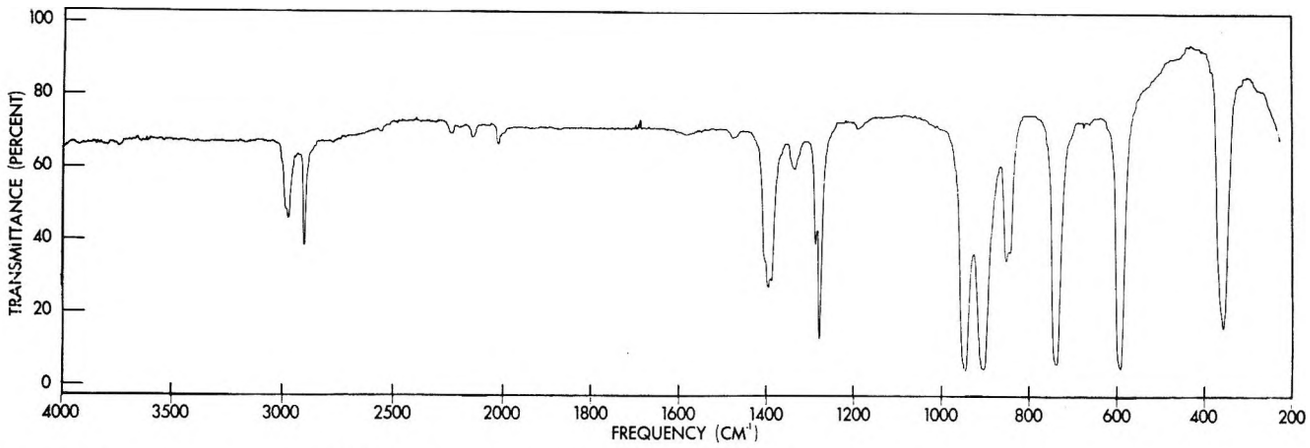

Figure 5. Infrared spectrum of $(CH_3)_2PSBr$ recorded as a contact film between CsBr plates.

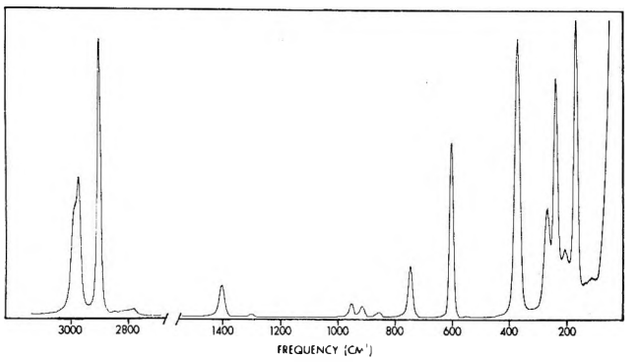

Figure 6. Raman spectrum of 5 ml of $(CH_3)_2PSBr$.

ting was found for the corresponding Cl—P=O bending modes. (See Table II for spectra of $(CH_3)_2PSCl$.)

Dimethylphosphinothioic Bromide. In the case of the two chlorides just discussed, the perturbation resulting from lowering the symmetry from C_{3v} to C_s was not enough to split the degeneracy of the two antisymmetric CH_3 stretching modes. The infrared and Raman spectra of dimethylphosphinothioic bromide, $(CH_3)_2PSBr$ (Figures 5 and 6), however, show a very definite shoulder on the high-frequency side of the band at around 3000 cm^{-1}. Both bands are depolarized and are located at 2990 and 2976 cm^{-1} in the Raman spectrum. It would, therefore, appear that the introduction of the bromide atom onto the molecule was sufficient to remove the degeneracy of the two antisymmetric stretching fundamentals. The strong polarized band at 2905 cm^{-1} is then assigned to the symmetric stretching. There is, however, still no coupling of the two methyl groups for these motions. Consequently, all three bands represent both one A′ and an A″ vibration which are coincident in frequency.

In the Raman spectrum of $(CH_3)_2PSBr$, only one band is found in the region of the methyl antisymmetric deformations. In the infrared spectrum, however, three bands are observed at 1406, 1397, and 1389 cm^{-1}. If the splitting of the degeneracy or the coupling of the methyl groups were greater, one would expect to see four bands in this region. It is believed that the four absorptions are so close together that an accidental degeneracy occurs. The symmetric deformations are again split into the out-of-phase and the in-phase motions at 1297 and 1286 cm^{-1}. The infrared spectrum of the $(CH_3)_2PSBr$ molecule shows four bands at 954, 913, 895, and 861 cm^{-1}; the first two frequencies are represented by polarized Raman bands at 947 and 909 cm^{-1}, respectively, while the corresponding Raman frequency of the fourth band at 848 cm^{-1} is depolarized. No Raman counterpart to the 895-cm^{-1} band was observed. Using the same arguments as were used for the two previous molecules, we have assigned the 954-cm^{-1} band to the in-phase symmetric CH_3 rocking whereas the 913-cm^{-1} band is ascribed to the in-phase motion of the antisymmetric methyl rocking mode. The out-of-phase A″ rocking vibrations are assigned at 895 cm^{-1} for the symmetric mode and at 861 cm^{-1} for the antisymmetric fundamental.

The three remaining bands in the infrared spectrum are all due to skeletal modes. For reasons discussed in the previous section, the band at 744 cm^{-1} is assigned to both the A′ and the A″ PC_2 stretching vibrations. The polarized band at 600 cm^{-1} is readily assigned as the P=S stretching mode whereas the other band, also strongly polarized, is ascribed to the P—Br stretching vibration of symmetry species A′ and is found at 368 cm^{-1} in the infrared spectrum and at 373 cm^{-1} in the Raman effect.

The far-infrared and Raman spectra of $(CH_3)_2PSBr$ each contain four bands below 300 cm^{-1}. The bands

Table III: Infrared and Raman Spectra of $(CH_3)_2PSBr$[a]

Infrared, liquid, cm^{-1}	Intens	Raman, liquid, cm^{-1}	Intens	Depolarization	Assignment
2982	m	2990	39	6/7 dp	ν_1, ν_{16} antisym CH_3 str
		2976	50	6/7 dp	ν_2, ν_{17} antisym CH_3 str
2905	m	2905	100	0.10 p	ν_3, ν_{18} sym CH_3 str
		2780	2	0.18 p	$2 \times (\nu_4, \nu_5, \nu_{19}, \text{or } \nu_{20}) = 2786\ cm^{-1}$
		2560	1	0.47 p	$2 \times (\nu_6 \text{ or } \nu_{21}) = 2576\ cm^{-1}$
2240	w	2247	1	6/7 dp	$(\nu_4, \nu_5, \nu_{19}, \text{or } \nu_{20}) + \nu_{23} = 2241\ cm^{-1}$
2202	vw	2205	1	0.64 p	$(\nu_6 \text{ or } \nu_{21}) + \nu_7 = 2235\ cm^{-1}$
2140	w	2140	1	6/7 dp	$(\nu_4, \nu_5, \nu_{19}, \text{or } \nu_{20}) + (\nu_9 \text{ or } \nu_{24}) = 2137\ cm^{-1}$
2027	w				$(\nu_6 \text{ or } \nu_{21}) + \nu_{24} = 2032\ cm^{-1}$
1415	sh				
1397	m	1393	12	6/7 dp	ν_5, ν_{19}, ν_{20} antisym CH_3 def
1389	sh				
1347	w				$\nu_{10} + \nu_{24} = 1344\ cm^{-1}$
1297	sh				
1286	s	1288	1	6/7 dp	ν_6, ν_{21} sym CH_3 def
1199	w				$2\nu_{10} = 1200\ cm^{-1}$
954	s	947	5	0.31 p	ν_7 sym CH_3 rock (in-phase)
913	s	909	4	0.64 p	ν_8 antisym CH_3 rock (in-phase)
895	sh				ν_{22} sym CH_3 rock (out-of-phase)
861	m	848	2	6/7 dp	ν_{23} antisym CH_3 rock (out-of-phase)
852	sh				$\nu_{10} + \nu_{12} = 864\ cm^{-1}$
746	s	744	18	6/7 dp	ν_9, ν_{24} sym and antisym PC_2 str
601	s	600	63	0.13 p	ν_{10} P=S str
		544	2	0.40 p	$\nu_{11} + \nu_{14} = 536\ cm^{-1}$
368	s	373	98	0.23 p	ν_{11} P—Br str
263	s	264	33	0.70 p	ν_{12} PC_2 wag, ν_{25} Br—P=S bend
239	s	235	79	0.50 p	ν_{13} Br—P=S bend
201	w	202	16	6/7 dp	ν_{26} PC_2 twist
168	s	163	97	0.78 p	ν_{14} PC_2 def
...		...			ν_{15}, ν_{27} CH_3 torsions

[a] Abbreviations used as in Table I.

which are observed in the far-infrared region (Figure 7) are too high in frequency to possibly be ascribed to the two methyl torsions. In the spectrum of $(CH_3)_2POCl$ is was observed that the PC_2 wagging mode was an extremely weak band, and this fact was used in assigning the strong band at 278 cm^{-1} in $(CH_3)_2PSCl$ to an accidental degeneracy of the PC_2 wagging and the S=P—Cl bending modes. The spectrum of $(CH_3)_2PSBr$ has a relatively strong absorption in this region, 263 cm^{-1}, which is again assigned to an accidental degeneracy of the PC_2 wagging and S=P—Br bending modes. An alternative explanation is that the PC_2 wagging mode is simply too weak to be observed in the spectra of $(CH_3)_2PSBr$ and $(CH_3)_2PSCl$, and the two strong bands may be ascribed simply to the X—P=S bending motions. The Br—P=S in-plane bending is ascribed to the strong, polarized Raman line at 235 cm^{-1}. The weak, depolarized band at 202 cm^{-1} is assigned to the PC_2 twisting mode of symmetry species A''. The final observed band is found at 163 cm^{-1} and is polarized; it is, therefore, assigned to the PC_2 deformation which is symmetric to the plane of symmetry. (See Table III for spectra of $(CH_3)_2PSBr$.)

Table IV is a summary of the fundamental frequencies of the three molecules studied in this work.

Summary

One of the interesting observations in this study is the demonstrated coupling of the PC_2 symmetric stretching vibration with the P=S stretching mode. In the spectrum of $(CH_3)_2POCl$, two definite absorptions are attributable to the PC_2 stretching modes: one at 751 cm^{-1} assigned to the antisymmetric vibration and the other at 696 cm^{-1} ascribed to the symmetric motion. However, in the spectra of $(CH_3)_2PSCl$ and $(CH_3)_2PSBr$ only one band can be assigned to the stretching motions of the PC_2 bonds, and these are found at 750 and 746 cm^{-1}, respectively. The vibrational energy levels of $(CH_3)_2POCl$ are thought to be unperturbed, and the two PC_2 stretching motions ab-

Table IV: Summary of the Fundamental Frequencies

Description of mode	$(CH_3)_2POCl$	$(CH_3)_2PSCl$	$(CH_3)_2PSBr$
A′ Symmetry Species			
Antisym CH_3 str	2988	2990	2990[b]
Antisym CH_3 str	2988	2990	2976[b]
Sym CH_3 str	2916	2915	2905
Antisym CH_3 def[a]	1412	1408	1415
Antisym CH_3 def[a]	1400	1408	1397
Sym CH_3 def	1303	1299	1297
P=O or P=S str	1246	608	601
Sym CH_3 rock	930	954	954
Antisym CH_3 rock	906	915	913
PC_2 str	696	750	746
P—X (X = Cl, Br) str	488	455	368
O=P—X or S=P—X bending	334	278	239
PC_2 wag	298	278	263
PC_2 twist	237	217[b]	201
CH_3 torsion	...	...	...
A″ Symmetry Species			
Antisym CH_3 str	2988	2990	2990[b]
Antisym CH_3 str	2988	2990	2976[b]
Sym CH_3 str	2916	2915	2905
Antisym CH_3 def[a]	1412	1408	1389
Antisym CH_3 def[a]	1400	1408	1389
Sym CH_3 def	1292	1289	1286
Sym CH_3 rock	865	857	895
Antisym CH_3 def	865	857	861
PC_2 str	751	750	746
O=P—X or S=P—X bending	367	...	263
PC_2 def	237	196	168
CH_3 torsion	...	...	...

[a] The exact assignment of these frequencies to the four modes is unknown. [b] Raman frequencies; all others are infrared frequencies.

sorb quite independently. In the case of $(CH_3)_2PSCl$ and $(CH_3)_2PSBr$, however, the unperturbed vibrational energies of the symmetric PC_2 stretching mode and P=S stretching motion are believed to be sufficiently close to one another to cause a strong repulsion of the two symmetric levels. The result is that the A′ PC_2 stretching fundamental is shifted to a higher frequency and covers the A″ PC_2 stretching mode. These conclusions are in agreement with the work of Hooge and Christen,[17] who state that the isolated P=S stretching frequency should be 675 cm^{-1}.

Chittenden and Thomas[3] have done considerable work on the P=S stretching fundamentals, and they state that two bands arise from the P=S motion, similar to the P=O doublets discussed earlier. The two bands of the doublet, however, are split by some 150 cm^{-1}, the over-all regions being 685–862 and 550–730 cm^{-1}. The evidence that both bands arise from the P=S motion is the fact that both bands disappear during the isomerization of phosphorothionates to phosphorothioates

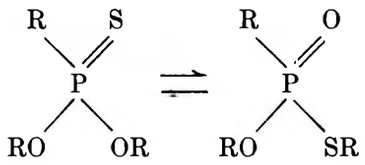

This evidence seems extremely weak if one considers the fact that, upon isomerization, the P—C bond also disappears and, as mentioned in the text, that is the region expected for the PC stretching modes. Thus, it would appear that the disappearance of both bands upon isomerization is in excellent agreement with the assignments put forth in this paper. In conclusion, we believe many of the assignments for the P=S stretching vibration which were classified as band I by Chittenden and Thomas[3] are more appropriately described to other motions in the organophosphorus compounds. In order to give more convincing data for two P=S stretching modes of vastly different frequencies, complete vibrational assignments are needed for the molecules in question.

Acknowledgment. The authors gratefully acknowledge the financial support given this work by the National Science Foundation.

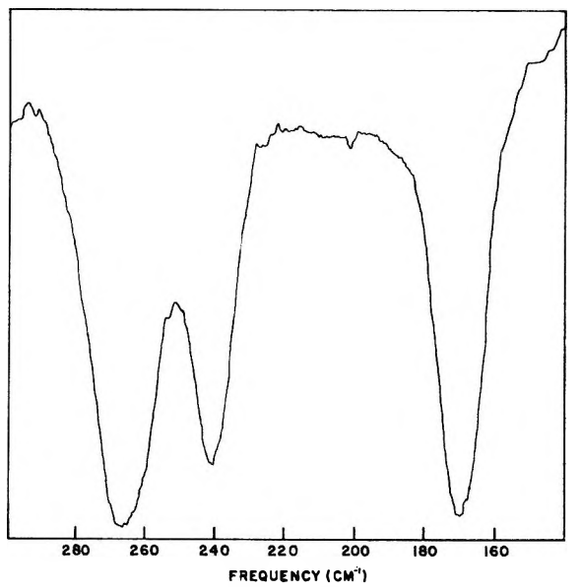

Figure 7. Region of absorption of $(CH_3)_2PSBr$ in the far-infrared region. The spectrum was recorded as a benzene solution in 1-mm polyethylene liquid cells.

(17) F. N. Hooge and P. J. Christen, *Rec. Trav. Chim.*, **77**, 911 (1958).

The Electrical Conductivity of Aqueous 0.03 to 4.0 *M* Potassium Chloride Solutions under Hydrostatic Pressure

by R. A. Horne and R. P. Young

Arthur D. Little, Inc., Cambridge, Massachusetts *(Received April 5, 1967)*

The electrical conductivity of aqueous KCl solutions has been measured over the concentration range 0.03–4.0 *M*, the temperature range −8 to +20°, and at pressures up to 4000 kg/cm². The effect of these variables on conductivity is similar to their effect on viscosity—generally speaking, they all tend to destroy the regions of structure in water and cause water to behave more like a "normal" liquid. Inasmuch as their effects are similar, the operancy of one variable tends to diminish the relative effectiveness of a second. Thus, increasing the temperature or adding electrolyte tends to smear out the anomalous minimum in the pressure dependence of the relative viscosity or the anomalous maximum in the pressure dependence of the relative conductance.

Introduction

A great many measurements have been reported on the electrical conductivity of aqueous electrolytic solutions under hydrostatic pressure;[1] for example, Körber;[2] Tamann and Rohmann;[3] Adams and Hall;[4] Zisman;[5] Buchanan and Hamann;[6] Hamann and Strauss;[7] Ellis;[8] Fischer, Mann, and Vaughan;[9] Brummer and Hills;[10] Fischer;[11] Horne, Myers, and Frysinger;[12] and Horne and Courant[13] all have examined the system H_2O–KCl, but the more recent work has been concerned with solutions 0.10 *M* or more dilute with particular emphasis given to the estimation of limiting conductances under pressure, and more concentrated solutions have been neglected.

Measurements of the viscosity of water under pressure have shown that pressure is even more effective than temperature in destroying the less-dense structured regions in liquid water.[1,14] Walden's rule is a good approximation for aqueous electrolytic solutions thereby indicating that the effect of temperature on the hydration atmospheres of ions in solution, at least that part of its hydration that an ion takes with it when it moves, is relatively modest; whereas the application of pressure tends to break up the water structure near ions and by thus in effect decreasing their radii, gives rise to a more abrupt increase in electrical conductivity with increasing pressure than expected from the viscosity and volume changes.[1,5,15,16] In addition to temperature and pressure the presence of an electrolyte is known to affect the structure of water both in the immediate neighborhood of the ions (electrostriction) and more remotely (the total hydration atmosphere). The over-all effect of some ions is to enhance the water structure whereas others are structure breakers.[17] At 1 atm and 20° a structure-making ion such as Na^+

(1) R. A. Horne, *Advan. High Pressure Res.*, in press.

(2) F. Körber, *Z. Physik. Chem.*, **67**, 212 (1909).

(3) G. Tamann and A. Rohmann, *Z. Anorg. Allgem. Chem.*, **183**, 1 (1929).

(4) L. H. Adams and R. E. Hall, *J. Phys. Chem.*, **35**, 2145 (1931).

(5) W. A. Zisman, *Phys. Res.*, **39**, 151 (1932).

(6) J. Buchanan and S. D. Hamann, *Trans. Faraday Soc.*, **49**, 1425 (1953).

(7) S. D. Hamann and W. Strauss, *ibid.*, **51**, 1684 (1955).

(8) A. J. Ellis, *J. Chem. Soc.*, 3689 (1959).

(9) A. Fischer, B. R. Mann, and J. Vaughan, *ibid.*, 1093 (1961).

(10) S. R. Brummer and G. J. Hills, *Trans. Faraday Soc.*, **57**, 1823 (1961).

(11) F. H. Fisher, *J. Phys. Chem.*, **66**, 1607 (1962).

(12) R. A. Horne, B. R. Myers, and G. R. Frysinger, *J. Chem. Phys.*, **39**, 2666 (1963).

(13) R. A. Horne and R. A. Courant, *J. Chem. Soc.*, 3548 (1964).

(14) R. A. Horne and D. S. Johnson, *J. Phys. Chem.*, **70**, 2182 (1966).

(15) R. A. Horne, *Nature*, **200**, 418 (1963).

(16) R. A. Horne, *Water Resources Res.*, **1**, 263 (1965).

(17) R. W. Gurney, "Ionic Processes in Solution," McGraw-Hill Book Co., Inc., New York, N. Y., 1953, Chapter 9.

has four water molecules tightly bound in its electrostricted innermost solvation sheath, but it has a total of 37 waters in its total structure-enhanced hydration atmosphere or almost exactly the same number of waters as in the average Frank–Wen cluster at the same temperature.[18] Water is only 55.6 *M* in water; clearly then, between 1 and 2 *M* the ions will begin to compete seriously with one another for solvent molecules. In the cases of Li^+ and Na^+, but not K^+, Good[19] has actually observed inflections in the Arrhenius activation energy of viscous flow *vs.* electrolyte concentration curves presumably corresponding to the onset of overlap of the ions' hydration envelopes.[18]

In view of the foregoing considerations it seemed of interest to examine the transpost properties of aqueous electrolytic solutions under the simultaneous influence of all three structure-altering parameters—temperature, pressure, and electrolyte—in order to clarify the nature of the relationships among these several factors.

Experimental Section

The apparatus and procedures for measuring the electrical conductivity of aqueous solutions under pressure have been described previously.[20] A capillary-type conductivity cell was used.

Results

Figure 1 shows the equivalent conductances at 1 atm as a function of temperature with values from the literature also shown for purposes of comparison. The agreement is satisfactory.

Figures 2–6 show the relative specific conductances, $K_p/K_{1\ atm}$, of 0.03, 0.10, 0.30, 1.00, and 3.00 *M* KCl solutions as a function of hydrostatic pressure. In order to obtain absolute specific conductances it is only necessary to convert the equivalent conductances in Figure 1 to 1-atm specific conductances and multiply by the relative conductances in Figures 2–6. The calculation of absolute equivalent conductances at pressure entails a correction for volume changes. In Figure 6, the old data of Körber[2] for 3.0 *M* KCl at 20° are also plotted, and their agreement with the present results is only fair; in particular, the curve does not fall off as steeply above the maximum with increasing pressure as do more modern measurements. The measurements of Adams and Hall[4] on 15% (approximately 2.6 *M*) NaCl at 30° appear to be commensurate with the present results on 3.0 *M* KCl at 20°.

Discussion

The application of hydrostatic pressure, in addition to destroying the less-dense structured regions in bulk liquid water, unlike temperature, is also effective at destroying the local water structure of the hydration

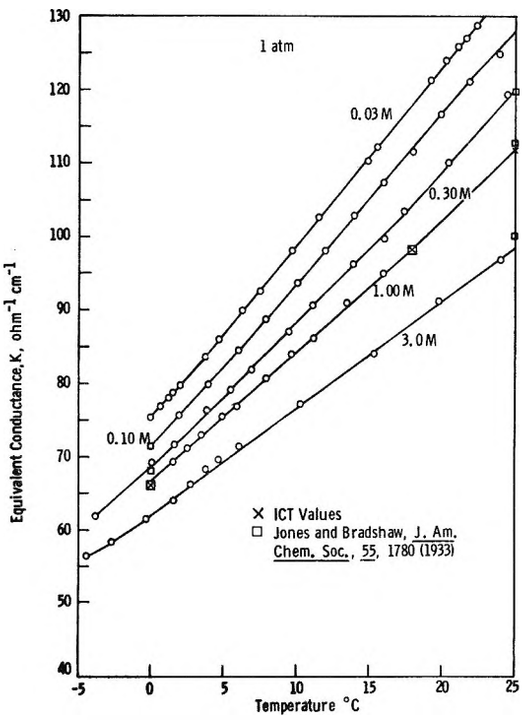

Figure 1. Temperature dependencies of the equivalent conductivities of aqueous 0.03, 0.10, 0.30, 1.00, and 3.00 *M* KCl solutions at 1 atm.

atmosphere of ions in solution (see above) and recently the dehydration of solid hydrated salts at 25° by high pressure has been demonstrated.[21] As a consequence of the dehydration of ions in solution the relative conductance increases more steeply with pressure (Figures 2–6) than does the product $(V_1/V_p)(\eta_1/\eta_p)$ of the reciprocal of the relative specific volume and relative viscosity (Figure 7). Figure 7 shows the product of the reciprocals of the relative viscosities and specific volumes of pure water as a function of pressure. For pure water the specific volume data at 0, 10, 20, and 30° of Bridgman, as quoted by Dorsey,[22] and the viscosity data of Horne and Johnson[14] at 2, 10, and 20° and of Bett and Cappi[23] at 30° are used. Comparison of the Figures for $K_p/K_{1\ atm}$ *vs.* *P* for the dilute solutions with Figure 7 confirms the dehydration phenomenon. However, the pressure dependence of $K_p/K_{1\ atm}$

(18) R. A. Horne and J. D. Birkett, *Electrochim. Acta*, **12**, 1153 (1967).

(19) W. Good, *ibid.*, **9**, 203 (1964).

(20) R. A. Horne and G. R. Frysinger, *J. Geophys. Res.*, **68**, 1967 (1963).

(21) R. R. Sood and R. A. Stager, *Science*, **154**, 388 (1966).

(22) N. E. Dorsey, "Properties of Ordinary Water-Substance," Reinhold Publishing Corp., New York, N. Y., 1940.

(23) K. E. Bett and J. B. Cappi, *Nature*, **207**, 620 (1965).

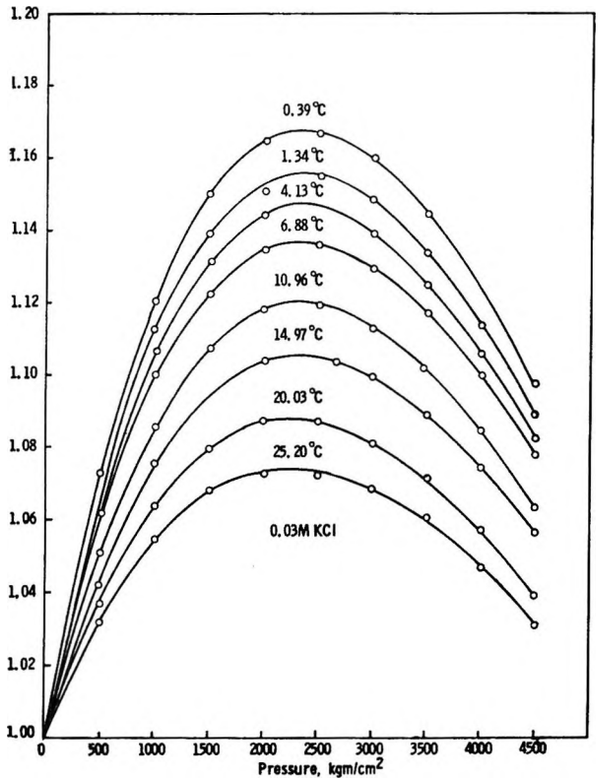

Figure 2. Relative specific conductance of an aqueous 0.03 *M* KCl solution.

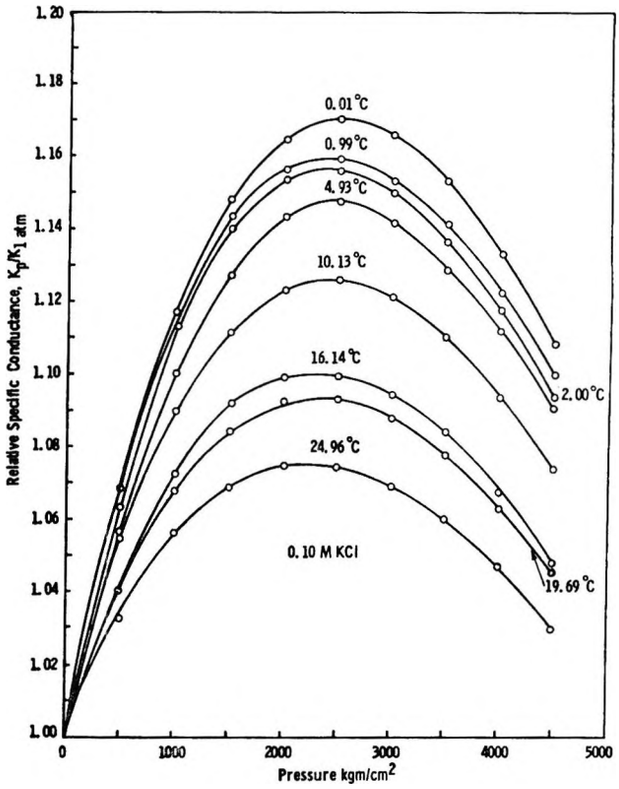

Figure 3. Relative specific conductance of an aqueous 0.10 *M* KCl solution.

for the more concentrated solutions should not be compared with $(V_1/V_p)(\eta_1/\eta_p)$ for pure water. Unfortunately, the only aqueous electrolytic solution for which there appears to exist reliable data for both specific volumes and viscosities under pressure is sea water. $(V_1/V_p)(\eta_1/\eta_p)$ for sea water is shown in Figure 7 as dashed curves. The specific volume data are for 25.568 °/₀₀ salinity sea water at 1.23, 10.15, and 20.05°[24] and the viscosity data for 35.00 °/₀₀ salinity sea water (approx 0.5 *M* NaCl) at 0.84, 10.13, and 20.14°.[25] The sea water values (Figure 7) indicate that electrolyte addition lowers $(V_1/V_p)(\eta_1/\eta_p)$; thus, although the K_p/K_1 for 3.0 *M* KCl at 20° and 2000 kg/cm² has fallen to only 1.03, there is no reason for supposing that this ratio is not still greater than the corresponding value of $(V_1/V_p)(\eta_1/\eta_p)$.

Figure 8 is a plot of the K_p/K_1 at 2000 kg/cm² near 0 and 20° as a function of electrolyte concentration. Perhaps an even more instructive plot would be $(K_pK_1)(V_1/V_p)(\eta_1/\eta_p)$ *vs.* concentration, but unfortunately, insufficient data are available. Figure 8 indicates that as the concentration increases the extent of dehydration at a given pressure diminishes, as evidenced by a decrease in the value of $K_p/K_{1\ atm}$. Alternatively, the maximum value of $K_p/K_{1\ atm}$ can be plotted *vs.* temperature for various pressures. The resulting Figure 9 indicates that the dehydrating effects of both temperature and pressure become less marked as the concentration increases, for in the more concentrated solutions the competition for waters is keen, and the waters upon which a given ion can make a claim are held more strongly; that is to say, in more concentrated solutions there are no, or at least fewer, weakly bound waters. The curves for the 0.03 and 0.10 *M* solutions fall very nearly on the shown curve for the 0.30 *M* solution.

When an electrolyte is dissolved in water the coulombic fields of the ions, especially the cations, electrostrict the nearby water dipoles, binding them strongly and compactly so that the reaction is accompanied by

$$M^+ + H_2O \longrightarrow M(H_2O)^+ \text{ solution} \qquad (1)$$

an over-all volume decrease. Therefore, simply by

(24) W. Wilson and D. Bradley, "Specific Volume, Thermal Expansion, and Isothermal Compressibility of Sea Water," U.S.N. Ordnance Laboratory Report NOLTR-66-103, June 2, 1966.

(25) R. A. Horne and D. S. Johnson, *J. Geophys. Res.*, **71**, 5275 (1966).

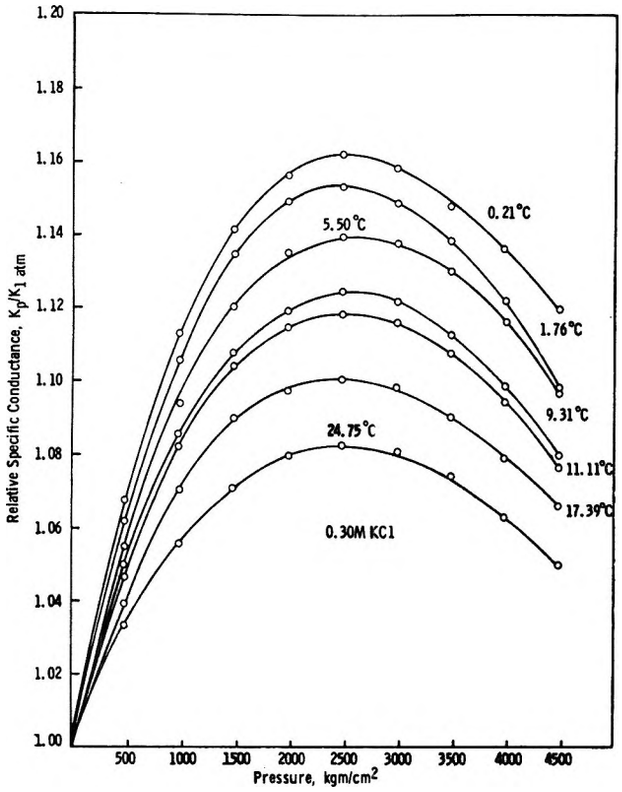

Figure 4. Relative specific conductance of an aqueous 0.30 *M* KCl solution.

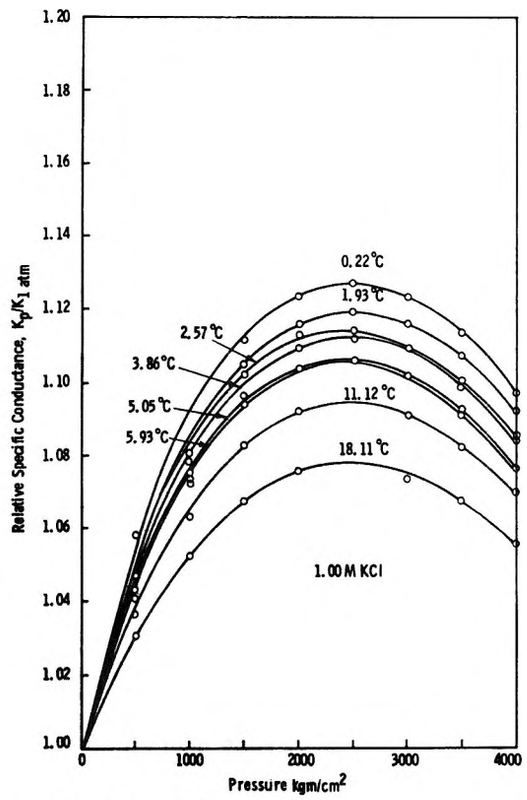

Figure 5. Relative specific conductance of an aqueous 1.00 *M* KCl solution.

the application of the principle of LeChatelier, one expects that the application of pressure should stabilize rather than disrupt ionic hydration, which is an exactly opposite conclusion from that drawn above on the basis of the more rapid increase in conductivity with increasing pressure than expected from the specific volume and viscosity changes.

In order to resolve this difficulty we have proposed that the structure-enhanced zone of the Frank–Wen model of ionic hydration[26] (which consists of an inner water structure-enhanced zone surrounded by an outer structure-broken zone) can in turn be subdivided into two further zones: an inner zone immediately adjacent to the ion consisting of tightly bound electrostricted water more dense than the water at some great distance from the ion, and a second zone which is in effect a Frank–Wen cluster and which is less dense than the water at some great distance from the ion.[1,18] In the case of NaCl the total number of molecules in the structure-enhanced zone (electrostricted *plus* cluster water) can be estimated from the concentration dependence of the activation energy of viscous flow[19] and comes out to be the same as the average number of molecules in a Frank–Wen cluster in pure water at the

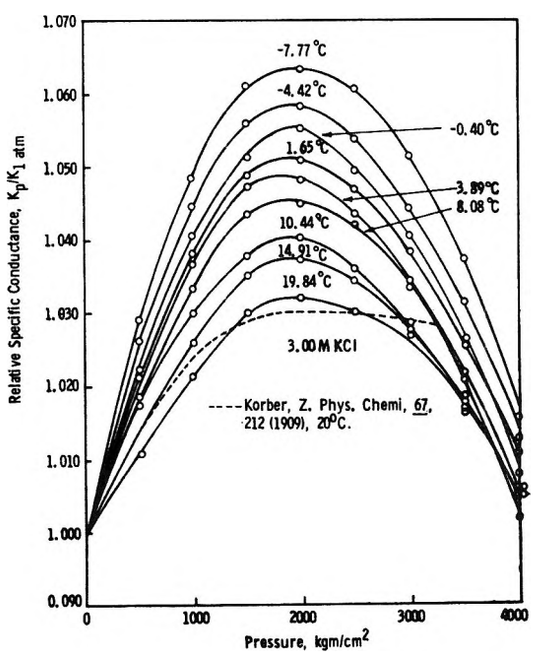

Figure 6. Relative specific conductance of an aqueous 3.00 *M* KCl solution.

(26) H. S. Frank and W. Y. Wen, *Discussions Faraday Soc.*, **24**, 133 (1957).

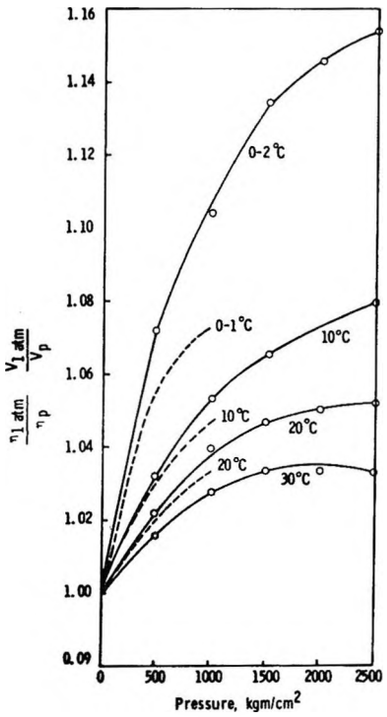

Figure 7. Pressure dependencies of the product of the reciprocals of the relative specific volume and viscosities of pure water and sea water (dashed curves).

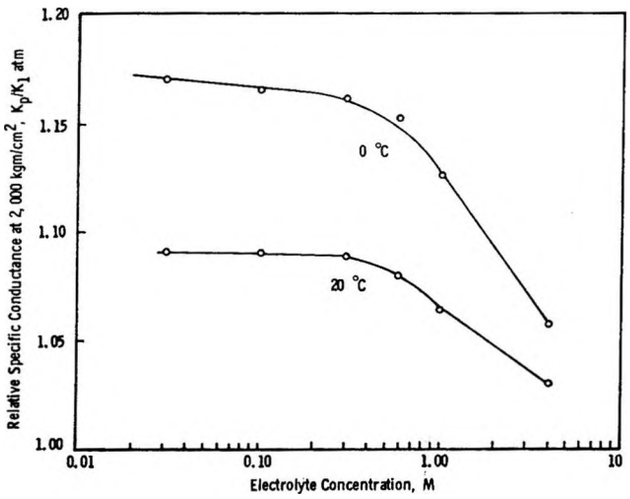

Figure 8. Relative specific conductances at 2000 kg/cm² as a function of electrolyte concentration.

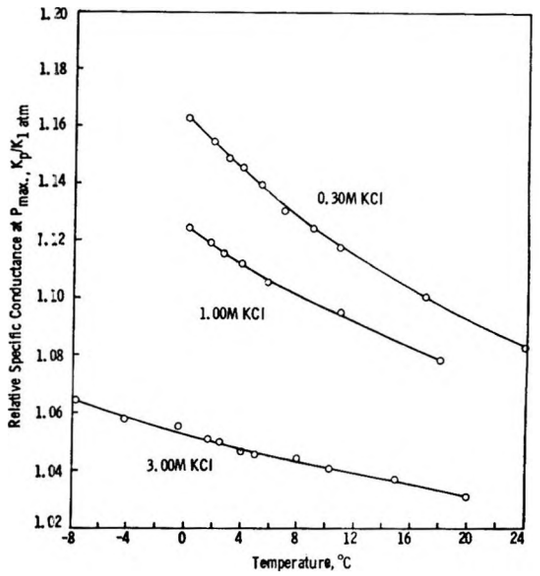

Figure 9. Maximum relative specific conductances as a function of temperature.

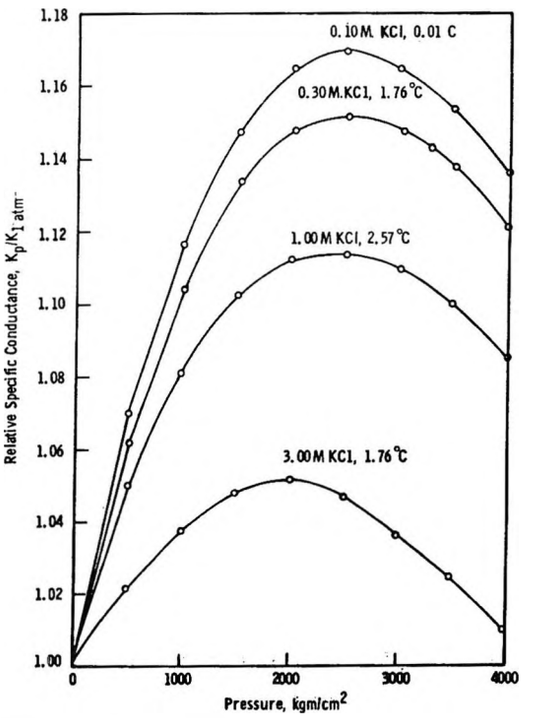

Figure 10. The temperature dependence of the pressure effects on conductivity near 2°.

same temperature as estimated by Némethy and Scheraga.[27]

As the hydrostatic pressure is increased the less dense Frank–Wen clusters surrounding the ions are destroyed. Then, inasmuch as the dense electrostricted region is relatively incompressible, a pressure is reached at which the density of the bulk water exceeds that of the electrostricted water and the electro-

(27) G. Némethy and H. A. Scheraga, *J. Chem. Phys.*, **36**, 3382 (1962).

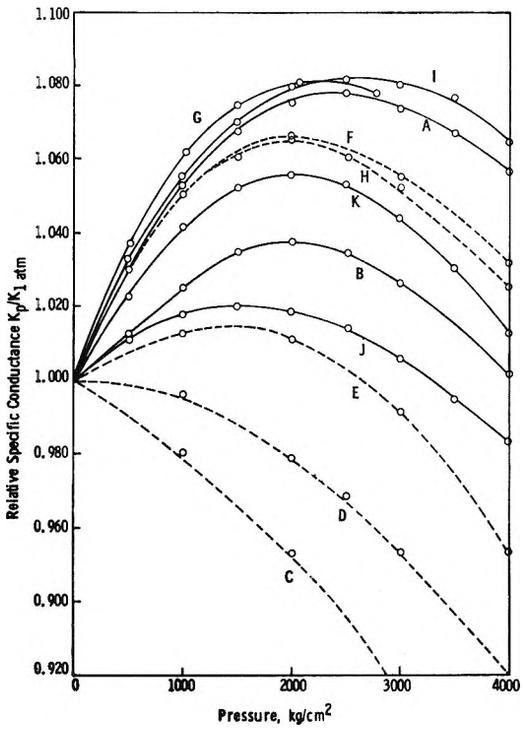

Figure 11. The concentration dependence of the pressure effects on conductivity in the 15–30° range: (A) 1.00 *M* KCl at 18.114°, (B) 3.00 *M* KCl at 14.91°, (C) 4.5 *m* NaCl at 30°, (D) 3.5 *m* NaCl at 30°, (E) 2.6 *m* NaCl at 30°, (F) 0.5 *m* NaCl at 30°, (G) 0.05 *m* KCl at 25° [for (C)–(G), $R_{1\ atm}/R_p$],[4] (H) 0.01 *N* NaCl at 30°,[5] (I) 0.30 *M* KCl at 24.74°, (J) 4.00 *M* KCl at 19.89°, (K) 2.00 *M* KCl at 19.92°.

stricted region begins to break up. Previously we estimated[28] that by 5000 kg/cm² the number of water molecules in the first hydration sheath or electrostricted region of Na^+ is reduced from 4 to 1.

If eq 1 is rewritten in more detail as

$$M^+ + (e + c + B)H_2O \longrightarrow M^+(H_2O)_e(H_2O)_c(H_2O)_B \quad (2)$$

where the subscripts e, c, and B represent electrostricted and clustered water and the region of broken water structure, respectively, then for electrostriction to be observed it is only necessary that

$$|\Delta V_{H_2O,B}| + |\Delta V_{H_2O,e}| > |\Delta V_{H_2O,c}| \quad (3)$$

and hence the observed volume change becomes

$$|\Delta V_{H_2O,B}| + |\Delta V_{H_2O,e}| - |\Delta V_{H_2O,c}|$$

and not

$$|\Delta V_{H_2O,e}|$$

The concentration dependence of the pressure effects is shown more clearly in Figures 10 and 11, where the relative specific conductances are plotted *vs.* pressure at a low (near 2°) and a higher (near 20°) temperature for various concentrations of KCl. Notice that Figure 11 also reports results of measurements on 2.0 and 4.0 *M* KCl. Comparison of Figures 10 and 11 indicates that the effect of the presence of electrolyte becomes more important and makes a correspondingly larger change in the pressure effect at lower temperatures which is what one might expect since there is more water structure to be perturbed by the combined effects of electrolyte and pressure at lower temperatures. In Figure 11 the relative resistance reciprocal, $R_{1\ atm}/R_p$, for NaCl solutions as measured by Adams and Hall[4] are also plotted (as dashed lines) for purposes of comparison. The curves for NaCl and KCl exhibit the same general features, namely the maximum in $K_p/K_{1\ atm}$ *vs.* P tends to diminish with increasing electrolyte concentration. However, in detail the two curves differ widely and increasing the concentration of KCl is much less effective at lowering $(K_p/K_{1\ atm})_{max}$ than increasing the concentration of NaCl. In fact, in the latter case $(K_p/K_{1\ atm})_{max}$ has disappeared by the time a 3.5 *M* solution is reached. Adams and Hall[4] also measured a 0.05 *M* KCl solution at 25° and obtained results in agreement with the present experiments; hence, the differences between KCl and NaCl are presumably real. The much more pronounced concentration dependence in the case of NaCl may be due to the fact that at 25° NaCl is a structure maker with a viscosity *B* coefficient of +0.078, whereas KCl is a weak structure breaker with a *B* coefficient of only −0.014.[17] Na^+ is more heavily hydrated than K^+; at 25° the former has 34 and the latter 10 water molecules in their *total* water-structure-enhanced hydration atmospheres.[18] One might expect that, inasmuch as the anomalously steep increase of $K_p/K_{1\ atm}$ with P arises from the dehydration of the ions, $d(K_p/K_{1\ atm})/dP$ below 1000 kg/cm² should always be greater for NaCl than for KCl which is contrary to Figure 11. But, as pointed out earlier,[15] direct comparisons between structure makers and breakers are uncertain. The most valid way of comparison would be to contrast the relative conductivities with the reciprocal of the relative volume–viscosity product. Recent work[14,23] has indicated that older studies of the viscosity of compressed pure water are unreliable and that the addition of an electrolyte,[25,29] again, has much less effect on the viscosity of water under pressure than reported in the old

(28) R. A. Horne, R. A. Courant, and D. S. Johnson, *Electrochim. Acta*, 11, 987 (1966).

(29) R. A. Horne and D. S. Johnson, *J. Phys. Chem.*, 71, 1147 (1967).

work of Cohen.[30] And, as a final difficulty, there are no reliable measurements on the viscosities of concentrated aqueous KCl solutions under pressure.

The values of $(K_p/K_{1\ atm})_{max}$ and the pressure at which it appears, P_{max}, both decrease with increasing concentration in a nonlinear fashion (Figures 2–6, 10, and 11). The former phenomenon is represented in greater detail in Figure 12 where $(K_p/K_{1\ atm})_{max}$ is plotted *vs.* electrolyte concentration on a logarithmic scale for a low (near 2°) and a higher (near 20°) temperature. At 20° and for KCl concentrations below approximately 0.5 *M* there appears to be plenty of water to satisfy the hydration needs of the ions, the hydration atmospheres are relatively independent of one another, and there is little concentration dependence of $(K_p/K_{1\ atm})_{max}$. However, above approximately 0.5 *M* there are insufficient water molecules, a given ion can lay exclusive claims on fewer waters, and as a result $(K_p/K_{1\ atm})_{max}$ begins to decrease steeply with increasing electrolyte concentration. In going from 20° to near 2°, just as the number of water molecules in the Frank–Wen clusters increases, the number of waters in a cation's total hydration atmosphere increases. This greater hydration makes $(K_p/K_{1\ atm})_{max}$ greater and causes it to begin to diminish at smaller concentrations (Figure 12). Extrapolation of the curve for KCl near 20° gives $(K_p/K_{1\ atm})_{max}$ intercepting unity at some concentration between 4 and 6 *M*, a range which, interestingly enough, straddles the saturation concentration. This intercept also corresponds to roughly 10 waters per K^+ (neglecting anion hydration) which is not too different from the above-mentioned estimate of the number of waters in the total structure-enhanced hydration atmosphere. With a certain amount of imagination an analogous curve (dashed curve in Figure 12) can be drawn for NaCl at 30° on the basis of the results of Adams and Hall.[4] This curve intercepts unity at a concentration corresponding to roughly about 15 waters per Na^+ which is smaller than the number of waters in the total hydration atmosphere (see above). Hitherto we had felt that the number of strongly bound, electrostricted waters in the hydration atmosphere of an ion (the "hydration number" in the conventional sense) is small, being 4 for Na^+. However, consideration of the electrostriction and densities of NaCl solutions[31] leads to the conclusion that of the total hydration atmosphere of Na^+ half the waters are electrostricted and half are cluster water. The number of electrostricted waters is then 17 which is comparable to the number yielded above by the intercept. That the interpretation of the KCl and NaCl intercepts should be different, the former corresponding to the ion's total hydration atmosphere, the latter to the electrostricted sub-zone of the total

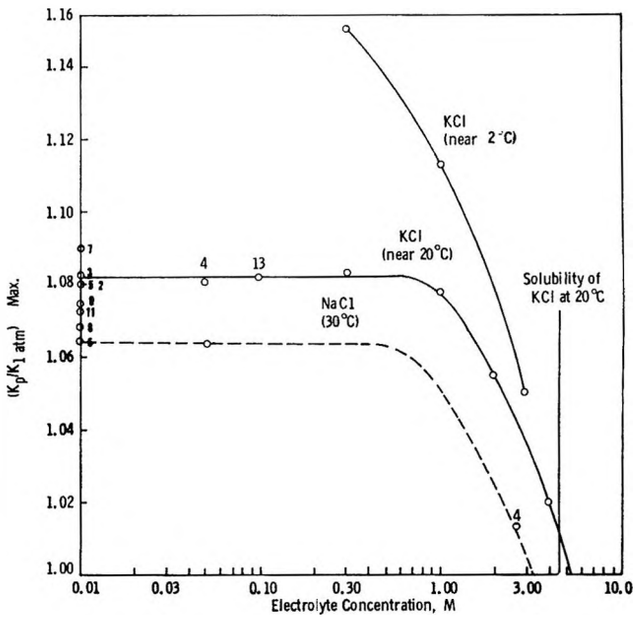

Figure 12. Dependence of the maximum relative conductance on electrolyte concentration (the numbers beside some of the points are references).

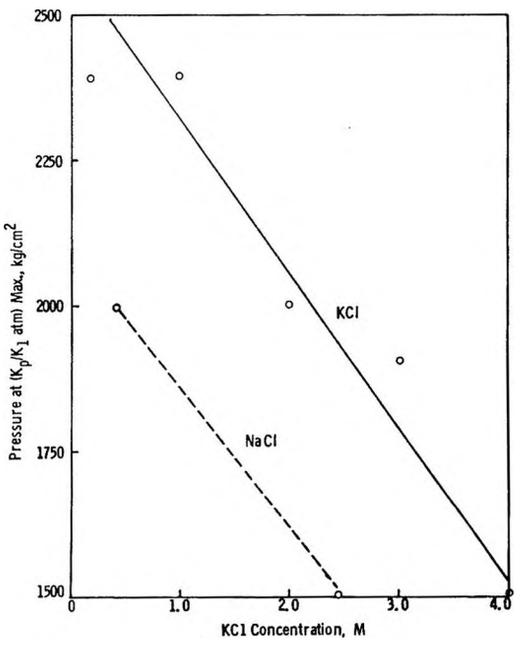

Figure 13. Concentration dependence on the pressure of maximum relative conductivity.

hydrated atmosphere, is not entirely implausible inasmuch as the two ions are fundamentally different, the

(30) R. Cohen, *Ann. Physik*, **45**, 666 (1892).

(31) R. A. Horne, "Electrostriction and the Dehydration of Ions Under Pressure," Arthur D. Little, Inc., Technical Report 26, Office of Naval Research Contract Nonr-4424(00), Nov 30, 1966.

one being a water structure breaker, the other a structure maker.

Figure 13 shows a plot of the pressure at which $(K_p/K_{1\ atm})_{max}$ appears near 20° for KCl (based on Figure 11) and NaCl (based on data from Adams and Hall[4]). As noted above, P_{max} decreases with increasing electrolyte concentration.

In the past we have found it useful to analyze transport processes using the Arrhenius activation energy, E_a, simply calculated from the relations

$$K = Ce^{-E_a/RT} \tag{4}$$

and

$$E_a = (\log K_2 - \log K_1)4.576(T_2T_1)\ \Delta T \tag{5}$$

since that parameter appears to be highly dependent on structural changes in liquid water.[28] Despite its utility this procedure is not entirely rigorous. For example we have assumed that the preexponential C is a "constant" and have thereby introduced an error by neglecting volume changes. If, as in the present experiments, E_a is calculated over at ΔT of 2°, for 1.0 *M* KCl at 2000 kg/cm², for example, the E_a calculated from eq 5 is about 1.7% larger than E_a corrected for the volume changes. If a larger ΔT of 10° were used the error would have increased to 3.3%. In an earlier paper[12] we tried to circumvent this difficulty by calculating E_a of the molal conductances but it soon became clear that this served only to confuse the readers; hence, since the correction involved is less than experimental error, the usage was abandoned.

The Arrhenius energy of activation of the electrical conductivity of "normal," strong, 1:1 electrolytes exhibits a maximum near 4°.[32] The decrease in E_a above 4° with increasing temperature is attributable to the facilitation of solvent vacancy formation, the rate-determining step, by thermal expansion of the liquid while the decrease in E_a below 4° with decreasing temperature has been attributed to the greater ease of hole formation in less-dense structured forms of liquid water more prevalent in that temperature region.[32] In the case of sea water the maximum decreases in value and shifts to lower temperatures as the electrolyte concentration increases.[33] If D_2O is substituted for H_2O, the maximum shifts to higher temperatures although the shift is less marked than the corresponding shift in the temperature of maximum density.[34] The maxima occur both for water structure makers (LiCl) and structure breakers (CsCl)[35] but do not occur for the electrical conductance of acid solutions as long as the solution is sufficiently dilute so that the Grotthuss contribution dominates the protonic conductance:[36] for the conductance of very heavily hydrated electro-

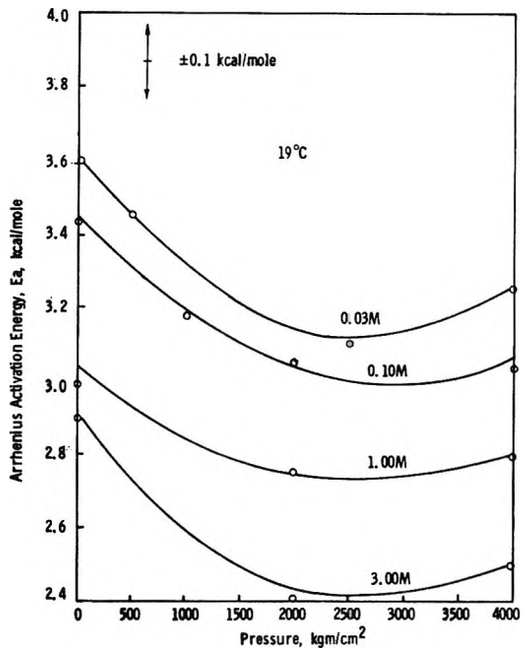

Figure 14. The pressure dependence of the Arrhenius activation energy of electrical conduction for various concentrations at 19°.

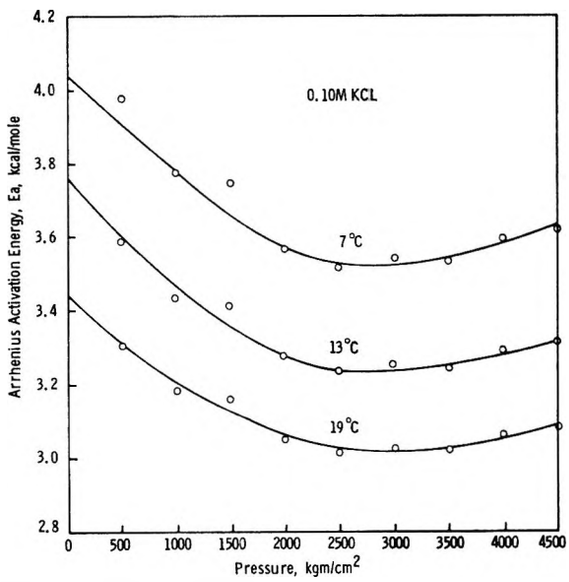

Figure 15. E_a *vs.* P curves for 0.10 *M* KCl at various temperatures.

(32) R. A. Horne and R. A. Courant, *J. Phys. Chem.*, **68**, 1258 (1964).

(33) R. A. Horne and R. A. Courant, *J. Geophys. Res.*, **69**, 1152 (1964).

(34) R. A. Horne and D. S. Johnson, *J. Phys. Chem.*, **71**, 1936 (1967).

(35) R. A. Horne and D. S. Johnson, *J. Chem. Phys.*, **45**, 21 (1966).

(36) R. A. Horne and R. A. Courant, *J. Phys. Chem.*, **69**, 2224 (1965).

lytes such as $MgSO_4$,[37] or for the viscosity of water at 1 atm;[38] although, rather unexpectedly, maxima do appear in E_a of viscous flow of water under pressure,[14] thereby indicating that these other transport processes involve a mechanism different from that of normal conductivity.[28]

The present results confirm earlier observations that E_a decreases with increasing electrolyte concentration (Figure 14). At elevated pressures and in the more concentrated solutions the maximum in E_a *vs.* T appears to shift to *higher* temperature values, which is just exactly the opposite of what one might expect inasmuch as the temperature of maximum density of pure water decreases with increasing pressure. We have no explanation for this phenomenon nor are we entirely convinced of its reality since it appears to be contingent on the way in which the curves are weighted through the experimental values. No such uncertainty, however, attaches to the pressure dependence of E_a (Figures 14 and 15). As reported earlier[12] E_a *vs.* P exhibits a minimum between 2000 and 3000 kg/cm^2. For a given electrolyte concentration (0.10 M, for example) E_a *vs.* P gives a family of parallel curves for different temperatures (Figure 15).

Acknowledgment. This work was supported in part by the Office of Naval Research.

(37) R. A. Horne and D. S. Johnson, *J. Chem. Phys.*, **44**, 2946 (1966).

(38) R. A. Horne, R. A. Courant, D. S. Johnson, and F. F. Margosian, *J. Phys. Chem.*, **69**, 3988 (1965).

The Effect of Crystallization Temperature and Molecular Weight on the Melting Temperature of Linear Polyethylene[1]

by M. Gopalan and L. Mandelkern

Department of Chemistry and Institute of Molecular Biophysics, Florida State University, Tallahassee, Florida
(Received April 7, 1967)

A theoretical and experimental study is reported of the dependence of the apparent melting temperature on the crystallization temperature for molecular-weight fractions of linear polyethylene. Particular attention is given to the influence of molecular weight and level of crystallinity. A critical examination is given of the extrapolation methods that have been proposed to obtain the equilibrium melting temperature from this kind of data. It is found that for very high molecular weights, at extremely low levels of crystallinity, a linear extrapolation of the data yields an equilibrium melting temperature of 146.0 ± 0.5°. This value is in very good accord with independent theoretical expectations. However, for high levels of crystallinity erroneously low values of the equilibrium melting temperature are obtained by the same extrapolation procedures. For low molecular weights, theory indicates that a linear extrapolation would not be valid. This latter conclusion is borne out by the experimental results.

Introduction

The equilibrium melting temperature, T_m^0, of a crystallizable long-chain molecule is defined as the melting temperature of crystals formed from infinitely long chains which are devoid of nonequilibrium internal defects and are sufficiently large so that there is no influence of interfacial effects. This quantity is important in describing the relationship of polymer properties to structure and in the analyses of crystallization kinetics and nucleation processes. For the latter phenomena the temperature dependence of the free energy of fusion, which depends on T_m^0, is of major importance.[2] A similar definition holds for the melting temperature of crystals formed from chains of finite length. Despite the extreme importance of these quantities, their experimental determination has been very elusive and no satisfactory direct determination has as yet been made for any long-chain molecule. The reasons for this difficulty are well recognized[2,3] and reside in the morphological characteristics of the crystalline system that is usually formed. For polymers of high molecular weight the crystallite sizes that are attained in the chain direction are usually much smaller than the extended chain length and associated with the crystallites is a large excess interfacial free energy.[2-4] Therefore, a significant melting-point depression results even under the most stringent conditions of crystallization and subsequent heating.[3,5]

To alleviate the problem of direct experimental determination several extrapolation methods have been devised. Among the most potent of these is a theoretical method developed by Flory and Vrij[6] where from an analysis of the equilibrium melting temperatures of monomeric homologs (wherein molecular crystals are formed) the equilibrium melting temperature for the infinite chain can be calculated. By utilizing the data available for the *n*-paraffins, up to c_{100}, the equilibrium melting temperature for the infinitely long linear polyethylene molecule was deduced to be 145.5 ± 1°. This

(1) This work was supported by a grant from the Army Research Office (Durham).

(2) L. Mandelkern, "Crystallization of Polymers," McGraw-Hill Book Co., Inc., New York, N. Y., 1964.

(3) L. Mandelkern, *J. Polymer Sci., Part C*, No. 15, 129 (1967).

(4) L. Mandelkern, J. M. Price, M. Gopalan, and J. G. Fatou, *J. Polymer Sci., Part A-2*, 4, 385 (1966).

(5) J. G. Fatou and L. Mandelkern, *J. Phys. Chem.*, 69, 417 (1965).

(6) P. J. Flory and A. Vrij, *J. Am. Chem. Soc.*, 85, 3548 (1963).

value is substantially greater than any directly observed melting temperature for this polymer.[5] The theoretical procedure of Flory and Vrij[6] has only been applied to polyethylene to date since the necessary data for the monomeric homologs of other polymers are not available.

Another method for extrapolating or estimating the equilibrium melting temperature involves measurements on the polymers themselves. It is based on the widespread observation that the actual measured melting temperature of a crystalline polymer depends on the crystallization temperature.[2,7,8] In this method the observed melting temperature T_m^* is plotted against the crystallization temperature T_c and the data extrapolated linearly to the line representing the relation $T_m^* = T_c$. The point of intersection is then taken to represent the equilibrium melting temperature of the sample. The theoretical basis for the procedure adopted will be detailed below and a brief critique of the method has already been given.[2] This method has been used to extrapolate T_m^0 for a variety of polymers, and it is universally found that this estimated quantity is greater than the directly observed melting temperatures.[7-9]

In the present paper we attempt to assess critically this extrapolation procedure by studying the fusion properties of molecular-weight fractions of linear polyethylene. The importance of utilizing molecular-weight fractions in investigating the crystallization behavior of polymers has recently become quite clear from studies of the course of fusion, melting temperatures, and thermodynamic and mechanical properties.[3,5,10] It has been shown that the utilization of unfractionated material, particularly with the very broad molecular-weight distribution characteristic of polyethylene, can easily lead to incorrect conclusions. Particular attention is given in the present paper to the influence of chain length and of the level of crystallinity on the apparent melting temperature and to the problems involved in the extrapolation to the equilibrium melting temperature.

The melting temperature, T_m^* of a crystallite comprising ζ repeating units in the chain direction, with unrestricted size in lateral directions, formed from a collection of chains each of which is x units long is given by[3,5,11]

$$\frac{1}{T_m^*} - \frac{1}{T_m^0} = \frac{R}{\Delta H_u}\left[\frac{2\sigma_{ec}}{RT_m^*\zeta} - \frac{1}{\zeta}\ln\left(\frac{x-\zeta+1}{x}\right) + \frac{1}{x}\right] \quad (1)$$

here ΔH_u is the heat of fusion per repeating unit of the infinite chain and σ_{ec} is the excess interfacial energy per chain emerging from the 001 interface of the actual mature crystallite formed. For large x, eq 1 reduces to the classical expression for the melting of crystals of finite size.[4] This equation can be compared with the relation between the equilibrium melting temperature T_m and chain length

$$\frac{1}{T_m} - \frac{1}{T_m^0} = \frac{R}{\Delta H_u}\left[\frac{1}{x} + \frac{1}{x-\zeta_e+1}\right] \quad (2)$$

where ζ_e, the equilibrium crystallite size, is given by

$$2\sigma_{ec}^e = RT_m\left[\frac{\zeta_e}{x-\zeta+1} + \ln\left(\frac{x-\zeta_e+1}{x}\right)\right] \quad (3)$$

Here σ_{ec}^e represents the excess interfacial free energy for the equilibrium crystallite characteristic of the given chain length.[6,11] (For reasons cited previously[3,5] for long-chain molecules irrespective of molecular weight, the equilibrium model is represented by crystalline sequences whose length is less than the extended chain length. In other words, the molecular crystal model is not appropriate since chains of exactly uniform length are not obtained. Strictly speaking, these equations only apply when a chain supplies one sequence to a crystallite. However, they can be shown to be excellent approximations, at high molecular weights where more than one sequence from the same chain can participate in a crystallite.)

From nucleation theory pertinent to long-chain molecules,[12] it is shown that for three-dimensional homogeneous nucleation, the critical size in the chain direction ζ^* at the crystallization temperature T_c is

$$\frac{\zeta^*}{2}\left[\Delta f_u(T_c) - \frac{RT_c}{x} + \frac{RT_c}{x-\zeta^*+1}\right] = 2\sigma_{en} - RT_c\ln\left(\frac{x-\zeta^*+1}{x}\right) \quad (4)$$

where Δf_u is the free energy of fusion per repeating unit for the infinite chain at T_c and σ_{en} is the interfacial free energy per chain that is associated with the nucleation process. The physical significance of the three interfacial free energies that have been introduced are quite different. It is thus inappropriate and incorrect

(7) L. Mandelkern, *J. Polymer Sci.*, **47**, 494 (1960).

(8) J. D. Hoffman and J. J. Weeks, *J. Res. Natl. Bur. Std.*, **66A**, 13 (1962).

(9) K. F. Wisbrun, *J. Polymer Sci., Part A-2*, **4**, 827 (1966).

(10) L. Mandelkern, J. G. Fatou, R. Denison, and J. Justin, *ibid.*, **38**, 803 (1965).

(11) P. J. Flory, *J. Chem. Phys.*, **17**, 223 (1949).

(12) L. Mandelkern, J. G. Fatou, and C. Howard, *J. Phys. Chem.*, **68**, 3386 (1964).

to equate them with one another without independent evidence. If the usual approximation is made that $\Delta f_u(T_c) = \Delta H_u(T_m^0 - T_c)/T_m^0$, then eq 1 and 4 can be combined to give an expression for the dependence of the melting temperature of a crystal of finite thickness on the crystallization temperature. When x becomes large, it is found that

$$T_m^* = \frac{a}{2n} T_c + T_m^0\left(1 - \frac{a}{2n}\right) \tag{5}$$

which has been previously given.[2] Here $a = \sigma_{ec}/\sigma_{en}$ and $n = \zeta/\zeta^*$. For large x and the special case where simultaneously $\zeta = \zeta^*$ and $\sigma_{ec} = \sigma_{en}$, a further reduction to

$$T_m^* = {}^1/_2(T_m^0 - T_c) \tag{6}$$

is achieved. Equation 6 is the form originally presented as the basis of the extrapolation method[7,13] and obviously involves a major set of simplifying assumptions.

Equation 6 predicts a simple linear relation between the apparent melting temperature T_m^* and T_c. It thus allows for a linear extrapolation, with slope equal to 0.5, to the $T_m^* = T_c$ line in order to obtain the equilibrium melting temperature. However, according to eq 5 this extrapolation will only be valid if the quantities a and n are independent of the crystallization temperature in both the experimentally accessible range and at the higher temperatures involved in the extrapolation. A more detailed analysis of eq 1 and 4 indicates that the expected linear relation would be disturbed for low molecular weights. The experimental assessment of this extrapolation procedure requires that the melting temperatures be determined in such a manner that there be no changes in crystallite size and morphology subsequent to crystallization. Although the equations have been derived for lamellar-type crystallites, the same functional forms result if the lateral dimension of the crystallite is restricted.[2]

The essence of the method outlined lies in relating the crystallite thickness to the critical dimensions of a nucleus. In the examples cited so far a three-dimensional homogeneously formed nucleus was used. Similar equations are obtained for three-dimensional heterogeneous nucleation.[2] For nucleation involving the unimolecular deposition of chain units on an already existing crystal face, it is found that[14]

$$\zeta^* = \frac{2\sigma_{en} - RT \ln \dfrac{(x - \zeta^* + 1)}{x}}{\Delta f_u - RT/x} \tag{7}$$

which reduces in the high molecular weight approximation to

$$\zeta^* = \frac{2\sigma_{en}}{\Delta f_u(T_c)} \tag{8}$$

Corresponding to eq 5 there is then obtained

$$T_m^* = \frac{a}{n} T_c + T_m^0\left(1 - \frac{a}{n}\right) \tag{9}$$

For the special case of both a and n being simultaneously equal to unity

$$T_m^0 - T_m^* = T_m^0 - T_c \tag{10}$$

Equation 10 states simply that T_m^* will equal T_c under the conditions specified. Thus melting should occur with an infinitesimal increase in temperature above the crystallization temperature when $a = n = 1$. This conclusion is contrary to all known facts in regard to the melting of bulk crystallized polymers.[2] Hence for this type of nucleus the special conditions leading to eq 10 cannot be imposed. According to eq 9 for the crystals to be thermodynamically stable above the crystallization temperature, the ratio a/n must be less than unity. Therefore σ_{ec} would have to be less than σ_{en} or ζ greater than ζ^*. Since it is highly unlikely that the interfacial free energy of a mature crystallite would be less than that of the nucleus from which it is formed, it is necessary that substantial growth occur in the chain direction subsequent to nucleation to satisfy the experimental stability observations. Formally, this requirement presents no problem as long as it is consistent with the molecular nature of the interface. (The theory that has been constructed for the nucleation of regularly folded chains yields an additional term to eq. 8 which is the order of 10 A and independent of undercooling.[13,15] It has been recognized[15] that this additional term has only a very minor effect on the thermodynamic stability of the crystallites.) No problem arises with respect to the thermodynamic stability of a crystallite whose size is controlled by a three-dimensional nucleation process. Stability in this case is achieved with $\zeta = \zeta^*$ so that growth in the chain direction is not required. Equations 5 and 9 are of the same functional form. Therefore, solely from the observations of the dependence of the apparent melting temperature no definitive conclusions can be drawn as to the kind of nucleation processes that is involved. At best it can be hoped that the propositions set forth will allow for an estimation of the equilibrium melting temperature.

(13) J. I. Lauritzen, Jr., and J. D. Hoffman, *J. Res. Natl. Bur. Std.*, **64A**, 73 (1960).

(14) L. Mandelkern, J. G. Fatou, and C. Howard, *J. Phys. Chem.*, **69**, 956 (1965).

(15) J. D. Hoffman, *Soc. Plastics Engrs. J.*, **4**, 315 (1964).

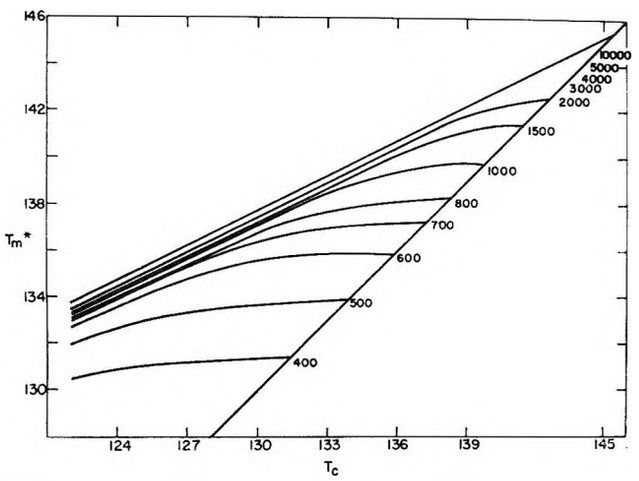

Figure 1. Theoretical plot, according to eq 5, of T_m* as a function of T_c for indicated chain lengths. For this example $\zeta/\zeta^* = 1$ and $\sigma_{ec}^e = \sigma_{en} = \sigma_{ec} = 4600$ cal/mole.

An illustrative example is given in Figure 1 of the expected dependence of the melting temperature on the crystallization temperature for different molecular weights. The curves plotted were calculated in accordance with eq 1 and 4. The simplifying assumption was made, for illustrative purposes, that $\sigma_{en} = \sigma_{ec} = \sigma_{ec}^e$. The value taken for the interfacial free energy was 4600 cal/mole of chain emanating from the 001 interface. T_m^0 was taken here as 145.5°[6] and ΔH_u as 950 cal/mole of CH_2 units.[16] The choice of parameters made and the assumed equality of the interfacial free energies do not sensibly alter the general conclusions that can be drawn from this model calculation. The further assumption is made in this illustration that ζ is identically equal to ζ^*. The point at which the curves for each x intersects the straight line $T_m^* = T_c$ gives the equilibrium melting temperature for the particular chain length.

Despite the simplifying assumptions that have been introduced T_m^* is not predicted to vary linearly with T_c in the molecular weight range $x \leq 10^4$. The curves characteristic of the lower molecular weights indicate, however, that a linear region does exist whose breadth becomes smaller with decreasing chain length. In anticipation of the analyses of the experimental results, it should be recognized that the range of crystallization temperatures accessible to experiment is restricted by kinetic factors. At high temperatures the times for crystallization will be intolerably long, while at lower temperatures the crystallization process becomes so rapid so that it is virtually impossible to achieve isothermal conditions.[2] For linear polyethylene, depending on molecular weight, the usually accessible crystallization temperatures range from about 124 to 130°.[2,17] For the highest molecular weights, in accord with eq 5, a straight line of slope 0.5 is expected for the complete range of crystallization temperatures. As the molecular weight decreases, however, the slope of the linear region decreases and becomes very small when x is the order of 400 or less.

The discussion above has been intended to serve primarily as background and as a guide to the presentation and analyses of new experimental data. In addition to a detailed investigation of the influence of molecular weight, we focus attention on the effect of the level of crystallinity on T_m^*, at a fixed T_c, and assess the reliability of the extrapolation procedure.

Experimental Section

Materials. The procedures adopted for the molecular-weight fractionation of the linear polyethylene and the characterization of the fractions have been previously described in detail.[5] Other pertinent crystallization properties of the fractions studied here, such as the density and enthalpy of fusion, have been reported elsewhere.[3-5] Standard dilatometric procedures[5] were employed to study the fusion process and determine the apparent melting temperatures. The temperature control of the silicone oil thermostat in which the dilatometers were immersed was better than 0.1°, and melting temperatures could be obtained with an uncertainty of ±0.2°.

Procedures. Prior to the initiation of crystallization the samples were rendered completely molten by immersion of the dilatometer in the thermostat at 160° for 30 min. The dilatometer was then quickly transferred to another thermostat, set at a predetermined temperature, and crystallization was allowed to ensue isothermally until the desired level of crystallinity was attained. The degree of crystallinity was calculated from the dilatometer scale readings and the specific volume relations given by Chiang and Flory,[18] assuming the additivity of volumes. The heating schedule that was adopted subsequent to crystallization was developed to ensure the melting of the actual crystalline system formed at the crystallization temperature. Fast heating must be avoided to prevent superheating which results in erroneously high melting temperatures. On the other hand, too slow a heating rate leads to the well-known partial melting and recrystallization which is characteristic of the fusion of polymers and results in a concomitant change in morphology and crystallite

(16) F. A. Quinn, Jr., and L. Mandelkern, *J. Am. Chem. Soc.*, **80**, 3178 (1958); **81**, 6533 (1959).

(17) W. Banks, M. Gordon, R. J. Roe, and A. Sharples, *Polymer*, **4**, 61 (1963).

(18) R. Chiang and P. J. Flory, *J. Am. Chem. Soc.*, **83**, 2857 (1961).

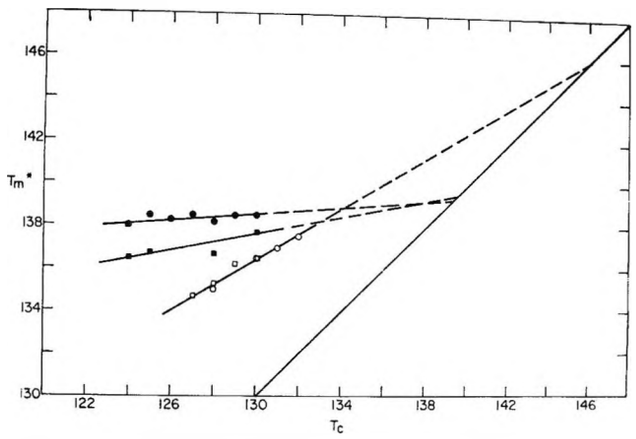

Figure 2. Plot of experimentally determined T_m^* as a function of T_c for two highest molecular-weight fractions. $M = 1.0 \times 10^6$: low level of crystallinity, □; high level of crystallinity, ■. $M = 4.7 \times 10^5$: low level of crystallinity, ○; high level of crystallinity, ●.

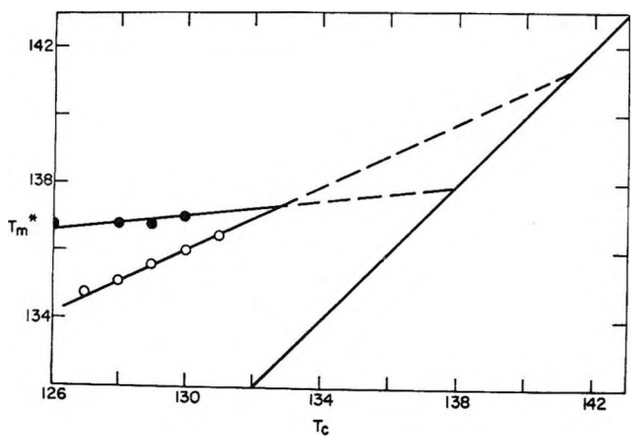

Figure 3. Plot of experimentally determined T_m^* as a function of T_c for $M = 2 \times 10^4$: low level of crystallinity, ○; high level of crystallinity, ●.

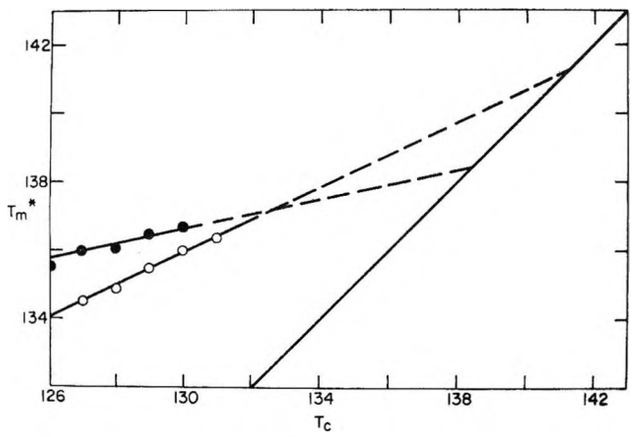

Figure 4. Plot of experimentally determined T_m^* as a function of T_c for $M = 1.25 \times 10^3$: low level of crystallinity, ○; high level of crystallinity, ●.

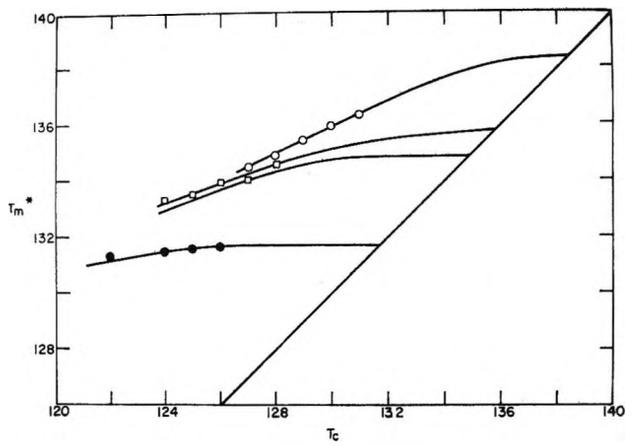

Figure 5. Plot of experimentally determined T_m^* as a function of T_c for two lowest molecular-weight fractions. $M = 5.3 \times 10^3$: low level of crystallinity, ○; high level of crystallinity, ●. $M = 3.3 \times 10^3$: low level of crystallinity, □; high level of crystallinity, ■.

size. Extensive preliminary studies of the kinetics of melting allowed a heating schedule to be developed which gave constant dilatometer readings at each temperature between T_c and T_m^*. The factors which are involved in establishing the heating rate are the initial levels of crystallinity, the molecular weight, and the temperature range.

For experiments involving the lowest amounts of crystallinity, of the order of 3–5%, constant readings could be obtained between 2 and 20 min below 130°. Above this temperature a heating rate of 1°/20 min was found adequate. For the higher levels of crystallinity that were studied, which were of the order of 70–80%, the heating rate was 1°/20 min up to 135° for all samples except the very highest molecular weights. For the higher temperatures and higher molecular weights, the heating rate was reduced to 1°/6 hr. Reducing the heating rate to as low as 0.5°/day at the higher temperatures does not sensibly alter the observed melting temperature.

Results and Discussion

The experimental results are given in Figures 2–5 for each of the molecular-weight fractions. The data are presented as plots of the apparent melting temperature T_m^* against T_c for the indicated levels of crystallinity $1 - \lambda$. These experiments encompass the very wide molecular-weight range of from 3.3×10^3 to 1.0×10^6. A crystallization temperature as high as 132° has been utilized for $M = 4.7 \times 10^5$ (for low levels of crystal-

Table I: Summary of Pertinent Quantities Obtained from Linear Plots of T_m^* against T_c

		Slope[a]				T_m[b]				Max T_m^*[c]			
		—Crystallinity (1 − λ)—				—Crystallinity (1 − λ)—				—Crystallinity (1 − λ)—			
Mol wt	x	~0.05	0.26	0.56	0.80	~0.05	0.26	0.56	0.80	~0.05	0.26	0.56	0.80
3.3×10^3	236	0.15			0	132.4			132.4	131.6			132.5
5.3×10^3	379	0.30			0	137.5			134.6	134.5			134.6
12.5×10^3	893	0.5			0.2	141.3 ± 0.3			138.3 ± 0.2	136.4			136.7
20.0×10^3	1,429	0.5			0.15	141.3 ± 0.3			137.9 ± 0.2	136.5			137.0
4.70×10^5	33,571	0.6		0.1		146.0 ± 0.5		139.3 ± 0.3		137.5		138.5	
1.00×10^6	71,428	0.62	0.2			146.0 ± 0.5	139.5 ± 0.3			136.5	137.7		

[a] Slope of linear region of plots of T_m^* *vs.* T_c in Figures 2–5. [b] From linear extrapolation of linear region. [c] Highest directly observed apparent melting temperature under prescribed conditions.

linity) and 131° for $M = 2.0 \times 10^4$. These temperatures represent the highest thus far utilized in experiments of this type for polyethylene. From purely an experimental point of view the results, for a given molecular weight and level of crystallinity, can be represented by a linear relation between T_m^* and T_c as is indicated by the solid straight lines in each of the figures. The continuation of these straight lines, beyond the experimentally accessible region, to the intersection of the line $T_m^* - T_c$, yield the melting temperatures listed in Table I. These temperatures are termed the equilibrium melting temperature obtained by a linear extrapolation of the experimental data. Other important quantities that are obtained from the plots in Figures 2–5 are also listed in Table I.

It is convenient, when analyzing the results in more detail, to consider first the three highest molecular weight fractions. From the theoretical analyses that have been given and the plots in Figure 1, it is to be expected that the complexities due to finite chain length would be minimal in this molecular weight range. Hence the linear extrapolation method should be valid. The experimental conditions that need to be fulfilled are expected to be best achieved at the lowest possible level of crystallinity that is susceptible to quantitative study. Under these circumstances any complications resulting from crystallite growth in the chain direction, subsequent to nucleation, would be minimized as would be any changes in the character of the residual noncrystalline regions. Both these factors must influence the apparent melting temperature. For these reasons, as well as for the distinct possibility that a crystallite size distribution can develop with increasing levels of crystallinity, the experiments performed at very low levels of crystallinity are of major importance.

In accordance with eq 5 for high molecular weight, the slope in the plot of Figure 2 should be equal to $^1/_2(\zeta^*/\zeta)(\sigma_{ec}/\sigma_{en})$. A unique assignment of each of the factors involved obviously cannot be made. For the two highest molecular weights, the observed slope of 0.6 is so close to the value 0.5 expected for $\zeta = \zeta^*$, $\sigma_{ec} = \sigma_{en}$, that a reasonable conclusion could be made that the ratios ζ^*/ζ and σ_{ec}/σ_{en} do not each depart very much from unity. The linearly extrapolated melting temperature that is obtained for $M = 4.70 \times 10^5$ and 1.0×10^6 is 146.0 ± .5°. These molecular weights are sufficiently high so that this melting temperature can be identified with T_m^0, the equilibrium melting temperature of an infinite chain.[5,6] This extrapolated melting temperature is in excellent accord with the theoretical predictions of Flory and Vrij.[6] It is somewhat higher than the revised estimate of 144.7° recently given by Broadhurst.[19] The melting temperature extrapolated from the plot in Figure 2 should probably best be considered a lower limit since the linear extrapolation is predicated on the assumption that the ratios of σ_{ec}/σ_{en} and ζ^*/ζ will remain constant for the higher crystallization temperatures where data are not available.

In other experiments of this type, using unfractionated linear polyethylene, an extrapolated value of 143 ± 2° was obtained.[8] However, it was concluded in this work that the best estimate of the equilibrium melting temperature lies between 141 and 143°.[8] A linear extrapolation of T_m^* against T_c yielding a value of 145.5° has also been reported.[20] This extrapolated

(19) M. G. Broadhurst, *J. Res. Natl. Bur. Std.*, **70A**, 481 (1966).
(20) J. J. Weeks, *ibid.*, **67A**, 441 (1963).

value was dismissed, and 142 ± 1° was taken to represent the equilibrium melting temperature.[15,20]

For the molecular weight fraction $M = 2.0 \times 10^4$, a slope of 0.5 is obtained at the low levels of crystallinity. This slope is compatible with the simultaneous fulfillment of the condition $\zeta = \zeta^*$ and $\sigma_{ec} = \sigma_{en}$ although not necessarily unique to it. The linear extrapolation of the T_m^* against T_c plot yields a melting temperature of 141.3 ± 3° (Figure 3). If this temperature represents the equilibrium melting temperature for this molecular weight, then from eq 2 and 3, σ_{ec}^e is found to be 4700 cal/mole of chains for $T_m^0 = 145.5°$. If $T_m^0 = 146.5°$, then σ_{ec}^e is found to be 6300 cal/mole for this molecular weight. These values of the interfacial free energy are close to those deduced from droplet nucleation experiments.[21,22] and from the fusion of random copolymers of polyethylene.[23] In these experiments the interfacial free energy was found to be 4600 cal/mole, which corresponds to 170 ergs/cm² for polyethylene. (In their original publication[22] Gornick, Ross, and Frolen reported a value for σ_{en} which was more than a factor of two less than that reported previously by Cormia, Price, and Turnbull.[21] A revision of this work (private communication and paper in press) has now resulted in virtually complete quantitative agreement between the two sets of investigations.) Although the possibility of an unusual coincidence cannot be dismissed, the striking similarity in the values for σ_{ec}^e and σ_{en} in this molecular weight range is apparent.

A unique value of σ_{ec} cannot be obtained from these results without arbitrarily setting the value of ζ/ζ^*. There is, however, an independent experimental report[4] of the relationship between the melting point, molecular weight, and crystallite size. From these data, σ_{ec} can be calculated. It was found, for samples crystallized to high levels of crystallinity, to increase with molecular weight in the lower molecular weight range and reach an asymptotic value of 8000–9000 cal/mole for molecular weights greater than 5.6×10^4.[3,4] For a molecular weight of 2×10^4, σ_{ec} was 5000–6000 cal/mole. This quantity is only slightly greater than that deduced in the present work for σ_{ec}^e and also for σ_{en} if the latter quantity is independent of chain length. The ratio of σ_{ec}/σ_{en} for this molecular weight is thus estimated to be in the range of 1.0–1.3. Consistent with the observed slope of 0.5 the corresponding value ζ/ζ^* would also be in this same range. If σ_{en} is independent of molecular weight, a fact which has not as yet been experimentally established, then for the two highest molecular weight fractions, σ_{ec}/σ_{en} is estimated to be in the range of 1.7–1.8 based on previous deductions for σ_{ec}.[4] Since the slope is 0.6 for the higher molecular weights, the estimates of ζ/ζ^* vary from 1.4 to 1.5. The above analysis is a rough estimate based on the best values of the different interfacial free energies that are presently available. Definitive relations between σ_{ec} and σ_{en}, and ζ and ζ^* cannot be obtained from these experiments without additional assumptions.

The above discussion has been predicated on the concept that a three-dimensional nucleation process is size controlling. If, however, nucleation occurs by a unimolecular deposition process (see above) then the slopes in Figures 2 and 3 will be equal to $(\sigma_{ec}/\sigma_{en})(\zeta^*/\zeta)$. In this case a significant increase of ζ over ζ^* is mandatory to allow for the observed thermodynamic stability. For the most favorable situation, σ_{ec} will be equal to σ_{en}. Hence, at least a twofold increase in crystallite thickness would be required to account for the observed slope. It can be expected that for the higher molecular weights σ_{ec} will be greater than σ_{en} so that an increase in crystallite size even greater than a factor of two would be required. In a formal algebraic sense the data satisfy these conditions. However, this large increase in crystallite thickness over that of the initiating nucleus must occur when the level of crystallinity is only a few per cent.

As the level of crystallinity is increased, at a constant crystallization temperature, the apparent melting temperature also increases. This increase in melting temperature varies from 2 to 3° at the lower crystallization temperatures to 1° or less at the higher ones. At the maximum level of crystallinity that can be attained for each of the three highest molecular-weight fractions there is then a large decrease in the slope (see Table I). The extrapolated melting temperatures in this case differ by no more than 1–2° from those actually observed. For a molecular weight of 2×10^4 the difference between the extrapolated melting temperature at high levels of crystallinity and that directly observed is less than a degree. The values of the slope have now been reduced to the range of 0.1–0.2. As a consequence, the linearly extrapolated melting temperatures are much smaller than when evaluated at the lower levels of crystallinity. For example, for $M = 1.0 \times 10^6$ the difference in extrapolated melting temperature is 7° as the level of crystallinity increases from 0.05 to 0.26.

At the high levels of crystallinity, if σ_{ec}/σ_{en} is implicitly taken as unity,[8,15,20] or the same value prevail-

(21) R. L. Cormia, F. P. Price, and D. Turnbull, *J. Chem. Phys.*, 37, 1333 (1962).

(22) F. Gornick, G. S. Ross, and L. J. Frolen, Abstracts, Polymer Division, Meeting of the American Chemical Society, Phoenix, Ariz., Jan 1966.

(23) M. J. Richardson, P. J. Flory, and J. B. Jackson, *Polymer*, 4, 221 (1963).

ing at the low levels of crystallinity, then a substantial growth would have to take place to satisfy the value of the slopes. For example, with this assumption, for $M = 1.0 \times 10^6$, ζ/ζ^* would increase from unity to 2.5 for three-dimensional control and fivefold for a unimolecular controlled nucleation process as $1 - \lambda$ increased to 0.26. Similarly for $M = 4.70 \times 10^5$ a further increase in growth by a factor of two over each of the values just cited would be indicated for $1 - \lambda = 0.56$. As crystallization progresses from the very small levels of crystallinity, many complexities in morphology and structure are to be expected. Thus the burden in interpretation should not be placed solely on crystallite growth in the chain direction. The distinct possibilities exist for σ_{ec} to increase, for the development of very diffuse and complex interfacial regions and for the constitution and structure of the residual noncrystalline regions to change. These factors are quite involved and do not lend themselves to a quantitative description at present. Until these and related matters can be more explicitly described the empirical extrapolation to the equilibrium melting temperature is best limited to the simplest morphological and structural situation attainable. This latter condition is best fulfilled by experiments conducted at the lowest levels of crystallinity feasible for study.

We have also investigated the change in apparent melting temperature as a function of time during the final portions of the crystallization process. In this crystallization region only small changes in the level of crystallinity occur.[2] The results are summarized in Table II. Over at least a decade of time, in the crystallization range cited, there is only a slight increase in the level of crystallinity. The increase in the apparent melting temperature is a few tenths of a degree at most. If it is assumed that this small increase in melting temperature results from growth in the chain direction, with no change occurring in the molecular nature of the interface, it follows that

$$\frac{\Delta T_1}{\Delta T_2} = \frac{\zeta_2}{\zeta_1} \tag{11}$$

where ΔT_1 and ΔT_2 are melting point depressions, calculated from the equilibrium melting temperature, corresponding to the crystallite sizes ζ_1 and ζ_2. Hence for a maximum increase in melting temperature of 0.3° the crystallite thickness will increase by no more than 3% for at least a decade of time in the tailing-off region of the crystallization isotherm. This analysis, therefore, does not indicate any major growth in the chain direction in this region of the crystallization process.[20,24]

The interpretation of the data for the lower molecular weights presents complications which are related to the curvature in the plots for the model calculations in Figure 1. For the two lowest molecular weight fractions crystallized to the highest level of crystallinity attainable ($1 - \lambda \sim 0.80$), the apparent melting temperatures are independent of the crystallization temperature. Thus, as is indicated in Figure 5, the extrapolation to the line $T_m^* = T_c$ is easily accomplished. This observation is in obvious contrast to the higher molecular weight samples. For $M = 5.3 \times 10^3$ the extrapolated melting temperature is 3° lower than the one obtained from the low level of crystallinity data. However, for $M = 3.3 \times 10^3$ although the slope for the low level of crystallinity data is 0.15 the extrapolated melting temperatures are identical within experimental error. In this molecular weight range, however, since the approximation of large x is not applicable there is no theoretical validity for a linear extrapolation. The observed invariance of T_m^* with T_c at the high levels of crystallinity is suggestive of a constancy in crystallite size and in the ratio of interfacial free energies irrespective of the crystallization temperature. This suggestion is supported by electron microscope observations[4,25] in this molecular weight range which have shown that at the high levels of crystallinity the crystallite sizes are virtually identical with the extended chain length of the molecules and are independent of the crystallization temperature. The constancy of the melting temperature thus receives a natural explanation. The observed melting temperatures (at the high levels of crystallinity) can thus be identified with the equilibrium melting temperature for the lower molecular weight samples as long as σ_{ec} is equal to or very close to the value of σ_{ec}^e.

Table II: Apparent Melting Temperature during Final States of Crystallization

M_η	T_c°, °C	Time, min	$1 - \lambda$	T_m^*
425,000	128	980	0.625	138.3
	128	11,000	0.65	138.5
	126	755	0.63	138.1
	126	11,000	0.66	138.2
20,000	128	660	0.82	136.5
	128	11,160	0.85	136.6
	126	755	0.86	136.5
	126	11,000	0.87	136.8

(24) J. D. Hoffman and J. J. Weeks, *J. Chem. Phys.*, **42**, 4301 (1965).

(25) F. R. Anderson, *J. Appl. Phys.*, **35**, 64 (1964); *J. Polymer Sci.*, **C3**, 123 (1963).

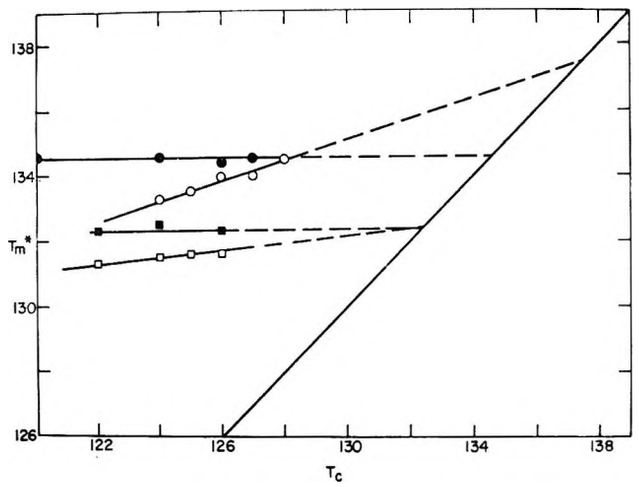

Figure 6. Comparison between theory and experiment for lowest molecular weight fractions at low levels of crystallinity. $M = 1.25 \times 10^4$: O for $\sigma_{en} = 4600$ cal/mole, $\sigma_{ec} = 5200$ cal/mole, and $\sigma_{ec}^e = 5200$ cal/mole. $M = 5.3 \times 10^3$: □ for $\sigma_{en} = \sigma_{ec} = \sigma_{ec}^e = 2400$ and 2800 cal/mole. $M = 3.3 \times 10^3$: ● for $\sigma_{en} = \sigma_{ec} = \sigma_{ec}^e = 2000$ cal/mole. $\zeta/\zeta^* = 1$ for all cases.

An analysis, but not necessarily a unique one, for the data obtained at the very low levels of crystallinity is given in Figure 6 for the two lower molecular weight samples. The solid lines are calculated from eq 1 and 4 with the assumption that $\zeta = \zeta^*$ and $\sigma_{en} = \sigma_{ec}^e$. For $M = 3.3 \times 10^3$, the experimental data are well represented with interfacial free energies of 2000 cal/mole. The curvature in this plot is apparent, and the equilibrium melting temperature is found to be 131.8°. This latter quantity depends solely on the value taken for σ_{ec}^e and compares favorably with the melting temperature of 132.4° obtained directly at the higher levels of crystallinity. If molecular crystals were formed from polymer chains of this molecular weight, then the melting temperature should be 131.3 ± 0.2° according to the analyses of Flory and Vrij.[6] As is also indicated in Figure 6, similar results are obtained for the fraction $M = 5.3 \times 10^3$. In this case the data for the low levels of crystallinity can be fitted by $\zeta = \zeta^*$ and interfacial free energies that lie in the range 2400–2800 cal/mole. The calculated equilibrium melting point is between 134.7 and 135.8° as compared to the value of 134.5° that is directly observed at the higher levels of crystallinity. Thus, in contrast to the results for the very high molecular weights, equilibrium melting temperatures are most easily obtained at high levels of crystallinity for the lowest molecular weight fractions.

The experimental data, at low levels of crystallinity, for $M = 1.25 \times 10^4$ can be well represented by a straight line of slope 0.5 and yield a linearly extrapolated melting temperature of 141.3 ± 0.3°. The interfacial free energy, σ_{ec}^e, that corresponds to this melting temperature has a value of 2300 cal/mole. However, eq 1 and 4 indicate that a linear plot is not to be theoretically expected in this molecular-weight range. Hence, the equilibrium melting temperature should be somewhat less than the above value with a corresponding increase in σ_{ec}^e. The theoretical curves that can fit the data in this case depend very crucially on the ratio of ζ/ζ^* that is taken. An example is also given in Figure 6 for $\zeta/\zeta^* = 1$ and $\sigma_{en} = 4600$ cal/mole and $\sigma_{ec} = \sigma_{ec}^e = 5200$ cal/mole. The equilibrium melting temperature for these parameters is 138.5°. However, if ζ is allowed to increase to 15% above ζ^*, slightly lower values of σ_{en}, σ_{ec}, and σ_{ec}^e can be employed to fit the experimental data. The resulting theoretical curves which fit the data yield melting temperatures which are between 138.5 and 141.3°. Therefore, the extrapolation of the experimental data of this fraction is extremely sensitive to the choice of parameters that are made. Hence in this case only limits can be placed on the equilibrium melting temperature.

The experimental results and analyses thereof that have been presented indicate that caution must be exercised in extrapolating apparent melting point data in order to obtain equilibrium melting temperatures. A great sensitivity to molecular weight and level of crystallinity is apparent. For very high molecular weight fractions crystallized to low levels of crystallinity valid extrapolations leading to a lower limit for the equilibrium melting temperature can be obtained. The theory developed and the conclusions reached are based on general considerations and do not depend on the crystallite morphology or on the details of the molecular nature of the interfacial region.[8,15]

The Kinetics of the Reaction of Some Pyrophoric Metals with Oxygen

by Thomas M. Gorrie,[1] Peter W. Kopf,[2] and Sidney Toby

School of Chemistry, Rutgers, The State University, New Brunswick, New Jersey 08903
(Received April 10, 1967)

Pyrophoric bismuth, cobalt, copper, iron, lead, nickel, and tin were prepared by the decomposition of the metal citrate, oxalate, or tartrate *in vacuo* at 350–450°. The rates of oxidation were first order in oxygen pressure, and the rate constants gave linear Arrhenius plots in the range −120 to +75°. The entropies of activation were very similar to the standard entropies of the reactions with 1 mole of oxygen. A compensation effect was observed which was shown to be due to the fact that the free energy of activation was approximately constant at 18 kcal mole^{-1} for the oxidation of all of the metals studied.

Introduction

The kinetics of the oxidation of metals is a subject of great theoretical and enormous practical interest. However, the rate-determining step in the oxidation of metals, as usually measured, is governed by diffusion processes in the solid phase. This complicates the kinetics considerably and the resulting rate laws have been described as linear, parabolic, cubic, or logarithmic, according to conditions.[3] A meaningful comparison of rate constants for metals which obey different rate laws during oxidation is not possible.

In a previous paper[4] it was shown that the study of the reaction of pyrophoric lead with oxygen could give an insight into metal oxidation processes that was free of the usual complexities resulting from diffusion through oxide layers. In addition, an attempt was made to correlate the (kinetic) entropy of activation with the (thermodynamic) entropy of the reaction. This papers extends the investigation to other pyrophoric metals and describes what we believe to be the first comparison of the kinetic parameters for the oxidation of several metals.

Experimental Section

The apparatus was similar to that previously described[4] except that a smaller reaction volume was used. In the course of repeating measurements on the oxidation of pyrophoric lead, we found an increase in the rate of oxygen uptake when the reaction volume was disconnected from associated tubing. This was presumably due to a viscous drag slowing the flow of oxygen. By eliminating dead space the reaction volume was reduced from its previous[4] value of 580 cm^3 to approximately 120 cm^3 at which the rate of oxygen uptake appeared to be independent of reaction volume. Tubing used throughout the apparatus had a minimum i.d. of 6 mm.

Approximately 0.5-g samples in break-seals were exposed to oxygen in the range −120 to 75°. Initial oxygen pressures were kept below 1.0 torr to minimize local heating and to conserve sample. Oxygen pressures were measured on a thermocouple gauge which had been calibrated against a McLeod gauge. It was noted that the calibration for oxygen was appreciably different from that for air. The most rapid pressure changes that could be measured with our apparatus corresponded to a rate constant of about 1.0 sec^{-1}. This value was approached at the highest temperatures used. As previously,[4] rate constants were measured in the earlier stages of oxidation before the metal was exhausted.

The pyrophoric metals were prepared by decomposing the appropriate salts at 350–450° in a vacuum system with continuous pumping. All salts were commercially available and were used without further purification.

(1) NSF Undergraduate Research Participant, 1966–1967.

(2) NSF Undergraduate Research Participant, 1965–1966.

(3) O. Kubaschewski and B. E. Hopkins, "Oxidation of Metals and Alloys," Academic Press Inc., New York, N. Y., 1962.

(4) J. Charles, P. W. Kopf, and S. Toby, *J. Phys. Chem.*, **70**, 1478 (1966).

Table I: Results of Decomposition of 20 Salts at 350–450° *in Vacuo*

	Bi(III)	Cd(II)	Ce(III)	Co(II)	Cu(II)	Fe(II)	Mn(II)	Ni(II)	Pb(II)	Sn(II)	Zn(II)
Citrate	Pyro metal	Carbon and massive metal			Pyro metal		Massive metal	Pyro metal in poor yield	Pyro metal		
Formate					Red oxide			Pyro metal in poor yield	Massive metal		
Oxalate		Green oxide and massive metal	Brown oxide	Pyro metal	Brown-red oxide			Pyro metal		Pyro metal	Oxide
Tartrate		Carbon and massive metal				Pyro metal			Feebly active metal	Pyro metal	

Table II: Kinetic and Thermodynamic Parameters for Oxidation of Metals

Reaction	E, kcal/mole	Log A (A in sec^{-1})	$\Delta S^{\ddagger}$, cal/mole of O_2 deg	ΔS°, cal/mole of O_2 deg
$^4/_3Bi + O_2 \rightarrow {}^2/_3Bi_2O_3$	1.7 ± 0.1	0.97 ± 0.1	−56 ± 1	−43.0
$2Co + O_2 \rightarrow 2CoO$	5.2 ± 0.6	3.5 ± 0.6	−44 ± 3	−41.6
$2Cu + O_2 \rightarrow 2CuO$	3.8 ± 0.5	1.9 ± 0.5	−52 ± 3	−44.1
$^4/_3Fe + O_2 \rightarrow {}^2/_3Fe_2O_3$	4.9 ± 0.7	3.1 ± 0.6	−46 ± 3	−43.3
$2Ni + O_2 \rightarrow 2NiO$	3.1 ± 0.3	2.1 ± 0.4	−50 ± 2	−45.0
$2Pb + O_2 \rightarrow 2PbO$	3.0 ± 0.3	2.1 ± 0.4	−51 ± 2	−46.8
$2Sn + O_2 \rightarrow 2SnO$	4.7 ± 0.6	3.0 ± 0.7	−47 ± 3	−46.6

Results

Qualitative results of the decomposition of 20 different salts are given in Table I. Pyrophoric bismuth, cobalt, copper, iron, lead, nickel, and tin were prepared, and each metal showed the first-order uptake of oxygen expected from previous consideration.[4] Although the reactivity was high in each case, pyrophoric copper and tin were found to lose their activity much more rapidly than the other metals. It is noteworthy that, as in the case for lead,[4] pyrophoric bismuth and tin were formed at temperatures considerably higher than the melting points of the metals.

Arrhenius plots for rates of oxygen uptake are given in Figures 1 and 2. In all cases more than one sample of pyrophoric metal was used. The Arrhenius parameters with estimated errors are collected in Table II. Also given are the standard entropy changes for the reactions per mole of oxygen. In the case of Bi_2O_3, Fe_2O_3, and PbO, the identity of the oxide was confirmed by gravimetric analysis with a correction for the carbon contained in the pyrophoric metal. For the other metals it was assumed that the stable oxide would be formed.

Discussion

All of the pyrophoric metals described here have been made previously,[5] but there are no accounts of quantitative kinetic comparisons. We were unable to make pyrophoric cadmium, cerium, manganese, or zinc by decomposition, but these metals have been made in pyrophoric form by hydrogen reduction methods. It may be significant that the enthalpies of reaction of the latter three metals with 1 mole of oxygen are considerably higher than those of the other metals. In the case of cadmium, appreciable sublimation of the

(5) A useful compilation has been made by G. S. Bahn, Fall Meeting, Western States Section, The Combustion Institute, 1964, paper 64-31.

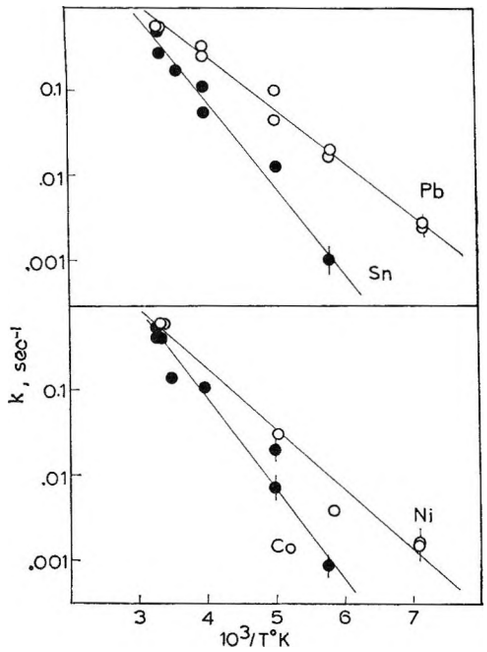

Figure 1. Arrhenius plots for the oxidation of pyrophoric cobalt, nickel, lead, and tin.

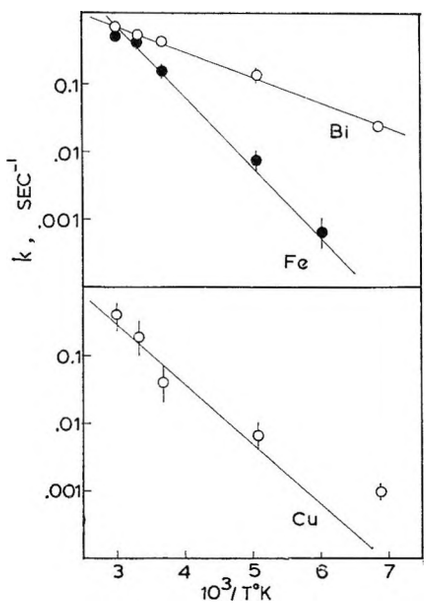

Figure 2. Arrhenius plots for the oxidation of pyrophoric copper, bismuth, and iron.

metal was observed during the decomposition *in vacuo*, and the volatility of the metal probably precluded its formation in a finely divided state.

The possibility exists that the observed rates were in part governed by gas-phase diffusion effects, and it was indeed found that the rate of oxygen uptake was

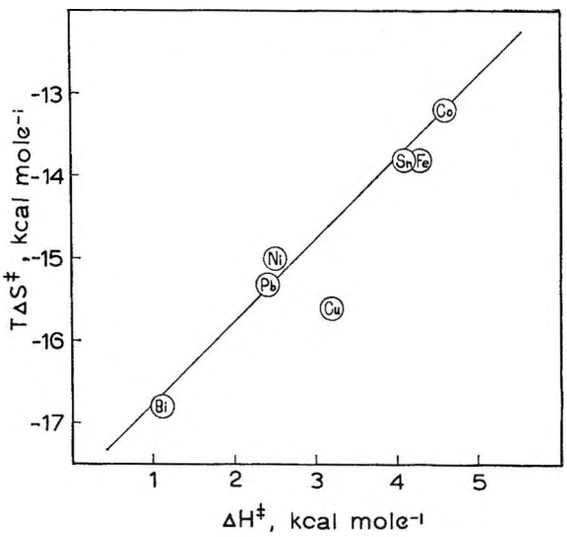

Figure 3. Compensation effect: plot of $T\Delta S^{\pm}$ *vs.* $\Delta H^{\pm}$ for the oxidation of seven pyrophoric metals. The line drawn has a slope of unity.

measurably decreased by a constriction in the connecting tubing. This decrease affected the observed A factors but not the activation energies. If diffusion were paramount, one would not expect to find appreciably different activation energies for various metals. Although diffusion effects cannot be entirely ruled out, we do not think they play an important part in our data.

The similarity between entropies of activation and entropies of reaction shown in Table II is quite striking. Although lessened somewhat, this similarity would still be apparent if appreciable quantities of a lower oxide were also formed [*e.g.*, $\Delta S^{\circ}(Cu_2O) = -35$ cal (mole of O_2)$^{-1}$ deg^{-1}]. The restriction on reaction between metals and oxygen evidently is an entropy rather than an enthalpy effect, and the transition state resembles the products far more than the reactants. Our values of $\Delta S^{\pm}$ are insufficiently precise for detailed speculation to be justified. However, there appears to be a slight increase in entropy in going from transition state, which presumably consists of adsorbed oxygen molecules, to the oxide product.

A comparison of the A factors and activation energies in Table II reveals that variations in the two parameters are parallel. For similar reactions it was noted by Hinshelwood and Legard[6] that log A was proportional to E. This so-called compensation effect was observed for solute diffusion in metals[7] and is to be

(6) C. N. Hinshelwood and A. R. Legard, *J. Chem. Soc.*, 587 (1935).
(7) R. H. Swalin, *J. Appl. Phys.*, 27, 554 (1956).

expected for a series of reactions involving similar bonds. Laidler[8] has considered the compensation effect for reactions in solution in terms of the free energy of activation, $\Delta G^{\ddagger}$. Taking this approach and assuming that $\Delta G^{\ddagger}$ is approximately constant for the oxidation of all metals, then a plot of $T\Delta S^{\ddagger}$ *vs.* $\Delta H^{\ddagger}$ should be linear with a slope of unity. Using the simple transition-state theory formulation, we have evaluated $T\Delta S^{\ddagger}$ (at 298°K) and $\Delta H^{\ddagger}$ from our Arrhenius parameters, and the results are plotted in Figure 3. The data agree well with the line drawn with a slope of unity, suggesting that $\Delta G^{\ddagger}$ is constant for the oxidation of pyrophoric metals and possibly for all metals when a layer of oxide does not retard subsequent oxidation.

Acknowledgment. We are most grateful to the National Science Foundation for support of this work.

(8) K. J. Laidler, *Trans. Faraday Soc.*, **55**, 1725 (1959).

The Oxidation of Aquopentaammine and of Hexaamminecobalt(III) Ions

by Darwin D. Thusius and Henry Taube

Department of Chemistry, Stanford University, Stanford, California 94305 *(Received April 10, 1967)*

When $S_2O_8^{2-}$ decomposes in the presence of $Co(NH_3)_5OH_2^{3+}$ under the influence of Ag^+ as catalyst, reduction of Co(III) to Co^{2+} is observed with O_2 as the major component of the gaseous product. Tracer experiments with O^{18}-enriched aquo ion show that in at least 0.7 of the acts leading to the reduction of Co^{2+}, complex bound oxygen is transferred to the gas phase. Indirect arguments are presented which indicate that the external oxidizing agent attacking the Co(III) complex is neither HO nor SO_4^-. Direct experiments using a solution containing Ag^{2+} show that this ion (or some species in labile equilibrium with it) oxidizes the Co(III) coordinated water to oxygen. The water coordinated to Co(III) is shown to be more readily oxidizable than is other water in the system. The spontaneous decomposition of $S_2O_8^{2-}$ in the presence of either $Co(NH_3)_5OH_2^{3+}$ or $Co(NH_3)_6^{3+}$ leads to the production of Co^{2+}. The rate of production of Co^{2+} as the concentration of $Co(NH_3)_5OH_2^{3+}$ increases reaches a limiting value which is very close to one-half the limiting rate of production of HO by the spontaneous decomposition of $S_2O_8^{2-}$. The dominant intrinsic gaseous product of the reaction is N_2, at least when Co(III) is within 25% of the saturation value. Striking effects of substituting D for H are observed. These experiments taken together with others suggest that although NH_3 is the coordination sphere of $Co(NH_3)_5OH_2^{3+}$ is oxidized, HO does not attack the NH_3 directly. The reaction is interpreted as involving oxidation of Co(III) to the Co(IV) state, Co(IV) then being reduced by coordinated NH_3 by a $2e^-$ change.

Introduction

The effect of a metal ion on the reactivity of an associated ligand is becoming of increasing interest. A specialized part of this subject area is comprised of the reactions in which a ligand upon being oxidized by an external oxidizing agent brings about reduction of the metal ion center to which it is attached.[1] One direction in which this interest is being pursued[2] is

(1) (a) P. Saffir and H. Taube, *J. Am. Chem. Soc.*, **82**, 13 (1960); (b) J. P. Candlin and J. Halpern, *ibid.*, **85**, 2518 (1963).

to use complex ligands which call for electron transfer between remote positions if the central metal ion is to be implicated. But much remains to be done also for simple systems in which the external oxidizing agent and the internal are separated by perhaps only a single atom in the activated complex for the reaction. Some work along this line has been described dealing with the oxidation of coordinated halides.[3] In the present work we have turned our attention to understanding the course of the reactions in which H_2O or NH_3 coordinated to Co(III) is oxidized. The experiments on the oxidation of coordinated water seem to us to be especially significant because the mechanisms of the important class of reactions in which water is oxidized[4,5] are not well understood.

It should be appreciated at the outset that the ions we have studied, $Co(NH_3)_5OH_2^{3+}$ (= $RoOH_2^{3+}$)[6] and $Co(NH_3)_6^{3+}$ (= $RoNH_3^{3+}$), are rather inert to oxidizing agents so that to get reactions of the kind we were interested in, we were obliged to resort to very powerful oxidizing systems.

Experimental Section

Preparation of Cobalt(III) Pentaammine Complexes and Special Reagents. Aquopentaamminecobalt(III) Perchlorate. Carbonatopentaamminecobalt(III) nitrate was prepared by the method of Lamb and Mysels.[7] This salt was converted to the aquo complex by treatment with 2 *M* perchloric acid and recrystallized three times from 0.1 *M* perchloric acid (see Table I).

O^{18}-Enriched Aquopentaamminecobalt(III) Perchlorate. Aquopentaamminecobalt(III) perchlorate of normal O^{18} content was enriched by the method of Hunt and Taube.[8] A saturated solution of the complex in 1.5% H_2O^{18}, made 0.01 *M* in perchloric acid, was heated at 65–75° for 6 hr. The enriched complex was recovered by cooling the mixture to 0° and filtering the precipitate. The crystals were washed with methanol and ether and dried under vacuum at 40°.

Hexaamminecobalt(III) Perchlorate. Hexaamminecobalt(III) bromide (furnished to us by Dr. R. B. Jordan) was dissolved in hot water, and perchloric acid was added dropwise to it until the solution became cloudy. The perchlorate salt which precipitated upon cooling was recrystallized three times from redistilled water.

$Co(ND_3)_5OH_2(ClO_4)_3$. A nearly saturated solution of $RoOH_2(ClO_4)_3$ in 99.8% D_2O at pH 6 (adjusted by using OD^- prepared by adding Na to D_2O) was kept at room temperature for 15 hr. At the end of this time the small amount of cobalt(III) oxide which had formed was filtered off and the solution made acidic with trifluoroacetic anhydride. The complex was precipitated with perchloric acid and recrystallized once from redistilled H_2O at a pH of 1.

$Co(ND_3)_6(ClO_4)_3$. The protonated species was placed in neutral 99.8% D_2O and heated at *ca.* 90° for 1 hr. At this time a small amount of cobalt(III) oxide was visible, and the solution was cooled to room temperature. The pH was 9.0 at this point; $(CF_3CO)_2O$ was added to pH of 2, then several drops of concentrated perchloric acid were added and the solution was cooled to 0°. The crystals which formed were filtered, washed with ether and methanol, and dried in a vacuum oven at 45°.

N^{15}-Enriched Ammonium Perchlorate. A mixture of ACS reagent grade NH_4NO_3 and 90% $N^{15}H_4N^{14}O_3$ (distributed by Bio-Rad Laboratories) was dissolved in redistilled water, and the ammonium perchlorate salt was precipitated by adding perchloric acid to the chilled solution. The N^{15}-enriched salt was recrystallized from hot, redistilled water by adding just enough perchloric acid to give a cloudly solution, then cooling to 0°. It was washed with ether and dried under vacuum at 40°.

Silver(II) Nitrate Solutions. Silver(II) nitrate in 6 *M* perchloric acid was prepared by the method of

Table I: Analysis of Pentaamminecobalt(III) Perchlorates[a]

Compound	Calcd	Found	Lit. value
$Co(NH_3)_5OH_2(ClO_4)_3$			
ϵ_{490}		47.3	47.5[b]
ϵ_{345}		44.5	44.8[b]
% N	15.2	15.4	
% H	3.7	3.7	
$Co(NH_3)_6(ClO_4)_3$			
ϵ_{475}		55.7	55.0[c]
ϵ_{340}		45.5	45.0[c]
% ClO_4^-	64.9	65.2	
% N	18.3	18.4	
% H	4.0	3.9	

[a] N and H determinations were performed by the microanalytical laboratory, Stanford Chemistry Department; ClO_4^- analysis was done gravimetrically by Mr. E. Deutsch, who precipitated the ClO_4^- as the tetraphenylarsonium salt. [b] H. Taube, *J. Am. Chem. Soc.*, **82**, 524 (1960). [c] A. Zwickel, Ph.D. Dissertation, University of Chicago, 1959.

(2) R. Robson and H. Taube, to be published.

(3) A. Haim and H. Taube, *J. Am. Chem. Soc.*, **85**, 495 (1963).

(4) H. Taube, *J. Gen. Physiol.*, **49**, 29 (1965).

(5) D. D. Thusius and H. Taube, *J. Am. Chem. Soc.*, **88**, 850 (1966).

(6) The radical $Co(NH_3)_5$ will in the following often be represented by the symbol Ro.

(7) A. Lamb and K. Mysels, *J. Am. Chem. Soc.*, **67**, 468 (1945).

(8) H. Hunt and H. Taube, *ibid.*, **80**, 2642 (1958).

Kirwin, *et al.*[9] The solution of redistilled water and perchloric acid was first purged with ozone to remove oxidizable impurities. Then the desired amount of silver perchlorate was added and ozone was bubbled through the iced solution until no further change was detected in the intensity of the dark brown color of the solution. Dissolved ozone was then removed with nitrogen.

Stock Reagents. The water for both the spontaneous and silver-catalyzed persulfate reactions was first deionized and then distilled from alkaline permanganate. For use in the spontaneous reactions, this water was heated (*ca.* 60°) with alkaline potassium persulfate until decomposition was complete, then distilled from the potassium sulfate. For use in the silver-catalyzed reactions, the water was heated (*ca.* 60°) with potassium persulfate, cobaltous perchlorate, and silver nitrate, and after complete decomposition of the persulfate, was collected by distillation. All water was stored in glass-stoppered bottles.

O^{18} water (1.5%) was supplied by Bio-Rad Laboratories. All O^{18} water was heated with silver nitrate and potassium persulfate in the presence of cobaltous perchlorate, then distilled and stored in glass bottles. D_2O (99.8%) was obtained from Bio-Rad Laboratories. Before use it was treated with Ag^+, $S_2O_8^{2-}$, and Co^{2+}, as in the case of H_2O^{18}. Thallic oxide furnished by Fisher Scientific Co. was dissolved in twice its weight of concentrated hydrochloric acid. To ensure that oxidation to the +3 state was complete, a small amount of sodium chlorate was added. The solution was cooled and filtered to give hexachlorothallic acid. Standard ampoules of NaOH manufactured by P. H. Tamm were diluted with boiled water which had been redistilled from alkaline permanganate. For solutions more concentrated than 0.1 *N*, ACS reagent grade NaOH was dissolved in water distilled from both alkaline permanganate and alkaline persulfate. H_2O_2 (3%) was obtained from the Braun–Knecht–Heimann Co., San Francisco, Calif. Cobaltous perchlorate, cerous perchlorate, and ceric perchlorate were supplied by the G. Frederick Smith Chemical Co. and were used without further purification. All other chemicals were ACS reagent grade and used without further purification.

Analyses. Cobalt(II) was determined spectrophotometrically as the thiocyanate complex according to the method of Kitsen.[10] Hydrochloric rather rather than chlorostannous acid was used because the latter was found to reduce the cobalt(III) ammine complexes. Excess $Fe(NH_4)_2(SO_4)_2$ in 2 *N* H_2SO_4 was added to the persulfate solution and back-titrated potentiometrically with primary standard $Ce(NH_4)_2(NO_3)_6$ in H_2SO_4 (G. Frederick Smith Chemical Co.). The concentration of a stock cerium(III) perchlorate solution was determined spectrophotometrically by oxidizing the colorless cerous ion to the yellow ceric carbonate complex. This method has been described by Sandell.[11] pH determinations were made with a Beckman Expandomatic pH meter equipped with microelectrodes. To determine the pH of a solution at an elevated temperature, the instrument was standardized at room temperature and the pH was then read directly by setting the temperature compensator control to the desired temperature. In the case of D_2O solutions, the meter was standardized using the empirical relation pD = pH + 0.4.[12]

The deuterium content of aquopentaammine and hexaamminecobalt(III) perchlorate was estimated by comparing the relative peak heights of the N–D and N–H stretching modes at 2400 and 3200 cm^{-1}, respectively. For $Co(ND_3)_5OH_2^{3+}$ the decrease at 850 cm^{-1} was also used. The per cent of nitrogen-15 in the N^{15}-enriched ammonium perchlorate was determined by the method of Riley, *et al.*,[13] in which the ammonium salt in base is oxidized by hypobromite. The nitrogen mass ratio 29/28 was read by peak heights with the mass spectrometer. The CO_2 equilibration method described by Hunt[14] was used to determine the O^{18} enrichment of the aquopentaammine complex.

Kinetics. The study of the spontaneous decomposition of persulfate in the presence of the cobalt(III) ammines was carried out at high and low phosphate concentrations, as well as in solutions containing no phosphate. For high phosphate concentrations the desired amounts of potassium persulfate and disodium phosphate were added to redistilled (from persulfate) water and the mixture was heated at 50° for 4–6 hr to purge the solution of oxidizable impurities. The solution was then cooled to room temperature and used as a stock reagent over a period of days. The pH of these solutions was 7–8. For more acidic reaction media the pH of this stock solution was adjusted by dropwise addition of concentrated perchloric acid. In the case of slow reactions, the cobalt(III) complex was added prior to the pH adjustment and the reaction was

(9) J. B. Kirwin, F. D. Peat, P. J. Proll, and L. H. Sutcliffe, *J. Phys. Chem.*, **67**, 1617 (1963).

(10) R. E. Kitsen, *Anal. Chem.*, **22**, 664 (1950).

(11) E. Sandell, "Colorimetric Determinations of Traces of Metals," 3rd ed, Interscience Publishers, Inc., New York, N. Y., 1954, p 385.

(12) R. G. Bates, "Determination of pH," John Wiley and Sons, Inc., New York, N. Y., 1964, p 219.

(13) R. F. Riley, E. Richter, M. Rotheram, N. Todd, L. S. Myers, Jr., and R. Nusbaum, *J. Am. Chem. Soc.*, **76**, 3301 (1954).

(14) H. R. Hunt, Ph.D. Dissertation, University of Chicago, 1957.

started by swirling the reaction mixture in the constant-temperature bath. For rapid reactions the persulfate solution (at the desired pH) was brought to reaction temperature and then either a solution of the complex or the salt itself was added with stirring. In the persulfate solutions with little or no phosphate, the preheating brings the pH down to 2–3. Following the preheating primary standard sodium carbonate was used to adjust the pH for reactions at pH 3–4 and sodium hydroxide for reactions at pH > 4. The sodium hydroxide was prepared with water redistilled from persulfate.

Kinetic measurements of the spontaneous decomposition were made by following the initial rate of cobalt(II) production. Aliquots were pipetted from the hot reaction solution, chilled, and diluted with thiocyanate, acetone, and hydrochloric acid. The optical density was determined with a Beckman Model DU spectrophotometer. In the case of high cobalt(III) hexaammine concentrations, centrifuging was necessary to remove the turbidity caused by precipitation of the salt by the acetone. In all runs the sample OD was corrected by using a cobalt(III) ammine blank of the appropriate concentration.

In neutral solutions cobalt(III) oxide was the principal product. It was produced as a fine suspension so that the above sampling procedure was still feasible. The sample was first added to hydrochloric acid, to convert the oxide to cobalt(II), and then diluted with thiocyanate and acetone. The data so obtained gave the rate of production of (cobalt(II) + cobalt(III)) oxide. In some runs, only the rate for cobalt(III) oxide was determined. In these cases the sampled suspension was filtered, washed with dilute perchloric acid, dissolved in hydrochloric acid, washed through the filter into a volumetric flask, and diluted to volume with thiocyanate, acetone, and water.

The initial rate of production of released cobalt (released cobalt is represented by Co_p was determined from the slope of the plot of $((Co)_p)$ *vs.* time. The specific rate constant for the process is defined as

$$k = \frac{d(Co)_p}{dt} \Big/ (S_2O_8^{2-})$$

The kinetics of the silver-catalyzed reaction were followed in much the same way as for the spontaneous reaction. Reaction solutions were prepared by first mixing all the reagents except the silver nitrate in redistilled (from Ag^+–$S_2O_8^{2-}$–Co^{2+}) water at room temperature. After adjusting the pH with concentrated perchloric acid, the solution was brought to the desired temperature in the constant temperature bath. Within 5 min the reaction was started by addition of the silver nitrate solution. Aliquots were quenched by chilling and sodium chloride was added to precipitate the silver. After removing the silver chloride by filtration the samples were diluted and read as described above.

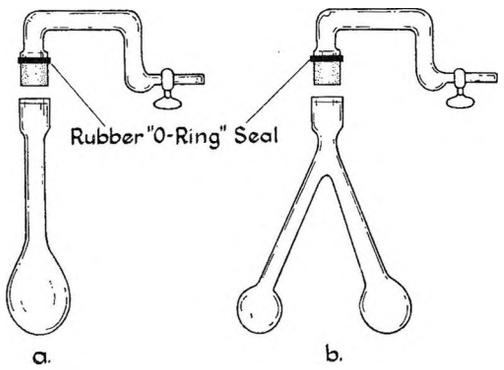

Figure 1. (a) Reaction vessels used for the uncatalyzed reaction; (b) vessels used for the Ag^+-catalyzed reaction.

Gas Analysis of Products. In the persulfate–cobalt(III) ammine reactions the general procedure was the same for both the spontaneous and silver-catalyzed reactions. It entailed the following steps: (1) degassing the reaction solution under vacuum, (2) starting the reaction and maintaining the solution at the selected temperature, usually 50°, (3) freezing the reaction solution and collecting the gas in a Urey tube, (4) measuring the amount of gas by means of a manometer, and (5) retrieving the gas from the manometer and analyzing it with the mass spectrometer. The vacuum reaction flasks used in these experiments are pictured in Figures 1a and b. The stopcock assembly was designed to prevent leaching of grease into the reaction mixture by evaporated solvent.

In the case of the uncatalyzed reactions, the reaction mixture was first prepared as described earlier. It was then transferred to the reaction flask and degassed by freezing the solution with a Dry Ice–alcohol sludge, then opening the stopcock and evacuating the flask, and finally closing the stopcock and thawing the mixture. This procedure was repeated at least two more times to ensure complete removal of dissolved air. The reaction was initiated by swirling the flask in the 50° bath for several minutes. A stream of warm air was directed on the stopcock assembly to minimize condensation of water vapor. After the desired length of time the reaction was quenched by swirling the flask in an ice bath.

The silver-catalyzed reaction solutions were degassed in the same fashion, with a solution of the cobalt(III) ammine, potassium persulfate, and perchloric acid in the large bulb (see Figure 1b) and the silver nitrate solution in the small bulb. After degassing,

the solutions were brought to 50° and mixed by tipping the flask to transfer the silver nitrate solution to the persulfate solution. An ice bath was used to quench the reaction.

In both the spontaneous and silver-catalyzed reactions the gas was transferred from the reaction flask to a Urey tube by means of a Toepler pump. To dry the gas a Dry Ice–alcohol trap was placed between the reaction flask and the Toepler pump. The amount of gas produced was measured by means of a vacuum manometer of calibrated volume.

Results

I. The Ag^+-Catalyzed Reaction of $S_2O_8^{2-}$ with $Co(NH_3)_5OH_2^{3+}$. General Observations on the Reactions in the $RoOH_2^{3+}$–Ag^+–$S_2O_8^{2-}$ System. When a solution of $AgNO_3$ is added to one containing $K_2S_2O_8$ and $RoOH_2(ClO_4)_3$ in dilute $HClO_4$, $S_2O_8^{2-}$ is reduced to SO_4^{2-}, O_2 is formed, and Co^{2+} is produced. Nitrogen gas comprises less than 2% of the gaseous products except when the pH becomes much higher. The rate of $S_2O_8^{2-}$ destruction is not materially affected by the presence of $RoOH_2^{3+}$, nor by the buildup of Co^{2+} or of other reaction products. Thus the specific rate of reduction of $S_2O_8^{2-}$, k_{Ag}, as defined by

$$-d(S_2O_2^{2-})/dt = k_{Ag}(Ag^+)(S_2O_8^{2-})$$

in an experiment at 50° and $\mu = 0.58$ was found to be $2.9 \times 10^{-2}\ M^{-1}\ sec^{-1}$ which can be compared to $2.4 \times 10^{-2}\ M^{-1}\ sec^{-1}$ as reported by Gupta and Ghosh[15] based on work in which Mn^{2+} was the reductant at $\mu = 1.0$. The difference in rate is slight and can be attributed to the difference in ionic strength; Gupta and Ghosh find k_{Ag} at $\mu = 0.64$ compared to $\mu = 1.0$ to be 1.2. Our specific rate for $\mu = 0.58$ compared to that measured by Gupta and Ghosh at $\mu = 1.0$ is also 1.2.

Figure 2 shows that the rate of production of Co^{2+} declines fairly rapidly as the reaction progresses. Even the initial rate of production is small compared to that of SO_4^{2-}, and it is therefore impossible on the basis of the rate laws alone to decide whether the reaction of $RoOH_2^{3+}$ with $S_2O_8^{2-}$ represents an additional path for the destruction of $S_2O_8^{2}$ or whether, in common with so many systems involving Ag^+ and $S_2O_8^{2-}$, the complex reacts with an intermediate generated by the action of $S_2O_8^{2-}$ on Ag^+. Because even with reducing agents more reactive than $RoOH_2^{3+}$ the latter situation obtains, we believe it obtains also in the present system. This view is corroborated by data appearing in Table II. When the results of expt 2 and 4 in Table II are compared, it is clear that the yield of Co^{2+} is independent of (Ag^+) and thus the reaction for Co^{2+} production and that which leads to the other product, O_2, have the same dependence on (Ag^+).

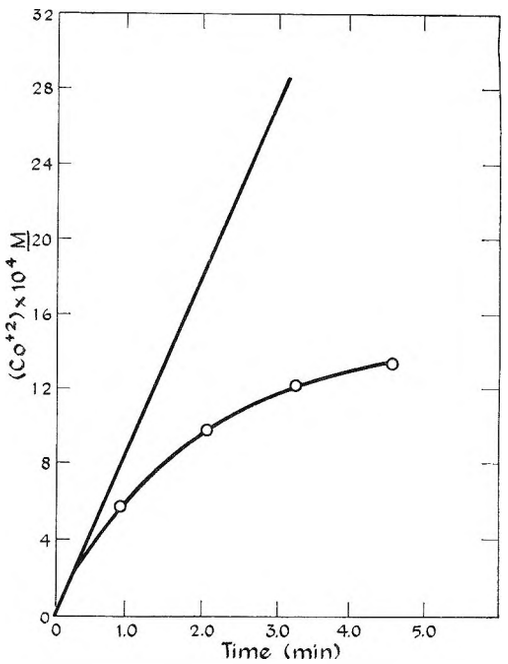

Figure 2. The production of Co^{2+} as a function of time in the Ag^+-catalyzed reaction: $AgNO_3 = 0.084\ M$; $K_2S_2O_8 = 0.050\ M$; $RoOH_2(ClO_4)_3 = 0.043\ M$; temp = 50.0°; pH 2.0 ± 3; $\mu = 0.6 \pm 0.1$. The initial slope is indicated by the straight line. It corresponds to $dCo^{2+}/dt = 1.5 \times 10^{-5}\ M\ sec^{-1}$.

Table II: Yields of Co^{2+} in the $RoOH_2^{3+}$–Ag^+–$S_2O_8^{2-}$ Reaction[a]

Expt no.	$(AgNO_3)$	$(K_2S_2O_8)$	$(RoOH_2(ClO_4)_3)$	$(Co^{2+})/(SO_4^{2-})$[b]
1	0.050	0.051	0.0064	0.0050
2	0.043	0.040	0.023	0.0140
3	0.046	0.039	0.023	0.0108[c]
4	0.083	0.037	0.023	0.0135
5	0.084	0.050	0.043	0.022
6	0.100	0.041	0.078	0.032
7	0.050	0.046	0.40	0.135[d]

[a] pH variable—*ca.* 1.9 → *ca.* 1.2 during course of reaction; temp 50.0°; $\mu = 0.6 \pm 0.1$; concentration in molarity. [b] Co^{2+} and SO_4^{2-} after complete decomposition of $S_2O_8^{2-}$. [c] $(Co(ClO_4)_2)_0 = 6.4 \times 10^{-4}\ M$; $(Co^{2+})_{final} = 14.8 \times 10^{-4}\ M$. [d] Temp 81°; $\mu = 2.5$.

The data of Table II show that the yield of Co^{2+} is proportional to the concentration of $RoOH_2^{3+}$, a circumstance which is quite compatible with the conclusion reached in the foregoing paragraph as long as

(15) Y. K. Gupta and S. Ghosh, *J. Inorg. Nucl. Chem.*, 9, 178 (1959).

Table III: Ag^+–$S_2O_8^{2-}$–$RoO^{18}H_2^{3+}$ Tracer Results[a]

Expt no.	$(AgNO_3)$	$(K_2S_2O_8)$	$(RoOH_2-(ClO_4)_3)$	E_R	t, min	$(Co^{2+}) \times 10^3$	$(O_2) \times 10^3$ [b]	E_O	O^*/Co^{2+} [c]
1	0.043	0.101	0.043	7.25	3.0	1.12	7.75	1.290	0.64
2	0.043	0.101	0.059	7.00	3.0	1.35	8.20	1.338	0.68
3	0.043	0.100	0.179	7.00	3.0	2.16	6.26	1.643	0.62
4	0.087	0.101	0.044	7.00	1.5	1.03	7.90	1.240	0.61
5	0.086	0.101	0.044	7.25	2.3	1.13	12.5	1.211	0.75[d]
6	0.086	0.101	0.022	7.25	1.5	0.69	8.88	1.175	0.73
7	0.084	0.051	0.043	7.25	3.0	1.11	7.27	1.285	0.60
8	0.043	0.048	0.042	7.00	3.0	0.96	...	...	...
9	0.043	0.049	0.042	7.25	3.0	1.24	3.88	1.293	0.61[e]
10	0.080	0.094	0.041	7.00	2.3	3.05	12.5	1.058	0.79[f]
11	0.043	0.101	0.043	7.00	3.0	0.78	7.02	1.240	0.72[g]
12	0.043	0.102	0.044	7.00	3.0	0.64	2.61	1.388	0.53[h]
13	0.038	0.098	0.098	7.00	2.3	1.90	2.84	2.370	0.17[i]

[a] Temp 50.0°; pH 1.7 ± 0.2; μ = 0.6 ± 0.1; concentrations in molarity; solvent and $S_2O_8^{2-}$ of normal isotopic composition. [b] (Moles of O_2 evolved)/(liter of reaction mixture). [c] Number of gram-atoms of aquo oxygen in the gas phase compared to the number of gram-atoms of Co^{2+} produced. [d] $(S_2O_8^{2-})$ = 0.0690 M at end of reaction. [e] $Co(ClO_4)_2$ = 6.43 × 10^{-4} M, t = 0 min. [f] $Co(ClO_4)_2$ = 2.74 × 10^{-3} M, t = 0 min. [g] pH 0.38. [h] $N^*H_4ClO_4$ = 86 × 10^{-3} M, t = 0 min. [i] 0.02 M NaOH present, t = 0; Co(III) as oxide = 6.1 × 10^{-3} M at end of reaction; Co^{2+} in O^*/Co^{2+} refers to sum of Co(III) oxide + Co^{2+}; N_2/O_2 = 0.61.

it is true that $RoOH_2^{3+}$ consumes only a small fraction of the intermediate generated by the Ag^+–$S_2O_8^{2-}$ reaction. Experiment 3 compared to experiment 2 shows that Co^{2+} somewhat inhibits the production of Co^{2+}.

O^{18}-Tracer Results. Although it has been shown that Co(III) in the aquopentaamminecobalt(III) complex is reduced to Co^{2+}, this fact does not prove that coordinated water is oxidized to oxygen. Tracer experiments which have been done, using oxygen-labeled $RoOH_2^{3+}$ in water of normal isotopic composition, and examining the isotopic composition of the oxygen which is formed do, however, prove that the oxygen which is contained in the complex is in good yield converted to O_2 (*cf.* Table III).

In the table, E_R and E_O represent enrichment ratios (that is, the isotopic ratio O^{18}/O^{16} in the sample compared to that in one of normal isotopic composition) of the complex and the evolved oxygen, respectively. The ratio O^*/Co^{2+} in the last column represents the number of gram-atoms of labeled oxygen placed in the gas phase per gram-atom of Co^{2+} produced. For completely efficient transfer to the gas phase of coordinated oxygen, this ratio would be 1.00. While the values of O^*/Co^{2+} do not reach this limit, they do get to be as high as ~0.075 and show that most of the Co^{2+} produced is accompanied by coordinated oxygen being transferred to the gas phase.

It should be mentioned, also, that having $RoOH_2^{3+}$ present protects the system from the deposition of solid products. Cobaltous ion alone serves this purpose, presumably acting by scavenging the oxidized form of silver which otherwise forms solid and providing an efficient route for the oxidation of water.

To sum up the conclusions reached in the foregoing, two reactions are necessary to describe the net change

$$S_2O_8^{2-} + H_2O = 2SO_4^{2-} + {}^1/_2O_2 + 2H^+ \quad (1)$$

$$3H^+ + {}^1/_2S_2O_8^{2-} + Co(NH_3)_5OH_2^{3+} = SO_4^{2-} + Co^{2+} + 5NH_4^+ + {}^1/_2O_2 \quad (2)$$

Reaction 2 waits on the formation of an intermediate generated by the interaction of Ag^+ and $S_2O_8^{2-}$. The intermediate for the most part reacts to form O_2 and in small part attacks $RoOH_2^{3+}$ forming Co^{2+}.

The values of O^*/Co^{2+} shown in Table III are seen to be somewhat variable even for experiments which are duplicates. The cause of this variability as well as of the defect in the values of O^*/Co^{2+} from 1.00 is that processes besides oxidation of coordinated water can produce Co^{2+}.

The variability may in part have an extrinsic cause. It is difficult to ensure that all carbonaceous material has been eliminated even by the pretreatment used. All of the gas samples contain CO_2 in addition to O_2; the CO_2 content is variable but for the experiments reported on in Table III it does not exceed 2 mole %. In an earlier series of experiments, a sample of the complex salt was used which had become contaminated with carbonaceous material. The gases collected in the experiments done with this material contained as much as 30 mole % CO_2 and the values of O^*/Co^{2+} calculated from the results were of the order of 0.45.

In one of the experiments, an initial sample of gas was withdrawn showing a CO_2/O_2 ratio of 0.40; for this portion O^*/Co^{2+} was determined as 0.46. A second sample was then withdrawn which showed CO_2/O_2 as 0.010 and gave for O^*/Co^{2+} a value of 0.67. These results suggest that stray carbonaceous material does reduce Co(III) to Co^{2+} but without delivering complex-bound oxygen to the gas phase as O_2.

Several experiments were undertaken with carbonaceous material of known identity to investigate the reduction of $RoOH_2^{3+}$ by carbon radicals. In one series of experiments, Ce(IV) was added dropwise to a solution containing $RoOH_2^{3+}$ and $H_2C_2O_4$. The Co^{2+} content of the solution after reaction was determined and a tracer experiment on the CO_2 was done in which the gas was swept from the solution by a stream of He and the CO_2 was collected in a liquid air trap. A complication in the experiments is that a precipitate may form. The precipitate contains $RoOH_2^{3+}$, Ce(IV), and oxalate; its formation can be avoided by adjusting the concentrations of the solutes, including that of $HClO_4$.

In one experiment with $H_2C_2O_4$ at 0.072 *M*, $[RoOH_2](ClO_4)_3$ at 0.0142 *M*, $HClO_4$ at 1.5 *M*, and Ce(IV) perchlorate at 0.016 *M* (the concentrations correspond to those which would have obtained after mixing but before reaction), the ratio of Co^{2+}/CO_2 produced was 0.197. In a second experiment the concentrations were substantially the same but Ce(IV) was 0.028 *M;* in this case the ratio Co^{2+}/CO_2 was observed to be 0.145. The second experiment was done using O^{18}-enriched aquo ion, but no enrichment appeared in the CO_2. A qualitative experiment was undertaken with $KMnO_4$ as the oxidant; this reagent, oxalic acid, and aquo ion were each a *ca.* 0.05 *M* and perchloric acid was at 0.2 *M*. In this system as well considerable reduction of Co(III) to Co^{2+} occurred. The three experiments demonstrate that the radical obtained by $1e^-$ oxidation of oxalate has the capacity to reduce aquopentaamminecobalt(III).

Carbon-containing radicals are extrinsic to the system and come into question only because carbonaceous matter is difficult to eliminate completely. (Though the actual content of carbonaceous material is very small, the products of its oxidation represent a substantial part of the gas formed because reaction occurs only to a small extent and carbonaceous matter is destroyed preferentially.) Radicals derived from H_2O_2 may, however, well be intrinsic to the system because hydrogen peroxide is a likely intermediate in the oxidation of water to oxygen. We did an experiment to learn whether the reaction of Ce(IV) with H_2O_2 induces the reaction of the aquo complex. In the experiment, 3.00 ml of 0.050 *M* Ce(IV) in 0.6 *M* $HClO_4$ was added dropwise over 10 min to a well-stirred solution, 6.00 ml in volume at 50–60°, which was 0.13 *M* in $[RoOH_2](ClO_4)_3$ and 0.15 *M* in H_2O_2. After the addition of Ce(IV), the solution was found to be 9.5×10^{-4} *M* in Co^{2+}; no measureable amounts of Co^{2+} are produced by Ce(IV)–$RoOH_2^{3+}$ or H_2O_2–$RoOH_2^{3+}$ mixtures under similar conditions. An additional blank experiment showed that the Co(III) salt without the "inductor" system would account for less than 1×10^{-4} *M* Co^{2+}. The induced reduction of Co(III), though small in extent, is definite. It is, of course, difficult to extrapolate from conditions of these experiments to those obtaining for the $[RoOH_2](ClO_4)_3$–Ag^+–$S_2O_8^{2-}$ system. In the former the radical HO_2, which we may reasonably assume to be the intermediate, is destroyed by Ce(IV) and in the latter by a different oxidizing agent or perhaps by disproportionation. It is possible, therefore, that the radical HO_2 plays a much greater role in reducing Co(III) in the latter system than is indicated by the induction factor uncovered in the $[RoOH_2]^{3+}$–Ce(IV)–H_2O_2 system.

Still another intrinsic process which may lead to reduction of Co(III) without concomitant production of O_2 is oxidation of coordinated NH_3. About 0.5–2.0% of the gas is N_2, which blank experiments as well as the magnitude of the Ar peak showed could not have come from contamination by air. That most of the N_2 does not arise from the oxidation of NH_4^+ was shown by doing an experiment (0.043 *M* $AgNO_3$, 0.100 *M* $K_2S_2O_8$, 0.097 *M* $RoOH_2(ClO_4)_3$, pH 1.7, $t = 3.0$ min) in the presence of 0.010 *M* NH_4ClO_4, 16-fold enriched in N^{15}. Only 3% of the N_2 evolved was found to have originated from the NH_4^+. The major product of the oxidation of NH_4^+ is presumably NO_3^-. The oxidation to nitrate of ammonia released as NH_4^+ by the reduction of the complex may also contribute to the defect of the values of O^*/Co^{2+} from the maximum of 1.00. In expt 12 of Table III, 8.6×10^{-2} *M* NH_4ClO_4 was added at the beginning of the experiment. Compared to expt 1, which is similar except that NH_4^+ was not added initially, the yield of oxygen is seen to be much diminished and the value of O^*/Co^{2+} is significantly less. The amount of NH_4^+ formed in the course of the reaction such as expt 1, Table III, is only of the order of 5×10^{-3} and thus the effect of the accumulated NH_4^+ on the results is expected to be considerably less than shown in expt 12. Nevertheless the factor referred to will be significant in depressing the values of O^*/Co^{2+}.

The check on the consumption of $S_2O_8^{2-}$ which was made in expt 5 of Table III proves that reactions 1 and 2 do not account for the disappearance of all of the

$S_2O_8^{2-}$. Making allowance in the total stoichiometry also for the reduction of Co(III) (reaction 2), it appears that 22% of the $S_2O_8^{2-}$ is found to disappear without producing an equivalent amount of O_2. The oxidation of carbonaceous material and the production of N_2 account for only a small part (2%) of the excess persulfate consumed, and it is likely that most is taken up in producing NO_3^-.

There is no dearth of processes to explain the excess production of Co^{2+} which is observed. Correction for the oxidation of carbonaceous material can raise O^*/Co^{2+} to *ca.* 0.80 and, assuming oxidation of coordinated NH_3, it can be brought to ~0.90. In view of the effects demonstrated, it seems likely that in those acts in which coordinated oxygen is oxidized, O^*/Co^{2+} is in fact close to 1.00.

Other Experiments. A tracer experiment was done using $S_2O_8^{2-}$ (0.100 *M*) of normal isotopic composition, 0.043 *M* $AgNO_3$, and 2.6×10^{-4} *M* $Co(ClO_4)_2$ (the latter reagent prevents the formation of the black precipitate) and in water threefold enriched in O^{18}. The oxygen gas was collected and was found to be of the same isotopic composition as the solvent.

In acting on our concern about the nature of the intermediates which give rise to the effects which have been described for $RoOH_2^{3+}$, experiments were done adding dilute solutions of Ag^{2+} to $RoOH_2^{3+}$. In one experiment at 58° with $(AgNO_3) = 0.25$ *M*, $(HClO_4) = 3.0$ *M*, $(RoOH_2^{3+}) = 0.014$ *M*, $\Delta(Co^{2+})/\Delta Ag^{2+}$ was found to be 0.009; in another at 52°, with $(AgNO_3) = 0.49$ *M*, $(HClO_4) = 3.0$ *M*, and $(RoOH_2^{3+}) = 0.086$, $\Delta Co^{2+}/\Delta Ag^{2+} = 0.070$. The effects are seen to be of the order of magnitude of those observed in the $RoOH_2^{3+}$–Ag^+–$S_2O_8^{2-}$ system.

II. The Uncatalyzed Oxidation of $RoOH_2^{3+}$ by $S_2O_8^{2-}$. A solution of $RoOH_2^{3+}$ when heated with $S_2O_8^{2-}$ even in the absence of Ag^+ produces Co^{2+}. The stoichiometry of the reaction, however, differs in important respects from that observed when Ag^+ is a catalyst. The results obtained in the study of the stoichiometry and kinetics of the reaction are summarized in this section.

(a) The $RoOH_2^{3+}$–$S_2O_8^{2-}$ System in the pH Range 3.2–4.4. A summary of the results obtained on the rate of Co^{2+} production as a function of several variables is given in Table IV. The specific rate appearing in the last column of the table is defined by the rate law

$$k = [d(Co^{2+})/dt]/(S_2O_8^{2-})$$

In Figure 3 the results of most of the experiments are displayed as a plot of k against $(RoOH_2^{3+})$. The figure also summarizes the results of some isotopic experiments which will be considered in a later section.

Table IV: Rates of Co^{2+} Production in the $S_2O_8^{2-}$–$RoOH_2^{3+}$ Reaction[a]

Expt no.	$K_2S_2O_8$	$RoOH_2(ClO_4)_3$ (× 10^4)	pH	k[b] (× 10^6 sec^{-1})
1	0.147	1.6	3.4	0.43[c]
2	0.145	1.9	3.6	0.53
3	0.147	2.1	3.6	0.48
4	0.147	2.0	3.4	0.40[c]
5	0.141	3.7	3.6	0.58
6	0.141	7.4	3.6	0.82
7	0.148	14.2	3.5	0.92[c]
8	0.148	28.3	3.2	1.07[c]
9	0.0357	40.3	3.4	1.08
10	0.141	1.25	4.2	0.52
11	0.148	5.0	4.3	0.87
12	0.148	19.5	4.3	1.00
13	0.148	36.5	4.4	0.98
14	0.142	452.0	4.1	0.32[c,d]

[a] pH 3.4–4.4; *T* 50.0°; sodium phosphate = 0.050 *M*; perchlorate media; μ = 0.5–0.8; concentrations in molarity. [b] $k = [d(Co^{2+})/dt]/(S_2O_8^{2-})$. [c] No phosphate. [d] $(Ce^{3+}) = 9.5 \times 10^{-4}$ *M*.

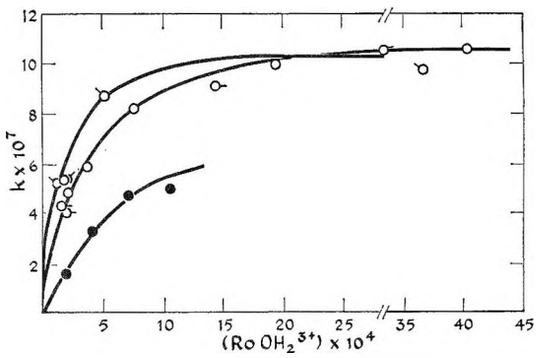

Figure 3. The rate of the Co^{2+} production in the uncatalyzed reaction as a function of $(RoOH_2^{3+})$ under various conditions (temp 50°, $(NaH_2PO_4) = 0.05$ *M* except where otherwise specified, μ = 0.60, $(K_2S_2O_8) = 0.13 \pm 0.01$ *M*): O, pH 3.2–3.6; O-, pH 3.2–3.6 (no phosphate); ○, pH 3.3 (NH_3 in complex, *ca.* 80% deuterated); ○, pH 4.1–4.2; ●, pD 3.7–3.9 (in D_2O, complex deuterated, no phosphate). A data point (●) corresponding to $k = 9.8 \times 10^{-7}$ M^{-1} sec^{-1} when $(RoOD_2^{3+}) = 203 \times 10^{-4}$ is not shown on the graph.

The most striking feature of the data (*cf.* Figure 3) is that though the rate of Co^{2+} production does increase with $(RoOH_2^{3+})$ when $(RoOH_2^{3+})$ is low, it becomes independent of this variable as its magnitude increases. The rate of Co^{2+} production does, however, vary directly with the concentration of $S_2O_8^{2-}$ (*cf.* expt 8 and 9 of Table IV) even after the rate has reached a "saturation" value with respect to $(RoOH_2^{3+})$.

Some evidence[16] has been adduced supporting the conclusion that when $S_2O_8^{2-}$ decomposes in not too acidic solution, the radical HO is produced.[17] The specific rate of production of HO on this basis at 50° is 2.0×10^{-6} sec^{-1} which is just twice the rate at which Co^{2+} forms. The data of Table V show that the 2:1 relationship is maintained over a range of conditions. We conclude therefore that the 2:1 ratio at saturation is not coincidence, but has stoichiometric significance.

Table V: Saturation Specific Rate for the Production of Co^{2+} Compared to the Rate of Production of HO from $S_2O_8^{2-}$

T, °C	pH	k at saturation, sec^{-1}	Specific rate of HO production, sec^{-1}
50.0	4.2	1.0×10^{-6}	2.0×10^{-6}
50.0	3.4–3.6	1.0×10^{-6}	2.0×10^{-6}
60.0	3.4–3.6	5.2×10^{-6}	1.0×10^{-5}
69.9	3.4–3.6	1.9×10^{-5}	4.5×10^{-5}

The conclusion cited in the previous paragraph is corroborated by the observations made on the total stoichiometry at rate saturation. In an experiment at 50°, with pH 3.6 (phosphate buffer), $(RoOH_2(ClO_4)_3) = 3.9 \times 10^{-3}$ continuing for 68 min, cobaltous ion was formed at a concentration of 5.9×10^{-4} M, and the amount of N_2 formed per liter of reaction solution was 2.7×10^{-4} mole. Excluding CO_2, always present in small amount as a result of carbonaceous material which was not eliminated, N_2 is the only gaseous product of the reaction at rate saturation and the main net change expressed in terms of HO is therefore represented by the equation

$$3H^+ + Co(NH_3)_5OH_2^{3+} + 2HO = Co^{2+} + 4NH_4^+ + {}^1/_2N_2 + 3H_2O \quad (3)$$

Two HO and one Co(III) are involved in the oxidation of one coordinated NH_3 to nitrogen, thus accounting for the 2:1 ratio of HO/Co^{2+} observed at rate saturation.

Even when the rate of Co^{2+} production is well below the saturation value, the yield of oxygen remains small. In an experiment at pH 3.4 with $(RoOH_2^{3+})$ initially at 0.119×10^{-4} M, after 60 min of heating, $(RoOH_2^{3+})$ had decreased to 1.04×10^{-4} M and 0.83×10^{-4}, 0.44×10^{-4}, and 0.055×10^{-4} moles of Co^{2+}, N_2, and O_2, respectively, were produced. If the production of Co^{2+} had proceeded at the saturation rate, the (Co^{2+}) at the end of the experiment would have been 5.4×10^{-4} M. The production of O_2, Co^{2+}, and N_2 by no means accounts for the consumption of $S_2O_8^{2-}$, and it is clear that some process or processes not yet described provides for the consumption of HO radicals. In all likelihood, what is involved is the oxidation of nitrogen to states above zero in oxidation number. Mass spectrometer analysis revealed the presence of N_2O (*ca.* 10 mole %) in the products of a reaction similar to that referred to above, but with the initial concentration of $RoOH_2^{3+}$ *ca.* 3.5-fold higher and with the pH at 4.5. The amount of N_2O was not great enough to account for the defect in the production of oxidized products and probably NO_3^- was also a product.

(*b*) *Variation with pH.* In Table VI and Figure 4 are shown data obtained at pH 2.4 and in the range 1.2–1.8. A definite decrease in the saturation value of the specific rate is observed as the pH falls: it is *ca.* 0.8×10^{-6} sec^{-1} at pH 2.4 and 0.7×10^{-6} sec^{-1} at the lower pH range. The concentration of $RoOH_2^{3+}$ needed to bring the rate of Co^{2+} production to one-half the saturation value is about 3×10^{-4} M at pH 2.4 and increases somewhat at lower pH. The increase as

Table VI: Rates of Co^{2+} Production in the $S_2O_8^{2-}$–$(NH_3)_5CoOH_2^{3+}$ Reaction[a]

Expt no.	$(K_2S_2O_8)$	$(RoOH_2(ClO_4)_3) \times 10^3$	pH	k ($\times 10^7$ sec^{-1})
1	0.147	0.127	2.4	3.3
2	0.147	0.61	2.4	5.3
3	0.147	1.56	2.4	5.8
4	0.147	1.52	2.4	5.8[b]
5	0.147	4.20	2.4	7.0
6	0.143	1.03	2.4	5.2[c]
7	0.189	3.07	2.4	6.3[c]
8	0.160	10.50	2.4	8.3[c]
9	0.154	19.00	2.4	7.7[c]
10	0.130	51.00	2.4	7.5[c]
11	0.098	2.00	1.2	5.2[d]
12	0.099	3.40	1.2	6.0[d]
13	0.145	2.20	1.4	5.8
14	0.145	10.00	1.8	6.7
15	0.147	20.30	1.2	7.2[d]
16	0.142	46.00	1.8	2.5[d,e]

[a] pH 1.2–2.4; T 50.0°; sodium phosphate = 0.050 M; perchlorate media; concentrations in molarity. [b] $NH_4ClO_4 = 1.3 \times 10^{-3}$ M. [c] Solvent was distilled only from MnO_4^-; no preheating with $S_2O_8^{2-}$. [d] No phosphate. [e] $Ce^{3+} = 8.6 \times 10^{-4}$ M.

(16) W. K. Wilmarth and A. Haim, "Peroxide Reaction Mechanisms," J. O. Edwards, Ed., Interscience Publishers, Inc., New York, N. Y., 1962, pp 199–200.

(17) I. M. Kolthoff and J. K. Miller, *J. Am. Chem. Soc.*, **73**, 3055 (1951).

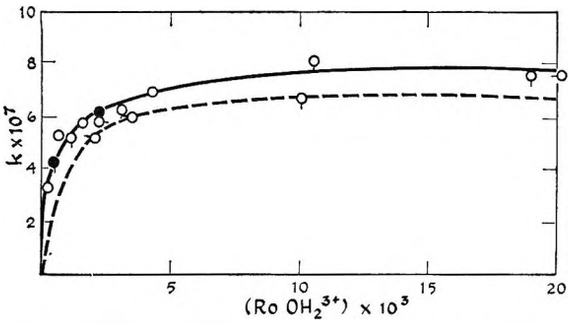

Figure 4. The rate of Co^{2+} production in the uncatalyzed reaction as a function of ($RoOH_2^{3+}$) under the same conditions as in Figure 3, but in more acidic solution: O, pH 2.4; ♀, pH 2.4 (no preheating of $S_2O_8^{2-}$); O-, pH 1.4; -O, pH 1.2 (no phosphate); ●, pH 1.4 (NH_3 in complex, *ca.* 80% deuterated); ●, pH 2.3 (NH_3 in complex, *ca.* 80% deuterated).

pH is lowered, even if not regular, is at least monotonic over the pH range 4–1.4. An analysis of the gas was performed for one experiment at pH 2.4. In this experiment ($RoOH_2^{3+}$) = 0.019 *M* and ($S_2O_8^{2-}$) = 0.147; *ca.* 6% of the gas was observed to be O_2 and the ratio of $\Delta N/\Delta Co^{2+}$ was ~0.9.

Figure 4 shows that the prepurification has little effect on Co^{2+} production, even though the CO_2 content of the gas was *ca.* 50 mole % in the samples not subject to pretreatment. Even after pretreatment, the CO_2 content was in the range 10–25%, but again no effect on Co^{2+} production could be related to the variability in CO_2 production. We are led to conclude that carbonaceous matter disappears by a chain reaction with $S_2O_8^{2-}$ and that there is little interaction between this chain process and the processes leading to the reduction of $RoOH_2^{3+}$. In terms of the earlier discussion, one hydroxyl radical can in principle lead to the destruction of several equivalents of carbonaceous matter by catalyzing its chain reaction with $S_2O_8^{2-}$. Experiment 4 of Table VI compared to expt 3 shows that moderate concentrations of NH_4^+ do not inhibit Co^{2+} production even short of rate saturation. The active intermediate apparently does not react readily with NH_4^+.

At high pH's, the reaction stoichiometry changes markedly. In an experiment at 50° with ($S_2O_8^{2-}$) = 0.125, ($RoOH_2^{3+}$) = 11.7 × 10^{-3}, and pH 6.9 ((Na_2HPO_4) = 1.2 × 10^{-3} *M*), *k* (where this now measures the total rate of destruction of Co(III) and not the rate of formation of Co^{2+}) was observed as 1.1 × 10^{-6} sec^{-1}. A black precipitate formed which we take to be a cobalt oxide, but which analysis proved as containing only 12% of the cobalt in the 2+ state, the balance presumably being in the 3+ state. The gas under these conditions contained oxygen in addition to nitrogen, the former component comprising about 30% of the total. Several additional experiments were done to provide information on the mode of formation of the cobaltic oxide. They revealed that neither O_2 nor H_2O_2 oxidize Co^{2+} to Co(III) under similar experimental conditions and further that the oxide does not form simply as a result of a bimolecular reaction of $S_2O_8^{2-}$ and Co^{2+}. A tracer experiment showed that only 5% of the oxygen formed contained atoms derived from the Co(III) complex.

(*c*) *H–D Isotope Effects.* A data point in Figure 3 (see legend) shows that there is no effect on the rate of Co^{2+} production by D substitution in the coordinated ammonias of $Co(NH_3)_5OH_2^{3+}$. At the pH of the experiment, 3.2, it was shown by infrared analysis of the hexachlorothallium(III) salt that 30% exchange of D for H had occurred, thus weakening the conclusion to some extent. At lower pH's, the rate of $-NH_3-D$ exchange is diminished and the conclusion is upheld by the data shown in Figure 4, taken at pH's 1.4 and 2.3.

However, when $Co(ND_3)_5OD_2^{3+}$ reacts in D_2O, there is a marked decrease in the rate. The results of Figure 3 demonstrate that the rate of Co^{2+} release as measured by the initial slope is 4.5–5 times less rapid than in the corresponding reaction of $Co(NH_3)_3OH_2^{3+}$ in H_2O. In considering the observations account should be taken of the fact that although the exchange of hydrogen in coordinated NH_3 with D_2O is slow in acid, it is very rapid in coordinated H_2O. The result at high ($RoOH_2^{3+}$) as reported in the legend to Figure 3 indicates that the saturation value of rate is insensitive to H–D substitution.

III. The Oxidation of $RoNH_3^{3+}$ by $S_2O_8^{2-}$. In the reaction of $RoNH_3^{3+}$ with $S_2O_8^{2-}$, Co^{2+} is produced and at the higher values of ($Ro(NH_3)_6^{3+}$), just as with $RoOH_2^{3+}$, N_2 is the gaseous product of the reaction. The kinetic data obtained with $RoNH_3^{3+}$ are summarized in Table VII and in part are displayed in Figure 5.

Rate saturation is observed also with $RoNH_3^{3+}$ as reductant but the saturation value of the specific rate ~0.7 × 10^{-6} sec^{-1} is considerably below that observed with $RoOH_2^{3+}$. The efficiency of $RoNH_3^{3+}$ in competing for the intermediate generated by the decomposition of $S_2O_8^{2-}$ is considerably less than that of $RoOH_2^{3+}$ (note that the concentration of $RoNH_3^{2-}$ to reach one-half rate saturation with the former agent is ~2 × 10^{-3} compared to ~2 × 10^{-4} for the latter). A profound difference between the systems is observed in the effects of deuteration. In the present system there is a marked decrease in rate when $Co(ND_3)_6^{3+}$ is used in place of $Co(NH_3)_6^{3+}$. Because exchange

Table VII: Rates of Co^{2+} Production in the $S_2O_8^{2-}$–$Co(NH_3)_6^{3+}$ Reaction[a]

Expt no.	$(K_2S_2O_8)$	$(Co(NH_3)_6(ClO_4)_3)$ × 10^4	Solvent	Acidity pH	Acidity pD	k (× 10^6 sec^{-1})
1	0.14	1.0	H_2O	3.5		0.17
2	0.14	3.1	H_2O	3.3		0.53
3	0.14	10.4	H_2O	3.3		0.68
4	0.15	20.0	H_2O	3.3		0.70
5	0.14	3.2	H_2O	3.3		0.18[b]
6	0.12	10.0	H_2O	3.3		0.35[b]
7	0.15	10.5	99% D_2O		3.8	0.13[c]
8	0.15	22.2	99% D_2O		3.4	0.25[c]
9	0.15	1.9	H_2O	2.5		0.58
10	0.15	9.8	H_2O	2.5		0.58
11	0.14	5.6	H_2O	2.5		~0.15[d]

[a] T 50.0°; sodium phosphate = 0.050 M; perchlorate media; concentrations in molarity. [b] The complex was ~70% deuterated ($Co(ND_3)_6^{3+}$. [c] The complex was 99% deuterated $Co(NH_3)_6^{3+}$. [d] $(Co(ClO_4)_2)_0 = 1.3 \times 10^{-3}$ M.

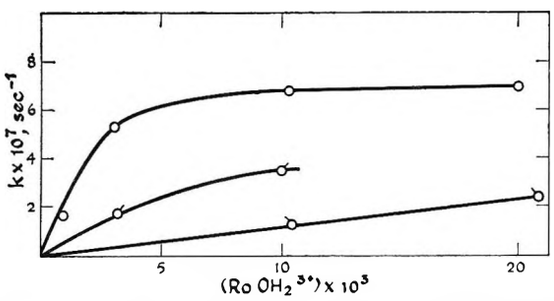

Figure 5. The rate of production of Co^{2+} from $RoNH_3^{3+}$ in the uncatalyzed reaction (temp = 50°, NaH_2PO_4 0.05 M, μ = 0.6): O, pH 3.3–3.5; ☌, pH 3.3 (complex 70% deuterated); ☋, pH 3.4–3.8 (complex 99% deuterated in D_2O).

during reaction is extensive, it is difficult to get a good measure of the H–D effect. Taking account of the exchange, a decrease of perhaps 8 or 9 in rate is indicated on replacing H by D in the coordination sphere. If in addition the solvent is deuterated, the decrease in rate as judged by the slope at low Co^{2+} in Figure 5 is by a factor of about 18. Thus a solvent isotope effect by a factor of about 2 is indicated.

It seems certain that the rate decreases recorded on deuteration are not the result of impurities in the deuterated hexaammine. Experiment 3 of Table VI was run after first allowing $Co(ND_3)_6^{3+}$ to exchange with solvent and the rate is seen to be normal. Experiment 8 was done by allowing $Co(NH_3)_6^{3+}$ to exchange with D_2O, then initiating the reaction. Experiments 9 and 10 at pH 2.5 suggest that rate saturation in this system, as in the aquo, sets in more sharply at lower pH's and indicate furthermore that the limiting value of k becomes less at lower pH. The data are too sparse to provide firm support for either conclusion. Taken together with the results of expt 11, they do seem to show that Co^{2+} has a striking inhibitory effect on the rate.

Discussion

The evidence uncovered for the oxidizing system Ag^+–$S_2O_8^{2-}$ acting on $RoOH_2^{3+}$ shows that this reducing agent in common with many others waits on the formation of an intermediate resulting from the interaction of Ag^+ with $S_2O_8^{2-}$. The reactivity of the intermediate to $RoOH_2^{3+}$ is not great, however, and a concentration far beyond the limit imposed by the solubility of $RoOH_2(ClO_4)_3$ would be required to reach the saturation rate in this case.

An important question to settle is the identity of the intermediate which reacts with $RoOH_2^{3+}$. When account is taken of the chemistry of the system, the only reasonable candidates appear to be (i) Co^{3+}, (ii) Ag(II) (or Ag(III)), and (iii) HO or SO_4^-. Our observations suffice to distinguish between the three categories but not to make the distinctions within the categories (ii) or (iii).

Direct experiments testing the action of Co^{3+} on $RoOH_2^{3+}$ as well as the fact that buildup of Co^{2+} decreases the rate of production of Co^{2+} from $RoOH_2^{3+}$ in the Ag^+–$S_2O_8^{2-}$ reaction show that neither Co^{3+} nor a species of higher oxidation number derived from it can be the active species. As the later discussion shows, the radical HO (or SO_4^-) is apparently involved in the uncatalyzed reaction where the reaction takes a markedly different stoichiometric course and the N_2 rather O_2 is the gaseous product. By elimination we are directed to the conclusion that highly oxidized silver species attack $RoOH_2^{3+}$. This conclusion is supported by the fact that a solution containing Ag^{2+} does produce Co^{2+} from $RoOH_2^{3+}$. It is also reasonable on the grounds that Ag^+, being present in high concentration in acidic solution, would be expected to convert HO or SO_4^-, if produced, to Ag(II) or Ag(III). Our data suggest that the same intermediate attacks water in $RoOH_2^{3+}$ as attacks other water, but does not lead to a decision between the states Ag(II) and Ag(III) which are in labile equilibrium.[9,18] In principle, a decision could be reached by a kinetic study of the direct reaction of Ag(II)(Ag(III)) with $RoOH_2^{3+}$.

Two distinct mechanisms for the oxidation of coordinated water need to be considered, and both are

(18) B. M. Gordon and A. C. Wahl, *J. Am. Chem. Soc.*, **80**, 273 (1958).

consistent with the stoichiometry and the oxygen tracer experiment.

A. $(NH_3)_5CoOH_2^{3+} \longrightarrow (NH_3)_5Co^{IV}OH_2 + e^-$ (4)

$$(NH_3)_5Co^{IV}OH_2 + OH_2 \longrightarrow Co^{2+} + HOOH + H^+ + NH_4^+ \quad (5)$$

B. $(NH_3)_5CoOH_2^{3+} + H_2OAg(II) \longrightarrow Co^{2+} + HOOH + Ag^+ + NH_4^+$ (6)

By either mechanism H_2O_2 is formed as an intermediate but it is, of course, readily oxidized in the Ag^+–$S_2O_8^{2-}$ system. In mechanism A, the O–O bond formation takes place by a $2e^-$ change generated on a single oxygen; in mechanism B, two one-electron changes cooperate in making formation of the O–O bond possible. As will appear presently, we find it necessary to invoke Co(IV) as the means by which coordinated NH_3 is oxidized and therefore conclude that mechanism B operates in the reaction under present discussion. The mechanism has much in common with the "reduction" of halopentaamminecobalt(III) species brought about by halogen atoms or other oxidizing radicals.[3] In the present system, however, the radical external to coordinated ligand is not pre-formed but is formed in the act of constructing the O–O bond. A mechanism such as B may also operate in the oxidation of water by Co^{3+}. An important path for this reaction is second order in (Co^{3+}) and inverse second order in (H^+).[19]

$$Co^{III}OHHOCo^{III} \longrightarrow 2Co^{2+} + H_2O_2 \quad (7)$$

In many cases, coordination of a ligand to a metal center protects the ligand from oxidation. This is notably the case for oxalate whether bound to $Co(NH_3)_5^{3+}$[1] or to Cr^{3+}.[20] In the $RoOH_2^{3+}$–Ag^+–$S_2O_8^{2-}$ system, there is kinetic assistance from the $Co(NH_3)_5^{3+}$ in oxidizing coordinated water. When account is taken of the rates at which water coordinated to Co(III) and other free water are oxidized and their respective abundance, the reactivity of water coordinated to Co(III) to the oxidizing intermediate is found to be approximately 100 times that of free water.

The $RoOH_2^{3+}$–$S_2O_8^{2-}$ system differs from that containing also Ag^+ in two important respects, namely, that the gaseous product is now N_2 rather than O_2 and that the reactivity to $RoOH_2^{3+}$ of the intermediate is very much higher. The reactivity is so great that a a concentration of 10^{-3} M suffices (see Figure 3) to divert all of the intermediate to reaction with $RoOH_2^{3+}$. Our results do not distinguish between SO_4^- and HO as the intermediate which attacks $RoOH_2^{3+}$. We can, however, rely on the testimony of Wilmarth and Haim[16] to the effect that a labile equilibrium

$$HO + H^+ + SO_4^{2-} = H_2O + SO_4^- \quad (8)$$

is maintained and thus the position of the equilibrium is such that at the low concentration of H^+ and SO_4^{2-} obtaining in our experiments the one-electron oxidizing agent is HO rather than SO_4^-.

The reaction[21] of HO with cobaltammines has been suggested as one of the processes involved in the radiation chemistry of aqueous solutions of amminecobalt(III) complexes. Our results agree with those of Katakis and Allen in the major respect that N_2 is the dominant gaseous product derived from the reaction of the cobaltammines in their system as in ours. There is, however, an important difference which we are quite unable to account for, namely, that in the irradiated system, Co^{2+} accelerates the rate of the Co^{2+} production, but in ours it is clearly inhibitory (*cf.* expt 11, Table VII).

The large diminution in rate which is observed when $Co(ND_3)_6^{3+}$ reacts in place of $Co(NH_3)_6^{3+}$ strongly suggests that HO attacks by H-atom abstraction, as it does in its reaction with most compounds containing H–C bonds.

$$(NH_3)_5Co^{III}NH_3^{3+} + OH \longrightarrow (NH_3)_5CoNH_2^{3+} + H_2O \quad (9)$$

The species with oxidized NH_3 in the first coordination sphere can probably be regarded as equivalent to Co(IV).

$$[(NH_3)_5Co^{III}NH_2]^{3+} \equiv [(NH_3)_5Co^{IV}NH_2^-]^{3+}$$

The formulation of the mechanism by which $RoOH_2^{3+}$ is oxidized by HO as involving Co(IV) seems to be required also by the data obtained for the aquo ion. Despite the fact that coordinated NH_3 is oxidized, there is no effect on the rate of replacing NH_3 by ND_3. There is, however, a substantial isotopic effect (decrease by a factor of 4.5–5) when the coordinated water and the solvent water are deuterated. Part of this effect resides in the solvent—the data obtained for the $RoNH_3^{3+}$ reaction suggest a factor of 2 for this part of the process—but a substantial effect in the coordinated water is probably still left. The isotopic results show that HO does not attack the coordinated NH_3 directly, but attacks elsewhere in the molecule, probably at the coordinated water.

(19) (a) D. Weiser, Ph.D. Dissertation, University of Chicago, 1955; (b) J. H. Baxendale and C. F. Wells, *Trans. Faraday Soc.*, **53**, 800 (1957).

(20) J. E. Teggins, M. T. Wang, and R. M. Milburn, Advances in Chemistry Series, No. 37, American Chemical Society, Washington, D. C., 1963, p 226.

(21) D. Katakis and A. O. Allen, *J. Phys. Chem.*, **68**, 1359 (1964).

$$(NH_3)_5CoOH_2^{3+} + HO \longrightarrow (NH_3)_5CoOH^{3+} + H_2O \quad (10)$$

Here again Co(IV) is generated, which as in the $Ro(NH_3)_6^{3+}$ case, is reduced by an ammonia molecule in the first coordination sphere.

We are unable to describe the further course of the reaction in any definite detail, but some reasonable suggestions about it can be offered. It seems likely that NH is produced when Co(IV) is reduced

$$Co(IV)NH_3 \longrightarrow Co^{2+} + 2H^+ + NH$$

and at least when (HO) is kept low by the cobaltammine at high concentration, the NH dimerizes and is then oxidized to N_2. When the concentration of the cobaltammine is low, NH is to some extent oxidized before it dimerizes and the nitrogen is produced in oxidation states above zero.

The specific rates of the reactions of HO with a number of reducing agents have been reported. The inhibition of the production of Co^{2+} by Ce^{3+} therefore makes it possible to estimate the specific rate for the reaction of HO with $RoOH_2^{3+}$. In expt 14 of Table IV, HO is consumed by reaction with $RoOH_2^{3+}$ and by reaction with Ce^{3+}. Since the total rate of production of HO (at 1 M $S_2O_8^{2-}$) is 2.0×10^{-6} M sec^{-1}, the relation to be given holds

$$[d(Co^{2+})/dt]\Big/\frac{d(Ce^{IV})}{dt} = \frac{0.33 \times 10^{-6}}{(2.0 - 2 \times 0.33) \times 10^{-6}} = 0.23$$

The factor 2 multiplying 0.33 in the denominator enters because each Co^{2+} produced consumes two hydroxyl radicals. The relation

$$[d(Co^{2+})/dt]/d(Ce)^{IV}/dt = \frac{0.5k_{Co^{2+}}(RoOH_3^{3+})(HO)}{k_{Ce^{IV}(Ce^{3+})(HO)}}$$

defines the rate law for the two processes, again making allowance for the 2:1 stoichiometry in the HO–Co(III) reaction. Combining the two relations and using for $k_{Ce^{IV}}$ the value 2.2×10^8 M^{-1} min^{-1} at 25° as determined from results obtained in radiation chemistry,[22] $k_{Co^{2+}} = 2 \times 10^6$ M^{-1} sec^{-1}. This is a minimum value because $k_{Ce^{IV}}$ at 50° will be somewhat greater than at 25°, though not much because the rates are close to diffusion-controlled values. The value of $k_{Co^{2+}} = 1.4 \times 10^6$ M^{-1} is calculated from the experiment with Ce^{3+} added at pH 1.8 (*cf.* Figure 3). The agreement is by no means perfect, but the numbers do at least suggest the order of magnitude of the specific rate in question. The specific rates are low enough to be consistent with a significant activation energy (~5 kcal) for the reaction of HO with $RoOH_2^{3+}$.

It is interesting to note that NH_3 coordinated to Co(III) is much more reactive to hydroxyl radicals than when it is coordinated to H^+. Studies in radiation chemistry[23] have shown that the attack of NH_4^+ by the hydroxyl radicals is extremely slow. An experiment done in the course of the present work (under conditions similar to those of the first entries of Table VI but with N^{15}-enriched NH_4ClO_4 present at 0.01 M) showed that not more than 3% of the N_2 evolved originated from NH_4^+ (the gas obtained had an unusually large proportion of CO_2 but it is unlikely that this affects the conclusion that N_2 originates from Co–NH_3 rather than from NH_4^+). It is possible that Co(III) cooperating in the $2e^-$ change

$$NH_3 \rightarrow NH + 2H^+ + 2e^-$$

is at least partly the cause of the greater reactivity of the coordinated NH_3.

A disturbing feature of the observations is the fact that the limiting specific rate varies with conditions. A diminution is expected as the concentration of acid increases because the mechanism of $S_2O_8^{2-}$ decomposition undergoes a change in acid. However, the decrease in k registered as the pH decreases to 2.4 and to 1.8 is too large to be accounted for on this basis. It is likely that there are changes with pH in the stoichiometric course of the reaction which account for this difference and for the difference between the saturation specific rate for $Co(NH_3)_5OH_2^{3+}$ as compared to $Co(NH_3)_6^{3+}$. This feature deserves more study as do the stoichiometry and kinetics below saturation. In our present work we have only sketched the general outlines of the behavior of the systems and have restricted our attention in the discussion to major conclusions which will, we trust, survive a more detailed investigation.

Acknowledgments. Financial support by the Atomic Energy Commission is gratefully acknowledged. Funds for purchase of the Cary spectrophotometer were made available by the National Science Foundation under Grant G-22611.

(22) T. S. Sworski, *Radiation Res.*, **4**, 483 (1956); **6**, 695 (1957).
(23) T. Rigg, G. Scholes, and J. Weiss, *J. Chem. Soc.*, 3034 (1952).

Activity Coefficients of Calcium Ions in Mixed Solutions

by Adam Shatkay

Isotope Department, The Weizmann Institute of Science, Rehovoth, Israel *(Received April 11, 1967)*

Activity coefficients of Ca^{2+} in $CaCl_2$ solutions approximately 10^{-3} M were measured with ion-specific electrodes in the presence of NaCl and of $MgCl_2$, in the range of the foreign salt concentrations from 0 to 1 M. A comparison is made between a simple equation allowing an approximate calculation of the activity coefficients of single ions in mixed solutions and more elaborate equations suggested by Guggenheim and Glueckauf. It is shown that the simple equation yields results which are closer to the experimental values than the results of Glueckauf's equation. However, the lowering of the activity coefficients in the presence of foreign salts appears to be even greater than the ionic strength of the mixture leads us to expect.

Introduction

In a previous publication,[1] we have suggested a convenient method for the assessment of ion specificity of electrodes. The method was based on the simple assumption stated by Lewis and Randall[2] that "in dilute solutions the activity coefficient of any ion depends solely upon the total ionic strength of the solution." While the simplicity of the above method made it a convenient tool for practical purposes, it is interesting to compare the results obtained by it with the results obtained by more sophisticated (and laborious) methods, such as the evaluation of single ion activities according to the derivations of Guggenheim[3] or of Glueckauf.[4] The results of such comparisons are presented in this paper.

Theoretical Section

Our discussion refers to activities of single ions, as measured by an ion-specific electrode against a reference calomel electrode. The concept of single ion activities has been thoroughly criticized.[2,5,6] The activity of Ca^{2+} is certainly no more (and no less) defensible than the activity of H^+ measured by a hydrogen reversible electrode against a reference calomel electrode. The following discussion is, therefore, subject to the same limitations as a discussion of pH measurements.

We consider an aqueous solution of $CaCl_2$ in which the concentration of Ca^{2+} is C_{Ca} and which contains also foreign salts, so that the ionic strength of the solution is I. The activity coefficient of Ca^{2+} in such a solution is $f_{Ca,I}$ and in general it is different from the activity coefficient $f_{Ca,C}$ of calcium in a pure solution of the same concentration of calcium C_{Ca}. Another solution of pure $CaCl_2$ may be considered, having the same ionic strength I as the original mixed solution, in which the concentration of the pure $CaCl_2$ is now C^*. The mean activity coefficient of such a solution is $f^{\pm}_{Ca,C^*}$. It is thermodynamically well defined and can be found from the values listed in literature.[7] We suggested[1] that

$$f_{Ca,I} \approx f^{\pm}_{Ca,C^*} \quad (1)$$

As an alternative to eq 1, we might consider some form of the Debye–Hückel equations, but two independent reasons prevent us from using such equations. First, the Debye–Hückel treatment would be expected to give a poorer approximation in the case of an asymmetric salt like $CaCl_2$ than in the case of symmetric electrolytes.[8] Next, the "ion size parameter" of the Debye–Hückel treatment loses its conventional physical meaning and ceases to be constant in mixtures of electrolytes.[9] These difficulties led Guggenheim[3] to a

(1) A. Shatkay, *Anal. Chem.*, **39**, 1056 (1967).

(2) G. N. Lewis and M. Randall, *J. Am. Chem. Soc.*, **43**, 1112 (1921).

(3) E. A. Guggenheim, *Phil. Mag.*, **19**, 588 (1935).

(4) E. Glueckauf, *Nature*, **163**, 414 (1949).

(5) D. A. MacInnes, *J. Am. Chem. Soc.*, **41**, 1086 (1919).

(6) E. A. Guggenheim, *J. Phys. Chem.*, **33**, 842 (1929).

(7) R. A. Robinson and R. H. Stokes, "Electrolyte Solutions," Butterworth and Co., Ltd., London, 1965, p 478.

(8) *Cf.* ref 7, Chapters 4 and 9.

different approach toward the calculation of activity coefficients.

Guggenheim develops an equation for the thermodynamically valid mean activity coefficient of a salt in a mixture (eq 52 in ref 3). Introducing the "Guggenheim convention," it is possible to express also the single ion activity. For the case discussed above, we may write (eq 101 in ref 3)

$$\log f_{Ca,I} = -0.50\frac{Z_+^2 I^{1/2}}{1 + I^{1/2}} + \Sigma_X \lambda_{R,X} C_X \qquad (2)$$

where Z_+ is the valence of the cation (2 in our case), R and X are, respectively, the cation and the anion of the salt considered, C_i is the concentration of i, and $\lambda_{\alpha,\beta}$ for any cation α and anion β is defined as

$$\lambda_{\alpha,\beta} = \frac{1}{\ln 10}\int [1 - \exp(-W_{\alpha\beta}^{spec}/kT)]d\omega \qquad (3)$$

In eq 3 $W_{\alpha\beta}^{spec}$ is the contribution of the specific interactions between α and β to the total potential energy $W_{\alpha\beta}$ of the pair of ions $\alpha\beta$. This total energy is divided by Guggenheim into the potential energy of some standard electrolyte of the same valence type $W_{\alpha\beta}^{stand}$ and into $W_{\alpha\beta}^{spec}$, so that

$$W_{\alpha\beta} \equiv W_{\alpha\beta}^{spec} + W_{\alpha\beta}^{stand} \qquad (4)$$

The term $d\omega$ in eq 3 denotes the element of volume occupied by the anion β relatively to the cation α and the integral extends over all the relative configurations of the two ions.

For the practical purpose of the evaluation of $f_{Ca,I}$ in any mixture, eq 2 cannot be employed directly, as the complicated λs cannot as yet be calculated from first principles. Discussion of λs can be found in the original publications cited.[3,4]

Following Guggenheim's treatment, Glueckauf[4] developed an equation suitable to the limited case of one electrolyte dissolved in the presence of one foreign salt, having a common anion with the electrolyte considered (*i.e.*, X′ = Cl^- in our case). Glueckauf's equation can be written, using our previous notation

$$\log f_{Ca,I} = \log f_{Ca,C} - \frac{C_{R'}}{4I}\left[K_1 \log f_{Ca,C} - K_2 \log f_{R'X'} - \frac{K_3}{1 + I^{-1/2}}\right] \qquad (5)$$

The coefficients K appearing in eq 5 are defined as follows, using q_i as the value of the ionic charge of the ion i

$$K_1 \equiv q_{R'}(2q_{R'} - q_{Ca} + q_{Cl}) \qquad (6)$$

$$K_2 \equiv q_{Ca}(q_{R'} + q_{Cl})^2(q_{Ca} + q_{Cl})^{-1} \qquad (7)$$

$$K_3 \equiv {}^1/_2 q_{Ca} q_{R'} q_{Cl}(q_{Ca} - q_{R'})^2(q_{Ca} + q_{Cl})^{-1} \qquad (8)$$

Thus when the foreign salt is NaCl, $K_1 = 1$, $K_2 = 2.67$, and $K_3 = 0.333$, while when the foreign salt is $MgCl_2$, $K_1 = 6$, $K_2 = 6$, and $K_3 = 0$.

Equation 5 can be used in practice to calculate $f_{Ca,I}$, provided the activity coefficient $f_{Ca,C}$ of the pure $CaCl_2$ solution is known and the activity coefficient of the pure foreign salt solution is known, while eq 1 required the knowledge of the activity coefficients of only pure $CaCl_2$ solutions. The effort involved in the employment of eq 5 as compared to eq 1 is obvious. As to the theoretical limitations to the use of eq 5, they are referred to in a later publication by Glueckauf, *et al.*[10]

Employing eq 1 and 5 to solutions of $CaCl_2$ of varying concentration in the presence of NaCl of varying concentration, it can be seen that the two methods of calculation give results which are similar qualitatively, but which differ quantitatively, especially in the case of dilute solutions of $CaCl_2$ in the presence of concentrated solutions of foreign salts. Glueckauf's method indicates that the lowering of the activity coefficient of Ca^{2+} will be fairly small—at most from about 0.89 for a pure 10^{-3} *M* $CaCl_2$ solution to about 0.76 in 1 *M* NaCl solution. Our method predicts much greater depressions of the activity coefficients; in the example cited above, $f_{Ca,I}$ should fall to about 0.46. However to test the two methods in such optimal conditions would require a highly specific Ca^{2+} electrode, which could measure a_{Ca} of a 10^{-3} *M* solution of calcium in the presence of NaCl 1000 times as concentrated. Such electrodes are not yet available. Use of electrodes specific to Ca^{2+} in a solution of NaCl 100 times as concentrated as the $CaCl_2$ solution can, however, be attempted.[1] Such a case corresponds, for instance, to 10^{-2} *M* $CaCl_2$, where eq 5 predicts a decrease of $f_{Ca,I}$ from about 0.73 for pure $CaCl_2$ to a minimum of about 0.66 at 1 *M* C_{NaCl}, while eq 1 predicts a decrease to about 0.46. Such a difference between the two predictions corresponds to an emf of about 5×10^{-3} v, which can be experimentally measured. We shall now present a number of such measurements, compared with calculations based on eq 1 and 5.

Experimental Section

The activities of Ca^{2+} were measured with two electrodes (Orion commercial electrode and solid polymer membrane electrode constructed by us) considered to be ion specific toward Ca^{2+} in at least a considerable part of the range of concentrations investigated. As refer-

(9) H. S. Harned and B. B. Owen, "The Physical Chemistry of Electrolytic Solutions," Reinhold Publishing Corp., New York, N. Y., 1964, Chapter 14.

(10) E. Glueckauf, H. A. C. McKay, and A. R. Matheson, *J. Chem. Soc.*, S-299 (1949).

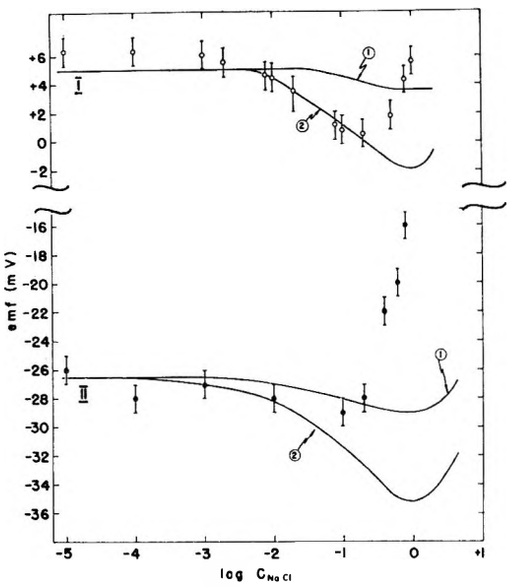

Figure 1. The emf's of Ca^{2+} specific electrodes *vs.* calomel electrodes in solutions of $CaCl_2$ in the presence of NaCl. Curves 1 were calculated with eq 5, curves 2 were calculated with eq 1, and the circles are experimental results: I (○), 1.52×10^{-3} *M* $CaCl_2$ measured with Orion electrode; II (●), 5.33×10^{-4} *M* $CaCl_2$ measured with solid polymer membrane electrode.

ence electrode we used a calomel (saturated KCl salt bridge) Radiometer electrode. The details of the experimental procedure were as given in a previous publication.[1]

Results and Discussion

Part I of Figure 1 presents the behavior of a solution of 1.52×10^{-3} *M* $CaCl_2$ in the presence of NaCl in varying concentrations, in the range of 10^{-5} to 1 *M*. The emf's calculated with the aid of eq 1 and 5 are drawn as continuous lines, while the points represent the emf's obtained by the use of the Orion electrode. It can be seen that up to a concentration of NaCl of about 2×10^{-1} *M* the experimental emf's tend to follow the theoretical curves.

At concentrations of NaCl $> 2 \times 10^{-1}$ *M* there is a large increase of emf for small increases of C_{NaCl}, and we doubt whether the electrode is specific to Ca^{2+} in this range. Assuming that the electrode is specific to Ca^{2+} for $C_{NaCl} < 2 \times 10^{-1}$, the experimental values appear to be better approximated by the use of eq 1 than by the use of eq 5.

The values of $f_{Ca,I}$ calculated according to eq 1 and 5 and from the experimental emf's are compared in Table I. As the experiments were conducted originally merely to assess the ion specificity of some membrane electrodes, the accuracy of the measurements was only within $\pm 10^{-3}$ v and the $f_{Ca,I}$ based on the experimental values are therefore accurate only within ± 0.01. To increase further the accuracy of the potentiometric measurements would require a considerable expenditure of equipment and time, which did not appear justified for the above purpose. We should remark, however, that while the values of the activity coefficients of Ca^{2+} listed currently in the literature[11] are given to within 10^{-3}, yet the discrepancies between the various sources are also of the order of 10^{-2}. Thus, in the absence of any other similar data, our experimental results may serve as provisional values for activity coefficients of $CaCl_2$ in mixed solutions.

Table I: Values of $f_{Ca,I}$ in Solutions of $CaCl_2$ in the Presence of NaCl

C_{NaCl}, *M*	$f_{Ca,I}$ for 1.52×10^{-3} *M* $CaCl_2$, measured with "Orion" electrode			$f_{Ca,I}$ for 5.33×10^{-4} *M* $CaCl_2$, measured with solid polymer membrane		
	Eq 1	Eq 5	Exptl	Eq 1	Eq 5	Exptl
10^{-5}	...	...	...	0.91	0.91	0.97
10^{-4}	...	...	...	0.91	0.91	0.81
10^{-3}	0.86	0.87	0.87	0.89	0.89	0.90
2×10^{-3}	0.85	0.87	0.80	...	...	...
8×10^{-3}	0.80	0.86	0.74	...	...	...
10^{-2}	0.79	0.86	0.72	0.81	0.83	0.81
2×10^{-2}	0.75	0.85	0.65	...	...	...
8×10^{-2}	0.62	0.80	0.55	...	...	...
10^{-1}	0.60	0.80	0.55	...	...	...
2×10^{-1}	0.54	0.77	0.51	...	...	...

A similar experiment was carried out with a solution of 5.33×10^{-4} *M* $CaCl_2$. In this case the emf was measured with the aid of the solid polymer membrane. The results presented in part 2 of Figure 1 indicate that the membrane is Ca^{2+} specific only up to about $C_{NaCl} < 2 \times 10^{-2}$ *M*. The tenfold loss of specificity as compared with previous measurements may be understood partly as the effect of the higher dilution of the $CaCl_2$ solution; the ratio of C_{NaCl} to C_{CaCl_2} at the point in which the membrane ceases to be specific in the previous experiment was about 130, while in the present case it is still about 40. However, the fact that the membrane is not specific to Ca^{2+} in the more interesting range of $C_{NaCl} \approx 1$ *M* does not allow us to compare critically eq 1 and 5.

Within the experimental error, eq 1 and 5 may both be considered as consistent with the results. The change of $f_{Ca,I}$ with the increasing concentration of NaCl is shown in the last three columns of Table I.

(11) *Cf.* ref 9, pp 550, 735, and 738.

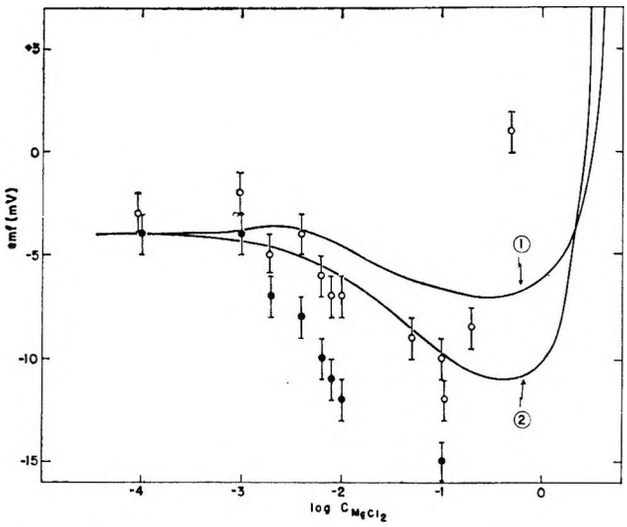

Figure 2. The emf's of Ca^{2+} electrodes *vs.* calomel electrodes in a solution of 3.80×10^{-3} *M* $CaCl_2$ in the presence of $MgCl_2$. Curve 1 was calculated with eq 5, curve 2 was calculated with eq 1: ○, experimental results with Orion electrode; ●, experimental results with solid polymer membrane electrode.

To investigate the effect of $MgCl_2$ on $CaCl_2$ we used a 3.80×10^{-3} *M* solution of $CaCl_2$, measured with the two different ion-specific electrodes. The results are presented in Figure 2, after deducing 1.85×10^{-2} v from the results obtained by the Orion electrode, in order to facilitate the graphical comparison.

It can be seen that the experimental results obtained by the two electrodes are similar, though the solid polymer membrane indicates an even greater effect of the $MgCl_2$ than the Orion electrode. Assuming that the electrodes are Ca^{2+} specific for $C_{MgCl_2} < 10^{-1}$ *M*, it appears again that eq 1 gives better results than eq 5, but the effect of $MgCl_2$ on $f_{Ca,I}$ is stronger than even eq 1 predicts. The comparison of the theoretical and experimental values of $f_{Ca,I}$ in this experiment is presented in Table II.

Table II: Values of $f_{Ca,I}$ in 3.80×10^{-3} *M* Solution of $CaCl_2$ in the Presence of $MgCl_2$

C_{MgCl_2}, *M*	$f_{Ca,I}$			
			Exptl	
	Eq 1	Eq 5	Orion	Solid polymer
10^{-4}	0.81	0.81	0.92	0.79
10^{-3}	0.79	0.83	1.00	0.79
2×10^{-3}	0.78	0.83	0.79	0.63
4×10^{-3}	0.75	0.83	0.84	0.58
6×10^{-3}	0.73	0.81	0.71	0.50
8×10^{-3}	0.71	0.79	0.66	0.47
10^{-2}	0.70	0.77	0.66	0.42
5×10^{-2}	0.56	0.71	0.55	
10^{-1}	0.52	0.67	0.49	0.34

The experimental evidence seems thus to support, on the whole, the use of our eq 1 instead of the more elaborate eq 5 as an aid in approximate calculations of activity coefficients in mixed solutions; not only is eq 1 easier to apply, but it yields also results which are closer to the experimental values. Finally, it appears that the activity coefficients of Ca^{2+} in mixed solutions are lowered even more than the mere ionic strength of the mixture leads us to expect.

Acknowledgments. We are greatly indebted to Professor M. Anbar of the Isotope Department of the Weizmann Institute of Science, under whose direction this investigation was carried out. This paper is based on work performed under Grant No. 5x5121 of the National Institutes of Health, to whom we offer our thanks.

Electrical Phenomena Associated with the Transport of Ions and Ion Pairs in Liquid Ion-Exchange Membranes. I. Zero Current Properties[1a]

by J. Sandblom,[1b] G. Eisenman, and J. L. Walker, Jr.[1c]

Department of Physiology, University of Chicago, Chicago, Illinois 60637 *(Received April 12, 1967)*

A theoretical examination has been carried out of the steady-state properties of a homogeneous, ideally permselective, liquid ion-exchange membrane in which sites and counterions are incompletely dissociated. Dissociated species are assumed to be in chemical equilibrium with neutral ion pairs at every point in the membrane, their concentrations being interconnected by the law of mass action. The flux equations, which describe the complete behavior of the system, are derived by considering the free ions and their combined forms as separately flowing entities, and the boundary conditions are obtained by assuming the sites to be completely trapped in the membrane phase (although free to move within it) while the counterions are free to undergo ion exchange. In the present paper, under the restriction of zero membrane current, a general expression for the membrane potential is deduced in terms of external solution conditions and membrane parameters (*e.g.*, mobilities, dissociation constants). From this expression, the factors governing the electrode properties of liquid ion-exchange membranes are discussed not only for the steady state but for certain transient situations as well. It is concluded that the steady-state expressions derived for convection-free systems describe the situations usually encountered with membrane electrodes made from liquid ion exchangers where the instantaneous values of successive potentials are measured with electrode systems which are not in the steady state and even when no precautions are taken to avoid convective mixing within the electrode. The parameters controlling electrode specificity are also discussed.

Introduction

Systems composed of a water-immiscible liquid interposed between two aqueous solutions were among the first "membranes" in which electric properties and selective ion permeabilities were studied.[2-5] When such membranes contain an appreciable concentration of an ionizable species which is preferentially soluble within the membrane phase (*e.g.*, a fatty acid or an aliphatic amine), they function as liquid ion exchangers whose properties are of interest not only because they can be made into electrodes specific for various ions,[6-10] but also because they constitute a model for one of the conceivable mechanisms of ion permeation through biological membranes.[11]

Despite their long history, the theory of such liquid ion-exchange membranes is not as advanced as that for solid ion-exchange membranes,[12] no doubt because the lack of fixation in a liquid of the ion-exchange sites introduces additional complexities in obtaining explicit solutions to the flux equations. Thus, theoretical considerations for liquid ion exchangers prior to that

(1) (a) This work was supported by National Science Foundation Grant GB-4039 and USPHS Grant GM 14404-01. It was assisted by USPHS General Research Support Grant FR-5367 and an NIH postdoctoral fellowship to J. L. Walker, Jr. (b) Institute of Physiology and Medical Biophysics, University of Uppsala, Uppsala, Sweden. (c) Department of Physiology, University of Utah, College of Medicine, Salt Lake City, Utah.

(2) (a) W. Nernst and E. H. Riesenfeld, *Ann. Phys.*, **8**, 600 (1902); (b) M. Cremer, *Z. Biol.*, **47**, 562 (1906).

(3) F. G. Donnan and W. E. Garner, *J. Chem. Soc.*, **115**, 1313 (1919).

(4) R. Beutner, "Physical Chemistry of Living Tissues and Life Processes," Williams and Wilkins Co., Baltimore, Md., 1944.

(5) W. J. V. Osterhout, *Cold Spring Harbor Symp. Quant. Biol.*, **8**, 51 (1940).

(6) K. F. Bonhoeffer, M. Kahlweit, and H. Strehlow, *Z. Physik. Chem.* (Frankfurt), **1**, 21 (1954).

(7) K. Sollner and G. M. Shean, *J. Am. Chem. Soc.*, **86**, 1901 (1964).

(8) O. D. Bonner and J. Lunney, *J. Phys. Chem.*, **70**, 1140 (1966).

of Conti and Eisenman[13] have been restricted to the potentials or fluxes observed under zero current conditions.[6,14-19] In addition, most treatments have either assumed the diffusion potential to be negligible[15] or have made particular assumptions about the concentration profiles within the membrane (*e.g.*, linear mixtures of the Henderson type[14-16] or linear concentration profiles[18]).

However, for the case of a liquid ion-exchange membrane with complete dissociation between sites and counterions, it has been shown recently that closed solutions to the flux equations can be obtained in the steady state without making *a priori* assumptions about the concentration profiles.[13] The characteristic features of such a membrane result from the redistribution of sites and are therefore related to such classical concentration polarization phenomena as occur in depletion layers at the interface between an electrode and an aqueous solution.[20-22]

As was recognized by Conti and Eisenman, the restriction of their treatment to completely dissociated systems constitutes a serious limitation when attempting to apply the results to the usual liquid ion-exchange membranes in view of the relatively low dielectric constant normally characteristic of these. In the present paper, we shall therefore consider the effects of incomplete dissociation in order to deduce the properties of a liquid ion-exchange membrane having any degree of dissociation. Additional complexities appear in our treatment as a result of association of the sites and counterions to form electrically neutral species. In particular, when an external force is applied to the system so as to perturb the concentration of the dissociated species, the concentration of the associated species is also perturbed by virtue of the dissociation equilibrium which couples the concentrations of dissociated and undissociated species at all points within the membrane. Despite these complexities, explicit expressions have been obtained for the membrane potential at zero current and also for certain nonzero current properties (in the case of a single counterion species).

Experimental Section

Description of the System. The system to be studied (see Figure 1) is isothermal and consists of a membrane separating two homogeneous solution phases (*e.g.*, aqueous) whose electric potentials are ψ' and ψ''. The membrane is composed of a single liquid phase immiscible with the external solutions. In the membrane is dissolved a "site" species S bearing a charge $z_s = \pm 1$ (given a negative sign in Figure 1). The sites are assumed to be completely reflected at the boundaries,

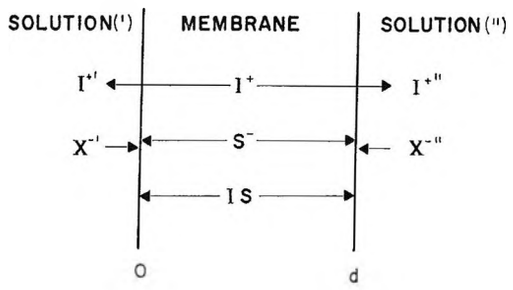

Figure 1. Diagram of the system; I^+, S^-, and X^- refer to the counterion, the site, and the co-ion species, respectively.

0 and d (as indicated by the arrows), but are free to move within the interior of the membrane. The system also contains n number of permeable univalent counterion species I whose charge z_i is opposite to that of the sites and which are free to cross the membrane solution interfaces as indicated by the arrows in Figure 1. Any number of co-ion species may be present in the external solutions although the co-ions are assumed to be completely excluded from the membrane.

Even species which behave as strong electrolytes in aqueous solutions will in general not be completely dissociated in a liquid ion-exchange membrane. We shall therefore assume that species I and S are in chemical equilibrium at every point in the membrane with the associated species IS through reactions of the type

$$I^+ + S^- \rightleftharpoons IS \qquad (1)$$

indicating that the only reactions assumed to occur in the membrane are those in which electrically neutral

(9) J. W. Ross, *Science*, **156**, 1378 (1967).

(10) Corning Ca^{2+} Electrode Specification. Corning Glass Works Ca^{2+} electrode data sheet No. EL-Ca RPP 2/67.

(11) G. Eisenman, J. Sandblom, and J. L. Walker, Jr., *Science*, **155**, 965 (1967).

(12) F. Helfferich, "Ion Exchange," McGraw-Hill Book Co. Inc., New York, N. Y., 1962, pp 19, 20.

(13) F. Conti and G. Eisenman, *Biophys. J.*, **6**, 227 (1966).

(14) K. H. Meyer, H. Hauptmann, and J. F. Sievers, *Helv. Chim. Acta*, **19**, 946 (1936).

(15) F. M. Karpfen and J. E. B. Randles, *Trans. Faraday Soc.*, **49**, 823 (1953).

(16) M. Dupeyrat, *J. Chim. Phys.*, **61**, 306, 323 (1964).

(17) H. L. Rosano, P. Duby, and J. H. Schulman, *J. Phys. Chem.*, **65**, 1704 (1964); H. L. Rosano, J. H. Schulman, and J. B. Weisbuch, *Ann. N. Y. Acad. Sci.*, **92**, 457 (1961).

(18) J. T. Davies, *J. Phys. Chem.*, **54**, 185 (1950).

(19) M. Kahlweit, *Archiv. Ges. Physiol.*, **271**, 139 (1960).

(20) E. Warburg, *Ann. Physik Chem.*, **67**, 493 (1899).

(21) P. Delahay, "New Instrumental Methods in Electrochemistry," Interscience Publishers, Inc., New York, N. Y., 1954; I. M. Kolthoff and J. J. Lingane, "Polarography," 2nd ed, Interscience Publishers, Inc., New York, N. Y., 1952.

(22) F. Helfferich, "Ion Exchange," McGraw-Hill Book Co., Inc., New York, N. Y., 1962, pp 360–363.

complexes are formed. For simplicity, we have also restricted considerations to the smallest complex possible (*i.e.*, the ion pair). Such behavior is often characteristic of weak electrolytes where the formation of triple ions and higher order aggregates is negligible over wide concentration ranges.[23]

The chemical potentials corresponding to reaction 1 are everywhere in the membrane related through

$$\mu_i + \mu_s = \mu_{is} \qquad (i = 1, \ldots, n) \tag{2}$$

where μ_i, μ_s, and μ_{is} are the chemical potentials of the counterions, sites, and ion pairs, respectively. For simplicity, we will assume activities to be equal to concentrations. Under this assumption, the concentrations of the species (c_i, c_s, c_{is}) are related to the dissociation constants K_i through a simple law of mass action

$$K_i = \frac{c_i c_s}{c_{is}} \qquad (i = 1, \ldots, n) \tag{3}$$

which, in effect, describes a chemical coupling between the various species within the membrane. In addition, the concentrations of the charged species are coupled electrically through the condition of electroneutrality

$$c_s = \sum_i c_i \tag{4}$$

Flux Equations

In describing ionic transport processes in a liquid ion-exchange membrane, it is useful to consider separately the flows of associated and dissociated species. The total flux of each species through the membrane can be written as a sum of partial fluxes

$$J_i^* = J_i + J_{is} \tag{5a}$$

$$J_s^* = J_s + \sum_i J_{is} \tag{5b}$$

where J_i^* and J_s^* are the total fluxes of counterions and sites, J_i and J_s are the fluxes of the species in their dissociated state, and J_{is} are the fluxes of the ion pairs.

Since counterions, sites, and associated pairs are treated as separately flowing entities, it is possible to write separate linear relationships between forces and fluxes for each of the species. By the Curie principle, the chemical reactions introduce no additional driving forces since the membrane is assumed to be isotropic, and assuming diffusion only in the x direction, we can therefore write the flux equations in the classical manner as

$$J_i = -u_i c_i \frac{\partial}{\partial x}(RT \ln c_i + z_i F\psi) \tag{6a}$$

$$J_s = -u_s c_s \frac{\partial}{\partial x}(RT \ln c_s + z_s F\psi) \tag{6b}$$

$$J_{is} = -u_{is} c_{is} \frac{\partial}{\partial x}(RT \ln c_{is}) \tag{6c}$$

where u_s, u_i, and u_{is} are the mobilities of sites, counterions, and ion pairs, respectively, ψ is the electric potential, R is the gas constant, F is the Faraday constant, and T is the absolute temperature. We will assume u_s, u_i, and u_{is} to be constants.

Continuity Equations

The law of conservation of mass leads to a set of continuity equations for the total fluxes and concentrations

$$\mathrm{div} J_i^* = \frac{\partial J_i^*}{\partial x} = \frac{\partial c_i^*}{\partial t} \tag{7a}$$

$$\mathrm{div} J_s^* = \frac{\partial J_s^*}{\partial x} = \frac{\partial c_s^*}{\partial t} \tag{7b}$$

where the asterisks refer to total quantities ($c_i^* = c_i + c_{is}$; $c_s^* = c_s + \sum_i c_{is}$).

At steady state, the total fluxes are constant as seen from eq 7, a conclusion which is not necessarily valid for the partial fluxes. In fact, as will be seen later, the partial fluxes are generally functions of distance (*cf.* Figure 3 of part II, the following article) and the membrane may be thought of as containing local sources and sinks. Because we can invoke the continuity equations only for the total fluxes, the number of variables is increased by n (the number of partial fluxes J_{is}) over that in the usual Nernst–Planck treatment. The n additional equations needed to solve the problem are given by eq 2.

Boundary Conditions

Assuming that boundary processes are not rate limiting, the boundary conditions for the counterions follow from the continuity of electrochemical potentials. Hence we may equate the electrochemical potentials of the counterions across each of the two boundaries 0 and d as

$$RT \ln a_i' + \mu_i^0 + z_i F\psi' = RT \ln c_i(0) + \mu_i^0(\mathrm{m}) + z_i F\psi(0) \qquad (i = 1, \ldots, n) \tag{8a}$$

and

$$RT \ln a_i'' + \mu_i^0 + z_i F\psi'' = RT \ln c_i(d) + \mu_i^0(\mathrm{m}) + z_i F\psi(d) \qquad (i = 1, \ldots, n) \tag{8b}$$

respectively. The quantities on the left-hand side of eq 8a and 8b refer to the solution phases, while the

(23) R. A. Fuoss and C. A. Kraus, *J. Am. Chem. Soc.*, **55**, 476 (1933); R. A. Fuoss, *ibid.*, **57**, 488 (1935); *Trans. Faraday Soc.*, **32**, 594 (1936).

quantities on the right-hand side refer to the membrane phase. μ_i^0 and $\mu_i^0(\mathrm{m})$ are the standard chemical potentials in the solution and membrane phases, respectively, and the superscripts (′) and (″) refer to the two solution phases (*cf.* Figure 1).

Subtracting any pair of eq 8a and rearranging gives

$$\frac{a_i'k_i}{c_i(0)} = \frac{a_j'k_j}{c_j(0)} \tag{9}$$

where the constants k_i and k_j are defined as

$$k_i = \exp\left(\frac{\mu_i^0 - \mu_i^0(\mathrm{m})}{RT}\right); \quad k_j = \exp\left(\frac{\mu_j^0 - \mu_j^0(\mathrm{m})}{RT}\right) \tag{10}$$

Equations 9 can be written for all the ions

$$\frac{a_1'k_1}{c_1(0)} = \frac{a_2'k_2}{c_2(0)} = \cdots = \frac{a_n'k_n}{c_n(0)} = \frac{\sum_i a_i'k_i}{c_s(0)} \tag{11}$$

where the condition of electroneutrality (4) has been used to obtain the last term. From eq 11 the membrane concentrations $c_i(0)$ can be expressed in terms of the solution concentration c_i' as

$$c_i(0) = c_s(0) \times \frac{a_i'k_i}{\sum_i a_i'k_i} \tag{12}$$

Similar expressions hold for the other membrane boundary.

Subtracting eq 8a from eq 8b gives the expression for the total membrane potential ($V = \psi'' - \psi'$) in terms of internal potential ($\Delta\psi = \psi(d) - \psi(0)$) and the concentrations at the boundaries as

$$z_iFV = z_iF\Delta\psi + RT \ln \frac{a_i'k_i}{c_i(0)} - RT \ln \frac{a_i''k_i}{c_i(d)} \tag{13}$$

Combining eq 12 and 13 yields an expression in terms of the activities of the counterions in the solutions and ratio of the site concentrations at 0 and d

$$V = \Delta\psi + \frac{RT}{z_iF} \ln \frac{c_s(d)}{c_s(0)} + \frac{RT}{z_iF} \ln \frac{\sum_i a_i'k_i}{\sum_i a_i''k_i} \tag{14}$$

This equation will be used to express the total potential in terms of external conditions and membrane parameters.

The boundary conditions for the sites follow from the assumption that the sites are completely reflected at the membrane boundaries, which leads directly to the equations

$$\frac{1}{d}\int_0^d c_s^* \mathrm{d}x = \bar{c}_s^* \tag{15}$$

$$J_s^* = 0 \tag{16a}$$

Equation 16a is valid for all values of x at steady state, but in the nonsteady state it is only valid at the boundaries where

$$J_s^*(t,0) = J_s^*(t,d) = 0 \tag{16b}$$

Equation 15 expresses the condition that the total number of sites contained in the membrane is constant, regardless of their concentration profile. Expressed per unit area, this number is equal to the average total concentration $\bar{c}_s^*$ times the membrane thickness d. Equation 16a states that the total flow of sites must be zero at all points in the membrane in the steady state, whereas eq 16b indicates that for nonsteady state J_s^* is zero only at the membrane–solution interfaces.

If eq 5b is introduced in eq 16a we get

$$J_s = -\sum_i J_{ts}$$

which indicates that a "circulation" of sites exists in the steady state as a result of equal and opposite flows of sites in their dissociated and associated forms. This circulation of material is characteristic of membranes containing "carriers"[24-26] and the neutral ion pairs may therefore be viewed as ionic carriers.

Equations 1–16 describe the total behavior of the system, but we shall only consider special cases: (1) the membrane potential at zero current here and (2) the complete steady-state properties for the case of a single counterion species, in the following paper.

Results

Since the electric current I is carried only by the charged species, it is given by

$$I = F\sum_i z_iJ_i + Fz_sJ_s = Fz_i\left(\sum_i J_i - J_s\right) \tag{17}$$

Substituting eq 5 in eq 17 yields

$$I = F\sum_i z_iJ_i^* + Fz_sJ_s^* \tag{18}$$

from which it is seen that the electric current is also given by the sum of the *total* flows. The potential gradient at zero current can now be expressed by inserting eq 6a and 6b into eq 17 for $I = 0$ and rearranging to yield

(24) J. B. Best and J. Z. Hearon, "Minerals and Metabolism," Vol. 1A, C. L. Comar and F. Bronner, Ed., Academic Press, Inc., New York, N. Y., 1960, p 11.

(25) A. H. Katchalsky and P. Curran, "Nonequilibrium Thermodynamics in Biophysics," Harvard University Press, Cambridge, Mass., 1965, p 204.

(26) A. Finkelstein, *Biophys. J.*, **4**, 421 (1964).

$$\frac{\partial\psi}{\partial x} = -\frac{RT}{z_t F}\frac{1}{\sum_i u_i c_i + u_s c_s}\frac{\partial}{\partial x}\left(\sum_i u_i c_i - u_s c_s\right) \quad (19)$$

which is recognized as the usual expression for the potential gradient in a "Planck" liquid junction. The difference appears when eq 19 is integrated since the presence of ion pairs will influence the profiles of c_t and c_s. In order to perform this integration, we shall derive another expression containing $\partial c_s/\partial x$.

Combining eq 5b, 6b, and 6c, we get

$$J_s^* = -u_s c_s\frac{\partial}{\partial x}(RT\ln c_s + z_s F\psi) - \sum_i u_{ts} c_{ts}\frac{\partial}{\partial x} RT\ln c_{ts} \quad (20)$$

and inserting the mass-law eq 3, this yields directly

$$J_s^* = -RTu_s\frac{\partial c_s}{\partial x} - Fu_s z_s c_s\frac{\partial\psi}{\partial x} - RT\sum_i\frac{u_{ts}}{K_t}c_s\frac{\partial c_t}{\partial x} - RT\sum_i\frac{u_{ts}}{K_t}c_t\frac{\partial c_s}{\partial x} \quad (21)$$

Equation 21 is now combined with eq 19 to eliminate $\partial c_s/\partial x$ and solving for the potential gradient, we get

$$\frac{Fz_t}{RT}\frac{\partial\psi}{\partial x} = -\frac{\left(u_s + \sum_i\frac{u_{ts}}{K_t}c_t\right)\sum_i u_i\frac{\partial c_t}{\partial x} + u_s c_s\sum_i\frac{u_{ts}}{K_t}\frac{\partial c_t}{\partial x} - \frac{u_s J_s^*}{RT}}{\left(u_s + \sum_i\frac{u_{ts}}{K_t}c_t\right)\sum_i u_i c_i + u_s c_s\sum_i\frac{u_{ts}}{K_t}c_t} \quad (22)$$

By rearranging this equation, we finally obtain the expression

$$\frac{Fz_t}{RT}\frac{\partial\psi}{\partial x} = -\frac{\sum_i u_i\frac{\partial c_t}{\partial x}}{\sum_i u_i c_i} - t\left[\frac{\sum_i\frac{u_{ts}}{K_t}\frac{\partial c_t}{\partial x}}{\sum_i\frac{u_{ts}}{K_t}c_t} - \frac{\sum_i u_i\frac{\partial c_t}{\partial x}}{\sum_i u_i c_i}\right] - \frac{\frac{u_s J_s^*}{RT}}{\left(u_s + \sum_i\frac{u_{ts}}{K_t}c_t\right)\sum_i u_i c_i + u_s c_s\sum_i\frac{u_{ts}}{K_t}c_t} \quad (23)$$

where

$$t = \frac{u_s c_s}{\left(\frac{u_s c_s}{\sum_i u_{ts} c_{ts}} + 1\right)\sum_i u_i c_i + u_s c_s} \quad (24)$$

(That eq 23 is identical with eq 22 can be checked by recombining the various terms in eq 23 to obtain a common denominator.) When eq 23 is integrated between the two boundaries 0 and d, we obtain the internal potential at zero current, designated as $\Delta\psi_0$

$$\frac{Fz_t}{RT}\Delta\psi_0 = -\ln\frac{\sum_i u_i c_i(d)}{\sum_i u_i c_i(0)} - \int_0^d t\,\mathrm{d}\ln\frac{\sum_i\frac{u_{ts}}{K_t}c_t}{\sum_i u_i c_i} - \int_0^d\frac{\frac{u_s J_s^*}{RT}\,\mathrm{d}x}{\left(u_s + \sum_i\frac{u_{ts}}{K_t}c_t\right)\sum_i u_i c_i + u_s c_s\sum_i\frac{u_{ts}}{K_t}c_t} \quad (25)$$

In order to arrive at an expression for V_0, the total membrane potential at zero current, eq 25 is combined with the boundary conditions (12) and (14) to yield

$$\frac{Fz_i}{RT}V_0 = -\ln\frac{\sum_i u_i k_i a_i''}{\sum_i u_i k_i a_i'} - \int_1 - \int_2 \quad (26)$$

where $\int_1, \int_2$ are the two integrals appearing in eq 25.

Since in the derivation of eq 26 no equations based on the assumption of steady state were used, eq 26 is valid for nonstationary as well as stationary states. The V_0 of a liquid ion-exchange membrane is therefore seen from eq 26 to be composed of three terms, only the first of which is independent of site distribution.

This is in contrast to the situation in a fixed site membrane where $u_s = 0$ and $J_s^* = 0$, so that, as can be seen from eq 24 and 25, V_0 reduces to the first term in eq 26 which is the usual equation for such a membrane.[27,28]

Steady State

General Considerations. In the steady state when, according to eq 16a, $J_s^* = 0$, V_0 is described by the two first terms in eq 26. Examining the parameter t, given by eq 24 and which determines the behavior of the second term in eq 25, it is seen that the degree of dissociation enters through the quantity

$$\frac{u_s c_s}{\sum_i u_{ts} c_{ts}} \quad (27)$$

The second term is therefore affected by the total concentration of sites, $\bar{c}_s^*$, since c_{ts} and c_s do not vary pro-

(27) F. Helfferich, "Ion Exchange," McGraw-Hill Book Co., Inc., New York, N. Y., 1962, see eq 8-90.

(28) F. Conti and G. Eisenman, *Biophys. J.*, **5**, 247 (1965); see eq 38.

portionally when the total number of sites is changed. This fact is most easily illustrated by adding the mass laws (3) and inserting the condition of electroneutrality (4). We get

$$c_s^2 = \sum_i K_i c_{is}$$

and from this it is seen that the quantity given by eq 27 varies inversely as the concentration of free sites, c_s. As the degree of dissociation is varied, for example by varying c_s from zero to infinity keeping all K_i constant, it follows therefore that the quantity t varies from zero to t_s, where t_s, the transference number of free sites, is given by

$$t_s = \frac{u_s c_s}{\sum_i u_i c_i + u_s c_s}$$

Consequently, the membrane potential at zero current depends on the site concentrations at intermediate degrees of dissociation. However, when the degree of dissociation is small and the quantity given in eq 27 is small compared to unity, the potential becomes independent of the degree of dissociation. This behavior is analogous to that of fixed-site membranes where V_0 depends on the fixed-site density for intermediate values (*cf.* Teorell,[29] eq 22–24), but for fixed-site density values high enough to achieve co-ion exclusion, the potential becomes independent of the site concentration (see below, eq 32).

Limiting Case of Complete Dissociation. In this case $\int_1$ is zero ($t = 0$) and since $\int_2$ is also zero in the steady state, the potential is described by the first term of eq 26

$$\frac{z_i F}{RT} V_0 = -\ln \frac{\sum_i u_i k_i a_i''}{\sum_i u_i k_i a_i'} \qquad (28)$$

which can be seen to be the proper value for this limit from its agreement with Conti and Eisenman's eq 35.[13]

Special Case of Two Counterions and Strong Association. If we confine ourselves to two counterions and strong association, *i.e.*, when eq 27 is much less than unity, the integral $\int_1$ in eq 26 can be written as

$$\int_1 = \int_0^d \frac{u_s\left(\frac{c_1}{c_2} + 1\right)}{(u_1 + u_s)\frac{c_1}{c_2} + u_2 + u_s} \times \mathrm{d} \ln \frac{\frac{u_{1s}}{K_1}\frac{c_1}{c_2} + \frac{u_{2s}}{K_2}}{u_1\frac{c_1}{c_2} + u_2} \qquad (29)$$

where the condition of electroneutrality has been taken into account and where we have divided through by c_2. The only independent variable now appearing is c_1/c_2, and the integral can therefore be solved explicitly. This gives

$$\int_1 = (1 - \tau) \ln \frac{\sum_{i=1}^{2} (u_i + u_s) c_i(d)}{\sum_{i=1}^{2} (u_i + u_s) c_i(0)} + \tau \ln \frac{\sum_{i=1}^{2} \frac{u_{is}}{K_i} c_i(d)}{\sum_{i=1}^{2} \frac{u_{is}}{K_i} c_i(0)} - \ln \frac{\sum_{i=1}^{2} u_i c_i(d)}{\sum_{i=1}^{2} u_i c_i(0)} \qquad (30)$$

where

$$\tau = \frac{u_s\left(\frac{u_{2s}}{K_2} - \frac{u_{1s}}{K_1}\right)}{(u_1 + u_s)\frac{u_{2s}}{K_2} - (u_2 + u_s)\frac{u_{1s}}{K_1}} \qquad (31)$$

Equation 30 depends only on the values of c_i of the boundaries and is therefore profile independent, which has important consequences to be discussed later.

When the boundary conditions (9) are inserted and eq 30 combined with eq 26, taking into account that $\int_2 = 0$ in the steady state since $J_s^* = 0$, then we obtain for the total potential

$$\frac{Fz_i}{RT} V_0 = (1 - \tau) \ln \frac{\sum_{i=1}^{2} (u_i + u_s) k_i a_i'}{\sum_{i=1}^{2} (u_i + u_s) k_i a_i''} + \tau \ln \frac{\sum_{i=1}^{2} \frac{u_{is}}{K_i} k_i a_i'}{\sum_{i=1}^{2} \frac{u_{is}}{K_i} k_i a_i''} \qquad (32)$$

The form of eq 32 can be illustrated by plotting the exponent of the potential against the mole fraction of one of the counterions in the external solution. The external solution is kept constant on one side of the membrane and varied on the other in such a way that the total ionic strength is always kept constant. Under these circumstances eq 32 can be written in the following way when solution (′) is constant and solution (″) is varied.

(29) T. Teorell, *Progr. Biophys.*, **3**, 305 (1953).

$$\frac{Fz_iV_0}{RT} = \text{constant} + (1 - \tau) \times \ln\left(1 + \left[\frac{u_1 + u_s}{u_2 + u_s}\frac{k_1}{k_2} - 1\right]X_1''\right) + \tau \ln\left(1 + \left[\frac{u_{1s}}{u_{2s}}\frac{K_2}{K_1}\frac{k_1}{k_2} - 1\right]X_1''\right) \quad (32a)$$

where X_1'' is the mole fraction of species 1 in the external solution on the side which is being varied. This equation is represented in Figure 2 where the exponent of $[(Fz_iV_0/RT) - \text{constant}]$ is plotted against X_1'' for various values of τ. Experimental data can be represented directly by such a plot, but since it can be seen from Figure 2 that the curves are approximately straight lines regardless of the value of τ, eq 32a might alternatively be represented to a good approximation by a single logarithmic term, defining a set of "average ionic selectivities."

It should be emphasized that eq 32 has been derived using only the condition that $J_s^* = 0$ and does not require the counterions to be in a steady state. This important fact will be used in the following section.

All the parameters appearing in eq 32 are measurable by classical methods except u_{is}, the mobilities of the ion pairs. These can be calculated from the current–voltage characteristics as will be shown in the following paper.

An interesting limit of eq 32 is obtained by putting all $u_i = u_s$. In this case $\tau = 0.5$, and from eq 19 it is apparent that the internal potential vanishes. Although V_0 is then due to the boundary potentials alone, its value can be seen to depend not only on the expected equilibrium parameters k_i and K_i but also, somewhat surprisingly, on the mobilities u_{is} of the ion pairs.

Transient State

Despite the many studies of the electrode properties of liquid ion exchangers, none of the measurements published to date appears to correspond to the convection-free steady state to which we have restricted considerations to this point. This is because the membrane phase has either been deliberately stirred[7,8,17] or because precautions to prevent convective mixing in its interior have not been taken[4,5,15,16] (the membrane phase being so thick that steady states have generally not been reached and because moreover, stable concentration gradients could only be established in the relatively static layers just internal to the solution interfaces). We will show here that the transient behavior of V_0 depends not only on the membrane parameters (particularly the degree of dissociation) but also on the experimental arrangement. Nevertheless,

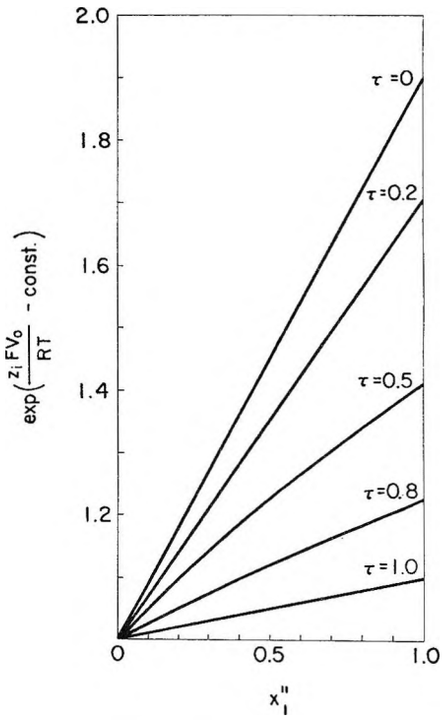

Figure 2. The form of eq 32. Equation 32 is represented by plotting $\exp[(Fz_iV_0/RT) - \text{constant}]$ as a function of mole fraction (X_1) of species 1 in the external solution. The parameters are chosen arbitrarily so that eq 32 may be written as $\exp[(Fz_iV_0/RT) - \text{constant}] = \exp[(1 - \tau)\ln(1 + 0.9X_1'') + \tau \ln(1 + 0.1X_1'')]$. This function is plotted for the following values of τ: 0, 0.2, 0.5, 0.8, and 1.0.

the present results are directly applicable to a number of experimental situations, not restricted to the steady state. For a more thorough discussion of the different experimental situations and their implications for the observed electrode potential properties, the reader is referred to Eisenman.[30]

Case of Simple Dilution. It is seen from eq 11, 15, and 16 that a simple dilution of the external solution on one side of the membrane (*i.e.*, all the a_i'' are changed by the same proportionality factor) will not alter the interior concentrations. (The concentration ratio of counterions is not changed by dilution (*cf.* eq 11); the remaining two boundary conditions, (15) and (16), needed to solve for the individual concentrations are independent of the external solution conditions.) The first two terms in eq 14 are therefore unaltered by such a dilution, and the potential will vary with the natural logarithm of the concentration with a Nernst slope (*i.e.*, RT/z_iF) as given by the third term. This behavior is a consequence of assuming complete co-ion

(30) G. Eisenman, *Anal. Chem.*, in press.

exclusion and completely trapped sites. Since eq 14 is valid at all times, this has the important practical consequence that *the membrane potential will respond in a step fashion to a step change in solution conditions whenever this corresponds to a simple dilution.*

More General Considerations. Except for the above case, however, a step change in external solution conditions will be accompanied by a redistribution of the sites until a new steady state is reached, which has the following consequences for the behavior of electrode potentials.

When a step change is made from a previous steady state, the profiles are initially unaltered. J_s^* is therefore zero in the interior of the membrane at zero time. At the boundaries J_s^* is zero at all times by virtue of the boundary conditions (16b). The last integral in eq 26, $\int_2$, is therefore zero instantaneously following a step change in solution conditions. *This is due to the fact that the initial ion exchange takes place across one of the membrane solution interfaces where the sites cannot move.*

Since in the limit of complete dissociation $\int_1$ of eq 26 is zero while in the limit of strong association $\int_1$ is a profile independent (being given by eq 30), we reach the important practical conclusion that the instantaneously observed potential is given by the steady-state expressions (26a) for complete dissociation and (32) for strong association in these two limiting cases, respectively. It should be emphasized that this conclusion is true not only for convection-free systems but also for stirred systems because $\int_1$ is independent of the concentration profiles. *Equations 26a and 32 therefore can be used to describe measurements carried out by holding solutions (′) constant and comparing the instantaneous values of successive potentials observed for various conditions of solutions (″) even when no precautions are taken to avoid convection*[4,5,15,16] or when the membrane phase is deliberately stirred.[7,8,17]

In addition, if the membrane interior is deliberately stirred, a *quasi-steady state* of potential will be rapidly established (again described by eq 26a and 32) since in this case $\int_2$ is zero because the uniform *distribution* of sites in the stirred interior reduces J_s^* to zero there long before the interior concentrations attain their steady-state values. This situation is analogous to that existing in a co-ion excluding fixed-site membrane where V_0 is time independent, although the profiles are not in a steady state.[28]

For systems of intermediate dissociation, it is difficult to ascertain the behavior of V_0 even when $\int_2$ is zero since the quantity t (eq 24) cannot be expressed in terms of c_1/c_2 in this case.

Liquid Junctions within the Membrane Phase. By virtue of the boundary condition (16b), the second integral $\int_2$ was shown to be zero both in a membrane in a stirred interior and instantaneously following a step change in external solution conditions.

In certain other experimental conditions,[19] the membrane phase has been preequilibrated with different solutions, and the V_0 is measured across the liquid junction which is formed when two such membrane phases, each in equilibrium with their respective solutions, are brought in contact. In this case the sites are not constrained by any boundary and J_s^* $\left(\text{and therefore}\int_2\right)$ is not necessarily zero. In fact, the membrane potential in these cases has been calculated from eq 19 assuming linear mixtures of free sites and counterions.[16]

The Parameters Controlling Electrode Specificity

We shall here only discuss the parameters as they appear in eq 32 for strongly associated systems. This equation applies instantaneously and at steady state to convection-free membranes as well as in stirred membranes. Each logarithmic term appearing in eq 32 defines a set of ion selectivities. In the first logarithmic term, the only parameter depending on the properties of the sites is seen to be u_s. This affects the selectivity in a particularly simple way since the sum $(u_i + u_s)$ is given directly by the limiting value at infinite dilution of the equivalent conductance Λ_{is}^0. On the other hand, the parameters k_i are related to the limiting values at infinite dilution of the distribution coefficients S_{ix}^0 of the salt between the solution phase and the pure solvent of the membrane. If the same anion X^- is used in measuring the distribution coefficients of two salts, IX and JX, the ratio $[S_{ix}^0/S_{jx}^0]^2$ is equal to k_i/k_j, regardless of the anion species. The standard chemical potentials determine S_{ix}^0 according to the treatment of Shedlovsky and Uhlig,[31] which has been carried out under the same assumptions used in the present paper, and the square appears because k_i/k_j is the ratio of the distribution coefficients of the counterions while S_{ix}^0/S_{jx}^0 is the ratio of the distribution coefficients of the salt.[32]

(31) T. Shedlovsky and H. H. Uhlig, *J. Gen. Physiol.*, **17**, 563 (1933).
(32) *Cf.* p 161 of L. W. Holm, *Arkiv Kemi*, **5**, 151 (1956).

It follows then that the selectivity between I and J is given by

$$\frac{(u_j + u_s)k_j}{(u_i + u_s)k_i} = \frac{\Lambda_{js}^0}{\Lambda_{is}^0}\left[\frac{S_{jx}^0}{S_{ix}^0}\right]^2 \quad (33)$$

Notice that since the parameters on the right-hand side of eq 33 are all defined for infinite dilution, they are completely independent of ion–site interactions, and the first logarithmic term of eq 32 therefore depends *only on the properties of the solvent* despite the fact that we are considering a system which is strongly associated.

On the other hand, the selectivity between I and J for the second logarithmic term of eq 32 is given by

$$\frac{u_{js}}{u_{is}}\frac{k_j}{k_i}\frac{K_i}{K_j} = \frac{u_{js}}{u_{is}}K_{ij} \quad (34)$$

where K_{ij} is the ion-exchange equilibrium constant for the reaction

$$J^+(\text{aqueous}) + IS(\text{membrane}) \rightleftharpoons JS(\text{membrane}) + I^+(\text{aqueous}) \quad (35)$$

This result was deduced by combining eq 2 and 3 and introducing the expressions for k_i and k_j from eq 10, to yield

$$\frac{k_j}{K_j}\frac{K_i}{k_i} = \exp\left(\frac{\mu_j^0 - \mu_i^0 - \mu_{js}^0(\text{m}) + \mu_{is}^0(\text{m})}{RT}\right) = K_{ij} \quad (36)$$

From eq 34, the ion-exchange equilibrium constant K_{ij} is seen to be the product of a term $[(k_j/k_i) = (S_{jx}^0/S_{ix}^0)^2]$ dependent on the properties of the solvent and a term (K_i/K_j) dependent on ion–site interactions.

Finally, it should be noted that if the mobilities of the associated pairs are approximately the same for all counterion species (as seems likely to be approximately true for the usual long-chain liquid ion exchangers), the selectivity of eq 34 reduces to K_{ij} and is therefore the same as that characteristic for equilibrium ion exchange. Thus the selectivity of the second logarithmic term of eq 32 is *characteristic of the properties of the site as well as of the solvent.*

Electrical Phenomena Associated with the Transport of Ions and Ion Pairs in Liquid Ion-Exchange Membranes. II. Nonzero Current Properties[1a]

by J. Sandblom,[1b] G. Eisenman, and J. L. Walker, Jr.[1c]

Department of Physiology, University of Chicago, Chicago, Illinois 60627 *(Received April 12, 1967)*

This paper continues the theoretical examination of the steady-state properties of liquid ion-exchange membranes in which sites and counterions are incompletely dissociated. The flux equations derived in the preceding paper are integrated for the case where only a single counterion species is present without the restriction of that paper to zero membrane current. The current–voltage relationship is deduced, and the steady-state fluxes and internal concentration profiles are related to the total membrane potential. On the basis of these relationships, the effects of association between sites and counterions are examined. A comparison is also made between the theoretically expected properties of liquid ion-exchange membranes having complete dissociation *vs.* strong association, as well as between the expectation for liquid *vs.* solid ion exchangers. It is concluded that increasing association makes a mobile-site membrane progressively more difficult to distinguish from a fixed-site membrane on the basis of its purely electrical properties, but progressively easier to distinguish on the basis of a comparison of electrical and flux properties. Some biological implications of these results are also discussed.

In a previous paper, the effects of association on the properties of a mobile-site membrane were examined.[2] The membrane under consideration was formally treated as a multicomponent system containing ionic as well as nonionic (ion pairs) species, assumed to be in chemical equilibrium at every point in the membrane but flowing independently of each other. Having chosen this approach as the basis for a quantitative treatment, the flux equations and boundary conditions for all the species were derived and the equations were solved under conditions of zero current.

This paper constitutes the second part of the same treatment and deals primarily with the behavior of the system under nonzero current conditions. The equations are written and solved for the case of a single counterion in steady state. Expressions are obtained relating concentration profiles, fluxes, and resistance to the total membrane potential and from these expressions the various effects of association on the membrane properties are deduced.

In the case where only a single counterion species is present in the system, the following set of equations can be deduced from eq 1 to 16 in part I.[2]

$$J_1 = -RTu_1 \frac{\partial c_1}{\partial x} - z_1 F u_1 c_1 \frac{\partial \psi}{\partial x} \quad (1)$$

$$J_s = -RTu_s \frac{\partial c_s}{\partial x} - z_s F u_s c_s \frac{\partial \psi}{\partial x} \quad (2)$$

$$J_{1s} = -RTu_{1s} \frac{\partial c_{1s}}{\partial x} \quad (3)$$

$$c_1 = c_s \quad (4)$$

$$\frac{c_1 c_s}{c_{1s}} = K \quad (5)$$

$$\int_0^d (c_s + c_{1s})\mathrm{d}x = \bar{c}^* d \quad (6)$$

(1) (a) This work was supported by National Science Foundation Grant GB-4039 and USPHS Grant GM 14404-01. It was assisted by USPHS General Research Support Grant FR-5367 and an NIH postdoctoral fellowship to J. L. Walker, Jr. (b) Institute of Physiology and Medical Biophysics, University of Uppsala, Uppsala, Sweden. (c) Department of Physiology, University of Utah, College of Medicine, Salt Lake City, Utah.

(2) J. Sandblom, G. Eisenman, and J. L. Walker, Jr., *J. Phys. Chem.*, 71, 3862 (1967).

$$V = \Delta\psi + \frac{RT}{z_1F}\ln\frac{c_s(d)}{c_s(0)} + \frac{RT}{z_1F}\ln\frac{a'}{a''} \quad (7)$$

$$J_1^* = J_1 + J_{1s} = \frac{I}{z_1F} \quad (8)$$

$$J_s^* = J_s + J_{1s} = 0 \quad (9)$$

Equations 8 and 9 are obtained from the condition of steady state, but all other expressions are valid in the nonsteady state as well.

We shall solve this system of differential equations to obtain fluxes and concentration profiles in terms of total membrane potential and external solution conditions. Dividing eq 8 by u_1 and eq 9 by u_s and adding the resulting expressions, we obtain

$$\frac{I}{z_1Fu_1} = \frac{J_1}{u_1} + \frac{J_s}{u_s} + \frac{2J_{1s}}{\bar{u}_{1s}} \quad (10)$$

where $\bar{u}_{1s}$ is a constant defined as

$$\bar{u}_{1s} = 2\frac{u_1u_s}{u_1 + u_s} \quad (11)$$

which we shall call the interdiffusion mobility of the dissociated species. Inserting eq 1–3 into eq 10 and using the condition of electroneutrality (4), we get

$$\frac{I}{z_1Fu_1} = -2RT\frac{dc_s}{dx} - 2RT\frac{u_{1s}}{\bar{u}_{1s}}\frac{dc_{1s}}{dx} \quad (12)$$

This equation can be integrated directly from 0 to x to yield

$$\frac{Ix}{z_1Fu_1} = -2RT[c_s(x) - c_s(0)] - 2RT\frac{u_{1s}}{\bar{u}_{1s}}[c_{1s}(x) - c_{1s}(0)] \quad (13)$$

Equation 12 is then integrated from 0 to d, and, taking into account eq 6, we get

$$\frac{Id}{2z_1Fu_1} = -2RT\frac{u_{1s}}{\bar{u}_{1s}}Q + 2RT\left[c_s(0) + \frac{u_{1s}}{\bar{u}_{1s}}c_{1s}(0)\right] \quad (14)$$

where the quantity Q is given by

$$Q = \bar{c}^* + \frac{1}{d}\left[\frac{\bar{u}_{1s}}{u_{1s}} - 1\right]\int_0^d c_s\,dx \quad (15)$$

In general, Q is a function of the electric current, but it is seen from eq 15 that in a number of limiting cases it is a constant, *e.g.*, when $\bar{u}_{1s} = u_{1s}$ or when the degree of dissociation is so small that the second term can be neglected in comparison with the first term. In certain other cases, it has been found justifiable to approximate Q by a constant.[3]

Equations 13 and 14 can be combined to eliminate $c_s(0)$ and $c_{1s}(0)$. This gives

$$2RT\frac{u_{1s}}{\bar{u}_{1s}}c_{1s}(x) + 2RTc_s(x) = 2RT\frac{u_{1s}}{\bar{u}_{1s}}Q + \frac{Id}{2z_1Fu_1}\left(1 - \frac{2x}{d}\right) \quad (16)$$

and finally, eq 4 and 5 are used to express eq 16 in terms of $c_s(x)$. After rearrangement, this gives an expression for the concentration at any point x, $c_s(x)$, in terms of the electric current and the various membrane parameters

$$c_s^2(x) + \frac{K\bar{u}_{1s}}{u_{1s}}c_s(x) = KQ + \frac{IdK\bar{u}_{1s}}{4z_1RTFu_1u_{1s}}\left(1 - \frac{2x}{d}\right) \quad (17)$$

from which $c_s(x)$ can be solved in terms of the electric current. The quantity Q may then be evaluated by inserting the resulting expression in (15) and integrating, as will be discussed in the section, "Concentration Profiles."

In order to relate the concentrations at the membrane boundaries to the total membrane potential, eq 2 and 3 are added, divided by u_s/z_1, and integrated using the steady-state condition (9) for the flow of sites. This gives

$$\Delta\psi = \frac{RT}{z_1F}\ln\frac{c_s(d)}{c_s(0)} + \frac{RT}{z_1F}\frac{u_{1s}}{u_s}\int_0^d\frac{dc_{1s}(x)}{c_s(x)} \quad (18)$$

After expressing $c_{1s}(x)$ in terms of $c_s(x)$ through eq 4 and 5, the integral is solved, and when this is introduced into eq 7, we obtain an expression for the total potential

$$V = \frac{RT}{z_1F}\ln\frac{a'}{a''} + \frac{2RT}{z_1F}\ln\frac{c_s(d)}{c_s(0)} + \frac{2RT}{z_1F}\frac{u_{1s}}{Ku_s} \times [c_s(d) - c_s(0)] \quad (19)$$

The solution to the equations is essentially complete since eq 19 can be combined with eq 17 to yield explicit expressions for the concentration profile and electric current in terms of the total membrane potential and external solution conditions.

Limiting Currents. Equations 17 and 19 indicate that the steady-state current–voltage relationship for a single counterion species depends on the mobilities of the undissociated as well as the dissociated species, the total concentration of sites, and the degree of dissocia-

(3) J. L. Walker, Jr., G. Eisenman, and J. Sandblom, *J. Phys. Chem.*, in press.

tion. The left side of eq 17 contains only positive quantities, and by inspecting the right-hand side after setting the left side of eq 17 equal to zero for $x = 0$ and $x = d$ (*i.e.*, $c_s(0) = 0$ and $c_s(d) = 0$, the respective concentrations at 0 and d for strong applied voltages), it can be seen that the electric current is confined to an interval given by

$$-\frac{4RTFu_1}{d}\frac{u_{1s}}{\bar{u}_{1s}}Q \leq I \leq \frac{4RTFu_1}{d}\frac{u_{1s}}{\bar{u}_{1s}}Q \qquad (20)$$

Thus, we find that a finite limiting current, previously deduced as being characteristic of a mobile-site membrane in the limit of complete dissociation,[4] is characteristic of mobile-site membranes quite generally regardless of their degree of dissociation. The end values of the interval in eq 20 define the values of the limiting currents I_1 whose absolute values are given by

$$|I_1| = \frac{4RTFu_1}{d}\frac{u_{1s}}{\bar{u}_{1s}}Q \qquad (21)$$

Concentration Profiles. In order to simplify the expressions, we shall introduce a quantity ϕ defined as

$$\phi = \frac{IdJ_{1s}}{4RTFu_1u_{1s}Q}$$

Note that $\phi \to 1$ as $I \to I_1$. Substituting this definition in eq 17 and solving for $c_s(x)$, we get an explicit expression for the concentration at any x as a function of ϕ

$$c_s(x) = -\frac{K}{2}\frac{\bar{u}_{1s}}{u_{1s}} + \sqrt{\left(\frac{K}{2}\frac{\bar{u}_{1s}}{u_{1s}}\right)^2 + KQ\left[1 + \frac{\phi}{z_1}\left(1 - \frac{2x}{d}\right)\right]} \qquad (22)$$

However, in order to calculate the concentration profiles, an expression for Q must be obtained. This is done by inserting eq 22 in eq 15 and integrating, which yields

$$Q = \bar{c}^* - \left\{\frac{\bar{u}_{1s}}{u_{1s}} - 1\right\} \times \left[\frac{\left[\left(\frac{K}{2}\frac{\bar{u}_{1s}}{u_{1s}}\right)^2 + KQ(1+\phi)\right]^{3/2} - \left[\left(\frac{K}{2}\frac{\bar{u}_{1s}}{u_{1s}}\right)^2 + KQ(1-\phi)\right]^{3/2}}{3\phi KQ} - \frac{K\bar{u}_{1s}}{2u_{1s}}\right] \qquad (23)$$

from which Q can be calculated graphically or by successive approximation.[3]

Figure 1 illustrates the concentration profiles for the indicated values of ϕ calculated from eq 22 and 23 for a membrane in which $K = 4 \times 10^{-7}$ mole/cm^3, $\bar{c}^* = 10^{-6}$ mole/cm^3, and $\bar{u}_{1s}/u_{1s} = 1/3.04$. (These particular values were chosen because they correspond to those characteristic of HCl in isopropyl alcohol, a liquid system in which the present theory has been tested).[3] Examining this figure, we notice that the concentration profiles are parabolic in form, in contrast to the linear profiles expected[4] and observed[5] in a completely dissociated mobile-site membrane. We also see that the concentration of sites becomes increasingly skewed as the applied field is increased, so that in the limit as $\phi \to 1$, the site concentration is reduced to zero at one side of the membrane, as noted in deducing eq 20.

Current–Voltage Relationship. An explicit relationship between current and voltage is obtained by expressing $c_s(0)$ and $c_s(d)$ in eq 19 in terms of eq 22. This gives

$$\bar{V} = \frac{RT}{z_1F}\ln\frac{a'}{a''} + \frac{2RT}{z_1F} \times \ln\frac{\sqrt{\left(\frac{K}{2}\frac{\bar{u}_{1s}}{u_{1s}}\right)^2 + KQ(1-\phi)} - \frac{K}{2}\frac{\bar{u}_{1s}}{u_{1s}}}{\sqrt{\left(\frac{K}{2}\frac{\bar{u}_{1s}}{u_{1s}}\right)^2 + KQ(1+\phi)} - \frac{K}{2}\frac{\bar{u}_{1s}}{u_{1s}}} + \frac{2RT}{z_1F}\frac{u_{1s}}{u_sK}\left[\sqrt{\left(\frac{K}{2}\frac{\bar{u}_{1s}}{u_{1s}}\right)^2 + KQ(1-\phi)} - \sqrt{\left(\frac{K}{2}\frac{\bar{u}_{1s}}{u_{1s}}\right)^2 + KQ(1+\phi)}\right] \qquad (24)$$

The general shape of the current–voltage relationship for varying values of the dissociation constant K and constant total concentration is illustrated in Figure 2 for a membrane in which $\bar{u}_{1s}/u_{1s} = 1/3.04$.

Figure 2 indicates that the voltage range over which the I–V relationship is nearly linear becomes increasingly extended with increasing association. This is because the increasing number of undissociated ion pairs, which are not acted on by electric forces, acts as a "reservoir" of sources and sinks for the dissociated species. Therefore, significant skewing of the concentration profiles does not occur until the field is so high that the fluxes are large enough to overcome the capacity of the "reservoir."

Examining the curves for successively smaller values of K, it can also be seen that, for a membrane in which $\bar{c}^*$ is constant, the steady-state resistance initially decreases as the association increases, which can be ex-

(4) F. Conti and G. Eisenman, *Biophys. J.*, **6**, 227 (1966).

(5) J. L. Walker, Jr., and G. Eisenman, *Ann. N. Y. Acad Sci.*, **137**, 777 (1966); *Biophys. J.*, **6**, 513 (1966).

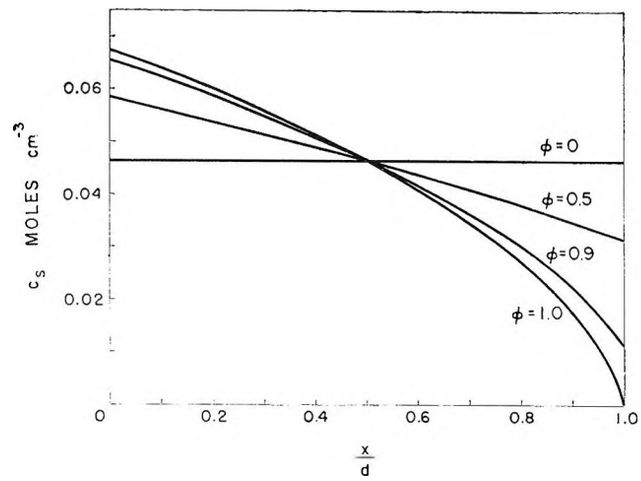

Figure 1. Concentration profiles are plotted for ϕ = 0, 0.5, 0.9, and 1.0. $K = 4 \times 10^{-7}$ mole/cm^3, $\bar{c}^* = 10^{-6}$ mole/cm^3, $u_{1s} = 3.04\bar{u}_{1s}$. Note that all the profiles intersect at the same point, $d/2$, a fact which may also be deduced from eq 17.

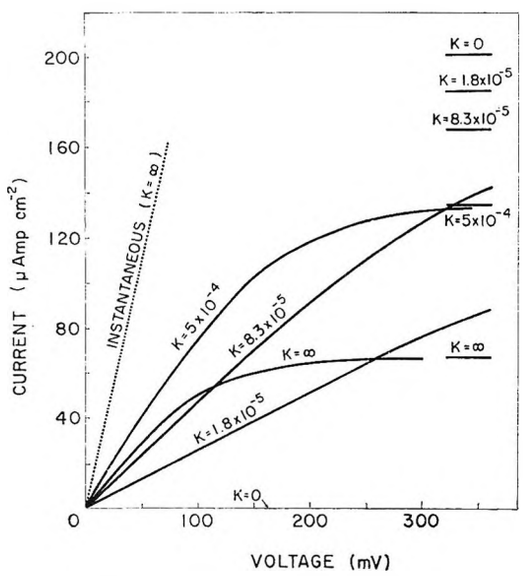

Figure 2. Theoretical current–voltage relationships for a membrane having the indicated degrees of dissociation (K is expressed in moles/liter) and $u_{1s} = 3.04\bar{u}_{1s}$ corresponding to the measured values for HCl in 2-propanol. $\bar{c}^*$ has been held constant at 10^{-3} mole/l. Note the initial decrease in resistance and subsequent increase as K is varied from infinity to zero. Also note that the limiting current at high positive voltage increases monotonically as K is varied from infinity to zero.

plained by the following considerations. For the case of complete dissociation ($K = \infty$), the electric current at steady state is carried only by the counterions. This follows from the fact that in a completely dissociated sytem $J_s^* = J_s = 0$. In an incompletely dissociated system, however, movement of the sites also contributes to the electric current within the membrane even in the steady state (the sites move as free ions in one direction and as neutral species combined with counterions in the other direction) so as to preserve the balance of eq 9 which in steady state requires J_s^* to be zero. In this way, the associated sites act as "carriers." If the mobility (u_{1s}) of the neutral species is larger than the mean mobility ($\bar{u}_{1s}$) of the ions, the steady-state resistance will initially decrease as the association increases (compare $K = 5.0 \times 10^{-4}$ with $K = \infty$), but as the association becomes still stronger the sites will be "consumed" and the resistance will increase (compare $K = \infty$ with $K = 8.3 \times 10^{-5}$ and $K = 1.8 \times 10^{-5}$).

Except for the special case where $u_{1s} = \bar{u}_{1s}$ the degree of association also affects the magnitude of the limiting current as can be deduced from eq 20 and is illustrated in Figure 2 (*cf.* the limiting values at the right). When $u_{1s} > \bar{u}_{1s}$, as in Figure 2, the backflow of the neutral species has a larger effect than the depletion of free sites, and the limiting current increases with increasing association. The reverse will be the case when $u_{1s} < \bar{u}_{1s}$.

Membrane Resistance. The instantaneous resistance R_∞ of the membrane, as measured using a step change in current or by a high-frequency alternating current is given by

$$R_\infty = \frac{1}{F^2(u_1 + u_s)} \int_0^d \frac{dx}{c_s(x)} \tag{25}$$

When the integration is performed, this gives

$$R_\infty = \frac{d}{F^2(u_1 + u_s)KQ\phi} \times \left\{\frac{K\bar{u}_{1s}}{2u_{1s}} \ln\left[\frac{c_s(d)}{c_s(0)}\right] + c_s(d) - c_s(0)\right\} \tag{26}$$

where, again, $c_s(d)$ and $c_s(0)$ may be expressed in terms of K, $\bar{u}_{1s}/u_{1s}$, ϕ, and Q through eq 22.

The steady-state resistance R_0 is given by

$$R_0 = \frac{V - V_0}{I} \tag{27}$$

and is obtained from eq 24 recalling that $\phi = I/|I_1|$.

A comparison between the steady-state resistance R_0 and the instantaneous resistance R_∞ is most easily made in the limit of zero current ($\phi = 0$). In this case, eq 25 and 27 reduce, respectively, to

$$R_\infty(\phi = 0) = \frac{d}{F^2(u_1 + u_s)c_s} \tag{28a}$$

and

$$R_0(\phi = 0) = \frac{u_s + u_{1s}\frac{c_s}{K}}{F^2\left[u_1u_sc_s + (u_1 + u_s)\frac{u_{1s}c_s^2}{K}\right]} \times d \qquad (28b)$$

From these expressions it is seen that as the association increases ($K \rightarrow 0$), the instantaneous resistance approaches the steady-state resistance. In the other limit of complete dissociation ($K \rightarrow \infty$), the following relationship is obtained between the two resistances

$$R_\infty(\phi = 0) = (1 - t_s) \times R_0(\phi = 0) \qquad (29)$$

where t_s is the transference number of the dissociated form of the sites, given by

$$t_s = \frac{u_s}{u_1 + u_s}$$

The relationship expressed by eq 29 was found and experimentally verified by Walker and Eisenman.[5]

Fluxes. Recalling that for the present single counterion case, $J_1^* = I/F$, the dependence of the total flux of the counterion species on the solution conditions and applied electric potential can be obtained from eq 24 and is shown in Figure 2. It has been mentioned that only the total fluxes are constant throughout the membrane, whereas the partial fluxes are subject to sources and sinks. This is seen by deriving explicit expressions for the partial fluxes J_1, J_s, and J_{1s}. The partial flux J_{1s} is obtained from eq 3–5

$$J_{1s} = -RTu_{1s}\frac{dc_{1s}}{dx} = -\frac{RTu_{1s}}{K}\frac{dc_s^2}{dx} = -\frac{2RTu_{1s}c_s}{K}\frac{dc_s}{dx} \qquad (30)$$

from which dc_s/dx and dc_{1s}/dx may be expressed in terms of J_{1s}. Inserting these expressions in eq 12, we get after rearrangement, recalling that $J_1^*F = I$

$$\frac{J_{1s}}{J_1^*} = \frac{t_sc_s}{c_s + \frac{K}{2}\frac{\bar{u}_{1s}}{u_{1s}}} \qquad (31)$$

Recalling the dependence of c_s on x in eq 22, eq 31 indicates the distance dependence of the partial flux J_{1s} in the steady state for constant J_1^* (*i.e.*, constant current). This dependence is illustrated in Figure 3, which presents flux profiles of J_1 as a fraction of the total flux J_1^* calculated from eq 31, 22, and 8 using the same values of the parameters and currents as those given for Figure 1. Note that the ratio J_1/J_1^* is smaller than unity for all currents less than the limiting one.

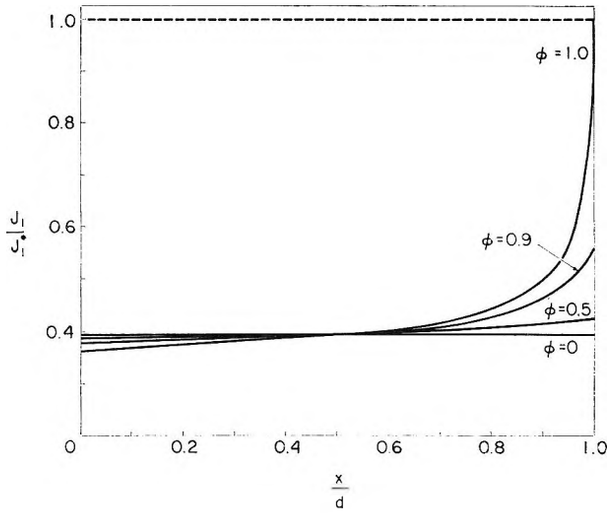

Figure 3. The partial flux J_1 of the counterion is plotted as a function of x in terms of the fraction of total flux (J_1/J_1^*) for ϕ = 0, 0.5, 0.9, and 1.0. The dotted line represents the total flux $J_1^* = I/F$.

It is only when $\phi = 1$ and the sites are depleted at one end of the membrane that the counterions are seen to carry the total current. Notice that for small currents (*i.e.*, for low values of ϕ) the flux of counterion species is essentially constant for a given applied field, being independent of the position within the membrane. This is comparable to the situation for all applied currents in a fixed-charge membrane in the steady state. Moreover, notice that this flux (J_1) is less than 40% of the total flux, demonstrating that circulation of sites contributes significantly to the flow of electric current even in the steady state despite the fact that the sites cannot cross the membrane–solution interfaces. Indeed, notice that as ϕ becomes increasingly large, it can be seen that the flux of the counterion becomes a function of distance, an effect which is surprisingly small until ϕ is greater than 0.5. The slope of the curve is of course the rate of change of the flux of the counterion species with x, which determines the rate of transformation from the dissociated form to the undissociated form. J_1^* (namely the total flux of species 1 in all of its forms within the membrane) is exactly equal to the fluxes of species 1 entering and leaving the membrane. This can be seen to be constant throughout the membrane in the steady state, as required by eq 8 (see dotted line in Figure 3). The difference between curves J_1^* and J_1 for each applied field represents the flux of the site species J_s, which is directly equal and opposite in this case to the flux of the associated pairs (see eq 9).

Diffusion Coefficients. For the present single counterion treatment, one interesting property of an associated

mobile site membrane which contrasts with the situation in a fixed-site membrane is that the diffusion coefficient measured by tracer flux (D_{tr}) differs from that measured from the high-frequency electrical resistance (D_{el}). Since the labeled and nonlabeled isotopes have the same properties, there will not be any potential gradient or site gradient at zero current regardless of the concentrations in the solution phases. The total tracer flux J_1^{*tr} can therefore be written directly in terms of concentration gradients of the tracer in the membrane.

When the tracer is added to one of the external solutions and the rate of appearance J_1^{*tr} is measured on the other side, we obtain

$$J_1^{*tr} = -RTu_1 \frac{dc_1^{tr}}{dx} - RTu_{1s} \frac{dc_{1s}^{tr}}{dx} =$$

$$RT\left[u_1 + \frac{c_s u_{1s}}{K}\right]\frac{dc_1^{tr}}{dx} = -\frac{RT}{d}\left[u_1 + \frac{c_s}{K}u_{1s}\right]sM_1c_1 \tag{32}$$

where s is the specific activity (curies/g), M_1 the molecular weight of the counterion, and c_1^{tr} the concentration of tracer in the membrane which is measured in curies cm^{-3}. c_1 is the (uniform) concentration of counterion as defined before and is measured in moles cm^{-3}. J_1^{*tr} is measured in curies sec^{-1} cm^{-2}. The measurement of tracer flux can be compared with the measurement of electric conductance performed at zero current and high-frequency alternating current.

This conductance is obtained from eq 28a, recalling that for a single counterion $c_1 = c_s$

$$G_\infty(\phi = 0) = \frac{F^2(u_1 + u_s)c_1}{d} \tag{33}$$

Dividing eq 32 and 33, we get

$$\frac{-J_1^{*tr}}{G_\infty}\frac{F^2}{RT}sM_1 = \frac{\left[u_1 + \frac{c_s}{K}u_{1s}\right]}{u_1 + u_s} = \frac{u_1}{u_1 + u_s} + \frac{u_{1s}}{u_1 + u_s}\frac{c_s}{K} \tag{34}$$

Equation 34 is seen to define a ratio between a diffusion coefficient measured by diffusion ($D_{diff} = RT[u_1 + (c_s/K)u_{1s}]$) and an electrically measured diffusion coefficient ($D_{el} = RT(u_1 + u_s)$).

For the limit of complete dissociation ($K \to \infty$), this ratio is given by the transference number of the counterion (see eq 34). On the other hand, for strong association ($K \to 0$), $c_s^2 = Kc_{1s} \to K\bar{c}^*$ and eq 34 reduces to

$$\frac{D_{diff}}{D_{el}} = \frac{u_{1s}}{u_1 + u_s}\sqrt{\frac{\bar{c}^*}{K}}$$

The discrepancy between diffusion coefficient measured electrically and that measured by tracer diffusion is therefore inversely proportional to the square root of K for strong association ($K \to 0$).

Discussion

Physical Systems to Which the Present Analysis Is Applicable. The present analysis is restricted to membranes in which (a) univalent counterions and sites are assumed to behave ideally except insofar as they can associate through a simple law of mass action to form neutral ion pairs, and in which (b) the sites are assumed to be unable to cross the membrane-solution interface, (c) the concentration of co-ions is assumed to be negligible, and (d) the mobilities of species are assumed to be constant. (e) In addition, we have considered only the situations in which the diffusion of counterions is membrane controlled (*i.e.*, we have assumed that negligible concentration polarization occurs in the solutions adjacent to the membrane and have neglected interfacial effects). Membranes for which these assumptions are expected to be approximately valid are those containing the usual monofunctional liquid ion exchangers[6] dissolved in water-immiscible solvents over some as yet undefined range of dielectric constant. Notice that for solvents of very low dielectric constant, the assumption (a) may no longer be correct since association is likely to be complicated by the formation of "triple ions" and other higher order aggregates.[7] Indeed, typical liquid ion exchangers such as diisooctyl hydrogen phosphate are known to form associated complexes in low dielectric constant solvents whose degree of aggregation is a function of the size and charge of the counterions.[8] The present system may also be thought of as a model for certain types of "carrier transport" mechanisms postulated for biological membranes.[9]

The conditions under which the present treatment is expected to apply to membranes made from the usual liquid ion exchangers are examined in more detail below; however, it is worth noting here that a simple physical system has been devised and studied by Walker, Eisenman, and Sandblom[3] to test the principal expectations of the present theory. This system,

(6) C. F. Coleman, C. A. Blake, Jr., and K. B. Brown, *Talanta*, **9**, 297 (1962).

(7) R. A. Fuoss and M. Krauss, *J. Am. Chem. Soc.*, **55**, 476 (1933); R. A. Fuoss, *ibid.*, **57**, 488 (1935); *Trans. Faraday Soc.*, **32**, 594 (1936).

(8) G. J. Janz and S. S. Danyluk, *Chem. Rev.*, **60**, 209 (1960); *cf.* pp 228–230.

(9) W. Wilbrandt and T. Rosenberg, *Pharmacol. Rev.*, **13**, 109 (1961).

in which all of the present assumptions are satisfied, consists of a solution of hydrochloric acid in 2-propanol bounded by two chloridized silver plates. In this system, chloride ions can enter or leave the aqueous phase, but hydrogen ions can only redistribute within it. We have therefore only one species of counterion—the chloride ion, while the hydrogen ion corresponds to the mobile site. The mobile associated species is the HCl molecule, whose dissociation is governed by a simple law of mass action. After conventional measurements had been made of the dissociation constant for HCl and of the individual mobilities of H^+ and Cl^-, the mobility of the undissociated HCl species was measured from the value of the limiting current density using eq 21 of the present theory. With the value of this parameter known, the steady-state current–voltage relationship is completely specified for all HCl concentrations and so are the concentration profiles, electric potential profiles, and instantaneous conductances for the steady state of any applied current. Measurements were therefore made of all of these properties and were found to be in quantitative agreement with the expectations of the present paper.

The Conditions under Which Assumptions b and e Are Satisfied Simultaneously. Assumption b that the sites are completely trapped within the membrane is an idealization whose validity is a function of the solubility of both the membrane phase and of the sites in the external solution phases. Since the site species must have a finite solubility in the external solutions which can be considered as infinite reservoirs, some fraction of the sites must be transported across the membrane under nonequilibrium conditions. Thus, if an electric field is applied to the equilibrium situation of a membrane separating two identical solutions, accumulation of sites will occur in the solution at one of the membrane–solution interfaces, together with a corresponding depletion of sites in the solution at the other interface as the system passes to the stationary state. Consequently, the number of sites contained in the membrane will change during the process. If, however, the ionic redistribution within the membrane is rapid compared to the rate of loss or gain of sites, the sites will transiently act as if they were trapped. Therefore, the physical situation which might be realized in a liquid ion exchanger corresponding to assumption b is that the transport of sites must be rate limited by the membrane boundaries (*e.g.*, film controlled)[10] whereas to satisfy assumption e the transport of permeant species must be rated limited by the membrane phase (*e.g.*, membrane controlled).[10] Since the activation energies for counterion diffusion across the membrane–solution interfaces may be much larger than within the membrane phase,[11] it is necessary to have a sufficiently thick system in order to ensure that this effect is negligible, while at the same time being certain that the membrane is sufficiently thin to maintain rate-limiting surfaces for the diffusion of sites.

The above conditions can be formulated quantitatively for the situation where the limiting part of the membrane boundaries may be attributed to an unstirred layer of thickness δ in the external solutions adjacent to the membrane surfaces. Confining ourselves to the case of a single counterion species and completely dissociated sites and counterions, the time constant of establishing interior profiles, τ_D, is given by

$$\tau_D = \frac{d^2}{\pi^2 D_m} \tag{35}$$

where d is the membrane thickness and $D_m = RT\bar{u}_{1s}$.

In order to calculate the time constant τ_s for the loss of sites, we shall consider the case when the electric current is zero and the concentration of sites in the external solution is zero initially. If the ionic redistribution within the membrane is rapid compared to the rate of loss of sites, the concentration profile within the membrane is essentially uniform. The rate at which the sites disappear must therefore be given by

$$\frac{d\bar{c}^*}{dt} = -\frac{2D_f}{d\delta S}\bar{c}^* \tag{36}$$

where S is the distribution coefficient of the sites, $S = [\bar{c}^*(m)/\bar{c}_s^*(f)]$, and D_f is the diffusion coefficient ($RT\bar{u}_{1s}$) in the film. The time constant τ_s calculated from eq 36 is

$$\tau_s = \frac{d\delta S}{2D_f} \tag{37}$$

and the condition for trapped sites may therefore be expressed as

$$\tau_s \gg \tau_D$$

or

$$S\frac{\delta}{d}\frac{D_m}{D_f} \gg \frac{2}{\pi^2} \tag{38}$$

A quantitative formulation can also be given to the condition (e) that the counterions are membrane controlled. Helfferich[10] (eq 8-8) has derived such an expression by considering self-diffusion in the stationary state, and under these conditions his treatment is also

(10) F. Helfferich, "Ion Exchangers," McGraw-Hill Book Co., Inc., New York, N. Y., 1962.

(11) J. T. Davies, *J. Phys. Chem.*, **54**, 185 (1950).

valid for a dissociated liquid ion-exchange membrane. The expression he obtains is

$$\frac{\bar{c}^*}{c}\frac{\delta}{d}\frac{u_{1m}}{u_{1f}} \ll 2 \tag{39}$$

where $\bar{c}^*$ is the total concentration in the membrane, c is the total concentration in the external solutions, and u_{1m}, u_{1f} are the mobilities of the counterion in the membrane and film, respectively. Note that $\bar{c}^*/c$ in (39) is not necessarily equal to S in (38) since we have assumed the presence of impermeable co-ions in the external solutions. In deriving eq 38 and 39 we have only considered completely dissociated systems. However, if the mobilities of associated and dissociated species are equal, these equations are also valid for membranes containing ion pairs.

We can also conclude that in order to satisfy both eq 38 and 39, *the sites should have a high affinity for the membrane (i.e., large S) and the ratio $\bar{c}^*/c$ (i.e., total site concentration to total external concentration) should be chosen to be as small as possible.*

Activity Coefficient Effects. It is possible in calculating the I–V curve for a single counterion to take varying activity coefficients into account. To introduce variable activity coefficients, we shall approximate them with the rather generally observed empirical relationship

$$\frac{\mathrm{d} \ln a_i}{\mathrm{d} \ln c_i} = n \tag{40}$$

where n is a constant characteristic of the nonideal behavior. This leaves the flux equations unaltered except for the relationship between diffusion coefficient and mobility for the ions which becomes

$$D_i = nRTu_i \tag{41}$$

The solution to the problem then follows the same line as presented above.

Biological Implications. Many types of ion-exchange membranes have been proposed as possible models for biological membranes and the liquid ion-exchange membrane treated here is a conceivable model for the postulated lipid soluble carriers. Some of the important features described in this paper may therefore be used as criteria for distinguishing this type of permeation mechanism from other types, *e.g.*, permeation through pores lined by fixed charges.

We have shown that in general mobile-site membranes are distinguishable from fixed-site membranes by the presence of limiting currents although in the case of strong association this property becomes increasingly difficult to assess. On the other hand, we have also demonstrated that a discrepancy between diffusion coefficients measured electrically and by tracers is to be expected, and this discrepancy becomes more pronounced for stronger association. This is a classical example of what is called exchange diffusion in the biological literature.[12] This effect may be thought of as a consequence of the fact that association leads to a transport of the counterion in an electrically neutral form due to combination with the oppositely charge mobile site.

In summary, we can therefore state that increasing association makes a mobile-site membrane progressively more difficult to distinguish from a fixed-site membrane on the basis of its purely electrical properties, but progressively easier to distinguish on the basis of a comparison of electrical and flux properties, and that therefore the latter measurements should be used in trying to distinguish the two permeation mechanisms in a biological membrane.

(12) H. Ussing, *Advan. Enzymol.*, 13, 21 (1952).

Thermodynamic Properties at 25° of Aqueous Solutions of *p*-Ethylbenzenesulfonic Acid and Its Alkali Metal Salts. Comparisons with Cross-Linked Polystyrenesulfonate Type Cation Exchangers[1]

by G. E. Boyd, F. Vaslow, A. Schwarz,[2] and J. W. Chase

Oak Ridge National Laboratory, Oak Ridge, Tennessee 37830 (*Received April 13, 1967*)

Molal osmotic and mean molal activity coefficients, ϕ and γ, and apparent molal heat contents, ϕ_L, of aqueous solutions of *p*-ethylbenzenesulfonic acid (*p*-EBSA) and its alkali metal salts were determined at 25° for a wide range of concentrations. The strength of the acid was inferred to be less than that of HNO_3, and evidence was obtained for ion-pair formation with the cesium salt. The concentration dependence of ϕ_L was unusual in that values above the Debye–Hückel limiting slope were observed with all but Cs *p*-EBS. Calculations of solvent relative partial molal entropies, $S_1 - S_1°$, indicated that the *p*-ethylbenzenesulfonate anion possessed "water structure forming" properties. Free energies of dilution, ΔG_D, were computed from ϕ and γ, and the differences between these were compared with the standard free energy changes, $\Delta G_{ex}°$, for ion-exchange reactions between the alkali metal cations and hydrogen ion in cross-linked polystyrenesulfonic acid type cation exchangers. Differences in ϕ_L were also compared with standard heats of cation exchange, $\Delta H_{ex}°$. The concordance between the various thermodynamic quantities indicated that the analogy between concentrated electrolyte mixtures and cation exchangers was valid.

The objective of this research has been to conduct the measurements necessary for a comparison of the differences in the thermodynamic properties at 25° of aqueous solutions of the alkali metal salts of *p*-ethylbenzenesulfonic acid with the standard enthalpies, free energies, and entropies of ion exchange for the corresponding cations in cross-linked polystyrenesulfonic acid type cation exchangers. Justification for this comparison lies in the existence of numerous analogies in the equilibrium behavior of organic ion exchangers with concentrated aqueous electrolyte solutions. The electrochemical properties of sulfonic acid groups in cross-linked polystyrenesulfonates, for example, appear to be virtually the same as those for the same groups in low molecular weight analogs such as in *p*-ethylbenzenesulfonic acid or *p*-toluenesulfonic acid. The pH titration curves for the cross-linked polymer acid and its heat of neutralization indicate strong acid behavior. Further, Raman spectral[3] and nmr[4] measurements on polystyrenesulfonic acid and on ethylbenzenesulfonic acid have shown that the amount of associated hydrogen ion must be quite small.

Comparisons between the thermodynamic properties for alkali metal cation-exchange reactions and those for concentrated aqueous alkali metal chloride solutions have been attempted.[5,6] However, only a poor correspondence was observed for several reasons. The properties of aqueous alkali metal salt solutions are strongly dependent on the nature of the anion, as may

(1) Research sponsored by the U. S. Atomic Energy Commission under contract with the Union Carbide Corp.

(2) Radiochemistry Department, Israel Atomic Energy Commission, Soreq Nuclear Research Center, Yavne, Israel.

(3) S. Lapanje and S. A. Rice, *J. Am. Chem. Soc.*, **83**, 496 (1961).

(4) L. Kotin and M. Nagasawa, *ibid.*, **83**, 1026 (1961).

(5) E. Cruickshank and P. Meares, *Trans. Faraday Soc.*, **53**, 1299 (1957).

(6) O. D. Bonner and J. R. Overton, *J. Phys. Chem.*, **65**, 1599 (1961).

be seen by comparing the activity coefficients and apparent molal heat content values for the chlorides with those for the nitrates. Comparisons of the properties of concentrated electrolyte solutions with those of cation exchangers therefore should be made with aqueous solutions of the "model compounds." Further, in one instance[5] it was mistakenly assumed that a hydrostatic pressure exists inside a cross-linked ion exchanger. Consequently, the free energies and heats of dilution for the alkali metal chloride solutions were corrected by estimated free energies and heats of compression (or decompression), respectively. In acttuality, the pressure in an ion-exchange gel is the same as the ambient pressure, which is usually 1 atm. A probe placed in the gel, for example, would not register a pressure different from that outside the gel. The free energy of the molecular network of an ion exchanger varies with its volume; formally this variation has the units of pressure and the derivative has been termed the "swelling pressure," although a better term would have been the "strain free energy."[7]

The lithium, sodium, potassium, and cesium salts of the "model" compound, *p*-ethylbenzenesulfonic acid, were employed in this investigation of the analogy between cation exchangers and concentrated electrolyte solutions. Molal osmotic coefficients, ϕ, for these salts in aqueous solution were measured with the gravimetric isopiestic vapor pressure comparison method and with a vapor pressure osmometer.[8,9] These determinations were employed to compute mean molal activity coefficients, γ, and free energies of dilution, ΔG_D, as a function of concentration. Calorimetric determinations of the heats of dilution of aqueous solutions of the acid and its alkali metal salts also were made and values of their apparent molal heat contents, ϕ_L, as a function of concentration were derived. The values of ΔG_D and ϕ_L thus obtained were employed to estimate free-energy differences, $\Delta(\Delta G_D)$, and enthalpy differences, $\Delta\phi_L$, for comparison with standard free energies and enthalpies of cation exchange.

Experimental Section

Materials. The synthesis of *p*-ethylbenzenesulfonic acid and its lithium and sodium salts have been described.[10] Measurements of the infrared and nmr spectra of the barium salt of the acid indicated at least 99% *para* substitution. The potassium and cesium salts were prepared from the barium salt, which was converted by ion exchange to give an aqueous solution of the acid which was neutralized with pure K_2CO_3 or Cs_2CO_3, respectively. The salts were recrystallized from absolute ethanol and vacuum-dried at 60°. Equivalent weights, determined by titration of the acid released when solutions containing known weights of salt were passed through a deep bed of H-form cation exchanger, were 224 and 318 for the potassium and cesium salts compared with theory values of 226 and 317, respectively.

Osmotic Coefficient Determinations. The gravimetric isopiestic vapor pressure comparison apparatus and techniques employed in measuring the concentrations of the model compound solutions in vapor pressure equilibrium with standard sodium chloride solutions have been described.[11] Concentrated stock solutions of the alkali metal *p*-ethylbenzenesulfonates were made up by weight, and weight burets were employed in the preparation of more dilute solutions as required. A vapor pressure osmometer was employed in the measurements with solutions of concentrations less than 0.5 *m*. The precision of these measurements was lower than with the gravimetric technique, particularly below 0.1 *m;* however, the speed and convenience with which determinations can be made on dilute solutions are important advantages. Approximately 6–8 min was needed for the system to come to a steady-state temperature difference and give a constant resistance reading. Repetitive measurements were made and the data were averaged to increase precision.

Molalities of the isopiestic NaCl and alkali metal *p*-ethylbenzenesulfonate solutions of 25° observed with the gravimetric technique are presented in Table I. Molal osmotic coefficients were computed from these data with

$$\nu_x m_x \phi_x = \nu_r m_r \phi_r \qquad (1)$$

where the number of ions, $\nu = 2$, m_x is the sulfonate molality, ϕ_x is its osmotic coefficient, and m_r and ϕ_r are the molality and osmotic coefficient of the reference electrolyte (NaCl), rsepectively.

The osmotic coefficients given in Table II were computed with the equation

$$(m\phi)_x = (\Delta R_x/\Delta R_r)(m\phi)_r \qquad (2)$$

where $(\Delta R_x/\Delta R_r)$ is the measured resistance ratio. Values for the osmotic coefficient, ϕ_r, of the reference electrolyte solution (NaCl) at 25° were computed from m_r with the equation[12]

(7) For a further discussion see J. J. Hermans, "Flow Properties of Disperse Systems," North-Holland Publishing Co., Amsterdam, 1953, Chapter III.

(8) O. D. Bonner and O. C. Rogers, *J. Phys. Chem.*, **65**, 981 (1961).

(9) G. E. Boyd, A. Schwarz, and S. Lindenbaum, *ibid.*, **70**, 821 (1966).

(10) S. Lindenbaum and G. E. Boyd, *ibid.*, **71**, 581 (1967).

(11) S. Lindenbaum and G. E. Boyd, *ibid.*, **68**, 911 (1964).

(12) E. A. Guggenheim and J. C. Turgeon, *Trans. Faraday Soc.*, **51**, 747 (1955).

$$1 - \phi = 0.3903m^{1/2}\sigma(m^{1/2}) - \beta m \qquad (3)$$

using $\beta = 0.15$.

Mean molal activity coefficients were calculated from the osmotic coefficients with the Gibbs–Duhem equation. The required integrations were performed numerically with a CDC 1604 digital computer. The necessary extrapolation of the ϕ_x values to zero concentration was performed with eq 3 with β taking the values 0.11, 0.08, −0.035, and −0.19 ± 0.03 for the lithium, sodium, potassium, and cesium salts, respectively. A value, $\beta = -0.047$, derived from the measurements of Bonner,[13] was employed for the acid. Osmotic and activity coefficients computed for interpolated concentrations are given in Table III. The concentration dependence of the measured osmotic coefficients including those for the acid is exhibited in Figure 1, where it may be seen that the sequence of values for the *p*-ethylbenzenesulfonates taken at a constant concentration resembles that for the corresponding nitrates. Interestingly, the sodium and potassium salts were relatively insoluble; the sodium salt in fact was the least soluble alkali metal *p*-ethylbenzenesulfonate.

Table I: Molalities of Isopiestic Solutions at 25°

m_{NaCl}	Li *p*-EBS	Na *p*-EBS	K *p*-EBS	Cs *p*-EBS
0.1994	...	...	...	0.2150
0.3493	...	0.3596	...	...
0.3973	...	0.4150	...	...
0.4316	...	...	0.4840	0.5143
0.4561	...	...	0.5170	0.5499
0.4646	...	0.4953	...	...
0.4886	0.5128	0.5274	...	...
0.5947	0.6375	0.6641	...	...
0.6674	0.7270	0.7678	...	...
0.6862	...	...	0.8788	0.9646
0.7837	...	...	1.097	1.213
0.8187	...	...	1.180	1.310
0.8732	1.008	1.135	...	...
0.9937	...	...	1.690	1.855
1.104	...	...	2.085	2.227
1.208	1.548	1.939	...	...
1.221	...	1.974	...	...
1.4525	...	...	3.167	3.346
1.537	2.0905	2.723	...	...
1.764	2.441	3.218	...	...
2.084	...	...	4.927	4.849
2.1635	3.006	...	...	...
2.211	3.085	4.026	...	...
2.533	...	...	...	5.874
2.741	3.751	...	...	...
2.971	...	...	...	6.9405
3.3845	...	...	...	7.873
3.385	4.520	...	...	...
3.392	...	...	...	7.894
4.009	...	...	...	9.473
4.155	5.410	...	...	...
4.210	...	...	...	10.044
4.808	...	...	...	11.739
5.1195	...	...	...	12.624

Table II: Osmotic Coefficients for Dilute Solutions from Vapor Pressure Osmometer Measurements at 25°

$m_{K\ p\text{-}EBS}$	$\phi_{K\ p\text{-}EBS}$	$m_{Cs\ p\text{-}EBS}$	$\phi_{Cs\ p\text{-}EBS}$
0.02129	(0.9368)	0.10012	0.9044
0.04998	0.9379	0.15001	0.8868
0.10000	0.9165	0.19420	0.8642
0.14996	0.9011		
0.19954	0.8865		

Calorimetric Measurements. The calorimeter and accessories employed in the heat of dilution measurements have been described.[14] Several improvements to the electrical measuring circuits were effected,[15] thereby increasing the temperature sensitivity to approximately 15 μdeg. Solutions of accurately predetermined concentration were measured into the calorimeter pipet from weight burets. The initial volume of water in the calorimeter was *ca.* 500 ml accurately measured by weight; the final concentration after dilution was less than 0.01 *m* in all cases. Over-all checks on the calorimetric system were made by measuring the heat of solution of KCl(c). The reaction temperature was 25.2° and the results are expressed in terms of the defined calorie (*i.e.*, 1 cal = 4.1840 absolute joules).

Corrections to the observed heats for "dilution to infinite dilution," $\phi_L(m_f)$, were computed with the equation proposed by Guggenheim and Prue[16] following a procedure outlined elsewhere.[17] In this procedure requisite values of the coefficient (dB/dT) were obtained from the correlation between (dB/dT) and $(B_{MX} - B_{KCl})$ computed from the values of B_{MX} =

(13) O. D. Bonner, G. D. Easterling, D. L. West, and V. F. Holland, *J. Am. Chem. Soc.*, **77**, 242 (1955).

(14) G. E. Boyd and F. Vaslow, *J. Chem. Eng. Data*, **7**, 237 (1962).

(15) S. Lindenbaum and G. E. Boyd, *J. Phys. Chem.*, **69**, 2374 (1965).

(16) E. A. Guggenheim and J. E. Prue, *Trans. Faraday Soc.*, **50**, 710 (1954).

(17) G. E. Boyd, J. W. Chase, and F. Vaslow, *J. Phys. Chem.*, **71**, 573 (1967).

Table III: Osmotic and Activity Coefficients for Interpolated Molalities of Aqueous Alkali Metal Salt Solutions of *p*-Ethylbenzenesulfonic Acid at 25°

	H *p*-EBS[a]		Li *p*-EBS		Na *p*-EBS		K *p*-EBS		Cs *p*-EBS	
m	ϕ	γ	ϕ	γ	ϕ	γ	ϕ	γ	ϕ	γ
0.1	0.915	0.749	0.932	0.773	0.929	0.769	0.916	0.752	0.904	0.734
0.2	0.891	0.683	0.918	0.723	0.915	0.717	0.888	0.683	0.864	0.652
0.3	0.871	0.637	0.906	0.688	0.902	0.682	0.864	0.634	0.834	0.595
0.4	0.852	0.600	0.893	0.659	0.885	0.650	0.841	0.593	0.804	0.548
0.5	0.832	0.568	0.880	0.634	0.862	0.617	0.817	0.557	0.777	0.509
0.6	0.813	0.539	0.866	0.611	0.839	0.587	0.792	0.524	0.751	0.475
0.7	0.793	0.513	0.852	0.590	0.819	0.560	0.767	0.494	0.725	0.444
0.8	0.772	0.488	0.838	0.569	0.795	0.534	0.741	0.466	0.700	0.417
0.9	0.754	0.466	0.827	0.550	0.772	0.508	0.715	0.440	0.675	0.392
1.0	0.737	0.446	0.808	0.531	0.751	0.485	0.689	0.415	0.650	0.369
1.2	0.709	0.412	0.781	0.498	0.712	0.445	0.642	0.373	0.603	0.329
1.4	0.687	0.385	0.757	0.469	0.676	0.409	0.604	0.338	0.568	0.298
1.6	0.672	0.363	0.738	0.445	0.640	0.377	0.567	0.309	0.538	0.272
1.8	0.665	0.347	0.722	0.424	0.606	0.348	0.538	0.284	0.511	0.250
2.0	0.660	0.333	0.711	0.407	0.584	0.326	0.514	0.264	0.488	0.232
2.5	0.661	0.309	0.705	0.379	0.554	0.288	0.476	0.227	0.454	0.199
3.0	0.682	0.297	0.713	0.362	0.536	0.260	0.455	0.201	0.435	0.176
3.5	0.706	0.290	0.737	0.355	0.538	0.242	0.440	0.182	0.425	0.160
4.0	0.735	0.288	0.768	0.355	0.548	0.230	0.429	0.167	0.420	0.147
4.5	0.773	0.290	0.802	0.357	0.563	0.222	0.421	0.154	0.423	0.138
5.0	0.822	0.298	0.837	0.363	0.582	0.215	0.418	0.145	0.428	0.130
5.5	0.870	0.308	0.874	0.372					0.433	0.124
6.0	0.917	0.320							0.438	0.119
7.0	1.009	0.349							0.448	0.110
8.0	1.100	0.385							0.462	0.104
9.0									0.469	0.098
10.0									0.474	0.093

[a] Computed from gravimetric isopiestic vapor pressure comparison data supplied by Professor O. D. Bonner, private communication.

$2\beta/2.303$ employed above in fixing the osmotic and activity coefficients at 0.1 m. Values of dB/dT of 0.00338, 0.00138, 0.00175, 0.00323, and 0.00473 were employed for the acid and the lithium, sodium, potassium, and cesium salts, respectively.

The ϕ_L values in Table IV are believed to be reliable to ± 10 cal mole^{-1} or to $\pm 2\%$, whichever is the larger. Initial and final concentrations in moles per kilogram of water are indicated as m_i and m_f, respectively, and Q is the heat absorbed in calories per mole of solute on diluting from m_i to m_f. Graphically smoothed ϕ_L values for interpolated molalities, m, and calculated relative partial molal heat contents, $\bar{L}_1$ and $\bar{L}_2$ of solvent and solute, respectively, are given in Table V. The calculations of $\bar{L}_1$ and $\bar{L}_2$ employed the smoothed ϕ_L values and the defining equations for these quantities.[18]

Heats of solution for the crystalline compounds are summarized in Table VI, where Q is the observed heat, m_f is the concentration of the final solution, and $\Delta H_\infty°$ is the "heat of solution to infinite dilution" obtained by correcting Q as in Table IV. The dissolution of the alkali metal *p*-ethylbenzenesulfonates appears to be more exothermic than for any other salts of these cations thus far measured. Interestingly, the difference in $\Delta H_\infty°$ values between the lithium and cesium *p*-ethylbenzenesulfonates was smaller than for any other of the alkali metal salts.

The concentration dependence of the ϕ_L values is shown in Figure 2, wherein the unique thermal behavior of aqueous ethylbenzenesulfonate solutions becomes apparent. An evolution of heat occurred on dilution from initial concentrations of 1 m and less with all salts. Further, a plot of ϕ_L against $\sqrt{m}$ revealed that the

(18) H. S. Harned and B. B. Owen, "The Physical Chemistry of Electrolytic Solutions," 3rd ed, Reinhold Publishing Corp., New York, N. Y., 1958, p 176.

Table IV: Experimental Heats of Dilution of the *p*-Ethylbenzenesulfonates at 25°

	m_i	$\sqrt{m_f}$	Q	ϕ_L		m_i	$\sqrt{m_f}$	Q	ϕ_L
H *p*-EBS	0.0929	0.0411	−192	209	Li *p*-EBS	0.0577	0.0413	−123	141
	0.182	0.0418	−338	355		0.0935	0.0413	−182	200
	0.451	0.0406	−583	599		0.201	0.0425	−306	324
	0.837	0.0393	−848	864		0.449	0.0400	−546	563
	1.797	0.0409	−1060	1076		0.494	0.0425	−556	574
	3.190	0.0426	−1122	1139		0.950	0.0413	−911	929
	4.300	0.0411	−1201	1218		1.016	0.0436	−943	962
	4.860	0.0399	−1255	1271		1.509	0.0480	−1092	1113
	6.340	0.0422	−1351	1368		2.003	0.0425	−1147	1165
	6.890	0.0423	−1384	1401		2.53	0.0447	−1186	1205
	7.870	0.0413	−1498	1515		3.28	0.0425	−1226	1244
	13.22	0.0427	−1867	1884		4.39	0.0436	−1271	1290
						5.24	0.0425	−1325	1343
Na *p*-EBS	0.0566	0.0413	−126	144		6.39	0.0425	−1397	1415
	0.206	0.0436	−265	284		8.00	0.0436	−1542	1561
	0.478	0.0413	−413	431		8.57	0.0443	−1594	1613
	0.967	0.0413	−554	572					
	1.457	0.0425	−573	591	K *p*-EBS	0.0528	0.0413	−82	97
	1.87	0.0413	−511	529		0.1369	0.0417	−188	205
	2.15	0.0413	−430	448		0.334	0.0426	−274	291
	2.60	0.0413	−311	329		0.553	0.0413	−382	399
	3.04	0.0425	−235	253		0.573	0.0501	−376	396
	3.31	0.0425	−181	198		0.919	0.0408	−488	505
						1.055	0.0400	−481	497
Cs *p*-EBS	0.0918	0.0409	−99	115		1.429	0.0423	−450	467
	0.192	0.0417	−153	169		1.909	0.0591	−318	340
	0.477	0.0417	−216	232		2.019	0.0426	−334	351
	0.681	0.0416	−263	279		2.628	0.0421	−190	207
	0.902	0.0405	−268	283		2.89	0.0423	−106	123
	1.46	0.0415	−197	213		3.402	0.0430	−8	25
	1.986	0.0422	−59	75		4.078	0.0648	142	−118
	2.60	0.0412	25	−9		4.26	0.0438	130	−112
	3.16	0.0423	218	−202					
	3.96	0.0426	324	−308					
	4.95	0.0423	479	−463					
	6.10	0.0419	704	−688					

heat of dilution for all but the cesium salt was greater than that given by the Debye–Hückel limiting law, $\phi_L = 472\sqrt{c}$, in the concentration range 0.1–1 *m*. No other strong electrolyte solutions show this unusual thermal behavior,[19] although solutions of tetra-*n*-propylammonium fluorides[20] and tetra-*n*-butylammonium chloride[21] and (β-hydroxyethyl)benzyldimethylammonium fluoride[22] may be examples.

Discussion

The Physical Chemistry of p-Ethylbenzenesulfonate Solutions. The *p*-ethylbenzenesulfonates exhibit a distinctive behavior in their aqueous solutions, as might be anticipated from the nature and structure of the anion. Considering the osmotic coefficients (Figure 1), it may be noted that the curve for the acid falls below that for the lithium salt at all concentrations and, at concentrations less than 1 *m*, below the curve for the sodium salt. Moreover, the measurements at 0.1 *m* show that the osmotic coefficient for the acid is also smaller than for the potassium salt. This behavior suggests that a slight association of hydrogen ion must occur.

Ion association may be significant with the cesium salt, as indicated by the relatively small osmotic coefficients it shows in dilute solutions. The magnitude of the "unlike ion interaction parameter," β of eq 3, has been suggested[12] as an approximate measure of association; for $\beta < -0.12$ kg mole^{-1} association has

(19) V. B. Parker, "Thermal Properties of Aqueous Uni-univalent Electrolytes," National Standard Reference Data Series, NSRDS-NBS 2, National Bureau of Standards, U. S. Government Printing Office, Washington, D. C., 1965, p 18.

(20) R. H. Wood, H. L. Anderson, J. D. Beck, J. R. France, W. E. deVry, and L. J. Soltzberg, *J. Phys. Chem.*, **71**, 2149 (1967).

(21) S. Lindenbaum, *ibid.*, **70**, 814 (1966).

(22) G. E. Boyd, J. W. Chase, and F. Vaslow, *ibid.*, **71**, 573 (1967).

Table V: Apparent Molal and Relative Partial Molal Heat Contents for Aqueous Solutions of the *p*-Ethylbenzenesulfonates at 25°

	H *p*-EBS			Li *p*-EBS			Na *p*-EBS			K *p*-EBS			Cs *p*-EBS		
m	ϕ_L	$-\bar{L}_1$	$10^{-2}\bar{L}_2$	ϕ_L	$-\bar{L}_1$	$10^{-2}\bar{L}_2$	ϕ_L	$\bar{L}_1$	$10^{-2}\bar{L}_2$	ϕ_L	$\bar{L}_1$	$10^{-2}\bar{L}_2$	ϕ_L	$\bar{L}_1$	$10^{-2}\bar{L}_2$
0.1	223	0.3	3.9	203	0.3	3.5	185	−0.2	2.8	154	−0.1	2.3	110	−0.15	1.8
0.2	357	0.8	5.7	321	0.8	5.3	264	−0.5	4.1	224	−0.5	3.5	165	−0.3	2.4
0.4	553	2.5	9.0	520	2.5	8.5	383	−1.3	5.6	324	−1.3	5.0	230	−0.7	3.2
0.6	706	4.4	11	705	4.9	11	462	−2.2	6.7	409	−2.3	6.2	263	−0.8	3.4
0.8	825	5.6	12	850	8.3	14	520	−2.7	7.1	460	−1.7	5.8	280	−0.5	3.1
1.0	902	5.8	12	960	8.5	14	559	−2.7	7.1	481	−1.0	5.4	280	1.7	1.8
1.5	1000	6.0	12	1113	8.7	14	576	2.9	4.7	443	5.9	2.2	202	8.1	−1.1
2.0	1050	6.0	12	1165	8.8	14	490	17	0.14	351	16	−0.78	80	17	−3.8
2.5	1083	7.9	13	1199	8.7	14	358	26	−2.1	230	30	−4.3	−28	24	−5.7
3.0	1120	12	13	1224	8.4	14	258	30	−2.9	104	37	−5.9	−135	33	−7.5
3.5	1155	16	14	1251	12	15	163	39	−4.6	10	38	−5.9	−232	42	−8.9
4.0	1191	21	15	1280	16	15	85	40	−4.7	−76	49	−7.6	−323	52	−10.5
4.5	1228	26	16	1306	20	16	20	45	−5.4				−413	65	−12
5.0	1263	33	16	1335	25	16	−40	48	−5.7				−500	80	−14
6.0	1338	48	18	1390	42	18							−660	110	−17
7.0	1410	65	19	1464	70	20									
8.0	1485	86	21	1560	90	22									
9.0	1560	110	22												
10.0	1632	130	24												
11.0	1708	160	25												
12.0	1781	180	26												
13.0	1855	210	28												

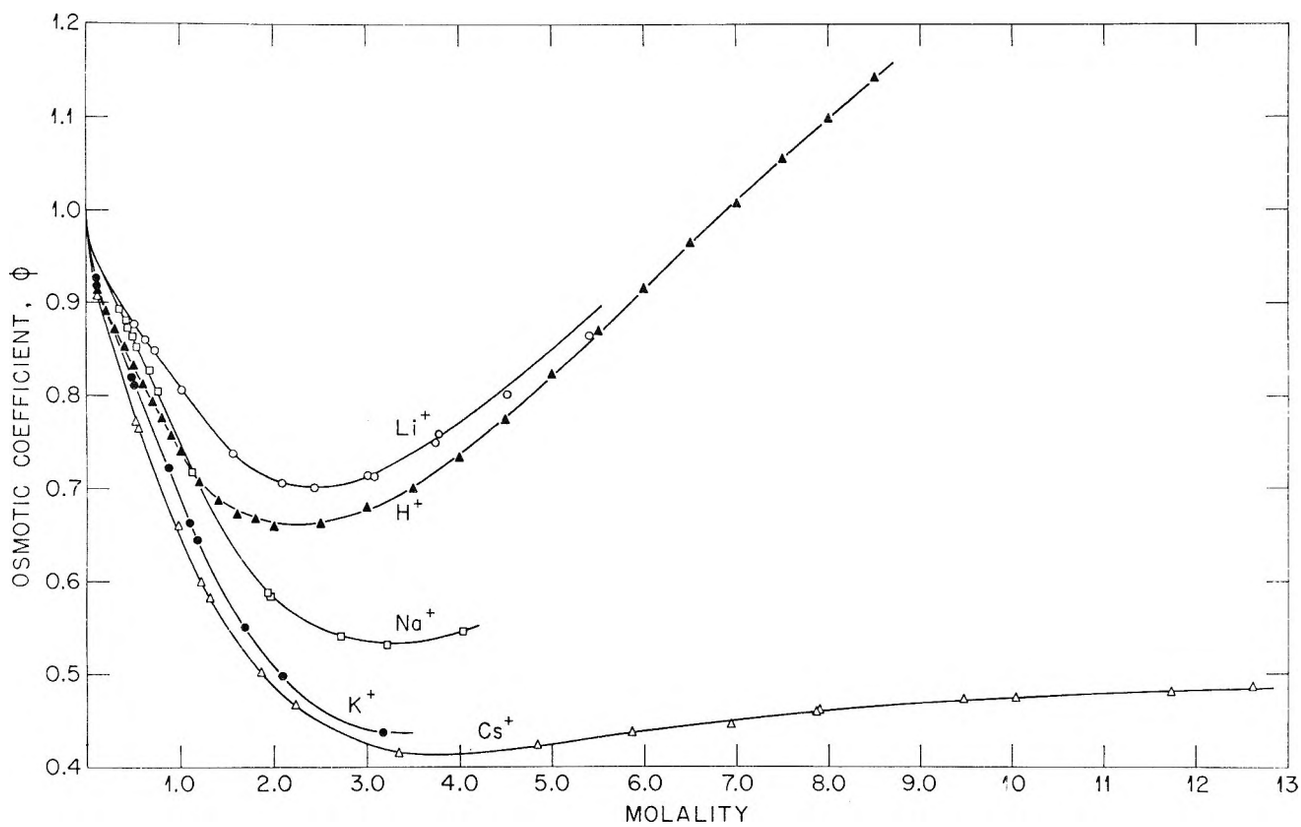

Figure 1. Concentration dependence of the molal osmotic coefficient, ϕ, for *p*-ethylbenzenesulfonic acid and its alkali metal salts in aqueous solution at 25°. (Experimental points shown are computed from isopiestic molalities given in Table I.)

Table VI: Heat of Solution (cal mole^{-1}) in Water of *p*-Ethylbenzenesulfonic Acid and Its Crystalline Alkali Salts at 25°

Compound	Q^a	$\sqrt{m_f}$	$\Delta H_\infty°$
p-EBSA·H_2O	−4260 ± 80	0.0401	−4275 ± 80
Li *p*-EBS	−1660 ± 5	0.0436	−1680 ± 5
Na *p*-EBS	1780 ± 2	0.0400	1760 ± 2
K *p*-EBS	3305 ± 5	0.0406	3290 ± 5
Cs *p*-EBS	5410 ± 10	0.0421	5395 ± 10

[a] Average of duplicate determinations.

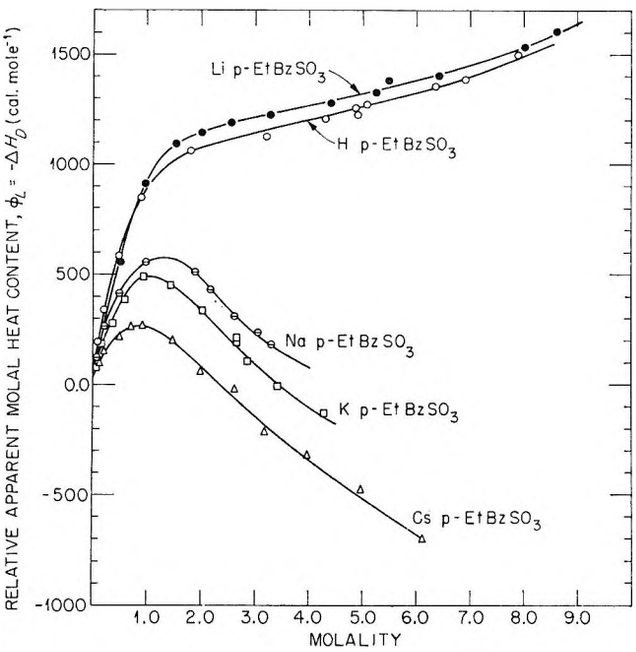

Figure 2. Concentration dependence of the relative apparent molal heat content, ϕ_L, for *p*-ethylbenzenesulfonic acid and its alkali metal salts in aqueous solution at 25°. (Experimental points are from data in Table IV.)

been said to be important, although small. Cesium *p*-ethylbenzenesulfonate shows $\beta = -0.19 \pm 0.03$.

The large, amphipolar *p*-ethylbenzenesulfonate anion undoubtedly interacts in an unusual way with the water molecules surrounding it in aqueous solutions. The hydrocarbon portions of this ion should exert a "structure-forming" action on the adjacent water molecules, while the sulfonate group may be slightly "structure-breaking," possibly analogous to nitrate or chlorate ions in aqueous solution which show negative viscosity *B* coefficients.[23] The question as to which effect predominates may be explored by comparing the relative partial molal entropies of water given by eq 4[24]

$$\bar{S}_1 - S_1° = \bar{L}_1/T - R \ln (a_1/N_1) \qquad (4)$$

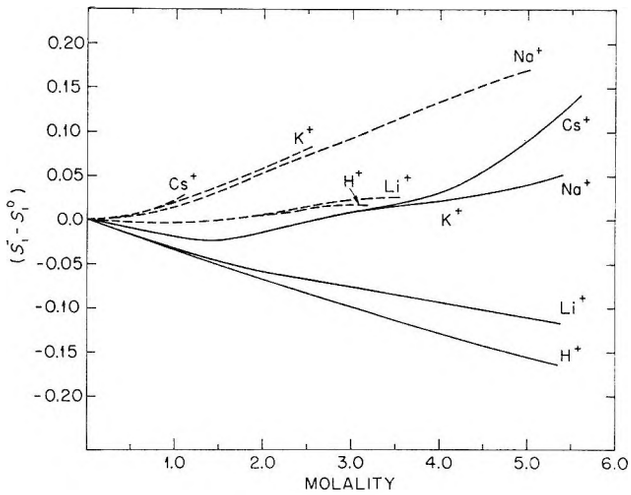

Figure 3. Concentration dependence of the solvent relative partial molal entropy $(\bar{S}_1 - S°_1)$ at 25° for aqueous nitrate (dashed lines) and *p*-ethylbenzenesulfonate (solid lines) solutions.

in solutions of the alkali metal nitrates and *p*-ethylbenzenesulfonates, respectively. In all cases with solutions with a common cation, the excess entropy of the solvent was lower (Figure 3) when the anion was *p*-ethylbenzenesulfonate rather than nitrate. This observation suggests that the former ion possesses a net water structure forming tendency. Measurements[25] of the volume change accompanying the ion-exchange reaction of *p*-ethylbenzenesulfonate anion in aqueous solution with fluoride ion on a lightly cross-linked strong-base anion exchanger are of interest and appear to support this conclusion. A value $\Delta V = -0.58$ ml equiv^{-1} was observed as expected when the former ion was extracted and replaced by fluoride ion.

The abnormal concentration dependence of ϕ_L noted above may be given a qualitative explanation if, following the hypothesis of Frank and Wen,[26] it may be assumed that cagelike structures of hydrogen-bonded water molecules surround the *p*-ethylbenzenesulfonate anion in solution. As the salt is diluted the hydrogen-bridged regions around the anion are completed because there is less overlap between the regions surrounding each anion and heat is evolved because the total amount of hydrogen bonding in the solution increases. Dilution of solutions containing structure-making cations (*viz.* H^+, Li^+) would give a relatively small

(23) R. W. Gurney, "Ionic Processes in Solution," McGraw-Hill Book Co., Inc., New York, N. Y., 1953, p 168.

(24) H. S. Frank and A. L. Robinson, *J. Chem. Phys.*, **8**, 933 (1940).

(25) G. E. Boyd and K. Bunzl, unpublished data.

(26) H. Frank and W. Y. Wen, *Discussions Faraday Soc.*, **24**, 133 (1957).

additional increase in structure, while structure breakers (*i.e.*, Cs^+) would act in an opposite sense. The order in ϕ_L is therefore $H^+ \approx Li^+ > Na^+ > K^+ > Cs^+$, as with inorganic anions. Friedman[27] has proposed that in the concentration range (*i.e.*, 1–3 *M*) where overlap is the main contribution to the value of ϕ_L that the overlap and hence ϕ_L will be approximately linear in concentration (*cf.* Figure 2).

Comparisons with Heats and Standard Free Energies of Cation Exchange. The osmotic coefficient and heat of dilution values measured in this research will now be applied to determine the adequacy of the analogy between cross-linked organic ion exchangers and concentrated aqueous electrolyte solutions. This test will be performed by computing the standard free energies, ΔG°, and enthalpies, ΔH°, for a hypothetical ion-exchange reaction between alkali metal cations, M_1 and M_2, or hydrogen ion, where X signifies the *p*-ethylbenzenesulfonate anion, when the products and reactants are in their standard states.

$$M_1X(m_i) + M_2^+(m = 0) \overset{\Delta H^\circ}{\rightleftharpoons} M_2X(m_f) + M_1^+(m = 0) \quad (A)$$

Reaction A may be regarded as the sum of two partial processes: (a) the dilution of M_1X to infinite dilution from an initial concentration of m_i

$$M_1X(m_i) \rightleftharpoons M_1^+(m = 0) + X^-(m = 0) \quad (B)$$

and (b) the concentration of M_2^+ and X^- initially at infinite dilution to a final concentration, m_f

$$M_2^+(m = 0) + X^-(m = 0) \rightleftharpoons M_2X(m_f) \quad (C)$$

The heat evolved in reaction B will be $\Delta H_D(m_i) = -\phi_L(m_i)$, that in (C) will be $-\Delta H_D = \phi_L(m_f)$, and for reaction A, $\Delta H^\circ = \phi_L(m_f) - \phi_L(m_i) = \Delta\phi_L$. To the extent that *p*-ethylbenzenesulfonic acid and its alkali metal salts are "model" compounds for the corresponding cation forms of cross-linked polystyrenesulfonate type cation exchangers, ΔH° may be compared with the standard heat of cation exchange, ΔH_{ex}°

$$\Delta H^\circ = \phi_L(m_f) - \phi_L(m_i) = \Delta\phi_L = \Delta H_{ex}^\circ \quad (5)$$

Similarly, the standard free energy of cation exchange, ΔG_{ex}°, for the cross-linked exchanger, corrected for the decrease in the free energy of its molecular network, $\int \pi dV_e$, accompanying the standard-state reaction, may be compared with the difference in the apparent molal free energy of dilution, $\Delta(\Delta G_D)$, of the "model" compound solutions

$$\Delta G_D(m_i) - \Delta G_D(m_f) = \Delta(\Delta G_D) = \Delta G_{ex}^\circ - \int_{V_i}^{V_f} \pi dV_e \quad (6)$$

The ΔG_D values required by eq 6 and the values of the integral $\int_{V_i}^{V_f} \pi dV_e$ were computed following the method previously described.[17]

Values of $\Delta(\Delta G_D)$ and $\Delta\phi_L$, computed with the data in Tables II and IV, respectively, for values of m_i and m_f corresponding to the water contents of the pure cationic forms of the cross-linked ion exchangers in their respective standard states, are compared in Table VII with the values of $\Delta G_{ex}^\circ - \int \pi dV_e$ and ΔH_{ex}° derived from equilibrium distribution and heat measurements,[28] respectively, on the same cation exchangers. Comparisons unfortunately could not be made with exchangers of greater than nominal 8% DVB cross linking because of the limited solubility of sodium *p*-ethylbenzenesulfonate. However, the agreement between $\Delta\phi_L$ and ΔH_{ex}° for the 2, 4, and 8% DVB exchangers appears satisfactory excepting with the potassium–sodium ion-exchange reaction where $\Delta\phi_L$ was sig-

Table VII: Comparison of Standard Free Energies, ΔG_{ex}°, and Enthalpies, ΔH_{ex}°, of Cation Exchange with Free Energy and Heat of Dilution Differences for Aqueous Solutions of the Salts of *p*-Ethylbenzenesulfonate (kcal mole^{-1})[a]

Cross linking	m_i	m_f	$-\Delta H_{ex}^\circ$	$-\Delta\phi_L$	$-\Delta G_{ex}^\circ - \int \pi dV_e$	$-\Delta(\Delta G_D)$
			Na^+/H^+ Exchange			
2	1.06	1.95	0.46	0.42	0.05	−0.56
4	2.4	2.9	0.86	0.86	0.14	−0.18
8	4.6	5.4	1.18	1.30	0.23	0.00
			Na^+/Li^+			
2	1.6	1.95	0.65	0.61	0.05	0.06
4	(2.8)	2.9	1.08	0.95	0.20	0.14
8	5.1	5.4	1.46	1.41	0.32	0.31
			K^+/Na^+			
2	1.95	2.0	0.29	0.16	0.17	0.14
4	2.9	3.2	0.41	0.20	0.18	0.15
8	5.4	6.6	0.55	0.34	0.19	0.17
			Cs^+/Na^+			
2	1.95	2.9	0.56	0.61	0.21	0.07
4	2.9	(4.3)	0.62	0.65	0.24	0.14
8	5.4	7.0	0.77	0.76	0.26	0.275

[a] Values for m_i, m_f, $-\Delta H_{ex}^\circ$, and $-\Delta G_{ex}^\circ$ from ref 28.

(27) Y. C. Wu and H. L. Friedman, *J. Phys. Chem.*, **70**, 166 (1966).

(28) G. E. Boyd, F. Vaslow, and S. Lindenbaum, *ibid.*, **68**, 590 (1964).

nificantly smaller than ΔH_{ex}°. Because of the unknown contribution of the enthalpy of swelling, $\Delta H^{\circ}_{network}$, to ΔH_{ex}° a quantitative agreement cannot be expected. The concordance between $\Delta\phi_L$ and ΔH_{ex}° obtained with the alkali metal *p*-ethylbenzenesulfonates, however, is demonstrably much better than that obtained with the chlorides. The correspondence between the corrected standard free energy of exchange, $\Delta G_{ex}^{\circ} - \int \pi dV_e$, and the dilution free-energy difference, $\Delta(\Delta G_D)$, is satisfactory except with the ion-exchange reaction involving hydrogen ion for reasons not immediately evident. The majority of the thermodynamic data (Table VII) nevertheless is believed to be consistent with the hypothesis that the gel solutions of cross-linked polystyrenesulfonate cation exchangers are analogous to concentrated aqueous electrolyte mixtures. Interestingly, this analogy appears to be valid at lower cross linkages in cation than in anion[17] exchangers. Presumably the alkali metal "counterions" are distributed in a much more diffuse double layer surrounding the negatively charged cation-exchange polymer chains and the counterion atmospheres about the chains overlap sufficiently for the "homogeneous gel solution" model to become a good approximation.

Theoretical Treatment of Hydrogen-Ion Effects on Hydrolytic Enzyme Systems Involving Two Enzyme–Substrate Complexes[1,2]

by James A. Stewart and Hung S. Lee[3]

Department of Chemistry, University of North Dakota, Grand Forks, North Dakota *(Received April 13, 1967)*

An exact mathematical solution is given for a general mechanism, which is applicable to hydrolytic enzyme systems. This three-step mechanism takes into consideration that all or any of the ionizable species at the active site may be functional even though they are protonated. General equations are derived for both transient and steady-state kinetics. The transient-phase equations are solved under the experimental conditions of excess enzyme and excess substrate, but the steady state, which is not attained with excess enzyme, is treated only for excess substrate. Complete general expressions are given for the pH dependence of the specific rate constants and the so-called Michaelis constant. These expressions are complex, but they become simple when the pH of the reaction medium is either above or below the optimum for catalysis. To illustrate the wide applicability of the proposed mechanism, specific examples are given for chymotrypsin and trypsin systems. A new system of nomenclature is proposed for the ionization constants, Ka_{000}, of functional groups and specific rate constants, k_{000}, for the catalytic stages. The system uses three-digit subscripts. The first digit represents the stage of catalysis, the second digit gives the number of ionizable hydrogens on the functional groups of the site, and the last digit refers to the number of ionizable hydrogens on the substrate.

According to early Michaelis–Menten theory,[4] an enzyme and its substrate form a complex which decomposes directly to products. For a typical hydrolytic system, this decomposition results in three products and insinuates that the products of hydrolysis are released simultaneously from the enzyme surface, as shown by eq 1.

$$E + S \rightleftharpoons ES \longrightarrow E + P_1 + P_2 \qquad (1)$$

In this equation, E = enzyme, S = substrate, ES = enzyme–substrate complex, and P_1 and P_2 = products.

In order to explain the experimental results for the hydrolysis of *p*-nitrophenyl acetate with chymotrypsin,[5] it was postulated that the enzyme–substrate complex decomposed in two sequential stages rather than simultaneously.

$$E + S \rightleftharpoons ES \longrightarrow ES' \longrightarrow E + P_2 \qquad (2)$$
$$\searrow P_1$$

Since only two products of reaction result at each stage, this mechanism is kinetically more acceptable than the classical mechanism. In several publications,[6-8] this mechanism has been shown to be applicable to a wide variety of enzyme reactions, especially where the substrate is hydrolyzed or converted into two products.

The prime purpose for studying the effects of hydrogen-ion concentration on enzyme reactions is to identify the functional groups at the enzymic site, which are

(1) This investigation was supported in part by U. S. Public Health Service Research Grant RG-09038-OI from the Division of General Medical Sciences.

(2) Presented in part at the 145th National Meeting of the American Chemical Society, New York, N. Y., Sept 1963.

(3) National Institutes of Health Predoctoral Fellow.

(4) L. Michaelis and M. L. Menten, *Biochem. Z.*, 49, 333 (1913).

(5) B. S. Hartley and B. A. Kilby, *Biochem. J.*, 56, 288 (1954).

(6) M. L. Bender, F. J. Kézdy, and C. R. Gunter, *J. Am. Chem. Soc.*, 86, 3714 (1964).

(7) J. A. Stewart and L. Ouellet, *Can. J. Chem.*, 37, 751 (1959).

(8) J. R. Whitaker and M. L. Bender, *J. Am. Chem. Soc.*, 87, 2728 (1965).

responsible for either binding or catalytic activity. The criterion used is that the hydrogen-ion inhibition constants evaluated from a study of the variation of hydrogen-ion concentration are the acid–base equilibrium constants of ionizable groups required for catalysis as well as binding of substrate. Since the range of such constants for carboxyl, sulfhydryl, imidazoyl, amino, and other free groups in proteins is known, it is possible to postulate the type of group involved. However, when this approach is used to establish the intricate details of an enzyme mechanism, it becomes necessary to relate these ionization constants to an elementary reaction rather than the over-all chemical rate process. This can only be done by isolating and studying the influence of hydrogen-ion concentration on the specific rate constants for each stage of catalysis, including the binding of substrate to the enzyme surface. To accomplish this end, it is essential to have a thorough treatment of the proposed mechanism in terms of hydrogen-ion equilibria.

The significance of hydrogen-ion effects on the steady-state constants as derived from classical enzyme kinetics has been discussed in detail by Laidler[9] and Dixon and Webb.[10] They outline several methods that may be used to evaluate the experimental results in terms of the rate constant for the rate-controlled stage and the Michaelis constant. Unfortunately, when the release of products is a sequential or two-stage process, as given by eq 2, the Michaelis constant obtained by conventional steady-state methods is a complex entity,[11] and it is not possible to interpret the significance of its pH dependence unless supplementary data are available from transient-phase kinetics.

By applying the condition of steady state to the first complex formed in eq 2, Gutfruend[11] derived the rate equations for the steady-state and transient-phase kinetics of a system involving two enzyme–substrate complexes. However, without applying a steady-state condition to the first complex, Ouellet and Stewart[12] derived the steady-state and transient-phase relationships in detail.

Although the influence of hydrogen ion has been applied to the rate equations for mechanism 2 in specific cases, no thorough treatment has been given. Work in this laboratory using the enzymes chymotrypsin and trypsin with a variety of substrates suggests that each enzyme–substrate system is a special case of the general mechanism illustrated in Figure 1. This mechanism takes into consideration the possibility that the protonated as well as the unprotonated forms of functional groups may be active. The difficulty of treating such a complex system has been pointed out.[13,14] It is the purpose of this paper: (a) to consider that any

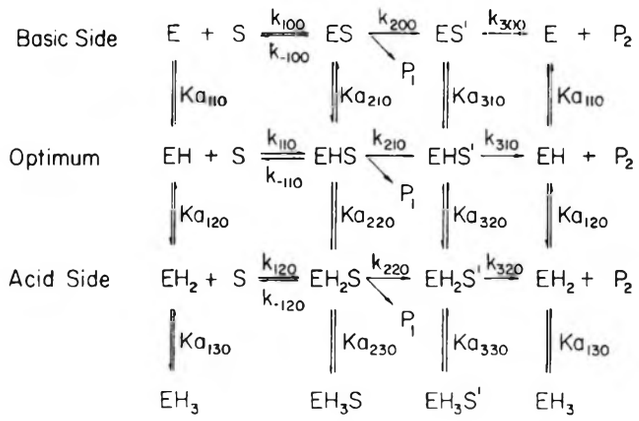

Figure 1. The general mechanism of enzyme-catalyzed hydrolysis. E, EH, EH_2, and EH_3 are the different protonated forms of the enzymic site; ES, EHS, EH_2S, and EH_3S are the different protonated forms of the enzyme–substrate complex; ES′, EHS′, EH_2S', and EH_3S' are the different protonated forms of the acylated or alkoxylated, etc., enzyme intermediate; and P_1 and P_2 are the products of hydrolysis. The specific rate constants, k_{000}, are designated by the use of three-digit subscripts; the first digit represents the stage of catalysis, the second digit the number of ionizable protons on the groups concerned with the active site, and the third digit is reserved for the case of an ionizable substrate. The acid–base equilibrium constants, Ka_{000}, for the functional groups likewise are represented by three-digit subscripts; the first digit indicates the stage of catalysis, the second digit the number of ionizable protons on the site in its associated form, and the third digit is reserved for the possibility of an ionizable substrate. The optimum kinetic pathway is designated arbitrarily by the k_{f10} rate constants.

of the protonated forms in Figure 1 can yield products, (b) to derive the steady-state equations for this mechanism, (c) to give the exact mathematical treatment of the transient-phase kinetics without any special assumptions such as steady state or equilibrium between the reactants and the first complex, and (d) through the use of examples, to show how the theory can be applied to the experimental results of any hydrolytic enzyme system.

Theoretical Section

The general mechanism in Figure 1 is applicable to those hydrolytic enzyme systems that involve two intermediates. It excludes those cases where an

(9) K. J. Laidler, "The Chemical Kinetics of Enzyme Action," Oxford University Press, New York, N. Y., 1958, p 117.

(10) M. Dixon and E. C. Webb, "Enzymes," Academic Press Inc., New York, N. Y., 1958, p 120.

(11) H. Gutfreund, *Discussions Faraday Soc.*, **20**, 167 (1955).

(12) L. Ouellet and J. A. Stewart, *Can. J. Chem.*, **37**, 737 (1959).

(13) K. J. Laidler, "The Chemical Kinetics of Enzyme Action," Oxford University Press, New York, N. Y., 1958, p 125.

(14) F. J. Kézdy and M. L. Bender, *Biochemistry*, **1**, 1097 (1962).

ionizable group belonging to the substrate interacts with the active site or where a coenzyme is required. Although it is quite likely that no systems behave according to the entire scheme, the complete scheme is required to analyze the experimental results and thereby assign the ionization constants of plausible functional groups to the elementary processes to which they correspond.

The entire scheme may be formulated by a single set of equations, but these are not too convenient to apply to experiment. Rather, it is far simpler first to consider the conditions under which the experimental results are to be obtained and arrive at solutions on this basis. Experimental conditions can be placed in four categories: (a) acidic solution, excess substrate, (b) acidic solution, excess enzyme, (c) basic solution, excess substrate, and (d) basic solution, excess enzyme. The steady-state equations are applicable only to the condition of excess substrate, whereas the equations for the transient-phase kinetics can be employed for either condition, excess substrate or excess enzyme.

By letting the concentration of each reacting species and resultant product be represented by the symbols defined in Figure 1, the following differential equations result

$$[\dot{E}S] = k_{100}[E\cdot S] + ka_{210}[EHS] - (k_{-100} + k_{200} + ka_{-210}a_H)[ES] \quad (3)$$

$$[\dot{E}HS] = k_{110}[EH\cdot S] + ka_{220}[EH_2S] + ka_{-210}[ES]a_H - (k_{-110} + k_{210} + ka_{210} + ka_{-220}a_H)[EHS] \quad (4)$$

$$[\dot{E}H_2S] = k_{120}[EH_2\cdot S] + ka_{-220}[EHS]a_H + ka_{230}[EH_3S] - (k_{-120} + k_{220} + ka_{220} + ka_{-230}a_H)[EH_2S] \quad (5)$$

$$[\dot{E}S'] = k_{200}[ES] + ka_{310}[EHS'] - (k_{300} + ka_{-300}a_H)[ES'] \quad (6)$$

$$[\dot{E}HS'] = k_{210}[EHS] + ka_{320}[EH_2S] + ka_{-310}[ES']a_H - (k_{310} + ka_{310} + k_{-320}a_H)[EHS'] \quad (7)$$

$$[\dot{E}H_2S'] = k_{220}[EH_2S] + ka_{-320}[EHS']a_H + ka_{330}[EH_3S'] - (k_{320} + ka_{320} + ka_{-330}a_H)[EH_2S'] \quad (8)$$

$$[\dot{P}_1] = k_{200}[ES] + k_{210}[EHS] + k_{220}[EH_2S] \quad (9)$$

$$[\dot{P}_2] = k_{300}[ES'] + k_{310}[EHS'] + k_{320}[EH_2S'] \quad (10)$$

The above equations may be simplified by defining the apparent rate constants or the over-all rate constants for the three possible ionization forms of the enzyme and each intermediate as

$$k'_i = (k_{i10} + k_{i20}a_H/Ka_{i20} + k_{i00}Ka_{i10}/a_H)/h_i \quad (11)$$

where $i = 1, 2, 3$, and

$$k'_{-1} = (k_{-110} + k_{-120}a_H/Ka_{220} + k_{-100}Ka_{210}/a_H)/h_2 \quad (12)$$

The h_i term is given by

$$h_i = 1 + a_H/Ka_{i20} + Ka_{i10}/a_H + a_H^2/Ka_{i20}Ka_{i30} \quad (13)$$

where $i = 1, 2$, or 3, and a_H is the hydrogen-ion activity. In the above relationships the ionization constants are

$$Ka_{110} = a_H[E]/[EH] = ka_{110}/ka_{-110} \quad (14)$$

$$Ka_{210} = a_H[ES]/[EHS] = ka_{210}/ka_{-210} \quad (15)$$

$$Ka_{310} = a_H[ES']/[EHS'] = ka_{310}/ka_{-310} \quad (16)$$

$$Ka_{120} = a_H[EH]/[EH_2] = ka_{120}/ka_{-120} \quad (17)$$

$$Ka_{220} = a_H[EHS]/[EH_2S] = ka_{220}/ka_{-220} \quad (18)$$

$$Ka_{320} = a_H[EHS']/[EH_2S'] = ka_{320}/ka_{-320} \quad (19)$$

$$Ka_{130} = a_H[EH_2]/[EH_3] = ka_{130}/ka_{-130} \quad (20)$$

$$Ka_{230} = a_H[EH_2S]/[EH_3S] = ka_{230}/ka_{-230} \quad (21)$$

$$Ka_{330} = a_H[EH_2S']/[EH_3S'] = ka_{330}/ka_{-330} \quad (22)$$

When the total concentration of the enzyme, $[E]_T$, and its intermediates, $[ES]_T$ and $[ES']_T$, are defined by

$$[E]_T = [E] + [EH] + [EH_2] + [EH_3] = [EH] \times h_1 \quad (23)$$

$$[ES]_T = [ES] + [EHS] + [EH_2S] + [EH_3S] = [EHS] \times h_2 \quad (24)$$

and

$$[ES']_T = [ES'] + [EHS'] + [EH_2S'] + [EH_3S'] = [EHS'] \times h_3 \quad (25)$$

the general mechanism in Figure 1 may be condensed to a simple scheme

$$E_T + S \underset{k'_{-1}}{\overset{k'_1}{\rightleftharpoons}} ES_T \xrightarrow{k'_2} ES'_T \xrightarrow{k'_3} E_T + P_2 \quad (26)$$

$$ES_T \xrightarrow{k'_2} P_1$$

This condensed scheme allows the eight differential equations, (3) through (10), to be written as

$$[\dot{E}HS] = k'_1[E]_T\cdot[S]/h_2 - ([S] + K'_m)[EHS] - (k'_1[S]h_3/h_2)[EHS'] \quad (27)$$

$$[\dot{E}HS'] = (k'_2h_2/h_3)[EHS] - k'_3[EHS'] \quad (28)$$

$$[\dot{P}_1] = k'_2[EHS] \times h_2 \quad (29)$$

$$[\dot{P}_2] = k'_3[EHS'] \times h_3 \quad (30)$$

The apparent Michaelis constant K'_m, has the same form as the true K_m and is

$$K'_m = (k'_{-1} + k'_2)/k'_1 \quad (31)$$

where k'_1, k'_2, and k'_3 refer to scheme 26 and are defined by eq 11 and 12.

The steady-state and transient-phase kinetics of scheme 26 has been published in detail for the condition of excess substrate,[12] except that the rate constants were true rather than apparent. By analogy of the two schemes, it is possible to write many of the solutions for the general mechanism in Figure 1 without solving the differential equations. This has been verified by Lee,[15] who found that the solutions had forms that were symmetrical to those of Ouellet and Stewart.[12]

Experiments in Acid Media. Since in acid solution Ka_{t10} is always smaller than the concentration of hydrogen ion, the expressions (11) and (12) for the apparent rate constants and (13) for the h_t term can be simplified. The Ka_{t10}/a_H term becomes negligible, and if $k_{t10} > k_{t00}$

$$k'_1 = (k_{t00} + k_{t20}a_H/Ka_{t20})/h_t \quad (11a)$$

$$k'_{-1} = (k_{-110} + k_{-120}a_H/Ka_{220})/h_2 \quad (12a)$$

$$h_t = 1 + a_H/Ka_{t20} + a_H^2/Ka_{t20}Ka_{t30} \quad (13a)$$

and where $i = 1$, 2, or 3.

Experiments in Basic Media. Since k_{t20} is in most instances probably less than k_{t10} and the hydrogen-ion concentration in basic solution is less than Ka_{t20} or Ka_{t30}, eq 11, 12, and 13 become

$$k'_1 = (k_{t10} + k_{t00}Ka_{t10}/a_H)/h_t \quad (11b)$$

$$k'_{-1} = (k_{-110} + k_{-100}Ka_{210}/a_H)/h_2 \quad (12b)$$

$$h_t = 1 + Ka_{t10}/a_H \quad (13b)$$

and where $i = 1$, 2, or 3.

Steady-State Kinetics. By using methods similar to Ouellet and Stewart,[12] an equation for the steady-state kinetics of the general mechanism can be written in terms of products, from the differential equations (27) through (30). Although the equation is applicable to the results obtained by conventional enzyme kinetic techniques and has the same form as the original Michaelis–Menten law,[4] the constants take on new meaning.

$$\text{rate} = [\dot{P}_1] = [\dot{P}_2] = k'_2k'_M[S]_0[E]_0/([S]_0 + k'_MK'_m) \quad (32)$$

$$k'_M = k'_3/(k'_2 + k'_3) \quad (33)$$

where $[S]_0$ and $[E]_0$ refer to the initial concentrations of substance and enzyme, respectively. The apparent rate constants k'_2 and k'_3 are given by eq 11, and K'_m is defined by eq 31.

When steady-state studies are employed, two special cases of eq 32 usually result.

Case I: $k'_2 > k'_3$. The rate-controlled step, when $k'_2 > k'_3$, is the release of the second product, P_2. Under this circumstance

$$\text{rate} = [\dot{P}_1] = [\dot{P}_2] = k'_3[S]_0[E]_0/([S]_0 + k'_3K'_m/k'_2) \quad (32a)$$

and should $k'_2 > k'_{-1}$, as well as k'_3, then

$$\text{rate} = [\dot{P}_1] = [\dot{P}_2] = k'_3[S]_0[E]_0/([S]_0 + k'_3/k'_1) \quad (32b)$$

If an enzyme system belongs to this latter case, it is possible to evaluate the apparent rate constant for enzyme–substrate complex formation, k'_1, by the steady-state method.

In the instance that $k'_{-1} > k'_2 > k'_3$, the apparent Michaelis constant, K'_m, is the equilibrium constant between the reactants and the first intermediate. The rate under these conditions is given by

$$\text{rate} = [\dot{P}_1] = [\dot{P}_2] = k'_3[S]_0[E]_0/([S]_0 + k'_3K'_{eq}/k'_2) \quad (32c)$$

Here, k'_3 can be readily isolated, but the quantity $k'_3 \cdot K'_{eq}/k'_2$, which is usually referred to as K_m in the literature, is not the equilibrium constant, K'_{eq}, between the reactants and their complex.

Case II: $k'_3 > k'_2$. If k'_2 is the rate constant for the rate-controlled step, the second complex has fleeting existence and the steady-state kinetics for the Hartley–Kilby type of mechanism reverts to a two-stage process. The rate equation is

$$\text{rate} = [\dot{P}_1] = [\dot{P}_2] = k'_2[S]_0[E]_0/([S]_0 + K'_m) \quad (32d)$$

As before, if $k'_2 > k'_{-1}$, when $k'_3 > k'_2$

$$\text{rate} = [\dot{P}_1] = [\dot{P}_2] = k'_2[S]_0[E]_0/([S]_0 + k'_2/k'_1) \quad (32e)$$

or should $k'_{-1} > k'_2$, the Michaelis constant K'_m is the equilibrium constant, and

$$\text{rate} = [\dot{P}_1] = [\dot{P}_2] = k'_2[S]_0[E]_0/([S]_0 + K'_{eq}) \quad (32f)$$

where $K'_{eq} = k'_{-1}/k'_1$.

For experiments performed in media on the acid side of the pH optimum, the specific rate constants are given by eq 11a, 12a, and 13a; on the base side, eq 11b, 12b, and 13b are used.

Transient-Phase Kinetics. Excess Substrate. For the experimental conditions where the concentration of sub-

(15) H. S. Lee, Doctoral Dissertation, University of North Dakota, 1963.

strate exceeds that of the enzyme, Ouellet and Stewart[12] have shown that the concentration of enzyme–substrate complex can be expressed in the form of a linear second-order differential equation with constant coefficients. If the same method is applied to eq 27 and 28, the following expression results

$$[\ddot{EHS}] + [k'_1([S]_0 + K'_m) + k'_3][\dot{EHS}] + [k'_1(k'_2 + k'_3)([S]_0 + k'_M K'_m)][EHS] = k'_1 k'_3 [S]_0 [E]_0/h_2 \quad (34)$$

The solution of eq 34 has the form

$$EHS = r/q + (m \exp ft) + (n \exp gt) \quad (35)$$

where

$$f = -p/2 + [(p/2)^2 - q]^{1/2} \quad (36)$$

$$g = -p/2 - [(p/2)^2 - q]^{1/2} \quad (37)$$

$$p = k'_1([S]_0 + K'_m) + k'_3 \quad (38)$$

$$r = k'_1 k'_3 [S]_0 [E]_0/h_2 \quad (39)$$

$$q = k'_1(k'_2 + k'_3)([S]_0 + k'_M K'_m) \quad (40)$$

$$m = -(r/q)(k'_3 g + q)/k'_3(g - f) \quad (41)$$

$$n = (r/q)(k'_3 f + q)/k'_3(g - f) \quad (42)$$

An equation for the rate of release of the first product

$$[\dot{P}_1] = k'_2 h_2 [r/q + (m \exp ft) + (n \exp gt)] \quad (43)$$

is obtained by substituting eq 35 into eq 29, which integrates to

$$[P_1] = k'_2 h_2 [rt/q + (m/f)(\exp ft - 1) + (n/g)(\exp gt - 1)] \quad (44)$$

A differential equation also may be set up in terms of the second complex, [EHS'].

$$[\ddot{EHS'}] + [k'_1([S]_0 + K'_m) + k'_3][\dot{EHS'}] + [k'_1(k'_2 + k'_3)([S]_0 + k'_M K'_m)][EHS'] = k'_1 k'_2 [S]_0 [E]_0/h_3 \quad (45)$$

This equation may be written as

$$[\ddot{EHS'}] + p[\dot{EHS'}] + q[EHS'] = r' \quad (45a)$$

where p and q are defined by eq 38 and 40, respectively, but r' is

$$r' = k'_1 k'_2 [S]_0 [E]_0/h_3 \quad (46)$$

Except for r', the solution of eq 45a is the same as that for eq 34, so that the concentration of second complex can be expressed as

$$[EHS'] = r'q + m' \exp ft + n' \exp gt \quad (47)$$

where f and g are given by eq 36 and 37, but m' and n' are

$$m' = -r'g/q(q - f) \quad (48)$$

$$n' = r'f/q(q - f) \quad (49)$$

Substitution of eq 47 into eq 30 leads to the rate of change of P_2, the second product with time

$$[\dot{P}_2] = k'_3 h_3 (r'/q + m' \exp ft + n' \exp gt) \quad (50)$$

Since f and g are negative, when t is large, eq 43 and 50 become identical.

$$[\dot{P}_1] = [\dot{P}_2] = k'_2 h_2 r/q = k'_3 h_3 r'/q$$

and is equivalent to steady-state eq 32.

Equation 50 can be integrated to give a relationship for the concentration of second product at any time t

$$[P_2] = k'_3 h_3 [r't/q + (m'/f)(\exp ft - 1) + (n'/g)(\exp gt - 1)] \quad (51)$$

Experiments in Acid and Base Media. As for steady-state kinetics, the apparent rate constants for transient-phase experiments in solutions, which are more acidic than the pH optimum of the system, are given by eq 11a and 12a, and the constants h_2 and h_3 are defined as h_t, by the general eq 13a. If a medium with a pH on the basic side of the pH optimum is employed, then eq 11b, 12b and 13b are applicable.

The General Rate Equation. The qualitative behavior of eq 44 and its various terms is illustrated in Figure 2. When t is appreciable, steady-state conditions are attained, and the exponential terms vanish. Under these conditions, eq 44 reduces to

$$[P_1] = k'_2 h_2 (rt/g - m/f - n/g) \quad (44a)$$

This equation describes the steady state, and according to Ouellet and Stewart[12] its extrapolation to the product and time axis yields two useful quantities π_1 and τ_1. The evaluation of these quantities has been discussed.[12]

When the release of the second product is studied, eq 51, which gives the concentration of P_2 at any time t, applies. The qualitative behavior of P_2 is the same as P_1, but the constants take on new meaning. For steady-state conditions, t is large, and eq 51 can be simplified to

$$[P_2] = k'_3 h_3 (r't/q - m'/f - n'/g) \quad (51a)$$

In a manner similar to π_1 and τ_1, the quantities π_2 and τ_2 can be found.

By setting $t = 0$, and $[P_2] = \pi_2$, and substituting the appropriate quantities into eq 51a, the value of π_2 is obtained

$$\pi_2 = [-k'_1k'_2k'_M[S]_0[E]_0([S]_0 + K'_m) + k'_2k'_3k'_M[S]_0[E]_0]/k'_1(k'_2 + k'_3)([S]_0 + k'_MK'_m)^2 \quad (52)$$

which is the intercept on the product, $[P_2]$, axis when (51a) is extrapolated to $t = 0$.

If $k'_2 > k'_3$, the value of π_2 reduces to, *i.e.*, when k'_1 is large

$$\pi_2 = -k'_3[E]_0/k'_2 \quad (52a)$$

provided $[S]_0$ is in excess of K'_m. Likewise, if $k'_3 > k'_2$, π_2 becomes

$$\pi_2 = -k'_2E_0/k'_3 \quad (52b)$$

In each case, the value of π_2 is only a small fraction of the initial enzyme concentration.

The intercept on the time axis can be found by letting $t = \tau_2$, when $[P_2 = 0]$. Equation 51a then becomes

$$\tau_2 = [k'_1([S]_0 + K'_m) + k'_3]/k'_1(k'_2 + k'_3) \times ([S]_0 + k'_MK'_m) \quad (53)$$

when $k'_2 > k'_3$ and $k'_1[S]_0 > k'_3$, this equation condenses to

$$\tau_2 = 1/k'_2$$

provided $[S]_0$ is adjusted to be larger than K'_m. Similarly, when $k'_3 > k'_2$, and $k'_1([S]_0 + K'_m) > k'_3$, $\tau_2 = 1/k'_3$. In both instances τ_2 gives useful quantities.

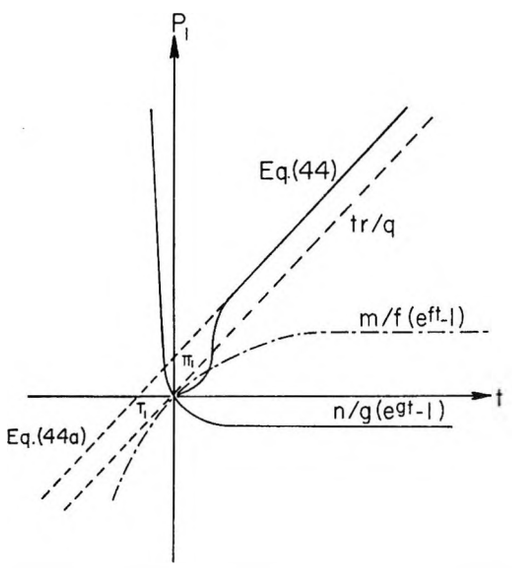

Figure 2. A hypothetical plot of the general rate equation (44). The individual behavior of the three main terms tr/q, $(m/f)(e^{ft} - 1)$, and $(n/g)(e^{gt} - 1)$ is shown. Equation 44a, the steady-state form of (44) is also illustrated. The quantities π_1 and τ_1, the intercepts of (44a) on the product and time axes, respectively, have been defined previously.[12]

Derivation of Applicable Forms of the Rate Equation. The constants f and g, which are the roots of the auxiliary eq of (34) or (45a), are given by (36) and (37). Both constants contain a $[(p/2)^2 - q]^{1/2}$ term. This term can be expanded into a series, which converges so rapidly that all but the first two terms become negligible.

$$[(p/2)^2 - q]^{1/2} = p/2 - q/p \quad (54)$$

Substitution of this result into (36) and (37) leads to

$$f = -q/p \quad (36a)$$

$$g = -p + q/p \quad (37a)$$

Since f and g must be real, the value of q/p never exceeds the value of $p/4$, and is probably always less than $p/4$. Therefore, eq 37a can be reduced to

$$g = -p \quad (37b)$$

This means that

$$q = fg \quad (40a)$$

which is also the case when (36) and (37) are considered without simplification.

When p (38) and q (40) are substituted into eq 36a and 37b, it is found that

$$f = -k'_1(k'_2 + k'_3)([S]_0 + k'_MK'_M)/[k'_1([S]_0 + K'_m) + k'_3] \quad (36b)$$

$$g = -[k'_1([S]_0 + K'_m) + k'_3] \quad (37c)$$

If k'_3 is rate controlling, *i.e.*, $k'_3 < k'_2$ and k'_1, and $[S]_0 \approx K'_m$

$$f = -k'_2[S]_0/([S]_0 + K'_m) \quad (36c)$$

$$g = -k'_1([S]_0 + K'_m) \quad (37d)$$

However, if k'_2 is rate controlling

$$f = -k'_1([S]_0 + K'_m) \quad (36d)$$

or

$$f = -k'_3 \quad (36e)$$

and g is given by (37d), or

$$g = -k'_3 \quad (37e)$$

depending upon the magnitude of k'_3 with respect to $k'_1([S]_0 + K'_m)$.

For the case where k'_3 is rate controlling, eq 44 can be shown to be equivalent to

$$[P_1] = k'_3[E]_0t + [E]_0(1 - \exp ft) \quad (44b)$$

Gutfreund[11] applied the Guggenheim[16] technique to a similar equation and found that

$$\ln([P_{11}] - 2[P_{12}] + [P_{13}]) = \text{constant} + ft_1 \quad (55)$$

where $[P_{11}]$, $[P_{12}]$, and $[P_{13}]$ are any readings proportional to the concentrations of product P_1 at times t_1, $t_1 + \Delta$, and $t_1 + 2\Delta$, respectively. The constant interval, Δ, should be at least twice the half-life of the reaction.

An appropriate plot of eq 55 allows one to evaluate f, and therefore, k'_2 and K'_m from a plot of $1/f$ *vs.* $1/[S]_0$, according to

$$-1/f = 1/k'_2 + K'_m/k'_2[S]_0 \quad (36f)$$

In terms of $[P_2]$, similar consideration which led to eq 44b gives

$$[P_2] = k'_3[S]_0[E]_0t/([S]_0 + k'_M K'_m) + [E]_0k'_M[\exp(ft - 1)] \quad (51b)$$

that is, provided k'_3 is rate controlling and k'_1 is very large compared to k'_2. The result shows that eq 51b is symmetrical with eq 44b and a Guggenheim[16] treatment evaluates f. Therefore, it does not appear to make any difference whether $[P_1]$ or $[P_2]$ is followed experimentally; the end result is the same.

Excess Enzyme. Under the condition of excess enzyme when the release of the first product, P_1, is considered, steady-state kinetics are nonexistent. This can be proven mathematically, but in essence the steady state cannot be attained; since the catalyst is in excess it can never become saturated with substrate.

The concentration of substrate at any time t is given by

$$[S] = [S]_0 - [EHS] - h_2 - [P_1] \quad (56)$$

From scheme 26 it is seen that

$$[\dot{E}S]_T = k'_1([E]_0 - [ES]_T - [ES']_T) \times ([S]_0 - [ES]_T - [P_1]) - [ES]_T(k'_2 + k'_1) \quad (57)$$

Since $[E]_0 > [ES]_T$ or $[ES']_T$, and $[ES]_T$ is given by eq 24, it follows that

$$[\dot{E}HS] = k'_1[E]_0[S]_0(1 - [P_1]/[S]_0)/h_2 - k'_1([E]_0 + K'_m)[EHS] \quad (57a)$$

Using eq 29 and differentiating eq 57a, we obtain

$$[\dot{E}\dot{H}S] + k'_1([E]_0 + K'_m)[\dot{E}HS] + k'_1k'_2[E]_0[EHS] = 0 \quad (58)$$

The general solution of this equation is

$$[EHS] = a \exp bt + c \exp dt \quad (59)$$

where b and d are always negative, and given by

$$b = -J/2 + (J^2 - 4L)^{1/2}/2 \quad (60)$$

$$d = -J/2 - (J^2 - 4L)^{1/2}/2 \quad (61)$$

here

$$J = k'_1([E]_0 + K'_m) \quad (62)$$

and

$$L = k'_1k'_2[E]_0 \quad (63)$$

The general eq 59 can be expressed in terms of product (P_1) by substituting this eq into eq 29, and integrating the resultant differential equation

$$[P_1] = k'_2h_2a[(\exp bt - 1)/b - (\exp dt - 1)/d] \quad (64)$$

where

$$a = -c = [S]_0[E]_0/h_2([E]_0 + K'_m) \quad (65)$$

If a solution is attempted in terms of the second product, P_2, a third-order differential equation results. Since the auxiliary equation is quadratic, a solution cannot be obtained readily.

Applicable Forms of the Rate Equation. By applying arguments similar to the derivation of (36a) and (37b)

$$b = -1/J \quad (60a)$$

and

$$d = -J \quad (61a)$$

Upon substitution of (62) and (63) into these equations, we find

$$b = -k'_2[E]_0/([E]_0 + K'_m) \quad (60b)$$

and

$$d = -k'_1([E]_0 + K'_m) \quad (61b)$$

If the appropriate values of a, b, and d are substituted into eq 64, the general rate equation becomes

$$[P_1] = [S]_0[1 - \exp -([S]_0[E]_0t/([E]_0 + K'_m)] - k'_2[S]_0[E]_0/[k'_2[E]_0 - k'_1([E]_0 + K'_m)^2] \times \exp -[k'_1([E]_0 + K'_m) - k'_2[E]_0/([E]_0 + K'_m)]t \quad (64a)$$

This complex equation simplifies to

$$[P_1] = [S]_0\,[1 - \exp -(k'_2[E]_0t/([E]_0 + K'_m)] \quad (64b)$$

or

$$[P_1] = [S]_0\,(1 - \exp bt) \quad (64c)$$

(16) E. A. Guggenheim, *Phil. Mag.*, 2, 538 (1926).

because, as for eq 44, the second exponential term approaches zero very rapidly.

The value of b, and hence k'_2 and K'_m, can be determined experimentally by the Guggenheim method.[16] The result is

$$\ln ([P_{12}] - [P_{11}]) = \text{constant} + bt_1 \qquad (65a)$$

An appropriate plot of $\ln ([P_{12}] - [P_{11}])$ *vs.* t_1 produces a straight line, the slope of which is b. This means that k'_2 and K'_m can be found by varying $[E]_0$ and plotting $-1/b$ against $1/[E]_0$ according to (60b)

$$-1/b = 1/k'_2 + K'_m/k'_2[E]_0 \qquad (60c)$$

Experiments in Acid and Base Media. When experiments are performed in media on the acid side of the pH optimum, the rate constants k'_1, k'_{-1}, and k'_2 are defined by eq 11a, 12a, and 13a. However, if the work is carried out on the basic side, eq 11b, 12b, and 13b apply.

Discussion

There are two aspects to the study of the influence of hydrogen-ion concentration on enzyme systems: (a) the calculation of true specific rate constants and (b) the determination of acid–base equilibrium constants of the functional groups at the enzymic site. The theoretical relationships derived can be used to determine apparent specific rate constants, k'_t, for each stage of the catalyzed hydrolysis. However, except under special circumstances, it is not possible to measure k'_1 for the first stage.[12] Once the apparent rate constants are known at several hydrogen-ion concentrations, it is possible to calculate the true rate constants, k_{i00}, k_{i10}, and k_{i20}, from eq 11 and 12. Since these equations are cumbersome to handle, some simplifications are necessary before the true rate constants can be found conveniently. As discussed earlier, eq 11 and 12 simplify to eq 11a and 12a when the pH of the solution is less than the pH optimum for enzyme activity, and to eq 11b and 12b when the pH is greater than the optimum. Using these equations, it is possible to obtain the intrinsic ionization constants, Ka_{i10}, Ka_{i20}, and Ka_{i30}, for ionizable groups which function as part of the enzymic site. From the magnitude of these constants, not only can the ionizable groups be identified, but their mechanistic role in each stage of catalysis can be established. This latter information is extremely significant, since it is necessary in order to characterize the involvement of the enzyme's functional groups during each stage of hydrolysis. Because a thorough understanding of the Ka values for a system is of such utmost importance, methods which can be used for their determination and assignment will be discussed in detail using eq 11 and 12. It should be realized that regardless of the hydrogen-ion concentration, all ionization forms of the enzymic site are present, at least in microscopic quantities. Therefore, although one form predominates in concentration, there is always the possibility that other forms may contribute to catalysis as well.

pH Profiles. A simple method for examining equations of types (11) and (12) is to plot the logarithm of the apparent rate constant, k'_1, *vs.* pH.[17] From the shape of the curve, it is possible to recognize what portion of the general scheme must be retained to explain the experimental results. Once this much is known, the appropriate equation can be written from (11) and (12). To illustrate this procedure, a discussion of pH profiles and their significance will be presented. However, it should be emphasized that to realize complete success, the specific rate constants for every phase of catalysis should be isolated and identified.

For each stage of the mechanism shown in Figure 1, 18 pH profiles are required to depict the different pH dependencies that a rate constant can have. The simplest case is complete pH independence, where a plot of log k'_1 *vs.* pH has zero slope over a wide pH range. Of the remaining possibilities, ten are bell-shaped and

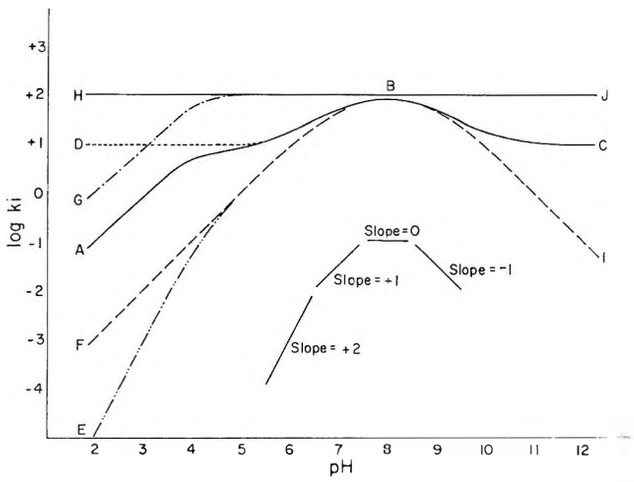

Figure 3. A plot of log k'_i *vs.* pH where k'_i is the apparent rate constant for a single stage of catalysis; 18 different pH profiles are illustrated. The arbitrary quantities used were as follows: $k_{i10} = 100$, $k_{i00} = k_{i20} = 10$, $Ka_{i10} = 10^{-9}$, $Ka_{i20} = 10^{-7}$, and $Ka_{i30} = 10^{-4}$. Each possible profile is designated by three alphabetical letters. All profiles are listed in Table II along with the corresponding mechanism number (see Table I) and mathematical expression.

(17) K. J. Laidler, "The Kinetics of Enzyme Action," Oxford University Press, New York, N. Y., 1958, p 140.

Table I: The 18 Possible Mechanisms for Stage i of the Scheme Shown in Figure 1

I.
$$\begin{array}{ccc} (E + S)_i & \xrightarrow{k_{i00}} & \\ {\scriptstyle Ka_{i10}}\downarrow\uparrow & & \\ (EH + S)_i & \xrightarrow{k_{i10}} & \\ {\scriptstyle Ka_{i20}}\uparrow\downarrow & & \\ (EH_2 + S)_i & \xrightarrow{k_{i20}} & \\ {\scriptstyle Ka_{i30}}\uparrow\downarrow & & \\ (EH_3 + S)_i & & \end{array}$$

II.
$$\begin{array}{ccc} (E + S)_i & \xrightarrow{k_{i00}} & \\ {\scriptstyle Ka_{i10}}\downarrow\uparrow & & \\ (EH + S)_i & \xrightarrow{k_{i10}} & \\ {\scriptstyle Ka_{i20}}\downarrow\uparrow & & \\ (EH_2 + S)_i & \xrightarrow{k_{i20}} & \end{array}$$

III.
$$\begin{array}{ccc} (E + S)_i & \xrightarrow{k_{i00}} & \\ {\scriptstyle Ka_{i10}}\downarrow\uparrow & & \\ (EH + S)_i & \xrightarrow{k_{i10}} & \\ {\scriptstyle Ka_{i20}}\downarrow\uparrow & & \\ (EH_2 + S)_i & & \\ {\scriptstyle Ka_{i30}}\downarrow\uparrow & & \\ (EH_3 + S)_i & & \end{array}$$

IV.
$$\begin{array}{ccc} (E + S)_i & \xrightarrow{k_{i00}} & \\ {\scriptstyle Ka_{i10}}\downarrow\uparrow & & \\ (EH + S)_i & \xrightarrow{k_{i10}} & \\ {\scriptstyle Ka_{i20}}\downarrow\uparrow & & \\ (EH_2 + S)_i & & \end{array}$$

V.
$$\begin{array}{ccc} (E + S)_i & \xrightarrow{k_{i00}} & \\ {\scriptstyle Ka_{i10}}\uparrow\downarrow & & \\ (EH + S)_i & \xrightarrow{k_{i10}} & \\ {\scriptstyle Ka_{i20}}\uparrow\downarrow & & \\ (EH_{(3)} + S)_i & & \end{array}$$

VI.
$$\begin{array}{ccc} (E + S)_i & \xrightarrow{k_{i00}} & \\ {\scriptstyle Ka_{i10}}\uparrow\downarrow & & \\ (EH + S)_i & \xrightarrow{k_{i10}} & \end{array}$$

VII.
$$\begin{array}{ccc} (E + S)_i & & \\ {\scriptstyle Ka_{i10}}\downarrow\uparrow & & \\ (EH + S)_i & \xrightarrow{k_{i10}} & \\ {\scriptstyle Ka_{i20}}\uparrow\downarrow & & \\ (EH_2 + S)_i & \xrightarrow{k_{i20}} & \\ {\scriptstyle Ka_{i30}}\uparrow\downarrow & & \\ (EH_3 + S)_i & & \end{array}$$

VIII.
$$\begin{array}{ccc} (E + S)_i & & \\ {\scriptstyle Ka_{i10}}\downarrow\uparrow & & \\ (EH + S)_i & \xrightarrow{k_{i10}} & \\ {\scriptstyle Ka_{i20}}\uparrow\downarrow & & \\ (EH_2 + S) & \xrightarrow{k_{i20}} & \end{array}$$

IX.
$$\begin{array}{ccc} (E + S)_i & & \\ {\scriptstyle Ka_{i10}}\downarrow\uparrow & & \\ (EH + S)_i & \xrightarrow{k_{i10}} & \\ {\scriptstyle Ka_{i20}}\uparrow\downarrow & & \\ (EH_2 + S)_i & & \\ {\scriptstyle Ka_{i30}}\uparrow\downarrow & & \\ (EH_3 + S)_i & & \end{array}$$

X.
$$\begin{array}{ccc} (E + S)_i & & \\ {\scriptstyle Ka_{i10}}\downarrow\uparrow & & \\ (EH + S)_i & \xrightarrow{k_{i10}} & \\ {\scriptstyle Ka_{i20}}\uparrow\downarrow & & \\ (EH_2 + S)_i & & \end{array}$$

XI.
$$\begin{array}{ccc} (E + S)_i & & \\ {\scriptstyle Ka_{i10}}\downarrow\uparrow & & \\ (EH + S)_i & \xrightarrow{k_{i10}} & \\ {\scriptstyle Ka_{i30}}\uparrow\downarrow & & \\ (EH_{(2)} + S)_i & & \end{array}$$

XII.
$$\begin{array}{ccc} (E + S)_i & & \\ {\scriptstyle Ka_{i10}}\downarrow\uparrow & & \\ (EH + S)_i & \xrightarrow{k_{i10}} & \end{array}$$

XIII.
$$\begin{array}{ccc} (EH + S)_i & \xrightarrow{k_{i10}} & \\ {\scriptstyle Ka_{i20}}\uparrow\downarrow & & \\ (EH_2 + S)_i & \xrightarrow{k_{i20}} & \\ {\scriptstyle Ka_{i30}}\uparrow\downarrow & & \\ (EH_3 + S)_i & & \end{array}$$

XIV.
$$\begin{array}{ccc} (EH + S)_i & \xrightarrow{k_{i10}} & \\ {\scriptstyle Ka_{i20}}\uparrow\downarrow & & \\ (EH_2 + S)_i & \xrightarrow{k_{i20}} & \end{array}$$

XV.
$$\begin{array}{ccc} (EH + S)_i & \xrightarrow{k_{i10}} & \\ {\scriptstyle Ka_{i20}}\uparrow\downarrow & & \\ (EH_2 + S)_i & & \\ {\scriptstyle Ka_{i30}}\uparrow\downarrow & & \\ (EH_3 + S)_i & & \end{array}$$

XVI.
$$\begin{array}{ccc} (EH + S)_i & \xrightarrow{k_{i10}} & \\ {\scriptstyle Ka_{i20}}\uparrow\downarrow & & \\ (EH_2 + S)_i & & \end{array}$$

XVII.
$$\begin{array}{ccc} (EH + S)_i & \xrightarrow{k_{i10}} & \\ {\scriptstyle Ka_{i30}}\uparrow\downarrow & & \\ (EH_{(3)} + S)_i & & \end{array}$$

XVIII. $(EH + S)_i \xrightarrow{k_{i10}}$

seven are sigmoid. The 18 profiles are shown in Figure 3, and the related mechanisms are tabulated in Table I. These mechanisms are listed by number in Table II, along with the corresponding mathematical expressions derived from eq 11 and alphabetical letters which refer to the profiles in Figure 3. For the reverse stages of catalysis, eq 12 must be used.

Once a pH profile for a specific rate constant of an individual stage of catalysis is obtained experimentally, it is possible from its shape to tell which of the 18 possible mechanisms are operative. Should the whole general scheme apply, at first, it appears that this situation is difficult to handle because equations 11 and 12 are quite cumbersome. On the other hand, the experimental pH profile might be simple and the evaluation of the constants presents no problem.

Even if the profile indicates that the mechanism is complex, it is still possible to determine the various rate constants and acid–base equilibrium constants given by eq 11 and 12. These equations simplify when experiments are performed either on the acidic or basic side of the pH optimum for catalysis as well as near this optimum.

Experiments near the pH Optimum of Catalysis.

Table II: pH Profiles (Figure 3) and Theoretical Expressions (Eq 11 and 12) for the 18 Mechanisms Given in Table I

Mechanism no.	pH profile	Theoretical expression for k'_i, eq 11 and 12
I	ABC	$\frac{k_{i10} + k_{i20}a_H/Ka_{i20} + k_{i00}Ka_{i10}/a_H}{1 + a_H/Ka_{i20} + Ka_{i10}/a_H + a^2_H/Ka_{i20}Ka_{i30}}$
II	DBC	$\frac{k_{i10} + k_{i20}a_H/Ka_{i20} + k_{i00}Ka_{i10}/a_H}{1 + a_H/Ka_{i20} + Ka_{i10}/a_H}$
III	EBC	$\frac{k_{i10} + k_{i00}Ka_{i10}/a_H}{1 + a_H/Ka_{i20} + Ka_{i10}/a_H + a_H^2/Ka_{i20}Ka_{i30}}$
IV	FBC	$\frac{k_{i10} + k_{i00}Ka_{i10}/a_H}{1 + a_H/Ka_{i20} + Ka_{i10}/a_H}$
V	GBC	$\frac{k_{i10} + k_{i00}Ka_{i10}/a_H}{1 + a_H/Ka_{i30} + Ka_{i10}/a_H}$
VI	HBC	$\frac{k_{i10} + k_{i00}Ka_{i10}/a_H}{1 + Ka_{i10}/a_H}$
VII	ABI	$\frac{k_{i10} + k_{i20}a_H/Ka_{i20}}{1 + a_H/Ka_{i20} + Ka_{i10}/a_H + a_H^2/Ka_{i20}Ka_{i30}}$
VIII	DBI	$\frac{k_{i10} + k_{i20}a_H/Ka_{i20}}{1 + a_H/Ka_{i20} + Ka_{i10}/a_H}$
IX	EBI	$\frac{k_{i10}}{1 + a_H/Ka_{i20} + Ka_{i10}/a_H + a_H^2/Ka_{i20}Ka_{i30}}$
X	FBI	$\frac{k_{i10}}{1 + a_H/Ka_{i20} + Ka_{i10}/a_H}$
XI	GBI	$\frac{k_{i10}}{1 + a_H/Ka_{i30} + Ka_{i10}/a_H}$
XII	HBI	$\frac{k_{i10}}{1 + Ka_{i10}/a_H}$
XIII	ABJ	$\frac{k_{i10} + k_{i20}a_H/Ka_{i20}}{1 + a_H/Ka_{i20} + a_H^2/Ka_{i20}Ka_{i30}}$
XIV	DBJ	$\frac{k_{i10} + k_{i20}a_H/Ka_{i20}}{1 + a_H/Ka_{i20}}$
XV	EBJ	$\frac{k_{i10}}{1 + a_H/Ka_{i20} + a_H^2/Ka_{i20}Ka_{i30}}$
XVI	FBJ	$\frac{k_{i10}}{1 + a_H/Ka_{i20}}$
XVII	GBJ	$\frac{k_{i10}}{1 + a_H/Ka_{i30}}$
XVIII	HBJ	k_{i10}

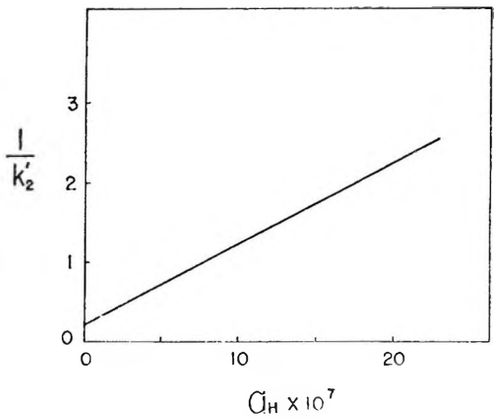

Figure 4a. A typical plot of eq 11c, which can be used to evaluate experimental results on the acid side near the pH optimum for catalysis. The plot shown is for the acetylation of chymotrypsin.[15] The intercept is $1/k_{210}$, and the slope is $1/Ka_{220}k_{210}$. The results are given in Table III. The shape of the pH profile is DBJ (Figure 3) and the mechanism is XIV (Table I) for the second catalytic stage.

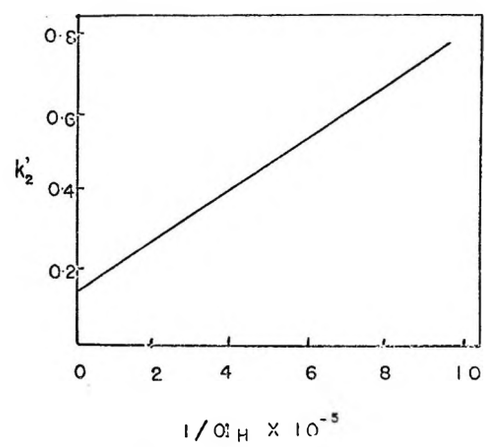

Figure 4b. A plot of the results on the extreme acid side of the pH optimum, see eq 11d. The plot shown is for the chymotrypsin-catalyzed hydrolysis of 2,4-dinitrophenyl acetate[15] and evaluates k_{220} and Ka_{220}. The results are given in Table III. The pH profile for this system is DBJ (Figure 3) and the mechanism is XIV (Table I) for the second stage of catalysis, *viz.*, acetylation.

When a series of rate measurements is performed at pH values near the pH optimum, then eq 11, 12, and 13 can be simplified to

$$k'_1 = k_{t10}/hi \qquad (11c)$$

$$k'_{-1} = k_{-110}/h_2 \qquad (12c)$$

and

$$h_t = 1 + a_H/Ka_{t20} + Ka_{t10}/a_H \qquad (13c)$$

Since the k_{t10} constants represent the major kinetic pathway, these constants are much larger than k_{t00} or k_{t20}. Therefore, the determination of k_{t10}, Ka_{t20}, and Ka_{t10} can be performed as shown in Figures 4a and 5a, numerous examples of which appear in the literature.[9]

Experiments in Acidic Media Compared to pH Optimum. In order to find the rate constants k_{t00} and k_{t20}, which are small compared to k_{t10}, it is necessary to use eq 11a, 11b, 12a, and 12b. In each of these instances, rate studies must be run at pH values which are either considerably greater or less than the pH optimum. Since experiments can be restricted to either

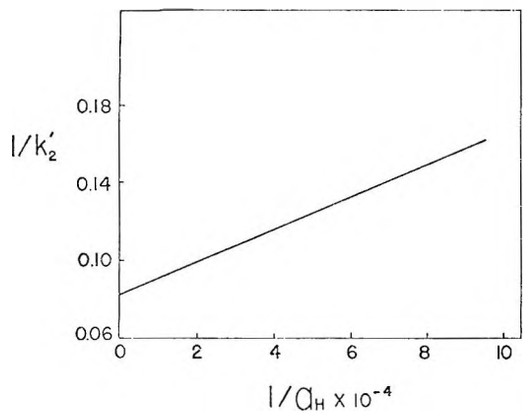

Figure 5a. A plot of $1/k_i$ *vs.* $1/a_H$, used to obtain the constants shown in eq 11g. The experimental results used must be on the basic side near the pH optimum. A typical example is shown using the trypsin–lysine methyl ester system.[18] The constants evaluated correspond to k_{212} and Ka_{212} in Figure 1. Note the third digit subscript indicates that the ionizable substrate is in the complete associated form. Because of an ionizable substrate, the mechanism is more complex than those in Table I. However, the pH profile is bell-shaped and at least near the optimum the behavior is represented by mechanism X (Table I) and pH profile FBI (Figure 3).

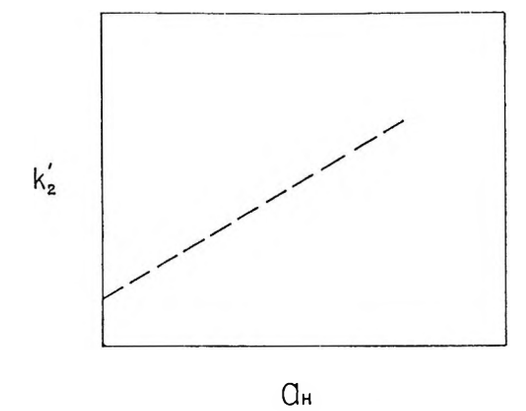

Figure 5b. The dashed line is for a hypothetical plot of eq 11h. This plot evaluates k_{i00} and Ka_{i10} by utilizing experimental results on the alkali side of the pH optimum for catalysis, where the profile has the shape BC (Figure 3).

the acid or base side, these will be considered individually.

When a series of rate studies is made in media which are quite acid compared to the optimum, eq 11a and 12a apply. If $Ka_{i30} > a_H$ or is nonexistent

$$k'_i = k_{i20} + k_{i10}Ka_{i20}/a_H \qquad (11d)$$

since $a_H/Ka_{i20} > 1$. This means that a plot of k'_i *vs.* $1/a_H$ will produce a straight line whose slope is $k_{i10} \cdot Ka_{i20}$ and intercept is k_{i20}. Similarly, if k'_{-1} can be determined, under the same experimental conditions eq 12b becomes

$$k'_{-1} = k_{-120} + k_{-110}Ka_{220}/a_H \qquad (12d)$$

and k_{-120} can be evaluated.

Examples of $1/k'_i$ *vs.* a_H plots as shown in Figure 4a for the inverse of eq 11c appear in the literature.[7] However, there is no evidence for k'_i *vs.* $1/a_H$ plots of eq 11d, as illustrated by Figure 4b.

Using the excess enzyme method, *i.e.*, eq 65, Lee[15] studied the acylation kinetics of chymotrypsin with 2,4-dinitrophenyl acetate. The pH dependency of k'_2 did not fit a simple titration curve. This was explained on the basis that a protonated form of the normal active site could lead to catalysis. The results for k'_2 were plotted according to Figures 4a and 4b. Values for k_{210}, k_{220}, and Ka_{220} were obtained. These are listed in Table III. As expected, $k_{210} > k_{220}$. Also, it should be noted that the Ka_{220} values, as determined from the two different plots (Figures 4a and 4b), agree within experimental error.

Table III: Acylation Constants for 2,4-Dinitrophenyl Acetate with Chymotrypsin[15]

Rate constant	k_{210}, sec^{-1} 2.18	k_{220}, sec^{-1} 0.13
pKa_{220}	6.76	6.63

Since Ka_{i30} is always greater than Ka_{i20}, at low pH values eq 11a and 12a reduce to

$$k'_i = (k_{i20} + k_{i10}Ka_{i20}/a_H)/(1 + a_H/Ka_{i30}) \qquad (11e)$$

$$k'_{-1} = (k_{-120} + k_{-110}Ka_{220}/a_H)/(1 + a_H/Ka_{230}) \qquad (12e)$$

Under normal circumstances these equations can be simplified further. Since $a_H \gg Ka_{i20}$ at low pH, the term involving these constants can be neglected, and therefore

$$k'_i = k_{i20}/(1 + a_H/Ka_{i30}) \qquad (11f)$$

$$k'_{-1} = k_{-120}/(1 + a_H/Ka_{230}) \qquad (12f)$$

the inverse forms of these equations are linear, and the constants can be evaluated from a $1/k'_i$ *vs.* a_H plot, as shown in Figure 4a.

Experiments in Basic Media Compared to pH Optimum. In order to evaluate k_{i10} and Ka_{i10}, it is necessary to use eq 11b, 12b and 13b. Near the pH optimum, $k_{i10} > k_{i00}Ka_{i10}/a_H$, and these equations reduce to

$$k'_i = k_{i10}/(1 + Ka_{i10}/a_H) \qquad (11g)$$

$$k'_{-1} = k_{-110}/(1 + Ka_{210}/a_H) \qquad (12g)$$

These indicate that a plot of $1/k'_t$ *vs.* $1/a_H$ will be linear and both k_{t10} and Ka_{t10} can be evaluated, *i.e.*, Figure 5a. A plot of this type was used by Parnell[18] to determine the k_{212} and Ka_{212} constants for the lysine methyl ester–trypsin system.

In basic media, where $Ka_{t10} \gg a_H$, eq 11b and 12b take on still other forms.

$$k'_t = k_{t00} + k_{t10}a_H/Ka_{t10} \quad (11h)$$

$$k'_{-1} = k_{-100} + k_{-110}a_H/Ka_{210} \quad (12h)$$

Both these equations are linear and a plot of k'_t *vs.* a_H, as shown in Figure 5b, will evaluate the constants k_{t00}, k_{t10}, and Ka_{t10}.

Influence of Hydrogen-Ion Concentration on K'_m, k'_M. The interpretation of the Michaelis constant is rather complex. This is due to the fact that any of the specific rate constants involved in eq 31 may or may not be hydrogen-ion dependent. To complicate matters further, the Michaelis constant for the three-step mechanism in Figure 1 is given by

$$K'_m k'_M = k'_3(k'_{-1} + k'_2)/k'_1(k'_2 + k'_3) \quad (66)$$

where K'_m is designated by eq 31 and k'_M by eq 33. Since according to eq 11, 12, and 13 the apparent rate constants, k'_t, are complex entities, the interpretation of the effect of hydrogen-ion concentration on K_m (classical) cannot be made without further information as to the magnitude and behavior of each specific rate constant. With this in mind, special cases will be presented to aid in the interpretation of the pH dependency of K_m (classical).

Case IA: $k'_3 > k'_2$. Under this special condition, $k'_M = 1$, and eq 66 reduces to eq 31, which refers to K'_m for a two-step mechanism. Table IV shows that there are eight possibilities for this case. However, if the behavior of k'_2 is known, then the pH dependence of K'_m can be narrowed down to four different cases.

Case IB: $k'_3 > k'_2 < k'_{-1}$. Under these conditions, $K'_m k'_M = K'_{eq}$, and as listed in Table IV there are four possible conditions of behavior.

Case IC: $k'_3 > k'_2 > k'_{-1}$. When this condition applies, there are four kinds of pH dependencies as shown in Table IV. However, since the influence of hydrogen ion on both k'_2 and K'_m can be determined, it is possible to select the condition which applies.

Case IIA: $k'_3 < k'_2$. For this condition, the final stage of catalysis is the rate-controlled step and eq 66 simplifies to

$$K'_m k'_M = k'_3(k'_{-1} + k'_2)/k'_1 k'_2 \quad (66a)$$

Table III shows the 16 different conditions that can exist, but these reduce to eight if the pH dependency of k'_3 is known. If the behavior of k'_2 is known as well, then the different possibilities are limited to four. In some instances K'_m might be equal to K'_{eq}, and it then would be possible to examine the results in a manner similar to case IB, Table IV.

Case IIB: $k'_3 < k'_2 > k'_{-1}$. Since $K'_m k'_M$ reduces to k'_3/k'_1, only four different types of pH behavior can exist. The pH dependency of k'_3 and $K'_m k'_M$ can be determined experimentally, which means that the pH

Table IV: Influence of Hydrogen-Ion Concentration on $K'_m k'_M$

Case	Condition	pH dependent	pH independent[a]
IA	1	k'_{-1}, k'_2, k'_1	
$k'_3 > k'_2$	2	k'_{-1}, k'_2	k'_1
	3	k'_{-1}, k'_1	k'_2
	4	k'_1, k'_2	k'_{-1}
	5	k'_1	k'_{-1}, k'_2
	6	k'_2	k'_{-1}, k'_1
	7	k'_{-1}	k'_2, k'_1
	8		k'_{-1}, k'_2, k'_1
IB	1	k'_{-1}, k'_1	
$k'_3 > k'_2 < k'_{-1}$	2	k'_1	k'_{-1}
	3	k'_{-1}	k'_1
	4		k'_{-1}, k'_1
IC	1	$k'_2 k'_1$	
$k'_3 > k'_2 > k'_{-1}$	2	k'_2	k'_1
	3	k'_1	k'_2
	4		$k'_2 k'_1$
IIA[b]	1	k'_1, k'_{-1}, k'_2, k'_3	
$k'_3 < k'_2$	2		k'_1, k'_{-1}, k'_2, k'_3
	3	k'_1, k'_{-1}, k'_2	k'_3
	4	k'_1, k'_{-1}, k'_3	k'_2
	5	k'_1, k'_2, k'_3	k'_{-1}
	6	k'_{-1}, k'_2, k'_3	k'_1
	7	k'_1	k'_{-1}, k'_2, k'_3
	8	k'_{-1}	k'_1, k'_2, k'_3
	9	k'_2	k'_1, k'_{-1}, k'_3
	10	k'_3	k'_1, k'_{-1}, k'_2
	11	k'_1, k'_{-1}	k'_2, k'_3
	12	k'_1, k'_2	k'_{-1}, k'_3
	13	k'_1, k'_3	k'_{-1}, k'_2
	14	k'_{-1}, k'_2	k'_1, k'_3
	15	k'_{-1}, k'_3	k'_1, k'_2
	16	k'_2, k'_3	k'_1, k'_{-1}
IIB	1	k'_3, k'_1	
$k'_3 < k'_2 > k'_{-1}$	2	k'_3	k'_1
	3	k'_1	k'_3
	4		$k'_3 k'_1$

[a] Note when k'_i's are pH independent, $k'_i = k_{i10}$. [b] There is also the possibility that $k_{-1} > k_2$, so that $K'_m = K'_{eq}$. K'_{eq} can be determined from eq 66, if k'_2 and k'_3 are known; *e.g.*, $k'_M K'_m = (k'_3/k'_2)K'_{eq}$.

(18) D. R. Parnell, Senior Research Thesis, University of North Dakota, 1964.

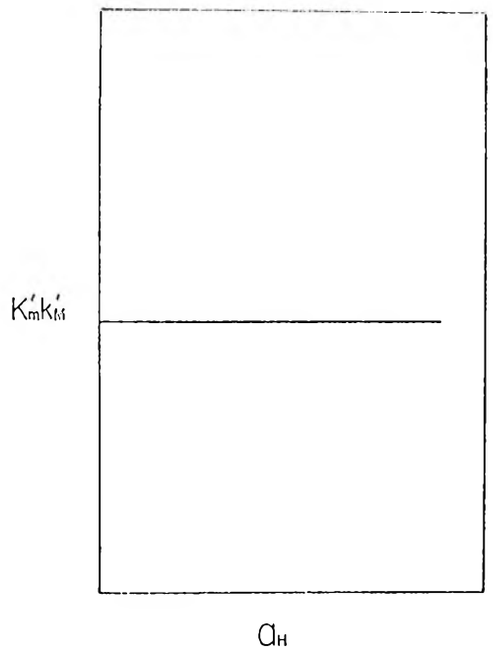

Figure 6a. A plot of the Michaelis constant *vs.* a_H, which shows pH independency when rate constants in the numerator and denominator exhibit similar pH behavior. Typical example is the chymotrypsin-catalyzed hydrolysis of methyl hydrocinnamate.[19]

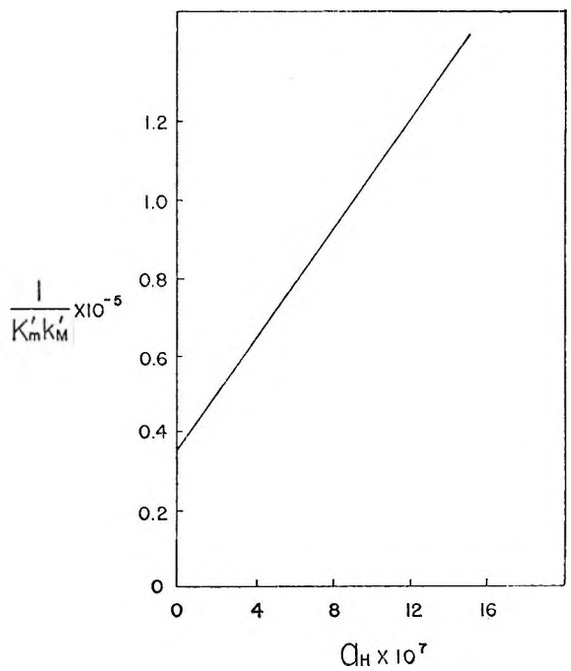

Figure 6b. A linear plot of the inverse of the Michaelis constant *vs.* a_H. The plot shown is for the *p*-nitrophenyl monochloroacetate–chymotrypsin system.[15] These steady-state results suggest that the numerator of eq 66 is pH dependent.

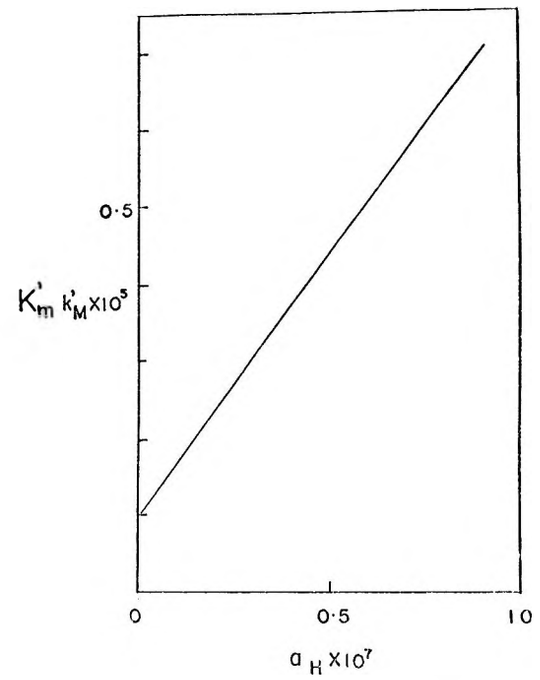

Figure 6c. A plot of the Michaelis constant *vs.* a_H, which shows positive slope. The plot given is for the deacylation kinetics of 2,4-dinitrophenyl acetate with chymotrypsin.[15] The result suggests that the denominator of eq 66 is pH dependent.

dependence of K_m (classical) can be narrowed down to a single condition.

Some Experimental Evidence. The need for a thorough treatment of the influence of hydrogen-ion concentration on enzyme-catalyzed hydrolysis is exemplified by the experimental results reported for the behavior of chymotrypsin.

If both the numerator and denominator of eq 66 have the same type of pH dependence, K_m (classical) will appear to be pH independent. This has been reported for the methyl hydrocinnamate–chymotrypsin system.[19] A plot of this type is illustrated in Figure 6a. On the other hand, when a plot of $1/K_m$ (classical) *vs.* a_H is linear, this insinuates that the numerator of eq 66 is pH dependent as shown in Figure 6b, which is typical of acetyl-L-tyrosine ethyl ester behavior with chymotrypsin.[15]

Finally, only the denominator of eq 66 might show pH dependence. Such is the case for the 2,4-dinitrophenylacetate–chymotrypsin system.[15] Both $K'_mk'_M$ and K'_m as determined by steady-state and transient-phase kinetics, respectively, exhibited the kind of behavior shown in Figure 6c.

(19) K. J. Laidler and M. L. Barnard, *Trans. Faraday Soc.*, **52**, 497 (1956).

In conclusion, it should be stated that there are other instances than those cited where a general scheme, as presented in Figure 1, is required to explain experimental results. The scheme is by no means restricted to trypsin and chymotrypsin behavior. Where the pH dependence of a system does not follow either a simple sigmoid (Figure 3, FBJ or HBI) or bell-shaped curve (Figure 3, FBI), and the curve shows "tailing," this is an indication that a protonated or unprotonated form of the active site can act as an alternate kinetic pathway.

Besides the alternate kinetic pathway aspect, the proposed scheme is required to explain the different pH behavior of rate constants. For the same enzyme, each catalytic stage can have dissimilar pH dependencies. To complicate matters further, different substrates with the same enzyme can possess different pH dependencies for corresponding catalytic stages. Therefore, each system has to be treated on its own merits. Work in this laboratory seems to indicate that it will be undoubtedly necessary to expand the general scheme in Figure 1. This is true particularly for those systems which involve ionizable substrates.

Acknowledgment. The authors wish to extend their appreciation to Dr. J. K. Tseng for his suggestions and assistance in preparing the manuscript.

The Adsorption and Oxidation of Hydrocarbons on Noble Metal Electrodes. V. Relation of "Reduced Carbon Dioxide" to Adsorbed Hydrocarbons

by S. B. Brummer and M. J. Turner

Tyco Laboratories, Inc., Waltham, Massachusetts 02154 *(Received April 17, 1967)*

The adsorption of a product—"reduced CO_2"—on smooth Pt electrodes in CO_2-saturated solutions of 12 *M* H_3PO_4 at 130° has been studied by anodic stripping and cathodic H atom deposition. The amount of adsorbate is a maximum at low potentials ($\theta \simeq 0.8$ at 0.2 v *vs.* rhe) and declines to zero at ~0.7 v. *vs.* rhe. Anodic desorption studies show that this absorbate has a constant structure in the range 0.15–0.35 v and may consist of two parts. The major part releases 1.2 electrons per site when oxidized back to CO_2 and is the same as the O-type adsorbed material reported previously for C_3H_8 and n-C_6H_{14}. The minor part of the adsorbate may be equivalent to the CH-β product reported earlier for C_3H_8 and n-C_6H_{14}. It is shown that the O-type material found with the hydrocarbons must have been produced directly from them and not from the reduction of CO_2 evolved from their anodic oxidation.

I. Introduction

This paper is part of a study of the basic mechanisms of the anodic oxidation of saturated hydrocarbons. Previously, we reported results for the oxidative adsorption of C_3H_8[1-3] and n-C_6H_{14}[4] on Pt from solutions in 12 *M* H_3PO_4 at 130°. An important result was the distinguishing of three generically different species in the steady-state adsorbate of the hydrocarbons. These species were of two main types: O type and CH types. The O type is predominant in terms of coverage at all potentials. It is the most highly oxidized of all of the species and the easiest to oxidize further (to CO_2) at high potentials. It was suggested that most of the C–H bonds of the original hydrocarbon had been converted to C–O bonds in forming the O type[5] (hence the name). The CH types, CH-β and CH-α, were much less oxidized than the O type. They are harder to oxidize at high potentials (0.70 v) and probably represent a polymeric material and (partly dehydrogenated) alkyl radicals, respectively. Unlike O type, which appears to be a single adsorbed species, the composition of the CH types changes with formation potential and probably with hydrocarbon structure. The further purpose of our research program is to examine the properties of these materials and to attempt to define their roles in the over-all hydrocarbon-to-CO_2 reaction.

The O-type species is of particular interest since the same material is found with various hydrocarbons[3,4] and the coverage is always so high. It is clear that the path whereby it is formed is of great importance in defining the chemical mechanism of anodic oxidation. For these reasons, we have investigated the structure and reactions of O-type adsorbed hydrocarbons in some detail. The present paper describes a comparison of the oxidation state of the O-type adsorbed on smooth Pt at 130° with "reduced CO_2."

The importance of "reduced CO_2" in the anodic

(1) S. B. Brummer, J. I. Ford, and M. J. Turner, *J. Phys. Chem.*, **69**, 3424 (1965).

(2) S. B. Brummer and M. J. Turner, "Hydrocarbon Fuel Cell Technology," B. S. Baker, Ed., Academic Press Inc., New York, N. Y., 1965, p 409.

(3) S. B. Brummer and M. J. Turner, *J. Phys. Chem.*, **71**, 2825 (1967).

(4) Part IV: S. B. Brummer and M. J. Turner, *ibid.*, **71**, 3494 (1967).

(5) S. B. Brummer, *J. Electrochem. Soc.*, **113**, 1042 (1966).

reactions of partially oxygenated fuels was first pointed out by Giner.[6] He investigated the products formed from methanol and formic acid solutions on platinized platinum electrodes and compared the anodic stripping curves for these materials with a product he had found adsorbed from CO_2-saturated solutions. This product he had called "reduced CO_2."[7] Subsequently,[8] he reported that a number of saturated hydrocarbons also give rise to "reduced CO_2" at 95° in 2 N H_2SO_4 solution.

Niedrach and co-workers[9] have reported evidence similar to that of Giner for the presence of "reduced CO_2" on electrodes exposed to saturated hydrocarbons. Their studies were with Teflon-bonded platinum fuel cell anodes in $HClO_4$ and H_3PO_4, working from 60 to 120°. Following Gilman,[10] they distinguished two parts of their adsorbates on the basis of waves in their anodic stripping curves. The first of these, at less anodic potentials, they identified with a "CO-like" material similar to $HCOOH_{ads}$ and "reduced CO_2." Their evidence for this conclusion, like Giner's, is based on the qualitative similarity of the peak positions for their so-called "type I" wave and the wave found in the presence of CO_2.

The purpose of the present investigation was to examine the properties of reduced CO_2 using the anodic desorption method developed earlier.[11,12] This method was used to characterize quantitatively the oxidation states of adsorbed C_3H_8[3] and n-C_6H_{14}[4] and therefore allows a quantitative and much less ambiguous comparison between the adsorbates.

II. Experimental Section

Most of the details of the experimental procedure have been described.[1-4] Experiments were carried out in purified 80% H_3PO_4 at 130° using annealed Pt microwire electrodes. CO_2 was "Instrument grade" (Coleman, 99.99 vol. %) and was presaturated with water before being passed into the cell. Potentials are reported against the reversible hydrogen electrode in the same solution (rhe) although they were actually measured against the dynamic hydrogen reference electrode of Giner.[13] Results are quoted "per real cm²," based on 210 μcoulombs for cathodic galvanostatic H atom deposition on a clean electrode.[14]

The adsorption and analysis procedure was as follows. The electrode was potentiostated at 1.35 v for 2 min with gas stirring, to oxidize any adsorbed impurities. The last 30 sec was without stirring if an experiment in quiescent solution was to be done. Oxide formed at 1.35 v was reduced at the adsorption potential (0.15–0.35 v *vs.* rhe). After appropriate adsorption (usually 5 min with gas stirring, then 1 min without) the electrode potential was raised to a region where no adsorption normally occurs. Preliminary experiments (Figure 1) showed that at 0.75 v there was no adsorption from CO_2-saturated solutions and this potential was chosen. At 0.75 v, the adsorbate formed at the lower potential was gradually oxidized.

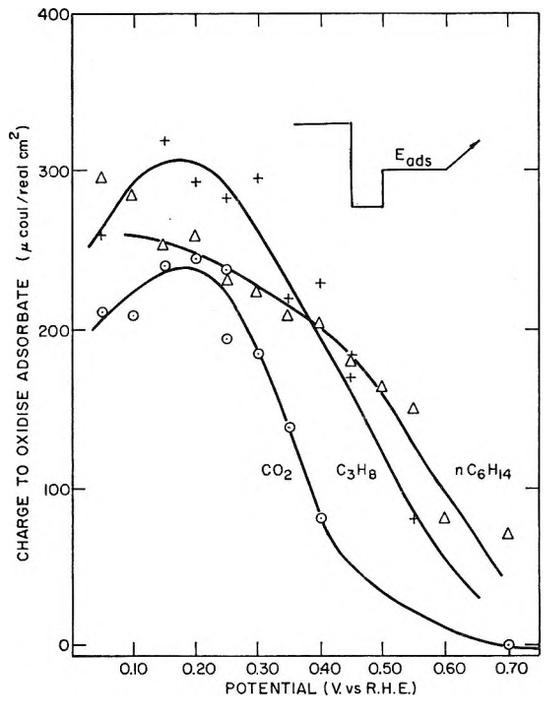

Figure 1. Charge to oxidize adsorbate as a function of potential at 130°: ⊙, 223 mm of CO_2; +, noncathodically desorbable residue under 223 mm of C_3H_8;[13] Δ, noncathodically desorbable residue under 102 mm of n-C_6H_{14}.

The anodic desorption method consists of interrupting this gradual oxidation process to sample the residual absorbate. The adsorbate is sampled in each of two ways: either we oxidize that part of the adsorbate not yet oxidized (Q) or we measure the residual coverage of the electrode with the adsorbate (θ_{org}). Q is measured with an anodic current (~50 ma/real cm²), all the charge to O_2 evolution being integrated and appropri-

(6) J. Giner, *Electrochim. Acta*, 9, 63 (1964).

(7) J. Giner, *ibid.*, 8, 857 (1963).

(8) J. Giner, paper presented at 15th CITCE (Comité Internationale de Thermodynamique et Cinetique Electrochimique) Meeting, London, 1964.

(9) L. W. Niedrach, S. Gilman, and I. Weinstock, *J. Electrochem. Soc.*, 112, 1161 (1965).

(10) S. Gilman, *Trans. Faraday Soc.*, 61, 2546, 2561 (1965).

(11) S. B. Brummer, *J. Phys. Chem.*, 69, 562 (1965).

(12) S. B. Brummer and J. I. Ford, *ibid.*, 69, 1355 (1965).

(13) J. Giner, *J. Electrochem. Soc.*, 111, 376 (1964).

(14) This has been discussed in some detail in ref 1–4 and 11.

ate subtraction of the charge for electrode oxidation being made.[3,15] The coverage, θ_{org}, is measured by plating H atoms onto the surface. This procedure gives θ^{c}_{H}, the fraction of the maximum H atom charge on a clean electrode. θ_{org} is defined as $1 - \theta^{c}_{H}$.[16]

Q is plotted against θ_{org} and changes in the slope of this relation are taken as indicative of changes in the structure of the original adsorbate. On the basis that the cathodic H atom charging method leads to a monolayer of H atoms,[14] the slope of the Q *vs.* θ_{org} plot gives [e], the number of electrons released per covered surface atom when the adsorbate is completely oxidized to CO_2. This quantity is obviously of crucial importance in helping to define the chemical structure of the adsorbed species for these complex adsorbates. In addition, it provides the soundest and most unequivocal comparison between adsorbates found (with varying coverages) with different starting materials.

III. Results and Discussion

Coverage. The coverage of smooth Pt at 130° with "reduced CO_2" is shown in Figure 1. We see a typical coverage–potential relation found for an organic species. For comparison we also show the coverage with the noncathodically desorbable "residue" (≡O type and CH-β) for C_3H_8[3] and n-C_6H_{14}.[4]

Since the relationship between Q and θ_{org} is almost linear (see later), the curve gives a good idea of the "reduced CO_2" coverage. Maximum coverage at low potentials is ~0.85. At 0.4 v, the coverage is less than 0.25, and by 0.70 v it is zero. The shape of the curve reflects the increasing rate of reduction of CO_2 at low potentials and its increasing rate of oxidation at high potentials.

Oxidation State of Reduced CO_2. The Q *vs.* θ_{org} plots for reduced CO_2 adsorbed at various potentials are shown in Figure 2. The process of desorption occurs from the right to the left of the figure. That is to say that the material most easily oxidized for a given adsorbate, *i.e.*, the first material to be oxidized at 0.75 v, is at the top right-hand corner of the figure.

For adsorption at saturation coverage (the 6-min data) at 0.25 v, Q *vs.* θ initially (*i.e.*, high θ) follows a line with a slope, [e], of 1.2 electrons per covered site. Coverages with this material are from <0.1 to 0.85. The data for adsorption in the range 0.15–0.35 v are indistinguishable, save that the coverage varies with potential. The last part of the adsorbate to be removed at 0.75 v is more reduced ([e] ≃ 4 electrons per site). It would be possible to draw a single line of slope 1.35 electrons per site through all of the 6-min adsorption data. However, least-square analysis indicates that the division of the Q–θ plot into two regions is the most reasonable.

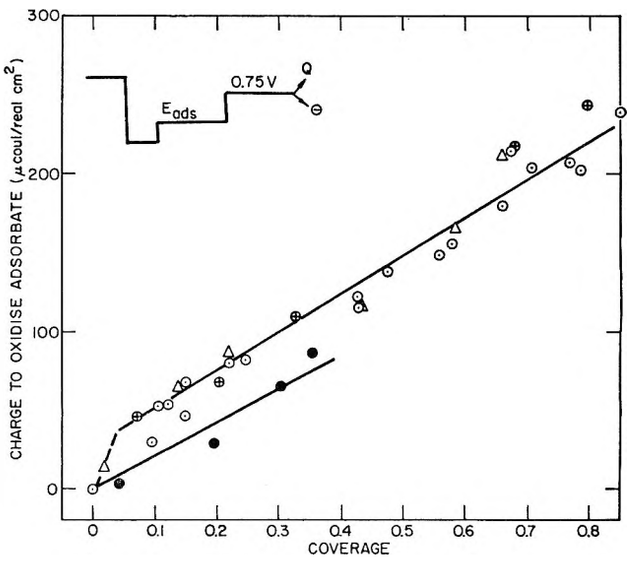

Figure 2. Anodic desorption (Q *vs.* θ) plots for reduced CO_2 adsorbed under various circumstances at 130°: ⊕, 0.15 v for 6 min; ⊙, 0.25 v for 6 min; ●, 0.25 v for 100 sec; Δ, 0.35 v for 6 min.

These two regions of the Q–θ plots are similar to those found previously for C_3H_8[3] and n-C_6H_{14}.[4] Thus for C_3H_8, we reported a slope of 1.3 electrons per covered site for the O-type adsorbate; for n-C_6H_{14}, we found $[e]_{O\ type}$ to be 1.4 electrons per site. These values are in reasonably good agreement with the above value for $[e]_{reduced\ CO_2}$. On this basis, we would confirm the observations of Giner[8] and Niedrach, *et al.*,[9] concerning the relationship between reduced CO_2 and adsorbed hydrocarbons, and, specifically, we would equate O-type hydrocarbons with reduced CO_2. Furthermore, since the previous conclusions[8,9] were based on the oxidation kinetics of the adsorbate and ours is based on its oxidation state, the results are complementary on this point.

It is not clear whether the small differences among the [e] values for reduced CO_2 (1.2), O-type C_3H_8 (1.3), and O-type n-C_6H_{14} (1.4) are significant, but probably they are within experimental error. Hence, we believe that the most reasonable interpretation is to equate the O-type materials with one another and with reduced

(15) The best way to correct for double-layer effects in these experiments has been discussed by S. B. Brummer, *J. Phys. Chem.*, 71, 2838 (1967).

(16) The general use of this method for adsorbate coverage determination was discussed in ref 11 and further during the International Symposium on Electrode Processes, Cleveland, Ohio, May 1966; see S. B. Brummer, *J. Electrochem. Soc.*, 113, 1044 (1966).

CO_2. We cannot rule out, however, that there is a slight change in the structure of the O-type materials formed in the series CO_2, C_3H_8, and n-C_6H_{14}, with the product increasing in average reduction state as the hydrocarbon homologous series is ascended.

Similarly, the small "tail" close to the Q–θ origin is reminiscent of the CH-β material found for C_3H_8 and n-C_6H_{14}. This may represent the further reduction of CO_2 from O-type to CH-β material. However, the amount of material involved is small (<0.05 of a monolayer in 6 min; 5 min with stirring) and we cannot rule out the possibility that this is from a small amount of adsorbable impurity in the solution. Data taken after 100 sec without stirring do not show this effect (Figure 2).

Composition of O-Type Hydrocarbons and Reduced CO_2. Relation to Hydrocarbon-to-CO_2 Reaction. The finding of the same adsorbed product for C_3H_8, n-C_6H_{14}, and CO_2 and, from others' work, for a variety of oxygenated compounds[6] and hydrocarbons[8,9] is significant in helping to define the structure of the adsorbate. Almost certainly, the material is a C_1 species. The [e] value of 1.2 shows that it must contain considerable oxygen; *i.e.*, it is close to CO_2 in oxidation state. There is considerable controversy about its exact composition, however. Niedrach, *et al.*,[9] referred to it as "CO-like." The data of Piersma, Warner, and Schuldiner,[17] albeit at low temperatures, show that reduced CO_2 is not CO, however. Frumkin, *et al.*,[18] have studied the product formed on platinized Pt at room temperature from MeOH solutions. From Giner's work,[6] this should be reduced CO_2. Giner[6] had suggested a composition –COOH but Frumkin, *et al.*,[18] postulated an adsorbed product $\geqslant$C(OH). This would release 3 electrons on oxidation to CO_2 and, since it occupies 3 sites, [e] should be 1. Their [e] value and ours are not in significant conflict,[19] but we cannot distinguish between these two structures.

The presence of reduced CO_2 as a substantial part of the adsorbate for a large number of organic compounds on Pt led to the suggestion of two general mechanisms for the anodic processes;[5] thus *the reaction, e.g.*, HCOOH oxidation,[20] *could proceed in spite of the adsorbed product, viz.*

$$\text{HCOOH or } CO_2 \longrightarrow \text{reduced } CO_2\ (\theta) \qquad (1)$$

$$\text{HCOOH} \longrightarrow CO_2 + 2H^+ + 2e^- \qquad (2)$$

Here, the main reaction goes on that part of the surface not occupied by reduced CO_2 $(1 - \theta)$. In these reactions, the production of reduced CO_2 is harmful. Alternatively, *the reaction could proceed via reduced CO_2* with the reduced $CO_2 \rightarrow CO_2$ step being rate limiting, *viz.* eq 3 and 4.

$$C_3H_8 \xrightarrow{\text{fast}} \text{reduced } CO_2 \qquad (3)$$

$$\text{reduced } CO_2 \xrightarrow{\text{slow}} CO_2 \qquad (4)$$

In this scheme, those situations which favor formation of reduced CO_2 at the expense of other adsorbed products (*e.g.*, CH-α and CH-β) would be desirable.

Niedrach, *et al.*,[9,21] have argued that reduced CO_2 formation (their type I) is to be encouraged. We have argued[3,4] that the virtual independence of $\theta_{O\ type}$ on hydrocarbon pressure is contrary to the prediction of the latter mechanism (reactions 3 and 4). This is because it has been reported that C_3H_8[22] and n-C_6H_{14}[23] oxidation are first order in gas pressure. On this basis, reduced CO_2 formation is undesirable.[24]

This question cannot be resolved at the present. However, our data do show that the O-type adsorbate is formed from the fuel and not from reduction of anodically evolved CO_2. Thus, the amount of adsorbed noncathodically desorbable residue (mainly O type) is greater for C_3H_8 and n-C_6H_{14} than for CO_2 above ~0.40 v. Similarly at lower potentials, *e.g.*, 0.30 v, the rate of production of reduced CO_2 from CO_2-saturated solutions is less than the rate of production of O type from C_3H_8.[2,3] Thus, the reduced CO_2 found in presence of hydrocarbons is produced from them *per se* and not from the reduction of anodically produced CO_2.

IV. Summary and Conclusions

(1) The amount of reduced CO_2 on smooth Pt at 130° shows a typical bell-shaped "isotherm." Adsorption is highest at ~0.2 v. *vs.* rhe (~0.8 monolayer) and decreases to zero at ~0.7 v.

(2) Anodic desorption experiments show that the structure of this adsorbate is constant as a function of

(17) B. J. Piersma, T. B. Warner, and S. Schuldiner, *J. Electrochem. Soc.*, **113**, 841 (1966).

(18) O. A. Petry, B. I. Podlovchenko, A. N. Frumkin, and H. Lal, *J. Electroanal. Chem.*, **10**, 253 (1965).

(19) Their value is based on anodic H atom charging; ours, on cathodic charging. If the cathodic charging method gives a lower charge than the anodic method, as suggested, for example, by the results of Gilman (*J. Electroanal. Chem.*, **7**, 382 (1964)), the agreement is even better.

(20) S. B. Brummer and A. C. Makrides, *J. Phys. Chem.*, **68**, 1448 (1964).

(21) L. W. Niedrach and M. Tochner, *J. Electrochem. Soc.*, **114**, 17 (1967).

(22) Report by E. Gileadi, G. Stoner, and J. O'M. Bockris to U. S. Army Engineer Research and Development Laboratories, Fort Belvoir, Va., April 1966, AD 632 319.

(23) Report by G. Stoner and J. O'M. Bockris to U. S. Army Engineer Research and Development Laboratories, Fort Belvoir, Va., Oct 1966, AD 643 386.

(24) The experiments reported in ref 22 and 23 may not be relevant, however. Thus, at the relevant potentials ($\leq$0.30 v), we have found zero or even negative order for the over-all $C_3H_8 \rightarrow CO_2$ reaction.

potential in the investigated range 0.15–0.35 v. *vs.* rhe and that the adsorbate may consist of two parts.

(3) The major part releases 1.2 electrons per covered site when oxidized and is the same as the O-type product found adsorbed from hydrocarbon-saturated solutions.[3,4]

(4) The minor part (<0.05 monolayer) may be equivalent to the previously reported CH-β product from hydrocarbon-containing solutions.

(5) The O-type material found adsorbed from hydrocarbon solutions cannot have originated from reduction of CO_2 produced anodically from the hydrocarbon. It is produced directly from the hydrocarbon itself.

Acknowledgment. It is a pleasure to acknowledge support of this work by the U. S. Army Engineer Research and Development Laboratories, Fort Belvoir, Va., under Contract DA 44-009-AMC-1408(T).

Volume Changes on Mixing Solutions of Potassium Halides and Symmetrical Tetraalkylammonium Halides. Evidence of Cation–Cation Interaction[1]

by Wen-Yang Wen and Kenichi Nara

Chemistry Department, Clark University, Worcester, Massachusetts 01610 *(Received April 19, 1967)*

Volume changes on mixing aqueous solutions of potassium bromide and symmetrical tetraalkylammonium bromides [$(CH_3)_4NBr$, $(C_2H_5)_4NBr$, $(C_3H_7)_4NBr$, and $(HOC_2H_4)_4NBr$] have been measured at constant total ionic strengths (I = 0.5, 1.0, and 2.0) at 25° using an apparatus similar to that described by Wirth, Lindstrom, and Johnson. In addition, the volume changes on mixing potassium chloride and tetra-*n*-butylammonium chloride were measured at constant total ionic strengths of 0.2, 0.5, and 1.0. The results obtained were discussed in terms of the ionic solution theory of Friedman. Friedman's theory, when applied to the volume of mixing of AX and BX, gives the two relations $\Delta_m V^{ex}/[I^2 y(1-y)] = 2\bar{v}_{AB}^* - \bar{v}_{AA}^* - \bar{v}_{BB}^* + \ldots$ and $[V^{ex}(AX) - V^{ex}(BX)]/I^2 = \bar{v}_{AA}^* + 2\bar{v}_{AX}^* - \bar{v}_{BB}^* - 2\bar{v}_{BX}^* + \ldots$, where $\bar{v}_{ij}^*$ is the part of the volume change on mixing due to the structural effects when ion i is in the neighborhood of ion j and y is the mole fraction of AX in the mixture. For $(C_3H_7)_4NBr$–KBr and $(C_4H_9)_4NCl$–KCl systems at $I = y = 0.5$, $\bar{v}_{AA}^*$ was found to be predominant over the rest of the terms with values of −9 and −11 ml/mole for A = $(C_3H_7)_4N^+$ and A = $(C_4H_9)_4N^+$, respectively. The large negative values of $\bar{v}_{AA}^*$ are taken as evidence of a significant contribution of the cation–cation interaction to the volume of the aqueous solutions. As expected, terms other than $\bar{v}_{AA}$ are no longer negligible for smaller cations like $(C_2H_5)_4N^+$ and $(CH_3)_4N^+$. For the $(HOC_2H_4)_4NBr$–KBr system, the values of $\Delta_m V^{ex}$ were found to be zero at total ionic strengths of 0.5, 1.0, and 2.0, in striking contrast to the large values obtained for the $(C_3H_7)_4$-NBr–KBr system. These studies clearly indicate that the volume changes on mixing are strongly governed by the solvent structural properties of the ions.

Introduction

Investigations by various workers have shown the solutions of tetraalkylammonium salts to possess many interesting physical properties.[2-14] Particularly noteworthy are recent works by Lindenbaum[15] and Wood, *et al.*,[16] on the enthalpy and entropy of dilution of these salts. These and other studies on the thermodynamic and transport properties[3,9-12] of the quaternary ammonium salt series seem to offer strong support to the notion that, in aqueous solutions, the peculiarities of the tetraalkylammonium ions are due not only to their large ionic sizes but also to the significant modification of water structure around the cations.

The apparent and partial molal volumes of these salts in aqueous solutions have been measured by Wen and Saito,[5] Conway and Verrall,[13,14] and Franks[17] at different concentration ranges. When the apparent molal volumes, φ_2, were plotted against $\sqrt{c}$, where c is the molar concentration, they found some of these salts to

(1) Presented before the Division of Physical Chemistry, 153rd National Meeting of the American Chemical Society, Miami Beach, Fla., April 9–14, 1967; see Abstract R-147.

(2) H. S. Frank and W. Y. Wen, *Discussions Faraday Soc.*, **24**, 133 (1957).

(3) J. N. Agar, *Advan. Electrochem. Electrochem. Eng.*, **3**, 96 (1963).

(4) S. Lindenbaum and G. E. Boyd, *J. Phys. Chem.*, **68**, 911 (1964).

(5) W. Y. Wen and S. Saito, *ibid.*, **68**, 2639 (1964).

(6) W. Y. Wen, S. Saito, and C. M. Lee, *ibid.*, **70**, 1244 (1966).

(7) H. G. Hertz and M. D. Zeidler, *Ber. Bunsenges. Physik. Chem.*, **68**, 821 (1964).

(8) H. S. Frank, *J. Phys. Chem.*, **67**, 1554 (1963); *Z. Physik. Chem.* (Leipzig), **228**, 364 (1965).

(9) R. L. Kay and D. F. Evans, *J. Phys. Chem.*, **69**, 4216 (1965).

(10) D. F. Evans and R. L. Kay, *ibid.*, **70**, 336 (1966).

(11) R. L. Kay and D. F. Evans, *ibid.*, **70**, 2325 (1966).

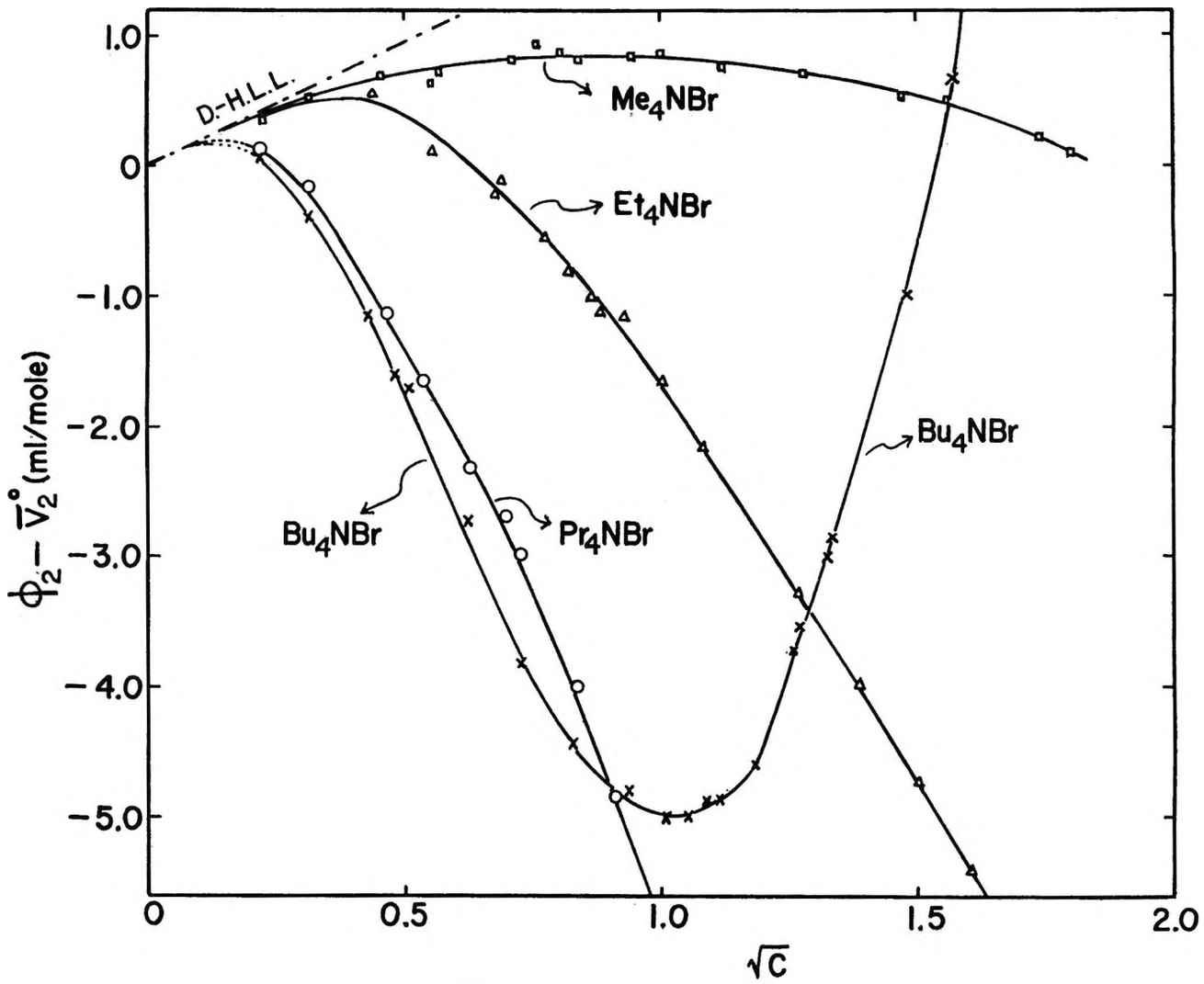

Figure 1. Relative apparent molal volumes, $\varphi_2 - \bar{V}_2^0$, of four tetraalkylammonium bromides (Me_4NBr, Et_4NBr, Pr_4NBr, and Bu_4NBr) plotted against $\sqrt{c}$ at 25°.

show substantial negative deviations from the Debye–Hückel limiting law at relatively low concentrations. At higher concentrations the plot of $\bar{V}_2$ *vs.* $\sqrt{c}$ for $(C_3H_7)_4NBr$ and $(C_4H_9)_4NBr$ go through a minimum and then turn upward with the increase of c.[5] These observations (see Figure 1) were explained in terms of water structure promoting influence of the cations in general and the formation of a clathrate-like structure for $(C_4H_9)_4NBr$ in particular. In view of the qualitative nature of this explanation, it seems desirable to us to find a more convincing evidence of cation–cation interaction among the large tetraalkylammonium ions in aqueous solutions. A promising avenue of approach in this regard is the ionic solution theory of Friedman[18] applied to the volume of mixing.

Friedman has extended Mayer's ionic solution theory[19] to mixed electrolyte solutions and derived the excess free energy of mixing

(12) R. L. Kay, T. Vituccio, C. Zawoyski, and D. F. Evans, *J. Phys. Chem.*, **70**, 2336 (1966).

(13) R. E. Verrall, Ph.D. Thesis, University of Ottawa, 1966.

(14) B. E. Conway and R. E. Verrall, *J. Phys. Chem.*, **70**, 3952 (1966); **70**, 3961 (1966).

(15) S. Lindenbaum, *ibid.*, **70**, 814 (1966).

(16) R. H. Wood, H. L. Anderson, J. D. Beck, J. R. France, W. E. deVry, and L. J. Soltzberg, *ibid.*, **71**, 2149 (1967).

(17) F. Franks, private communication. In very dilute solutions ($c < 0.01$), Franks has observed that the curves do turn over to give agreement with the behavior predicted by Debye and Hückel (see Figure 1).

(18) H. L. Friedman, *J. Chem. Phys.*, **32**, 1134 (1960); H. L. Friedman, "Ionic Solution Theory," Interscience Publishers, Inc., New York, N. Y., 1962.

(19) J. E. Mayer, *J. Chem. Phys.*, **18**, 1426 (1950).

$$\Delta_m G^{ex}(y,I) = I^2RTy(1 - y) \times [g_0 + g_1(1 - 2y) + g_2(1 - 2y)^2 + \ldots] \quad (1)$$

where R and T have their usual meaning, I is the molal ionic strength, y is the fraction of the ionic strength due to an electrolyte in a mixture of two electrolytes, and the g's are interaction parameters. Friedman's theory predicts that the leading term, g_0, is the major term for 1–1 common ion mixtures and that the major interactions contributing to g_0 are those of like-charged ion pairs. Similar equations can be obtained for the volume of mixing

$$\Delta_m V^{ex}(y,I) = I^2y(1 - y)[v_0 + v_1(1 - 2y) + v_2(1 - 2y)^2 + \ldots] \quad (2)$$

where $v_0 = RT(\partial g_0/\partial P)$, $v_1 = RT(\partial g_1/\partial P)$, etc., in which P is the pressure. It seems likely that useful results can be obtained only if terms beyond v_0 in eq 2 are negligible. In order to see whether the cation–cation interaction makes a significant contribution to the volume, we have measured the values of $\Delta_m V^{ex}$ for solutions of potassium halides and tetraalkylammonium halides and calculated v_0 by eq 2 and then proceeded to analyze and compare the values of V_0 according to Friedman's theory.[20]

Wirth, Lindstrom, and Johnson[21] have measured the volume changes on mixing two solutions of equal ionic strength for the six combinations of the four electrolytes, NaCl, HCl, $NaClO_4$, and $HClO_4$, at two concentrations. They showed that the volume changes at constant ionic strength accompanying the mixing of the two heteroionic combinations could be calculated from the observed volume changes on mixing four homoionic pairs (the so-called "cross-square rule").[22] This implies that the mixing of four ions involves no ion–ion interactions not already taken into account in the mixtures containing three ions. It will be of interest to extend the measurements so that the "cross-square rule" for the volumes can be tested for systems of electrolytes which include tetraalkylammonium salts.

Experimental Section

Materials. Fisher Certified potassium chloride and bromide[23] were recrystallized twice from water and dried carefully before use. The halides were analyzed gravimetrically and found to be in 99.9% or better agreement with the calculated value. Four tetraalkylammonium salts (Me_4NBr, Et_4NBr, Pr_4NBr, and Bu_4NCl) were obtained from the Distillation Products Industries of Rochester, N. Y., and each was recrystallized twice or more from the suitable solvents[24] and dried at proper temperatures[25] before use. The gravimetric analyses of the cations[26] and the anions indicated their purities to be at least 99.9%. Tetrakis(2-hydroxyethyl)ammonium bromide (also known as tetraethanolammonium bromide) was prepared by the method of Wen and Saito.[27,28] After several recrystallizations, the bromide content determined gravimetrically as the silver salt was 100.00 ± 0.01%, mp 102° with slight decomposition. Most solutions were made by direct weighing of the salts and water; dilute solutions were prepared by weight dilution of stock solutions. The reagent grade mercury obtained from the Fisher Scientific Co. was used without further purification. Experiments on mixing solutions of KBr and Bu_4NBr were also carried out, but Bu_4NBr and mercury reacted to give a small amount of white solid particles when the mixture was stirred vigorously at 25°. The data obtained from mixing KBr and Bu_4NBr were, therefore, excluded from this report.

Apparatus and Procedure. Volume changes on mixing solutions of equal molal ionic strength were measured by use of a dilatometer (Figure 2) similar to that described by Wirth, Lindstrom, and Johnson.[21] About 65 ml of one solution was introduced from bulb B into A (volume 300 ml) through a three-way stopcock a. The amount introduced was determined by weighing the mercury displaced through the capillary tube (diameter 1 mm) at the right of the apparatus. A second solution filled the bulb C and all connecting tubing. Stopcock b was opened and mercury from A displaced the second solution into the first in A through another three-way stopcock a′. The bulbs permitted the addition of 1, 3, or 13 ml of the second solution and were calibrated by weighing the mercury required to fill them to reference marks on the connecting capillary tubing. After addition of the second solution, the solution in A was thoroughly mixed by the magnetic stirrer S. Any volume change was reflected by an increase or decrease in weight of mercury in a weighing beaker D around the capillary tip. Weight changes were determined to ±1 mg, corresponding to a volume change of

(20) H. L. Friedman, private communications. We are indebted to Professor Friedman for these suggestions.

(21) H. E. Wirth, R. E. Lindstrom, and J. N. Johnson, *J. Phys. Chem.*, **67**, 2339 (1963).

(22) Y. C. Wu, M. B. Smith, and T. F. Young, *ibid.*, **69**, 1873 (1965).

(23) Products of Fisher Scientific Co., Pittsburgh, Pa.

(24) See ref 13, p 111.

(25) A. K. R. Unni, Ph.D. Thesis, McGill University, Montreal, 1958.

(26) Tetraalkylammonium cations were precipitated as tetraalkylammonium tetraphenylboride using the standard procedure.

(27) W. Y. Wen and S. Saito, *J. Phys. Chem.*, **69**, 3569 (1965).

(28) D. F. Evans, G. P. Cunningham, and R. L. Kay, *ibid.*, **70**, 2974 (1966).

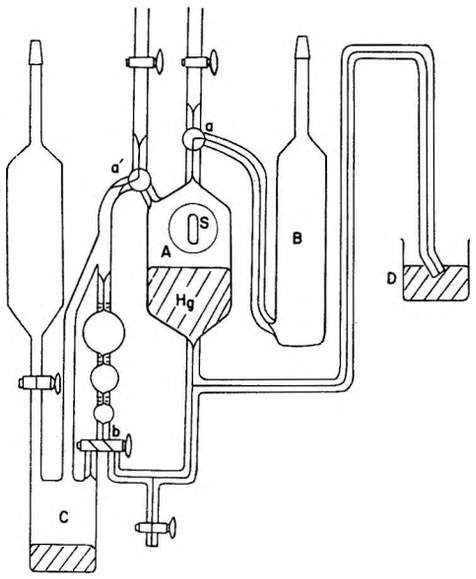

Figure 2. Dilatometer for measuring the volume changes on mixing two solutions.

$\pm 1 \times 10^{-4}$ ml. Stopcock b was turned to permit the mercury in the bulbs to flow into the bottom of C, and more of the second solution could be added. It was found essential to keep the mercury levels in A and D nearly identical so that the pressure at the capillary tip would be equal to the pressure on the solution in A. This was accomplished by adjusting the position of beaker D containing the mercury and also by changing the length of capillary tip near D. All the stopcocks were made of Teflon inserts. The apparatus was immersed in a thermostat at a temperature of 25° maintained constant to ±0.001°. The precision for values of $\Delta_m V^{ex}$ obtained in our experiments at $y = 0.5$ is to ±0.008 ml at $I = 0.5$, ±0.004 ml at $I = 1.0$, and ±0.002 ml at $I = 2.0$.

Results and Discussion

We define the excess function on mixing

$$\Delta_m V^{ex}(y,I) \equiv V^{ex}(y,I) - (1 - y)V^{ex}(0,I) - yV^{ex}(1,I) \quad (3)$$

where I is the total molal ionic strength, y is the fraction of the molal ionic strength due to AX in a mixture of AX and BX, and $V^{ex}(y,I)$ is the excess volume of the solution whose composition is specified by y and I. For systems under consideration, A denotes R_4N^+, B denotes K^+, and X denotes Br^- (or Cl^-). Suppose the first solution contains n_1 moles of AX and the second solution contains n_2 moles of BX and, on mixing two solutions of an equal molality, Δu is the observed change in volume, then it can be easily shown[21] that

$$\Delta_m V^{ex}(y,I) = \Delta u/(n_1 + n_2) \quad (4)$$

The experimentally obtained values of $\Delta_m V^{ex}$ are given in Tables I–V and plotted against y (the mole fraction of R_4NX) for some selected systems in Figures 3–6 for comparison.

Table I: Volume Changes (ml/mole) on Mixing Solutions of Pr_4NBr and KBr at 25°

	I = 0.500		I = 1.000		I = 1.996	
y	$\Delta_m V^{ex}$	Z^a	$\Delta_m V^{ex}$	Z	$\Delta_m V^{ex}$	Z
0.1	0.193	8.58	0.306	3.39	0.500	1.40
0.2	0.338	8.45	0.555	3.46	0.894	1.40
0.3	0.455	8.67	0.764	3.63	1.167	1.39
0.4	0.533	8.88	0.884	3.67	1.270	1.33
0.5	0.570	9.12	0.905	3.60	1.260	1.27
0.6	0.541	9.02	0.843	3.50	1.180	1.24
0.7	0.469	8.93	0.710	3.37	1.025	1.23
0.8	0.351	8.78	0.516	3.21	0.731	1.45
0.9	0.195	8.67	0.283	3.13	0.394	1.10

[a] $Z = \Delta_m V^{ex}/[I^2 y(1 - y)]$.

Table II: Volume Changes (ml/mole) on Mixing Solutions of Et_4NBr and KBr at 25°

	I = 0.500		I = 1.000		I = 2.000	
y	$\Delta_m V^{ex}$	Z^a	$\Delta_m V^{ex}$	Z	$\Delta_m V^{ex}$	Z
0.1	0.097	4.33	0.161	1.79	0.280	0.780
0.2	0.175	4.38	0.305	1.91	0.524	0.819
0.3	0.249	4.75	0.411	1.96	0.710	0.845
0.4	0.294	4.90	0.475	1.98	0.795	0.828
0.5	0.318	5.08	0.491	1.96	0.800	0.800
0.6	0.297	4.95	0.458	1.91	0.741	0.771
0.7	0.252	4.80	0.390	1.86	0.627	0.747
0.8	0.185	4.63	0.295	1.85	0.463	0.723
0.9	0.098	4.35	0.151	1.68	0.257	0.713

[a] $Z = \Delta_m V^{ex}/[I^2 y(1 - y)]$.

Table III: Volume Changes (ml/mole) on Mixing Solutions of Me_4NBr and KBr at 25°

	I = 0.50		I = 1.00		I = 2.00	
y	$\Delta_m V^{ex}$	Z^a	$\Delta_m V^{ex}$	Z	$\Delta_m V^{ex}$	Z
0.1	0.016	0.71	0.032	0.36	0.059	0.164
0.2	0.031	0.78	0.060	0.38	0.117	0.183
0.3	0.040	0.76	0.082	0.39	0.160	0.190
0.4	0.046	0.77	0.096	0.40	0.197	0.205
0.5	0.049	0.78	0.099	0.40	0.208	0.208
0.6	0.045	0.75	0.090	0.38	0.195	0.203
0.7	0.038	0.72	0.075	0.36	0.160	0.190
0.8	0.028	0.70	0.053	0.33	0.116	0.181
0.9	0.015	0.67	0.029	0.32	0.060	0.166

[a] $Z = \Delta_m V^{ex}/[I^2 y(1 - y)]$.

Table IV: Volume Changes (ml/mole) on Mixing Solutions of Bu_4NCl and KCl at 25°

	I = 0.20		I = 0.50		I = 1.00	
y	$\Delta_m V^{ex}$	Z^a	$\Delta_m V^{ex}$	Z	$\Delta_m V^{ex}$	Z
0.1	0.110	30.6	0.223	9.89	0.323	3.59
0.2	0.202	31.6	0.411	10.28	0.584	3.65
0.3	0.281	33.5	0.548	10.43	0.785	3.74
0.4	0.338	35.2	0.645	10.75	0.912	3.80
0.5	0.361	36.1	0.680	10.88	0.945	3.78
0.6	0.341	35.5	0.642	10.70	0.890	3.71
0.7	0.288	34.3	0.552	10.52	0.760	3.62
0.8	0.207	32.3	0.412	10.31	0.571	3.57
0.9	0.111	30.8	0.223	9.93	0.316	3.51
Mean value of Z		33.3 ± 1.8		10.41 ± 0.27		3.66 ± 0.08

[a] $Z = \Delta_m V^{ex}/[I^2 y(1 - y)]$.

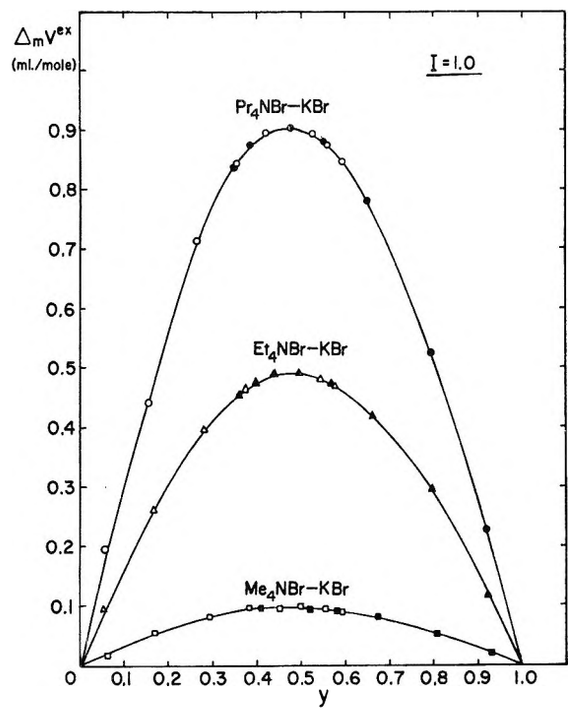

Figure 3. Volume changes, $\Delta_m V^{ex}$, on mixing R_4NBr and KBr solutions plotted against the mole fraction, y, at a constant ionic strength of I = 1.0 at 25°: R = Pr, Et, and Me.

According to Friedman[20] relations 5 and 6 can be derived for mixed electrolyte solutions

$$\Delta_m V^{ex}/[I^2 y(1 - y)] = v_0 + \text{rem}_1 = 2\bar{v}_{AB}^* - \bar{v}_{AA}^* - \bar{v}_{BB}^* + \text{rem}_2 \quad (5)$$

$$[V^{ex}(AX) - V^{ex}(BX)]/I^2 = \bar{v}_{AA}^* + 2\bar{v}_{AX}^* - \bar{v}_{BB}^* - 2\bar{v}_{BX}^* + \text{rem}_3 \quad (6)$$

where

$$V^{ex}(AX) = I(\varphi_{AX} - \overline{V}_{AX}^0) \text{ and } V^{ex}(BX) = I(\varphi_{BX} - \overline{V}_{BX}^0) \quad (7)$$

In contrast to eq 5, eq 6 relates the difference of excess volumes of two separate solutions at an identical ionic strength I. In these equations $\bar{v}_{ij}^*$ is the part of the volume which changes on mixing due to the structural effects when ion i is in the neighborhood of ion j, while rem_1, rem_2, and rem_3 are the remainder terms which can be shown to be small compared to other terms for dilute

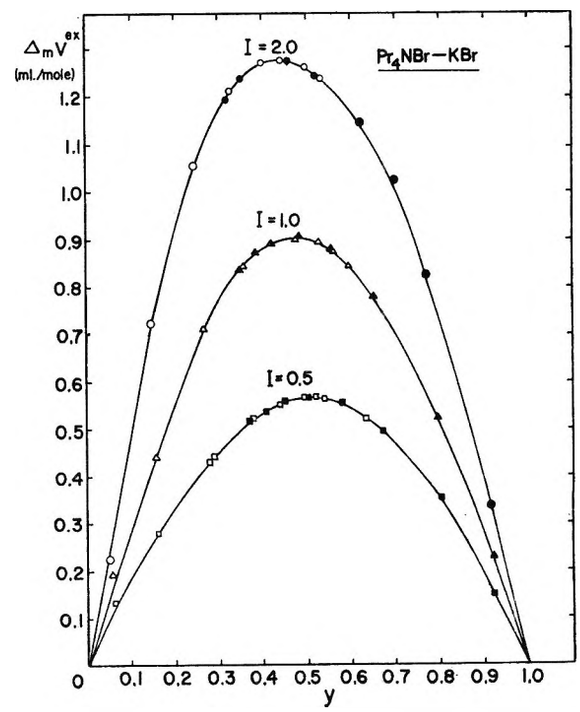

Figure 4. Volume changes on mixing Pr_4NBr and KBr solutions plotted against the mole fraction of Pr_4NBr at constant ionic strengths of I = 0.5, 1.0, and 2.0 at 25°.

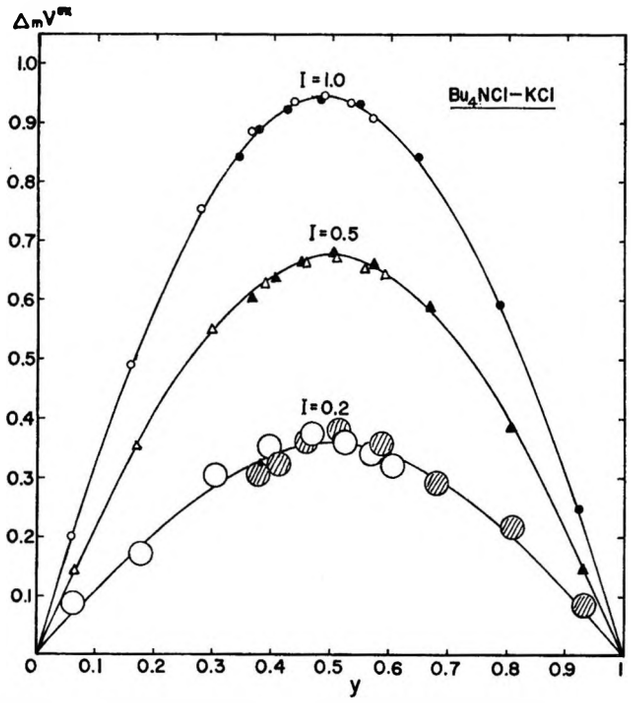

Figure 5. Volume changes on mixing Bu_4NCl and KCl solutions plotted against the mole fraction of Bu_4NCl at constant ionic strengths of I = 0.2, 0.5, and 1.0 at 25°.

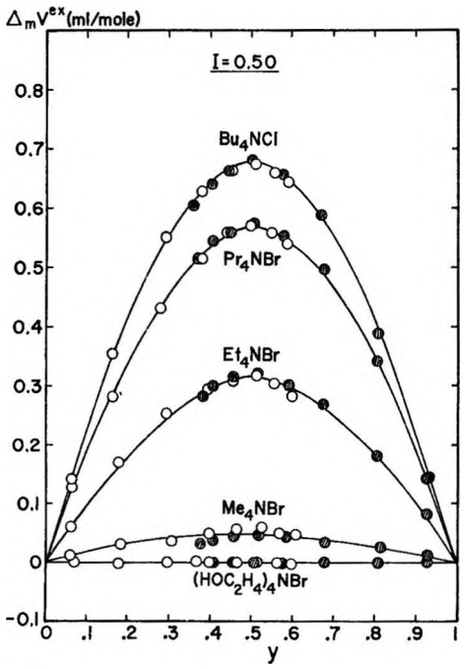

Figure 6. Volume changes for $(HOC_2H_4)_4NBr$–KBr, Me_4NBr–KBr, Et_4NBr–KBr, Pr_4NBr–KBr, and Bu_4NCl–KCl mixings at I = 0.50 at 25°.

solutions. Comparing eq 5 and 6 we see that if $\bar{v}_{AA}^*$ is much larger than the other terms (comparing absolute values), then both eq 5 and 6 will be large, while if $\bar{v}_{AX}^*$ dominates then (6) will be much larger than (5). A large absolute value of $\bar{v}_{AA}^*$ may be taken to indicate a large contribution of the R_4N^+–R_4N^+ interaction to the solution volume. The fact that the absolute values of $\bar{v}_{AA}^*$ are indeed large for Pr_4N^+ and Bu_4N^+ ions can be seen from the following example. Using the data obtained at I = 0.50 and y = 0.50 for Pr_4NBr–KBr (from Table I) and for Bu_4NCl–KCl (from Table IV), we write $Z = \Delta_m V^{ex}/[I^2 y(1 - y)]$ = 9.12 ml/mole for

Table V: Volume Changes (ml/mole) on Mixing Solutions of $(HOC_2H_4)_4NBr$ and KBr at 25°

I = 0.50		I = 1.00		I = 2.00	
y	$\Delta_m V^{ex}$	y	$\Delta_m V^{ex}$	y	$\Delta_m V^{ex}$
0.071	−0.0011	0.059	+0.0030	0.054	−0.0005
0.176	−0.026	0.166	+0.0017	0.153	−0.0018
0.299	+0.0032	0.284	−0.0007	0.316	+0.0006
0.390	+0.0028	0.374	+0.0002	0.352	−0.0007
0.460	+0.0029	0.450	+0.0001	0.420	+0.0004
0.506	+0.0015	0.493	−0.0016	0.466	0.0000
0.516	+0.0014	0.500	0.0000	0.475	+0.0005
0.561	+0.0003	0.544	−0.0001	0.521	−0.0002
0.578	−0.0026	0.565	+0.0020	0.537	−0.0003
0.599	−0.0014	0.582	−0.0011	0.559	+0.0003
0.672	+0.0021	0.661	−0.0012	0.635	−0.0004
0.804	−0.0068	0.780	−0.0006	0.777	+0.0011
0.928	−0.0020	0.925	−0.0004	0.917	0.0000
Mean value	−0.002		+0.0001		−0.0001

Table VI: List of Data Used for Calculation of $(V^{ex}(AX) - V^{ex}(BX))/I^2$ (ml/mole)

Salt	I	φ_{AX}	φ_{BX}	$\varphi_{AX} - \bar{V}_{AX}^{0}$ [a]	$\varphi_{BX} - \bar{V}_{BX}^{0}$ [b]	W
Pr_4NBr	0.5	236.7	35.4	−2.5	1.7	−8.4
	1.0	234.5	35.8	−4.7	2.1	−6.8
	2.0	231.8	36.5	−7.4	2.8	−5.1
Et_4NBr	0.5	173.0	35.4	−0.3	1.7	−4.0
	1.0	172.0	35.8	−1.3	2.1	−3.4
	2.0	170.4	36.5	−2.9	2.8	−2.9
Me_4NBr	0.5	115.2	35.4	0.8	1.7	−1.8
	1.0	115.3	35.8	0.9	2.1	−1.2
	2.0	115.1	36.5	0.7	2.8	−1.1
Bu_4NCl	0.2	292.7	27.6	−1.4	0.9	−11.5
	0.5	291.0	28.2	−3.1	1.5	−9.2
	1.0	288.9	28.8	−5.2	2.1	−7.3

[a] $\bar{V}_{AX}^{0}$, 239.2 for Pr_4NBr,[17] 173.3 for Et_4NBr,[17] 114.4 for Me_4NBr,[17] and 294.1 for Bu_4NCl.[13] [b] $\bar{V}_{BX}^{0}$, 33.7 for KBr and 26.7 for KCl (for both values, see H. E. Wirth, *J. Am. Chem. Soc.*, **59**, 2549 (1937)).

Table VII: Comparison of Values Obtained by Eq 5 at $y = 0.5$ and by Eq 6

	Pr_4NBr–KBr		Et_4NBr–KBr		Me_4NBr–KBr		Bu_4NCl–KCl		NaCl–KCl[a]	
I	(5)	(6)	(5)	(6)	(5)	(6)	(5)	(6)	(5)	(6)
0.5	9.12	−8.4	5.08	−4.0	0.78	−1.8	10.88	−9.2	−0.089	−0.43
1.0	3.60	−6.8	1.96	−3.4	0.40	−1.2	3.78	−7.3		
2.0	1.27	−5.1	0.80	−2.9	0.21	−1.1				

[a] H. E. Wirth, *J. Am. Chem. Soc.*, **59**, 2549 (1937).

Pr_4NBr and 10.88 ml/mole for Bu_4NCl. On the other hand from Table VI we have $W = [V^{ex}(AX) - V^{ex}(BX)]/I^2 = -8.4$ ml/mole for Pr_4NBr and -9.2 ml/mole for Bu_4NCl. Since the values of Z and W are large and opposite in sign for both systems, we see that $\bar{v}_{AA}^*$ must be much larger than the other terms in eq 5 and 6. It is concluded, therefore, that the cation–cation interaction induces a decrease in solution volume by approximately the amounts given at $I = 0.50$: $\bar{v}_{AA}^* = -9$ ml/mole for Pr_4N^+ and -11 ml/mole for Bu_4N^+.

Similar comparisons have been carried out for these and other systems at different ionic strengths and the results are summarized in Table VII. For Pr_4NBr–KBr system at higher ionic strengths ($I = 1.0$ and 2.0) the values calculated by eq 5 and 6 show greater discrepancies than at $I = 0.50$, indicating that the remainder terms (rem_2 and rem_3) are no longer negligible. At higher concentrations multiplet interactions among cations are expected to become important in addition to the pairwise interaction. The fact that the higher v_n (v_1, v_2, v_3, etc.) are more important at larger I can also be seen from the greater skewness of the curves in Figure 4. As expected, the contribution to the volume by the cation–cation interaction decreases with the cationic size in the order of $Bu_4N^+ > Pr_4N^+ > Et_4N^+ > Me_4N^+ > Na^+$. It is to be noted that the values of $\Delta_m V^{ex}$ for Bu_4NX–KX and Pr_4NX–KX systems are relatively close to each other in contrast to the large differences found between Pr_4NX–KX and Et_4NX–KX as well as between Et_4NX–KX and Me_4NX–KX systems. These results seem to be related to the behavior of $\varphi_2 - \overline{V}_2^0$ *vs.* $\sqrt{c}$ shown in Figure 1 for R_4NX salts in the concentration region of $c = 0.5$–1.0 mole/l. As can be observed from Figure 1, the difference between Bu_4NX and Pr_4NX is relatively small when compared to the large differences between Pr_4NX and Et_4NX as well as between Et_4NX and Me_4NX. In other words, the mixing experiments gave results which are parallel to those of dilution experiments. Similar observation was made recently by Wood and Anderson[29] based on their heat of mixing and heat of dilution studies.

If the peculiar interaction of the large tetraalkylammonium ion with water is, in most part, due to the hydrophobic surface of the cation, the substitution of the terminal methyl groups of Pr_4N^+ with hydroxyl groups should drastically alter the nature of its interaction with water; $(HOC_2H_4)_4N^+$ ion is expected to prevent the "iceberg" formation of water molecules around it. With this expectation we have investigated the volume changes on mixing $(HOC_2H_4)_4NBr$ and KBr solutions at constant ionic strengths. The results obtained are given in Table V and the values of $\Delta_m V^{ex}$ at $I = 0.50$ are plotted against y in Figure 6 for comparison with other systems. These results are striking, since $\Delta_m V^{ex}$ is found to be zero to within our experimental errors at $I = 0.5$, 1.0, and 2.0. The ion seems to behave ideally in water and there is no contribution due to the cation–cation interaction. This finding is in agreement with the view expressed by Frank and Wen[2] that the solutes containing hydrogen-bonding groups like NH_2 or OH do not alter the water structure much, if at all. Our results are also consistent with the experimental findings on molal volumes by Wen and Saito,[27] conductance and viscosity by Kay, *et al.*,[28] heats of transport by Agar,[3] and heat capacities by Frank and Wen.[30]

Conclusion

When an aqueous tetraalkylammonium halide (R_4NX) solution is mixed with a potassium halide solution at 25°, a volume increment over and above the sum of the two solution volumes is observed. The molal excess volumes on mixing ($\Delta_m V^{ex}$) are found to be very large for the salts containing large tetraalkylammonium cations (Bu_4N^+ and Pr_4N^+). The main reasons for this large volume increase on mixing may be understood from the structural viewpoint of the solute–water interaction. The mixing at constant total ionic strengths will result in a partial elimination of the causes for the abnormally small volume of solution containing Bu_4NX or Pr_4NX. The solution volume before mixing

(29) R. H. Wood and H. L. Anderson, *J. Phys. Chem.*, **71**, 1871 (1967).

(30) In 1958, Frank and Wen found that $(HOC_2H_4)_4NBr$ in water gave almost no extra apparent molal heat capacity in sharp contrast to the large excess observed for $(C_4H_9)_4NBr$.[2]

is abnormally small in the concentration range under discussion owing to the overlap of the "hydration cospheres"[31] and also to the caging effect.[32]

If, now, a KX solution is mixed with an R_4NX solution, the concentration of R_4N^+ ion will decrease in spite of the fact that the total ionic strength is kept constant. The decrease of R_4N^+ ion concentration will, of course, diminish the cation–cation overlap and result in the increase of volume. The introduction of K^+ ions will disrupt the caging effect and cause the volume to increase.

The large volume increase of mixing Pr_4NX and KX solutions cannot be attributed entirely to the ion size difference between Pr_4N^+ and K^+ without consideration of the solvent structural changes. This becomes particularly obvious in view of the fact that the mixing of solutions of tetraethanolammonium bromide and potassium bromide gave zero value for $\Delta_m V^{ex}$, although the size of $(HOC_2H_4)_4N^+$ ion is about the same as that of Pr_4N^+ ion. The observation is explicable in terms of the ion–water interaction, since, in contrast to Pr_4N^+ ion, there is no "hydration cosphere" nor "cagelike structure" around the $(HOC_2H_4)_4N^+$ ion. In conclusion the present studies clearly indicate that the volume changes on mixing are strongly governed by the solvent structural properties of the ions.

Acknowledgments. We wish to thank Professor Harold L. Friedman for many valuable comments and suggestions. This research was supported by the U. S. Department of the Interior, Office of Saline Water, through Grant No. 14-01-0001-456.

(31) The overlap of "hydration cospheres" of the two cations will cause the decrease of the number of hydrogen bonds of water per cation and lead to the decrease of the solution volume, since less hydrogen bonding will result in smaller volume for water.

(32) The caging effect denotes the tendency of water molecules to form cagelike structure to "hide" the hydrocarbon tails of the R_4N^+ ion inside. When two cations approach to a suitable distance, their cage systems will tend to link up and stabilize each other, leading to a smaller total volume (see also ref 5 and 8).

The Spectra of Amides. Theoretical Considerations[1a]

by John A. Schellman and Eigil B. Nielsen[1b]

Chemistry Department, University of Oregon, Eugene, Oregon *(Received April 20, 1967)*

The first strong absorption band of the amide group or peptide link is interpreted as an intramolecular charge transfer in a highly simplified, semiempirical treatment. The effect of substitution and solvent on the position and integrated intensity of the bands is introduced *via* the ionization potential of the constituent amine group as a part of the charge-transfer energy. Agreement with experiment of the calculated transition moment vector (length and direction) is good. The resulting wave functions are used to calculate the matrix elements which are of importance in the theory of amide and peptide optical rotation.

The calculation of the contribution of a chromophore to the optical rotation of a molecule usually requires more information about its electronic transitions than is available from conventional spectroscopy, which normally supplies only the energy of the excited states and the magnitudes of the electric transition dipole moments. For optical rotation caused by interband[2a] or intraband[2b] coupling among the chromophores, the direction of the transition moments must be known as well. In such calculations it is frequently necessary

to treat the transition moments as distributed charges (transition monopoles[3]) rather than as point dipoles because the size of the charge distributions is commensurate with the distance between them. This requires information concerning the wave functions of the ground and excited states.

If the optical rotation arises from static perturbations of the chromophore,[4a] unusual spectroscopic quantities such as transition magnetic moments and transition quadrupole moments enter into the theory. Since these are not ordinarily susceptible to direct observation,[4b,5] recourse must be made to calculation on the basis of assumed wave functions.

The electronic structure and spectrum of the amide groups has been the subject of a number of investigations.[6-13] In general, it is found with structures containing heteroatoms that semiempirical methods produce better agreement with experiment, especially with regard to more subtle features such as the direction of transition moments. In the case of amides there is a particularly fortunate array of experimental facts with which to test a model of electronic structure. There are (1) the position of the π,π^* band and of the n,π^* band in a variety of derivatives, (2) the direction and magnitude of the transition dipole of the π,π^* transition,[7] and (3) the direction and magnitude of the permanent dipole moment.[11]

The Two-Transition Model

The excited states on which experimental work is normally focused are the n,π^* transition (210–230 mμ) and the π,π^* transition (175–200 mμ). The variations represent a systematic dependence on solvent and substitution.[12] We first develop a discussion which considers only these two excited states. We shall see in the next section that the addition of another state does not materially change the general results. The treatment may either be regarded as a simplification of the treatment of Nagakura[13] and of Longuet-Higgins and Murrell[14] in which locally excited states are left out or as a transposition of the "method of structures" of Simpson and Rosa[10] into the language of molecular orbital theory. The basis functions for the calculation are

$$|A\rangle = (6!)^{-1/2}|N\bar{N}\pi\bar{\pi}n\bar{n}|$$

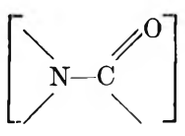

corresponding to a trigonal amine adjacent to a carbonyl group (see ref 13 for a discussion of the physical model associated with the basis functions). N, π, and n refer, respectively, to the $2P_z$ orbital of the N atom, the π_x orbital of C=O, and the nonbonding orbital of C=O which has $y = 0$ as a nodal plane (Figure 1).

$$|B\rangle = [(2)(6!)]^{-1/2}\{|\pi^*\bar{N}\pi\bar{\pi}n\bar{n}| + |N\bar{\pi}^*\pi\bar{\pi}n\bar{n}|\}$$

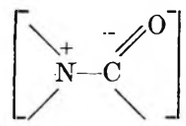

corresponding to the singlet charge-transfer state and

$$|D\rangle = [(2)(6!)]^{-1/2}\{|N\bar{N}\pi\bar{\pi}\pi^*\bar{n}| + |N\bar{N}\pi\bar{\pi}n\bar{\pi}^*|\}$$

corresponding to the locally excited singlet n,π^* state of C=O. Note that in this treatment $|B\rangle$ is not the usual valence bond resonance structure.[13]

$|A\rangle$ and $|B\rangle$ are of A′ symmetry and combine in the diagonalization of the amide Hamiltonian.[15,16] $|D\rangle$ is of A″ symmetry and does not combine with $|A\rangle$ or $|B\rangle$ in the absence of perturbations external to the amide group. Setting the energy of $|A\rangle$ equal to zero, the secular equation becomes

$$\begin{vmatrix} -E & H_{AB} \\ H_{AB} & E_B - E \end{vmatrix} = 0$$

with solutions

$$E = \frac{E_B \pm \sqrt{E_B^2 + 4H_{AB}^2}}{2}$$

(1) (a) This research was supported by grants from the National Institutes of Health (Cancer Institute CA-4216) and the National Science Foundation; (b) Research Laboratory, Tuborg Breweries Ltd., Hellerup, Copenhagen, Denmark.

(2) (a) J. G. Kirkwood, *J. Chem. Phys.*, **5**, 479 (1937); (b) W. Moffitt, *ibid.*, **25**, 467 (1956).

(3) F. London, *J. Phys. Chem.*, **46**, 305 (1942).

(4) (a) E. U. Condon, W. Altar, and H. Eyring, *J. Chem. Phys.*, **5**, 753 (1937); (b) a magnetic dipole transition in formaldehydes has been observed recently.[5]

(5) J. H. Callomon and K. K. Innes, *J. Mol. Spectry.*, **10**, 166 (1963).

(6) J. S. Ham and J. R. Platt, *J. Chem. Phys.*, **20**, 335 (1952).

(7) D. L. Peterson and W. T. Simpson, *J. Am. Chem. Soc.*, **79**, 2375 (1957).

(8) S. Nagakura, *Bull. Chem. Soc. Japan*, **25**, 164 (1952).

(9) M. Suard-Sender, *J. Chim. Phys.*, **62**, 79 (1965).

(10) E. J. Rosa and W. T. Simpson, "Physical Processes in Radiation Biology," L. Augenstein, P. Mason, and B. Rosenberg, Ed., Academic Press Inc., New York, N. Y., 1964.

(11) R. Kurland and E. B. Wilson, *J. Chem. Phys.*, **27**, 585 (1957).

(12) E. B. Nielsen and J. A. Schellman, *J. Phys. Chem.*, **71**, 2297 (1967).

(13) S. Nagakura, *J. Mol. Phys.*, **3**, 105 (1960).

(14) H. C. Longuet-Higgins and J. N. Murrell, *Proc. Phys. Soc.* (London), **A68**, 601 (1955).

(15) This analysis implies that $|A\rangle$ and $|B\rangle$ are orthogonal. If the one-electron functions are linear combinations of atomic orbitals, they fail to be so by a first-order overlap correction. Orthogonality would be obtained by the use of orthoganilized atomic orbitals.[16] The valence bond functions of Rosa and Simpson[10] are orthogonal to a second-order overlap correction.

(16) P.-O. Löwdin, *J. Chem. Phys.*, **18**, 365 (1950).

Defining θ by

$$\tan \theta = 2H_{AB}/E_B$$

we have

$$E = (E_B/2)(1 \pm \sec \theta)$$

Symbolizing the ground state by $|0\rangle$, the excited state by $|\beta\rangle$, and the n,π^* state by $|\alpha\rangle$, we have in summary

$$|0\rangle = \cos \theta/2|A\rangle - \sin \theta/2|B\rangle$$

$$E_0 = (E_B/2)(1 - \sec \theta)$$

$$|\beta\rangle = \sin \theta/2|A\rangle + \cos \theta/2|B\rangle$$

$$E_\beta = (E_B/2)(1 + \sec \theta)$$

$$|\alpha\rangle = |D\rangle$$

$$E_\alpha = E_D$$

where E_D is the excitation energy of the n,π^* state of the C=O group. The energy relationship of these states is shown in Figure 2.

H_{AB} may be evaluated by the Pariser–Parr procedure. This has been done by Nagakura.[13] Alternatively, the off-diagonal element associated with valence bond structures has been estimated from spectral data.[10] The disparity between the resulting values (23.9 and 20.3 kK, respectively) is not serious and a mean value of 22 kK will be selected.

In the evaluation of E_B, the terms which survive the Pariser–Parr approximations are entirely electrostatic

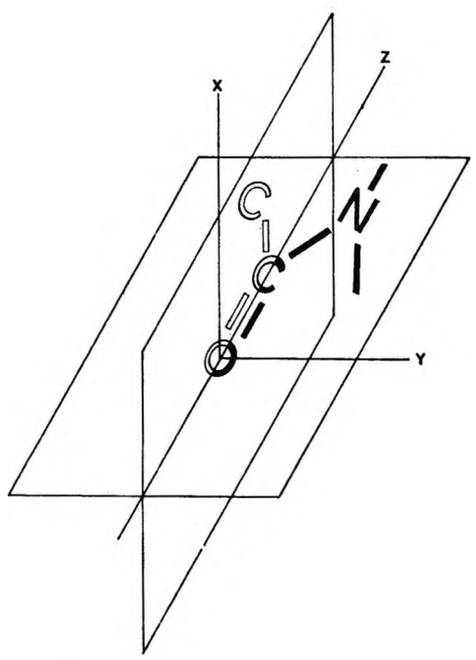

Figure 1. The coordinate system for the amide group.

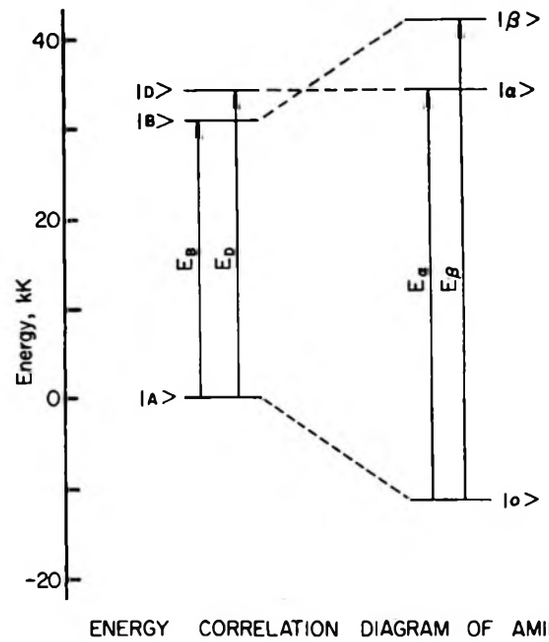

ENERGY CORRELATION DIAGRAM OF AMIDE

Figure 2. Energy correlation diagram for the amide group; compare ref 10. Numerical values selected are those appropriate for N-ethylacetamide in a nonpolar solvent. See text for definitions of the energy symbols.

and have a simple interpretation. E_B consists of the energy required to remove an electron from the nitrogen atom to infinity (the ionization potential of the amine plus the charge–dipole interaction of the electron with the polar C=O group) plus the energy of its return to the C=O group (the electron affinity of C=O plus the charge–charge interaction of the electron with the N atom which now possesses a positive charge). Thus

$$E_B = I - A + \text{electrostatic terms}$$

where I is the ionization potential of the amine, A is the electron affinity of the carbonyl group, and the other electrostatic terms are lumped together in the last term. Both I and A depend on the substituents and solvation of the respective groups. The ionization potentials of a number of substituted amines have been determined by Watanabe and Mottl.[17] Some of their results converted to units of kilokaisers are shown in Table I. As a satisfactory reference substance for the amide R_1-$(R_2)NC(=O)$ we select the amine $R_1(R_2)NCH_3$. The ionization potentials of mixed amines are estimated by interpolation between the values for the symmetrical amines.[18]

(17) K. Watanabe and J. R. Mottl, *J. Chem. Phys.*, 26, 1773 (1957).

(18) For the present calculation we require, in fact, the vertical ionization potential of a trigonal amine and not the standard ionization potential. As will be seen shortly, an empirical parameter

Table I: Ionization Potentials of Amines

Amine	R	Ionization, ev	Potential, kK
NH_3		10.154	81.84
RNH_2	Me	8.97	72.3
	Et	8.86	71.4
	Pr	8.78	70.8
	i-Pr	8.72	70.3
	Bu	8.71	70.2
R_2NH	Me	8.24	66.4
	Et	8.01	64.6
	Pr	7.84	63.2
	i-Pr	7.73	62.3
	Bu	7.69	62.0
R_3N	Me	7.82	63.0
	Et	7.50	60.4
	Pr	7.23	58.3

The electron affinity of the carbonyl group is unknown and may even be negative.[13] This forces the introduction of an empirical parameter into the calculations, into which we might as well incorporate the rest of the electrostatic terms, writing $E_B = I + P$, where P is determined by fitting the spectrum of one amide in the series. The others of the series are then determined by the variation of I. The energy of the π,π^* transition is given by

$$E_{\pi\pi^*} = E_\beta - E_0 = E_B \sec\theta = 2H_{AB}/\sin\theta$$

where the dependence on ionization potential is contained in $\sin\theta$. Inverting this equation

$$\lambda_{\pi\pi^*} = (\lambda_{H_{AB}}/2)\sin\theta = 227\sin\theta\ (m\mu)$$

where $\lambda_{H_{AB}}$ is the wavelength associated with the energy H_{AB}. The value of 22 kK has been substituted in the final form.

Figure 3 shows the result of applying this formula to a number of amides of acetic acid in cyclohexane solution. The smooth curve results from assigning to P the value of -35.7 kK. The experimental points compare the spectral data of ref 12 with the interpolated ionization potential data of Watanabe and Mottl. The correlation between the two experimental quantities is unmistakable. The fact that the experimental plot of I and $\lambda_{\pi\pi^*}$ does not really form a smooth curve could arise either from the oversimplifications of the theory or from the fact that the experimental ionization potentials are not quite the appropriate quantities to be used in the comparison.

Though experimental evidence is more sparse concerning the absorption properties of the amides of

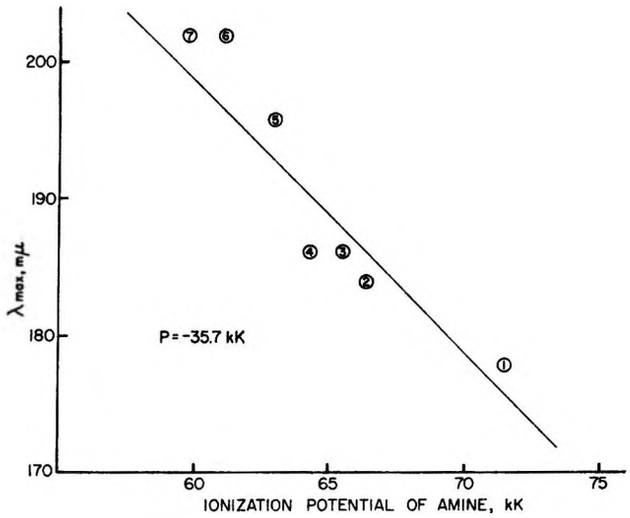

Figure 3. λ_{max} *vs.* the ionization potential of the constituent amine for a series of amides of acetic acid: 1, acetamide; 2, N-methylacetamide; 3, N-ethylacetamide; 4, N-butylacetamide; 5, N,N-dimethylacetamide; 6, N,N-diethylacetamide; 7, N,N-dipropylacetamide. The solvent is cyclohexane. The absorption maximum for acetamide is an estimate.[12]

formic acid, propionic acid, etc., it can be inferred from the available data that the appropriate value of P varies from one series to another. In the context of the present discussion, this would be expected to arise from the effect of substitution on the electron affinity A. The substitution of CH_3 for H (acetic for formic acid) produces the most profound changes, as would be expected. For the few comparisons which can be made,[12] an increased electron affinity in formic acid derivatives is required to account for the spectral changes which are observed.

There are also significant shifts with solvent. Since the excited state of the π,π^* transition is more polar than the ground state, the energy of the absorption will depend on the polarity and polarizability of the solvent, in accordance with the considerations of Bayliss and McRae.[19] When amides are transferred from a completely nonpolar solvent to water, there is a large red shift for primary amides, a smaller red shift for sec-

enters the evaluation of E_B. As a result, only the differences in ionization potential of the various amines is of significance in the calculations. In utilizing the standard ionization potentials, we are therefore not identifying these ionization potentials but making the less drastic assumption that the difference in ionization potentials between two amines is not changed when they are transformed to the virtual trigonal form used in constructing $|A\rangle$ and $|B\rangle$. There is a further difficulty in that electron impact ionization potentials diverge from those determined by photoionization as substitution is increased. This is discussed by Watanabe and Mottl.

(19) N. S. Bayliss and E. G. McRae, *J. Chem. Phys.*, **58**, 1002 (1954).

ondary amides, and a blue shift for tertiary amides. The red shifts evidently arise from the hydrogen bonding of the amine hydrogen atoms with the polar solvent. This lowers the effective ionization potential, leading to a lower transition energy by the discussion given above. With tertiary amides, the nitrogen atom is evidently insulated from direct polar contact with solvent by the substituent groups, and polarizability, rather than polarity, plays the dominant role. In this case the less polarizable water produces a blue shift. Hydrogen bonding to the carbonyl group does not appear to be very effective in producing shifts in the π,π^* transition.

Transition Moments of the π,π^* and the n,π^* Transitions. For the estimation of spectral properties we require the matrix elements for a one-electron operator f among the various states. f represents the electric moment, magnetic moment, transition density, quadrupole moment, etc. For the π,π^* transition we have, utilizing the expressions for $|0\rangle$ and $|\beta\rangle$ and the formulas for reducing determinantal matrix elements

$$\begin{aligned}\langle 0|f|\beta\rangle &= -\frac{\sin\theta}{2}\{\langle B|f|B\rangle - \langle A|f|A\rangle\} + \cos\theta\langle A|f|B\rangle \\ &= -\frac{\sin\theta}{2}\{\langle B|f|B\rangle - \langle A|f|A\rangle\} + \sqrt{2}\cos\theta\,\langle N|f|\pi^*\rangle \\ &\cong -\frac{\sin\theta}{2}\{\langle B|f|B\rangle - \langle A|f|A\rangle\}\end{aligned}$$

The term in $\langle N|f|\pi^*\rangle$ has been dropped by the approximation of zero differential overlap. Hansen has recently examined the circumstances under which this approximation is applicable to the evaluation of various one-electron operators.[20] We have, in fact, evaluated all the correction terms which are eliminated by this approximation and have found them to be small. They almost invariably tend to improve the results slightly (*e.g.*, the direction of the transition moment of the π,π^* transition), but it would be hard to justify adorning so crude a theory with arbitrary refinements. Applied to the electric transition moment, we have

$$\vec{\mu}_{\pi\pi^*} = -\frac{\sin\theta}{2}\vec{\mu}_{ct}$$

where $\vec{\mu}_{ct}$ is the charge-transfer moment, *i.e.*, the moment which is generated by moving an electron from the N atom to a π^* orbital. The dipole strength is given by

$$D = (\vec{\mu}_{\pi\pi^*})^2 = \frac{\sin^2\theta}{4}(\vec{\mu}_{ct})^2$$

The other matrix elements are

$$\begin{aligned}\langle\alpha|f|0\rangle &= \cos\theta/2\langle D|f|A\rangle - \sin\theta/2\langle D|f|B\rangle \\ &= \sqrt{2}\cos\theta/2\langle\pi^*|f|n\rangle + \sin\theta/2\langle N|f|n\rangle \\ &\cong \sqrt{2}\cos\theta/2\langle\pi^*|f|n\rangle \\ \langle\alpha|f|\beta\rangle &= \sin\theta/2\langle D|f|A\rangle + \cos\theta/2\langle D|f|B\rangle \\ &= \sqrt{2}\sin\theta/2\langle\pi^*|f|n\rangle - \cos\theta/2\langle N|f|n\rangle \\ &\cong \sqrt{2}\sin\theta/2\langle\pi^*|f|n\rangle\end{aligned}$$

Further progress requires the assumption of specific forms for the orbitals: π, π^*, N, and n. We select the carbonyl orbitals of Hansen[21] which have been derived using the Pariser–Parr–Pople procedures and permit a realistic discussion of the n,π^* transition. In particular, the n orbital is not localized on the oxygen atom as is often assumed, but extends to the antisymmetric combination of σ orbitals which link the carbonyl group to two other atoms. The coefficients of these orbitals are given in Table II.

Table II: Carbonyl Wave Functions

	Coefficients			
Symbol	$2P_z(O)$	$2P_z(C)$	$2P_y(O)$	X_y[a](C)
n	...	...	0.775	−0.631
π	0.879	0.478	...	...
π^*	0.478	−0.879	...	...

[a] X_y is the combination of σ bonding orbitals (sp^2 hybrids linked to atoms adjacent to C=O) which is antisymmetric in y (Figure 1). Hansen approximates this united orbital as a $2P_y$ orbital of carbon.

With this assumption of wave functions, the calculation of matrix elements is a straightforward matter. The electric transition moment is seen to be always parallel to $\vec{\mu}_{ct}$, which is determined by the mean position of an electron in the π^* orbital of the carbonyl group relative to the N nucleus. The angle between the calculated transition moment and the line connecting the O and N atoms is 17°. The observed angle in myristamide crystals is 9°.[7] It is also seen that the magnitude of the transition moment depends on the parameter θ, which in turn depends on the degree and nature of the substitution. Taking average values of θ for primary, secondary, and tertiary amides, we predict transition moments of 2.8, 3.0, and 3.1 D., respectively. The ob-

(20) A. Hansen, *Theoret. Chim. Acta*, 6, 341 (1966).

(21) A. Hansen, Ph.D. Thesis, University of Copenhagen, 1965. The orbitals used in Table II are a revised version which was kindly made available to us.

served values in water are 2.8, 3.3, and 3.5 D., respectively.[12] The transition dipole for primary amides in a nonpolar solvent has not been measured, but for secondary and tertiary amides the values are 2.8 and 3.0 D., respectively. Quantitatively, the agreement is quite satisfactory, but more important is the correct prediction of the qualitative features of the data. Increasing the degree of substitution on the amine decreases the effective ionization potential and therefore increases $\sin\theta$ and $\vec{\mu}_{\pi\pi^*}$ as is observed experimentally.[22-24]

The magnetic moment of the n,π^* transition is given by

$$\langle\alpha|\vec{m}|0\rangle = \sqrt{2}\cos\theta/2\langle\pi^*|\vec{m}|\mathrm{n}\rangle$$

Utilizing the coefficients for the n and π^* orbitals, this becomes

$$\langle\alpha|\vec{m}|0\rangle = i\sqrt{2}\cos\theta/2(0.925)\beta\vec{k}$$

where β is the Bohr magneton and $\vec{k}$ designates the positive z direction (Figure 1). θ is always determinable by the relation $\sin\theta = \lambda_{\mathrm{obsd}}/227\ \mathrm{m}\mu$, where $\lambda_{\mathrm{obsd}} = \lambda_{\pi\pi^*}$ in mμ.

In calculations of optical rotation by the Condon mechanism, one is required to evaluate either the quadrupole moment or the electronic transition density associated with the n,π^* transition. It is current practice to represent transition densities as point charges evaluated by the London method of integrating separately over regions between nodal surfaces of $\psi_i\psi_j$, where ψ_i and ψ_j are one-electron wave functions associated with the initial and final states. In each of these regions α is assigned a charge

$$\rho_a = e\int_\alpha \psi_i\psi_j d\tau$$

which is located at

$$\vec{R}_\alpha = \frac{\int_\alpha \psi_i\vec{R}\psi_j d\tau}{\int_\alpha \psi_i\psi_j d\tau}$$

In the case of an n,π^* transition, the appropriate nodal boundaries are the planes $x = 0$ and $y = 0$. $\langle\alpha|f|\beta\rangle$ is required for the Condon, Altar, and Eyring mechanism of optical rotation and $\langle\alpha|f|0\rangle$ for a dipole-quadrupole coupling mechanism. We have

$$\langle\alpha|\vec{R}|0\rangle_{x,y>0} = \sqrt{2}\cos\theta/2\langle\pi^*|\vec{R}|\mathrm{n}\rangle_{x,y>0} \cong \sqrt{2}\cos\theta/2[0.555\langle 2\mathrm{P}_{x\mathrm{C}}|\vec{R}|\chi_{\mathrm{C}}\rangle_{x,y>0} + 0.370\langle 2\mathrm{P}_{x\mathrm{O}}|\vec{R}|2\mathrm{P}_{y\mathrm{O}}\rangle_{x,y>0}]$$

The two integrals suggest a representation by two charges, one associated with the carbon atom and the other with the oxygen atom. The magnitudes of the charges are given by $(\sqrt{2}e/2\pi)\cos\theta/2$ multiplied by 0.555 and 0.370, respectively. Since Slater orbitals are known to give a poor representation of wave functions close to the nucleus and such regions dominate in the quadrupole integrals, we have used self-consistent Hartree–Fock orbitals to locate the monopoles on the oxygen atom. The first-quadrant monopole is located at $x,y = 0.44$ A. The equivalent calculation for the carbon monopole would not be meaningful, since we are using a $2\mathrm{P}_y$ orbital as a crude representation of the antisymmetric combination of σ orbitals. (In our work on the theory of amide Cotton effects we arbitrarily use the same x,y coordinates as for the O atom.) The other six charges are found by the quadrupole symmetry of the distribution about the z axis. The net result is a pair of quadrupole charge distributions about the C and O atoms of the same sign (in a given quadrant) but of different magnitudes. Had there been a reversal in sign, an octant rather than a quadrant rule would be appropriate for the n,π^* Cotton effects of the amide group.

The transition monopoles associated with $\beta \rightarrow \alpha$ have identical positions. The charges may be found by substituting $\sin\theta/2$ rather than $\cos\theta/2$ in the above expressions.

The Charge-Transfer Model of Nagakura

In his treatment of the electronic structure of formamide Nagakura[13] introduced an additional configuration, the locally excited state, which in our notation is given by

$$|\mathrm{C}\rangle = [(2)(6!)]^{-1/2}\{|\mathrm{N}\bar{\mathrm{N}}\pi\bar{\pi}^*\mathrm{n}\bar{\mathrm{n}}| + |\mathrm{N}\bar{\mathrm{N}}\pi^*\bar{\pi}\mathrm{n}\bar{\mathrm{n}}|\}$$

This electronic configuration is of A′ symmetry and mixes with $|\mathrm{A}\rangle$ and $|\mathrm{B}\rangle$ to give a 3×3 secular equation. The energy of this state is assumed to be the π,π^*

(22) Prior to utilizing the wave functions of Hansen for the C=O group for this calculation, we used those of Sidman.[23] The agreement of the direction of the π,π^* transition moment was better than reported above. In this case the transition moments tended to have slightly larger values than are observed. The difference lies in the polarity of the π and π^* orbitals. Hansen worked with an eight-electron problem and to keep his calculations both tractable and self-consistent he assumed no polarity in the σ bonding system. The result is that the entire dipole moment of the C=O group is vested in the π electrons. Sidman is explicitly critical of π electrons which are so strongly polar,[23] but his discussion does not permit a self-consistent discussion of the n,π^* transition. There still exists a need for a better treatment of so simple a group as the carbonyl. Parks and Parr have performed extensive calculations on the formaldehyde molecule in which specific attention is given to the polarity and to changes in polarity of the σ system.[24] This treatment demonstrates the complexity of the problem. The results are primarily concerned with the evaluation of energy parameters and would be very difficult to use in the present context.

(23) J. W. Sidman, *J. Chem. Phys.*, **27**, 429 (1957).

(24) J. M. Parks and R. G. Parr, *ibid.*, **32**, 1657 (1960).

excitation energy of the carbonyl group and the additional off-diagonal elements have been estimated by Nagakura.

Our initial approach to the problem consisted in a somewhat expanded version of Nagakura's calculations. E_B was taken to be a parameter which varied with substitution and solvation of the amide as in the previous section; Sidman and Hansen's wave functions for the carbonyl group were used rather than those of Kon;[25] six electrons rather than four were used to describe the electronic configurations so that the n,π^* transition and its matrix elements could be considered. We shall not give the details of these calculations, since with regard to agreement with experimental results nothing seems to be gained by the inclusion of the additional state. The direction of the transition moment is changed but not significantly improved. The angle which the transition moment makes with the O–N direction is predicted to be 3°, which is to be compared with the experimental value of 9° and the value of 17° obtained in the previous section. This constitutes an improvement of 2°, which is not significant, since the experimental value itself has a possible error of about 10°. The principal reason for the difference in direction of the transition moment between the two theories results from the presence of a considerable admixture of state C in the π,π^* excited state of the amide. This introduces the C=O transition moment, thereby turning the total transition moment toward the oxygen atom. An additional effect of this admixture is an increase in the predicted magnitude of the transition moment which is in the neighborhood of 4.0 D. for primary, secondary, and tertiary amides and greater than the experimental values. Predictions of the correlation of the transition energy with the ionization potential of the amine are as good with this model as with the simpler model, but the correlation of intensity with substitution disappears entirely. As a consequence, there is no practical reason for preferring the more complex model, which does not lead to simple formulas for the energies and matrix elements of the transitions.

The three-configuration model permits an investigation of the variation of the amide π,π^* transition moment direction with substitution. This is not possible with the two-configuration model, since the transition moment is forced by the assumptions to coincide in direction with $\vec{\mu}_{ct}$. The direction of this transition moment has been determined for a primary amide[7] and the results are assumed to be correct in discussions of the α and collagen helices where secondary and tertiary amides are prevalent. We investigated the variation of the direction of the transition moment as a function of E_B over the values of this parameter appropriate for primary, secondary, and tertiary amides and found that it did not vary more than 1°. This calculation is reassuring but has validity only in the framework of the model. It shows only that the inclusion of a potential source of variation of the transition moment (the locally excited state) does not lead to significant changes.

Discussion

If an empirical configuration interaction calculation involving only two electronic configurations gives good results for both the ground and an excited state, it must mean that the initial configurations which have been selected are associated with relevant empirical parameters, unless agreement with experiment is fortuitous. The latter is unlikely in the present instance. The correlation of the positions of absorption bands with the ionization potential of the constituent amines is easily seen on a qualitative level and indicates that an electron configuration involving separation of an electron from the nitrogen atom should at least be an important part of the description of the states. Once this trend is granted, the agreement between calculated and observed energies for the transition is not especially significant, since the basis for the selection of the parameter P was that it moves the progression of predicted energies into agreement with the observed progression. What is significant is that the selected value of the parameter simultaneously establishes good agreement with the experimentally determined dipole strengths. This indicates that the main features of the π,π^* transition of amides are representable by an intramolecular charge transfer as previously proposed by Nagakura[13] and by Simpson and Rosa.[10]

A complete calculation would have to include many other configurations. Four excited states of the C=O group have now been observed and have been assigned by Johnson and Simpson[26] as n $\rightarrow \pi^*$, n $\rightarrow \sigma^*$, n $\rightarrow \sigma'^*$, and $\pi \rightarrow \pi^*$, in order of increasing energy. When incorporated in an amide group, the first is of A'' symmetry and cannot combine with the A' states. The $\pi \rightarrow \pi^*$ transition was included by Nagakura as discussed in the previous section. The n $\rightarrow \sigma^*$ states are of A' symmetry but arise from the wrong symmetry species (B_2) in the parent carbonyl group. This results in a much lower interaction with A' in the amide group. This indicates that the mixing with the n $\rightarrow \sigma^*$ state would be considerably smaller than the states selected by Nagakura in his treatment. Consequently, an extension of the calculations would require the use of a number of hypothetical configurations such as $|B\rangle$ and

(25) H. Kon, *Bull. Chem. Soc. Japan*, 28, 275 (1955).

(26) C. Johnson, Ph.D. Thesis, University of Washington, 1966.

deprive the method of its extensive use of empirical data.

It was the latter consideration which caused us to represent the n $\rightarrow \pi^*$ state as a single configuration. To be consistent, we should have included a charge-transfer state with A'' symmetry. This state would involve double occupation of the π^* orbital of C=O. However, the present state of information concerning the n orbital is sufficiently crude that such refinements would not have real significance. The use of an n orbital which preserves its antisymmetry in y is one deficiency; the uncertainty in the extent of delocalization of the n orbital is another. It is likely that a large fraction of the absorption intensity of the n,π^* transition of the amide group results from the distortion of the n orbital by the N atom.[27,28] It must be concluded that we are still a rather long way from a complete understanding of the n,π^* transition of the amide. With regard to the prediction of n,π^* Cotton effects, there is at least a practical consolation. We have used a number of different theoretical approaches including self-consistent molecular orbitals and a wide variety of proposed wave functions. Although quantitatively predicted results vary by a factor of about 4, the qualitative predictions of signs and orders of magnitudes of rotatory strengths generally remain the same.

Acknowledgment. We are grateful to W. T. Simpson for stimulating discussions and for pointing out the orthogonality problem associated with the basis functions.

(27) If the n orbital of the carbonyl group is localized on the O atom, the n,π^* transition is "locally forbidden" in the sense discussed by Platt.[28] If, on the other hand, it is delocalized into the σ system of the amide, this is no longer the case.

(28) J. R. Platt, *J. Chem. Phys.*, **18**, 1168 (1950).

Exciton Bands in Disordered Molecular Crystals

by R. E. Salomon

Department of Chemistry, Temple University of the Commonwealth System of Higher Education, Philadelphia, Pennsylvania *(Received April 27, 1967)*

A theory of exciton bands in disordered molecular crystals is described. The treatment is based on the use of pseudo-Bloch functions which diagonalize the secular equation in the average and with negligible deviations in the infinite crystal limit. A quadratic dependence of the exciton band edge on mole fraction is predicted.

Introduction

A number of molecular solid solutions can be formed over the entire range of composition without any accompanying phase change and with only minor change in lattice dimensions. The electronic spectra of these systems may be used to obtain information about the intermolecular interactions between host and guest molecules. A theoretical analysis is needed for this purpose as well as for the tailoring of alloy compositions to achieve specific spectral results such as the adjustment of spectral peaks at desired wavelengths.

A theoretical treatment of ordered molecular crystals, using a Green's function technique, has recently been reported[1] although the disordered system, which is the one most likely to be encountered in the laboratory, has not been subjected to the same level of analysis. The elucidation of the electronic structure of a disordered solid solution is complicated by the fact that the crystal Hamiltonian is not invariant to the space group operations.

(1) D. P. Craig and M. R. Philpott, *Proc. Roy. Soc.* (London), **A290**, 583 (1966).

The nature of the energy bands in disordered metallic alloys has received a considerable amount of attention.[2-15] Unfortunately the results of these investigations cannot be directly carried over to the present problem for the following reason. The usual starting point in discussions of the disordered metallic alloy is an assumed one-electron random potential. The one-electron eigenstates and eigenfunctions are found using some approximate method and then the building-up principle is applied. Thus the effects of composition on spectra in metallic alloys is due to a change in potential and in some cases to a change in the number of electrons in a band. The work in this area is divided into approximate specific methods[2-11] and exact methods which provide some general theorems against which these approximate treatments can be tested.[2-14] The latter is exhaustively treated in a recent review.[15]

In the case of molecular solids and molecular solid solutions this nearly free electron approach is known to be unrealistic and unwarranted. This is because the free molecule wave functions are rather good basis functions with which to build crystal orbitals. This in turn is related to the weakness of the intermolecular interactions.

The exciton problem in pure molecular crystals is described elsewhere.[16] The approach is based on the formation of Bloch functions using localized excitation functions which themselves are products of free molecule wave functions. In this manner, the secular equation is diagonalized (at least in the case in which there is only one molecule per unit cell) and the roots are the diagonal matrix elements.

If Bloch sums are formed for solid solutions in which explicit account is taken of the different free molecule wave functions for the two species, then there is no group theoretical argument which will guarantee that the secular equation will be diagonalized. In the following, an argument will be presented to demonstrate that this approach does, in the infinite crystal, lead to a diagonal matrix whose roots approach those of the secular equation.

The Model

For purposes of simplicity the argument is restricted to a one-dimensional, random, binary (A–B) alloy, in the rigid-lattice and nearest-neighbor interaction approximation. It is also assumed that there is only one molecule per unit cell. The Hamiltonian H of the crystal may be written

$$H = \sum_{i=1}^{N} H_i + \sum_r V_{r,r+1} = H_0 + V \qquad (1)$$

where H_i is the free A molecule Hamiltonian or the free B molecule Hamiltonian according as site i is occupied by an A or B molecule. In a similar manner it is to be understood that $V_{r,r+1}$ is the interaction potential between an A or B molecule on site r and an A or B molecule on site $r + 1$ according to the manner in which sites r and $r + 1$ are occupied. The interaction potential operators are V_{AA}, V_{AB}, and V_{BB}. Continuing in this manner we let ϕ_i be the ground-state wave function and ϕ_i^s be the excited-state wave function for free A and B molecules according to whether site i is occupied by A or B [$\phi_i(A)$, $\phi_i(B)$, $\phi_i^s(A)$, or $\phi_i^s(B)$].

The corresponding energies are ϵ_A, ϵ_A^s, ϵ_B, and ϵ_B^s. The ϕ's are taken to be real and orthonormal. We define Θ_l, the localized, excitation function, by the relation

$$\Theta_l = \phi_1\phi_2 \ldots \phi_l^s \ldots \phi_N \qquad (2)$$

The orthonormal pseudo-Bloch functions $\Phi(k)$ are defined by the relation

$$\Phi(k) = \frac{1}{\sqrt{N}} \sum_{l=1}^{N} \Theta_l \exp(2\pi ikl/N) \qquad (3)$$

where k is the wave vector.

Because the expectation value of the energy depends on the crystal configuration, which is assumed to be random, we make the approximation that its value in any state is the ensemble average (denoted by a bar) over representative crystals. This approximation will be justified later by an analysis of the fluctuation and an appeal to the fact that the observed spectra do not vary erratically from sample to sample.

Since we are ultimately to be concerned with spectroscopic transitions, we shall express the energy relative to the ground state which has a wave function $\Psi^0 = \phi_1\phi_2 \ldots \phi_N$. The ensemble average of the ground-state energy, E_0, is

(2) E. A. Stern, *Phys. Rev.*, **144**, 143 (1966).
(3) R. H. Parmenter, *ibid.*, **97**, 587 (1954).
(4) R. H. Parmenter, *ibid.*, **99**, 1759 (1955).
(5) R. H. Parmenter, *ibid.*, **104**, 22 (1956).
(6) J. L. Beeby, *ibid.*, **135**, A130 (1964).
(7) J. Friedel, *Advan. Phys.*, **3**, 446 (1954).
(8) J. Korringa, *J. Phys. Chem. Solids*, **7**, 252 (1958).
(9) J. S. Faulkner and J. Korringa, *Phys. Rev.*, **122**, 390 (1961).
(10) J. Des Cloizeaux, *ibid.*, **139**, 1531 (1965).
(11) H. M. James, *ibid.*, **76**, 1611 (1949).
(12) H. M. James and A. Ginzbarg, *J. Phys. Chem.*, **57**, 840 (1953).
(13) P. L. Taylor, *Proc. Phys. Soc.* (London), **90**, 233 (1967).
(14) E. H. Kerner, *ibid.*, **A69**, 234 (1956).
(15) *Progr. Theoret. Phys. Suppl.*, **36**, 3 (1966).
(16) D. P. Craig and S. H. Walmsley, "Chemistry and Physics of the Organic Solid State," Interscience Publishers, Inc., New York, N. Y., 1963, p 586.

$$\overline{E_0} = N(m_A\epsilon_A + m_B\epsilon_B + m_A^2F_{AA} + 2m_Am_BF_{AB} + m_B^2F_{BB}) \quad (4)$$

where m_A and m_B are mole fractions of A and B and $\langle\phi_r\phi_{r+1}|V_{r,r+1}|\phi_r\phi_{r+1}\rangle = F_{AA}$, F_{AB}, or F_{BB} according to the manner in which sites r and $r+1$ are occupied. The N pseudo-Bloch functions, $\Phi(k)$, lead, according to the variation theorem, to the usual secular equation. The ensemble average diagonal elements, $\overline{H_{kk}}$, are

$$\overline{H_{kk}} = \overline{\langle\Phi(k)|H - E_0|\Phi(k)\rangle} = \zeta + \Delta_F + \Delta_G[\exp(2\pi ik/N) + \exp(-2\pi ik/N)] \quad (5)$$

where

$$\zeta = (\epsilon_A^s - \epsilon_A)m_A + (\epsilon_B^s - \epsilon_B)m_B$$

$$\Delta_F = 2m_A[m_A(F_{AA}^s - F_{AA}) + m_B(F_{AB}^s - F_{AB})] + 2m_B[(m_A(F_{BA}^s - F_{BA}) + m_B(F_{BB}^s - F_{BB})] \quad (6)$$

$$\Delta_G = m_A^2G_{AA} + 2m_Am_BG_{AB} + m_B^2G_{BB}$$

$\langle\phi_r^s\phi_{r+1}|V_{r,r+1}|\phi_r^s\phi_{r+1}\rangle = F_{AA}^s$, F_{AB}^s, F_{BA}^s, or F_{BB}^s, as sites r and $r+1$ are occupied by A's or B's, accordingly. $\langle\phi_r^s\phi_{r+1}|V_{r,r+1}|\phi_r\phi_{r+1}^s\rangle = G_{AA}$, G_{AB}, or G_{BB}, as sites r and $r+1$ are occupied by A's or B's, accordingly.

The off-diagonal elements $H_{kk'} = \langle\Phi(k)|H - E_0|\Phi(k')\rangle$ are zero in the ensemble average. The standard deviation in $H_{kk'}$ averaged over representative crystals is taken as the order of magnitude of $H_{kk'}$. This quantity $\sigma_{kk'}$ is given by the relation

$$\sigma_{kk'} = \overline{\langle\Phi(k)|H - E_0|\Phi(k')\rangle\langle\Phi(k)|H - E_0|\Phi(k')\rangle}^{1/2} \quad (7)$$

It proves convenient, however, to take as the order of magnitude of $\sigma_{kk'}$ the quantity $\gamma_{kk'}$ which satisfies the relation

$$\gamma_{kk'} = \overline{R_{kk'}R_{kk'}^* + J_{kk'}J_{kk'}^* + P_{kk'}P_{kk'}^*}^{1/2} > 3^{-1/2}\sigma_{kk'} \quad (8)$$

where

$$R_{kk'} = \langle\Phi(k)|H_0|\Phi(k')\rangle \quad (9)$$

$$J_{kk'} = \frac{1}{N}\sum_{m=1}^{N}\langle\Theta_m|V|\Theta_m\rangle\exp\left[2\pi\frac{im}{N}(k' - k)\right] \quad (10)$$

and

$$P_{kk'} = \frac{1}{N}\sum_{r=1}^{N}\langle\Theta_r|V_{r,r+1}|\Theta_{r+1}\rangle\left[\exp\left(2\pi\frac{ik'}{N}\right) + \exp\left(-2\pi\frac{ik}{N}\right)\right]\exp\left[2\frac{\pi i}{N}(k' - k)r\right] \quad (11)$$

It is simple to show that

$$\overline{RR^*} = \frac{m_Am_B}{N}(\epsilon_A^s - \epsilon_A - \epsilon_B + \epsilon_B^s)^2 \quad (12)$$

$$\overline{J_{k'k}J_{k'k}^*} = \frac{1}{N}\left[F_{(0)} - F_{(2)} + (F_{(1)} - F_{(2)})\cos\frac{2\pi}{N}(k' - k)\right] \quad (13)$$

$$\overline{P_{k'k}P_{k'k}^*} = \frac{2}{N}\left(1 + \cos 2\pi\frac{(k' + k)}{N}\right)\times\left\{[G_{(0)} - G_{(2)} + 2\left[\cos 2\pi\frac{(k' - k)}{N}\right](G_{(1)} - G_{(2)})]\right\} \quad (14)$$

where $F_m = \langle\Theta_m|V|\Theta_m\rangle$, $F_{(0)} = \overline{F_m^2}$, $F_{(1)} = \overline{F_mF_{m+1}}$, $\overline{F_mF_l} = F_{(2)}$ for $m \neq l$ and $m \neq l \pm 1$, $G_r = \langle\Theta_r|V_{r,r+1}|\Theta_{r+1}\rangle$, $\overline{G_m^2} = G_{(0)}$, $\overline{G_mG_{m+1}} = G_{(1)}$, and $\overline{G_mG_l} = G_{(2)}$ for $m \neq l$ and $m \neq l \pm 1$. $F_{(0)}$, $F_{(1)}$, $F_{(2)}$, $G_{(0)}$, $G_{(1)}$, and $G_{(2)}$ can all be evaluated. The results are quite lengthy and since we are only interested in orders of magnitude, it is sufficient to observe that $F_{(0)} - F_{(2)}$ and $F_{(1)} - F_{(2)}$ are of magnitude $(\Delta_F)^2$, $G_{(0)} - G_{(2)}$ and $G_{(1)} - G_{(2)}$ are of magnitude $(\Delta_G)^2$ and $m_Am_B[\epsilon_A^s - \epsilon_A + \epsilon_B^s - \epsilon_B]^2$ is of magnitude ζ^2. Therefore we may write

$$H_{kk'} = \frac{\alpha}{\sqrt{N}}(\zeta + \Delta_F + \Delta_G) \quad (15)$$

where α is a function of kk' and is of the order of unity.

The Secular Equation

The diagonal elements of the secular equation are given in eq 5. The off-diagonal elements are obtained by combining eq 8, 12, 13, and 14. It is quite clear that as N approaches infinity the off-diagonal elements vanish. However, the size of the secular equation is equal to N and it is not immediately obvious that the off-diagonal elements can be ignored with impunity (no general proof of this is presently available). If, on the other hand, all the off-diagonal elements were given by eq 15 with α equal to unity, the resulting secular equation can be solved and the result is that half the roots satisfy the relation

$$E_{(k)} = \zeta + \Delta_F + 2\Delta_G\cos\left(2\frac{\pi k}{N}\right) - \frac{\zeta + \Delta_F + \Delta_G}{\sqrt{N}}$$

The remaining roots can be shown to lie between $E_{(k)}$ and $E_{(k+1)}$. As N approaches infinity the roots approach the diagonal elements. In the pure crystal, each root is doubly degenerate. The degeneracy is removed in the disordered solid solution. This result

was also observed by Faulkner.[9] Although $\gamma_{kk'}$ (the measure of the deviation of $H_{kk'}$ from zero) is dependent on k and k', this dependence is slight if $|\epsilon_A^s - \epsilon_A|$ and $|\epsilon_B^s - \epsilon_B|$ are large compared to the intermolecular interaction energies. This is the situation that actually occurs in molecular crystals.

Concentration Dependence

The separation of the band edge from the ground state and the band width are, in general, quadratic functions of concentration (eq 5 and 6). The theory does allow, however, for a linear dependence of the band edge on composition. This occurs, in particular, if

$$F_{AA}^s - F_{AA} + F_{BB}^s - F_{BB} = F_{AB} - F_{AB}^s + F_{BA} - F_{BA}^s$$

and

$$G_{AB} = \frac{G_{AA} + G_{BB}}{2}$$

This treatment can be readily extended to three-dimensional systems and to considerations of the Davydov splitting. Nothing can be said at present about selection rules since k has no group theoretical significance.

Acknowledgments. The author wishes to thank Drs. F. Verderame and S. Eisman of the Pitman–Dunn Laboratory, Frankford Arsenal, Philadelphia, Pa., and Professor L. Steinberg of the Mathematics Department of Temple University, Philadelphia, Pa., for helpful discussions.

The Conductance and Association Behavior of the Alkali Metal Perchlorates and Tetraphenylborides in Anhydrous Acetonitrile

by Robert L. Kay,[1] Brian J. Hales, and G. P. Cunningham

Mellon Institute, Pittsburgh, Pennsylvania 15213 *(Received May 3, 1967)*

Equivalent conductances of the alkali metal perchlorates and tetraphenylborides (Ph_4B) in anhydrous acetonitrile at 25° are reported. The lithium salts were too unstable or too hygroscopic for precise measurements, although an estimated ionic mobility for the Li^+ ion is reported. All the perchlorates show some ion pair association, whereas the tetraphenylborides are all completely dissociated with the possible exception of cesium. The limiting ionic conductances, obtained from a Fuoss–Coplan split for this solvent, are compared to similar data for methanol and ethanol solutions. For very large ions, the conductance–viscosity products are about the same. For ions of intermediate size, the dipole moment and size of the solvent molecules appear to be the mobility-determining factors, whereas for small ions, the relative acid–base strength of the solvent molecules rather than their dipole moments appears to be the important factor.

Introduction

Preliminary transference measurements carried out in this laboratory indicate that the Fuoss–Coplan split[2] for ionic conductances is approximately correct for acetonitrile solutions. This split is based on the assumption that both large ions of triisobutylammonium tetraphenylboride (i-Bu_3NPh_4B) have the same equivalent conductance equal to 58.13. However, on this basis, it was very difficult to explain the rather high conductances for the alkali metal ions obtained from the data of Minc and Werblan[3] after recalculation[4] to bring the conductance parameters into conformity with the Fuoss–Onsager theory.[5] Further evidence that these data are too high can be obtained from recent results for KI[6] and BuNI[4] that give $\lambda_0(K^+) = 84.1$ compared with Minc and Werblan's value of 101.9. Owing to this exceedingly large discrepancy, we remeasured the alkali metal perchlorates in acetonitrile at 25° and include the tetraphenylborides as a check.

Experimental Section

The complete apparatus, with the exception of the salt cup dispensing device, and general techniques used for these measurements have been described adequately in a previous publication.[4] The absolute temperature was set within 0.003° by a platinum resistance thermometer. An improved salt cup dispensing device[7] for the introduction of salt samples to the cell without exposing the cell contents to the atmosphere is shown in Figure 1. With the exception of the Teflon disks, C and D, and the metal pins, A and B, it can be constructed entirely of Pyrex glass by a glassblower, thereby eliminating all epoxy seals between Lucite and glass. Such seals were found to be the source of leaks and cracks in the older design owing to the different coefficient of expansion of glass, Lucite, and epoxy resin. By lubricating the large 60/50 standard taper joint,[8] the top Teflon disk can be rotated relative to the disk D which is restrained by one of the pins B. This permits

(1) To whom all correspondence should be addressed.

(2) M. A. Coplan and R. M. Fuoss, *J. Phys. Chem.*, **68**, 1181 (1964).

(3) S. Minc and L. Werblan, *Electrochim. Acta*, **7**, 257 (1962).

(4) D. F. Evans, C. Zawoyski, and R. L. Kay, *J. Phys. Chem.*, **69**, 3878 (1965).

(5) R. M. Fuoss and F. Accascina, "Electrolytic Conductance," Interscience Publishers, Inc., New York, N. Y., 1959.

(6) G. J. Janz, A. E. Marcinkowsky, and I. Ahmed, *Electrochim. Acta*, **9**, 1687 (1964).

(7) J. L. Hawes and R. L. Kay, *J. Phys. Chem.*, **69**, 2420 (1965).

(8) An error in the drawing of the earlier model should be noted in our previous publication.[7] The large 55/50 standard taper joint is slanting in the wrong direction.

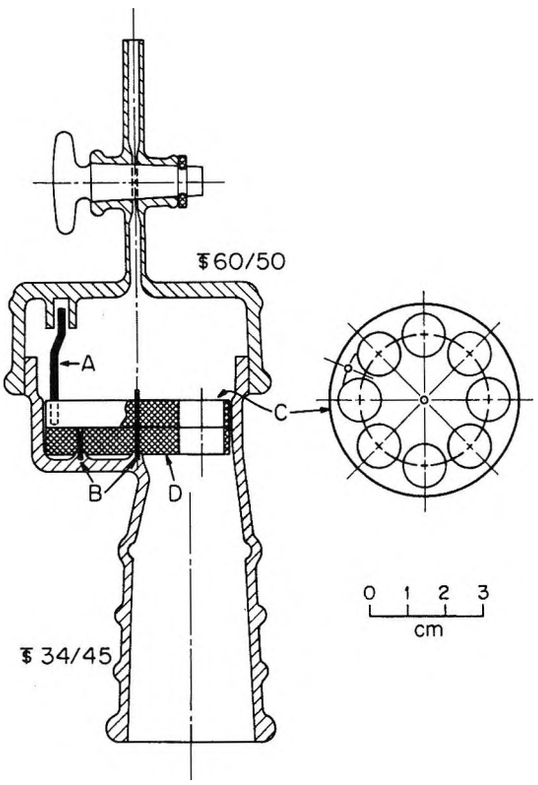

Figure 1. An improved salt cup dispensing device.

the eight openings in C to be brought into line in succession with the single opening in D. The tungsten pins, B and D, are sealed into the glass, while the copper pin, A, fits tightly into C but loosely into a short section of glass tubing sealed into the underside of the top. In later models the metal pins B have been replaced by glass tubing for greater stability. Further details concerning the salt cups and their manipulation can be found in the original publication.[7] It should be added here, however, that no problem of splashing has been encountered nor has loss of salt from the cups been detected even in the case of extremely fluffy crystals. One further improvement has been the replacement of nitrogen by argon as the flushing gas.

The tetraphenylborides were prepared by adding the appropriate alkali halide to $NaPh_4B$ (Fisher Scientific) in aqueous solution. The resulting precipitate in each case was dissolved in acetone and reprecipitated by water eight to ten times or until successive runs gave the same results. The salts were not hygroscopic and were dried in a vacuum oven at 60–80°.

$LiClO_4$ (K & K), $NaClO_4$, and $KClO_4$ (Fisher) were purified by precipitation both from a minimum amount of ethyl acetate by ethylene dichloride and from acetone solution by the addition of chlorobenzene. $RbClO_4$ and $CsClO_4$ were prepared by precipitation by adding $NaClO_4$ to a solution of the corresponding chlorides in anhydrous methanol and were recrystallized eight to ten times from a water–methanol mixture, 1:1 by volume. All the perchlorates were dried at 200° in a vacuum oven. The purification of the sodium salt was most difficult owing to its limited solubility and extreme hygroscopic nature. All the perchlorates were handled in a drybox and weighed in capped weighing bottles.[9] We were unable to dry $LiClO_4$ sufficiently so as to obtain constant results (see following section).

Reagent grade acetonitrile was further purified by the Coetzee method[10] to give a product well below 1×10^{-3} M in water content.

Results

The measured equivalent conductances for the alkali metal perchlorates and tetraphenylborides are given in Table I. In these measurements, the solvent specific conductance varied between 3 and 8 ohm^{-1} cm^{-1}. The solution density increments were obtained from density measurements on the most concentrated solution studied in each case and amounted to 0.12–0.19 and 0.09–0.19 g/ml mole kg of solution for the tetraphenylborides and perchlorates, respectively. All salts were recrystallized between the two runs recorded for each salt in Table I.

Owing to the considerable disagreement found in the literature for the physical properties of acetonitrile at 25°, we have measured the density, viscosity, and dielectric constant with considerable care and obtained 0.7767 g ml^{-1}, 0.3412 cp, and 35.95,[11] respectively. This value of the viscosity was the average obtained from measurements[11] using Ubbelohde- and Fenske-type viscometers.[12] The viscometer constants measured were reproducible to 0.05% using as calibrating liquids[12] n-decane, η/ρ = 0.1175 cstokes; n-hexane at 25°, η/ρ = 0.4496 cstokes; and n-hexane at 10°, η/ρ = 0.5132 cstokes. These liquids provided a 2.5 variation in flow time and n-hexane at 25° has almost the same flow time as acetonitrile. No kinetic energy correction was required.[13]

The conductance parameters and the standard deviation of the individual points, σ_A, in Table II for all the

(9) R. L. Kay, C. Zawoyski, and D. F. Evans, *J. Phys. Chem.*, **69**, 4208 (1965).

(10) J. F. Coetzee, G. P. Cunningham, D. K. McGuire, and G. R. Padmanabhan, *Anal. Chem.*, **34**, 1139 (1962).

(11) G. P. Cunningham, G. A. Vidulich, and R. L. Kay, *J. Chem. Eng. Data*, **12**, 336 (1967).

(12) Cannon Instrument Co., State College, Pa.

(13) A calibration with water at 25° gave viscometer constants that were almost 1.5% lower owing presumably to the need for a surface tension correction. This difference points out the care which must be exercised in measuring viscosities of liquids.

Table I: Measured Equivalent Conductances in Acetonitrile at 25°

10^4C	Λ	10^4C	Λ	10^4C	Λ	10^4C	Λ
$NaClO_4$		$KClO_4$		$RbClO_4$		$CsClO_4$	
4.138	172.14	7.177	175.65	5.796	178.60	10.809	175.15
9.760	167.55	13.817	170.62	13.885	171.82	17.706	170.24
15.051	164.43	21.777	166.16	20.760	167.58	24.337	166.40
20.858	161.59	28.432	163.00	27.233	164.31	29.871	163.63
26.170	159.42	39.555	158.63	40.925	158.47	35.267	161.18
32.489	157.17	48.079	155.77	48.727	155.76	42.059	158.42
38.649	155.18	56.471	153.24			47.514	156.43
5.591	170.89	9.772	173.57	6.331	178.06	5.484	180.19
10.378	167.19	16.560	169.00	14.140	171.71	11.798	174.33
15.060	164.33	26.032	164.12	20.959	167.56	18.492	169.75
19.776	161.90	34.226	160.63	27.435	164.35	25.363	165.88
29.857	157.75	43.942	157.12	34.570	161.23	30.434	163.41
35.055	155.89	53.798	154.07	42.451	158.20	38.908	159.76
		62.001	151.76	49.396	155.80	46.663	156.83
$NaPh_4B$		KPh_4B		$RbPh_4B$		$CsPh_4B$	
5.381	127.53	9.774	131.69	3.126	137.86	4.701	137.77
12.317	124.18	14.886	129.70	6.672	135.36	9.345	134.57
18.798	122.05	20.403	128.04	10.570	133.38	13.772	132.26
25.663	120.26	26.037	126.62	13.950	131.99	18.387	130.29
30.936	119.10	32.006	125.34	17.910	130.62	23.725	128.32
37.528	117.80	37.321	124.32	21.004	129.69	29.535	126.44
44.656	116.58	42.680	123.41	24.825	128.65	33.663	125.24
52.966	115.34			27.904	127.88	38.292	124.00
5.277	127.66	5.119	134.39	3.797	137.13	4.299	138.00
11.927	124.38	9.735	131.86	8.124	134.36	9.062	134.66
18.733	122.10	14.062	130.18	12.347	132.45	13.860	132.15
24.522	120.57	18.878	128.68	17.023	130.78	18.595	130.11
32.052	118.90	24.339	127.23	21.368	129.45	22.896	128.52
37.970	117.77	29.666	126.01	25.469	128.34	27.002	127.11
43.806	116.77	35.501	124.86	30.014	127.26	32.341	125.51
49.713	115.87			34.573	126.27	36.819	124.27

perchlorates and for the second entry for $CsPh_4B$ were obtained from the Fuoss–Onsager theory[5] in the form

$$\Lambda = \Lambda_0 - S(C\gamma)^{1/2} + EC\gamma \log C\gamma + (J - B\Lambda_0)C\gamma - K_A C\gamma\Lambda f^2 \quad (1)$$

The remaining entries were obtained from eq 1 by assuming complete dissociation and setting $\gamma = 1$ and $K_A = 0$. The parameters were obtained from a computerized least-squares analysis of the unweighted data. A good approximation for the viscosity B coefficients for the tetraphenylborides was obtained by assuming an equal split for both ions in Bu_4NPh_4B as reported by Tuan and Fuoss.[14] This leads to a value of $B = 0.7$ for all the tetraphenylborides after small allowance is made for the cations. The only change resulting from this correction is an increase in $\mathring{a}$ of only 0.2, which is almost negligible. In light of this, the smaller viscosity correction for the perchlorates was assumed to be negligible.

For acetonitrile at 25°, the constants α, β, E_1, and E_2 are equal to 0.7374, 233.6, 5.473, and 253.9, respectively, where $S = \alpha\Lambda_0 + \beta$ and $E = E_1\Lambda_0 - E_2$. The change in $\mathring{a}$ per unit change in J can be estimated from $\partial J/\partial\mathring{a}$, which varies between 430 and 490 for the perchlorates and between 310 and 380 for the tetraphenylborides.

The association of the perchlorates is evident from the definite curvature of the Λ' plots shown in Figure 2, where Λ' is given by

$$\Lambda' \equiv \Lambda - \Lambda_0 + SC^{1/2} - EC \log C = (J - B\Lambda_0)C \quad (2)$$

The value of Λ_0 used in Figure 2 was that obtained from an application of eq 1 to the data. The excellent

(14) D. F. Tuan and R. M. Fuoss, *J. Phys. Chem.*, **67**, 1343 (1963).

Table II: Conductance Parameters for Acetonitrile Solution at 25°

Salt	Λ_0	$\mathring{a}$	K_A	σ_A	$J - B\Lambda_0$
$NaClO_4$	180.32 ± 0.03	3.7 ± 0.2	9 ± 1	0.02	1980
	180.63 ± 0.07	3.7 ± 0.4	11 ± 2	0.03	1965
$KClO_4$	187.41 ± 0.06	3.0 ± 0.2	13 ± 1	0.03	1710
	187.52 ± 0.05	3.1 ± 0.1	14 ± 1	0.02	1750
$RbClO_4$	189.55 ± 0.08	3.2 ± 0.3	19 ± 1	0.04	1860
	189.49 ± 0.09	3.4 ± 0.3	19 ± 1	0.04	1920
$CsClO_4$	190.98 ± 0.04	3.0 ± 0.1	20 ± 1	0.01	1760
	191.08 ± 0.06	3.5 ± 0.2	23 ± 1	0.03	1980
$NaPh_4B$	135.4 ± 0.1	5.1 ± 0.1	...	0.09	1940
	135.4 ± 0.1	5.2 ± 0.1	...	0.07	1940
KPh_4B	141.79 ± 0.06	5.5 ± 0.1	...	0.06	2120
	141.84 ± 0.05	5.7 ± 0.1	...	0.06	2191
$RbPh_4B$	143.86 ± 0.03	5.3 ± 0.06	...	0.03	2080
	143.72 ± 0.05	5.2 ± 0.07	...	0.06	2060
$CsPh_4B$	145.38 ± 0.02	2.8 ± 0.02	...	0.02	1200
	145.31 ± 0.02	2.8 ± 0.01	...	0.02	1200
$CsPh_4B$	145.47 ± 0.02	3.3 ± 0.1	2.7 ± 0.6	0.02	1400
	145.36 ± 0.02	3.1 ± 0.1	1.7 ± 0.6	0.01	1320

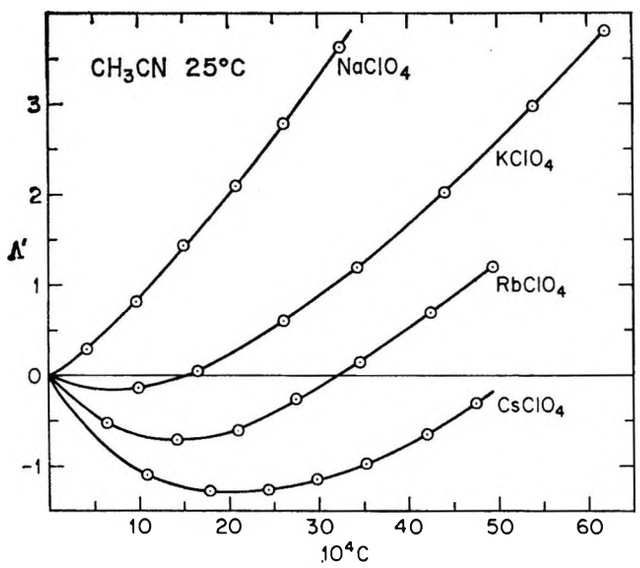

Figure 2. Plots of eq 2 for the alkali metal perchlorates in acetonitrile at 25°.

linearity of the tetraphenylboride Λ' plots shown in Figure 3 indicates complete dissociation of these salts. However, the lower Λ' values for $CsPh_4B$ as reflected in the lower $\mathring{a}$ values in Table II suggested this salt may be associated to some extent, although the amount of curvature in the Λ' plot is small. An analysis by the Fuoss–Onsager eq 1 seemed to confirm this, as is shown by the bottom entry in Table II. Although the slight curvature in the Λ' plot for this salt might be experimental error, the decrease of three conductance units in Λ' compared to the other tetraphenylborides at the highest concentration is far too large to be attributed to any error in the measurements. If the Λ' plot for $CsPh_4B$ is made to coincide with those for the other tetraphenylborides ($\mathring{a}$ = 5.3), the much larger association constant, K_A = 12, would be required, indicating significant association into ion pairs.

The average Λ_0's for the various salts are given in Table III along with the cation limiting conductances. The latter were obtained from $\lambda_0(ClO_4^-)$ = 103.8 ± 0.2 and $\lambda_0(Ph_4B^-)$ = 58.1, which in turn are based on

Table III: Limiting Salt and Cation Conductances in Acetonitrile at 25°

Salt	Λ_0	λ_0^+
$NaClO_4$	180.4	76.6
$NaPh_4B$	135.4	77.3
$KClO_4$	187.5	83.7
KPh_4B	141.8	83.7
$RbClO_4$	189.5	85.7
$RbPh_4B$	143.8	85.7
$CsClO_4$	191.0	87.2
$CsPh_4B$	145.4	87.3

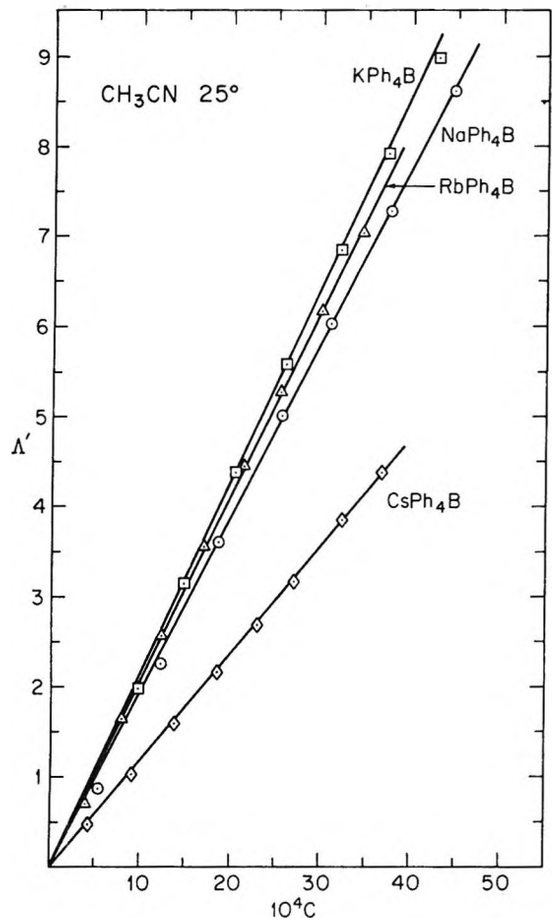

Figure 3. Plots of eq 2 for the alkali metal tetraphenylborides in acetonitrile at 25°.

the Fuoss–Coplan split[2] (see above) and known conductances for two perchlorates.[15] Considering the difficulties encountered with the hygroscopic perchlorates and the difficulties encountered in purification, the agreement in λ_0^+ is better than expected and the checks with both Janz's value[6] of λ_0 (K^+) = 84.1 and Popov's[16] λ_0 (Na^+) = 76.1 are as good as is to be expected. However, the Λ_0 values reported here are all considerably lower than those reported by Minc and Werblan,[3,4] the differences being 10.8, 18.3, 11.9, and 13.5 units in Λ_0 for the Na, K, Rb, and Cs salts, respectively. They prepared their salts by the addition of perchloric acid to the appropriate chloride followed by heating to eliminate HCl. Since $HClO_4$ is the only strong acid in acetonitrile, its occlusion could have led to their high results.

We attempted to measure the lithium salts of these two anions without success. $LiPh_4B$ was far too unstable in acetonitrile for accurate measurements and $LiClO_4$ was too hygroscopic to obtain free of water. Repeated recrystallizations of $LiClO_4$ resulted in a continuously increasing Λ_0 and all that can be stated is that $\lambda_0(Li^+) > 69$.[17]

Discussion

In a previous work,[4] we established that the association of the tetraalkylammonium halides in acetonitrile was controlled primarily by direct coulombic interaction on an ionic size basis. The larger the crystallographic radii of the ions involved, the smaller the degree of association. In contrast, the alkali metal perchlorates show the reverse behavior, namely, a slight increase in association as the cation crystallographic radii increase. This is the same behavior found in methanol,[18] ethanol–water,[7] and dioxane–water,[19] solvents in which the alkali metal cations are known to be extensively solvated. In acetonitrile, consequently, the association behavior of alkali metal salts appears to be governed on the one hand by the degree of solvation of the cations and on the other hand by the size of the anions involved. Size is the important factor in the case of the anions owing to the general lack of solvation of even small anions by acetonitrile. The tetraethanolammonium halides are an exception to the rule since they are extensively associated[20] owing to the inability of acetonitrile to solvate a hydroxyl group as a result of its poor acid–base properties.

In Figure 4, the limiting Walden products for the alkali metal, the halide, the tetraalkylammonium, and the perchlorate ions in acetonitrile, methanol, and ethanol at 25° are plotted as a function of the reciprocal measured or estimated crystallographic radii. References to the data and to the precise transference numbers on which the split into ionic conductances is based have already been tabulated in a previous publication[21] except for the perchlorate ion.[15,22]

The conductance–viscosity product for the large Bu_4N^+ ion is approximately the same in the three sol-

(15) J. F. Coetzee and G. P. Cunningham, *J. Am. Chem. Soc.*, **87**, 2529 (1965).

(16) A. I. Popov and R. E. Humphrey, *ibid.*, **81**, 2043 (1959). Only Λ_0 was reported for $NaPh_4B$. Their reported data for acetonitrile solutions indicate a precision of ±0.4 Λ unit when fitted by the Fuoss–Onsager theory.

(17) One of the referees pointed out that our estimate is confirmed by recent data for $LiClO_4$ in acetonitrile reported by F. Accascina [*Ric. Sci. Rend.*, **7**, 556 (1966)], who obtained $\lambda_0(Li^+)$ = 69.2 and $K_A(LiClO_4)$ = 4.

(18) R. L. Kay and J. L. Hawes, *J. Phys. Chem.*, **69**, 2787 (1965).

(19) T. L. Fabry and R. M. Fuoss, *ibid.*, **68**, 971 (1964).

(20) G. P. Cunningham, D. F. Evans, and R. L. Kay, *ibid.*, **70**, 3998 (1966).

(21) R. L. Kay and D. F. Evans, *ibid.*, **70**, 2325 (1966).

(22) E. D. Copley and H. Hartley, *J. Chem. Soc.*, 2488 (1930); M. Barak and H. Hartley, *Z. Physik. Chem.* (Leipzig), **165**, 272 (1933); E. D. Copley, D. M. Murray-Rust, and H. Hartley, *J. Chem. Soc.*, 2492 (1930).

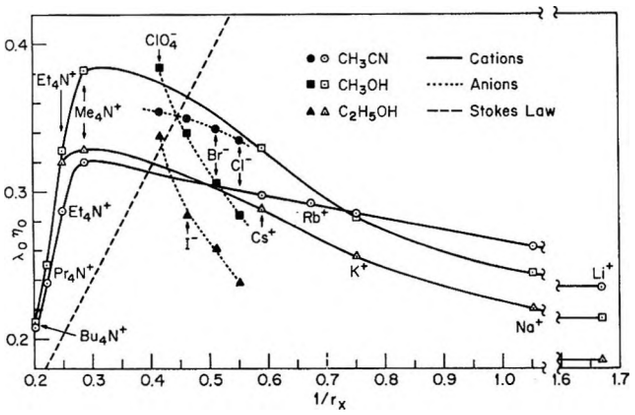

Figure 4. Limiting ionic conductance–viscosity products for cations and anions in methanol, ethanol, and acetonitrile at 25°.

vents; but as the size of the R_4N^+ ions decreases, large differences in this product result. The ions are relatively more mobile in methanol and in ethanol than in acetonitrile. This could be a result of differences in solvation owing to the large dipole moment of acetonitrile of 4.0 D. compared to 1.7 D. for methanol and ethanol.[23] The difference between ethanol and methanol could be attributed to the larger size of the ethanol molecule. The most interesting fact evident in Figure 4 is the crossover that occurs for acetonitrile solutions as the size of the cations decreases further. The alkali ions with the smallest crystallographic radii have larger Walden products in acetonitrile than in the two alcohols, whereas the difference between the two alcohols remains about the same. This crossover cannot be the result of a solvation effect based to any great extent on the dipole moment of the solvent, but this behavior could be attributed to the less predominant basic properties of acetonitrile compared to the alcohols. Thus, it appears that as the cations become small, the availability of a free electron pair in the solvent molecule determines solvation effects to a great extent. In methanol, the interaction between a small cation and the free electron pairs of the oxygen is greater than in acetonitrile, resulting in more solvation and, consequently, lower mobilities in methanol solutions. As the size of the cations increases and the distance of closest approach of cation and solvent molecule becomes greater, the charge-dipole interaction predominates and the crossover in the Walden product curve results.

Identical behavior is exhibited by the anion in that the halide ions are progressively more extensively solvated as their size decreases by the relatively strongly acidic alcohols but poorly solvated by the weakly acidic acetonitrile. The larger perchlorate ion is not affected by acid properties of the solvent; but, if at all, its solvation sheath is determined by the larger dipole moment of acetonitrile compared to methanol.

Thus, from these results it would appear that the degree of solvation of large ions is determined predominantly by the dipole moment of the solvent molecules, whereas the degree of solvation of small ions is determined predominately by the acid–base properties of the solvent molecules. The crossover effect found here cannot be explained by a solvent dielectric relaxation effect,[24] as will be discussed in detail in a future publication.[25]

Acknowledgment. This work was supported by the Office of Saline Water, U. S. Department of the Interior, under Contract No. 14-01-0001-359.

(23) A. L. McCellan, "Tables of Experimental Dipole Moments," W. H. Freeman and Co., San Francisco, Calif., 1963.

(24) R. Zwanzig, *J. Chem. Phys.*, **38**, 1603 (1963).

(25) After submitting this paper for publication, three papers by S. Minc and L. Werblan [*Roczniki Chem.*, **40**, 1537, 1753, 1989 (1966)] dealing with the alkali metal perchlorates in acetonitrile have come to our attention. They have repeated their earlier measurements[3] at 25° and now quote substantially lower values of Λ_0 that, however, are now from 6 to 8 units lower than our values given in Table II and in equally poor agreement with the data of other workers.[6,16,17] On the other hand, their $\lambda_0(Et_4N^+)$ is close to our value. This suggests that hydration of the alkali metal cations produces their lower conductances. Their solvent purification procedure was entirely different than our own. Also, the much higher values obtained for the dielectric constant (36.77) and viscosity (0.3439 cp) substantiate this conclusion. It should be noted also that their data show a change of conductance with concentration that is 40% greater than our data. In light of the poor agreement in Λ_0 and the possibility of extensive hydration, their association constants and the conclusions reached from their temperature dependence must be viewed with considerable suspicion.

Substituent Effects on the Optical Activity of Some Purine Nucleosides[1]

by Daniel W. Miles, Roland K. Robins, and Henry Eyring

Department of Chemistry and Institute for the Study of Rate Processes, University of Utah, Salt Lake City, Utah *(Received May 4, 1967)*

The circular dichroism of some 3,5′-purine cyclonucleosides of known geometry has been calculated and compared to the experimental data. The dipole–dipole interactions among electronic transition moments of the base and sugar residue appear to be responsible for at least 50% of the observed circular dichroism. Agreement between the calculations and experiment is very satisfactory when an explicit assumption regarding the $\pi \rightarrow \pi^*$ magnetic moment is made. The theory used accounts for the substituent effects observed for the 3,5′-purine nucleosides and provides a basis for the understanding of certain trends in the optical rotatory dispersion of ordinary purine ribonucleosides. Moreover, the experimental results indicate that sugar–base interactions in the rigid systems can give rise to rotational strengths of the same order of magnitude as those observed for dinucleoside phosphates.

I. Introduction

In a previous paper[2] we reported the optical rotatory dispersion (ORD), circular dichroism (CD), and absorption properties of some naturally occurring ribonucleosides and related derivatives and identified the type of electronic transition ($\pi \rightarrow \pi^*$ or $\eta \rightarrow \pi^*$) responsible for the observed Cotton effects. The results on some 3,5′-purine cyclonucleosides of fixed conformation with different substituents at C-2 and C-6 (see Figure 1 for numbering system) were of particular interest. The signs and magnitudes of the B_{2u}, B_{1u}, and E_{1u} Cotton effects were found to be quite sensitive to the type of substituent at these sites. This paper is an attempt to calculate the rotational strengths of the observed Cotton effects of these cyclonucleosides and hence gain a better understanding of the mechanisms that produce the optical activity. There are several distinct intramolecular interactions that are currently held to be responsible for optical activity[3,4] and all predict substantial changes in the optical rotation when the chromophore is altered by chemical substitution. The rigid 3,5′-purine cyclonucleosides are more amenable to quantitative treatment and should provide a basis for the understanding of certain trends in the signs and magnitudes of the $\pi \rightarrow \pi^*$ Cotton effects observed for ordinary purine ribonucleosides.

Recent attempts to calculate the optical rotation of dinucleoside phosphates by including only base–base interactions *via* the coupled oscillator mechanism and excluding all base–sugar and base–phosphate interactions have not been wholly successful.[5,6] Our results on the 3,5′-purine cyclonucleosides indicate that for this conformation the sugar–base interactions can give rise to fairly large rotational strengths.

II. Experimental Procedures

Absorption, optical rotatory dispersion, and circular dichroism curves were determined, respectively, using the Cary Model 14 spectrophotometer, the Cary Model 60 spectropolarimeter, and a prototype circular dichroism attachment built by Cary Instruments for the Model 60. The prototype CD unit was calibrated using the Cary Model 1401 circular dichroism attachment for the Model 14. The standard used was an aqueous solution of *d*-10-camphorsulfonic acid (J. T. Baker lot N. 9-361) with an $\epsilon_L - \epsilon_R$ of 2.2 at 290 mμ.

To ensure against artifacts in the optical rotation

(1) This research was supported by Research Grant GM-12862-02 from the National Institutes of Health and by Research Grant CA-8019-02 from the National Cancer Institute of the National Institutes of Health, Public Health Service.

(2) D. W. Miles, R. K. Robins, and H. Eyring, *Proc. Natl. Acad. Sci.* U. S., **57**, 1138 (1967).

(3) J. A. Schellman, *J. Chem. Phys.*, **44**, 55 (1966).

(4) D. J. Caldwell and H. Eyring, *Rev. Mod. Phys.*, **35**, 577 (1963).

(5) C. A. Bush and J. Brahms, *J. Chem. Phys.*, **46**, 79 (1967).

(6) C. A. Bush and I. Tinoco, *J. Mol. Biol.*, **23**, 601 (1967).

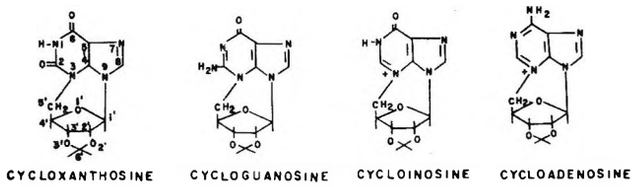

Figure 1. Structural formulas of the 3,5′-purine cyclonucleosides studied in this paper. This figure also displays the numbering system used.

or circular dichroism data concentrations were chosen to be well under the instrument's peak toleration absorbance level of 3.0, and further dilution of each sample did not alter the shape of the dispersion or circular dichroism curves.

All compounds were made and purified in the laboratory of Professor Roland K. Robins.[7] The values of the molecular rotations, $[M]$, or molecular ellipticity, $[\theta]$, have variable accuracy depending on the signal-to-noise ratio encountered. The measurements in the regions of high absorbancy have the following accuracy ranges: cyclonucleosides, 5–10%; and ordinary noncyclic ribonucleosides, 10–15%.

III. Results

The absorption and circular dichroism for 2′,3′-isopropylidene-3,5′-xanthosine cyclonucleoside (cycloxanthosine), 2′,3′-isopropylidene-3,5′-guanosine cyclonucleoside (cycloguanosine), 2′,3′-isopropylidene-3,5′-inosine cyclonucleoside *p*-tolylsulfonate (cycloinosine), and 2,3′-isopropylidene-3,5′-adenosine cyclonucleoside *p*-tolylsulfonate (cycloadenosine) are given in Figures 2–5.[8,9] Structural formulas are given in Figure 1. Replacement of the tolylsulfonate ion with the iodide ion in cycloinosine or cycloadenosine was found to have no effect on the optical activity.[10] It is most interesting to observe that Cotton effects of similar electronic origin are quite variable in regards to both magnitude and sign. For example, it is interesting to compare the CD curve of cycloinosine with the CD curve of cycloxanthosine. The effect of removing the keto group from the position 2 carbon of cycloxanthosine is to reverse the signs of the first three Cotton effects. This striking reversal of signs is predicted by our calculations in the next section.

Figure 6 displays the ORD of a series of 8-substituted guanine nucleosides. All 8-substituted guanine nucleosides have an intense absorption band in the 250–260-mμ region. Guanosine and 8-bromoguanosine give negative Cotton effects in this region whereas 8-hydroxyguanosine and 8-aminoguanosine give positive Cotton effects. An explanation of these substituent effects will be given in section VI.

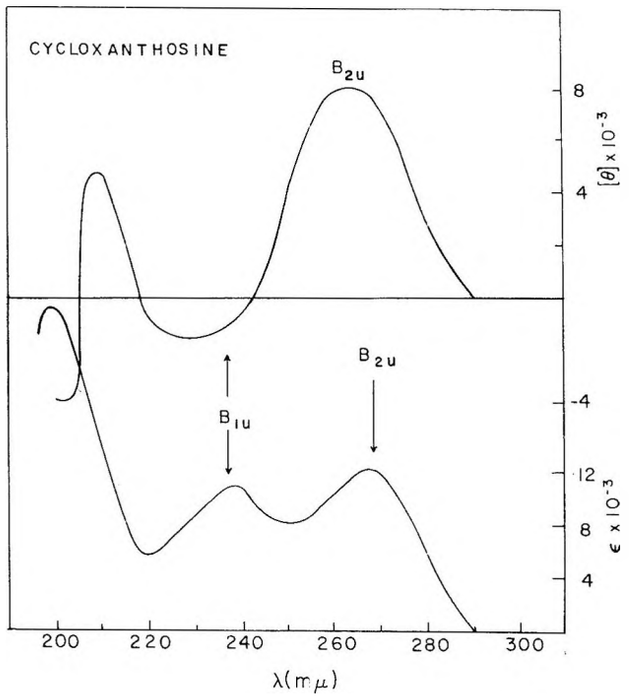

Figure 2. The circular dichroism and absorption curves of 2′,3′-isopropylidene-3,5′-xanthosine cyclonucleoside (cycloxanthosine) in aqueous solution at pH 7.

Figure 7 reports the ORD of some 6-substituted purine nucleosides and Figure 8 gives the ORD of some 8-substituted adenine nucleosides. Although the sign of the long-wavelength Cotton effect is negative for all 6-substituted purine nucleosides and 8-substituted adenine nucleosides, interesting changes in the magnitude of this Cotton effect are observed. These results will be discussed in more detail in section VI.

IV. Theory

If one assumes isolated groups interacting through

(7) R. E. Holmes and R. K. Robins, *J. Org. Chem.*, **28**, 3483 (1963); R. E. Holmes and R. K. Robins, *ibid.*, **86**, 1242 (1964); R. E. Holmes and R. K. Robins, *ibid.*, **87**, 1772 (1965).

(8) The circular dichroism reported in Figures 2–5 is somewhat less than the circular dichroism previously reported in ref 1, owing to the calibration procedure discussed in the Experimental Section.

(9) Reference 2 should be consulted for justification of the band assignments. The B_{2u}, B_{1u}, and E_{1u} transitions are found not only in the spectra of benzene and its derivatives, but also in the class of polynuclear aromatic hydrocarbons known as the catacondensed hydrocarbons (naphthalene, for example) (see P. E. Stevenson, *J. Chem. Educ.*, **41**, 234 (1964), and references cited therein) and in the nucleic acid bases (see also L. B. Clark and I. Tinoco, *J. Am. Chem. Soc.*, **87**, 11 (1965)).

(10) The ORD of 2′,3′-isopropylidene-3,5′-cycloadenosine iodide has been previously reported by T. R. Emerson, R. J. Swan, and T. L. V. Ulbricht, *Biochem. Biophys. Res. Commun.*, **22**, 505 (1966). They reported a positive Cotton effect for this compound in the 260-mμ region. We have discovered that this compound decays in a matter of days unless the solution is buffered on the acidic side. The ORD curve of the decomposed product resembles the curve reported by Ulbricht, *et al.*

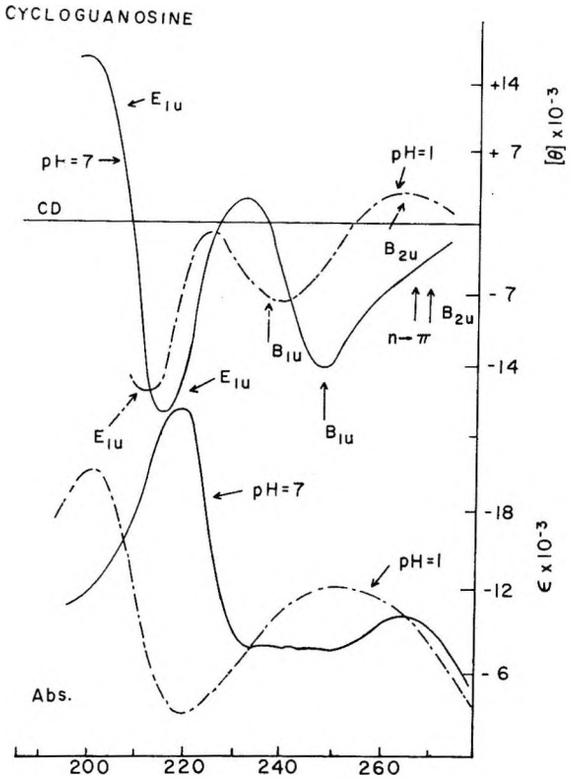

Figure 3. The circular dichroism and absorption curves of 2′,3′-isopropylidene-3,5′-guanosine cyclonucleoside (cycloguanosine) in aqueous solution at pH 7 and 1. The pH effect is discussed in ref 2.

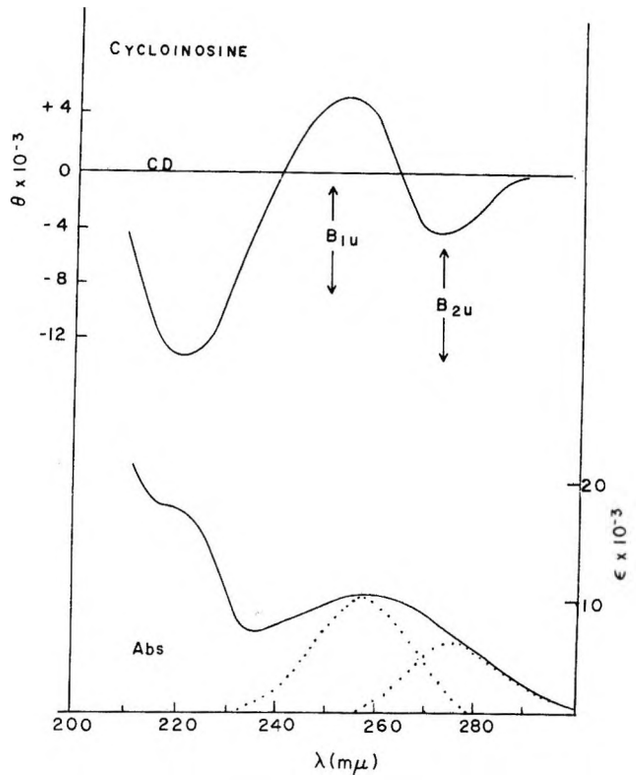

Figure 4. The circular dichroism and absorption curves of 2′,3′-isopropylidene-3,5′-inosine cyclonucleoside *p*-tolylsulfonate (cycloinosine) in aqueous solution at pH 7. A rough resolution of the absorption curve is given by the dotted lines.

space and applies first-order perturbation theory to the appropriate zeroth-order wave functions in conjunction with the Rosenfeld[11] equation

$$\beta = \frac{2}{3\pi}\sum_{A}\frac{R_A}{V_{0A}^2 - V^2} = \frac{2}{3\pi}\sum_{A}\mathrm{Im}\,\frac{\vec{\mu}_{0A}\cdot\vec{m}_{A0}}{V_{0A}^2 - V^2} \quad (1)$$

one obtains[12]

$$R_A = \mathrm{Im}\,\vec{\mu}_{i0a}\cdot\vec{m}_{ia0} \quad (2a)$$

$$-2\sum_{j\neq i}\sum_{b\neq a}\mathrm{Im}\,\frac{V_{i0a;j0b}(\vec{\mu}_{i0a}\cdot\vec{m}_{jb0_{\nu_a}} + \vec{\mu}_{j0b}\cdot\vec{m}_{ia0_{\nu_b}})}{h(\nu_b^2 - \nu_a^2)} \quad (2b)$$

$$-\sum_{j\neq i}\sum_{b\neq a}\mathrm{Im}\,\frac{V_{iab;j00}(\vec{\mu}_{i0a}\cdot\vec{m}_{ib0} + \vec{\mu}_{i0b}\cdot\vec{m}_{ia0})}{h(\nu_b - \nu_a)} \quad (2c)$$

$$-\sum_{j\neq i}\sum_{b\neq a}\mathrm{Im}\,\frac{V_{i0b;j00}(\vec{\mu}_{i0a}\cdot\vec{m}_{iab} + \vec{\mu}_{iab}\cdot\vec{m}_{ia0})}{h\nu_b} \quad (2d)$$

$$-\sum_{j\neq i}\mathrm{Im}\,\frac{V_{i0a;j00}(\vec{\mu}_{iaa} - \vec{\mu}_{i00})\cdot\vec{m}_{ia0}}{h\nu_a} \quad (2e)$$

$$-\frac{2\pi}{c}\sum_{j\neq i}\sum_{b\neq a}\frac{V_{i0a;j0b_{\nu_a\nu_b}}(\vec{R}_j - \vec{R}_i)\cdot\vec{\mu}_{j0b}\vec{\mu}_{i0a})}{h(\nu_b^2 - \nu_a^2)} \quad (2f)$$

in which the basic intramolecular interactions responsible for optical activity such as the coupled oscillator effects[13,14] and the one-electron effect[15] arise as terms. In eq 1 and 2, R_A is the rotational strength of the Ath transition in the molecule; $\vec{\mu}_{0A}$, $\vec{m}_{A0}$ are the electric and magnetic dipole moments of transitions in the molecule as a whole; $\vec{\mu}_{0a}$, $\vec{\pi}_{0b}$, $\vec{m}_{a0}$ $\vec{m}_{b0}$ are electric and magnetic dipole moments of transitions in individual groups; ν_a, ν_b are the group transition frequencies; $V_{i0a;j0b}$, etc. $= \int\psi_{i0}\psi_{ia}\psi_{j0}\psi_{jb}V_{ij}d\psi_i d\psi_j$; and V_{ij} is the interaction between groups i and j.

In eq 2, term 2a is seen to measure the partial rotation of a transition in an isolated group and is zero in the nucleosides since these molecules can formally be divided into groups having inversion and reflection symmetry elements. Term 2b arises from the inter-

(11) L. Rosenfeld, *Z. Physik*, **52**, 161 (1928).
(12) I. Tinoco, *Advan. Chem. Phys.*, **4**, 113 (1962).
(13) J. G. Kirkwood, *J. Chem. Phys.*, **5**, 479 (1937).
(14) L. L. Jones and H. Eyring, *Tetrahedron*, **13**, 235 (1961).
(15) W. J. Kauzmann, J. E. Walter, and H. Eyring, *Chem. Rev.*, **3**, 339 (1940).

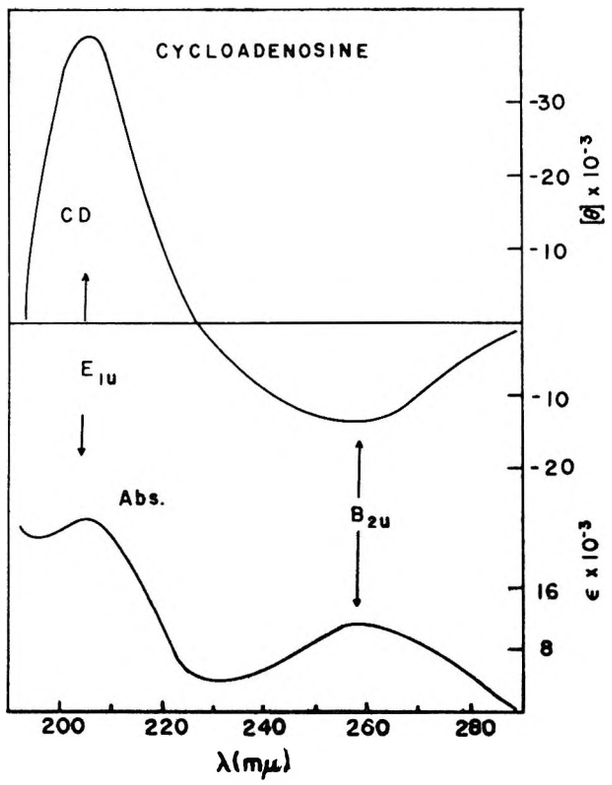

Figure 5. The circular dichroism and absorption curves of 2′,3′-isopropylidene-3,5′-adenosine cyclonucleoside *p*-tolylsulfonate (cycloadenosine) in aqueous solution at pH 7.

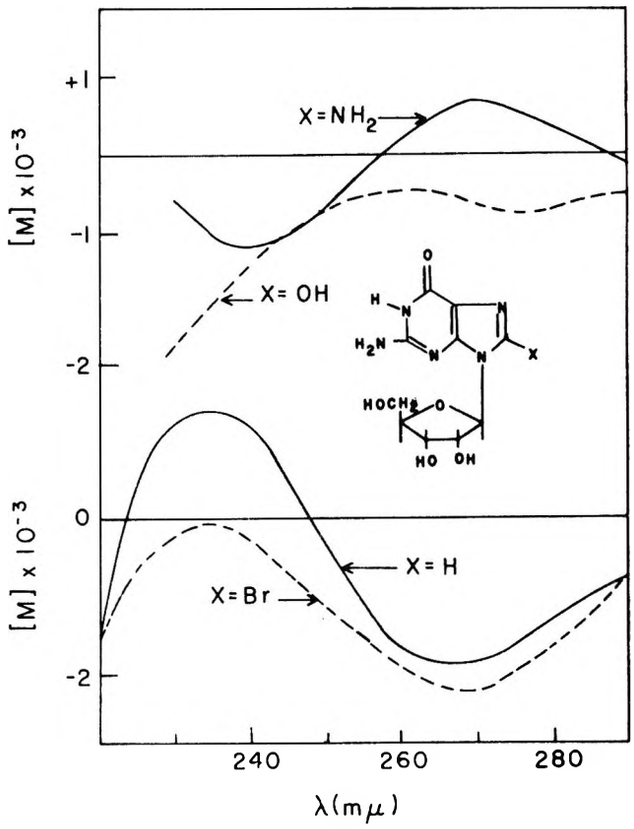

Figure 6. The optical rotatory dispersion of a series of 8-substituted guanine nucleosides in aqueous solution at pH 7.

action of an electric dipole transition in one group with a magnetic dipole transition in another. Bush and Brahms[16] have recently used this term to help explain the optical activity of some dinucleoside phosphates. In their treatment they assumed that the magnitudes of the $\pi \rightarrow \pi^*$ magnetic transition moments are of the order of 0.1 BM. In the cyclonucleoside systems we have found that the interaction of a magnetic moment of this magnitude with the electric dipole transitions of the sugar residue contributes only about 10% of the observed rotation. We will discuss this term in more detail later.

Terms 2c and 2d are due to the mixing of parallel or antiparallel components of the electric and magnetic dipole transitions within the same group. These are the one-electron terms where it is the function of the static field of the disymmetrically arrayed vicinal groups to add in the conjugate transition moment. There are several reasons why the one-electron terms may make substantial contributions to $\pi \rightarrow \pi^*$ rotational strengths. In the first place, Schellman[17] has shown that the optical rotation induced by the static mechanism should be relatively larger for chromophores of low symmetry such as the nucleic acid bases. Secondly, the $n \rightarrow \pi^*$ transitions in the nucleic acid bases can provide the prerequisite in-plane magnetic moment, m_{ib0}, of term 2c. Moreover, as a consequence of the fact that there are $n \rightarrow \pi^*$ and $\pi \rightarrow \pi^*$ transitions lying in approximately the same region of the spectrum (*ca.* 260 mμ), the denominator of term 2c will be quite small. Nevertheless, since there is no simple way to estimate the contribution of the one-electron terms they have been neglected in this treatment. Term 2e is usually neglected owing to the large denominator, $h_a{}^{\nu}$, and the smaller interaction matrix element, $V_{i0a;j00}$.

Term 2f accounts for the dynamic coupling mechanism of Kuhn and Kirkwood.[18] This term is expected to be large for transitions with large electric dipole moments such as the $\pi \rightarrow \pi^*$ transitions in the base chromophores.

V. Application of Theory to 3,5′-Purine Cyclonucleosides

What we propose to do in this study is to evaluate

(16) See ref 4.

(17) J. A. Schellman, *J. Chem. Phys.*, **44**, 55 (1966).

(18) W. Kauzmann in "Quantum Chemistry," Academic Press Inc., New York, N. Y., 1957, Chapter 15.

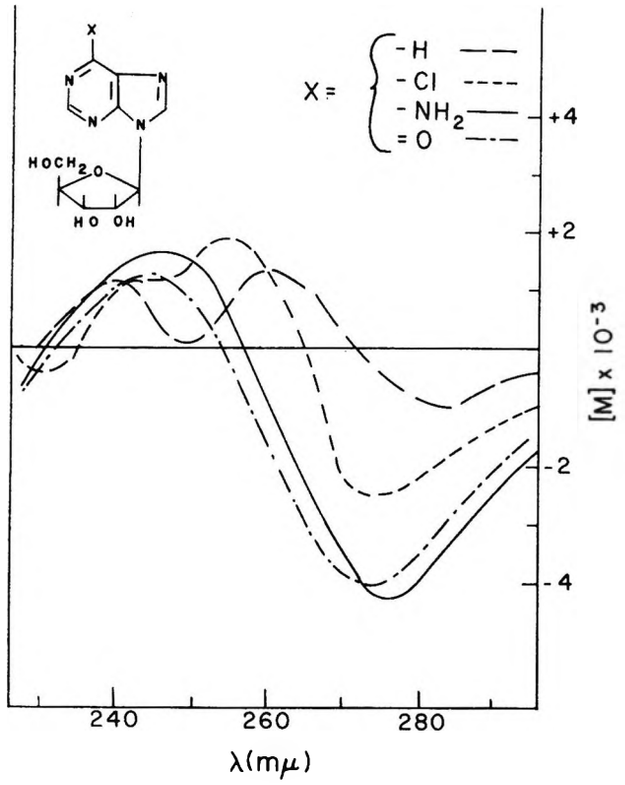

Figure 7. The optical rotatory dispersion of a series of 6-substituted purine nucleosides in aqueous solution at pH 7.

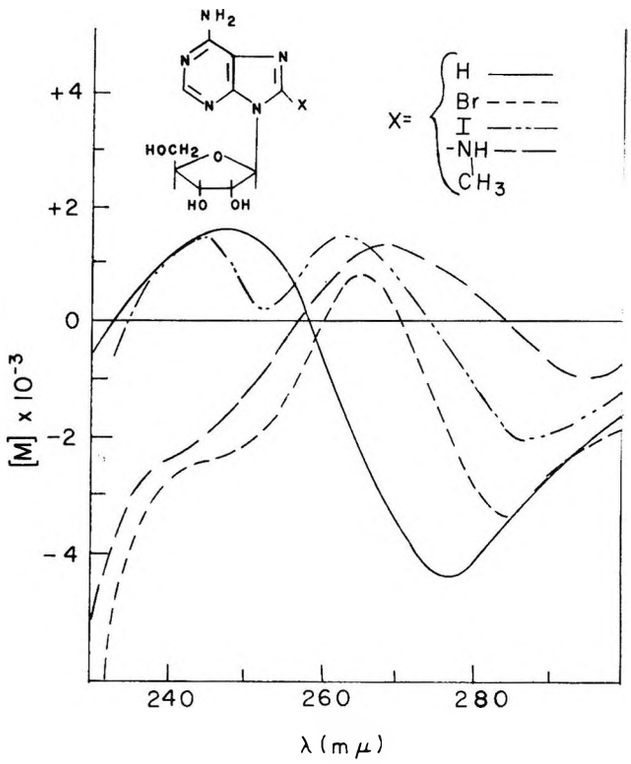

Figure 8. The optical rotatory dispersion of a series of 8-substituted adenine nucleosides in aqueous solution at pH 7.

terms 2b and 2f and compare the results with the measured rotational strengths of the $\pi \rightarrow \pi^*$ Cotton effects. In this manner we can gauge the importance of the coupling mechanisms in the optical activity of ribonucleosides. Poor comparison between theory and experiment would emphasize the importance of the one-electron effects.

Approximate expressions for terms 2b and 2f are given below.

$$R_A^{(2b)} = -\sum_{j \neq i} \frac{\nu_0^2}{\nu_0^2 - \nu_a^2} \mu_{i0a} m_{ia0} (\alpha_{33} - \alpha_{11})_j G_{ij} \frac{\hat{e}_j \cdot \hat{e}_i'}{r_{ij}^3} \quad (3)$$

$$R_A^{(2f)} = \sum_{j \neq i} \frac{\pi}{c} \frac{\nu_a \nu_0^2}{\nu_0^2 - \nu_a^2} \mu_{i0a}^2 (\alpha_{33} - \alpha_{11})_j G_{ij} \frac{\hat{e}_i \hat{e}_j \cdot \vec{r}_{ij}}{r_{ij}^3} \quad (4)$$

$$G_{ij} = \hat{e}_i \cdot \hat{e}_j - \frac{3(\vec{r}_{ij} \cdot \hat{e}_i)(\vec{r}_{ij} \cdot \hat{e}_j)}{r_{ij}^2}$$

The derivation of eq 3 is given in the Appendix of this paper while the derivation of eq 4 is found in ref 5 or 12. In eq 3 and 4 $\hat{e}_j$ is the unit vector in the direction of the symmetry axis of group j; $\hat{e}_i$ is the unit vector in the direction of the electric dipole moment, $\vec{\mu}_{i0a}$, of the transition 0 to a in group i, and ν_a is its frequency; $\hat{e}_i'$ is a unit vector in the direction of $\vec{m}_{ia0}$ (perpendicular to the base plane); α_{33} and α_{11} are the electronic polarizabilities at zero frequency parallel and perpendicular to the symmetry axis of group j and can be approximated by the Na D line values; $\vec{r}_{ij}$ is the distance from group i to group j; and ν_0 can be approximated by a frequency midway between the first absorption band in group j and its ionization frequency.

In application of eq 3 and 4 we prefer to use bond instead of group polarizabilities as the effect of molecular geometry can be better taken into account with this approach. The bond polarizabilities, the wavelength of the first absorption band, and the ionization frequency of the bonds in the sugar residue are given in Table I. It is noted that the C–H bond contributes very little to the rotation since this bond is isotropic. The atomic coordinates of the sugar residue are given in Table II[19] and the $\hat{e}_j$ and $\vec{r}_{ij}$ vectors based on these coordinates are given in Table III. The coordinates are to be referred to the primed coordinate system given

(19) The atomic coordinates are taken from the X-ray data of J. Zussman, *Acta Cryst.*, 6, 504 (1953), on cycloadenosine. The coordinates are assumed to be applicable to the other 3,5′-purine cyclonucleosides.

Table I: The Polarizabilities, Wavelength of the First Absorption Band, and Ionization Frequency of the Bonds in the Ribose Residue of the Cyclonucleosides

Bond	α_{33}[a] × 10^{+24} cc	α_{11}[a] × 10^{+24} cc	λ_{max},[b] A	λ_{ion},[c] A	ν_0[d] × 10^{-15} sec^{-1}
C–C	1.02	0.27	1470	980	2.3
C–H	0.63	0.63	1250	940	2.7
C–OC	0.89	0.46	1900 1700	1150	2.0

[a] R. J. W. LeFevre and C. G. LeFevre, *J. Chem. Soc.*, 3549 (1956); R. J. W. LeFevre, A. Sundaram, and R. K. Pierens, *ibid.*, 479 (1965); M. Aroney and R. J. W. LeFevre, *ibid.*, 3002 (1958). [b] L. W. Pickett, M. Muntz, and E. M. McPherson, *J. Am. Chem. Soc.*, **73**, 4864 (1951); P. G. Wilkinson, *J. Mol. Spectry.*, **6**, 1 (1961). [c] F. A. Matsen in "Technique of Organic Chemistry," Vol. IX, W. West, Ed., Interscience Publishers, Inc., New York, N. Y., 1956, pp 657–659. [d] ν_0 is approximated by a frequency midway between the first absorption band in group j and its ionization frequency.

Table II: Atomic Coordinates for the 3,5′-Purine Cyclonucleosides

Atom	x	y	z	Atom	x	y	z
C_1'	0.15	0.45	3.55	O_3'	−1.81	2.04	4.76
C_2'	−1.28	0.02	3.72	C_4'	0.23	−1.85	3.33
O_2'	−1.90	0.18	4.90	O_1'	0.82	−0.60	3.86
C_3'	−1.08	−1.59	3.76	C_5'	0.54	−2.28	1.88
				C_6'	−1.97	−0.90	5.66

in Figure 9; the center of the coordinate system was taken as the center of positive charge of the chromophore.

The transition frequencies, ν_a, and the dipole strengths, μ_{i0a}^2, have been estimated from the absorption curves as accurately as possible by using the following approximate expression[20]

$$\mu_{i0a}^2 = 0.92 \times 10^{-38}\sqrt{\pi}\epsilon_a^0 \frac{\Delta_a}{\lambda_a^0}$$

$$\lambda_a^0 = \frac{c}{\nu_a}$$

ϵ_a^0 = maximum value for the molar extinction

$$\Delta_a = |\lambda_a - \lambda_a^0| \text{ where } \epsilon_a = \frac{1}{0.368}\epsilon_a^0$$

Similarly the experimental rotational strengths, R_{0a}^{exptl}, can be taken from the expression of Moscowitz (see ref 20)

$$R_A^{exptl} = 0.696 \times 10^{-42}\sqrt{\pi}\frac{\Delta_a}{\lambda_a^0}[\theta_a^0]$$

POSITIVE X AND X' ARE DOWN

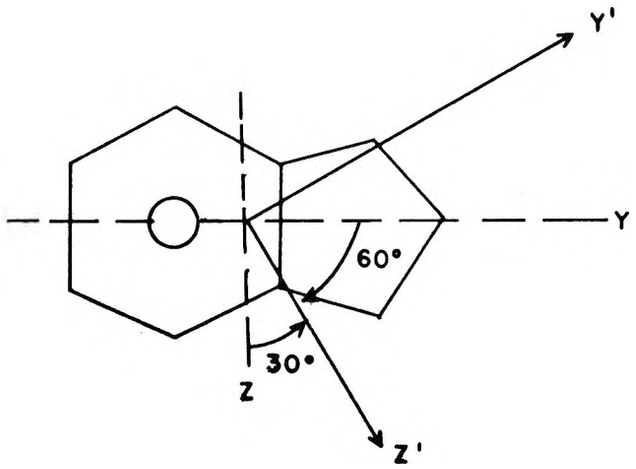

Figure 9. The primed coordinate system (chosen for convenience in using the data of Zussman) is used throughout this paper. The polarization angle, γ, is taken as positive for e_i vectors oriented counterclockwise relative to the primed coordinate system.

where $[\theta_a^0]$ is the maximum ellipticity from the CD curve. Table IV contains the calculated dipole strengths and R_A^{exptl}.

VI. Results of Calculation

All the necessary data are thus available for the evaluation of terms 2b and 2f except for the polarization direction, $\hat{e}_i = \hat{j}\sin\gamma + \hat{k}\cos\gamma$, and the sign and magnitude of $\vec{m}_{ia0}$. The polarization angle, γ, is defined in Figure 9. Several authors have used the expression.[21,22]

$$\gamma = \tan^{-1}\frac{\Sigma_p c_{kp} c_{lp} y_p}{\Sigma_p c_{kp} c_{lp} z_p} \qquad (5)$$

In eq 5 c_{kp} and c_{lp} stand for the coefficients of the pth atomic orbital in the MO's k and l, respectively, and z and y are the components of the position vector $\vec{r}_p$ of the pth nucleus. The use of this method has shown that the direction of a particular transition moment is quite sensitive to the set of parameter values used. Because of the lack of experimental information regarding the transition moments and because of our lack of complete confidence in eq 5, we have calculated, with the aid of a computer, eq 3 and 4 for all possible directions of the $\hat{e}_i$ vector. The results for the B_{2u} transition

(20) C. Djerassi, "Optical Rotatory Dispersion," McGraw-Hill Book Co., Inc., New York, N. Y., 1960.

(21) H. DeVoe and I. Tinoco, *J. Mol. Biol.*, **4**, 518 (1962).

(22) T. A. Hoffman and J. Ladik, *Advan. Chem. Phys.*, **7**, 96 (1964

Table III: The $\hat{e}_j$ Bond Vectors and $\vec{r}_{ij}$ Vectors for the 3,5′-Purine Cyclonucleosides

Bond	$\hat{e}_j$ x	$\hat{e}_j$ y	$\hat{e}_j$ z	$\hat{r}_{ij}$ x	$\hat{r}_{ij}$ y	$\hat{r}_{ij}$ z
C_1'–O_1'	0.51	−0.82	0.24	0.50	−0.08	3.70
C_1'–C_2'	−0.98	−0.27	0.11	−0.56	0.22	3.63
C_2'–O_2'	−0.43	0.11	0.83	−1.59	0.10	4.31
C_2'–C_3'	0.12	−0.99	0.03	−1.18	−0.79	3.74
C_3'–O_3'	−0.56	0.34	0.76	−1.45	−1.81	4.26
C_3'–C_4'	0.94	−0.12	−0.31	−0.45	−1.72	3.55
C_4'–O_1'	0.41	0.84	0.36	0.53	−1.22	3.60
C_4'–C_5'	0.20	−0.28	−0.94	0.38	−2.06	2.60
O_2'–C_6'	−0.05	−0.82	0.58	−1.94	−0.36	5.28
O_3'–C_6'	−0.11	0.78	0.62	−1.88	−1.47	5.20

Table IV: Calculated Contribution of Terms 2b and 2f to the Rotational Strength

Molecule	Transition	γ,[a] deg	$\mu_{i0a}^2 \times 10^{36}$ [b] cgs	$R_{0b} \times 10^{40}$ cgs	$R_{calcd} \times 10^{40}$ cgs: Term 2f	$R_{calcd} \times 10^{40}$ cgs: Term 2b
Cycloadenosine	B_{2u}	10	1.63	−12	−4.6	−5.7
	B_{1u}	145			small positive predicted[c]	
	E_{1u}	80	1.82	+28	+13.0	+4.0
Cycloinosine	B_{2u}	26	0.33	−1.30	−0.60	−0.70
	B_{1u}	82	0.82	+2.40	+1.00	0.30
	E_{1u}	165		large negative	large negative predicted[c]	
Cycloxanthosine	B_{2u}	70	1.10	6.0	+3.00	+1.00
	B_{2u}	20	0.54	−1.0	−1.20	−1.30
	E_{1u}	115		large positive	large positive predicted[c]	
Cycloguanosine	B_{2u}	5	1.00	−5.5	−3.00	−3.6
	B_{1u}	80		−8.0	small positive predicted[c]	
	E_{1u}	2	1.98	−11.0	−7.0	−8.0

[a] Direction of transition moment from LCAO–MO theory. [b] The dipole strength, μ_{i0a}, and the observed rotational strength, R_{0a}, were estimated from the absorption and CD curves. [c] Prediction based on Figure 9.

of cycloadenosine is given in Figure 10. (Plots for other transitions in the cyclonucleosides will differ only with respect to magnitudes since the same geometry was assumed for these systems.) Figure 10 shows that term 2b makes a contribution of similar magnitude and usually of the same sign for any particular value of γ if $\vec{m}_{ia0} = +0.5$ BM. Stewart and Jensen[23] have found two possible transition moment directions for the B_{2u} transition of the adenine chromophore consistent with the crystal symmetry and dichroic ratio. These directions, in conformity with the convention of Figure 9, are -33 ± 3 or $15 \pm 3°$. If we take the latter angle for the direction of the electric moment of the B_{2u} transition and assume that its magnetic moment is 0.5 BM, we find that

$$R_{B_{2u}}^{(2b)} = -5.7 \times 10^{-40}$$
$$R_{B_{2u}}^{(2f)} = -4.6 \times 10^{-40}$$
$$R_A = -10.3 \times 10^{-40}$$

which agrees quite closely with $R_{B_{2u}}^{exptl} = -12 \times 10^{-40}$.

For the other transitions we have resorted to the LCAO–MO method (eq 5) to estimate the polarizations. Table IV contains the rotational strengths of many of the $\pi \rightarrow \pi^*$ transitions as calculated from eq 3 and 4 ($\vec{m}_{ia0}$ in term 2b was taken as 0.5 BM). The polarization angles, γ, were calculated by constructing the appropriate secular determinants for each cyclo-

(23) R. F. Stewart and L. H. Jensen, *J. Chem. Phys.*, **40**, 2071 (1964).

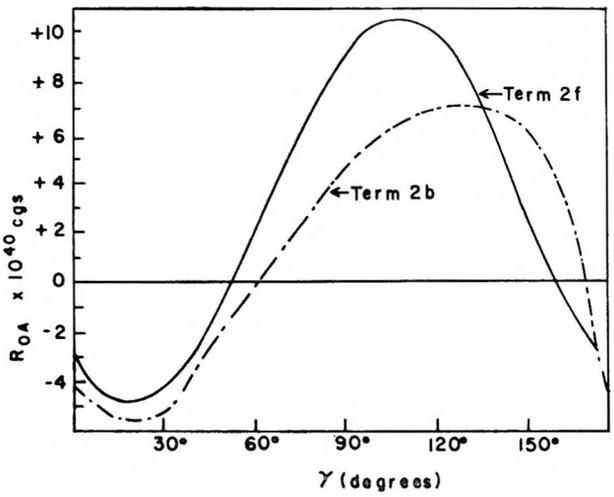

Figure 10. The calculated contribution of terms 2b and 2f to the rotational strength of the B_{2u} transition of cycloadenosine as a function of the direction of the B_{2u} electric transition moment. The polarization angle, γ, is defined in Figure 9.

nucleoside and solving the determinantal equations with the aid of a computer. Ladik's parameters[22] were used since they were found to give polarizations that compare favorably (within 5°) with the results of polarized absorption studies on several pyrimidine derivatives[24-26] and because they also give the polarization of the B_{2u} moment of adenine at 10° (with reference to Figure 9). This agrees closely with the 15 ± 3° option of Stewart and Jensen. The polarizations of the first three transitions of lowest energy ($k \rightarrow k + 1$, $k \rightarrow k + 2$, $k - 1 \rightarrow k + 1$, where k denotes the quantum number of the highest filled MO) were determined and are labeled B_{2u}, B_{1u}, and E_{1u} in Table IV.

VII. Discussion

A detailed evaluation of all the terms that might contribute to the rotation of compounds as complex as the purine nucleosides is very difficult at the present time. We have shown, however, that term 2f can be evaluated by means of eq 4 if the dipole approximation is valid for complex and extensive chromophores such as the nucleic acid bases and when the direction of the transition moment and the coordinates of the molecule are known. For cycloadenosine, where this experimental information is available, we have found that term 2f accounts for approximately 50% of the observed rotation. Similarly the results given in Table IV (where the LCAO–MO method was used to find the polarizations) show that term 2f again accounts for about one-half of the measured rotation (the only major exception is for the B_{1u} band of cycloguanosine) of the 3,5′-purine cyclonucleosides.

Evaluation of term 2b also depends on the validity of the dipole approximation. For this term we also lack experimental information regarding the sign and magnitude of $\vec{m}_{ia0}$. By assuming that $\vec{m}_{ia0}$ is of the order of 0.5 BM, we get a rather remarkable agreement (when terms 2b and 2f are added) between theory and experiment. It is unfortunate that no experimental criterion (such as the Kuhn's anisotropy factor) is available to provide information regarding the magnetic moments of transitions that are both electrically and magnetically allowed. Nonetheless, while it is more difficult to visualize $\pi \rightarrow \pi^*$ transitions with intrinsic magnetic moments than, for example, the $n \rightarrow \pi^*$ transitions, symmetry considerations tell us that $\pi \rightarrow \pi^*$ transitions in the bases may have large magnetic moments. Therefore, it does not seem prudent to ignore this term altogether. Thus it has been included here to show the magnitude of the magnetic moment required before the magnetic–electric term becomes competitive with the Kirkwood term and to demonstrate its dependence on the polarization of the transitions.

In summary, this paper demonstrates that term 2f is very important in the optical activity of nucleosides. It shows that term 2b is relevant only if the $\pi \rightarrow \pi^*$ transition of the bases have relatively large magnetic moments. Our study provides little information about the importance of the one-electron effects.

These calculations explain the origin of the substituent effects on the optical activity of optically active substances containing aromatic-ring chromophores. Substituent effects on terms 2b and 2f are best discussed by referring to Figure 10. Chemical substitution on an aromatic-ring chromophore alters the dipole strength, μ_{i0a}^2, and the frequency, ν_a, of the transition responsible for the Cotton effect. The magnitude of both terms are affected by these changes. However, sign changes reflect the influence of the substituent group on the orientation of the $\hat{e}_i$ vector. The removal, for instance, of a keto group from C-2 of cycloxanthosine changes the orientation of $\hat{e}_i$ sufficiently to reverse the sign of that Cotton effect. Figure 10 suggests that a series of substituents at C-2 known progressively to rotate $\hat{e}_i$ from, say, $\gamma = 40$ to $\gamma = 70°$ should gradually change the sign of the Cotton effect from positive to negative. This idea is used in the next section to explain certain trends in the optical activity of ordinary purine nucleosides where the geometrical factors are not known well enough to allow for quantitative cal-

(24) R. F. Stewart and N. Davidson, *J. Chem. Phys.*, 39, 255 (1963).
(25) L. E. Lyons, *ibid.*, 20, 1814 (1952).
(26) W. E. Seeds, *Progr. Biophys. Biophys. Chem.*, 3, 27 (1953).

culations. Such a treatment assumes that the substituent does not produce any conformational changes.

VIII. Extension of Theory to Ordinary Nucleoside Systems

The objective of this section is quite simple. We intend to show that changes in the magnitude and sign of the first long-wavelength Cotton effect exhibited by several series of purine nucleosides vary progressively with the direction of the transition moment. Our procedure is simply to plot the amplitude, A

$$A = [M]_1 - [M]_2$$

where $[M]_1$ is the molecular rotation of the extremum of longer wavelength and $[M]_2$ is the molecular rotation of the extremum of shorter wavelength, against the spectroscopic moment of the theory of Platt,[27] Moffitt,[28] and Petruska.[29,30] (The spectroscopic moments used are taken from ref 30.) The changes in the polarization angle of a particular transition is related to the spectroscopic moment of the substituent and the site of substitution. Although this method is not expected to be completely applicable to the strong perturbations present here, it does constitute a basis for making estimates of the changes in polarization induced by the substituents. We have not normalized our data with respect to dipole strength or transition frequency since changes in these parameters due to substitution are less than 20% in the compounds studied, nor have we made any attempt to correct for background rotation.

In Figure 11 we have plotted the amplitude of the long-wavelength Cotton effect against the spectroscopic moment, m, of the substituent for the 8-substituted guanosine derivatives (see Figure 6). The amplitude is observed to increase progressively in the positive direction with increasing magnitude of the spectroscopic moment. Moreover this plot appears to represent a segment of a curve (centered near a node) similar to those of Figure 10. This observation suggests that the small amplitudes of the 250–260-mμ Cotton effects of variable sign exhibited by these guanosine derivatives is a consequence of the shifting of the polarization angle through a nodal region of the hypothetical R_A *vs.* γ plot.

Figures 12a and 12b represent similar plots for the purine and adenine nucleoside derivatives. In both series the measured amplitudes vary progressively with increasing spectroscopic moment. It is interesting to note that for 6-substituted purine nucleosides the amplitude is observed to become more negative with increasing spectroscopic moment while the opposite is observed for the 8-substituted adenine nucleosides. Since 6-aminopurine is the same compound as X equals

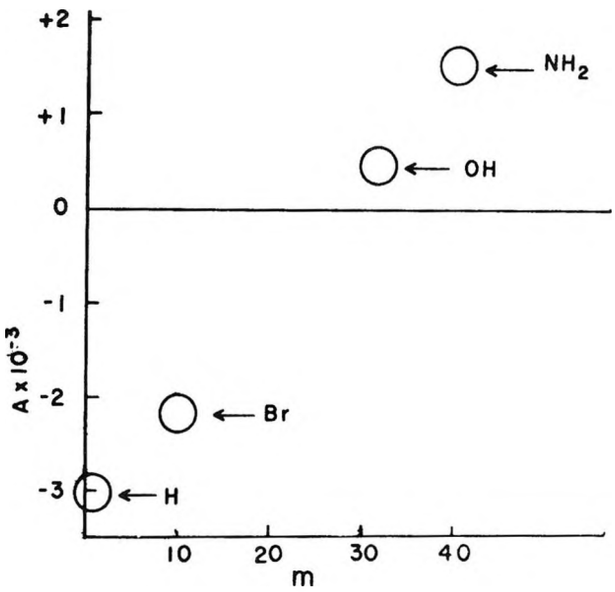

Figure 11. The amplitude of the long-wavelength Cotton effect of 8-substituted guanosines plotted against the spectroscopic moment, m, of the substituents.

H for the 8-substituted adenines, we could think of the two series as representing the substituent effects on 6- and 8-substituted purine. Substituents in the 6 position increase the rotation with increasing magnitude of their spectroscopic moments while 8 substitution decreases the rotation with increasing magnitude of the spectroscopic moments. A possible interpretation is that in one case the polarization angle is rotated clockwise and in the other counterclockwise. This interpretation is supported by an extrapolation of the theory of Platt, Moffitt, and Petruska. It has been observed that imidazole I, benzimidazole II, and purine III form a series of diminishing basic strength and increasing acid strength,[31] indicating that the benzene and, more particularly, the pyrimidine nucleus exerts an electron-withdrawing effect on the imidazole ring, or, to look at it from the other viewpoint, the imidazole ring exerts an electron-donating effect on the pyrimidine or benzene ring. Consequently its spectroscopic moment

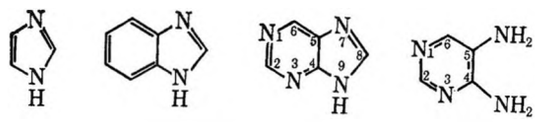

I II III IV

(27) J. R. Platt, *J. Chem. Phys.*, 19, 263 (1951).

(28) W. M. Moffitt, *ibid.*, 22, 320 (1954).

(29) J. Petruska, *ibid.*, 34, 1120 (1961).

(30) J. N. Murrell, "The Theory of the Electronic Spectra of Organic Molecules," John Wiley and Sons Inc., New York, N. Y., 1963, p 207.

(31) A. Albert and R. Brown, *J. Chem. Soc.*, 2062 (1954).

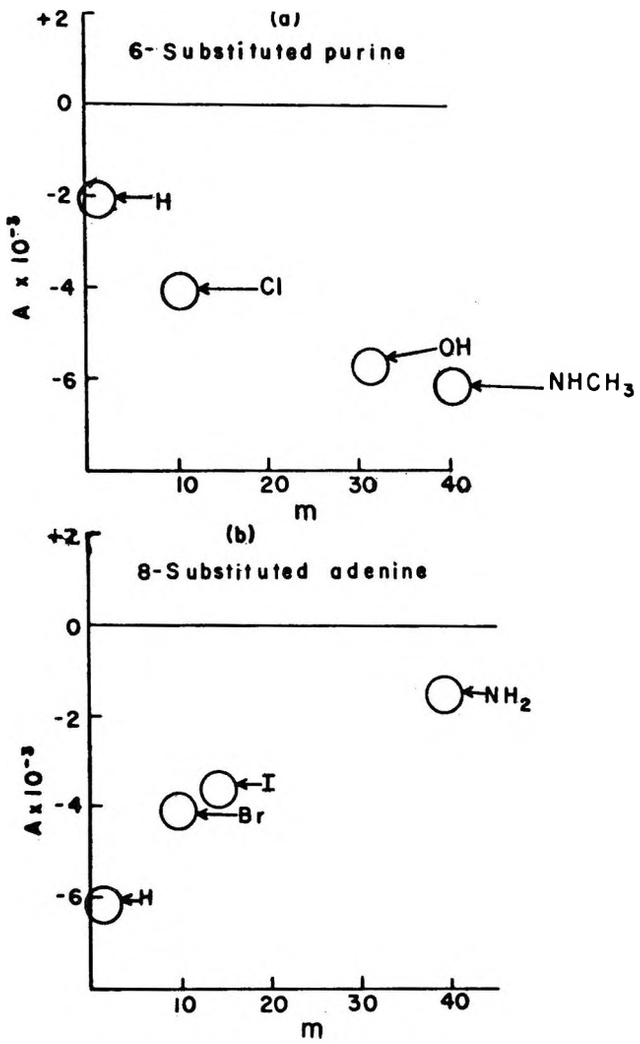

Figure 12. The amplitude of the long-wavelength Cotton effect of 6-substituted purines (a) and 8-substituted adenine nucleosides (b) as a function of the spectroscopic moment, m, of the substituents.

should be positive and this moment will be further enhanced by electron-donating substituents on the glyoxaline ring by virtue of the mesomeric effect. Moreover the ultraviolet spectrum of III is virtually not distinguishable from that of 4,5-diaminopyrimidine VI.[32] Consequently, the spectroscopic moment of the function 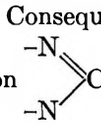 can be approximated by the vector sum of the spectroscopic moments of the $-NH_2$ groups attached at position 4 and position 5 of purine and also an electron-donating substituent at position 8 will increase this moment. Making use of the spectroscopic moments and their directions we can add moments vectorially to give the resultant moment for adenine

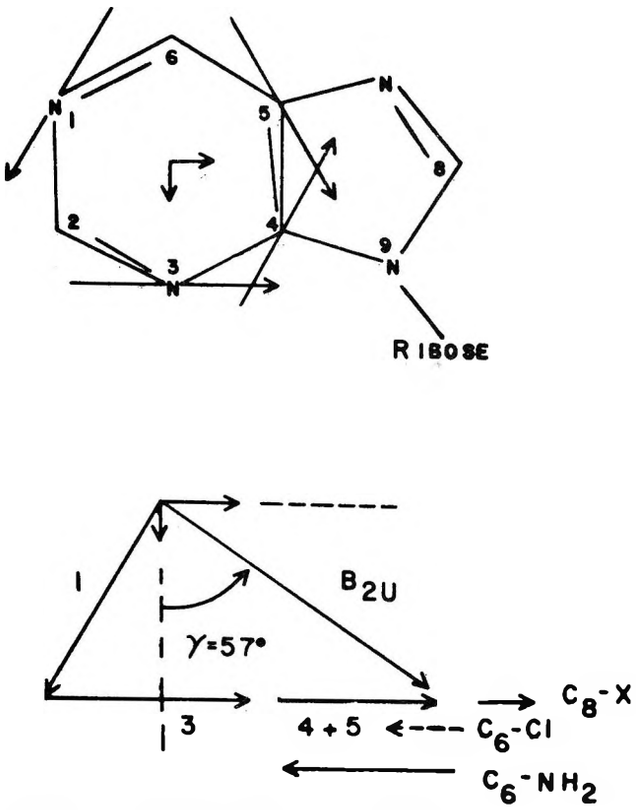

Figure 13. The B_{2u} transition moment is shown (bottom drawing) as the vector sum of the spectroscopic moments of the substituents in the purine ring (top drawing). Electron-donating substituents at site 8 will increase γ (counterclockwise) while electron-donating substituents at site 6 will decrease γ.

and purine (see Figure 13). From Figure 13 it is evident that 6-substituents with positive spectroscopic moments will tend to rotate the polarization direction clockwise, while positive 8-substituents will tend to rotate the polarization angle counterclockwise. Thus the substituent effects of Figure 12 appear to be the result of this shifting of the polarization angle back and forth.

Acknowledgments. We wish to thank Dr. Dan Urry and the Institute for Biomedical Research for the use of the Cary 6001 circular dichroism attachment to the Cary 60 and for the use of their facilities in preparing the manuscript. We also thank Mr. Douglas Miles for his help in performing the optical rotatory dispersion measurements and Miss Barbara Davis for drawing the figures and typing the manuscript.

Appendix

We wish to transpose term 2b into eq 3 after the method of Tinoco (see ref 12, p 151). The treatment

(32) S. F. Mason, *J. Chem. Soc.*, 2071 (1954).

given here is applicable to any system having a chromophore with C_s symmetry which interacts with vicinal groups having transitions only in the far-ultraviolet. We dissect the sugar residue into C–C, C–O, and O–H bond groups (the summation of j is taken over these bonds) and assume that these groups are sufficiently displaced from the base chromophore (group i) that it is sufficient to retain only the dipole term in the multiple expansion of the potential, $V_{i0a;j0b}$, of their interaction

$$V_{i0a;j0b} = \vec{\mu}_{i0a} \cdot \vec{T} \cdot \vec{\mu}_{j0b} \qquad \text{(A-1)}$$

$$\vec{T} = \frac{1}{r_{ij}^3}\left[1 - \frac{\vec{r}_{ij}\vec{r}_{ij}}{r_{ij}^2}\right]$$

The substitution of eq A-1 in term 2b gives

$$R_A^{(2b)} = -2 \sum_{j \neq i} \sum_{b \neq a} \mathrm{Im} \frac{\vec{\mu}_{i0a} \cdot \vec{T} \cdot \vec{\mu}_{j0b}}{h(\nu_b^2 - \nu_a^2)} \times [\vec{\mu}_{i0a} \cdot \vec{m}_{jb0} \nu_a + \vec{\mu}_{j0b} \cdot \vec{m}_{ia0} \nu_0] \qquad \text{(A-2)}$$

We expand this expression in a Taylor series about the frequency ν_0. Retaining only the first term in the expansion

$$R_A^{(2b)} = -2 \sum_{j \neq i} \frac{1}{h(\nu_0^2 - \nu_a^2)} \times [\mathrm{Im} \sum_b \nu_a \vec{\mu}_{i0a} \cdot \vec{T} \cdot \vec{\mu}_{j0b} \vec{m}_{jb0} \cdot \vec{\mu}_{i0a} + \nu_b \vec{\mu}_{i0a} \cdot \vec{T} \cdot \vec{\mu}_{j0b} \vec{\mu}_{j0b} \cdot \vec{m}_{ia0}] \qquad \text{(A-3)}$$

The summation $\sum_b \vec{\mu}_{j0b} \cdot \vec{m}_{jb0}$ in (A-3) is zero for cylindrically symmetrical groups in the sugar residue since symmetry prohibits $\vec{\mu}_{j0b}$ and $\vec{m}_{jb0}$ from having parallel components and the summation over $\sum_b \vec{\mu}_{j0b} \vec{\mu}_{jb0}$ can be replaced by the expression (see ref 12, p 151)

$$[(\alpha_{33} - \alpha_{11})_j \hat{e}_i \hat{e}_j + (\alpha_{11})_j 1] \frac{h\nu_0}{2}$$

Making this substitution we obtain

$$R_A^{(2b)} = -\sum_{j \neq i} \frac{\nu_0^2}{\nu_0^2 - \nu_b^2} \mu_{i0a} m_{ia0} (\alpha_{33} - \alpha_{11})_j G_{ij} \frac{\hat{e}_j \cdot \hat{e}_i'}{r_{ij}^3}$$

where we have also used the identities

$$\hat{\mu}_{i0a} = \mu_{i0a} \hat{e}_i$$

$$\vec{m}_{ia0} = m_{ia0} \hat{e}_i$$

and the expression for the dipole tensor, T. All symbols are as defined previously.

Vibrational Spectra of the Hydrogen Dihalide Ions. IV. $BrHBr^-$ and $BrDBr^-$

by J. C. Evans and G. Y-S. Lo

Chemical Physics Research Laboratory, The Dow Chemical Company, Midland, Michigan 48640
(Received May 5, 1967)

Infrared and Raman spectra of the series of salts, $R_4N^+ \cdot BrHBr^-$, where R is methyl, ethyl, *n*-propyl, *n*-butyl, or *n*-pentyl, were examined in the solid phase and in solution; some spectra were recorded of selected samples at low temperature. The data indicate that the anion may exist either in a linear, symmetrical form or in a linear, unsymmetrical form, the environment being the determining factor. Structure which was observed in the extremely broad absorption region, 1300–500 cm^{-1}, shown by the salts of the linear, symmetrical anion was assigned to $\nu_3 \pm n\nu_1$ where ν_3 and ν_1 are, respectively, the antisymmetric and symmetric stretching modes of the anion. It is suggested that this interpretation may be extended to the large class of compounds which contain very strong hydrogen bonds, –OHO–, and which show a similar, very broad absorption region the origin of which has not been satisfactorily explained.

Introduction

Earlier papers in this series[1] described and interpreted the vibrational spectra of several tetraalkylammonium salts of the hydrogen dihalides $ClHCl^-$, $ClHBr^-$, and FHX^-, where X was Cl, Br, or I. A striking result was the observation that the spectra of the anions, particularly $ClHCl^-$ and $ClDCl^-$, were markedly dependent upon the nature of the cation present. Two different structures were postulated for $ClHCl^-$ in different salts; for example, in tetraethylammonium hydrogen dichloride a linear, symmetrical anion was indicated while in the tetramethylammonium salt a linear, unsymmetrical anion in which the proton or deuteron residue in a single-minimum, unsymmetrical potential well was favored. Nuclear quadrupole resonance data[2,3] supported these conclusions. In this paper it is shown that the hydrogen dibromide ion is also very sensitive to its environment and that the vibrational spectra data again demand interpretation in terms of different anion structures in different salts.

Experimental Section

Infrared spectra were recorded using Beckman IR 9 and IR 11 instruments over the 50–3800-cm^{-1} range. Solid samples were dispersed in Nujol or Fluorolube for examination; solution spectra were obtained with dried, fractionally distilled methylene chloride, acetonitrile, and benzene as solvents. Anion absorption bands were broad and this factor determined the uncertainties in band frequency measurements. All sample handling was done in a glove box purged with dry nitrogen; only in this manner could the appearance of bands of H_3O^+ and its deuterated analogs in the spectra be avoided. Some infrared spectra were recorded of samples cooled to approximately 100°K. Raman spectra were obtained for the solid salts, sealed in glass cells, using a Hilger E612 (*f*/5.7) spectrograph with photographic recording (16 A/mm at 4358 A) and mercury arc excitation (4358-A line).

Eastman grade tetra-*n*-alkylammonium bromide samples were further purified by recrystallization if their infrared spectra were not satisfactory; all were dried by azeotropic distillation with benzene followed by further drying by warming under vacuum. Anhydrous HBr (Matheson, 99.8% min) reacted with the solid bromides readily. To ensure complete reaction the gas was con-

(1) J. C. Evans and G. Y-S. Lo, *J. Phys. Chem.*, **70**, 11, 20, 543 (1966).

(2) J. C. Evans and G. Y-S. Lo, *ibid.*, **70**, 2702 (1966).

(3) J. C. Evans and G. Y-S. Lo, *ibid.*, **71**, 3697 (1967).

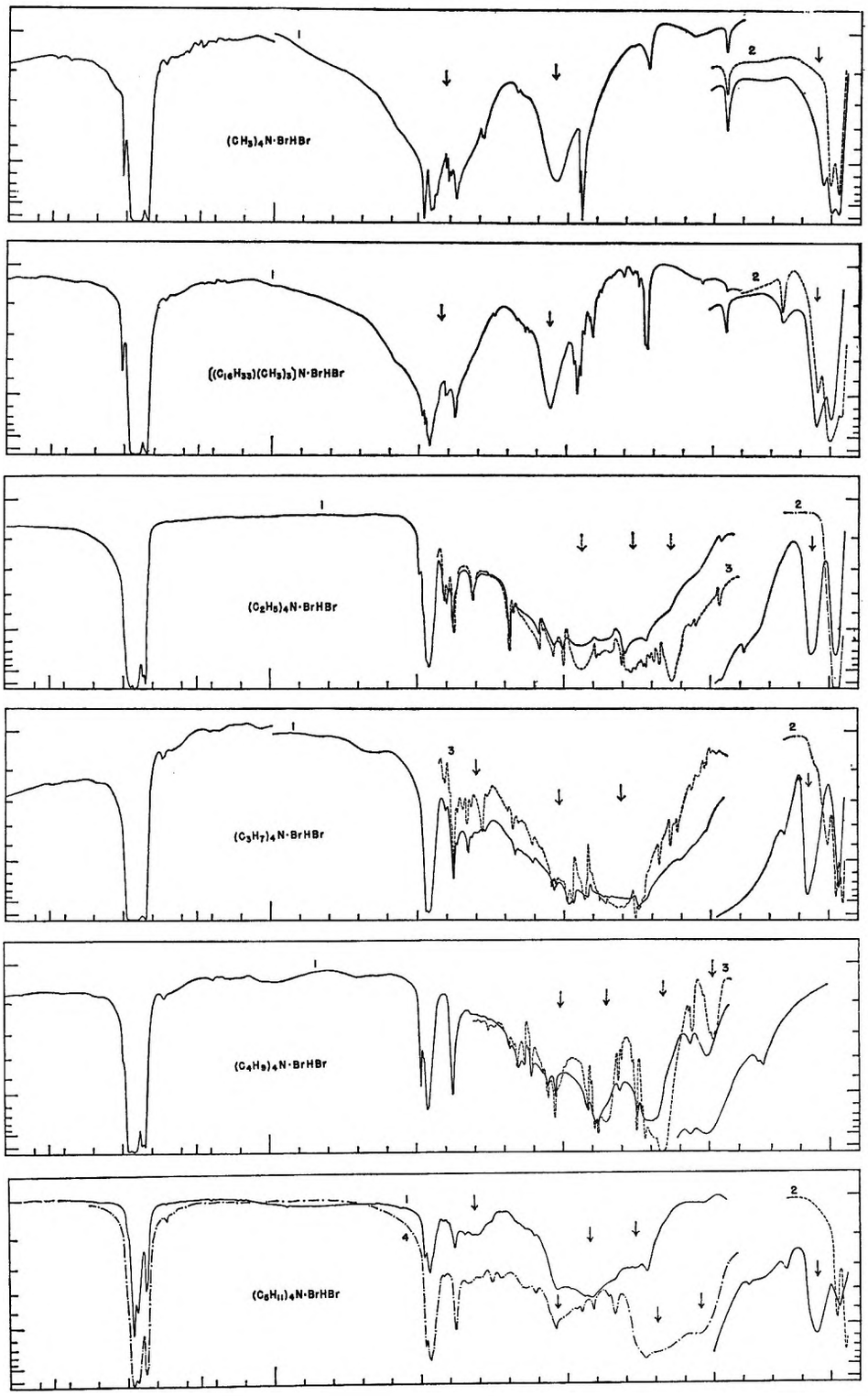

Figure 1. Infrared absorption spectra of Nujol mulls of protium dibromide salts. Traces numbered 1 are room-temperature spectra; those marked 3 were obtained at approximately 100°K; those marked 2 are the spectra (far-infrared only) of the corresponding bromides obtained at room temperature and included here to illustrate the lattice-mode absorption region. Arrows indicate bands assigned to the anions. The C_6H_{11} spectra were of liquid films; spectrum 4 is that of the deuterium dibromide salt of $(C_6H_{11})_4N^+$.

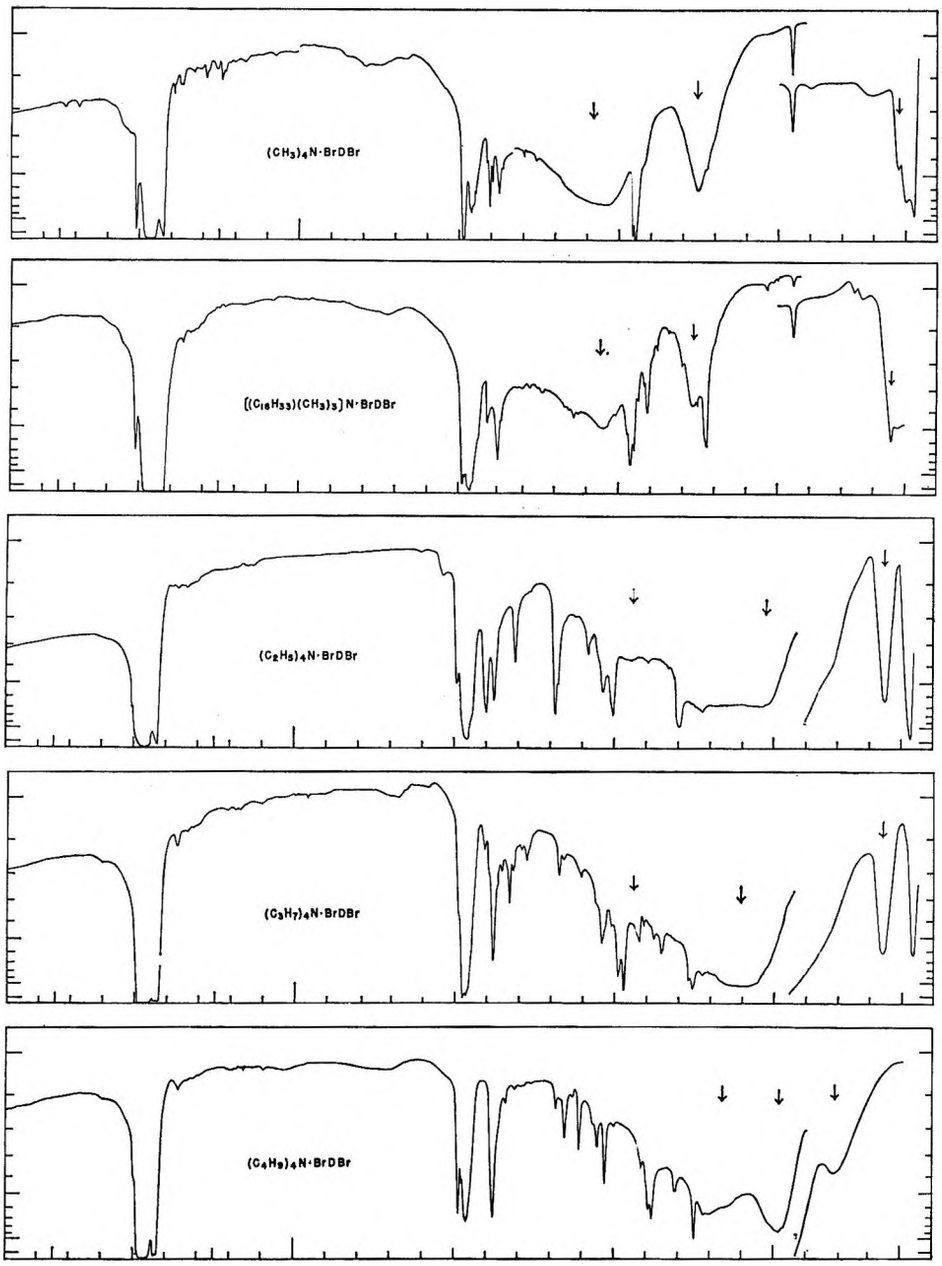

Figure 2. Infrared absorption spectra of Nujol mulls of deuterium dibromide salts.

densed onto the salt at low temperature (approximately −78°), the mixture was allowed to equilibrate, and the excess HBr was evaporated away carefully to yield the 1–1 salts; this ratio was determined by titration of an aqueous solution of the product with standard alkali. Another method of preparation was also used for several salts; the appropriate bromide was dissolved in methylene chloride at room temperature and HBr was bubbled through the solution. Addition of cyclohexane induced crystallization of the desired 1–1 salts. DBr was prepared by the reaction of D_2O (99.7%) with benzoyl bromide and used immediately to prepare the deuterium dibromide salts.

Results

Infrared spectra are reproduced in Figures 1–3 while wavenumber data for the species of interest, the anions, are collected in Tables I–III. Arrows on the diagrams indicate all bands assigned to the anions; overlapping cation bands, which are readily identified, make the

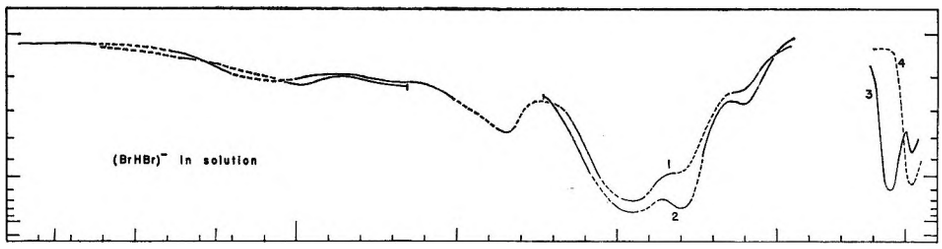

Figure 3. Infrared absorption spectra of $BrHBr^-$ in methylene chloride (1), in acetonitrile (2), and in benzene solution (3). Spectrum 4, which is that of $(C_6H_{11})_4N{\cdot}Br$ in benzene in the far-infrared region only, illustrates the presence of bands of ion aggregates. Concentrations were approximately 0.15 *M*; cell thickness was approximately 0.1 mm in the mid-infrared region; in the far-infrared region 1-mm cells with concentrations approximately 0.2 *M* were used.

Table I: Vibrational Bands Assigned to the Protium and Deuterium Dibromide Ions in Solid Type I Salts[a]

$(CH_3)_4N^+$			$(CH_3)_8$-*n*-$C_{16}H_{33}N^+$		
Infrared		Raman	Infrared		Assignment
$BrHBr^-$	$BrDBr^-$	$BrHBr^-$	$BrHBr^-$	$BrDBr^-$	
~1850 vb, w			~1850 vb, w		$2\nu_2$
1420 ± 30 vb, vs	1070 ± 20 vb, vs	1380 ± 30 vb, vw	1420 ± 30 vb, vs	1070 ± 30 vb, vs	ν_3
1038 ± 4 vs	752 ± 3 vs	1030 ± 15 b, vw	1053 ± 3 s	765 ± 5 s	ν_2
126 ± 3 b, w	123 ± 3 b, w	...	~130 (obscured partly)	~130 b	ν_1

[a] vb = very broad; vs = very strong; b = broad; s = strong; w = weak; vw = very weak; m = medium intensity.

choice of band centers uncertain in many cases. A limited comparison with previously reported spectra is possible. Bands at 1670 and 1170 cm^{-1} were reported[4] for the anion in tetraethylammonium hydrogen dibromide, at 1700 cm^{-1} for the same salt,[5] at 1690 and 1170 cm^{-1} for tetra-*n*-butylammonium hydrogen dibromide,[4] and at 1297 and 870 cm^{-1} for tetra-*n*-butylammonium deuterium dibromide.[6] The spectra obtained for the same salts during the present study were markedly different and it is suggested that the bands previously reported should be reassigned. Brief exposure of tetraethylammonium hydrogen dibromide to atmospheric moisture during the sample preparation for infrared examination yielded prominent bands near 2900 (vs), 2500 (sh), 2160 (w), 1680 (m), 950 m, and 550 cm^{-1} (w), all of which are H_3O^+ bands;[7] the other feature reported at 1170 cm^{-1}, a sharp, prominent band which is unaffected by exposure of the sample to moisture and which is prominent also in the spectrum of tetraethylammonium bromide, is a cation band. Exposure of several DBr_2^- salts to atmospheric moisture yielded complex spectra probably attributable to $H_nD_{3-n}O^+$ species, but no prominent features near 1297 and 870 cm^{-1} were observed. However, D_3O^+ bands occur near 1250 and 800 cm^{-1} in $D_3{}^+O{\cdot}Cl^-$.[7] This may be the proper interpretation for the previously observed bands but if this is so it seems surprising that the strongest D_3O^+ band near 1900 cm^{-1} was overlooked.

Most of the salts were examined in solution in acetonitrile and in methylene chloride; although HBr and acetonitrile react readily, there was no indication of reaction in these solutions during the time required to record infrared and Raman spectra. For the far-infrared region benzene was the only suitable solvent found and only the longer chain cation salts were sufficiently soluble. The spectra given in Figure 3 are composites of several spectra; the regions of uncertainty, due largely to solvent absorption bands, are indicated by dotted lines.

The Raman spectra of the solid salts and of their solutions showed numerous cation bands but in only one case, that of tetramethylammonium hydrogen dibromide, were weak, broad anion bands observed.

Discussion

Structural information is not yet available for any hydrogen dibromide salt, nor has a residual entropy determination, analogous to that made for tetramethylammonium hydrogen dichloride,[8] been made. Inter-

(4) D. H. McDaniel and R. E. Vallee, *Inorg. Chem.*, **2**, 997 (1963).
(5) D. G. Tuck and E. J. Woodhouse, *Proc. Chem. Soc.*, **53** (1963).
(6) J. A. Salthouse and T. C. Waddington, *J. Chem. Soc., Sect. A*, 28 (1966).
(7) C. C. Ferriso and D. F. Hornig, *J. Chem. Phys.*, **23**, 1464 (1955).
(8) S. Chang and E. F. Westrum, *ibid.*, **36**, 2571 (1962).

Table II: Absorption Bands Assigned to the Protium and Deuterium Dibromide Ions in Solid Type II Salts[a]

$(C_2H_5)_4N^+$				$(n\text{-}C_3H_7)_4N^+$				$(n\text{-}C_4H_9)_4N^+$				$(n\text{-}C_5H_{11})_4N^+$		Assignment
BrHBr⁻		BrDBr⁻		BrHBr⁻		BrDBr⁻		BrHBr⁻		BrDBr⁻		BrHBr⁻	BrDBr⁻	
300°K	100°K	300°K		300°K	100°K	300°K		300°K	100°K	300°K	100°K	300°K	300°K	
1350 ± 20 w		~950 w		1300 ± 20 w		~950 w		...				1320 ± 20 w	970 ± 20 w	ν_2
very broad, unresolved	940 ± 10 s 780 ± 10 s 630 ± 5 s	very broad, unresolved		very broad, unresolved, center ~820	~1000 s ~820 s	~800 s ~600 s		~1040 w ~870 m 700 ± 10 s 510 ± 10 m	1030 ± 10 m 860 ± 10 s 670 ± 10 vs 495 ± 10 w	650 ± 10 m 490 ± 5 s 320 ± 5 w	480 s ...	920 ± 20 s, b 770 ± 10 s, b	700 ± 20 s, b 550 ± 10 s, b	$\nu_2 + 2\nu_1$ $\nu_3 + \nu_1$ ν_3 $\nu_3 - \nu_1$
~330 vvw														$2\nu_1$
160 ± 5 vw		155 ± 5 vw		170 ± 5 vw		165 ± 5 vw		...		...		150 ± 5 vw		ν_1

[a] See Table I for key to abbreviations.

pretation of the vibrational spectra is, however, greatly assisted by the available data for the unsymmetric $ClHBr^-$ ion and the two types of $ClHCl^-$ ions.[1] An analogous classification into type I and type II salts is applicable here also.

Type I Salts. Two of the salts showed spectra reminiscent of the $ClHBr^-$ and type I $ClHCl^-$ salts; these are the tetramethyl- and hexadecyltrimethylammonium hydrogen dibromides. Both showed a very broad band near 1400 cm^{-1}, a narrower band near 1050 cm^{-1}, and a weak band near 130 cm^{-1}. Deuterium substitution shifted these to the 1070-cm^{-1} region ($\nu^H/\nu^D = 1.33$) and the 750-cm^{-1} region ($\nu^H/\nu^D = 1.38$), while the lowest wavenumber band, which was partly overlapped by lattice modes, appeared to move to lower wavenumber by about 3 cm^{-1} ($\nu_H/\nu_D \sim 1.02$). Lowering the temperature to approximately 100°K sharpened the spectra slightly but did not significantly affect the two higher wavenumber bands; the temperature dependence study was confined to the region above 200 cm^{-1}. The two higher frequency bands were also observed in the Raman spectrum of tetramethylammonium hydrogen dibromide. Arguments closely analogous to those which are given in detail in paper I of this series lead to the assignment of the linear, unsymmetrical structure, with single-minimum potential for the hydrogen, to the $BrHBr^-$ ion in these type I salts. The existence of the type II salts with their markedly different spectra supports this conclusion.

Type II Salts. The outstanding feature of the infrared spectra of the type II salts, which include the tetraethyl-, tetra-*n*-propyl-, tetra-*n*-butyl-, and tetra-*n*-pentylammonium hydrogen dibromides, was an extremely broad region, 1300–500 cm^{-1}, of strong absorption. The band showed some structure, which was best defined in the case of the tetrabutylammonium salt for which four components could be discerned. At approximately 100°K these features were rather better defined and it appeared that the lowest frequency band, near 500 cm^{-1}, was reduced in intensity relative to the others although it was sharper. The tetraethylammonium salt also showed structure at the lower temperature and here, also, the components were evenly separated by wavenumber intervals of about 160 cm^{-1}. In the far-infrared region, the tetrabutylammonium salt showed no absorption near 160 cm^{-1} but a well-defined, weak band appeared here for all the other type II salts. It is assigned to ν_1, the symmetric stretching mode of $BrHBr^-$. A reasonable assignment for the structure observed within the broad absorption is then to $\nu_3 \pm n\nu_1$, where ν_3 is the antisymmetric stretching mode. Where the features are sufficiently well defined they are so assigned in Table II. The strongest feature in the

Table III: Anion Absorption Bands in Spectra of Solutions of Tetraalkylammonium Protium and Deuterium Dibromides[a]

Acetonitrile	Methylene chloride		Benzene		Assignment
$BrHBr^-$	$BrHBr^-$	$BrDBr^-$	$BrHBr^-$	$BrDBr^-$	
	1350 ± 10 w	980 ± 20 w			ν_2
1050 ± 20 s	1050 ± 20 s,b	~740 s			$\nu_3 + \nu_1$
790 ± 10 s	800 ± 20 s	580 ± 20 s			ν_3
610 ± 10 w	630 ± 20 w				$\nu_3 - \nu_1$
			150 ± 5 vw	145 ± 5 vw	ν_1

[a] See Table I for key to abbreviations.

low-temperature spectra is in each case assigned to ν_3; this is in accord with the assignment ν_3–ν_1 in tetrabutylammonium hydrogen dibromide.

The absence of a band, assignable to ν_1, from this salt's spectrum is probably due to the high site symmetry at the anion in this crystal; the anion behaves as expected for a linear, symmetric $D_{\infty h}$ species for which ν_1 is infrared inactive. Further support for this structure is provided by the ratio ν_3^H/ν_3^D of 1.41 which is reminiscent of symmetrical FHF^- [9] and by the force constant values computed for a valence force field with two constants—k_1, the bond stretching, and k_{12}, the bond–bond interaction constant—applied to the linear, symmetrical model, with $\nu_3 = 670$ and $\nu_1 = 170$ cm^{-1}, $k_1 = 0.75$ and $k_{12} = 0.62$ mdyne/A. The exceptionally high k_{12}/k_1 ratio is also reminiscent of HF_2^-.

There is no obvious choice of band for assignment to ν_2, the degenerate bending mode, in the spectra of type II salts. There is, in the spectrum of tetrapentylammonium hydrogen bromide, which was examined as a liquefied film, a broad absorption near 1330 cm^{-1} which shifts to near 1000 cm^{-1} in the deuterium-substituted salt. Thick films of solid tetrapropylammonium salts show the same features but less clearly. Assignment of these to ν_2 is favored.

Solution spectra in methylene chloride show the analogous bands at 1350 and 980 cm^{-1}. If the assignment to ν_2 is accepted, the remaining three, broad overlapping bands in the 1200–500-cm^{-1} region must be assigned to ν_3 and its combinations with ν_1; $\nu_3 + \nu_1$, ν_3, and $\nu_3 - \nu_1$ seem to be suitable and the ratio ν_3^H/ν_3^D is close to the expected 1.41. However, the intensity ratios are anomalous with $\nu_3 + \nu_1$ showing an unusually high intensity. An energy level diagram of the type proposed by Stepanov[10] may be used to rationalize this. Sheppard[11] had discussed the scheme in detail more recently and the present description will merely outline briefly the main assumptions. The observed transitions in the vicinity of the fundamental ν_3 transition are considered to be transitions between energy levels, of the mode ν_1, which are drawn in the two Morse-type (potential energy *vs.* Br···Br distance) curves, the lower of which describes the system with ν_3 unexcited while the upper curve describes the system with ν_3 excited by one quantum; *i.e.*, the Born–Oppenheimer approximation is assumed to be valid for the vibrational motions of ν_3 and ν_1. A difference in position of the potential minima of the two curves and the assumption that the Franck–Condon principle is applicable supplies the mechanism for an intense $\nu_3 + \nu_1$ transition. This transition occurs between the 0 level of the lower curve and 1 level of the upper curve. Since the interaction energy is not large, approximately 13 kcal/mole,[4] external influences such as solvent, cation structure, and unit-cell dimension changes produced by temperature reduction would be expected to influence such potential energy curves and the transitions between them, significantly. Another factor which contributes to the temperature dependence of the spectra is the influence of upper-stage transitions involving not only ν_1 but also the lattice mode levels.

Conclusion

The most significant result is the clear evidence which is given for the nature of the extremely broad absorption region, 500–1300 cm^{-1}, shown by the type II salts which are believed to contain linear, symmetrical anions. It is probable that the proposed explanation can be extended to the large class of compounds containing strong –O···H···O– bonds which also show a similar broad absorption region; it appears that in no case of this class has there yet been observed a well-defined band progression in this region.[12]

(9) J. A. Ibers, *J. Chem. Phys.*, **41**, 25 (1964).

(10) B. I. Stepanov, *Zh. Fiz. Khim.*, **19**, 507 (1945).

(11) N. Sheppard, "Hydrogen Bonding Symposium Proceedings," D. Hadzi, Ed., Pergamon Press, Inc., New York, N. Y., 1959.

(12) D. Hadzi, *Pure Appl. Chem.*, **11**, 435 (1965).

The Concentration Dependence of Zeolitic Sorption

by W. W. Brandt[1] and W. Rudloff

Department of Chemistry, Illinois Institute of Technology, Chicago, Illinois 60616 (*Received May 7, 1967*)

The concentration dependence of sorption rates of selected gases on chabazite has been determined and interpreted in terms of the various rate-controlling mechanisms present. Argon and several other gases exhibit concentration-independent activated diffusion into the bulk of the zeolite. Freon 21 occupies only the pores or crevices of the mineral and the rates are probably controlled by Knudsen or gaseous bulk diffusion, depending on the concentration range. Finally, carbon dioxide sorption rates at low sorbate concentrations appear to be controlled by a relatively slow chemisorption on the internal sites, while at higher concentrations the diffusion rate of the gas into the bulk of the zeolite becomes important. Sorption isotherms obtained in this study and differential heats of sorption and infrared evidence reported in the literature are consistent with this interpretation.

Introduction

The concentration dependence of apparent sorption or desorption rate coefficients is measured only rarely with the primary goal of gaining insight into the nature of the rate process present. This is largely due to the mathematical and computational difficulties encountered in the evaluation.[2] Especially if the sorbate concentration changes appreciably during a given experiment and if the rate is controlled by different steps of the over-all sorption process as the sorbate concentration changes, the approach becomes impractical. In earlier studies, this latter effect, that is, the apparent concentration dependence of measured sorption rates, has been rendered harmless by refining the experimental techniques to the point where only very small changes in the sorbate concentrations occur during a given sorption rate experiment (small-step experiments).[3,4] The resulting sorption rate data were fitted at various stages of the process, using the solution to the diffusion equation involving constant, *i.e.*, concentration-independent, diffusion coefficients. In this way, the changes of the rate coefficient at various stages of the process, but at essentially constant sorbate concentrations, were obtained and then interpreted in terms of different possible rate-controlling steps present, or in terms of the sorbent heterogeneity as demonstrated by microscopic methods.

In the present study, many additional small-step (and other) experiments have been carried out, as described above, at widely differing sorbate concentrations. The inherent concentration dependence of the observed sorption rate coefficient has thus been determined as contrasted to the apparent concentration dependence discussed above. The question as to what constitutes a "small-step" experiment will be discussed after the presentation of the results.

The inherent concentration dependence of the rate coefficients, for example, those obtained at the beginning of each step experiment (where a single-step experiment would involve very small changes of sorbate concentration, but the steps were performed at widely differing concentration levels), will be used to gain information on the nature of the rate-controlling step present. The analysis will be aided by analyzing the variation of the apparent diffusion coefficients during each individual step.

Natural chabazite is a rather interesting sorbent for studies of this type; its crystal structure has been carefully investigated.[5,6] The diffusion paths, at least in

(1) To whom correspondence should be addressed at the Chemistry Department, University of Wisconsin, Milwaukee, Wis.

(2) (a) J. Crank, "The Mathematics of Diffusion," Oxford University Press, 1957; (b) E. Bruecke and H. Ley, *Z. Physik. Chem.* (Frankfurt), **26**, 187, 202 (1960).

(3) W. W. Brandt and W. Rudloff, *J. Phys. Chem. Solids*, **25**, 167 (1964).

(4) W. W. Brandt and W. Rudloff, *Z. Physik. Chem.* (Frankfurt), **42**, 201 (1964).

(5) J. V. Smith, *J. Chem. Soc.*, 3759 (1964).

(6) J. H. Fang and J. V. Smith, *ibid.*, 3749 (1964).

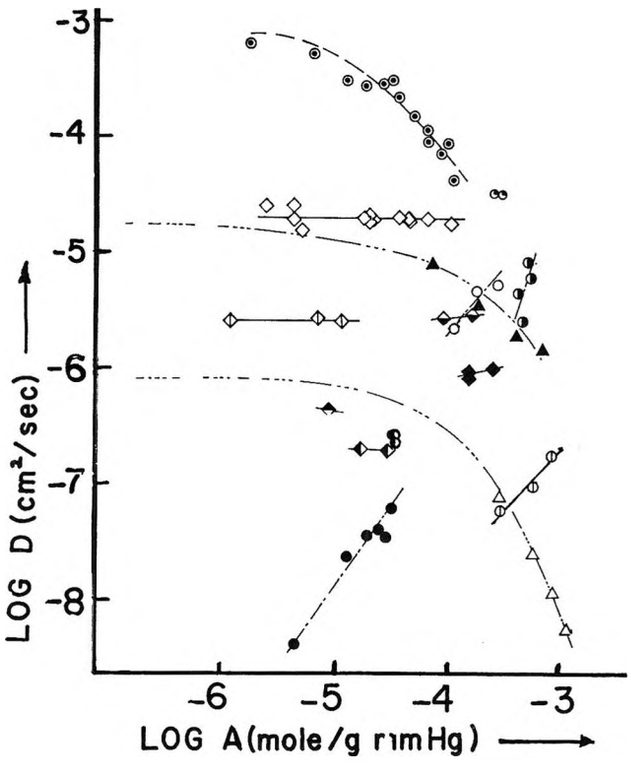

Figure 1. Apparent diffusion coefficients, D, as a function of the total final uptake of sorbate in the sorbent, A. All data are reported in Table I unless otherwise indicated. A sample of chabazite, grain diameter 0.81 cm,[3] was degassed at experimental temperature: ⊙, Freon 21 sorption and desorption at 13.6° (the points corresponding to runs 25/66 and 25/77 practically coincide in this figure); ◈, methane sorptions at about 100° (see runs 13/232 and 13/233 of ref 4 and run 13/231 of Figure 2 ($D^* = D/a^2$, where a is the radius of the grains); ◆, methane sorption at 50°; O, carbon dioxide sorption at 100°; ◔, carbon dioxide desorption at 100°; ⊙, carbon dioxide sorption at 5.7°. A sample of chabazite powder, average grain diameter 0.19 cm, was degassed at 350°; ◆, methane sorption at 150°; ◆, methane sorption at 100°; ◑, carbon dioxide sorption at 150°. A sample of small chabazite grains, average diameter 0.68 cm, was degassed above 250°: ◇, methane sorption at 50°. A sample of chabazite powder, average grain diameter 0.0088 cm, was degassed at the experimental temperature: ●, carbon dioxide sorption at 100°; ◑, carbon dioxide desorption at 100°. A similar sample: ◈, methane sorption at 100° (see runs 25/120 and 25/122 of ref 4). The experiments ◇, ◆, ◆, and ◑ are somewhat less precise than the others; they are reported in this figure only while the other D values are taken from Table I: ▲, propane sorption on chabazite at 150°; △, methylene chloride sorption on same chabazite at 0° (both curves from data given in ref 10 but shifted to higher D values by seven units on the logarithmic scale).

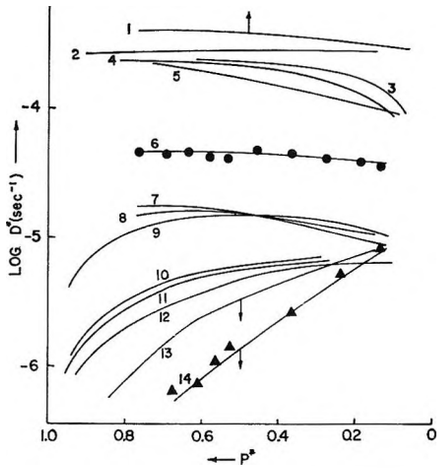

Figure 2. Apparent diffusion rates, D^*, against fractional amount of sorbate yet to be sorbed or desorbed in a given run, P^*: $D^* \equiv D/a^2$, where D is the diffusion coefficient and a is the (equivalent) radius of the sorbent grains. The top curve is displaced to lower values and the two bottom curves, 13 and 14, are displaced to higher values of log D^*, always by one decade. The curve numbers, gases, and experimental temperatures are given here, with the experiment reference numbers in parentheses: 1, Freon 21, sorption at 13.6° (25/64); 2, same, but higher concentration (25/74); 3, carbon dioxide, desorption at 50.6° (25/13); 4, argon, desorption at 97.7° (13/235); 5, argon desorption at 97.7° (13/236); 6, argon, sorption at 50.3° (13/257); 7, methane, sorption at 97.8° (13/231); 8, methane, desorption at 97.8° (13/234); 9, carbon dioxide, sorption at 99.7° (25/8); 10, sorption at intermediate sorbate concentration at 50.6° (25/12); 11, same (25/15); 12, same (25/10); 13, carbon dioxide sorption at relatively high sorbate concentration at 5.7° (25/7); 14, at lower concentration, at the same temperature (25/5). Runs 13/231, 13/235, and 13/257 are reported in ref 4; the others are in Table I. The individual points of D^* as a function of P^* were obtained by fitting the appropriate solution to the diffusion equation to portions of the experimental desorption curves (see text). The individual points thus obtained are shown for two of the curves, 6 and 14, to demonstrate the magnitude of the uncertainties in this graphical procedure. The reproducibility of the results from one run to the next is seen by comparing curves 7 and 8.

the case of intracrystalline diffusion, as opposed to defect diffusion, are defined by the eight-membered apertures or windows of about 3–4-A diameter, connecting the large cavities of 6–7-A diameter and 10-A length.

The sorbate molecules used varied greatly in diameter: H_2 has a diameter of 2.97 A, or 2.43 A; CH_4, 3.88 A; CO_2, 4.00 A; and Freon 21 or dichlorofluoromethane, roughly a 4.9-A diameter.[7] Comparing these diameters with the size of the aperatures in the crystal structure, one may well expect very different predominant diffusion mechanisms in the various gas chabazite systems.

Experimental Section

The principal sample of crystalline chabazites used

(7) J. O. Hirschfelder, C. F. Curtiss, and R. B. Bird, "Molecular Theory of Gases and Liquids," John Wiley and Sons, Inc., New York, N. Y., 1954, pp 1110 and 1111. The value for Freon 21 is interpolated.

Table I: Basic Experimental Data on Sorption and Desorption Experiments[a]

Run	t_d, hr	T, °C	p_1, mm	p_0, mm	p_∞, mm	s, moles/g mm	D, cm²/sec
Sample: chabazite grain, diameter 0.81 cm; degassed at the experimental temperature, T							
				Argon			
13/236	...	97.7	212.64	0.077	12.40	16×10^{-7}	2.9×10^{-5}
13/321	12	9.4	0	201.89	160.36	2.8×10^{-7}	1.5×10^{-6}
				Methane			
13/232	15	97.8	0	27.10	23.96	1.0×10^{-7}	1.0×10^{-6}
13/234	...	97.8	76.11	0.18	13.79	2.5×10^{-7}	2.6×10^{-6}
13/259	...	50.2	93.8	1.85	24.06	7.4×10^{-7}	4.7×10^{-7}
				Hydrogen			
25/28	...	99.5	184.44	1.40	3.70	...	9.2×10^{-4}
25/30	...	99.5	236.03	0.42	3.43	...	8.1×10^{-4}
25/32	...	49.1	211.2	0.52	4.29	...	5.5×10^{-4}
25/34	...	49.1	255.42	0.78	5.30	...	6.0×10^{-4}
25/39	...	3.8	211.34	409.50	403.50	3.1×10^{-8}	3.8×10^{-4}
25/40	...	3.6	403.50	249.63	253.71	3.2×10^{-8}	3.3×10^{-4}
25/41	...	3.6	253.71	10.00	16.57	7.3×10^{-8}	3.6×10^{-4}
				Carbon Dioxide			
25/8	24	99.7	0	44.11	28.65	7.3×10^{-6}	2.3×10^{-6}
25/17	12	99.5	0	22.23	13.33	9.0×10^{-6}	2.3×10^{-6}
25/19	12	99.5	0	21.14	12.15	1.0×10^{-5}	2.5×10^{-6}
25/20	...	99.5	12.15	36.39	28.70	7.9×10^{-6}	4.8×10^{-6}
25/21	...	99.5	28.70	52.86	46.90	6.5×10^{-6}	5.3×10^{-6}
25/22	...	99.5	46.90	0.21	38.52	6.8×10^{-6}	3.3×10^{-6}
25/23	...	99.5	38.52	0.30	32.57	6.9×10^{-6}	3.5×10^{-5}
25/10	7	50.6	0	42.39	15.43	2.4×10^{-5}	1.1×10^{-6}
25/12	...	50.6	15.43	43.51	28.25	2.0×10^{-5}	1.2×10^{-6}
25/13	...	50.6	28.25	0.63	26.94	2.0×10^{-5}	1.8×10^{-5}
25/15	12	49.4	0	224.69	107.4	1.5×10^{-5}	1.1×10^{-6}
25/16	12	49.4	0	21.76	6.76	3.0×10^{-5}	1.1×10^{-6}
25/5	70	5.7	0	45.67	2.58	2.3×10^{-4}	1.3×10^{-6}
25/6	...	5.7	2.58	44.31	5.97	1.9×10^{-4}	1.4×10^{-6}
25/7	...	5.6	5.97	45.91	10.76	1.5×10^{-4}	1.5×10^{-6}
				Freon 21			
25/64	12	13.6	0	31.3	27.9	1.2×10^{-7}	6.4×10^{-4}
25/65	...	13.6	27.9	77.3	71.9	1.3×10^{-7}	5.3×10^{-4}
25/66	...	13.6	71.9	128.0	122.0	1.2×10^{-7}	3.2×10^{-4}
25/67	...	13.6	122.0	179.4	173.8	1.2×10^{-7}	2.9×10^{-4}
25/68	...	13.6	173.8	231.3	225.0	1.2×10^{-7}	2.9×10^{-4}
25/69	...	13.6	225.0	276.6	272.9	1.2×10^{-7}	2.2×10^{-4}
25/70	...	13.6	272.9	323.9	317.4	1.3×10^{-7}	2.3×10^{-4}
25/71	...	13.6	371.4	394.6	381.8	1.4×10^{-7}	1.6×10^{-4}
25/72	...	13.6	381.8	489.5	472.1	1.5×10^{-7}	9.2×10^{-5}
25/73	...	13.6	472.1	592.6	568.7	1.7×10^{-7}	7.3×10^{-5}
25/74	...	13.6	568.7	628.1	608.3	1.9×10^{-7}	4.3×10^{-5}
25/75	...	13.6	608.3	475.4	513.8	1.5×10^{-7}	9.1×10^{-5}
25/76	...	13.6	513.8	368.9	398.8	1.2×10^{-7}	1.2×10^{-4}
25/77	...	13.6	398.8	203.3	232.2	...	3.3×10^{-4}
Sample: grain of same chabazite, average diameter 0.67 cm; degassed at above 250°							
				Methane			
13/30	12.5	50	0	27.3	24.0	4.3×10^{-7}	1.6×10^{-5}
13/32	2	50	0	15.5	13.9	3.6×10^{-7}	2.5×10^{-5}
13/33	15	50	0	26.3	23.5	3.7×10^{-7}	2.6×10^{-5}
13/34	2	50	0	28.1	25.1	3.8×10^{-7}	2.3×10^{-5}

Table I (*Continued*)

Run	t_d, hr	T, °C	p_1, mm	p_0, mm	p_∞, mm	s, moles/g mm	D, cm²/sec
Sample: grain of same chabazite, average diameter 0.67 cm; degassed at above 250°							
				Methane			
13/35	19	50	0	108.0	95.6	4.0×10^{-7}	2.1×10^{-5}
13/36	19	50	0	110.7	97.8	4.1×10^{-7}	2.1×10^{-5}
13/37	2	50	0	108.6	95.8	4.1×10^{-7}	2.1×10^{-5}
13/38	15	50	0	110.3	97.4	4.1×10^{-7}	1.9×10^{-5}
13/39	2	50	0	201.2	177.7	4.1×10^{-7}	2.1×10^{-5}
13/40	16	50	0	113.2	99.2	4.4×10^{-7}	2.0×10^{-5}
13/41	...	50	99.2	114.1	112.4	3.9×10^{-7}	2.1×10^{-5}
13/42	...	50	112.4	130.8	128.4	3.5×10^{-7}	1.9×10^{-5}
13/43	13	50	0	112.7	98.5	4.5×10^{-7}	2.0×10^{-5}
13/44	...	50	98.5	211.2	198.6	4.2×10^{-7}	2.0×10^{-5}
13/45	...	50	198.6	307.8	296.0	4.0×10^{-7}	1.8×10^{-5}
Sample: chabazite powder, average grain diameter 0.0088 cm; degassed at the experimental temperature, T							
				Carbon Dioxide			
13/183	19	99.2	0	13.2	1.74	5.6×10^{-6}	4.2×10^{-9}
13/184	...	99.2	1.74	13.6	4.67	3.7×10^{-6}	2.4×10^{-8}
13/185	...	99.2	4.67	14.6	7.62	3.0×10^{-6}	3.7×10^{-8}
13/186	...	99.2	7.62	16.4	10.8	2.6×10^{-6}	4.1×10^{-8}
13/187	...	99.2	10.8	17.5	13.1	2.4×10^{-6}	3.6×10^{-8}
13/188	...	99.2	13.1	18.7	15.3	2.3×10^{-6}	6.3×10^{-8}
13/189	...	99.2	15.3	10.6	11.3	3.0×10^{-6}	2.3×10^{-7}
13/190	...	99.2	11.3	7.89	8.74	3.8×10^{-6}	2.8×10^{-7}
13/191	...	99.2	8.74	5.75	6.62	4.9×10^{-6}	2.7×10^{-7}

[a] t_d, degassing time; T, experimental temperature; p_1, p_0, p_∞, the gas pressure above the sample before, at the beginning, and a long time after the start of a run, respectively; s, total amount of gas sorbed during the experiment and preceding step experiments (if any), divided by p_∞; D, apparent initial diffusion coefficient (see text).

in the present work was the same one described previously.[3,4] Certain additional samples of a related nature were introduced and are discussed in the legends to Figures 1 and 2 and Table I.

The experimental methods employed in this work were described in some detail earlier.[3] Essentially, the sample was housed in a closed and thermostated vessel and the pressure of gas in sorptive equilibrium with the sample before the experiment, designated p_1, was measured. Next, the pressure was quickly changed to another nonequilibrium value, p_0, and its change with time due to sorption or desorption of some of the gas was recorded.

The evaluation of the resulting data can be approached in several ways. In particular, diffusion rate controlled sorption data would normally be fitted by the appropriate solution to the diffusion equation and chemisorption rate data by the Elovich equation[8] or a related expression.

In the present study it seems best to fit all data to the solution of the diffusion equation with constant coefficients, so as to make comparisons of the different results easy. This in no way implies that all measured rates are truly diffusion controlled.

A graphical method similar to that used in earlier work[4] was used to derive apparent or effective diffusion coefficients at various stages of each sorption or desorption run. As mentioned above, the appropriate solution to the diffusion equation was fitted at various portions of the experimental data, for example, near the beginning of the run, close to the end, or at various intermediate points (see Figure 2). In this way, the apparent rate coefficients were obtained and compared.

Results

Table I summarizes most of the results for the present series of sorption runs. The run numbers indicated in this table allow one to correlate the present data with those reported previously; in particular, consecutive sorption steps can be identified as such.

Figure 1 shows a plot of apparent initial diffusion coefficients as a function of the final uptake of sorbate

(8) M. J. D. Low, *Chem. Rev.*, **60**, 267 (1960).

during a given run and preceding step experiments (if any). Some of the earlier precise data[3,4] and some data of lower precision obtained on different samples are included in Figure 1 since the resulting comparisons will aid in the interpretation (see legend to Figure 1 for details).

Figure 2 shows apparent or effective diffusion coefficients for selected experiments as a function of the fraction of sorbate yet to be sorbed or desorbed in a given run, P^*. These were derived as described above. A sorption rate experiment which conforms well to the solution of the diffusion equation with a constant diffusion coefficient corresponds to a straight horizontal line in Figure 2; $P^* = 1.0$ represents zero uptake, *i.e.*, the beginning of a run, while $P^* = 0$ corresponds to the end.

From the above data it is clear that sometimes the pressure change at the start of the experiment $p_1 - p_0$ was quite appreciable. Whenever the observed diffusion coefficients are independent of concentration, or nearly so, the actual magnitude of $p_1 - p_0$ is assumed to be of no consequence.

In the case of carbon dioxide the apparent diffusion coefficient of course is not concentration independent. A study of curves 14 and 13 of Figure 2 obtained at low and intermediate sorbate concentrations, respectively, shows that the changes in D or D^* due to the change in average concentration in going from one run to the next (run 25/5 (of Table I) or 14 of Figure 2 to run 25/6 and then to 25/7, or 13 of Figure 2) are less important than the change in D^* during each of these runs. In this sense, one is dealing with "small-step experiments" as discussed in the Introduction.

Further refinements of the experimental techniques could lead to even smaller concentration changes, or of $p_1 - p_0$, and thus to slight changes in the type of data presented here, but such refinement would hardly affect the basic conclusions from this work.

Discussion

The results obtained for argon and methane are very simple. For one, the diffusion coefficients are essentially constant during each run (see Figure 2, horizontal lines of D *vs.* P) and they are independent of concentration over the range investigated (Figure 1). The sorption of these gases therefore seems to be diffusion rate controlled, in accord with the conclusion reached earlier.[3,4]

The Freon 21 data indicate a somewhat more complicated situation. As in the case of argon and methane, the rates conform to the solution of the diffusion equation and the sorption and desorption results agree well (Figure 2), but the Freon 21 rates show a strong negative concentration dependence, especially at the higher sorbate concentrations used (Figure 1). The diffusion coefficients of Freon 21 are very large, compared to those of the smaller diffusate molecules, argon, and methane. This of course is not consistent with the molecular sieve effect and shows that diffusion into the well-ordered crystalline regions of the sorbent cannot be the rate-controlling step in the sorption of Freon 21. Only coarse grains of the zeolite, consisting of many individual pieces of different crystalline orientation, were found to sorb Freon 21, while a fine-grain sample of the same zeolite containing far fewer grain boundaries did not.[4] Ames recently discussed the relation of this structural heterogeneity to the measured rate coefficients.[9] Also, Barrer and Brook[10] found diffusion coefficients, for molecules of comparable size in chabazite, which decrease with increasing concentration, while Habgood[11] found upward and downward trends for small molecule diffusion coefficients in Linde 4A zeolite, depending on the pretreatment of the sorbent. The apparent diffusion coefficients differ widely in all these cases and again the molecular sieve effect cannot be the primary cause of this.

On the other hand, the present data on Freon 21 and most of the literature results are readily explained if we assume Knudsen diffusion in crevices and gross defects to be the rate-controlling step at low pressures, while gaseous bulk diffusion becomes important at the higher sorbate concentrations. Correspondingly,[12] the apparent or effective diffusion coefficient is nearly concentration independent at low pressures and roughly inversely proportional to sorbate concentration at high gas pressures.

It is conceivable that surface diffusion plays a minor role in these data; if this were pronounced, one should expect an increase of the apparent diffusion rates with increasing vapor pressure and increasing surface concentration. This of course is not the case.

The results obtained for carbon dioxide, finally, are striking in that there is a distinct increase of the apparent initial sorption rates with concentration (Figure 1). There are a few literature data showing similar trends. For example, Barrer and Fender determined diffusion coefficients of sorbed H_2O from D_2O–H_2O exchange rate measurements on several zeolites;[13] they

(9) L. L. Ames, *Am. Mineralogist*, **50**, 465 (1965).

(10) R. M. Barrer and D. W. Brook, *Trans. Faraday Soc.*, **49**, 1049 (1953).

(11) H. W. Habgood, *Can. J. Chem.*, **36**, 1384 (1958).

(12) C. N. Satterfield and T. K. Sherwood, "The Role of Diffusion in Catalysis," Addison-Wesley Publishing Co., Reading, Mass., 1963, pp 12–28, especially eq 1-26 to 1-32.

(13) R. M. Barrer and B. E. F. Fender, *J. Phys. Chem. Solids*, **21**, 12 (1961).

noted that in the laminar silicate heulandite these coefficients markedly increase with increasing H_2O concentration. H_2O causes the mineral to expand[14] and this presumably leads to the increased mobility of the diffusing molecules.

Interestingly, Barrer and Fender's data also show that the H_2O diffusion coefficients in gmelinite, a typical framework zeolite, increase somewhat with sorbate concentration. Thus, the widening of a lattice, as established for heulandite, is not necessarily the only possible reason for the observed upward trend. Tiselius obtained similar results on certain other zeolites.[15]

The present data also show that D at the end of a given sorption run ($P^* \rightarrow 0$) is higher than that measured at the beginning of a subsequent run (see Figure 2). This means that the concentration dependence seen in the carbon dioxide data of Figure 1 does not, by itself, explain the D/P^* curves reviewed in Figure 2. It also means that the sorption does not involve a rate-controlling diffusion step followed by an instantaneous immobilization of the sorbate on (internal) sorption sites, regardless of whether a linear or nonlinear sorption isotherm is assumed.[16] Next, we note that desorption rates correspond well to the diffusion equation (see Figure 2) and the derived diffusion coefficients are much higher than those for the sorption processes (see Figure 1). Finally, considering the sorption and desorption isotherm data given in Table I, one finds that there is a strong sorption hysteresis; only a small portion of the sorbed CO_2 is given off at intermediate vapor pressures.

The positive concentration dependence of the effective rate constants, the increasing compliance of the experimental rates with the diffusion equation, the high diffusion coefficients obtained for the desorption runs, and the sorption hysteresis are readily explained if we assume that a good part of the CO_2 taken up is chemisorbed at active sites and is not released at intermediate pressures used in the present desorption runs. In addition, some of the gas is physically sorbed only and can easily be recovered by a fast diffusion rate controlled process. Earlier work[3] indicated that the relatively slow chemisorption is even more important at low experimental temperatures. Kington and MacLeod[17] have noted that the sorption sites of carbon dioxide in chabazite are energetically very heterogeneous, consistent with above interpretation. There is considerable infrared evidence for the existence of two types of sorbed CO_2 in several other zeolites.[18] In view of the problems in interpreting the infrared data, it is important that the present sorption and desorption rate measurements and their comparison permit this distinction of several species to be made.

In the past, compliance of the sorption rate data to the Elovich equation has often been used as a criterion for chemisorption rate control. Figure 3 shows that the argon data can be fitted better by this equation than those for carbon dioxide. Obviously, this equation is too general to permit a reliable distinction of diffusion and chemisorption rate control and recent work by Allen and Scaife tends to keep it that way.[19] Much literature data on heterogeneous catalytic rates may require a reinterpretation if analyzed on the basis of the Elovich equation only.

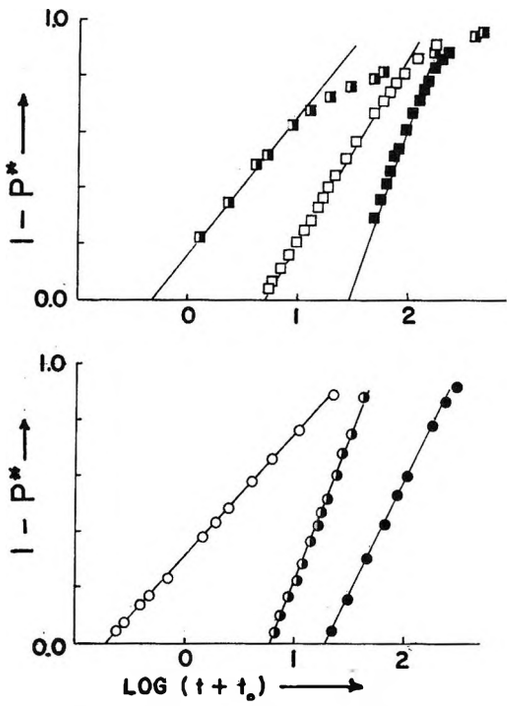

Figure 3. Elovich plot of sorption runs. According to the Elovich equation,[8] $(1 - P^*)$ should be linearly dependent on log $(t + t_0)$, where t is the time and $(1 - P^*)$ is the fractional amount of gas sorbed in given run (t_0 is a constant, chosen to produce the best curve fit): ◨, carbon dioxide sorption on chabazite powder, average grain diameter 0.0088 cm, degassed at the experimental temperature, 99.5°; □, ■, carbon dioxide sorption on chabazite grain, 0.81 cm diameter, at 99.5 and 5.7°, respectively; ◑, argon sorption on same powder, at 97.6°; ○, ●, argon sorption on same grain, at 97.7 and 9.4°, respectively.

(14) R. M. Barrer and B. E. F. Fender, *J. Phys. Chem. Solids*, 21, 1 (1961).

(15) A. Tiselius, *Z. Physik. Chem.* (Leipzig), A169, 425 (1934); A174, 401 (1935).

(16) See ref 2a, p 121, eq 8-3.

(17) G. L. Kington and A. C. MacLeod, *Trans. Faraday Soc.*, 55, 1799 (1959).

(18) L. Bertsch and H. W. Habgood, *J. Phys. Chem.*, 67, 1621 (1963); J. W. Ward and H. W. Habgood, *ibid.*, 70, 1178 (1966).

(19) J. A. Allen and P. H. Scaife, *Australian J. Chem.*, 19, 2015 (1966).

Calculation of Stability Constants of Hydrogen-Bonded Complexes from Proton Magnetic Resonance Data. Interactions of Phenol with Dimethylacetamide and Various Ketones. Solvent Effect[1a]

by Masahiro Nakano, Naomi I. Nakano, and Takeru Higuchi[1b]

School of Pharmacy, University of Wisconsin, Madison, Wisconsin 53706 *(Received May 8, 1967)*

A new iterative method of calculating stability constants of hydrogen-bonded complexes from pmr data is presented. Unlike earlier procedures which require large excesses of one of the interactants, the proposed approach is particularly applicable to systems containing nearly equivalent concentrations of the donor and acceptor species, successive corrections being made for the amount of the interactants present in the complexed form. Data and results are presented for phenol complexes of dimethylacetamide, acetone, 3-methylcyclohexanone, and some α,β-unsaturated ketones in carbon tetrachloride. Effects of several solvents on the stability constant and chemical shift of the bonded proton of the phenol–isophorone complex have also been studied with this method.

Although proton magnetic resonance (pmr) data have been used to compute stability constants of hydrogen-bonded complexes[2] and charge-transfer complexes[3] in ternary systems, published methods of calculation, which are analogous in equations to the Benesi–Hildebrand expression for spectrophotometric data, leave much to be desired. These methods require that the concentration of one of the interactants (usually the hydrogen acceptor for hydrogen bonding studies) be substantially in excess of the other so that the effect of complex formation on the concentration of the major component can be neglected. Such a condition is often difficult to achieve in practice because of limited solubilities of the interactants in the solvent under study and the relative lack of sensitivity of the pmr method. Lower concentrations would normally be preferable even when solubilities permit since higher concentrations of the interactants present may (1) change the properties of the solvent itself, (2) favor formation of higher order complexes,[4] and (3) be responsible for other anomalies encountered in the spectroscopic method in general.[5,6]

An iterative method suitable for computation of stability constants from pmr measurements on systems where the concentrations of the two interactants are comparable is described in the present report. The proposed procedure takes into account the amount of both reactants present in the complexed form by successive approximation. A similar iterative approach[7] based on solving a quadratic expression to obtain approximate concentration of the complexed species was proposed earlier for treatment of optical rotatory dispersion data but was found to be too cumbersome for the present purpose. The suitability of the proposed method has been tested on data corresponding to interactions of phenol with dimethylacetamide, acetone, 3-methylcyclohexanone, isophorone, mesityl oxide, and phorone in carbon tetrachloride. The effect of vary-

(1) (a) This study was supported in part by grants from the National Institutes of Health (GM-05830) and from funds supplied by Smith, Kline & French Laboratories; (b) address all inquiries to T. Higuchi, 314 Malott Hall, University of Kansas, Lawrence, Kan. 66045.

(2) R. Mathur, E. D. Becker, R. B. Bradlay, and N. C. Li, *J. Phys. Chem.*, **67**, 2190 (1963).

(3) (a) M. W. Hanna and A. L. Ashbaugh, *ibid.*, **68**, 811 (1964); (b) R. Foster and C. A. Fyfe, *Trans. Faraday Soc.*, **61**, 1626 (1965).

(4) S. D. Ross and M. M. Labels, *J. Am. Chem. Soc.*, **79**, 76 (1957).

(5) P. H. Emslie, R. Foster, C. A. Fyfe, and I. Horman, *Tetrahedron*, **21**, 2843 (1965).

(6) R. Foster and I. Horman, *J. Chem. Soc., Sect. B*, 1049 (1966).

(7) J. Meier and T. Higuchi, *J. Pharm. Sci.*, **54**, 1183 (1965).

ing the solvent environment on the stability constant and the chemical shift of the bonded proton of the phenol–isophorone complex has also been determined.

A General Method of Computing Stability Constants by Pmr. If two species A and B interact reversibly in solution to form a 1:1 complex C according to

$$A + B \overset{K_c}{=} C \tag{1}$$

the stability constant, K_c, in the concentration unit can be expressed by

$$K_c = \frac{C_c}{(C_a - C_c)(C_b - C_c)} \tag{2}$$

where C_a and C_b are the added concentrations of A and B, respectively, and C_c is the concentration of the complex at equilibrium. Since these equilibria usually involve very rapid reactions, the observed chemical shift of the protons on A, δ_{obsd}, will be the time-weighted average of the chemical shift of the protons in the complexed form, δ_c, and that in the uncomplexed form, δ_a.[8] Therefore, the δ_{obsd} is related to δ_a and δ_c by eq 3.

$$\delta_{obsd} = \frac{C_{c\delta_c}}{C_a} + \frac{C_a - C_{c\delta_c}}{C_a} \tag{3}$$

Equation 3 can be rearranged to give

$$C_c = \frac{\delta_{obsd} - \delta_a}{\delta_c - \delta_a} C_a \tag{4}$$

Equation 2 can be rearranged to give

$$K_c C_a C_b - K_c C_c (C_a + C_b - C_c) = C_c \tag{5}$$

From eq 4 and 5, eq 6 is obtained

$$\frac{C_b}{\Delta\delta_{obsd}} = \frac{1}{\delta_c - \delta_a}(C_a + C_b - C_c) + \frac{1}{K_c(\delta_c - \delta_a)} \tag{6}$$

where $\Delta\delta_{obsd} = \delta_{obsd} - \delta_a$. Equation 6 contains two unknowns, C_c and δ_c, which can be calculated by means of a simple iterative procedure based on successive approximations.

Plot of $C_b/\Delta\delta_{obsd}$ *vs.* $(C_a + C_b)$ yield, according to eq 6, a line with a slope value approximately equal to $1/(\delta_c - \delta_a)$. This can be substituted into eq 4 to obtain the first approximate values of C_c. The C_c values thus obtained are then used in eq 6 to calculate an improved value of the slope. These steps are repeated until two successive cycles yield essentially identical convergent values for the slope. The final stability constant, K_c, is then calculated from the limiting slope and intercept values. The chemical shift of the bonded proton in the complex δ_c can also be obtained from the final slope.

If $C_b \gg C_c$, eq 6 reduces to the equivalent relationships given by eq 7 and 8, *i.e.*, (1) Hanna and Ashbauth's form (see also ref 1)

$$\frac{1}{\Delta\delta_{obsd}} = \frac{1}{K_c(\delta_c - \delta_a)} \frac{1}{C_b} + \frac{1}{\delta_c - \delta_a} \tag{7}$$

and (2) Foster and Fyfe's form

$$(\Delta\delta_{obsd}/C_b) + \Delta\delta_{obsd} K_c = (\delta_c - \delta_a)K_c \tag{8}$$

It can be shown that eq 6 can also be directly developed from these equations if the higher order terms were not neglected during their derivation. It is evident that the equation is generally applicable to pmr data for computation of both stability constants and δ_c values of 1:1 complexes in ternary systems, not only resulting from hydrogen bonding but also from other types of rapidly reversible intermolecular interactions in solution.

Experimental Section

Reagents. Reagent grade phenol (J. T. Baker Analyzed reagent), dimethylacetamide (Eastman White Label), and 3-methylcyclohexanone were distilled under vacuum. Acetone (J. T. Baker Analyzed reagent) was dried over anhydrous potassium carbonate and distilled at 55°. Isophorone (Aldrich) after repeated fractional distillation under vacuum showed no evident impurity in the pmr spectrum. Mesityl oxide was repeatedly distilled at 129°. Phorone (J. T. Baker) was recrystallized several times from ethanol, mp 27°. All solvents used were of commercially available spectroscopic grade.

Instrumentation. A Varian Model Z-60A analytical spectrometer with a V-6057 variable-temperature accessory was used.

Procedure. Samples (10 ml) were prepared by mixing solutions of phenol and those of the hydrogen acceptors and diluted with appropriate solvents. The concentration ranges of both phenol and the hydrogen acceptors employed are given in Table I. For computation of stability constants of the phenol–isophorone system in various solvents, two different concentrations of phenol within the range of 4–10 $\times$ 10^{-3} M were used, the concentrations of isophorone being varied between 0.02 and 0.10 M.

All chemical shift measurements were carried out against tetramethylsilane (TMS) as the internal reference at 25 ± 0.5°. The chemical shifts were reproducible to better than 0.5 cps. For each sample, data from at least three field sweeps were used for computing the stability constants. Since at the concentration of

(8) H. S. Gutowsky and A. Saika, *J. Chem. Phys.*, 21, 1688 (1953).

Table I: Proton Magnetic Resonance Data for Interactions of Phenol with Some Carbonyl Compounds in Carbon Tetrachloride at 25°

Carbonyl hydrogen acceptor	C_a (concn of phenol), $M \times 10^{-3}$	C_b (concn of hydrogen acceptor), $M \times 10^{-3}$	K_c, l./mole	δ_c[a]
DMA	5.04	7.21–36.1		
	4.73	8.59–21.5		
	4.56	2.40–38.4	145	513.3
	6.84	2.40–14.4		
	9.12	2.40–33.6		
Acetone	6.83	5.72–80.0	10.7	443.0
Isophorone	5.44	5.13–51.3	29.7	482.7
	9.59	10.0–139		
3-Methylcyclohexanone	7.71	10.7–74.8	15.3	444.8
Mesityl oxide	6.71	7.55–45.3	15.6	456.3
Phorone	6.43	6.43–57.9	14.7	453.6

[a] Based on δ_a = 257.5; the numbers in cycles per second are in reference to TMS.

phenol employed there still was some tendency for hydroxyl signal to change on further dilution, the values of δ_a were estimated for each solvent by extrapolating the curve obtained at the concentration range of above 4×10^{-3} M to infinite dilution as shown in Figure 1. The slope values were calculated throughout by the method of least squares and each K_c value was obtained from the slope and intercept of the final regression line.

Applications of the Method

Interactions of Phenol with Dimethylacetamide (DMA) and Other Carbonyl Compounds in Carbon Tetrachloride. The suitability of the iterative procedure base on eq 6 for computing stability constants from pmr data is evident in Figure 2, the specific case being for interaction of phenol with DMA. In this experiment the added concentration of phenol was fixed at 5.04×10^{-3} M, the concentrations of DMA being varied from 7.21 to 36.1×10^{-3} M. As a first approximation, line 1 was constructed by plotting $C_b/\Delta\delta_{obsd}$ against $C_a + C_b$, ignoring for the moment the C_c term in eq 6. The slope of this line was then used to calculate the first approximate concentrations of the complex species in solution, $C_c = C_a\Delta\delta_{obsd}$ (slope), according to eq 4. Line 2 was then obtained by replotting $C_b/\Delta\delta_{obsd}$ now against $C_a - C_b - C_c$ based on these values of C_c. The slope of line 2 was then employed to yield more refined values of C_c which were used in turn to give line 3, which essentially coincided with line 4 and succeeding lines. The indicated value of K_c = (slope/intercept) of the final convergent line was 145 l./mole.

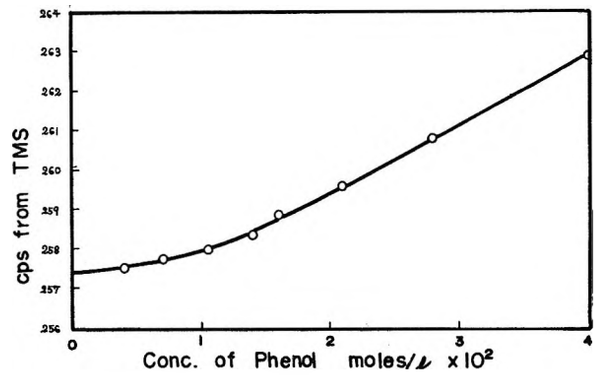

Figure 1. Hydroxyl signal of phenol in carbon tetrachloride.

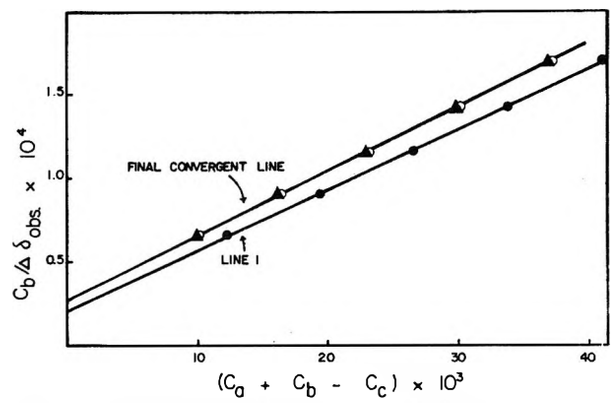

Figure 2. Plots showing the application of the iterative method for calculation of the stability constant from pmr data for interaction of phenol with DMA in carbon tetrachloride at 25°. Line 1 corresponds to the first approximation with C_c set equal to zero. Points indicated by O on the final convergent line are for the second approximation and ▲ for the final convergent values of C_c.

It can be seen that essentially one iterative cycle brought the values of C_c very close to the final convergent values for this relatively strong interaction. The number of iterations normally necessary would be expected to be dependent upon the concentration ratio of two interactants as well as the degree of interaction. This method of analysis seems to have an advantage over the previously suggested iterative method[7] based on successive approximation of C_c by a quadratic relationship. In the latter method the initial line occasionally yields a negative intercept, particularly with strongly interacting systems, a situation which is rather difficult to cope with. The proposed procedure is much simpler to apply in practice and seems to be free of such problems.

The final convergent line must be independent of phenol concentrations in the range where dimerization is not a factor, although the number of iteration cycles required may differ, and in the process of iteration sepa-

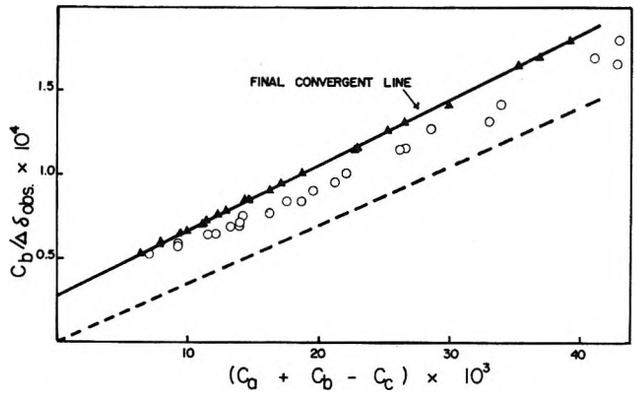

Figure 3. Plots showing the final convergent line for five independent experiments corresponding to interaction of phenol with DMA. The circles represent the first approximation plots of $C_b/\Delta\delta_{obsd}$ *vs.* $C_a + C_b$ (see the text for the dashed line).

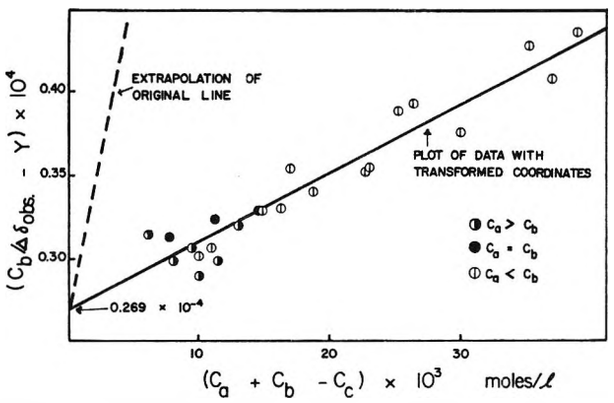

Figure 4. Plots showing the same data given in Figure 3 but with the ordinate scale expanded. The ordinate values represent the differences between the observed values and those given by the arbitrary dashed line in Figure 3.

rate lines are usually established for different phenol concentrations. In Figure 3 the results of five independent experiments, as shown in Table I, obtained at several but low concentrations of added phenol, have been pooled and plotted according to eq 6. Only the first approximation, *i.e.*, plots of $C_b/\Delta\delta_{obsd}$ *vs.* $C_a + C_b$ and the final plots of $C_b/\Delta\delta_{obsd}$ *vs.* $C_a + C_b - C_c$ are shown (separate initial lines corresponding to the several added phenol concentrations are not shown). It is clear that the points have converged as expected into one straight line irrespective of the phenol concentration after incorporation of the convergent C_c values.

Since the final points obtained for several phenol concentrations and defining the convergent regression line fall so well on the line, it is difficult to determine from the plot shown in Figure 3 the exact nature of the residual deviations from the theoretical relationship. In Figure 4 an attempt has been made to magnify the residual scatter by increasing the ordinate scale by a factor of 10 and plotting $C_b/\Delta\delta_{obsd} - Y$ against the same abscissa values where $Y = 3.50 \times 10^{-3}(C_a + C_b - C_c)$, an arbitrary line represented by dashes in Figure 3. The points shown in Figure 4 were analyzed with respect to the relative concentration of phenol to that of DMA, *i.e.*, $C_a > C_b$, $C_a = C_b$, and $C_a < C_b$. It is evident from this magnified plot that the deviations from the regression line of the points arising from different ratios of the concentration of phenol to that of DMA are more or less random and that the line represents a common solution. The results strongly support the validity of the general method of calculation and the underlying assumptions.

In Table I the stability constants and the chemical shifts of bonded protons calculated from pmr data in the above manner for complexes formed by phenol

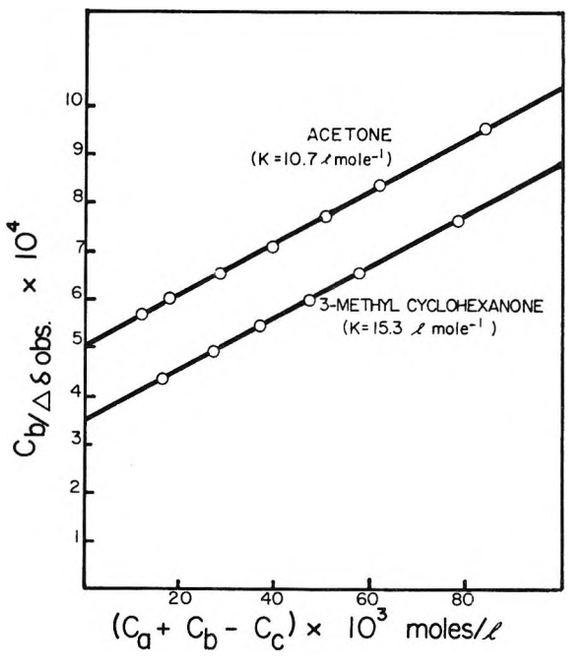

Figure 5. Final plots of $C_b/\Delta\delta_{obsd}$ *vs.* $C_a + C_b - C_c$ for phenol–acetone–carbon tetrachloride and phenol–3-methylcyclohexanone–carbon tetrachloride systems at 25°.

with DMA, acetone, 3-methylcyclohexanone, mesityl oxide, phorone, and isophorone in carbon tetrachloride at 25° are listed. The corresponding additional plots, shown in Figures 5–7, appear to adhere equally well to eq 6. On the basis of the observed precision of the pmr data and other factors, the reproducibility of these constants appears to be of the order of ±4%.

In Table II the stability constant obtained for the phenol–DMA complex is compared with those obtained by other investigators from infrared and ultraviolet

spectroscopic measurements. The agreement is certainly as good as can be expected. In Table III the value for the phenol–acetone complex is compared with five others determined by different workers using the infrared technique. Again it would appear that the present result is certainly as reliable as the others.

Table II: Summary of Available Data on the Interaction of Phenol with DMA in Carbon Tetrachloride

Method	Temp, °C	K_c, l./mole	Ref
Ultraviolet	25	134 ± 3	*a*
Ultraviolet	32	108	*b*
Infrared	20	270	*c*
Infrared	25[d]	184	*c*
Infrared	30	136	*c*
Pmr	25	145	Present work

[a] M. D. Joesten and R. S. Drago, *J. Am. Chem. Soc.*, **84**, 2037 (1962). [b] F. Takahashi and N. C. Li, *J. Phys. Chem.*, **69**, 1622 (1965). [c] S. Mizushima, M. Tuboi, T. Shimanouchi, and Y. Tsuda, *Spectrochim. Acta*, **7**, 100 (1955). [d] Interpolated value.

Table III: Summary of Available Data on the Interaction of Phenol with Acetone in Carbon Tetrachloride

Method	Temp, °C	K_c, l./mole	Ref
Infrared	25	13.5	*a*
Infrared	24.5	8.5	*b*
Infrared	20	12.31	*c*
Infrared	50	6.01	*c*
Infrared	23	12.3	*d*
Infrared	30	8.35	*e*
Pmr	25	10.7	Present work

[a] M. D. Joesten and R. S. Drago. *J. Am. Chem. Soc.*, **84**, 3817 (1962). [b] J. M. Widom, R. J. Philippe, and M. E. Hobbs, *ibid.*, **79**, 1383 (1957). [c] T. Gramstad, *Spectrochim. Acta*, **19**, 497 (1963). [d] W. Heinen, *Rec. Trav. Chim.*, **82**, 859 (1963). [e] S. Mizushima, M. Tuboi, T. Shimanouchi, and Y. Tsuda, *Spectrochim. Acta*, **7**, 100 (1955).

It has been reported from infrared spectral shift studies that the conjugation with ethylenic double bonds does not appreciably alter the basicities of ketones.[9,10] It can be seen, however, from the data shown in Table I that the cyclic α,β-unsaturated ketone, isophorone, is apparently significantly more basic toward phenolic hydrogen than α,β-unsaturated ketones in which ethylenic double bonds are conjugated with noncyclic aliphatic ketone groups. Such observations suggest the possible utility of stability constant determination such as described above in eliciting structural information.

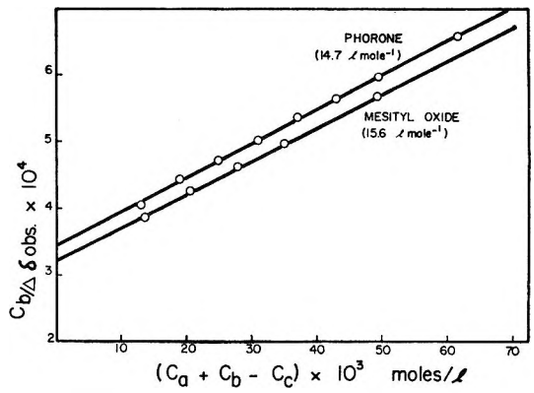

Figure 6. Final plots of $C_b/\Delta\delta_{obsd}$ *vs.* $C_a + C_b - C_c$ for phenol–phorone–carbon tetrachloride and phenol–mesityl oxide–carbon tetrachloride systems at 25°.

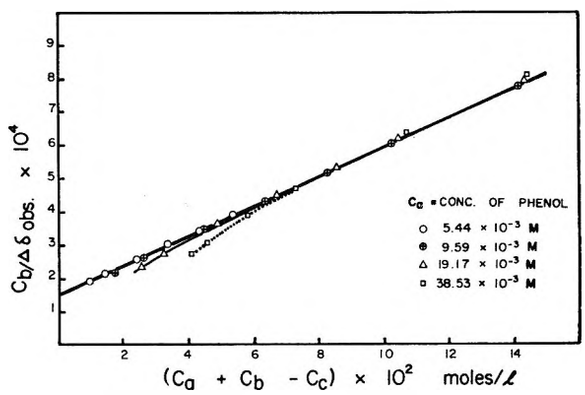

Figure 7. The effect of concentration of phenol on the plots of $C_b/\Delta\delta_{obsd}$ *vs.* $C_a + C_b - C_c$ for interaction of phenol with isophorone in CCl_4 at 25°. The straight line drawn is the regression line for $C_a = 5.44 \times 10^{-3}$ and 9.59×10^{-3} *M* only.

Effect of Higher Phenol Concentrations. Since associated forms of phenol appear to hydrogen bond more readily than the monomeric species,[7,11] higher concentration of the hydrogen donor may be expected to produce significant deviations from eq 6. Figure 7 shows the plots of $C_b/\Delta\delta_{obsd}$ *vs.* the final values of $C_a + C_b - C_c$ for interaction of phenol with isophorone covering a wide range of phenol concentrations. Theoretically, all points should converge into one straight line after an appropriate number of the iteration cycles, if the determination of the stability constant were totally independent of phenol concentrations. For the higher

(9) A. W. Baker and G. Harris, *J. Am. Chem. Soc.*, **82**, 1923 (1960).
(10) L. J. Bellamy and R. J. Pace, *Spectrochim. Acta*, **19**, 1831 (1963).
(11) L. J. Bellamy and R. J. Pace, *ibid.*, **22**, 525 (1966).

concentrations of phenol, however, the experimental points did not converge into the same straight line as for the lower concentrations and the observed deviations were progressively greater as the concentration of phenol was increased. The effect was particularly pronounced when the ratio of the concentration of phenol to that of isophorone was high and can probably be attributed to the presence of the associated forms of phenol at the higher concentrations as was the case in our previous camphor–phenol system.[7] Below phenol concentration of about 10×10^{-3} M, this effect appears to be unimportant, as can be seen in Figure 7. From the infrared studies, it is believed that the presence of dimeric forms of phenol is less than 1% under this condition.[12]

The observed chemical shift of the phenolic proton at these concentrations differed from that of infinite dilution by, at the most, 2 cps in all solvents studied. It was because of this observation that the concentration of phenol was kept below 10×10^{-3} M for determination of the stability constants; on the other hand, the sensitivity of the nmr spectrometer necessitated concentrations at least of the order of 4×10^{-3} M. The use of an nmr spectrometer of greater sensitivity and having a higher resolution can be expected to improve the accuracy and precision of determination of K_c values by this method.

Effect of Solvents on Pmr Data. The values of stability constants of complexes formed by hydrogen bonding are, of course, dependent upon the solvent in which the measurements are made. More recently the solvent effect has been attributed largely to competing equilibria between the solutes and the solvent rather than to some bulk dielectric effect of the solvent.[13-16] Experimental observations arising from the present study based on pmr measurements have shed some light on this situation in part because of the greater precision of the method.

Stability constants of the phenol–isophorone complex obtained by the present method at 25° in carbon tetrachloride, carbon disulfide, tetrachloroethylene, and various saturated hydrocarbon solvents are listed in Table IV. The values of K_c were observed to be much larger for the saturated hydrocarbon solvents than for the three nonhydrocarbon solvents. This effect may be due to specific interactions between the solutes and the latter solvents, as has been pointed out by earlier investigators.[14,17-19] From purely entropic considerations it would appear that these constants should vary directly with the molar volume of the solvent. Although a trend in this direction appears to be the case for the saturated hydrocarbon solvents, it seems less than expected.

Table IV: Pmr Data for Interaction of Phenol with Isophorone in Various Solvents at 25°

Solvent	K_c, l./mole	Chemical shift of unbonded phenolic hydrogen[a]	Chemical shift of bonded phenolic hydrogen[a]
CCl_4	29.6	257.5	482.7
C_2Cl_4	39.7	256.5	479.7
CS_2	39.8	255.5	482.8
n-Pentane	67.9	240.0	481.5
n-Hexane	65.1	240.5	485.0
n-Heptane	67.2	241.5	485.4
Cyclopentane	63.2	241.5	483.0
Cyclohexane	69.8	242.5	484.6
Methylcyclohexane	71.0	243.3	485.4
Isooctane	81.0	240.6	482.7
Decalin	78.3	243.8	489.8

[a] Units are in cycles per second in reference to TMS.

One of the interesting outcomes of this pmr study in various solvents was the observation that the chemical shift of the bonded proton of the phenol–isophorone complex, δ_c, appeared to be relatively independent of the solvents used, although that of the free phenol, δ_a, and the K_c values were distinctly different for the nonhydrocarbon and hydrocarbon solvents (see Table IV). This may be attributable to the fact that the hydrogen atom involved in bonding is shielded from the solvent molecules, its chemical shift being relatively independent of the nature of the solvent shell and dependent largely upon the properties of the hydrogen acceptor (see Table I). Further investigations are required on interactions of phenol with a wide variety of hydrogen acceptors in various solvents, however, before definitive conclusions can be drawn. On the other hand, the chemical shift of the free phenolic proton, as shown in Table IV, depended upon the nature of the solvent. This effect may be looked upon as interaction of free phenol with solvent molecules to form weakly hydrogen-bonded complexes.

(12) For example, the dimerization constant of phenol in CCl_4 at 30° is reported to be 0.70 l./mole: M. M. Maguire and R. West, *Spectrochim. Acta*, **17**, 369 (1961). Based on this value at 0.01 M, the concentration of the dimer present is calculated to be 0.70×10^{-4} M.

(13) J. Rubin and G. S. Panson, *J. Phys. Chem.*, **69**, 3089 (1965).

(14) R. J. Bishop and L. E. Sutton, *J. Chem. Soc.*, 6100 (1964).

(15) R. S. Drago, T. F. Bolles, and R. J. Niedzielski, *J. Am. Chem. Soc.*, **88**, 2717 (1966), and references cited therein.

(16) M. Horak and J. Pliva, *Spectrochim. Acta*, **21**, 911 (1965).

(17) T. Gramstad, *Acta Chem. Scand.*, **15**, 1337 (1961).

(18) T. Gramstad, *ibid.*, **16**, 1969 (1962).

(19) T. Gramstad, *Spectrochim. Acta*, **19**, 1363 (1963).

Polarographic and Spectral Studies of Charge-Transfer Complexes

by Roger D. Holm, W. R. Carper,[1] and James A. Blancher

Chemistry Department, California State College at Los Angeles, Los Angeles, California *(Received May 15, 1967)*

Formation constants for some charge-transfer complexes have been evaluated polarographically. Complexation was found to perturb the energy levels of the acceptor (7,7,8,8-tetracyanoquinodimethane) causing an energy decrease in the lowest unfilled level and, consequently, reduction at more positive potentials for hexamethylbenzene and pentamethylbenzene. For durene and mesitylene, on the other hand, the lowest empty acceptor level was shifted to higher energy, causing reduction at more negative potentials. Corrections for these energy level perturbations were obtained from spectral shifts of the first acceptor transition and were applied to the observed half-wave potentials in computing formation constants. The relative order of donor character was found to be hexamethylbenzene > pentamethylbenzene > durene > mesitylene in chloroform solution using tetrabutylammonium perchlorate as the supporting electrolyte. This relative donor order differs from that indicated by Benesi–Hildebrand investigations in chloroform, but the polarographic values do follow the relative order of the donors in many other solvents and probably reflect the true sequence in chloroform as well.

Introduction

Several studies of charge-transfer complexes have been conducted in which shifts in polarographic half-wave potentials are utilized in obtaining formation constants.[2] In these investigations, it has been assumed that the potential shift is entirely due to the formation of the complex.[3] In several cases very poor agreement has been obtained between formation constants obtained polarographically and those obtained spectrally. It is the purpose of this paper to show that acceptor half-wave potentials depend not only upon the value of the complex formation constant, but also on the energy of the vacant molecular orbital of the acceptor which changes upon complexation.

Experimental Section

Solvents. Spectroquality carbon tetrachloride was used as received. Preliminary addition of tetracyanoethylene to the solvent yielded no observed donor–acceptor interaction. Hexamethylbenzene, pentamethylbenzene, and durene were obtained from Eastman and pyrene was from K & K Laboratories, all as reagent grade and used without purification. Mesitylene from Eastman was distilled through a spinning-band column at a temperature of 164°. Tetrabutylammonium perchlorate (Southwestern Analytical Chemicals) was recrystallized from methanol and dried *in vacuo* over anhydrous magnesium perchlorate at 100° for at least 5 hr. Tetrabutylammonium chloride (Southwestern Analytical Chemicals) was recovered from aqueous solution by evaporation under reduced pressure, followed by drying *in vacuo* at 50° over magnesium perchlorate. Chloride solutions in chloroform were prepared from this salt with great rapidity and it was experimentally verified that the amount of moisture acquired in dissolving the tetrabutylammonium chloride had no significant effect on the stability of the observed potentials. 7,7,-8,8-Tetracyanoquinodimethane (TCNQ) was recrystallized from specifically purified acetonitrile three times and dried *in vacuo* over P_2O_5 at 80°.

Spectral Studies. Spectral measurements were made on a Cary 14 spectrophotometer at 25 ± 0.1°. The first absorption band position of the acceptor could be located to ±3 A and the charge-transfer band maxima to ±5 mμ. All solutions contained 0.1 *M* tetrabutylammonium perchlorate as an inert electrolyte in

(1) Address correspondence to this author at Wichita State University, Wichita, Kan. 67208.

(2) H. Irving, "Advances in Polarography," Vol. 3, Pergamon Press Inc., New York, N. Y., 1960, p 42.

(3) (a) M. E. Poever, *Trans. Faraday Soc.*, 58, 2370 (1962); (b) *J. Chem. Soc.*, 4540 (1962).

order to preserve the same solution environment for both spectral and polarographic studies.

The TCNQ concentration was generally about 10^{-4} M and the donor concentrations were varied from 0.10 to 1.0 M depending on solubility. All solutions were thoroughly deoxygenated with purified nitrogen which was presaturated with chloroform before being transferred to degassed absorption cells. For spectrophotometric measurements of the formation constants, dilutions of the most concentrated solutions were taken and constants were obtained at several wavelengths from the expression[4]

$$\frac{(D)(A)b}{d_i} = \frac{1}{K\epsilon_i} + \frac{(D)}{\epsilon_i}$$

in which (D) and (A) are the concentrations of donor and acceptor, respectively, K is the formation constant, b is the path length, and d_i and ϵ_i are the absorbance and molar absorptivity, respectively, for wavelength λ_i. If one complex species exists in solution, the K is generally reasonably constant over the charge-transfer band.

Polarographic Studies. A three-compartment cell was used with a central working compartment which was isolated from the auxiliary and reference compartments with fine frits. The working solution level was kept higher in this compartment than in the other compartments to ensure a net outflow through the frits and preclude contamination of the working solution. Provision was made to degas the solutions in all three cells to prevent entry of oxygen which not only is electroactive but also complexes with the TCNQ. Salt bridge solutions in the auxiliary and reference compartments were of freshly prepared chloroform solutions of 0.1 M tetrabutylammonium perchlorate. The working solutions contained 0.1 M tetrabutylammonium perchlorate, 0.1–1.0 M donor, and typically 10^{-4} M TCNQ. These solutions were thoroughly degassed in a fritted cell, transferred under nitrogen to the polarographic cell, and degassed further. During all measurements, chloroform-saturated nitrogen was passed over the working solutions.

A Sargeant XV polarograph was employed in conjunction with a Sargeant infrared compensator and a three-electrode cell system. The chart paper divisions were calibrated by measuring the potentials of the bridge windings with a Leeds and Northrup Model K-3 potentiometer. The infrared compensator was periodically balanced so that the potential of the dropping mercury electrode (dme) was within ±0.5 mv of the nominal bridge potential.

Plots of applied potential *vs.* log $(i_d - i)/i$ were made and the potential at which the log term became zero was taken as the half-wave potential. The plots consistently exhibited slopes within 10% of 59.1 mv. Values for the half-wave potential for the same solution were reproducible to ±1 mv. Preliminary trials using a silver–silver iodide electrode[5] were unsuccessful owing to erratic drifting of the electrode. More stable potentials were obtained with a silver–silver chloride electrode composed of a helix of silver wire anodized in a solution of tetrabutylammonium chloride and immersed in a chloroform solution containing 0.10 M tetrabutylammonium perchlorate and approximately 0.01 M tetrabutylammonium chloride. The electrode contained in a 1-cm fritted tube was found to vary only 4–5 m during a 12-hr period when compared to a similarly prepared electrode. Although the concentration of chloride was only approximately known, the reference potential was stable enough so that alternate polarograms could be run repeatedly for the acceptor and for the complex. The differences in half-wave potential were obtained over a time period short enough so that the reference electrode was essentially constant within experimental error. The shifts in half-wave potential are felt to be reliable to ±1.5 mv.

Results and Discussion

Spectral investigations revealed that the first transition of the TCNQ was shifted slightly to higher energies (from 4015 to as much as 4000 A) upon complexation with durene and mesitylene and to slightly lower energies (from 4015 to 4025 A) with hexamethylbenzene and pentamethylbenzene. At the higher concentration of donors, the absorption is believed to be predominantly due to the complexed TCNQ as is indicated by an apparent limiting amount of shift at the higher donor concentrations of each system. Since the complexes are rather weak, the spectral shifts and corrections may be considered minimum values. The charge-transfer bands for TCNQ–hexamethylbenzene and pentamethylbenzene are sufficiently far removed from the TCNQ band so that no overlapping occurs. Although the charge-transfer bands of durene and mesitylene do overlap considerably with the TCNQ band at 4015 A, little error is involved in measuring the peak intensity of the acceptor band since the absorbance of this band is roughly 100 times as great as the charge-transfer bands. In addition, the latter bands are very broad with little change in absorption over a 20- or 30-A region.

(4) H. A. Benesi and J. H. Hildebrand, *J. Am. Chem. Soc.*, 71, 2703 (1949).

(5) M. E. Poever, *Trans. Faraday Soc.*, 60, 417 (1964).

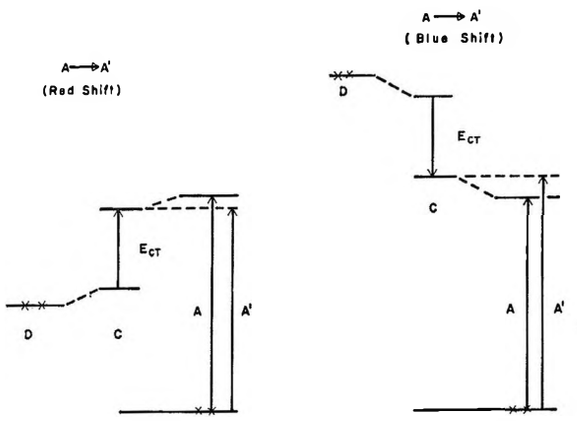

Figure 1. Perturbation of acceptor levels upon complexation. Filled levels of the donor, D, and acceptor, A, are shown as well as the small perturbations, A′, and the first unfilled acceptor level when the complex, C, is formed. The E_{CT} represents the first charge-transfer band of the molecular complex. Upon complexation the donor level and the first unfilled acceptor level are shifted slightly toward each other.

The spectral shift of the TCNQ band may be interpreted as reflecting a perturbation of the acceptor orbitals upon complexation as is shown in Figure 1. Though all levels may be somewhat affected, it is the lowest unfilled acceptor level which participates most in complex formation and which probably undergoes the greatest perturbation effect. The filled level of the acceptor is likely to be relatively unaffected and the extent of the spectral energy shift of the first transition (A → A′) is therefore probably close to the true change in energy of the lowest unfilled level.

The reference energy level of the calomel electrode may be thought of as lying above the acceptor levels. In the red shift case in Figure 1, complexation perturbs the acceptor level to a lower value (closer to the donor level), causing a greater energy separation between the reference electrode and the acceptor level and requiring a more negative potential for electron transfer. A slightly more negative half-wave potential is observed for this reduction process in addition to the conventional negative potential shift from complexation, giving rise to an apparent formation constant which is too large. The observed half-wave potential is therefore a function of the energy level perturbation from complexation, as well as of concentration of donor and formation constant of the complex. The energy correction calculated in this manner from the perturbation of both filled and unfilled orbitals represents a maximum correction for the half-wave potential of the complex. Since the filled level is probably little affected, however, the correction is probably close to the true correction.

It has been shown that molecular complexation is accompanied by a shift of the reversible polarographic half-wave potential to more negative potentials according to the relation

$$\Delta E_{1/2} = \frac{RT}{nF} \ln [1 + K(\mathrm{D})]$$

for a 1:1 complex of small formation constant K and donor concentration (D). It is reasonable to assume that at the prevailing concentrations only 1:1 complexes are involved and the treatment in this study has ignored any higher complexes. It is assumed that the activity coefficients of acceptor and complex are identical and that the diffusion current constants for acceptor and complex are also identical. The first condition is reasonable and the latter condition appears to be true. Reports[5] of a reversible and diffusion-controlled reduction wave for TCNQ were confirmed. The donors were all reduced at potentials roughly 2 v more negative than the TCNQ. The perchlorate ion is probably of little complexing effect as its donor strength for TCNQ is less than that of the π donors used which are present in equal or greater concentration.

The observed shift in half-wave potential for durene is greater (more negative) than that produced by the equilibrium effect by the amount of perturbation shift and the formation constant can be calculated once the spectral potential component in the potential shift is deducted. This component may be evaluated by measuring the wavelength shift in the band maximum of the acceptor. Since 1 ev equals 1.60×10^{-12} erg, one may express the energy difference in millielectron volts

$$\Delta E_{1/2} = hc\Delta(1/\lambda)$$

$$\Delta E_{1/2} = \frac{hc(10^3)}{(1.6 \times 10^{-12})}\left[\frac{1}{\lambda_A} - \frac{1}{\lambda_{DA}}\right]$$

$$= (0.124)\left[\frac{1}{\lambda_A} - \frac{1}{\lambda_{DA}}\right]$$

where h and c are Planck's constant and velocity of light, respectively, and λ_A and λ_{DA} are the band maxima expressed in cm^{-1} for the uncomplexed and complexed acceptor.

In a similar manner, TCNQ complexation with hexamethylbenzene and pentamethylbenzene results in a lowering of empty acceptor level as is seen from the diminution in the energy of the TCNQ transition. The energy level shift will partially compensate the equilibrium effect and the observed half-wave potential shift to negative values will be too small. It was found in

Table I: Formation Constants of Complexes

Donor concn, M	$\Delta E_{1/2}$, mv	Cor term, mv	K_{uncor}, l./mole	K_{cor}, l./mole
		TCNQ–Hexamethylbenzene		
0.10	7	+1.5	3.12	3.93
0.20	11	+3.0	2.68	3.61
0.30	17	+6.0	3.14	4.83[a]
0.40	16	+7.0	2.16	3.62
0.50	20	+7.0	2.36	3.72
		Av	2.69 ± 0.44	3.72 ± 0.15
		TCNQ–Pentamethylbenzene		
0.10	4	0.0	1.68	1.68
0.20	8	+1.0	1.83	2.10
0.30	12	+1.5	1.99	2.30
0.40	14	+3.1	1.82	2.36
0.50	16	+3.8	1.73	2.33
		Av	1.81 ± 0.12	2.15 ± 0.28
		TCNQ–Durene		
0.20	5	−1.4	1.08	0.750
0.40	8	−2.4	0.91	0.608
0.60	18	−7.7	1.69	0.822
0.80	24	−11.0	1.93	0.825
1.00	24	−6.3	1.55	0.991
		Av	1.43 ± 0.43	0.799 ± 0.14
		TCNQ–Mesitylene		
0.20	3	0.0	0.36	0.62
0.40	8	0.0	0.91	0.92
0.60	23	−3.1	2.42	1.96[a]
0.80	14	−4.5	0.91	0.561
1.00	20	−5.4	1.18	0.77
		Av	1.15 ± 0.77	0.72 ± 0.51

[a] These values were rejected with better than 95% confidence before computing average values.

this study that the spectral potential shifts can amount to 30% of the observed shift in half-wave potential. In Table I are listed the observed half-wave potential shifts at different donor concentrations, the corresponding correction term in millivolts computed from TCNQ spectral shifts, the formation constant computed from the observed half-wave potential alone, and the constant computed from the corrected half-wave potentials. As would be expected, the effect of the spectral shift correction is seen in an increase in the constant for hexamethylbenzene and pentamethylbenzene and a diminished constant for durene and mesitylene. Moreover, the standard deviations listed are generally smaller for the corrected constants. The donor strengths observed were in the order hexamethylbenzene > pentamethylbenzene > durene > mesitylene. Such a sequence is reasonable since the inductive effect of six methyl groups would be expected to make the π-cloud more available in a charge-transfer complex. Melby, *et al.*,[6] have reported that the constant in methylene chloride for TCNQ–hexamethylbenzene exceeds that of durene. In a polarographic study in chloroform, Poever obtained a value of 2.0 ± 0.2 for TCNQ–hexamethylbenzene in ionic strength 0.5 M. This value essentially corresponds to the uncorrected constant of this study, though at a different ionic strength.

For comparison with the polarographic results, spectral measurements were made of each solution and constants were calculated using the Benesi–Hildebrand equation. Comparison of the constants obtained from the two methods, presented in Table II, shows that the values not only disagree but the relative order of donor strength is different. A similar order of spectrally determined donor strength in chloroform has been obtained by Thompson and de Maine[7] for trinitrobenzene with the same donor molecules, indicating that the progression of values from the Benesi–Hildebrand equation is at least reproducible with other acceptors in chloroform, although it may not produce real values. Spectrally determined donor–acceptor constants in other solvents yield relative donor strengths which parallel that progression observed polarographically in this study. Such is the case for complexes of tetracyanoethylene with the same donors in methylene chloride.[8] The same relative progression of constants was found by Thompson and de Maine[7] for trinitrobenzene with the donors in carbon tetrachloride, *n*-heptane, *n*-hexane, and cyclohexane. Moreover, in the study reported in this paper the charge-transfer bands exhibited a regular trend toward higher energy from hexamethylbenzene to mesitylene, suggesting that this really is the true order of decreasing stability for these complexes in chloroform rather than as suggested by the Benesi–Hildebrand treatment. Maxima could be obtained only for TCNQ–hexamethylbenzene (6010 ± 50 A) and pentamethylbenzene (5400 ± 50 A) since the other two bands partially overlapped the TCNQ band. It would appear that the absorptions used in the Benesi–Hildebrand extrapolations in chloroform arise from some effect more complicated than merely the excitation of an isolated complex. The origin of this effect is unknown but may be related to interaction of the solvent dipole in the absorption by the complex.

Since the polarographic constants (both corrected

(6) L. R. Melby, R. J. Harder, W. R. Hertler, W. Mahler, R. E. Benson, and W. E. Mochel, *J. Am. Chem. Soc.*, 84, 3374 (1962).

(7) C. C. Thompson, Jr., and P. A. D. de Maine, *J. Phys. Chem.*, 69, 2766 (1965).

(8) G. Briegleb, "Elektronen-Donator-Acceptor-Komplexe," Springer-Verlag, Berlin, 1961, p 129.

Table II: Comparison of Polarographic and Spectral Constants in Chloroform

Donor	Polarographic constants in $CHCl_3$ (cor)	Benesi–Hildebrand constants in $CHCl_3$ (this study)
Hexamethylbenzene	3.7 ± 0.2	0.30 ± 0.03
Pentamethylbenzene	2.2 ± 0.3	1.36 ± 0.05
Durene	0.8 ± 0.1	0.18 ± 0.05
Mesitylene	0.7 ± 0.5	0.07 ± 0.03

and uncorrected) are consistent with the usual donor strengths, it is probable that values obtained from the Benesi–Hildebrand treatment in chloroform are suspect and that the true values are close to those obtained polarographically.

Calculations.—During the course of our investigation, several observations were made concerning the spectral shifts associated with the acceptor, TCNQ.

First of all there is a shift, a fact which is hardly surprising in view of Mulliken's early papers[9] and consideration of perturbation theory. In his paper concerning the molecular orbital treatment of charge-transfer complexes, Flurry[10] provides a review of the various perturbation treatments and points out the difficulties of such calculations. However, he does provide a simple molecular orbital treatment (neglecting overlap) of the problem in question.

Returning to the experimental results once again, it is seen that both red and blue shifts are observed for the acceptor first transition energy. This would suggest several interesting possibilities: (a) a simple energy scheme (as shown in Figure 1) wherein a red shift implies that the empty acceptor orbital is of higher energy than the filled donor orbital; (b) a more complicated picture wherein either one or both orbitals have been perturbed by the solvent molecules before (or during) complexation. Obviously, case b would not permit a simple correlation between shifts and the relative energies of the donor and acceptor orbitals except in rather fortuitous cases.

Having pointed out the problems concerning the interpretation of the spectroscopic shifts, we would like to confine ourselves to an examination of a, or a special case of b, where the solvent effects are treated as a constant factor.

Utilizing the one-electron molecular orbital treatment,[10] the energy of the charge-transfer transition (ΔE_{CT}) is

$$\Delta E_{CT} = (b^2 - a^2)(D - A + V_{es}) - 4ab\beta_{DA}$$

where D = negative of donor ionization potential, A = negative of electron affinity of acceptor, V_{es} = potential resulting from complete charge-transfer, β_{DA} = resonance integral between donor and acceptor, and a and b = molecular orbital coefficients ($a^2 + b^2 = 1$).

The value of A for TCNQ was taken as -1.70 ev.[11] D values were taken from Flurry's calculations[10] and Watanabe's values.[12] The charge-transfer band maxima were obtained from spectral results and, where necessary, from ΔE_{CT} *vs.* electron affinity plots. The latter plots are seldom linear unless the acceptor molecules are similar (*p*-benzoquinone, chloranil, and TCNE gave linear relationships for the donors benzene, toluene, *o*-xylene, mesitylene, durene, pentamethylbenzene) and the donor molecules are of the same series.

Special emphasis must be placed upon both geometric and orbital (atomic) similarities in acceptor molecules if any reliance is to be placed on such plots. Recently, a reexamination of X-ray data[13,14] has revealed that bond distances in the

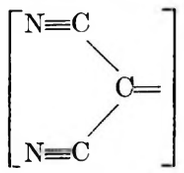

group of TCNQ are the same as those in TCNE. Furthermore, the bond distances in the ring of *p*-benzoquinone are similar to those found in the ring of TCNQ. X-Ray information concerning the methylbenzene[15] indicates that the standard benzene ring distance is relatively unaltered by the addition of the methyl groups.

While all of the above information may not be conclusive, it gives us encouragement. Proceeding to the next problem, there is the choice of V_{es}. As Flurry pointed out,[10] the choice of V_{es} is somewhat arbitrary in view of the limited information available.[10] With this in mind, we have set the complex equilibrium distance equal to three different values (3.25, 3.35, and 3.65 A) and compiled three sets of data (Table III). The values of a and b ($a = 0.88$ and $b = 0.47$) for the TCNQ

(9) R. S. Mulliken, *J. Phys. Chem.*, **56**, 801 (1952); *J. Am. Chem. Soc.*, **74**, 811 (1952), and other related papers.

(10) R. L. Flurry, Jr., *J. Phys. Chem.*, **69**, 1927 (1965).

(11) G. Briegleb, *Angew. Chem. Intern. Ed. Engl.*, **3**, 617 (1964).

(12) K. Watanabe, *J. Chem. Phys.*, **26**, 542 (1957).

(13) C. J. Fritchie, Jr., *Acta Cryst.*, **20**, 107 (1966).

(14) R. E. Long, R. A. Sparks, and K. N. Trueblook, *ibid.*, **18**, 932 (1965).

(15) "Tables of Interatomic Distances and Configuration in Molecules and Ions," Supplement, 1956–1959, The Chemical Society, London, 1965.

complexes are almost identical with those values (a = 0.89 and b = 0.45) obtained for the TCNE complexes.[10]

A distance of 3.25 A produces the only reasonable values of complex formation constants (see Tables I and II). This may be compared with a value of 3.26 A, the $TCNQ^-$–$TCNQ^-$ distance found by Fritchie[16] in the unit cell of N-methylphenazinium tetracyanoquinodimethanide.

While it can be correctly argued[10] that equilibrium constants calculated by this method are subject to doubt, there still remains the fact that the MO method should still correctly predict the relative order of constants. (See Table IV.)

Table III: Variations in Potential (V_{es}) and Resonance Integral (β_{DA}) with Intermolecular Distance (r)[a]

r, A	V_{es}, ev	$-\beta_{DA}$, ev
3.25	4.44	0.78
3.35	4.30	0.73
3.65	3.95	0.61

[a] $a^2 + b^2 = 1$ (a = 0.88, b = 0.47).

Table IV: Equilibrium Constants (K) Calculated from Molecular Orbital Theory with r = 3.25 A

TCNQ complex	Log (K/K^0)	K[a]
Hexamethylbenzene	1.65	43.7
Pentamethylbenzene	1.10	12.6
Durene	0.74	5.5
Mesitylene	0.00	1.0

[a] All K's normalized to the mesitylene–TCNQ complex.

Acknowledgment. Financial support was provided by National Science Foundation Grant GP-6031 and an institutional grant. W. R. C. wishes to acknowledge helpful discussions with R. L. Flurry concerning the calculations.

(16) C. J. Fritchie, Jr., *Acta Cryst.*, **20**, 892 (1966).

Effects of Structure on the Reactions of Hydrocarbon Ions

by M. S. B. Munson

Esso Research and Engineering Company, Baytown Research and Development Division, Baytown, Texas *(Received May 15, 1967)*

Mass spectrometric experiments on butane and isobutane at pressures as high as 1.4 torr confirm the previously reported hydride-transfer reactions and the low reactivity of the butyl ions. Formation of $C_3H_7^+$ is also observed possibly by a methide-transfer reaction. Only very small differences are observed in the rate constants for reactions of several ions with butane and isobutane. From studies on mixtures of the butanes and butenes, it was possible to observe differences in reactivities between i-$C_4H_8^+$ and 1- or 2-$C_4H_8^+$. The relative concentration of $C_3H_3^+$ exhibits a peculiar pressure dependence which suggests that two types of this ion are also formed.

There has been a continued effort in these laboratories to make a systematic study of the reactions of hydrocarbon ions. The present paper is concerned with reactions of ions with the butanes and with reactions of the isomeric butene ions. A previous study on the reactions of ions in butane has been reported from these laboratories.[1] The butane and isobutane systems and mixtures of each of these compounds with olefins have been investigated to confirm our previous findings and extend the pressures of the experiments to about 1 torr, to check for differences in the reactivities of ions with the isomeric butanes, and to check for differences in reactivities of isomeric ions.

Experimental Section

The instrument has been adequately described previously.[2] The *n*-butane and isobutane used in these experiments were Phillips Research grade hydrocarbons (stated purity 99.95+ mole %) for which no successful further purification was achieved. The purity of the other hydrocarbons was 99 mole % or better. The electron energy was approximately 800 v; the source temperature was 200 ± 10°, and the repeller was 5 v, field strength of 12.5 v/cm.

Results and Discussion

Reactions of Ions with Isomeric Butanes. Experiments were done on butane and mixtures of butane with a few per cent of other compounds: propylene, 1-butene, isobutylene, 1-pentene (6.4%), and 2,2,4-trimethylpentane (3.5%). Experiments were also performed on isobutane and similar mixtures of isobutane with these hydrocarbons. Let us first consider the reactions in the butanes.

The major process is hydride transfer as indicated by the predominance of $C_4H_9^+$ (predominantly *sec*-$C_4H_9^+$).[3] $C_4H_9^+$ reacts slowly, if at all, with butane since the concentration of $C_4H_9^+$ is substantially constant for pressures of 0.5–1.2 torr. Very similar results were noted for isobutane, the major difference being that 0.92 of the total ionization was present as $C_4H_9^+$ (predominantly t-$C_4H_9^+$)[3] in isobutane and 0.76 in butane.

Figure 1 shows plots of the pressure dependence of the logarithms of the relative ionic concentrations for $C_2H_5^+$ and $C_3H_7^+$ in butane and in mixtures of butane with the olefins. Since the rate constants for reactions of the primary ions (those produced from direct ionization by the electrons) with the two butanes are large, the presence of a few per cent of added material should not change the rate constants for reaction of these primary ions. The points of different shapes indicate experiments on the various mixtures and it is apparent that the rates of reaction are the same in all of the mixtures.

The linear plot in Figure 1 for the decrease in the

(1) M. S. B. Munson, J. L. Franklin, and F. H. Field, *J. Phys. Chem.*, 68, 3098 (1964).

(2) M. S. B. Munson and F. H. Field, *J. Am. Chem. Soc.*, 88, 2621 (1966).

(3) (a) P. G. Ausloos, S. G. Lias, and A. A. Scala, Advances in Chemistry Series, No. 58, American Chemical Society, Washington, D. C., 1966, pp 264–277; (b) M. S. B. Munson, *J. Am. Chem. Soc.*, 89, 1772 (1967).

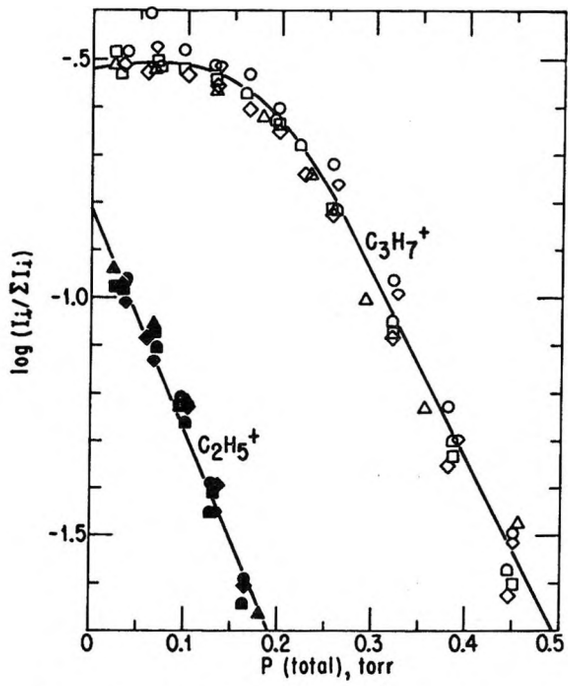

Figure 1. Log $I_1/\Sigma I_1$ *vs.* P.

relative ion current of $C_2H_5^+$ is precisely what one would expect from these experiments

$$C_2H_5^+ + n\text{-}C_4H_{10} \longrightarrow C_4H_9^+ + C_2H_6 \quad (1)$$

$$d(C_2H_5^+)/dt = -k(C_2H_5^+)(C_4H_{10}) \quad (2)$$

$$\log (I_{29}/\Sigma I_i) = A - 2.3k(C_4H_{10})t \quad (3)$$

since $(C_4H_{10}) \gg (C_2H_5^+)$ and the kinetics should be pseudo first order. I is the ion current, assumed to be proportional to ion concentration for all ionic species, k is the rate constant, parentheses indicate concentration, and t is the residence time of the ion calculated from simple electrostatics.

On the other hand, the curve for the logarithm of the relative ion current for $C_3H_7^+$ as a function of pressure is sufficiently different in shape from the curve for $C_2H_5^+$ to correspond to a more complicated process. This curve for $C_3H_7^+$ indicates that it is being formed and consumed by ionic reactions with butane. The reaction may be a methide-transfer reaction for C_1 or C_2 ions

$$R^+ + C_4H_{10} \longrightarrow C_3H_7^+ + RCH_3 \quad (4)$$

or perhaps H_2 transfer to $C_3H_5^+$. Similar behavior is observed for $C_3H_7^+$ ion isobutane, so similar reactions occur. The possibility of a methide-transfer reaction was suggested for propane,[4] but subsequent experiments attributed the products to other reactions.[5] The maximum ion energy in these experiments is 2.5 v, but at pressures of 0.1–0.2 torr it is likely that the primary ions react before they attain that energy. However, the amount of CH_3^- transfer (or dissociative proton transfer) with $C_2H_3^+$ was shown to increase relative to H^- transfer when the ion energy was increased from quasi-thermal to only 1 v;[5] consequently, the reaction forming $C_3H_7^+$ may be dissociative proton transfer assisted by the translational energy of the ion.[5]

Table I lists the rate constants for reaction of some of the primary ions formed by electron impact with the isomeric butanes. The rate constants are calculated from the slopes of the plots for the logarithms of relative ion current *vs.* pressure for pressures of 0.03–0.2 torr, generally. Since the pressure measurement is direct and more accurate in these experiments, the present set of rate constants is to be preferred over the earlier values reported from these laboratories.[1] The rates of reaction of $C_3H_7^+$, $C_4H_8^+$, and $C_4H_9^+$ with the butanes were calculated from the data at pressures above a few tenths of a torr and are less reliable. The upper limits indicated in Table I are obtained from the constancy of ionic concentrations at high pressures and the absence of higher molecular weight products.

Table I: Rate Constants for Reactions of Ions with Butanes

	k, 10^{-10} cc/molecule sec			
	n-C_4H_{10}		i-C_4H_{10}	
Ion	These data	Literature	These data	Literature
$C_4H_9^+$	<0.007	...	<0.001	...
$C_4H_8^+$	<0.01	...	2.1 ± 0.3[c]	...
$C_3H_7^+$	3.9 ± 0.3	...	4.0 ± 0.3	...
$C_3H_6^+$	5.1 ± 1.1	4.1–4.5[a]	6.7 ± 1.0	4.0–4.6[a]
$C_3H_5^+$	5.0 ± 0.6	8.5[b]	5.8 ± 0.4	2.8[b]
$C_2H_5^+$	7.5 ± 0.9	6.6 ± 2.8[b]	10.1 ± 1.3	3.9[b]
$C_2H_4^+$	11.4 ± 1.3	12 ± 4[b]	...	...
$C_2H_3^+$	8.5 ± 1.0	6.0 ± 1.8[b]	11.4 ± 1.3	9.8[b]

[a] L. W. Sieck and J. H. Futrell, *J. Chem. Phys.*, **45**, 560 (1966). [b] See ref 1. [c] Does not include experiments with 1-C_4H_8 and *t*-2-C_4H_8.

The structures of these primary ions are not known. However, since the primary ions are produced by 800-v electrons, it is reasonable to suppose that isomerization to the most stable structures is rapid. Even if the propyl ions which are produced by ion–molecule reactions in these isomeric butanes are formed with initially different structures, there is some evidence that isomerization of primary to secondary ions by

(4) K. R. Ryan and J. H. Futrell, *J. Chem. Phys.*, **42**, 819 (1965).
(5) L. I. Bone and J. H. Futrell, *ibid.*, **46**, 4084 (1967).

H^- shifts is very rapid even when compared to the times of these experiments.[6] The butyl ions have been shown to have different structures[3] and later in this paper differences in reactivities of the butene ions will be interpreted to show that these ions have different structures.

Let us consider possible differences in the rate constants for the reactions of this set of ions with the two isomeric butanes. Only the butenes, which are expected to have different structures, show an appreciable difference in rate constants for reaction with these two isomers. There does, however, appear to be a small difference: the ions may react slightly more rapidly with isobutane than with *n*-butane. The average value of the ratio of the rate constants is 1.2. Sieck and Futrell[7] find rate constants for reaction of $C_3H_6^+$ with butane and isobutane which are equal within experimental error (estimated at $\pm 10\%$). In their experiments the residence times of the ions are more precisely determined than in the present experiments, but the pressure measurements are probably less reliable than the present ones. The two sets of data are not contradictory and they do indicate that the effect of this structural variation is small, if real.

Borkowski and Ausloos,[8] however, observed in radiation chemistry experiments that the ratio of rate constants for reaction of $C_3H_7^+$ with isobutane and $C_3H_7^+$ with *n*-butane was 0.67 in contrast to the value of 1.0 ± 0.1 from the present set of experiments. There is no ready explanation for this discrepancy.

One may expect with confidence that the C_1 and C_2 ions can abstract primary, secondary, and tertiary hydrogens from the isomeric butanes. Consequently, the rate constants for reactions of the C_2 ions with the butanes should be nearly the same because the polarizabilities of the butane isomers are essentially equal.[9] For $C_3H_6^+$, H_2^- transfer from either butane and H^- transfer from the tertiary carbon atom of isobutane are exothermic and H^- transfer from a secondary carbon atom is about thermoneutral.[10] Since there are energetically similar reactions for both butanes, one would not expect appreciable differences in rate constants. However, if the propyl ions have the secondary structure, as appears to be the case from radiation studies,[8] then only one hydrogen is available for H^- transfer in isobutane compared with four in *n*-butane. More detailed studies are necessary to decide whether this apparent preference for a tertiary hydrogen is real.

Reactions of Isomeric Butene Ions. Figure 2 shows plots of the concentrations of butene ions (as fractions of the total ionization) as functions of pressure for butane and mixtures of butane with several olefins. The nonreactivity of the butene ions with butane is

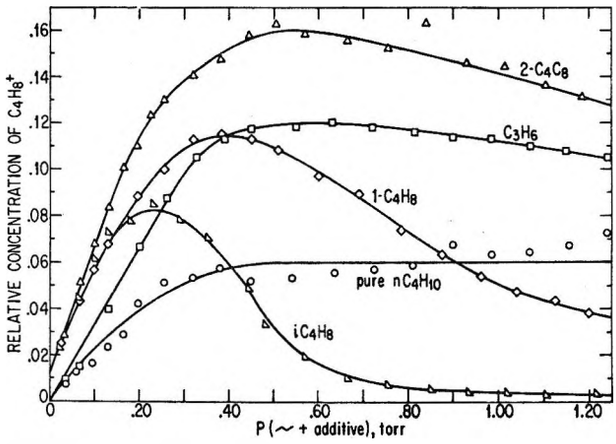

Figure 2. Relative concentrations of butene ions.

shown by the constancy of the concentration of $C_4H_8^+$ for pressures above about 0.5 torr. It will be remembered from the data in Table I that the analogous ion in isobutane did indicate a rapid reaction. $C_4H_8^+$ is formed as a product ion in butane by H_2^- transfer reactions. The data of Sieck and Futrell[7] on H_2^- transfer reactions from partially deuterated *n*-butane to $C_3H_6^+$ indicate that the ratio $1\text{-}C_4H_8^+/2\text{-}C_4H_8^+$ should be about 0.7. Consequently, this nonreactivity of butene ions with butane suggests that neither $1\text{-}C_4H_8^+$ nor $2\text{-}C_4H_8^+$ reacts with butane.

In the mixture of *n*-butane and 6.5% propylene, there are notably more butene ions produced than in butane alone. These ions are probably produced by both H_2^- transfer reactions[1,7]

$$C_3H_6^+ + n\text{-}C_4H_{10} \longrightarrow C_3H_8 + C_4H_8^+ \qquad (5)$$

and by H_2 transfer reaction[11,12]

$$C_4H_{10}^+ + C_3H_6 \longrightarrow C_4H_8^+ + C_3H_8 \qquad (6)$$

The small decrease in relative concentration of $C_4H_8^+$ in this mixture of butane and propylene for pressures above 0.8 torr is equal to the small amount of $C_7H_{14}^+$ produced by a collision-stabilized addition of butene ions to propylene

(6) P. S. Skell and R. J. Maxwell, *J. Am. Chem. Soc.*, **84**, 3963 (1962).

(7) See footnote *a* of Table I.

(8) R. P. Borkowski and P. Ausloos, *J. Chem. Phys.*, **40**, 1128 (1964).

(9) H. H. Landolt and R. Bornstein, "Zahlenwerte und Functionen," Part 3, 6th ed, Springer-Verlag, Berlin, 1950.

(10) Heats of formation of ions are taken from F. H. Field and J. L. Franklin, "Electron Impact Phenomena," Academic Press Inc., New York, N. Y., 1957, Table 45.

(11) P. Ausloos and S. G. Lias, *J. Chem. Phys.*, **43**, 127 (1965).

(12) F. P. Abramson and J. H. Futrell, *J. Phys. Chem.*, **71**, 1233 (1967).

$$C_4H_8^+ + C_3H_6 \rightleftarrows (C_7H_{14}^+)^* \quad (7)$$

$$(C_7H_{14}^+)^* + C_4H_{10} \longrightarrow C_7H_{14}^+ + C_4H_{10}^* \quad (8)$$

Collision-stabilized addition of olefin ions to olefins was reported previously for ethylene.[13]

The butene ions produced in this mixture of butane and propylene do not react with butane either. These observations support the previous statement that 1-$C_4H_8^+$ and 2-$C_2H_8^+$ do not react with butane.

The greater abundance of $C_4H_8^+$ ions in the mixtures of *n*-butane with the butenes is attributable primarily to charge-exchange reactions with these additives. Only the amount indicated by the zero pressure intercept can be attributed to direct ionization.

The butene ions produced in the mixture with 2-butene do not react rapidly with 2-butene and do not react at all with *n*-butane. The decrease in relative concentration of $C_4H_8^+$ ions in the mixture for pressures above 0.5 torr can be attributed in a large part to a collision-stabilized reaction with butene, analogous to (7) and (8)

$$C_4H_8^+ + t\text{-}2\text{-}C_4H_8 \rightleftarrows (C_8H_{16}^+)^* \quad (9)$$

$$(C_8H_{16}^+)^* + C_4H_{10} \longrightarrow C_4H_{10}^* + C_8H_{16}^+ \quad (10)$$

In addition, second-order products have been reported previously from reaction of butene ions with butene: $C_4H_7^+$ and $C_4H_9^+$,[14] and $C_5H_9^+$.[14,15] There is no evidence for any reaction of the 2-butene ions with butane. These collision-stabilized addition reactions are observed at pressures of several tenths of a torr in the present experiments and could not be observed at the lower pressures of the other experiments (of the order of 0.01 torr).

It is apparent from Figure 2 that 1-$C_4H_8^+$ reacts more rapidly in the mixture with 1-butene than 2-$C_4H_8^+$ does in the mixture with 2-C_4H_8. Only about one-half of the loss of $C_4H_8^+$ can be explained by the formation of $C_8H_{16}^+$ through reactions analogous to (10). However, it is known that second-order reactions of 1-$C_4H_8^+$ with 1-C_4H_8 are about four times as fast as second-order reactions of 2-$C_4H_8^+$ with 2-C_4H_8.[14,15] Consequently, it is not possible to obtain an accurate balance on $C_4H_8^+$ to decide whether or not reaction occurs with *n*-butane.

The isobutylene ion reacts even more rapidly in the mixture of *n*-butane and isobutylene than does the 1-butene ion in the mixture of 1-butene and *n*-butane by a factor of approximately 3. Only about one-fourth of the decrease in concentration of $C_4H_8^+$ above 0.2 torr can be accounted for by the formation of $C_8H_{16}^+$ from collision-stabilized addition of olefin ions to olefins. In addition, it is known that the cross section for second-order reactions of *i*-$C_4H_8^+$ with *i*-C_4H_8 is about one-half the cross section for second-order reactions of 1-$C_4H_8^+$ with 1-C_4H_8.[15] Consequently, *i*-$C_4H_8^+$ must react with *n*-C_4H_{10}, in all likelihood by H transfer

$$i\text{-}C_4H_8^+ + n\text{-}C_4H_{10} \longrightarrow t\text{-}C_4H_9^+ + sec\text{-}C_4H_9 \quad (11)$$

for which the heat of reaction is zero or slightly negative. H^- transfer to give *sec*-$C_4H_9^+$ and *t*-C_4H_9 is endothermic and less likely to occur. This difference in reactivity between the isobutylene ion and the 1- and 2-butene ions with butane suggests a difference in structure and a slow rate of isomerization. The discussion of distinguishable 1- and 2-butene ions is based primarily on the slightly different heats of formation of these ions and the present results provide no information about possible differences between them.

As mentioned previously in this paper, the butene ions produced in isobutane react rapidly with isobutane. The reaction is

$$i\text{-}C_4H_8^+ + i\text{-}C_4H_{10} \longrightarrow t\text{-}C_4H_9^+ + t\text{-}C_4H_9 \quad (12)$$

since there is no product other than $C_4H_9^+$ of sufficient concentration to account for the decrease in the concentration of $C_4H_8^+$. The rate constants for reaction of the butene ions are essentially the same in isobutane and in the mixtures of isobutane with the additives, except for the mixtures with 1-butene and 2-butene. Small amounts of collision-stabilized olefin addition products were observed. The fact that the rate constant for the disappearance of the ions of *m/e* 56 in the mixture of isobutane and isobutylene is the same as that in isobutane supports the idea that charge exchange with isobutylene and H_2^- transfer with isobutane produce the same butylene ions, *i*-$C_4H_8^+$.

The rate constant for the disappearance of *m/e* 56 in the mixture of isobutane and 1-butene is 1.4×10^{-10} cc/molecule sec (assuming that the reactant is isobutane). This value is lower than that given in Table I by an amount which is probably greater than the experimental error and suggests that some of the butene ions have different reactivities (and possibly different structures).

The rate constant for the disappearance of ions of *m/e* 56 in the mixture of isobutane and 2-butene is 0.34×10^{-10} cc/molecule sec (assuming the neutral reactant to be isobutane). This difference of a factor of 7 is well beyond experimental error and shows clearly that the butene ions from 2-butene are different from the butene ions from isobutane. The reactions analogous to (12)

(13) F. H. Field, *J. Am. Chem. Soc.*, **83**, 1523 (1961).

(14) I. Koyano, *J. Chem. Phys.*, **45**, 706 (1966).

(15) R. Fuchs, *Z. Naturforsch.*, **16a**, 1026 (1961).

$$2\text{-}C_3H_8^+ + i\text{-}C_4H_{10} \begin{cases} \xrightarrow{X} t\text{-}C_4H_9^+ + sec\text{-}C_4H_9 & (13a) \\ \xrightarrow{X} sec\text{-}C_4H_9^+ + t\text{-}C_4H_9 & (13b) \end{cases}$$

are both endothermic and the reactions should be less favored than (12).

These observations suggest that the isobutylene and 2-butene ions have the different structures that one would intuitively assume and that the rate of interconversion is slow. Because of the already established differences in reactivities of $1\text{-}C_4H_8^+$ with $1\text{-}C_4H_8$ and $2\text{-}C_4H_8^+$ with $2\text{-}C_4H_8$, it is not possible to be certain that these results indicate any difference between these two ions.

Reactivities of $C_3H_3^+$. In these butane systems there is another indication of isomeric ions of different reactivities—the very unusual pressure plot of the relative concentration of $C_3H_3^+$ shown in Figure 3. This initial steep decrease to an essentially constant value is unique among the ions in these mixtures. This behavior suggests strongly that there are two types of $C_3H_3^+$ ions formed in butane—one which is as reactive as the majority of the other ions and another which is essentially unreactive. Equally surprising is the nonreactivity with olefins and the lack of hydride transfer of the tertiary hydrogen in 2,2,4-trimethylpentane. The only compound with which reaction occurs is isobutylene, but it is not possible to identify the products. Essentially the same results are observed for isobutane, an initial steep decrease to an essentially constant value. The final concentration of $C_3H_3^+$ in isobutane is slightly higher than in *n*-butane, 0.03 and 0.02. This difference may represent a difference in the ratios of the two forms of $C_3H_3^+$ produced in the two gases.

These data may be taken as support for the suggestion that there is a $C_3H_3^+$ ion of energy lower than the accepted value of 270 kcal/mole.[16] It is not possible in the present series of experiments to establish what are the reactions of $C_3H_3^+$. However, possible reactions are

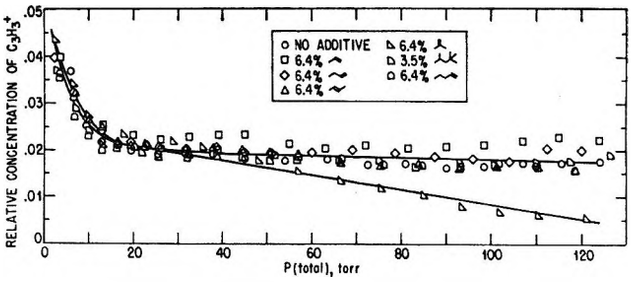

Figure 3. Relative concentration of $C_3H_3^+$ as a function of pressure in $n\text{-}C_4H_{10}$ and certain mixtures with $n\text{-}C_4H_{10}$.

$$C_3H_3^+ + n\text{-}C_4H_{10} \begin{cases} \longrightarrow C_3H_5^+ + C_4H_8 & (14a) \\ \longrightarrow C_4H_9^+ + C_3H_4 & (14b) \end{cases}$$

Similar reactions have been reported for $C_3H_3^+$ ions with propane.[5] Both reactions are exothermic if the heat of formation of $C_3H_3^+$ is 270 kcal/mole. If there is a nonreactive form of $C_3H_3^+$ and reaction 14 is prohibited for energetic reasons, then perhaps the heat of formation of this lower energy species is less than 250–255 kcal/mole. This suggestion is admittedly highly speculative, but perhaps it will lead to more definitive experiments.

Acknowledgments. The author is grateful to Drs. J. L. Franklin and F. H. Field and to the reviewer for helpful comments about this paper.

(16) G. B. Kistiakowsky and J. V. Michael, *J. Chem. Phys.*, **40**, 1447 (1964).

The Reactions of Hydrogen Atoms with Benzene and Toluene Studied by Pulsed Radiolysis: Reaction Rate Constants and Transient Spectra in the Gas Phase and Aqueous Solution[1]

by Myran C. Sauer, Jr., and Barry Ward[2]

Chemistry Division, Argonne National Laboratory, Argonne, Illinois 60439 *(Received May 19, 1967)*

The rate constants at 25° for the gas-phase reactions of hydrogen atoms with benzene and toluene have been determined by the technique of pulsed radiolysis and are, in units of M^{-1} sec^{-1}, 0.37×10^8 and 1.0×10^8, respectively. The activation energy in the case of benzene is about 3 kcal/mole. In aqueous solution, the corresponding rate constants have been determined to be 1.1×10^9 and 2.6×10^9, respectively. The limits of error on these rate constants are *ca.* ±20%. The rate constants were measured by following, as a function of time, the formation of the optical absorption due to radicals produced when hydrogen atoms, produced by an electron pulse, react with the aromatic compound. Benzene and toluene yield the cyclohexadienyl radical and the methylcyclohexadienyl radical, respectively, with absorption maxima at 302 and 307 mμ, respectively, in the gas phase. The half-widths of the absorption peaks are about 30 mμ. In aqueous solution, the absorption maxima are 311, (ϵ^{311} (5.4 ± 0.5) $\times 10^3$ M^{-1} cm^{-1}) and 315 mμ, respectively, with half-widths similar to those in the gas phase. The combination of two cyclohexadienyl radicals proceeds at least as fast as once every ten collisions in the gas phase at 25°, indicating a "loose" activated complex. In the liquid phase, the combination is diffusion controlled.

Introduction

The use of the pulsed-radiolysis technique as a means of producing oxygen atoms in the gas phase and studying their reaction with molecular oxygen has been described.[3,4] When a system consisting of about 50 atm of argon and a few centimeters of oxygen was irradiated with a 1-μsec pulse of 12–15-Mev electrons, a "pulse" of oxygen atoms was found to be produced essentially simultaneously. The formation of ozone due to the reaction of this pulse of oxygen atoms with molecular oxygen was observed and analyzed to obtain information on the rate constant of the reaction $O + O_2 + Ar \rightarrow O_3 + Ar$.

The present work describes how the same technique has been used to produce a pulse of hydrogen atoms by pulsed radiolysis of a system containing, for example, 50 atm of argon and 5 atm of hydrogen. By introducing a few centimeters of benzene or toluene, the reactions of hydrogen atoms with these materials were followed after the electron pulse by measuring the rates of formation of the optical absorptions of the resulting radicals.

Because of the limited number of reactions for which rate constants have been determined in both the gaseous and condensed phases,[5] we have used similar techniques to investigate the rates of reaction of hydrogen atoms with benzene and toluene in aqueous solution.

(1) Based on work performed under the auspices of the U. S. Atomic Energy Commission.

(2) Shell Research Ltd., Thornton Research Centre, Chester, England.

(3) M. C. Sauer, Jr., and L. M. Dorfman, *J. Am. Chem. Soc.*, **86**, 4218 (1964).

(4) M. C. Sauer, Jr., and L. M. Dorfman, *ibid.*, **87**, 3801 (1965).

(5) K. J. Laidler, "Chemical Kinetics," McGraw-Hill Book Co., Inc., New York, N. Y., 1965, p 199.

Experimental Section

General. Detailed descriptions of the techniques of high-pressure pulse radiolysis and the methods of spectrophotometric observation have been given earlier.[4,6] However, the pressure gauge and the freeze-out arm were removed from the high-pressure irradiation cells used in this investigation since it was suspected that they might cause errors in the results due to incomplete mixing in the "dead-ends." Useful results were also obtained from a 17 cm long quartz irradiation vessel containing a total pressure of only 1 atm.

Materials. The argon (Linde) and hydrogen (National Cylinder Gas) were used without purification directly from the cylinder, the purity of the argon having been checked in an earlier investigation.[4] As for the hydrogen, the stated purity was 99.97%, with less than 10 ppm O_2 and 5 ppm hydrocarbons. The benzene and toluene (Phillips research grade) and chlorobenzene (La Pine and Co.) were degassed by several trap-to-trap distillations on a conventional vacuum line before vaporizing into the irradiation cell. The deuterated benzene and toluene (Merck Sharp and Dohme) were handled in a similar manner.

Aqueous Solutions. The aqueous solutions of the aromatic compounds were prepared in nominal concentrations by first dissolving the hydrocarbon in methanol (Baker) and then adding an aliquot of this solution to triply distilled water.

Degassing was effected in 100-cc syringes by adding argon to the solution and shaking vigorously for about 1 min before expelling the gases. After five or six such cycles, the oxygen concentration is about 10^{-7} M. The technique of filling and emptying the 4-cm quartz irradiation cell using a differential gas pressure has been described previously.[7] The experimental arrangement for monitoring the optical transmission of the solutions was almost identical with that used in the gas-phase experiments except that the path length (within the irradiation vessel) of the light beam was only 8 cm as compared to 26 cm.

The determination of the hydrocarbon concentrations was not simple since the high volatility of the solutes caused immediate loss from a solution on exposing it to a liquid–gas interface. Eventually, the analytical method adopted was gas chromatography on a silicon gum rubber column at 50°. Standard solutions were prepared in 100-cc syringes, containing glass mixing disks but no gas space, by injection of an appropriate amount of hydrocarbon from a calibrated microsyringe into a known volume of methanol. This operation was followed by an identical one in which a portion of the hydrocarbon–methanol mixture was injected into water (to give a solution of required concentration). Signal strengths from the degassed experimental solutions, prepared by normal volumetric techniques, were then compared with those from the standard solutions. Using this method, we estimate the uncertainty in the hydrocarbon concentrations to be not more $\pm 10\%$, including a correction for the loss of solute which occurs when the solution is forced into an empty cell.

The solutions were adjusted to a pH of about 3 with sulfuric or perchloric acids in order to convert the solvated electrons produced by the pulse into hydrogen atoms and prevent possible radical formation by reaction of the aromatics with the electrons followed by protonation of the resulting anion. Methanol was added to the system, not only to facilitate solution of the aromatics, but also to scavenge hydroxyl radicals[8] which add to the benzene ring[9] ($k = 4.3 \times 10^9$ M^{-1} sec^{-1}) to form the hydroxycyclohexadienyl radical, absorbing[9] in the same region as the product of the hydrogen atom reaction. Unfortunately, methanol also reacts with hydrogen atoms at a non-negligible rate[10] ($k = 1.6 \times 10^6$ M^{-1} sec^{-1}) such that under optimum conditions (benzene $\sim 10^{-4}$ M, methanol $\sim 2.5 \times 10^{-2}$ M) only about 70% of the hydrogen atoms formed add to the benzene. In a case such as this, the experimentally determined pseudo-first-order rate constant is given by k_1[benzene] + k_2[methanol] where k_1 and k_2 are the second-order rate constants for the reactions of hydrogen atoms with benzene and methanol. Since k_2 and the alcohol concentration are known, it is a simple matter to apply a correction to the kinetic measurements.

In order to minimize this correction, experiments were repeated using completely deuterated methanol (Merck Sharp and Dohme) as an OH scavenger. Deuteration has the effect that while the rate constant for OH reaction is little changed (from 4.4[8] to 2.5[11] $\times$ 10^8 M^{-1} sec^{-1}), that for the hydrogen atom reaction decreases from 1.6×10^6 [10] to 8×10^4 M^{-1} sec^{-1}.[11] Here we have assumed that the reactivity of CD_3OD is the same as that of CD_3OH; we feel this is a reasonable assumption since radical attack on alcohols occurs mainly at a C–H bond.[11] Because of this decrease in

(6) M. C. Sauer, Jr., S. Arai, and L. M. Dorfman, *J. Chem. Phys.*, **42**, 708 (1965).

(7) E. J. Hart and J. W. Boag, *J. Am. Chem. Soc.*, **84**, 4090 (1962).

(8) G. E. Adams, J. W. Boag, J. Currant, and B. D. Michael, "Pulse Radiolysis," M. Ebert, *et al.*, Ed., Academic Press, New York, N. Y., and London, 1965, p 131.

(9) L. M. Dorfman, I. A. Taub, and R. E. Buhler, *J. Chem. Phys.*, **36**, 3051 (1962).

(10) J. P. Sweet and J. K. Thomas, *J. Phys. Chem.*, **68**, 1363 (1964).

(11) OH + CD_3OD: M. Anbar, D. Meyerstein, and P. Neta, *J. Chem. Soc.*, [B], 742 (1966); H + CD_3OD: M. Anbar and D. Meyerstein, *J. Phys. Chem.*, **68**, 3184 (1964).

the hydrogen atom reaction rate, the correction in the experiments with CD_3OD was less than 3%, and for this reason the results from this system are more reliable. While the contribution of the hydroxycyclohexadienyl radical to the absorption could approach 5% of the maximum in these runs, its effect on the formation curves will be negligible since, to a good approximation, this absorption will be a constant cancelling out in the expression used in the first-order plot.

Treatment of Data. The reactions after the pulse were monitored on an oscilloscope by displaying the intensity of transmitted light as a function of time. Photographs of the oscillographic traces were analyzed by a completely automatic, computerized technique, details of which may be found in ref 12, 13, and 14.

Preparation of Gas-Phase Samples. The samples were prepared by first letting into the irradiation vessel the required pressure of the aromatic compound, followed by the desired pressures of hydrogen and/or argon. The samples were allowed to stand overnight to ensure complete mixing.

A few samples were run in which excess liquid benzene or toluene was present. It was found that the rate of transient formation was larger than expected, based on the vapor pressure of benzene at room temperature and 1 atm. This anomaly is accounted for by the elevation of saturated vapor pressures caused by high gas pressure.[15]

Product Analysis. Gas chromatographic analysis of the products formed during the pulsed radiolysis of gas-phase samples was carried out by trapping the nonvolatile contents of the irradiation vessel in a stainless steel U-shaped trap containing some glass wool, at liquid nitrogen temperature. This was done on a vacuum line so that the argon and hydrogen were pumped away. After 2 hr or more of distillation from the vessel to the trap, the trap was placed directly before the column on a flame detector apparatus. A 6-ft silicon–gum rubber column, temperature programmed from 25 to 210°, was used for the dimer analysis. An 8-ft β,β'-oxydipropionitrile column at room temperature was used for the cyclohexadiene analysis. An analysis of products from the aqueous solutions was not attempted.

Results

Transient Spectra. Figure 1 shows the spectra observed when samples of argon and hydrogen (ratio about 10:1), or just hydrogen, containing much smaller amounts (*ca.* 7 cm) of benzene or toluene were pulse irradiated. The spectra were the same over the entire time range of the transient formation and decay, except that the decay at 270–280 mμ was slightly slower than at wavelengths longer than 280 mμ, indicating absorption at lower wavelengths due to another species, possibly a permanent product. The assignment of these spectra to the cyclohexadienyl radical, $C_6H_7\cdot$ (λ_{max} 302 mμ), and methylcyclohexadienyl radical, $C_7H_9\cdot$ (λ_{max} 307 mμ), will be discussed.

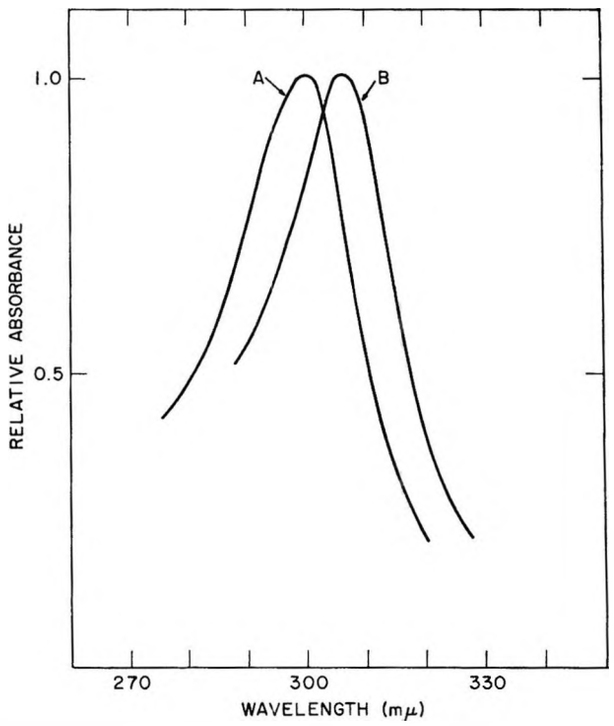

Figure 1. Gas-phase spectra of cyclohexadienyl (A) and methyl cyclohexadienyl (B) radicals. (Both spectra are arbitrarily normalized to 1.0 at maximum absorption.)

Although the wavelength of maximum absorption did not vary, for a given aromatic compound, from one sample to another, or with changes in pressure, the precise shape and half-width of the absorption did. No general trends could be established with changes in pressure or composition. (Most of the results gave half-width of about 30 mμ, but a few variations of about ±20% occurred.) The spectra shown in Figure 1 are intended to indicate only the approximate shapes of the absorptions. Since a band-pass of 3.2 mμ was used in the spectrophotometric determination of these spectra, some structural features may be lost. The use of completely deuterated benzene or toluene also had no effect on the wavelength of maximum absorption,

(12) S. Arai and M. C. Sauer, Jr., *J. Chem. Phys.*, **44**, 2297 (1966).

(13) M. C. Sauer, Jr., Argonne National Laboratory Report, ANL-7113, Oct 1965.

(14) M. C. Sauer, Jr., Argonne National Laboratory Report, ANL-7146, Jan 1966.

(15) S. Robin and B. Vodar, *Discussions Faraday Soc.*, **15**, 233 (1953).

and the half-width did not change more than would be expected from the variations noted above for the non-deuterated compounds.

When samples of argon plus benzene or toluene *without* hydrogen gas were irradiated, an absorption about 30–50% as strong was observed in the same spectral region, with the same wavelength of maximum absorption. The spectra were not appreciably different in shape except for a tendency toward stronger absorption at wavelengths below the maxima. However, there was an initial absorption which disappeared within about 5 μsec after the pulse and which had a maximum absorption around 330–340 mμ in the case of benzene. A similar, but weaker, absorption was also present in the case of toluene. The identity of the species responsible for these rapid decays is unknown. The decay of the main absorption was similar to that observed in the experiments where hydrogen was present (see later section on transient decay). For the sake of completeness, it should be mentioned that "blank" experiments on argon or hydrogen alone gave no absorbing transients. These facts will be discussed later.

The absorption spectra obtained from the reaction of hydrogen atoms with benzene (λ_{max} 311 mμ) and toluene (λ_{max} 315 mμ) in aqueous solution are shown in Figure 2. These spectra were taken at about 20 μsec after the pulse; the decay was considerably slower at lower wavelengths than at the wavelength of maximum absorption and higher. This indicates either an absorption due to a product or the presence of another transient which absorbs at lower wavelengths but decays slowly. The half-widths are somewhat uncertain because of the increase in absorption at low wavelengths, but are not appreciably different from the gas-phase results. We estimate that a maximum of 5% of the absorption is due to $\cdot C_6H_6OH$ and $\cdot CH_2OH$ formed in reactions of OH and H with the aromatic solute and methanol. The spectrum of the methanol radical $\cdot CH_2OH$, in an aqueous solution of 2.5×10^{-2} *M* CH_3OH is included in Figure 2. The absorption of $\cdot CH_2OH$ is considerably weaker than that of the cyclohexadienyl radical (see later section on absorption coefficients), but it has been plotted on a comparable scale for convenience.

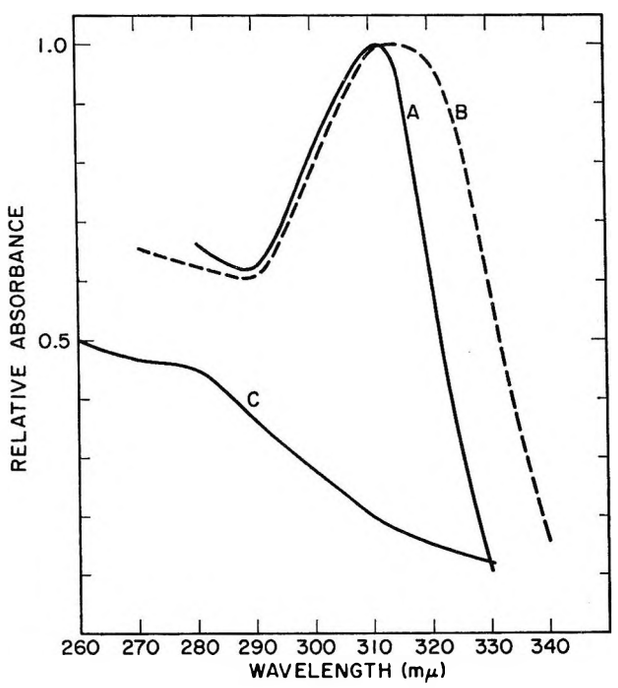

Figure 2. Spectra in aqueous solution: A, cyclohexadienyl radical; B, methylcyclohexadienyl radical; C, $\cdot CH_2OH$ radical. A and B are both arbitrarily normalized to 1.0 at maximum absorption, and C is arbitrarily normalized to 0.5 at 270 mμ. The actual absorption coefficient of C is much smaller than shown, relative to A and B: ϵ_A^{311} 5.4×10^3 M^{-1} cm^{-1}; ϵ_C^{311} 25 M^{-1} cm^{-1}.

Rate Constants for Hydrogen Atom Reactions. Figures 3 and 4 show oscilloscope traces representing the concentration of transient as a function of time when a system containing 53 atm of argon, 7 atm of hydrogen, and 0.1 atm of benzene is pulse irradiated. The initial relatively sharply curved part represents the transient formation, and the subsequent more slowly changing part of the trace represents the decay of the transient. As will be shown, the formation of the transient is due to the reaction of hydrogen atoms with benzene and the decay is due to the dimerization and disproportionation

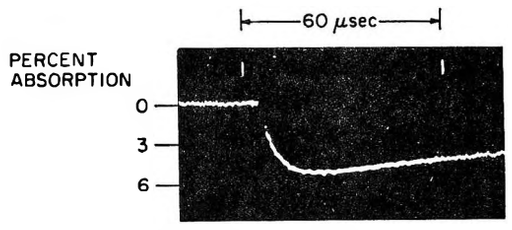

Figure 3. Formation of cyclohexadienyl (gas phase), higher intensity pulse; λ = 302 mμ.

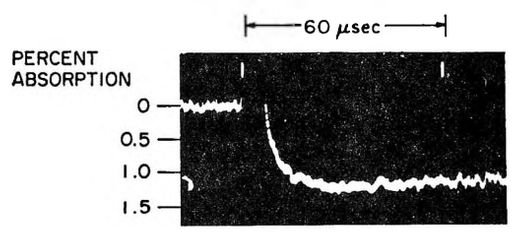

Figure 4. Formation of cyclohexadienyl (gas phase), lower intensity pulse; λ = 302 mμ.

of the resulting cyclohexadienyl radical. Similar curves are obtained in the case of toluene.

The analysis of such curves for the rate constants of the reactions of hydrogen atoms with the aromatic compounds must take into account the fact that the transient undergoes decay by radical–radical reaction even during the time period of its formation. Experimentally, one can minimize the importance of this fact by decreasing the electron pulse intensity and increasing the amplification of the signal. That is, the rate of the pseudo-first-order reaction of hydrogen atoms with the aromatic compound is proportional to the initial hydrogen atom concentration, but the rate of the second-order radical–radical reaction will depend on [radical]^2. The result of this effect can be seen by comparing Figures 3 and 4.

An iterative method for computer analysis of such curves (where decay is not negligible) has been described[14] and was used to determine rate constants from curves such as Figure 3.[16-18] Figure 5 shows the optical density (circles) as determined from the trace shown in Figure 4, and the corrected optical density (triangles), as a function of time. The corrected optical density is the actual optical density corrected to the hypothetical situation in which no decay of the cyclohexadienyl radical occurs. Figure 6 shows the first-order plot for the approach to the plateau of the corrected optical density curve. The slope of this plot is equal to the rate constant for reaction of hydrogen atoms with benzene multiplied by the benzene concentration. In the case of curves such as Figure 4, where the decay is nearly negligible, the analysis was often carried out by the usual method[4] of making a first-order plot of the approach to the uncorrected plateau. The rate constants obtained from the analysis of curves such as those shown in Figures 3 and 4 were in agreement.

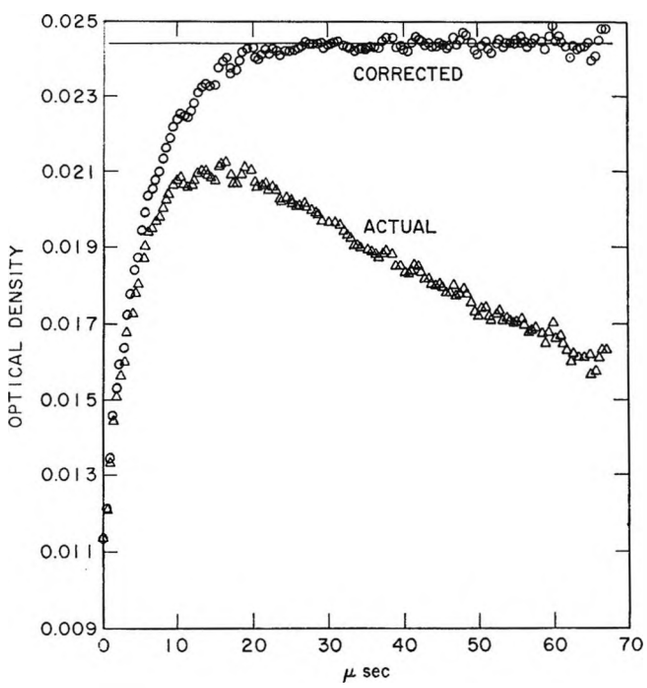

Figure 5. Optical densities *vs.* time, calculated from Figure 3: Δ, actual optical density; O, corrected optical density.

Table I summarizes the rate constants obtained for the reactions of hydrogen atoms with benzene and toluene. Although the rate constant for benzene seems to increase slightly with total pressure, the effect is almost within the experimental scatter, and apparently there is no marked effect of pressure on the rate constants. It is worthwhile to note that removal of hydrogen atoms by diffusion to the walls is ruled out by the data, since this would cause an increase in the rate constant at lower pressure. The average values of the rate constants and the experimental uncertainties may be stated as $k(H + C_6H_6) = (0.37 \pm 0.06) \times 10^8$, and $k(H + C_6H_5CH_3) = (1.0 \pm 0.1) \times 10^8$, in units of M^{-1} sec^{-1}.

(16) In order to make a complete correction to a curve such as Figure 3, the values of the rate constants for the reactions between two hydrogen atoms and between hydrogen atoms and the aromatic radical must be known relative to the rate constant for the reaction between two aromatic radicals. The latter reaction is responsible for the decay in Figure 3. As will be shown, the gas-phase rate constant for this reaction is between 10^{10} and 10^{11} M^{-1} sec^{-1}, with the lower value being more probable, and the liquid phase value is about 1.8×10^9 M^{-1} sec^{-1}. In the gas phase, the reaction between two hydrogen atoms is dependent upon the third body, and for argon, the rate constant[17] is 2.3×10^9 M^{-2} sec^{-1}. Therefore, at the highest argon concentrations used in this work, the rate constant times argon concentration is about 10^{10} M^{-1} sec^{-1}, which is about the same as the rate constant for reaction between two cyclohexadienyl radicals. In the analysis of experimental curves, it was found that when the H + H reaction was given a relative value of from 0 to 1 times the cyclohexadienyl dimerization rate constant, there was little change in the result for the rate constant derived for the addition reaction. Data on the reaction rate constant of hydrogen atoms with the cyclohexadienyl radical are not available, so the reaction was assumed to proceed with the same rate constant as H + H. Again, the exact value had little effect on the result obtained.

In aqueous solution, the rate constant for reaction between two hydrogen atoms is known to be[18] about 10^{10} M^{-1} sec^{-1}, which is higher than the value obtained for reaction of two cyclohexadienyl radicals of 1.8×10^9 M^{-1} sec^{-1} (see Discussion section). The value for k_{H+R}. was assigned values intermediate to those for k_{H+H} and k_{R+R}, but nearer to that for k_{H+H}. When relative values (to k_{R+R}) of 10.0 for k_{H+H} and 5.0 for k_{H+R} were used, the first-order formation plots were no longer linear, and all indications are that relative of 5.0 for k_{H+H} and 2.5 for k_{H+R} are reasonable. The value obtained for the rate constants for the reaction of hydrogen atoms with benzene and toluene did not change by more than 15 to 20% when the relative values of k_{H+H} and k_{H+R} were changed from 1.0 and 1.0 to 10.0 and 5.0, so the effect of these values on the result is small. Also, the results from experiments which were done with the smallest pulses, where the corrections for H + H and H + R would be at a minimum, are in agreement with values which were obtained from the higher intensity pulses.

(17) B. A. Thrush, *Progr. Reaction Kinetics*, **3**, 64 (1965).

(18) M. Anbar and P. Neta, *Intern. J. Appl. Radiation Isotopes*, **16**, 227 (1965).

Table I: Summary of Rate Constants Obtained for Reactions of Hydrogen Atoms

Reaction of H with	Conditions	$k \times 10^{-8}$, M^{-1} sec^{-1}
	Gas Phase	
Benzene	0.9 atm of Ar, 0.12 atm of H_2, 0.13 atm of benzene	0.31 ± 0.05
Benzene	6 atm of Ar, 0.8 atm of H_2, 0.09 atm of benzene	0.36 ± 0.05
Benzene	54 atm of Ar, 7 atm of H_2, 0.09 atm of benzene	0.43 ± 0.05
Toluene	11 atm of Ar, 0.8 atm of H_2, 0.03 atm of toluene	0.94 ± 0.1
Toluene	54 atm of Ar, 7 atm of H_2, 0.03 atm of toluene	1.1 ± 0.1
Toluene–methyl-d_3	11 atm of Ar, 0.8 atm of H_2, 0.03 atm of toluene	0.94 ± 0.2
		Av values over a number of runs
	Aqueous Solution: pH 3	
Benzene	2.5×10^{-2} M CH_3OH, 7.9×10^{-5} M benzene	13 ± 2^a
Benzene	2×10^{-2} M CD_3OD, 6.1×10^{-5} M benzene	10 ± 1^a
Toluene	2.5×10^{-2} M CH_3OH, 2.9×10^{-5} M toluene	39 ± 6^a
Toluene	2×10^{-2} M CD_3OD, 3.3×10^{-5} M toluene	18 ± 2^a

[a] Corrected for reaction of hydrogen atoms with methanol (see text).

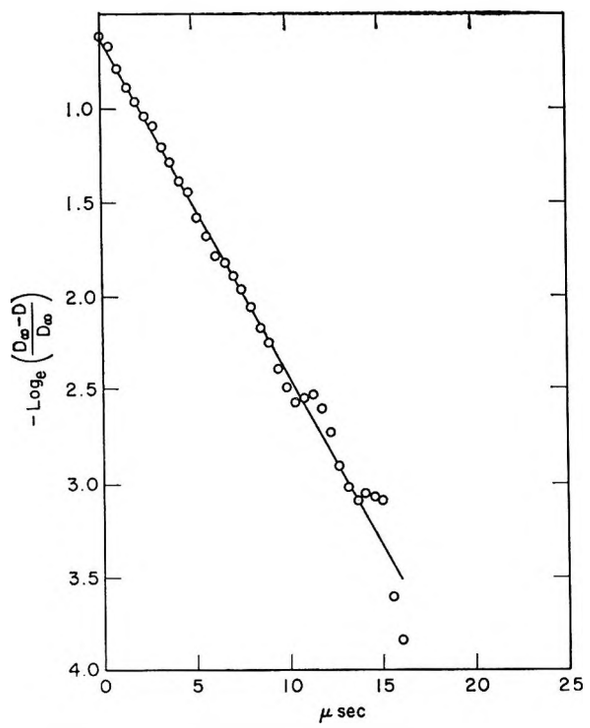

Figure 6. First-order plot of approach to plateau (D_∞) of corrected curve in Figure 5.

Some experimental results are not included in Table I because low values of the rate constants were found, evidently because of absorption of benzene or toluene by the small amount of grease on the O-rings (the results in the table are from samples where the O-rings had no grease). Even though the rate constants were on the average about 30% lower for these samples, several qualitative aspects of these results should be noted.

First, the rate constant was not dependent on benzene or toluene concentration, within about ±20%. Second, when no argon was used, but instead the hydrogen pressure was 50 to 100 atm, the rate constants were the same as those for the argon-containing samples, again within about 20%. Third, the use completely of deuterated benzene had no effect on the rate constant within an experimental error of about 15%. The latter indicates that abstraction from the benzene is not important. This is in agreement with the negligible amount of biphenyl found in the product spectrum, which will be described later.

In the case of toluene, use of toluene–methyl-d_3 (Table I) had no effect on the rate constant within an experimental error of 10 to 15%. Hence, deuteration of the methyl causes, at most, a 15% decrease in the rate constant. If abstraction from the methyl group were important in the case of ordinary toluene, deuteration of the methyl should, because of the large kinetic isotope effect expected, eliminate most of the abstraction, and therefore lower the observed rate constant by a percentage nearly as large as the percentage of the hydrogen atoms which abstract from the methyl group in the reaction with ordinary toluene. Therefore, the ratio of abstraction to addition in the case of ordinary toluene is no greater than 1:6. This is in agreement with the relative unimportance of bibenzyl in the product spectrum, which will be described later.

The ratio of H atom abstraction to addition was examined also in another manner. Both ethylene and toluene were used to scavenge atomic hydrogen in the Co^{60} radiolysis of ethane. It is known that in the radiolysis of pure ethane at very low conversion, 64% of the hydrogen yield results from atomic hydrogen abstracting hydrogen from the ethane.[19,20] (That these hydrogen atoms behave "properly" has been shown by Yang,[21] who has used the radiolysis of propane as a source of hydrogen atoms to measure relative rate constants, which appear to be very reasonable when compared with other work.) Therefore, we added about 2 mole % ethylene to ethane and measured the hydrogen yield. This concentration of ethylene should scavenge about 99.8% of the atomic hydrogen. Under the same conditions, the hydrogen yields from ethane samples containing about 2 mole % toluene were determined. About 99.7% of the atomic hydrogen should react with the toluene, but the hydrogen yield will be higher than in the case of the ethylene scavenger if abstraction occurs in the reaction of H with toluene. The results of these experiments are shown in Table II. The hydrogen production actually seems to be about 6% lower

Table II: H_2 Production in the Co^{60} Radiolysis of Ethane Scavenged by Ethylene and Toluene

Mole % scavenger	$10^5 \times$ ratio of H_2 produced to C_2H_6[a]
2.0, ethylene	2.06
2.1, ethylene	1.96
1.7, toluene	1.90
1.9, toluene	1.85

[a] All samples contained about 5×10^{-3} mole of ethane at a pressure of about 1 atm.

when toluene is the scavenger; however, this could be due to experimental error. A consideration of possible experimental errors indicates that the hydrogen production when toluene is the scavenger could not be more than about 6% greater than when ethylene is the scavenger, so an upper limit for the ratio, R, of abstraction to addition in the reaction of H with toluene is given by

$$R = \frac{Y_T - Y_E}{\frac{A}{M}(Y_E)}$$

where Y_T and Y_E are the relative yields of hydrogen with toluene and ethylene scavengers, respectively, and A/M is the ratio of atomic to molecular hydrogen in the radiolysis of pure ethane (*i.e.*, 64:36). This yields an upper limit of about 3% for R.

In the case of the experiments performed on aqueous solutions, the same methods were used to extract the rate constants for the reactions of hydrogen atoms with benzene and toluene from the experimental curves. (See footnote 16.) The rate constants obtained are shown in Table I. The values obtained using deuterated methanol involve a smaller correction for H + methanol, and are therefore more reliable, as has been pointed out in the Experimental Section. The average results may be stated as $k(H + C_6H_6) = 1.1 \pm 0.1 \times 10^9$ and $k(H + C_6H_5CH_3) = 2.6 \pm 0.8 \times 10^9$, in units of M^{-1} sec^{-1}.

Temperature Dependence of the Reaction of Hydrogen Atoms with Benzene. The temperature dependence of the rate constant of the gas-phase reaction of hydrogen atoms with benzene was investigated by determining the rate constant at 27 and 84°. These experiments yielded the result that the rate constant was 2.4 ± 0.4 times greater at the higher temperature. This leads to the Arhennius expression

$$k = 10^{9.9} \times 10^{\left(\frac{-3.3 \pm 0.6}{4.58 \times 10^{-3}T}\right)} M^{-1} \text{ sec}^{-1}$$

where the error limits have arbitrarily been put in the activation energy term. The actual barrier for the reaction is 2.9 ± 0.6 kcal/mole (instead of 3.3) if one considers the theoretical $T^{1/2}$ dependence of the preexponential factor. This gives the alternate expression

$$k = 10^{8.3}T^{1/2} \times 10^{\left(\frac{-2.9 \pm 0.6}{4.58 \times 10^{-3}T}\right)}$$

A similar increase in rate constant in going from 25 to 100° was observed in the case of toluene, but a quantitative study was not carried out.

Decay of Transients. Figure 7 shows an oscilloscope trace, taken at a slower sweep-rate at 302 mμ, of the transient from hydrogen atoms reacting with benzene in the gaseous phase. Similar curves were obtained in the case of toluene and in the aqueous solution experiments. When these decay curves for the gas-phase samples are plotted to test for first- and second-order decay, much better linearity is obtained in the case of the second-order test (reciprocal of optical density *vs.* time). Often, good linearity is obtained over a decrease in optical density by a factor of 6, as is shown in Figure

(19) R. A. Back, *J. Phys. Chem.*, **64**, 124 (1960).

(20) K. Yang and P. L. Gant, *ibid.*, **65**, 1861 (1961).

(21) (a) K. Yang, *J. Am. Chem. Soc.*, **84**, 3795 (1962); (b) *ibid.*, **84**, 719 (1962).

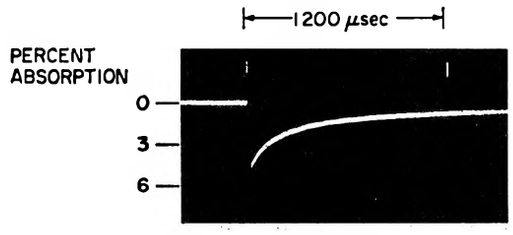

Figure 7. Decay of cyclohexadienyl radical, gas phase; $\lambda = 302$ mμ.

8, which is the second-order plot corresponding to Figure 8. This indicates that the transient decays by bimolecular radical–radical reaction.

However, the situation with respect to the decay of the transient is not completely understood, because the second-order plots show two anomalous characteristics. First, as the pulse intensity is increased, the second-order plots eventually become nonlinear, with the slope decreasing with time. Second, the slope (or initial slope where the plot shows curvature) is greater the smaller the pulse intensity. These effects will be considered further in the Discussion section. The slopes of the second-order plots (determined at the wavelength of maximum absorption) fall mainly in the range of 1.5 to 3.5 $\times$ 10^5 sec^{-1} in the cases of both benzene and toluene.

In the gas-phase experiments, we have determined that the energy absorbed from the electron beam decreases by a factor of between $^1/_4$ to $^1/_3$ from the front to the back of the cell. The question of whether the resulting nonuniformity of transient concentration causes a significant error in the determination of the slope of the second-order plots has been dealt with elsewhere.[22] Under the conditions of nonhomogeneity stated above, the slopes should be no more than about 5% too high, if the curves are analyzed over 2 to 3 half-lives.[22] This error is obviously small compared with other errors, and no attempt has been made to correct for it.

In the liquid-phase experiments, the slopes of second-order plots of the absorptions due to the cyclohexadienyl and methylcyclohexadienyl radicals show less variation, and for both benzene and toluene the slope is (1.7 $\pm$ 0.3) $\times$ 10^5 sec^{-1}, at the wavelength of maximum absorption. The decay of the methanol radical (determined in the absence of benzene or toluene) was complex and second-order plots were nonlinear, reflecting the probable formation of an absorbing product. At 2900 A, the initial slope of the second-order plot was 1.4 $\times$ 10^5 sec^{-1}.

Product Analysis. The products formed during the pulsed radiolysis of the gas-phase benzene and toluene

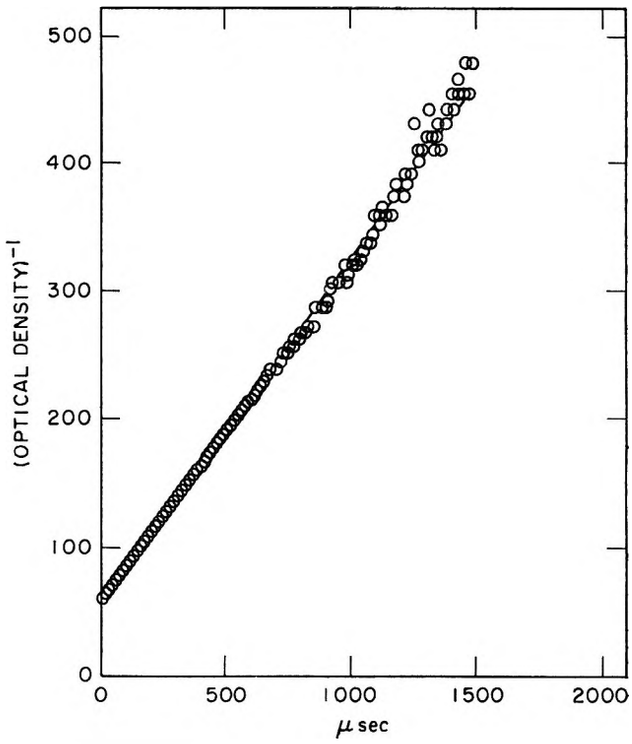

Figure 8. Second-order plot of Figure 7.

systems were examined by giving the system a sufficient number of pulses so that the sum of the maximum transient optical densities was about unity. The contents of the irradiation vessel were then analyzed as has been described in the Experimental Section.

In the case of the products resulting from the reaction of hydrogen atoms with benzene, the dimer products and the cyclohexadiene were determined. The results of the gas chromatographic analyses showed three partially separated peaks slightly before the expected position of biphenyl (which was determined by running a separate "authentic" sample of biphenyl). These three peaks are apparently due to isomers of bicyclohexadienyl formed when two cyclohexadienyl radicals combine. About one-half as much 1,4-cyclohexadiene was found, indicating that two cyclohexadienyl radicals disproportionate about one-half as often as they combine. (The reaction of hydrogen atoms with the cyclohexadienyl radical may contribute slightly to the formation of cyclohexadiene, but under the conditions of these experiments, hydrogen atoms react mainly with benzene.) The relative unimportance of 1,3-cyclohexadiene is interesting, there being less than 25% as much of the 1,3 isomer as the 1,4 iso-

(22) M. C. Sauer, Jr., Argonne National Laboratory Report, ANL-7327, May 1967.

mer. These results are similar to those found in another study on the cyclohexadienyl radical,[23] and the predominance of 1,4-cyclohexadiene is in agreement with the principle of least motion[24] applied to the cyclohexadienyl radical. Also, the formation of 1,4-cyclohexadiene predominates in the radiolysis of liquid benzene.[25]

In the case of toluene, only the analysis for the dimers was successful. Again, several partially separated peaks were observed, which came mainly before the position of bibenzyl. Bibenzyl was less than 25% of the total dimer.

The results described above apply to samples in which molecular hydrogen was present in amounts large compared to benzene or toluene. In experiments where no hydrogen was present, *i.e.*, argon was present at high pressure and benzene or toluene near the vapor pressure at room temperature, the biphenyl accounted for 80 to 90% of the dimer in the case of benzene, and the bibenzyl accounted for more than 50% of the dimer in the case of toluene. Even though the optical density due to transient formation was only 30–50% of that formed when hydrogen was present, the total amount of dimer formed was approximately the same.

Optical Absorption Coefficients. The results of the product analyses can be used to obtain approximate values for the absorption coefficients of the transient radicals from the relationship

$$D_{\text{total}} = \epsilon c l$$

where D_{total} is the sum of the maximum optical densities produced in the individual pulses, ϵ is the absorption coefficient of the transient, c is the sum of the maximum transient concentrations produced in the individual pulses, and l is the optical path length. The value of c is estimated from the chromatographic analyses of the products. The result of these considerations is that for the transients produced from both benzene and toluene, $\epsilon = 10^{4.18 \pm 0.40}\ M^{-1}\ \text{cm}^{-1}$. The value for ϵ is more likely to be less than $10^{4.18}$ because errors made in the analyses are likely to be due mainly to incomplete recovery of products and possibly to appearance of the absorbing radical in minor products not determined in the analyses or not included in the list of products believed to result from the radical in question.

The absorption coefficient of the cyclohexadienyl radical in aqueous solution was determined on the basis of $G(e_{sol}^-) + G(H) = 3.1$. Dosimetry on the electron beam was done under exactly the same conditions as the observation of the cyclohexadienyl radical, using a 10^{-3} M KI solution, and observing the I_2^- at 385 mμ, where the absorption coefficient[26] is $1.4 \times 10^4\ M^{-1}\ \text{cm}^{-1}$ and $G(I_2^-) = G(OH) = 2.4$. The pulse intensity was thereby determined to be 4.7×10^{18} ev $l.^{-1}$, and the resulting value for the absorption coefficient of the cyclohexadienyl radical at 311 mμ is $(5.4 \pm 0.5) \times 10^3\ M^{-1}\ \text{cm}^{-1}$. (This value includes an estimated correction of 18% due to hydrogen atoms which do not add to benzene, and cyclohexadienyl radicals which disappear before observation at the maximum optical density.) The observation of the cyclohexadienyl radical was carried out in solutions containing CD_3OD (see section on aqueous solutions). The value of ϵ for the $\cdot CH_2OH$ radical is estimated to be about $25\ M^{-1}\ \text{cm}^{-1}$ at 311 mμ, on the basis of experiments where benzene was not present.

In view of the facts that the determination of the absorption coefficient in the liquid phase is more straightforward and the shapes of the gas-phase and aqueous absorption spectra are similar, the value obtained for the liquid phase probably indicates that the gas-phase value of $1.5 \times 10^4\ M^{-1}\ \text{cm}^{-1}$ is too high, due to discrepancies in the product analyses, as has been discussed.

Discussion

Evidence That the Observed Transients Are Due to Reaction of a Pulse of Thermal Hydrogen Atoms with the Aromatic Compound. In order to obtain from these experiments, in a straightforward manner, meaningful rate constants for reactions of atomic hydrogen, the production of hydrogen atoms by the electron pulse must be complete before their reaction with the aromatic compound has proceeded to a significant extent, and the hydrogen atoms must be essentially thermalized before reacting. Also, the observed transients must not be produced in other reactions occurring simultaneously with the reaction of hydrogen atoms with the aromatic compound. Evidence that these conditions prevail is given by the following considerations.

Experimentally, evidence for the above is provided by the fact that wide variations in experimental conditions of the gas-phase experiments, such as pressures of various components and pulse intensity, produced no effect on the value derived for the rate constants of the reaction of hydrogen atoms with benzene and toluene.

Hydrogen atoms are probably formed mainly by ion–molecule reactions and neutralization reactions such as the following.

(23) D. G. L. James and R. D. Suart, *Chem. Commun.*, **14**, 484 (1966).

(24) J. Hine, *J. Org. Chem.*, **31**, 1236 (1966); summarized in *Chem. Eng. News*, **44**, No. 16, 57 (1966).

(25) M. K. Eberhardt, *J. Phys. Chem.*, **67**, 2856 (1963).

(26) J. K. Thomas, *Trans. Faraday Soc.*, **61**, 702 (1965).

$$Ar^+ + H_2 \longrightarrow ArH^+ + H$$
$$ArH^+ + e^- \longrightarrow Ar + H$$

or, when argon is not present, by the processes

$$H_2^+ + H_2 \longrightarrow H_3^+ + H$$
$$H_3^+ + e^- \longrightarrow H_2 + H$$

The ion–molecule reactions are very fast, and would proceed almost simultaneously with the electron pulse; neutralization would also be rapid[4] due to the high intensity in the pulse-radiolysis experiments.

If production of hydrogen atoms after the pulse were occurring by neutralization processes, an effect of pulse intensity would be expected, which was not observed. If long-lived excited states were responsible for production of hydrogen atoms (or the observed transient) after the pulse, one might expect changes in the measured rate constant with sample composition. No such changes were observed; in fact, the same rate constant was obtained when argon was not used, but hydrogen was the main gas.

The possible importance of hot hydrogen atoms has also been considered. If hydrogen atoms are formed with excess kinetic energy, they may react with the aromatic before they become thermalized by collisions. However, one can show, using standard equations for transfer of kinetic energy, that the probability of a hydrogen atom reacting with the aromatic before it has become thermalized is small, and furthermore, any hydrogen atoms which do react while hot have to do so in a time considerably shorter than the observed half-time for transient formation. This is because of the fact that a large number of collisions of a hydrogen atom with argon occur before a collision with benzene, due to the large argon pressure used. Even in experiments where the argon pressure was only 1 atm, the formation rate constant was the same.

The importance of electronically excited hydrogen atoms can be ruled out on the basis of lifetimes given by Bethe and Salpeter.[27]

In summary, the above considerations lead to the conclusion that the observed transients result from the reaction with the aromatic of a pulse of thermal hydrogen atoms which essentially coincides in time with the electron pulse.

The parallel results from the aqueous solutions are consistent with hydrogen atom reactions since other reactive intermediates, e_{sol}^- and OH, were removed by suitable scavengers. There is a small probability that part of the observed spectrum is the result of the addition of methanol radicals, $\cdot CH_2OH$, to the benzene ring. However, in view of the simplicity of the kinetic curves and the likelihood that the $\cdot CH_2OH$ radical will add slowly[28,29] to the benzene ring in comparison with hydrogen atom addition, it is felt that such a complication is unlikely.

Identification of the Transients. In the case of samples where hydrogen was present as a source of hydrogen atoms, the results of the product analyses show that in the case of benzene, the dimer was definitely not biphenyl. Therefore, abstraction of hydrogen from benzene is not an important process. The lack of an isotope effect on the formation rate constant when deuterated benzene was used also argues strongly against abstraction as do the negative results from experiments in which we looked for phenyl absorption in the 5000-A region.[30] Since the dimer products appear to have resulted from combination of cyclohexadienyl radicals, and 1,4-cyclohexadiene is an important product, probably formed by disproportionation of two cyclohexadienyl radicals, the proposal that the observed transient results from addition of hydrogen atoms to benzene seems eminently reasonable. The spectrum obtained here is similar to that reported for the cyclohexadienyl radical trapped in an organic glass at low temperature.[31] A similar spectrum was found for the radical formed when hydroxyl radicals add to benzene.[9]

In the case of toluene (with H_2 present in excess of the toluene), abstraction of hydrogen from the methyl group, forming the benzyl radical, is apparently not important. In the section on rate constants it is concluded that the ratio of addition to abstraction is apparently at least 6:1, on the basis of a lack of a deuterium isotope effect, and greater than 30:1 on the basis of the relative scavenging efficiencies to toluene and ethylene in the γ radiolysis of ethane. The unimportance of bibenzyl in the product spectrum also supports this conclusion.

Although the evidence favors the hypothesis that the observed transients result from addition of the hydrogen atom to the aromatic compound, the possibility has been considered that the transient actually results from the further addition of the cyclohexadienyl radical to

(27) H. A. Bethe and E. E. Salpeter, "Quantum Mechanics of One- and Two-Electron Atoms," Academic Press Inc., New York, N. Y., 1957, p 266.

(28) The rate constant for addition of $\cdot CH_2OH$ to benzene would probably be approximately the same order of magnitude as that for methyl radical, which is very slow, judging from the value of about 10 M^{-1} sec^{-1} at 25° for the gas-phase addition of methyl radicals to the toluene ring.[29]

(29) M. Cher, C. S. Hollingsworth, and F. Sicilio, *J. Phys. Chem.*, **70**, 877 (1966).

(30) G. Porter and B. Ward, *Proc. Roy. Soc.* (London), **A287**, 457 (1965).

(31) W. H. Hamill, J. P. Guarino, M. R. Ronayne, and J. A. Ward, *Discussions Faraday Soc.*, **36**, 169 (1963).

another benzene molecule. The latter hypothesis apparently is not, however, supported by the product spectrum; furthermore, the rate constant for addition of phenyl-type radicals to aromatic rings in liquid aromatic hydrocarbons has been estimated[32] as being about $5 \times 10^4\ M^{-1}\ \text{sec}^{-1}$. This is about three orders of magnitude smaller than necessary to explain the results observed here.

As has been described in the sections on transient spectra and product analysis, transient spectra with peaks at 302 and 340 mμ[33] in the case of benzene were observed in samples from which hydrogen was omitted, but with only 30–50% the intensity of absorption at 302 mμ, compared to samples where hydrogen was present. However, the amount of dimer products formed was approximately the same in both cases. The nature of the dimers is quite different in the absence of hydrogen, and indicates that the phenyl radical and the benzyl radicals are the important species in the case of samples containing benzene and toluene, respectively. The similarity of the absorption spectra in the presence and absence of hydrogen must mean either that the phenyl and benzyl radicals have similar absorption spectra to the cyclohexadienyl and methylcyclohexadienyl radicals, respectively, or the cyclohexadienyl radical is responsible for the absorption, but mainly reacts with the larger amount of phenyl radical to lose a hydrogen atom, forming two benzene molecules. The absorption maximum for the benzyl radical is in the same region,[34] but a phenyl radical absorption in the 300-mμ region is not known.[30] Since one expects that some hydrogen atoms will be produced from the aromatic in the absence of hydrogen gas, the absorption spectra in the absence of hydrogen seem likely to be due to the cyclohexadienyl type radicals, with possibly some contribution from phenyl and benzyl radicals.

Even though the transient absorption spectra in the presence and absence of hydrogen are similar, the observed transient curves are different, and the dimer products of the reaction are different. In addition, the formation rate constants are invariant with changes in the ratios of Ar or H_2 to the aromatic when hydrogen is present in excess of the aromatic compound, indicating that the formation mechanism is not influenced by absorption of energy by the aromatic. Hence, it seems reasonable that the mechanisms for observed transient formation are different in the two cases, and that little transient formation occurs by direct absorption of energy by the aromatic or transfer of energy from Ar or H_2 to the aromatic when hydrogen is present.

Rate Constants. The rate constants for the reactions of hydrogen atoms with benzene and toluene determined here should be reliable, as they are measured in a rather direct method from the transient curves (*e.g.*, Figures 3 and 4), and in principle, are determined from a simple first-order plot of the approach to a plateau. In contrast to the case of the decay of the transient, the absorption coefficient of the transient need not be known to obtain the rate constant. The rate constants obtained represent the sum of all reactions for the hydrogen atom with the aromatic. In the case of benzene, the reaction is completely addition to form the cyclohexadienyl radical, but in the case of toluene, the rate constant may include a small contribution of abstraction from the methyl group.

The value obtained for the room temperature rate constant of the gas-phase reaction of hydrogen atoms with benzene is about midway between the values obtained by Allen, *et al.*,[35] and Yang.[21a] The former value is $1.1 \times 10^8\ M^{-1}\ \text{sec}^{-1}$, and while it is an absolute rate constant, there is some doubt as to the quantitative accuracy of the experimental method.[36] The latter is $0.1 \times 10^8\ M^{-1}\ \text{sec}^{-1}$ measured relative to the abstraction of hydrogen from propane. Yang[21a] measured the temperature dependence of the reaction and obtained

$$k = 10^{8.6} T^{1/2} \times 10\left(\frac{-3.5}{4.58 \times 10^{-3} T}\right)$$

which is in satisfactory agreement with the expression obtained in this work. The value obtained here indicates that hydrogen atoms react with benzene at room temperature about once every 2×10^4 collisions.

Another determination, by a discharge-flow method, of the rate constant for the reaction of hydrogen atoms with benzene[37] yields the value $2.9 \times 10^9\ M^{-1}\ \text{sec}^{-1}$, at 298°K, which is almost 2 orders of magnitude higher than that determined in this work. The reason for this discrepancy is not apparent, although in the work

(32) A. MacLachlan and R. L. McCarthy, *J. Am. Chem. Soc.*, **84**, 2519 (1962).

(33) The identity of the short-lived species (see section on transient spectra) absorbing at 330–340 mμ is a matter of conjecture. It is formed during the pulse after which the absorption decays in an almost first-order fashion with a half-life of about 2 μsec. Such reactivity is unlikely to be associated with a neutral radical and is more characteristic of an ion or an excited state. Such possibilities as $C_6H_6^-$, $C_6H_6^+$, and transitions between excited states of benzene are ruled out on the basis of their known spectra. It is possible that the transient is a charged phenyl species $C_6H_5^{\pm}$, but in view of the sparse evidence, this assignment must remain in the realm of speculation.

(34) G. Porter and B. Ward, *J. Chim. Phys.*, 1517 (1964).

(35) P. E. M. Allen, H. W. Melville, and J. C. Robb, *Proc. Roy. Soc.* (London), **A218**, 311 (1953).

(36) R. J. Cvetanovic, *Advan. Photochem.*, **1**, 115 (1963); (see p 162).

(37) H. Girouard, F. M. Graber, and B. F. Meyers, NASA Accession No. N64-13061, Report No. NASA-CR-52376, AE-63-0078; 93 pp (1963).

mentioned,[37] benzene was only one of many compounds studied, and was not studied extensively.

Allen, *et al.*,[35] also measured the rate constant of the reaction of hydrogen atoms with toluene, and obtained a value of $0.24 \times 10^8\ M^{-1}\ \text{sec}^{-1}$, which is only about one-fourth as high as the value obtained here.

The values obtained in this work for the rate constants of the reactions of hydrogen atoms with benzene and toluene in aqueous solution are about 30 times greater than the corresponding values in the gas phase. A similar ratio has been obtained in the case of the reaction of hydrogen atoms with ethylene in the gas phase[38,39] as compared with aqueous solution.[40] Also, some reactions of methyl radicals seem to show a similar (but generally smaller) ratio.[41] This increase in rate constant in going to the liquid phase is contrary to most of the previous evidence,[5] but for a nondiffusion controlled bimolecular reaction, such an increase in the liquid-phase rate constant has been predicted.[42]

In order to estimate the gas-phase rate constant for the reaction between two cyclohexadienyl (or methylcyclohexadienyl) radicals, the absorption coefficient was measured by determining the amounts of products formed for a given optical density of transient. The experimental decay curves when plotted as a reciprocal of optical density *vs.* time yield a slope which is related to the rate constant by $k = \epsilon l/2 \times (\text{slope})$, where ϵ is the absorption coefficient and l is the optical path length through the sample.

Only an approximate value of k can be obtained here because of two experimental difficulties. First, the slopes of the second-order plots increase somewhat with smaller initial optical density. This would seemingly be explainable on the basis of a concurrent first-order disappearance of the transient, but the fact that the second-order plots show excellent linearity for the lowest initial optical densities argues against this. Other experimental variations, when added to this effect, make the total uncertainty in the second-order slope large, *i.e.*, $(2.5 \pm 1.0) \times 10^5\ \text{sec}^{-1}$. However, the second experimental difficulty introduces even more uncertainty in the value of ϵ. That is, the product analysis was not very reproducible, and the identification of products was not complete. Hence, the value of ϵ obtained is $10^{4.18 \pm 0.40}\ M^{-1}\ \text{cm}^{-1}$. (The lower end of the range is probably more likely, because products are more likely to be incompletely recovered, and this leads to a high value of ϵ.) Using these values of the second-order slope and ϵ, and assuming that the cyclohexadienyl radicals decay only by reactions with themselves, we obtain $k = 5 \times 10^{10}\ M^{-1}\ \text{sec}^{-1}$. This value of k seems rather large, because it indicates that reaction proceeds nearly on every collision ($k = 10^{11}\ M^{-1}\ \text{sec}^{-1}$, from simple collision theory if the diameter of the cyclohexadienyl radical is 5 A). If the value of ϵ determined for the gas phase is too high, and the $5.4 \times 10^3\ M^{-1}\ \text{sec}^{-1}$ value obtained in the liquid phase is more nearly correct, $k = 1.6 \times 10^{10}\ M^{-1}\ \text{sec}^{-1}$. The important point to note is that the rate constant for reaction between two cyclohexadienyl radicals is large, and at least 0.1 times the collision frequency. This indicates, therefore, that similar to the case of alkyl radicals,[43] the activated complex for the reaction is "loose." This is in contrast to the case of the alkyl + allyl reaction where the rate constant is about 5×10^{-3} times the collision frequency and the activated complex is "tight."[44]

In the case of the aqueous solution results, the rate constant for reaction between two cyclohexadienyl radicals can also be estimated, using the second-order slope of $(1.7 \pm 0.3) \times 10^5\ \text{sec}^{-1}$ and $\epsilon = 5.4 \times 10^3\ M^{-1}\ \text{cm}^{-1}$. A correction for the reactions of the $\cdot CH_2OH$ radical with the cyclohexadienyl radical must be made since these radicals are present at a concentration nearly the same as the cyclohexadienyl radical due to reaction of hydroxyl radicals with the methanol. As a reasonable approximation, the rate constants for reactions among these radicals can be assumed to be the same, except that the statistical factor of 2 has to be applied to the reaction between $\cdot CH_2OH$ and the cyclohexadienyl radical. The result of this assumption is an additional factor of one-half in the relation between the second-order slope and the desired rate constant. Thus, $k = \epsilon l/4 \times (\text{slope})$. Since $l = 8$ cm, $k = 1.8 \times 10^9\ M^{-1}\ \text{cm}^{-1}$. The result justifies the approximation, since the rate constant for the combination of two $\cdot CH_2OH$ radicals is probably not much different from the value for the $\cdot CH_2CH_2OH$ radical[45] of 1.4×10^9. Thus, the liquid-phase rate constant appears to be approximately an order of magnitude smaller than the gas phase value. This is in the opposite direction compared to the case of the addition of hydrogen atoms to benzene or toluene, where the rate constant is about 30 times

(38) J. M. Brown, P. B. Coates, and B. A. Thrush, *Chem. Commun.*, 22, 843 (1966).

(39) J. V. Michael and R. E. Weston, Jr., *J. Chem. Phys.*, 45, 3632 (1966).

(40) J. K. Thomas, Proceedings of the Third International Congress on Radiation Research, Cortina, Italy, 1966.

(41) J. K. Thomas, private communication.

(42) S. W. Benson, "The Foundations of Chemical Kinetics," McGraw-Hill Book Co., Inc., New York, N. Y., 1960, pp 504–507.

(43) J. A. Kerr and A. F. Trotman-Dickenson, *Progr. Reaction Kinetics*, 1, 105 (1961).

(44) F. H. Doer and B. S. Rabinovitch, *J. Phys. Chem.*, 69, 1952 (1965).

(45) I. A. Taub and L. M. Dorfman, *J. Am. Chem. Soc.*, 84, 4053 (1962).

greater in the liquid phase. This difference is related to the diffusion-controlled nature of the radical–radical reactions in the liquid phase.

Future Work. The techniques described here are being applied in the extension of this work to a series of substituted benzenes, in which similar reactions and transients are found. For example, the gas-phase reaction of hydrogen atoms with chlorobenzene has a rate constant of about $4 \times 10^8\ M^{-1}\ \text{sec}^{-1}$ and the resulting transient absorbs in the same region as in the case of benzene or toluene. This result, indicating that chlorobenzene is more reactive toward hydrogen atoms than benzene or toluene, is of some interest since it conflicts (although the fact that toluene is more reactive than benzene does not conflict) with the idea that the hydrogen atom is an electrophilic reagent.[46] The work on other substituted benzenes should enable this hypothesis to be fairly tested as well as providing data amenable to a theoretical treatment. Similarly, rate constants and transient spectra are being determined for the reactions of oxygen atoms with aromatic compounds.

Acknowledgments. We wish to thank B. E. Clifft, B. J. Naderer, and E. Backstrom for operating the Linac, D. G. Truhlar for his contributions and participation in the early part of this work, C. Connally for his contributions to various aspects of the work, especially for performing the scavenger experiments on the γ radiolysis of ethane, and D. Meyerstein for discussions and suggestions concerning this work.

(46) M. Anbar, D. Meyerstein, and P. Neta, *Nature*, **209**, 1348 (1966).

Photolysis of Ketene in the Presence of Carbon Monoxide

by B. A. DeGraff and G. B. Kistiakowsky

Department of Chemistry, Harvard University, Cambridge, Massachusetts 02138 *(Received May 22, 1967)*

The reaction of photochemically generated singlet and triplet methylene with carbon monoxide to form ketene has been studied at several wavelengths. It is found that triplet methylene reacts more readily with carbon monoxide than with ketene or butene, whereas the reverse is true for singlet methylene. The relative rates for the reactions

$$^1CH_2 + CH_2CO \longrightarrow \text{products} \qquad k_1$$
$$^1CH_2 + CO \longrightarrow CH_2CO \qquad k_2$$
$$^3CH_2 + CH_2CO \longrightarrow \text{products} \qquad k_3$$
$$^3CH_2 + CO \longrightarrow CH_2CO \qquad k_4$$
$$^1CH_2 + M \longrightarrow {}^3CH_2 + M \qquad k_5$$

are presented. The ratio k_4/k_3 for the triplet is 3.6 at 3160 A and might be somewhat wavelength dependent. The ratio k_2/k_1 for the singlet is 0.14 ± 0.02 over the wavelength region 2900–3340 A. The ratio k_5/k_1 is approximately 0.01 when M is nitrogen and/or carbon monoxide. When methylene reacts with *trans*-butene, the ratio of rates for the singlet is substantially the same as with ketene (0.10 ± 0.02), but the corresponding ratio for the triplet is somewhat lower (1.3 ± 0.3). Using the reaction with carbon monoxide as the diagnostic, the percentages of singlet methylene were found to be 67% at 2900 A, 59% at 3160 A, 39% at 3340 A, and much less than 40% at 3660 A.

Introduction

Since Herzberg and Shoosmith showed that methylene exists in two long-lived electronic states of different multiplicity,[1] there has been considerable interest in the relative abundance of these spin states produced by the common sources of methylene (*e.g.*, ketene, diazomethane, and diazirine). The relative population of singlet and triplet states is important in understanding the extensively studied reactions of methylene with hydrocarbons and is relevant to the problem of spin inversion leading to the formation of triplet methylene from its precursors.[2] It appears that each form is capable of distinct reactions, and hence quantitative interpretation of reaction mechanisms is difficult without fairly accurate estimates of the initial amounts of singlet and triplet methylene formed from the precursor. As the singlet can "relax" to the triplet state, an additional complication is introduced in inferring initial populations by estimating the relative amounts of methylene that ultimately react as singlet or triplet.[3]

Several workers have made estimates as to the singlet and triplet yields in the photolysis of ketene at various wavelengths.[4] The technique used was to allow methylene to react with a substituted olefin and follow the product distribution as a function of various experimental parameters. Using the Doering–Skell hypothesis,[5] mechanistic arguments can be made that certain products arise only from reactions of triplet

(1) (a) G. Herzberg and J. Shoosmith, *Nature*, **183**, 1801 (1959); (b) G. Herzberg, *Proc. Roy. Soc.* (London), **A262**, 291 (1961).

(2) (a) For recent reviews see J. A. Bell, *Progr. Phys. Org. Chem.*, **2**, 1 (1964); (b) W. B. DeMore and S. W. Benson, *Advan. Photochem.*, **2**, 219 (1964); (c) H. M. Frey, *Progr. Reaction Kinetics*, **2**, 131 (1964); see also (d) J. W. Simons and B. S. Rabinovitch, *J. Phys. Chem.*, **68**, 1322 (1964).

(3) (a) H. M. Frey, *J. Am. Chem. Soc.*, **82**, 5947 (1960); (b) R. F. W. Bader and J. I. Generosa, *Can. J. Chem.*, **43**, 1631 (1965).

(4) (a) S. Ho, I. Unger, and W. A. Noyes, Jr., *J. Am. Chem. Soc.*, **87**, 2297 (1965); (b) R. W. Carr, Jr., and G. B. Kistiakowsky, *J. Phys. Chem.*, **70**, 118 (1966).

(5) P. S. Skell and R. C. Woodworth, *J. Am. Chem. Soc.*, **78**, 4496 (1956); **81**, 3383 (1959).

Table I: Effect of Added Carbon Monoxide in Ketene–*trans*-Butene-2 Mixtures on the C_6 Product Yields at 3160 A

Pressures, mm				Normalized yields				
Ketene	Butene	Other	[CO]/[butene]	TDMC[a]	CDMC[a]	*trans*-2-pentene	2-Methyl-butene-2	3-Methyl-butene-1
5.0	45.0		...	1.94	0.208	1.51	0.339	0.106
5.0	45.0	65.0 (CO)	1.45	1.49	0.074	1.29	0.288	0.038
5.0	45.0	125.0 (CO)	2.78	1.23	0.046	1.09	0.244	0.023
5.0	45.0	250.0 (CO)	5.55	1.11	0.020	1.02	0.228	0.011
5.0	45.0	338.0 (CO)	7.50	1.00	0.010	0.92	0.206	...
5.0	45.0	485.0 (CO)	10.8	0.84	0.00	0.78	0.177	...
5.0	45.0	10.0 (O_2)	...	1.63	0.020	1.48	0.314	...

[a] The letters TDMC and CDMC denote *trans*- and *cis*-dimethylcyclopropane, respectively.

methylene, while other products must have their origin in singlet reactions. Unfortunately, the product mixtures from such studies are rather complex. Thus, while there seems to be general agreement on the trends, there are differences on the quantitative aspects.

Earlier, it had been shown that methylene reacts with carbon monoxide to re-form ketene.[6] It seemed worthwhile to reinvestigate the photolysis of the ketene–carbon monoxide system in the hope that like the isoelectronic species, O atoms, singlet methylene would be more reactive toward CO, and thus a direct measure of the rate of triplet production could be obtained.[7] The results of this study are described below.

Experimental Section

The photolysis apparatus consisted of a cylindrical, I-shaped quartz cell connected in series with a magnetically operated mixing pump and trap, and through a bakable metal valve to a high-vacuum line. The cell and related accessories were enclosed in a thermostat whose temperature could be controlled to ±0.5°. The cell pressure was measured by means of a Wallace and Tiernan 0–50-torr differential gauge in conjunction with a standard mercury manometer. The optical train was composed of an Osram HBO-500 high-pressure mercury arc whose output was isolated into various bands centered at 3660, 3340, 3160, and 2900 A by means of a Bausch and Lomb high-intensity monochromator. The band width was 64 A in each region. The emergent beam was passed through a Corning CS7-54 filter to remove scattered visible light, was collimated by a series of lenses and stops, was passed through the cell, and was focused on the cathode of an RCA 935 phototube. The signal from the phototube was displayed on a Moseley 680 recorder. The light fluxes for the various spectral regions were frequently measured using ferrioxalate actinometry as described by Hatchard and Parker with suitable reflection corrections.[8] Extinction coefficients were determined at each temperature and wavelength region using the described photometer.

The hydrocarbon products were analyzed using a Perkin-Elmer flame ionization detector mounted in a Model 154 vapor fractometer. Standard analyses were done with a 2-m silica gel column (30–60 mesh) operated at 70°. Products from the reaction of methylene with butene were analyzed using a 6-m column packed with 60–80 mesh firebrick coated with 33% by weight of dimethyl sulfolane, operated at room temperature. The carrier gas was helium at a flow rate of 60 cc/min in each case. The response of the detector was calibrated before each analysis by use of a known gas mixture which closely approximated in both size and composition the experimental sample.

In a typical experiment the cell was brought to the desired temperature and pressurized with condensable gases; then, after condensing these at liquid nitrogen temperature, the cell was pressurized with the noncondensable gases, and finally the condensed material was allowed to vaporize. The gases were then stirred for 1.5–2 hr. The completeness of mixing had previously been checked by following the absorption as a function of mixing time. After irradiation, the mixture was passed through a packed trap at solid nitrogen temperature. When an analysis for carbon monoxide was made, the noncondensable fraction was circulated over CuO at 220° and the resultant CO_2 was condensed and then measured in a calibrated gas buret. The hydrocarbon fraction was transferred to a sample bulb which contained a small amount of acetic anhydride to destroy the excess ketene. The sample was then

(6) T. Wilson and G. B. Kistiakowsky, *J. Am. Chem. Soc.*, **80**, 2934 (1958).

(7) (a) O. F. Raper and W. B. DeMore, *J. Chem. Phys.*, **40**, 1053 (1964); (b) R. Klein, *Trans. Faraday Soc.*, **62**, 3135 (1966); (c) M. Clerc and F. Barat, *J. Chem. Phys.*, **46**, 107 (1967).

(8) C. G. Hatchard and C. A. Parker, *Proc. Roy. Soc.* (London), **A235**, 518 (1956).

Table II: Quantum Yields of Ethylene, Ethane, and Acetylene from Ketene–Carbon Monoxide Mixtures at 50°

Pressures, mm				Quantum yields			
Ketene	CO	Other	[CO]/[ketene]	C_2H_4	C_2H_6	C_2H_2	Other
			Part 1. 3160 A				
25.0				0.90	0.015	...	2.0_2 (CO)
10.0		185.4 (N_2)		0.87	0.036	0.046	1.9_0 (CO)
10.0		323.4 (N_2)		0.83	0.044	0.044	1.8_0 (CO)
10.0	5.0	100.0 (N_2)	0.5	0.58	0.008	0.007	
10.0	10.6	94.4 (N_2)	1.1	0.49	0.003	0.005	
10.0	20.0	86.0 (N_2)	2.0	0.41	0.001	0.003	
10.0	50.0	50.0 (N_2)	5.0	0.33	tr[a]	0.002	
10.0	70.0	30.5 (N_2)	7.0	0.28	tr	tr	
10.0	107.5		10.8	0.22	tr	tr	
10.0	107.8		10.8	0.23	tr	tr	
10.0	2.6	211.3 (N_2)	0.26	0.63	0.006	0.012	
10.0	5.0	207.5 (N_2)	0.50	0.51	0.005	0.01_0	
10.0	10.6	182.6 (N_2)	1.0_6	0.46	0.002	0.007	
10.0	21.0	184.2 (N_2)	2.1	0.34	0.001	0.004	
10.0	20.8	184.5 (N_2)	2.1	0.35	0.001	0.003	
10.0	54.0	158.6 (N_2)	5.4	0.27	0.001	0.002	
10.0	75.0	134.6 (N_2)	7.5	0.23	tr	tr	
10.0	100.0	101.2 (N_2)	10.0	0.20	tr	tr	
10.0	200.0		20.0	0.14	tr	tr	
50.0	200.0		4.0	0.33	nm[b]	nm	
25.0	200.0		8.0	0.25	nm	nm	
20.0	337.4		16.9	0.16	nm	nm	
13.2	200.0		15.2	0.17	nm	nm	
8.0	242.0		30.2	0.10	nm	nm	
5.0	200.0		40.0	0.06	nm	nm	
5.0	200.0		40.0	0.06	nm	nm	
50.0	10.0		0.20	0.75	0.003	0.005	
50.0	19.5		0.39	0.69	0.002	nm	
49.0	26.0		0.53	0.66	0.002	0.005	
50.5	49.5		0.98	0.61	tr	0.004	
50.0	105.2		2.1	0.52	tr	0.002	
40.0	20.0	212.4 (N_2)	0.50	0.62	tr	0.004	
20.0	10.0	100.7 (N_2)	0.50	0.61	0.001	0.004	
19.1	9.6	71.1 (N_2)	0.50	0.59	0.002	0.005	
10.0	5.0	53.0 (N_2)	0.50	0.61	0.004	nm	
5.0	2.5	18.5 (N_2)	0.50	0.66	0.006	0.009	
21.6	8.4		0.39	0.77	0.005	nm	
			Part 2. 3340 A				
10.0				0.61	0.067	0.067	1.3_0 (CO)
10.0				0.62	0.062	0.061	1.3_5 (CO)
10.0		107.8 (N_2)		0.61	0.062	0.062	
10.0	2.1	103.9 (N_2)	0.21	0.41	0.016	0.022	
10.0	5.3	100.5 (N_2)	0.53	0.27	0.003	0.007	
10.0	10.6	95.4 (N_2)	1.0_6	0.21	tr	0.006	
10.0	21.2	84.8 (N_2)	2.1	0.19	tr	0.003	
10.0	50.0	50.0 (N_2)	5.0	0.14	tr	0.001	
10.0	80.0	25.2 (N_2)	8.0	0.11	tr	tr	
10.0	107.0		10.7	0.09_2	tr	tr	
10.0	112.2		11.2	0.09_1	tr	tr	
5.0	104.5		20.9	0.05_6	tr	tr	

analyzed by vpc. All portions of the apparatus in contact with the products were equipped with grease-free stopcocks.

To test the procedure for handling and isolating the products, several known mixtures which approximated a typical reaction mixture were processed using the

Table II (*Continued*)

Pressures, mm				Quantum yields			
Ketene	CO	Other	[CO]/[ketene]	C_2H_4	C_2H_6	C_2H_2	Other
			Part 3. 2900 A				
10.0		106.2 (N_2)		0.93	0.018	0.02_0	2.0 (CO)
10.0	4.2	103.3 (N_2)	0.42	0.66	0.01_0	0.02_0	
10.0	18.5	88.5 (N_2)	1.85	0.49	0.004	nm	
10.0	25.0	81.5 (N_2)	2.5	0.45	tr	0.01_0	
10.0	38.7	68.8 (N_2)	3.87	0.40	tr	0.008	
10.0	77.6	29.4 (N_2)	7.8	0.29	tr	tr	
10.0	106.5		10.6	0.26	tr	tr	
10.0	206.8		20.6	0.16	tr	tr	
			Part 4. 3660 A				
50.0				0.021	5×10^{-4}	5×10^{-4}	
50.0		51.0 (N_2)		0.021	4×10^{-4}	4×10^{-4}	
50.0	52.4		1.05	0.003	3×10^{-5}	nm	
50.0	25.2		0.50	0.005	5×10^{-5}	nm	

[a] tr indicates trace amounts. [b] nm indicates that peak of product was not measurable.

Table III: Special Experiments

Pressures, mm			λ,	Cell temp,	Quantum yields			
Ketene	Other	Other	A	°C	C_2H_4	C_2H_6	C_2H_2	Other
10.0	186.7 (CO)	1.0 (O_2)	3160	50	0.13	tr	tr	
10.0	180.0 (CO)	5.0 (O_2)	3160	50	0.13	tr	tr	
25.0	106.2 (N_2)	0.5 (O_2)	3160	50	0.64	tr	0.005	2.95 (CO)
25.0	106.5 (N_2)	0.7 (O_2)	3160	50	0.65	tr	0.004	3.00 (CO)
50.0	104.4 (CO)		3160	22	0.53	nm	nm	
50.0	106.0 (CO)		3160	85	0.50	nm	nm	
10.0	2.0 (O_2)	81.5 (N_2)	3340	50	0.21	tr	0.003	2.41 (CO)
10.0	5.0 (O_2)	102.0 (N_2)	3340	50	0.17	tr	0.004	
10.0	2.0 (O_2)	101.3 (N_2)	2900	50	0.67	tr	tr	3.02 (CO)
10.0	5.0 (O_2)	103.2 (N_2)	2900	50	0.66	tr	tr	2.97 (CO)

routine procedures. In each case the values determined by this method agreed to within 2% of the known values.

Ketene was prepared by the pyrolysis of acetic anhydride, using the method described by Jenkins.[9] After purification, a ketene sample treated with acetic anhydride showed a light hydrocarbon (C_1–C_3) impurity level of less than 100 ppm. Nitrogen and carbon monoxide with less than 1 ppm of oxygen were supplied in 1-l. Pyrex flasks by J. T. Baker. The hydrocarbon gases were Phillips research grade. About 0.2% propane was added to the *trans*-butene-2 to act as an "internal standard."

As the usual conversion was about 1%, impurity levels were critical. To check the possibility of trace oxygen impurity, the quantum yields in a ketene–nitrogen–carbon monoxide mixture were determined at 0.5, 1.0, and 2.0% conversion with no apparent trend in the values. Several samples of less pure CO were used in preliminary experiments with no change in the results.

Results

Table I shows the effect of added carbon monoxide on the C_5 products for the methylene–*trans*-butene reaction at 3160 A and 50°. The yields are normalized in the sense that they are relative to the internal standard and corrections have been made for the differences in the percentage decomposition. Since carbon monoxide production could not be used to measure the rate of decomposition, the latter was determined by multiplying the absorbed intensity by $0.5\phi_{CO}$ for a ketene–nitrogen mixture of equivalent composition (*i.e.*, one in which the ketene pressure was assumed to be the

(9) A. D. Jenkins, *J. Chem. Soc.*, 2563 (1962).

sum of the ketene and butene pressures while the nitrogen pressure was the same as that of carbon monoxide). With added oxygen the primary decomposition rate was assumed to be the same as that in the absence of oxygen.

The values shown in this table are subject to some error owing to the fact that the large excess of butene, unavoidably injected along with the sample into the vpc column, made estimation of the base line very difficult. To reduce the error, several chromatograms were usually made for a given sample. The peaks were cut out and weighed, with the average value being used for subsequent calculations. *cis*-Pentene-2 is not shown in the table since the column used for this study could not isolate it.

Table II, parts 1–4, is a collection of the quantum yields of the observed products in other experiments. No products higher than C_2 were observed in mixtures containing carbon monoxide. In ketene–nitrogen mixtures small amounts of propane, cyclopropane, and propylene were found at higher conversions.

The experimental variables included total pressure, mole fraction of ketene, carbon monoxide, and nitrogen, temperature, and wavelength. Illumination times varied from 15 min for high ketene pressures at 3160 A to 5 hr at 3660 A. Several blank experiments were performed which showed that thermal decomposition was negligible at the temperatures of these experiments (*i.e.*, 20–80°).

Product quantum yields which are less than 10^{-2} of the ethylene quantum yield are not quantitatively reliable and are shown as trace amounts. The estimated error in the ethylene and carbon monoxide values is $\pm 5\%$. For the other C_2 products the error is likely to be as high as $\pm 10\%$. These error limits should not be confused with reproducibility, as individual values were reproducible to better than $\pm 5\%$. The major sources of systematic error were in determining the light flux and vpc response.

Table III is a compilation of results from experiments with added oxygen at various wavelengths. In addition to the products shown, carbon dioxide was found when oxygen was added, but no attempt was made to measure it. Also included are the results of a temperature-dependence study done at 3160 A.

Discussion

Since the decomposition quantum yield for ketene has been shown to be pressure dependent for $\lambda > 2700$ A, it was necessary to determine the pressure effect on the primary decomposition yield for our conditions so that collisional relaxation effects could be distinguished from recombination quenching.[10] As nitrogen would be expected to be similar to carbon monoxide in its ability to deactivate excited ketene, experiments were performed in which the decomposition quantum yield of ketene was measured as a function of increasing nitrogen pressure at various wavelengths. It was found (see Table II) that addition of 100 torr of N_2 caused essentially no change in the quantum yield at 2900, 3160, and 3340 A, while 50 torr produced no change at 3660 A. Further, ~200 torr of N_2 lowered the yield at 3160 A only 4–5% as compared to a 17–18% decrease for a comparable pressure of pure ketene.[10] These results are consistent with the findings of others that nitrogen is quite inefficient in deactivating excited ketene.[6] Thus, no corrections for the "pressure effect" of added CO and N_2 were necessary except for the series of experiments done at 3160 A with a total CO and N_2 pressure of 200 torr or greater. For these experiments the correction was determined by measuring $\phi(C_2H_4)$ with a pressure of nitrogen equal to the combined pressures of nitrogen and carbon monoxide used. The ratio of the ethylene yield with added nitrogen to the value found in the absence of any added gas was used as the pressure correction.

Preliminary experiments showed that the two forms of methylene did indeed react with CO at different rates and that a definite trend with wavelength was present which was contrary to that expected if the singlet were the more reactive species.[4b]

To obtain additional information as to the spin multiplicity of the more reactive methylene, the effect of carbon monoxide on the methylene–*trans*-butene reaction was studied. Previous work indicated that *cis*-dimethylcyclopropane and 3-methylbutene-1 could be used as triplet diagnostics, while *trans*-pentene-2 could be used for the singlet.[4b] Figure 1 shows the yields of these products relative to the CO-free value as a function of the [carbon monoxide]/[butene] ratio. The rapid removal of the triplet products compared to those of the singlet indicates that relative to butene, triplet methylene is more reactive toward CO than is singlet. We conclude that this is also the case in the ketene–carbon monoxide system.

Additional evidence for this assignment is obtained from the observation that even at small [CO]/[ketene] ratios the quantum yields of ethane and acetylene are dramatically reduced. Both ethane and acetylene are reported to arise as a result of triplet methylene abstraction from ketene.[11] That these C_2's are quenched by CO more rapidly than ethylene, which can come from both singlet and triplet methylene, gives credence to

(10) B. T. Connelly and G. B. Porter, *Can. J. Chem.*, **36**, 1640 (1958).

(11) K. H. Sauer, Ph.D. Thesis, Harvard University, 1957.

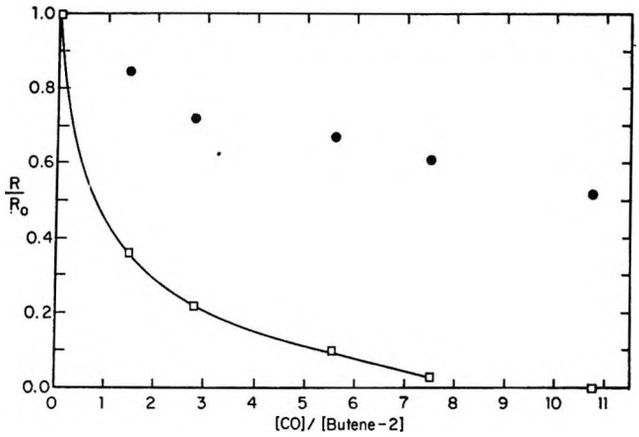

Figure 1. Rate of selected C_5 hydrocarbon formation at 3160 A in a ketene–*trans*-butene-2 mixture with added carbon monoxide relative to the CO-free rate: ●, *trans*-pentene-2; □, CDMC + 2-methylbutene-1.

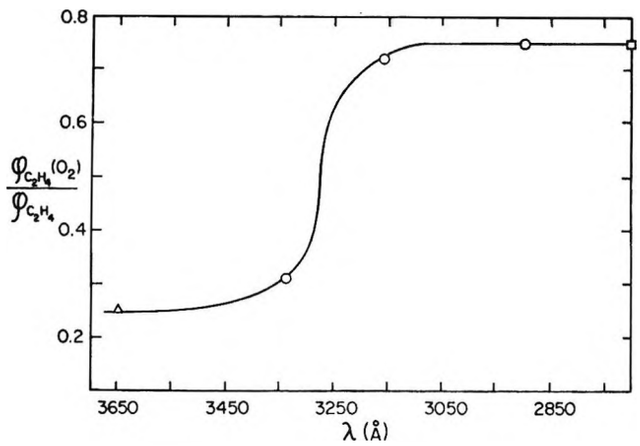

Figure 2. Quantum yield of ethylene with added oxygen relative to the O_2-free value: O, this work; △, G. B. Porter (1957); □, A. N. Strachan and W. A. Noyes, Jr. (1954).

the greater reactivity of triplet methylene toward carbon monoxide. This same effect is found in the ketene–butene system. That is, with no added carbon monoxide the C_2 fraction is about 60% ethylene and 40% ethane, whereas at a [CO]/[butene] ratio of 10.8 the C_2 fraction is 100% ethylene.

Oxygen has been used as a means of selectively removing triplet species. However, the ethylene quenching action of O_2 in the photolysis of ketene is not well understood. As shown in Figure 2, the relative quenching curve of O_2 as a function of exciting wavelength has two distinct regions. They differ not only in the magnitude of the quenching effect but also in that, at the wavelengths (*i.e.*, 3660 and 3340 A) where O_2 is particularly effective, the ethylene quantum yield is dependent on O_2 pressure, whereas in the region of less complete quenching the O_2 pressure may be varied within wide limits with little effect on the yield of ethylene.

Because of the oxygen pressure effect, it has been suggested that O_2 reacts with excited ketene at 3660 A[12] and this seems to be the case at 3340 A as well. Whether only triplet excited molecules are scavenged at these wavelengths is not clear.

Recent isotopic studies on the mechanism of oxygen quenching in methylene–olefin systems shows that oxygen reacts with the secondary radicals rather than with the methylene.[13] Consequently, the quantitative aspects of oxygen quenching as a triplet diagnostic are open to question; however, it does provide a qualitative, indirect means of ascertaining triplet participation.

Comparison of Table III and Table II, Part 1, shows that, within experimental error, oxygen has no effect on the ethylene quantum yield at high [CO]/[ketene] ratios and 3130-A radiation. This is in contrast to the 25–30% reduction in the ethylene yield by oxygen in the absence of CO (see Figure 2) and is further evidence that the triplet methylene has been preferentially removed by the CO before it reacts with the ketene.

The remainder of the discussion will be more explicit if the following mechanism is considered

$$CH_2CO + h\nu \longrightarrow {}^1CH_2 + CO \quad \phi_s I_a$$

$$\searrow \; {}^3CH_2 + CO \quad \phi_t I_a$$

$$^1CH_2 + CH_2CO \longrightarrow C_2H_4 + CO \quad k_1$$

$$^1CH_2 + CO \longrightarrow CH_2CO \quad k_2$$

$$^3CH_2 + CH_2CO \longrightarrow C_2H_4 + CO \quad k_3$$

$$^3CH_2 + CO \longrightarrow CH_2CO \quad k_4$$

$$^1CH_2 + M \longrightarrow {}^3CH_2 + M \quad k_5$$

where ϕ_s and ϕ_t denote the quantum yields of singlet and triplet methylene, respectively. This simplified mechanism, which omits the details of the primary processes in ketene, tacitly assumes that the pressure is high enough to stabilize all re-formed ketene. The validity of this assumption will be shown later. All hydrocarbon products other than ethylene are ignored. Additionally, the assumption is made that CO and N_2 are equally effective in promoting reaction 5.

Using the conventional steady-state treatment, the above yields

(12) G. B. Porter, *J. Am. Chem. Soc.*, 79, 1878 (1957).

(13) C. McKnight and F. S. Rowland, *ibid.*, 88, 3179 (1966).

$$\phi(C_2H_4) = \phi_s\left\{1 + \frac{k_2[CO]}{k_1[\text{ketene}]} + \frac{k_5[M]}{k_1[\text{ketene}]}\right\}^{-1} + \frac{\phi_t + \dfrac{\phi_s}{1 + (1/k_5[M])(k_1[\text{ketene}] + k_2[CO])}}{1 + \dfrac{k_4[CO]}{k_3[\text{ketene}]}}$$

This expression is cumbersome, but under some conditions simplifying approximations can be made. For experiments at [CO]/[ketene] ratios such that essentially all of the triplet methylene reacts with carbon monoxide and further that [CO] $\simeq$ [M], the above expression simplifies to

$$1/\phi(C_2H_4) = (1/\phi_s)\left[\frac{(k_2 + k_5)[CO]}{k_1[\text{ketene}]} + 1\right]$$

Thus a plot of $1/\phi(C_2H_4)$ *vs.* [CO]/[ketene] should be linear if the triplet has been removed. Figure 3 shows such a plot for data taken at 3160 A and 50°. The least-squares intercept is 1.88 ± 0.1 which corresponds to $\phi_s = 0.53 \pm 0.03$. The slope was found to be $0.26_6 \pm 0.01$, whence $(k_2 + k_5)/k_1 = 0.14_1 \pm 0.007$. A similar plot for data taken at 3340 A gives a slope of 0.62 ± 0.03 and an intercept of 4.1 ± 0.2. Data at 2900 A when plotted in the foregoing manner give an intercept of 1.7 ± 0.1 and the slope as 0.22 ± 0.01.

If $k_1 > k_2$ and, as one may assume from previous work, $k_5 \ll k_1$, then at low [CO]/[ketene] ratios with no added inert gas, the approximation holds

$$\phi' \equiv \frac{\phi_t}{\phi(C_2H_4) - \phi_s} \simeq 1 + \frac{k_4[CO]}{k_3[\text{ketene}]}$$

A series of experiments were done at 3160 A in which the ketene pressure was held constant and the [CO]/[ketene] ratio varied from 0 to 0.98. Since ϕ_s is given by the intercept in Figure 3, ϕ_t could be obtained by difference (*i.e.*, 0.90 − 0.53 = 0.37 = ϕ_t as only ethylene was considered). Figure 4 shows ϕ' plotted as a function of the [CO]/[ketene] ratio. From the observed slope we find $k_4/k_3 = 3.6 \pm 0.3$.

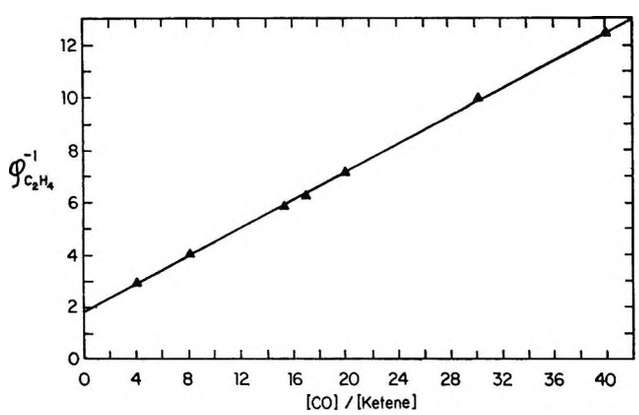

Figure 3. Reciprocal ethylene quantum yield for ketene–carbon monoxide mixtures at 3160 A.

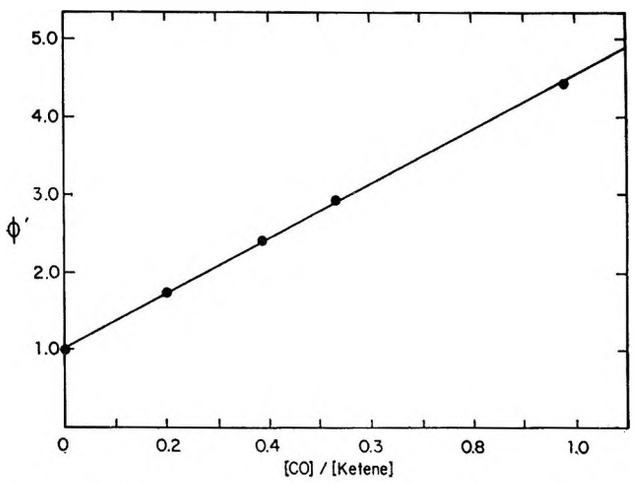

Figure 4. Determination of the ratio k_4/k_3 at 3160 A.

If the [CO]/[ketene] ratios are chosen such that the triplet contribution to ethylene formation is small and further that [CO] + [N_2] = [M] $\simeq$ constant, then

$$1/\phi(C_2H_4) = (1/\phi_s)\left\{\frac{k_2[CO]}{k_1[\text{ketene}]} + \frac{k_5[M]}{k_1[\text{ketene}]} + 1\right\}$$

which, when [M]/[ketene] is constant can be written as

$$1/\phi(C_2H_4) = (1/\phi_s)\left\{\frac{k_2[CO]}{k_1[\text{ketene}]}\right\} + C;$$

$$C = (1/\phi_s)\left(\frac{k_5[M]}{k_1[\text{ketene}]} + 1\right)$$

Figure 5 shows data taken at 2900, 3160, and 3340 A under the conditions described above. Two different total pressures were used at 3160 A to test the pressure sensitivity of the ratio k_2/k_1. The slope values found were combined with the previously determined values of ϕ_s and $(k_2 + k_5)/k_1$ to compute the rate constant ratios and singlet quantum yields shown in Table IV.

The trend of ϕ_s shown in Table IV is similar to that found for other carbonyl compounds. The values listed are strictly correct only for our experimental conditions. At longer wavelengths the excited ketene is sufficiently long-lived that environmental factors (*e.g.*, pressure and temperature) could alter the relative amounts of singlet and triplet formed.

Table IV: Kinetic Parameters for the Ketene–Carbon Monoxide System

λ, A	[M]/[ketene]	ϕ_a	% singlet	k_2/k_1	k_4/k_3	k_5/k_1
2900	10.5	0.60 ± 0.03	67 ± 4	0.12 ± 0.01	3.4 ± 0.3	<0.01
3160	10.5	0.53 ± 0.03	59 ± 3	0.14 ± 0.01	3.6 ± 0.3	0.01
3160	20.5	0.5[illegible] ± 0.03	59 ± 3	0.14 ± 0.01	3.6 ± 0.3	0.01
3340	10.5	0.24 ± 0.01	39 ± 2	0.15 ± 0.01	6.4 ± 0.6	>0.01

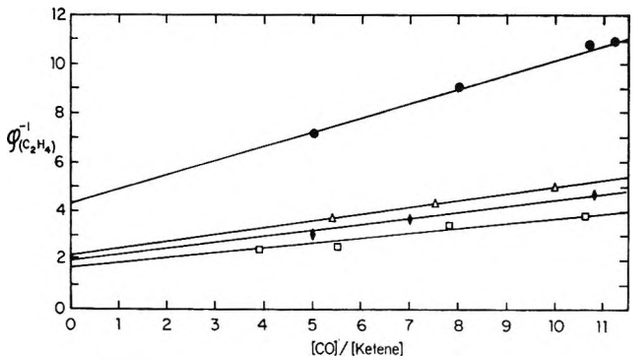

Figure 5. Reciprocal ethylene quantum yield for ketene–carbon monoxide–nitrogen mixtures at constant total pressure: ●, 3340 A and 115 torr total pressure; △, 3160 A and 215 torr total pressure; ◆, 3160 A and 115 torr total pressure; □, 2900 A and 115 torr total pressure.

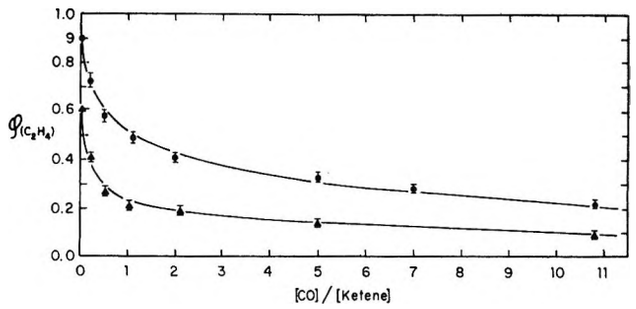

Figure 6. Comparison of computed effect of carbon monoxide on the ethylene quantum yield using quantities from Table IV with experimental points: ●, 3160 A and 115 torr total pressure; ▲, 3340 A and 115 torr total pressure.

The k_5/k_1 ratios shown have only semiquantitative significance because of the uncertainties in the intercepts of Figure 5 and because the alternate method of computing their value involves taking the small difference between the experimental values of k_2/k_1 and $(k_2 + k_5)/k_1$. The value of k_5/k_1 will depend on the nature of M, the quenching gas, which in this study was nitrogen and/or carbon monoxide.

To test the derived rate parameters, the carbon monoxide quenching of the ethylene quantum yield was computed for each wavelength using the complete kinetic equation. While the expression is not very sensitive to small changes in the various parameters, changes of 10% or more in the ratios result in a noticeable deterioration of the fit between experimental and calculated points.

Figure 6 shows both the computed curves and the experimental points for 3340 and 3160 A. The agreement is sufficiently good to give some confidence in the parameters used. The data at 3660 A are too few to allow a detailed discussion, but it appears that the percentage of singlet formed is substantially less than at 3340 A and that k_4/k_3 might be somewhat greater.

The value of k_5/k_1 when M is nitrogen or carbon monoxide, while accurate to only order of magnitude, is about the same as a similar ratio which can be computed from the data of Frey,[3a] who used argon as a quenching gas. Defining a simplified mechanism as

$$^1CH_2 + M \longrightarrow {}^3CH_2 + M \qquad k_5$$

$$^1CH_2 + \textit{cis}\text{-butene} \longrightarrow \text{CDMC} \qquad k_6$$

$$^3CH_2 + \textit{cis}\text{-butene} \longrightarrow \text{TDMC} + \text{CDMC} \qquad k_7$$

and assuming that triplet methylene gives *cis*- and *trans*-cyclopropane with equal probability and that diazomethane photolysis in Frey's experiments initially yields only singlet methylene, one can, from his data, derive a value of 0.8×10^{-2} for k_5/k_6.

The ratio k_2/k_1 shows no significant change with exciting wavelength whereas k_4/k_3 appears to change significantly. This may be interpreted as a change in k_3 with photon energy; that is, the triplet reactivity is related to the energy that the methylene carries from the photodecomposition of ketene. However, the error limits on the data are such that no strong case can be made for a wavelength dependence of the k_5/k_3 ratio. The insensitivity of the ratio k_2/k_1 to photon energy and to temperature suggests that these singlet reactions have virtually no energy barrier and that statistical factors determine the ratio.

From the data in Table I on the effect of CO on the methylene–*trans*-butene reaction, one obtains k_2/k_8 and k_4/k_9 as 0.10 ± 0.02 and 1.3 ± 0.3, respectively, where

$$^1CH_2 + \textit{trans}\text{-butene} \longrightarrow \text{TDMC} \qquad k_8$$

$^3CH_2$ + *trans*-butene ⟶

TDMC + CDMC + 3-methylbutene-1 k_9

The amount of TDMC due to singlet methylene was estimated by subtracting 1.6 times the yield of CDMC in the absence of carbon monoxide from the observed yield of TDMC.[4b]

Using these ratios and those in Table IV, one obtains $k_3/k_1 = 1.5 \pm 0.4$ and $k_9/k_3 = 2.8 \pm 0.7$. The ratio for the singlet is not significantly different from unity. However, these figures indicate that triplet methylene does show a small degree of discrimination as to the nature of the double bond. The magnitude of the effect is similar to that found by Cvetanovic for a series of olefins.[14] This fact may limit the effectiveness of carbon monoxide as a triplet getter in some systems. However, the reaction described in this paper has a distinct advantage over other techniques in that methylene itself is removed rather than some later intermediate.

As in other work on methylene, the results appear as ratios of rate constants. Using 3160-A radiation, the triplet methylene formed appears to be about 24 times more reactive toward CO than is the singlet, relative to their reactivities toward ketene. The question of whether the absolute reactivity of $^3CH_2$ toward CO is greater than that of singlet is of considerable interest but also one which cannot be answered definitively from our data. The crucial assumption is that $k_1 \simeq k_3$, that is, that the rate of reaction with the C=C bond is about the same for both singlet and triplet. This has never been demonstrated, but a survey of the relevant literature, especially the experiments with flash sources, reveals no evidence to the contrary. Thus, provisionally we will assume that $k_1 \simeq k_3$ and hence that the reactivity of the triplet methylene toward CO is higher than that of the singlet.

A rational explanation of this difference in reactivity is provided by a simplified potential energy diagram of ketene, Figure 7, showing it as a function of the C=C bond distance alone.[15] The $^1A_2$ state reached on absorption in the near-ultraviolet region is assumed to be sufficiently coupled to the $^3A_2$ state that intersystem crossing occurs over the entire range of energies of the transition.[16] The lowest points on both the $^1A_2$ and $^3A_2$ curves have been placed below the dissociation energy of ketene into $CH_2(^3\Sigma)$ + $CO(X^1\Sigma)$ to allow for the observed weak absorption extending into the visible[17] region and the very low dissociation quantum yield at 3700 A.[18,19]

According to Figure 7, $CH_2(^3\Sigma)$ + $CO(X^1\Sigma)$ form a bound state and hence could form "hot" triplet molecules on virtually every collision. Experiments were made with a [CO]/[ketene] ratio of 0.5 ranging in

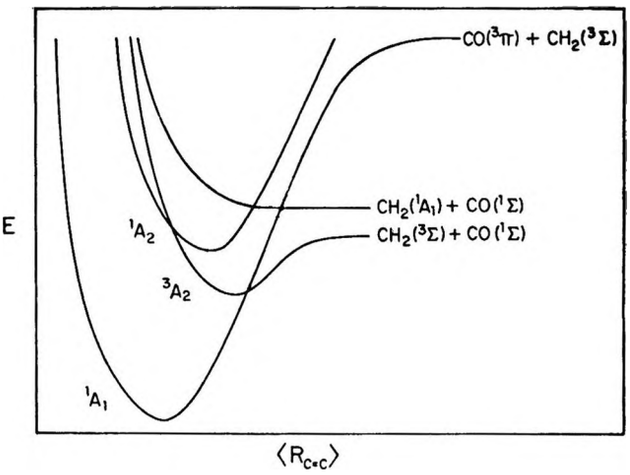

Figure 7. Potential energy diagram for ketene as a function of the C=C bond distance.

total pressure from 200 to 26 torr to determine whether the k_4/k_3 ratio is pressure dependent (see Table II, part 1). Down to 50 torr the ratio remained constant but was slightly lower at 26 torr. This indicates that the stabilization of the hot $^3A_2$ molecules is incomplete at this pressure and with the assumption that stabilization occurs on every collision indicates a lifetime of about 10^{-9} sec or greater. The foregoing implies that over the pressure range 50–200 torr the yield of triplet methylene was constant. This explanation seems more plausible than invoking exactly balanced changes in k_4/k_3 and ϕ_t.

The comparatively low reactivity of the $CH_2(^1A_1)$–$CO(X^1\Sigma)$ pair is due to the proposition that they do not correlate with the lowest singlet bound state and in the adiabatic approximation form a nonbonding state. Thus recombination must occur *via* curve crossing and could have a rather low collisional efficiency. Data from Tables I–IV show no effect of temperature or wavelength on the k_1/k_2 ratio so that the $CH_2(^1A_1)$ + $CO(X^1\Sigma)$ curve must be rather flat in the crossing region. Changing the pressure from 100 to 200 torr

(14) R. J. Cvetanovic and R. S. Irwin, *J. Chem. Phys.*, 46, 1694 (1967).

(15) We are indebted to Dr. G. Herzberg for suggesting to us that in the "adiabatic approximation" the dissociation products of the normal $^1A_1$ state of ketene are $CO(^3\Pi)$ and $CH_2(^3\Sigma)$.

(16) Whether the transition is a true kinetic process or an overlap of the two absorption systems will not be discussed here.

(17) R. N. Dixon and G. H. Kirby, *Trans. Faraday Soc.*, 62, 1406 (1966).

(18) G. B. Porter, *J. Am. Chem. Soc.*, 79, 827 (1957).

(19) Because temperature has a strong effect on the quantum yield of dissociation, decomposition may occur as a result of a transition from a vibrationally excited ground state, *i.e.*, "hot band absorption."

(see Table IV) leaves the ratio k_1/k_2 unchanged so that the stabilization of the hot $^1A_2$ state is not the rate-determining step. What happens to the system in this state is not clear, but crossing into the $^3A_2$ state seems probable. In this state the molecule could either relax to the ground state or dissociate to triplet methylene and carbon monoxide. The net result of this latter process would be indistinguishable from reaction 5.

Some of the results and conclusions of this paper have already been published.[20]

Acknowledgments. The authors wish to thank the Research Grants Branch, National Center for Air Pollution Control, Bureau of Disease Prevention and Environmental Control, for the funds which made this work possible.

(20) B. A. DeGraff and G. B. Kistiakowsky, *J. Phys. Chem.*, 71, 1553 (1967).

Reactions of Carbonylic Compounds with Hydrated Electrons[1]

by Edwin J. Hart, E. M. Fielden,[2] and M. Anbar[3]

Chemistry Division, Argonne National Laboratory, Argonne, Illinois 60439 *(Received May 22, 1967)*

The reactivity of the hydrated electron with carbonyl compounds of the type R_1COR_2 has been measured. Their rate constants, k_1, vary from 3.0×10^5 M^{-1} sec^{-1} for urea to 8.0×10^9 M^{-1} sec^{-1} for cyclohexanone. For aldehydes, ketones, and carboxylic acids a linear correlation is obtained between log k and Taft's σ^* function. The slope, ρ, equals -0.74. Amides and esters deviate from this relation because of mesomeric forms, in which the electrophilic center is localized on either the nitrogen or the alkoxy oxygen. For a group of these compounds, a ρ of $+1.16$ is found. Hydrated electron rate constants, as demonstrated by these and previous studies, provide a new parameter for exploring the electronic configuration of organic compounds.

Introduction

The hydrated electron, e_{aq}^-, has been suggested as a new nucleophilic reactant for studying the structure of organic molecules and ions in aqueous solutions.[4-6] In many reactions e_{aq}^- transfers directly to an electrophilic center. Halogen atoms, for example, act as such centers on aliphatic coupounds.[5] Another functional group displaying appreciable reactivity toward e_{aq}^- is the carbonyl group.[6] Since no systematic studies on these compounds have been carried out we supplement previous reports[4,5,7-9] by providing rate constants for a series of organic compounds, characterized by the general formula R_1COR_2. R_1 and R_2 are H, alkyl, alkoxy, NH_2, or OH (O^-) groups.

Experimental Section

The rate constants were measured by an electron-pulse technique similar to that described in earlier work.[10,11] The set-up appears in Figure 1. It differs

(1) Based on work performed under the auspices of the U. S. Atomic Energy Commission.

(2) Physics Department, Institute of Cancer Research, Belmont, Sutton, Surrey, England.

(3) Weizmann Institute of Science, Rehovoth, Israel.

(4) M. Anbar and E. J. Hart, *J. Am. Chem. Soc.*, 86, 5613 (1964).

(5) M. Anbar and E. J. Hart, *J. Phys. Chem.*, 69, 271 (1965).

(6) M. Anbar, Advances in Chemistry Series, No. 50, American Chemical Society, Washington, D. C., 1965, p 55.

(7) E. J. Hart, J. K. Thomas, and S. Gordon, *Radiation Res. Suppl.*, 4, 74 (1964).

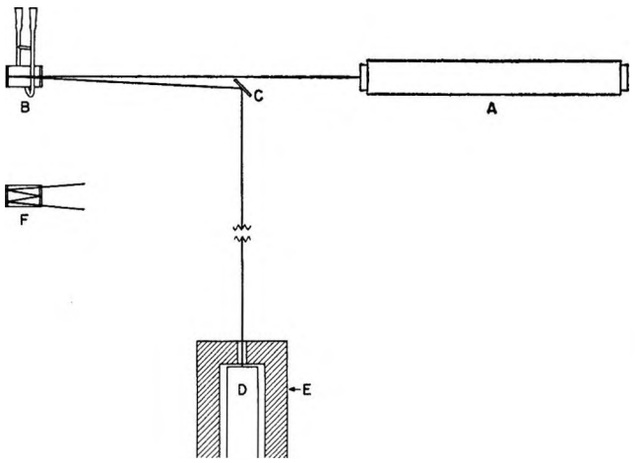

Figure 1. Electron pulse radiolysis set-up using a gas laser light source: A, helium neon laser with continuous output at 6328 A; B, 4 × 2 cm diameter silica irradiation cell with silvered Suprasil end windows; C, plane mirror; D, Amperex Type XP1002 photomultiplier; E, 2-in. thick lead pot with 0.25-in. diameter hole in lid; F, top view of optical path in cell.

from previous arrangements in the use of a gas laser (A) as a light source. Benefits gained by its use are (1) a major simplification in the optical system, and (2) complete suppression of "Cerenkov noise" during the pulse. These advantages are offset, to some extent, by the inherent instability of the laser and its 60-cycle fluctuations in intensity. For microsecond sweep rates for which most of our work was done, these instabilities posed no problems. The laser was a Perkin-Elmer Model 5200 D.C. excited helium neon laser, giving a continuous output at 6328. A. The laser emits a parallel beam of light approximately 0.5 mwatt power. The irradiation cell (B) consisted of a quartz tube 4 cm long and 2 cm in diameter with optically polished high-purity quartz end windows. The windows of the cell were completely silvered with the exception of two small diametrically opposed areas (little larger than the laser beam diameter of 3 mm) on the front face of the cell. These unsilvered portions served as entrance and exit windows for the laser beam. By adjusting the angle at which the laser beam entered the cell, the beam was reflected back and forth (F) between the mirrored ends of the cell before emerging. Between 2 and 10 passes of the beam along the length of the cell were readily obtained in this manner. The beam emerging from the cell was reflected by a plane mirror (C) onto a photomultiplier (D) (Amperex Type XP1002) encased in a 2-in. thick lead shield (E). The monochromatic and parallel nature of the light eliminated the monochromater and quartz lens assembly normally required.[10] The system of electronic amplifiers and oscilloscope used to record the transient absorption due to the radiation-induced hydrated electron was identical with that described previously.[10]

Preparation of Solutions

The compounds were irradiated in unbuffered solutions, and in solutions buffered at pH 7.2 with NaH_2PO_4–Na_2HPO_4 and at pH 11 with NaOH. In the solutions where 1.0 mM ethanol was used to destroy hydroxyl radicals, the ethanol was purified by distillation through a fractionation column. The solutions were injected[8] into the deaerated matrix[11] to produce a solution of the desired solute concentration. In this procedure, 5 ml of the stock solution (0.01–0.05 M) or the pure organic liquid was first deaerated by shaking with an equal volume of helium in a 10-ml syringe. After 2 to 3 min shaking, the gas was expelled and 5 cc of helium again added and the shaking repeated. By chromatographic analysis we found that each shaking reduced the oxygen concentration of the solution by a factor of 20. Consequently, the concentration of oxygen in our stock solution was reduced to about 0.5 μM after two equilibrations. Normally of the order of 0.25 ml of this solution was then injected into 50 ml of the preirradiated hydrogen saturated matrix. Previous studies[11] showed that the concentration of oxygen in these solutions was less than 10^{-7} M.

Analysis of Decay Curves

The rate constants were calculated directly from a first-order plot of the logarithm of optical density *vs.* time. The oscillograms were analyzed by CHLOE, an automatic film scanning machine developed by the Applied Mathematics Division of Argonne.[12] CHLOE, with a maximum resolution of 1024 "bits" in both the X and Y coordinates scans an oscillogram photograph and stores the data in digital form. These data were then fed into a CDC 3600 computer which printed out the optical density (or any similar function such a log OD) *vs.* time. A graph of log OD *vs.* time with the "least mean squares" slope was also produced automatically. This method not only saved time but it also eliminated personal errors in the measurements of oscillograms and in calculating the errors involved in such reading. Figure 2 shows a typical decay curve

(8) E. J. Hart, S. Gordon, and J. K. Thomas, *J. Phys. Chem.*, **68**, 71 (1964).

(9) A. Szutka, J. K. Thomas, S. Gordon, and E. J. Hart, *ibid.*, **69**, 289 (1965).

(10) J. K. Thomas, S. Gordon, and E. J. Hart, *ibid.*, **68**, 1524 (1964).

(11) E. J. Hart and E. M. Fielden, ref 6, p 253.

(12) D. Hodges, Applied Mathematics Division Technical Memorandum No. 61, 1963.

Table I: Hydrated Electron Rate Constants for Some Organic Compounds

Compound	Source	Matrix	pH	Concn, mM	Slope[a]	k, M^{-1} sec^{-1}	k_{av}
CH_3COCN	*c*	H_2O	7.15	38.3	0.4839	2.9×10^7	
		H_2O	7.15	9.56	0.1461	3.5×10^7	3.0×10^7
		H_2O	7.15	9.56	0.1288	2.7×10^7	
CH_3CHNOH	*d*	Alk	10.82	6.54	0.2050	7.2×10^7	
		Alk	10.82	6.54	0.1981	7.0×10^7	7.2×10^7
		Alk	10.82	6.54	0.2086	7.3×10^7	
$(CH_3)_2CNOH$	*e*	H_2O	7.75	0.25	0.0337	3.1×10^8	3.0×10^8
		H_2O	7.75	0.25	0.0310	2.9×10^8	
FCH_2COCH_3	*f*	H_2O	6.7	0.500	0.2255	1.04×10^9	1.0×10^9
		H_2O	6.7	0.150	0.0685	1.04×10^9	
		Alk	10.86	0.500	0.1755	8.1×10^8	8.8×10^8
		Alk	10.86	0.250	0.1025	9.4×10^8	
$COO^-(CH_2)_2COO^-$	*g*	Alk	10.0	10.0	0.133	3.1×10^7	
$COO^-(CH_2)_2COOH$	*g*	H_2O	6.0	2.0	0.100	1.2×10^8	
CF_3COCH_3	*d*	H_2O	5.19	1.00	0.0289	6.6×10^7	
NH_2COCOO^-	*h*	Alk	11.2	0.40	0.6510	3.7×10^9	4.0×10^9
		Alk	11.04	0.133	0.2442	4.2×10^9	
CF_3COOCH_3	*d*	Alk	10.62	0.406	0.3277	1.9×10^9	
$OHCH_2COOCH_3$	*f*	Alk	10.65	0.519	0.1092	4.8×10^8	
$CH_3CH_2COOCH_3$	*d*	H_2O	6.81	4.16	0.1843	9.0×10^7	
$(CH_3)_3CCOOCH_3$	*c*	H_2O	5.91	15.33	0.1511	2.3×10^7	
$CH_3COOC_2H_5$	*b*	H_2O	6.53	20.45	0.5217	5.9×10^7	
CH_3COCN	*d*	Alk	10.94	5.60	0.3659	1.5×10^8	
$NH_2CH_2COOCH_3$	*c*	Alk	10.66	1.00	0.1268	2.92×10^8	2.91×10^8
		Alk	10.66	1.00	0.1259	2.90×10^8	
$CNCH_2COOC_2H_5$	*c*	Alk	10.92	0.906	0.1259	3.2×10^8	

[a] Log OD/μsec (corrections have been made for the standard matrix and for effect of pH on the matrix). [b] BDH Analar. [c] Fluka puriss. [d] Fluka purum. [e] BDH Lab. [f] K & K Laboratories, Inc. [g] Baker CP; recrystallized three times. [h] G. F. Smith Chem. Co.

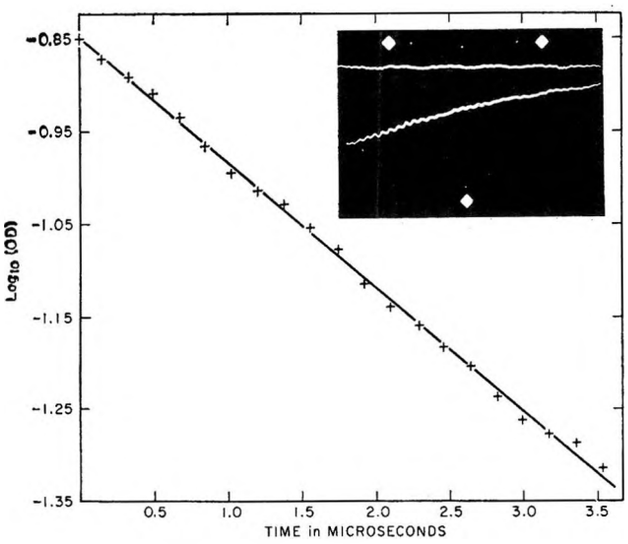

Figure 2. Reaction of 0.001 M methyl glycinate with e_{aq}^- at pH 10.66: +, points on decay curve calculated by CHLOE and presented on a calcomp plot; ———, least-square curve. Slope = 0.1346 log OD/μsec.

and its graphical printout of the optical density data. The rate constant was calculated from the difference between the slopes of the solute and matrix under identical irradiation conditions. The complete equation is

$$k = 2.3 \times 10^6 \times \frac{[\log (OD/\mu\text{sec}) \text{ solute} - \log (OD/\mu\text{sec}) \text{ matrix}]}{C}$$

where OD = optical density, μsec = unit of time of decay curve, C = concentration in moles/l., k = rate constant in M^{-1} sec^{-1}. Data obtained from the compounds studied appear in Table I. The estimated error is ±10%.

Results and Discussion

The carbonyl group is highly reactive with e_{aq}^- but its reactivity is influenced to a major extent by the nature of adjoining groups. For example, the rate constants decrease by a factor of 20,000 when the methyl groups of acetone are replaced by the amine groups of urea. In an attempt to explain this behavior we studied

Table II: The Rates of Reaction of Carbonylic Compounds (R_1COR_2) with Hydrated Electrons

Compound	R_1	R_2	k, M^{-1} sec^{-1}	Log k	$\sigma^*_{R_1}$	$\sigma^*_{R_2}$	$\sigma^*_{R_1} + \sigma^*_{R_2}$
Acetaldehyde	CH_3	H	3.5×10^9	9.54	0	0.49	0.49
Acetone	CH_3	CH_3	6.3×10^9	9.80	0	0	0
Fluoroacetone	CH_3	FCH_2	9.5×10^8	8.98	0	1.10	1.10
Trifluoroacetone	CH_3	F_3C	6.6×10^7	7.82	0	2.58	2.58
Acetic acid	CH_3	OH	1.8×10^8	8.26	0	1.55	1.55
Pyruvate ion	CH_3	COO^-	6.8×10^9	9.83	0	0	0
Acetamide	CH_3	NH_2	1.7×10^7	7.23	0	1.2	1.2
Pyruvonitrile	CH_3	CN	3.0×10^7	7.48	0	3.6	3.6
N-Acetylglycinate ion	CH_3	$HNCH_2COO^-$	2.0×10^7	7.30	0	1.1	1.1
Cyclohexanone	CH_2–	$-CH_2(CH_2)_3$	8.0×10^9	9.90	−0.1	−0.1	−0.2
Formic acid	H	OH	1.4×10^8	8.15	0.49	1.55	2.04
Formamide	H	NH_2	4.2×10^7	7.62	0.49	1.2	1.69
Pivalic acid	OH	$(CCH_3)_3C$	9.7×10^7	7.99	1.55	−0.30	1.25
Succinic acid	OH	$-CH_2COO^-$	1.2×10^8	8.08	1.55	0	1.55
Oxamate ion	NH_2	COO^-	4.0×10^9	9.60	1.2	0.0	1.2
Urea	NH_2	NH_2	3.0×10^5	5.48	1.2	1.2	2.4
Ethyl acetate	CH_3CH_2O	CH_3	5.7×10^7	7.76	1.35	0	1.35
Methyl propionate	CH_3O	CH_3CH_2	9.0×10^7	7.96	1.45	−0.10	1.35
Methyl glycolate	CH_3O	$HOCH_2$	4.8×10^8	8.68	1.45	0.55	2.00
Methyl glycinate	CH_3O	H_2NCH_2	2.9×10^8	8.46	1.45	0.43	1.88
Methyl fluoroacetate	CH_3O	FCH_2	9.8×10^8	8.99	1.45	1.10	2.55
Ethyl cyanoacetate	CH_3CH_2O	$NCCH_2$	3.2×10^8	8.51	1.35	1.30	2.65
Methyl trifluoroacetate	CH_3O	F_3C	1.9×10^9	9.28	1.45	2.58	3.03
Methyl pivalate	CH_3O	$(CH_3)_3C$	2.3×10^7	7.36	1.45	−0.30	1.15
Formoxime	CH_3[a]	H[a]	7.2×10^7	7.86	0	0.49	0.49
Acetoxime	CH_3[a]	CH_3[a]	3.0×10^8	8.48	0	0	0
Glycine	OH	H_2NCH_2	8.0×10^6	6.91	1.55	0.43	1.98
Alanine	OH	$H_3C(NH_2)CH$	5.9×10^6	6.77	1.55	0.33	1.88

[a] Oxime.

the effect of the substituents on the CO group. Table I lists our data for the new compounds and Table II summarizes the available rate constants and Taft σ^* values for these and other carbonyl compounds.[13] The compounds considered include aldehydes, ketones, carboxylic acids, amides, esters, and oximes.

Taft's σ^* values[14] again provide us with a suitable parameter for correlating our rate constants of carbonyl compounds. We had previously found them suitable for explaining the behavior of haloaliphatic and aromatic compounds. As the σ^* values are expected to be additive,[14,15] we list the sum of the polar substituent constants σ^* of R_1 and R_2 in Table II and plot them *vs.* log $k(e_{aq}^- + R_1COR_2)$ in Figures 3 and 4. We had to estimate σ^* values for the COO^- and NH_2 groups. For COO^-, σ^* was assumed equal to that of CH_3 ($\sigma^*_{COO^-} = 0.0$). This is justified since the values of σ_p, σ_m, σ_p^+, and σ_m^+ for COO^- are all very close to zero.[14] In the case of NH_2, $\sigma^* = 1.2$ was estimated on the basis of the polarity of the C–N bond manifested by its dipole moment.[13] Thus $\sigma^*_{NH_2}$ is comparable with that of $\sigma^*_{FCH_2}$ and is intermediate between σ^*_H and σ^*_{OH}.

The linear dependence of log k on σ^* illustrated in Figure 3 describes the behavior of aldehydes, ketones, and carboxylic acids. This curve has a slope ρ, equal to −0.74. The rate constants of substituted carbonyl compounds decrease linearily under the influence of electron-withdrawing substituents by a factor of two hundred from acetone to pyruvonitrile. In order to explain this result we assume that e_{aq}^- adds to an orbital of the carbonyl oxygen atom. This assumption is plausible since an ion radical, $CH_3\dot{C}(O^-)CH_3$, has been identified in the case of acetone.[16,17] Electron-

(13) M. Anbar and P. Neta, *Intern. J. Appl. Radiation Isotopes*, **18**, 493 (1967).

(14) R. W. Taft in "Steric Effects in Organic Chemistry," M. S. Newman, Ed., John Wiley and Sons, Inc., New York, N. Y., 1956, p 556.

(15) J. E. Leffler and E. Grunwald, "Rates and Equilibria of Organic Reactions," John Wiley and Sons, Inc., New York, N. Y., 1963, p 219.

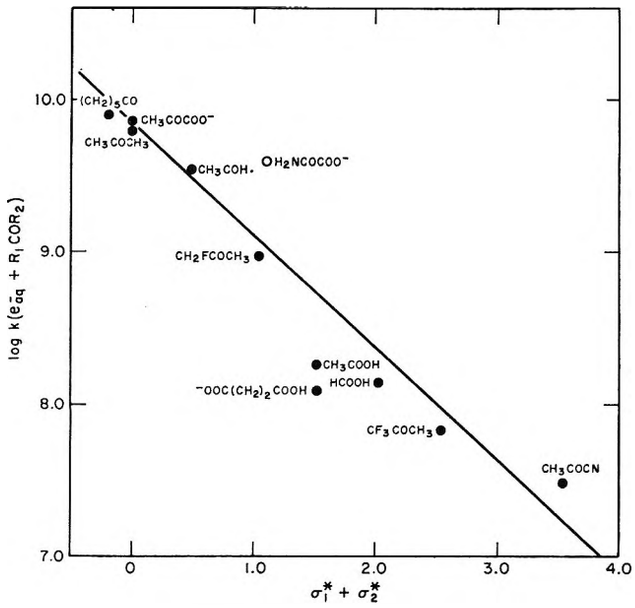

Figure 3. Relationship between hydrated electron rate constants of carbonyl compounds and Taft's σ^* function.

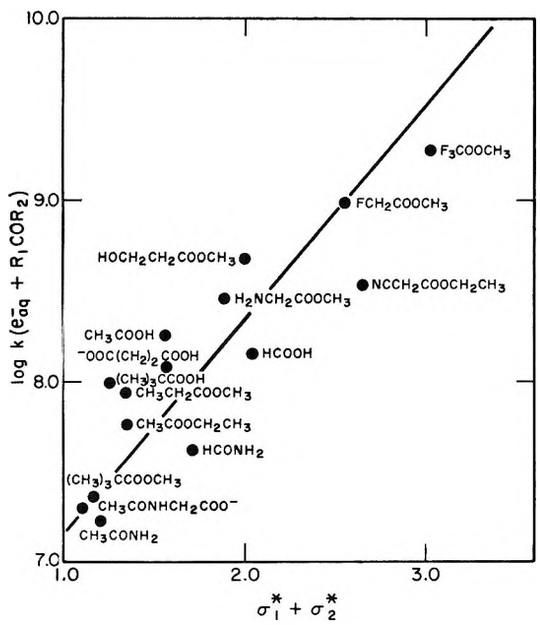

Figure 4. Relationship between hydrated electron rate constants of esters and amides and Taft's σ^* function.

withdrawing groups induce a shortening of the C=O bond, a result inferred from the increase in the stretching frequency, $\nu_{C=O}$.[18] This bond shortening, which is directly related with σ^*,[19] implies a higher electron density in the π orbitals, resulting in a decreased tendency to accommodate an additional electron.[4]

Oximes behave like carbonyls and they have a comparable ρ value. Their reactivity is lower than that of ketones because of the inductive effect of the OH group on the nitrogen atom. This effect lowers the dipole moment from 1.3 for propylamine to 0.9 Debye units for acetoxime. By contrast the dipole moments increase from 1.6 D. for 2-propanol to 2.9 for acetone.[20]

Amides and esters exhibit a completely different log k *vs.* σ^* free-energy relationship from that of substituted ketones and acids. Note especially that the slopes of the lines of Figures 3 and 4 change from plus to minus. The retarding effect of the NH_2 or OR groups on the reactivity of the carbonyl group with e_{aq}^- is more extensive than expected from their inductive effects. We attribute this behavior to the mesomeric effect of these substituents, an effect that can also be inferred from the change in $\nu_{C=O}$.[18] The mesomeric forms

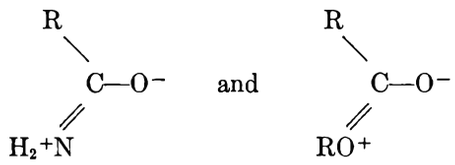

depress the double-bond character of the C=O group, make the carbonyl bond nonreactive toward e_{aq}^- and create new electrophilic centers of lower reactivity.

The mesomeric form of esters

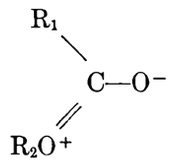

while nonreactive at the carbonyl bond still has a finite electron affinity at the alkoxy oxygen. This electron affinity will obviously *increase* with the electron-withdrawing capability of R_1. The higher reactivity of esters toward e_{aq}^- correlates with an increase in σ^* of R_1. In Figure 4 note that there is a hundredfold increase in reactivity between $(CH_3)_3CCOOCH_3$ ($\sigma^* = 1.15$) and CF_3COOCH_3 ($\sigma^* = 3.03$). Because of the mesomeric character of these molecules the reactive center moves from the carbonyl to the alkoxy group.

(16) S. Gordon, E. J. Hart, and J. K. Thomas, *J. Phys. Chem.*, **68**, 1262 (1964).

(17) L. Kevan, P. N. Moorthy, and J. J. Weiss, *J. Am. Chem. Soc.*, **86**, 771 (1964).

(18) R. N. Jones and C. Sandorfy in "Chemical Applications of Spectroscopy, Techniques in Organic Chemistry," Vol. IX, Interscience Publishers, New York, N. Y., 1956, p 443.

(19) L. N. Ferguson, "The Modern Structure Theory of Organic Chemistry," Prentice-Hall, Englewood Cliffs, N. J., 1963, Chapter V.

(20) A. L. McClellan, "Tables of Experimental Dipole Moments," Freeman and Co., San Francisco, Calif., 1963.

The reactivities of formamide and acetamide also seem to be due to the

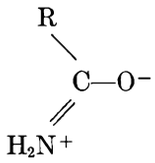

mesomeric form and they fit satisfactorily on the same log k–σ^* curve as the esters.

The unusually low reactivity of urea and the unusually high reactivity of the oxamate ion deserve special consideration. Urea may be represented by the formula

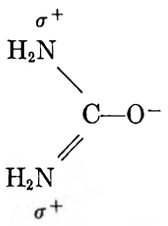

without any well-defined electrophilic center. Consequently low reactivity is expected. Furthermore, in the 0.10 M urea used, this compound may be partly in a dimeric, less-reactive form.

Stabilization of the mesomeric form of the oxamate ion by hydrogen bonding may account for the high reactivity of this compound. The oxamate ion may exist in the forms

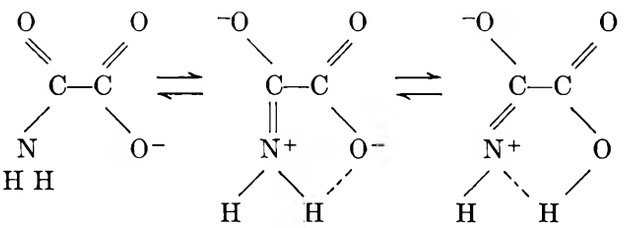

Hydrogen bonding stabilizes the carbonyl group on the carboxylate ion thereby providing the oxamate ion with two highly reactive electrophilic centers. This assumption explains the high rate constant of 4×10^9 M^{-1} sec^{-1} for this compound. A much lower value would have been predicted from the σ^* of its functional groups.

The carboxylic acids studied, HCOOH, CH_3COOH, $^-OOC(CH_2)_2COOH$, and $(CH_3)_3CCOOH$, fit fairly well on either Figure 3 or 4. Consequently, it is hard to decide whether the inductive or mesomeric effects predominate in these acids. Formic acid fits better on Figure 3, whereas $(CH_3)_3CCOOH$ and $^-OOC(CH_2)_2$-COOH fit better on Figure 4. Possibly both inductive and mesomeric effects contribute to the reactivity of carboxylic acids. The reactivity of e_{aq}^- with carboxylic acids has also been interpreted in terms of a Brönsted relationship (*i.e.*, taking the hydroxylic hydrogen as the reactive center) with reasonable success.[21] However, one would predict succinic acid (pK_{a_2} = 5.6) to be considerably less reactive than acetic acid (pK_a = 4.75) and the latter less reactive than formic acid (pK_a = 3.75). On the contrary, the rate constants differ by only a factor of 2. We conclude, therefore, that the reactivity of carboxylic acids with e_{aq}^- may be accounted for by their carbonylic functional group and that the "general acid" correlation[21] is probably not applicable in this case.

The rate constants of glycine and alanine are 8×10^6 and 6×10^6 M^{-1} sec^{-1}, respectively.[22] This low reactivity of amino acids is expected because these acids are predominantly in the form of the nonreactive zwitterion. Much higher rate constants would be predicted from the inductive effects of the amino and hydroxyl groups on the carbonyl bond. Peptides, on the other hand, like glycylglycine are more reactive than the amino acids.

In conclusion, the reactivity of hydrated electrons with carbonyl compounds behaves like other systems previously studied.[6] Reactivity depends on the electron density at a specific reaction center. Any parameter which decreases the electron density at this center enhances the rate of attack by e_{aq}^-. Thus, hydrated electrons are again shown to be an adequate probe for estimating the electron distribution on a given substrate molecule.

(21) J. Rabani, ref 6, p 242.

(22) J. V. Davies, M. Ebert, and A. J. Swallow, in "Pulse Radiolysis," J. H. Baxendale, *et al.*, Ed., Academic Press Inc., New York, N. Y., 1965, p 165.

The Thermal Decomposition of Oxygen Difluoride in a Flow System[1]

by L. Dauerman,[2] G. E. Salser, and Y. A. Tajima

Department of Chemical Engineering, New York University, New York, New York *(Received May 23, 1967)*

Oxygen difluoride in helium gas carrier has been decomposed at temperatures from 773 to 973°K and at residence times from 1 to 10 msec using a tubular flow reactor coupled to a mass spectrometer. The rate expression found for the bimolecular rate coefficient was $\log k = 9.78 - 7065/T$ l./mole sec over the temperature range from 723 to 923°K. No evidence for the oxyfluoride (OF) radical was found. This thermal decomposition does not appear to be a simple unimolecular decomposition.

Introduction

The kinetics of the thermal decomposition of oxygen difluoride, OF_2, have been studied by Koblitz and Schumacher.[3] This study has been treated as a representative unimolecular decomposition reaction by Trotman-Dickenson.[4] He equated the activation energy for this reaction with the bond dissocation energy and concluded that the strength of the first oxygen–fluorine bond is 41 kcal. On the other hand, Dibeler, Reese, and Franklin[5] concluded from appearance potential measurements on OF_2 that the first oxygen–fluorine bond is approximately 60 kcal.

The heat of atomization of OF_2 is approximately 90 kcal from a summation of the heat of formation of OF_2 and the bond dissociation energies of oxygen and fluorine, respectively. It follows from the kinetic study that the first oxygen–fluorine bond is 10 kcal weaker than the second one; in contrast, the conclusion from the appearance potential measurement study is that the first oxygen–fluorine bond is 30 kcal stronger than the second one. Arkell, Reinhard, and Larson[6] concluded from a study in which they produced the oxyfluoride radical (OF) at 4°K by photolysis of OF_2 in a N_2 or Ar matrix that the second oxygen–fluorine bond is stronger than the first. These authors suggested that a value of 56 kcal/mole for the second oxygen–fluorine bond is reasonable.

In the present work an attempt has been made to clarify the conflicting conclusions through a kinetic study whose aim was to detect the oxyfluoride radical (OF) in the gas phase. Whereas Koblitz and Schumacher[3] followed the thermal decomposition of OF_2 manometrically over the temperature range from 250 to 270°, in this study, OF_2 in a carrier gas was decomposed in a flow reactor over the temperature range from 500 to 700° and the system was sampled directly into a mass spectrometer. It was thought that the detection of OF would disprove the conclusion of Dibeler and co-workers. The deduction from their reported bond energy for the first oxygen–fluorine bond is that at the temperature at which the first oxygen–fluorine is broken, the resulting OF species will be thermally unstable.

Experimental Section

The kinetics of the decomposition of OF_2 were studied using a flow reactor combined with a mass spectrometer.[7] A nickel reactor was used, 3 in. long × 0.25 in. i.d. Thermocouples in the wall of the reactor were used to measure the reactor temperature. The reactor fitted over a cone-shaped nickel probe with a 0.002-in. leak which was attached to the mass spectrometer. The distance between the leak and the electron beam was 1.5 in. The probe, reactor,

(1) Preliminary results were presented by L. Dauerman at the 150th National Meeting of the American Chemical Society, Atlantic City, N. J., Sept., 1965.

(2) To whom inquiries should be sent.

(3) W. Koblitz and H. J. Schumacher, *Z. Physik. Chem.* (Leipzig), B25, 283 (1934).

(4) A. F. Trotman-Dickenson, "Gas Kinetics," Academic Press Inc., New York, N. Y., 1955, p 80.

(5) V. H. Dibeler, R. M. Reese, and J. L. Franklin, *J. Chem. Phys.*, 27, 1296 (1955).

(6) A. Arkell, R. R. Reinhard, and L. P. Larson, *J. Am. Chem. Soc.*, 87, 1016 (1965).

(7) F. P. Lossing in "Mass Spectrometry," C. A. McDowell, Ed., McGraw-Hill Book Co., Inc., New York, N. Y., 1963, pp 442–505.

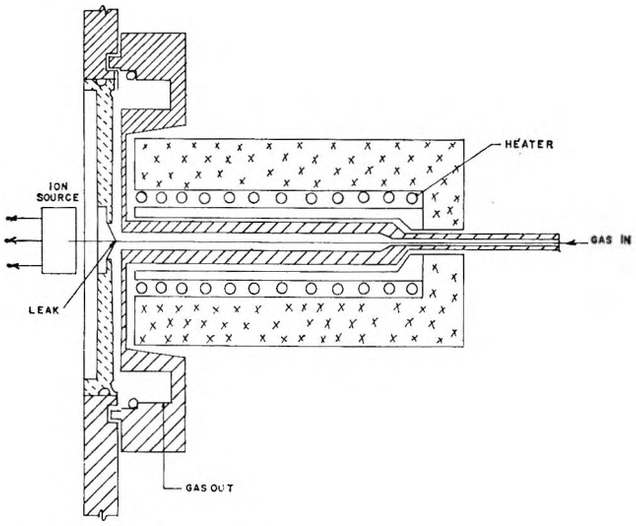

Figure 1. Gas flow reactor.

and ion source relationships are shown schematically in Figure 1. The reactor and probe were passivated in a stream of fluorine at 350° until the intensity due to fluorine as observed in the mass spectrum remained constant.

External thermocouples were used because of the difficulties involved in using internal thermocouples with OF_2. The reactor was profiled internally by using mixtures of CO_2, instead of OF_2, diluted with helium over the temperature range, and the stay times reported in this study. The equivalent kinetic temperatures were calculated using the method of Fabuss, Smith, and Satterfield.[8]

The equivalent kinetic temperature is the temperature at which the reacting system, if held isothermally for a time equal to the actual contact time in the reactor, would show the same per cent conversion as that actually found. It was assumed in making these calculations that the system was a first-order reaction with an activation energy of 30 kcal/mole. This situation approximates the OF_2 pyrolysis. Rather than reporting the individual temperature corrections, the accuracy of which are questionable because of the assumptions made in the calculations, the reported temperatures are considered to be good to within $\pm 10°$, based upon the maximum spread between the equivalent kinetic temperature and the measured external temperature.

The residence times were calculated assuming plug flow from the flow rates, the reactor dimensions, and the pertinent pressure and temperature conditions. Flow rates were measured with a calibrated rotometer. Flow rates were controlled by one of a series of valves across which a constant pressure differential was maintained by a Moore diaphragm regulator. The mass spectrometer, built at this facility, is of the 60° sector-type and was designed for kinetic studies. It has a relatively "open" ion source which sits on a large pump.

The maximum pressure in the flow reactor that could be accommodated by the mass spectrometer was 100 mm, a high pressure with respect to mass spectrometers in general, but a significant limitation in regard to kinetic studies.

The diluent gas, helium, contained 1 mole % argon. Argon was used as a reference for oxygen difluoride. The flow of gas through it is affected to some extent by the temperature, pressure, and flow rate. These effects are minimized by referencing to argon. The mixtures of OF_2, helium, and argon were prepared outside the flow system. The OF_2 obtained from Allied Chemical Co., was 99% pure, the major impurity being oxygen. It was not further purified. Helium, obtained from Matheson Gas Co., Inc., was 99.95% pure. Argon obtained from the same company was 99.99% pure.

It was not possible to change the surface-to-volume ratio by a significant factor and maintain comparable conditions. On the other hand, Koblitz and Schumacher found that this system was not susceptible to heterogeneous effects except when glass was used.

Results and Discussion

Turning to Table I, it can be seen that the thermal decomposition of OF_2 was studied at five 50° temperature intervals over the range from 773 to 973°K.

Table I: The Pseudo-First-Order and Bimolecular Rate Coefficients

Mole % OF_2	P_{total}, mm	T, °K	$k_{pseudo-first}$, sec^{-1}	$k_{bimolecular}$, l. $mole^{-1}$ sec^{-1}
1	60	773	1.46	120
0.1	100	773	2.60	126
1	60	823	5.44	465
0.1	100	823	9.20	472
1	100	823	11.2	574
1	60	873	14.3	1309
0.1	100	873	22.6	1228
1	100	873	27.5	1495
1	60	923	46.8	4500
0.1	100	923	75.9	4387
1	100	923	59.7	3451
1	60	973	91.7	9291
0.1	100	973	155	9394
1	100	973	152	9212

(8) B. M. Fabuss, J. O. Smith, and C. N. Satterfield, *Chem. Eng.*, **70**, No. 8, 153 (1963).

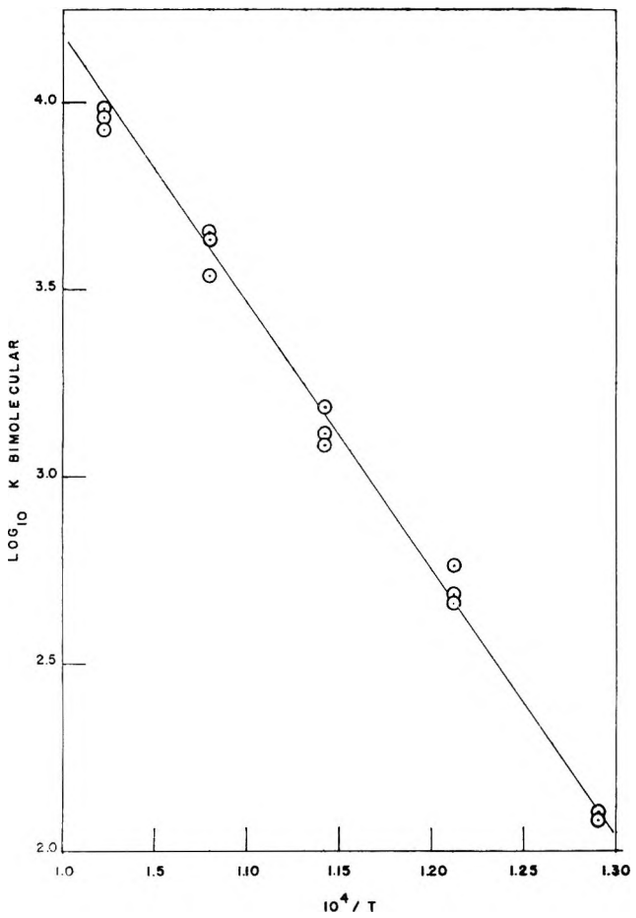

Figure 2. Arrhenius plot of k in units of liters per mole second.

At each of these temperatures the mole % OF_2 was varied from 0.1 to 1 and the pressure from 60 to 100 mm. To repeat what is stated in the Experimental Section, it was not possible to obtain higher pressures because of the high vacuum requirement of the mass spectrometer. At each temperature, the residence time was varied from 1 to 10 msec. First-order plots were obtained and the calculated rate coefficients are listed under $k_{\text{pseudo-first}}$. From these rate coefficients, the second-order rate coefficients were calculated by dividing by the helium concentration. The values obtained are listed under $k_{\text{b molecular}}$.

The log $k_{\text{b molecular}}$ values are plotted in Figure 2 as a function of $1/T$, an Arrhenius plot, and an activation energy of 32.5 kcal is found. From this value the preexponential factor, log $(A/T^{1/2})$ l./mole sec, was calculated for each rate coefficient and the average value is 9.78. Thus the bimolecular rate coefficient is

$$\log k = 9.78 - 7065/T$$

for 773–973°K. The comparable rate expression from the work of Koblitz and Schumacher is

$$\log k = 13.3 - 8478/T$$

for 523–543°K. It is difficult to assess the source of this discrepancy. We had the advantages of continuous analysis and in coverting a wider temperature range; on the other hand, Koblitz and Schumacher were able to work at higher pressures. However, what is significant from the point of departure of this work is that if one equates the activation energy with the first bond dissociation energy, then the radical, OF, should be thermally more stable than OF_2.

We did not detect the radical OF. Parenthetically, many studies have been carried out in an attempt to observe OF in the gas phase. Since the results have been negative they have not, in general, appeared in the general literature but rather have either been privately communicated or reported in government contract reports.[9-12] Returning to the results of this study, the only species that we observed with certainty are oxygen, fluorine, and oxygen difluoride. In trying to detect OF we used the appearance potential technique and, also, we tried to detect any change in the ratio of the intensities at masses 35 and 54 from the normal ratio for OF_2. Concerning the latter point, an increase in the ratio of the intensities at masses 35 and 54 would indicate the formation of OF.

The inability to observe OF by a variety of techniques means either that OF is so chemically reactive that in the experimental systems used to date it has reacted with probes, wall, etc., or that the decomposition of OF_2 is like that of N_2O_5, OF being the analog of NO_3. In either case, shock tube studies would appear to be of value.

Conclusions

Based upon the results in this study it does not appear that the thermal decomposition kinetics for OF_2 represent a simple unimolecular decomposition reaction. Furthermore, in the absence of definitive data with respect to the bond energies of the first and second oxygen–fluorine bonds, it is considered premature to formulate a plausible mechanism.

Acknowledgment. The aid of Mr. E. R. Allen in reducing the mass spectrometry data is gratefully

(9) T. J. Malone and H. A. McGee, Jr., *J. Phys. Chem.*, 69, 4338 (1955).

(10) A. Arkell, Texaco Inc., private communication.

(11) J. Holmes, Allied Chemical Corp., private communication.

(12) T. D. Nevitt, *et al.*, "The FO Radical and Pressure Reactions of N_2F_2," U. S. Army Research Office (Durham), 1963.

acknowledged. This investigation was supported by the National Aeronautics and Space Administration under Contract No. NASR-183. The mass spectrometer was built in part by support from the Propulsion Research Division, Air Force Office of Scientific Research, under Contract No. AF 49(638)-173.

Solubility and Thermodynamics of Solution of Argon in Water–Methanol System

by A. Ben-Naim[1]

Department of Physical Chemistry, Hebrew University, Jerusalem, Israel *(Received May 26, 1967)*

The solubility of argon in mixtures of water and methanol was measured at several temperatures in the range of 5–25°. The thermodynamic functions of solution $\Delta\mu_s°$, $\Delta\overline{S}_s°$, and $\Delta\overline{H}_s°$ were calculated. An interpretation in terms of structural changes in the system water–methanol is suggested.

Introduction

Recently,[2] the thermodynamic behavior of argon in water–ethanol and water–*p*-dioxane mixtures was studied. This report extends the previous work to include the water–methanol system as a solvent. The main issue of this investigation has been the attempt to account for the anomalously large negative entropy and enthalpy of solution of gases in water. The study of the changes of these quantities when changing continuously the solvent from pure water to pure organic solvent provides some clues to the origin of the anomalous behavior in pure water. In addition, it provides some information on the structural changes in the system water–organic solvent which has some interesting features and deserves investigation in its own right. A review of the properties of the system water–alcohol was recently published by Franks and Ives.[3] At present, no complete theory of aqueous solutions of nonelectrolytes is available. Therefore, a quantitative analysis of the results of this investigation is impossible. However, some characteristic features of the results could be partially interpreted by using a simple "mixture model" for liquid water. Undoubtedly, data of this sort will be needed in the future in order to test proposed theories of aqueous solutions.

Experimental Section and Results

The solubility of argon in water–methanol mixtures was measured over the entire range of concentrations. The solubility measurements (consisting of direct reading of the volume of gas absorbed in a given volume of liquid) were carried out according to a method described elsewhere.[4] Mixtures of different compositions were prepared by weighing. No correction was made for the slight change of composition while outgassing.[2a] The solubility of argon was measured at five temperatures: 5, 10, 15, 20, and 25°. The mean values obtained are given in Figures 1 and 2 in terms of the Ostwald absorption coefficient,[5] defined

(1) Address all correspondence to the author at Bell Telephone Laboratories, Murray Hill, N. J. 07971.

(2) (a) A. Ben-Naim and S. Baer, *Trans. Faraday Soc.*, **60**, 1736 (1964); (b) A. Ben-Naim and G. Moran, *ibid.*, **61**, 821 (1965).

(3) F. Franks and D. J. G. Ives, *Quart. Rev.* (London), **20**, 1 (1966).

(4) A. Ben-Naim and S. Baer, *Trans. Faraday Soc.*, **59**, 2735 (1963).

(5) J. H. Hildebrand and R. L. Scott, "The Solubility of Nonelectrolytes," 3rd ed, Reinhold Publishing Corp., New York, N. Y., 1950.

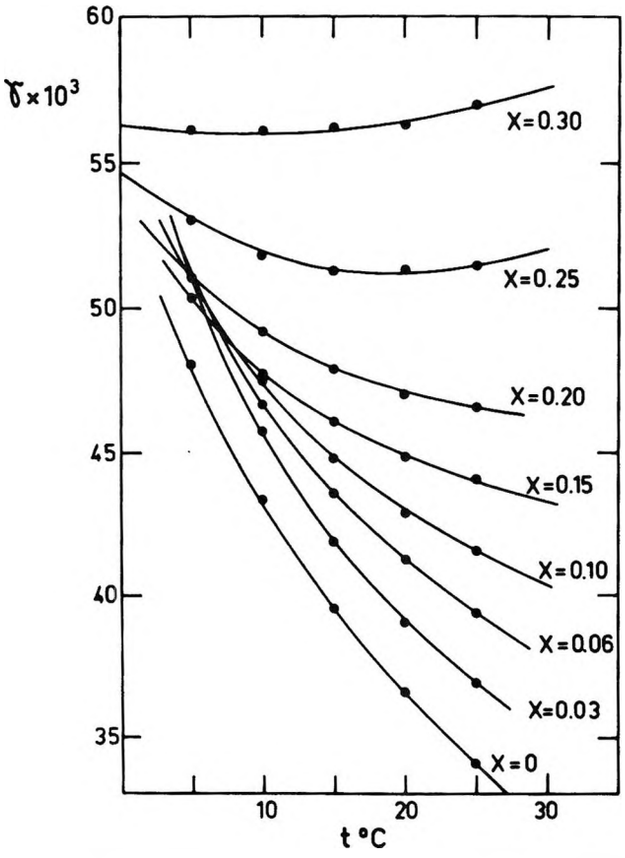

Figure 1. Ostwald coefficients (γ) as a function of temperature for different mixtures of water–methanol ($0 \leq X \leq 0.3$).

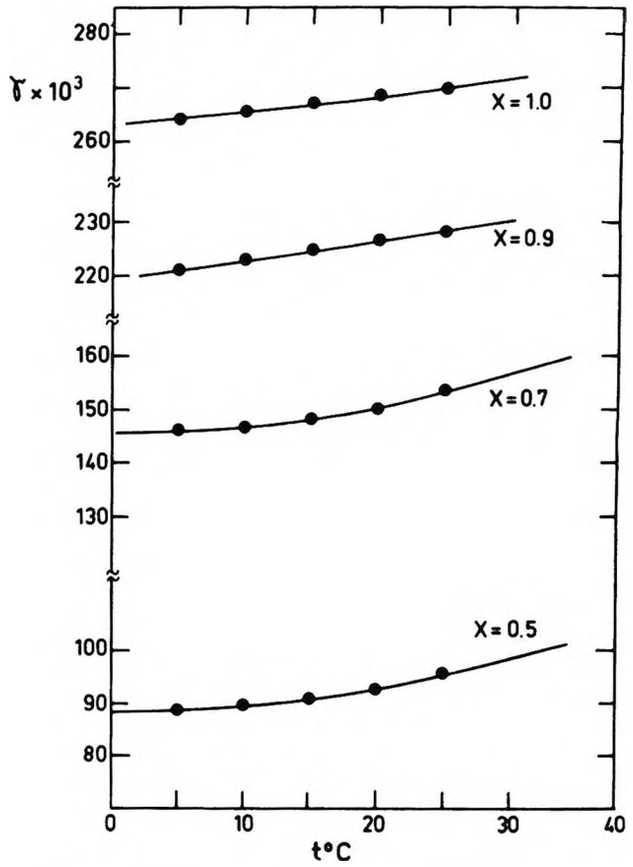

Figure 2. Ostwald coefficients (γ) as a function of temperature for different mixtures of water–methanol ($0.3 \leq X \leq 1$).

by γ = volume of gas at T/volume of liquid at T (at total pressure of 1 atm). Figure 3 shows γ as a function of the mole fraction X of methanol for different temperatures. Regarding the accuracy of the measurements, it is worthwhile to note that the absolute precision decreases for the mixtures of high concentration of methanol. However, the relative error remains nearly constant over the entire range (between 0.2 and 0.25%).

From the temperature dependence of the solubility, the values of $\Delta\mu_s^\circ$, $\Delta\bar{S}_s^\circ$, and $\Delta\bar{H}_s^\circ$ of solution of argon were calculated. The pertinent relations are[6]

$$\Delta\mu_s^\circ = -RT \ln \gamma$$

$$\Delta\bar{S}_s^\circ = R\frac{\partial(T \ln \gamma)}{\partial T} - RT\frac{\partial \ln \rho}{\partial T} - R$$

$$\Delta\bar{H}_s^\circ = \Delta\mu_s^\circ + T\Delta\bar{S}_s^\circ$$

Values of the densities ρ were taken from the International Critical Tables. Values of $\Delta\mu_s^\circ$, $\Delta\bar{S}_s^\circ$, and $\Delta\bar{H}_s^\circ$ are recorded in Figures 4, 5, and 6. These functions refer to the process argon (g) → argon (soln) at equal molar concentration of argon in the two phases. (For more details, see ref 6.)

General Features of the Thermodynamic Functions of Solution of Argon in Some Water and Organic Solvent

We shall summarize some of the salient features of the curves obtained for the various systems. It is obviously impossible to give a full interpretation of all the details; however, a partial interpretation of the major trends can be given based on some previous study of the anomalous behavior of aqueous solutions of noble gases.[6,7]

A. Solubility Curves. Both water–ethanol and water–methanol systems show a maximum and then a minimum at low temperatures. As temperature increases the maxima and minima approach each other forming a curve with an inflection point. At higher temperatures a monotonic increase of solubility is exhibited. The corresponding curves in water and

(6) A. Ben-Naim, *J. Phys. Chem.*, 69, 3240, 3245 (1965).
(7) A. Ben-Naim, *ibid.*, 69, 1922 (1965).

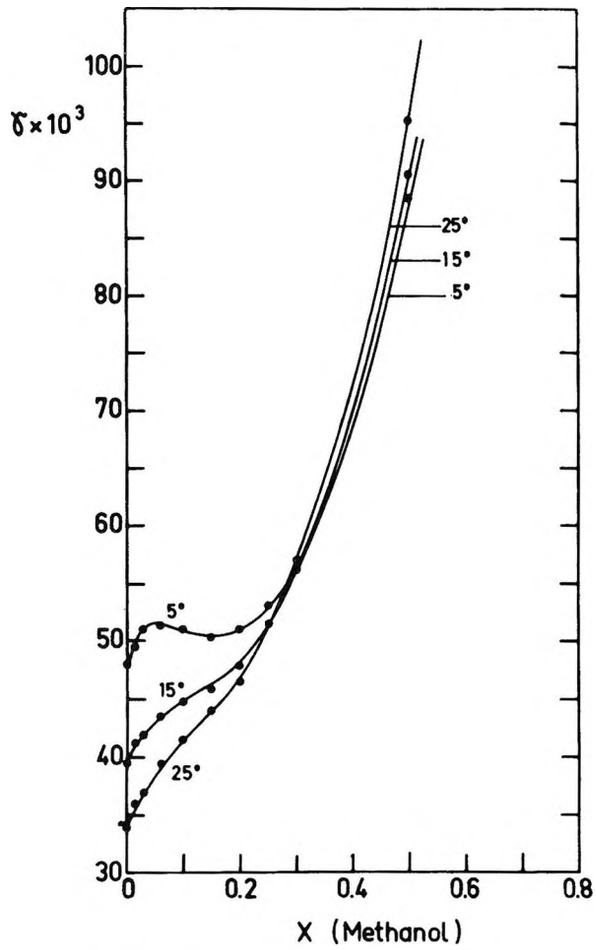

Figure 3. Ostwald coefficients as a function of mole fraction of methanol. At $X \geq 0.5$ the curves of γ as a function of X are almost linear in X, though not demonstrated by this figure.

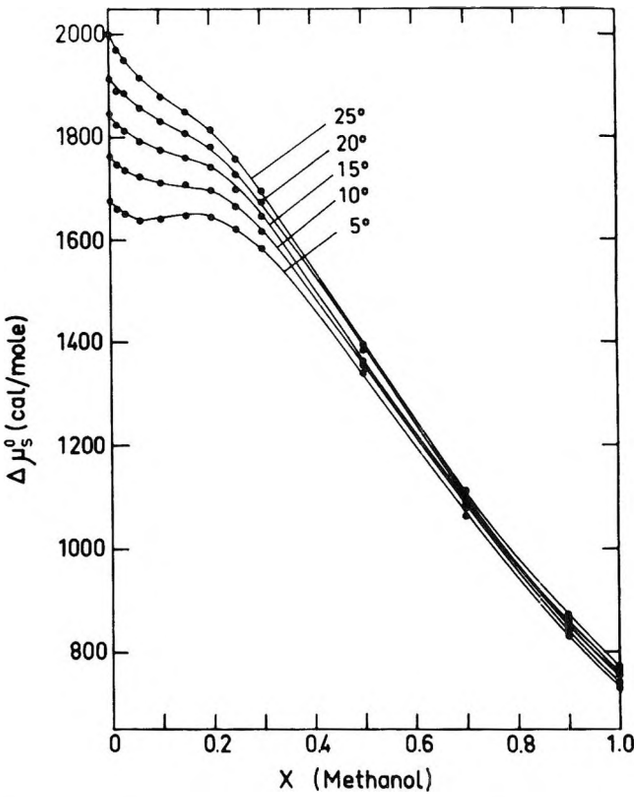

Figure 4. $\Delta\mu_s^\circ$ of solution of argon as a function of mole fraction of methanol at different temperatures.

p-dioxane system show no maxima but only minima. In anticipating the subsequent interpretation, we believe that the main feature of these curves arises from both the effects of argon and of the organic liquid on the structure of water. We also note that these peculiarities of the solubility curves occur approximately between $\gamma \approx 3 \times 10^{-2}$ to 5×10^{-2}; this is only a small portion of the whole solubility range which extends from $\gamma \approx 3 \times 10^{-2}$ to 2.8×10^{-1}.

B. Entropy and Enthalpy of Solution. The $\Delta\overline{H}_s^\circ$ and $\Delta\overline{S}_s^\circ$ curves (Figures 5 and 6) have a common trend for all the systems which have been studied. The fine structure, observed earlier in these curves,[2a] might not have any significance since the relative error of the calculated values is much larger compared to those in the solubility curves. The main feature is a steep increase of $\Delta\overline{H}_s^\circ$ and $\Delta\overline{S}_s^\circ$ in the range of $0 \lesssim X \lesssim 0.25$ followed by a flat, sometimes constant, change in the high concentration range.

Discussion and Interpretation

In the following discussion we shall use the two-structure model for liquid water. This model, although very simple, provides a satisfactory qualitative explanation for the properties of both pure water[8] and aqueous solutions of nonelectrolytes.[6,7] Let n_i and n_p be the number of moles of the icelike form and the monomeric form, respectively, n_s and n_o the number of moles of the gas (s) and the organic solute (o). Following a previous notation,[9,10] the partial molar quantity, $\overline{E}_s$, of the gas (s) is given by

$$\overline{E}_s = \left(\frac{\partial E}{\partial n_s}\right)_{n_w,n_o} = \left(\frac{\partial E}{\partial n_s}\right)_{n_i,n_p,n_o} + \left[\frac{\partial E}{\partial n_i} - \frac{\partial E}{\partial n_p}\right]\left(\frac{\partial n_i}{\partial n_s}\right)_{n_w,n_o} \quad (1)$$

(8) G. Wada, *Bull. Chem. Soc. Japan*, 34, 955 (1961).

(9) Note that whenever the two-structure model is employed for a qualitative discussion, we prefer to use the equilibria $i \rightleftarrows p$ (as in ref 8) rather than the more exact set of reactions $c_n \rightleftarrows np$ (as in ref 6 and 7). The use of the latter is inevitable when one wants to include effects which depend on the surface of the cluster. These two points of view were also discussed by Frank.[10]

(10) H. S. Frank, *Federation Proc.*, 24 (III), 51 (1965).

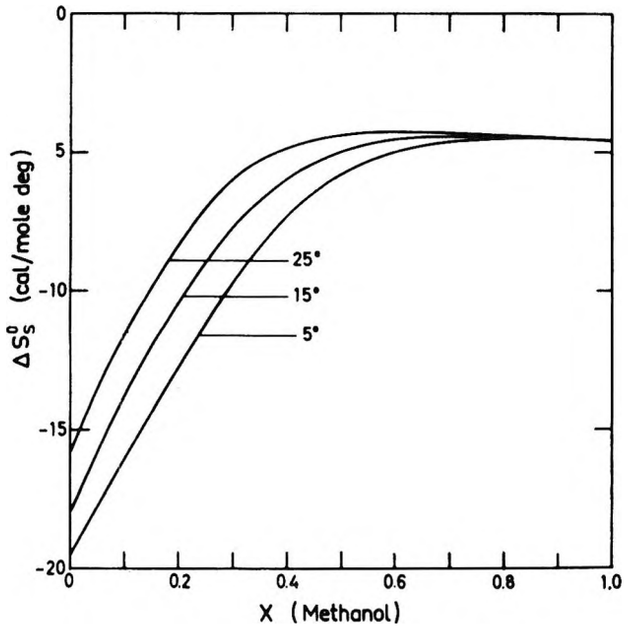

Figure 5. $\Delta\bar{S}_s°$ of solution of argon as a function of mole fraction of methanol at different temperatures.

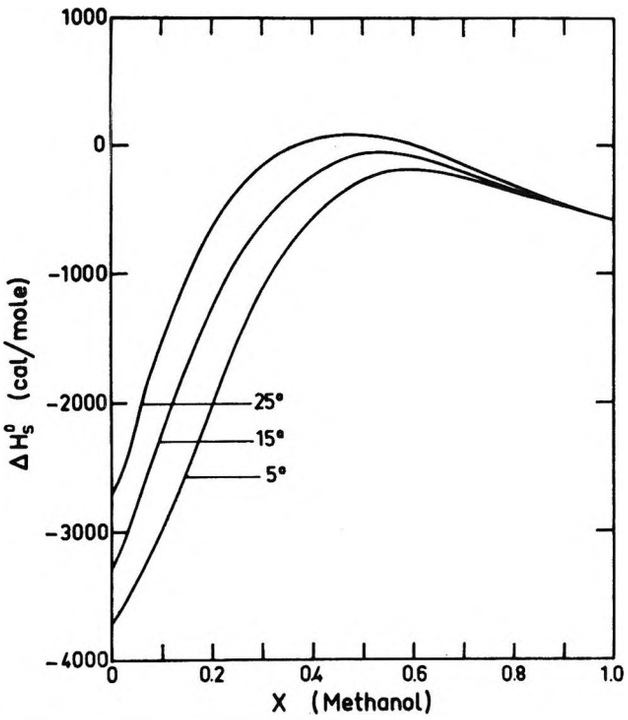

Figure 6. $\Delta\bar{H}_s°$ of solution of argon as a function of mole fraction of methanol at different temperatures.

where n_w is the total number of moles of water, *i.e.*, $n_w = n_i + n_p$. (The temperature and pressure are also assumed to be constant, but are omitted from the notation.) We also denote by

$$E_s^* = \left(\frac{\partial E}{\partial n_s}\right)_{n_i,n_p,n_o}, \quad \Delta\bar{E}_s^r = (\bar{E}_i - \bar{E}_p)\left(\frac{\partial n_i}{\partial n_s}\right)_{n_w,n_o}$$

and get

$$\bar{E}_s = E_s^* + \Delta E_s^r \tag{2}$$

We shall first proceed to interpret the $\Delta\bar{H}_s°$ and $\Delta\bar{S}_s°$ curves (Figures 5 and 6). If water were a normal liquid, we should expect that when mixing it with a second normal liquid, the properties of the system will change smoothly as a function of the mole fraction of one of the components. In particular, let us fix our attention on the partial molar enthalpy, $\bar{H}_s$, of an inert gas s in this system. $\bar{H}_s$ depends mainly on the interaction of s with its immediate surroundings. As we change continuously the composition of the solvent mixtures, we should expect a smooth change in $\bar{H}_s$ too. The experimental observation is different. The steep increase of $\Delta\bar{H}_s°$ in the range of $X \lesssim 0.2$ and then an abrupt change to a slowly varying function of X strongly suggests that there exists at least one more property of the water–organic liquid system that changes steeply in the low-concentration range, while remaining nearly constant for the rest of the concentration range. This property should be responsible, at least for the major part, for the anomalously low negative values of $\Delta\bar{H}_s°$ and $\Delta\bar{S}_s°$ of solution of noble gases in water. This argument led us recently[7] to suggest that this peculiar feature is the existence of large compact clusters of water molecules linked by hydrogen bonds. Some theoretical consideration of a very simplified model for liquid water shows that if one assumes the existence of large compact clusters of water molecules, a stabilization effect[7] of noble gases on the structure of water is expected under some circumstances. Moreover, the examination of that model shows that this effect is proportional to the average cluster size. We expect that a similar dependence on the cluster's size will be valid in real water too. If we accept this explanation, we can immediately extend it to water–organic liquid mixtures, to obtain a plausible explanation to the $\Delta\bar{H}_s°$ and $\Delta\bar{S}_s°$ curves. We write $\Delta\bar{H}_s°$ of solution in the form[6]

$$\Delta\bar{H}_s° = \Delta H_s^* + \Delta H_s^r$$

(ΔH_s^* is the standard enthalpy of solution in a hypothetical system in which the equilibrium i $\rightleftarrows$ p is "frozen in.") Now, H_s^* depends mainly on the total interaction energy between s and its surroundings. In a dilute solution with respect to s, we expect that the interaction of s with a water molecule is almost the same whether the water molecule is a monomeric

one or part of a large cluster. Thus we expect that addition of alcohol to the system will change H_s^* gradually from its value in pure water to that in pure alcohol. The same argument holds for ΔH_s^*. The quantity, ΔH_s^r, on the other hand, is strongly dependent on the average cluster size. Addition of organic liquid to water will cause a steep decrease of the average cluster size;[11] as a result of that the stabilization effect will decrease steeply in the range $0 \lesssim X \lesssim 0.2$. At about $X \approx 0.2$ we expect that large clusters of water molecules do not exist any more (although small ones probably exist) and as far as these quantities are concerned, the gas molecule "sees" a normal liquid for the remaining range of concentration. We have been discussing mainly the partial molar enthalpy of solution since $\bar{H}_s$ and $\bar{H}_s^\circ$ are almost identical. For the entropy, however, one has to include the ideal mixing term in the discussion. Nevertheless, as far as the relaxation part of $\bar{S}_s$ and $\bar{H}_s$ are concerned, the relation[6,7] $T\Delta S_s^r = \Delta H_s^r$ assures that the same composition dependence will be expected from both ΔS_s^r and ΔH_s^r.

Next we shall look at the solubility curves (as a function of X). The arguments presented in the beginning of this section apply equally well to this case; namely, that there exists at least one more feature in the system water–organic liquid which is responsible for the occurrence of the maxima and the minima. Now instead of dealing directly with the changes of the solubility, we found it more feasible to handle the changes of the chemical potential μ_s at the saturation point with respect to a gas phase containing s. Changes of μ_s at this state will reflect the change in solubility. Let us look at the following process, which although not exactly the one actually carried out in the measurements, is simple enough to describe thermodynamically. It is also useful since it clearly demonstrates how the mutual effects of s and o on the structure of water give rise to some peculiar features of the solubility curves. We start with a system described by (n_i, n_p, n_s, n_o) in equilibrium with a gas phase and add dn_o moles of organic liquid keeping n_s and n_w constant. The variation of μ_s in the liquid phase will be

$$(d\mu)_{n_s,n_w} = \left(\frac{\partial \mu_s}{\partial n_o}\right)_{n_i,n_p,n_s} dn_o + \left(\frac{\partial \mu_s}{\partial n_i}\right)_{n_p,n_s,n_o} dn_i + \left(\frac{\partial \mu_s}{\partial n_p}\right)_{n_i,n_s,n_o} dn_p \quad (3)$$

Rearranging and using the relation $dn_i + dn_p = 0$, we get

$$\left(\frac{\partial \mu_s}{\partial n_o}\right)_{n_s,n_w} = \left(\frac{\partial \mu_s}{\partial n_o}\right)_{n_i,n_p,n_s} + \left(\frac{\partial \Delta\mu}{\partial n_s}\right)_{n_i,n_p}\left(\frac{\partial n_i}{\partial n_o}\right)_{n_s,n_w} \quad (4)$$

where $\Delta\mu = \mu_i - \mu_p$. The first term on the right-hand side of eq 4 is the change of μ_s due to the addition of dn_o in a "frozen" system, the second term exhibits the mutual effect of o and s on the structure of water. We can write eq 4 in a more symmetrical way by using the identity[7]

$$0 = \left(\frac{\partial \Delta\mu}{\partial n_s}\right)_{n_o,n_w} = \left(\frac{\partial \Delta\mu}{\partial n_s}\right)_{n_i,n_p\,n_o} + (\mu_{ii} - 2\mu_{ip} + \mu_{pp})\left(\frac{\partial n_i}{\partial n_s}\right)_{n_o,n_w} \quad (5)$$

where $\mu_{\alpha\beta} = \partial\mu_\alpha/\partial n_\beta$. Substituting from eq 5 into eq 4 we get

$$\left(\frac{\partial \mu_s}{\partial n_o}\right)_{n_s,n_o} = \left(\frac{\partial \mu_s}{\partial n_o}\right)_{n_i,n_p,n_s} - (\mu_{ii} - 2\mu_{ip} + \mu_{pp})\left(\frac{\partial n_i}{\partial n_s}\right)_{n_o,n_w}\left(\frac{\partial n_i}{\partial n_o}\right)_{n_s,n_w} \quad (6)$$

since $(\mu_{ii} - 2\mu_{ip} + \mu_{pp}) > 0$, we see that the product of $(\partial n_i/\partial n_s)_{n_o,n_w}$ and $(\partial n_i/\partial n_o)_{n_s,n_w}$ determines the sign of the second term on the right-hand side of eq 6. $(\partial\mu_s/\partial n_o)_{n_s,n_w}$ and $(\partial\mu_s/\partial n_o)_{n_i,n_p,n_s}$ should be negative as required by the stability condition; however, their difference changes sign according to the different effects of o and s on the structure of water. We now suggest that the difference between these two slopes imposes a division of the composition range into three parts. For $X \lesssim 0.03$ both the gas s and the alcohol o stabilize the structure of water; *i.e.*, the product $(\partial n_i/\partial n_s)_{n_o,n_w}(\partial n_i/\partial n_o)_{n_s,n_w}$ is positive and thus the second term on the right-hand side of eq 6 gives a negative superimposed slope to $(\partial\mu_s/\partial n_o)_{n_i,n_p,n_s}$. In the range $0.03 \lesssim X \lesssim 0.2$ the gas molecules still stabilize the structure of water (*i.e.*, $\partial n_i/\partial n_s > 0$) while the alcohol destabilizes it (*i.e.*, $\partial n_i/\partial n_o < 0$), thus giving a positive superimposed slope to $(\partial\mu_s/\partial n_o)_{n_i,n_p,n_s}$. At $X \gtrsim 0.2$ both solutes destabilize the structure of water, since the clusters are now smaller than the critical size required for the existence of a stabilizing effect. This will again give a negative contribution to the right-hand side of eq 6. These arguments apply to the systems water–methanol and water–ethanol. In the system water–*p*-dioxane (and also for water–ethylene glycol[12]) the organic

(11) Apart from a possible stabilization by alcohol which might occur for very low concentration. This might produce a fine structure to the $\Delta\bar{H}_s^\circ$ and $\Delta\bar{S}_s^\circ$ curves; however, their interpretation would be very uncertain because of the large relative inaccuracy in their measurements.

solvent is supposed to destabilize the structure of water from the very beginning; thus the first region does not exist in this case. These systems will therefore show only a minimum and not a maximum in the solubility curve. As a conclusion to the above discussion, it will be fair to say that the two-structure model for water, in spite of its great simplicity, is capable of providing some qualitative explanation to the major trends observed in this work. Obviously, the interpretation suggested above does not give any sound support for the model used. This is a matter which is still under controversy. The most we can say at present is that the assumption of a mixture model for liquid water is not inconsistent with the observations.

Acknowledgment. The assistance of Mr. A. Ben-Shaul is gratefully acknowledged.

(12) A. Ben-Naim, unpublished results.

Configurational Properties of Poly(ethylene oxide) and Poly(tetramethylene oxide)[1]

by K. Bak,[2a] G. Elefante, and J. E. Mark[2b]

The Department of Chemistry, The Polytechnic Institute of Brooklyn, Brooklyn, New York 11201
(Received May 29, 1967)

Mean-square dipole moments of poly(ethylene oxide) and poly(tetramethylene oxide) chains from 20 to 60° have been determined from dielectric constant measurements on dilute solutions of the polymers in benzene. These moments and their temperature coefficients are in good agreement with values predicted using rotational isomeric state models for these chain molecules. In addition, the temperature dependence of the unperturbed dimensions of the poly(tetramethylene oxide) chain has been determined from force–temperature measurements on cross-linked networks; again, good agreement between theory and experiment is obtained.

Introduction

The family of polyoxides of repeat unit $-[(CH_2)_mO]-$ are ideally suited for studies of the effect of structure on statistical properties of chain molecules. The relatively simple, regular chemical structure of these polymers makes their representation by the well-known rotational isomeric state model[3,4] straightforward. In addition, the availability and low melting point of several members of the series[5] make their detailed experimental study quite feasible.

Studies of chain dimensions have been carried out for several polyoxides of high degrees of polymerization x: poly(oxymethylene), $-[CH_2O]-_x$;[6-8] poly(ethylene oxide), $-[(CH_2)_2O]-_x$;[9-10] poly(trimethylene oxide), $-[(CH_2)_3-$

(1) Presented at the 154th National Meeting of the American Chemical Society, Chicago, Ill., Sept 1967.

(2) (a) On leave of absence from Chemistry Department A, The Technical University of Denmark, Lyngby, Denmark; (b) to whom correspondence should be addressed at the Department of Chemistry, The University of Michigan, Ann Arbor, Mich.

(3) S. Mizushima, "Structure of Molecules and Internal Rotation," Academic Press Inc., New York, N. Y., 1954.

(4) M. V. Volkenstein, "Configurational Statistics of Polymeric Chains," Interscience Publishers, Inc., New York, N. Y., 1963.

(5) H. Tadokoro in "Macromolecular Reviews," Vol. 1, Interscience Publishers Inc., New York, N. Y., 1967.

O]$_x$;[11,12] and poly(tetramethylene oxide), $-[(CH_2)_4$-O]$_x$.[13,14] In addition, investigations of electric dipole moments have been reported for oligomers of oxymethylene,[15] oligomers and polymers of ethylene oxide,[16-21] and polymers of tetramethylene oxide.[14,22] In two of these studies,[14,21] rotational isomeric state calculations employing results obtained for these molecules and also for the limiting case of polyethylene[23] were used to predict several unmeasured properties of such chains. Specifically, values of the following quantities in the limit of long chain length were predicted: (i) the temperature dependence of the dipole moment of the poly(ethylene oxide) chain,[21] (ii) the dipole moment and its temperature dependence for poly(tetramethylene oxide),[14] and (iii) the temperature coefficient of the unperturbed dimensions[24] $\langle r^2\rangle_0$ of the poly(tetramethylene oxide) chain.[14]

It is the purpose of this study to obtain experimental values of the above quantities, and to use them to evaluate the rotational isomeric state representation of these polymers.

Experimental Section

Polymer Fractions. A sample[25] of poly(ethylene oxide) having a molecular weight of approximately 4×10^3 was fractionated by lowering the temperature of a solution of the polymer in a mixture of benzene and *n*-hexane. The first fraction, obtained at 55°, was discarded. The second fraction, obtained at 50° and consisting of approximately 10% of the original weight of polymer, was used in this study. Purification of this material consisted of precipitation from the benzene–hexane mixture into 2-propanol and drying under vacuum at 35°. Its intrinsic viscosity in water at 25° was found to be 0.127 dl g^{-1}; this corresponds to a molecular weight of 4.26×10^3 (average degree of polymerization $\bar{x} = 97.8$) on the basis of the Mark–Houwink relationship for this system.[26]

A fraction of poly(tetramethylene oxide) was obtained by isothermally adding *n*-hexane to a solution of the polymer[27] in benzene at 60°. The fraction chosen for the dielectric studies constituted approximately 10% of the unfractionated material. Its molecular weight, calculated from its intrinsic viscosity, 3.00 dl g^{-1}, in benzene at 30° and the appropriate Mark–Houwink relationship,[13] is 4.08×10^5 ($\bar{x} = 5.36 \times 10^3$).

Purification of Solvents. Chromatographic grade (Fisher, 99 mole % pure) cyclohexane and benzene were dried by repeated passage through a Linde Type 4A molecular sieve. Di-*n*-butyl ether was purified by two consecutive distillations and was stored over sodium in the absence of light, as suggested by Mecke and Specht.[28]

Dielectric Constants and Indices of Refraction. A DM01 dipole meter[29] operating at a fixed frequency of approximately 2.0 Mcps and a cylindrical, gold-plated, thermostated cell were used for all dielectric determinations. The instrument was calibrated at each temperature of measurement using solvents purified as described in the preceding section and established values of their dielectric constants. Values used for 20° were: benzene, 2.285;[30] cyclohexane, 2.023;[30] and di-*n*-butyl ether, 3.083.[28] Separate solutions of the polymers in benzene, made up by weight, were used for each of five concentrations.

Indices of refraction were measured using a Zeiss dipping refractometer. The same solutions were used for both the dielectric and refractometric measurements.

Preparation of Cross-Linked Networks. Dicumyl

(6) P. J. Flory and J. E. Mark, *Makromol. Chem.*, 75, 11 (1964).

(7) V. Kokle and F. W. Billmeyer, Jr., *J. Polymer Sci.*, B3, 47 (1965).

(8) W. H. Stockmayer and L.-L. Chan, *ibid.*, A2, 4, 437 (1966).

(9) F. E. Bailey, Jr., and R. W. Callard, *J. Appl. Polymer Sci.*, 1, 56 (1959); F. E. Bailey, Jr., J. L. Kucera, and L. G. Inhof, *J. Polymer Sci.*, 32, 517 (1958.

(10) J. E. Mark and P. J. Flory, *J. Am. Chem. Soc.*, 87, 1415 (1965).

(11) K. Yamamoto, A. Teramoto, and H. Fujita, *Polymer*, 7, 267 (1966).

(12) J. E. Mark, *J. Polymer Sci.*, B4, 825 (1966).

(13) M. Kurata, H. Utiyama, and K. Kamada, Makromol. *Chem.*, 88, 281 (1965).

(14) J. E. Mark, *J. Am. Chem. Soc.*, 88, 3708 (1966).

(15) T. Uchida, Y. Kurita, and M. Kubo, *J. Polymer Sci.*, 19, 365 (1956).

(16) W. J. Svirbely and J. J. Lander, *J. Am. Chem. Soc.*, 67, 2189 (1945).

(17) J. Marchal and H. Benoit, *J. Chim. Phys.*, 52, 818 (1955); *J. Polymer Sci.*, 23, 223 (1957).

(18) T. Uchida, Y. Kurita, N. Koizumi, and M. Kubo, *ibid.*, 21, 313 (1956).

(19) C. Rossi and V. Magnasco, *ibid.*, 58, 977 (1962).

(20) A. Kotera, K. Suzuki, K. Matsumura, T. Nakano, T. Oyama, and U. Kambayashi, *Bull. Chem. Soc. Japan*, 35, 797 (1962).

(21) J. E. Mark and P. J. Flory, *J. Am. Chem. Soc.*, 88, 3702 (1966).

(22) R. E. Wetton and G. Williams, *Trans. Faraday Soc.*, 61, 2132 (1965).

(23) A. Abe, R. L. Jernigan, and P. J. Flory, *J. Am. Chem. Soc.*, 88, 631 (1965), and references given therein.

(24) P. J. Flory, "Principles of Polymer Chemistry," Cornell University Press, Ithaca, N. Y., 1953.

(25) Carbowax 4000, provided by the Union Carbide Corp.

(26) W. Ring, H.-J. Cantow, and W. Holtrup, *European Polymer J.*, 2, 151 (1966).

(27) Samples were supplied by Prof. H. Tadokoro of Osaka University, Dr. G. S. Trick of the Goodyear Tire and Rubber Co., and Dr. P. Dreyfuss of the B. F. Goodrich Co.

(28) R. Mecke and H. Specht, *Z. Elektrochem.*, 62, 500 (1958).

(29) Wissenschaftlich-Technische Werkstätten, GMBH, Weilheim Oberbayern, Germany. Available in this country from the Kahl Scientific Instrument Co., El Cajon, Calif.

(30) W. M. Heston, Jr., and C. P. Smyth, *J. Am. Chem. Soc.*, 72, 99 (1950).

peroxide and sulfur were dispersed in a concentrated solution of unfractionated, high molecular weight poly(tetramethylene oxide)[27] in benzene. A dried sheet of this material was kept under vacuum at 70° for 3 days to assure the absence of oxygen, and was then cured at 150° under nitrogen for 3 hr. Soluble constituents, extracted with benzene at 70°, amounted to from 7 to 9% of the vulcanizate. An inhibitor to reduce oxidative degradation of the network was introduced by swelling the samples in a benzene solution of N-phenyl-β-naphthylamine.

Sample 1 was prepared using dicumyl peroxide amounting to 6%, and sulfur 0.6%, of the weight of polymer. Since the resulting network was rather highly cross-linked, the remaining samples (2–5) were prepared using a lower peroxide content, 4%.

Force–Temperature Measurements. The stress–strain apparatus employed has been described in detail elsewhere.[31] Forces exhibited by the poly(tetramethylene oxide) networks in the amorphous state, at constant length in a nitrogen atmosphere, were determined over the range 60–100°. Lower temperatures were unsuitable because of the possibility of crystallization;[32] higher temperatures introduced the problem of instability due to chain scission. Forces were recorded when they became sensibly constant, up to 3 days being required in some cases.

The cubical thermal expansion coefficient β of the networks over the temperature range studied was found by dilatometry to be 0.73×10^{-3} deg^{-1}.

Results and Discussion

Dipole Moments and Their Temperature Coefficient. Mean-square dipole moments $\langle\mu^2\rangle$ were calculated using the method of Guggenheim[33] and Smith[34] which results in the equation

$$\langle\mu^2\rangle = \left[\frac{27kTM}{4\pi N d_1(\epsilon_1 + 2)^2}\right]\left[\frac{\mathrm{d}(\epsilon - \epsilon_1)}{\mathrm{d}w} - \frac{\mathrm{d}(n^2 - n_1^2)}{\mathrm{d}w}\right] \quad (1)$$

where k is the Boltzmann constant, N the Avogadro number, T the absolute temperature, d_1 the density of the solvent, M the molecular weight of the polymer, ϵ and ϵ_1 the dielectric constants of solution and solvent, respectively, w the weight fraction of polymer, and n and n_1 the indices of refraction of solution and solvent, respectively. In Figure 1, the quantitites $(\epsilon - \epsilon_1)$ and $(n^2 - n_1^2)$ are shown as a function of w for poly(ethylene oxide); slopes in the limit[33] $w \to 0$ required in eq 1 were obtained directly from such plots and are given in Table I. Data at 30, 40, and 50° were omitted from Figure 1 for clarity; similar results at all temperatures were obtained for poly(tetramethylene oxide).

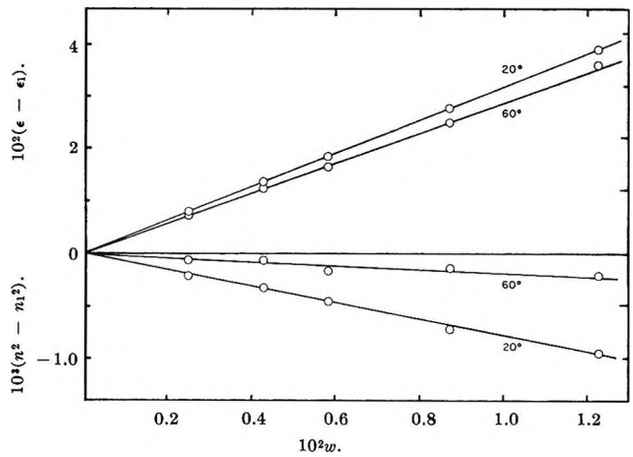

Figure 1. The quantities $(\epsilon - \epsilon_1)$ and $(n^2 - n_1^2)$ plotted against the weight fraction of polymer, for poly(ethylene oxide) in benzene.

Dipole moments thus calculated were expressed in Debyes and each value of $\langle\mu^2\rangle$ was divided by nm^2, where n is the number of skeletal bonds in the chain and m^2 is the mean square of the bond moments.[14] Thus, the dipole moment ratio $\langle\mu^2\rangle/nm^2$ represents the observed mean-square moment of the chain relative to the mean-square moment of the same chain in the idealization that the skeletal bonds are freely jointed. Values of this ratio for poly(ethylene oxide) and poly(tetramethylene oxide) over the range 20–60° are given in Table I. The quantity $\ln \langle\mu^2\rangle/nm^2$ is plotted against temperature in Figure 2; the lines shown have been drawn according to the method of least squares. The value $\langle\mu^2\rangle/nm^2 = 0.62$ for poly(ethylene oxide) at 20° is in agreement with the range 0.57 to 0.59[21] found in other studies of this polymer.[16,17,19] The temperature coefficient $\mathrm{d} \ln \langle\mu^2\rangle/\mathrm{d}T$, estimated from the upper line in Figure 2, was found to have the value 2.6×10^{-3} deg^{-1}.

Rotational isomeric state theory has given a remarkably consistent interpretation of the unperturbed dimensions and their temperature coefficient for poly(ethylene oxide)[10] and dipole moments and their temperature dependence for ethylene oxide chains of any length.[21] This model predicts $\mathrm{d} \ln \langle\mu^2\rangle/\mathrm{d}T = 2.5 \times 10^{-3}$ deg^{-1} for ethylene oxide chains at 25° in the limit of long chain length.[21] (The marked increase in $\langle\mu^2\rangle$ with increasing temperature results primarily from

(31) J. E. Mark and P. J. Flory, *J. Am. Chem. Soc.*, **86**, 138 (1964).

(32) On the basis of differential thermal analysis, these samples have melting points in the vicinity of 40°.

(33) E. A. Guggenheim, *Trans. Faraday Soc.*, **45**, 714 (1949); *ibid.*, **47**, 573 (1951).

(34) J. W. Smith, *ibid.*, **46**, 394 (1950).

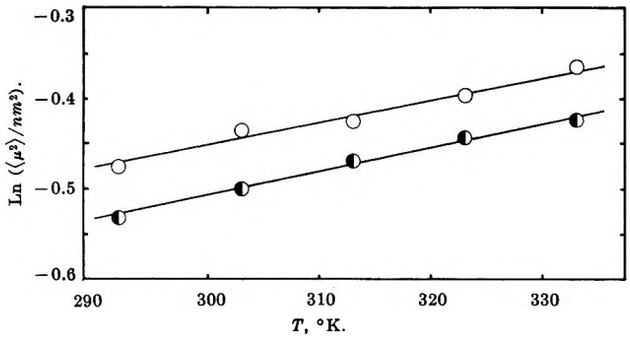

Figure 2. Dependence of the logarithm of the dipole moment ratio on temperature. Open circles refer to poly(ethylene oxide), half-filled circles to poly(tetramethylene oxide).

Table I: Dielectric Results, Poly(ethylene oxide) and Poly(tetramethylene oxide)

	20°	30°	40°	50°	60°
	Poly(ethylene oxide)				
$d(\epsilon - \epsilon_1)/dw$	3.13	3.10	2.97	2.92	2.87
$d(n^2 - n_1^2)/dw$	−0.08	−0.06	−0.05	−0.04	−0.02
$\langle\mu^2\rangle/nm^2$	0.621	0.646	0.653	0.672	0.693
	Poly(tetramethylene oxide)				
$d(\epsilon - \epsilon_1)/dw$	1.70	1.68	1.66	1.64	1.61
$d(n^2 - n_1^2)/dw$	−0.11	−0.09	−0.07	−0.04	−0.02
$\langle\mu^2\rangle/nm^2$	0.586	0.606	0.625	0.640	0.654

trans to *gauche* transitions about CH_2–O and O–CH_2 skeletal bonds.[21] Such transitions are departures from the all-*trans* conformation, for which $\lim_{n\to\infty} \langle\mu^2\rangle/nm^2 = 0$ for any polyoxide $-[(CH_2)_mO]-$ having an even value of m.) The agreement between theory and experiment found here is remarkably good.

For poly(tetramethylene oxide) chains the data yield $\langle\mu^2\rangle/nm^2 = 0.59$ at 20°, and $d \ln \langle\mu^2\rangle/dT = 2.7 \times 10^{-3}$ deg^{-1}. These quantities could not be predicted with certainty using rotational isomeric state theory since the energy of one important interaction occurring in this chain, that between an oxygen atom and the methylene groups separated from it by three skeletal bonds, is not known. Use of a rough estimate of this energy obtained by comparison of this interaction with a similar interaction[6] occurring in the poly(oxymethylene) chain yields, however, $\langle\mu^2\rangle/nm^2 = 0.5$ to 0.6 and $d \ln \langle\mu^2\rangle/dT = 1.0$–$1.5 \times 10^{-3}$ deg^{-1}.[14] (The large, positive temperature coefficient predicted for $\langle\mu^2\rangle$ results primarily from the occurrence of *trans* to *gauche* transitions about C–O, O–C, and one of the C–C bonds in the repeat unit as the temperature is increased.[14]) The experimental value of the ratio is in excellent agreement with this prediction, and also with a preliminary experimental result $\langle\mu^2\rangle/nm^2 = 0.53$ to 0.64[14,22] for poly(tetramethylene oxide) chains in the amorphous, undiluted state. Approximate agreement is also obtained between experimental and predicted values of $d \ln \langle\mu^2\rangle/dT$; detailed correlation of theory with experiment would, however, more properly await experimental determinations of both $\langle\mu^2\rangle/nm^2$ and $d \ln \langle\mu^2\rangle/dT$ as a function of chain length.

The Temperature Coefficient of the Unperturbed Dimensions. Forces exhibited by the poly(tetramethylene oxide) networks on temperature increasing and temperature decreasing portions of a cycle agreed within 1%. They were expressed in dynes per square centimeter of undistorted cross section at the highest temperature of measurement for that sample, and are plotted as a function of temperature in Figure 3. The method of least squares was used to locate the lines shown. Each line is labeled with the elongation ratio $\alpha = L/L_i$ at the highest temperature, where L and L_i are the distorted and undistorted lengths of the sample, respectively. The force f at the mean temperature T, the slope $(\partial f/\partial T)_{p,L}$ obtained from Figure 3, and the coefficient $[\partial \ln (f/T)/\partial T]_{p,L}$ calculated from these two quantities are listed in columns 3, 4, and 5 of Table II.

Table II: Force–Temperature Results, Poly(tetramethylene oxide)

Sample	α	$f \times 10^{-6}$, dynes cm^{-2}	$(\partial f/\partial T)_{p,L} \times 10^{-4}$	$[\partial \ln (f/T)/\partial T]_{p,L} \times 10^{3}$	$\beta(\alpha^3 - 1)^{-1}, \times 10^{3}$	$-f_e/f$	$-d \ln \langle r^2\rangle_0/dT \times 10^{3}$
1	1.359	4.62	1.52	0.46	0.50	0.34	0.96
2	1.383	3.50	1.30	0.92	0.45	0.49	1.37
3	1.388	3.68	1.35	0.98	0.44	0.50	1.42
4	1.391	3.54	1.40	1.01	0.44	0.52	1.45
5	1.424	3.58	1.42	1.08	0.39	0.51	1.47
					av	0.47	1.33
						±0.05	±0.15

The temperature coefficient $d \ln \langle r^2\rangle_0/dT$ of the unperturbed chain dimensions may be calculated from the first of two relationships given by the molecular theory of rubber elasticity of gaussian networks[35,36]

$$\frac{d \ln \langle r^2\rangle_0}{dT} = -\left[\frac{\partial \ln (f/T)}{\partial T}\right]_{p,L} - \frac{\beta}{\alpha^3 - 1} = \frac{f_e}{fT} \quad (2)$$

(35) A. Ciferri, C. A. J. Hoeve, and P. J. Flory, *J. Am. Chem. Soc.*, **83**, 1015 (1961).

(36) P. J. Flory, A. Ciferri, and C. A. J. Hoeve, *J. Polymer Sci.*, **45**, 235 (1960); P. J. Flory, *Trans. Faraday Soc.*, **57**, 829 (1961).

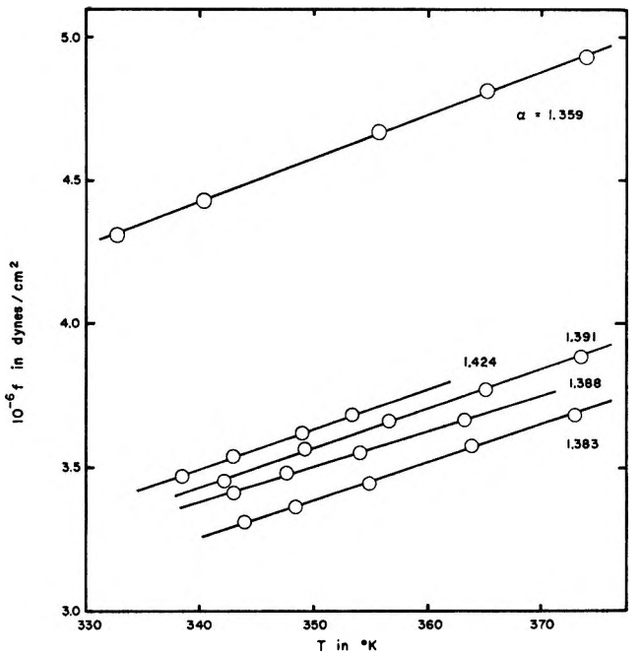

Figure 3. Force *vs.* temperature at constant length for poly(tetramethylene oxide) networks. Values of the extension ratio at the highest temperature of measurement are indicated.

The quantity $f_e = (\partial E/\partial L)_{V,T}$ is the internal energy component of the total force f, and thus f_e/f serves as a measure of the nonideality of the elastomeric network. Values of f_e/f and d ln $\langle r^2\rangle_0/dT$ calculated from eq 2 are given in columns 7 and 8, respectively, of Table II. The reason for the increase in the temperature coefficient of $\langle r^2\rangle_0$ with increasing α, if significant, is not known. The average value, d ln $\langle r^2\rangle_0/dT = -1.33 \times 10^{-3}$ deg^{-1} in the vicinity of 60°, is in excellent agreement, however, with the range -1.2 to -1.3×10^{-3} deg^{-1} predicted from rotational isomeric state calculations.[14] (The pronounced decrease in $\langle r^2\rangle_0$ with increasing temperature is due primarily to the same *trans* to *gauche* transitions which give rise to a *positive* temperature coefficient of $\langle \mu^2\rangle$. This striking difference results from the fact that $\lim_{n\to\infty} \langle \mu^2\rangle/nm^2 = 0$ but $\lim_{n\to\infty} \langle r^2\rangle_0/nl^2 = \infty$, where l^2 is the mean square bond length, for all the *trans* poly(tetramethylene oxide) chain.[14])

Conclusions

These experimental results show that the rotational isomeric state model for poly(ethylene oxide) and poly(tetramethylene oxide) chains gives a surprisingly good account of several very different properties of these molecules in very dissimilar environments: their dielectric properties in dilute solution and their dimensions in the amorphous, *undiluted* state. These results thus add considerably to the confidence with which such models can be used to predict or interpret statistical properties of chain molecules.

Acknowledgments. It is a pleasure to acknowledge that Dr. G. S. Trick of the Goodyear Tire and Rubber Co. provided very useful information on the preparation of poly(tetramethylene oxide) networks. Financial support to K. B. from Statens teknisk-videnskabelige Fond, Denmark, is also gratefully acknowledged.

Simple Attractive-Disk Monolayer Isotherms with Phase Transitions

by F. Tsien and G. D. Halsey, Jr.

Department of Chemistry, University of Washington, Seattle, Washington 98105 *(Received May 29, 1967)*

Monolayer adsorption isotherms for the model of disks showing repulsion and inverse power attraction are discussed. The van der Waals (mobile) and Fowler (immobile) isotherms are put in compatible form. One adjustable parameter reflects the assignment of the reduced value of the van der Waals parameter a. Solid, liquid, and gaslike phases are identified and critical and triple points are calculated. The theory is applied to the data for krypton on exfoliated graphite, with reasonable success.

1. Introduction

Theoretical treatment for adsorption isotherms has been given in detail both for mobile and localized cases. Stebbins and Halsey[1] treated the phase transitions between the localized and mobile isotherms for hard disks on a structureless surface. We shall consider molecules here as disks with attractive force varying according to an inverse power law. The surface is assumed to be structureless to simplify the treatment.

2. Mobile Monolayers

The two-dimensional analog of the van der Waals equation had been used to represent a mobile monolayer.[2,3] It can be expressed as

$$\left(\phi + \frac{a'N^2}{A^2}\right)(A - Nb) = NkT \qquad (2.1)$$

where ϕ is the spreading pressure, A is the area of the film, N is the number of molecules adsorbed, and a' and b are parameters. b is sometimes referred to as the "co-area" per molecule, in analogy to the co-volume in the van der Waals equation. We shall choose b so that the area occupied by an adatom in the completed monolayer is

$$b = \sqrt{3}/2(r^*)^2 \qquad (2.2)$$

where r^* is the distance between the centers of atoms in closest array.

If the adatom has no permanent dipole, the correction term a' is then the attraction which arises from the London dispersion forces. In calculating a', we assume a uniform radial distribution function outside of $r = r^*$, and zero inside. The molecular interaction will be described on a pairwise basis and in terms of the Sutherland potential

$$u(r) = -\epsilon^*(r^*/r)^6 \qquad (r \geq r^*) \qquad (2.3)$$

$$u(r) = \infty \qquad (r < r^*)$$

We can then calculate a,[4] where $a = a'/kT$

$$a = \frac{1}{2}\int_{r^*}^{\infty} \frac{u(r)}{kT} 2\pi r dr \qquad (2.4)$$

$$= \frac{\pi}{4}\frac{(r^*)^2}{kT}\epsilon^* \qquad (2.5)$$

and

$$\frac{a}{b} = \frac{\pi}{2\sqrt{3}}\frac{\epsilon^*}{kT} \qquad (2.6)$$

We shall, in the following calculations, assume the same temperature dependence, but will express a as

$$\frac{a}{b} = \frac{C}{2T^*} \qquad (2.7)$$

where C is an adjustable parameter, and the reduced temperature

$$T^* = kT/\epsilon^* \qquad (2.8)$$

With this relation for a/b, the two-dimensional equation of state eq 2.1 can be related to the adsorption isotherm

(1) J. P. Stebbins and G. D. Halsey, Jr., *J. Phys. Chem.*, **68**, 3863 (1964).

(2) T. L. Hill, *Advan. Catalysis*, **4**, 211 (1952).

(3) S. Ross and J. P. Olivier, "On Physical Adsorption," Interscience Publishers, Inc., New York, N. Y., 1964.

(4) T. L. Hill, *J. Chem. Phys.*, **14**, 441 (1946).

via the Gibbs adsorption equation which takes the form

$$d\phi = kT\Gamma \, d \ln p \tag{2.9}$$

where p is the gas pressure and Γ is the surface concentration per unit area. Equations 2.1 and 2.9 give us the mobile isotherm

$$\ln p = -\ln k_v + \ln \frac{\theta}{1-\theta} + \frac{\theta}{1-\theta} - \frac{2a}{b}\theta \tag{2.10}$$

or

$$\ln p = -\ln k_v + \ln\left(\frac{\theta}{1-\theta}\right) + \left(\frac{\theta}{1-\theta}\right) - \frac{C}{T^*}\theta \tag{2.11}$$

where θ is the fractional coverage. k_v can be written as

$$k_v = \frac{b}{\Lambda^2} f_\perp [\exp(-\chi/kT)] e^{\mu^0/kt} \tag{2.12}$$

where μ^0 is the standard chemical potential, χ is the minimum energy required to evaporate an adsorbed atom from its lowest energy state in the monolayer, $f_\perp$ is the partition function for motion normal to the surface, and

$$\Lambda = \frac{h}{(2\pi mkT)^{1/2}} \tag{2.13}$$

3. Localized Monolayers

We assume that the sites are fixed and that each adsorbed molecule interacts with its nearest neighbors only. Each lattice site has z nearest neighbor sites. The approximate adsorption isotherm for a random distribution as derived by Fowler and Guggenheim[5] (referred to as the Fowler isotherm from now on), after rearranging and taking $z = 6$ for a triangular close packed two-dimensional lattice, has the form

$$\ln p = -\ln k_F + \ln\left(\frac{\theta}{1-\theta}\right) - \frac{6}{T^*}\theta \tag{3.1}$$

where

$$k_F = f_x f_y f_\perp [\exp(-\chi/kT)] e^{\mu^0/kT} \tag{3.2}$$

and f_x and f_y are the partition function for motion parallel to the surface. Equation 3.1, combined with the Gibbs adsorption equation, yields

$$\frac{\phi A}{NkT} = \frac{1}{\theta} \ln\left(\frac{1}{1-\theta}\right) - \frac{3}{T^*}\theta \tag{3.3}$$

4. Corresponding States

For convenience, we define K as[6]

$$K = k_v/k_F \tag{4.1}$$

which, after cancellation, becomes

$$K = \left(\frac{b}{\Lambda^2}\right) \Big/ f_x f_y \tag{4.2}$$

$$= \frac{b}{\Lambda^2} \Big/ \left[\frac{\exp(-\theta_E/2T)}{1-\exp(-\theta_E/T)}\right]^2 \tag{4.3}$$

where θ_E is the Einstein "characteristic temperature." θ_E will be approximated in the following fashion. The Lennard-Jones (6–12) potential is summed over the nearest neighbors in the hexagonal lattice and then differentiated twice with respect to r. This gives

$$\theta_E = \frac{1}{2\pi}\frac{h}{k}\sqrt{\frac{216\epsilon^*}{m(r^*)^2}} \tag{4.4}$$

$$= \frac{3\sqrt{6}}{\pi}\frac{\epsilon^*}{k}\Lambda^* \tag{4.5}$$

where

$$\Lambda^* = \frac{h}{r^*\sqrt{m\epsilon^*}} \tag{4.6}$$

θ_E values for argon and krypton, calculated by this method, are 46 and 36°K, respectively.[7] These values are close to the ones used by McAlpin and Pierotti,[8] which are 45 and 34°K, respectively. K can now be expressed as

$$K = \frac{\left[\frac{\sqrt{3}\pi T^*}{\Lambda^{*2}}\right]}{\left[\frac{\exp\left(-\frac{3\sqrt{6}\Lambda^*}{2\pi\ T^*}\right)}{1-\exp\left(-\frac{3\sqrt{6}\Lambda^*}{\pi\ T^*}\right)}\right]^2} \tag{4.7}$$

The adsorption isotherms can be expressed in a much simpler form if we define

$$p^* = pk_v \tag{4.8}$$

The mobile isotherm is then

$$\ln p^* = \ln\left(\frac{\theta}{1-\theta}\right) + \frac{\theta}{1-\theta} - \frac{C}{T^*}\theta \tag{4.9}$$

(5) R. H. Fowler and E. A. Guggenheim, "Statistical Thermodynamics," Cambridge University Press, London, 1949.

(6) We have used the same form of definition for K as by Stebbins and Halsey. However, K in their eq 31 and 32 as well as in Figure 4 should be replaced by $1/K$.

(7) Values of ϵ^* and r^* are taken from J. O. Hirschfelder, C. F. Curtiss, and R. B. Bird, "Molecular Theory of Gases and Liquids," John Wiley and Sons, Inc., New York, N. Y., 1954.

(8) J. J. McAlpin and R. A. Pierotti, *J. Chem. Phys.*, **41**, 68 (1964).

and the Fowler isotherm becomes

$$\ln p^* = \ln K + \ln\left(\frac{\theta}{1-\theta}\right) - \frac{6}{T^*}\theta \quad (4.10)$$

5. Classical Case

The classical law of corresponding states is correct when the mass of the molecule is sufficiently large, or when Λ^* is negligibly small. In such a case, we can expand the exponentiation term $e^x \approx 1 + x$ so that $1 - e^{-x} \approx x$. The ratio K can then be approximated as

$$K = \frac{\frac{\sqrt{3}\pi T^*}{\Lambda^{*2}}}{\left[\frac{1}{1 - \exp\left(-\frac{3\sqrt{6}}{\pi}\frac{\Lambda^*}{T^*}\right)}\right]^2} \quad (5.1)$$

after expansion

$$K = \frac{\frac{\sqrt{3}\pi T^*}{\Lambda^{*2}}}{\left(\frac{1}{\frac{3\sqrt{6}}{\pi}\frac{\Lambda^*}{T^*}}\right)^2} \quad (5.2)$$

$$\approx 30/T^* \quad (5.3)$$

so that our classical Fowler isotherm then becomes

$$\ln p^* = \ln 30 - \ln T^* + \ln\left(\frac{\theta}{1-\theta}\right) - \frac{6}{T^*}\theta \quad (5.4)$$

6. Critical Conditions

Much work has been done on the two-dimensional condensation for the mobile isotherms[3] and the Fowler isotherm.[5] Designating the reduced critical temperature by T_c^*

$$T_c^*(\text{mobile}) = \frac{4}{27}C \quad (6.1)$$

$$T_c^*(\text{Fowler}) = 1.5 \quad (6.2)$$

so that for T^* lower than $^4/_{27}\,C$ and 1.5 first-order phase changes occur for both the mobile and Fowler isotherms. Under these conditions, we will show that first-order phase changes occur between the mobile and Fowler isotherms.

7. Phase Transitions

We will refer this section to Figure 1, and the subscripts A, B, C, etc., to the points A, B, C, etc. For the mobile isotherm ABCDEFGH, the criteria for phase transition are satisfied when the two phases have equal pressure, and also when they have equal spreading pressure. Expressed in mathematical form, they are

$$\ln p_B^* = \ln p_G^* \quad (7.1)$$

and

$$\phi_B = \phi_G \quad (7.2)$$

The expression $\phi_B = \phi_G$ is equivalent to saying that the area BDEB is equal to the area EFGE. The spreading pressure can be calculated *via* the Gibbs adsorption equation

$$d\phi = kT\Gamma \, d\ln p \quad (7.3)$$

$$= kT\Gamma \frac{\partial \ln p}{\partial \theta} d\theta \quad (7.4)$$

Integration of eq 7.4 gives

$$\phi = \int_0^\theta kT\Gamma \frac{\partial \ln p}{\partial \theta} d\theta \quad (7.5)$$

when applied to the mobile isotherm

$$\phi_G - \phi_B = \Gamma_\infty kT\left[\frac{1}{1-\theta_G} - \frac{C}{2T^*}\theta_G^2 - \left(\frac{1}{1-\theta_B} - \frac{C}{2T^*}\theta_B^2\right)\right] = 0 \quad (7.6)$$

where Γ_∞ is the maximum surface concentration as the pressure approaches infinity.

The criteria for phase transitions are also satisfied between the mobile and Fowler isotherms. Taking the two hypothetical isotherms ABGH (mobile) and IJKO (Fowler), we will find that at points H and N

$$\ln p_H^* = \ln p_N^* \quad (7.7)$$

and

$$\phi_H = \phi_N \quad (7.8)$$

where, after integration

$$\phi_H = \Gamma_\infty kT\left[\frac{\theta_H}{1-\theta_H} - \frac{C}{2T^*}\theta_H^2\right] \quad (7.9)$$

and

$$\phi_N = \Gamma_\infty kT\left[-\ln(1-\theta_N) - \frac{3}{T^*}\theta_N^2\right] \quad (7.10)$$

At sufficiently low coverage, the stable isotherm is the mobile isotherm, and at extremely high coverage, the stable isotherm is the Fowler isotherm. Therefore, the stable isotherm path must then be ABEGHNO. It can also be shown that, at any given p^*, the stable isotherm path has a lower chemical potential than the other isotherm paths. We shall designate the expanded phase AB, the condensed phase GH, and the ordered phase NO as the two-dimensional gas phase, liquid phase, and solid phase, respectively.

Under certain conditions, when the mobile transition pressure is close to the Fowler transition pressure, there is also a phase transition between the unstable mobile isotherm and the stable Fowler isotherm. Thus the unstable two-dimensional gas–solid transition is represented by the path CM.

When T^* gets sufficiently low, another type of phase transition takes place. The equilibrium between the two isotherms takes place before the mobile transition. The stable isotherm path now follows PQLO which has the lower chemical potential. OL is then the two-dimensional gas–solid transition.

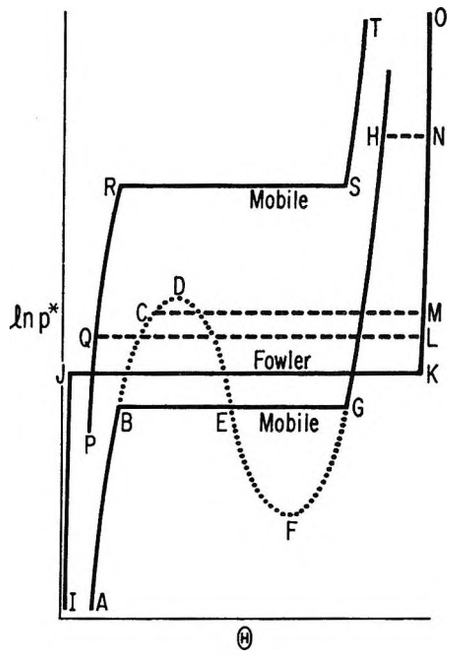

Figure 1. Phase transitions between mobile and Fowler isotherms, indicated by long dotted lines, as explained in text.

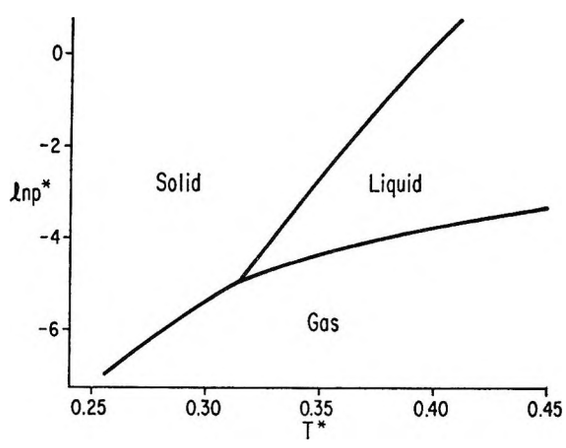

Figure 2. Two-dimensional reduced phase diagram for $C = 4.2$.

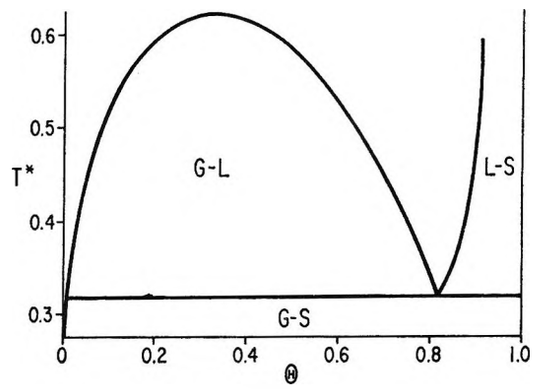

Figure 3. Plot of coverage at which transition occurs as a function of reduced temperature for $C = 4.2$.

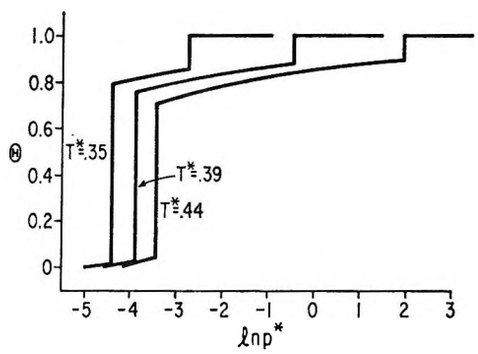

Figure 4. Adsorption isotherm for reduced temperature of 0.35, 0.39, and 0.44. $C = 4.2$.

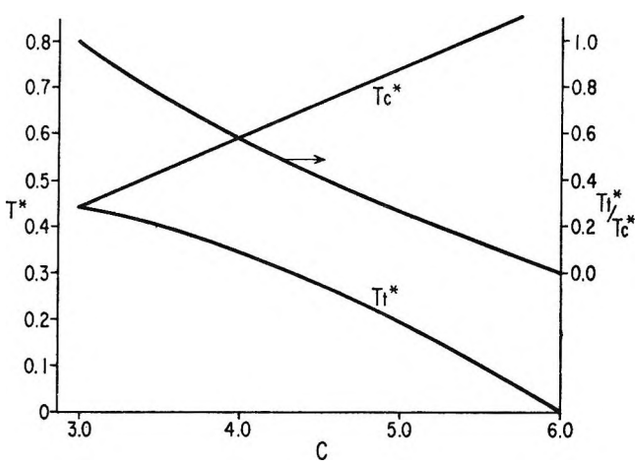

Figure 5. Plot of reduced critical temperature and reduced triple point as a function of C. The ratio of triple point and critical temperature is also shown.

A typical phase diagram is shown for $C = 4.2$ (Figure 2). The corresponding coverage for which the phase transitions occur as a function of reduced temperature is shown in Figure 3. Some typical isotherms

are shown in Figure 4. For analysis of data, however, C is available as an adjustable parameter. It determines the values of the reduced triple point and critical temperatures, and thus the ratio of the unreduced temperatures. To show the dependence on C, T^* of the critical point and of the triple point are plotted as a function of C, in Figure 5. The ratio of the critical temperature to the triple point is also shown.

8. Application to Data for Krypton on Graphite

The recent data of Thomy and Duval[9] resemble the isotherms of Figure 4 and appear to be suitable for analysis. Although these data do not quite reach a two-dimensional triple point at their lowest temperature of 77.4°K, the short vertical riser that appears to correspond to a "solid–liquid" equilibrium is almost on top of the longer "gas–liquid" riser at that temperature. A short extrapolation suggests a triple-point temperature of about 77°K. The observed critical temperature is about 86°K. The ratio of 0.9 (Figure 5) yields a value of $C = 3.2$ These results may be contrasted with the values for bulk krypton where the ratio of triple-point to critical temperature is 0.55 for a value of $C = 4.1$.

From the reduced value of the critical temperature at $C = 3.2$, ϵ^*/k is calculated to be 180°. This result is close to the free gas pair interaction energy of 171°,[7] but rather far from the pair interaction calculated for the case of krypton on a graphite surface (144°).[8]

9. Discussion

Both the mobile and immobile isotherms that are used in this analysis are of the lowest degree of approximation to the exact isotherms, and at least are consistent. The application of a Sutherland potential to the mobile case and a harmonic oscillator model to the solid is not consistent. At high temperature ($T^* = 30$), eq 5.3 predicts a reversal in the stability of the low density mobile film for this reason. This temperature would be of the order of 5000°K for krypton and is thus not physically important.

Reference to Figure 5 indicates that if $C < 3$ no liquid ever forms, and the transition is always from mobile gas to solid, at any value of T^*. There are thus no critical or triple-point temperatures below this value. For $C > 6$, the liquid phase is stable down to $T^* = 0$, and only the critical temperature remains. It should be noted that if we use eq 2.3 to calculate C, a value of 1.8 is obtained. This value is below the range of interest, and this is the reason we have left C as an empirical parameter. A similar difficulty is encountered if the equation is used in three-dimensional form to estimate van der Waals constants.

The existence of an unstable transition from an overcompressed gas to the solid (Figure 1) may have a bearing on the difficulty of observing the two-step gas–liquid–solid condensation. If the equilibrium solid–liquid region is typically as short as it is for krypton on graphite, the triple point could easily be lost if nucleation for the liquid is difficult. Although a true critical point would then be missing, a crude sampling of data would indicate that one existed. All that actually would happen is that a wide step would change into a narrow one just below $\theta = 1$. This phenomenon would occur near the lattice critical temperature, and the narrow step might be missed in the onset of second-layer formation, and so one could be misled into seeing "T_c."

Note that aside from this possibility, a direct manifestation of a lattice critical temperature is not present in our results. In order to find such a temperature, one must explore the region where K in eq 5.3 is less than unity, and thus the underlying surface favors a lattice gas.

(9) A. Thomy and X. Duval, Colloques Internationaux Du Center National de La Recherche Scientifique, No. 152, 1965.

Nuclear Magnetic Resonance of Iodine–Alkyl Sulfide Complexes[1]

by E. Thomas Strom, Wilson L. Orr, Brinkley S. Snowden, Jr., and Donald E. Woessner

Field Research Laboratory, Mobil Oil Corporation, Dallas, Texas 75221 *(Received June 9, 1967)*

Equilibrium constants (K_f's) were determined by high-resolution nmr for iodine complexes of 11 cyclic and aliphatic sulfides in CCl_4 at 25°. In the majority of cases the precision is better than 10% and compares favorably with absorption spectroscopy. The K_f's agree reasonably well for the five obtained by conventional absorption spectroscopy. The chemical shifts of the protons in the complexes were tabulated. Substitution of methyl groups for α protons increases the K_f, but this effect is subject to steric hindrance. The large K_f of the thiacyclopentane–iodine complex is discussed.

It has long been known that iodine and alkyl sulfides form molecular complexes.[2] Hastings found that iodine and aliphatic sulfide complexes have large absorptivities in the near-ultraviolet region.[3] Effective absorptivities are a function of the absorptivity of the complex and the position of equilibrium 1 for each sulfide. Equilibrium constants and absorptivities have

$$RSR' + I_2 \rightleftharpoons RSR' \cdot I_2 \qquad (1)$$

been evaluated for a number of alkyl sulfides by spectrophotometric methods.[4-6] Our goals are to determine the effect of complexing on the chemical shifts of the protons, to compare equilibrium constants meaured by nmr with those determined by absorption pectroscopy, and to elucidate the structural features ontrolling the strength of the complex formation.

Results

If a proton undergoes a fast exchange between two different chemical species, a single proton resonance is observed at a position which depends on a weighted average of the position of proton resonance and the relative abundance of the two species.[7,8] For the specific example of the protons α to the sulfur atom in an alkyl sulfide, we denote the chemical shifts of the α protons in the uncomplexed sulfide and the iodine-complexed sulfide as δ^{α}_S and δ^{α}_C, respectively. For a dynamic system in which reaction 1 occurs, the experimentally measured chemical shift of the α protons, δ^{α}_{ex}, is given by

$$\delta^{\alpha}_{ex} = \delta^{\alpha}_C\Delta + \delta^{\alpha}_S(1 - \Delta) \qquad (2)$$

where Δ is the mole fraction of iodine-complexed sulfide and $(1 - \Delta)$ is the mole fraction of uncomplexed alkyl sulfide. The mole fraction of complexed alkyl sulfide is thus given by

$$\Delta = \frac{\delta^{\alpha}_{ex} - \delta^{\alpha}_S}{\delta^{\alpha}_C - \delta^{\alpha}_S} \qquad (3)$$

Remembering that the sum of concentrations of complexed and uncomplexed sulfide must equal the original alkyl sulfide concentration, $[RSR']^0$, expression 4 for the molar concentration of alkyl sulfide–iodine complex can be obtained. The equilibrium constant

$$[RSR' \cdot I_2] = \Delta[RSR']^0 \qquad (4)$$

for complex formation, K_f, is thus given by eq 5.

$$K_f = \frac{\Delta[RSR']^0}{([RSR']^0 - \Delta[RSR']^0)([I_2]^0 - \Delta[RSR']^0)} \qquad (5)$$

Many previous nmr studies of charge-transfer complexes have dealt with complexes in which the K_f's are not large, and it was impossible to determine chem-

(1) Presented at the 153rd National Meeting of the American Chemical Society, Miami Beach, Fla., April 1967.

(2) G. Patein, *Bull. Soc. Chim. Paris*, **50**, 201 (1888).

(3) S. H. Hastings, *Anal. Chem.*, **25**, 420 (1953).

(4) (a) N. W. Tideswell and J. D. McCullough, *J. Am. Chem. Soc.*, **79**, 1031 (1957); (b) J. D. McCullough and D. Mulvey, *ibid.*, **81**, 1291 (1959).

(5) H. Tsubomura and R. P. Lang, *ibid.*, **83**, 2085 (1961).

(6) M. Tamres and S. Searles, Jr., *J. Phys. Chem.*, **66**, 1099 (1962).

(7) (a) H. S. Gutowsky and A. Saika, *J. Chem. Phys.*, **21**, 1688 (1953); (b) H. S. Gutowsky, D. W. McCall, and C. P. Slichter, *ibid.*, **21**, 279 (1953).

(8) H. M. McConnell, *ibid.*, **28**, 430 (1958).

ical shifts for the protons in the complex directly.[9,10] The shifts for pure complex and the K_f's must then be determined by modified Benesi–Hildebrand plots.[9-11] The K_f's for the sulfide–iodine complexes are large; hence, the chemical shifts for the protons in the complex are readily determined, and the K_f's are conveniently evaluated numerically.

Equilibrium constants in CCl_4 were determined in the following manner. First, the chemical shifts for the uncomplexed sulfide were measured. These were concentration independent for the ranges studied. Then chemical shifts for the protons in the complex were measured by diluting successively smaller amounts of 0.1 M stock sulfide solution to 1 ml total volume with 0.05 M I_2 solution. Addition of iodine caused a downfield shift of the proton resonances. When further addition of iodine no longer caused changes in proton frequencies, the measured proton chemical shifts were assumed to be the shifts for the pure complex. The basic splitting patterns appeared unchanged by complexing. If more concentrated I_2 solutions were used to determine the shifts for pure complex, any or all of the following happened: the proton frequencies never reached a limiting value, peaks broadened markedly, and new peaks appeared. Reasons for this behavior may include formation of complexes not obeying eq 1, oxidation to sulfoxides,[12] or other side reactions. Even sulfide solutions containing excess 0.05 M I_2 showed signs of decomposition after several hours. The shifts for pure complex, therefore, were always determined within 10 min of preparation.

Measurements (usually 8–12) were then made for several ratios of $[I_2]^0$ to $[RSR']^0$ in the range of total sulfide concentrations from 0.02 to 0.0025 M. Solutions containing excess sulfide or only small excesses of I_2 gave constant values of proton frequencies for periods of at least 24 hr. Nevertheless, in general, measurements were made within 8 hr. Figure 1 shows plots of K_f *vs.* $[I_2]^0$ for typical runs. The deviations appear to be random.

The K_f's were determined, whenever possible, from α shifts. When a choice was available between two different α proton resonances, that of lower multiplicity was chosen. The K_f for the diisopropyl sulfide–iodine complex, however, was determined from the β shifts. Spectra of the aliphatic sulfides were amenable to first-order analysis, and the determined K_f's and measured chemical shifts are given in Table I. Rather broad lines were found for the α protons in thiacyclohexane while the spectrum of thiacyclobutane was of higher order. This caused a marked decrease in the accuracy of measurement. The properties of the cyclic sulfide–iodine complexes are also recorded in Table I.

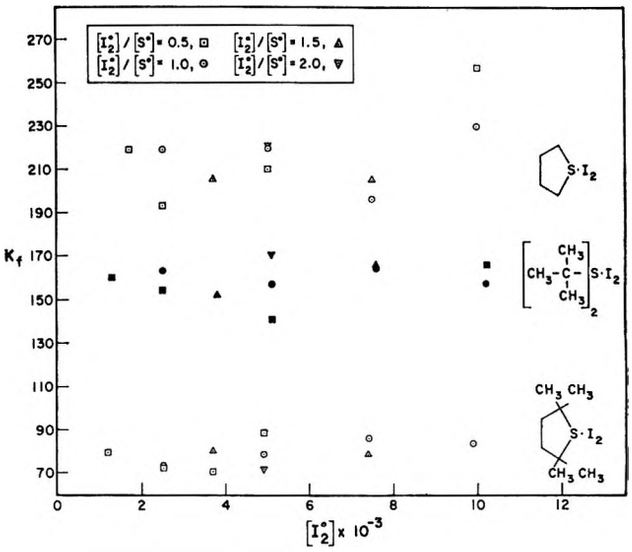

Figure 1. Plot of K_f *vs.* $[I_2]^0$ for three iodine–alkyl sulfide complexes.

Discussion

One expects from simple considerations of local diamagnetic currents that complexing of the sulfur atom should deshield the α protons, and this is what is observed experimentally. If we compare methylene protons, the results for di-*n*-propyl sulfide and thiacyclopentane indicate that deshielding of β protons is approximately half that of the α protons. Methyl protons α to the sulfur are deshielded by 0.29–0.31 ppm. This range is relatively narrow when compared with the 0.10–0.15-ppm deshielding range of the β-methyl protons. In the aliphatic series the amount of deshielding seems to increase with increasing methyl substitution. This may simply reflect the closer approach of the β-methyl group to the iodine.

A remarkable chemical shift is found for the diisopropyl sulfide–iodine complex. The α-methine proton is *shielded* on complexation. This should be compared to the complex with methylisopropyl sulfide where the methine proton is deshielded by ~0.1 ppm. It seems probable that, in the iodine–diisopropyl sul-

(9) (a) M. W. Hanna and A. L. Ashbaugh, *J. Phys. Chem.*, 68, 811 (1964); (b) H. A. Sandoval and M. W. Hanna, *ibid.*, 70, 1203 (1966).

(10) (a) R. Foster and C. A. Fyfe, *Trans. Faraday Soc.*, 61, 1626 (1965); (b) R. Foster and C. A. Fyfe, *ibid.*, 62, 1400 (1966).

(11) H. A. Benesi and J. H. Hildebrand, *J. Am. Chem. Soc.*, 71, 2703 (1949).

(12) T. Higuchi and K.-H. Gensch, *ibid.*, 88, 5486 (1966).

Table I: Properties[a] of Iodine–Alkyl Sulfide Complexes in CCl_4 at 25°

Sulfide	δ^{α}_S	δ^{β}_S	$\delta^{\alpha}_C - \delta^{\alpha}_S$	$\delta^{\beta}_C - \delta^{\beta}_S$	K_f (no. of measurements)
Me_2S	2.054	...	0.294	...	71.1 ± 4.8(9)
MeEtS	2.037,[b] 2.441[c]	1.245	0.298,[b] 0.209[c]	0.097	136.2 ± 15.8(11)
Me-*i*-PrS	2.020,[b] 2.728[d]	1.241	0.314,[b] 0.10[d]	0.118	155.4 ± 11.8(10)
Et_2S	2.474	1.234	0.213	0.118	170.8 ± 23.3(8)
n-Pr_2S[e]	2.412	1.578	0.227	0.123	168.8 ± 17.1(11)
i-Pr_2S	2.890	1.224	−0.015	0.139	184.7 ± 14.7(12)
t-Bu_2S	...	1.380	...	0.148	159.3 ± 8.0(11)
Thiacyclobutane	3.180[f]	2.962[f]	0.218	...	95.8 ± 10.6(6)
Thiacyclopentane	2.755	1.914	0.305	0.161	215.9 ± 16.9(11)
2,2,5,5-Tetramethyl-thiacyclopentane	...	140.0,[b] 190.7[c]	...	0.118,[b] 0.063[c]	78.4 ± 5.7(11)
Thiacyclohexane[g]	2.522	1.807[f]	0.210	...	136.0 ± 29.4(6)

[a] Shifts are given in ppm. Errors are standard deviations. [b] Value for methyl protons. [c] Value for methylene protons. [d] Value for the methine proton. [e] $\delta^{\gamma}_S = 0.998$, $\delta^{\gamma}_C - \delta^{\gamma}_S \approx 0.006$. [f] This is the position of the highest point of a complex envelope rather than a true chemical shift. The chemical shifts for thiacyclobutane are $\delta^{\alpha}_S = 3.43$ and $\delta^{\beta}_S = 3.17$: E. Lippert and H. Prigge, *Ber. Bunsenges. Physik. Chem.*, **67**, 415 (1963). [g] The γ-proton resonance is centered about 1.643.

Table II: Measured K_f's for Iodine–Alkyl Sulfide Complexes at 25°

Sulfide	$K^{nmr}_{CCl_4}$	$K^{vis}_{CCl_4}$	$K^{vis}_{n\text{-heptane}}$[a]	$K^{uv}_{n\text{-heptane}}$[a]
Me_2S	71.1 ± 4.8	71 ± 2[b]	...	...
Et_2S	170.8 ± 23.3	...	187.1 ± 3.4	168,[c] 180.4 ± 7.3
Thiacyclobutane[d]	95.8 ± 10.6	87 ± 4,[e] 79.2[a]	90.3 ± 1.8	111.4 ± 0.9
Thiacyclopentane	215.9 ± 16.9	186 ± 2[e]	210.7 ± 4.8	251.4 ± 1.9
Thiacyclohexane	136.0 ± 29.8	148[f]	153.3 ± 1.1	155.3 ± 1.5

[a] Except where noted from ref 6. Error limits are for the 50% confidence level. [b] From ref 4a. Error is standard deviation. [c] Calculated from data in ref 5. [d] The value determined in ref 6 in CCl_4 by ultraviolet spectroscopy is 79.0 ± 2.7. [e] From ref 4b. Errors are standard deviations? [f] Work of J. D. McCullough cited in ref 6. The value given in ref 4b is 110.

fide complex, the methine protons have a preferred conformation with respect to the iodine–sulfur bond.

The K_f's for some of the complexes covered in this study have previously been determined by visible and ultraviolet spectroscopy. Table II compares the results from this nmr study with those obtained by absorption spectroscopy. The agreement is reasonable, even excellent for some compounds. Each method has definite advantages in specific cases. Solvent considerations will at times restrict either method. It is experimentally easier to determine a K_f from a line position, as in the nmr method, than from line intensities, as in absorption spectroscopy. Balancing this advantage is the inherently greater sensitivity of absorption spectroscopy. Analysis of the ultraviolet spectra of iodine–alkyl sulfide complexes in certain cases is complicated by the overlapping of the charge-transfer bands with the sulfide absorption. Also, one has to *assume* that the absorption of the complex follows Beer's law. These difficulties are obviated by the nmr method. For sulfides where there are large numbers of uncoupled protons, the nmr method seems excellent. However, the accuracy of the nmr method decreases with a decrease in the number of protons contributing to a given resonance and with an increase in the multiplicity of the resonance. When K_f's can be determined by either method, the nmr method may be preferred because of its experimental convenience although the sensitivity is less than that of the absorption spectroscopy method.

For donor–acceptor complexes, such as the iodine–alkyl sulfide complexes, simple theory predicts that substitution of electron-donating groups about the donor atom should increase the strength of the complex. This prediction is amply realized. Substitution of a single methyl group for one of the hydrogens of dimethyl sulfide results in a 92% increase in the K_f. More modest effects ensue from further substitution of methyl groups. It appears that either the inductive effect from increased methyl substitution is saturated

or the inductive effect is cancelled by increased steric hindrance to complex formation. The results for the cyclic sulfides (*vide infra*) seem to indicate the latter. The lower K_f for the iodine–di-*t*-butyl sulfide complex than for the diethyl sulfide complex clearly indicates that steric hindrance occurs in the former compound.

Comparison of the thiacyclopentane–iodine complex and the diethyl sulfide complex shows a 26% increase in K_f for the cyclic compound. The results for the five-membered ring may be rationalized in the following manner. When methyl groups are substituted for α hydrogens, there will be repulsions between the methyl groups and the electron pairs on the iodine molecule in certain conformations of the complex which will tend to destabilize the complex. The situation has been interpreted in terms of front strain or "*F* strain."[13] When the β-alkyl groups are "tied back" in a five-membered ring, these repulsions are minimized and the K_f of the complex is increased. Prototypes for this concept are the trimethylboron–amine complexes.[14,15]

There is a drastic decrease in K_f when every α position in thiacyclopentane is methylated. If conditions are optimum for complex stability in the thiacyclopentane–iodine complex, the decrease of stability in the 2,2,5,5-tetramethylthiacyclopentane–iodine complex is understandable. The K_f of the latter complex is about half that of the corresponding di-*t*-butyl sulfide complex. This difference may reflect the increase in rotational freedom of the methyl groups in the aliphatic sulfide, thus allowing a conformation with stronger sulfur–iodine bonding.

More subtle structural factors influencing the strength of the complex in cyclic sulfides will be examined in the future. Furthermore, iodine complexation can be used as an aid in interpretation of the nmr spectra of bicyclic sulfides. The nmr spectrum of I shows on cursory examination the presence of only

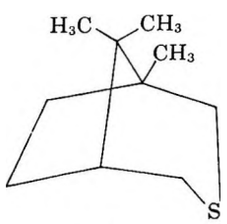

I

two protons α to the sulfur. Iodine complexation, however, indicates the existence of two other α protons whose resonances fall under the methylene envelope in the uncomplexed compound.[16]

Experimental Section

The following commercially available sulfides, which were found to be free of impurities by gas–liquid partition chromatography (glpc), were used: diethyl sulfide, methyl isopropyl sulfide, diisopropyl sulfide, and di-*t*-butyl sulfide (Aldrich); dimethyl sulfide and thiacyclohexane (J. T. Baker, "Baker grade"); di-*n*-propyl sulfide (J. T. Baker, Technical grade); and thiacyclopentane (Eastman). Thiacyclobutane was an API standard sample containing less than 0.05 mole % impurities. The compound was vacuum distilled immediately prior to use, and the distillate showed no impurities by glpc. A glpc analysis showed that methyl ethyl sulfide (J. T. Baker, Technical grade) and 2,2,5,5-tetramethylthiacyclopentane (gift from Bureau of Mines, Bartlesville, Okla.) contained significant impurities. The 2,2,5,5-tetramethylthiacyclopentane was purified by preparative scale glpc while methyl ethyl sulfide was purified through mercuric chloride complexation, according to the procedure of McAllan, *et al.*[17] Iodine was Baker Analyzed reagent grade. The carbon tetrachloride was redistilled. Tetramethylsilane (TMS) was then added to the solvent to make up a 3% solution of TMS in carbon tetrachloride.

The iodine and sulfides were weighed into separate volumetric flasks and diluted with solvent to volume. The components were mixed directly in the nmr sample tubes which were then covered with Teflon caps. Accurate transfers were made with microliter syringes. In preliminary experiments anomalous broadenings were noted on occasion when acid-cleaned tubes were used; therefore, new sample tubes were used which were subsequently cleaned only with organic solvents.

Spectra were measured on a Varian HR-100 nmr spectrometer. An internal lock of TMS was used. All frequencies were measured on a Hewlett-Packard 522-B electronic counter which has a precision of ± 0.1 c. The accuracy of the line position measurements ranged from ± 0.1 cps for the highest sulfide concentrations to ± 0.3 cps for the dilute samples. To make certain that iodine had no effect on the chemical shift of TMS, the chemical shift of the protons in a 3% cyclohexane solution was determined for both pure CCl_4 and 0.05 *M* I_2 in CCl_4, with TMS as an internal

(13) H. C. Brown, H. Bartholomay, Jr., and M. D. Taylor, *J. Am. Chem. Soc.*, **66**, 435 (1944).

(14) H. C. Brown and M. Gerstein, *ibid.*, **72**, 2926 (1950).

(15) H. C. Brown and S. Sujishi, *ibid.*, **70**, 2878 (1948).

(16) W. L. Orr, *et al.*, unpublished results.

(17) D. T. McAllan, T. V. Cullum, R. A. Dean, and F. A. Fidler, *J. Am. Chem. Soc.*, **73**, 3629 (1951).

lock. The measured chemical shifts were identical. The temperature of the probe for the K_t determinations was 25.0 ± 1.0° as measured from ethylene glycol calibrations.

Equilibrium constants were calculated from eq 5 on the CDC 1604B computer of the Field Research Laboratory.

Acknowledgments. The authors wish to thank L. E. Nelson for operation of the HA-100 nmr spectrometer and C. H. Calvert for purifying the sulfide compounds. We are grateful to the staff of API Project 48 (Bartlesville, Okla.) for the sample of 2,2,5,5-tetramethylthiacyclopentane and to Mobil Oil Corp. for permission to publish this work.

On Dielectric Relaxation Due to Chemical Rate Processes

by Gerhard Schwarz

Max-Planck-Institut für physikalische Chemie, Göttingen, Germany,[1]
and Institut für molekulare Biologie, Biochemie und Biophysik, Stöckheim/Braunschweig, Germany

Accepted and Transmitted by The Faraday Society (March 28, 1967)

The effect of chemical relaxation on the dielectric behavior of dipolar reaction systems is examined. When only small electric field densities are applied, the equilibrium of the over-all reaction is not perturbed so that the static dielectric constant remains unchanged. Nevertheless, the chemical process may affect the dielectric relaxation by providing an alternate means of orienting dipoles. In principle, this should be measurable in cases where chemical relaxation proceeds at least with about the same rate as the rotation of dipoles. If the reaction rate is much faster than rotational diffusion, a distinct dielectric relaxation effect occurs which reflects directly the chemical relaxation process. Owing to the unfavorably large rotational diffusion coefficients of small molecules in solution, pertinent reaction systems can be expected, first of all, among those systems which involve macromolecular particles. Potential applications of the phenomenon aiming at the determination of chemical rate data are discussed, including even cases which originally could not be studied because of dipole rotation being too fast.

I. Introduction

Dielectric polarization of an isotropic and homogeneous medium is described by the expression

$$P = M/V = \epsilon_0(\epsilon - 1)E \qquad (1)$$

relating the electric dipole moment per unit volume, P, to the electric field density, E, which induces it (M = over-all dipole moment, V = volume, $\epsilon_0 = 8.854 \times 10^{-14}$ f/cm). The quantity ϵ represents the (relative) dielectric constant of the system. Owing to the finite rate of formation, the actual value of the dipole moment M will lag behind its equilibrium value, if the field is changed fast enough. This is of particular significance for periodic fields of sufficiently high frequencies. In such cases a phase shift between M and E will occur, resulting in an energy absorption (dielectric loss). Also the amplitude of M will be changed. Using complex notation, this dielectric dispersion is adequately described by writing $E = E_0 e^{i\omega t}$ (E_0 = amplitude of the field, $i = \sqrt{-1}$, ω = angular frequency, t = time) and introducing a complex dielectric constant

$$\epsilon = \epsilon^* = \epsilon' - i\epsilon'' \qquad (2)$$

(1) Send inquiries to the author at this address.

The (real) dielectric constant, ϵ', as well as the dielectric loss factor, ϵ'', become functions of ω within the dispersion range (for frequencies outside this region ϵ' is independent of ω, while ϵ'' vanishes). Both quantities are accessible experimentally by means of electrical impedance measurements. The capacitive part yields ϵ', the conductive one ϵ''.

Dielectric polarization may be the result of various effects. First of all, individual molecules can be polarized owing to slight deformations of their atomic and electronic charge distribution. This is generally brought about in extremely short times, corresponding to dielectric dispersion at optical frequencies. Another important mechanism becomes effective if permanent molecular dipoles exist in the system. Then, an applied electric field tends to cause preferential orientation of the dipole axes—which are originally distributed at random—thus giving rise to an over-all nonvanishing dipole moment (orientational polarization). The rate of this process is ordinarily determined by the rotational diffusion of the molecules perpendicularly to their dipole axes. This results in dielectric relaxation at sufficiently high frequencies. The corresponding dispersion is observed at microwave frequencies ($\approx 10^4$ Mc) as far as small molecules in liquids are concerned.

Since the time which is required to rotate a molecule increases rapidly with its length, orientational polarization in macromolecular systems may display relaxation at fairly low frequencies, *e.g.*, at radiofrequencies as in the case of polypeptides[2] or polynucleotides[3] in solution. In macromolecular systems considerable dielectric polarization and relaxation may occur also owing to polarization of the ionic atmosphere of polyions[4] or colloidal particles[5] as well as to the effect of heterogeneities in the dielectric properties of the medium[6] (Maxwell–Wagner effect). The respective relaxation frequencies are usually also rather low (kilocycle–megacycle range); they may decrease even below the kilocycle range for sufficiently large polarizable particles.[7]

Apart from the mentioned physical effects there is a potential chemical mechanism of dielectric polarization and relaxation. It can be anticipated for systems where dielectric properties are changed during the course of a chemical reaction. The chemical equilibrium of such a process is shifted by an applied electric field as can be shown thermodynamically. Thus a field tends to change the dielectric polarization of the system *via* the initiated chemical reaction. In this case the rate of dielectric polarization is, of course, determined by the respective chemical relaxation process. As an important consequence we conclude that an investigation of the corresponding dielectric dispersion can, in principle, be utilized to measure chemical relaxation times. These quantities may be interpreted then in terms of the underlying chemical kinetics.[8]

The fundamental potentiality of chemically induced dielectric relaxation and its inherent significance for the study of fast reactions in solution has been pointed out recently by Bergmann, Eigen, and De Maeyer.[9] These authors directed attention also to a restrictive peculiarity of the phenomenon, namely, that any chemical contribution to the dielectric constant vanishes for $E \rightarrow 0$. Thus it cannot be measured by means of the conventional impedance-measuring techniques which employ fairly low field densities. The effect should be measurable, however, in the presence of a sufficiently high static electric field. By imposing such a condition upon a special system (200 kv/cm on the dimerization of 6-hexanolactam (ϵ-caprolactam)) it has actually been observed experimentally and interpreted in terms of kinetic properties.[9]

On fundamental grounds and in view of the comparatively difficult and inconvenient experimental problems involved in the application of high field densities, the question may arise whether a chemical reaction could nevertheless induce dielectric effects without a strong static field being present. This is indeed possible as is to be shown in this article. Our result does not contradict the above-mentioned conclusion provided we express it in the more precise form: "Small field densities do not perturb a chemical equilibrium sufficiently to produce a chemical contribution to the static dielectric constant." It will turn out that actually not the dielectric polarization but the dielectric relaxation may be affected by a chemical reaction even for $E \rightarrow 0$.

In the above-mentioned experiment, strong fields were predicted to be absolutely necessary for any chemically induced dielectric effect. As a matter of fact, this rests upon the implicit assumption that the relaxation time of dipole rotation, τ_r, is small compared with the chemical relaxation time, τ_{ch}. Such an assumption is very well

(2) (a) H. Watanabe, K. Yoshioka, and A. Wada, *Biopolymers*, **2**, 91 (1964); (b) S. Takashima, *ibid.*, **1**, 171 (1963).

(3) S. Takashima, *J. Phys. Chem.*, **70**, 1372 (1966).

(4) (a) G. Schwarz, *Z. Physik. Chem.* (Frankfurt), **19**, 286 (1959); (b) M. Mandel and A. Jenard, *Trans. Faraday Soc.*, **59**, 2158, 2170 (1963).

(5) (a) H. P. Schwan, G. Schwarz, J. Maczuk, and H. Pauly, *J. Phys. Chem.*, **66**, 2626 (1962); (b) G. Schwarz, *ibid.*, **66**, 2636 (1962).

(6) (a) C. T. O'Konski, *ibid.*, **64**, 605 (1960); (b) H. Pauly and H. P. Schwan, *Z. Naturforsch.*, **14b**, 125 (1959).

(7) H. P. Schwan, *Advan. Biol. Med. Phys.*, **5**, 147 (1957).

(8) (a) M. Eigen and L. De Maeyer in "Technique of Organic Chemistry," S. L. Friess, E. S. Lewis, and A. Weissberger, Ed., 2nd ed, Vol. VIII, Part 2, Interscience Publishers, Inc., New York, N. Y., 1963, p 895; (b) G. Schwarz, *Rev. Mod. Phys.*, in press.

(9) K. Bergmann, M. Eigen, and L. De Maeyer, *Ber. Bunsenges. Physik. Chem.*, **67**, 819 (1963).

justified in that special case as well as for other small molecular dipoles which can freely rotate in a liquid ($\tau_{ch} > 10^{-10}$ sec $\gg \tau_r \approx 10^{-11}$ sec). That explains, of course, why actually no chemical effect has been observed so far at low fields. Nevertheless, there might be cases where the reverse relation $\tau_r \gg \tau_{ch}$ holds true. Under that condition a low-field dielectric dispersion caused by a chemical reaction can, in principle, occur. This may apply especially to macromolcular reaction systems (among them many of biological significance). There the rotational diffusion could well proceed more slowly than a chemical relaxation process. Furthermore, by manipulating systems this behavior might be achieved deliberately in order to utilize the resulting dielectric relaxation effect for kinetic measurements.

In the following the problem is treated in more detail from a quantitative point of view. At first we shall establish the thermodynamic relations describing the effect of an electric field on a chemical equilibrium. Then a model reaction will be discussed which is especially suited to demonstrate clearly the fundamental aspects of the phenomenon under consideration. This will clarify under which circumstances a chemical mechanism of dielectric relaxation at low fields can be expected. Finally a reaction process of more practical interest is to be investigated with regard to potential experimental applications.

II. Thermodynamic Foundation

The general chemical reaction process

$$\nu_1'\mathrm{R}_1' + \nu_2'\mathrm{R}_2' + \ldots \rightleftarrows \nu_1''\mathrm{R}_1'' + \nu_2''\mathrm{R}_2'' + \ldots \quad (3)$$

may proceed in a solution which is assumed to be a closed and dielectrically isotropic system. Any changes in the numbers of moles, n_i, of the reaction partners R′ and R″ are determined then by

$$\delta n_i = \nu_i \delta\xi \quad (4)$$

where ν_i equals the respective stoichiometric coefficient, ν'', for any R″ species, but is taken as the negative ν' value for the reactants R′. The quantity ξ is introduced as the extent of reaction. The Gibbs free energy, G, of the system is to be considered a function of T (absolute temperature), p (pressure), E, and ξ. Its total differential can be expressed by the well-known relation[10]

$$\mathrm{d}G = -S\mathrm{d}T + V\mathrm{d}p - M\mathrm{d}E - A\mathrm{d}\xi \quad (5)$$

(S = entropy). The affinity

$$A = -\sum \nu_i \mu_i \quad (6)$$

is related to the chemical potentials μ_i of all the individual reaction partners. The condition of chemical equilibrium is given by $A = 0$. Conventionally μ_i is expressed in terms of activity coefficients, f_i, and concentrations, c_i

$$\mu_i = \mu_i^0 + RT \ln f_i + RT \ln c_i \quad (7)$$

The standard chemical potentials μ_i^0 depend on T, p, E (and on the nature of the solvent), but not on ξ. Using (7) eq 6 may be transformed to

$$A/RT = \ln K^* - \sum_i \nu_i \ln c_i \quad (8)$$

with

$$\ln K^* = \ln K - \sum_i \nu_i \ln f_i \quad (9)$$

$$K = \exp\{-\textstyle\sum \nu_i \mu_i^0/RT\} \quad (10)$$

where K is the thermodynamic equilibrium constant. According to (8) we have at equilibrium

$$\ln \bar{K}^* = \textstyle\sum \nu_i \ln \bar{c}_i \quad (11)$$

(equilibrium quantities are always to be denoted by a bar). Since we are interested in the change of the equilibrium concentrations by an applied field, the effect of E on $\bar{K}^*$ (="apparent equilibrium constant") will be investigated now.

On account of the fact that the order of differentiation is immaterial when computing second derivatives of G, eq 5 leads at once to

$$\left(\frac{\partial A}{\partial E}\right)_{T,p,\xi} = \left(\frac{\partial M}{\partial \xi}\right)_{T,p,E} \equiv \Delta M \quad (12)$$

The quantity ΔM represents the molar change of the over-all dipole moment M which is produced by reaction 3 (proceeding from the left to the right) while keeping the intensive variables T, p, and E constant. Inserting A from (8) into (12) yields

$$\left(\frac{\partial \ln K^*}{\partial E}\right)_{T,p,\xi} = \frac{\Delta M}{RT} \quad (13)$$

provided the concentrations are measured in molalities (n_i/1000 g of solvent). The use of molarities (n_i/1000 ml of solution) requires, strictly speaking, to take into account the effect of E on V (electrostriction). This is done by adding the term $-(1/V)(\partial V/\partial E)_{T,p,\xi}\sum_i \nu_i$ on the right side of (13). However, even for $\sum_i \nu_i \neq 0$ we may generally neglect it in those cases we are interested in, *i.e.*, reactions with an appreciable ΔM at $E \to 0$.

(10) *Cf.*, *e.g.*, A. H. Wilson, "Thermodynamics and Statistical Mechanics," Cambridge University Press, London, 1957.

In order to describe the perturbation of equilibrium caused by the field E we differentiate K^* for $A = 0$ instead of keeping ξ constant

$$\left(\frac{\partial \ln \overline{K^*}}{\partial E}\right)_{T,p} = \left(\frac{\partial \ln K^*}{\partial E}\right)_{T,p,A=0} = \left(\frac{\partial \ln K^*}{\partial E}\right)_{T,p,\xi} + \left(\frac{\partial \ln K^*}{\partial \xi}\right)_{T,p,E}\left(\frac{\partial \xi}{\partial E}\right)_{T,p,A=0} \quad (14)$$

By using the relation

$$\left(\frac{\partial \xi}{\partial E}\right)_{T,p,A} = -\frac{(\partial A/\partial E)_{T,p,\xi}}{(\partial A/\partial \xi)_{T,p,E}} \quad (15)$$

as well as eq 8, 9, 12, and 13 we finally obtain

$$\left(\frac{\partial \ln \overline{K^*}}{\partial E}\right)_{T,p} = f_{T,p}\frac{\Delta M}{RT} \quad (16)$$

with

$$f_{T,p} = \left\{1 - \left(\frac{\partial \ln K^*}{\partial \xi}\right)_{T,p,E}\Gamma_{T,p}\right\}^{-1} \quad (17a)$$

$$\Gamma_{T,p} = \left\{\left(\frac{\partial \sum \nu_i \ln c_i}{\partial \xi}\right)_{T,p,E}\right\}^{-1} \quad (17b)$$

Since $(\partial \ln K^*/\partial \xi)_{T,p,E} = -(\partial \Sigma \nu_i \ln f_i/\partial \xi)_{T,p,E}$, one sees immediately that $f_{T,p} = 1$ if the activity coefficients are not changed during the reaction. This is frequently the case in practical work (*e.g.*, if the f_i are essentially determined by an excess of a nonreacting electrolyte).

In principle, eq 16 may not apply to the actual conditions of the reaction system. Chemical rate processes which produce measurable contributions to dielectric relaxation would be very fast. Hence they can be expected to proceed at constant S and V rather than at constant T and p. Let us therefore evaluate the pertinent quantity

$$\left(\frac{\partial \ln \overline{K^*}}{\partial E}\right)_{S,V} = \left(\frac{\partial \ln K^*}{\partial E}\right)_{S,V,A=0} = \left(\frac{\partial \ln K^*}{\partial E}\right)_{S,V,\xi} + \left(\frac{\partial \ln K^*}{\partial \xi}\right)_{S,V,E}\left(\frac{\partial \xi}{\partial E}\right)_{S,V,A=0} \quad (18)$$

where K^* is considered a function of S, V, E, and ξ. Because of (8) we may write

$$\left(\frac{\partial \ln K^*}{\partial E}\right)_{S,V,\xi} = \left(\frac{\partial (A/RT)}{\partial E}\right)_{S,V,\xi} = \frac{1}{RT}\left(\frac{\partial A}{\partial E}\right)_{S,V,\xi} - \frac{A}{RT^2}\left(\frac{\partial T}{\partial E}\right)_{S,V,\xi} \quad (19)$$

The second term on the right side vanishes because $A = 0$, while the first one may be expressed in terms of M by means of

$$\left(\frac{\partial A}{\partial E}\right)_{S,V,\xi} = \left(\frac{\partial M}{\partial \xi}\right)_{S,V,E} \quad (20)$$

This latter relation is readily established when computing second derivatives of $G + TS - pV$ using the exact differential

$$\mathrm{d}(G + TS - pV) = T\mathrm{d}S - p\mathrm{d}V - M\mathrm{d}E - A\mathrm{d}\xi \quad (21)$$

(Equation 21 is immediately obtained from eq 5.)

Now, a procedure which is analogous to that used for deriving (16) and (17) may be employed to evaluate the final form of (18), namely

$$\left(\frac{\partial \ln \overline{K^*}}{\partial E}\right)_{S,V} = f_{S,V}\frac{1}{RT}\left(\frac{\partial M}{\partial \xi}\right)_{S,V,E} \quad (22)$$

with

$$f_{S,V} = \left\{1 - \left(\frac{\partial \ln K^*}{\partial \xi}\right)_{S,V,E}\Gamma_{S,V}\right\}^{-1} \quad (23a)$$

$$\Gamma_{S,V} = \left\{\left(\frac{\partial \sum \nu_i \ln c_i}{\partial \xi}\right)_{S,V,E}\right\}^{-1} \quad (23b)$$

Obviously this result differs from (16) and (17) only by the fact that all of the derivatives with respect to ξ are taken at constant S and V instead of taking them at constant T and p. Both kinds of derivatives can, of course, be related to each other. For instance, we have

$$\left(\frac{\partial M}{\partial \xi}\right)_{S,V,E} = \left(\frac{\partial M}{\partial \xi}\right)_{T,p,E} + \left(\frac{\partial M}{\partial T}\right)_{p,E,\xi}\left(\frac{\partial T}{\partial \xi}\right)_{S,V,E} + \left(\frac{\partial M}{\partial p}\right)_{T,E,\xi}\left(\frac{\partial p}{\partial \xi}\right)_{S,V,E} \quad (24)$$

The variations of T and p due to the reaction (under the condition S, V = constant) can be expressed by measurable thermodynamic quantities. Using well-known methods of evaluation[11] (compare also ref 8a) leads to

(11) *Cf.*, *e.g.*, H. Margenau and G. M. Murphy, "The Mathematics of Physics and Chemistry," D. Van Nostrand Co., Inc., Princeton, N. J., 1943.

$$\left(\frac{\partial T}{\partial \xi}\right)_{S,V,E} = -\frac{(\partial S/\partial \xi)_{T,V,E}}{(\partial S/\partial T)_{V,E,\xi}} = \frac{-\Delta H + (\alpha T/\varkappa)\Delta V}{\rho V c_V} \tag{25}$$

$$\left(\frac{\partial p}{\partial \xi}\right)_{S,V,E} = -\frac{(\partial V/\partial \xi)_{S,p,E}}{(\partial V/\partial p)_{S,E,\xi}} = \frac{\Delta V - (\alpha/c_p\rho)\Delta H}{V[\varkappa - (\alpha^2 T/c_p\rho)]} \tag{26}$$

(ΔH and ΔV = molar change of enthalpy and volume, respectively, due to the reaction at constant T, p, E; ρ = density; α = thermal expansion coefficient, $\varkappa$ = compressibility, c_p = specific heat, all taken at constant values of the respective intensive variables; c_V = specific heat at constant volume; α, $\varkappa$, c_p, and c_V do not include contributions of the chemical reaction.) Thus—under adiabatic and isochoric conditions—a field E may affect a chemical equilibrium even for $\Delta M = 0$. This will occur if M (or the dielectric constant of the system, respectively) depends on T or p, while ΔH or ΔV does not vanish. However, these effects can usually be neglected for systems with a ΔM of appreciable magnitude.

Application of (24) to $\Sigma\nu_i \ln c_i$ and $\ln K^*$, respectively, instead of M yields practically no difference between $f_{T,p}$ and $f_{S,V}$ except for cases where ΔH, ΔV, and the concentrations of the reaction partners are extremely large. We may finally conclude that for many reaction processes of interest with a ΔM of considerable magnitude and no change of activity coefficients the simple relation

$$\left(\frac{\partial \ln \overline{K^*}}{\partial E}\right)_{S,V} = \left(\frac{\partial \ln \overline{K^*}}{\partial E}\right)_{T,p} = \frac{\Delta M}{RT} \tag{27}$$

holds true as far as practically meaningful accuracy is concerned.

Because of the general relation (1) we may expect that in ordinary reactions $\partial M/\partial \xi$ is proportional to E, no matter what the thermodynamic conditions are. Hence $\partial \ln \overline{K^*}/\partial \xi \to 0$ for $E \to 0$; *i.e.*, the chemical equilibrium will not be perturbed at very low field densities. Consequently no chemically induced dielectric polarization due to additionally produced dipoles can occur. The situation will be different in this respect at sufficient high field densities. However, as is to be shown in the next section, the chemical process contributes, in principle, to the dielectric properties of the reaction system also at low fields. This does not contradict the preceding conclusion because only the dielectric relaxation is affected, while the static dielectric constant remains unaltered.

III. A Simple Model Process

For the sake of simplifying the mathematical effort, let us consider a special model reaction which is as uncomplicated as possible but nevertheless discloses clearly the basic aspects of our problem. The unimolecular reaction process

$$A_1 \underset{k^0_{21}}{\overset{k^0_{12}}{\rightleftharpoons}} A_2 \tag{28}$$

turns out to be well suited for this purpose. The quantities k^0_{12} and k^0_{21} denote the rate constants for the forward and reverse reactions, respectively. They are related to the equilibrium concentrations $\bar{c}^0_1$ and $\bar{c}^0_2$ and the "apparent equilibrium constant" $\overline{K^*}_0$ by the well-known relation

$$\bar{k}^0_{12}/\bar{k}^0_{21} = \bar{c}^0_2/\bar{c}^0_1 = \overline{K^*}_0 \tag{29}$$

We assume the rotational diffusion coefficients of both species A_1 and A_2 to be equal ($=D_r$); furthermore A_2 may have a permanent molecular dipole moment μ, while A_1 has none. Actually such reactions might be encountered—to some approximation—even in practical work, *e.g.*, among rotational isomerizations or proton transfer in zwitterions.

In the molecules of A_2 an axis is defined by the direction of the dipole μ. This axis is to be conserved for the transition $A_2 \to A_1$. Thus also an axis for the molecules of A_1 is introduced. There will be a distribution of the axes with respect to the direction of an applied field E. The concentrations of these molecules which have axes pointing at the time t into the solid angle $d\Omega = 2\pi \sin\theta\, d\theta$ (θ being the angle between E and a molecular axis) can be expressed as

$$dc_1 = \gamma_1(\theta, t)d\Omega,\ dc_2 = \gamma_2(\theta, t)d\Omega \tag{30}$$

The distribution functions γ_1 and γ_2 (=concentrations per solid angle) may change owing to the chemical reaction process (28), but also on account of rotational diffusion and—in the case of A_2—because of the momentum of force exerted by the field. This is described by the two partial differential equations

$$\frac{\partial \gamma_1}{\partial t} = -v_{12} + D_r\nabla^2\gamma_1 \tag{31a}$$

$$\frac{\partial \gamma_2}{\partial t} = v_{12} + D_r\nabla^2\gamma_2 - \operatorname{div} j_E \tag{31b}$$

The effect of the reaction rate is represented by

$$v_{12} = -\left(\frac{\partial \gamma_1}{\partial t}\right)_{chem} = \left(\frac{\partial \gamma_2}{\partial t}\right)_{chem} = k_{12}\gamma_1 - k_{21}\gamma_2 = k_{21}(\overline{K^*}\gamma_1 - \gamma_2) \tag{32}$$

It should be emphasized that—owing to the perturbation of equilibrium by the field—the rate constants k_{12}

and k_{21} as well as the corresponding $\overline{K^*}$ depend on E and θ. For $E = 0$ they are, of course, identical with k^0_{12}, k^0_{21}, or $\overline{K^*}_0$, respectively. The term $D_r\nabla^2\gamma_i$ ($i = 1, 2$) in (31a, b) results from rotational diffusion according to Fick's law. Application of the Laplace operator ∇^2 yields in our case

$$\nabla^2\gamma_i = \frac{1}{\sin\theta}\frac{\partial}{\partial\theta}\left\{\sin\theta\frac{\partial\gamma_i}{\partial\theta}\right\} \tag{33}$$

Finally the angular flux of axes directed by the field E can be introduced as

$$j_E = -\gamma_2\frac{D_r}{kT}\mu E_r \sin\theta \tag{34}$$

This is simply the product of concentration (γ_2) and angular velocity, the latter being expressed analogously to Stokes' law as angular mobility ($= D_r/kT$) times the momentum of force ($= -\mu E_r \sin\theta$). The electric field attempting to rotate the molecular dipole is given by the directing field E_r (according to Onsager[12]). This field is parallel to the applied field E, but generally of different magnitude. The contribution of j_E to the temporal change of γ_2 is given by

$$-\text{div}\, j_E = \frac{\mu E_r}{kT}D_r\frac{1}{\sin\theta}\frac{\partial}{\partial\theta}\{\gamma_2 \sin^2\theta\} \tag{35}$$

Fortunately it will not be necessary to find the general solution of (31a, b). Since $\mu E_r/kT \ll 1$ (usually by orders of magnitude), the field causes only very slight deviations from the state corresponding to $E = 0$, *i.e.*, random distribution of axes. Therefore we set

$$\gamma_1 = \gamma_1^0 + \frac{\mu E_r}{kT}\Phi_1(\theta, t); \quad \gamma_2 = \gamma_2^0 + \frac{\mu E_r}{kT}\Phi_2(\theta, t) \tag{36}$$

with

$$\gamma_1^0 = \frac{\bar{c}_1^0}{4\pi}, \gamma_2^0 = \frac{\bar{c}_2^0}{4\pi}, \gamma_2^0/\gamma_1^0 = \overline{K^*}_0 \tag{37}$$

corresponding to equilibrium at $E = 0$. Any terms of second or higher order in E_r will be neglected. Now, inserting (36) into the rate term v_{12} according to (32) leads to

$$v_{12} = \frac{\mu E_r}{kT}\{k^0_{12}\Phi_1 - k^0_{21}\Phi_2\} + k^0_{21}\gamma_2^0\frac{\partial \ln \overline{K^*}}{\partial E_r}E_r \tag{38}$$

Suppose the conditions of eq 27 apply here; then

$$\frac{\partial \ln \overline{K^*}}{\partial E_r} = \frac{N_A\mu\cos\theta}{RT} = \frac{\mu\cos\theta}{kT} \tag{39}$$

(N_A = Avogadro's number) since the molar change of the dipole moment due to the reaction 28 equals $N_A\mu\cos\theta$ (only the components in the direction of the field E have to be taken into account). Upon putting

$$\Phi_1 E_r = F_1(t)\cos\theta, \Phi_2 E_r = F_2(t)\cos\theta \tag{40}$$

(with F_1 and F_2 being independent of θ), we finally transform (31a, b) to a system of two ordinary and linear differential equations for F_1 and F_2

$$\frac{dF_1}{dt} = -\{k^0_{12} + 2D_r\}F_1 + k^0_{21}F_2 - k^0_{21}\gamma_2^0 E_r \tag{41a}$$

$$\frac{dF_2}{dt} = k^0_{12}F_1 - \{k^0_{21} + 2D_r\}F_2 + \{k^0_{21} + 2D_r\}\gamma_2^0 E_r \tag{41b}$$

There are two cases of degeneracy. One of them concerns $D_r = 0$, *i.e.*, no rotational diffusion. It is described by only one relaxation time, namely, the chemical relaxation time pertaining to process 28, τ_{ch}, which is obtained according to

$$\frac{1}{\tau_{ch}} = k^0_{12} + k^0_{21} \tag{42}$$

On the other hand, if there is no chemical rate process ($k^0_{12} = k^0_{21} = 0$) but a finite D_r, a relaxation time due to rotational diffusion

$$\tau_r = \frac{1}{2D_r} \tag{43}$$

is found (of course, two rotational relaxation times would exist in the more general case of different D_r values for A_1 and A_2). In any event, however, the degeneracy will be destroyed if both the chemical as well as the rotational effect must be taken into account. In this case the characteristic equation of (41a, b) yields, in principle, two different eigenvalues. Their negative reciprocals represent two relaxation times, τ_1 and τ_2. As is readily determined, we have $\tau_1 = \tau_r$, while for τ_2 the relation

$$\frac{1}{\tau_2} = \frac{1}{\tau_r} + \frac{1}{\tau_{ch}} \tag{44}$$

holds true. The final solution in terms of γ functions is obtained by means of standard procedures. For a periodic field of angular frequency ω, the function γ_2 takes the form

$$\gamma_2 = \gamma_2^0\left\{1 + \frac{\mu E_r}{kT}(\cos\theta)\varphi(\omega)\right\} \tag{45}$$

with the relaxation function

(12) *Cf.*, *e.g.*, C. J. F. Böttcher, "Theory of Electric Polarization," Elsevier Publishing Co., Amsterdam, 1952.

$$\varphi(\omega) = \left(\frac{\overline{K^*}_0}{1 + \overline{K^*}_0}\frac{1}{1 + i\omega\tau_r}\right) + \left(\frac{1}{1 + \overline{K^*}_0}\frac{1}{1 + i\omega\tau_2}\right) \quad (46)$$

The average dipole moment per unit volume, ΔP, which is due to the permanent molecular dipoles of A_2, results from integration over the contributions of any direction ($0 \leq \theta \leq \pi$). The effect of the reaction fields of the dipoles on the atomic and electronic polarization can be taken into account by a factor $g_\alpha \gtrapprox 1$. Because of (1) the result is easily related to the corresponding complex dielectric increment $\Delta\epsilon^*$

$$\Delta P = g_\alpha N_A \int_0^\pi \mu(\cos\theta)\gamma_2 2\pi(\sin\theta)d\theta = \epsilon_0\Delta\epsilon^* E \quad (47)$$

After evaluation it follows

$$\Delta\epsilon^* = \varphi(\omega)\Delta\epsilon^0 = \frac{\Delta\epsilon_r{}^0}{1 + i\omega\tau_r} + \frac{\Delta\epsilon_2{}^0}{1 + i\omega\tau_2} \quad (48)$$

with

$$\Delta\epsilon^0 = g_r\frac{N_A\mu^2}{3\epsilon_0 kT}\bar{c}^0{}_2,\ \Delta\epsilon_r{}^0 = \frac{\overline{K^*}_0}{1 + \overline{K^*}_0}\Delta\epsilon^0,$$

$$\Delta\epsilon_2{}^0 = \frac{\Delta\epsilon^0}{1 + \overline{K^*}_0} \quad (49a, b, c)$$

The factor g_r comes in because of the difference between the directing field and the applied field. It is to include also the factor g_α. For spherical particles g_r could be expressed as[12]

$$g_r = \frac{\epsilon(n^2 + 2)^2}{(2\epsilon + n^2)^2}\frac{2\epsilon + 1}{3} \quad (50)$$

(n = refractive index of A_2) provided the static dielectric constant of the system, ϵ, is essentially determined by the solvent and its dispersion occurs at frequencies $\gg 1/\tau_2$. Otherwise g_r should be smaller ($g_r \to 1$ in the limit), although this is generally difficult to ascertain quantitatively.

Splitting $\Delta\epsilon^*$ into its real and imaginary parts enables us to determine the increments of the dielectric constant, $\Delta\epsilon'$, and the respective dielectric loss, $\Delta\epsilon''$ (according to (2)). Apparently, the dielectric relaxation behavior depends very much on the order of magnitude by which τ_r and τ_2 ($\leq\tau_r$) differ from each other. Let us consider the three possible cases.

Case I. $\tau_r \ll \tau_{ch}$, *i.e.*, rotational diffusion proceeds much faster than chemical relaxation. Upon this condition eq 44 yields practically $\tau_2 = \tau_r$. Hence, the relaxation function $\varphi(\omega)$ reduces to the simple expression $1/(1 + i\omega\tau_r)$. Consequently the dielectric dispersion is completely controlled by the rotational diffusion of the molecular dipoles, no matter whether there is a chemical reaction or not.

Case II. $\tau_r \approx \tau_{ch}$, *i.e.*, rotational diffusion and chemical relaxation proceed with comparable rates. Under these circumstances τ_r and τ_2 are different. However, since the difference is not large enough to distinguish them clearly from the measured dispersion curves (this requires $\tau_r \gtrapprox 10\tau_{ch}$), merely a flattening of the curves will occur. Thus a direct determination of the individual relaxation times is not possible. Nevertheless their effect on the dielectric constant and the dielectric loss might be measurable provided sufficiently sensitive experimental techniques are available. For instance, at the high-frequency limit of the dispersion range we obtain

$$\lim_{\omega\to\infty}\frac{\omega\Delta\epsilon''}{\Delta\epsilon^0} = \frac{\Delta\varkappa_\infty}{\epsilon_0\Delta\epsilon^0} = \frac{1}{\tau^*} = \frac{1}{\tau_r} + \left(\frac{1}{1 + \overline{K^*}_0}\frac{1}{\tau_{ch}}\right) \quad (51)$$

($\Delta\varkappa_\infty$ = total conductivity increase due to the respective dielectric loss), where τ^* may be introduced as the mean reciprocal relaxation time[8b] according to

$$\frac{1}{\tau^*} = \left(\frac{\overline{K^*}_0}{1 + \overline{K^*}_0}\frac{1}{\tau_r}\right) + \left(\frac{1}{1 + \overline{K^*}_0}\frac{1}{\tau_2}\right) \quad (52)$$

The corresponding arithmetic mean $\bar{\tau}$ results from measurements at the low-frequency limit because of

$$\lim_{\omega\to 0}\frac{\Delta\epsilon''}{\omega\Delta\epsilon^0} = \bar{\tau} = \tau_r\left\{1 - \left(\frac{1}{1 + \overline{K^*}_0}\frac{\tau_r}{\tau_r + \tau_{ch}}\right)\right\} \quad (53)$$

Combining (51) and (53) can, in principle, be used to separate τ_r and τ_{ch}.

Of course, the chemical relaxation term affects not only the above limiting values, but also $\Delta\epsilon'$ and $\Delta\epsilon''$ at any frequency within the dispersion range. This could eventually be utilized for an alternate access to the chemical effect.

Case III. $\tau_r \gg \tau_{ch}$, *i.e.*, rotation proceeds much more slowly than chemical relaxation. Now, application of (44) results in $\tau_2 \approx \tau_{ch} \ll \tau_r$. This means that $\Delta\epsilon^*$ displays generally two distinctly different dispersion ranges. One—caused by rotational relaxation—appears at comparatively low frequencies; another one—which is due to the chemical rate process—occurs at higher frequencies. Apparently their amplitudes ($\Delta\epsilon_r{}^0$ and $\Delta\epsilon_{ch}{}^0 = \Delta\epsilon_2{}^0$, respectively) are equal for $\overline{K^*}_0 = 1$ (*i.e.*, $\bar{c}^0{}_1 = \bar{c}^0{}_2$). This is also the condition for a maximum of the absolute amplitude of the chemical relaxation effect, $\Delta\epsilon_{ch}{}^0$ (the latter being determined by $\bar{c}^0{}_2/(1 + \overline{K^*}_0) = [\overline{K^*}_0/(1 + \overline{K^*}_0)^2]c_0$, where $c_0 = \bar{c}_1 + \bar{c}_2$ = constant). As is easily to be seen, this maximum value amounts to one-fourth of the maximum

of the total dielectric increment, $\Delta\epsilon^0_{max}$ (at $\overline{K^*}_0 \rightarrow \infty$, *i.e.*, $\bar{c}^0_2 = c_0$, $\bar{c}^0_1 = 0$).

IV. Fundamental Aspects

Let us summarize the essentials of the actual physical mechanism of the phenomenon under consideration as they have been disclosed by the discussion in the preceding section. By application of an electric field a new equilibrium distribution of dipole axes is determined, namely, a preferential orientation with respect to the direction of the field. The system tends to establish this equilibrium state as fast as possible. Ordinarily this is achieved *via* rotational diffusion. In principle, however, a chemical process as introduced above provides an alternate means of orienting dipoles without actually rotating them. This works in the way that unfavorably oriented dipoles vanish *via* the reaction $A_2 \rightarrow A_1$, while favorably oriented ones are formed by the reverse reaction $A_1 \rightarrow A_2$. Both mechanisms of orientation compete with each other. Thus the chemical process causes no observable dielectric relaxation if it is too slow with respect to rotation. In the converse case (fast chemical relaxation, but slow rotation) orientation *via* the chemical process will be reflected directly in the dielectric relaxation behavior. However, the chemically induced dielectric increment $\Delta\epsilon_{ch}{}^0$ is generally smaller than the total increment $\Delta\epsilon^0$ because the perturbation of chemical equilibrium by E does not suffice to produce complete preferential orientation as determined by the applied field. Hence a certain part of it is always controlled by the rotational mechanism. Accordingly there will be, in any event, a dielectric relaxation effect in the range of rotational relaxation frequencies.

It should be emphasized that the field does not cause changes of the total concentrations of A_1 and A_2 (*i.e.*, $\delta\bar{c}_i = \int_0^\pi \gamma_i \, d\Omega = 0$; $i = 1, 2$). In compliance with the conclusions at the end of section II an appreciable perturbation of the over-all equilibrium (28) can be expected only at high field densities.

As is quite apparent from the discussion, the fundamental results obtained for our special model process may be qualitatively extended to any type of a chemical reaction which brings about changes of dipole moments. In such cases there is always a chemical mechanism of dipole orientation. This will be of no practicable significance if rotational diffusion of all of the reacting molecules proceeds much more rapidly than the reaction rate. Otherwise, the chemical effect must be reflected in the dielectric relaxation behavior. This should be especially pronounced if chemical relaxation is much faster than rotational diffusion. One can generally anticipate then a distinct dielectric dispersion effect solely controlled by the chemical rate process.

As far as only small molecules in liquid systems are concerned, relevant chemical contributions to the dielectric behavior can only rarely be expected because ordinarily the relation $\tau_r \ll \tau_{ch}$ holds true (as pointed out already in the Introduction). Nevertheless there might be a number of very fast reaction processes with $\tau_r \approx \tau_{ch}$ so that sensitive microwave techniques could detect the chemical effect along the lines suggested in the discussion of case II (as given in the preceding section). The relation $\tau_r \gg \tau_{ch}$—which results in distinctive rotational and chemical dispersion ranges—may very well apply to certain macromolecular reaction systems. This has been discussed elsewhere for the special case of conformational changes of biopolymers.[13] Among other biologically relevant systems similar effects may be encountered.

The phenomenon under consideration is also of considerable practicable importance because of the implied potentialities to determine chemical relaxation data by means of dielectric dispersion measurements at low field densities. Unfortunately many reactions of interest would not be measurable in this way owing to unfavorably high rates of rotational diffusion. In taking this as their restricted situation, the question arises whether such reaction systems can be manipulated somehow so that the dielectric method may be applied after all. Apparently it will be necessary to eliminate the detrimental influence of rotational diffusion by slowing it down. This problem is to be discussed in the following section.

V. The Effect of Retarding Rotational Diffusion

We consider a simple reaction process which is of much more practical significance than the intramolecular transformation (28), namely, the general recombination–dissociation process

$$A + B \underset{k\theta_D}{\overset{k^0_R}{\rightleftharpoons}} AB \qquad (54)$$

(k^0_R, k^0_D = respective rate constants). The molecules of the individual reaction partners may possess the respective permanent dipole moments μ_A, μ_B, and μ_{AB}. By

$$\overline{K^*}_0 = \frac{\bar{c}^0_{AB}}{\bar{c}^0_A \bar{c}^0_B} = \frac{k^0_R}{k^0_D}; \quad \frac{1}{\tau_{ch}{}^0} = k^0_R(\bar{c}^0_A + \bar{c}^0_B) + k_D \qquad (55a, b)$$

(13) G. Schwarz in "Molecular Relaxation Processes," Chemical Society Special Publication No. 20, Academic Press Inc., New York, N. Y., 1966, p 191.

the apparent equilibrium constant, $\overline{K^*}_0$, and the chemical relaxation time, τ_{ch}^0, respectively, are introduced. The latter will usually be much larger than the rotational relaxation times for small molecules. As we know, this is the most unfavorable case with regard to the effect we are interested in. A favorable situation, however, would exist if one of the reaction partners is a macromolecular particle with $\tau_r \gg \tau_{ch}^0$. Apparently the reactant could as well be only a small group which is rigidly fixed to such a macromolecule. This indicates a potential means to generate a chemical mechanism of dielectric relaxation in systems which ordinarily would display none. Evidently such an effect may be achieved by attaching the molecules of at least one of the reaction partners to sufficiently large macromolecules (*e.g.*, by chemical binding). They must be bound firmly enough so that they cannot rotate freely, but only together with the big particle. Of course, the binding must not interfere with the reaction process to be investigated. In principle, the procedure should be feasible in many cases of practical interest.

A quantitative discussion is to be carried out now with respect to the special process (54). We assume that the species B is a reaction site which is rigidly bound to big particles with a large rotational relaxation time $\tau_r^{(M)}$. The molecules of A are to be free in solution, their rotational relaxation time $\tau_r^{(A)}$ being so small that the equilibrium distribution of the dipole axes is always established during the course of the chemical reaction. It is reasonable to assume furthermore that the reaction product AB remains fixed to the macromolecular carrier. It should be emphasized that no specific assumptions will be made as to how the individual groups B and AB are located relative to each other and the carrier. The dipole moment μ_{AB} will generally not have the same direction as μ_B. Hence, the change in the fixed dipole moments due to the reaction has to be calculated as a vector difference

$$\vec{\mu}_D = \vec{\mu}_{AB} - \vec{\mu}_B \tag{56}$$

so that

$$\mu_D^2 = \mu_{AB}^2 + \mu_B^2 - 2\mu_{AB}\mu_B \cos\psi \tag{57}$$

where ψ represents the angle between $\vec{\mu}_{AB}$ and $\vec{\mu}_B$.

The direction of $\vec{\mu}_D$ is suitably chosen as the axis of the AB as well as the B groups. Then the concentrations of group axes pointing in a certain solid angle $d\Omega$ can be introduced analogously as in section III

$$dc_{AB} = \gamma_{AB}d\Omega,\ dc_B = \gamma_B d\Omega \tag{58}$$

That part of the original reaction (54) which involves any A molecule but only those B and AB groups having axes in the θ direction (with respect to the applied field E) may be written as

$$A + B(\theta) \underset{k_D}{\overset{k_R}{\rightleftharpoons}} AB(\theta) \tag{59}$$

Its apparent equilibrium constant

$$\overline{K^*} = k_R/k_D = \bar{\gamma}_{AB}/(\bar{c}_A\bar{\gamma}_B) \tag{60}$$

will depend on θ and E. Employing (27) we obtain at small field densities

$$\delta \ln \overline{K^*} = \ln(\overline{K^*}/\overline{K^*}_0) = \frac{1}{kT}\left\{\mu_D(\cos\theta)E_r - \frac{\mu_A^2}{3kT}E_r'^2\right\} \approx \frac{\mu_D E_r}{kT}\cos\theta \tag{61}$$

The first term in the braces represents the change of dipole moments due to B → AB (E_r denotes the respective directing field). The second term takes into account the disappearance of an A dipole in compliance with the assumption that the distribution of A axes is always at equilibrium (E_r' designates the directing field pertaining to A). This latter term is proportional to E^2 and may be neglected at small field densities.

Random distribution of axes—as present for $E = 0$—is described by

$$\gamma^0_{AB} = \bar{c}^0_{AB}/4\pi,\quad \gamma^0_B = \bar{c}^0_B/4\pi \tag{62}$$

Since $\gamma_{AB} + \gamma_B$ must remain constant we may write in the general case

$$\gamma_{AB} = \gamma^0_{AB} + x,\ \gamma_B = \gamma^0_B - x \tag{63}$$

Only slight deviations will be caused by the field, thus $|x| \ll \gamma^0_{AB}, \gamma^0_B$.

During a time interval $\Delta t \ll \tau_r^{(M)}$ we have

$$\frac{\partial\gamma_{AB}}{\partial t} = \frac{\partial x}{\partial t} = k_R c_A\gamma_B - k_D\gamma_{AB} = k_D\{\overline{K^*}c_A\gamma_B - \gamma_{AB}\} \tag{64}$$

because γ_{AB} can be changed then *via* chemical reaction 59 but not by rotation. Expression 64 equals zero at $E = 0$; after applying a small field density E (so that $k^0_D \to k_D = k^0_D + \delta k_D$, $\bar{c}^0_A \to \bar{c}^0_A + \delta c_A$), it becomes

$$\frac{\partial x}{\partial t} = k^0_D\{-(\overline{K^*}_0\bar{c}^0_A + 1)x + \overline{K^*}_0\gamma^0_B\delta c_A + \gamma^0_{AB}\delta \ln \overline{K^*}\} \tag{65}$$

as is found by neglecting all terms which are small of the second or higher order. The quantity $\delta \ln K^*$ is inserted according to (61). Then we may set

$$x = F(t)\frac{\mu_D \cos\theta}{kT} \tag{66}$$

where $F(t)$ does not depend on θ. Under these circumstances

$$\delta c_A = \delta c_B = -\delta c_{AB} = -\int_0^\pi x d\Omega = 0 \qquad (67)$$

i.e., the already mentioned condition that the total concentrations of the reaction partners are not changed. Using eq 66, eq 65 is finally transformed to

$$\frac{dF}{dt} = -\frac{1}{\tau_{ch}}\left(F - \frac{\beta(1-\beta)}{4\pi} c_0 E_r\right) \qquad (68)$$

($c_0 = c_B + c_{AB}$ = constant, $\beta = \bar{c}^0_{AB}/c_0$ = degree of complex formation) with

$$\frac{1}{\tau_{ch}} = k^0_R \bar{c}^0_A + k^0_D \qquad (69)$$

This chemical relaxation time, τ_{ch}, differs from that shown in (55b) because it actually pertains to process 59 which—according to (67)—is buffered with respect to A. Equation 68 is easily solved; subsequently we immediately obtain x by means of (60).

The dipole moment per unit volume induced by the chemical effect is given by

$$\Delta P = g_\alpha N_A \int_0^\pi \mu_D(\cos\theta) x \, d\Omega \qquad (70)$$

(g_α has the same meaning as in eq 47). This is to be evaluated for a periodic field of angular frequency ω—with $1/\tau_r^{(M)} \ll \omega \ll 1/\tau_r^{(A)}$— and interpreted in terms of the chemical contributions to the dielectric constant, $\Delta\epsilon_{ch}'$, and the dielectric loss, $\Delta\epsilon_{ch}''$, respectively (using eq 1 and 2). The result reads

$$\Delta\epsilon_{ch}' = \frac{1}{1+\omega^2\tau_{ch}^2}\Delta\epsilon_{ch}^0, \quad \Delta\epsilon_{ch}'' = \frac{\omega\tau_{ch}}{1+\omega^2\tau_{ch}^2}\Delta\epsilon_{ch}^0 \qquad (71a, b)$$

where

$$\Delta\epsilon_{ch}^0 = g_r \frac{N_A \mu_D^2}{3\epsilon_0 kT}\beta(1-\beta)c_0 \qquad (72)$$

The factor g_r is defined analogously to that in (49a); it depends on the special system under consideration. For dipole moments which are parallel to the long axis of a rodlike macromolecule one can expect $g_r = 1$. In any event, an uncertainty in the exact value of g_r does not interfere with a determination of the kinetic quantity τ_{ch}.

For a potentional application of the phenomenon as a chemical relaxation method it is required that $\tau_r^{(M)} \gg \tau_{ch} \gg \tau_r^{(A)}$; *i.e.*, the rotational dispersion ranges of the macromolecules (at lower frequencies) and the small molecules (at higher frequencies) must be sufficiently far off the intermediate range of chemical relaxation. Macromolecules with a $\tau_r^{(M)}$ below 10^{-5} sec are readily available. Sufficiently rigid binding of small reacting groups to such large carriers might well be encountered in certain systems of interest or could be, in principle, achieved deliberately by appropriate procedures. Thus the method would be adequate for dipole reactions with relaxation frequencies in the megacycle range (*i.e.*, $\tau_{ch} \approx 10^{-6}$–$10^{-9}$ sec). In order to form an idea of the magnitude of the effect, eq 72 may be evaluated numerically for a special case with $\beta = 0.5$, $\mu_D = 3$ D., $c_0 = 1$ M, and $g_r = 1$. The result is $\Delta\epsilon_{ch}^0 = 0.15$. For solvents with a dielectric constant $\epsilon \lesssim 10$ we find for the corresponding loss angle $\Delta\epsilon_{ch}''/\epsilon' \approx 10^{-2}$–$10^{-1}$. This is far above the limit of measurability, at least as far as (nonaqueous) solutions with little electrolytic conductivity are concerned. In the case of cooperative reactions even considerably larger effects can be expected (*cf.* ref 13).

Acknowledgments. Stimulating discussions with Professor M. Eigen and Dr. L. de Maeyer are gratefully acknowledged. The author is also indebted to Mrs. M. Barnes for proofreading the manuscript.

Determination of the Average Desorption Time of Cyclohexane and Benzene on a Nonuniform Surface by Gas–Solid Partition Chromatography

by Claire Vidal-Madjar and Georges Guiochon

Laboratoire du Professeur L. Jacque, Ecole Polytechnique, Paris 5, France

Accepted and Transmitted by The Faraday Society (June 24, 1966)

The average desorption time of cyclohexane and benzene on a nonuniform solid support (benzophenone on firebrick) has been experimentally determined by gas–solid partition chromatography from the value of the kinetic mass transfer term of the plate height equation. This time is less than 10^{-4} sec for cyclohexane, while for benzene it depends on the temperature and varies between 10^{-4} and 10^{-3} sec. This last value may be explained by the existence on this surface of active sites with higher adsorption energy. The differential enthalpy of adsorption of benzene on the most active sites of the surface which can be derived from the variation of the average desorption time with temperature was found to be between 11.5 and 14.5 kcal/mole, while the differential enthalpy of adsorption on the average surface, calculated from the variation of the retention volume of benzene with temperature, is only 8.3 kcal/mole.

Introduction

The study of the adsorption properties of a solid support is conveniently made by gas–solid partition chromatography using a systematic investigation of the elution peaks of several organic compounds.[1] Retention volumes and their variation with temperature are a measure of the solute–adsorbent interaction while the zone profile depends on the rate of desorption. However, whereas retention volume measurements have been extensively used to derive adsorption isotherms, heat of adsorption, and entropy of adsorption,[1–4] information derived from the zone profile has been much less used, probably because it is more difficult to account for.

In linear gas–solid partition chromatography the zone profile eluted out of the column has a gaussian shape. By definition the average plate height, $\bar{H}$, is related to the standard deviation of the gaussian peak by

$$\bar{H} = \frac{\sigma^2}{L} \tag{1}$$

Several physical processes are responsible of the zone broadening during its elution: molecular diffusion in the gas phase, mass transfer in gas and liquid phases, and unevenness of the carrier gas flow. Assuming that these processes are independent and symmetrical, we can calculate the plate height in terms of the sum of the individual variances of these processes.[5] The result is known as the plate height equation,[6] which may be written as

$$\bar{H} = H_g f + C_k j u_0 \tag{2}$$

In this equation H_g is the sum of the terms which originates in the gas phase (molecular diffusion, resistance to mass transfer, unevenness of the flow pattern, etc); all of these terms are proportional to $u_0 D_g^{-1}$ and therefore are constant all along the column. According to Littlewood,[6] H_g is given by

$$H_g = \frac{2\gamma D_g}{u_0} + C_g u_0 + \frac{K u_0}{D_g + a d_p u_0} \tag{3}$$

(1) A. V. Kiselev, *Gas Chromatog., Proc. Symp., 5th, Brighton, 1964*, 238 (1965).

(2) R. L. Gale and R. A. Beebe, *J. Phys. Chem.*, **68**, 555 (1964).

(3) R. D. Oldenkamp and G. Houghton, *ibid.*, **67**, 597 (1963).

(4) C. G. Scott. *Gas Chromatog., Proc. Symp., 4th, Hamburg, 1962*, 36 (1963).

(5) J. C. Giddings, "Chromatography," E. Heftmann, Ed., Reinhold Publishing Corp., New York, N. Y., 1961, p 20.

(6) A. B. Littlewood, *Anal. Chem.*, **38**, 2 (1966).

D_g is measured at the outlet pressure; f and j are pressure correction factors which allow for the influence of the zone expansion during its progression along the column.[7] This results from the carrier gas decompression. f and j are given by the relations

$$f = \frac{9}{8}\frac{(P^4 - 1)(P^2 - 1)}{(P^3 - 1)^2} \quad (4)$$

$$j = \frac{3}{2}\frac{P^2 - 1}{P^3 - 1} \quad (5)$$

f varies only from 1 to 1.125 when inlet pressure varies from P_0 to infinity and may sometimes be neglected. In the same conditions j decreases from 1 to 0.

C_k in eq 2 is the term of resistance to mass transfer in the fixed phase and is known as the kinetic mass transfer term. This term has been related by Giddings to the average desorption time.[8]

The main purpose of our work is to prepare new specific adsorbents for gas chromatography from solid organic compounds. However, crystals of organic compounds have generally no mechanical stability and have a very low specific surface; it is therefore necessary to disperse them on a solid support. Several solid supports can be used. Our work originated from Scott's experiments on benzophenone-coated firebrick.[4]

Excellent efficiencies can be obtained for alkanes when using this phase under the melting point of benzophenone. Unfortunately, the efficiency of the same column for polar compounds and even benzene is quite poor and, especially with this last compound, varies largely with experimental conditions.[9] This observation leads us to make a more detailed study of the kinetic mass transfer term.

In a previous paper[9] we have discussed the properties of the adsorbents obtained by coating benzophenone on graphitized carbon black, crushed firebrick C_{22}, and chromosorb W. Graphitized carbon black is a well-known nonspecific adsorbent with a very homogeneous surface.[1] When benzophenone is coated on this support, a new adsorbent is obtained which has all the properties of an adsorbent of type III of Kiselev's classification[1] as expected; nonspecific adsorption is observed for saturated hydrocarbons, benzene, and ether, as well as for other molecules with π bonds and unshared electron pairs. The adsorption enthalpy of these molecules is lower than or near their vaporization enthalpy. Molecules with acidic hydrogen, on the contrary, such as alcohols and amines, undergo specific interaction with this surface, they have a much higher adsorption enthalpy, and their peaks tail badly.

When benzophenone is coated on the diatomaceous supports, the result is quite different. The adsorbent has properties of type II and III adsorbents at the same time. Specific interactions are observed with all compounds except paraffins. The ether peak has a large tailing even with a very low sample amount (less than 0.1 μg). Its retention volume is 8 cm^3/m^2 of adsorbent surface instead of 1 cm^3/m^2 on benzophenone-coated graphitized carbon black, and its adsorption enthalpy is 2.5 kcal/mole more on the first packing than on the last. The difference between the two supports is much less for benzene peak; the retention volume and adsorption enthalpy are the same on both supports; however, the benzene peak tails somewhat on the diatomaceous phase and never on the carbon black phase, whatever the benzophenone ratio be.

All of these results show that the surface of the adsorbent obtained by coating benzophenone on diatomaceous supports is heterogeneous, as could be expected from the difficulties to coat an organic solid compound on a solid surface. The surface of the adsorbent obtained by coating benzophenone or anthraquinone on graphitized carbon black is also heterogeneous,[10] although the influence of the heterogeneity is much less important for practical purposes.

We have studied the variations of the kinetic mass transfer term of benzene and cyclohexane, and we discuss here the relations between this coefficient and the desorption rate constant of these two compounds.

Experimental Section

The apparatus was made in our laboratory. The columns can be thermostated at any temperature between -20 and $+90°$ at $\pm 0.1°$, with a water or a water and glycol bath. The inlet pressure of the column is regulated with a Negretti and Zambra valve. The flame ionization detector is of a design described by Halasz and Schreyer[11] with a grounded platinum burner and a platinum cage electrode. A splitting system[12] allows reproducible injection of very small samples in the column.

A splitting ratio of 1:1000 is used for liquid samples and a ratio of 1:10 for methane. The other part of the sample is discarded to the atmosphere. The internal volume of the injector is 0.3 cm^3; since it is

(7) J. C. Giddings and P. D. Schettler, *Anal. Chem.*, **36**, 1483 (1964).
(8) J. C. Giddings, *ibid.*, **36**, 1170 (1964).
(9) C. Vidal-Madjar and G. Guiochon, *Bull. Soc. Chim. France*, 1096 (1966).
(10) C. Vidal-Madjar and G. Guiochon, *Separation Sci.*, **2**, 155 (1967).
(11) I. Halasz and G. Schreyer, *Chem. Ingr-Tech.*, **32**, 675 (1960).
(12) H. Bruderreck, W. Schneider, and I. Halasz, *Advan. Chromatog.*, 91 (1967); *J. Gas Chromatog.*, **5**, 217 (1967).

upstream to the splitter, its contribution to the apparatus dead volume is divided by the splitting ratio. The detector volume is 10 μl. These contributions are negligible compared to the column gas holdup of 5 cm^3.

Columns were made with copper tubing of 2-mm i.d. and 2-m length. The sieved firebrick C_{22} (125–160 μ) is acid-washed. The benzophenone is dissolved in acetone, the liquid is mixed up with firebrick, and the solvent is removed at a temperature above the melting point of benzophenone (49°). The amount of the benzophenone deposited on the support is given as a percentage of the total weight of packing. The amount of solute injected into the column is about 0.1 μg, except when the influence of a large load is studied.

The outlet linear velocity of the carrier gas is obtained from the retention time, t_m, of an unretained component multiplied by j for the pressure correction

$$u_0 = \frac{L}{jt_m}$$

Methane, which is not adsorbed by either the diatomaceous support or the benzophenone, is injected into the column at the same time as the solutes to be studied; so for each experimental determination of the plate height equation the outlet linear velocity is known with accuracy.

The kinetic mass transfer term, C_k, has been calculated as indicated by Giddings and Schettler.[7] Two series of measurements of $\bar{H}$ at various values of the carrier gas velocity are carried out using two different carrier gases, hydrogen and argon. Equation 2 may be rearranged to

$$\frac{\bar{H}}{f} = H_g + C_k \frac{jD_g}{f}\frac{u_0}{D_g} \qquad (6)$$

As pointed out earlier, H_g depends only on $x = u_0/D_g$. j/f is a function of u_0 as well as $\bar{H}/f$. If the experimental values of $\bar{H}/f$ and jD_g/f are plotted *vs.* $x = u_0/D_g$, for the two series of measurements, as was done in Figures 1 and 2, we have for a given value of x

$$\left(\frac{\bar{H}}{f}\right)_1 = H_g(x) + C_k x\left(\frac{jD_g}{f}\right)_1 \qquad (7')$$

$$\left(\frac{\bar{H}}{f}\right)_2 = H_g(x) + C_k x\left(\frac{jD_g}{f}\right)_2 \qquad (7'')$$

where subscripts 1 and 2 relate to the values obtained with hydrogen and argon as carrier gas, respectively. In these two equations x and $H_g(x)$ are the same. Therefore

$$C_k = \frac{\Delta(\bar{H}/f)}{x\Delta(jD_g/f)} \qquad (8)$$

where $\Delta(\bar{H}/f)$ and $\Delta(jD_g/f)$ are, respectively, the differences between the values measured or interpolated for $\bar{H}/f$ on the two curves in Figure 1 and for jD_g/f on the two curves in Figure 2 at the same value of x.

D_g is the diffusion coefficient of the solute in the gas phase. It has been calculated according to the Chapman–Enskog equation.[13] At 20°, D_g is 0.073 and

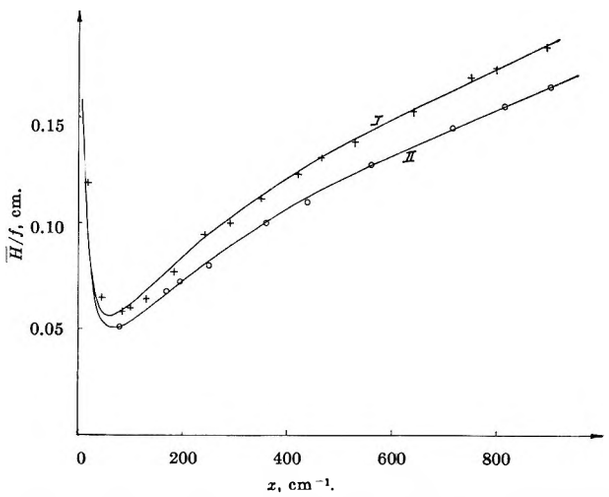

Figure 1. Determination of the coefficients of the plate height equation for benzene at −9°. Column (2 m) packed with 3% benzophenone on firebrick. Plot of $\bar{H}/f$ *vs.* x: I, hydrogen; II, argon.

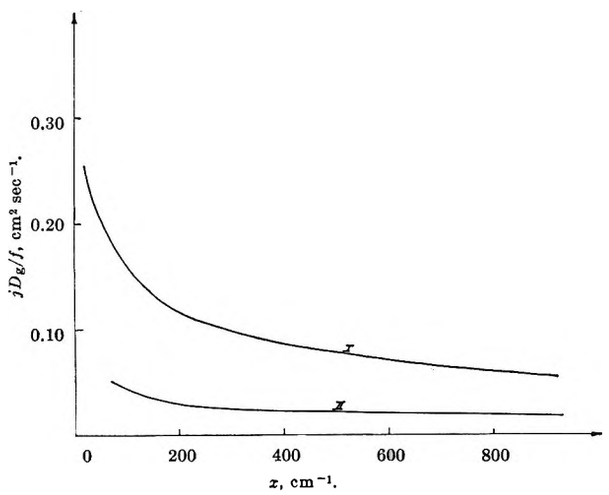

Figure 2. Determination of the coefficients of the plate height equation for benzene at −9°. Column (2 m) packed with 3% benzophenone on firebrick. Plot of jD_g/f *vs.* x: I, hydrogen; II, argon.

(13) J. O. Hirschfelder, C. F. Curtiss, and R. B. Bird, "Molecular Theory of Gases and Liquids," John Wiley and Sons, Inc., New York, N. Y., 1954, p 539.

0.34 cm^2 sec^{-1} for cyclohexane in argon and hydrogen, respectively, and 0.077 and 0.40 cm^2 sec^{-1} for benzene.

The C_k term of benzene at $-9°$ is thus obtained from the curves given in Figures 1 and 2. The mean of ten values of C_k obtained for x = 100, 200, ..., 1000 cm^{-1} is 0.60 msec, and the standard deviation is 0.02 msec.

To measure C_k with accuracy, it is necessary to work at great linear velocities where H_g is well represented by eq 3. In the experiments discussed here the numerical values of the constants are a = 0.24, d_p = 140 μ, and γ = 0.75.

Equation 3 can also be written to compare the performances obtained with different carrier gases

$$H_g = \frac{2\gamma}{x} + C_gD_gx + \frac{Kx}{1 + ad_px} \qquad (9)$$

where C_gD_g is independent of the nature of the carrier gas; it is well known that the resistance to mass transfer in the gas phase is inversely proportional to the diffusion coefficient.[5] K and C_g have been experimentally determined from a plot of $[(H_g/x) - (2\gamma/x^2)]\cdot(1 + ad_px)$ *vs.* x, which according to the theory should be a straight line that intercepts the x = 0 axis at $K + C_gD_g$. The slope of this straight line should be $C_gD_gad_p$ = 3.36 × $10^{-3}C_gD_g$ (Figure 3). The experimental points are in excellent agreement with this theoretical statement; the points corresponding to the experiments made with the two carrier gases are on a common straight line at high linear velocities (x = 180). No data are shown, Figure 3, in the low velocity range where molecular diffusion in the gas phase is dominant. A value of 0.75 has been assumed for the tortuosity factor which characterizes the contribution of the axial diffusion, as suggested in the literature for packed columns.[6] It has not been experimentally determined, which may introduce a small systematic error only in the lower velocity range. Least-square fit analysis of the experimental data obtained for cyclohexane and for benzene at x = 180 and at all temperatures studied give in each case the same numerical values: C_gD_g = 7 × 10^{-5} cm^2 and K = 40 × 10^{-5} cm^2.

This result is a confirmation of the validity of eq 2, and at the same time it indicates that the large dif-

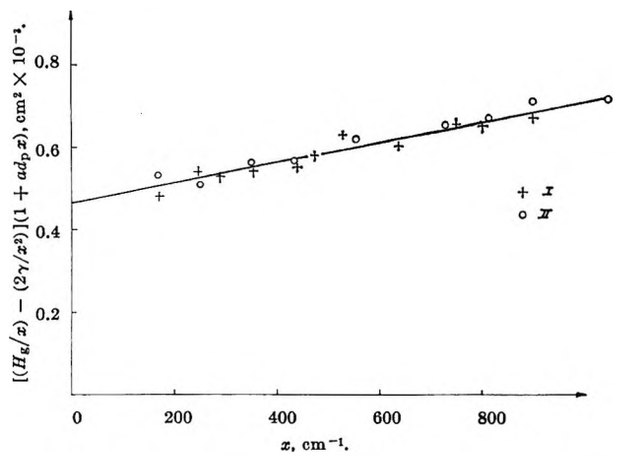

Figure 3. Determination of the coefficients of the plate height equation for benzene. Plot of $[(H_g/x) - (2\gamma/x^2)](1 + ad_px)$ *vs.* x: I, hydrogen; II, argon. Same conditions as for Figures 1 and 2.

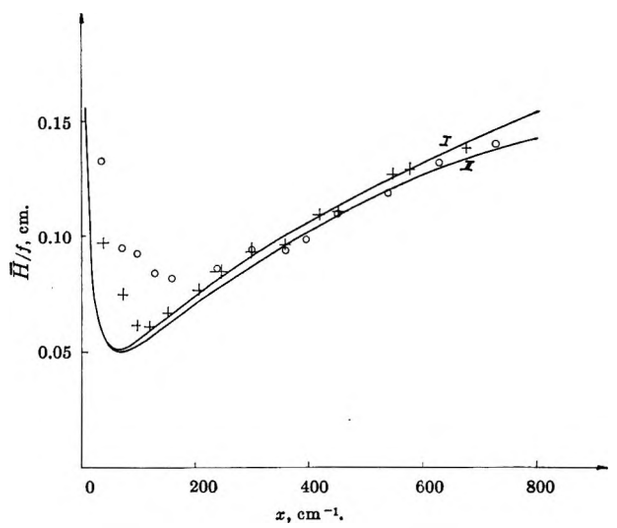

Figure 4. Determination of the kinetic mass transfer term of the plate height equation for benzene at 20° (same column as for Figures 1 and 2). Plot of $\bar{H}/f$ *vs.* x: I, hydrogen; II, argon.

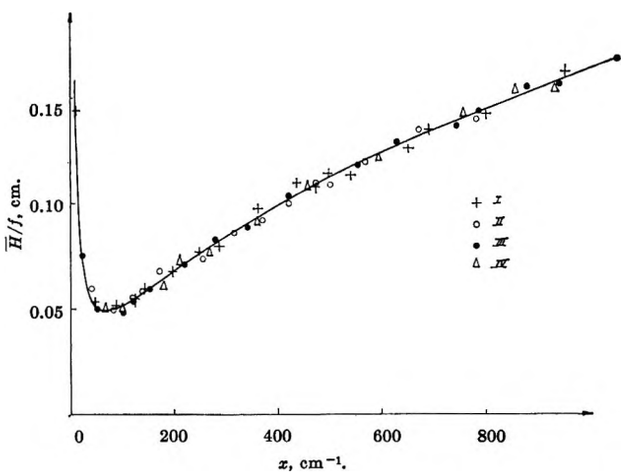

Figure 5. Determination of the kinetic mass transfer term of the plate height equation for cyclohexane at 20 and −9° (same column as for Figures 1 and 2). Plot of $\bar{H}/f$ *vs.* x: I, 20° hydrogen; II, 20° argon; III, −9° hydrogen; IV, −9° argon.

Table I: Kinetic Mass Transfer Term, Experimental Time of Desorption, and Calculated Value for a Perfectly Uniform Surface, Heterogeneity Factor, and Difference in the Adsorbent Energy of the Active Sites

		Solute						
		Cyclohexane		Benzene				
T, °K		293	264	293	285	277.5	268.5	264
R		0.36	0.14	0.27	0.22	0.15	0.10	0.07
C_k (exptl), msec		<0.05	<0.05	0.15 ± 0.05	0.25 ± 0.05	0.35 ± 0.05	0.50 ± 0.05	0.60 ± 0.05
t_d (exptl), msec		<0.1	<0.2	0.4 ± 0.1	0.7 ± 0.2	1.3 ± 0.2	2.8 ± 0.3	4.6 ± 0.4
$\alpha = 1$	$t_d^0 \times 10^5$, msec	0.8	2.8	1.2	1.6	2.5	4.0	6.0
	$S \times 10^{-4}$	<1	<1	3	4	5	7	8
	ΔH_1, kcal mole^{-1}	<6.2	<5.4	6.9 ± 0.2	6.8 ± 0.2	6.8 ± 0.2	6.7 ± 0.2	6.6 ± 0.2
$\alpha = 0.1$	$t_d^0 \times 10^5$, msec	8	28	12	16	25	40	60
	$S \times 10^{-4}$	<0.1	<0.1	0.3	0.4	0.5	0.7	0.8
	ΔH_1, kcal mole^{-1}	<5.0	<4.2	5.6 ± 0.2	5.5 ± 0.2	5.5 ± 0.2	5.5 ± 0.2	5.4 ± 0.2

ference between the values of $\bar{H}$ measured for these two compounds are to be found in the term of resistance to mass transfer in the adsorbed phase. In Figures 1, 4, and 5 the experimental data $\bar{H}/f$ are plotted *vs.* u_0/D_g for benzene at temperatures of −9° (Figure 1) and 20° (Figure 4) and for cyclohexane at the same temperatures (Figure 5). In these figures the theoretical curves given by eq 2 with numerical coefficients determined as indicated above are drawn.

The kinetic mass transfer terms, C_k, are reported in Table I, for cyclohexane and benzene on the column packed with 3% benzophenone on firebrick.

The differential enthalpy of adsorption ΔH_0, given in Table II, is calculated from the slope of the straight line obtained by plotting the logarithm of the capacity factor $k' = (1 - R)/R$ *vs.* the reciprocal of the absolute temperature.

Table II: Differential Enthalpies of Adsorption on Firebrick Uncoated and Coated with Benzophenone

Solute	ΔH_v, kcal mole^{-1}	ΔH_0, kcal mole^{-1}	
		3% benzophenone on firebrick	Firebrick
Cyclohexane	7.9	7.9	8.2
Benzene	8.1	8.3	13.6
n-Heptane	8.7	9.1	10.0
Isooctane	8.4	9.2	10.2

The latent heat of vaporization ΔH_v is determined from the variation of the vapor pressure with absolute temperature.[14]

The surface areas of the samples of firebrick coated with different ratios of benzophenone were measured with the BET method. They are given in Figure 6a.

Results

Chromatographic Properties of Firebrick Coated with Benzophenone. They are summarized in Figure 6 which gives the variations with the ratio of benzophenone on firebrick of: (a) the specific surface area of the adsorbent, (b) the retention volume per unit surface area of packing of four compounds at 20°, and (c) the efficiency of the column for these compounds.

The surface area of the adsorbent decreases markedly only at very large ratios of benzophenone. Qualitatively however, the surface properties are changed even for a small ratio of benzophenone; the surface becomes more homogeneous and its specific interaction with π electrons is weaker.

The surface is more homogeneous. The enthalpy of adsorption (Table II) and the specific retention volume of paraffins (Figure 6b) are smaller on the benzophenone–firebrick adsorbent than on the bare firebrick; also the adsorption isotherm is linear for a much larger range of sample size. On the bare firebrick even peaks of 0.1-μg samples of paraffins tail.

The specific interaction of the surface with benzene is weaker. The retention volume is much decreased by the first addition of benzophenone (Figure 6b) and the peak tailing due to nonlinearity of the isotherm at small sample size[3] disappears. The elution order changes; benzene is eluted after *n*-heptane and isooctane on bare firebrick and before them on firebrick coated with 3% benzophenone.

The heat of adsorption of benzene on this last adsorbent is almost equal to its heat of vaporization and is 5 kcal/mole less than the heat of adsorption on the bare firebrick (this last value is calculated from benzene retention times at zero sample size, derived by extrap-

(14) C. D. Hodgman, Ed., "Handbook of Chemistry and Physics," 42nd ed, The Chemical Rubber Publishing Co., Cleveland, Ohio, 1961.

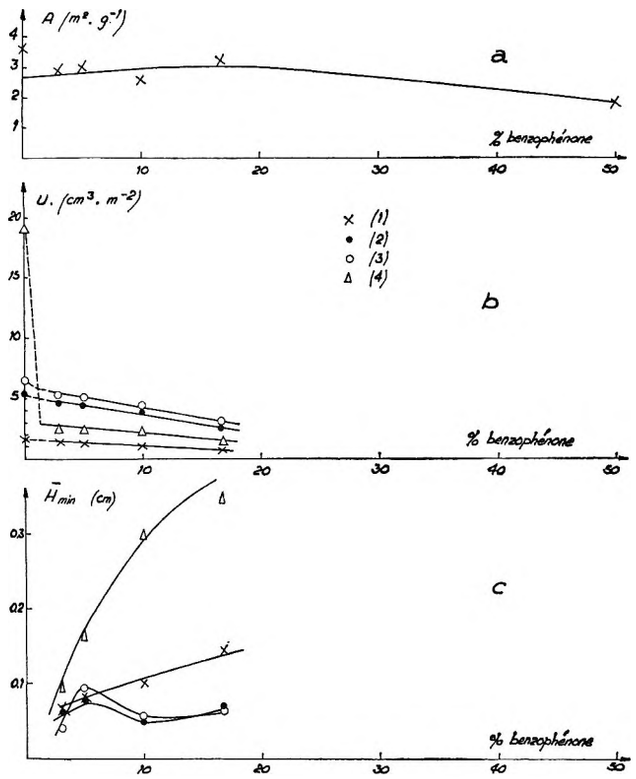

Figure 6. Variations with the percentage of benzophenone of (a) the specific surface area of crushed firebrick coated with benzophenone, (b) the retention volume per surface area of this packing at 20°, and (c) the minimum plate height of the column: (1) cyclohexane; (2) *n*-heptane; (3) isooctane; (4) benzene.

olation from measurements of retention times with various sample sizes in the 0.1–10-μg range).

On the other hand, when benzophenone is coated on graphitized carbon black, no tailing is observed, either for ether or for benzene peaks.

Kinetic Mass Transfer Term. The kinetic mass transfer term has been calculated according to the eq 2. This equation is valid as far as the elution curve is gaussian. Accordingly, the C_k term has been measured only for the column packed with 3% benzophenone deposited on firebrick (Table I). The elution peak of cyclohexane is gaussian at all temperatures and for all of the carrier gas velocities as it is shown on the chromatograms of Figures 7 and 8. For benzene, however, the elution peak presents a slight tailing at temperatures higher than 15° when the linear velocity is smaller than about 30 cm sec^{-1}. As can be seen in Figure 4 the efficiency measured for benzene is smaller than expected from theoretical considerations at these small linear velocities, so that eq 2 does not fit accurately the experimental points in the velocity range 5–30 cm sec^{-1}. This phenomenon

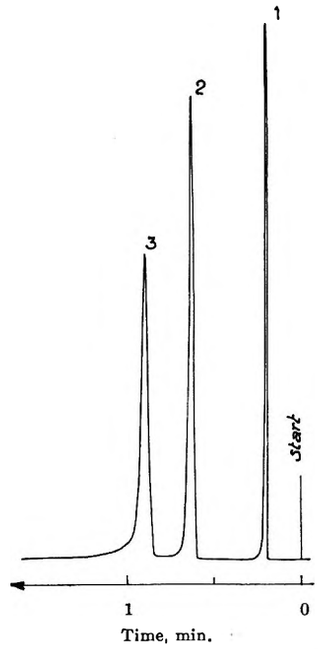

Figure 7. Chromatograms of methane (1), cyclohexane (2), and benzene (3) at 20° (same column as for Figures 1 and 2). Carrier gas, hydrogen; inlet pressure, 2.45 atm.

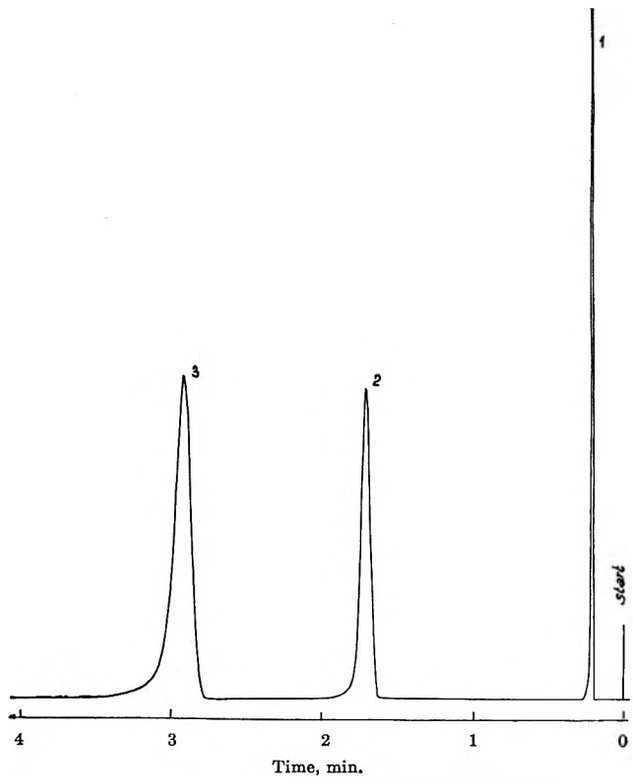

Figure 8. Chromatograms of methane (1), cyclohexane (2), and benzene (3) at −9° (same column as for Figures 1 and 2). Carrier gas, hydrogen; inlet pressure, 2.45 atm.

happens also with the column packed with 16.7% benzophenone deposited on firebrick; in this case tailing is more pronounced although the adsorption isotherm is still linear in the range of pulse sizes studied.

For the column packed with 3% benzophenone deposited on firebrick, the experimental points are quite well represented by the theoretical plate height equation whenever the peak has a gaussian shape (Figures 1, 2, and 5).

Average Time of Desorption. The average time of desorption $\bar{t}_d$ on the different kinds of sites is related to C_k by the equation[15]

$$C_k = 2R(1 - R)\bar{t}_d \qquad (10)$$

The values of $\bar{t}_d$ are reported in Table I.

The average desorption time of cyclohexane on this surface is too small to be measured by this method. The two plots of H/f *vs.* x for argon and hydrogen carrier gas cannot be distinguished because of the scattering of the experimental points. From the standard deviation of these data from eq 10 it results that the average desorption time of cyclohexane is certainly less than 10^{-4} sec. The value predicted for a perfectly uniform and inert surface is however about 10^{-8} sec.[8] The average desorption time of benzene is large enough to be measured. In the temperature range studied here, it varies between 10^{-3} and 10^{-4} sec.

A plot of the logarithm of the average desorption time of benzene *vs.* the reciprocal of the absolute temperature (Figure 9) is linear. The errors made on the different values are given in Figure 9. Relatively great absolute errors are made, which vary from 25 to 10% of the value of the desorption time (Table I). The differential enthalpy of adsorption of benzene on the most active sites has been derived from this plot according to eq 17 below. It is between 11.5 and 14.5 kcal/mole.

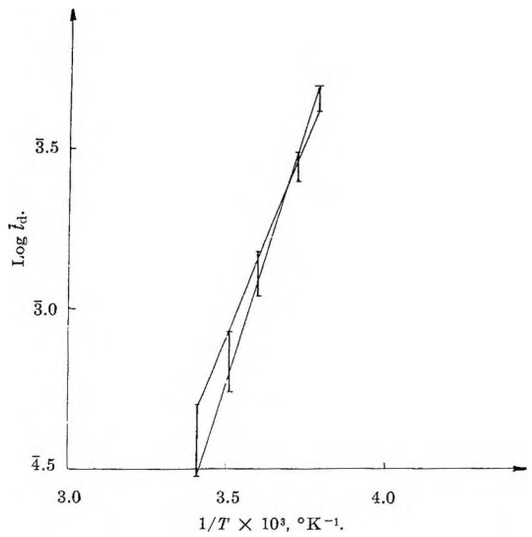

Figure 9. Plot of log $\bar{t}_d$ *vs.* $1/T$(°K) for benzene (same column as for Figures 1 and 2).

Discussion

A surface prepared by coating crushed firebrick with benzophenone should be expected to show a high degree of heterogeneity toward compounds with π bonds or unshared electron pairs because it is known that on the firebrick surface there are OH groups with strong electron affinity whereas the benzophenone surface has a relatively high density of negative charges from π bonds. However such a high degree of heterogeneity as exhibited by this surface and illustrated by the high values of the average desorption time of benzene may be accounted for either by geometrical defects of the surface such as micropores or by heterogeneity of the adsorption energy of some active sites.

As an example of the first phenomenon Eberly,[16] in the course of a study of the adsorption kinetics of *n*-butane on silica gels, has measured very large desorption times (up to 10 sec) which, he could show, were caused by micropores on the silica gel surface.

The existence of micropores or other geometrical defects on the benzophenone surface cannot, of course, be completely ruled out. In fact, it is probable that micropores appear at high ratios of benzophenone and therefore that some eventually exist at the lower ratios. When carrying out the surface area measurements, a slight hysteresis was observed during nitrogen desorption from the surface of the 16.7% benzophenone sample; a strong hysteresis was observed in the same conditions with the 50% sample. Furthermore, with the 16.7% benzophenone packing the benzene peaks show a marked tailing with no change of the retention volume when the sample size varies between 0.1 and 20 μg. Cyclohexane and alkanes have a similar behavior. On the contrary, packings with 10% or less benzophenone ratios do not exhibit such chromatographic properties which are in agreement with the existence of a sizable number of micropores at high benzophenone ratios and few if any at the lower ratios.

In the present case therefore, where systematic measurements were carried out on a 3% benzophenone packing, the heterogeneity of the surface resulting from different types of sites is a much more probable explanation. It is highly improbable that the firebrick surface be uniformly covered by benzophenone

(15) J. C. Giddings, *J. Chromatog.*, **3**, 443 (1960).
(16) P. E. Eberly, *J. Appl. Chem.*, **14**, 330 (1964).

crystals because of its intricate geometrical structure[17] and because 3% by weight is only approximately the amount corresponding to a monolayer. An X-ray diffraction diagram of the crushed firebrick coated with 3% benzophenone shows the same diffraction line profiles as the diagram obtained for the powder of pure benzophenone; the lack of any line broadening shows that the average dimensions of the benzophenone crystals in the packing exceed 0.1 μ or so.[18] Careful examination of the packing particles with an optical microscope fails, however, to reveal organic crystals which therefore have average dimensions of less than 1 μ. A simple calculation shows that if the average crystal dimensions are 0.1 μ, their density would be $2.5/\mu^2$ which would leave practically all of the firebrick surface uncovered. Although the intensity of the X-ray diffraction lines accounts roughly for the known amount of benzophenone in the packing, it would be possible that a limited fraction of benzophenone exist as a monolayer or very small crystallites.

The difference of the behavior of benzene and ether, which have the same electronic properties as far as physical adsorption is concerned and behave similarly on homogeneous surfaces,[1,9] is another argument for a broad spectrum of adsorption energies; if the large values of the heterogeneity factors result from adsorption in micropores, the two compounds would have the same chromatographic behavior. On the contrary, benzene gives symmetrical peaks and linear isotherms on firebrick coated with 3% benzophenone whereas ether gives strongly tailing peaks and nonlinear isotherms with 0.1-μg samples. This difference can be explained if there are different types of adsorption sites because benzene has a zero dipole moment and therefore its interactions with the most active sites can be more easily decreased.

Thus there is conclusive evidence that the benzophenone-coated firebrick has a heterogeneous surface, most active sites for benzene adsorption being on the firebrick surface as previously shown[9] by comparison of the benzene and ether elution peaks on packings made with benzophenone coated either on firebrick or on graphitized carbon black. A quantitative study of this adsorption energy heterogeneity is possible if one assumes the simple model of a surface with only two kinds of adsorption sites, the most active sites being very few and covering a very small part of the surface area.

For a completely uniform surface the desorption time is given by[8]

$$t_d^0 = \frac{4V_G}{\alpha \bar{c} A} \frac{1 - R}{R} \tag{11}$$

t_d^0 is the average time that a molecule stays on the surface of the adsorbent. It is identical with the "adsorption time" defined by De Boer[19] and from the temperature variation of which the adsorption enthalpy may be derived.[16] It is obvious from eq 11 that the change of t_d^0 with temperature follows that of $(1 - R)/R$ since the temperature dependence of $\bar{c}$ is very small in comparison

$$\Delta H_0 = r \frac{\partial \ln t_d^0}{\partial (1/T)} = r \frac{\partial \ln \frac{1 - R}{R}}{\partial (1/T)} \tag{12}$$

Accordingly the differential enthalpy of adsorption ΔH_0 is derived from gas chromatographic measurement of the column capacity factor, $k' = (1 - R)/R$, at various temperatures. The contribution of adsorption kinetics to the mass transfer term of the plate height equation for a completely uniform surface is given by combination of eq 10 and 11

$$C_k = \frac{8(1 - R)^2 V_G}{\alpha \bar{c} A} \tag{13}$$

For a nonuniform surface Giddings has defined the heterogeneity factor as

$$S = \sum \frac{(x_i)^2}{a_i} = C_k \frac{\alpha \bar{c} A}{8(1 - R)^2 V_G} \tag{14}$$

x_i and a_i denote, respectively, the fraction of the molecules which are adsorbed on the ith type of sites and the fractional area of these type of sites. The density of adsorption is then $\rho_i = x_i/a_i$. S is the ratio of the experimental kinetic mass transfer coefficient to the value of this coefficient calculated for a uniform surface. As previously explained we assume the existence of only two kinds of sites on the surface made by depositing benzophenone on firebrick, the most active sites being very few and so covering a very small part of the surface area ($a_1 \sim 1$; $a_2 \ll 1$). Then the summation term becomes as indicated by Giddings

$$S = \frac{x_1^2}{a_1} + \frac{x_2^2}{a_2} = x_1 x_2 \frac{\rho_2}{\rho_1} \tag{15}$$

The product $x_1 x_2$ reaches a maximum value of 0.25 for $x_1 = x_2 = 1/2$.

For a nonuniform surface, the temperature variations of $(1 - R)/R$ will still give ΔH_0, the differential adsorption enthalpy on the first type of sites, those numerous

(17) D. M. Ottenstein, *J. Gas Chromatog.*, 1 [4], 11 (1963).

(18) B. D. Cullity, "Elements of X-Ray Diffraction," Addison-Wesley Publishing Co., Reading, Mass., 1956, pp 98, 261.

(19) J. H. De Boer, "The Dynamical Character of Adsorption," Clarendon Press, London, 1953.

sites which cover most of the surface. The variation of $\bar{t}_d$ with the temperature will give the differential adsorption enthalpy on the most active sites. Combining eq 10, 14, and 15 and assuming that x_1x_2 is maximum we obtain

$$\bar{t}_d = \frac{V_G}{\alpha \bar{c} A} \frac{1 - R}{R} \frac{\rho_2}{\rho_1} \tag{16}$$

The variation of $\bar{t}_d$ with temperature will therefore be given by

$$r\frac{\partial \ln \bar{t}_d}{\partial(1/T)} = \Delta H_0 + r\frac{\partial \ln (\rho_2/\rho_1)}{\partial(1/T)} = \Delta H_0 + \Delta H_1 \tag{17}$$

ΔH_0 is derived from the temperature variation of the capacity factor. Equation 17 allows us therefore to calculate the difference in the adsorption energies of the two kinds of sites.

Values of the average desorption time, $\bar{t}_d$, for benzene and cyclohexane at various temperatures on the column packed with 3% benzophenone deposited on firebrick were derived from experimental values of C_k according to eq 10. They are given in Table I, together with the corresponding values t_d^0 for a completely uniform surface calculated according to eq 11 with $V_G = 5$ cm^3, $A = 9 \times 10^4$ cm^2, 3 g of a packing with a specific surface area of 3 m^2/g, $\bar{c} = 5 \times 10^4$ cm sec^{-1}, and with two values of the accommodation coefficient, 0.1 and 1. In the same table is given the heterogeneity factor determined as the ratio of the experimental and calculated C_k values (eq 14).

The values of the surface heterogeneity factor for benzene are very large at any temperature, the accommodation coefficient being 0.1 or 1. The heterogeneity factor is at least ten times smaller for cyclohexane. The comparison of the adsorption mechanisms of benzene and cyclohexane would have been an indication of the exact contribution of the difference in the adsorption energies of the two kinds of sites to the benzene heterogeneity factor. Unfortunately, this comparison is impossible since it would have been necessary to measure the average desorption time of cyclohexane, or an upper limit of it, with a 100-fold smaller error, which is impossible in the present state of the art (Table I).

Some interesting results, however, may be derived from the data obtained for benzene; they too confirm that the large kinetic mass transfer term observed for benzene results from the surface heterogeneity. If the only difference between the adsorption properties of two kinds of sites is a difference, ΔH_1, in their adsorption energies, then ΔH_1 is given by[8]

$$\Delta H_1 = rT \ln \frac{\rho_2}{\rho_1} \tag{18}$$

ρ_2/ρ_1 is derived from the heterogeneity factor by eq 15. As results from data given in Table I, ΔH_1 is between 5.5 and 7 kcal/mole for benzene at any temperature if the accommodation coefficient is between 0.1 and 1. The adsorption energy on the most active sites, $\Delta H_0 + \Delta H_1$, is thus between 13.8 and 15.3 kcal/mole.

The adsorption enthalpy on the most active sites may also be derived from the temperature variation of the average desorption time

$$\Delta H = r\frac{\partial \ln \bar{t}_d}{\partial(1/T)} \tag{19}$$

From the experimental data (Figure 9) it results that ΔH is between 11.5 and 14.5 kcal/mole. Both values of the adsorption energy on the most active sites, derived from the values of the heterogeneity factor and from the temperature variation of the average desorption time, are in good agreement with the differential adsorption enthalpy of benzene on uncoated crushed firebrick, 13.6 kcal/mole (Table II).

Whenever the elution peak is gaussian, the determination of the plate height and the derivation of the kinetic term of resistance to mass transfer are straightforward. Then the experimental results are in good agreement with the theoretical predictions by Giddings for a surface having active sites of high adsorption energy. When peaks are tailing, however, it is not possible to account for the experimental results this way; the plate height which is directly related to the standard deviation of a gaussian curve has no more sense. A more sophisticated theory would be needed to account for these tailing peaks, when tailing has a kinetic origin and is not related directly to the curvature of the adsorption isotherm.

Even when there are on the surface some active sites of high adsorption energy, leading to measurable band broadening, the kinetic term of resistance to mass transfer is relatively small. In the particular case studied here, this term is between 0.1 and 1 msec for benzene. With the same column, at a temperature above the melting point of benzophenone (49°) the term of resistance of mass transfer of benzene in the liquid phase is 1.6 msec, a value which is typical of what is currently obtained in gas–liquid partition chromatography. This comparison illustrates fairly well why the potentialities of gas–solid partition chromatography are much brighter than those of gas–liquid partition chromatography while this work shows the great experimental difficulties still to be overcome: the energetic heterogeneity of most exist-

ing surfaces and the large term of resistance to mass transfer in the gas phase which most often is the major contribution to the plate height at large carrier gas velocities.

Acknowledgment. This work was made under contract to the Direction des Recherches et Moyens d'Essais, Ministère des Armées, Paris, France.

Appendix

Nomenclature

A, cm^2	Surface area of the packing
a	Constant of the coupling term of the plate height equation
a_i	Fractional area occupied by ith type of sites
C_g, sec	Gas-phase mass transfer term of the plate height equation
C_k, sec	Kinetic mass transfer term of the plate height equation
$\bar{c}$, cm sec^{-1}	Mean molecular velocity
d_p, cm	Packing particle size
D_g, cm^2 sec^{-1}	Diffusion coefficient in the gas phase
f	Pressure correction term
j	Pressure correction term
H, cm	Plate height
H_g, cm	Part of plate height which originates in the gas phase
K, cm^2	Constant of the coupling term of the plate height equation
k'	Column capacity factor
L, cm	Column length
P	Ratio of inlet to outlet pressure
P_0, kg cm^{-2}	Outlet pressure
R	Ratio of air peak retention time to component retention time
r, kcal/deg	Gas constant
S	Heterogeneity factor
T, °K	Temperature
f_d^0, sec	Desorption time for a completely uniform surface
$\bar{t}_d$, sec	Average desorption time
t_m, sec	Elution time of methane
U, cm^3/m^2	Retention volume per surface area of packing corrected for dead volume
u_0, cm sec^{-1}	Outlet linear velocity
V_G, cm^3	Gas volume of a column
x, cm^{-1}	$x = u_0/D_g$
x_i	Fraction of adsorbed molecules on ith types of sites
α	Accommodation coefficient
ΔH_0, kcal mole^{-1}	Differential enthalpy of adsorption on the average surface
ΔH, kcal mole^{-1}	Differential enthalpy of adsorption on the most active sites of the surface
ΔH_1, kcal mole^{-1}	Difference in the adsorption energy on a heterogeneous surface
ΔH_v, kcal mole^{-1}	Latent heat of vaporization
γ	Tortuosity factor
ρ_i	Adsorption density on ith type of sites
σ	Standard deviation

A Modified Equation for Pore Volume and Area Distributions in Finely Divided and Porous Materials

by P. T. John and J. N. Bohra

National Physical Laboratory, New Delhi, India *(Received January 4, 1967)*

The Pierce equation has been modified, and using this equation, the pore volume and surface area have been computed from the desorption isotherm using the film thickness and Kelvin's radius. The equation is first solved for the pore volume using the pore radius, film thickness, and the observed desorbed volume. Substituting this value of pore volume in the equation, which relates the volume, surface, and radius of an open-ended cylinder, the surface area is determined. The computed values show good agreement with the experimental values.

Introduction

The determination of pore volume and surface area distributions in a porous system gives an insight into its physical structure. Shull[1] was one of the first to determine pore size distribution from gas desorption data. Barrett, Joyner, and Halenda[2] have described a theory and method for calculating the distributions. Pierce[3] has described a simplified method based on Kelvin's equation radii for computation of the pore size and surface area distributions from nitrogen desorption isotherms. The method involves fewer parameters when compared to those of Barrett, *et al.*[2] Orr and Dallavalle[4] have followed the method of Pierce[3] using modified values of film thickness. Their values seem to have been computed from an empirical equation, whereas those of Pierce are from experimental observations. According to Shull[1] it is probably better to use the flat-surface experimental data of film thickness.

Method of Computation

The BJH data[2] published by Pierce[3] are used in the present computations. The data are taken from the nitrogen desorption isotherm for bone-char. The derivation of the equation of Pierce, modified by the authors, is given below. Initially, at saturation pressure P_0, all the pores of adsorbent are supposed to be completely full. It implies that there is no surface available for adsorption. Let the vapor pressure be reduced in small decrements from P_0 to P_1. For nitrogen adsorption the capillary radius corresponding to any pressure P is given by Kelvin's equation.[3]

$$r = 4.14/\ln (P_0/P) \quad (1)$$

When pressure is reduced from P_0 to P_1, capillaries of radii larger than r_1 will be emptied. Let the pore size of capillaries of radius r_1 be R_1 and the corresponding film thickness is then t_1. Hence

$$R_1 = r_1 + t_1 \quad (2)$$

Let the mean values of pore radius, capillary radius, and film thickness in the vapor pressure range P_0–P_1 be $\bar{R}_1$, $\bar{r}_1$, and $\bar{t}_1$, respectively. Note that

$$\bar{R}_1 = (R_1 + R_0)/2,\ \bar{r}_1 = (r_1 + r_0)/2,$$

$$\text{and } \bar{t}_1 = (t_1 + t_0)/2$$

The volume of vapor desorbed, when pressure changes from P_0 to P_1, from the pores of mean pore radius, $\bar{R}_1$, may be looked upon as the difference between the pore volume of pores of mean radius, $\bar{R}_1$, and the volume of vapor adsorbed on the walls of those pores. Let the volume of these pores be v_1. The area contributed by these pores can be written as

(1) C. G. Shull, *J. Am. Chem. Soc.*, **70**, 1405 (1948).

(2) E. P. Barrett, L. G. Joyner, and P. P. Halenda, *ibid.*, **73**, 373 (1951).

(3) C. Pierce, *J. Phys. Chem.*, **57**, 149 (1953).

(4) C. Orr and J. M. Dallavalle, "Fine Particle Measurements," Macmillan and Co., London, 1959, p 272.

$$\Delta A_1 = (2v_1)(0.001558)/10^{-8}\bar{R}_1 \text{ cm}^2$$

$$\Delta A_1 = (2v_1)(0.001558)/10^{-4}\bar{R}_1 \text{ m}^2 \quad (3)$$

Area ΔA_1 is determined after finding the value of v_1 (see eq 6). Pore volume, v_1, multiplied by 0.001558 is the volume of the pore when v_1 is expressed in cc of gas volume. Radius and thickness are measured in angstroms. The volume F_1 (in cc of gas) that remains adsorbed on the walls of the pores is given by

$$F_1 = \Delta A_1(\bar{t}_1/3.6)0.23 \quad (4)$$

The film thickness divided by 3.6 gives the number of layers of molecules, since one molecule is 3.6 A in size. A unimolecular layer of nitrogen on 1 m^2 is equal to 0.23 cc of gas at STP. Substituting eq 3 in eq 4 we get

$$F_1 = (2v_1)(0.001558)(0.23\bar{t}_1)/3.6 \times 10^{-4}\bar{R}_1 \quad (5)$$

The amount desorbed (which is the observed value) when the pressure changes from P_0 to P_1 is given by

$$V_0 - V_1 = \Delta V_1 = v_1 - F_1 \quad (6)$$

Substituting the values of F_1 in eq 6, v_1, the only unknown quantity in eq 6, can be determined. Consider the next decrement of vapor pressure from P_1 to P_2. At P_2, let the pore radius, capillary radius, and film thickness be R_2, r_2, and t_2, respectively, and the corresponding mean values for the range P_1–P_2 be $\bar{R}_2$, $\bar{r}_2$, and $\bar{t}_2$, respectively. When pressure is changed from P_1 to P_2, there will be desorption from pores whose mean pore radius is $\bar{R}_2$. Let the volume of these pores be v_2. The contribution of area by these pores is given by

$$\Delta A_2 = (2v_2)(0.001558)/10^{-4}\bar{R}_2 \text{ m}^2 \quad (7)$$

The volume of vapor (in cc of gas at STP) that remains on the walls of the pores of mean pore radius $\bar{R}_2$ is given by

$$F_2 = \Delta A_2(\bar{t}_2/3.6)0.23 \quad (8)$$

where

$$\bar{t}_2 = (t_2 + t_1)/2$$

In addition to the above-mentioned desorption, when the vapor pressure is changed from P_1 to P_2 there will be thinning of the adsorbed layer from the walls of pores whose radii are larger than $\bar{R}_2$. The area of such pores has already been found to be ΔA_1. The volume f_2 evaporated from these walls is given by the expression

$$f_2 = \Delta A_1[(t_1 - t_2)/3.6]0.23$$

$$f_2 = \Delta A_1(\Delta t_2/3.6)(0.23) \quad (9)$$

Hence

$$V_1 - V_2 = \Delta V_2 = v_2 - F_2 + f_2 \quad (10)$$

Referring to eq 6 it may be stated that f_1 is zero since there existed no area from where evaporation could take place. Similarly, when vapor pressure is changed from P_2 to P_3

$$V_2 - V_3 = \Delta V_3 = v_3 - F_3 + f_3 \quad (11)$$

where

$$F_3 = \Delta A_3(\bar{t}_3/3.6)(0.23)$$

where

$$\bar{t}_3 = (t_3 + t_2)/2$$

and

$$f_3 = (\Delta A_1 + \Delta A_2)(\Delta t_3/3.6)(0.23)$$

where

$$\Delta t_3 = t_2 - t_3$$

Hence, the general equation can be written as

$$V_{m-1} - V_m = \Delta V_m = v_m - F_m + f_m \quad (12)$$

where V_{m-1} and V_m are, respectively, the volume of all the pores whose radii lie between R_{m-2} and R_{m-1}, and R_{m-1} and R_m.

$$F_m = (2v_m)(0.001558\bar{t}_m/3.6)(0.23)/10^{-4}\bar{R}_m = \Delta A_m(\bar{t}_m/3.6)(0.23)$$

where

$$\bar{R}_m = (R_{m-1} + R_m)/2$$

and

$$\bar{t}_m = (t_{m-1} + t_m)/2$$

and

$$\Delta A_m = (2v_m)(0.001558)/10^{-4}R_m \quad (13)$$

$$f_m = (\Delta A_1 + \ldots + \Delta A_{m-1})[(t_{m-1} - t_m)/3.6](0.23)$$

$$f_m = (\Delta t_m/3.6)(0.23)\sum_{i=1}^{i=m-1}\Delta A_i$$

This type of calculation is carried out to a pore size where capillary condensation is almost negligible.

Sample Calculations. (1) Referring to Table I, consider the desorption when the relative pressure is changed from 1.00 to 0.967. Substituting the value of ΔA_1 from eq 3 in eq 4, when $m = 1$ we get

$$F_1 = 2v_1(0.001558)(t_1/3.6)(0.23)/\bar{R}_1 \times 10^{-4}$$

$$F_1 = 2v_1(0.001558)(15.25 \times 0.23)/500 \times 10^{-4}$$

where $\bar{t}_1/3.6 = \bar{n}_1$ ($\bar{n}_1$ is the mean number of molecular

Table I: Calculation of Pore Volume and Surface Area Distribution for Bone-char

P/P_0	V	R	n	v^b	v^c	v^d	ΔA^b	ΔA^c	ΔA^d
1.000	152.0	...	19.0	...	...	...	...	...	...
0.967[a]	145.2	340	11.5	8.8	8.7	1.9	0.54	0.54	...
0.961	142.5	280	10.4	3.4	3.43	4.9	0.34	0.34	0.40
0.953	138.0	240	9.2	5.8	5.83	1.5	0.69	0.70	0.72
0.950	135.2	230	8.8	3.4	3.66	3.5	0.45	0.48	0.51
0.947	130.5	220	8.5	6.2	6.29	6.5	0.85	0.87	0.53
0.941	127.3	190	7.9	3.7	3.91	3.2	0.56	0.59	1.09
0.937	123.5	180	7.5	4.9	4.93	4.7	0.82	0.83	0.89
0.932	119.2	160	7.1	5.4	5.63	5.3	1.06	1.03	1.06
0.927	115.3	150	6.8	5.0	5.20	4.8	1.00	1.04	1.04
0.921	110.3	140	6.5	6.6	6.78	6.2	1.41	1.46	1.44
0.915	105.9	130	6.2	5.7	5.82	5.5	1.31	1.34	1.47
0.906	99.8	120	5.8	8.6	8.76	8.5	2.13	2.18	2.24
0.897	93.0	110	5.4	7.9	8.06	8.1	2.13	2.18	2.38
0.886	86.3	100	5.1	8.9	8.98	8.6	2.62	2.66	2.82
0.870	77.5	88	4.7	11.4	11.66	11.6	3.77	3.87	4.26
0.850	68.5	75	4.3	11.5	11.88	11.8	4.40	4.57	4.88
0.823	58.7	65	3.9	12.4	12.97	12.7	5.48	5.77	6.09
0.808	54.6	59	8.6	3.3	3.52	5.1	1.65	1.77	2.78
0.788	50.3	52	3.3	3.5	3.77	5.3	1.97	2.13	3.16
0.763	46.5	46	3.0	2.5	2.65	4.4	1.58	1.68	2.99
0.733	43.0	41	2.75	2.6	2.68	3.7	1.83	1.90	2.68
0.695	39.2	35	2.69	2.9	3.02	4.0	2.36	2.48	3.31
0.642	35.7	30	2.23	2.2	2.29	3.1	2.13	2.23	3.02
0.580	31.8	25	2.01	3.6	3.98	3.3	4 14	4.59	3.71
0.488	27.7	20	1.76	3.1	3.59	2.8	4.38	5.08	3.91
0.352	23.2	15	1.46	2.5	2.61	2.88	5.17	4.64	5.03
			Total calculated	145.8	150.56	143.8	54.77	56.91	62.33
			Total experimental		152.00			64.57	

[a] The mean pore radius corresponding to relative pressure 0.967 is taken as 500 A, $\bar{R}_1 = (R_0 + R_1)/2$, $\bar{R}_2 = (R_1 + R_2)/2$ ... etc. [b] See ref 3. [c] See eq 12. [d] Values determined by BJH.[2]

layers at relative pressure $P_1/P_0 = 0.967$). Hence, substituting the values from Table I in eq 12 we get

$$152 - 145.2 = v_1 - 2v_1(0.001558) \times (15.25 \times 0.23)/500 \times 10^{-4} + f_1$$

As stated earlier, $f_1 = 0$. Solving for v_1, we get $v_1 = 8.700$ cc. Substituting the value of v_1 in eq 3 we get

$$\Delta A_1 = 2 \times 8.7 \times 0.001558/500 \times 10^{-4} = 0.540 \text{ m}^2$$

(2) Now consider desorption from the relative pressures 0.967 to 0.961. In this case there is a wall-film contribution, f_2, toward desorption, since there exists an area of 0.540 m^2 at relative pressure P_1/P_0. Using eq 12 when $n = 2$

$$V_1 - V_2 = \Delta V_2 = v_2 - F_2 + f_2$$

or

$$145.2 - 142.5 = v_2 - 2v_2(0.001558) \times (10.95 \times 0.23)/310 \times 10^{-4} + 0.540 \times (11.5 - 10.4) \times 0.23$$

Solving for v_2, we get $v_2 = 3.432$ cc. Substituting this value of v_2 in eq 13 when $m = 2$, we get

$$\Delta A_2 = 2 \times 3.432 \times 0.001558/310 \times 10^{-4} = 0.3448 \text{ m}^2$$

Hence, the cumulative area would be

$$\Delta A_1 + \Delta A_2 = \sum_{i=1}^{i=2} A_i = 0.5420 + 0.3448 = 0.8868 \text{ m}^2$$

and the cumulative pore volume would be

$$v_1 + v_2 = \sum_{i=1}^{i=2} v_i = 8.700 + 3.432 = 12.132 \text{ cc}$$

All the succeeding distributions of area and pore volume have been computed in the similar manner.

Results and Discussion

The computed values of pore volume and surface area distributions are given in Table I, and the corresponding values by Pierce[3] and BJH[2] are also given for

comparison. The pore volume computed by the authors is in very good agreement with the experimental values whereas those by Pierce and BJH are lower. The surface area obtained by the authors shows better agreement with the experimental value when compared to that by Pierce but is lower than that by BJH. In the earlier methods[1-4] the determination of pore volume involved the squares of capillary and pore radius. It must be noted that errors are liable to occur in the values of capillary radius and film thickness due to the limitations of Kelvin's equation and the method of measurement of film thickness. Since they occur as squares, the error in the computation of pore volume will be greater and consequently it will be reflected in the value for the area. Since cumulative area is used in the succeeding calculations, the effect of earlier errors will give rise to more errors.

The modified equation for computation of pore volume contains two terms in the numerator. The second term involves the product of R and t. In the first step of computation (in the pressure range 1.00–0.967) the value of the second term is zero. In the succeeding computations the second term increases. Even for the last computation the value of the second term becomes only comparable to the first term. This implies that the error involved in the computations of pore volume by the modified equation is less when compared to that of Pierce. The computations of surface area by Pierce involve squares of the capillary radius whereas the modified equation avoids them. The computed value of the pore volume at each step has been used by Pierce as well as by the authors for the computation of area in the same step. Since the pore volume computed by the authors is more precise, as discussed earlier, their computed surface area will obviously be better.

Acknowledgment. The authors are thankful to Mr. G. D. Joglekar, scientist in charge of the division, for his continued interest in the work. We are also thankful to Mr. R. S. Sekhon for useful discussions. The authors express their gratitude to the Director of the National Physical Laboratory of India for the permission to publish the paper.

Proof of Structure of the Colored Photoproducts of Chromenes and Spiropyrans

by Jaroslav Kolc and Ralph S. Becker

Department of Chemistry, University of Houston, Houston, Texas 77004 *(Received March 13, 1967)*

Based on infrared, nuclear magnetic resonance, independent synthesis, and ultraviolet data, strong evidence for the structures of the colored photoproducts of the chromenes and spiropyrans is presented. The structure in the case of the chromenes is *o*-quinoneallide (II). A parallel structure is appropriate for the spiropyrans.

Introduction

In the course of investigation of spectroscopic and photochromic properties of spiropyrane, photochromism of the chromene half of such molecules was discovered in this laboratory[1] and structure II proposed for the colored form.[1]

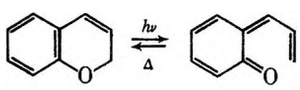

I II

Photochromism of spiropyrans has been known for some time, although, up to the present time, only one indirect piece of evidence has been given for the nature of the colored form of spiropyrans, which is considered to be as in IV

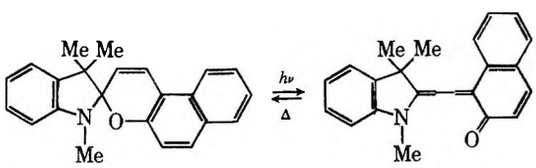

III IV

This evidence was based on the resemblance of the absorption spectrum to that of merocyanine dye.[2]

The purpose of this paper is to give more direct evidence for the structure of the colored photoproduct II. This will be based on the reduction of the photoproduct with lithium aluminum hydride at temperatures at which the photoproduct is being produced (−30 to −75°) and the identification of such reaction product. The reaction sequence would be expected to be

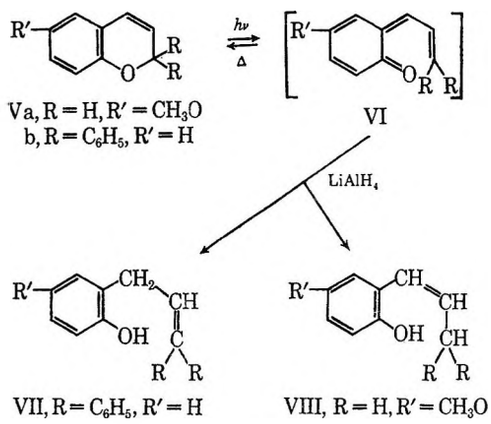

Va, R = H, R′ = CH_3O
b, R = C_6H_5, R′ = H

VI

VII, R = C_6H_5, R′ = H VIII, R = H, R′ = CH_3O

The colored product is expected to react with lithium aluminum hydride giving phenol VII or VIII. Such a phenol can be identified using infrared, nuclear magnetic resonance, and ultraviolet spectroscopy as well as by comparing such spectral data with those of independently synthesized compounds.

Experimental Section

For photoconversion of chromenes, quartz cells were immersed into a cooling bath (hexane–Dry Ice) in a quartz dewar flask and irradiated with ultraviolet light from a low-pressure mercury lamp, filtered through a Corning 9-30 filter.

For thin layer chromatography Chroma-Plates 7GF (Mallinckrodt) with Silicar (pH 6.5–7.2) were used, and detection was made by ultraviolet light.

(1) R. S. Becker and J. Michl, *J. Am. Chem. Soc.*, 88, 5931 (1966).

(2) R. Heiligman-Rim, Y. Hirshberg, and E. Fischer, *J. Chem. Soc.*, 156 (1961); *J. Phys. Chem.*, 66, 2465 (1962).

Infrared spectra (in carbon tetrachloride) were taken on Beckman IR-10 apparatus. The nuclear magnetic resonance (nmr) spectra (in the same solvent) were obtained on a Varian HA-100 high-resolution spectrometer. Ultraviolet spectra were taken on Cary Model 15 instrument using quartz optical cells.

The 2,2-diphenyl-2H-chromene was obtained from Dr. Livingstone of Huddersfield College of Technology, England; lapachenole (2,2-dimethyl-6-methoxy-7,8-benzo-2H-chromene) from Dr. J. W. Morgan of the Forest Products Research Laboratories, England; and 6-methoxy-2H-chromene from Sankyo Co., Ltd., Japan. The 2-allyl-4-methoxyphenol and 2-propenyl-4-methoxyphenol necessary for comparison were synthesized[3,4] from *p*-methoxyphenol (Eastman White Label).

The intense red color of the photoproduct, created by ultraviolet irradiation of the solution of 2,2-diphenyl-2H-chromene in 2-methyltetrahydrofuran (2-MeTHF) at −75°, rapidly disappeared by addition of lithium aluminum hydride at this temperature. The reaction mixture was treated with water and sodium hydroxide solution, acidified, extracted into ether, and evaporated to dryness. Thin layer chromatography revealed a spot with R_f 0.6 in addition to the main spot of the starting chromene (going with the front of the solvent mixture CCl_4–$CHCl_3$ = 2:1).

The same substance was produced in much greater quantity when a solution of the chromene in a slurry of lithium aluminum hydride in 2-MeTHF was simultaneously mixed and irradiated at −75° for 75 min. Whenever mixing during the irradiation was interrupted, the red color of the photocolored form of the chromene was created on the inner surface of the cell facing the source of irradiation and disappeared when the mixing was continued.

The reaction product was purified using column chromatography on neutral silica gel (pH 6.95) and spectra of the pure product (*ca.* 50% of weight of starting chromene) were taken. No such product was detected when the chromene was treated with a slurry of lithium aluminum hydride in 2-MeTHF under the same conditions (temperature, time) *without* irradiation.

6-Methoxy-2H-chromene and lapachenole were converted into phenols under similar conditions. Again, no products were detected when the chromenes were treated with lithium aluminum hydride *without* irradiation.

Results and Discussion

Conversion of 2,2-Diphenyl-2H-chromene into Phenol VII. There are two peaks in the infrared O–H region of the product, Figure 1A (plus a shoulder at higher concentrations). The same pattern is obtained for *o*-allylphenols,[5] where the peak at higher energy corresponds to the O–H frequency of the free OH group, and the second one, to the intramolecular hydrogen-bonded OH species of the type

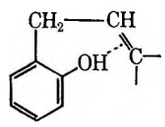

The nmr spectrum, Figure 2A, shows a doublet of two protons at τ 6.75 ($-CH_2-$), a triplet of one proton centered at τ 3.98 (—CH=C—, conjugated), and a set of 14 aromatic protons (τ 2.7–3.6).

Both the infrared and nmr spectra are fully consistent with structure VII.

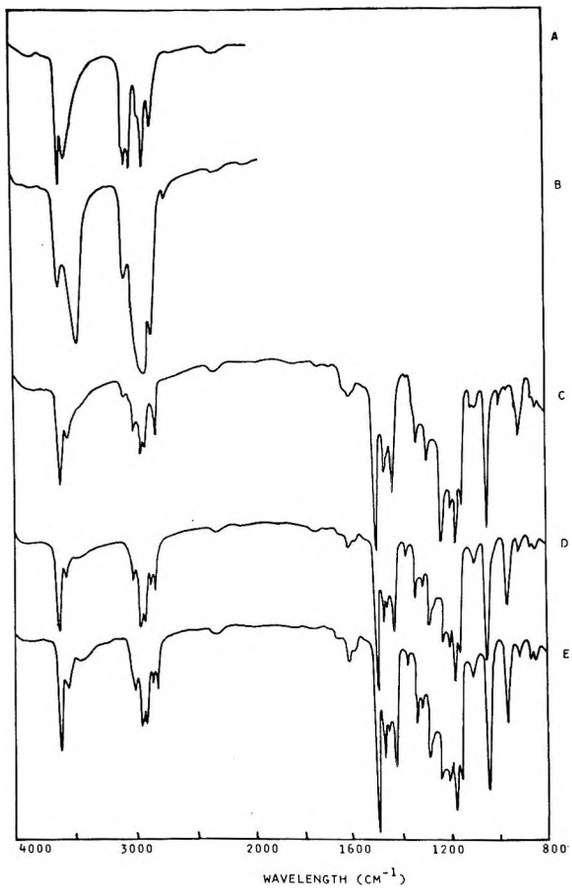

Figure 1. Infrared spectra: (A) phenol VII, (B) phenol IX, (C) 2-allyl-4-methoxyphenol, (D) phenol VIII, and (E) 2-propenyl-4-methoxyphenol.

(3) D. S. Tarbell in "Organic Reactions," Vol. 2, John Wiley and Sons, Inc., New York, N. Y., 1947, pp 1–48.

(4) J. H. Fletcher and D. S. Tarbell, *J. Am. Chem. Soc.*, **65**, 1431 (1943).

(5) A. W. Baker and A. T. Shulgin, *ibid.*, **80**, 5358 (1958).

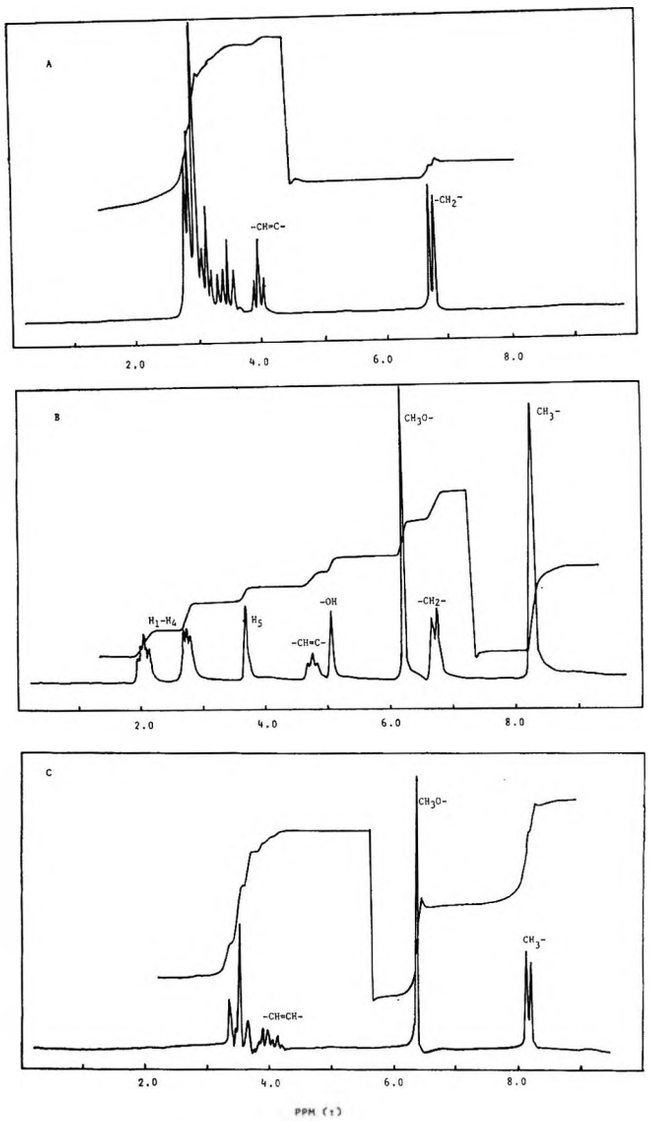

Figure 2. Nmr spectra: (A) phenol VII, (B) phenol IX, and (C) phenol VIII.

Conversion of Lapachenole (2,2-Dimethyl-6-methoxy-7,8-benzo-2H-chromene) into Phenol IX. As in the previous case, the infrared spectrum of the product, Figure 1B, shows two peaks in the O–H region (a free OH and intramolecular bonded OH). In this case, the peak corresponding to the intramolecular bonded OH is especially strong. It seems to be due to the fact that basicity of the π electrons in the double bond of the side chain are increased by the presence of two attached methyl groups, which increases the strength of the hydrogen bond.[5]

The spectrum of the deuterated phenolic product shows essentially no change in the mutual ratio of both O–D peaks compared with the O–H peaks.

Nmr peaks in Figure 2B corresponding to four aromatic protons H–H_4 in IX as well as the singlet τ 6.20 (MeO–) are at the same position as in the lapachenole. A single $>CMe_2$ in the lapachenole (τ 8.58) was changed to the singlet τ 8.25 in the product, corresponding to $C{=}CMe_2$. Further, there is a doublet of two protons at τ 6.72 ($-CH_2-$), a triplet of one proton at τ 4.75 ($-CH{=}C-$, nonconjugated), a singlet at τ 3.70 belonging to the H_5 in IX, and a singlet at τ 5.06 which can be depressed by deuteration with D_2O and thus corresponds to OH.

The ultraviolet spectrum of the product in 3-methylpentane at room temperature is quite similar to the spectrum of the simple 1-naphthol.

On the basis of the foregoing evidence we can write the reaction product as

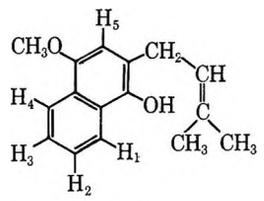

IX

Conversion of 6-Methoxy-2H-chromene into Phenol VIII. In this case the structure of the product was proved by comparison of the infrared, Figure 1D, and nmr data, Figure 2C, with those of the independently synthesized authentic 2-allyl-4-methoxyphenol, Figure 1C, and 2-propenyl-4-methoxyphenol, Figure 1E. The spectra are identical with those of the last named compound. Creation of the propenylphenol in this case is possible to explain as a consequence of the absence of conjugative substituents and/or steric effects of substituents in the photoproduct.

Results obtained from the three investigated chromenes with different structures are fully consistent with structure II as that for the photocolored product of a chromene. Moreover, the indoline portion of indolinospiropyrans does not play an active role in the formation of their colored form. At least studies by us on 1,3,3-trimethyl-2-phenyl-2-hydroxyindoline show that the indoline does not exhibit photochromism. This, plus the results on the chromenes, provides strong evidence that the structure of the indolinospiropyran photoproduct is that given (IV). Other photochromic spiropyrans such as dibenzo-, N-methylquinolino-, acridinospiropyran, etc., should have colored photoproducts with parallel structures.

Acknowledgments. We wish to thank Dr. M. R. Willcott of this university for his assistance in the interpretation of the nmr data as well as those who

gave us compounds as noted in the Experimental Section. This investigation was sponsored by U. S. Air Force, Systems Engineering Group, Wright-Patterson AFB, Ohio, Contract AF 33(615)-1733.

Relationship between the Intrinsic Viscosity and the Sedimentation Coefficient of a Monodisperse Polymer

by Ichiro Noda, Satoshi Saito, Teruo Fujimoto, and Mitsuru Nagasawa

Department of Synthetic Chemistry, Nagoya University, Furo-cho, Chikusa-ku, Nagoya, Japan
(Received April 3, 1967)

To study the hydrodynamic properties of dilute polymer solutions, the measurements of intrinsic viscosity and sedimentation coefficient of monodisperse poly(α-methylstyrene) in toluene (t) at 25° and in cyclohexane (c) at 39° were carried out. The observed sedimentation coefficient was extrapolated to meniscus to obtain the sedimentation coefficient at 1 atm by using Fujita's equation. From the comparison between the intrinsic viscosity $[\eta]$ and the frictional coefficient $[f]$ in the same solvent, the relationship of $[\eta]_t/[\eta]_c = ([f]_t/[f]_c)^{2.4}$ was obtained. This relationship is discussed in comparison with the current theories.

Introduction

To investigate the hydrodynamic properties of dilute polymer solutions, it is no doubt pertinent to study both the intrinsic viscosity and the sedimentation coefficient (or diffusion coefficient) simultaneously, since different types of flow of the polymer coil are observed in those measurements, that is, the rotational flow in intrinsic viscosity and the translational flow in sedimentation and diffusion.[1] It cannot always be assumed that both the intrinsic viscosity and the sedimentation coefficient can be interpreted by using the same hydrodynamic radius.

The intrinsic viscosities of flexible polymers have been extensively studied, but the rotational flow is so complicated that we are usually obliged to introduce some approximations into a theory which gives a relationship between intrinsic viscosity and molecular parameters.[2] In contrast to the intrinsic viscosity, according to the Kirkwood general theory of irreversible processes in polymer solutions,[3] the translational frictional coefficient can be unambiguously related to the segmental distribution of polymer coil, *i.e.*, to the molecular parameters at partial drainage as well as at the limit of nondrainage, whether the excluded volume effect exists or not. We believe that the translational frictional coefficient can be more clearly understood than the intrinsic viscosity. Unfortunately, however, it seems to us that most data of the sedimentation coefficients of flexible polymers should be carefully reexamined, because of the ambiguity arising from the polydispersity of the samples and also because the effect of the hydrostatic pressure on the sedimentation coefficient in organic solvents was not properly taken into account in the experiments so far reported. In particular, there are only a few reliable and consistent data to clarify the relationship between the sedimentation coefficient and the intrinsic viscosity of flexible polymers.[4,5] The purpose of the present paper

(1) J. G. Kirkwood and J. Riseman, *J. Chem. Phys.*, 16, 565 (1948).
(2) M. Kurata and H. Yamakawa, *ibid.*, 29, 311 (1958).
(3) J. G. Kirkwood, *J. Polymer Sci.*, 12, 1 (1954).

Table I: Molecular Weights of the Samples

	Sample													
	S-1	S-2	S-3	S-4	S-5	S-6	S-7	S-8	S-9	S-10	S-11	S-12	S-13	S-14
$M_n \times 10^{-4}$		3.54		7.16	11.5		20.4		27.2	38.5				
$M_w \times 10^{-4}$		3.94[a]		6.76[a]		13.5[b]		28.1[b]		40.0[b]	46.0[b]	60.0[b]	117[b]	136[b]
$M_v \times 10^{-4}$[c]	2.20	3.69	4.25	6.53	11.0	12.2	18.3	26.0	27.8	41.0	43.6	62.2	122	146
M_w/M_n		1.11		0.95						1.04				

[a] Determined by the Archibald method. [b] Determined by the light-scattering method. [c] M_v is calculated from eq 8.

is to report some experimental data on the relationship between the intrinsic viscosity and the sedimentation coefficient of a linear polymer. Special attention is given to the pressure dependence of the sedimentation coefficient and the rate of shear dependence of the intrinsic viscosity.

Experimental Section

Samples. The monodisperse poly(α-methylstyrenes) were prepared in our laboratory by an anionic polymerization technique previously reported.[6] All samples were repeatedly purified by precipitation from benzene solution using methyl alcohol. Two samples of lower molecular weights, S-1 and S-2, were fractionated by using toluene as solvent and methyl alcohol as nonsolvent at 25° to make their molecular weight distribution sharper, since the molecular weight distribution of a polymer of lower molecular weight is broader than that of higher molecular weight when they are prepared by an anionic polymerization. Then the samples were freeze-dried, followed by evacuation for about 24 hr at 80°. Before use, they were again evacuated for more than 8 hr at 80°.

The molecular weights of the samples given in Table I were determined by using light-scattering techniques or the Archibald method of sedimentation in cyclohexane and also by osmotic pressure measurement in toluene. The detailed results of the light-scattering and the osmotic pressure measurements will be described elsewhere. The ratios of weight-average molecular weight to number-average molecular weight, M_w/M_n, are given in Table I, but, presumably, must be as small as 1.01 if they are determined from the sedimentation study, which is believed to be more suitable for determining M_w/M_n of the samples having very narrow molecular weight distributions, as previously reported.[6]

Toluene of the first grade was shaken with concentrated H_2SO_4 until the H_2SO_4 layer did not show any color and then was dried with $CaCl_2$ and sodium metal, followed by fractional distillation over sodium metal at 1 atm. No impurity in toluene thus purified was detected by gas chromatography. Cyclohexane of a practical grade was passed through a silica gel column and dried with sodium metal, followed by fractional distillation over sodium metal at 1 atm. Neither ultraviolet spectroscopy nor gas chromatography showed any impurity, especially benzene, in cyclohexane thus purified.

Measurement of Intrinsic Viscosity. The measurements of viscosity were carried out in toluene at 25 ± 0.01° and in cyclohexane at 39 ± 0.01° using viscometers of the Ubbelohde type, one of which had three bulbs for giving rate of shear corrections to measured values. The dimensions of the viscometers used are given in Table II. The correction for the kinetic energy was less than 0.3% in all viscometers. The intrinsic viscosities at the limit of negligible rate of

Table II: Dimensions of the Viscometers[a]

Viscometer	10^2r, cm	h, cm	l, cm	Q, ml	γ, sec^{-1}	K, %
VS-53	1.80	15.3	14.3	1.4	$983/\eta_{rel}$	0.3 (in toluene at 25°)
VS-54	2.00	15.3	14.3	1.6	$742/\eta_{rel}$	0.3 (in cyclohexane at 39°)
		3.62		1.06	$315/\eta_{rel}$	0.2 (in toluene at 25°)
VS-56	2.28	6.13	20	1.1	$542/\eta_{rel}$	0.1 (in toluene at 25°)
		8.64		1.06	$754/\eta_{rel}$	0.1 (in toluene at 25°)

[a] r, radii of capillaries; h, heights of bulbs; l, lengths of capillaries; Q, volumes of bulbs; γ, rate of shear; K, contribution of the kinetic energy term.

(4) H. Lütje and G. Meyerhoff, *Makromol. Chem.*, **68**, 180 (1963); *Z. Physik. Chem.* (Frankfurt), **38**, 364 (1963).

(5) M. N. Ho-Duc and H. Daoust, report presented at the International Symposium on Macromolecular Chemistry of IUPAC, Kyoto, Japan, Oct 1966.

(6) T. Fujimoto, N. Ozaki, and M. Nagasawa, *J. Polymer Sci.*, **A3**, 2259 (1965).

shear were confirmed by using a viscometer of the Zimm type (rotational viscometer).[7] The values obtained using both types of viscometer agreed within the limit of experimental error (with Ubbelohde viscometer VS-56: $[\eta] = 2.44$ for S-13 and 2.77 for S-14; with Zimm viscometer: $[\eta] = 2.44$ for S-13 and 2.81 for S-14).

Measurement of Sedimentation Coefficient. Ultracentrifugation was carried out in toluene at 25 ± 0.2° and in cyclohexane at 39 ± 0.2° by using a Spinco Model E ultracentrifuge equipped with a schlieren optical system and an RTIC temperature control unit. An angular velocity of a rotor was chosen as slow as possible to reduce the pressure effect. The center pieces used in this work were 3, 12, and 30 mm and were chosen according to the molecular weight and the concentration of the polymer solution used. The sedimentation coefficient was calculated from the position of the maximum of the refractive index gradient which was determined using a microcomparater, since the schlieren patterns were of good gaussian distribution curves.

Since the pressure effect in organic solvents[8,9] is generally very large owing to their large compressibilities, we extrapolated apparent sedimentation coefficients to the meniscus by using Fujita's equation[10] (1) to have the values at 1 atm

$$S_{app} \equiv \frac{\ln (x_h/x_m)}{\omega^2(t - t_0)} = S^\circ\{1 - G[(x_h/x_m)^2 - 1]\} \quad (1)$$

and

$$G = [m(1 + 2kC_0) - kC_0]/2(1 + kC_0)$$

$$m = {}^1/_2\gamma\omega^2 x_m{}^2\rho_0{}^\circ$$

where ω is the angular velocity, t_0 the initial time correction, C_0 the initial concentration, k the concentration dependence coefficient of the sedimentation coefficient, S_{app} the apparent sedimentation coefficient defined by eq 1, S° the sedimentation coefficient at 1 atm, x_h the position of the maximum of the refractive index gradient, x_m the position of meniscus, γ the pressure dependence coefficient of sedimentation coefficient, and $\rho_0{}^\circ$ the density of the solvent at 1 atm. The true sedimentation coefficient S° is given from the intercept of the straight line when S_{app} is plotted against $(x_h/x_m)^2 - 1$. To calculate S_{app}, however, we must know the initial time correction t_0 which cannot be given directly from the experiments. Although the time when an angular velocity reaches two-thirds of the final speed is usually used to estimate t_0, this method is not precise enough to obtain t_0 used in eq 1.[9] Since both S° and t_0 are unknown, it is quite difficult to determine S° without ambiguity. In this work, therefore, we used two

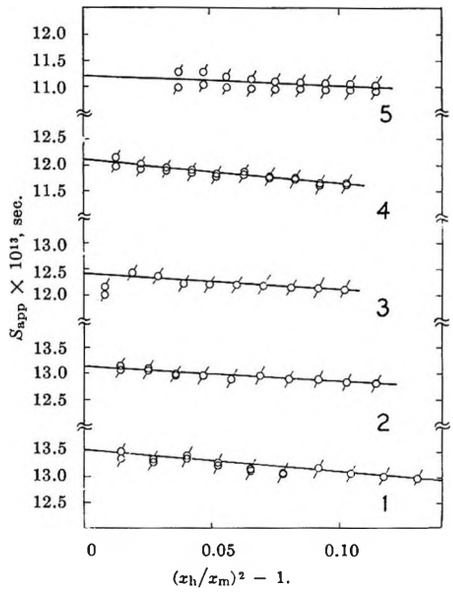

Figure 1. Change of the apparent sedimentation coefficient of S-11 calculated from the first method (○) and the second method (○) in cyclohexane at 39°: (1) C = 0.054 g/dl, ω = 42,040 rpm; (2) 0.093 g/dl, 39,460 rpm; (3) 0.190 g/dl, 39,460 rpm; (4) 0.282 g/dl, 39,460 rpm; (5) 0.386 g/dl, 39,460 rpm.

approximate methods and obtained almost the same results. The first method follows. Since a linear relationship was experimentally found to hold between $(x_h{}^2 - x_m{}^2)$ and time t if t is not very large,[11] the initial time correction t_0 is determined as the time when $x_h = x_m$ is reached. Then, S_{app} can be calculated from eq 1 by using this t_0 value. In the second method, both S° and t_0 are determined so that a standard deviation of the difference between the left-hand term and the right-hand term of eq 1

$$\Delta = \frac{\ln (x_h/x_m)}{\omega^2(t - t_0)} - S^\circ\{1 - G[(x_h/x_m)^2 - 1]\}$$

becomes minimum by using a high-speed electronic computer.[12] Almost the same values of sedimentation coefficient were obtained from both methods as shown in Figure 1. The relative differences between both S° values were from 2 to 0.5%.

The ultracentrifugation was carried out at different

(7) B. H. Zimm and D. Crothers, *Proc. Natl. Acad. Sci., U. S.*, **48**, 905 (1962).

(8) J. Oth and V. Desreux, *Bull. Soc. Chim. Belges*, **63**, 133 (1954).

(9) I. H. Billick, *J. Phys. Chem.*, **66**, 1941 (1962).

(10) H. Fujita, "Mathematical Theory of Sedimentation Analysis," Academic Press Inc., New York, N. Y., 1962.

(11) H. G. Elias, *Makromol. Chem.*, **24**, 30 (1959).

(12) A. Soda, T. Fujimoto, and M. Nagasawa, submitted for publication.

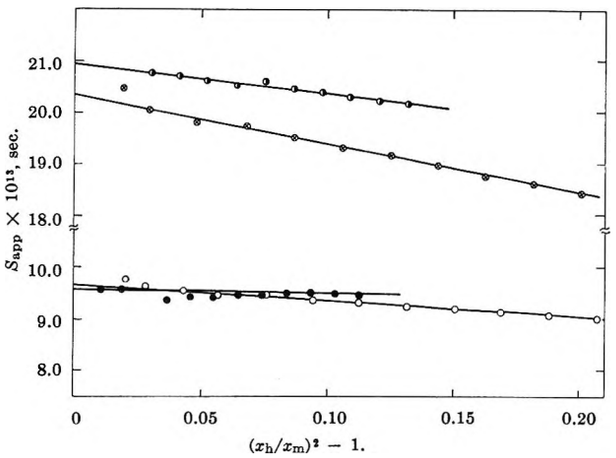

Figure 2. Effects of the angular velocity on the apparent sedimentation coefficient of S-13 (calculated from the first method): The circles ◑ and ⊗ show data at 31,410 and 59,780 rpm in cyclohexane at 39° (C = 0.132 g/dl), while the circles ● and ○ show data at 42,040 and 59,780 rpm in toluene at 25° (C = 0.180 g/dl).

velocities to confirm the applicability of these methods to the extrapolation. The intercepts of the straight lines for different angular velocities did not perfectly agree with each other as shown in Figure 2, but the relative differences between $S°$ values obtained at different velocities may be smaller than about 2%, which is as small as the ambiguity arising from the different methods of extrapolation described above. The tangent of the straight line, G, is larger in the poor solvent than in the good solvent.

The pressure dependence coefficient, γ, of sedimentation coefficient in eq 1 is defined by an equation giving the dependence of the apparent sedimentation coefficient on the actual hydrostatic pressure in solution, p. Thus, if pressure dependence of density, viscosity coefficient, and partial specific volume of the solvent used are known, γ can be calculated by

$$\gamma = \lambda + \frac{\bar{v}_0\rho_0^\circ(\kappa - \varphi)}{1 - \bar{v}_0\rho_0^\circ} \qquad (2)$$

where κ, λ, and φ are constants defined by Baldwin and van Holde.[13] Assuming φ to be zero in this range of pressure and using $\kappa = 0.12 \times 10^{-9}$, $\lambda = 1.7 \times 10^{-9}$ for toluene, $\kappa = 0.088 \times 10^{-9}$, $\lambda = 0.74 \times 10^{-9}$ for cyclohexane, which are given in a table summarized by Baldwin and van Holde, we have $\gamma = 1.00 \times 10^{-9}$ cm/dyne in toluene and $\gamma = 1.96 \times 10^{-9}$ cm/dyne in cyclohexane. The average values of γ obtained from the present sedimentation measurements with various molecular weights and various speeds of centrifugation are 1.1×10^{-9} cm/dyne in toluene and 2.3×10^{-9} cm/dyne in cyclohexane. The agreement between the values calculated and observed may be considered satisfactory. Therefore, it is probably safe to conclude that the correct sedimentation coefficients at 1 atm can be obtained by one of the methods described above.

Partial Specific Volume. A modified Gay-Lussac type of pycnometer having a volume of about 100 ml was used to determine the solution density. Then, the partial specific volume ($\bar{v}_0$) of poly(α-methylstyrene) was found to be 0.886 ml/g in cyclohexane at 39° and 0.873 in toluene at 25°.

Results

Since no definite experimental conclusion has yet been reached concerning the concentration dependence of viscosity of polymer solution, the viscosity data were extrapolated to infinite dilution by using not only Huggins' equation[14] (3) but also Mead and Fuoss' equation[15] (4) and Schulz and Blaschke's equation[16] (5)

$$\eta_{sp}/C = [\eta] + k'[\eta]^2C \qquad (3)$$

$$(\ln \eta_{rel})/C = [\eta] + k_m'[\eta]^2C \qquad (4)$$

$$\eta_{sp}C = [\eta] + k_s'[\eta]\eta_{sp} \qquad (5)$$

As shown in Figure 3, the values of intrinsic viscosity obtained by these methods agree within experimental error for the samples of high molecular weights, although deviations from linearity are observed if eq 4 and 5 are used in toluene and eq 3 in cyclohexane. The relationship between the Huggins constant k' and the molecular weight is given in Table III.

The sedimentation data were extrapolated to infinite dilution by using eq 6. It gives a good linear relationship even in good solvent as shown in Figure 4, whereas deviations from linearity are observed if eq 7 is used.

$$1/S° = (1/S_0°)(1 + kC) \qquad (6)$$

$$S° = S_0°(1 - kC) \qquad (7)$$

The relationship between the coefficients k and the molecular weight is also given in Table III.

The experimental results of $[\eta]$ and $S_0°$ are summarized in Table III. The double logarithmic plots of the intrinsic viscosity against the molecular weight in toluene and in cyclohexane are given in Figure 5. The relationships between them are expressed by

$$[\eta] = 1.01 \times 10^{-4}\,\bar{M}^{0.72} \text{ (in toluene at 25°)} \qquad (8)$$

$$[\eta] = 7.13 \times 10^{-4}\,\bar{M}^{0.51} \text{ (in cyclohexane at 39°)} \qquad (9)$$

(13) R. L. Baldwin and K. E. van Holde, *Fortschr. Hochpolymer. Forsch.*, 1, 451 (1960).

(14) M. L. Huggins, *J. Am. Chem. Soc.*, 64, 2712 (1942).

(15) D. F. Mead and R. M. Fuoss, *ibid.*, 64, 277 (1942).

(16) G. V. Schulz and F. Blaschke, *J. Prakt. Chem.*, 158, 130 (1941).

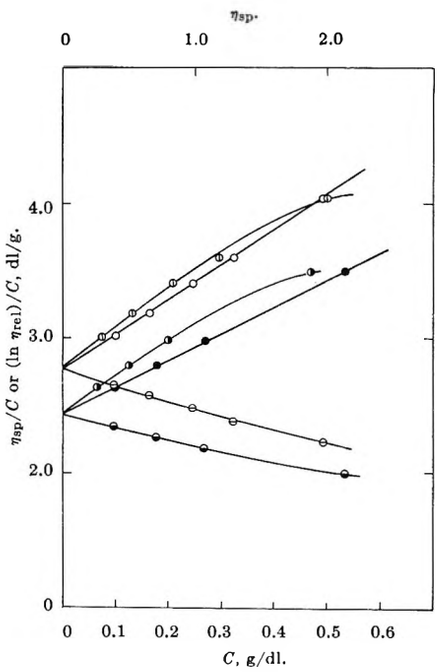

Figure 3. Concentration dependence of the specific viscosities of S-13 and S-14 in toluene at 25° according to eq 3 (● and ○), eq 4 (◒ and ⊖), and eq 5 (◑ and ⦶).

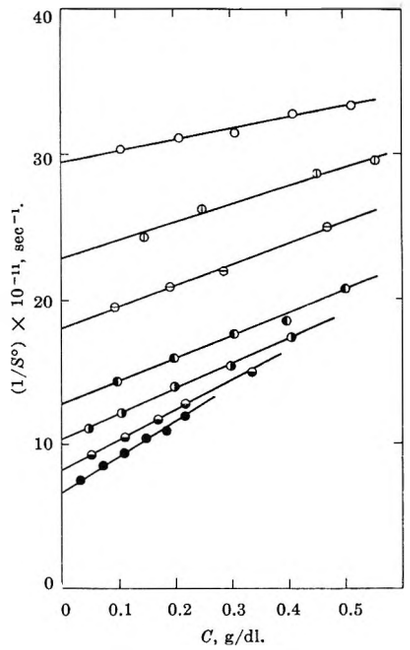

Figure 4. Concentration dependence of the sedimentation coefficient of poly(α-methylstyrene) in toluene at 25°: ○, S-3; ⦶, S-4; ⊖, S-6; ◐, S-8; ◑, S-11; ◒, S-12; ●, S-13.

Table III: Intrinsic Viscosity and Sedimentation Coefficient of Poly(α-methylstyrene) in Toluene and in Cyclohexane

Sample	In toluene at 25° [η], dl/g	k′	$10^{13}S_0°$, sec	k, dl/g	In cyclohexane at 39° [η], dl/g	k′	$10^{13}S_0°$, sec	k, dl/g
S-1	0.135	0.59			0.110	1.45		
S-2	0.196	0.42			0.150	0.71		
S-3	0.217	0.30	3.40	0.261	0.160	0.80	4.17	0.22
S-4	0.296	0.39	4.39	0.542	0.204	0.58	5.17	0.14
S-5	0.430	0.35						
S-6	0.463	0.34	5.56	0.81	0.274	0.85	7.08	0.22
S-7	0.621	0.37						
S-8	0.799	0.35	7.87	1.25	0.406	0.70	10.8	0.41
S-9	0.838	0.36						
S-10	1.11	0.37			0.512	0.80		
S-11	1.16	0.37	9.72	1.69	0.521	0.81	13.8	0.56
S-12	1.50	0.32	12.2	2.45	0.628	0.76	17.6	0.67
S-13	2.44	0.33	15.2	3.90	0.938	0.60[a]	22.7	1.19
S-14	2.77	0.34			1.03	0.55[a]		

[a] Obtained from eq 5.

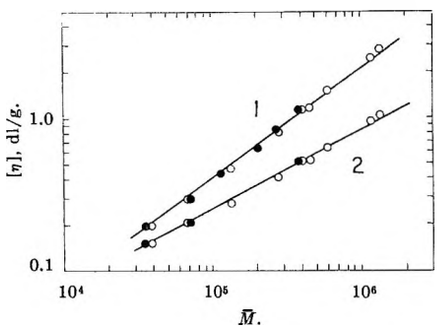

Figure 5. Log [η] *vs.* log M plot for poly(α-methylstyrene) in toluene at 25° (1) and in cyclohexane at 39° (2): ○, M_w; ●, M_n.

Equation 8 is in good agreement with the data previously reported.[17-19] The double logarithmic plots of the sedimentation coefficient against the molecular weight are shown in Figure 6. The relationships between them are given by

$$S_0° = 3.01 \times 10^{-15}\bar{M}^{0.44} \text{ (in toluene at 25°)} \quad (10)$$

$$S_0° = 2.04 \times 10^{-15}\bar{M}^{0.50} \text{ (in cyclohexane at 39°)} \quad (11)$$

From eq 9, 39° in cyclohexane may not be exactly the Θ point but is very close to it. This slight departure from the Θ point would not give any effect on our following discussion.

If we compare the sedimentation coefficient $S_0°$ and the intrinsic viscosity [η] obtained in the same solvent, the results are as shown in Figure 7. From the figure, we know that

$$[\eta]_t/[\eta]_c = ([f]_t/[f]_c)^{2.4} \quad (12)$$

(17) H. W. McCormick, *J. Polymer Sci.*, **41**, 327 (1959).

(18) A. F. Sirianni, D. J. Worsfold, and S. Bywater, *Trans. Faraday Soc.*, **55**, 2124 (1959).

(19) D. E. Burge and D. B. Bruss, *J. Polymer Sci.*, **A1**, 1927 (1963).

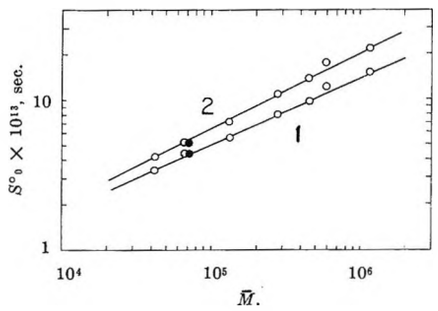

Figure 6. Log S°_0 *vs.* log M plot for poly(α-methylstyrene) in toluene at 25° (1) and in cyclohexane at 39° (2): ○, M_w (or M_v); ●, M_n.

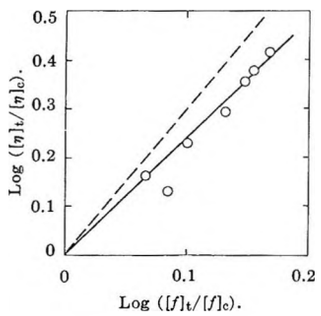

Figure 7. Relationship between the intrinsic viscosity and the frictional coefficient: ———, $\delta = 2.4$; – – – –, $\delta = 3.0$.

where the subscripts t and c denote toluene and cyclohexane, respectively.

Discussion

It is well known that the hydrodynamic properties of flexible polymers are determined by two fundamental factors, that is, the draining effect which is a purely hydrodynamic effect and the excluded volume effect which is a thermodynamic one. If we assume that a polymer coil is nondraining, according to Flory and Fox[20] and Mandelkern and Flory,[21] the intrinsic viscosity and the sedimentation coefficient of a flexible linear polymer are given by

$$[\eta] = \Phi_0\langle r^2\rangle^{3/2}/M = \Phi_0^2(\langle r^2\rangle_0^{3/2}/M)\alpha^3 = [\eta]_\theta\alpha^3 \quad (13)$$

$$[f] = f/\eta_0 = P_0\langle r^2\rangle^{1/2} = [f]_\theta\alpha \quad (14)$$

where $\langle r^2\rangle^{1/2}$ and $\langle r_0^2\rangle^{1/2}$ are the root-mean-square end-to-end distance and its value at the Θ point, and α is the expansion factor defined by

$$\alpha^2 = \langle r^2\rangle^{1/2}/\langle r^2\rangle_0^{1/2} \quad (15)$$

However, since the configuration statistics of polymer chain depart appreciably from that of a random-flight Gaussian chain as the molecular weight or the solvent power is increased, the hydrodynamic radius of the polymer chain is not proportional to the radius of gyration in good solvents. Strictly speaking, moreover, the hydrodynamic radius estimated from the intrinsic viscosity and that estimated from the translational frictional coefficient cannot be the same. The difference between two kinds of the hydrodynamic radius as well as the difference between the hydrodynamic radius and the radius of gyration was pointed out by several authors.[2,22,23]

Kurata and Yamakawa[2] used the theory of Kirkwood and Riseman,[1] assuming that the ratio between $\langle r_{ij}^{-1}\rangle$ and the corresponding quantity at the Θ point, $\langle r_{ij}^{-1}\rangle_0$, may be replaced by the average value over all pairs of i and j and also that $\sum_{i<j}\langle r_{ij}^{-1}\rangle$ may be replaced by $\sum_{i<j}\alpha_{ij}^{-1}\langle r_{ij}^{-1}\rangle_0$ as in

$$1/\tilde{\alpha} = \frac{\langle r_{ij}^{-1}\rangle}{\langle r_{ij}^{-1}\rangle_0} = \frac{\Sigma\langle r_{ij}^{-1}\rangle}{\Sigma\langle r_{ij}^{-1}\rangle_0} = \frac{\Sigma\alpha_{ij}^{-1}\langle r_{ij}^{-1}\rangle_0}{\Sigma\langle r_{ij}^{-1}\rangle_0} \quad (16)$$

where $\alpha_{ij}^2 = \langle r_{ij}\rangle^2/\langle r_{ij}\rangle_0^2$. Then, they obtained the results

$$[\eta] = [\eta]_\Theta(1 + 1.55z + \ldots) \quad (17)$$

$$[f] = [f]_\Theta(1 + 0.416z + \ldots) \quad (18)$$

Since

$$\alpha^2 = 1 + (4/3)z + \ldots \quad (19a)$$

and

$$\alpha_S^2 = \langle s^2\rangle/\langle s^2\rangle_0 = 1 + (134/105)z + \ldots \quad (19b)$$

where $\langle s^2\rangle^{1/2}$ and $\langle s^2\rangle_0^{1/2}$ are the radius of gyration and its value at the Θ point, respectively, it followed that

$$[\eta] = [\eta]_\Theta\alpha^{2.32} = [\eta]_\Theta\alpha_S^{2.43} \quad (20)$$

$$[f] = [f]_\Theta\alpha^{0.624} = [f]_\Theta\alpha_S^{0.652} \quad (21)$$

That is, we have $\delta = 3.73$, where δ is defined by

$$[\eta]/[\eta]_\Theta = ([f]/[f]_\Theta)^\delta \quad (22)$$

Differently from Kurata and Yamakawa, Stockmayer and Albrecht[22] calculated $\sum_{i>j}\langle r_{ij}^{-1}\rangle$ using the perturbation method of Fixman and introduced it into the following equation which is given by the Kirkwood general theory of irreversible processes in flexible polymer solutions[3]

(20) P. J. Flory and T. G. Fox, *J. Am. Chem. Soc.*, **73**, 1904 (1951).

(21) L. Mandelkern and P. J. Flory, *J. Chem. Phys.*, **20**, 312 (1952).

(22) W. H. Stockmayer and A. C. Albrecht, *J. Polymer Sci.*, **32**, 215 (1958).

(23) O. B. Ptitsyn and Y. E. Eizner, *Zh. Fiz. Khim.*, **32**, 2464 (1958); *Zh. Tekh. Fiz.*, **29**, 1117 (1959); O. B. Ptitsyn, *Vysokomolekul. Soedin.*, **3**, 1673 (1963).

$$f^{-1} = (n\rho)^{-1} + (3\pi\eta\, n^2)^{-1}\sum_{i>j}\langle r_{ij}^{-1}\rangle \qquad (23)$$

where ρ is the frictional coefficient of a segment and n is the number of segments in a polymer. Then, they obtained the result

$$[f] = 3\pi n^2 \frac{1}{\sum_{i>j}\langle r_{ij}^{-1}\rangle} = [f]_\Theta(1 + 0.609z + \ldots)$$
$$= [f]_\Theta\alpha^{0.914} \qquad (24)$$
$$= [f]_\Theta\alpha_s^{0.954}$$

Introducing this equation into eq 16 to calculate the intrinsic viscosity according to the method of Kurata and Yamakawa,[2] we obtain

$$[\eta] = [\eta]_\Theta(1 + 1.72z + \ldots) = [\eta]_\Theta\alpha^{2.58} \qquad (25)$$
$$= [\eta]_\Theta\alpha_s^{2.70}$$

Then, we have that the power of $[f]/[f]_\Theta$ in eq 22, δ, is 2.83.

On the other hand, assuming that the distance between i and j on a polymer chain in good solvents is given by $r_{ij} = b_0^2|i - j|^{1+\epsilon}$, Ptitsyn and Eizner[23] calculated the intrinsic viscosity and the frictional coefficient of polymer chain in good solvents from the theory of Kirkwood and Riseman[1] and the theory of Kirkwood[3] and then gave the equations in which universal constants, Φ_0 and P_0 in eq 13 and 14, are expressed by functions of ϵ as

$$[\eta] = 4.17 \times 10^{24}(1 - 2.63\epsilon + 2.86\epsilon^2) \times \langle s^2\rangle^{3/2}/M) \qquad (26)$$

$$[f] = 12.5(1 - 0.5\epsilon - 0.226\epsilon^2)\langle s^2\rangle^{1/2} \qquad (27)$$

Although they did not show the relationship between $[\eta]/[\eta]_\Theta$ and $[f]/[f]_\Theta$ in good solvents, it can be estimated from the values of $[\eta]/[\eta]_\Theta$ and $[f]/[f]_\Theta$ calculated for n (degree of polymerization) = 10^4, 10^5, and 10^6, and ϵ = 0.05, 0.10, 0.15, and 0.20.[4] The δ thus obtained is about 2.7 which is almost equal to the value of Stockmayer and Albrecht (2.83), but smaller than that of Kurata and Yamakawa (3.73).

Now the present experimental result gives the relationship of $[\eta]_t/[\eta]_c = ([f]_t/[f]_c)^{2.4}$ as shown in Figure 7. The result obtained here differs from the result of Lütje and Meyerhoff,[4] who demonstrated the relationship of $[\eta]/[\eta]_\Theta = ([f]/[f]_\Theta)^{3.0}$, but agrees with the result recently reported by Ho-Duc and Daoust.[5] Although there is no current theory which can give a really satisfactory explanation to the experimental relationship between intrinsic viscosity and frictional coefficient, it may be concluded that the experimental results are quite well explained by the theory of Ptitsyn and Eizner. Moreover, if we accept eq 28 obtained by

$$[\eta]/[\eta]_\Theta = (\langle s^2\rangle^{1/2}/\langle s^2\rangle_0^{1/2})^{2.2-2.4} \qquad (28)$$

experiments,[4,24] and also if the theory obtained by using perturbation method is applicable to the experiments in good solvents, we may use eq 24 and 28 to calculate δ. The value of δ thus obtained is from 2.3 to 2.5. The result seems to indicate that the theory of Stockmayer and Albrecht on sedimentation is valid.

Very recently, it was suggested that, in order to interpret the experimental results of intrinsic viscosity of polystyrene,[25] it is necessary to take into account not only the excluded-volume effect but also the draining effect of a polymer coil. Even if the draining effect is not negligible in a polymer coil, the conclusion obtained here would not be affected, because the ratio $[\eta]/[f]^3$ is not markedly influenced by the draining effect.[1,2] However, more data of the samples having higher molecular weights may be required to confirm the speculation.

Based on their conclusion that the higher terms of z in eq 17 are not important even in good solvents, Stockmayer and Fixman[26] presented eq 29 to estimate the unperturbed dimension of a polymer chain from the relationship between $[\eta]$ and M in good solvents.

$$[\eta]/M^{1/2} = K_v + 0.51\Phi_0 BM^{1/2} \qquad (29)$$

where $K_v = \Phi_0[\langle r^2\rangle_0/M]^{1/2}$ and $\Phi_0 = 2.87 \times 10^{21}$. Similarly, the unperturbed dimension may be estimated from the relationship[27] between $[f]$ and M by using eq 30. Equation 30 can be transformed from eq 24 when the expansion of a polymer coil is not very large.

$$[f]/M^{1/2} = K_f + 0.201P_0^3K_f^{-2}BM^{1/2} \qquad (30)$$

where $K_f = P_0[\langle r^2\rangle_0/M]^{1/2}$ and $P_0 = 5.2$. Figure 8 shows the plot of $[\eta]/M^{1/2}$ *vs.* $M^{1/2}$ while Figure 9 shows that of $[f]/M^{1/2}$ *vs.* $M^{1/2}$. The unperturbed dimensions of poly(α-methylstyrene), $(\langle r^2\rangle_0/M)^{1/2}$, which are obtained from the intercepts in Figures 7 and 8 are 6.45×10^{-9} and 7.11×10^{-9}, respectively. Considering the ambiguities in the absolute values of Φ_0 and P_0^2, it may be concluded that both values agree with each other. Similar deviations from linearity are observed in both plots if the solvent is good and the molecular weight is high. The deviation is well known in the study of intrinsic viscosity of linear polymer. On the same idea

(24) W. R. Krigbaum and D. K. Carpenter, *J. Phys. Chem.*, **59**, 1166 (1955).

(25) G. C. Berry, *Polymer Letters*, **4**, 161 (1966).

(26) W. H. Stockmayer and M. Fixman, *J. Polymer Sci.*, **C1**, 137 (1963).

(27) J. M. G. Cowie and S. Bywater, *Polymer*, **6**, 197 (1965).

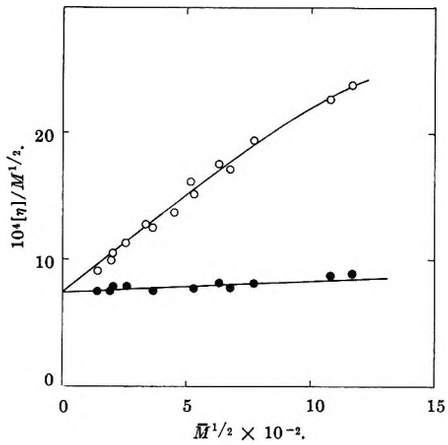

Figure 8. Plot of $[\eta]/M^{1/2}$ *vs.* $M^{1/2}$ in toluene at 25° (○) and in cyclohexane at 39° (●).

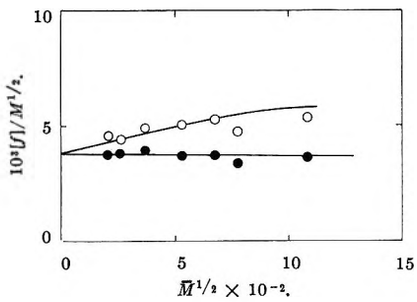

Figure 9. Plot of $[f]/M^{1/2}$ *vs.* $M^{1/2}$ in toluene at 25° (○) and in cyclohexane at 39° (●).

as in the derivation of eq 29, we can obtain a close form of the α^3 type from eq 24 by using the variational method of Fixman[28]

$$([f]/[f]_0)^3 = 1 + 1.83z \tag{31}$$

That is

$$([f]/M^{1/2})^3 = K_f{}^3 + 0.60P_0{}^3BM^{1/2} \tag{32}$$

However, the plot of $([f]/M^{1/2})^3$ against $M^{1/2}$ also shows the deviation from linearity and cannot improve the disagreement at high molecular weight in good solvents. The deviation may also be due to the neglect of higher terms.

Finally, the concentration dependence of sedimentation coefficient is briefly discussed. The theories on the concentration dependence of sedimentation coefficient were presented by Yamakawa[29] and Pyun and Fixman.[30] According to Pyun and Fixman, the concentration dependence of sedimentation coefficient, that is, k in eq 6 is given by

$$k = (7.16 - \kappa(A)) \frac{(4\pi/300)a^3N}{M} \tag{33}$$

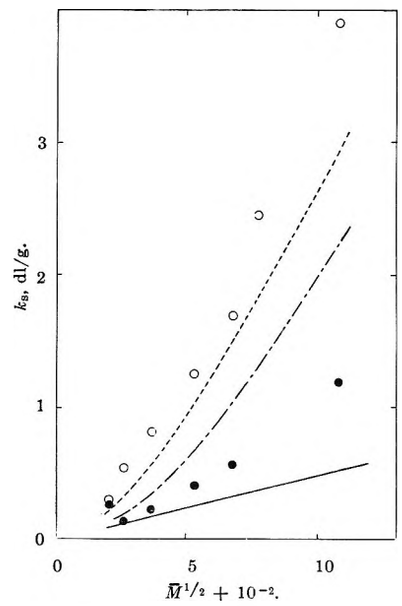

Figure 10. Variation of k with $M^{1/2}$ in toluene at 25° (○) and in cyclohexane at 39° (●): ———, Pyun and Fixman (in cyclohexane at 39°); – – – –, Pyun and Fixman (in toluene at 25°); — - —, Yamakawa (in toluene at 25°).

and $A = 3n^2X/8\pi a^3$, where a is the radius of a polymer chain, n is the number of segments per molecule, and X is the second virial coefficient for segment–segment interaction. According to Yamakawa, k is given by

$$k = 1.65[\eta]\lambda(x) \log (1 + 5.73x) \tag{34}$$

where $x = z/\alpha^3$.

It is clear from eq 33 and 34 that the concentration dependence of sedimentation coefficient remains finite and k is proportional to $M^{1/2}$ at the Θ point according to the theory of Pyun and Fixman, whereas the dependence disappears at the Θ point according to the theory of Yamakawa. In Figure 10, the curves calculated from both theories are compared with the experimental data. The theoretical values in toluene were calculated by using the excluded-volume function z which is estimated from the equation $\alpha_\eta{}^3 = 1 + 1.55z$, while the theoretical values in cyclohexane were calculated by using $\kappa_d(0) = 2.60$ instead of $\kappa(0)$ in eq 33.[30] If we take into account the ambiguities in z estimated from $\alpha_\eta{}^3$ and in the values of κ, we may conclude that the theory of Pyun and Fixman agrees with the experiments at least qualitatively in both good and poor solvents, whereas the theory of Yamakawa agrees with experiments in good solvent only.

(28) M. Fukatsu and M. Kurata, *J. Chem. Phys.*, **44**, 4539 (1966).
(29) H. Yamakawa, *ibid.*, **36**, 2995 (1962).
(30) C. W. Pyun and M. Fixman, *ibid.*, **41**, 937 (1964).

Production of Isomeric Nitrophenols in Radiolysis of Aqueous Nitrobenzene Solution

by R. W. Matthews and D. F. Sangster

Australian Atomic Energy Commission Research Establishment, Lucas Heights, Sutherland, N.S.W., Australia
(Received April 12, 1967)

The isomeric distribution of nitrophenols formed during the radiolysis of aerated aqueous nitrobenzene has been studied. The *o*-nitrophenol yield was affected by addition of 0.1 m*M* dichromate and varied with dose rate, whereas the *m*- and *p*-nitrophenol yields were substantially unaffected. The results show that all three isomers may be formed by unimolecular or pseudo-unimolecular decomposition of the corresponding oxygenated nitrobenzene–hydroxyl radical adduct. In the case of the *ortho* product there is, however, a competing reaction whereby pairs of *ortho* adducts undergo bimolecular dismutation giving half the number of nitrophenol molecules. The yield may be further reduced by a recombination reaction between the ·OH adduct and the nitrobenzene-reducing radical adduct. Dichromate reacts rapidly with the nitrobenzene–hydroxyl radical adduct preventing the two bimolecular reactions and giving nitrophenol in equivalent yield. The isomeric product ratios *ortho*:*meta*:*para* are 2:1:1. These ratios reflect the extent of attack of hydroxyl radical at different positions of the aromatic ring and are those expected of a very reactive homolytic reagent with some electrophilic character.

Introduction

As part of a program concerned with the reactions of the hydroxyl radical on aromatic solutes in aqueous solutions exposed to high-energy ionizing radiation,[1,2] we have been studying its reaction with nitrobenzene. The nitro group is particularly interesting as an aromatic substituent because it is an extreme case of substituent directional effect on an attacking reagent. Thus, a better understanding of the electrophilic reaction characteristics of the hydroxyl radicals may be obtained.

In this paper we report investigations on the isomeric distribution of the nitrophenols produced during radiolysis at air-equilibrated natural pH (pH 5.5). The yield of *o*-nitrophenol was markedly increased by low concentrations of dichromate whereas other electron scavengers had no effect. There was also a pronounced dependence of *o*-nitrophenol yield $G(o\text{-NP})$, on dose rate. The *meta* and *para* isomers varied only slightly under these conditions. These effects were further investigated and the corrected isomeric product ratios obtained are more nearly those expected for hydroxyl radical reactions than are those published previously.

Experimental Section

Materials and Irradiation. All reagents used were AR grade; the nitrobenzene was redistilled before preparing solutions of it in water distilled from acid dichromate and alkaline permanganate. Pyrex irradiation bottles (55 ml capacity) were soaked in nitric acid, thoroughly washed, and then heated for several hours at 550° before each irradiation. All solutions irradiated were 0.8 m*M* nitrobenzene, aerated, and at pH 5.5 unless otherwise stated. In all experiments the radiation dose was approximately 20 krads. Most of the irradiations were carried out using ^{60}Co γ rays. For some dose rate studies, spent reactor fuel elements were used. The dose was estimated using Fricke dosimetry and the correction applied for the difference in electron

(1) R. W. Matthews and D. F. Sangster, *J. Phys. Chem.*, **69**, 1938 (1965).

(2) D. F. Sangster, *ibid.*, **70**, 1712 (1966).

density between 0.8 N sulfuric acid and the irradiated solution.

Deaerated solutions of nitrobenzene containing added solutes were prepared in syringes by the technique of Hart, *et al.*[3] The solutions were irradiated in the syringes. Portions of unirradiated solutions were retained for nitrobenzene determination by spectrophotometric measurement at 268 mμ. In some other experiments, solutions were irradiated in a cell fitted with a sintered glass base through which nitrogen was bubbled continuously during the irradiation. The nitrogen had previously been passed through an aqueous nitrobenzene solution of approximately the same nitrobenzene concentration as that irradiated.

o-Nitrophenol Determination. To separate the *o*-nitrophenol, the irradiated solution was buffered to pH 6.8 with sodium phosphate and steam distilled. The distillate was adjusted to pH 12 with sodium hydroxide and the optical density measured at 416 mμ. A correction was necessary to allow for the 3% of *p*-nitrophenol which also was distilled under our experimental conditions. The contribution to the optical density from nitrobenzene was obtained from appropriate blanks.

To show that the steam-volatile product formed during irradiation from solutions containing dichromate was entirely *o*-nitrophenol, a solution containing 0.8 mM nitrobenzene and 0.2 mM dichromate was irradiated. After adjusting the pH to 13, the unchanged nitrobenzene was extracted with carbon tetrachloride. The aqueous solution was then buffered to pH 6.8. Steam distillation and optical density measurements were carried out as before. The value obtained by this method agreed with that for solutions without the extraction of nitrobenzene. The absorption spectra of the distillate at acid and alkaline pH were found to be essentially indistinguishable from authentic *o*-nitrophenol.

Hydrogen peroxide is formed during the radiolysis of aqueous solution. There is, therefore, the possibility of its reacting with dichromate and nitrobenzene to give nitrophenol. A yellow color, which increased in intensity with dichromate concentration, was noticed in the alkaline distillate from unirradiated solutions of nitrobenzene containing 4.0×10^{-5} M hydrogen peroxide and potassium dichromate. The unirradiated blank values were subtracted for dichromate concentrations up to 0.2 mM. At higher concentrations the blanks were large enough to introduce uncertainties especially since the appropriate hydrogen peroxide yield could not be estimated exactly. Because the G value for the production of hydrogen peroxide probably approaches the "molecular" yield of 0.7 at the higher concentrations of potassium dichromate, it was assumed that the hydrogen peroxide concentration in these solutions irradiated to 20 krads would be approximately 1.4×10^{-5} M. Blank determinations were consequently made using solutions of 0.8 mM nitrobenzene containing 1.4×10^{-5} M hydrogen peroxide and various concentrations of potassium dichromate. The solutions were allowed to stand for 30 min, which was the approximate time from the commencement of irradiation to the commencement of analysis. When the potassium dichromate concentration was less than 0.3 mM, the blank was insignificant but became appreciable at concentrations above this. The appropriate blank values were subtracted from the values obtained for irradiated solutions by the following modified procedure. The pH of the solution (50 ml) was adjusted to 4–5, and the nitrobenzene and nitrophenols were extracted with 25 ml of chloroform. The nitrophenols were then back-extracted with 50 ml of 0.01 M sodium hydroxide, buffered to pH 6.8, and steam distilled as before.

Determination of m- and p-Nitrophenols. The *m*- and *p*-nitrophenols were determined by the following method. Uniformly labeled C^{14} nitrobenzene obtained from Amersham Radiochemical Centre was purified by steam distillation. Aliquots of a stock solution were diluted to give solutions 0.8 mM in nitrobenzene of a convenient activity and in some experiments containing other solutes. The solutions irradiated were each approximately 1-ml total volume and were analyzed by paper chromatographic separation and Schöniger flask combustion of the active areas. A carrier solution of *o*-, *m*-, and *p*-nitrophenates (Na form) was added to each irradiated solution such that 0.1 ml of the diluted solution contained about 20 μg of each nitrophenol. Aliquots (0.1 and 0.2 ml) were spotted onto Whatman no. 1 paper with hot air drying (60° at the surface of the paper). The paper was exposed to HCl vapor, since this was found to restrict the spot size, before chromatographic development with benzene–diethylamine–water solvent system.[4] The developed chromatograms were air-dried and the nitrophenols were cut out, combusted in Schöniger flasks,[5] and counted by the liquid scintillation method. The activities were compared with the activity of the unirradiated nitrobenzene solutions by adding aliquots from a microsyringe to the counting solutions. Blanks were carried out on the unirradiated solutions in each

(3) E. J. Hart, S. Gordon, and J. K. Thomas, *J. Phys. Chem.*, 68, 1271 (1964).

(4) R. W. Matthews, *J. Chromatog.*, 20, 190 (1965).

(5) R. W. Matthews, Australian Atomic Energy Commission, AAEC, TM 216, 1963.

case. $G(o\text{-NP})$ could not be determined by this method because of its volatility from the paper.

High-Pressure Oxygen Experiments. In some experiments the concentration of molecular oxygen in the solution was increased by a high pressure of oxygen over the solution. A small pressure vessel of about 10-ml internal volume was provided with a lid which could be screwed down onto a rubber O ring. The lid also incorporated an O-ring valve which could be connected directly to an oxygen cylinder. Tests showed that the seals did not leak appreciably overnight. Five milliliters of the solution under investigation was contained in a glass tube fitted with a cone and standard taper glass plug. A hole was drilled in each end of the plug, and the apparatus was inverted as the pressure was raised slowly to ensure that the gas saturated the solution. After irradiation, the end of the pressure vessel was chilled by immersion in alcohol–Dry Ice mixture for 30 min. The gas pressure was released, and the frozen solution in the tube was allowed to melt before being analyzed for *o*-nitrophenol.

Results and Discussion

To establish that hydroxyl radicals were responsible for production of *o*-nitrophenol, various known radical-scavenger species were added to nitrobenzene solutions before irradiation. The hydroxyl radical scavengers ethanol, formate, bromide, ferrocyanide, and phenol decreased the radiolytic yield of *o*-nitrophenol. The hydrated electron scavengers nitrate, acetone, and oxygen had little or no effect. In the case of potassium dichromate, however, a marked increased was observed both in aerated and deaerated solutions. Since this effect does not appear to have been reported previously, it was investigated further.

Effect of Dichromate. $G(o\text{-NP})$ values as a function of dichromate concentration are given in Figure 1. Solutions containing 4.8 mM dichromate were at pH 4.3. The pH increased to 5.5 at 0.2 mM and was constant below this concentration. $G(o\text{-NP})$ was 1.0 in deaerated 0.8 mM nitrobenzene solutions containing 0.2 mM dichromate and 0.99 in nitrogen-flushed solutions. These values are in good agreement with the 1.03 found in aerated solution.

In order to explain the increase in $G(o\text{-NP})$ in the presence of dichromate, consideration was given to the possibility that the reducing radicals, the hydrated electrons and hydrogen atoms, might be converted by the dichromate to an hydroxylating species, although this is not allowed for in the published mechanisms for the radiolysis of dichromate in acid solutions.[6] The percentages of the hydrated electron reacting with dichromate can be calculated, from published rate constant data,[7] for each dichromate concentration. The change in these percentages bears no resemblance to the increase in $G(o\text{-NP})$ observed. Another possibility, that dichromate might react with the nitrobenzene–electron adduct[3,7] to give *o*-nitrophenol, can be discounted for similar reasons. Since $G(o\text{-NP})$ in 0.2 mM dichromate solutions is virtually the same in aerated and nitrogen-flushed solutions, the species $O_2\cdot^-$ cannot be implicated. Nor can the hydrogen atom, which reacts very readily with oxygen giving $HO_2\cdot$. At the pH used, $HO_2\cdot$ ionizes to $O_2\cdot^-$. For similar reasons, hydrogen atom–solute adducts cannot be involved.

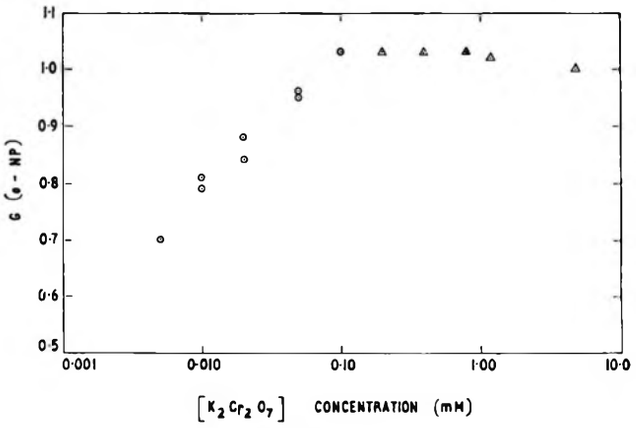

Figure 1. Addition of dichromate to aerated 0.8 mM nitrobenzene, pH 4.3–5.5, 20 krads, 1.8 krads/min: ⊙, standard determination; △, modified method.

The yields obtained for each isomer at different dose rates and in the presence of various solutes are given in Table I. Solutions were irradiated at their natural

Table I: Isomeric Nitrophenol Yields—0.8 mM Nitrobenzene

			20 krads, 1.8 krads/min		
Atm	mM	Solute	$G(o\text{-NP})$	$G(m\text{-NP})$	$G(p\text{-NP})$
Air	...	...	0.66	0.42	0.45
Air	0.2	$K_2Cr_2O_7$	1.03	0.48	0.51
N_2	0.2	$K_2Cr_2O_7$	0.99[a]	...	...
Air	...	...	0.95[b]	0.39[b]	0.41[b]
Air	...	...	0.36[c]	0.37[c]	0.46[c]
N_2	...	...	0.12	0.08	0.22
130 atm of O_2	...	...	0.71	...	...
65 atm of O_2	...	...	0.66	...	...

[a] Flushed with N_2 during irradiation. [b] Dose rate 0.2 krad/min. [c] Dose rate 14 krads/min.

(6) T. J. Sworski, *J. Phys. Chem.*, **63**, 823 (1959); A. R. Anderson and Farhatziz, *Trans. Faraday Soc.*, **59**, 1299 (1963). See also M. Lefort, *J. Chim. Phys.*, **54**, 782 (1957).

(7) M. Anbar and P. Neta, *Intern. J. Appl. Radiation Isotopes*, **16**, 227 (1965); Israel Atomic Energy Commission, I.A. 1079, 1966.

pH 5.5 for aerated and pH 7 for deaerated solution. In most cases values are the average of four determinations and reproducibility was within ±0.02.

The above contentions are supported by the fact that in the presence of dichromate the yields of *m*- and *p*-nitrophenol (Table I) increased only slightly (12%) compared with $G(o\text{-NP})$ (56%). The behavior is therefore not general, but peculiar to the formation of some or all of the *o*-nitrophenol. Particular attention must therefore be given to the reactions of the *ortho* adduct.

Dorfman, Taub, and Bühler[8] showed that in the case of aqueous solutions of aromatic solutes, the hydroxyl radical adds on to the benzene ring to give a hydroxycyclohexadienyl species. In aerated solutions, molecular oxygen adds on to this species readily to give a peroxy radical, which, they suggested, disappears in steady-state radiolysis by a first-order reaction to give phenols and $HO_2\cdot$.

The behavior of aqueous nitrobenzene solutions can be explained if it is assumed that in the absence of dichromate each *ortho* ·OH adduct (*o*-nitrophenol precursor) does not necessarily give a molecule of *o*-nitrophenol product. On the other hand, dichromate in aerated or deaerated solution oxidizes all nitrobenzene··OH adducts to the isomeric nitrophenols corresponding to the location of the –OH group on the cyclohexadienyl ring.

That oxygen is not essential for the formation of phenol from irradiated aqueous benzene was shown by Baxendale and Smithies.[9] They obtained high G(phenol) values from deaerated solutions containing ferric and cupric ions. Allen[10] considers that the metal ions may oxidize the benzene··OH radical adduct directly to the phenol in this case.

Figure 1 shows that some increase in $G(o\text{-NP})$ occurred even with a dichromate concentration below 0.01 mM. These concentrations are of the same order as those reached by slowly reacting radical species such as those which disappear by a bimolecular reaction. The results, therefore, suggest that, at dichromate concentrations below 0.1 mM, a dichromate–radical reaction producing *o*-nitrophenol competes with a radical–radical reaction which does not give *o*-nitrophenol or, at least, gives a lower yield.

Since the *o*-nitrophenol yield is not influenced by the addition of electron scavengers other than dichromate, the proposed radical–radical reaction which lowers the *o*-nitrophenol yield cannot be a recombination reaction between nitrobenzene··OH radical adduct and an electron adduct.

The possibility remains that the *o*-nitrophenol yield is reduced by a dismutation reaction in which two ·OH adducts give one molecule of product

$$2NO_2C_6H_5OHO_2\cdot \longrightarrow NO_2C_6H_4OH + NO_2C_6H_5 + H_2O + 2O_2 \quad (1)$$

similar to the reaction proposed by Nakken[11] in the radiolysis of aqueous *p*-aminobenzoic acid solution. In our case this competes with the reaction

$$NO_2C_6H_5OHO_2\cdot \longrightarrow NO_2C_6H_4OH + HO_2 \quad (2)$$

which has been suggested for aqueous benzene solutions[8] and in which each ·OH adduct gives a molecule of product.

Reaction 2 is unimolecular, or if reaction with another entity is necessary to bring about decomposition of the adduct, is pseudo-unimolecular. Reaction 1 is bimolecular. It follows that the extent of each will depend upon the steady-state concentration of the reacting radical species and hence upon the dose rate.

Effect of Dose Rate. $G(m\text{-NP})$ and $G(p\text{-NP})$ were found to be essentially independent of dose rate (Table I). Figure 2 shows that at the dose rate (1.8 krads/min) chosen for the dichromate investigations, $G(o\text{-NP})$ is in the rate-dependent region and at zero dose rate the value must approach the 1.03 found in the presence of dichromate.

From 1 to 10 krads/min, $G(o\text{-NP})$ decreased with dose rate, and this is attributed to competition between bimolecular reactions and reaction 2. However, if reaction 1 were the only significant bimolecular reac-

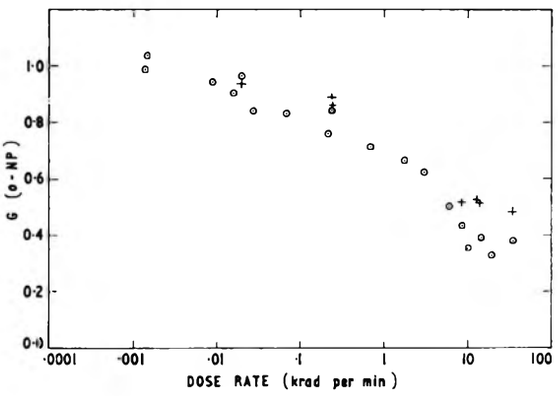

Figure 2. Effect of dose rate 0.8 mM nitrobenzene, 20 krads: ⊙, pH 5.5, no solute, aerated; +, pH 4, aerated.

(8) L. M. Dorfman, I. A. Taub, and R. E. Bühler, *J. Chem. Phys.*, **36**, 3051 (1962).

(9) J. H. Baxendale and D. Smithies, *J. Chem. Soc.*, 779 (1959).

(10) A. O. Allen, "The Radiation Chemistry of Water and Aqueous Solutions." D. Van Nostrand Co., Inc., Princeton, N. J., 1961, p 131.

(11) K. F. Nakken, *Radiation Res.*, **21**, 446 (1964).

tion, then G(*o*-NP) would not drop below 0.51 which is half its value at low dose rates. In fact it decreased to 0.36. This means that there must be another reaction which decreases the yield. This reaction becomes increasingly important with increasing dose rate indicating, once again, a second-order radical–radical reaction.

In studying the effect of hydrogen ion concentration (pH) on this system[12] we found that this reaction is the recombination reaction between the *ortho* ·OH adduct and the reducing radical–nitrobenzene adduct giving the original nitrobenzene and no net reaction. At pH 5.5 this reaction becomes important above 4–5 krads/min. At pH 4 or less the electron adduct is protonated and does not react with the *ortho* ·OH adduct. G(*o*-NP) at high dose rate and pH 4 (Figure 2) was found to be 0.52 which is just one-half the value at zero dose rate.

At dose rates greater than 10 krads/min, G(*o*-NP) remains constant, and in this region, therefore, it may be assumed that the unimolecular reaction 2 is negligible. There is a competition between the two bimolecular reactions and, since the relative extent of these two reactions is not affected by dose rate, G(*o*-NP) remains constant.

Since high oxygen concentration does not affect G(*o*-NP) greatly, the nitrobenzene–radical adducts are almost certainly completely oxygenated in aerated solution. The dose-rate dependence does confirm that the reaction giving *o*-nitrophenol at low dose rates is, indeed, first order. Nitrobenzene as a solute therefore resembles benzene[8] more nearly than *p*-aminobenzoic acid.[11]

Post-Irradiation Effect. No post-irradiation effects have been found in solutions irradiated at low dose rate (0.013 krad/min). At high dose rate (4.1 krads/min), G(*o*-NP) increased 5% over the first day and then remained steady. All measurements have therefore been made within 1 hr of removal from source. It is apparent that the dose-rate effects are not caused by post-irradiation phenomena. Any unstable species, *e.g.*, peroxides, might be decomposed by the analytical method which involves heating the solution.

$HO_2\cdot$ as a Hydroxylating Agent. The radical $HO_2\cdot$ or its ionized form $O_2\cdot^-$ is a well-known hydroxylating agent in organic chemical synthesis and is the active constituent in certain reagents.[13] There is no evidence from our investigations to suggest that, in the radiolysis of nitrobenzene solutions, these radicals act as significant hydroxylating agents. At high oxygen pressures when all the hydrated electrons would be expected to react with oxygen, the G(*o*-NP) values (0.66 and 0.71) are nearly the same (0.66) as when no more than a few per cent form $HO_2\cdot$. Nor is there any evidence that $O_2\cdot^-$ reacts with the ·OH adduct to form a phenol.[8,11]

meta and para Isomers. The virtual constancy of the yields of *m*-nitrophenol and *p*-nitrophenol means that all of these products arise from such reactions as (2), and their precursors do not undergo dismutation or recombination reaction to any great extent. There is however a slight effect, the yields being about 12% higher in the presence of dichromate than in its absence. This indicates that even at the low dose rates used there are some residual bimolecular reactions reducing the yields. Alternatively, these differences might be due to additional and unknown reactions in the presence of the strong oxidizing reagent dichromate.

In deaerated solution (Table I), G(*o*-NP) and G(*m*-NP) were about one-fifth of the values found in aerated solutions whereas G(*p*-NP) was about one-half. This shows that recombination is relatively more important for *ortho* and *meta* adducts than for *para*.

It is reasonable to assume that, in the case of dismutation reactions, at least one of the reactants must correspond in isomeric configuration to the final product of the reaction. An *ortho* adduct will undergo collision with *meta* or *para* adducts almost as frequently as with its fellow *ortho* adducts. Assuming that the yields in the presence of dichromate reflect the ratios of the isomeric precursors present during the irradiation, it is possible to obtain from our experimental results a semiquantitative idea of the results of these collisions, although there are insufficient data to solve the equations uniquely. *ortho–ortho* collisions give *ortho* product—perhaps at nearly every collision. Collisions involving *meta* or *para* adducts are much less effective.

Differences in Behavior. It is apparent that the behavior of the *ortho* adduct is different from that of the *meta* or *para* adducts and that there are also minor differences between the latter adducts.

The polarographic and electron spin resonance studies of Corvaja, Farnia, and Vianello[14] on nitrophenol radical anions are relevant to our irradiated system because the protonated forms of the nitrophenol–electron adducts are isoelectronic with the nitrobenzene–hydroxyl radical adducts.

Our radiolytic results are in qualitative agreement with their observations, the *ortho* adduct undergoing both dismutation and recombination reactions more readily than do either *meta* or *para* adducts. Alternatively or additionally, the unimolecular decom-

(12) R. W. Matthews and D. F. Sangster, to be published.

(13) W. T. Dixon and R. O. C. Norman, *Nature*, 196, 891 (1962).

(14) C. Corvaja, C. Farnia, and E. Vianello, *Electrochim. Acta*, 11, 919 (1966).

position of the *ortho* adduct may be particularly slow. The spatial configuration of the *ortho* adduct is such that the hydrogen of the OH group is close to the oxygens of the NO_2 group allowing it to form a six-membered ring by hydrogen bonding. This would be expected to confer stability and reduce the likelihood of unimolecular decomposition thus allowing bimolecular reactions to proceed.

Reaction 2 in the paper of Corvaja, *et al.*,[14] suggested that one of the products of radiolysis might be *o*-nitrosophenol. We therefore irradiated a solution of nitrobenzene at high dose rate (25 krads/min). These conditions would be expected to be the most favorable for such a bimolecular reaction. The light absorption at 472 mμ, where alkaline solutions of *o*-nitrosophenol exhibit a maximum,[15] could be completely accounted for by the known concentrations of the three isomeric nitrophenols. There is therefore no evidence for the formation of nitrosophenol under our experimental conditions.

·OH Radical Balance. The radiolytic yield of primary ·OH radical at this pH is 2.4. The nitrophenol product yield in the presence of 0.1 m*M* dichromate totals 2.02. This means that 84% of the ·OH radical reactions are accounted for. The remainder may be due to ·OH radical attack at either the C-1 position or nitro group and reactions giving products other than nitrophenols such as dialdehydes, dimers, and peroxide species.

Partial Rate Constants. It is usually assumed that, once interfering reactions have been eliminated, the isomeric product distribution reflects faithfully the extent of attack by the reagent on the different ring positions of the aromatic substrate. If this is taken as valid, we are able to calculate the reaction rate constants at the three different isomeric positions for hydroxyl-radical attack on the nitrobenzene molecule, free of any interference from dismutation or recombination reactions.

Taking $G_{OH} = 2.4$, the total reaction rate constant[7] $k_{\cdot OH+nitrobenzene} = 1.9 \times 10^9\ M^{-1}\ sec^{-1}$ and $G(o\text{-NP}) = 1.03$, $G(m\text{-NP}) = 0.48$, and $G(p\text{-NP}) = 0.51$, one obtains the following absolute rate constants in units of $10^9\ M^{-1}\ sec^{-1}$ for total attack at two *ortho* positions 0.81, two *meta* positions 0.40, and one *para* position 0.40. ·OH radical reactions unaccounted for total 0.30. The corresponding rate in unsubstituted benzene is 0.63 at each ring position (units $10^9\ M^{-1}\ sec^{-1}$).

Other Hydroxylating Reagents. Other authors have reported isomeric ratios for the nitrophenols formed in the hydroxylation of nitrobenzene using radiation[16] or chemical reagents[17-19] such as Fenton's reagent. The oxidizing species in the radiolysis of aqueous solutions is uncharged,[20] and there are very good reasons for claiming that it is the hydroxyl radical.[21]

Comparison of isomeric ratios and rates of attack can be used to indicate if the hydroxyl radical is the attacking species in the various chemical systems.

The dose rate used by Loebl, Stein, and Weiss[16] is about 2.2 krads/min so their *o*-nitrophenol yield will not reflect the extent of attack at the *ortho* position. Under the experimental conditions used for Fenton's reagent by Loebl, Stein, and Weiss[17] and by Norman and Radda,[18] the steady-state concentration of *ortho* adduct would be expected to be much higher than in our radiolysis experiments. This means that almost all the *o*-nitrophenol found by them probably came from a dismutation mechanism and must be allowed for by doubling their *ortho* yield. The total reaction rate relative to benzene noted by Norman and Radda is 0.14 which is much less than $k_{\cdot OH+nitrobenzene}/k_{\cdot OH+benzene} = 0.39/1.2$ reported by Matthews and Sangster[1] and a more recent unpublished measurement 0.5/1.2 made by us. After we had completed the experimental part of this work, the paper by Hamilton, Hanifin, and Friedman[19] appeared. The isomeric ratios they obtained, 2:1:1, is in striking agreement with our result. However, the reaction rates relative to benzene of anisole 1.4, chlorobenzene 0.6, and nitrobenzene 0.6 for their catalytic system are not in good agreement with our radiolytic values[1] phenol 0.9, chlorobenzene 0.9, and nitrobenzene 0.4.

The evidence shows that the hydroxyl radical is not the reactive entity in any of the chemical hydroxylating reagents.

·OH Reaction Characteristics. Important from the point of view of the reaction characteristics of the hydroxyl radical are the $2m:p$ and $2o:p$ product ratios of 1:1 and 2:1, respectively, which we have found.

The $2m:p$ ratio of about unity and the lower reaction rate compared with unsubstituted benzene are typical of a reagent exhibiting some degree of electrophilic character. This confirms the observations of Lindsay Smith and Norman[22] and of Anbar, Meyerstein, and Neta.[23]

(15) J. P. Phillips and F. C. Nachod, Ed., "Organic Electronic Spectral Data," Vol. II, Interscience Publishers, Inc., New York, N. Y., 1960, p 54.

(16) H. Loebl, G. Stein, and J. Weiss, *J. Chem. Soc.*, 2704 (1950).

(17) H. Loebl, G. Stein, and J. Weiss, *ibid.*, 2074 (1949).

(18) R. O. C. Norman and G. K. Radda, *Proc. Chem. Soc.*, 138 (1962).

(19) G. A. Hamilton, J. P. Friedman, and P. M. Campbell, *J. Am. Chem. Soc.*, **88**, 5266 (1966); G. A. Hamilton, J. W. Hanifin, and J. P. Friedman, *ibid.*, **88**, 5269 (1966).

(20) A. Hummell and A. O. Allen, *Radiation Res.*, **17**, 302 (1962).

(21) C. J. Hochanadel, *ibid.*, **17**, 286 (1962).

The $2o:p$ ratio of 2 shows no selectivity between these positions and is the ratio expected from such a highly reactive reagent as hydroxyl radical. This is in agreement with the high absolute reaction rates found.

Acknowledgments. The authors wish to thank Mr. D. F. O'Regan for technical assistance, Mr. B. M. O'Leary for carrying out the irradiations, and Dr. J. H. O'Donnell for loan of the pressure vessel.

(22) J. R. Lindsay Smith and R. O. C. Norman, *J. Chem. Soc.*, 2897 (1963).

(23) M. Anbar, D. Meyerstein, and P. Neta, *J. Phys. Chem.*, **70**, 2660 (1966).

Donor Properties of Diethers

by A. F. Garito and B. B. Wayland

John Harrison Laboratory of Chemistry and Laboratory for Research on the Structure of Matter, University of Pennsylvania, Philadelphia, Pennsylvania 19104 *(Received April 17, 1967)*

The equilibrium constants and thermodynamic values for 1:1 adduct formation of 1,4-dioxane, 1,3-dioxane, 1,1-dimethoxymethane, and 1,2-dimethoxyethane with iodine are reported. The donor properties of these diethers are discussed in terms of the effects of the two equivalent donor sites present.

Introduction

The donor properties of basic solvents containing a single ether oxygen have been extensively investigated.[1-4] With the exception of dioxane, little has been reported on the donor properties of solvents containing two ether oxygens. The bases 1,4-dioxane, 1,3-dioxane, 1,1-dimethoxymethane, and 1,2-dimethoxyethane have recently received wide attention as nonaqueous solvents, particularly as media for polymerization reactions. The interest in these bases as nonaqueous solvents prompts us to report the donor properties of these bases as measured by the thermodynamics of adduct formation with iodine.

Experimental Section

Reagents and Solutions. Reagent grade iodine was sublimed before use. Reagent grade phenol was distilled and sublimed once. The bases (Fisher reagent grade) were refluxed and distilled over Na metal immediately before use. Fisher Spectroanalyzed carbon tetrachloride was used without further purification. All solutions were prepared and used within a 1-hr period. No change in the electronic spectra of the solutions was observed over a 24-hr period.

Apparatus. Spectroscopic measurements were made with a Beckman DB spectrophotometer with a fluid-thermostated cell compartment. The temperature was measured by inserting a thermocouple directly into the cell. The temperature was maintained constant within $\pm 0.1°$. The solution concentrations were corrected for volume changes due to any change in temperature.

The phenol O–H frequency shifts were measured on a Perkin-Elmer 521 infrared spectrometer.

Procedure. The equilibrium constants at 25.0° (Table I) were obtained by analytical solution of the Rose–Drago equation

(1) M. Brandon, M. Tamres, and S. Searles, Jr., *J. Am. Chem. Soc.*, **82**, 2129, 2134 (1960).

(2) R. West, D. L. Powell, M. K. T. Lee, and L. S. Whatley, *ibid.*, **86**, 3227 (1964).

(3) T. M. Barakat, M. J. Nelson, S. M. Nelson, and A. D. E. Pullin, *Trans. Faraday Soc.*, **62**, 2674 (1966).

(4) W. Gerrard and E. D. Macklen, *Chem. Rev.*, **59**, 1105 (1959).

Table I: Data and Equilibrium Constants for 1 : 1 Adducts of the Diethers with Iodine at 25° and λ 450 mμ

Donor	C_A, M	C_B, M	$A - A^0$	$\epsilon_C - \epsilon_A$	K, l./mole
1,1-Dimethoxymethane	0.006890	0.04460	0.106		
		0.08919	0.208	573	0.63 ± 0.08
		0.2230	0.448		
		0.4459	0.872		
		0.8919	1.409		
1,2-Dimethoxyethane	0.005459	0.04248	0.166		
		0.08496	0.315	635	1.19 ± 0.08
		0.2124	0.692		
		0.4248	1.160		
1,3-Dioxane	0.005366	0.08027	0.191		
		0.2007	0.455	679	0.71 ± 0.03
		0.4013	0.812		
		0.8027	1.309		
1,4-Dioxane	0.005044	0.04087	0.1475		
		0.08173	0.288	705	1.08 ± 0.05
		0.2043	0.642		
		0.4087	1.092		
		0.8173	1.658		

Table II: Data and Thermodynamic Values for 1 : 1 Adducts of the Diethers with Iodine

Donor	C_A, M	C_B, M	$A - A^0$	$\epsilon_C - \epsilon_A$	Temp, °C	K, l./mole	$-\Delta H$, kcal/mole	ΔF, kcal/mole	$-\Delta S$, cal/mole
1,1-Dimethoxy-	0.006889	0.3012	0.488	573	25.2	0.636		0.27 ± 0.02	11.6 ± 0.8
methane	0.006852	0.2996	0.455		29.1	0.594			
	0.006818	0.2982	0.427		32.6	0.558			
	0.006787	0.2968	0.403		36.0	0.528	3.2 ± 0.2		
	0.006756	0.2957	0.380		39.2	0.500			
1,2-Dimethoxy-	0.005451	0.2124	0.692	635	25.2	1.182		−0.10 ± 0.02	12.1 ± 0.8
ethane	0.005431	0.2113	0.644		28.8	1.094	3.7 ± 0.3		
	0.005406	0.2103	0.603		32.2	1.017			
	0.005356	0.2084	0.530		39.6	0.889			
1,3-Dioxane	0.005673	0.2135	0.504	656	24.9	0.736		0.20 ± 0.02	13.1 ± 0.8
	0.005645	0.2124	0.468		28.5	0.683			
	0.005617	0.2114	0.437		32.0	0.638			
	0.005589	0.2104	0.407		35.5	0.595	3.7 ± 0.2		
	0.005567	0.2095	0.382		38.5	0.559			
1,4-Dioxane	0.005043	0.2043	0.642	705	25.0	1.080	3.8 ± 0.3	−0.05 ± 0.02	12.9 ± 0.8
	0.005016	0.2032	0.590		29.3	0.991			
	0.004971	0.2013	0.518		35.9	0.865			
	0.004948	0.2004	0.485		39.2	0.809			

$$K^{-1} = \frac{C_A C_B}{A - A^0}(\epsilon_C - \epsilon_A) - C_A - C_B + \frac{A - A^0}{\epsilon_C - \epsilon_A}$$

where C_A is the initial acid concentration, C_B is the initial base concentration, $A - A^\circ$ is the difference in the absorbance of a solution of acid at concentration C_A and a solution of acid and base at concentrations C_A and C_B, and $\epsilon_C - \epsilon_A$ is the difference in molar absorptivities of the complex (C) and acid (A).

The enthalpy measurements were made from the temperature dependence of the equilibrium constants. A single-solution technique that utilizes the Rose–Drago equation was used in the enthalpy calculations.[5] The ΔH values determined by the single-solution technique are insensitive to small errors in K and $\epsilon_C - \epsilon_A$. The value of ΔH is, however, very sensitive to the temperature dependence of $\epsilon_C - \epsilon_A$. The absorptivity difference $(\epsilon_C - \epsilon_A)$ was found to be temperature independent within experimental error. Several runs were

(5) R. L. Carlson and R. S. Drago, *J. Am. Chem. Soc.*, **84**, 2320 (1962).

made on each iodine–base system, and the measured values were found to be within experimental error.

The phenol frequency shift measurements were made on CCl_4 solutions containing 0.15 M phenol with several base concentrations. Two well-resolved O–H frequencies are observed for these solutions. The frequency shift $\Delta\nu$(OH) is the difference in the O–H stretching frequency for free and complexed phenol.

Results and Discussion

The equilibrium constants and the thermodynamic values for 1:1 adduct formation of diether donors with iodine are given in Tables I and II, respectively. The equilibrium constants and enthalpies for formation of diether adducts with iodine are significantly smaller than those of the monoether–iodine adducts. The dioxane–iodine thermodynamics have been redetermined and found to be in good agreement with previous work on this system[6] (Table III).

Table III: Comparative Thermodynamic Data for Formation of Iodine Adducts

Donor	Solvent	K, l./mole	$-\Delta H$, kcal/mole
1,4-$(CH_2)_4O_2$	CCl_4	1.08[a]	3.8[a]
		1.14[b]	
1,3-$(CH_2)_4O_2$[a]	CCl_4	0.71	3.7
$CH(OCH_3)_2$[a]	CCl_4	0.63	3.2
$(CH_2)_2(OCH_3)_2$[a]	CCl_4	1.19	3.7
$(CH_2)_2O$[c]	n-C_7H_{16}	0.94	3.8
$(CH_2)_3O$[c]	n-C_7H_{16}	3.85	6.4
$(CH_2)_4O$[c]	n-C_7H_{16}	2.54	5.3
$(CH_2)_5O$[c]	n-C_7H_{16}	2.51	4.9
$(C_2H_5)O$[d]	CCl_4	0.97	4.3

[a] This paper. [b] See ref 6; temperature 17°. [c] M. Brandon, M. Tamres, and S. Searles, Jr., *J. Am. Chem. Soc.*, **82**, 2129, 2134 (1960). Calculated using the Benesi–Hildebrand equation. Converted from mole fraction to liters per mole. [d] P. A. D. DeMaine, *J. Chem. Phys.*, **26**, 1192 (1957). Calculated using the Benesi–Hildebrand equation.

The difference in enthalpies of adduct formation for the diethers with iodine are small. The equilibrium constants are much more sensitive to small differences in donor properties and will be used here as a means of comparing donor properties.

An acid–base equilibrium involving more than one reactive site on the donor molecule is generally complicated by competitive equilibria taking place at the nonequivalent donor sites. For example, the thioanisole–phenol system involves competition in the phenyl π-donor site with the sulfide donor site for adduct formation with phenol, and the measured equilibrium constant of adduct formation for a system of this type has been shown to be the sum of the individual equilibrium constants associated with each site.[7] Thus, substituent effects reflected in the measured equilibrium constant even qualitatively are difficult to assess when the substituent itself is a potential donor site.

The diether donors used in this study, on the other hand, all have two equivalent ether oxygen donor sites; thereby, only one type of 1:1 adduct with the reference acid is formed. The donor, 1,4-dioxane, has been shown to form only a 1:1 and not a 2:1 adduct with iodine[8] and other reference acids,[3,4,8,9] so that the diethers provide a suitable system to observe the substituent effect of one ether oxygen on a second equivalent ether oxygen.

This substituent effect of one ether oxygen on the other is immediately evident on comparing the diether–iodine equilibrium constants with those of the corresponding monoethers. To do so requires a statistical correction to the measured values.[10] The diethers, having two equivalent donor sites, have twice the probability for adduct formation than a monoether. For example, the equilibrium constant for the cyclic diethers should be on a strict statistical basis just twice that of tetrahydropyran,[1] $2 \times 2.5 = 5.0$. This value is five times greater than that observed. Thus, the presence of a second ether oxygen drastically reduces the donor ability of the diether.

The diethers, within themselves, show this substituent effect. As shown in Table II, the ΔF values are positive for the diethers in which the oxygen atoms are separated by one methylene group, while the ΔF values are negative for those in which the oxygen atoms are separated by two methylene groups. Thus, as the distance between the oxygen atoms increases, the donor ability increases. This effect is not unexpected from simple inductive arguments, but it has been shown that adduct formation of ethers with iodine and other reference acids do not involve simple inductive effects alone.[1-3,11]

The possibility exists for these donors to utilize both

(6) R. S. Drago and N. J. Rose, *J. Am. Chem. Soc.*, 81, 6141 (1959).

(7) B. B. Wayland and R. S. Drago, *ibid.*, 86, 5240 (1964).

(8) See O. Hassel and C. Rømming, *Quart. Rev.* (London), **16**, 1 (1962), and references therein.

(9) S. C. Mohr, W. D. Wilk, and G. M. Barrow, *J. Am. Chem. Soc.*, 87, 3048 (1965).

(10) J. N. Brønsted, *Chem. Rev.*, **5**, 322 (1928); S. W. Benson, *J. Am. Chem. Soc.*, 80, 5151 (1958).

(11) V. I. Gol'danskii, O. Yu. Okhlobystin, V. Ya. Rochev, and V. V. Khrapov, *J. Organometal. Chem.* (Amsterdam), **4**, 160 (1965).

ether oxygens in forming adducts.[12] This is more likely for the donors 1,1-dimethoxymethane and 1,3-dioxane where both oxygens are bonded to a single carbon atom. Evidence has been presented for a three-body complex of tetramethylene sulfone with phenol where both donor oxygens are bonded to a single sulfur atom.[13] Although this effect may be important in hydrogen-bonded adducts, there is no reported evidence for its contribution in iodine adducts. The use of both ether oxygens in adduct formation is expected to result in unusually large entropy effects.[13] These effects are not apparent in the thermodynamic values for the adducts reported in this paper.

The usual correlations between donor ability of the diethers and such measurements as nmr proton shifts, solubility in halomethane solvents, and phenol OH vibrational frequency shifts can be made. The phenol frequency shifts for these bases are reported in Table IV. These data suggest a similar order of donor ability for the diethers toward hydrogen-bonding acids as that measured toward iodine. The diamines and disulfides show analogous behavior toward reference acids as the diethers.[9,14]

Table IV: Phenol Frequency Shift with the Diethers

	$\Delta\nu$(OH), cm^{-1} [a]
1,1-Dimethoxymethane	221
1,2-Dimethoxyethane	234
1,3-Dioxane	216
1,4-Dioxane	233

[a] Phenol concentration is 0.15 *M* in CCl_4. The data reported are extrapolated to infinite dilution of base. Estimated error in frequency shifts is ± 4 cm^{-1}.

Acknowledgments. The authors wish to acknowledge the Advanced Research Projects Agency for generous support of this research through Contract No. SD-69.

(12) For an excellent discussion of this point, see H. Tsubomura and R. P. Lang, *J. Am. Chem. Soc.*, **83**, 2085 (1961).

(13) R. S. Drago, B. B. Wayland, and R. L. Carlson, *ibid.*, **85**, 3125 (1963).

(14) J. D. McCullough and I. C. Zimmermann, *J. Phys. Chem.*, **66**, 1198 (1962).

Electron Capture by Nitrous Oxide in Irradiated Alkane and Alkene Gases. Subsequent Reactions of the O^- Ion[1]

by John M. Warman

Radiation Research Laboratories, Mellon Institute, Pittsburgh, Pennsylvania *(Received May 1, 1967)*

The yields of nitrogen formed on irradiation of alkane (C_2, C_3, C_4) and alkene (C_3, C_4) gases containing small amounts (<5%) of added nitrous oxide have been measured. The yield of nitrogen, $G(N_2)$, for a given hydrocarbon increases with increasing concentration of nitrous oxide up to ~2% above which $G(N_2)$ is approximately constant. This limiting yield, $G(N_2)_\infty$, depends upon the hydrocarbon used, being for the alkanes $1.55G_e$ (G_e = yield of electrons/100 ev), for propylene and isobutylene $\sim G_e$, and for the 1- and 2-butenes $\sim 2G_e$. These differences in the value of $G(N_2)_\infty$ are attributed to subsequent reactions of the O^- ion, formed on electron capture by the nitrous oxide, in the case of the alkane + N_2O systems with nitrous oxide and in the case of the alkene + N_2O systems with the alkene. Rate constant ratios for these reactions have been determined by studying mixed-hydrocarbon + N_2O systems and by the use of carbon dioxide and acetone as competitive scavengers of the O^- ion.

Introduction

Nitrous oxide has been used as a specific electron scavenger in irradiated liquid[2-4] and gaseous[5,6] hydrocarbons. In these systems nitrogen is formed by the dissociative capture of electrons

$$e + N_2O \xrightarrow{k_2} N_2 + O^- \qquad (1)$$

Accordingly the yield of nitrogen, $G(N_2)$, should equal the number of electrons captured. In both gaseous and liquid alkanes, nitrogen yields considerably in excess of the known yield of electrons (derived from the W value) have been found. In the gas phase it has been suggested[5] that this "excess" nitrogen is formed by the subsequent reaction of O^-, formed in (1), with nitrous oxide *via*

$$O^- + N_2O \longrightarrow N_2 + O_2^- \qquad (2)$$

The present work extends the study of nitrogen formation, from gaseous hydrocarbon + N_2O mixtures, to other alkanes and to the alkenes. An attempt is made to clarify the role of O^- in nitrogen formation in these systems.

Experimental Section

The hydrocarbons (Philips Research grade), nitrous oxide, carbon dioxide, and sulfur hexafluoride (Matheson) were distilled several times (through a cold spiral) on a vacuum line. Acetone (Fisher Scientific Spectroanalyzed) was used without further purification. All reagents were deaerated by a freeze–pump–thaw cycle.

The pressure of each constituent of the mixture to be irradiated was measured in a known volume prior to transfer to a common bulb at −196°. The resulting mixture was then warmed to room temperature and expanded into a volume containing the radiation vessels. The resultant total pressure was ~630 mm. The vessels were Pyrex cylinders of volume 160 cm^3 and length 20 cm.

A 2000-curie Co^{60} source was used to irradiate the samples. The products which were noncondensable at −196° were transferred to a gas buret by means of a

(1) Supported in part by the U. S. Atomic Energy Commission.

(2) G. Scholes and M. Simic, *Nature*, **202**, 895 (1964).

(3) W. V. Sherman, *J. Chem. Soc., Sect. A*, **5**, 599 (1966).

(4) S. Sato, R. Yugeta, K. Shinsaka, and T. Terao, *Bull. Chem. Soc. Japan*, **39**, 156 (1966).

(5) G. R. A. Johnson and J. M. Warman, *Nature*, **203**, 73 (1964).

(6) G. R. A. Johnson and J. M. Warman, *Trans. Faraday Soc.*, **61**, 512 (1965).

single-stage diffusion pump and a Toepler pump. After pressure–volume measurement, the gas composition was determined mass spectrometrically.

Dosimetry was based on $G(C_2H_4 \rightsquigarrow H_2) = 1.31$.[7] The energy absorbed by a gas mixture was taken to be the sum of the energies absorbed by all constituents of the mixture, using the relevant partial pressures and stopping powers.[7] The average dose rate in the present experiments was $\sim 2 \times 10^{13}$ ev/cm^3 sec. G values were calculated from the slopes of linear yield–dose plots (product yields at at least four different total doses were measured). The highest total dose used was 2×10^{17} ev/cm^3. G values are given in the text in terms of G_e (the yield of electrons per 100 ev absorbed) as calculated from the relevant W value (energy required to form one ion pair). The W values[7] for the hydrocarbons used lie within the range 23.9 ± 1.0 ev corresponding to $G_e = 4.20 \pm 0.17$.

Results and Discussion

Alkane + N_2O Mixtures. The formation of nitrogen, on irradiation of propane gas containing small amounts of nitrous oxide, has been shown to be due to the dissociative capture of electrons by the nitrous oxide,[5,6] reaction 1. The capture of electrons is presumed to compete with their disappearance by electron–ion recombination, $e + X^+$, where X^+ represents the positive ion or ions present at the time of recombination. According to the above competition the yield of nitrogen, $G(N_2)$, should vary with the concentration of nitrous oxide, $[N_2O]$, according to

$$G(N_2) = \frac{G_e}{1 + \dfrac{A}{[N_2O]}} \qquad (A)$$

where G_e is the yield of electrons, given by $100/W$, and A is a function of the rate constants for ion recombination and electron capture and the rate of formation of ions. According to (A), a plot of $G_e/G(N_2)$ *vs.* $1/[N_2O]$ should be a straight line of slope A. This linear behavior has been observed in the case of propane[6] and also in the present work for ethane, *n*-butane, and isobutane, Figure 1. According to the above mechanism, the yield of nitrogen when all electrons are captured by N_2O should be equal to the yield of electrons, G_e. This maximum yield, $G(N_2)_\infty$, given by the reciprocal of the intercept in Figure 1 is, however, found to be considerably greater than G_e, being for the four alkanes studied $1.55G_e$. This has previously been attributed to the subsequent reaction of O^- with N_2O,[5] reaction 2. If reaction 2 represented the sole fate of O^- ions, then one should observe $G(N_2) = 2G_e$. That the experimentally determined value, $G(N_2) = 1.55G_e$, is

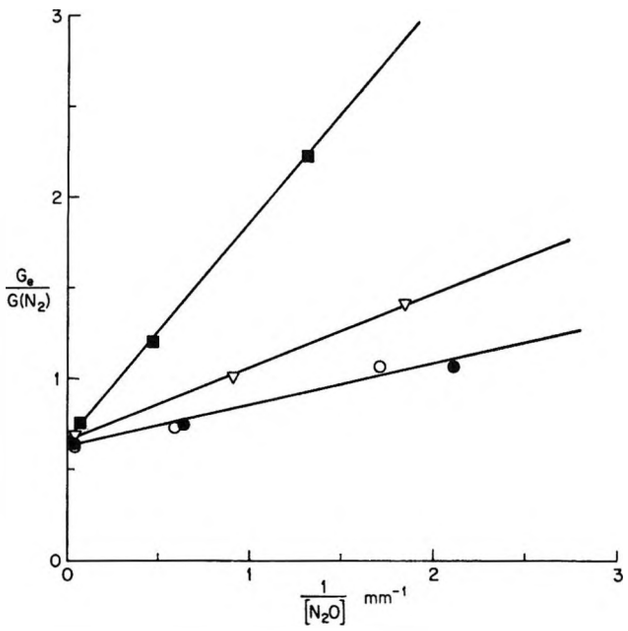

Figure 1. Dependence of the reciprocal nitrogen yield, from irradiated alkane (600 mm) + N_2O mixtures, on the reciprocal nitrous oxide concentration for ethane (■), propane (▽), *n*-butane (●), and isobutane (○).

lower than this can be explained if reaction 3, which has been found to occur concurrently with reaction 2 in the mass spectrometer,[8] also occurs in the present systems with $k_2/k_3 = 1.2$. The reaction between O^-

$$O^- + N_2O \xrightarrow{k_3} NO + NO^- \qquad (3)$$

and CO_2, reaction 4, has been found to be fast.[9,10] Ac-

$$O^- + CO_2 \xrightarrow{k_{CO_2}} CO_3^- \qquad (4)$$

cording to the above mechanism for nitrogen formation, the addition of CO_2 to the alkane + N_2O systems should, then, result in a competition between CO_2 and N_2O for O^- thereby decreasing $G(N_2)$, in the limit to G_e when all O^- ions are scavenged by the CO_2. CO_2 was, in fact, found to decrease $G(N_2)$, Figure 2, even for $[CO_2]/[N_2O]$ as low as 0.02, to a limiting value of G_e. CO_2 is not known to react with the free radical or ionic species produced in hydrocarbon radiolysis. The effect of CO_2 on $G(N_2)$ from alkane + N_2O mixtures therefore strongly supports the postulate that the reaction of O^- with N_2O is responsible for the "excess"

(7) G. G. Meisels, *J. Chem. Phys.*, **41**, 51 (1964).

(8) B. P. Burtt and J. Henis, *ibid.*, **41**, 1510 (1964).

(9) W. L. Fite and J. A. Rutherford, *Discussions Faraday Soc.*, **37**, 192 (1964).

(10) J. L. Moruzzi and A. V. Phelps, *J. Chem. Phys.*, **45**, 4617 (1966).

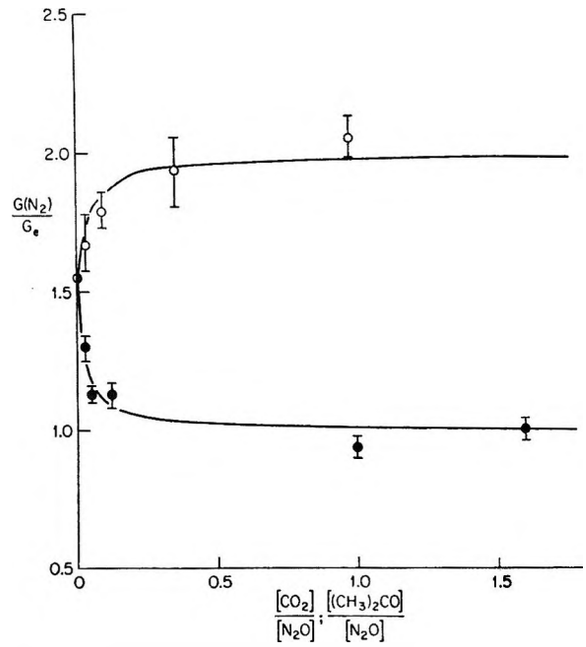

Figure 2. Effect of carbon dioxide (●) and acetone (○) on the yield of nitrogen from a propane (600 mm) + N_2O (25 mm) mixture.

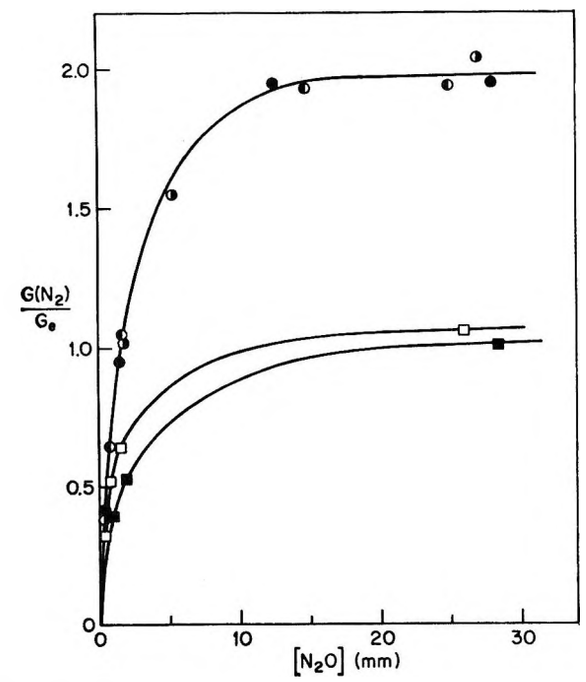

Figure 3. Dependence of the yield of nitrogen on concentration of nitrous oxide in ~600 mm of propylene (□), isobutene (■), 1-butene (●), *cis*-2-butene (◑), and *trans*-2-butene (◐).

yields of nitrogen (*i.e.*, $G(N_2) > G_e$) found in these systems.

Alkene + N_2O Mixtures. The addition of small amounts of N_2O to irradiated alkenes is found to yield nitrogen as for alkane + N_2O mixtures, Figure 3. The yield of nitrogen increases with increasing N_2O concentration below approximately 2%, and above this concentration it is nearly constant. A plot of $1/G(N_2)$ *vs.* $1/[N_2O]$ is linear for all of the alkenes studied in accordance with eq A. The limiting nitrogen yields, however, differ considerably from that found for the alkanes and from alkene to alkene. Thus for propylene and isobutene $G(N_2)_\infty \sim G_e$ whereas for 1-butene and the 2-butenes $G(N_2)_\infty \sim 2G_e$. The addition of 0.2% SF_6 (an efficient electron scavenger) to the systems C_3H_6 + N_2O (4%) and *trans*-2-C_4H_8 + N_2O (4%) inhibited the formation of nitrogen, Figure 4, indicating the electron to be the primary precursor of nitrogen in both cases. Since the simple alkenes (having negative electron affinities) cannot capture electrons, the primary process in nitrogen formation must be reaction 1 as in the alkane + N_2O systems. The observation that $G(N_2)_\infty$ for propylene and isobutene is $\sim G_e$ indicates that the subsequent reactions, (2) and (3), of O^- with N_2O are not occurring in these systems. The most obvious explanation of this is

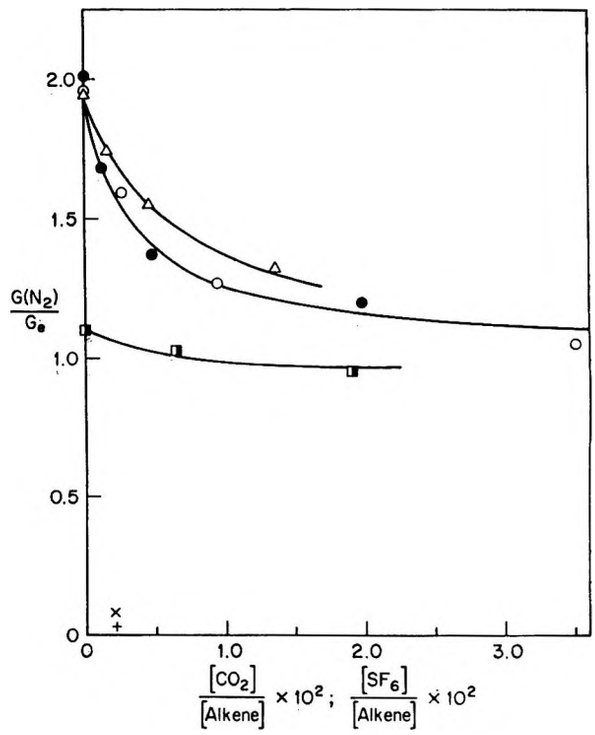

Figure 4. Effect of added carbon dioxide and sulfur hexafluoride on the yield of nitrogen from an alkene (600 mm) + N_2O (25 mm) mixture. The alkene and additive, respectively, are: (◨) C_3H_6, CO_2; (△) 1-C_4H_8, CO_2; (●) *cis*-2-C_4H_8, CO_2; (○) *trans*-2-C_4H_8, CO_2; (+) C_3H_6, SF_6; (×) *trans*-2-C_4H_8, SF_6.

that the O^- ion can react preferentially with the solvent alkene to form species which do not further react with N_2O to form nitrogen

$$O^- + D \xrightarrow{k_D} (DO)^- \qquad (5)$$

where D represents propylene or isobutene and $(DO)^-$ the product or products of the reaction of O^- with propylene or isobutene. The value of $G(N_2)_\infty \sim 2G_e$ found for 1-butene and the 2-butenes can then be explained by a reaction analogous to reaction 5 but the product(s) of which can subsequently react with N_2O to form N_2

$$O^- + E \xrightarrow{k_E} (EO)^- \qquad (6)$$

$$(EO)^- + N_2O \longrightarrow (EO_2)^- + N_2 \qquad (7)$$

where E represents 1-butene or 2-butene. Accordingly, on the addition of CO_2 to the latter systems, $G(N_2)$ should decrease, owing to competition between reactions 4 and 6, and tend toward G_e with increasing CO_2 concentration. This is found to be so, Figure 4. The addition of CO_2 to the propylene + N_2O system should not markedly affect $G(N_2)$ since neither reaction 4 nor reaction 5 leads to nitrogen formation. This is also found to be so, Figure 4.

The possibility that the "excess" nitrogen formed in the alkene systems is due to deactivation of metastable excited species by nitrous oxide cannot be completely ruled out on the basis of the present data

$$RH^* + N_2O \longrightarrow N_2 + O + RH$$

However, if this were the case, then, in order to explain the above results, the relative efficiencies for quenching of these species would have to give an alkene:N_2O:CO_2:SF_6 ratio of $1:\sim10^2:\sim10^3:\sim10^5$. This is to be compared with the relative efficiencies for deactivation of metastable Hg ($^3P_1$) atoms which are found to be in an alkene:N_2O:CO_2 ratio of 1:0.5:0.1.[11] Also the prerequisite that the yield (or nature) of such metastable species should differ markedly between propylene or isobutene and 1-butene or 2-butene would seem unlikely.

Mixed-Hydrocarbon + N_2O Mixtures. The above discussion has been concerned with substantiating the occurrence of reactions of the O^- ion in the systems studied and the effect of these reactions on the yield of nitrogen from irradiated hydrocarbon + N_2O mixtures. A more detailed study of the variation of the nitrogen yields, resulting from these reactions, should enable one to obtain kinetic data pertaining to the reactions which as well as being of intrinsic interest might also shed light on the nature of the reactions involved.

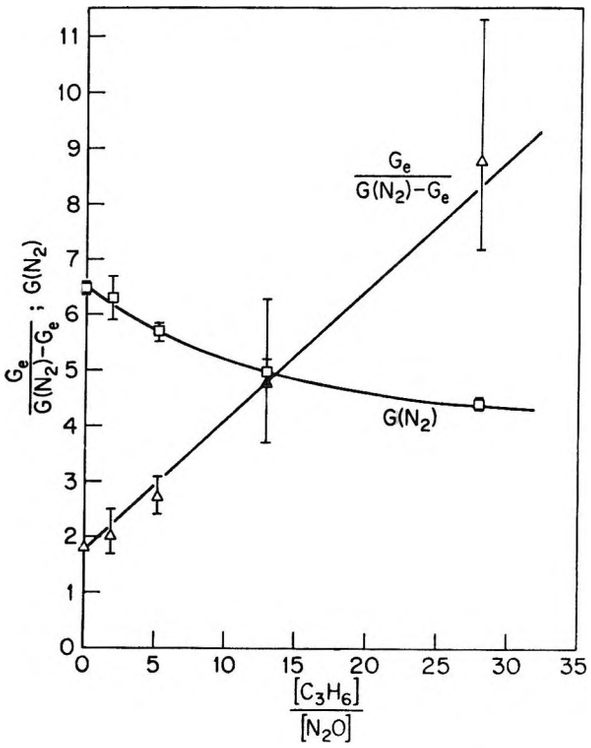

Figure 5. Dependence of the yield of nitrogen on partial pressure of propylene in the mixture propylene + propane (total pressure 600 mm) + N_2O (25 mm) (□). Above results plotted as $G_e/(G(N_2) - G_e)$ *vs.* $[C_3H_6]/[N_2O]$ which according to eq C (see Discussion) should be linear (△).

The yield of nitrogen, from propane + propylene mixtures (total pressure ~600 mm) containing ~4% N_2O, was measured for varying partial pressures of propylene, Figure 5. In these systems competition between propylene, reaction 5, and N_2O, reactions 2 and 3, for O^- should occur. The resulting decrease in $G(N_2)$ with increasing $[C_3H_6]/[N_2O]$ ratio should obey the expression

$$G(N_2) = G_e\left[1 + \frac{1}{\frac{k_2 + k_3}{k_2} + \frac{k_{C_3H_6}[C_3H_6]}{k_2[N_2O]}}\right] \qquad (B)$$

obtained from a steady-state treatment of reactions 1, 2, 3, and 5. Substitution for $k_2/k_3 = 1.2$ from above then gives

$$G(N_2) = G_e\left[1 + \frac{1}{1.83 + \frac{k_{C_3H_6}[C_3H_6]}{k_2[N_2O]}}\right] \qquad (C)$$

According to (C) a plot of $G_e/(G(N_2) - G_e)$ *vs.* $[C_3H_6]/[N_2O]$ should be a straight line of slope $k_{C_3H_6}/k_2$. Such

(11) R. J. Cvetanović, *Progr. Reaction Kinetics*, 2, 55 (1964).

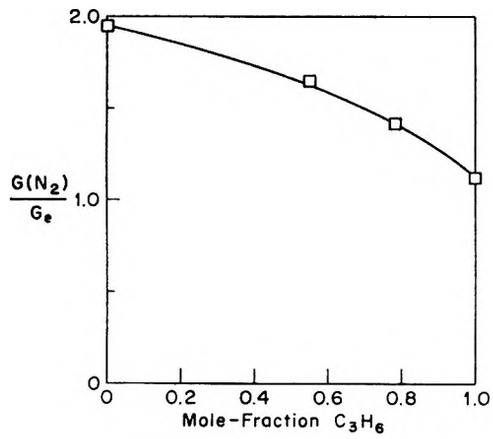

Figure 6. Dependence of the yield of nitrogen on mole fraction of propylene in the mixture propylene + 1-butene (total pressure 600 mm) + N_2O (25 mm).

a plot is shown in Figure 5 from which $k_2/k_{C_3H_6} = 4.5$ and hence $k_3/k_{C_3H_6} = 3.6$.

The yields of nitrogen, from propylene + 1-butene mixtures (total pressure ~600 mm) containing ~4% N_2O, were measured for different partial pressures of propylene, Figure 6, in order to determine the rate constant ratio $k_{1\text{-}C_4H_8}/k_{C_3H_6}$. A steady-state treatment of the competition involved, *i.e.*, between reactions 5 and 6, gives as the predicted dependence of $G(N_2)$ on $[C_3H_6]/[1\text{-}C_4H_8]$

$$G(N_2) = G_e\left[1 + \frac{1}{1 + \dfrac{k_{C_3H_6}[C_3H_6]}{k_{1\text{-}C_4H_8}[1\text{-}C_4H_8]}}\right] \quad \text{(D)}$$

Under the conditions of these experiments the reaction of O^- with N_2O takes place to a small but not negligible extent (*e.g.*, in propylene alone plus 4% N_2O, approximately 20% of the O^- ions will undergo reaction with N_2O). The inclusion of reactions 2 and 3 in the kinetic scheme is therefore necessary and results in a modification of (D) giving

$$G(N_2) = G_e \times \left[1 + \frac{\dfrac{k_2[N_2O]}{k_{C_3H_6}[C_3H_6]} + \dfrac{k_{1\text{-}C_4H_8}[1\text{-}C_4H_8]}{k_{C_3H_6}[C_3H_6]}}{1 + \dfrac{(k_2 + k_3)[N_2O]}{k_{C_3H_6}[C_3H_6]} + \dfrac{k_{1\text{-}C_4H_8}[1\text{-}C_4H_8]}{k_{C_3H_6}[C_3H_6]}}\right] \quad \text{(E)}$$

When the values for $k_2/k_{C_3H_6}$ and $k_3/k_{C_3H_6}$ determined above are substituted in (E), the rate constant ratio $k_{1\text{-}C_4H_8}/k_{C_3H_6}$ remains the only unknown. The value of $k_{1\text{-}C_4H_8}/k_{C_3H_6}$ giving the best fit to the data in Figure 6 was then determined by trial and error. This value was found to be $k_{1\text{-}C_4H_8}/k_{C_3H_6} = 2.0$. Using this value in (E), the curve in Figure 6 was computed.

Competitive Reactions Involving CO_2. The use of CO_2 as a scavenger of O^- ions has been discussed in the first two sections. From the decrease in $G(N_2)$ on addition of CO_2 to the 1-butene and 2-butene + N_2O systems, Figure 4, it is possible to obtain values for the rate constant ratios $k_{1\text{-}C_4H_8}/k_{CO_2}$ and $k_{2\text{-}C_4H_8}/k_{CO_2}$. The competition involved is that between reactions 4 and 6, a steady-state treatment of which gives as the dependence of $G(N_2)$ on $[CO_2]$ for 1-butene

$$G(N_2) = G_e\left[1 + \frac{1}{1 + \dfrac{k_{CO_2}[CO_2]}{k_{1\text{-}C_4H_8}[C_4H_8]}}\right] \quad \text{(F)}$$

According to (F) a plot of $G_e/(G(N_2) - G_e)$ *vs.* $[CO_2]/[1\text{-}C_4H_8]$ should be a straight line of slope $S = k_{CO_2}/k_{1\text{-}C_4H_8}$. Such a plot of the results in Figure 4 for 1-butene is linear and gives $S = 196$. When the contribution of reactions 2 and 3 (*i.e.*, those involving $O^- + N_2O$) are taken into account, the slope of the above plot is modified to

$$S = \frac{1}{1 + \dfrac{k_2[N_2O]}{k_{1\text{-}C_4H_8}[1\text{-}C_4H_8]}} \frac{k_{CO_2}}{k_{1\text{-}C_4H_8}} \quad \text{(G)}$$

The value for $k_2/k_{1\text{-}C_4H_8}$ is, from above, $(k_2/k_{C_3H_6}) \times (k_{C_3H_6}/k_{1\text{-}C_4H_8}) = 2.25$, and, since $[N_2O]/[1\text{-}C_4H_8]$ in the present experiments is 0.04, then $S = (1/1.09) \times (k_{CO_2}/k_{1\text{-}C_4H_8})$. The true value of $k_{CO_2}/k_{1\text{-}C_4H_8}$ is therefore 180. This value was used to compute the curve for 1-butene shown in Figure 4 and gives $k_2/k_{CO_2} = (k_2/k_{1\text{-}C_4H_8})(k_{1\text{-}C_4H_8}/k_{CO_2}) = 0.013$. Since for the 2-butenes the value of $k_2/k_{2\text{-}C_4H_8}$ is not known, a process of successive approximations is necessary to derive $k_{CO_2}/k_{2\text{-}C_4H_8}$ from the slope S of a plot of $G_e/(G(N_2) - G_e)$ *vs.* $[CO_2]/[2\text{-}C_4H_8]$ derived from the results in Figure 4. Thus, if S is taken as a first approximation to $k_{CO_2}/k_{2\text{-}C_4H_8}$, then $k_2/k_{2\text{-}C_4H_8}$ is given by $(k_2/k_{CO_2})S$ which on substitution in the expression for the slope

$$S = \frac{1}{1 + \dfrac{k_2[N_2O]}{k_{2\text{-}C_4H_8}[2\text{-}C_4H_8]}} \frac{k_{CO_2}}{k_{2\text{-}C_4H_8}}$$

gives a second approximation to $k_{CO_2}/k_{2\text{-}C_4H_8}$. The final, constant value of $k_{CO_2}/k_{2\text{-}C_4H_8}$ obtained was 400 which was used to compute the curve shown in Figure 4 for the 2-butenes.

Acetone As an O^- Scavenger. It was found that when acetone was added to the propylene + 4% N_2O system, $G(N_2)$ increased, tending to a value of $2G_e$ with increasing acetone concentration, [AO], Figure 7. It was thought that this was possibly due to the reaction of O^- with acetone (in competition with its

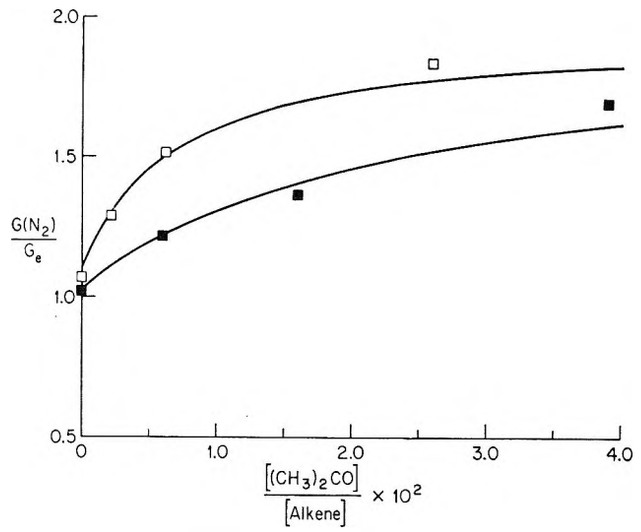

Figure 7. Dependence of the yield of nitrogen, from the mixtures C_3H_6 (600 mm) + N_2O (25 mm) (□) and *i*-C_4H_8 (600 mm) + N_2O (25 mm) (■), on the concentration of added acetone.

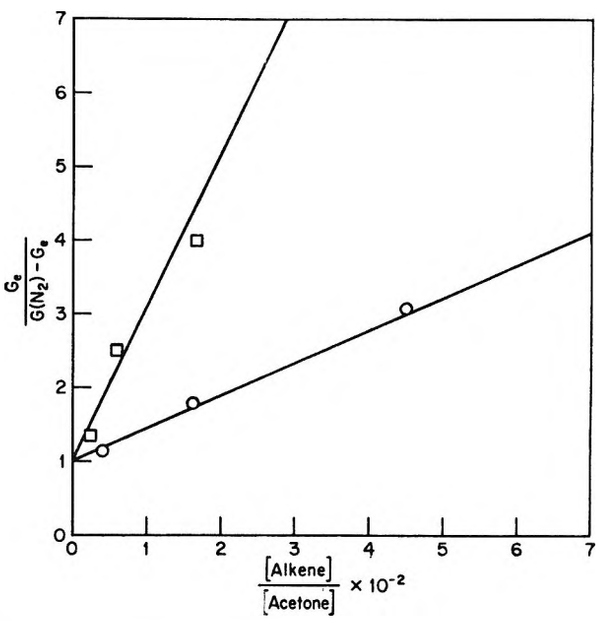

Figure 8. Plots of the points in Figure 7 as $G_e/(G(N_2) - G_e)$ *vs.* [alkene]/[acetone] which according to eq H (see Discussion) should be linear for propylene (○) and isobutene (□).

reaction with propylene) to give species which could further react with N_2O to form nitrogen, *i.e.*

$$O^- + AO \longrightarrow (AO_2)^- \quad (8)$$

$$(AO_2)^- + N_2O \longrightarrow (AO_3)^- + N_2 \quad (9)$$

According to this competition $G(N_2)$ from a mixture of propylene + N_2O + acetone should depend upon the concentration of acetone according to

$$G(N_2) = G_e + \left[\frac{1}{1 + \frac{k_{C_3H_6}[C_3H_6]}{k_{AO}[AO]}}\right] \quad (H)$$

A plot of $G_e/(G(N_2) - G_e)$ *vs.* $[C_3H_6]/[AO]$ derived from the results in Figure 7 is shown in Figure 8. The linear behavior found is to be expected if (H) were obeyed but is somewhat fortuitous since a slight curvature would be expected due to the occurrence of the reaction of O^- with N_2O in this system. When this is taken into account, a value for $k_{AO}/k_{C_3H_6} = 190$ is obtained. A similar though less pronounced increase in $G(N_2)$ was observed on addition of acetone to the isobutene + 4% N_2O system, Figure 7. A plot of $G_e/(G(N_2) - G_e)$ *vs.* $[i\text{-}C_4H_8]/[AO]$ as for propylene is shown in Figure 8. From the slope of this plot $k_{AO}/k_{i\text{-}C_4H_8} = 42$.

Summary of Kinetic Data. The values for the rate constant ratios, k_X/k_Y, obtained above by direct competition between reactants X and Y for the O^- ion are listed in Table I. The error limits indicated are estimated and represent the values outside of which

Table I: Rate Constant Ratios, k_X/k_Y, Determined by Direct Competition between Two Reactants, X and Y, for the O⁻ Ion

X	Y	k_X/k_Y
N_2O (→$N_2 + O_2^-$)	N_2O (→$NO + NO^-$)	1.2 ± 0.15
N_2O (→$N_2 + O_2^-$)	C_3H_6	4.5 ± 0.9
1-C_4H_8	C_3H_6	2.0 ± 0.3
CO_2	1-C_4H_8	180 ± 20
CO_2	2-C_4H_8	400 ± 40
$(CH_3)_2CO$	C_3H_6	190 ± 30
$(CH_3)_2CO$	*i*-C_4H_8	42 ± 6

calculation and experiment would disagree considerably. A sounder determination of errors is not possible owing to the differing errors incurred in each G value and the magnification of these errors in the kinetic plots (*e.g.*, see Figures 2 and 5 where the error limits, indicated by the vertical lines through the points, are calculated standard deviations of the mean). For ease of comparison, the rate constants for the reactions proposed relative to $k_{C_3H_6} = 1.0$ have been derived from the relevant rate constant ratios of Table I and are listed in Table II.

The internal consistency of the values in Table I was tested by deriving the ratios k_2/k_{CO_2}, k_3/k_{CO_2}, k_2/k_{AO}, and k_3/k_{AO} by combining the relevant ratios in Table I. These values were then used to compute the expected dependence of $G(N_2)$, from an alkane + 4% N_2O mixture, on concentration of added CO_2 and acetone.

Table II: Rate Constants for O^- Reactions Relative to the Rate Constant for Reaction of O^- with Propylene

Reactant (X)	$k_X/k_{C_3H_6}$
N_2O ($\rightarrow N_2 + O_2^-$)	4.5
N_2O ($\rightarrow NO + NO^-$)	3.7
C_3H_6	1.0
i-C_4H_8	4.5
1-C_4H_8	2.0
2-C_4H_8	0.9
$(CH_3)_2CO$	190
CO_2	360

The respective computed curves are shown in Figure 2 and agree well with the experimental points.

Possible Reactions. As noted above the reactions of the O^- ion with carbon dioxide and nitrous oxide have been previously observed and the product ions characterized by mass spectrometry. The postulated reactions of O^- with acetone and the alkenes have not been observed in the mass spectrometer. Suggestions as to the specific reactions involved are mere speculation and as such will not be dealt with at length.

It has been suggested[12] that, in part, the formation of mass 57 ions in the negative ion mass spectrum of acetone could be due to proton-abstraction reactions of the general type

$$R^- + CH_3COCH_3 \longrightarrow RH + CH_3COCH_2^-$$

Possibly the reaction of O^- with acetone is of this type. The OH radical so formed would react exclusively with the hydrocarbon which is present in large excess in the present systems. The formation of nitrogen would then be due to reaction of the ion $CH_3COCH_2^-$ with N_2O possibly *via* the reaction

$$CH_3COCH_2^- + N_2O \longrightarrow CH_3COCH_2O^- + N_2$$

The comparative stability of the allyl anion suggests the possibility that attack of O^- on the alkenes also involves proton abstraction, *e.g.*

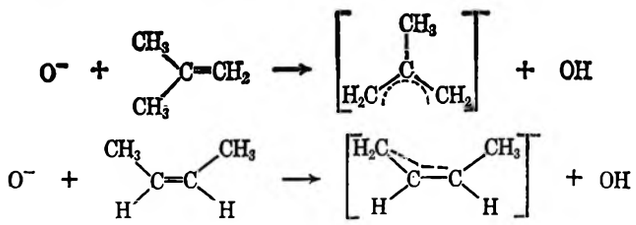

Why the product of this reaction should further react with nitrous oxide, to form nitrogen, in the case of 1-butene or the 2-butenes but not in the case of propylene or isobutene is not obvious. The presence of a four-carbon chain in the former as opposed to a three-carbon chain in the latter suggests that the possibility of butadiene formation from the former may be responsible for preferential reaction, *e.g.*

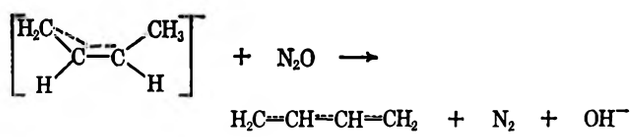

Acknowledgment. The author wishes to thank Mr. G. K. Buzzard for carrying out the mass spectrometric analyses.

(12) B. C. de Souza and J. H. Green, *J. Chem. Phys.*, **46**, 1421 (1967).

Infrared Study of Poly-L-proline in Aqueous Solution[1]

by Charles A. Swenson and Robert Formanek

Department of Biochemistry, University of Iowa, Iowa City, Iowa *(Received May 4, 1967)*

Infrared spectra were measured for aqueous solutions (H_2O and D_2O) of form II poly-L-proline in the fundamental region as a function of temperature. The temperature range includes the region where a reversible phase transition is known to occur. The spectral changes in the carbonyl absorption as this temperature range is approached are interpreted as a breakdown of solute–solvent interactions which result in destabilization of the solute in the solution phase. Simultaneously, there occurs a change in the C–H bending absorption which is interpreted as a small conformational change. Both of these absorptions show apparent isosbestic behavior as a function of temperature. A van't Hoff ΔH° of 60 ± 10 kcal/mole (residue) was estimated for the over-all process from the temperature dependence of the carbonyl absorption.

Introduction

Infrared spectroscopy in the fundamental region has been shown to be useful in elucidating the conformations of various proteins and synthetic polypeptides in oriented and unoriented dry films.[2,3] These studies have led to the assignment of some of the bands, notably amide I and amide II, to various conformations.[4,5] Few studies of this type have been carried out in aqueous solutions (H_2O or D_2O) primarily because of experimental difficulties arising from the large extinction coefficient of water throughout the region of interest. A considerable amount of specific information can be gained from such a study, some of which cannot be obtained in any other way. In the present communication we report the results of an infrared study of solute–solvent interactions for the peptide poly-L-proline in aqueous solution.

Poly-L-proline is of interest because of its similarities with the structural protein collagen which has proline as its second most abundant amino acid. It is well suited as a model for an infrared study because of its limited capabilities for hydrogen bonding. Inter- and intrapeptide-chain hydrogen bonding cannot occur as it can act only as a base in this interaction. Thus a study of hydrogen bonding with the solvent can be carried out and interpreted without the usual complications. In spite of the lack of intramolecular hydrogen bonds, the conformation of polyproline in solution might be expected to be semirigid due to the existence of a resonance stabilized imide peptide linkage and a pyrrolidine ring in the structure. These restrictions leave the polymer with rotational freedom only at the C_α—C=O linkage, and this is thought to be hindered.[6] Thus very few conformations are available to the polymer in aqueous solution. Poly-L-proline is known to exist in two forms, designated I and II, which differ in their configuration at the imide linkage.[7] Crystallographic analysis has shown that form II is a left-handed helix with all-*trans* imide linkages and a repeat distance of 3.1 A. Form I is a right-handed all-*cis* helix with a repeat distance of 1.9 A.[8] Forms I and II can be interconverted in solution by simply changing the solvent.[9]

When an aqueous solution of poly-L-proline is heated to 55°, precipitation occurs. This process is completely reversible and is analogous to the heat precipita-

(1) This research was supported by a grant from the National Science Foundation, GB 4385.

(2) A. Elliott and E. J. Ambrose, *Nature*, **165**, 921 (1950).

(3) M. Beer, G. B. B. M. Sutherland, K. N. Tanner, and D. L. Wood, *Proc. Roy. Soc.* (London), **A249**, 147 (1959).

(4) T. Miyazawa and E. R. Blout, *J. Am. Chem. Soc.*, **83**, 712 (1961).

(5) S. Krimm, *J. Mol. Biol.*, **4**, 528 (1962).

(6) W. F. Harrington and P. H. von Hippel, *Advan. Protein Chem.*, **16**, 1 (1961).

(7) F. Gornick, L. Mandelkern, A. F. Diorio, and D. E. Roberts, *J. Am. Chem. Soc.*, **86**, 2549 (1964).

(8) W. Traub and U. Shmueli, *Nature*, **198**, 1165 (1963).

(9) I. Z. Steinberg, A. Berger, and E. Katchalski, *Biochem. Biophys. Acta*, **28**, 647 (1958).

tion observed with tropocollagen.[10] Structurally there is also a similarity; X-ray crystallographic studies have shown that the conformational arrangement of poly-L-proline, form II, is the basis for the structure of collagen.[10] Our purpose for this study was to investigate the interactions of polyproline with the solvent as the precipitation temperature is approached and relate them to the stability of the solution phase and/or changes in the conformation.

Experimental Section

Poly-L-proline (mol wt 34,000) was obtained from Mann Research Laboratories (Lot R 1416). It existed entirely in form II as judged from the absence of the band at 965 cm^{-1} in the infrared spectrum of the solid. Two other lower molecular weight samples were also investigated. One was obtained from New England Nuclear (mol wt 1500), and the other was prepared in this laboratory (mol wt 2000). These two samples were predominantly form I and were converted to form II by dissolution in anhydrous formic acid prior to study. All the samples, after conversion to form II, had identical solid-state infrared spectra and were completely soluble in cold water. Although all three samples were investigated, the data reported here are almost exclusively on the Mann sample.

Solutions in water and deuterium oxide were prepared by weighing the dry polyproline. Complete dissolution was effected in a few minutes by cooling to about 0°. A concentration of 0.5% was used for most of these studies; however, a limited number of experiments were performed with concentrations as low as 0.1% and as high as 5%.

Spectra were recorded with a Perkin-Elmer Model 521 spectrometer at a spectral slit of approximately 4 cm^{-1}. The monochromator and the sample chamber were purged with dry air. This reduced atmospheric absorption and prevented the cells from sweating at low temperatures. The sample cells were thermostated by circulating water through a coil which was in thermal contact with the cell windows. The cell and water jacket were insulated from the surroundings by a layer of styrofoam. A thermistor in thermal contact with the cell window was used to monitor the temperature in the range 0–70°.

Two matched cells with CaF_2 windows and optical paths of 0.05 mm were used. The reference cell contained pure solvent. For the region 1700–1500 cm^{-1} the solvent was D_2O, and for the region 1550–1300 cm^{-1}, H_2O was used. D_2O would have been the solvent of choice for all of our studies except for the fact that HDO, which is difficult to eliminate entirely, absorbs at 1450 cm^{-1} and complicates the interpretation of changes in the band shapes in this region.

Results

The infrared spectrum of a 0.5% (w/v) solution of poly-L-proline form II is shown in Figure 1. Both water and deuterium oxide were employed as solvents to cover the spectral region of interest. The concentration was varied from 0.1 to 5% with no apparent changes in the details of the spectrum. It is notable that the spectra obtained in solution are slightly sharper than those obtained in the solid phase. No absorptions due to bands characteristic of form I at 965 and 1365 cm^{-1} were observed.[11] It is possible that these bands, which are often used to distinguish between form I and form II, are characteristic only of the solid-state spectrum. Several intense bands are present in the spectrum of polyproline in aqueous solution. Only two of these can be assigned with any degree of certainty; the band at 1624 cm^{-1}, which is predominantly a carbonyl-stretching motion, and the band at 1456 cm^{-1}, which is predominantly a C–H bending motion of the pyrrolidine ring.[12]

A variation in the solution temperature causes no observable effects on the spectrum until the precipitation temperature is approached. All the bands are then observed to change; the effects on most bands are changes in intensity with little or no shifting of the absorption frequencies. Large changes in intensity and frequency are observed to occur in the carbonyl and the C–H bending regions. Two new bands appear in these regions: one on the high frequency side of the original carbonyl absorption, and one on the low frequency side of the C–H bending absorption. In both cases the new band increases in intensity as the temperature is raised with simultaneous decreases in the original band. The isosbestic behavior of these two bands is shown in Figures 2 and 3.

Preliminary observations concerning the precipitation of the polymer showed the rate of heating to be critical. The nature of the precipitation has recently been studied carefully by Ciferri and Orofino so that further details need not be presented here.[13] The important point to note is that equilibrium is established only very slowly in aqueous poly-L-proline solutions at or near the precipitation temperature. Thus the curves

(10) A. Veis, "The Macromolecular Chemistry of Gelatin," Academic Press Inc., New York, N. Y., 1964.

(11) (a) E. R. Blout and G. D. Fasman, *Recent Advan. Gelatin Glue Res., Proc. Conf. Univ. Cambridge*, 122 (1958); (b) J. Kurtz, A. Berger, and E. Katchalsky, *ibid.*, 131 (1958).

(12) F. A. Miller, "Organic Chemistry," H. Gilman, Ed., Vol. 3, John Wiley and Sons, Inc., New York, N. Y., 1953, p 143.

(13) A. Ciferri and T. A. Orofino, *J. Phys. Chem.*, **70**, 3277 (1966).

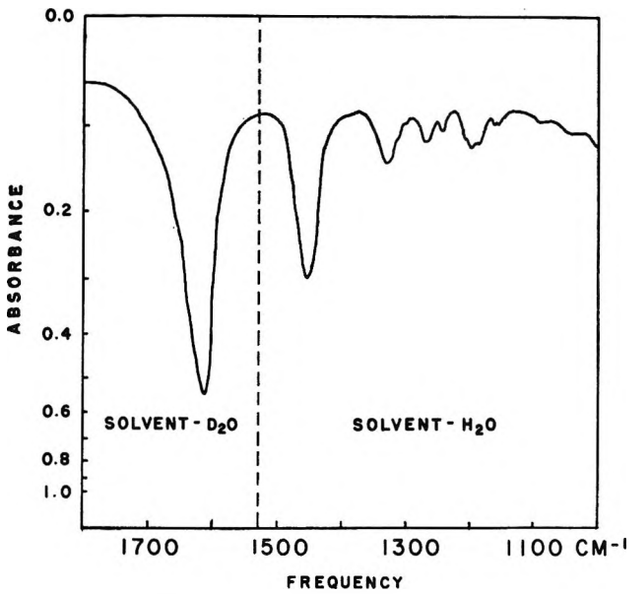

Figure 1. Infrared spectrum of a 1.0% aqueous solution of poly-L-proline in a 0.05-mm CaF_2 cell 31°. Solvents: D_2O, 1800–1530 cm^{-1}; H_2O, 1550–1000 cm^{-1}.

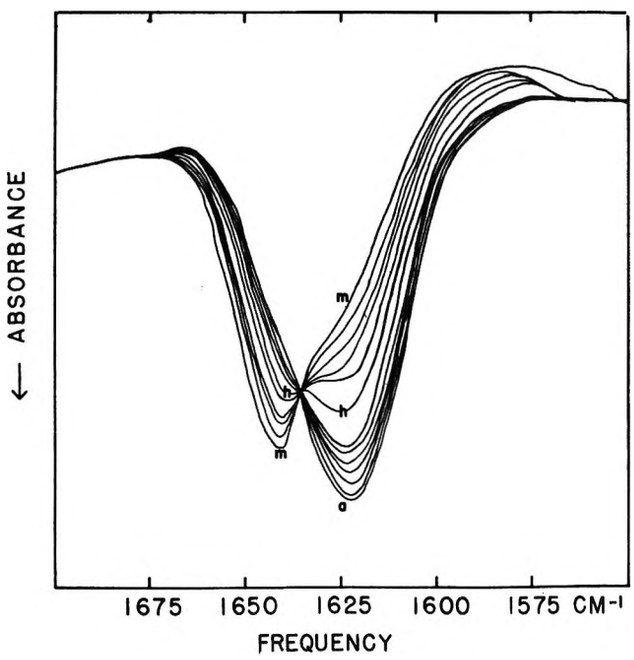

Figure 2. Spectra of the carbonyl region as a function of temperature: curve a, 45°; curve h, 53°; curve m, 65°.

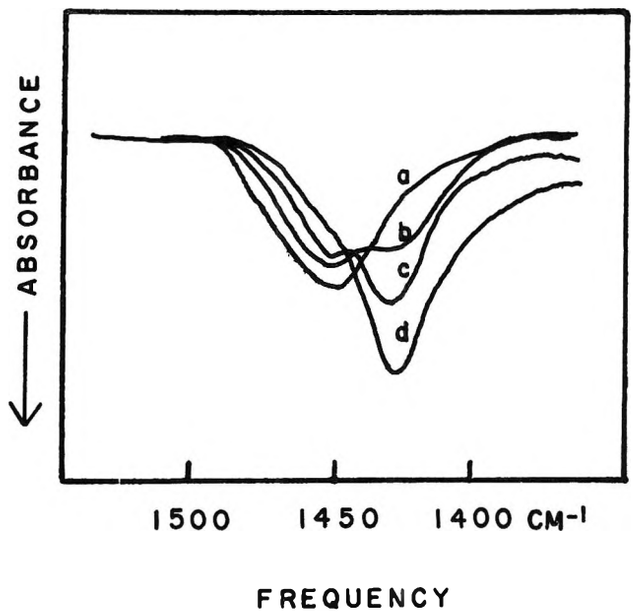

Figure 3. Spectra of the C–H bending region as a function of temperature: curve a, 45°; curve b, 52°; curve c, 57°; curve d, 67°.

shown in Figures 2 and 3 may not represent equilibrium values of the absorbance. In order to obtain them, a standard rate of heating of 1°/hr was adopted. We attempted to approach the 1°/day used by Ciferri and Orofino; however, the evaporation of solvent from the cells when maintained at these temperatures would not permit precise measurements.

Reversal of the precipitation or the spectral changes associated with it could not be achieved by cooling to room temperature. However, complete reversal occurs in a few minutes upon cooling to 0–5°, in agreement with earlier observations.[13] Only a very slight turbidity could be seen in the cells at the highest temperature during the time span of our study. If the solution was permitted to remain for 24 hr or longer at a temperature in the range of precipitation, precipitate was noted at the bottom of the cell. Spectra of this dried precipitate confirmed the earlier observation that intraconversion of form II–form I does not occur upon heating.[13]

Two other observations are notable. The precipitation temperature seemingly was dependent on concentration. At the higher concentrations it was apparently decreased by several degrees. No attempt was made to study this effect further. We also noted that the precipitation temperature in D_2O was several degrees lower than in water for equal concentrations of polymer.

Discussion

The temperature effect shown by the carbonyl absorption is typical of hydrogen bonding.[14] N-Methyl

(14) G. C. Pimentel and A. L. McClellan, "The Hydrogen Bond," W. H. Freeman and Co., San Francisco, Calif., 1960.

lactams which are suitable models for poly-L-proline show similar frequencies for the *free* and bonded states.[15] Since inter- and intrachain hydrogen bonding cannot occur for poly-L-proline, the observed changes are a measure of this interaction between carbonyl and the solvent D_2O. The temperatures at which an appreciable fraction of these hydrogen bonds are broken in D_2O coincides qualitatively with the range of temperatures where precipitation is known to occur in water.[13] At these temperatures the equilibrium may involve polyproline molecules which exist as an amorphous solid or a microcrystalline solid in suspension, in addition to those in true solution. The solid phase could exist even though no precipitate was discernible in the cell during the experiments. In spite of these various possibilities the experimental results suggest that the interaction of the carbonyl with the solvent is directly related to the stability of the solution phase. The results shown in Figure 2 were very reproducible as long as the rate of heating was duplicated. We were thus tempted to calculate the $\Delta H°$ for this process in spite of the large hysteresis effects known for the reverse process, which indicates that the system is slow to achieve equilibrium.[13] In Figure 4 is shown a plot of ln K *vs.* $1/T$. The equilibrium constants were calculated assuming two states as indicated by the spectra. The concentration of hydrated carbonyl, α, at a given temperature was calculated from the peak height of the band at 1624 cm^{-1}, assuming that the peak height at 30° represented the fully hydrated specie. Unhydrated carbonyl concentrations were then calculated by the difference, $1 - \alpha$. The equilibrium constant, K, is then $\alpha/(1 - \alpha)$. The overlapping bands were visually separated for this analysis.

A value of 60,000 ± 10,000 cal/mole (residue) was obtained for $\Delta H°$ from the slope. Although this $\Delta H°$ is only suggestive of the true energy due to the above indicated limitations, it still deserves comment. It is not likely to be $\Delta H°$ for the phase transition, as that is first order. The magnitude 60 kcal/mole (residue) is too large for just a dehydration of the carbonyl. This $\Delta H°$ could be associated with nucleation and/or some cooperative intramolecular process.

Occurring simultaneously with the changes in the carbonyl absorption are changes in the C–H bending absorption of the pyrrolidine ring. These changes parallel exactly the behavior of the carbonyl absorption. Since the C–H vibration is not directly affected by hydrogen bonding, the frequency shift results either from a nonspecific solvent effect, an inductive effect, or a conformational change. Solvent effects for C–H vibration are not generally this large.[16] Furthermore, a solvent effect such as raising the temperature would be

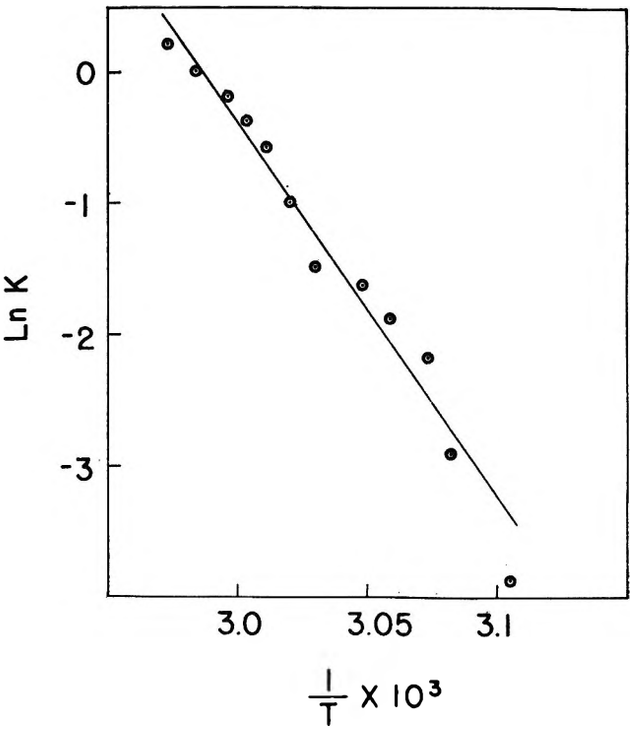

Figure 4. Van't Hoff plot for the carbonyl region.

expected to give rise to a gradually shifting frequency, not the isosbestic behavior observed here. An inductive effect is possible; however, the C–H bond is rather far removed from the carbonyl. It is also possible to explain the experimental observations in terms of a conformational change which occurs as the solvent interaction with the carbonyl group is decreased. Since the structure of polyproline is very rigid, the conformational change may be a slight rotation at the C_α—C=O bond, the only bond in the backbone with *free* rotation. At present we are not able to distinguish between these two possibilities.

This infrared study of poly-L-proline in aqueous solution has permitted the observation of some specific solvent–solute interactions for this macromolecule. Poly-L-proline, form II, in aqueous solution is likely to be a semirigid helix rather than a folded structure, and thus the solvent is able to interact with a large fraction of the peptide groups. Some of these interactions involve the solvent and the peptide carbonyl. They are easily broken by heating, presumably as part of some intramolecular cooperative process. These hy-

(15) O. E. Edwards and T. Singh, *Can. J. Chem.*, 32, 683 (1954).

(16) W. West, Ed., "Techniques of Organic Chemistry," Vol. IX. "Chemical Applications of Spectroscopy," Interscience Publishers, Inc., New York, N. Y., 1956.

drogen bonds between the solvent and the peptide carbonyl seem to be important for maintaining the balance of forces in favor of a stable solution form.

Acknowledgment. The authors wish to thank Mrs. Mary Clemmer for her assistance with the experimental work and the preparation of the manuscript.

The Thermal Decomposition of Nitronium Perchlorate[1]

by J. N. Maycock and V. R. Pai Verneker

Research Institute for Advanced Studies (RIAS), Martin Marietta Corporation, Baltimore, Maryland 21227 *(Received May 8, 1967)*

The thermal decomposition of nitronium perchlorate has been studied in the temperature range 100–160° by isothermal constant-volume techniques and by mass spectrometry. Kinetic analyses have been performed for all the major decomposition species, *e.g.*, O_2 NO, and Cl_2. The activation energy is found to be 15 ± 1 kcal mole^{-1}. This is found to be in good agreement with the activation energy derived from $E = h\nu\epsilon_0/\epsilon$ where $h\nu$ is the absorption edge and ϵ_0 and ϵ are the high- and low-frequency dielectric constants of the solid.

Introduction

The solid-state chemistry of the perchlorates is very important owing to their effectiveness as solid oxidizers. Considerable information is available relating to the metallic perchlorates,[2a] but the only nonmetallic perchlorate which has received considerable attention is ammonium perchlorate.[2b,3] Another nonmetallic perchlorate of interest is nitronium perchlorate, whose decomposition between 70 and 112° has been studied by Cordes[4] and at 65° by Marshall and Lewis.[5] The kinetic analysis performed by Cordes fitted the Mampel[6] theory of solid-state decompositions remarkably well. As a result of this kinetic analysis he postulated that the rate-controlling step in the decomposition was the transference of the anionic electron to the nitronium ion with subsequent gas phase reactions to produce NO_2, Cl_2, ClO_2, NO_3Cl, and O_2. This can be represented by

$$ClO_4^- \longrightarrow ClO_4\cdot + e^-$$

$$e^- + NO_2^+ \longrightarrow NO_2$$

with the subsequent gas phase reactions being

$$ClO_4\cdot \longrightarrow ClO_2 + O_2$$

$$NO_2 + ClO_2 \longrightarrow NO_3 + OCl$$

$$OCl + NO_2 \longrightarrow NO_3Cl$$

$$2OCl \longrightarrow Cl_2 + O_2$$

The isothermal decompositions of Marshall and Lewis have been interpreted such that nitronium perchlorate (NO_2ClO_4) decomposes into nitrosonium perchlorate ($NOClO_4$) and oxygen with subsequent decomposition of the nitrosonium perchlorate.

(1) Supported by the U. S. Army Missile Command, Huntsville, Ala., Contract No. DA-01-021-AMC-12596(Z).

(2) (a) R. D. Stewart, "Perchlorates," J. C. Schumacer, Ed., American Chemical Society Monograph, Reinhold Publishing Corp., New York, N. Y., 1960, p 46; (b) L. L. Bircumshaw and T. R. Phillips, *J. Chem. Soc.*, 4741 (1957).

(3) A. K. Galway and P. W. M. Jacobs, *Proc. Roy. Soc.* (London), **A254**, 455 (1960).

(4) H. F. Cordes, *J. Phys. Chem.*, **67**, 1693 (1963).

(5) M. D. Marshall and L. L. Lewis, *Advan. Chem. Ser.*, **54**, 82 (1966).

(6) K. L. Mampel, *Z. Physik. Chem.*, **A187**, 235 (1940).

$$NO_2ClO_4 \longrightarrow NOClO_4 + {}^1/_2O_2$$

$$NOClO_4 \longrightarrow NO_2 + ClO_2\ (Cl_2 + O_2) + {}^1/_2O_2$$

Both of these reaction schemes are derived from analysis of the condensed decomposition products and both investigators have observed remarkably large induction periods.

In this paper, results will be presented for the decomposition of NO_2ClO_4 whereby the experiments have been performed in a conventional closed volume system and also for time-of-flight mass spectrometric direct inlet decompositions such that the gaseous products formed are continuously being analyzed. The kinetic analyses have been performed using both the Prout–Tompkins equation[7] and the more general kinetic analysis technique of Jacobs and Kureishy.[8]

Experimental Section

Commercial grade nitronium perchlorate (Callery Chemical Co.) was used initially in the as-received form for some exploratory runs. However, the irreproducibility of the isothermal data with this material necessitated the standardization of all future material. The problem was undoubtedly the extreme hygroscopicity of the nitronium perchlorate. To eliminate this problem, all transference operations of material from the stock batch to the sample containers were performed in a drybox having a stream of pure, dry nitrogen passing through it. Even with this precaution it was found by differential thermal analysis (D.T.A.) that all samples invariably absorbed a certain amount of water. But by using D.T.A. and mass spectrometric analyses it was found that complete removal of water and products of hydrolysis could be accomplished by pumping on each individual sample for a period of 18 hr in a vacuum line maintained at 10^{-4} torr. Samples undergoing this treatment then gave reproducible data.

The isothermal decompositions were studied by means of a conventional constant-volume high-vacuum apparatus previously described,[9] the course of the reaction being followed by an ionization gauge and a Pirani gauge. Simultaneously, the course of the reaction was followed by bleeding the gaseous products through a Varian 951-5100 adjustable leak valve having a minimum leak rate of 1×10^{-9} torr l./sec into a Consolidated Electrodynamics 21-613 residual gas analyzer. Using this technique we could either run complete mass sweeps or, as was more often the case, gate on the oxygen, O_2, peak and follow its growth as a function of time. The use of the residual gas analyzer enabled us to determine the molecular species formed during decomposition. Owing to the complexity of this decomposition we have also followed the isothermal decompositions with a Bendix Model 14 time-of-flight mass spectrometer where we have been able to gate simultaneously on five different chemical species as a function of time. Again all samples underwent the pumping treatment prior to the isothermal decomposition data being obtained. Specifically we constructed a very simple, all-glass vacuum decomposition line which was attached to a variable leak on the inlet port of the Bendix mass spectrometer. The arrangement is shown diagrammatically in Figure 1.

The actual decomposition line was maintained at a pressure of approximately 10^{-3} torr and the main flight tube at 10^{-7} torr. At each experimental constant temperature, *e.g.* 100°, the preliminary procedure was to take a complete mass spectrum every minute for the complete duration of the run, the mass spectra being recorded by a Honeywell Visicorder. As a further check the spectrum was continuously displayed on an oscilloscope. All actual recorded runs were performed using an ionization voltage of 65 eV. Having established the fundamental mass spectrum, we then repeated the isothermal decompositions by gating simultaneously and continuously on five different mass species. This procedure allowed the establishment of the partial pressure *vs.* time curves for any spectral species. These isothermal decompositions have been studied in the temperature range 100–160°.

Results

After the elimination of the instrument background species, a typical mass analysis of the total decomposition products is given in Table I.

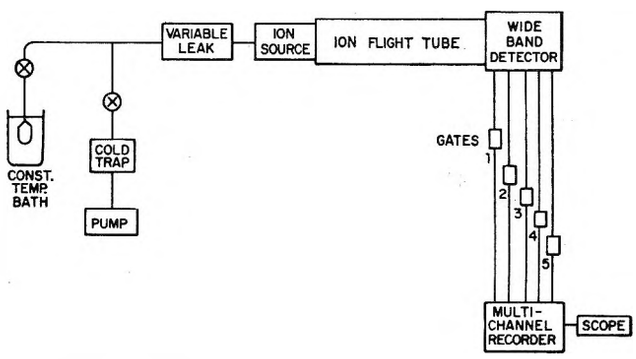

Figure 1. A diagrammatic display of the constant-volume apparatus connected *via* a variable leak to the Bendix time-of-flight mass spectrometer.

(7) E. G. Prout and F. C. Tompkins, *Trans. Faraday Soc.*, **40**, 488 (1944).

(8) P. W. M. Jacobs and A. R. T. Kureishy, *J. Chem. Soc.*, 910, 4718 (1964).

(9) J. N. Maycock, V. R. Pai Verneker, and L. Witten, *J. Phys. Chem.*, **71**, 2107 (1967).

Table I: Mass Species from the Thermal Decomposition of Nitronium Perchlorate at 140°

m/e	Peak height, current × 10^9 amp	Identification
14	1.6	N
16	10.2	O
28	0.2	N_2
30	13.3	NO
32	17.8	O_2
35	7.6	Cl^{35}
37	2.8	Cl^{37}
46	5.5	NO_2
51	1.7	OCl^{35}
53	0.8	OCl^{37}
67	1.4	ClO_2
70	6.9	Cl_2^{35-35}
72	4.8	Cl_2^{35-37}
74	1.2	Cl_2^{37-37}

The identification of the species has been based on the precalibrated cracking patterns for Cl_2, N_2, O_2, NO, N_2O, NO_2, and the oxides of chlorine. An important feature of these products is that we did not find any evidence of NO_3Cl as suggested by the Cordes[4] mechanism and also no evidence of the parent or fragments of $NOClO_4$ as suggested by the low-temperature study of Marshall and Lewis.[5] From Table I and the cracking patterns mentioned above, it is apparent that the only gaseous decomposition products are O_2, Cl_2, OCl, ClO_2, NO, and NO_2. All the pressure–time curves, Figure 2, both obtained in the conventional system and by the mass spectrometer gating method exhibited the usual sigmoid characteristics as observed by Cordes.[4] In the temperature range investigated the residue was either very small (~5%) or nonexistent above approximately 120°.

The kinetic data produced from the time-of-flight mass spectrographic study were initially in the pressure *vs.* time form since we gated on the O_2, Cl_2, and NO peaks simultaneously as a function of time. These data have been reduced into a fractional decomposition (α) as a function of time form. Kinetic analysis of the α–t data has been tried using the Prout–Tompkins[7] equation. As will be seen from Figure 3 a plot of log $\alpha/(1 - \alpha)$ *vs.* time gives a reasonably good straight line. This type of analysis has been used for O_2, Cl_2, and NO over the temperature range 100–160°. From these plots the rate constants k have been calculated and are presented for the three decomposition species as a function of temperature in Figure 4. By inspection of this figure it is apparent that the data for all three species agree reasonably well if possible experimental error is accounted for. A line drawn through these points gives a value of 14.3 kcal $mole^{-1}$ for the activation energy of thermal decomposition of nitronium perchlorate.

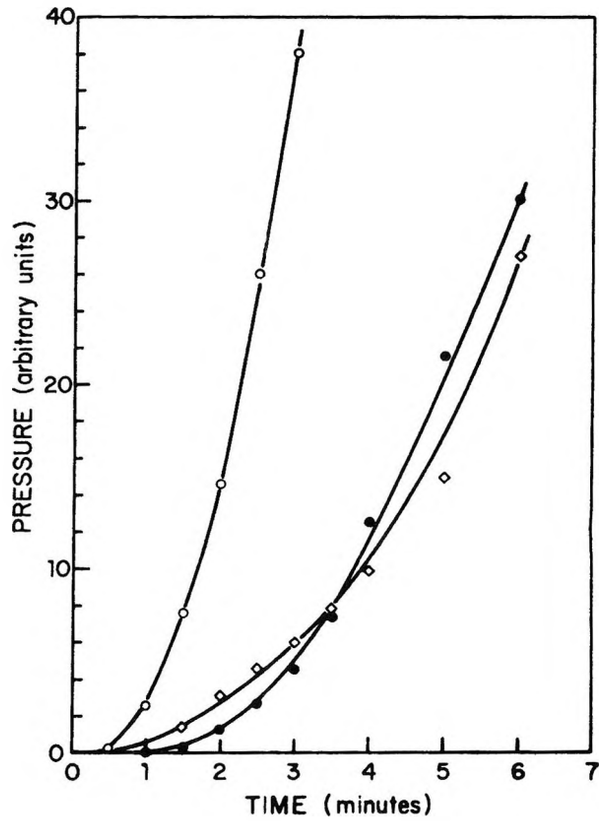

Figure 2. Pressure–time plot for the production of oxygen (○), chlorine (●), and nitric oxide (◇) from the thermal decomposition of nitronium perchlorate at 160°.

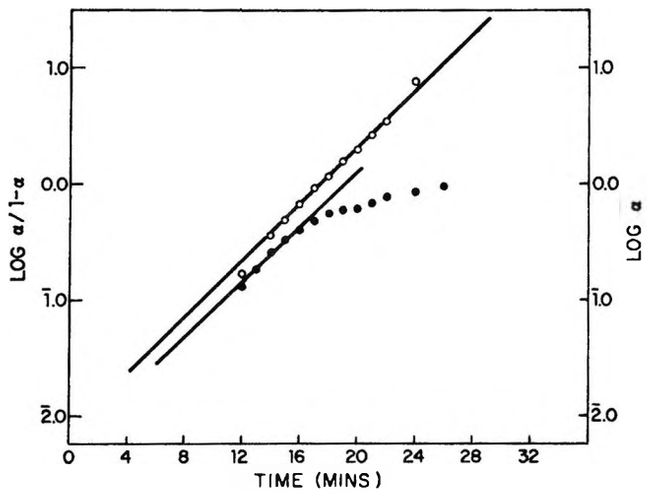

Figure 3. Log α *vs.* t analysis (●) and log $\alpha/(1 - \alpha)$ *vs.* t analysis (○) for the production of O_2 from the thermal decomposition of nitronium perchlorate at 120°.

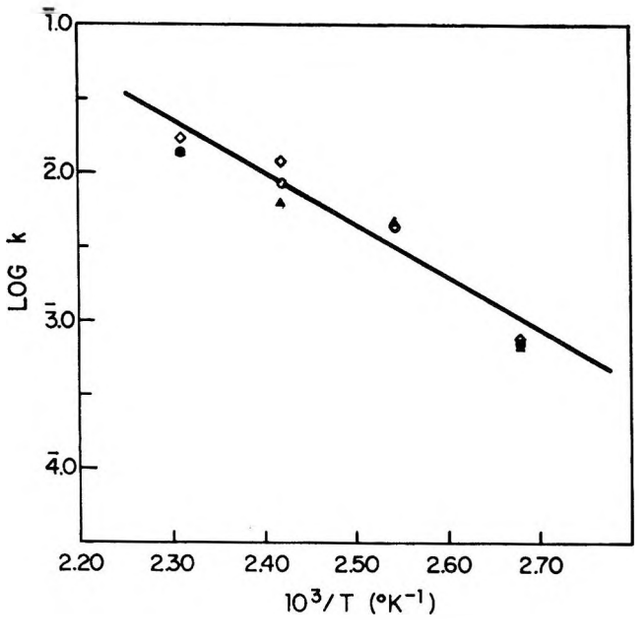

Figure 4. Relationship between log k (rate constant) and $10^3/T$ (°K^{-1}) for O_2 (▲), Cl_2 (◇), and NO (○).

The major difficulty in using the above analytical method is the uncertainty in the applicability of the Prout–Tompkins equation[7] to the experimental data. We have therefore reanalyzed the oxygen data using the Jacobs–Kureishy technique[8] whereby the rate equation can be expressed in the general form

$$f(\alpha) = kt$$

k being the rate constant and α_n, α_{n+1} values of the fractional decomposition (α) at times t_n and t_{n+1}. Thus, one sees that

$$F(\alpha_{n+1}) - F(\alpha_n) = k(t_{n+1} - t_n)$$

and for a different temperature, but the same values of α then

$$F(\alpha_{n+1}) - F(\alpha_n) = k'(t_{n+1}' - t_n')$$

and hence a plot of log $(t_{n+1} - t_n)$ against T^{-1} should be linear with a slope of $2.303R$. The data for the production of oxygen have been analyzed in this manner and gives an activation energy of 16.12 kcal mole^{-1}.

Discussion

After careful consideration of various molecular cracking patterns to be expected from the species produced during a thermal decomposition of nitronium perchlorate, it is apparent that the main species are O_2, NO, and Cl_2. We would like to propose the following, possible decomposition reactions which take place in the thermal degradation of nitronium perchlorate.

$$ClO_4^- \longrightarrow ClO_4^{\cdot} + e^- \quad \text{(conduction band)}$$

$$ClO_4^{\cdot} \longrightarrow ClO_2 + O_2 \quad \text{solid phase}$$

$$e^- + NO_2^+ \longrightarrow NO_2$$

The resultant gases, NO_2, O_2, and ClO_2 then undergo possible gas phase reactions in the following manner

$$ClO_2 + NO_2 \longrightarrow NO + O_2 + ClO$$

$$2OCl \longrightarrow O_2 + Cl_2$$

whereby the following complete reaction scheme can be written as

$$2NO_2ClO_4 = 5O_2 + Cl_2 + 2NO$$

The traces of OCl and ClO_2 as observed mass spectrometrically are undoubtedly intermediate products as shown in the proposed mechanism for the decomposition of nitronium perchlorate.

Owing to the complexity of the decomposition it is felt that the Jacobs–Kureishy[8] treatment of the kinetics is more valid than the approach using the Prout–Tompkins[7] equation. A survey of the activation energies obtained by these two different approaches is given in Table II.

Table II: Activation Energies (Least-Squares Calculation) for the Thermal Decomposition of Nitronium Perchlorate

1. Jacobs–Kureishy method	
O_2 data	E = 16.12 kcal mole^{-1}
2. Prout–Tompkins method	
O_2 data	E = 16.11 kcal mole^{-1}
Cl_2 data	E = 14.43 kcal mole^{-1}
NO data	E = 15.14 kcal mole^{-1}

The activation energy for all these products is the same, *i.e.*, 15 ± 1 kcal mole^{-1}. Cordes,[4] on the other hand, finds the activation energy to be 26 kcal mole^{-1}. This difference is too great to be an experimental error. Upon replotting the Cordes data, using the Jacobs–Kureishy type of analysis, we find that his log t *vs.* $1/T$ data exhibit a break at about 100° such that the activation energy above 100° is of the order of 15 kcal mole^{-1} and below 100° it is of the order of 25 kcal mole^{-1}. Hence the observed divergence of data appears to be due to a possible wrong usage of the Mampel theory. An estimate within 10% of the activation energy can be made from the relationship $E = h\nu\epsilon_0/\epsilon$ where $h\nu$ is the absorption edge and ϵ and ϵ_0 are the static and high-frequency dielectric constants of the solid. We have measured the absorption edge of nitronium perchlorate[9] (3400 A) and although the dielec-

tric constants are not known, these can be estimated from the ultraviolet and infrared absorption of the material.

From the dispersion theory of optics it is possible to show that the refractive index, n, of a material can be expressed by

$$n^2 - 1 = \sum \frac{qe^2N}{m\pi(\nu_0^2 - \nu^2)}$$

where e and m are the charge and mass of the electron, q the number of active electrons per molecule (ion), N the atomic density, ν_0 the characteristic frequency of oscillator, and ν the variable frequency. As the expression stands it is only applicable to electronic transitions, *i.e.*, ν_0 will be an ultraviolet frequency. To include effects at longer wavelengths where nuclear motion will become important, the formula will be

$$n^2 - 1 = \sum \frac{qe^2N}{m\pi(\nu_v^2 - \nu^2)} + \sum \frac{qe^2N}{M\pi(\nu_r^2 - \nu^2)}$$

ν_v and ν_r being the ultraviolet and infrared frequencies and M the mass of the ion. The low-frequency dielectric constant ϵ will therefore only involve the infrared frequency since the ultraviolet term will be negligible. Using the X-ray data of Truter, *et al.*,[10] we have calculated the atomic density of nitronium perchlorate to be 0.83×10^{22}. Assuming a value of 1 for q

$$\epsilon_0 \simeq 1 + \frac{0.83 \times 10^{22} \times (4.8 \times 10^{-10})^2}{9 \times 10^{-28} \times 3.142 \times (0.88 \times 10^{15})^2}$$

$$\therefore \epsilon_0 \simeq 1.87$$

Our calculation of ϵ, the static dielectric constant, is probably more approximate than that for ϵ_0 since the most intense infrared absorption band known for nitronium perchlorate is found by Nebgen, *et al.*,[11] to be at 1100 cm^{-1}. This band is the asymmetric Cl–O stretch of the ClO_4^- ion. Probably a more appropriate frequency would be the one corresponding to the motion of the NO_2^+ lattice against the ClO_4^- lattice. Acknowledging the shortcoming of this calculation we have calculated the static dielectric constant, ϵ, to be 13.3. Hence

$$E \approx 3.65 \times \frac{1.87}{13.3} = 0.514 \text{ ev} = 11.8 \text{ kcal mole}^{-1}$$

This value is in reasonably good agreement with our activation energy derived experimentally.

Thus one can say that the activation energy for the thermal decomposition is 15 kcal $mole^{-1}$ and is the same for O_2, NO, and Cl_2. Although we did not observe $NOClO_4$ mass spectrometrically, Marshall and Lewis' work using Raman spectroscopy positively shows that it is formed at 65°. However, Rosolovskii and Rumyantsev[12] report that the major product in the decomposition of $NOClO_4$ above 90° is NO_2ClO_4. From our recalculation of Cordes[4] data and the Marshall and Lewis[5] data concerning the formation of $NOClO_4$, it is a possibility that the decomposition of NO_2ClO_4 goes *via* two different mechanisms, one above 100° and the other below 100°. Further work on the low-temperature decomposition is in progress and will be reported later.

Acknowledgments. We wish to thank C. S. Gorzynski, Jr., and D. E. Grabenstein for their valuable assistance in the experimental part of this program.

(10) M. R. Truter, D. W. J. Cruikshank, and G. A. Jeffrey, *Acta Cryst.*, 13, 855 (1960).

(11) J. W. Nebgen, A. D. McElroy, and H. F. Klodowski, *Inorg. Chem.*, 4, 1796 (1965).

(12) V. Ya. Rosolovskii and E. S. Rumyantsev, *Russ. J. Inorg. Chem.*, 4, 1796 (1965).

Assignments of the Electronic Transitions in the Methoxy-Substituted Benzenediazonium Cations

by Earl M. Evleth[1] and Robert J. Cox

IBM Research Laboratory, San Jose, California *(Received May 17, 1967)*

The visible–ultraviolet absorption spectra of benzenediazonium, 2-, 3-, 4-methoxybenzenediazonium, 2,4-, 2,5-, 2,6-, 3,4-dimethoxybenzenediazonium, and 2,3,5-, 2,4,5-, 2,4,6-, 3,4,5-trimethoxybenzenediazonium cations were measured in the 200–450-mμ region. The assignments of the electronic transitions of these materials were made possible through the use of molecular orbital theory. An excellent quantitative correlation between the calculated and observed values of the transition energies is obtained. The assignments of the ^1L_a and ^1L_b transitions are in qualitative agreement with those previously assigned for other "strongly substituted" benzenes.

Introduction

Although a number of experimental studies have been reported on the spectroscopic properties of diazonium and diazo compounds,[2-22] a systematic theoretical treatment of the electronic structures of these materials has not been reported. The diazonium moiety (—$N^+{\equiv}N$) is reported to be the most electron-withdrawing substituent known;[21] an observation in agreement with expectations considering both the net positive charge of the substituent and the interaction of its π electrons with the aromatic nucleus. The diazonium moiety represents a strongly perturbing substituent on aromatic systems and in this manner resembles the nitro group.[23] Experimentally, aromatic diazonium cations do not exhibit the $n-\pi^*$ transitions which complicate the analysis of the spectra of aromatic nitro compounds.[23] The strong interaction of electron-donating groups (methoxy, dimethylamino) with benzenediazonium cation (I) is shown by an inordinately high shift in the N≡N stretching frequency on substitution.[3,5,22] This, in combination with the high photosensitivity[24-27] and variable chemical reactivity,[22,28] has prompted us to investigate the electronic absorption spectra of a number of structurally related aryldiazonium cations. We have analyzed the observed spectral properties of these materials within several theoretical frameworks.

Experimental Section

The syntheses of the aryldiazonium fluoroborates investigated here are reported elsewhere.[22] The vis-

(1) University of California at Santa Cruz, Santa Cruz, Calif.

(2) E. A. Boudreaux, H. B. Jonassen, and L. J. Theriot, *J. Am. Chem. Soc.*, 85, 2039, 2896 (1963).

(3) R. H. Nuttall, E. R. Roberts, and D. W. A. Sharp, *Spectrochim. Acta*, 17, 947 (1961).

(4) A. Wohl, *Bull. Soc. Chim. France*, 6, 1319 (1939).

(5) K. B. Whetsel, G. F. Hawkins, and F. E. Johnson, *J. Am. Chem. Soc.*, 78, 3360 (1956).

(6) A. F. Gremillion, H. B. Jonassen, and R. J. O'Connor, *ibid.*, 81, 6134 (1959).

(7) L. S. Gray, V. A. Fassel, and R. N. Kniseley, *Spectrochim. Acta*, 16, 514 (1960).

(8) E. S. Lewis and H. Suhr, *J. Am. Chem. Soc.*, 80, 1367 (1958).

(9) E. S. Lewis and M. D. Johnson, *ibid.*, 82, 5399 (1960).

(10) A. Hantzsch and J. Lifschitz, *Chem. Ber.*, 45, 3011 (1912).

(11) L. C. Anderson and J. W. Steedly, Jr., *J. Am. Chem. Soc.*, 76, 5144 (1954).

(12) L. C. Anderson and B. Manning, *ibid.*, 77, 3018 (1955).

(13) M. Aroney, R. J. W. Le Fevre, and R. L. Werner, *J. Chem. Soc.*, 276 (1955).

(14) R. J. W. Le Fevre, J. B. Sousa, and R. L. Werner, *ibid.*, 4686 (1954).

(15) W. von E. Doering and C. H. De Puy, *J. Am. Chem. Soc.*, 75, 5955 (1953).

(16) M. J. Amrich and J. A. Bell, *ibid.*, 86, 292 (1964).

(17) J. D. C. Anderson, R. J. W. Le Fevre, and I. R. Wilson, *J. Chem. Soc.*, 2082 (1949).

(18) L. C. Anderson and M. J. Roedel, *J. Am. Chem. Soc.*, 67, 955 (1945).

ible–ultraviolet absorption spectra of the diazonium salts were determined in spectral grade acetonitrile (Matheson Coleman and Bell) on a Cary Model 14 spectrophotometer. All solutions were prepared in actinic glassware, and subsequent dilutions and handling were done in such a way as to protect the materials from photodecomposition. Beer's law was obeyed in all cases over the concentration ranges tested.

Theoretical Computation. Initial attempts at SCF–CI calculations on benzenediazonium cation (I) (*vide infra*) proved unsuccessful.[29] As will be shown, Hückel molecular orbital calculations were successful. These calculations were conducted on an IBM 7094 using a FORTRAN IV program described elsewhere.[30] The computational application of Hückel theory is well discussed in standard texts.[31,32] The major problem in the application of the theory to polyatomic systems containing heteroatoms is the assignment of the Coulomb and resonance parameters, h and k, as defined by Streitwieser.[33] The values of the h and k parameters used here are listed in Table I. These parameters arbitrarily assigned with the exception of the h and k values for the $-N^{+}\equiv N$ moiety. These were assigned by conducting several calculations using various values for h_7, h_8, k_{78} until a reasonable pair of relative excitation energies were obtained for the first two electronic transitions in benzenediazonium cation (I).

Table I: Coulomb and Resonance Parameters

Atom type	Coulomb parameter h	Bond type	Resonance parameter k
N (diazo, 8)	1.0	N–N (7–8)	2.0
N (diazo, 7)	2.5	C–N (1–7)	0.7
C (1)	0.4	C–C (all)	1.0
O (methoxy)	2.0	C–O (methoxy)	0.7

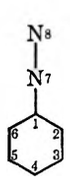

Discussion and Results

Table II contains the measured spectral characteristics of compounds I–XII. Graphical representations of the visible–ultraviolet spectra of these materials are given in Figures 1, 2, and 3. Also listed in Table II are the calculated energies for the lowest two electronic transitions and their respective transition moments, squared. The symmetry assignments given in Table II will be discussed later. Visual comparison of the spectral features of compounds I–XII shows that all but two of the materials possess two absorption maxima in the region above 250 mμ. Ad-

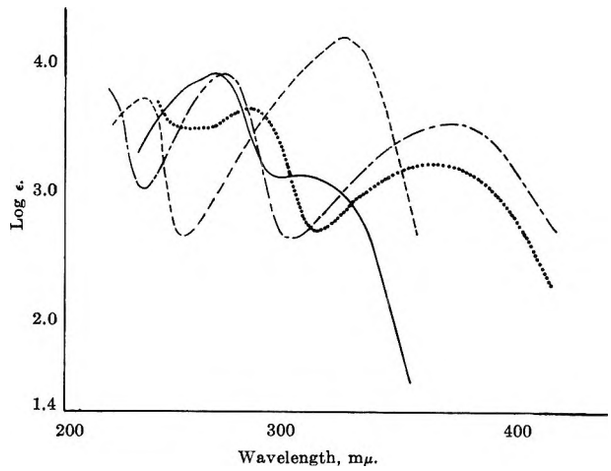

Figure 1. Ultraviolet–visible spectra of the unsubstituted and monosubstituted methoxybenzenediazonium cations:
— — —, benzenediazonium fluoroborate;
. . . ., 3-methoxybenzenediazonium fluoroborate;
– . – ., 2-methoxybenzenediazonium fluoroborate;
– – – –, 4-methoxybenzenediazonium fluoroborate.

(19) C. B. Moore and G. C. Pimentel, *J. Chem. Phys.*, **40**, 342, 329, 1529 (1964).

(20) L. L. Leveson and C. W. Thomas, *Tetrahedron*, **22**, 209 (1966).

(21) E. S. Lewis and M. D. Johnson, *J. Am. Chem. Soc.*, **81**, 2070 (1959).

(22) R. J. Cox and J. Kumamoto, *J. Org. Chem.*, **30**, 4254 (1965).

(23) For a discussion, see J. N. Murrell, "Theory of Electronic Spectra of Organic Molecules," John Wiley and Sons, Inc., New York, N. Y., 1964, pp 186, 187.

(24) J. deJonge, R. Dijkstra, and G. L. Wiggerink, *Rec. Trav. Chim.*, **71**, 846 (1952).

(25) C. F. Goodeve and L. J. Wood, *Proc. Roy. Soc.* (London), **A166**, 342 (1938).

(26) R. Moraw and J. Munder, "Kolliquim uber Wiss. Photographie," Section IV, II Zurick 1961, J. Kosar, "Light-Sensitive Systems," John Wiley and Sons, Inc., New York, N. Y., 1965, pp 194–320.

(27) J. G. Calvert and J. N. Pitts, Jr., "Photochemistry," John Wiley and Sons, New York, N. Y., 1966, pp 472, 473.

(28) H. Zollinger, "Azo and Diazo Chemistry," Interscience Publishers Inc., New York, N. Y., 1961.

(29) E. M. Evleth, unpublished results.

(30) E. M. Evleth, J. A. Berson, and S. L. Manatt, *Tetrahedron Letters*, **42**, 3087 (1964); J. A. Berson, E. M. Evleth, and S. L. Manatt, *J. Am. Chem. Soc.*, **87**, 2901 (1965).

(31) A. Streitwieser, Jr., "Molecular Orbital Theory for Organic Chemists," John Wiley and Sons, Inc., New York, N. Y., 1961.

(32) K. B. Wiberg, "Physical Organic Chemistry," John Wiley and Sons, Inc., New York, N. Y., 1964, pp 65–103.

(33) Reference 31, Chapter 4.

Table II: Ultraviolet–Visible Spectra of Methoxy-Substituted Diazonium Cations[a]

	Benzenediazonium derivative	Experimental λ_{max} (mμ)	Experimental Log ε	Calculated E_T[b]	Calculated μ_T^2[c]	Calculated Symmetry[d]	
I	Unsubstituted	296	3.28	1.337	0.19	$^1B_1$	^1L_b
		261	4.09	1.466	1.08	$^1A_1$	^1L_a
II	2-Methoxy	356	3.69	1.233	0.29	AB	^1L_b
		264	4.09	1.464	1.00	A	^1L_a
III	3-Methoxy	350	3.36	1.211	0.27	AB	^1L_b
		275	3.80	1.441	0.95	A	^1L_a
IV	4-Methoxy	313	4.39	1.324	1.19	$^1A_1$	^1L_a
		...	...	1.347	0.15	$^1B_1$	^1L_b
		231	3.89	...	...		
V	2,4-Dimethoxy	350 sh	4.02	1.239	0.37	AB	
		300	4.34	1.335	0.99	A	
		232	3.86	...	...		
		206	4.22	...	...		
VI	2,5-Dimethoxy	405	3.69	1.121	0.36	AB	^1L_b
		272	3.93	1.447	0.89	A	^1L_a
		220	4.26	...	...		
VII	2,6-Dimethoxy	380	3.66	1.170	0.22	$^1B_1$	^1L_b
		296	4.16	1.435	1.06	$^1A_1$	^1L_a
VIII	3,4-Dimethoxy	348	4.07	1.183	0.56	A	
		305	4.02	1.333	0.75	A	
		240	4.15	...	...		
		212	4.04	...	...		
IX	2,3,5-Trimethoxy	410	3.48	1.062	0.27	B	^1L_b
		307	3.77	1.358	0.90	A	^1L_a
		231	4.25	...	...	...	
X	2,4,5-Trimethoxy	377	3.96	1.111	0.51	A	
		308	4.19	1.329	0.82	A	
		240	4.02	...	...		
		218	4.09	...	...		
XI	2,4,6-Trimethoxy	340	3.69	1.180	0.17	$^1B_1$	^1L_b
		301	4.56	1.320	1.17	$^1A_1$	^1L_a
		208 sh	4.27	...	...		
XII	3,4,5-Trimethoxy	...	...	1.162	0.16	$^1B_1$	^1L_b
		356	4.11	1.204	1.08	$^1A_1$	^1L_a
		220	4.23	...	...		
		202	4.21	...	...		

[a] Fluoroborate salts in acetonitrile. [b] Calculated transition energy in β units, first two calculated transitions. [c] Square of the computed transition moment, angstrom units. [d] C_{2v} symmetry symbol and Platt nomenclature assignment, see Discussion for an explanation of the symbols, A, B, and AB, upper state symmetry given in all cases.

ditional bands appear in the region below 250 mμ; these will not be discussed further. In Figure 4 is shown a plot of the observed versus the calculated transitions. An adequate correlation (coefficient = 0.97) is obtained from a least-squares plot of this data. The slope yields a spectroscopic value for β (the resonance parameter) of 33,650 cm^{-1}.

The reasonable agreement between the observed and calculated spectral features of compounds I–XII is not particularly enlightening. Correlation curves of this type do not present a systematic understanding of the effect of structure on spectra but possibly demonstrate the adequacy of the theoretical method.

The first question to answer, however, is why the Hückel calculations are successful at all in quantitatively correlating the spectral features of these materials. It is generally accepted, although most certainly not true,[34] that Hückel calculations are unable to yield adequate spectral correlations. The methods developed by Pariser and Parr (ASMO–CI)[35] and Pople (SCF–CI)[36,37] have yielded adequate

(34) Reference 31, Chapter 8.

(35) R. Pariser and R. G. Parr, *J. Chem. Phys.*, 21, 466, 767 (1953).

(36) J. A. Pople, *Trans. Faraday Soc.*, 49, 1375 (1953).

(37) J. A. Pople, *Proc. Phys. Soc.* (London), 68A, 81 (1955).

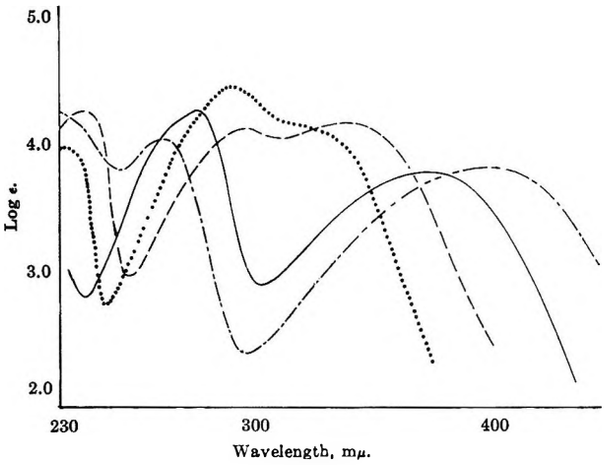

Figure 2. Ultraviolet–visible spectra of the disubstituted methoxybenzenediazonium cations:
———, 2,6-dimethoxybenzenediazonium fluoroborate;
. . . ., 2,4-dimethoxybenzenediazonium fluoroborate;
– . – ., 2,5-dimethoxybenzenediazonium fluoroborate;
– – – –, 3,4-dimethoxybenzenediazonium fluoroborate.

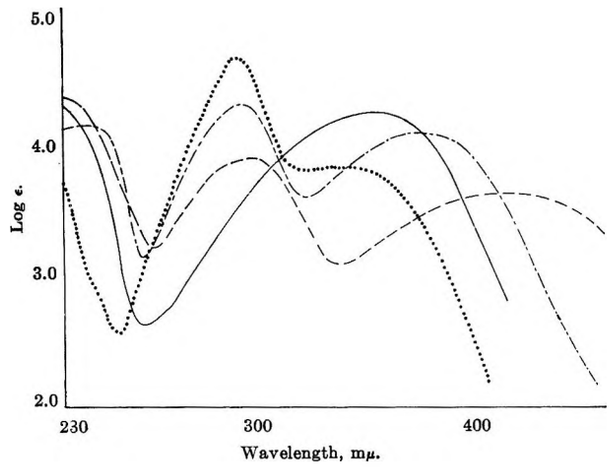

Figure 3. Ultraviolet–visible spectra of the trisubstituted methoxybenzenediazonium cations:
———, 3,4,5-trimethoxybenzenediazonium fluoroborate;
. . . ., 2,4,6-trimethoxybenzenediazonium fluoroborate;
– . – ., 2,4,5-trimethoxybenzenediazonium fluoroborate;
– – – –, 2,3,5-trimethoxybenzenediazonium fluoroborate.

results in the analysis of the spectral features of planar organic molecules. The essential accomplishment of these methods has been due to the introduction of configuration interaction under appropriate parameterization.[38–40] The major consequences of the inclusion of electron repulsion terms are that (i) a separation of the singlet and triplet states is predicted and (ii) degenerate or close-lying states of the same symmetry are split. This latter phenomena is particularly important under conditions where the pairing rule is obeyed.[38,41] The inadequacy of the Hückel method

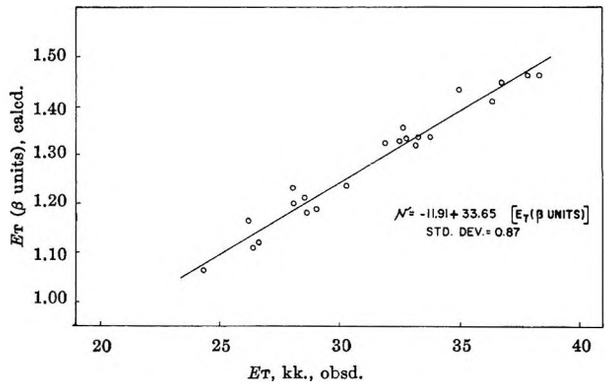

Figure 4. Correlation plot of the first two calculated electronic transitions *vs.* the observed electronic transitions of the aryldiazonium salts shown in Table II.

in correlating spectral properties is particularly evident where the pairing rule is obeyed;[38] *i.e.*, the polyacenes. If configuration interaction is not of importance in determining the relative intensities and positions of the electronic transitions from the ground state to the first or second excited states, simple Hückel theory may be useful in spectral interpretation.[42] Preliminary SCF–CI calculations on benzenediazonium cation (I) were carried out but yielded poor quantitative predictions of the first two transitions.[29] It was determined that configuration interaction was of little importance in lowering the calculated SCF energies of the first two excited states. Both transitions were nearly "pure," *i.e.*, the configurational weights were over 90% of a single excited-state SCF wave function. In addition the symmetries of the first two transitions were in the same order as predicted from the Hückel calculations (Table II). In the Hückel calculation the degree of the splitting of the transitions of a substituted benzene over the identical case for benzene (degenerate in the Hückel approximation) is dependent on the magnitude of the Coulomb and resonance parameters of the substituent.[43] Under such circumstances configuration interaction plays a diminished role and adequate spectral correlations can be anticipated using simple Hückel theory.[42] This is ap-

(38) R. Pariser, *J. Chem. Phys.*, 24, 250 (1956).

(39) Y. L'Haya in "Advances in Quantum Chemistry," P. O. Lowdin, Ed., Academic Press, New York, N. Y., 1964, Vol. 1, pp 203–240.

(40) I. Fischer-Hjalmars in "Molecular Orbitals in Chemistry, Physics, and Biology," P. O. Lowdin and B. Pullman, Ed., Academic Press, New York, N. Y., 1964, pp 361–383.

(41) A. D. McLochlan, *Mol. Phys.*, 2, 361 (1959).

(42) N. M. Atherton and J. N. Murrell, *Ann. Rept. Chem. Soc.*, 61, 197 (1964).

(43) C. R. Sandorfy, "Electronic Spectra and Quantum Chemistry," Prentice-Hall, Englewood Cliffs, N. J., 1964, p 217.

parently the case with the substituted benzenediazonium cations.

The main difficulty with a purely computational approach to spectral analysis is that it is unable to provide a systematic understanding of the spectral properties of a number of structurally related materials. Systematic spectral analyses have been provided from three main sources: (i) resonance theory,[44,45] (ii) free electron theory,[46] and (iii) charge-transfer calculations.[47,48] Too few valence-bond calculations have been done on organic molecules with regard to spectral analysis[45] to test the validity of resonance theory. As a consequence resonance arguments have no computational support.

Of the few charge-transfer resonance structures shown below for benzenediazonium cation (I), Ia, Ib, and Ic can be considered "traditional." There is no compelling reason to exclude Id and Ie from a truncated set of important valence-bond structures. In any case there is no noncomputational method of either assigning the weights or relative importance of these and other structures in the ground and particularly the excited states of I.[49]

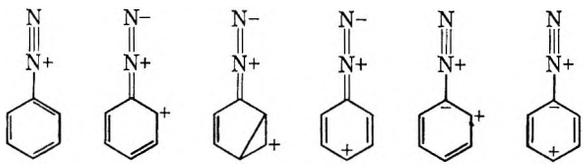

I Ia Ib Ic Id Ie

In the case of the monosubstituted methoxybenzenediazonium cations both II and III absorb at lower energies than IV. Traditional resonance arguments would compel using structures IIa, IIIa, and IVa to rationalize this observation. The charge-transfer caclulations of Murrell[47] on aminonitrobenzenes indicate that charge-transfer interactions of the donor or acceptor with the benzene ring are of more importance than with one another, especially in the case of IV. In addition, although the weaker intensity of II *vs.* IV can be explained on the basis of the shorter transition dipole, the weak intensity of III is anamolous in resonance terms. Also traditional spectral resonance arguments usually disregard other low energy transitions.

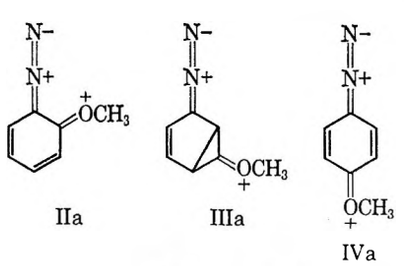

IIa IIIa IVa

N V_1 = 356 mμ 350 mμ 313 mμ

The systematic application of free electron theory has lead to the assignments of the two lowest energy transitions in benzene and substituted benzenes.[46,50,51] The weak 254-mμ band in benzene has been assigned as being $^1L_b \leftarrow {}^1A$. The stronger 204-mμ band has been assigned as being $^1L_a \leftarrow {}^1A$. Visual comparison of the known absorption spectra for the monosubstituted benzenes shows that the labeling of the two lowest energy electronic transitions as being L_a or L_b has general validity. For monosubstituted benzenes the molar extinction coefficient of the L_a transitions are in a region between 6000 and 13,000.[50,52] The L_b transitions, when observed, are much weaker, in the region between several hundred and 3000. For mildly perturbed systems, such as anisole, the energy shifts of the L_a and L_b transitions from their values in benzene are small.[50] As the number and charge-transfer characteristics of the substituents change, the L_a and L_b purity of the observed transitions become tainted by contributions from higher benzene transitions and charge-transfer structures of appropriate symmetry.[47] Stevenson has shown[50] that the spectral features of 191 substituted benzenes, previously experimentally investigated by Doub and Vandenbelt,[53] are adequately treated as perturbations of the L_a and L_b transitions in benzene. In all but ten cases the L_a and L_b transitions could be assigned on the basis of their different intensities.

Table II contains the assignments of the electronic transitions for compounds I–XII. Of these materials, compounds I, IV, VII, XI, and XII have C_{2v} symmetry.[54] For molecules having C_{2v} symmetry the $\pi-\pi^*$ electronic transitions are polarized in the plane of the molecule and either along the molecular axis ($^1A_1 \leftarrow {}^1A_1$) or perpendicular to it ($^1B_1 \leftarrow {}^1A_1$).

(44) G. W. Wheland, "Resonance in Organic Chemistry," John Wiley and Sons, Inc., New York, N. Y., 1955.

(45) Reference 43, Chapter 9.

(46) J. R. Platt, *J. Chem. Phys.*, **17**, 484 (1949); see also "Systematics of the Electronic Spectra of Conjugated Molecules," J. R. Platt, Ed., John Wiley and Sons, Inc., New York, N. Y., 1964.

(47) M. Godfrey and J. N. Murrell, *Proc. Roy. Soc.* (London), **A278**, 57 (1964).

(48) See K. Kimura and S. Nagakura, *Mol. Phys.*, **8**, 117 (1965), and references cited therein.

(49) For a recent discussion read E. Heilbronner, ref 39, pp 329–359.

(50) P. E. Stevenson, *J. Mol. Spectry.*, **15**, 220 (1965).

(51) P. E. Stevenson, *J. Chem. Educ.*, **41**, 234 (1964).

(52) J. Petruska, *J. Chem. Phys.*, **34**, 1120 (1961).

(53) L. Doub and J. M. Vandenbelt, *J. Am. Chem. Soc.*, **69**, 2714 (1947); **71**, 2414 (1949); **77**, 4535 (1955).

(54) Neglecting the symmetry of the O–CH_3 group.

These transitions correspond to, respectively, the L_a and L_b transitions of the perturbed benzene model. The other molecules shown have C_s symmetry and strictly speaking all excited π-electron states have the same symmetry. We have taken the liberty of assigning these transitions as being A, AB, or B. A and B are assigned on the basis of whether the computed squared transition moment acquired 70% or more of its strength from the x or y component of the transition moment. Transitions having approximately equal contributions of the x and y components were assigned AB. In this way a direct comparison of the molecules having C_{2v} and C_s symmetry can be made.

Based on their weak intensities the low-energy transitions of compounds I, II, III, VI, VII, IX, and XI are assigned as being L_b. This is agreement both with the polarization (B or AB) and weak computed squared transition moments obtained from the Hückel calculations. Conversely the second electron transitions of these materials are significantly stronger and are assigned as being L_a transitions. Compounds IV and XII only exhibit a single strong transition in the region above 250 mμ. These transitions are assigned as being L_a transitions on the basis of their intensities. The Hückel calculations indicate that the L_a and L_b transitions of these materials are nearly degenerate. The rationalization is that the weaker L_b transition is buried beneath the L_a transition. In some strongly perturbed systems, particularly the *para*-disubstituted benzenes, L_b transitions have not been observed[50,52] and are presumably buried beneath the stronger L_a transitions. The charge-transfer calculations by Murrell[47] on the 2-, 3-, and 4-aminonitrobenzenes and the SCF–CI calculations by Labhart[55] on 4-dimethylaminonitrobenzene also indicate a computed near degeneracy of the L_a and L_b transitions.

The three remaining materials, V, VIII, and X, exhibit two transitions in the region above 250 mμ having reasonably strong intensities ($\epsilon > 9000$). On the basis of intensity it is not possible to assign these as being either perturbed L_a or L_b transitions. The computed weaker intensity of the low-energy transitions (and certainly the AB character of the transition for V) would lead toward the L_b assignment for V, VIII, and X. The theoretical expectation is that the L_a and L_b interpretation will lose its meaning at a strongly perturbed stage. This is apparently the case for these latter three compounds. In Figure 5 is shown a comparison of the computed and observed positions of the L_a and L_b transitions for compounds I–XII. This figure graphically demonstrates that the low-energy transitions of V, VIII, and X are

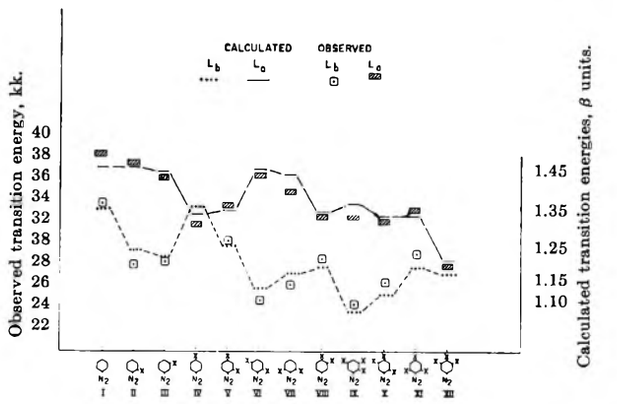

Figure 5. Platt diagram of the experimental and computed $^1A_1$–^1L_b and $^1A_1$–^1L_a electronic transitions.

systematically related to the other L_b transitions. The lack of symmetry (C_s) in these compounds coupled with a *para*-substituted electron-donating substituent gives rise (*vide infra*) to a strong red shift of the L_a transitions of I. This in turn will give rise to a closing of the energy gap between these transitions. A possible explanation is that this, coupled with the low symmetry of these substances will, conceptually, give rise to a mixing of the L_a and L_b transitions and thus increase in the intensity of the L_b transition by borrowing from the adjacent L_a transition.

A Qualitative Interpretation of the Spectra of I–XII. Neither the Hückel calculations nor the free electron theory interpretation gave a qualitative understanding of the effect of methoxy substitutions on the spectra of I. Perturbation theory is able to predict the effects of the substitution of methoxy groups on I. This requires knowledge of the wave functions in the ground and the excited states of I. Shown in Figure 6 are the calculated π-electron densities for I in the ground and L_a and L_b excited states as obtained by the Hückel approximation. In the ground state there is a slight positive charge at the *ortho* and *para* positions. In the L_b excited state the *ortho* and *meta* positions have a much higher positive charge than in the ground state while the *para* position shows a slight gain in electron density. The electron distribution of the L_a state is quite different in that the *para* position has a much higher positive character, the *meta* position a slightly greater positive charge, and the *ortho* position is essentially unchanged with regard to the ground-state electron distribution. These different changes in electron density at the *ortho*, *meta*, and *para* positions in going from the ground to the L_b and L_a states have great significance with

(55) H. Labhart and G. Wagnere, *Helv. Chim. Acta*, **46**, 1314 (1963).

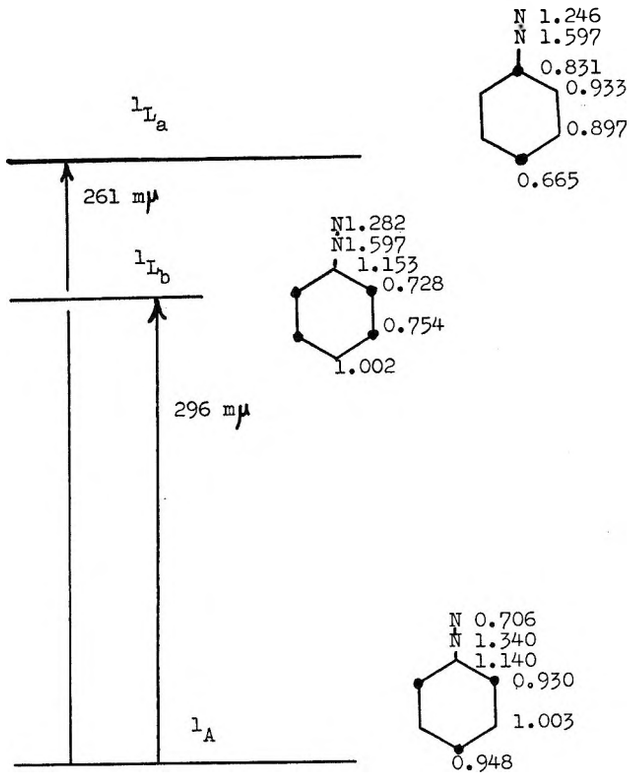

Figure 6. Computed electron densities of the ground and the first two excited states of I.

regard to the possible effect of methoxy substitution on the position of electronic transitions between these states. Since the electron demands of the benzene ring system are higher in the excited states than the ground state, it would intuitively be predicted that the presence of electron-donating substituents would have a greater stabilizing effect on the excited states than the ground state. This would give rise to a shift of the L_a and L_b transitions of methoxy-substituted benzenediazonium cations to lower energies (red shift) as compared to I. Simple perturbation theory shows that the energy E_m of a particular molecular orbital, m, will change on the substitution of a single atom, S (methoxy oxygen in this case), to a new energy E' according to the expression[56]

$$E'_m = (a_{mr}^2\beta_{rs}^2)/(E_m - \alpha_s)$$

where a_{mr}^2 is the coefficient, at the molecular orbital m at the position of substitution, r; β_{rs} is the resonance integral between r and s, and α_s the Coulomb parameter of s.

The change in the energy separation between two molecular orbitals, m and n, E'_m and E'_n, on substitution of S will be

$$E'_m - E'_n = \frac{(a_{mr}^2\beta_{rs}^2)}{E_m - \alpha_s} - \frac{(a_{nr}^2\beta_{rs}^2)}{E_n - \alpha_s} \quad (1)$$

which, in the Hückel approximation is equivalent to the change in the transition energy $\Delta E_{T(n-m)}$. Collecting all constant terms

$$\Delta E_{T(n-m)} = K_m a_{mr}^2 - K_n a_{nr}^2 \quad (2)$$

The constants K_m and K_n can be estimated from the experimental shifts of the L_a and L_b transitions (see Table II) and the computed values of a^2. For the simple case of monosubstitution on benzenediazonium cation into the *ortho*, *meta*, and *para* positions, six equations are generated. Using computed values for a^2 for the lowest unoccupied and two highest occupied molecular orbitals (from which the theoretical data shown in Table II were calculated for I), eq 3–5

ortho

$$\Delta E_{T(L_b \text{ transition})} = K_m(0.048) - K_b(0.250) = 4700 \text{ cm}^{-1}$$

$$\Delta E_{T(L_a \text{ transition})} = K_m(0.048) - K_a(0.044) = 400 \text{ cm}^{-1} \quad (3)$$

meta

$$\Delta E_{T(L_b \text{ transition})} = K_m(0.000) - K_b(0.250) = 5700 \text{ cm}^{-1}$$

$$\Delta E_{T(L_a \text{ transition})} = K_m(0.000) - K_a(0.108) = 1900 \text{ cm}^{-1} \quad (4)$$

para

$$\Delta E_{T(L_b \text{ transition})} = K_m(0.054) - K_b(0.000) = \text{not observed}$$

$$\Delta E_{T(L_a \text{ transition})} = K_m(0.054) - K_a(0.338) = 6400 \text{ cm}^{-1} \quad (5)$$

are found. K_a and K_b are the values of K_n for the L_a and L_b transitions. The resultant five equations and three unknowns are not suitable for regression analysis. In addition the broad nature of the absorption bands prevents an accurate evaluation of the shift in these transitions and the coefficients connected with K_m are small, preventing an accurate estimate of this quantity. Average values of 20,000 cm^{-1} are computed for both K_a and K_b. Using a value for β_{rs} of $-16{,}000$ cm^{-1} and the experimental values for $E_m - E_a$ and $E_m - E_b$ of 38,300 and 33,800 cm^{-1}, respectively, K_m is calculated to be in the order of 5000–5500 cm^{-1}. Using these values for K_a,

(56) M. J. S. Dewar, *J. Am. Chem. Soc.*, **74**, 3341 (1952).

K_b, and K_m the calculated shifts of the L_b and L_a transitions for (i) II are -4800 and -700 cm^{-1}, (ii) III are -5000 and -2200 cm^{-1}, and (iii) IV are $+300$ and -6500 cm^{-1}, respectively. Except for the unobserved L_b transition of IV all these computed values are within several hundred cm^{-1} of the observed values. This at very least shows the consistency of the argument.

An interesting qualitative aspect of eq 3–5 is that they demonstrate that the L_b transitions are more strongly affected (red shifted) by *ortho* and *meta* substitutions of methoxy substituents than the L_a transitions. Conversely, the L_a transitions are primarily red shifted by *para* substitution, *meta* substitution having a mild effect. The effects of di- and trisubstitution of methoxy groups are not additive. The effects are accumulative, however. Compounds II, III, VI, VII, and IX represent a family in which no *para* substitution occurs. The L_b transition in all these materials gradually moves to lower energies. *para* substitution has the effect of suppressing the degree of red shift of the L_b transition while enhancing the L_a transition in multiply substituted systems.[57]

Conclusion. The Hückel calculations and the free electron theory interpretation has made it possible to assign the L_b and L_a transitions of I, II, III, VI, VII, IX, and XI. Only the L_a transitions were observed in IV and XII, the weaker L_b transition presumably buried under the stronger band systems. Both the observed transitions in V, VIII, and X were too strong to be classified as L_b. This is presumably due to a breakdown in the model that assumes that the spectra of these materials can be treated as perturbations of benzene. An additional perturbation model was constructed which is able to rationalize the effect of substitution on the spectra of benzenediazonium cation (I).

(57) The referee showed in his comments that the application of eq 9, ref 49, yielded a fair correlation between the observed and calculated positions of the ^1L_a transitions of compounds II, III, and V through XII.

Oxidation Kinetics of Polydimensional Silicon Monoxide

by W. Hertl

Technical Staffs Division, Corning Glass Works, Corning, New York *(Received May 17, 1967)*

The oxidation kinetics of polydimensional SiO powder was studied in the temperature range 715–910°. The diffusion rate constants were calculated with a modified form of the Ginstling–Brounshtein equation. This modification allows one to obtain the specific diffusion constants in a system containing a wide spectrum of particle sizes. The rate-determining step of the reaction is the diffusion of molecular oxygen through the product silica (cristobalite) sheath formed on each reactant particle. Up to about 250 torr of oxygen, the rate increases linearly with increasing oxygen pressure; above 250 torr of oxygen, the increase in rate with increasing oxygen pressure is less, due to saturation of the surface or limiting solubility of oxygen in silica. The rate constants are in good agreement with published oxygen diffusion constants.

Introduction

Oxygen diffusion in silica has been studied by several techniques, which include permeation measurements,[1] isotopic exchange,[2,3] and kinetic studies of the oxidation of silicon[4,5] and silicon carbide.[6–8] Widely divergent activation energies for oxygen diffusion have been reported. Motzfeldt[9] critically reviewed the work done on these systems by converting the initial rates of the published data to rate constants. Assuming the rates are controlled by oxygen diffusion through silica, he shows that the experimental data are consistent throughout the temperature ranges covered. The rate dependence on the oxygen pressure, however, could not be conclusively determined due to meager data.

The air oxidation kinetics of SiO was studied in this laboratory and an oxygen diffusion activation energy obtained equal to 24 kcal.[10] However, that study did not yield an oxygen pressure dependence nor a value for the oxygen diffusion rate constant.

This paper describes the oxidation kinetics of particulate SiO over a range of ambient oxygen pressures from 25 to 710 torr in the temperature range 715–910°. The variation in particle size within the reactant mixture (0.5 to 45 μ) is also taken into account in analyzing the data to obtain the diffusion rate constants.

Experimental Section

1. Materials. Silicon monoxide for the oxidation experiments obtained from Linde Division of Union Carbide Co. was −325 mesh, select grade. The cation impurity level, determined by emission spectrographic analysis, was less than 0.1%. In the temperature range at which the oxidation experiments were carried out this silicon monoxide neither vaporizes nor disproportionates measurably.[11] The particle size distribution is given in Figure 1. X-Ray analysis of the oxidized silicon monoxide showed that the product silica formed was cristobalite. Matheson Co. extra dry oxygen was used without further purification.

2. Procedure. SiO charges weighing 0.600 g were used for each experiment. The SiO powder was placed in an alumina tray (25 × 14 × 4 mm) which was suspended *via* a platinum chain from the balance pan of an Ainsworth recording analytical balance (Type RZA-AU-1). The suspended charge was enclosed within a 2-in. i.d. 96% silica glass muffle, and the entire system

(1) F. J. Norton, "Transactions of the Eighth National Vacuum Symposium and Second International Congress on Vacuum Science and Technology," The Macmillan Co., New York, N. Y., 1961, p 8.

(2) E. W. Sucov, *J. Am. Ceram. Soc.*, **46**, 14 (1963).

(3) E. L. Williams, *ibid.*, **48**, 190 (1965).

(4) P. J. Burkhardt and L. V. Gregor, *Trans. AIME*, **236**, 299 (1966).

(5) B. E. Deal and A. S. Grove, *J. Appl. Phys.*, **36**, 3770 (1965).

(6) G. Ervin, *J. Am. Ceram. Soc.*, **41**, 347 (1958).

(7) P. J. Jorgensen, M. E. Wadsworth, and I. B. Cutler, *ibid.*, **42**, 613 (1959); **43**, 209 (1960).

(8) R. F. Adamsky, *J. Phys. Chem.*, **63**, 305 (1959).

(9) K. Motzfeldt, *Acta Chem. Scand.*, **18**, 1596 (1964).

(10) W. W. Pultz and W. Hertl, *J. Am. Ceram. Soc.*, **50**, 202 (1967).

(11) W. Hertl and W. W. Pultz, *ibid.*, **50**, 378 (1967).

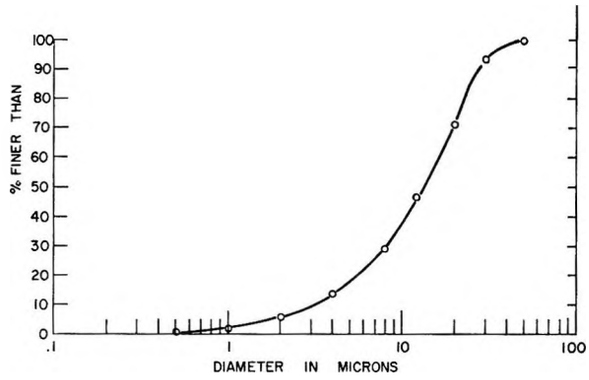

Figure 1. Silicon monoxide particle size distribution given as Stokes equivalent spherical diameter from sedimentation time in water.

was connected to a conventional glass vacuum rack. A platinum-wound tube furnace was mounted on a vertical track running along the muffle, allowing the furnace to be raised (and lowered) about the muffle. A monitoring thermocouple was mounted on the muffle opposite the point where the charge was suspended.

To carry out an experiment, the entire system was evacuated to at least 10^{-2} torr, the furnace was raised on the track to the point where the suspended charge was within a constant temperature zone of the tube furnace, and the desired pressure of oxygen was then added to the system. Due to the large volume of the system, no significant pressure changes were noted during the course of an oxidation experiment. The weight changes due to the oxidation of SiO to SiO_2 were automatically recorded on a strip chart.

Some preliminary runs at 940° with a different batch of SiO showed that the presence or absence of added argon to the oxygen atmosphere had no effect on the oxidation rate. Blank runs in 100 torr of argon pressure showed no weight change due to volatilization.

Derivation of Rate Equation

When a spherical particle oxidizes to form a nonvolatile oxide sheath, there are several steps in the oxidation process which can be rate determining. When the rate-determining step is the diffusion of oxygen through the oxide sheath, the rate at any time is given by Fick's law

$$dn/dt = -AD(dc/dx) \qquad (1)$$

where dn/dt is the number of molecules transported in unit time across the oxide sheath of thickness dx, A is the area across which diffusion is taking place, D is the diffusion coefficient, and dc is the oxygen concentration differential across dx. It is assumed that the oxygen concentration at the silica–silicon monoxide interface is substantially zero; *i.e.*, the oxidation reaction ($SiO + {}^1/_2O_2 = SiO_2$) is faster than the diffusion process. Accounting for spherical geometry, the increasing thickness of the oxide sheath, and the decreasing surface area of the reacting surface as the reaction proceeds, eq 1 may be integrated to obtain

$$1 - {}^2/_3\alpha - (1 - \alpha)^{2/3} = kt/R^2 \qquad (2)$$

where α is the fraction of total reaction in time t, R is the initial radius of the spherical particle, and k is the rate constant. The constant k is proportional to the diffusion coefficient, and in this case, includes the term dc. Then, k is here defined as a diffusion constant for a given ambient oxygen pressure and has the units $(\text{length})^2\,(\text{time})^{-1}$. Equation 2 is commonly known as the Ginstling–Brounshtein equation.[12] This equation neglects the difference in molar volumes of the reactant and product. This will not significantly affect the accuracy if the product to reactant volume ratio is less than about 2;[13] for SiO oxidizing to SiO_2 it is 1.35.

Due to the term for the initial particle radius (R) on the right-hand side of eq 2, it is clear that the equation in this form will not yield a true value for k in a system containing a spectrum of particle sizes. However, since each particle reacts independently, the following analysis of the system can be carried out when the size distribution of particles is known. Rearrange eq 2 as

$$R^2\{1 - {}^2/_3\alpha - (1 - \alpha)^{2/3}\} = kt \qquad (3)$$

At any given time during the course of oxidation there will be a range of α values, depending on the size of the individual particle; the value of α decreases with increasing R. If a value of α_1 is assigned to those particles which have radius R_1, eq 3 can be solved for kt. For a given value of kt the α corresponding to each R is uniquely determined. Thus, with this value of kt one takes a value of R_2 and calculates to what α this corresponds, say α_2. This is carried out for all values of R in the mixture. The average α ($\bar{\alpha}$) for this mixture at the given kt value must then be

$$\sum_0^i n_i\alpha_i = \bar{\alpha}$$

where n_i is the weight fraction of the mixture which has reacted to the extent α_i. This procedure is repeated for various assignments of α_1 until a table is built up of $\bar{\alpha}$ *vs.* kt values. It is the quantity $\bar{\alpha}$ which is experimentally observed. Table I gives the mean radius of

(12) A. M. Ginstling and B. I. Brounshtein, *J. Appl. Chem. USSR*, 23, 1327 (1950). A similar analysis had also been made by G. Valensi, *Compt. Rend.*, 201, 602 (1935).

(13) R. E. Carter, *J. Chem. Phys.*, 34, 2010 (1961); 35, 1137 (1961).

Table I: Calculation of $\bar{\alpha}$ and kt Value[a] (Each Fraction Contains 10% of the Total Amount of Material)

Fraction	Mean radius, μ	α
1	0.91	0.6700
2	2.17	0.3187
3	3.40	0.2101
4	4.65	0.1558
5	6.00	0.1218
6	7.40	0.0993
7	9.00	0.0819
8	10.65	0.0695
9	12.35	0.0600
10	15.90	0.0468
		$\bar{\alpha}$ = 0.1834

[a] $kt = 0.0627\ \mu^2$.

Table II: Partial List of $\bar{\alpha}$ *vs.* kt Values Generated by Computer for SiO Size Distribution Given in Figure 1

$\bar{\alpha}$	kt, μ^2	$\bar{\alpha}$	kt, μ^2	$\bar{\alpha}$	kt, μ^2
0.0074	0.00008	0.1771	0.05799	0.5281	1.21475
0.0225	0.00078	0.1898	0.06787	0.5723	1.61595
0.0377	0.00222	0.2030	0.07916	0.6086	2.04715
0.0480	0.00364	0.2166	0.09215	0.6513	2.66972
0.0584	0.00544	0.2384	0.11576	0.7099	3.82911
0.0689	0.00767	0.2625	0.14665	0.7512	4.99361
0.0795	0.01034	0.2911	0.19125	0.8019	6.93011
0.0903	0.01349	0.3251	0.25911	0.8618	10.51392
0.1067	0.01922	0.3512	0.33125	0.9122	16.09944
0.1179	0.02378	0.3783	0.41885	0.9503	23.8140
0.1293	0.02898	0.4169	0.56782	0.9779	35.2327
0.1408	0.03492	0.4485	0.71443	0.9880	44.8416
0.1526	0.04165	0.4839	0.91066	1.0000	84.2700
0.1647	0.04930				

each of the ten size fractions used for the calculation. Also given are the calculated values of α_i, $\bar{\alpha}$, and kt for an arbitrarily assigned value of $\alpha_1 = 0.6700$.

The complete table of $\bar{\alpha}$ *vs.* kt values were generated on a computer at $\bar{\alpha}$ intervals of about 0.01. Fraction 1 ($R = 0.91\ \mu$) was completely reacted when $\bar{\alpha}$ reached 0.3178. At this point α_2 (the next larger size fraction) was 0.5750. Values of $\alpha_1 = 1.000$ and $\alpha_2 = 0.5750$ were assigned and the procedure repeated by assigning values to α_2 until it also reached 1.000, and so on. Part of the table of $\bar{\alpha}$ *vs.* kt values (rounded off to five figures) generated by the computer is given in Table II.

Results

Reaction curves for the runs at 810 and 715° at various ambient oxygen pressures are shown in Figures 2 and 3.

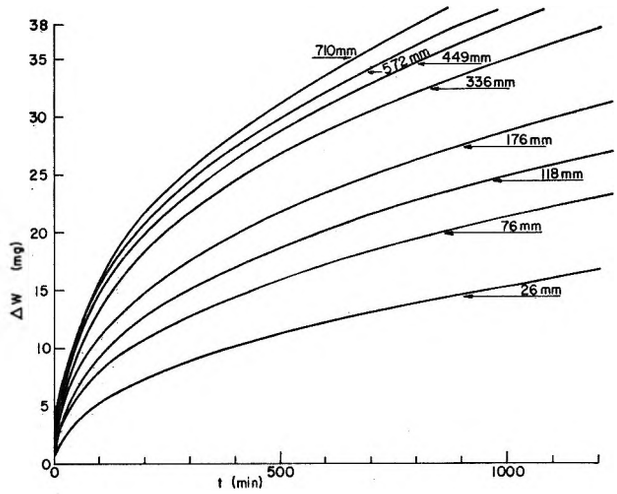

Figure 2. SiO weight gain, ΔW, *vs.* time at 810° for various ambient oxygen pressures. Charge weight, 0.600 g; 100% reaction would give a weight change of 219 mg.

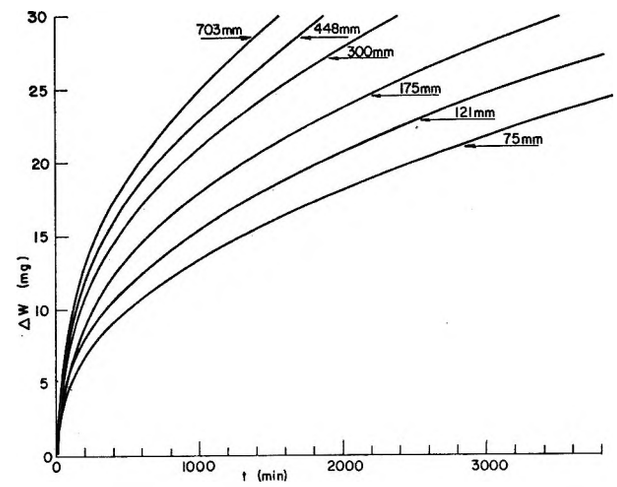

Figure 3. SiO weight gain, ΔW, *vs.* time at 715° for various ambient oxygen pressures. Charge weight, 0.600 g.

The data for two runs carried out at 910° were plotted (Figure 4) using the generated $\bar{\alpha}$ *vs.* kt values given in Table II. The values of kt for the experimentally observed $\bar{\alpha}$ are plotted against the time for that $\bar{\alpha}$. The slope of this plot gives the value of k (eq 2). Due to the long times needed (weeks) to obtain a large degree of oxidation (60%), only the higher pressure run was carried out to large $\bar{\alpha}$. The vertical lines on the points in Figure 4 indicate the limits of a $\pm 1.0\%$ error in $\bar{\alpha}$. The data fit a straight line to within the limits of $\pm 1.0\%$ accuracy, at least out to a value of $\bar{\alpha} = 0.6$ (*i.e.*, 60% reaction). The values in Table II can thus be confidently applied to runs with lesser extents of conversion. This is done in Figures 5 and 6 for runs at 810

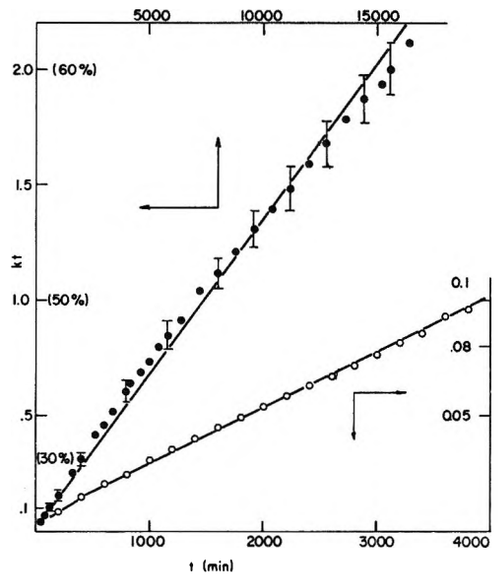

Figure 4. Plot of kt *vs.* t for two runs at 910°: ●, 706 torr of oxygen; O, 74 torr of oxygen. Vertical lines indicate ±1.0% error limits in per cent conversion. Units of k are μ^2/min.

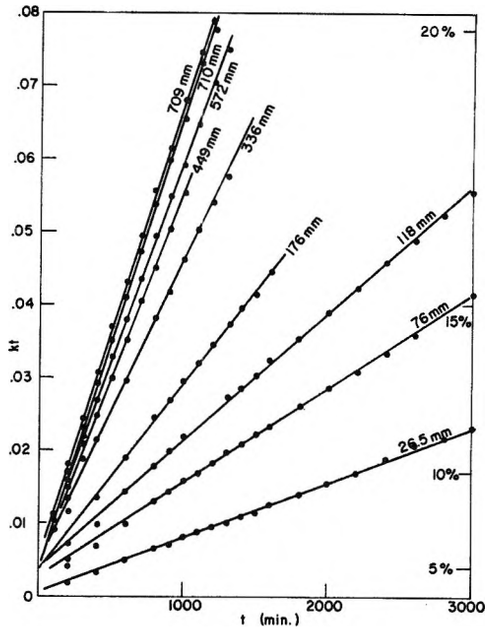

Figure 5. Plot of kt *vs.* t for runs with various ambient oxygen pressures at 810°. Units of k are μ^2/min.

and 715°. That the data fit the modified form of eq 2 shows that the reaction is indeed diffusion controlled.

The positive intercepts on the plots (Figures 4, 5, and 6) are probably due either to the surface roughness of the particles causing the reaction to proceed initially faster, or a not sufficiently small size interval at the smaller end of the size distribution, giving an apparently faster initial reaction. A calculation of the particle size from a BET surface area measurement (1.4 m^2/g) yields an apparent average diameter of only 2 μ.

The values of k obtained for various ambient oxygen pressures are summarized in Table III. Figure 7 is a plot of log k *vs.* log (P_{O_2}) where (P_{O_2}) is the ambient

Table III: Values of Calculated Rate Constant, k (μ^2/min), at Various Temperatures and Pressures

T = 715°		T = 810°		T = 910°[a]	
$k \times 10^6$	P_{O_2} torr	$k \times 10^6$	P_{O_2} torr	$k \times 10^6$	P_{O_2} torr
5.10	75	61.2	710	153	706
6.70	121	61.9	709	31.5	74
8.90	175	56.0	572		
13.8	300	49.8	449		
16.2	449	42.0	336		
21.0	703	25.7	176		
		17.6	118		
		12.9	76		
		7.0	26.5		

[a] The slopes used for the values at 910° are those up to 15% reaction, so as to be consistent with the slopes measured at 810 and 715°.

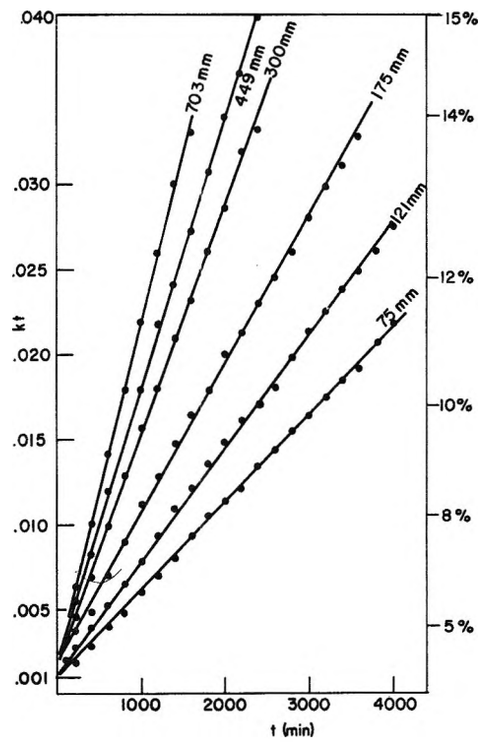

Figure 6. Plot of kt *vs.* t for runs with various ambient oxygen pressures at 715°. Units of k are μ^2/min.

oxygen pressure. The slopes of these plots give the oxygen pressure dependence of the diffusion process. For the runs at 715 and 810°: (a) the rate is directly

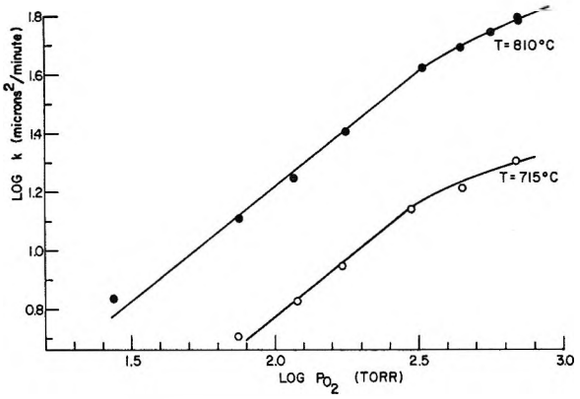

Figure 7. Plot of log k (Table III) *vs.* log P_{O_2} at 715 and 810°.

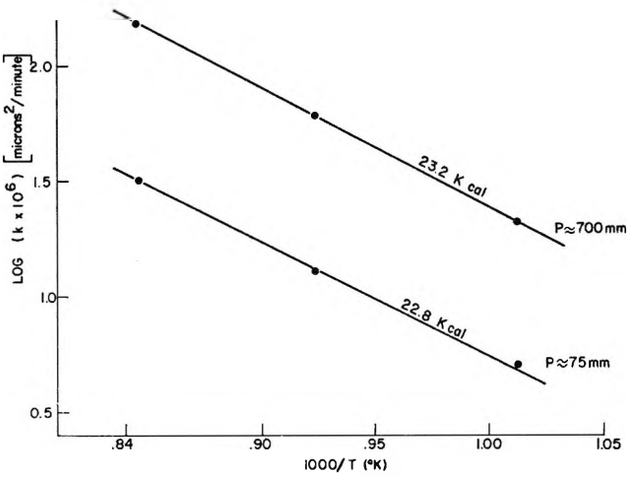

Figure 8. Arrhenius plot of k (Table III) measured at high pressure (~700 torr) and low pressure (~75 torr).

proportional to the oxygen pressure in the range 25 to 250 torr. A best fit to the points gives a power dependence between 0.80 and 0.90, however, rather than 1.00. (b) The rate dependence on pressure falls off in the range 250 to 710 torr.

Discussion

A pressure power dependence of 1.0 is expected when molecular oxygen is the diffusing species, and 0.5 when an oxygen atom or ion is the diffusing species. It is assumed here that molecular oxygen is the diffusing species, although it is possible that there is a contribution due to oxygen atoms which form when a chemisorbed oxygen molecule dissociates on the surface.

In Figure 8 are given Arrhenius plots of k for runs at high pressures (710 torr) and at low pressures (75 torr). The measured activation energies are (a) 23.1 ± 1.5 kcal for the 75-torr runs; (b) 23.2 ± 1.0 kcal for the 710-torr runs. Since the activation energies are essentially equal for the high- and the low-pressure region, the same species must be diffusing through the silica. If diffusion of a different species were to become rate controlling, the observed activation energies would depend on the ambient oxygen pressure. Therefore, when proceeding from low to high oxygen pressures, only the effective concentration gradient across the silica sheath changes. In the low-pressure region, the oxygen concentration gradient is determined principally by the ambient oxygen pressure; in the high-pressure region the outer part of the silica becomes saturated.

At the experimental temperatures used oxygen is not physically adsorbed on the silica surface. The diffusing oxygen molecules must, however, first adsorb on the surface and then dissolve in the silica. At sufficiently high pressures (in this case greater than about 250 torr) either the amount of oxygen chemisorbed on the surface approaches saturation, or the concentration of oxygen

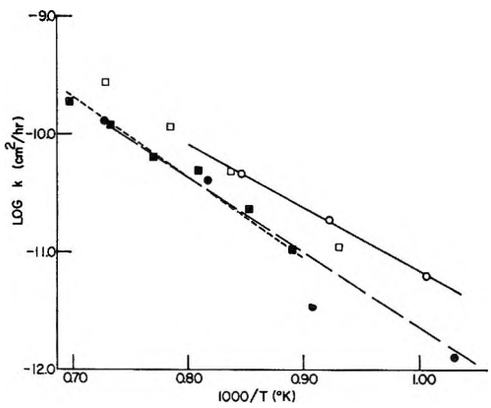

Figure 9. Comparisons of diffusion rate constants: O, this work in cristobalite; ●, Norton,[1] permeation in vitreous silica; ■, Williams,[3] isotopic oxygen exchange in fused silica; □, Deal and Grove,[5] silicon oxidation.

dissolved in the outer layer of silica is no longer directly proportional to ambient oxygen pressure. Since the solubility of oxygen in silica increases with increasing temperature,[1] it is obviously not behaving like a perfect gas going into solution. Hence, one would not expect Henry's law to be obeyed over a wide pressure range. Thus, the concentration gradient across the silica sheath tends to become independent of the ambient oxygen pressure. Saturation would only occur in the outermost layers, since oxygen is constantly diffusing inward to the reaction interface.

Due to equipment limitations it has not been possible to verify that the rate becomes completely oxygen independent at pressures higher than 1 atm.

It is of interest to compare the rate constants obtained here with the reported literature values for oxygen diffusion in fused silica. Motzfeldt[9] has converted

Norton's[1] permeation constants at 1 atm to rate constants in units of cm^2/hr. These are plotted in Figure 9, along with Williams'[3] diffusion constants measured by isotopic exchange and Deal and Grove's[4] parabolic rate constants of silicon oxidation in dry oxygen. In Figure 9 are also plotted the constants obtained here (converted to cm^2/hr and divided by a stoichiometric factor of 2) for the runs carried out in the vicinity of 1 atm.

The good agreement between the rate constants obtained here with the published oxygen diffusion constants confirms that the reaction is oxygen diffusion controlled and illustrates a method for obtaining the diffusion constants in a reactant mixture containing a wide spectrum of particle sizes.

Acknowledgment. The author wishes to thank Mrs. Janet Johnson for programming and generating the $\bar{\alpha}$ *vs.* kt table.

Gas-Phase Photolysis of Cyclohexane and Benzene in the Far-Ultraviolet Region

by Robert R. Hentz and Stefan J. Rzad

Department of Chemistry and the Radiation Laboratory,[1] University of Notre Dame, Notre Dame, Indiana 46556
(Received May 22, 1967)

The gas-phase photolyses (at 1–70 torr) of cyclohexane and of benzene were studied with the Xe and Kr resonance lamps. It is concluded that the primary quantum yield for cyclohexane conversion is unity over the range 1–70 torr. Four major primary dissociations of excited cyclohexane are proposed with products and approximate quantum yields as follows: (1) H_2 + c-C_6H_{10}*, ϕ(Xe) = 0.48, ϕ(Kr) = 0.27; (2) H + c-C_6H_{11}, ϕ(Xe) = 0.07, ϕ(Kr) = 0.09; (3) H_2 + X, ϕ(Xe) = 0.19, ϕ(Kr) = 0.21; (4) C_2H_4 + $\dot{C}H_2C_2H_4\dot{C}H_2$, ϕ(Xe) = 0.15, ϕ(Kr) = 0.43. Pressure dependence of the quantum yields of c-C_6H_{10}, C_2H_4, and 1,3-C_4H_6 confirms the secondary decomposition c-C_6H_{10}* → C_2H_4 + 1,3-C_4H_6 in competition with collisional deactivation. Essentially all H are assumed to form H_2 by abstraction from c-C_6H_{12}; such primary products as X, c-C_6H_{11}, and $\dot{C}H_2C_2H_4\dot{C}H_2$ are assumed to participate in "polymer" formation (observed as an intensity reducing deposit on the cell windows). In benzene photolysis with the Xe and Kr lamps, yields of simple decomposition products are higher than in photolysis at 1849 A; *e.g.*, ϕ(C_2H_2) is 0.083 and 0.067 at 1 torr of benzene with the Xe and Kr lamps, respectively, as compared to a reported value of ϕ(C_2H_2) = 0.013 in 1849-A photolysis of 0.08 torr of benzene. Polymer is a major photolysis product and, at equal pressures, $\phi(-C_6H_6)$ appears to be considerably larger than in 1849-A photolysis. In Xe-lamp photolysis, a suppression of quantum yields occurs with increase in pressure that is similar to that occurrent in 1849-A photolysis. In Kr-lamp photolysis, there is no effect on measured quantum yields of a change in benzene pressure from 1 to 66 torr; the implications of such a result are discussed. Presence of 3% NO in 1 torr of benzene reduces yields of polymer and certain other products but has no effect on yields of H_2, C_2H_2, and vinylacetylene.

Introduction

The behavior of yields in radiolysis of benzene–cyclohexane mixtures,[2] in both the liquid[3] and gas phases,[4] has been interpreted in terms of a "protective" effect[2] of benzene on the radiolysis of cyclohexane. In the liquid phase, evidence has been adduced for the conclusion that the predominant contribution to such a "protective" effect is nonchemical and attributable to an interaction between benzene and a precursor of the major decomposition modes of cyclohexane.[5] Although the evidence is less compelling, nonchemical interactions appear to contribute significantly to the "protective" effect in the gas phase as well.[4]

Burton recently has reviewed evidence for the conclusion that energy transfer in a cyclohexane system cannot involve excitation transfer from *single* excited (neutral) cyclohexane molecules,[6] owing to rapid decomposition of such excited molecules ($\tau \approx 10^{-13}$ sec). Such a conclusion has been implicit in the emphasis on ionic interpretations of sensitization[7] and "protective"

(1) The Radiation Laboratory of the University of Notre Dame is operated under contract with the U. S. Atomic Energy Commission. This is AEC Document No. COO-38-529.

(2) The work of J. P. Manion and M. Burton, *J. Phys. Chem.*, **56**, 560 (1952), is the prototype for many subsequent studies.

(3) The most recent study is that of J. F. Merklin and S. Lipsky, *ibid.*, **68**, 3297 (1964).

(4) J. M. Ramaradhya and G. R. Freeman, *Can. J. Chem.*, **39**, 1769 (1961); J. Blachford and P. J. Dyne, *ibid.*, **42**, 1165 (1964); L. M. Theard, *J. Phys. Chem.*, **69**, 3292 (1965).

(5) P. J. Dyne and W. M. Jenkinson, *Can. J. Chem.*, **39**, 2163 (1961); J. A. Stone and P. J. Dyne, *Radiation Res.*, **17**, 353 (1962).

(6) M. Burton, *Mol. Cryst.*, in press; the term "single excited molecules" is used to make a distinction from collective excitations which could be involved in the liquid.

(7) R. R. Hentz, D. B. Peterson, S. B. Srivastava, H. F. Barzynski, and M. Burton, *J. Phys. Chem.*, **70**, 2362 (1966).

effects in radiolysis of cyclohexane systems, both in the gas phase[4] and in liquids[8] (except perhaps at very high additive concentrations). In principle, it should be possible to assess the role of single excited cyclohexane molecules in the "protective" effect by study of the gas-phase photolysis of benzene–cyclohexane mixtures with both the Xe and Kr resonance lamps. The Xe resonance lamp provides lines of 1470 A (8.4 ev) and 1295 A (9.5 ev), the latter having an intensity 2% of that at 1470 A; the Kr lamp emits lines at 1236 A (10.0 ev) and 1165 A (10.6 ev), the latter with an intensity 28% of that at 1236 A.[9] Cyclohexane (ionization potential = 9.88 ev[10]) is not ionized by light of the Xe lamp, and benzene (ionization potential = 9.24 ev[10]) is ionized to a negligible extent. On the other hand, the Kr lamp should produce appreciable ionization in both benzene and cyclohexane. Thus, photolysis of the pure gases and their mixtures with the Xe lamp permits the study of processes peculiar to excitation alone; use of the Kr lamp should provide information on superimposed ionic processes. Motivated by such considerations, the present study of quantum yields in photolysis of benzene and of cyclohexane with the Xe and Kr resonance lamps was undertaken as a prelude to study of the mixtures.

Doepker and Ausloos[11] have reported a study of the photolysis of cyclohexane with Xe and Kr lamps. Emphasis was on elucidation of the decomposition modes; quantum yields were not determined. Photolysis of benzene with Kr and Xe lamps has not been reported.

Experimental Section

Materials. Cyclohexane, specified as 99.97% pure, was obtained from James Hinton. Such cyclohexane contained no significant impurities detectable by gas chromatography with a flame-ionization detector; therefore, it was used without further purification. The benzene used was Fisher Certified reagent; it was purified with an Aerograph Autoprep Model A-700 using a $^3/_8$ in. × 12 ft column which was packed with 20 wt % β,β'-oxydipropionitrile on 60–80 mesh Chromosorb W and operated at 70°. Benzene of purity better than 99.99 mole % was obtained. Nitric oxide, obtained from Matheson, was purified by low-temperature distillation. Matheson Research grade carbon dioxide, specified as better than 99.995 vol. % pure, was used for actinometry without further purification.

Light Sources and Photolysis Cells. The air-cooled electrodeless discharge lamps[9] were constructed from full-length inner 45/50 standard-taper joints with an upper tube of 4 cm o.d.; the lower tube was reduced to ~1.5 cm i.d., and, about 1.5 cm below the ground glass, a 2-mm LiF window (obtained from Harshaw Chemical Co.) was attached by means of a Pt–AgCl seal. The other end of the lamp was joined, about 10 cm above the ground glass, *via* a graded seal to a quartz finger which contained four channel-ring Ba–Al–Ni getters (size U-11) supplied by the Kemet Co.

Such lamps were evacuated to 10^{-6} torr for 48 hr at 350°. After flashing the getter, either 1 torr of 10% Xe in He or 0.3 torr of Kr[12] was introduced and the lamp was sealed. The discharge was initiated with a Tesla coil and sustained with a 2450-Mc sec^{-1}, 100-w Raytheon Model PGM10X1, which was operated at 60% of full power for the Xe lamp and 80% for the Kr lamp. Lamp spectra were checked with a 0.5-m Seya-Namioka monochromator and sodium salicylate detector.[9] Essentially only the resonance lines were detected below 2500 A in both kinds of lamp and with relative intensities in agreement with those reported by Okabe.[9] Emission purity of the lamps did not change over the period of the experiments.

Two different photolysis cells were used. For sample pressures of 1 and 10 torr, a 3-l. flask was equipped with an outer 45/50 standard-taper joint into which the lamps were fitted. The distance from lamp window to opposite cell wall was ~18 cm. A cold finger and a two-way stopcock were sealed to opposite sides of the 3-l. flask on a line normal to that of the light path. For photolyses at near 70 torr, the lamps were fitted into the outer 45/50 standard-taper joint of a 5-cm o.d. closed tube which was ~10 cm in length (exclusive of the joint); the cell volume was 190 ml, and the distance from lamp window to opposite wall was ~8 cm. This tube also was fitted with a cold finger and two-way stopcock.

Sample Preparation and Product Collection. Storage bulbs containing 20 ml of the pure benzene or cyclohexane were joined to the vacuum line *via* a Hoke bellows valve. The liquids were degassed by the microstill-reflux method.[13] In experiments at 1 torr, the gases were admitted to the desired pressure into a calibrated volume and then were condensed into the cold finger of the photolysis cell at 77°K. In experiments at higher pressures, the gases were admitted to the desired pressure directly into the photolysis cell. Pressures were measured at room temperature (~23°)

(8) See, *e.g.*, P. J. Dyne, *Can. J. Chem.*, **43**, 1080 (1965).

(9) H. Okabe, *J. Opt. Soc. Am.*, **54**, 478 (1964).

(10) K. Watanabe, *J. Chem. Phys.*, **26**, 542 (1957).

(11) R. D. Doepker and P. Ausloos, *ibid.*, **42**, 3746 (1965).

(12) J. J. Sparapany, *Appl. Opt.*, **4**, 303 (1965).

(13) W. Van Dusen, Jr., and W. H. Hamill, *J. Am. Chem. Soc.*, **84**, 3648 (1962).

with a Bourdon-tube gauge obtained from Wallace and Tiernan, Inc. All photolyses were at room temperature.

After photolysis, the cell was opened to a series of three traps at 77°K, and noncondensable gases were removed and measured with a standard Toepler pump and gas buret arrangement. The gases then were transferred into a sample bulb for analysis. To facilitate transfer of less volatile products from the cell into the traps at 77°K, the cell and tubing to the first trap were warmed with a hand torch after removal of the gases noncondensable at 77°K. The photolysis cell then was closed, ethyl bromide mush (−118°) was placed on the traps, and a second fraction of volatile products was collected for measurement and analysis. Measurement of this fraction was made in a calibrated volume on the mass spectrometer with a Consolidated membrane micromanometer. After removal of the two volatile fractions, the condensable fraction was transferred into a capillary at 77°K. During this procedure, the traps and connecting tubes were warmed with a hand torch. After 1 hr, the capillary was sealed off.

Analyses. The two volatile fractions (noncondensable at −196 and at −118°) were analyzed on a Consolidated 21-103A mass spectrometer. Identifications and determinations were made by comparison with fragmentation patterns of known amounts of the pure substances.

The condensable fraction was analyzed by gas chromatography. Cyclohexene and the cyclohexadienes were determined on an F & M Model 609 with a flame-ionization detector. Cyclohexadienes were analyzed with a 0.25 in. × 10 ft column packed with 20 wt % of succinate polyester of diethylene glycol on 60–80 mesh Chromosorb P and operated at 60°; cyclohexene was separated with a 0.25 in. × 20 ft column packed with 17 wt % β,β′-oxydipropionitrile on 60–80 mesh Chromosorb P and operated at room temperature. Biphenyl, dihydrobiphenyls, and bicyclohexyl were analyzed on an F & M Model 810 with a flame-ionization detector; the 0.25 in. × 4 ft column was packed with 9 wt % silicone grease on 60–80 mesh Chromosorb P and operated at 165°.

Actinometry. Quantum yields were determined with CO_2 as the actinometer for which $\phi(CO) = 1.0$ was assumed.[14] In the 3-l. cell, 15 torr of CO_2 was used for actinometry with the Xe lamp and 70 torr was used with the Kr lamp; in the 190 ml cell, 70 torr of CO_2 was used with both lamps. For the Xe lamp, an intensity of $7.1 \pm 0.5 \times 10^{15}$ quanta sec^{-1} was determined as the average of 25 measurements with both cells; no change in intensity of the Xe lamp occurred over the period of the experiments. Intensity of the Kr lamp decreased with time; *e.g.*, in one series of experiments the intensity decreased from 3.1×10^{15} to 2.1×10^{15} quanta sec^{-1} over a 23-hr period of operation. Because the maximum photolysis time was only 5 min, no appreciable change in lamp intensity occurred during an experiment. For most experiments the Kr-lamp intensity was near $1.5 \pm 0.1 \times 10^{15}$ quanta sec^{-1}.

The extinction coefficients of Table I permit an estimation of the fraction of light absorbed in the distance from lamp window to opposite cell wall. Such calculations indicate essentially complete light absorption (>99%) within the cells in all experiments except the Kr-lamp actinometry at 70 torr of CO_2 in the 190-ml cell. In the latter case, 92% absorption is calculated for the 8-cm path length. No significant difference was detected between intensities of the Kr lamp measured in the 3-l. and 190-ml cells; thus, any incompleteness of absorption in Kr-lamp actinometry with the 190-ml cell lies within the experimental deviation (∼±10%) of the intensity measurements.

Table I: Decadic Extinction Coefficients

λ, A	ε, atm^{-1} cm^{-1} (at 25°)		
	c-C_6H_{12}[a]	C_6H_6[a]	CO_2[b]
1550	208	151	...
1470	...	...	7.8
1467	408	159	...
1348	408	286	...
1236	...	...	1.5
1206	715	306	...

[a] The values for *c*-C_6H_{12} and C_6H_6 were obtained by S. Lipsky with an Ar lamp and were privately communicated. [b] *Cf.* ref 14.

Photolysis of all hydrocarbon samples produced a deposit on the cell windows which reduced the intensity being absorbed in the sample during the course of an experiment. To provide data requisite for calculation of quanta absorbed by the sample, each photolysis experiment was comprised of the following sequence of steps: (1) photolysis of CO_2, (2) photolysis of the sample, (3) photolysis of CO_2, (4) photolysis of ∼700 torr of O_2 for 30 min. The last step removed the deposit from the windows and restored the intensity transmitted into the cell to its original value.[15]

Results

Polymer Formation and Estimation of Absorbed

(14) B. H. Mahan, *J. Chem. Phys.*, **33**, 959 (1960), gives $\phi(CO) = 1.1 \pm 0.1$ at 1470 A and $\phi(CO) = 1.2 \pm 0.1$ at 1236 A; both values are stated to be upper limits.

(15) *Cf.*, A. G. Leiga and H. A. Taylor, *ibid.*, **41**, 1247 (1964).

Quanta. The fractional reduction in measured intensity as a consequence of 5-min photolyses is shown in Table II for a variety of experimental conditions. Such values provide a crude relative measure of the yield of nonvolatile material or "polymer." Not surprisingly, polymer formation is greater in benzene than in cyclohexane (assuming comparable values of ϵ for the two kinds of polymer); however, appreciable polymer formation in photolysis of cyclohexane is evident, particularly in photolyses with the Kr lamp and in the small cell at 70 torr with the Xe lamp. Reduced polymer formation from benzene in the presence of NO suggests the participation of free radicals in formation of the benzene polymer.

Table II: Values of I/I_0[a] for 5-Min Photolyses

Lamp	P, torr	I/I_0 c-C_6H_{12}	I/I_0 C_6H_6	I/I_0 C_6H_6 + 3% NO
Xe	1	0.95	0.30	0.65
Xe	10	0.89	0.15	...
Xe	70	0.65	0.15	...
Kr	1	0.62	0.30	0.54
Kr	10	0.50	0.30	...
Kr	70	0.45	0.30	...

[a] Ratio of intensity measured after photolysis to that measured initially.

Quantum yields were estimated by the use of curves (for each set of experimental conditions) such as that in Figure 1, where I represents the intensity measured by CO_2 actinometry after photolysis of a sample for a given time and I_0 is the initial intensity. The number of absorbed quanta was obtained as the product of I_0 and the area under such a curve for the photolysis time used.

An upper limit for per cent conversion can be estimated by use of the initial intensity and the assumption that $\phi = 1$ for consumption of the hydrocarbon. With the Xe lamp, per cent conversions so calculated for a 5-min photolysis are 2, 0.2, and 0.4% at 1, 10, and 70 torr, respectively. Corresponding values for the Kr lamp are 0.5, 0.05, and 0.1% at 1, 10, and 70 torr, respectively.

Cyclohexane. Hydrogen quantum yields are independent of pressure from 1 to 70 torr in photolysis of cyclohexane with either the Xe or Kr lamp. Over this pressure range, $\phi(H_2) = 0.74 \pm 0.02$ with the Xe lamp and $\phi(H_2) = 0.57 \pm 0.03$ with the Kr lamp. The yields of other major products are pressure dependent as shown in Table III. Quantum yields at each pressure represent the average of two to four determinations.

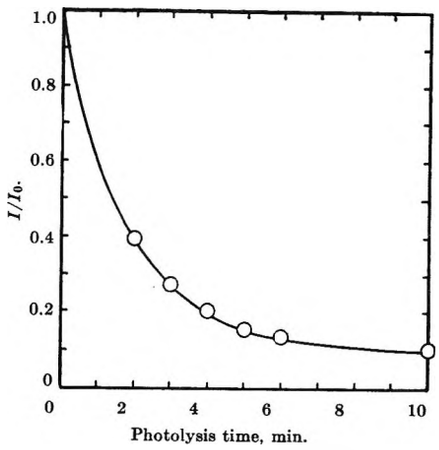

Figure 1. Actinometry curve for the photolysis of 66 torr of benzene with the Xe resonance lamp.

An increase in photolysis time from 2 to 5 min did not affect the quantum yields of the major products. Thus, any photolysis of polymer on the cell windows does not seem to affect appreciably the measured product yields.

Table III: Pressure Dependence of Quantum Yields in the Photolysis of Cyclohexane

P, torr	ϕ[a] c-C_6H_{10}	C_2H_4	1,3-C_4H_6	C_3H_6
		Xe Lamp		
1	0.27	0.38	0.18	0.04
10	0.39	0.24	0.08	0.03
70	0.49	0.10	0.02	0.02
		Kr Lamp		
1	0.11	0.60	0.16	0.10
10	0.17	0.53	0.09	0.07
70	0.19	0.48	0.08	0.06

[a] Average deviation is $\sim\pm0.01$ for $\phi \leqq 0.1$ and ±0.02–0.03 for $\phi > 0.1$.

Minor products included CH_4, C_2H_6, C_3H_8, and C_4H_8 with individual values of $\phi < 0.1$ and, at 1 torr, a summed value of $\phi = 0.07$ with the Xe lamp and of $\phi = 0.17$ with the Kr lamp. Addition of 4% NO to 1 torr of cyclohexane reduced the yields of such minor products but had no significant effect on yields of the major products, except for a small increase in ϕ(1,3-C_4H_6).

Benzene. The quantum yields of products that were identified in benzene photolysis are presented in Table IV. Each value is the average of at least two measurements. These were the only products detected in significant yield other than the polymer. Characteristically, the quantum yields of such decomposition products are low. Increase in pressure considerably

Table IV: Quantum Yields[a] in the Photolysis of Benzene

	Xe lamp		Kr lamp
	1 torr	66 torr	1 torr
$\phi(H_2)$	0.03	0.015	0.04
$\phi(C_2H_2)$	0.083	0.006	0.067
$\phi(C_2H_4)$	0.069	0.009	0.037
$\phi(C_3H_4)$[b]	0.042	0.005	0.037
$\phi(C_4H_4)$[c]	0.046	0.02	0.019
$\phi(c\text{-}C_6H_8)$[d]	0.024	0.016	0.016
$\phi(C_6H_5C_6H_5)$	0.023	0.010	0.012
$\phi(C_6H_5C_6H_7)$[e]	0.039	0.005	0.008

[a] Average deviation is $\sim\pm0.005$ for values given to the second decimal place and ±0.001–0.004 for values given to the third decimal place. [b] Propadiene. [c] Vinylacetylene. [d] Cyclohexadienes. [e] Dihydrobiphenyls.

depressed all quantum yields in the Xe-lamp photolyses (*cf.*, Table IV); surprisingly, however, quantum yields obtained in Kr-lamp photolyses at 66 torr were within experimental error of those given in Table IV for 1 torr, except for an increase in $\phi(C_4H_4)$ to ~0.04 and a small decrease in yields of cyclohexadienes and dihydrobiphenyls. Again, measured quantum yields were constant for photolysis times of 3–10 min, which indicates no appreciable effect owing to photolysis of the cell-window deposit.

In photolysis with either lamp, the presence of 3% NO in 1 torr of benzene almost completely eliminated C_3H_4, $c\text{-}C_6H_8$, $(C_6H_5)_2$, and $C_6H_5C_6H_7$. The other product yields were essentially unaffected by the presence of 3% NO, except for a significant decrease in $\phi(C_2H_4)$ with the Xe lamp.

Discussion

Cyclohexane. Certain results of this study are qualitatively in accord with those of Doepker and Ausloos[11] and support their conclusion with regard to an effect of pressure on one of the major decomposition modes. However, there are some significant differences between results of the two studies; in addition, measurement of quantum yields and observation of significant polymer formation reveal aspects of the decomposition not evident in the earlier study.

Doepker and Ausloos[11] have suggested that the major primary decomposition mode of excited cyclohexane is reaction 1, in which the H_2 is eliminated predominantly

$$c\text{-}C_6H_{12}^* \longrightarrow c\text{-}C_6H_{10}^* + H_2 \qquad (1)$$

from a single carbon atom; the resultant carbene, it is suggested, rearranges to a vibrationally or electronically excited cyclohexene, $c\text{-}C_6H_{10}^*$, which is collisionally deactivated or decomposes as in reactions 1a and 1b, respectively. The results shown in Table III are in

$$c\text{-}C_6H_{10}^* + M \longrightarrow c\text{-}C_6H_{10} + M \qquad (1a)$$

$$c\text{-}C_6H_{10}^* \longrightarrow 1,3\text{-}C_4H_6 + C_2H_4 \qquad (1b)$$

accord with the assignment of a significant role to reaction sequence 1. With either lamp, increase in pressure results in an increase in the yield of $c\text{-}C_6H_{10}$ and a complementary decrease in the yields of C_2H_4 and 1,3-C_4H_6. Also in agreement with Doepker and Ausloos,[11] the ratio $\phi(1,3\text{-}C_4H_6):\phi(c\text{-}C_6H_{10})$ is smaller in Xe-lamp photolyses (*cf.*, Table III) and more sensitive to pressure. However, we find that Δ of eq I is not zero.

$$\Delta = \phi(H_2) - \phi(c\text{-}C_6H_{10}) - \phi(1,3\text{-}C_4H_6) \qquad (I)$$

Rather, $\Delta = 0.26$ and 0.30 for the Xe and Kr lamps, respectively.

A portion of the discrepancy, Δ, can be accounted for in terms of reaction sequence 2

$$c\text{-}C_6H_{12}^* \longrightarrow H + c\text{-}C_6H_{11} \qquad (2)$$

$$H + c\text{-}C_6H_{12} \longrightarrow H_2 + c\text{-}C_6H_{11} \qquad (2a)$$

Doepker and Ausloos[11] studied the photolysis of a 1:1 mixture of $c\text{-}C_6H_{12}$ and $c\text{-}C_6D_{12}$ at 10 torr; the HD yield was essentially the same percentage of total hydrogen in the presence of 5% NO as in its absence and amounted to ~5 and $\sim8\%$ with the Xe and Kr lamps, respectively. We find that 4% NO in 1 torr of $c\text{-}C_6H_{12}$ has no effect on $\phi(H_2)$. Several authors[16–18] report that NO catalyzes H atom combination with no NO consumption.[18] However, even were NO merely to catalyze H atom combination, some reduction in $\phi(H_2)$ and percentage HD should have occurred if a reaction of H with NO competes with reaction 2a. Thus, absence of an effect of NO on $\phi(H_2)$ and percentage HD implies either (1) that all hydrogen, including HD in $c\text{-}C_6D_{12}$–$c\text{-}C_6H_{12}$ mixtures, is formed by a molecular elimination process or (2) that NO scavenges a negligible fraction of the H atoms produced in reaction 2.

In photolysis of 1:1 mixtures of $c\text{-}C_6H_{12}$ and $c\text{-}C_6D_{12}$, formation of 5–8% of total hydrogen as HD cannot be attributed to elimination of molecular hydrogen in a collision of $c\text{-}C_6H_{12}^*$ (or $c\text{-}C_6D_{12}^*$) with $c\text{-}C_6D_{12}$ (or $c\text{-}C_6H_{12}$); such an interpretation requires that excited cyclohexane have a lifetime of at least $\sim10^{-9}$ sec, which is not plausible.[6] Reaction sequence 2 may involve "hot" H atoms; however, it is also probable that 4–5% NO does not compete effectively with reaction 2a for

(16) R. Simonaitis, *J. Phys. Chem.*, **67**, 2227 (1963).

(17) M. A. A. Clyne and B. A. Thrush, *Discussions Faraday Soc.*, **33**, 139 (1962).

(18) M. A. A. Clyne and B. A. Thrush, *Trans. Faraday Soc.*, **57**, 1305 (1961).

thermal H atoms in the photolyses at 1–10 torr. With the extreme assumption of a reaction volume of only 1 ml at 1 torr (or 0.1 ml at 10 torr) in Xe-lamp photolyses, reaction 2a with $k_{2a} = 10^6\ M^{-1}\ \text{sec}^{-1}$ is ~500 times faster than termolecular H atom combination with $k = 10^{10}\ M^{-2}\ \text{sec}^{-1}$ (for H_2 as third body[19]). Thus, termolecular scavenging by NO with $k \approx 10^{10}\ M^{-2}\ \text{sec}^{-1}$ (again for H_2 as third body[16-18]) must compete with reaction 2a for H atoms; a straightforward calculation gives 20% of H being scavenged at 10 torr and 5% NO. Considering uncertainties in the k's and that H atoms scavenged by NO are combined into half as much H_2, absence of an observable effect of NO on $\phi(H_2)$ and percentage HD does not preclude attribution of the HD yield and an equivalent yield of $H_2 + D_2$ to reaction sequence 2.

The minimum percentage of $\phi(H_2)$ attributable to reaction sequence 2 is obtained with the assumption of no isotope effect in primary process 2. In such case, the values[11] of 5 and 8% HD give 10 and 16% of total hydrogen *via* reaction sequence 2 with the Xe and Kr lamps, respectively;[20] by subtraction of such a contribution of reaction sequence 2, the discrepancy of eq I is reduced to 0.19 for the Xe lamp and 0.21 for the Kr lamp. Consequently, our results require a third primary process

$$c\text{-}C_6H_{12}^* \longrightarrow H_2 + X \qquad (3)$$

in which molecular hydrogen and products other than C_2H_4, c-C_6H_{10}, and 1,3-C_4H_6 are formed; $\phi_3 \approx 0.2$ for both lamps. It is important to note that the foregoing considerations are but little affected even if all H atoms form H_2 by combination on the walls.[21] In such a case, no inhibition by NO would be observed. Assuming no difference in isotope effect for combination catalyzed by the walls or by NO, the percentage of total hydrogen from reaction 2, and therefore ϕ_3, would be unaltered; however, ϕ_2 would be twice the value given by reaction sequence 2, *i.e.*, 0.14 for the Xe lamp and 0.18 for the Kr lamp.

At 1 torr, the collisional deactivation of as little as 1% of c-$C_6H_{12}^*$ would require a c-$C_6H_{12}^*$ lifetime of at least $\sim 10^{-9}$ sec; the available evidence[6] seems to require that the primary quantum yield for cyclohexane conversion, $\phi_0(-c\text{-}C_6H_{12})$, be unity. Because our quantum yields are presumably upper limits,[14] another primary process that does not yield hydrogen is indicated. Doepker and Ausloos[11] have suggested primary process 4, which is followed by rapid decomposition of the

$$c\text{-}C_6H_{12}^* \longrightarrow C_2H_4 + \dot{C}H_2C_2H_4\dot{C}H_2 \qquad (4)$$

diradical into two molecules of ethylene. Evidence cited for instability of the diradical is failure of NO to affect the ratio H_2:C_2H_4 and the absence of C_4H_8 and c-C_4H_8 as products in the presence of NO. However, such observations may be interpreted equally well as evidence for a stable diradical which is scavenged by NO or contributes to polymer formation in the absence of NO. Further, the results of Table III are made compatible with the requirement $\phi_0(-C_6H_{12}) = 1$ by the assumption that $\phi_4 = \phi(C_2H_4) - \phi(1,3\text{-}C_4H_6)$. In photolyses with the Kr lamp (*cf.* Table III), $\phi(C_2H_4) - \phi(1,3\text{-}C_4H_6)$ is independent of pressure and has an average value of 0.43; the latter value added to $\phi(H_2) = 0.57$ gives $\phi_0(-C_6H_{12}) = 1$. With the Xe lamp, it seems likely that $\phi(1,3\text{-}C_4H_6)$ at 1 torr is somewhat low owing to some H atom and radical scavenging at the higher conversion used at this pressure. An observed increase in $\phi(1,3\text{-}C_4H_6)$ to 0.23 on addition of 4% NO at 1 torr of cyclohexane is consistent with such an argument. Addition of the average value of $\phi(C_2H_4) - \phi(1,3\text{-}C_4H_6) = 0.15$ to $\phi(H_2) = 0.74$ gives $\phi_0(-C_6H_{12}) = 0.89$. Agreement with $\phi_0(-C_6H_{12}) = 1$ is satisfactory in view of the presence of minor products and uncertainties in the actinometry and measurement of yields.

Additional support for a primary process such as (4) (that presumably contributes to polymer formation) is provided by the results shown in Table II. That appreciable polymer is formed in cyclohexane photolyses is especially evident in photolyses at 70 torr in the 190-ml cell (*i.e.*, under conditions most favorable to deposition on the cell window). Furthermore, intensity reduction is always greater with the Kr lamp in accord with $\phi_4 = 0.43$ for that lamp as compared to $\phi_4 = 0.15$ for the Xe lamp. It is also noteworthy that the shorter wavelengths of the Kr lamp favor C_2H_4 and polymer formation (or primary process 4) relative to hydrogen formation (*cf.* ref 11).

In summary, the major primary processes proposed for cyclohexane photolysis and their approximate quantum yields are

$$c\text{-}C_6H_{12}^* \longrightarrow H_2 + c\text{-}C_6H_{10}^*$$

$$\phi_1(\text{Xe}) = 0.48,\ \phi_1(\text{Kr}) = 0.27$$

$$c\text{-}C_6H_{12}^* \longrightarrow H + c\text{-}C_6H_{11}$$

$$\phi_2(\text{Xe}) = 0.07,\ \phi_2(\text{Kr}) = 0.09$$

(19) C. B. Kretschmer and H. L. Peterson, *J. Chem. Phys.*, **39**, 1772 (1963); T. C. Marshall, *Phys. Fluids*, **5**, 743 (1962).

(20) With the Xe lamp (5% HD), assumption of equal isotope effects in primary processes 1 and 2 gives ~11% as the contribution of primary process 2; assumption of no isotope effect in primary process 1 gives ~23% as the contribution of primary process 2.

(21) A rough estimate of the probability of H combination on the walls (in competition with reaction 2a) indicates that only combination on the windows need be considered; thus, the contribution of such a reaction to conversion of H into H_2 is necessarily less than 50% and is probably negligible.

$c\text{-}C_6H_{12}^* \longrightarrow H_2 + X \quad \phi_3(Xe) = 0.19, \phi_3(Kr) = 0.21$

$c\text{-}C_6H_{12}^* \longrightarrow C_2H_4 + \dot{C}H_2C_2H_4\dot{C}H_2 \quad \phi_4(Xe) = 0.15, \phi_4(Kr) = 0.43$

It is concluded that $\phi_0(-C_6H_{12}) = 1$.

Benzene. The photolysis of benzene[22-26] at wavelengths greater than ~1800 A is quite complex. Little or no measurable yields of simple decomposition products are obtained.[22,24,25] The isomers benzvalene and fulvene have been detected in photolysis of the liquid at 2537 A.[23] Photolysis of the vapor at 1849 A yields the ubiquitous polymeric material and a benzene isomer,[24,25] recently identified as fulvene.[26] At 1849 A, $\phi(-C_6H_6)$ shows a marked pressure dependence; thus, $\phi(-C_6H_6) \approx 1$[25] at ~0.09 torr of benzene and falls to 0.25[24] at 1 torr and 0.10[24] at 3 torr.

Photolysis with the Xe lamp exhibits certain features of the 1849-A photolysis. As might be expected, however, yields of simple decomposition products are higher and $\phi(-C_6H_6)$ is greater at corresponding pressures. The yields in Table IV can be used for estimation of a lower limit to $\phi(-C_6H_6)$ based on total hydrogen accounted for among the measured products. At 1 torr, values obtained with the Xe and Kr lamps are $\phi(-C_6H_6) \geqq 0.29 \pm 0.03$ and $\phi(-C_6H_6) \geqq 0.16 \pm 0.03$, respectively. Such values are to be compared with the value of $\phi(-C_6H_6) = 0.25$ obtained by measurement of benzene disappearance in 1849-A photolysis at 1 torr;[24] because Shindo and Lipsky[24] were unable to detect significant yields of decomposition products such as those in Table IV, the value $\phi(-C_6H_6) = 0.25$ at 1849 A largely represents conversion to polymer and benzene isomers. Although benzene isomers were not sought in this work, appreciable polymer formation is evident in the data of Table II. Thus, it is clear the Xe-lamp photolysis yields greater benzene conversion than does 1849-A photolysis at corresponding pressures. Such conclusions are additionally supported by comparison of the values for $\phi(C_2H_2)$ in Table IV with $\phi(C_2H_2) \approx 0.013$ obtained at 1849 A and ~0.08 torr by Foote, *et al.*[25]

The suppression of quantum yields with increase in pressure in Xe-lamp photolyses (*cf.* Table IV) is similar, though perhaps less pronounced, to that observed at 1849 A.[24,25,27] A mechanism such as that suggested by Shindo and Lipsky,[24] seems to be required. The initially excited state is assumed to convert internally with essentially 100% efficiency to a longer lived, energy-rich state that does not radiate and does not yield the lowest excited singlet or triplet state on collisional deactivation (see ref 24 for a summary of the pertinent evidence). Thus, loss of energy by collisional deactivation of the energy-rich benzene molecule competes with isomerization and decomposition. The greater decomposition and conversion yields obtained, relative to 1849-A photolysis, with the shorter wavelengths of the Xe lamp also are consistent with such a view.

The absence of an effect of pressure, from 1 to 66 torr, on the quantum yields measured in Kr-lamp photolysis is striking. In Kr-lamp photolysis, there are three possible processes whereby excitation of a benzene molecule may lead to its chemical conversion: (1) rapid decomposition of the excited state in competition with ionization,[28] (2) reaction of $C_6H_6^+$ with C_6H_6,[29,30] and (3) decomposition of $C_6H_6^+$ on neutralization.[31] The reaction modes and relative yields of the three processes, whose total quantum yield is denoted by ϕ_0, must be independent of pressure from 1 to 66 torr. The value of $1 - \phi_i \approx 0.4$[28] gives a lower limit for ϕ_0. Because of the probable importance of ion–molecule reactions and because capture of an electron by $C_6H_6^+$ in the gas phase may result in immediate decomposition,[32] it appears probable that $\phi_0 = 1$.

In view of the obvious complexity of benzene photolysis with Xe and Kr lamps and because the measured decomposition products of Table IV may represent minor products and in some cases are secondary products, presentation of a detailed mechanism for formation of individual products is not warranted at this

(22) W. A. Noyes, Jr., and D. A. Harter, *J. Chem. Phys.*, **46**, 674 (1967); W. A. Noyes, Jr., W. A. Mulac, and D. A. Harter, *ibid.*, **44**, 2100 (1966).

(23) K. E. Wilzbach, J. S. Ritscher, and L. Kaplan, *J. Am. Chem. Soc.*, **89**, 1031 (1967).

(24) K. Shindo and S. Lipsky, *J. Chem. Phys.*, **45**, 2292 (1966).

(25) J. K. Foote, M. H. Mallon, and J. N. Pitts, Jr., *J. Am. Chem. Soc.*, **88**, 3698 (1966).

(26) H. R. Ward, J. S. Wishnok, and P. D. Sherman, Jr., *ibid.*, **89**, 162 (1967); L. Kaplan and K. E. Wilzbach, *ibid.*, **89**, 1030 (1967).

(27) Note, however, that F. Mellows and S. Lipsky, *J. Phys. Chem.*, **70**, 4076 (1966), report values of $\phi(H_2) = 2.5 \pm 0.5 \times 10^{-3}$ and $\phi(H) = 0.01$–0.02 in photolysis at 1849 A that are independent of pressure.

(28) Evidence for such a process is provided by the observation of an isotope effect in the photoionization efficiency of benzene, $\phi_i(C_6D_6)/\phi_i(C_6H_6) = 1.07$, and by the benzene photoionization efficiencies of $\phi_i = 0.60$ at 10.0 ev and $\phi_i = 0.50$ at 10.6 ev; *cf.*, J. C. Person, *J. Chem. Phys.*, **43**, 2553 (1965).

(29) The little information available on ion–molecule reactions in benzene indicates considerable complexity; *cf.*, R. Barker, *Chem. Ind.* (London), 233 (1960), and A. Henglein, *Z. Naturforsch.*, **17a**, 44 (1962).

(30) Fragmentation of $C_6H_6^+$ is not significant at 10.0 or 10.6 ev; *cf.*, A. Terenin and F. Vilessov, *Advan. Photochem.*, **2**, 385 (1964).

(31) Because at least 10^3–10^4 collisions of $C_6H_6^+$ with C_6H_6 occur in an ion–electron combination lifetime, neutralization of $C_6H_6^+$ may be precluded by its ion–molecule reactions.

(32) From theoretical considerations, J. L. Magee and M. Burton, *J. Am. Chem. Soc.*, **72**, 1965 (1950), concluded that capture of an electron by an isolated complicated molecule ion appears to lead in most cases to immediate decomposition.

stage. It is sufficient to note that such products as C_3H_4, c-C_6H_8, $(C_6H_5)_2$, $C_6H_5C_6H_7$, and polymer (whose yields are appreciably affected by addition of 3% NO) are formed largely *via* free-radical precursors; free radicals also seem to contribute to C_2H_4 formation in photolysis with the Xe lamp. The other measured products are formed wholly by molecular elimination. Because of the efficiency of benzene as an H atom scavenger, $k = 5 \times 10^7\ M^{-1}\ \text{sec}^{-1}$ in the gas phase,[33] the hydrogen yield would be expected to be molecular, as in photolysis at 1849 A,[27] and not scavengeable by 3% NO (see the discussion of H atom reactions in the section on cyclohexane). The yields of c-C_6H_8, $(C_6H_5)_2$, and $C_6H_5C_6H_7$ (*cf.*, Table IV) suggest a contribution of the primary process $C_6H_6^* \rightarrow C_6H_5 + H$, followed by rapid addition of C_6H_5 and H to benzene and subsequent disproportionation reactions of the secondary radicals. The quantum yield of such a primary process appears to be of the same order as that of other decomposition processes in photolyses with the Xe and Kr lamps, and somewhat larger than at 1849 A[27] (perhaps by a factor of ~5 with the Xe lamp at 1 torr).

(33) M. C. Sauer, Jr., private communication. K. Yang, *J. Am. Chem. Soc.*, 84, 3795 (1962), gives $k = 2 \times 10^7\ M^{-1}\ \text{sec}^{-1}$.

Heats of Mixing of Nonelectrolyte Solutions.

IV. Mixtures of Fluorinated Benzenes[1]

by David V. Fenby and Robert L. Scott

Contribution No. 2094 from the Department of Chemistry, University of California, Los Angeles, California 90024 *(Received May 19, 1967)*

The heats of mixing of 34 of the 78 possible binary systems $C_6H_m F_{6-m} + C_6H_nF_{6-n}$ have been measured; in addition the systems *n*-propylbenzene + hexafluorobenzene, *n*-butylbenzene + pentafluorobenzene, and *n*-butylbenzene + hexafluorobenzene were studied. The great variety of results is striking; not only are some of these heats of mixing positive in sign and some negative, but nine systems show changes of sign at intermediate compositions. These heats of mixing are interpreted as the sums of several contributions, "physical" (positive) and "chemical" (negative).

Introduction

Solutions in which one of the components is an aliphatic or alicyclic fluorocarbon have been extensively investigated.[2] Many of these solutions show very much larger positive deviations from ideality than those predicted from solubility parameter theory,[3] while others conform quite well to the theory.[2] Here we report some extensive studies on parallel aromatic systems.

Benzene and hexafluorobenzene form a solid 1:1 molecular complex[4,5] generally accepted as being due to charge-transfer interactions, although there is as yet no direct evidence for this. Recently, we reported[6] the

(1) This work was supported by the U. S. Atomic Energy Commission, the National Science Foundation, and Allied Chemical Corporation. It is based on part of a dissertation by D. V. Fenby for the Ph.D. degree, University of California, Los Angeles, Calif., 1967.

(2) R. L. Scott, *J. Phys. Chem.*, 62, 136 (1958).

(3) J. H. Hildebrand and R. L. Scott, "Regular Solutions," Prentice-Hall, Inc., Englewood Cliffs, N. J., 1962.

(4) C. R. Patrick and G. S. Prosser, *Nature*, 187, 1021 (1960).

(5) W. A. Duncan and F. L. Swinton, *Trans. Faraday Soc.*, 62, 1082 (1966).

Table I: Materials Used

Material	Source, grade	Purity/ mole %	Principal impurities
Benzene	*a*, Spectroquality	~99.95	
Fluorobenzene	*a*, White Label	>99.9	
o-Difluorobenzene (1,2-Difluorobenzene)	*b*	>99.5	C_6H_5F
m-Difluorobenzene (1,3-Difluorobenzene)	*b*	>99.8	*o*-C_6H_4F
p-Difluorobenzene (1,4-Difluorobenzene)	*b*	>99.8	
1,3,5-Trifluorobenzene	*c*	~99.7	C_6HF_5, 1,2,3,5-$C_6H_2F_4$
1,2,3,4-Tetrafluorobenzene	*b*	96–98	1,2,4,5-$C_6H_2F_4$
1,2,3,5-Tetrafluorobenzene	*b*	98–99	1,2,4,5-$C_6H_2F_4$
1,2,4,5-Tetrafluorobenzene	*b*	98–98.5	1,2,3,4-$C_6H_2F_4$
Pentafluorobenzene	*c*	>98.5	1,2,3,5-$C_6H_2F_4$
Hexafluorobenzene	*b*	~99	C_6HF_5 and/or C_6H_6
	c, Anaesthetic	>99.9	
n-Propylbenzene	*d*, Eastman, White Label	...	
n-Butylbenzene	*e*, Research	~99.9	

[a] Matheson Coleman and Bell. [b] Pierce Chemical Co. [c] Imperial Smelting Corp. Ltd. [d] Eastman Organic Chemicals. [e] Phillips Petroleum Co.

molar heats of mixing (*i.e.*, the molar excess enthalpies, $\tilde{H}^E$) of benzene with hexafluorobenzene, pentafluorobenzene, and 1,2,4,5-tetrafluorobenzene; the surprising differences between these systems (see Figure 1 in ref 6) have led us to a systematic examination of the heats of mixing of other fluorinated benzenes. There are a total of 13 compounds of the type $C_6H_nF_{6-n}$ which together form 78 possible binary systems. We have now measured 34 of these and, in addition, the systems *n*-propylbenzene + hexafluorobenzene, *n*-butylbenzene + pentafluorobenzene, and *n*-butylbenzene + hexafluorobenzene. Many of these heats of mixing were determined at more than one temperature.

Experimental Section

The calorimeter and procedure have been described previously.[7]

Materials. In most cases no attempt was made to purify further the materials used. Most of these compounds were examined by gas–liquid chromatography (glc) which yielded an estimate of the amount of impurities present and often of their nature. In Table I are listed the materials used, the source and grade of these materials, the estimated purity (based on glc data), and the probable identity of the principal impurities. For several compounds more than one sample was used during the course of this research; except in the case of hexafluorobenzene these were obtained from the same source. The several samples of any particular compound had the same principal impurity although in a few cases the estimated purities were appreciably different (up to 2 mole %). (In such cases the range of purity for the various samples is given in Table I.)

Results

The results[8] were fitted by a least-squares computer program[9] to the expression

$$\tilde{H}^E = x_2(1 - x_2)\sum_{n=0}^{m} h_n(1 - 2x_2)^n \qquad (1)$$

in which x_2 is the mole fraction of the second component and the h_n are constants. Each result was weighted in proportion to the reciprocal of the square of the estimated deflection-time extrapolation error.[7] With the exception of the system $C_6H_6 + C_6HF_5$ (which required four parameters), the data for each system could be fitted satisfactorily with three parameters; in a few cases two parameters would have been just as good. Table II gives the parameters h_0, h_1, h_2, and h_3 for the system $C_6H_6 + C_6HF_5$ and the parameters h_0, h_1, and h_2 for all other systems. Also given are the standard de-

(6) D. V. Fenby, I. A. McLure, and R. L. Scott, *J. Phys. Chem.*, **70**, 602 (1966).

(7) J. A. Larkin, D. V. Fenby, T. S. Gilman, and R. L. Scott, *ibid.*, **70**, 1959 (1966).

(8) All the experimental results may be found in tabular and graphical form in the Ph.D. Dissertation of D. V. Fenby (UCLA, 1967), obtainable from the UCLA Library or from University Microfilms.

(9) D. B. Myers and R. L. Scott, *Ind. Eng. Chem.*, **55**, 43 (1963).

Table II

System	Temp/°C	h_0/joules mole^{-1}	h_1/joules mole^{-1}	h_2/joules mole^{-1}	h_3/joules mole^{-1}	σ/joules mole^{-1}
$C_6H_6 + C_6H_5F$	25.0	10.6 ± 0.2	−53.6 ± 1.1	−16.5 ± 1.8		0.2
$C_6H_6 + o$-$C_6H_4F_2$	25.0	742 ± 3	89 ± 7	111 ± 17		1.3
	40.0	699 ± 3	124 ± 9	91 ± 19		1.1
$C_6H_6 + m$-$C_6H_4F_2$	25.0	777 ± 6	24 ± 18	17 ± 29		1.8
	40.0	749 ± 3	19 ± 5	15 ± 15		0.9
$C_6H_6 + p$-$C_6H_4F_2$	25.0	270 ± 3	−226 ± 11	−112 ± 19		1.6
	40.0	248 ± 7	−192 ± 15	−51 ± 50		2.5
$C_6H_6 + 1,3,5$-$C_6H_3F_3$	25.0	1984 ± 5	224 ± 11	163 ± 30		1.8
	40.0	1915 ± 5	253 ± 19	239 ± 60		2.2
$C_6H_6 + 1,2,3,4$-$C_6H_2F_4$	25.0	1013 ± 5	512 ± 13	338 ± 28		2.1
	40.0	966 ± 6	445 ± 18	257 ± 39		2.4
$C_6H_6 + 1,2,3,5$-$C_6H_2F_4$	25.0	1480 ± 4	401 ± 10	207 ± 20		1.5
	40.0	1407 ± 7	339 ± 36	166 ± 65		2.5
$C_6H_6 + 1,2,4,5$-$C_6H_2F_4$	25.0	1193 ± 6	210 ± 12	117 ± 31		2.5
	38.7	1116 ± 5	195 ± 13	93 ± 27		2.0
$C_6H_6 + C_6HF_5$	25.3	230 ± 2	578 ± 8	409 ± 8	168 ± 19	0.7
	41.7	240 ± 2	562 ± 6	369 ± 14	185 ± 21	0.6
$C_6H_6 + C_6F_6$	10.1	−1790 ± 320	1676 ± 42	790 ± 450		3.0
	25.0	−1984 ± 22	1483 ± 35	1169 ± 77		9.8
	35.0	−1858 ± 18	1394 ± 20	988 ± 43		3.2
	45.0	−1757 ± 13	1342 ± 26	796 ± 64		3.9
$C_6H_5F + p$-$C_6H_4F_2$	25.0	220 ± 1	−5 ± 3	20 ± 5		0.5
$C_6H_5F + 1,3,5$-$C_6H_3F_3$	25.0	1000 ± 7	−31 ± 11	2 ± 26		2.0
$C_6H_5F + 1,2,4,5$-$C_6H_2F_4$	25.0	209 ± 1	50 ± 3	15 ± 9		0.5
$C_6H_5F + C_6HF_5$	25.0	−700 ± 5	166 ± 8	100 ± 15		1.1
$C_6H_5F + C_6F_6$	25.0	−1689 ± 14	603 ± 22	354 ± 55		5.1
o-$C_6H_4F_2 + m$-$C_6H_4F_2$	25.0	98 ± 2	−13 ± 6	6 ± 12		0.9
o-$C_6H_4F_2 + 1,2,3,4$-$C_6H_2F_4$	25.0	−342 ± 6	−9 ± 6	31 ± 12		1.0
o-$C_6H_4F_2 + 1,2,3,5$-$C_6H_2F_4$	25.0	−81 ± 2	−38 ± 3	53 ± 6		0.5
o-$C_6H_4F_2 + 1,2,4,5$-$C_6H_2F_4$	25.0	−49 ± 2	−97 ± 7	34 ± 12		0.8
m-$C_6H_4F_2 + 1,2,3,4$-$C_6H_2F_4$	25.0	−237 ± 1	49 ± 2	37 ± 3		0.3
m-$C_6H_4F_2 + 1,2,3,5$-$C_6H_2F_4$	25.0	−279 ± 10	33 ± 20	−21 ± 36		2.9
m-$C_6H_4F_2 + 1,2,4,5$-$C_6H_2F_4$	25.0	−236 ± 5	37 ± 9	27 ± 18		1.5
p-$C_6H_4F_2 + 1,3,5$-$C_6H_3F_3$	25.0	278 ± 3	−30 ± 6	33 ± 13		0.8
p-$C_6H_4F_2 + 1,2,3,4$-$C_6H_2F_4$	25.0	−200 ± 2	77 ± 4	16 ± 11		0.7
p-$C_6H_4F_2 + 1,2,3,5$-$C_6H_2F_4$	25.0	−257 ± 3	−17 ± 8	17 ± 12		0.9
p-$C_6H_4F_2 + 1,2,4,5$-$C_6H_2F_4$	25.0	−419 ± 7	9 ± 14	47 ± 25		2.2
p-$C_6H_4F_2 + C_6HF_5$	25.0	−762 ± 3	11 ± 5	55 ± 13		0.9
p-$C_6H_4F_2 + C_6F_6$	25.0	−1045 ± 8	141 ± 9	107 ± 20		1.7
$1,3,5$-$C_6H_3F_3 + 1,2,4,5$-$C_6H_2F_4$	25.0	118 ± 1	55 ± 5	18 ± 10		0.5
$1,3,5$-$C_6H_3F_3 + C_6HF_5$	25.0	−2.5 ± 1.6	53 ± 10	32 ± 21		0.9
$1,3,5$-$C_6H_3F_3 + C_6F_6$	25.0	−172 ± 3	13 ± 8	21 ± 15		1.0
$1,2,3,5$-$C_6H_2F_4 + C_6HF_5$	25.0	30.9 ± 0.3	−15.5 ± 0.7	10.0 ± 1.4		0.1
$1,2,3,5$-$C_6H_2F_4 + C_6F_6$	25.0	28 ± 3	103 ± 6	−9 ± 13		0.9
$C_6HF_5 + C_6F_6$	25.0	−51 ± 1	46 ± 2	−3 ± 4		0.3
n-Propylbenzene + C_6F_6	25.0	−2270 ± 14	300 ± 26	272 ± 59		4.6
n-Butylbenzene + C_6HF_5	25.0	98 ± 3	−425 ± 4	167 ± 10		1.0
n-Butylbenzene + C_6F_6	25.0	−1971 ± 15	122 ± 26	440 ± 45		2.6

viations of these parameters and the standard deviations of the molar excess enthalpies, σ, defined in the usual way.

$$\sigma = \left(\frac{(\text{sum of the squared deviations})}{(\text{number of observations}) - (\text{number of parameters})} \right)^{1/2} \quad (2)$$

The great variety of curves corresponding to eq 1 with the parameters listed in Table II (only a fraction of which are drawn here, see Figures 1–7) is noteworthy. Not only are some of these heats of mixing positive (endothermic change) and some negative (exothermic change), but nine systems show changes of sign at intermediate compositions. This sign change occurs

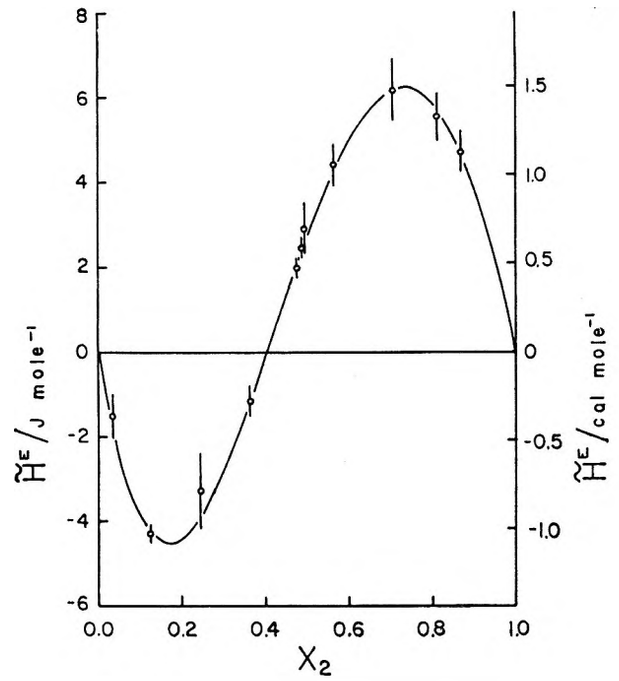

Figure 1. Heat of mixing of C_6H_6 + C_6H_5F at 25.0°.

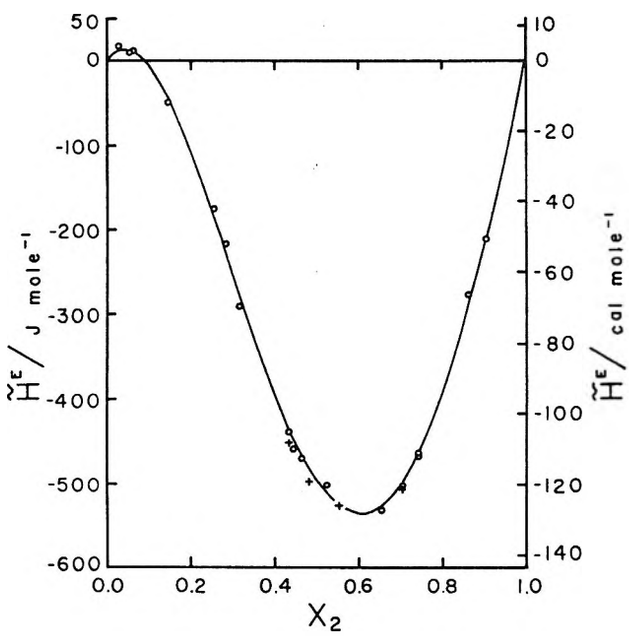

Figure 2. Heat of mixing of C_6H_6 + C_6F_6 at 25.0°: O, C_6F_6 sample 1 (Pierce Chemical Co.); +, C_6F_6 sample 2 (Imperial Smelting Corp. Ltd.).

whenever the magnitude of $(h_1 + h_3)$ exceeds that of $(h_0 + h_2)$ (*i.e.*, when $|h_1 + h_3| > |h_0 + h_2|$). The value of $\tilde{H}^E$ at $x = 0.5$ is simply $h_0/4$; these values at 25° are given in Table III.

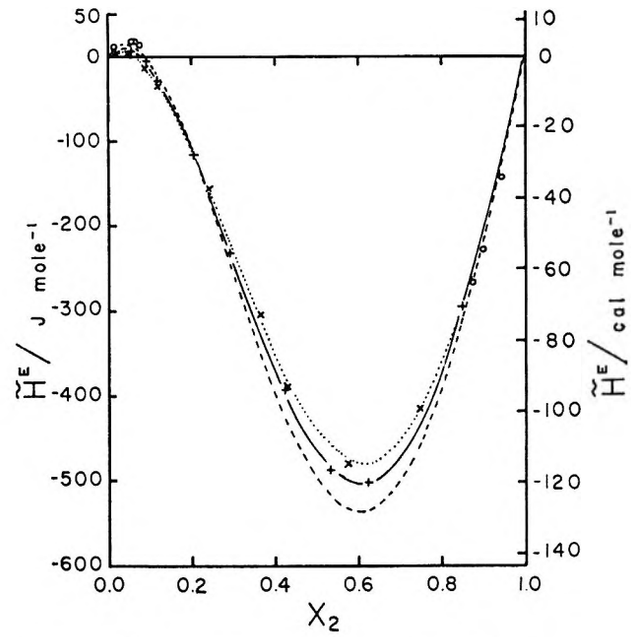

Figure 3. Heat of mixing of C_6H_6 + C_6F_6 at 10.1° (O, no curve), 35.0° (+, ———), and 45.0° (×, · · · ·). Also shown is curve corresponding to the heat of mixing at 25.0° (– – – –).

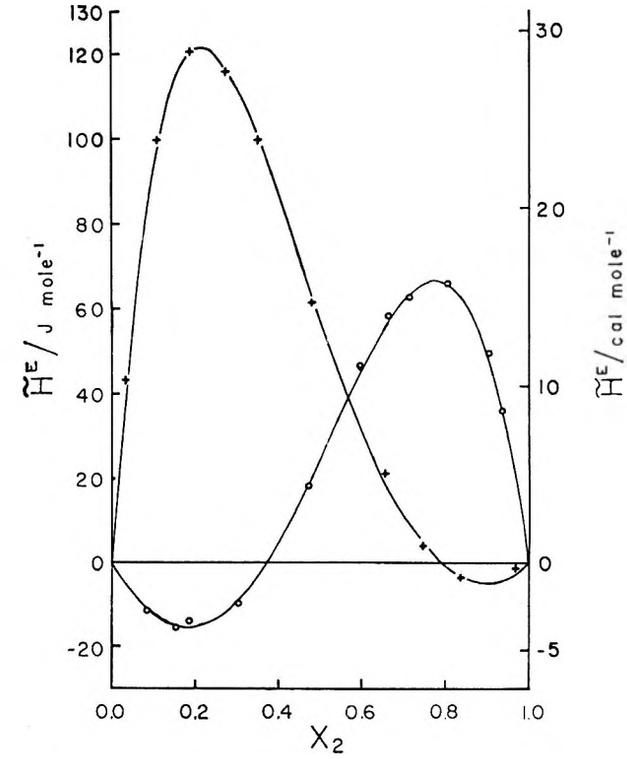

Figure 4. Heats of mixing of C_6H_6 + C_6HF_5 at 25.3° (+) and *n*-butylbenzene + C_6HF_5 at 25.0° (O).

A number of the systems studied have very small heats of mixing; this is most strikingly so for C_6H_6 +

Table III: $\tilde{H}^E$/Joules Mole^{-1} at 25° and $x = 0.5$ for the Systems $C_6H_mF_{6-m} + C_6H_nF_{6-n}$

	Component 1							
Component 2	C_6H_6	C_6H_5F	*o*-$C_6H_4F_2$	*m*-$C_6H_4F_2$	*p*-$C_6H_4F_2$	1,3,5-$C_6H_3F_3$	1,2,3,5-$C_6H_2F_4$	C_6HF_5
C_6H_6								
C_6H_5F	2.7							
o-$C_6H_4F_2$	186							
m-$C_6H_4F_2$	194		25					
p-$C_6H_4F_2$	67	55						
1,3,5-$C_6H_3F_3$	496	250			69			
1,2,3,4-$C_6H_2F_4$	253		−86	−59	−50			
1,2,3,5-$C_6H_2F_4$	370		−20	−70	−64			
1,2,4,5-$C_6H_2F_4$	298	52	−12	−59	−105	29		
C_6HF_5	57	−175			−191	−0.6	7.7	
C_6F_6	−496	−422			−261	−43	6.9	−13

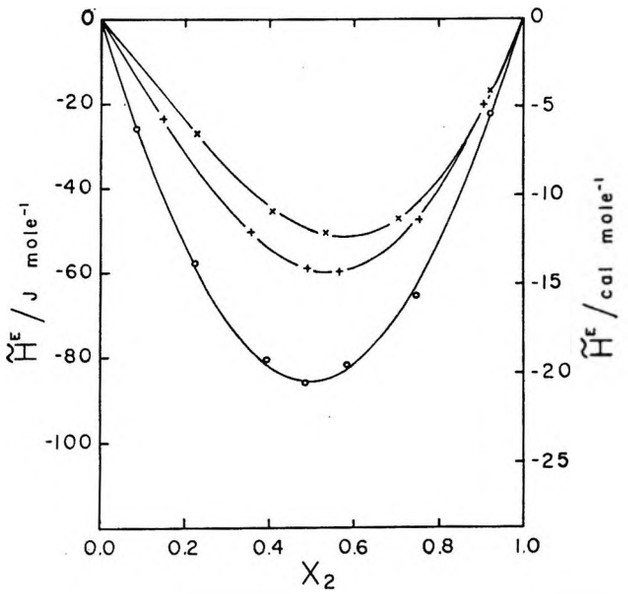

Figure 5. Heats of mixing of *o*-$C_6H_4F_2$ + 1,2,3,4-$C_6H_2F_4$ (O), *m*-$C_6H_4F_2$ + 1,2,3,4-$C_6H_2F_4$ (+), and *p*-$C_6H_4F_2$ + 1,2,3,4-$C_6H_2F_4$ (×) at 25.0°.

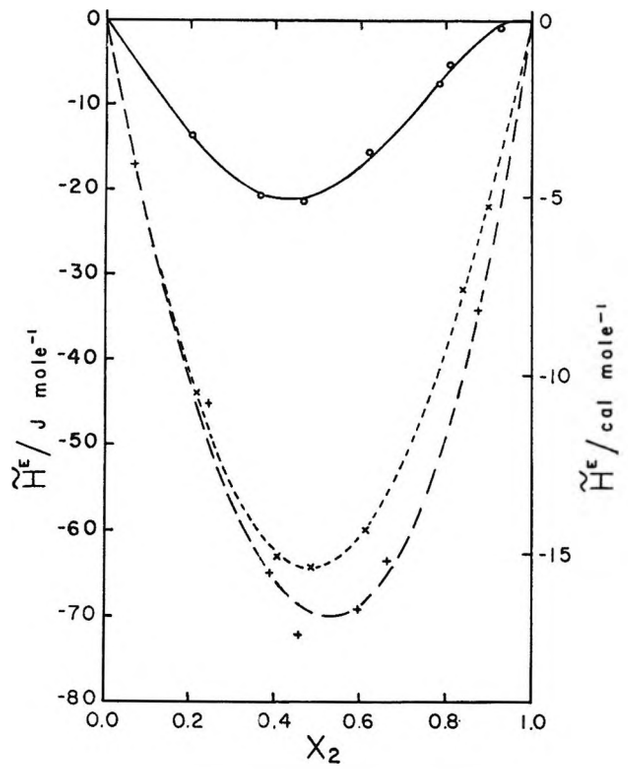

Figure 6. Heats of mixing of *o*-$C_6H_4F_2$ + 1,2,3,5-$C_6H_2F_4$ (O), *m*-$C_6H_4F_2$ + 1,2,3,5-$C_6H_2F_4$ (+), and *p*-$C_6H_4F_2$ + 1,2,3,5-$C_6H_2F_4$ (×) at 25.0°.

C_6H_6F (Figure 1). Runs for this system and for other cases in which the heat of mixing is very small involve no electrical compensation, and consequently the sign of the temperature change unequivocally determines the sign of $\tilde{H}^E$.

Morcom[10] has determined heats of mixing for C_6H_6 + C_6F_6 at 40° while Swinton[11] has obtained results at 25, 40, 55, and 70°. We have fitted their data to eq 1, assigning unit weight to each result. The parameters h_0, h_1, h_2, their standard deviations, and the standard deviations of the molar excess enthalpies, σ, are compared in Table IV with our results for C_6H_6 + C_6F_6 (Figures 2 and 3). Morcom's results are in good agreement with ours. The parallelism between the curves corresponding to Swinton's data and those corresponding to our data is quite striking, both sets showing minima at $x_2 \cong 0.62$, a sign change at low x_2, and maxima which decrease with increasing temperature. At 25°, however, our results in the neighborhood of the minimum are approximately 35 joules mole^{-1} more

(10) K. W. Morcom, private communication.

(11) F. L. Swinton, private communication.

Table IV

Ref	Temp/°C	h_0/joules mole^{-1}	h_1/joules mole^{-1}	h_2/joules mole^{-1}	σ/joules mole^{-1}
Morcom[10]	40	−1854 ± 14	1376 ± 31	847 ± 65	6.4
Swinton[11]	25	−1836 ± 10	1379 ± 23	879 ± 51	5.4
	40	−1733 ± 9	1270 ± 17	777 ± 38	4.1
	55	−1608 ± 5	1221 ± 9	565 ± 20	2.1
	70	−1404 ± 5	1068 ± 10	360 ± 24	2.1
This work	25	−1984 ± 22	1483 ± 35	1169 ± 77	9.8
	35	−1858 ± 18	1394 ± 20	988 ± 43	3.2
	45	−1757 ± 13	1342 ± 26	796 ± 64	3.9

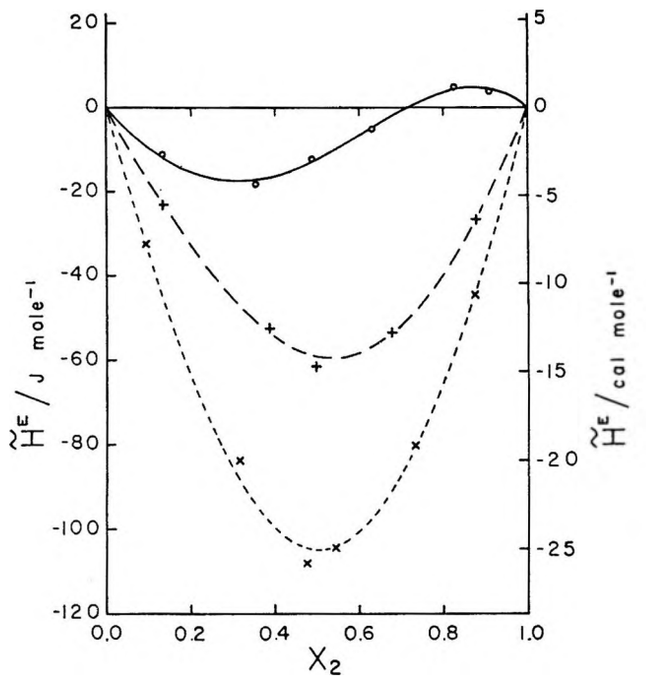

Figure 7. Heats of mixing of o-$C_6H_4F_2$ + 1,2,4,5-$C_6H_2F_4$ (○), m-$C_6H_4F_2$ + 1,2,4,5-$C_6H_2F_4$ (+), and p-$C_6H_4F_2$ + 1,2,4,5-$C_6H_2F_4$ (×) at 25.0°.

exothermic than those obtained by Swinton; at 40°, we differ by about 20 joules mole^{-1}. A few measurements using the hexafluorobenzene sample of high purity (Table I) yielded results not significantly different from those obtained with the less pure sample (see Figure 2), so the quality of our material does not seem to be the source of the discrepancy.

In general, for all the fluorinated benzenes the principal impurities were very similar to the substance itself (see Table I). Therefore, it is very unlikely that these will have any appreciable effect on the measured heat of mixing. In the case of the less pure samples (<99 mole %), the principal impurity is always another isomer of the same compound.

Discussion

It is apparent that any interpretation of the results summarized in Table II must treat the molar heat of mixing, $\tilde{H}^E$, as the sum of several terms differing in sign and mole fraction dependence;[12] indeed, the systems with sign changes virtually require this. We believe that the heat of mixing is made up of contributions from at least three different kinds of interactions:

1. A nonspecific "physical" interaction, $\tilde{H}_P{}^E$, typical of mixtures of hydrocarbons with fluorocarbons. This should be large and positive[2,12,13] and not necessarily symmetrical in mole fraction.

2. A specific "chemical" interaction, $\tilde{H}_C{}^E$, thought to arise from charge-transfer complex formation. This should contribute a negative (exothermic) term to $\tilde{H}^E$, which should be more nearly symmetrical in mole fraction than (1), and whose magnitude will depend upon the donor and acceptor strengths of the two components.[13a]

3. A specific interaction between matching hydrogen atoms and fluorine atoms on adjacent rings.[13a]

Regular solution theory[3] suggests that $\tilde{H}_P{}^E$ should fit a volume fraction equation such that the maximum is displaced in the direction of solutions rich in the component of smaller molar volume. This is demonstrated strikingly in the comparison of the molar heat of mixing of C_6H_6 ($\tilde{V}$ = 89 cm^3 mole^{-1}) + C_6HF_5 ($\tilde{V}$ = 110 cm^3 mole^{-1}) with that of n-butylbenzene ($\tilde{V}$ = 156 cm^3 mole^{-1}) + C_6HF_5 shown in Figure 4. In the former case, the hydrocarbon has the smaller molar volume and the maximum in the S-shaped curve appears on the

(12) *Cf.* the system $C_7F_{15}H$ + $(CH_3)_2CO$ reported by D. L. Andersen, R. A. Smith, D. B. Myers, S. K. Alley, A. G. Williamson, and R. L. Scott, *J. Phys. Chem.*, **66**, 621 (1962).

(13) A. G. Williamson and R. L. Scott, *ibid.*, **65**, 275 (1961).

(13a) NOTE ADDED IN PROOF. Professor M. W. Hanna (University of Colorado) has suggested to us that the entire "chemical" part of the energy may be electrostatic in origin, *i.e.* quadrupole–quadrupole interactions, bond dipole interactions, etc. In this view there is little or no stabilization of the complex by charge transfer and our second and third kinds of interaction are essentially similar in origin.

hydrocarbon-rich side; in the latter case, the hydrocarbon has the larger molar volume and the maximum in the S-shaped curve appears on the fluorocarbon-rich side. This effect is also present, but much less obviously, in a comparison of the systems C_6H_6 + C_6F_6 ($\bar{V}$ = 116 cm^3 mole^{-1}), *n*-propylbenzene ($\bar{V}$ = 139 cm^3 mole^{-1}) + C_6F_6, and *n*-butylbenzene + C_6F_6. Here the shift in the minimum to lower mole fractions, x_2, with increasing molar volume of the hydrocarbon is indicative of a shift in the maximum of the nonspecific contribution to higher mole fractions, a trend in the predicted direction.

Benzene and hexafluorobenzene form a crystalline 1:1 molecular complex[4,5] which has generally been accepted as a charge-transfer complex between the donor C_6H_6 and the acceptor C_6F_6. It seems reasonable to attribute the "chemical" part of the thermodynamic properties of the liquid mixtures to the presence of this complex. Swinton and co-workers[5,11,14,15] have investigated the effect of varying the donor species; their results suggest an increase in complex formation with increasing π-donor strength of the hydrocarbon. We interpreted[5] the variations in the magnitudes and temperature dependences of $\tilde{H}^E$ for the systems C_6H_6 + C_6F_6, C_6H_6 + C_6HF_5, and C_6H_6 + 1,2,4,5,-$C_6H_2F_4$ in terms of decreasing complex formation with decrease in the number of fluorine atoms in the acceptor. Although these thermodynamic measurements are strongly indicative of a charge-transfer interaction between benzene and hexafluorobenzene, there is at present no convincing nonthermodynamic evidence. If such an interaction is present in this system, it is plausible that similar interactions occur in other systems of the series $C_6H_mF_{6-m}$ + $C_6H_nF_{6-n}$ although these should on the whole be somewhat weaker.

The need for a third contribution to the heat of mixing, one dependent upon the arrangement of the hydrogen and fluorine atoms on the rings, is strikingly evident in Figures 5, 6, and 7 and Table III. These show that the matching "lock-and-key" systems (*o*-$C_6H_4F_2$ + 1,2,3,4-$C_6H_2F_4$, *m*-$C_6H_4F_2$ + 1,2,3,5-$C_6H_2F_4$, and *p*-$C_6H_4F_2$ + 1,2,4,5-$C_6H_2F_4$) have algebraically lower heats of mixing. The other "lock-and-key" systems (C_6H_6 + C_6F_6 and C_6H_5F + C_6HF_5) appear to exhibit similar behavior; *e.g.*, the heat of mixing of C_6H_5F + C_6HF_5 is appreciably more exothermic than that of C_6H_6 + C_6HF_5 although fluorobenzene is certainly not a markedly better π-donor than benzene. However, the argument for these systems is less convincing because of the parallel changes in the endothermic contribution, $\tilde{H}_P^E$, with varying $m - n$. The origin of this comparatively small effect is not clear. Conceivably, it could be a direct interaction between adjacent bond dipoles

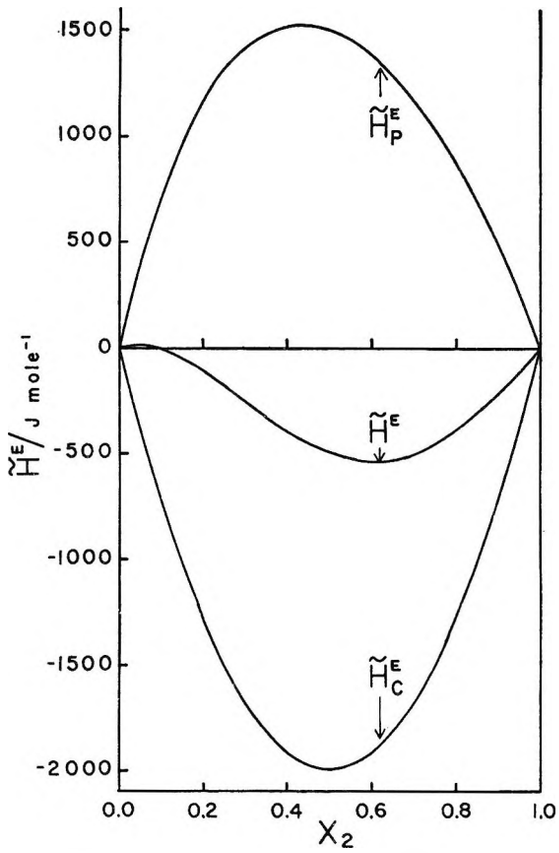

Figure 8. Division of the heat of mixing, $\tilde{H}^E$, of C_6H_6 + C_6F_6 at 25.0° into a "physical" contribution, $\tilde{H}_P^E$, and a "chemical" contribution, $\tilde{H}_C^E$.

C–H and C–F on neighboring molecules. (The net dipole moment of the whole molecule is certainly not a significant factor. It should be noted that C_6H_6, *p*-$C_6H_4F_2$, 1,3,5-$C_6H_3F_3$, 1,2,4,5-$C_6H_2F_4$, and C_6F_6 have zero net dipole moments; the other compounds do have dipole moments. No correlation is found that can be associated with the presence or absence of a net dipole moment in the fluorinated benzene.)

Unfortunately, unlike the system $C_7F_{15}H$ + acetone,[12] the systems $C_6H_mF_{6-m}$ + $C_6H_nF_{6-n}$ offer no method for quantitative separation of these contributions. There are no spectra from which one can deduce an equilibrium constant and heat of formation; there is no satisfactory substance to substitute for benzene without its electron-donor ability (as C_7F_{16} substituted[12] for $C_7F_{15}H$ without its hydrogen-bond forming ability). In order to estimate $\tilde{H}_P^E$, we make the plausible assumption (based upon the random probabilities of interac-

(14) W. A. Duncan, J. P. Sheridan, and F. L. Swinton, *Trans. Faraday Soc.*, 62, 1090 (1966).

(15) W. J. Gaw, Ph.D. Thesis, University of Strathclyde, 1966.

Table V: $\bar{H}_C^E$ (x = 0.5)/kjoules Mole^{-1} for Systems $C_6H_mF_{6-m}$ + $C_6H_nF_{6-n}$

	Component 1							
Component 2	C_6H_6	C_6H_5F	o-$C_6H_4F_2$	m-$C_6H_4F_2$	p-$C_6H_4F_2$	1,3,5-$C_6H_3F_3$	1,2,3,5-$C_6H_2F_4$	C_6HF_5
C_6H_6								
C_6H_5F	−0.04							
o-$C_6H_4F_2$	0.02							
m-$C_6H_4F_2$	0.03		0.03					
p-$C_6H_4F_2$	−0.10	0.01						
1,3,5-$C_6H_3F_3$	0.12	0.08			0.03			
1,2,3,4-$C_6H_2F_4$	−0.42		−0.25	−0.23	−0.22			
1,2,3,5-$C_6H_2F_4$	−0.30		−0.19	−0.24	−0.23			
1,2,4,5-$C_6H_2F_4$	−0.38	−0.33	−0.18	−0.23	−0.27	−0.01		
C_6HF_5	−0.99	−0.85			−0.57	−0.17	−0.03	
C_6F_6	−2.01	−1.47			−0.93	−0.42	−0.16	−0.05

tions between hydrogen and fluorine atoms on adjacent rings) that it is proportional to $(m - n)^2$. On the basis of a comparison with a number of hydrocarbon + fluorocarbon systems in which there is no complex formation, we estimate that $\bar{H}_P^E(x = 0.5)$ for the system $C_6H_6 + C_6F_6$ lies between 1 and 2 kjoules mole^{-1}; for purposes of discussion we assume a value of 1.50 kjoules mole^{-1}. Using this value of $\bar{H}_P^E$ and assuming the "chemical" contribution, $\bar{H}_C^E$, to be symmetrical in mole fraction, one obtains the division of $\bar{H}^E$ for the system $C_6H_6 + C_6F_6$ shown in Figure 8.

Using the assumptions above, one deduces for the systems $C_6H_mF_{6-m} + C_6H_nF_{6-n}$ that

$$\bar{H}_P^E(x = 0.5)/\text{kjoule mole}^{-1} = 0.042(m - n)^2$$

This can be subtracted from the $\bar{H}^E(x = 0.5)$ values given in Table III to yield the $\bar{H}_C^E(x = 0.5)$ values given in Table IV. Although there is no direct evidence (either from electron affinity or reduction potential data) to support the idea, one intuitively expects that acceptor strength should increase with increase in the number of fluorine atoms. For a particular π-donor (*i.e.*, column in Table V) the magnitude of $\bar{H}_C^E(x = 0.5)$ generally becomes more exothermic with increasing number of fluorine atoms in the π-acceptor. For a particular π-acceptor (*i.e.*, row in Table V) the magnitude of $\bar{H}_C^E(x = 0.5)$ generally becomes less exothermic with increasing number of fluorine atoms in the π-donor. Although this trend is what one would anticipate intuitively, it does not follow the ionization potentials[16,17] which suggest that fluorobenzene and p-difluorobenzene should be better π-donors than benzene. Although there are a number of exceptions to these generalizations, nonetheless in view of the crude approximations involved, the trends in Table V are quite impressive.

Acknowledgments. We wish to acknowledge helpful discussions with Dr. I. A. McLure, Dr. A. G. Williamson, Professor C. M. Knobler, Dr. D. McIntyre, and Professor M. E. Baur. We thank Mr. S. C. Durana for carrying out the chromatographic analyses. D. V. F. gratefully acknowledges the award of a Postgraduate Scholarship in Science by the University Grants Committee, New Zealand, and a Dupont Teaching Fellowship. We also gratefully acknowledge the gift of a sample of 1,3,5-trifluorobenzene from the Imperial Smelting Corporation, Ltd., Bristol, England.

(16) R. Bralsford, P. V. Harris, and W. C. Price, *Proc. Roy. Soc.* (London), **A258**, 459 (1960).

(17) J. R. Majer and C. R. Patrick, *Trans. Faraday Soc.*, **58**, 17 (1962).

The Ionization Potential and Heat of Formation of Thioformaldehyde[1]

by A. Jones[2] and F. P. Lossing

Division of Pure Chemistry, National Research Council of Canada, Ottawa, Ontario, Canada
(Received July 3, 1967)

Monomeric thioformaldehyde has been prepared transiently from the pyrolysis of thiacyclobutane and subjected to electron impact in a mass spectrometer. The ionization potential is 9.44 ± 0.05 v. From the appearance potential of H_2CS^+ ion from thiacyclobutane, $\Delta H_f(H_2CS^+) \leq 242$ kcal/mole. Taken with $IP(H_2CS) = 9.44$, this leads to $\Delta H_f(H_2CS) \leq 24 \pm 2.6$ kcal/mole, much lower than previous estimates. Derived bond dissociation energies are $D(H\text{–}H_2CS \text{ in } CH_3S\cdot) = 45$, $D(CH_3\text{–}H_2CS \text{ in } CH_3CH_2S\cdot) = 32$, and $D(H_2C{=}S) \sim 124$ kcal/mole.

Introduction

Thioformaldehyde, H_2CS, is unstable as a monomeric species under normal conditions[3] and all attempts to prepare it have given the cyclic polymer, trithioformaldehyde. At low pressures (*ca.* 10^{-3} torr), however, the monomer has an appreciable lifetime and we have observed it as a reaction product in the low-pressure $Hg(^3P_1)$ photosensitized decompositions of both CH_3SCH_3 and CH_3SSCH_3.[4] A thermochemical analysis of these reactions was not possible because of the lack of a reliable value for $\Delta H_f(H_2CS(g))$. It was the aim of this work to obtain a more accurate estimate of this quantity and to provide the first direct measurement of the ionization potential of H_2CS.

Two values for $\Delta H_f(H_2CS)$ have been employed in the literature. In an electron impact study of sulfur-containing compounds, Gallegos and Kiser[5] used a value of 76 kcal/mole based on appearance potential measurements for which H_2CS was one of the neutral fragments. This value was amended to 51 kcal/mole in later work.[6]

The method used here was based on appearance potential thresholds for the processes

$$\begin{matrix} CH_2CH_2 \\ | \quad | \\ CH_2S \end{matrix} + e \longrightarrow H_2CS^+ + C_2H_4 + 2e$$

$$\Delta H \leq AP(H_2CS)^+ \quad (1)$$

$$H_2CS + e \longrightarrow H_2CS^+ + 2e$$

$$\Delta H = IP(H_2CS^+) \quad (2)$$

The ionization potential measurement in (2) was carried out on H_2CS generated at low pressures in a reaction stream. It follows that

$$\Delta H_f(H_2CS) \leq AP(H_2CS^+) - IP(H_2CS) + \Delta H_f[(CH_2)_3S] - \Delta H_f(C_2H_4) \quad (3)$$

Experimental Section

The monomeric H_2CS was produced by pyrolysis at 1000° of thiacyclobutane at low pressure in a fused-silica capillary furnace leading to the ionization chamber of a mass spectrometer.[7] The other main product was ethylene. Small amounts of allyl radical and allene were also detected. The appearance potential curves were compared to those of xenon by a curve-matching procedure.[7]

Results and Discussion

With the furnace at room temperature, measurements of $AP(H_2CS^+)$ from undissociated thiacyclobutane gave an average value of 10.40 ± 0.1 v. With the furnace at 1000° thiacyclobutane was about 80% decomposed,

(1) Issued as National Research Council of Canada No. 9833.

(2) National Research Council of Canada Postdoctorate Fellow, 1965–1967.

(3) E. E. Reid, "Organic Chemistry of Bivalent Sulfur," Vol. III, Chemical Publishing Co., Inc., New York, N. Y., 1960, Chapter 2.

(4) A. Jones, S. Yamashita, and F. P. Lossing, submitted for publication.

(5) E. J. Gallegos and R. W. Kiser, *J. Phys. Chem.*, **66**, 136 (1962).

(6) B. G. Hobrock and R. W. Kiser, *ibid.*, **67**, 1283 (1963).

(7) R. Taubert and F. P. Lossing, *J. Am. Chem. Soc.*, **84**, 1523 (1962).

and measurements on the H_2CS produced gave IP(H_2CS) = 9.44 ± 0.05. The errors quoted represent standard deviations of several determinations rather than estimates of the absolute error. An attempt was made to measure AP($C_2H_4^+$) from $(CH_2)_3S$, and so obtain an independent value of $\Delta H_f(H_2CS)$ from the process

$$(CH_2)_3S + e \longrightarrow C_2H_4^+ + H_2CS + 2e \quad (4)$$

The intensity of the m/e 28 peak from thiacyclobutane was less than 3% of the base peak, however, and excessive tailing of the $C_2H_4^+$ curve precluded a reliable measurement of AP($C_2H_4^+$).

As a check on our measurements, the ionization potential of thiacyclobutane was also determined. The observed value, 8.8 ± 0.1 v, was in good agreement with two previous measurements of 8.9 + 0.15[5] (by electron impact) and 8.64 v[8] (by photoionization).

$\Delta H_f(H_2CS)$ and $\Delta H_f(H_2CS^+)$. The appearance potential for H_2CS^+ from $(CH_2)_3S$ measured in this work, 10.40 ± 0.1 v, is considerably lower than that found by Gallegos and Kiser,[5] 11.8 ± 0.2 v. The difference appears to be larger than can be accounted for by the difference in the method of comparing the ionization efficiency curves for the fragment ion with those for the standard gas. Values of $\Delta H_f(H_2CS^+)$ from the literature,[5,6,9] derived from electron-impact measurements on various sulfur compounds, show a spread from 215 to 252 kcal/mole, but in some cases the assumption has been made that the appearance potential includes the energy of dissociation of the neutral products as well. The present appearance potential and the assumption of the simplest dissociation process, reaction 1, lead to $\Delta H_f(H_2CS^+) \leq 242$ kcal/mole, using $\Delta H_f(C_2H_4)$ = 12.50 kcal/mole[10] and $\Delta H_f((CH_2)_3S)$ = 14.63 kcal/mole.[11,12] Substitution in eq 3 gives $\Delta H_f(H_2CS) \leq 24 \pm 2.6$ kcal/mole.

Support for this lower value of $\Delta H_f(H_2CS)$ comes from a consideration of the observed temperature range for the thermal decomposition of thiacyclobutane in the reactor, as compared with the temperature range observed for other compounds for which activation energies of decomposition are known. On this basis, the activation energy at high pressure (assuming similar decreases in activation energy at low pressure) should not be greater than 50–55 kcal/mole for the dissociation

$$(CH_2)_3S \longrightarrow H_2CS + C_2H_4 \quad (5)$$

From the relationship between the forward and reverse activation energies and the enthalpy for dissociation

$$E_{-5} = E_5 - \Delta H \quad (6)$$

and the experimental estimate of $E_5 \sim 50$ kcal/mole, one can estimate E_{-5} for various values of $\Delta H_f(H_2CS)$. For example, a value of $\Delta H_f(H_2CS)$ = 51 kcal/mole would give ΔH = 49 kcal/mole and hence $E_{-5} \sim 1$ kcal/mole. Such a low value for E_{-5} seems highly improbable. For analogous bimolecular association reactions, activation energies in the range 20–30 kcal/mole are generally found.[13] The value of $\Delta H_f(H_2CS)$ = 24 kcal/mole found in the present work leads to $E_{-5} \sim$ 28 kcal/mole, which seems to be a reasonable value.

It is of interest to calculate from the present data the heats of reaction for disproportionation and combination reactions of methylthio radicals

$$2CH_3S\cdot \longrightarrow H_2CS + CH_3SH \quad (7)$$

$$2CH_3S\cdot \longrightarrow CH_3SSCH_3 \quad (8)$$

Using $\Delta H_f(CH_3S\cdot)$ = 30.5 ± 5,[14] $\Delta H_f(CH_3SH)$ −5.46,[12] and $\Delta H_f(CH_3S_2CH_3)$ = −5.71 kcal/mole,[12] ΔH_7 becomes −42 ± 8 kcal/mole and ΔH_8 becomes −67 ± 7 kcal/mole. For the isoelectronic $CH_3O\cdot$ radical the analogous reactions are

$$2CH_3O\cdot \longrightarrow H_2CO + CH_3OH \quad (9)$$

$$2CH_3O\cdot \longrightarrow CH_3OOCH_3 \quad (10)$$

Using $\Delta H_f(CH_3O)\cdot$ = 2 ± 2,[15] $\Delta H_f(H_2CO)$ = −27.7,[16] and $\Delta H_f(CH_3OH)$ = −48.08[16] kcal/mole, ΔH_9 is −78 ± 2 kcal/mole and ΔH_{10} is −36.1 ± 1 kcal/mole.[15] It can be seen that for CH_3O radicals the disproportionation is thermochemically favored, in contrast to CH_3S for which the combination is favored over disproportionation, although by a smaller margin. It is interesting to note that the experimentally observed relative rates of these reactions are in qualitative agreement with the exothermicities: the combination of methoxyls is negligibly slow compared to the disproportionation, whereas the combination of CH_3S radicals is faster than the disproportionation.[4,17]

(8) L. D. Isaacs, W. C. Price, and R. G. Ridley in "The Threshold of Space," Pergamon Press Ltd., London, 1957, p 143.

(9) B. G. Hobrock and R. W. Kiser, *J. Phys. Chem.*, **66**, 1648 (1962); **67**, 648 (1963).

(10) F. D. Rossini, *et al.*, "Selected Values of Physical and Thermodynamic Properties of Hydrocarbons and Related Compounds," Carnegie Press, Pittsburgh, Pa., 1953.

(11) W. N. Hubbard, C. Katz, and G. Waddington, *J. Phys. Chem.*, **58**, 142, 396 (1954).

(12) H. Mackle and P. G. O'Hare, *Tetrahedron*, **19**, 961 (1963).

(13) See, for example, Table XII-8 in S. W. Benson, "The Foundations of Chemical Kinetics," McGraw-Hill Book Co. Inc., New York, N. Y., 1960.

(14) H. Mackle, *Tetrahedron*, **19**, 1159 (1963).

(15) J. A. Kerr, *Chem. Rev.*, **66**, 465 (1966).

(16) "Selected Values of Thermodynamic Properties," National Bureau of Standards Circular 500, U. S. Government Printing Office, Washington, D. C., 1952.

Calculations of the endothermicities of the radical dissociation processes

$$RCH_2S\cdot \longrightarrow R\cdot + H_2CS \quad (11)$$

which are analogous to the well-known alkoxy radical dissociations

$$RCH_2O\cdot \longrightarrow R\cdot + H_2CO \quad (12)$$

have recently been performed by Friswell and Gowenlock[18] using $\Delta H_f(H_2CS) = 51$ kcal/mole. Values recalculated using $\Delta H_f(H_2CS) = 24$ kcal/mole are given below, together with (in brackets) the corresponding values for reaction 12: R = H, 45 (22); R = CH_3, 32 (13); R = C_2H_5, 30 (9); R = n-C_3H_7, 30 (9). The heats of formation of alkyl and alkoxy radicals[15] and the alkylthio radicals[14] are taken from the literature. Although the thiyl radicals are on this basis less stable than the earlier estimates[18] indicated, they are still considerably more stable than the corresponding alkoxy radicals.

The Bond Dissociation Energy $D(H_2C{=}S)$. From the equation

$$H_2CS \longrightarrow CH_2 + S \quad (13)$$

it can be seen that

$$D(H_2C{=}S) = \Delta H_f(CH_2) + \Delta H_f(S) - \Delta H_f(H_2CS) \quad (14)$$

The heat of formation of CH_2 is not known precisely. $\Delta H_f(CH_2)$ used here is 86 ± 6 kcal/mole from data given by Bell and Kistiakowsky.[19] The heat of formation of atomic sulfur, $\Delta H_f(S(g))$, has been the subject of some uncertainty, but a value of 65.9 kcal/mole appears to be now established.[12] Substituting these quantities in reaction 14 gives $D(H_2C{=}S) = 124$ kcal/mole with an uncertainty of about 6–8 kcal/mole. The analogous dissociation energy $D(H_2C{=}O)$ is 173 ± 6 kcal/mole, using $\Delta H_f(O) = 59.5$[20] and $\Delta H_f(H_2CO) = -27.7$ kcal/mole.[15] Although these dissociation energies are subject to large errors, the difference $D(H_2C{=}O) - D(H_2C{=}S)$ is more precise since $\Delta H_f(CH_2)$ cancels. From the present data, this difference is 45.6 kcal/mole.

$IP(H_2CS)$. The measured value of 9.44 ± 0.05 v found in this work is much higher than the value of 6.7 v derived by Gallegos and Kiser, which was based on their initial value of $\Delta H_f(H_2CS) = 76$ kcal/mole.[5] It might be noted that $IP(H_2CO) \approx IP(CH_3OH)$, 10.87 and 10.85 v, respectively.[21] Correspondingly, the present value for $IP(H_2CS)$ is in good agreement with that of CH_3SH, 9.44 v.[21]

Peak Ratios in Mass Spectrum of H_2CS. The ratio of peak intensities for the parent, P-1 and P-2 peaks of H_2CS were measured by stripping contributions from undecomposed thiacyclobutane from the spectrum at 1000°. The ratios were m/e 46 (80%), m/e 45 (100%), and m/e 44 (19%). Peaks at lower mass numbers were subject to possible interference by other reaction products.[22]

Acknowledgment. The authors wish to thank Professor B. G. Gowenlock for correspondence concerning ref 18 in advance of publication.

(17) R. P. Steer, B. L. Kalra, and A. R. Knight, *J. Phys. Chem.*, 71, 783 (1967); P. M. Rao, J. A. Copeck, and A. R. Knight, *Can. J. Chem.*, 45, 1369 (1967).

(18) N. J. Friswell and B. G. Gowenlock in "Advances in Free Radical Chemistry," Vol. 2, G. H. Williams, Ed., Logos Press, London, 1967, p 27.

(19) J. A. Bell and G. B. Kistiakowsky, *J. Am. Chem. Soc.*, 84, 3417 (1962).

(20) T. L. Cottrell, "The Strengths of Chemical Bonds," 2nd ed, Butterworth and Co. Ltd., London, 1958.

(21) R. W. Kiser, "Introduction to Mass Spectrometry, and its Applications," Prentice Hall, Inc., Englewood Cliffs, N. J., 1965.

(22) NOTE ADDED IN PROOF. Reaction 11, with R = H, has been observed at 925° in this reactor [T. F. Palmer and F. P. Lossing, *J. Am. Chem. Soc.*, 84, 4661 (1962)]. Decomposition of CH_3S at this temperature is consistent with $D(H{-}H_2CS) = 45$ kcal/mole as given, but is incompatible with the 73 kcal/mole required for this reaction by the higher value for $\Delta H_f(H_2CS)$.

The Gaseous Hydroxides of Cobalt and Nickel

by G. R. Belton and A. S. Jordan[1]

School of Metallurgy and Materials Science, University of Pennsylvania, Philadelphia, Pennsylvania 19104
(Received April 4, 1967)

Measurements have been made, by means of the transpiration technique, of the volatility of cobalt and nickel in mixtures of water vapor, hydrogen, and argon. The volatilization reactions and their standard Gibbs energy changes are shown to be $Co + 2H_2O(g) = Co(OH)_2(g) + H_2(g)$ $\Delta G^\circ = 58{,}200 - 9.38T$ cal (1548–1739°K) and $Ni + 2H_2O(g) = Ni(OH)_2(g) + H_2(g)$ $\Delta G^\circ = 58{,}290 - 6.04T$ cal (1448–1695°K). These, and previous data, when combined with free energy functions based on reasonable structural parameters, lead to the following average bond energies for the iron group dihydroxides: Fe–OH, 98.2; Co–OH, 91.9; Ni–OH, 91.2 kcal. These energies are shown to be consistent with a pseudohalide character for the gaseous hydroxides.

Introduction

The enhanced volatility of iron in the presence of water vapor has been shown by Belton and Richardson[2] to be caused by the formation of the gaseous compound $Fe(OH)_2$. No direct evidence is available in the literature, however, for the existence of analogous species of the chemically similar transition metals Co and Ni. Indeed, Brewer and Elliott[3] concluded from experiments with solid NiO and water vapor at 1500° that decomposition to the elements was the only important vaporization process. In exploratory experiments, however, Morey[4] did observe an enhanced mobility of solid NiO in high-pressure steam (2100 atm) at 500°.

The purpose of the present study has been to establish the existence of the gaseous hydroxides of Co and Ni and to obtain thermodynamic data for their formation. This has been achieved by using the semimicro transpiration technique to measure the apparent vapor pressures of the metals in mixtures of water vapor, hydrogen, and argon which were insufficiently oxidizing to permit formation of a condensed oxide. A few measurements have been made with nickel under conditions in which NiO was the stable phase to help establish the number of metal atoms in the species.

Experimental Section

The transpiration apparatus and experimental procedure were essentially the same as have been described earlier[2,5] except for a small modification caused by reaction of the refractory tubes used to contain the metal specimens. In the case of nickel, a small slip cast thoria insert (Zircoa), 0.5 cm in i.d. and approximately 5 cm in length, was used to contain the spiral wire sample. This insert was carefully ground to fit into an outer alumina reaction tube and could be readily removed for weighing. For each change in experimental conditions, the insert was found to change in weight; hence, after each such change, the insert was subjected to a 5–8-hr saturation run. In subsequent experiments the weight of the insert fluctuated about a constant value (± 3–5×10^{-5} g). An insert of the same material could not be saturated when a cobalt specimen was used, but *hot-pressed* thoria (Thermal Syndicate Ltd.) could be readily saturated to constant weight ($\pm 2 \times 10^{-5}$ g) in about 1 hr. It was later found that negligible reaction occurred between oxidized nickel samples and the hot-pressed thoria.

Materials. High-purity wire (Johnson, Matthey and Co.) approximately 0.25 mm in diameter was used in the bulk of the experiments. The cobalt wire had a purity of 99.95% and the purity of the Ni wire was in excess of 99.99%. A few experiments were carried out with wires of lower purity (99.87% Co and 99.98%

(1) Bell Telephone Laboratories, Murray Hill, N. J.

(2) G. R. Belton and F. D. Richardson, *Trans. Faraday Soc.*, **58**, 1562 (1962).

(3) L. Brewer and G. R. B. Elliott, University of California Radiation Laboratory Report 1831, 1952.

(4) G. W. Morey, *Econ. Geol.*, **52**, 225 (1957).

(5) G. R. Belton and A. S. Jordan, *J. Phys. Chem.*, **69**, 2065 (1965).

Ni) but no difference in apparent volatilities could be detected. Experimental specimens which were approximately 25 mm long by 5 mm in diameter were constructed of two concentric coils of wire with a few short lengths in the center.

In order to obtain the necessary range of water vapor pressures and water vapor–hydrogen ratios, seven commercially prepared argon–hydrogen gas mixtures were used. In all cases the composition was known to better than 1% of the hydrogen content.

Results

It is now well established[2] that reliable equilibrium vapor pressures can be determined by the transpiration technique if the derived pressures can be shown to be independent of the flow rate of the transporting gas over a substantial range. Several typical sets of data, obtained in this work, for the apparent pressures of cobalt and nickel are presented in Figure 1. A vapor pressure plateau, similar to those illustrated, was obtained for each experimental condition. The average value of the standard deviations from the equilibrium pressures, calculated for those cases (12) showing at least five plateau results, was approximately 3.5%.

Cobalt. The equilibrium pressures for cobalt and the relevant experimental conditions are presented in Table I, where it will be noted that the data at 1436° were taken at two essentially constant water vapor–hydrogen ratios and several water pressures. The value of carrying out experiments in this way, as an aid in separating and identifying volatile species, has been pointed out in an earlier paper.[5] At constant water–hydrogen ratio, that part of the volatility which is independent of the water pressure must be due to the neutral vapor pressure of the metal plus any volatile oxides. The additional volatility and its functional dependence on the water pressure and water–hydrogen ratio may then be used to determine the stoichiometry of the hydrated species.

In Figure 2, the equilibrium pressures at 1436° are shown plotted *vs.* the water pressure. Within experimental error, a linear dependence is shown; hence the data were analyzed by the method of least mean squares to determine the best values for the intercepts and slopes. Each individual measurement was included in the analysis in order to yield meaningful probable errors.

For the data with an average value of p_{H_2O}/p_{H_2} = 6.02, the value of the slope is 24.24 (±0.66) × 10^{-6} atm *per atmosphere* of water vapor and the value of the intercept is 3.49 (±0.18) × 10^{-6} atm. For the data at p_{H_2O}/p_{H_2} = 10.82, the values are 45.80 (±1.60) × 10^{-6} and 3.70 (±0.30) × 10^{-6}, respectively. There

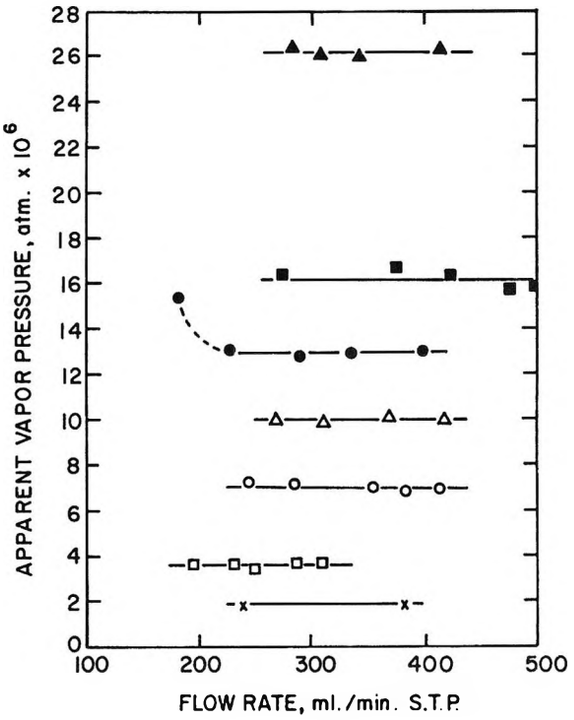

Figure 1. Typical results obtained from transpiration experiments with cobalt and nickel. Values of p_{H_2O}/p_{H_2}, p_{H_2O} (mm), and temperature are: ▲, Co, 9.56, 302.6, 1466°; ■, Co, 10.87, 237.0, 1427°; ●, Ni, 42.9, 307.6, 1422°; △, Co, 10.80, 109.8, 1436°; ○, Ni, 23.6, 374.1, 1390°; □, Co, 11.55, 336.2, 1275°; ×, Ni, 108.0, 400.6, 1175°.

Table I: The Volatility of Cobalt in the Presence of Water Vapor

Temp, °C	p_{H_2O}/p_{H_2}		p_{H_2O}, mm	App vapor pressure, atm × 10^6
1466	9.56		302.6	26.14
1466	9.68		69.9	11.17
1436	10.83		236.2	18.08
1436	10.80	10.82 av	109.8	9.96
1436	10.82		76.4	8.61
1436	5.96		328.7	13.72
1436	6.04	6.02 av	220.9	10.72
1436	6.04		151.4	8.42
1436	6.02		65.5	5.40
1427	10.87		237.0	16.15
1372	10.22		72.3	3.58
1370	10.07		312.1	9.95
1323	11.60		336.2	6.59
1275	11.55		336.2	3.66

are available two experimental studies of the vapor pressure of cobalt which are in excellent agreement, the

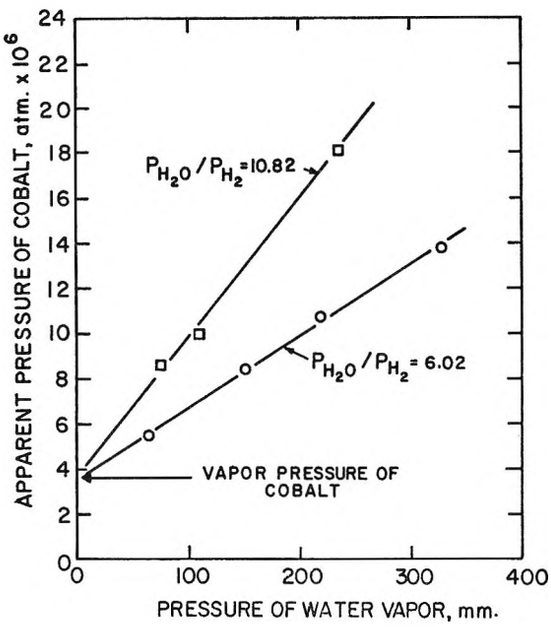

Figure 2. Dependence of volatility of cobalt on water pressure at constant water–hydrogen ratio at 1436°.

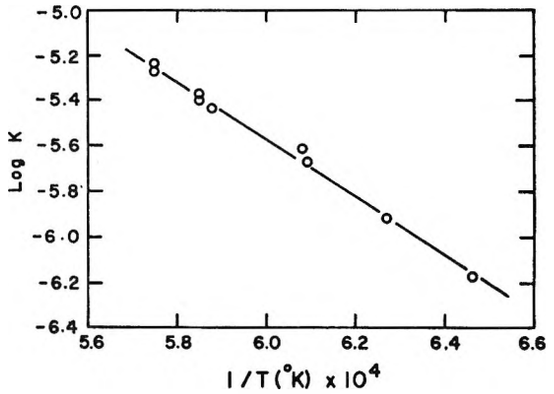

Figure 3. Temperature dependence of equilibrium constant for the reaction $Co + 2H_2O(g) = Co(OH)_2(g) + H_2(g)$.

Langmuir study of Edwards, *et al.*,[6] and the Knudsen cell work of Saxer.[7] These yield, when combined with published free energy functions,[8] a value of 101,400 ± 100 cal for ΔH°_{298} which in turn gives a value of 3.59 (±0.11) × 10^{-6} atm for the vapor pressure of cobalt at 1436°. Clearly, the values of the intercepts are experimentally indistinguishable from each other and from the vapor pressure of cobalt. Accordingly, it is assumed in the subsequent interpretation that no significant oxide contribution exists, this being consistent with the recently reported[9] vapor pressure of pure CoO, at this temperature, of approximately 2.7 × 10^{-8} atm.

Assuming that one atom of cobalt is incorporated in the hydrated species, the only stoichiometry which is consistent with the data within experimental error is $Co(OH)_2$. Considering this species, the formation reaction in the presence of H_2 and H_2O would be

$$Co + 2H_2O(g) = Co(OH)_2(g) + H_2(g) \qquad (1)$$

for which

$$K = (p_{Co(OH)_2})(p_{H_2})/(p_{H_2O})^2 \qquad (2)$$

At constant temperature, the apparent pressure of cobalt should be directly proportional to $(p_{H_2O}/p_{H_2})p_{H_2O}$. The necessary linear dependence on water pressure at constant water–hydrogen ratio is clearly shown in Figure 2, and the ratio of the slopes is 1.89 ± 0.11 for a ratio of the values of p_{H_2O}/p_{H_2} of 1.80. Any other single species would require errors of at least 50% in the measured equilibrium pressures.

Values of log K, derived from the slopes at 1436° and from the pressures listed in column 4 of Table I after deduction of the vapor pressure, are shown plotted against $1/T$(°K) in Figure 3. The best straight line calculated by the method of least squares is

$$\log K = -\frac{12{,}720\ (\pm 180)}{T} + 2.05\ (\pm 0.11) \qquad (3)$$

which gives for the standard Gibbs energy change of reaction 1

$$\Delta G^\circ = 58{,}200 - 9.38T \text{ cal} \qquad (4)$$

Nickel. The derived apparent vapor pressures of nickel and the corresponding experimental conditions are presented in Table II. In Figure 4 the data taken at 1390° with a value of p_{H_2O}/p_{H_2} of 23.6 are shown plotted against the pressure of water vapor. There is a clearly linear dependence with an intercept at zero water pressure which agrees with the vapor pressure of nickel, measured by means of an inert transporting gas.

The three most recent determinations[10] of the vapor pressure of nickel, when combined with the published free-energy functions,[8] yield a value for ΔH°_{298} of

(6) J. W. Edwards, H. L. Johnston, and W. E. Ditmars, *J. Am. Chem. Soc.*, 73, 4729 (1951).

(7) R. K. Saxer, Ph.D. Thesis, The Ohio State University, 1962.

(8) R. Hultgren, R. L. Orr, P. D. Anderson, and K. K. Kelley, "Selected Values of Thermodynamic Properties of Metals and Alloys," John Wiley and Sons, Inc., New York, N. Y., 1963.

(9) R. T. Grimley, R. P. Burns, and M. G. Inghram, *J. Chem. Phys.*, 45, 4158 (1966).

(10) J. P. Morris, G. R. Zellers, S. L. Payne, and R. L. Kipp, U. S. Bureau of Mines, Report of Investigations 5364, Mines Bureau, Pittsburgh, Pa., 1957; H. L. Johnston and A. L. Marshall, *J. Am. Chem. Soc.*, 62, 1382 (1940); G. P. Kovtun, A. A. Kruglykh, and V. S. Pavlov, *Ukr. Fiz. Zhur.*, 7, 436 (1962).

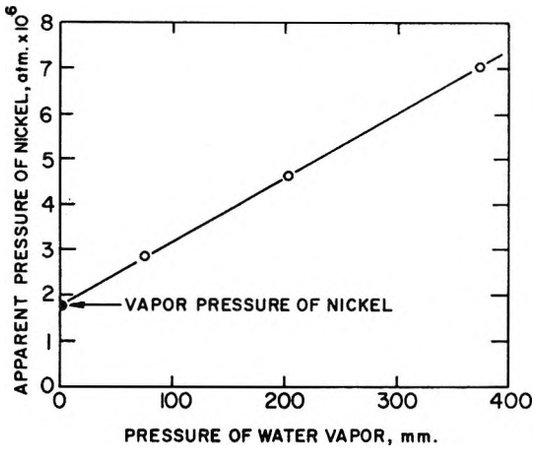

Figure 4. Dependence of volatility of nickel on water pressure at p_{H_2O}/p_{H_2} = 23.6 and 1390°.

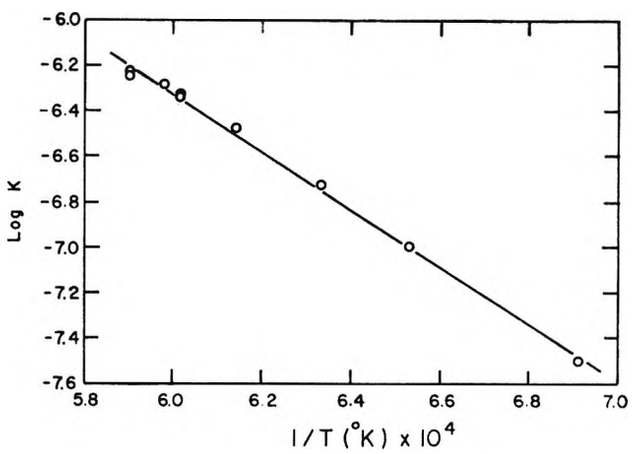

Figure 5. Temperature dependence of equilibrium constant for the reaction Ni + $2H_2O(g)$ = $Ni(OH)_2(g)$ + $H_2(g)$.

Table II: The Volatility of Nickel in the Presence of Water Vapor

Temp, °C	p_{H_2O}/p_{H_2}	p_{H_2O}, mm	App vapor pressure, atm × 10^6
1422	42.9	307.6	12.97
1422	16.0	307.6	7.00
1422	142.0[a]	307.6	28.10
1398	53.9	156.4	7.89
1398	53.9	91.6	5.86
1390	23.6	374.1	7.03
1390	23.6	204.0	4.62
1390	23.6	76.4	2.89
1390	53.9	348.0	13.26
1390	Inert Gas[b]		1.77
1356	80.1	342.0	13.22
1307	82.2	348.0	7.48
1258	81.3	348.0	3.90
1175	108.0	400.6	1.81

[a] Above the oxidation limit of nickel. [b] No significant difference could be detected between purified argon and hydrogen containing 3% water.

102,050 ± 490 cal, which gives 1.72 (±0.25) × 10^{-6} atm for the vapor pressure of nickel at 1390°. This is in agreement with the measured value of 1.77 × 10^{-6} atm and the least-mean-square value for the intercept of 1.82 (±0.09) × 10^{-6} atm. It is concluded that any contribution from NiO(g) may be safely ignored in the interpretation, and this is consistent with the mass spectrometric work of Grimley, Burns, and Inghram[11] on the vaporization of solid NiO. Their work gives, for unit activity of NiO at 1390°, p_{NiO} = 5 × 10^{-8} atm. At the reduced activity of NiO in the present work, the calculated contribution would be approximately 1.3 × 10^{-8} atm.

Again, if one metal atom is assumed to be incorporated in the gaseous species, the only equilibrium which is consistent with the data is

$$Ni + 2H_2O(g) = Ni(OH)_2(g) + H_2(g) \quad (5)$$

for which

$$K = (p_{Ni(OH)_2})(p_{H_2})/(p_{H_2O})^2 \quad (6)$$

The necessary linear dependence on water pressure at constant water–hydrogen ratio has already been shown in Figure 4. These same data yield a value for K of 4.66 (±0.12) × 10^{-7} from which one may readily calculate that, at the same temperature, with p_{H_2O}/p_{H_2} = 53.9 and p_{H_2O} = 348 mm, the expected total apparent pressure of nickel should be 12.80 (±0.34) × 10^{-6} atm. The experimentally determined value for these conditions (Table II) is 13.26 (±0.46) × 10^{-6} atm. In view of the similar behavior of iron and cobalt, this is considered to be sufficient evidence for the nature of the species.

Values of log K, derived from the data in Table II, after deduction of the vapor pressures, are shown plotted against $1/T$(°K) in Figure 5. The best straight line is given by

$$\log K = -\frac{12{,}740\ (\pm 210)}{T} + 1.32\ (\pm 0.13) \quad (7)$$

which gives for the standard Gibbs energy change of reaction 5

(11) R. T. Grimley, R. P. Burns, and M. G. Inghram, *J. Chem. Phys.*, **35**, 551 (1961).

$$\Delta G^\circ = 58{,}290 - 6.04T \text{ cal} \quad (8)$$

Although, in view of the stoichiometry of iron hydroxide,[2] it is reasonable to expect a single metal atom in the hydrated species of Co and Ni, it was considered desirable to obtain experimental confirmation for at least one of the species. Accordingly, experiments were carried out with nickel at 1422° with the water–hydrogen ratio adjusted to be well over the oxidation limit of nickel.

These experiments were carried out by using essentially the same procedure as before except that during the cooling cycle an argon–hydrogen gas mixture was passed over the samples in order to reduce the oxide film back to metal. A few preliminary experiments were carried out in which the nickel sample was exposed to the oxidizing atmosphere for about 1 min before cooling; these indicated that the errors introduced by the reduction step were negligible (approximately 1×10^{-5} g, *i.e.*, <1%). The experimental results are presented in Figure 6, and the derived pressure is given in Table II.

NiO is well known to form on Ni as a tenacious, nonporous layer;[12] hence, if equilibrium is assumed at the gas–solid interface, the activity of Ni may be readily calculated from the water–hydrogen ratio and a knowledge of the standard Gibbs energies of formation of NiO and H_2O. The study of Kiukkola and Wagner[13] indicates that the data for NiO in Coughlin[14] should be corrected by −930 cal to yield a value of −21.05 kcal for ΔG° at 1422°. This is in almost exact agreement with the value of −21.06 kcal extrapolated from the recent equation of Tomlinson and Young.[15] Using this value and the literature value of H_2O,[13] one readily calculates the activity of Ni to be 0.70 under the conditions of the experiment.

Combination of the above activity with the equilibrium constant from eq 7 and the partial pressures of hydrogen and water vapor yields a pressure of $Ni(OH)_2$ of 2.57×10^{-5} atm. Addition of the reduced vapor pressure of nickel gives a total apparent pressure of 2.79×10^{-5} atm: this is in excellent agreement with the measured apparent pressure of 2.81×10^{-5} atm. If a similar calculation is performed for the species $Ni_2(OH)_2$, the expected apparent pressure would be 2.02×10^{-5} atm. This latter value is well outside any reasonable experimental uncertainty.

As this interpretation depends strongly upon the accuracy of the thermodynamic data, a series of additional experiments was carried out at 1422°. In these, the water–hydrogen ratio which caused a distinct change in the surface of fresh nickel samples was determined. This gave a value for the oxidation limit of

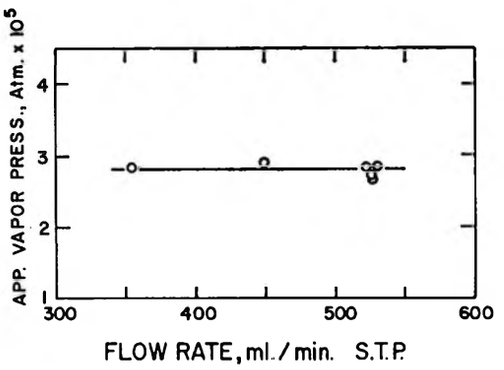

Figure 6. Results of transpiration experiments with nickel under oxidizing conditions at 1422°.

$p_{H_2O}/p_{H_2} = 97 \pm 1$, which compares very well with the value of 99 calculated from the above thermodynamic data.

Discussion

Errors. The uncertainties in the experimental variables are considered to be as follows: temperature, ±3°; p_{H_2O}, ±0.5%; weight losses, ±1.5%; gas volumes, ±1%. The combined effect of these uncertainties on the apparent pressure is estimated to be ±5%, this being consistent with the average standard deviation from the various plateaus of ±3.5%. In the absence of unknown systematic errors, the derived probable errors (eq 3 and 7) in the heat and entropy terms of the Gibbs energy equations (eq 4 and 8) of ±1 kcal and ±0.6 eu would appear to be realistic.

The Iron Group Hydroxides. The heats of formation and standard entropies of the iron group hydroxides, derived by combination of the literature data[8,16] with the Gibbs energy equations from this and the previous work,[2] are summarized in Table III. The relatively higher heat of formation of the iron species compared to those of the other species closely parallels the behavior of the gaseous dichlorides,[17] suggesting that the pseudohalide character noted for the hydroxides of the alkalis[18] and alkaline earths[19] may extend to the transi-

(12) O. Kubaschewski and B. E. Hopkins, "Oxidation of Metals," Butterworth and Co. Ltd., London, 1962.

(13) K. Kiukkola and C. Wagner, *J. Electrochem. Soc.*, **104**, 379 (1957).

(14) J. P. Coughlin, U. S. Bureau of Mines Bulletin 542, U. S. Government Printing Office, Washington, D. C., 1954.

(15) J. W. Tomlinson and D. R. Young, quoted by C. B. Alcock and T. N. Belford, *Trans. Faraday Soc.*, **60**, 822 (1964).

(16) "Joint Army–Navy–Air Force Thermochemical Tables," Dow Chemical Company, Midland, Mich., 1965.

(17) T. L. Allen, *J. Chem. Phys.*, **26**, 1644 (1953).

(18) R. C. Schoonmaker and R. F. Porter, *ibid.*, **31**, 830 (1959).

(19) F. E. Stafford and J. Berkowitz, *ibid.*, **40**, 2963 (1964).

tion metals. It is of interest, therefore, to derive the metal–hydroxyl radical bond energies for comparison with the halides.

Table III: Standard Heats of Formation and Standard Entropies of the Iron Group Gaseous Hydroxides at 1600°K

Species	$\Delta H_f°$, kcal	$S°$, eu
$Fe(OH)_2$[a]	80.9[a]	105.0[a]
$Co(OH)_2$	61.6	108.1
$Ni(OH)_2$	61.5	103.9

[a] Derived from Belton and Richardson (ref 2). Additional data for calculations taken from Hultgren, *et al.*, (ref 8) and "JANAF Tables" (ref 16).

No structural information is available for these gaseous molecules, and furthermore, in view of the high partial pressures of water vapor necessary in the formation equilibria, it is unlikely that spectroscopic studies can be made by existing techniques. Accordingly, in order to derive reasonable bond energies from the experimental data, it is necessary to estimate the structural parameters. The similarity of the experimental entropies at 1600°K strongly suggests that the species have similar basic structures; hence, estimates were first made in the manner of Stafford and Berkowitz[19] and then adjustments were made to give agreement between calculated and experimental entropies. The initial assignments were made as follows.

(1) A linear configuration was chosen for O–M–O in view of the evidence of Büchler, *et al.*,[20] for the linearity of the difluorides of these metals, and the hydrogen atoms were assumed to be in plane at 105° in a *cis* configuration.

(2) Brewer, *et al.*,[21] have assigned a bond length of 1.72 A for the difluorides; this was increased to 1.80 A for the M–O distance in view of the known difference in bond lengths between solid hydroxides and fluorides.[22] A distance of 0.96 A was selected for the O–H distance.[19]

(3) The symmetric and antisymmetric HO–M–OH stretching frequencies were estimated by applying the valence force method[23] to the stretching force constant for $NiF_2(g)$ of Milligan, *et al.*[24] This method gave 650 and 820 cm^{-1}. A value of 3650 cm^{-1}, based on water, was selected for the O–H stretching frequencies (2).

(4) The bending vibration for HO–M–OH was taken as 82 cm^{-1} by applying the valence force method and the Brewer, *et al.*,[21] estimate of the ratio of stretching to bending force constants for the transition metal halides. The two in-plane bending frequencies for the OH groups were taken as 1170 cm^{-1} by applying the method of Berkowitz, *et al.*,[25] to a comparison with water.

(5) The two out-of-plane torsional vibrations were taken as 230 cm^{-1}, similarly to gaseous H_2O_2.[26]

The values for the entropies at 1600°K calculated by standard methods[27] from the above parameters are 106.5, 106.7, and 105.9 eu for the Fe, Co, and Ni species, respectively. The electronic contributions were obtained, following Brewer and Chandrasekharaiah,[28] by a direct summation of the significant terms in the partition functions, taking the energy levels for Fe^{2+}, Co^{2+}, and Ni^{2+} from Moore's tabulation.[29] The calculated and experimental entropies are in surprisingly good agreement, thus demonstrating the reasonableness of the structure and the estimating procedure.

In order to obtain free energy functions better reflecting the experimental data, a change in the molecular parameters was made by adjusting the HO–Ni–OH bending vibration for the nickel species to give agreement with the experimental entropy. The derived ratio for stretching to bending force constants was then assumed to hold for the other species, and the three HO–M–OH vibrational frequencies adjusted accordingly to give agreement with the measured entropies. The assumed molecular parameters and derived free-energy functions are presented in Table IV.

The average bond energies M–OH, derived by the usual combination of thermochemical cycles and third-law calculations, are presented in Table V, the other data necessary to the calculations being taken from Hultgren, *et al.*,[8] and the "JANAF Tables."[16] Included in the same table are the single bond energies for the dichlorides and difluorides derived from Allen[17] and Brewer, *et al.*[21]

An assessment of the uncertainties in the derived bond energies is difficult, but on the basis of the in-

(20) A. Büchler, J. L. Stauffer, and W. Klemperer, *J. Chem. Phys.*, **40**, 3471 (1964).

(21) L. Brewer, G. R. Somayajulu, and E. Brackett, *Chem. Rev.*, **62**, 111 (1962).

(22) S. S. Batsanov and G. B. Bokii, *Zh. Strukt. Khim.*, **3**, 716 (1962).

(23) G. Herzberg, "Infrared and Raman Spectra of Polyatomic Molecules," D. Van Nostrand Co., Inc., New York, N. Y., 1945.

(24) D. E. Milligan, M. E. Jacox, and J. D. McKinley, *J. Chem. Phys.*, **42**, 902 (1965).

(25) J. Berkowitz, D. J. Meschi, and W. A. Chupka, *ibid.*, **33**, 533 (1960).

(26) R. L. Miller and D. F. Hornig, *ibid.*, **34**, 265 (1961).

(27) G. N. Lewis, M. Randall, K. S. Pitzer, and L. Brewer, "Thermodynamics," McGraw-Hill Book Co., Inc., New York, N. Y., 1961.

(28) L. Brewer and M. S. Chandrasekharaiah, University of California Radiation Laboratory Report UCRL 8713 (1959).

(29) C. E. Moore, "Atomic Energy Levels," Vol. 2, National Bureau of Standards Circular 467, U. S. Government Printing Office, Washington, D. C., 1952.

Table IV: Estimated Molecular Structure Parameters Used to Calculate the Free-Energy Functions of the Hydroxides

	Fe	Co	Ni
r_e (M–O), A	1.8	1.8	1.8
r_e (O–H), A	0.96	0.96	0.96
O–H (2), stretch, cm^{-1}	3650	3650	3650
M–OH, stretch, cm^{-1}	605	365	650
	770	460	820
O–M–O, bend, cm^{-1}	210	125	222
M–O–H (2), bend, cm^{-1}	1170	1170	1170
MO–H (2), torsion, cm^{-1}	230	230	230
M–O–H angle, deg	105°	105°	105°
Electronic fef (1600°K), eu	−5.75	−5.54	−4.89
Fef (1600°K), eu	−82.56	−83.50	−81.50

sensitivity of the results to a number of manipulations of the structural parameters, *e.g.*, assuming a *trans* configuration or free internal rotations of the OH groups, it is the authors' opinion that the values should be correct to about ±2 kcal, at least in comparison to the halides.

Table V: Average Bond Energies, 0°K, of Fe, Co, and Ni Difluorides, Dihydroxides, and Dichlorides[a]

	Fe	Co	Ni
M–F, kcal	114.3	110.8	109.3
M–OH, kcal	98.2	91.9	91.2
M–Cl, kcal	94.9	85.3	86.0

[a] Data for dichlorides and difluorides derived from Allen[17] and Brewer, *et al.*[21]

Thus it appears that treating the gaseous hydroxides as pseudohalides is a useful concept, and consistently with this, the bond energies may be taken to be approximately midway between the fluorides and chlorides.

Acknowledgment. This study, a contribution from the Laboratory for Research on the Structure of Matter, University of Pennsylvania, was supported by the Advanced Research Projects Agency, Office of the Secretary of Defense.

NOTES

The Influence of Pressure on the Velocity Constants of Bimolecular Ionic Reactions in Aqueous Solution

by E. A. Moelwyn-Hughes

Department of Physical Chemistry, The University, Cambridge, England

Accepted and Transmitted by The Faraday Society (March 10, 1967)

The bimolecular velocity constant for ionic reactions at zero ionic strength can be represented by the equation[1]

$$\ln k_2^0 = \ln Z_2^0 - \frac{E_n}{RT} - \frac{z_A z_B \epsilon^2}{DrkT} \qquad (1)$$

where Z^0 is the standard binary collision frequency in a solvent of dielectric constant D at temperature T. Concerning E_n, the nonelectrostatic component of the activation energy, little is known. The electrostatic component, $z_A z_B \epsilon^2/Dr$, is given by the electrovalencies, z, the electronic charge, ϵ, the dielectric constant, D, and the distance apart of the centers of the charges in the activated complex. By treating Z^0, E_n, and r as temperature independent, eq 1 has been shown adequate to explain high and low values of the preexponential term in the Arrhenius equation, $\ln k_2^0 = \ln A_2^0 - E_A/RT$. We have[2]

$$A_2^0 = Z_2^0 e^{-z_A z_B \epsilon^2 L/kDr} \qquad (2)$$

where $L = -(\partial \ln D/\partial T)_P$. The object of this communication is to find to what extent eq 1 may account for the variation of k_2^0 with respect to pressure at constant temperature.

(1) J. A. Christiansen, *Z. Physik. Chem.*, **113**, 35 (1924); G. Scatchard, *Chem. Rev.*, **10**, 229 (1932).

(2) E. A. Moelwyn-Hughes, *Proc. Roy. Soc.* (London), **A155**, 308 (1936).

By differentiating eq 1 and making use of the equation

$$\Delta V_c = -RT\left(\frac{\partial \ln k_2^0}{\partial P}\right)_T \quad (3)$$

we obtain for the molar volume of critical activation the expression

$$\Delta V_c = -RT\left(\frac{\partial \ln Z_2^0}{\partial P}\right)_T + \left(\frac{\partial E_n}{\partial P}\right)_T - \frac{z_A z_B \epsilon^2 N_0}{Dr}\left[\left(\frac{\partial \ln r}{\partial P}\right)_T + \left(\frac{\partial \ln D}{\partial P}\right)_T\right] \quad (4)$$

where N_0 is Avogadro's number. A rough estimate of the first term on the right-hand side may be made by assuming Z_2^0 to be proportional, directly or inversely, to the viscosity of the solvent. For water at 30°, the contribution to ΔV_c is -1.15 or $+1.15$ cc, respectively. Nothing is known about $(\partial E_n/\partial P)_T$ except that it may be considerable. If the reacting ions and the complex formed from them are all spherical, with evenly distributed charges, it is possible in principle to evaluate the term $(\partial \ln r/\partial P)_T$ in terms of the partial ionic compressibilities, β_i, as Hamann[3] has shown in the case of the ionization of ammonium hydroxide. None of the reacting species to be considered approaches such a simple electrostatic model and we remain in ignorance of the magnitude of $(\partial \ln r/\partial P)_T$. To evaluate the remaining term in eq 4, it is convenient to use the compressibility, β, and the density, ρ, of the solvent, as

$$\left(\frac{\partial \ln D}{\partial P}\right)_T = \left(\frac{\partial \ln D}{\partial V}\right)_T\left(\frac{\partial V}{\partial P}\right)_T = -\beta\left(\frac{\partial \ln D}{\partial \ln V}\right)_T = \beta\left(\frac{\partial \ln D}{\partial \ln \rho}\right)_T \quad (5)$$

The contribution to ΔV_c ascribable to the effect of pressure on the dielectric constant is thus

$$\Delta V_c = -\frac{N_0 z_A z_B \epsilon^2 \beta}{Dr}\left(\frac{\partial \ln D}{\partial \ln \rho}\right)_T \quad (6)$$

The compressibility of water at 20° is 4.68×10^{-5} atm^{-1} and $(\partial \ln D/\partial \ln \rho)_T$ is 1.34 ± 0.02.[4] Hence, with ΔV_c in cubic centimeters per mole and r in angstrom units

$$\Delta V_c = -\frac{10.7(z_A z_B)}{\mathring{r}} \quad (7)$$

Because ΔV_c varies with the pressure, we have used the experimental values relating to low pressures. These are given in Table I, where, unfortunately, only two of the data refer to temperatures near to that for which eq 7 applies. For these two reactions, the values of the critical interionic separation afforded by eq 7 compare favorably with the values found by numerous independent methods.[5] It therefore appears that the effect of pressure on the velocity of ionic reactions in aqueous solution is significantly, if not predominantly, to be traced to the effect of pressure on the dielectric constant of the medium.

Table I: Critical Interionic Distances Afforded by Eq 7

Reaction	Ref	Temp, °C	ΔV_c	$z_A z_B$	$\mathring{r}$, A
$CH_2ClCOO^- + OH^-$	*a*	40	−6.1	+1	1.75
$NH_4^+ + NCO^-$	*b*	60	+14	−1	0.76
$CH_2BrCOO^- + S_2O_3^{2-}$	*c*	24.5	−4.8	+2	4.46
$Co(NH_3)_5Br^{2+} + OH^-$	*c*	30	+8.5	−2	2.52

[a] R. O. Gibson, E. W. Fawcett, M. W. Perrin, and E. G. Williams, *Proc. Roy. Soc.* (London), **A150**, 223 (1935); **154**, 684 (1936). [b] H. G. David and S. D. Hamann, *Trans. Faraday Soc.*, **50**, 1188 (1954). [c] C. T. Buriss and K. J. Laidler, *ibid.*, **51**, 1497 (1955).

Christiansen's theory of bimolecular reactions in solution has been applied to interpret the effect of pressure on the velocity constants of ionic reactions at zero ionic strength. It is concluded that the effect of pressure on the reaction rate is significantly, if not predominantly, to be traced to the effect of pressure on the dielectric constant of the medium.

(3) "Physicochemical Effects of Pressure," Butterworth and Co., Ltd., London, 1957.

(4) I. S. Jacobs and A. W. Lawson, *J. Chem. Phys.*, **20**, 1161 (1952).

(5) E. A. Moelwyn-Hughes, "Kinetics of Reactions in Solution," 2nd ed, Oxford University Press, London, 1947, p 106.

The Dehydrogenation Reaction of Methanol during Electrosorption on Platinum

by R. E. Smith, H. B. Urbach, and N. L. Hatfield

U. S. Navy Marine Engineering Laboratory, Annapolis, Maryland *(Received March 22, 1967)*

Radiometric evidence of a reduction of hydrogen–carbon bond strengths in the methanol molecule when adsorbed from solution on a platinum black electrode has been obtained in a continuing study[1] of electrosorp-

(1) R. E. Smith, H. B. Urbach, J. H. Harrison, and N. L. Hatfield, *J. Phys. Chem.*, **71**, 1250 (1967).

tion processes undertaken as part of this laboratory's investigation of fuel cell electrodes.

A platinum black working electrode (effective area of 3 m^2) of an experimental three-electrode cell was maintained as a fixed potential of 0.2 v *vs.* the reversible hydrogen electrode (rhe) in the same system. The normal sulfuric acid solution of 40 ml was injected with sufficient ^3H- and ^{14}C-labeled methanol to produce a methanol concentration of 10^{-3} molarity. As reported previously,[1] methanol is adsorbed on platinum black so that the observed bulk methanol concentration decreases with time. Thus the anticipated concentration of methanol as indicated by the ^{14}C and ^3H assay should decrease. The activity of each isotope in the solution was determined as a function of time by analysis of 50-μl samples of the electrolyte with a liquid scintillation spectrometer in 15-min intervals. The results of these experimental assays are shown in Figure 1 as a plot of the individual isotope activities dpm (disintegrations per minute) in the electrolyte *vs.* time in minutes. The decrease in the ^{14}C activity with time due to methanol adsorption on the electrode was consistent with previous studies[1] employing ^{14}C-labeled methanol. However, the failure to detect a decrease in the ^3H activity is anomalous and may be attributed to the accelerated dehydrogenation and/or exchange of carbon-bonded hydrogen from methanol when the molecule is in the adsorbed state. The rate of these reactions must be at least as great as the over-all adsorption rate to preclude the detection of tritium removal from the solution.

This conclusion is validated by studies of the ^3H to ^{14}C ratio in methanol-containing aqueous solutions before and after contact with platinum (at open-circuit conditions). Solutions prepared from methanol labeled with ^3H and ^{14}C in 3:1 ratio were shaken together with various lengths of platinum wire coated with platinum black in a thermostated shaking bath for 16 hr. Methanol was removed from the aqueous solutions for analysis by liquid–liquid extraction with toluene.

Since the aqueous solution is insoluble in the organic phase, only ^3H bonded to the carbon atom in the methanol molecule can be detected. The ^3H to ^{14}C ratio after a 16-hr test at 30 and 63° is shown as a function of electrode area in Figure 2. The rapid decay of the ratio, which is observed at both temperatures, is indicative of the loss of ^3H from the organic molecule to the inorganic aqueous phase and confirms the hypothesis that carbon-bonded hydrogen on adsorbed methanol molecules undergoes rapid exchange or dehydrogenation. Examination of the temperature coefficient of the process indicates that the rate-limiting factor may be

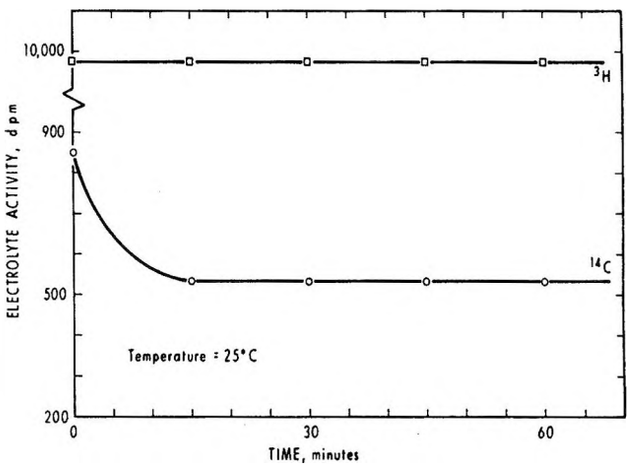

Figure 1. Isotopic activity of radio-labeled methanol solutions containing platinum electrodes. Electrode potential was maintained at 0.2 v rhe.

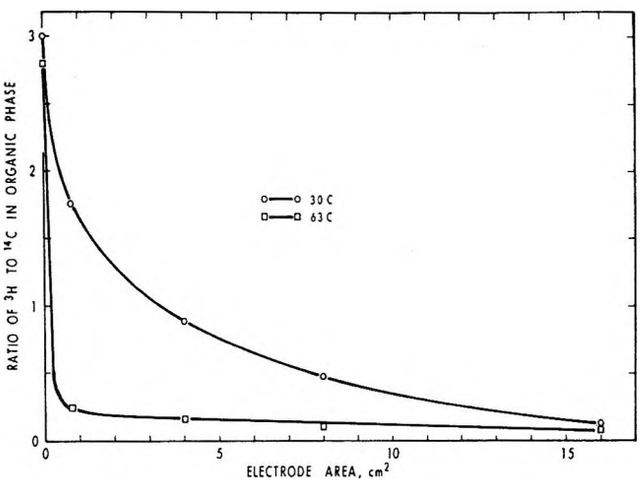

Figure 2. Effect of electrode area on isotope activity in the toluene phase after extraction from radio-labeled methanol–electrolyte solution.

diffusion since the rough activation energy is of the order of 4 kcal.

It is possible to interpret the observed data as both a dehydrogenation and an exchange phenomenon. It appears that the dehydrogenation process is more probable on the basis of the data of Podlovchenko and coworkers[2-4] and Bagotsky, *et al.*[5-8] The results re-

(2) B. I. Podlovchenko and Z. A. Jofa, *Zh. Fiz. Khim.*, **38**, 211 (1964).

(3) B. I. Podlovchenko and E. P. Gorgonova, *Dokl. Akad. Nauk SSSR*, **156**, 673 (1964).

(4) B. I. Podlovchenko, O. A. Petry, and A. N. Frumkin, *ibid.*, **153**, 379 (1963).

(5) V. S. Bagotsky and Yu. B. Vassiliev, *Electrochim. Acta*, **11**, 1439 (1966).

ported herein therefore constitute quite plausible direct evidence for the dehydrogenation mechanisms proposed on indirect grounds by previous investigators.[5,6] The existence of these mechanisms lends support to the dissociative theory of electrosorption and explains in part the activation of hydrocarbons undergoing anodic oxidation.

Acknowledgment. The motivation and encouragement of J. H. Harrison, who initiated this program of study, is gratefully acknowledged. The opinions or assertions expressed herein are those of the authors and are not to be construed as official or reflecting the views of the Department of the Navy or the naval service at large.

(6) D. A. Khazova, Yu. B. Vasiliev, and V. S. Bagotsky, *Elektrokhimiya*, 2, 267 (1966).

(7) M. W. Breiter and S. Gilman, *J. Electrochem. Soc.*, **109**, 622, 1099 (1962).

(8) J. Giner, *Electrochim. Acta*, 9, 63 (1963).

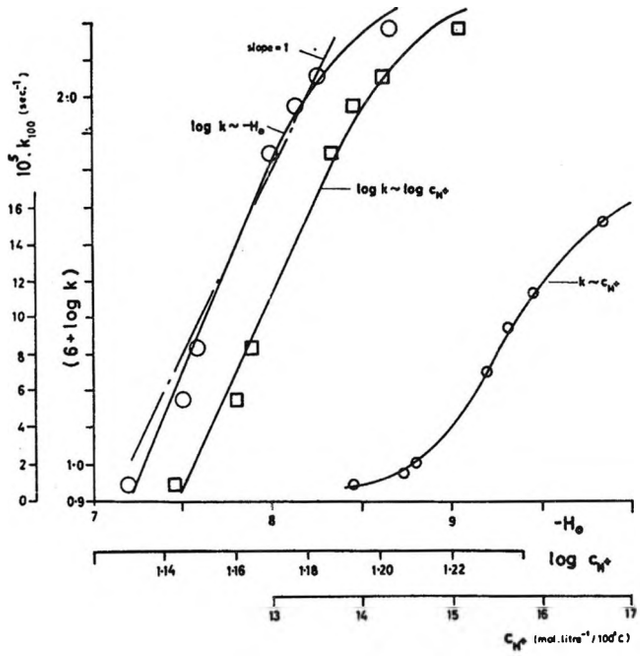

Figure 1. Variation of rate with sulfuric acid strength at 100°.

Kinetics of Isomerization of 1,8-Dichlorofluorenone in Sulfuric Acid Solution

by E. V. Murphy and W. E. Silbermann

Department of Chemistry, University College, Belfield, Dublin 4, Ireland

Accepted and Transmitted by The Faraday Society (March 28, 1967)

Observations reported[1] from investigations of the isomerization of 1,8-dichlorofluorenone and 1,6-dichlorofluorenone, each to 3,6-dichlorofluorenone, on heating in strong sulfuric acid solution suggest that the 1,6 isomer is an intermediate in the conversion of the 1,8 compound.

Preliminary experiments soon established that 1,8-dichlorofluorenone in fact isomerizes quantitatively to the 1,6 compound in aqueous sulfuric acid under relatively mild conditions. The kinetics of this change have been examined in sulfuric acid–water mixtures containing from 81.8 to 93.4% w/w H_2SO_4 and at temperatures between 100 and 116°. (The range of acidity in which accurate kinetic measurements can be made is limited at one end by insolubility of the compounds in weaker acid solutions and at the other by onset of side reactions in solutions of strength close to that of the concentrated acid.)

The isomerization has been found to be of simple first order; the experimental activation energy (E_a) has been determined as 32.9 kcal mole^{-1} in 93.3% H_2SO_4 solution and 34.8 kcal mole^{-1} in 84.0% H_2SO_4, subject to an estimated uncertainty of ±1.5 kcal mole^{-1}. The corresponding entropies of activation (ΔS^*) at 100°, calculated from the usual "absolute rate" formula,[2] $k = (kT/h) \exp(-\Delta H/RT) \exp(\Delta S^*/R)$, are 9.5 and 10.5 (±4.0) cal deg^{-1} mole^{-1}, respectively.

Figure 1 shows variation of the rate constant at 100° (k_{100}) with stoichiometric concentration of sulfuric acid (c_{H^+}) alongside plots of log k_{100} against the Hammett acidity function[3] ($-H_0$) for 25° and of log k_{100} against log c_{H^+}. Apart from the point for the highest acidity (at which quite possibly more complex changes begin to appear), the log $k \sim -H_0$ plot is very nearly linear with a best slope of 1.13; the slope of the log $k \sim$ log c_{H^+} plot is approximately 21. Thus the results fit fairly well the theoretical correlation[4] between rate and H_0 for a mechanism ("A-1") involving first-order conversion of the protonated reactant as the

(1) E. H. Huntress and E. R. Atkinson, *J. Am. Chem. Soc.*, 58, 1514 (1936).

(2) "Technique of Organic Chemistry," Vol. 8, Part 1, A. Weissberger, Ed., 2nd ed, Interscience Publishers, Inc., New York, N. Y., 1961, p 200.

(3) L. P. Hammett, "Physical Organic Chemistry," McGraw-Hill Book Co., Inc., New York, N. Y., 1940; Chapter IX; M. A. Paul and F. A. Long, *Chem. Rev.*, 57, 1 (1957).

(4) M. A. Paul and F. A. Long, *ibid.*, 57, 935 (1957).

rate-controlling step. The "A-2" (bimolecular) mechanism, which would be indicated by proportionality of the rate constant to c_{H^+}, is clearly excluded. This finding, together with the fairly large activation energy and the positive value of the entropy of activation, is considered to support the following sequence.

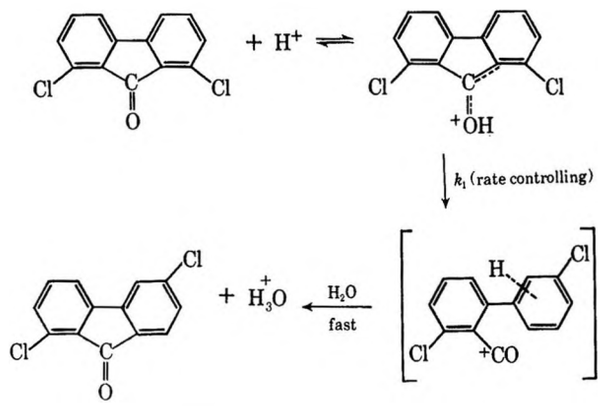

Experimental Section

Materials. 1,8-Dichlorofluorenone was prepared by the method of Huntress and Cliff.[5] The yellow product was crystallized from benzene to constant melting point (257° uncor, lit. mp 254°) and reproducible ultraviolet spectrum in cold concentrated H_2SO_4 solution.

1,6-Dichlorofluorenone was prepared for identification purposes essentially by the method of Huntress and Cliff.[5] The crude product was freed of acidic material by extraction with sodium bicarbonate solution; it was purified by sublimation *in vacuo* and by crystallization from benzene until bright yellow crystals, constant mp 215–216° uncor (lit. mp 218–219°), showing reproducible ultraviolet spectrum in cold concentrated H_2SO_4 were obtained.

Sulfuric acid solutions were prepared from AnalaR concentrated acid and triply distilled water.

Apparatus. Ultraviolet absorption measurements were made on a Unicam SP 500 spectrophotometer with matched 1-cm silica cells. Kinetic runs were carried out in 35-ml glass-stoppered Pyrex tubes held in a vapor bath thermostat as previously described.[6] Temperature constancy to within ±0.15° was maintained during each run.

Isomerization. Samples of 1,8-dichlorofluorenone were heated in approximately 93% aqueous H_2SO_4 at 100° for 24 hr; the solution was poured onto ice. Recovery of the precipitated yellow solid was quantitative. The purified product gave mp 215–216°, ultraviolet spectrum identical with that of 1,6-dichlorofluorenone prepared separately, and mixture melting point with the latter undepressed at 215–216°. (Heating of the 1,8 compound in 98% H_2SO_4 at somewhat above 200° resulted in failure to recover a solid product, probably because of sulfonation.)

Analytical Method. The dichlorofluorenones showed the following ultraviolet absorption properties in cold concentrated sulfuric acid solution.

Compd	λ_{max}, mμ	ε (264 mμ)	ε (274.5 mμ)
1,8	264	31,730	23,530
1,6	274.5	29,500	45,000

The Beer–Lambert law was accurately obeyed by each isomer; it was thus possible to analyze a solution containing both compounds by optical density measurements at each of the two wavelengths.[7] The spectrophotometric procedure was tested on synthetic mixtures of the isomers in cold concentrated H_2SO_4 and gave results good to within 2%.

Kinetic Procedure. Because of the slow rate of solution of 1,8-dichlorofluorenone in the aqueous acid, it was found convenient to start a run by adding 10 ml of a solution of the compound prepared in concentrated H_2SO_4 at room temperature to a measured volume (10 ml at room temperature) of aqueous acid preheated in the thermostat. At timed intervals, 2-ml pipet samples were taken from the reaction mixture, run into cold concentrated H_2SO_4, and at once diluted to large standard volume with the stock cold concentrated acid; the resulting solutions were analyzed as soon as possible. The sulfuric acid strength was determined at the end of each run by alkali titration of a weighed sample. Simultaneously with each run a "blank" solution of the same acid content as the reaction mixture was prepared for use in the spectrophotometric analysis.

The reaction always showed strictly first-order kinetics; runs were taken to as near completion as reasonably possible (more than 80%) and rate constants were evaluated from linear plots of log (A_0/A_t) against time (t); (A_t = instantaneous concentration of 1,8 isomer; A_0 = initial concentration of 1,8 isomer = sum of concentrations of the two isomers, which was also checked against the "made-up" concentration, with due correction for volume change on heating). Reproducibility of rate constants was tested by running duplicate reactions at the same temperature and taking samples alternately from one mixture and the other; ex-

(5) E. H. Huntress and I. S. Cliff, *J. Am. Chem. Soc.*, **55**, 2559 (1933).

(6) T. Henshall, W. E. Silbermann, and J. G. Webster, *ibid.*, **77**, 6656 (1955); W. E. Silbermann and T. Henshall, *ibid.*, **79**, 4107 (1957); D. M. March and T. Henshall, *J. Phys. Chem.*, **66**, 840 (1962).

(7) A. E. Gillam and E. S. Stern, "Electronic Absorption Spectroscopy," 2nd ed, Edward Arnold and Co., London, 1952, p 214; G. F. Lothian, "Absorption Spectrophotometry," Adam Hilger Ltd., London, 1949, p 59.

cellent conformity to a single plot of log $(A_0/A_t) \sim t$ was always obtained.

Activation Energy (E_a). Rate constants were measured at different temperatures for each of two acidities; E_a was found from the linear plots of $(5 + \log k)$ against T^{-1} (Table I).

Table I

T, °K	374.6	382.4	388.7	372.4	382.1	389.2
10^5k, sec^{-1}	15.2	38.8	77.5	1.50	5.38	11.2
	93.3% H_2SO_4			84.0% H_2SO_4		
E_a, kcal $mole^{-1}$	32.9			34.8		

Effect of Acidity. Rate constants were measured at 100° for each of seven acid strengths; the results are shown in Figure 1. Stoichiometric concentration of sulfuric acid (c_{H^+}) was calculated using standard density data.[8]

(8) "International Critical Tables," Vol. 3, McGraw-Hill Publishing Co., Inc., New York, N. Y., 1928, p 57.

The Critical Surface Tension of Sapphire[1]

by J. G. Eberhart

Sandia Laboratory, Albuquerque, New Mexico
(Received April 21, 1967)

Zisman[2] has shown that if a single solid is wet by a homologous series of liquids, then the cosine of the contact angle, $\cos\theta$, is a linear function of the surface tension of the liquid, σ_{LV}. Zisman calls the value of σ_{LV} corresponding to complete wetting ($\theta = 0$) the critical surface tension of wetting, σ_C, and has shown that σ_C is a property of the solid surface only. This linear relationship has been demonstrated primarily for low surface tension organic liquids on low surface tension solids such as polymers or metals covered by monolayers of long chain organic acids. The correlation also appears to be valid for liquids and solids with intermediate surface tensions, as was demonstrated by Olsen and Osteraas[3] in their consideration of existing data on the wetting of glass by low melting point metals.

In order to test Zisman's relationship for the wetting of high surface tension solids by high surface tension liquids, the studies of a number of authors on the wettability of sapphire by liquid transition metals[4,5] and the surface tension of liquid transition metals[6,7] are examined here.

Armstrong, Chaklader, and Clarke[4] measured the contact angle of pure liquid Ni and its alloys with Ti, Cr, and Zr, under vacuum, at 1500°, on a solid sapphire surface approximately coincident to the $\langle 10\bar{1}2\rangle$ plane. The alloys with Ti and Cr were explored over compositions ranging from pure Ni to 9% Ti and to 19% Cr. In both alloys the contact angle decreased through an inflection point (at ~1.5% Ti and 8% Cr) and then leveled off to a constant terminal value with increasing Ti or Cr composition. Additional experiments and calculations made by Armstrong, *et al.*, showed that Ti or Cr was preferentially adsorbed at the solid–liquid interface. Because of the strong preferential adsorption, it is assumed that the terminal value of θ is the value θ would have for pure Ti or Cr at that temperature. Only one composition of the Zr alloy was studied (10% Zr) and this was also assumed to be the value of θ for pure Zr. Thus from the data of Armstrong, *et al.*, values of 108, 85, 83, and 75° are extracted as representing the contact angle of the pure liquids Ni, Ti, Cr, and Zr, respectively, on Al_2O_3 at 1500°.

More recently, Ritter and Burton[5] published additional measurements of the contact angle of pure Ni and its alloys with Ti and Cr on a $\langle 10\bar{1}2\rangle$ sapphire surface at 1500°. Assuming again that θ for the highest alloy concentration is characteristic of the solute only, values of 111.3 and 90° are found for Ni and Cr, respectively, under vacuum. The Ti alloys were not studied under vacuum, but since the terminal Cr contact angle showed no atmospheric dependence, the Ar atmosphere value of 84° is employed for Ti.

The surface tension of the above pure liquids has been determined by numerous authors. The values selected here are 1924 dynes/cm[6] for Ni at 1550° and 1650, 1700, and 1480 dynes/cm[7] for liquid Ti, Cr, and Zr, respectively, at their melting points. These particular values are among the highest reported, which suggests high sample purity. Assuming a typical temperature

(1) This work was supported by the U. S. Atomic Energy Commission.

(2) (a) W. A. Zisman, *Ind. Eng. Chem.*, **10**, 19 (1963); (b) W. A. Zisman, Advances in Chemistry Series, No. 43, R. F. Gould, Ed., American Chemical Society, Washington, D. C., 1964, pp 1–51.

(3) D. A. Olsen and A. J. Osteraas, *J. Phys. Chem.*, **68**, 2730 (1964).

(4) W. M. Armstrong, A. C. D. Chaklader, and J. F. Clarke, *J. Am. Ceram. Soc.*, **45**, 115 (1962); and J. F. Clarke, M.Sc. Thesis, University of British Columbia, Canada, 1959.

(5) J. E. Ritter, Jr., and M. S. Burton, *Trans. Met. Soc. AIME*, **239**, 21 (1967).

(6) P. Kozakevitch and G. Urbain, *J. Iron Steel Inst.*, **186**, 167 (1957).

(7) B. C. Allen, *Trans. Met. Soc. AIME*, **227**, 1175 (1963); **230**, 1357 (1964).

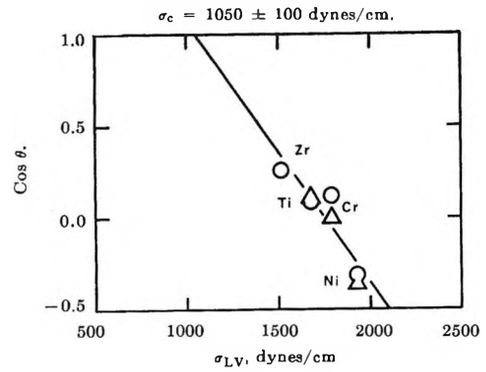

Figure 1. Cosine of the contact angle *vs.* surface tension for liquid transition metal sessile drops on solid sapphire at 1500° under vacuum: O, Armstrong, Chaklader, and Clarke;[4] △, Ritter and Burton.[5]

coefficient of $d\sigma_{LV}/dT = -0.1$ dyne/cm deg, the surface tension values of the liquids at 1500° are then estimated as approximately 1930, 1680, 1790, and 1515 dynes/cm for Ni, Ti, Cr, and Zr, respectively.

In Figure 1 the wetting and surface tension data considered above are plotted as prescribed by Zisman. The points do define the usual linear relationship between cos θ and σ_{LV} with the negative slope which has always been found characteristic of this correlation. The least-squares intercept of the linear curve at $\theta = 0$ gives a critical surface tension for Al_2O_3 at 1500° of $\sigma_C = 1050 \pm 100$ dynes/cm. The slope of the curve is $A = -0.00143$ cm/dyne. With these two parameters and the Zisman equation, $\cos\theta = 1 + A(\sigma_{LV} - \sigma_C)$, the contact angle of other liquid transition metals on sapphire can be estimated.

The view is held by some authors[8,9] that the critical surface tension, σ_C, is equal to the solid–vapor interfacial tension, σ_{SV}, *i.e.*, the solid–vacuum surface tension, σ_{SO}, minus the spreading pressure of any adsorbed layer present, π. Olsen and Osteraas[3] found excellent agreement between σ_C and $\sigma_{SO} - \pi$ in their analysis of glass wettability. Thus although this interpretation of σ_C has been criticized,[10] it is nonetheless of interest to compare the above value of σ_C with the surface tension of solid Al_2O_3. The surface tension of sintered solid Al_2O_3 has been determined by Kingery[11] to be $\sigma_{SV} = 905$ dynes cm at 1850°. Assuming a temperature coefficient of $d\sigma_{SV}/dT = -0.1$ dyne/cm deg the surface tension is estimated as 940 dynes/cm at 1500°. This value is in reasonably good agreement with the above critical surface tension of $\sigma_C = 1050 \pm 100$ dynes/cm.

The liquid transition metal–sapphire system considered here differs in several ways from the organic systems in which almost all previous Zisman-type analyses have been done. First, in liquid metal wetting, it is difficult at present to identify the analog of Zisman's requirement that the liquids be members of a homologous series. In the absence of data on a greater variety of liquid metals on sapphire, it would seem reasonable to restrict tentatively the above correlation to transition metals. Second, although steady contact angles were obtained in both the wetting studies employed,[4,5] evidence of chemical reaction was found at the solid–liquid interfaces in the form of the oxide of the liquid metal. Caution must always be exercised in dealing with wetting in reacting systems; for example, the validity of Young's equation is doubtful. However, Zisman's equation is empirical in nature and its applicability in reacting systems can only be decided by experimental test. The above linear correlation is preliminary evidence that the equation can be applied to some reacting systems.

(8) E. Wolfram, *Kolloid Z.*, **182**, 75 (1962).

(9) V. R. Gray, *Chem. Ind.* (London), 969 (1965).

(10) M. C. Phillips and A. C. Riddiford, *Z. Physik. Chem.*, **47**, 17 (1965).

(11) W. D. Kingery, *J. Am. Ceram. Soc.*, **37**, 42 (1954).

Helix Formation of Poly-L-lysine Thiocyanate in Aqueous Solutions

by D. Puett, A. Ciferri,

Chemstrand Research Center, Inc., Durham, North Carolina 27702

Estella Bianchi,[1a]

Istituto di Chimica Industriale dell'Universita' Genova, Genova, Italy

and Jan Hermans, Jr.[1b]

Department of Biochemistry, University of North Carolina, Chapel Hill, North Carolina *(Received May 17, 1967)*

Aqueous solutions of poly-L-lysine serve as a model for basic proteins, since, particularly under alkaline conditions, this polypeptide may form α-helices and can exist in a β conformation.[2,3] Furthermore, the polyelectrolyte effects occurring at low pH allow one to

(1) (a) Supported in part by the National Research Council of Italy (Centro Virus Vegetali). (b) Research Career Awardee of the U. S. Public Health Service (Grant GM-22015). Supported in part by a research grant from the National Institutes of Health.

(2) (a) K. Rosenheck and P. Doty, *Proc. Natl. Acad. Sci., U. S.*, **47**, 1775 (1961); (b) P. K. Sarkar and P. Doty, *ibid.*, **55**, 981 (1966).

(3) B. Davidson, N. Tooney, and G. D. Fasman, *Biochem. Biophys. Res. Commun.*, **23**, 156 (1966).

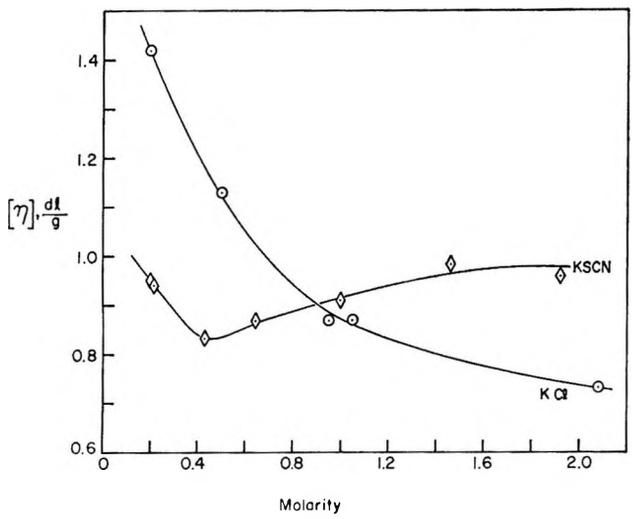

Figure 1. The dependence of the intrinsic viscosity $[\eta]$ of poly-L-lysine (Sigma Type I, Lot 115B-0700, M_w 150,000, obtained as hydrobromide) on KCl and KSCN concentration at pH 3.2 and at 25°. Measurements were performed as described elsewhere.[11]

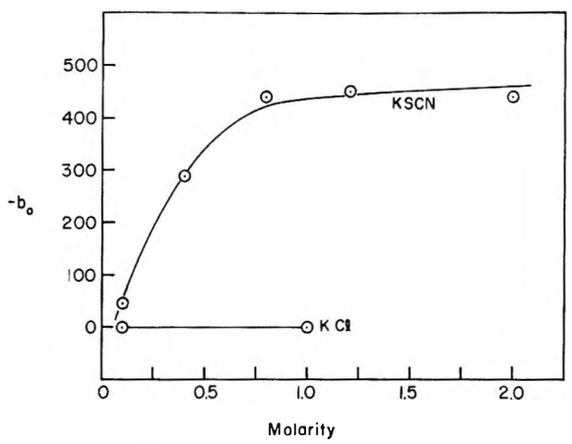

Figure 2. The variation of b_0 of poly-L-lysine with the concentration of KCl and KSCN at pH 3.2. (Measurements were obtained with a Durrum-Jasco ORD/UV-5 instrument using 1-, 5-, and 10-mm cells. The polymer concentration was varied between 0.4 and 4 mg/ml. The wavelength range was 300–550 mμ and λ_0 was taken to be 212 mμ. The refractive index of water was used in calculating the reduced mean residue rotation, and the refractive index dispersion was estimated from Table III of Fasman[14]). T, 25°.

study the stability of the various conformations by varying the degree of ionization. Thus, helix–coil transitions of poly-L-lysine in aqueous media have been studied by several investigators[4–7] and it was shown that the degree of dissociation of the ε-amino group affects the conformation of the molecule as expected from simple considerations of the electrostatic free energy.[8,9]

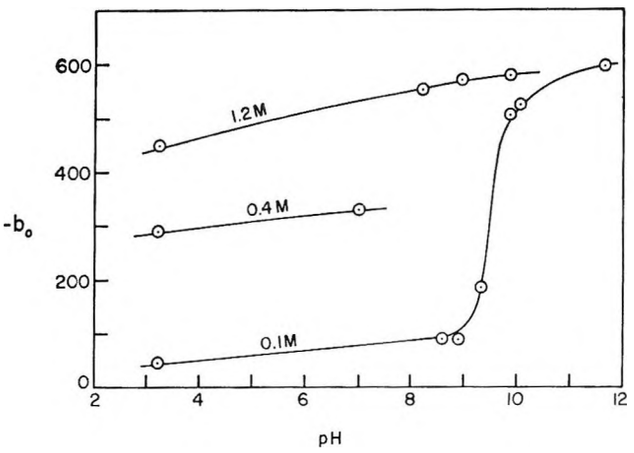

Figure 3. The dependence of b_0 of poly-L-lysine on pH at several KSCN concentrations; T, 25°.

The randomly coiled conformation was found to be stable at low pH.

We have extended these measurements to include the effects of neutral salts on ionizable polypeptides. These results are to be presented in another publication.[10] In the course of this work we noted some rather striking effects of the thiocyanate ion on the conformation of poly-L-lysine at low pH. For one, these effects are visible in the behavior of the intrinsic viscosity $[\eta]$ as the salt concentration is increased (see Figure 1; a part of these data has been reported[11]). The effect of KCl is to decrease $[\eta]$ as the concentration is raised, as generally found with randomly coiled polyelectrolytes.[12] At low concentrations, KSCN causes a more rapid decrease of $[\eta]$ than does KCl while at high concentrations $[\eta]$ becomes constant at a value above that found at identical concentrations of KCl. The data at low salt concentration indicate that the thiocyanate ion is more effective than Cl^- in reducing the electrostatic repulsion

(4) J. Applequist and P. Doty in "Polyamino Acids, Polypeptides, and Proteins," Proceedings of Symposium at University of Wisconsin, by M. A. Stahmann, Ed., University of Wisconsin Press, Madison, Wis., 1961, p 161.

(5) P. Appel and J. T. Yang, *Biochemistry*, **4**, 1244 (1965).

(6) J. Hermans, Jr., *J. Phys. Chem.*, **70**, 510 (1966).

(7) H. Noguchi, *Biopolymers*, **4**, 1105 (1966).

(8) B. H. Zimm and S. A. Rice, *Mol. Phys.*, **3**, 391 (1960).

(9) J. A. Schellman and C. Schellman in "The Proteins," Vol. II, H. Neurath, Ed., 2nd ed, Academic Press Inc., New York, N. Y., 1964, p 1.

(10) A. Ciferri, J. Hermans, Jr., D. Puett, and L. V. Rajagh, to be submitted.

(11) E. Bianchi, A. Bicchi, G. Conio, and A. Ciferri, *J. Macromol. Sci.*, in press.

(12) R. M. Fuoss and U. P. Strauss, *Ann. N. Y. Acad. Sci.*, **51**, 836 (1949).

of the positive charges of the ϵ-amino groups. At high KSCN concentrations, the data suggest that the polymer assumes a more rigid conformation. Measurements of the optical rotatory dispersion confirm this conclusion and allow one to conclude that the rigid conformation is very likely that of the α-helix.

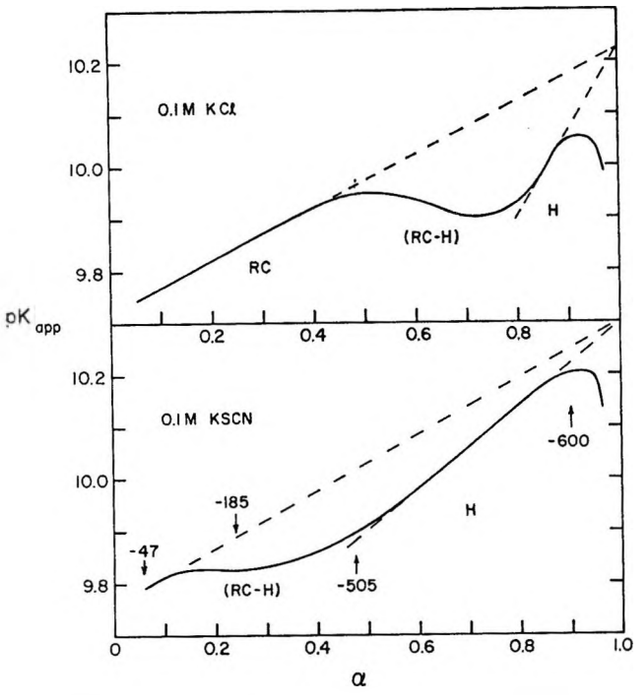

Figure 4. Titration curves (obtained using a Radiometer Type 4 pH meter as described earlier[6,14]) of poly-L-lysine in 0.1 *M* KCl and 0.1 *M* KSCN plotted as the apparent p*K* [pK_{app} = pH − log (α/1 − α)] *vs.* the degree of ionization, α. The curves can be divided into regions corresponding to coiled (RC) and helical (H) poly-L-lysine. In 0.1 *M* KCl, the helical region corresponds to a pH range of 10.72 to 10.95 (α = 0.85 to 0.89), whereas in 0.1 *M* KSCN the pH range is 9.97 to 11.01 (α = 0.52 to 0.87). b_0 values of poly-L-lysine in 0.1 *M* KSCN at various ionization values are indicated on the graph. The value of −600 at α = 0.9 corresponds to the value expected[21] for the α-helix. T = 25° for all measurements.

Figure 2 shows values of b_0 (calculated from the Moffitt and Yang[13] equation) for poly-L-lysine at pH 3.2 at various concentrations of KCl and KSCN. Quite clearly, the simplest conclusion (*cf.* ref 2, 3, and 9) from these data is that at high KSCN concentrations the α-helix is the stable conformation *even at low pH*. Similar data obtained at different pH values are shown in Figure 3. Here it is seen that the helix–coil transition accompanying the binding of protons to the $R-NH_2$ groups, observable in 0.1 *M* KSCN (or in KCl solutions[6,10] or 1 *M* KBr[6]) is not observed in solutions containing 1.2 *M* KSCN.

The phenomena reported above can be explained by two distinct (but not necessarily exclusive) assumptions. For one, it is possible that a physical property of the whole salt–water solution (such as the dielectric constant or the degree of ice-likeness) controls helix stabilization (as is the case with ethanol[14]). Secondly, it is possible that the thiocyanate ions bind to the (charged) ϵ-amino groups, thus reducing the electrostatic repulsion and allowing the intrinsically more stable helix to form.

The former assumption is in contrast with the destabilizing effect of the thiocyanate ion on isoelectric proteins[15,16] and nonionizable polypeptides.[17] For collagen, the depression of the melting by the thiocyanate ions is due to a binding of the anions to the protein.[18] Ion binding to isoelectric proteins is believed to occur mainly at the peptide bond as Bello, *et al.*,[19] have shown that the same melting temperature depressions are observed in gelatins in which the charged groups were blocked.

On the other hand, the second explanation, *i.e.*, binding of SCN^- to the $R-NH_3^+$ groups, is supported by potentiometric titrations as shown in Figure 4 for 0.1 *M* KCl and KSCN. These results clearly show that the slope of the apparent p*K*, pK_{app} *vs.* the degree of ionization, α, curves[5-8] for helical poly-L-lysine is considerably smaller in 0.1 *M* KSCN than in 0.1 *M* KCl. This suggests[8] that a large part of the $R-NH_3^+$ groups tightly hold SCN^- ions, with a concurrent reduction of the net charge of the molecule. Also, the curves in Figure 4 show that the helical conformation is stable over a much broader ionization range in 0.1 *M* KSCN than in 0.1 *M* KCl. The possibility that some SCN^- binds also to the peptide groups (especially when a substantial $R-NH_3^+SCN^-/R-NH_3^+$ ratio is reached) is not entirely dismissed.

(13) W. Moffitt and J. T. Yang, *Proc. Natl. Acad. Sci., U. S.*, **42** 596 (1956).

(14) J. Hermans, Jr., *J. Am. Chem. Soc.*, **88**, 2418 (1966).

(15) A. Ciferri, L. V. Rajagh, and D. Puett, *Biopolymers*, **3**, 461 (1965).

(16) P. H. von Hippel and K. Y. Wong, *Science*, **145**, 577 (1964); *J. Biol. Chem.*, **240**, 3909 (1965).

(17) A. Ciferri and T. A. Orofino, *J. Phys. Chem.*, **70**, 3277 (1966); **71**, 1165 (1967).

(18) D. Puett, R. Garmon, and A. Ciferri, *Nature*, **211**, 1294 (1966).

(19) J. Bello, H. C. A. Riese, and J. R. Vinograd, *J. Phys. Chem.*, **60**, 1299 (1956).

Evidence of the O_3^- Radical in Irradiated Sodium Bromate by Electron Spin Resonance

by T. Andersen, J. R. Byberg, and K. J. Olsen

Institute of Chemistry, University of Aarhus, Aarhus, Denmark

Accepted and Transmitted by The Faraday Society (April 21, 1967)

Radiolysis of alkali bromates at room temperature has been reported[1-5] to result in the formation of BrO_2^-, BrO^-, Br^-, $O_2(g)$, and possibly BrO_2. Recently, additional fragments such as $Br-BrO_3^-$, O_3^-, and BrO_3^{2-} were detected by chemical analysis, ultraviolet spectroscopy, and thermoluminescence measurements in crystalline $NaBrO_3$ and $KBrO_3$ after irradiation at room temperature.[6] The O_3^- radical is stable in the lattice below 80–100°.

Esr spectra of O_3^- trapped in various matrices have been described.[7-11] Therefore, esr measurements were undertaken to give additional information about the presence of O_3^- in $NaBrO_3$.

Single crystals of $NaBrO_3$ were irradiated with 10-Mev electrons at −78° or at room temperature (dose 2–3 Mrads). Esr spectra of a number of different paramagnetic centers may be observed immediately after the irradiation. Storing at 80–100° for several days destroys the majority of the paramagnetic centers. However, one center, A, survives this treatment. It decays in a few hours at 130°. Figure 1 presents typical esr spectra of A. The components in the spectra correspond to centers in magnetically distinct sites. No hyperfine interaction was detected.

$NaBrO_3$ crystallizes in the cubic tetrahedral class and belongs to the space group T^4 ($P2_13$). The unit cell contains four molecules. The anisotropy of the esr spectra shows that the centers A are located in four inequivalent sites of axial symmetry, the axes being parallel to the body diagonals of the unit cell. Thus, the geometrical arrangement is exactly that of the BrO_3^- ions.

The principal g values for A are given in Table I, which contains also the reported g values for O_3^-.

The g values for the A center are consistent with those reported for O_3^-, since the influence of the different host lattices may easily account for the observed discrepancies. On the other hand, the behavior of the center A under thermal treatment strongly indicates that A is identical with the species in $NaBrO_3$ identified as O_3^- by the alternative methods mentioned above. Thus, the esr results provide additional evidence of O_3^- in irradiated $NaBrO_3$. It may be noted that a very similar paramagnetic center has been detected but not identified in γ-irradiated $NaClO_3$[12] which is isomorphous with $NaBrO_3$.

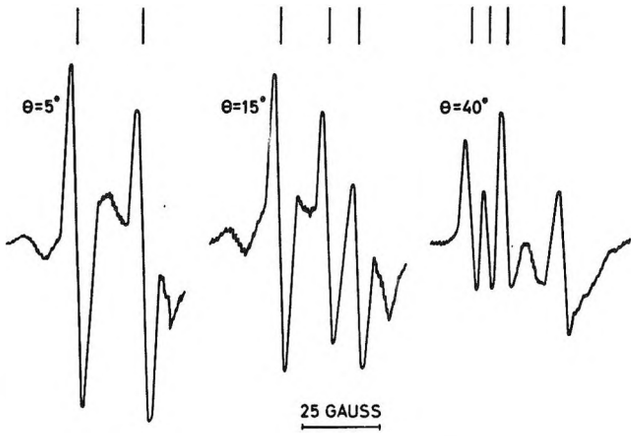

Figure 1. Esr spectra at −180° for an irradiated $NaBrO_3$ crystal stored for 3 days at 100°. The magnetic field was perpendicular to the [111] axis, and θ is the angle between the magnetic field and the [110] axis. Vertical lines indicate the absorption of the A centers. The remaining esr lines in the spectra originate in other types of paramagnetic centers.

Table I: Principal g Values for O_3^- and the A Center

Species	Matrix	g_{xx}	g_{yy}	g_{zz}	g_{av}
O_3^-	$KClO_4$[7]	2.0174	2.0113	2.0025	2.0104
O_3^-	$KClO_4$[8]	2.018	2.011	2.0034	2.011
O_3^-	NaO_3[9]				2.012
O_3^-	NaO_3[10]	2.015	2.015	2.003	2.011
A	$NaBrO_3$	2.022	2.022	2.006	2.017

(1) G. E. Boyd, E. W. Graham, and Q. V. Larson, *J. Phys. Chem.* **66**, 300 (1962).

(2) G. E. Boyd and Q. V. Larson, *ibid.*, **68**, 2627 (1964).

(3) G. E. Boyd and T. G. Ward, *ibid.*, **68**, 3809 (1964).

(4) G. E. Boyd and Q. V. Larson, *ibid.*, **69**, 1413 (1965).

(5) J. W. Chase and G. E. Boyd, ASTM Special Technical Publication No. 400, American Society for Testing and Materials, Philadelphia, Pa., 1966, p 17.

(6) T. Andersen, H. E. L. Madsen, and K. Olesen, *Trans. Faraday Soc.*, **62**, 2409 (1966).

(7) P. W. Atkins, J. A. Brivati, N. Keen, M. C. R. Symons, and P. A. Trevalion, *J. Chem. Soc.*, 4785 (1962).

(8) A. V. Dubovitskii and G. B. Manelis, *Kinetika i Kataliz*, **6**, 828 (1965).

(9) A. D. McLachlan, M. C. R. Symons, and M. G. Townsend, *J. Chem. Soc.*, 952 (1959).

(10) J. E. Bennett, D. J. E. Ingram, and D. Schonland, *Proc. Phys Soc.* (London), **A69**, 556 (1956).

(11) J. C. Fayet and B. Thieblemont, *Compt. Rend.*, **261**, 5420 (1965).

(12) F. T. Gamble, *J. Chem. Phys.*, **42**, 3542 (1965).

Thermodynamic Study of Silicon Sesquitelluride Using a Mass Spectrometer

by G. Exsteen, J. Drowart, A. Vander Auwera-Mahieu,

Laboratoire de Chimie Physique Moléculaire, Université Libre de Bruxelles, Brussels, Belgium

and R. Callaerts

Laboratorium voor Kristallografie en Studie van Vaste Stoffen, Rijksuniversiteit Gent, Ghent, Belgium

Accepted and Transmitted by The Faraday Society (March 20, 1967)

Increased attention has recently been paid to the electrical and optical properties of silicon telluride.[1-4] Whereas there is agreement concerning these and other physical properties of the compound studied, there is none for its formula. According to Weiss and Weiss[5] and Rau and Kannewurf,[3] the compound prepared by different techniques as red crystalline platelets is $SiTe_2$; according to Vennik and Callaerts[2] and Bailey[4] it is Si_2Te_3.

The experiments reported here were made to determine the partial pressures of the components of the vapor and to determine the heat of formation of the compound. Simultaneously, an independent confirmation of the formula Si_2Te_3 was obtained.

As for previous measurements,[2] the samples were grown in the vapor phase.[6] Very pure silicon and excess tellurium were placed at the extremities of an evacuated quartz ampoule 25 cm long inserted into a horizontal furnace with a temperature gradient 700 (Te) to 900° (Si). Fairly large red platelets were obtained near the middle.

The chemical analysis[6] was based on the gravimetric determination of both elements. The samples were oxidized with aqua regia, resulting in the formation of SiO_2 precipitate and Te^{4+} in solution. The former was filtered off, ignited, and weighed. The latter was reduced to metallic Te with SO_2 and $(NH_2)_2 \cdot 2HCl$ and weighed. The average formula is $SiTe_{1.57\pm0.04}$ compared to $SiTe_{1.54\pm0.08}$ given by Bailey.[4]

The vaporization and partial pressures were studied mass spectrometrically. The 60°, single-focusing instrument equipped with a conventional electron-impact ionization source and a secondary electron multiplier was described previously.[7] So was the general procedure.[8]

The Si_2Te_3 samples were vaporized from quartz cells having effusion orifices ranging from 7.43×10^{-3} to 1.15×10^{-2} cm^2. These were inserted into molybdenum shells and heated by radiation from two concentric tungsten loops. Temperatures were measured with Pt—Pt-10% Rh thermocouples.

The ions formed by ionization with 25-ev electrons are Te_2^+, $SiTe^+$, and $SiTe_2^+$. The ionization potentials obtained by the linear extrapolation method and calibrated against those of Hg and H_2O[9] are 8.7 ± 0.5 and 9.2 ± 0.5 ev for Te_2 and SiTe, respectively. The low intensity of the $SiTe_2^+$ peak did not allow such measurements. This ion is nevertheless considered as a parent ion by analogy with a number of similar molecules:[10] CO_2, CS_2, SiO_2,[11] SiS_2,[12] $SiSe_2$,[13] and $GeTe_2$.[14]

On the basis of the phase diagram[4] and the present results, the vaporization behavior can be described by the over-all reaction

$$Si_2Te_3(c) \longrightarrow (2 - x)Si(c) + [(3 - x)/2]Te_2(g) + xSiTe(g) \quad (1)$$

the $SiTe_2$ pressure being negligible.

The pressures were determined in the temperature interval 775–950°K by integrating the ion intensities for both Te_2 and SiTe with time and comparing these with the weight loss of the sample.[8] The residue, crystalline silicon, was identified by X-ray diffraction and shown by X-ray fluorescence to contain not more than 1% Te by weight. Per 100 mg of initial sample, there remained 11.23 mg of Si. The calculated Si content of Si_2Te_3 is 12.80 mg/100 mg. The difference, 1.57 mg, corresponds to the Si vaporized as SiTe(g).

(1) K. Smirous, L. Stourec, and J. Bednar, *Czech. J. Phys.*, **7**, 120 (1956).

(2) J. Vennik and R. Callaerts, *Compt. Rend.*, **260**, 496 (1965).

(3) J. W. Rau and C. R. Kannewurf, *Phys. Chem. Solids*, **27**, 1097 (1966).

(4) L. G. Bailey, *ibid.*, **27**, 1593 (1966).

(5) A. Weiss and A. Weiss, *Z. Anorg. Allgem. Chem.*, **273**, 124 (1953).

(6) Performed at the Laboratorium voor Kristallografie en Studie van Vaste Stoffen, Rijksuniversiteit Gent, Ghent, Belgium.

(7) J. Drowart and P. Goldfinger, *J. Chim. Phys.*, **55**, 721 (1958); M. Ackerman, F. E. Stafford, and J. Drowart, *J. Chem. Phys.*, **33**, 1784 (1960).

(8) M. G. Inghram and J. Drowart in "Proceedings of a Symposium on High Temperature Technology," McGraw-Hill Book Co., Inc., New York, N. Y., 1960, p 219; J. Drowart and P. Goldfinger, *Angew. Chem.*, **79**, 589 (1967); *Angew. Chem., Intern. Ed.*, **6**, 581 (1967).

(9) F. H. Field and J. L. Franklin, "Electron Impact Phenomena," Academic Press Inc., New York, N. Y., 1957.

(10) J. Drowart, *Bull. Soc. Chim. Belges*, **73**, 451 (1964).

(11) R. F. Porter, W. A. Chupka, and M. G. Inghram, *J. Chem. Phys.*, **23**, 216 (1955).

(12) J. C. Lievin, Licence Thesis, University of Brussels, Sept 1962; R. Colin, Ph.D. Thesis, University of Brussels, March 1965.

(13) G. Exsteen, R. Colin, and J. Drowart, to be published.

(14) R. Colin and J. Drowart, *J. Phys. Chem.*, **68**, 428 (1964).

Table I: Thermodynamic Data (kcal/mole)

Reaction	2nd law $\Delta H°_{850}$	2nd law $\Delta H°_{298}$	2nd law $\Delta H°_0$	3rd law $\Delta H°_{298}$	3rd law $\Delta H°_0$
$Si_2Te_3(c) \rightarrow 2Si(c) + {}^3/_2Te_2(g)$	76.2 ± 3	80.3 ± 4	81.1 ± 4	79.8 ± 4	80.6 ± 4
$Si(c) + {}^1/_2Te_2(g) \rightarrow SiTe(g)$	30.0 ± 3	30.8 ± 3	30.5 ± 3	31.7 ± 1	31.4 ± 1
$Si(c) + Te_2(g) \rightarrow SiTe_2(g)$	...	...	...	...	13.1 ± 4
$2Si(c) + 3Te(c) \rightarrow Si_2Te_3(c)$	−32.6 ± 4	−18.8 ± 4	−18.8 ± 4	−18.3 ± 4	−18.3 ± 4
$SiTe(g) \rightarrow Si(g) + Te(g)$	106.0 ± 3	105.1 ± 3	104.1 ± 3	104.2 ± 2	103.2 ± 2
$SiTe_2(g) \rightarrow Si(g) + 2Te(g)$	...	...	...	...	149 ± 5

The relative effective ionization cross section (*i.e.*, the product of the cross section σ_i and the secondary electron multiplier yield γ_i) calculated from these results and the measured ion intensities is $\sigma\gamma(Te_2)/\sigma\gamma(SiTe) = 1.4 \pm 0.2$. In independent experiments[13] with the Si + ZnTe system, $\sigma\gamma(Te_2)/\sigma\gamma(SiTe) = 1.6 \pm 0.2$ was obtained. Since the silicon content of $SiTe_2$ would be 9.90 mg/100 mg of initial sample, the composition Si_2Te_3 of the latter is confirmed solely from the vaporization experiments.

The partial pressures are given by the relations

$$-\log p_{atm}(Te_2) = [(11.1 \pm 0.4) \times 10^3/T] - (7.9 \pm 0.5) \quad (2)$$

$$-\log p_{atm}(SiTe) = [(12.1 \pm 0.3) \times 10^3 T] - (8.3 \pm 0.4) \quad (3)$$

The $SiTe_2$ pressures are $-\log P_{atm}(SiTe_2) = 7.27$, 7.07, and 6.52 at 879, 891, and 919°K, respectively.

The enthalpies (Table I) of the reactions

$$Si_2Te_3(c) \longrightarrow 2Si(c) + {}^3/_2Te_2(g) \quad (4)$$

$$Si(c) + {}^1/_2Te_2(g) \longrightarrow SiTe(g) \quad (5)$$

$$Si(c) + Te_2(g) \longrightarrow SiTe_2(g) \quad (6)$$

were calculated by the second and third laws. The free energy functions were taken from the literature for Si(c),[15] Te_2,[15] and SiTe.[16] The values for Te_2 were, however, decreased by 2.18 cal/deg mole (R ln 3) on the basis of recent spectroscopic data for Te_2.[17] The free energy function of $SiTe_2$ was calculated with the usual statistical mechanical formulas; a linear symmetric model and vibrational frequencies $\omega_1 = 204$, $\omega_2 = 172$, and $\omega_3 = 733$ cm^{-1} were chosen by comparison with CO_2;[18] the interatomic distances were taken the same as in SiTe. This gives $-(G° - H°_0)/T = 72.7$ cal/deg mole at 900°K.

The standard entropy $S°_{289}(Si_2Te_3) = 2S°_{298}(Si) + 3S°_{298}(Te) - 4.75 = 40 \pm 4$ cal/deg mole was estimated by comparing the experimental entropies[19] of CaTe, CdTe, SnTe, and PbTe with those of the corresponding metals and tellurium. The heat capacity was estimated as 6.35 cal/deg g-atom at 298°K and 7.25 cal/deg g-atom[19] at the melting point 1165°K.[4] This gives $-(G° - H°_{298})/T(Si_2Te_3) = 51.85$ and 54.34 cal/deg mole at 800 and 900°K, respectively.

Together with the heat of sublimation of Te_2,[15] corrected in keeping with its modified free energy function, 41.0 ± 1.0 kcal/mole, there results from $\Delta H°_{298}$ (4), $\Delta H_f°_{298}(Si_2Te_3) = -18.3 \pm 4$ kcal/mole for the standard heat of formation of Si_2Te_3. Together with the dissociation energy of Te_2, $D°_0(Te_2) = 55 \pm 2$ kcal/mole,[20] and the heat of sublimation of silicon, $\Delta H_s°_0(Si) = 107.1 \pm 1.0$ kcal/g-atom,[21] there follows from $\Delta H°_0(5)$ and $\Delta H°_0(6)$, $D°_0(SiTe) = 103.2 \pm 2$ kcal/mole and $\Delta H_{at}°_0(SiTe_2) = 149 \pm 5$ kcal/mole for the dissociation and atomization energies of SiTe(g) and $SiTe_2$(g), respectively, in agreement with the values[13] obtained in the Si + ZnTe system.

Acknowledgment. The authors wish to express their appreciation to Dr. R. Colin and Ing. J. Vennik for valuable comments. J. D. thanks the Fonds National de la Recherche Scientifique (Belgium) for a "Crédit aux Chercheurs" research grant and R. C. thanks the Comité d'Etude de l'Etat Solide, Institut pour l'Encouragement de la Recherche Scientifique dans l'Industrie et l'Agriculture (Belgium), for partial support of this investigation.

(15) D. R. Stull and G. Sinke, Advances in Chemistry Series, No. 18, American Chemical Society, Washington, D. C., 1956.

(16) K. K. Kelley, U. S. Bureau of Mines Bulletin 584, Department of the Interior, U. S. Government Printing Office, Washington, D. C., 1960; K. K. Kelley and E. G. King, U. S. Bureau of Mines Bulletin 592, Department of the Interior, U. S. Government Printing Office, Washington, D. C., 1961.

(17) R. P. Du Parcq and R. F. Barrow, *Chem. Commun.*, 270 (1966).

(18) G. Herzberg, "Infrared and Raman Spectra," D. Van Nostrand Co., Inc., Princeton, N. J., 1945.

(19) O. Kubaschewski and E. L. Evans, "Metallurgical Thermochemistry," Pergamon Press Inc., New York, N. Y., 1958.

(20) J. Drowart and P. Goldfinger, *Quart. Rev.* (London), **20**, 545 (1966).

(21) R. Hultgren, R. L. Orr, and K. K. Kelley, Supplements to "Thermodynamic Properties of Metals and Alloys," University of California, Berkeley, Calif., 1965.

Reaction Rates of Alkyl and Peroxy Radicals with Copper Ion—Pulse Radiolysis Studies

by A. MacLachlan

Contribution No. 1279 from the Central Research Department, Experimental Station, E. I. Du Pont de Nemours and Company, Wilmington, Delaware 19898 *(Received June 19, 1967)*

The pulse radiolysis technique[1] has been applied to observe directly the rates of interaction of substituted alkyl and peroxy radicals with Cu^{I} and Cu^{II} ions. Some effects of radical structure and ligands were also studied.

Pulse radiolysis of solutions involves subjecting the sample to a 5-μsec beam pulse of electrons (energy 5–8 Mev) which produces during that time a concentration of free radicals dependent on the G(solvent). If the solution is deoxygenated, only alkyl-type radicals are produced, and correspondingly, if the solution is saturated with oxygen before pulsing, high yields of peroxy radicals are obtained.[2] In this work, radicals were generated from three solvent systems: ethanol (EtOH), 98% ethanol–2% acetic acid (98–2 E–A), and glacial acetic acid (HOAc). The efficiencies and rates of interaction of Cu^{II} and Cu^{I} ions with the radicals produced were examined.

Table I lists the interaction efficiencies for $CuCl_2$ and $Cu(OAc)_2$. $CuCl_2$ in EtOH and in 98–2 E–A captures 2×10^{-4} M/pulse, in agreement with the known radical yield in ethanol.[2]

Table I: Capture Efficiencies of Alkyl Radicals by Cu^{II} Ions (2.00×10^{-3} M)

Compound	Solvent	Mole of Cu^{II} reduced/pulse
$CuCl_2$	EtOH	2.3×10^{-4}
$CuCl_2$	98–2 E–A	2.9×10^{-4}
$Cu(OAc)_2$	98–2 E–A	5.2×10^{-5}
$Cu(OAc)_2$	HOAc	4.5×10^{-5}
$Cu(OAc)_2$ + 1 M NH_4OAc	HOAc	1.0×10^{-4}
$Cu(OAc)_2$ + 1 M NH_4OAc	98–2 E–A	1.6×10^{-4}

Direct observation at 3400 A showed that reduction of Cu^{II} in 98–2 E–A follows the beam pulse shape even down to 2×10^{-4} M $CuCl_2$. Consequently, the rate constant is greater than 10^9 l./mole sec and is probably diffusion controlled. $Cu(OAc)_2$ could not be examined in pure ethanol because of the immediate precipitation of the Cu^{I} produced. However, in 98–2 E–A no precipitation problem occurred; surprisingly only 5×10^{-5} mole of Cu^{II} was reduced per pulse. From kinetic arguments, Kochi[3] has concluded that $Cu^{II}(OAc)_2$ dimer is unreactive toward alkyl radicals. The spectrum of $Cu(OAc)_2$ in 98–2 E–A clearly indicates the presence of dimer. Table I shows that the reduction yield of $Cu(OAc)_2$ is also low in pure HOAc (4.4×10^{-5} mole/pulse), another solvent where dimer is present.[4] This result could also be due to a low yield of substituted alkyl radicals or to the low reactivity of the $\cdot CH_2COOH$ radical as a reducing agent. To distinguish these possibilities, $Cu(OAc)_2$ in HOAc containing 1 M NH_4OAc was irradiated. Spectral evidence indicated a significant diminution in the dimer concentration, and the reduction yield increased to 1×10^{-4} mole/pulse. Addition of 1 M NH_4OAc to 98–2 E–A also dissociated $Cu(OAc)_2$, and as the last entry in Table I shows, there was a corresponding increase in reduction yield. These results agree with Kochi.[3] In addition, we find the $\cdot CH_2COOH$ radical to be a good reducing agent with a rate constant greater than 10^9 l./mole sec.

Cu^{I} ions were not reoxidized by substituted alkyl radicals to Cu^{II} in any of the solvents used; thus, this is a relatively slow reaction if it occurs at all.

Peroxy radicals were studied by presaturation of the solutions with oxygen. Since it has already been shown that the substituted alkyl radicals react at a diffusion-controlled rate, it is necessary to use low concentrations of Cu^{II} (2×10^{-4} M) to have peroxy radical formation compete with the alkyl radical reduction reaction. Transient observation and end product spectral analysis revealed no detectable reaction of α-ethanol peroxy radicals with Cu^{II} chloride or acetate. Cuprous ion was investigated by first reducing a $CuCl_2$ (2×10^{-4} M) solution in ethanol by electron irradiation of a deoxygenated solution. This sample was then saturated with oxygen and pulse radiolyzed. Transient analysis showed a reoxidation by the α-ethanol peroxy radical that followed the beam pulse duration. Thus the rate constant is at least 10^9 l./mole sec and may be diffusion controlled. It was not possible to run these experiments with cuprous acetate because of the rapid rate of reoxidation by dissolved oxygen. In future work, the effects of ligands on the rates of alkyl and peroxy radical reactions with cupric and cuprous ions will be studied.

(1) R. L. McCarthy and A. MacLachlan, *Trans. Faraday Soc.*, **56**, 1187 (1960).

(2) A. MacLachlan, *J. Am. Chem. Soc.*, **87**, 960 (1965).

(3) J. K. Kochi and R. V. Subramanian, *ibid.*, **87**, 4855 (1965).

(4) J. K. Kochi and R. V. Subramanian, *Inorg. Chem.*, **4**, 1527 (1965).

Acknowledgments. The author is indebted to J. R. Merrill for helpful discussions and to R. T. Edwards, Jr., and R. B. Uhlig for assistance in the experimental work.

On the Saturation–Recovery Method for Determining Nuclear Spin-Lattice Relaxation Times

by J. E. Anderson and Robert Ullman

Scientific Laboratory, Ford Motor Company, Dearborn, Michigan 48121 *(Received January 23, 1967)*

Perhaps the least complicated method of determining nuclear spin-lattice relaxation times (T_1) in liquids is that of saturation–recovery.[1-3] This method consists of saturating a particular resonance line with a large H_1 field[4] and following the subsequent recovery of the nuclear signal after H_1 has been reduced to a small, nonsaturating, value.[5] It is presumed that the v mode will recover exponentially with a time constant T_1. It is well known that residual saturation effects in the low H_1 field impose an effective upper limit on the T_1 values that can be determined by this method. The saturation–recovery method has been less critically examined in the range of short T_1 values. Experimentally, it has been observed in a number of laboratories[3,6] that there is large initial distortion in the recovery curve, due to a "transient" which seems to last about 200 msec. A typically distorted recovery curve is shown in Figure 1. The cause of this distortion has not been well understood: it has been attributed to both experimental and nuclear origins. The transient caused us considerable concern, for being uncertain of its true duration, we were unable to gauge the accuracy of short T_1 values obtained from saturation–recovery measurements. It is hoped that the following discussion will prove valuable to others who may face the same problem.

Torrey[2] has obtained a general solution to the Bloch equations, including transient terms. We shall restrict our attention to the case where $T_1 = T_2$. This case is easy to treat mathematically, and it describes the relaxation behavior found in many simple liquids. When $T_1 = T_2$, Torrey's solution for the v mode becomes

$$v(\delta,\tau) = e^{-\beta\tau}\left[\left(v_0 + \frac{\beta}{1+\beta^2+\delta^2}\right)\cos(s\tau) + \left(\delta u_0 - m_0 + \frac{\beta^2}{1+\beta^2+\delta^2}\right)\frac{\sin(s\tau)}{s}\right] - \left(\frac{\beta}{1+\beta^2+\delta^2}\right) \quad (1a)$$

$$\delta = (\omega - \omega_0)/\gamma H_1 \quad (1b)$$

$$s = (1 + \delta_0^2)^{1/2} \quad (1c)$$

$$\beta = 1/\gamma H_1 T; \quad T = T_1 = T_2 \quad (1d)$$

The quantities u_0, v_0, and m_0 are the initial values of u, v, and m_z, respectively, for a particular value of δ. Equation 1 describes the radiofrequency absorption of a particular "spin isochromat" a distance (δ) away from resonance. The experimental absorption signal is obtained from

$$v(\tau) = \int_{-\infty}^{\infty} g(\delta)v(\delta,\tau)\mathrm{d}\delta \quad (2)$$

where $g(\delta)$ is a weighting factor reflecting the H_0 field inhomogeneities. Specifically, we will take $g(\delta) = (a/\pi)[a_2 + \delta^2]^{-1}$, where $a = 1/\gamma H_1 T_2^*$ (T_2^* is the apparent value of T_2 in the inhomogeneous field). We are interested in $v(\tau)$ following the reduction of H_1 at $t = 0$. For this reason, it is convenient to let the symbol H_1

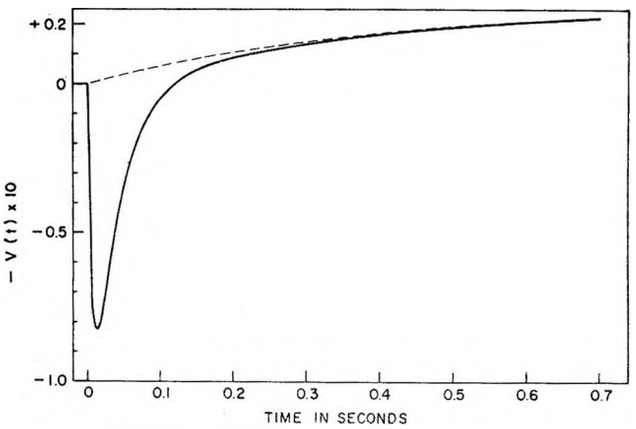

Figure 1. Solid curve: saturation–recovery curve obtained from eq 3. The initial and final H_1 values are 5.9 and 0.030 mg, respectively; $T_1 = T_2 = 0.40$ sec; $T_2^* = 0.04$ sec. Dashed curve: exponential recovery. The two curves have identical asymptotic behavior.

(1) See, for example, E. R. Andrew, "Nuclear Magnetic Resonance," Cambridge University Press, New York, N. Y., 1958, p 107 ff.

(2) H. C. Torrey, *Phys. Rev.*, **76**, 1059 (1949).

(3) A. L. Van Geet and D. N. Hume, *Anal. Chem.*, **37**, 983 (1965).

(4) The notation used in this article has become conventional. A complete exposition is given in ref 2.

(5) J. G. Powles and D. J. Neale, *Proc. Phys. Soc.*, **77**, 737 (1961), have used a variation of this saturation–recovery method which is preferable for long T_1 values. Following the reduction of the saturation H_1 field, they shift the H_0 field off resonance. The recovery of the magnetization is then monitored by periodic sweeps through resonance at low H_1 levels. The absence of a continuously resonant H_1 greatly reduces residual saturation effects. It does not circumvent the difficulties with short T_1 values, however.

(6) G. Weill (private communication, University of Strasbourg, France) has observed the transient on a Varian HA100 spectrometer.

represent the intensity of the smaller, nonsaturating radiofrequency field. In the following paragraphs, the parameters δ, s, and β also refer to values in the nonsaturating field (eq 1). We will use the symbol F to designate the ratio of the radiofrequency field intensity during saturation to that during recovery. In this notation, the boundary conditions become

$$u_0 = \frac{\delta F}{\beta^2 + \delta^2 + F^2} \tag{3a}$$

$$v_0 = -\frac{\beta F}{\beta^2 + \delta^2 + F^2} \tag{3b}$$

$$m_0 = \frac{(\beta^2 + \delta^2)}{\beta^2 + \delta^2 + F^2} \tag{3c}$$

Owing to the form of s in eq 1, we were unable to integrate the resulting equations analytically. $v(\delta,\tau)$ is a rapidly oscillating function of (δ), so that numerical integration is also difficult. We observed, however, that the small H_1 values used during recovery cause δ^2 to be $\gg 1$ for all nuclei except the small number very close to resonance (commonly, those within about ± 0.3 cps of resonance.) If s is approximated by δ, $v(\tau)$ may be obtained by integration of eq 2.[7,8] The result is

$$v(\tau) = -\frac{\beta}{K(a+K)} + e^{-\beta\tau}\left\{-\frac{\beta F(ae^{-L\tau} - Le^{-a\tau})}{L(a^2 - L^2)} + \frac{\beta(ae^{-K\tau} - Ke^{-a\tau})}{K(a^2 - K^2)} - \frac{\beta^2}{aL^2}\left[\frac{L^2e^{-a\tau} - a^2e^{-L\tau}}{a^2 - L^2)} + 1\right] + \frac{(aF - a)}{a^2 - L^2}\left(e^{-L\tau} - e^{-a\tau}\right) + \frac{\beta^2}{aK^2}\left[\left(\frac{K^2e^{-a\tau} - a^2e^{-K\tau}}{a^2 - K^2}\right) + 1\right]\right\} \tag{4}$$

The quantities K and L in eq 4 stand for $(1 + \beta^2)^{1/2}$ and $(F^2 + \beta^2)^{1/2}$.

In a typical experiment, F may be about 10^3, and $1 \ll \beta \ll F$. Under these conditions, $K \approx \beta$, $F \approx L$. The quantity a is normally larger than β and also substantially less than F or L. Keeping this in mind, a good approximation to eq 4 is

$$v(\tau) = \frac{-\beta}{Ka}\left(1 - \frac{\beta}{K}e^{-\beta\tau}\right) + e^{-(\beta+K)\tau}\left(1 - \frac{\beta}{K}\right) \times \left(\frac{\beta}{Ka}\right) - (a/F)(e^{-(F+\beta)\tau} - e^{-(a+\beta)\tau}) \tag{5}$$

The first term of eq 5 describes the expected exponential recovery. The second term, which has a time constant comparable to $(1/T)$, makes a significant contribution only when there is residual saturation. (Residual saturation effects cause $\beta \neq K$.) The third term describes the transient. This term arises from integration of $(u_0\delta/s)$ sin $(s\tau)$, an expression which is finite for those nuclei which are off-resonance and only partially saturated by the large radiofrequency field. During saturation, these nuclei are "locked" along the effective field,[9] and retain finite magnetization. When the radiofrequency field is reduced, these spins precess, producing a large nuclear signal which decays as T_2^*.[10,11]

From consideration of (4), one finds that the best experimental conditions consist of using the largest possible radiofrequency field for detection consistent with small residual saturation. Roughly, this means that $\gamma H_1 T < 0.3$. The use of a large H_1 means that the normal decay term is enhanced with respect to the large transient. If a slightly modified Varian A-60 spectrometer with a maximum H_1 of 10 mg is adapted for this experiment, $T \geq 0.2$ sec can be measured. If higher values of H_1 are accessible, it becomes possible to measure shorter relaxation times since the magnitude of the transient (see eq 4) is reduced by increasing H_1 without affecting the normal decay signal.

In ref 3, the authors often used experimental conditions where a is greater than F. Accordingly, the dominating terms of eq 4 are not those given in eq 5. A transient still exists and arises from the same source; its magnitude and persistence can be determined from eq 4.

It should be pointed out that the calculation of the transient is based on the assumption that $T_1 = T_2$. It is also evident that the form assumed for $g(\delta)$ (eq 2) is not precise in any real experimental situation. Accordingly, the transient obtained in an experiment will deviate from the results of the calculation, though the dependence on the significant parameters remains essentially valid.

(7) The difference between the values of $v(\tau)$ using the true and approximate values of s in the vicinity of $\delta = 0$ was determined by numerical integration on a Philco 212 computer. As expected, the difference produced no substantial changes in the shape of the (theoretical) recovery curve.

(8) With $T_2^* = 0.04$ sec, the distortion persists for 200 msec. This is approximately the duration of the experimental transient. Throughout this article we have implicitly assumed that there is no phase difference between the large and small radiofrequency fields. If there is a phase difference, the experimental transient is observed to alter its shape, direction, and magnitude.

(9) The effective field is the resultant of $H_0 - \omega/\gamma$ in the longitudinal direction and H_1 in a transverse direction. This is the net magnetic field imposed on the sample from the viewpoint of the rotating frame.

(10) Van Geet and Hume (ref 3) suggested that such unsaturated, "field-locked," nuclei might play some role in the saturation–recovery experiment. They did not relate these nuclei to the initial distortion of the recovery curve, however, and attributed the "transient" to a temporary malfunction of their spectrometer.

(11) N. Bloembergen, "Nuclear Magnetic Relaxation," W. A. Benjamin, Inc., New York, N. Y., 1961, p 75, speaks of "burning a hole in the resonance line." This phenomenon has the same basis as the transient discussed in this article.

Pressure Effects in the Photolysis of CH_3CD_3 at 1470 A

by Hajime Akimoto and Ikuzo Tanaka

Laboratory of Physical Chemistry, Tokyo Institute of Technology, Ohokayama, Meguroku, Tokyo, Japan *(Received June 9, 1967)*

Several studies[1-4] on the photolysis of ethane in the vacuum ultraviolet region have been reported in respect to the primary-decomposition modes and the nature of intermediate excited ethylene or ethylidene. As to the photolysis of CH_3CD_3, the following reaction scheme has been proposed both at 1470 and at 1236 A in the earlier paper.[1,2]

$$CH_3CD_3 + h\nu \longrightarrow H_2 + C_2HD_3^* \longrightarrow \begin{matrix} D_2 + C_2HD \\ HD + C_2D_2 \\ +M \searrow \\ C_2HD_3 \end{matrix} \qquad (1)$$

$$CH_3CD_3 + h\nu \longrightarrow D_2 + C_2H_3D^* \longrightarrow \begin{matrix} H_2 + C_2HD \\ HD + C_2H_2 \\ +M \searrow \\ C_2H_3D \end{matrix} \qquad (1')$$

$$CH_3CD_3 + h\nu \longrightarrow H + D + C_2H_2D_2 \qquad (2)$$

On the other hand, Hampson and McNesby[4] have studied the pressure dependence of the formation ratio of ethylene to acetylene for the photolysis of C_2H_6 and clarified that the intermediate excited ethylene decomposes into acetylene and hydrogen unimolecularly competing with collisional stabilization to ethylene. They have also suggested the presence of another intermediate ethylene species which cannot decompose even without collisional stabilization, and proposed the following scheme.

$$C_2H_6 + h\nu \longrightarrow H_2 + C_2H_4^{**} \qquad (3)$$

$$C_2H_6 + h\nu \longrightarrow 2H + C_2H_4 \qquad (4)$$

$$C_2H_4^{**} \longrightarrow C_2H_4^* \qquad (5)$$

$$C_2H_4^{**} \longrightarrow C_2H_2 + H_2 \qquad (6)$$

$$C_2H_4^{**} + M \longrightarrow C_2H_4 + M \qquad (7)$$

$$C_2H_4^* + M \longrightarrow C_2H_4 + M \qquad (8)$$

This work has been conducted in order to study the photolysis of CH_3CD_3 at 1470 A in more detail and to check the validity of reaction schemes 1 and 2 and 3–8.

Experimental Section

The experimental procedures used in these experiments are the same as described previously.[1,2] Since some of the experiments were performed under very low conversion (less than 0.01 %), C_2H_6 obtained from Takachiho Chem. Ind. Co. and CH_3CD_3 from Merck Sharp and Dohm Ltd. were purified by gas chromatography until the impurity ethylene was reduced to less than 0.0003%. Activated charcoal column was used to detect the ethylene and acetylene in the huge amount of unreacted ethane. The reaction cell composed of a magnetic circulator and glass tube of 15 mm o.d. was designed so that the reactant might be circulated most effectively especially near the window.

Results and Discussion

The data are presented in Figures 1 and 2. Figure 1 shows the pressure dependence of the ratio of ethylene to acetylene produced in the photolysis of C_2H_6 and CH_3CD_3 at 1470 A, room temperature, and at very low conversion less than 0.01%. The figure also con-

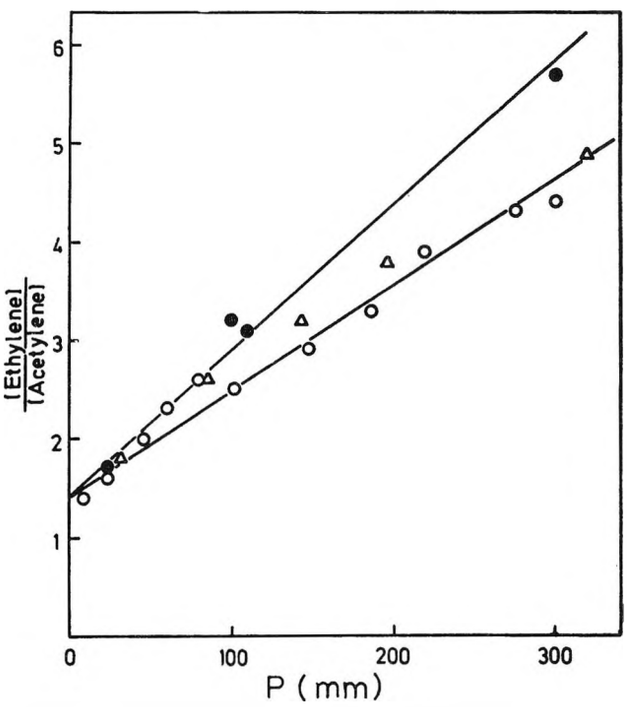

Figure 1. Ethylene to acetylene ratio *vs.* pressure of ethane in the photolysis of C_2H_6 (○) and CH_3CD_3 (●) at low conversion, and Hampson's data[4] (△) for C_2H_6 at 310°.

(1) R. F. Hampson, Jr., J. R. McNesby, H. Akimoto, and I. Tanaka, *J. Chem. Phys.*, **40**, 1099 (1964).

(2) H. Akimoto, K. Obi, and I. Tanaka, *ibid.*, **42**, 3864 (1965).

(3) R. F. Hampson, Jr., and J. R. McNesby, *ibid.*, **42**, 2200 (1965).

(4) R. F. Hampson, Jr., and J. R. McNesby, *ibid.*, **43**, 3592 (1965).

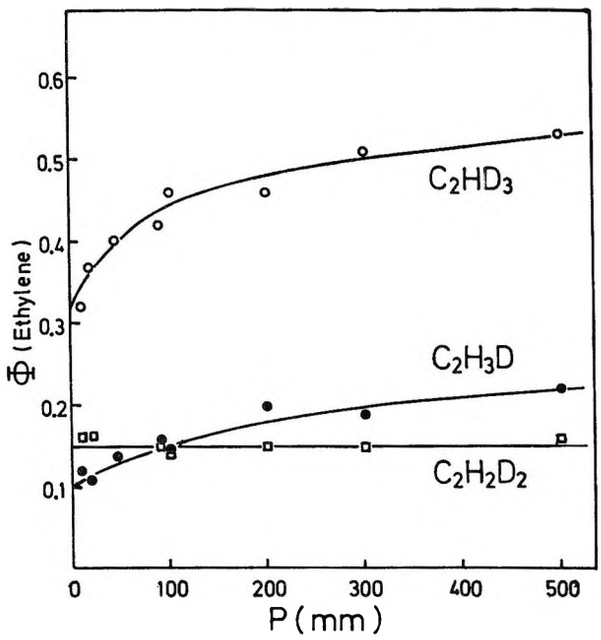

Figure 2. Yields of C_2HD_3 (○), C_2H_3D (●), and $C_2H_2D_2$ (□) *vs.* pressure in the photolysis of CH_3CD_3.

tains several plots of Hampson's data[4] at 310°. It has been shown[1] that internal scavenging of hydrogen atom produced in reaction 4 occurs at room temperature

$$C_2H_4 + H + M \longrightarrow C_2H_5 + M \qquad (9)$$

so that the ethylene to acetylene ratio should decrease as a function of conversion. On the other hand, no scavenging should occur at 310° as postulated by Hampson and McNesby.[3,4] The agreement of our present data with those at 310° implies that essentially no scavenging of hydrogen atom occurs at low conversion less than 0.01%, and therefore, the ratio in Figure 1 reflects the primary yields of ethylene and acetylene.

Now that the ratio of ethylene to acetylene has been found to be dependent on the ethane pressure, it must be instructive to investigate how the isotopic distribution in ethylene in the photolysis of CH_3CD_3 changes with pressure. Figure 2 shows each yield of C_2H_3D, $C_2H_2D_2$, and C_2HD_3 as a function of pressure. The yield is calculated based upon the isotopic distribution of ethylene and the primary formation ratio of ethylene to acetylene which has been obtained in Figure 1 and is normalized so that the total primary yield of ethylene and acetylene should be unity. Assuming that the isotopic distribution in ethylene is independent of conversion, the yield in Figure 2 can be recognized as the primary one of each ethylene.

According to reactions 1 and 2, the yields of C_2H_3D and C_2HD_3 must be zero when the pressure of CH_3CD_3 is extrapolated to zero. However, this is not the case in Figure 2, but the yields of C_2H_3D and C_2HD_3 start from a nonzero value at zero pressure and increase with pressure. This fact suggests directly that one part of C_2H_3D and C_2HD_3 results from some process which does not need collisional stabilization, and the other part of them descends from some excited ethylene species which can decompose competing with collisional stabilization. The presence of ethylene which can be formed without collisional stabilization strongly supports the assumption proposed by Hampson and McNesby.[4] On the other hand, the absence of pressure dependence of $C_2H_2D_2$ supports the assumption that the formation of $C_2H_2D_2$ corresponds to reaction 2.

Thus we have the modified reaction scheme

$$CH_3CD_3 + h\nu \xrightarrow{\varphi_1} H_2 + C_2HD_3^{**} \xrightarrow{k_d} D_2 + C_2HD$$
$$\qquad\qquad \xrightarrow[\varphi_3]{} \qquad\qquad \xrightarrow{k_s[M]} \quad HD + C_2D_2 \qquad (10)$$
$$H_2 + C_2HD_3^{*} \longrightarrow C_2HD_3 \qquad (11)$$

$$CH_3CD_3 + h\nu \xrightarrow{\varphi_1'} D_2 + C_2H_3D^{**} \xrightarrow{k_d'} H_2 + C_2HD$$
$$\qquad\qquad \xrightarrow[\varphi_3']{} \qquad\qquad \xrightarrow{k_s'[M]} \quad HD + C_2H_2 \qquad (10')$$
$$D_2 + C_2H_3D^{*} \longrightarrow C_2H_3D \qquad (11')$$

$$CH_3CD_3 + h\nu \xrightarrow{\varphi_2} H + D + CH_2CD_2 \qquad (12)$$

Assuming the above scheme, the following equations are obtained

$$\Phi(C_2H_2D_2) = \varphi_2 \qquad (13)$$

$$\Phi_0(C_2HD_3) = \varphi_3; \quad \Phi_0(C_2H_3D) = \varphi_3' \qquad (14)$$

$$\frac{1}{\Phi(C_2HD_3) - \Phi_0(C_2HD_3)} = \frac{1}{\varphi_1}\left(1 + \frac{k_d}{k_s}\frac{1}{[M]}\right) \qquad (15)$$

$$\frac{1}{\Phi(C_2H_3D) - \Phi_0(C_2H_3D)} = \frac{1}{\varphi_1'}\left(1 + \frac{k_d'}{k_s'}\frac{1}{[M]}\right) \qquad (15')$$

where $\Phi(C_2HD_3)$ is the normalized yield of C_2HD_3 and $\Phi_0(C_2HD_3)$ is that at zero pressure, etc. Figure 3 shows the plots of experimental values of the left-hand side of eq 15 and 15′ against the reciprocal of CH_3CD_3 pressure. Using the data in Figures 2 and 3, the values for φ_1, φ_3, φ_1', φ_3', φ_2, k_s/k_d, and k_s'/k_d' are obtained as follows: $\varphi_1 = 0.23$, $\varphi_3 = 0.32$, $\varphi_1' = 0.20$, $\varphi_3' = 0.10$, $\varphi_2 = 0.15$, $k_s/k_d = 0.010$ mm^{-1}, $k_s'/k_d' = 0.004$ mm^{-1}. It should be noticed that the present values of $\varphi_1 + \varphi_3 = 0.55$, $\varphi_1' + \varphi_3' = 0.30$, and φ_2 agree well with earlier ones,[1] 0.50, 0.35, and 0.15 respectively, which were calculated from isotopic distribution of ethylene and acetylene without knowledge of the pressure effect. This agreement assures the validity of the relative ratio of each primary process

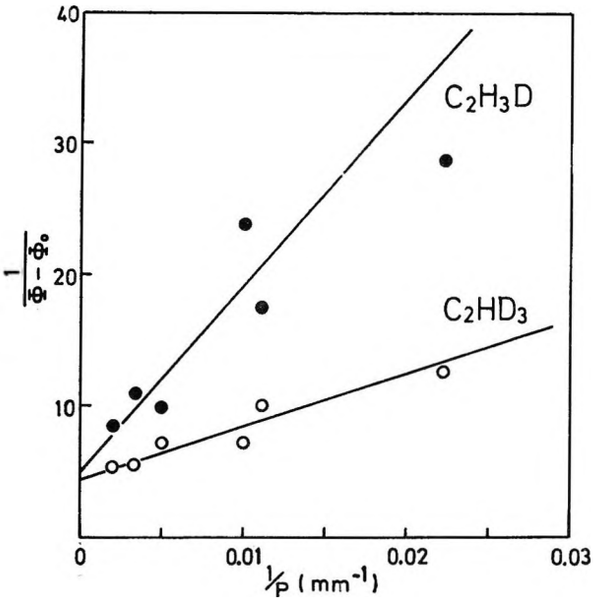

Figure 3. Reciprocals of $\Phi(C_2HD_3) - \Phi_0(C_2HD_3)$ (○) and $\Phi(C_2H_3D) - \Phi_0(C_2H_3D)$ (●) *vs.* reciprocal of pressure of CH_3CD_3.

reported earlier.[1] The present values of $\varphi_3/\varphi_1 = 1.4$ or $\varphi_3'/\varphi_1' = 0.5$, and $k_s/k_d = 0.010$ mm^{-1} or $k_s'/k_d' = 0.004$ mm^{-1} are also compared to 1.22 and 0.0047 mm^{-1} for the photolysis of C_2H_6 reported by Hampson and McNesby.[4]

As to the assignments of C_2HD_3** and C_2HD_3*, both of them can be distinguished from the electronic excited singlet state attained by direct light absorption in the point of reactivity. Direct photolysis of ethylene has been studied to give both hydrogen molecule and atoms following to the reaction[5]

$$C_2H_4 + h\nu \longrightarrow C_2H_2 + H_2 \qquad (16)$$

$$\searrow C_2H_2 + 2H \qquad (17)$$

The relative importance of each process has been determined to be $\varphi_{17}/\varphi_{16} = 1.0$[5] and 0.6[6] at 1470 and 1634 A, respectively. Since the C_2HD_3** produced in reaction 10 should have maximum energy 7.0 ev, which is equivalent to 1770 A, it should also yield hydrogen atoms if it is in the electronic excited singlet state. But this is not the case in our experiments, and the inclusion of such an atomic process could not explain the product analysis reported earlier.[1,3] The circumstances are the same for the photolysis of diazoethane,[7,8] methyldiazirine,[9] and methylketene,[10] and the formation of hydrogen atom was not reported in either case.

Our present data can also be interpreted by the alternative scheme which is equivalent to reactions 3–8

$$CH_3CD_3 + h\nu \longrightarrow H_2 + C_2HD_3^{**} \xrightarrow{k_d} D_2 + C_2HD$$
$$\qquad\qquad\qquad\qquad\quad \downarrow k_s[M] \quad\searrow\ HD + C_2D_2$$
$$\qquad\qquad\qquad\qquad\quad \downarrow k_2$$
$$\qquad\qquad\qquad\qquad C_2HD_3^{*} \longrightarrow C_2HD_3 \qquad (18)$$

etc., but we are not at the stage of choosing one of the alternatives.

Further work on the photolysis of ethane at the absorption edge is under investigation.

(5) M. C. Sauer, Jr., and L. M. Dorfman, *J. Chem. Phys.*, **35**, 497 (1961).

(6) H. Akimoto and I. Tanaka, unpublished data.

(7) H. M. Frey, *J. Chem. Soc.*, 2293 (1962).

(8) C. L. Kibby and G. B. Kistiakowsky, *J. Phys. Chem.*, **70**, 126 (1966).

(9) H. M. Frey and I. D. R. Stevens, *J. Chem. Soc.*, 1700 (1965).

(10) D. P. Chong and G. B. Kistiakowsky, *J. Phys. Chem.*, **68**, 1793 (1964).

The Magnetic Properties of Some Europium Chelates

by T. M. Shepherd

United Kingdom Atomic Energy Authority, Atomic Weapons Research Establishment, Aldermaston, Berks. England

Accepted and Transmitted by The Faraday Society (April 4, 1967)

Considerable interest has been shown recently in the coordination chemistry of europium diketone systems mainly on account of their liquid laser applications. The magnetic properties of europium chelates have only received limited attention.[1] This paper reports the results of magnetic susceptibility measurements of several salts of europium tetrakisbenzoyltrifluoroacetonate, $Eu(BTFA)_4^-$, over the temperature range $-150°$ to 100°.

Trivalent europium and samarium differ from the other trivalent lanthanides in exhibiting a relatively small spin–orbit coupling constant. With Eu^{3+}, the $^7F_1$ and $^7F_2$ states are sufficiently close to the lowest J state, the $^7F_0$, to be populated at ordinary temperatures. The Curie–Weiss relationship is therefore not obeyed and the magnetic susceptibility becomes a complicated function of temperature.[2] Experimental data obtained for europium salts have been in good agreement with Van Vleck's theoretical values except at very low temperatures.[2,3]

(1) T. Moeller, D. F. Martin, L. C. Thompson, R. Ferrús, G. R. Feistel, and W. J. Randall, *Chem. Rev.*, **65**, 1 (1965).

Experimental Section

Magnetic susceptibilities of five salts, the piperidinium (P), piperazinium (PZ), morpholinium (M), ammonium (A), and benzyltrimethylammonium (BTMA) of $Eu(BTFA)_4^-$ were measured by the Gouy technique.[4] Magnetic fields of up to 8500 gauss were obtained using a water-cooled Newport Type A electromagnet. Constant current circuitry gave a field stability of better than 0.01%. The temperature of the sample was controlled to within ±1° by passing nitrogen gas through a two-walled vessel surrounding the sample. Calibration was carried out using $Co(NCS)_4$-Hg.[5] The error in the magnetic susceptibilities is estimated to be less than 2%. Despite the good packing characteristics of the powdered samples, packing was the largest source of error.

The necessary corrections for the magnetism of the Gouy tube were made. Diamagnetic corrections for the sample were derived from Pascals' constants[3] and are given in Table I. Measurements were made throughout the temperature range at intervals not greater than 5°. No field strength dependence was found.

Table I

Temp, °C	Cor molar susceptibility (×10⁴) (diamagnetic correction) P (5.09)	PZ (5.04)	M (5.01)	A (4.56)	BTMA (5.50)
100	47.10	44.10	43.00	44.40	42.90
50	50.20	48.10	46.30	47.50	46.00
0	55.10	53.10	51.50	51.70	50.10
−50	59.90	58.70	57.00	57.10	54.20
−100	64.50	63.50	62.00	62.80	58.30
−150	68.00	67.30	66.30	68.00	61.60

Results and Discussion

The corrected molar susceptibilities of the europium ion in the compounds studied are given, at several temperatures, in Table I. Significant differences were found, the maximum spread in susceptibility at temperature being about 10%. With the exception of BTMA, the differences decrease with temperature and at −150° the spread is within experimental error. The effective magnetic moments derived from these figures are shown in Figure 1.

Also shown are Van Vleck's theoretical values corresponding to $^7F_0 \rightarrow {}^7F_1$ energy differences of 254 and 290 cm^{-1}. These calculations are based on a nondegenerate $^7F_1$, whereas the ^7F states (except the $^7F_0$) show ligand field splitting. The symmetries of the ligand field in these compounds belong to one of the point groups C_{1h}, C_1, C_2, or C_{2v}.[6] In order to apply Van Vleck's "intermediate" formula, the positions of the split components must be known. Spectral data at −196° are available[6] but the validity of applying these at other temperatures is dubious since the ligand field may be appreciably altered by lattice expansions. Quantitative correlations with theory would therefore require spectral data over the range of temperatures examined with the consequent difficulties associated with marked vibronic broadening at higher temperatures. The discussion is therefore limited to qualitative considerations.

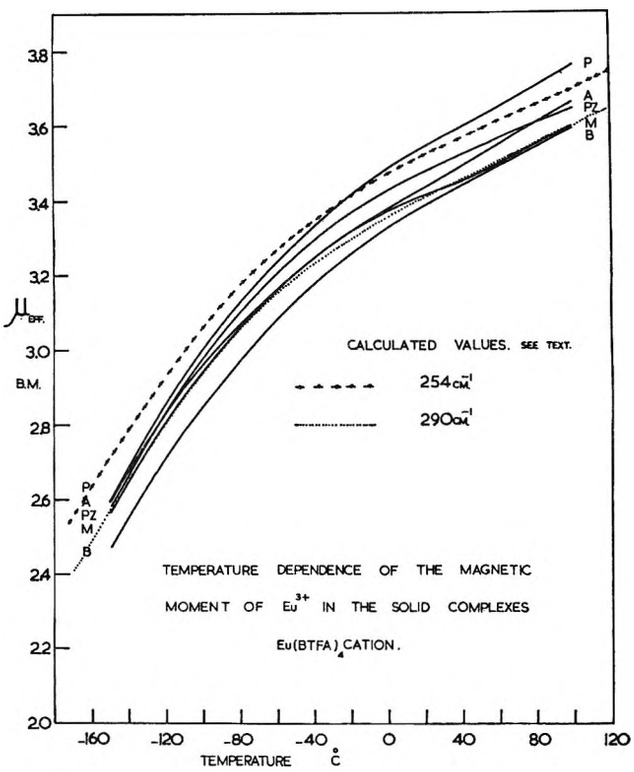

Figure 1.

The magnetic behavior of these compounds is in good general agreement with that expected for the Eu^{3+} ion. The close correspondence of P, PZ, and M at temperatures near −150° is reconcilable with the spectral similarities at −196°. It is tempting to attribute the lower paramagnetism of BTMA to the higher $^7F_0 \rightarrow {}^7F_1$ energy differences found in this case. However, the ammonium salt, which has energy differences comparable

(2) J. H. Van Vleck, "Electric and Magnetic Susceptibilities," Oxford University Press, London, 1932.

(3) P. W. Selwood, "Magnetochemistry," 2nd ed, Interscience Publishers, Inc., New York, N. Y., 1956.

(4) B. N. Figgis and R. S. Nyholm, *J. Chem. Soc.*, 331 (1959).

(5) B. N. Figgis and R. S. Nyholm, *ibid.*, 4190 (1958).

(6) T. M. Shepherd, *J. Inorg. Nucl. Chem.*, 29, 2551 (1967).

to BTMA, has a higher moment although deviation from a smooth curve in its susceptibility–temperature characteristic may reflect relatively large changes in the effective ligand field with temperature. Indeed, the increasing divergence of the susceptibilities of all the compounds studied with increasing temperature suggest that the ligand field strength and/or symmetry is markedly temperature dependent. In view of the complexity of the crystal structure, this behavior is not surprising.

Acknowledgment. The author thanks Dr. F. W. Bultitude and Mr. W. A. Fort who provided the samples.

The Sublimation of Aluminum Trifluoride and the Infrared Spectrum of $AlF_3(g)$[1]

by Alfred Büchler, Edward P. Marram, and James L. Stauffer

Arthur D. Little, Inc., Cambridge, Massachusetts
(Received July 21, 1967)

This note reports the mass-spectrometric determination of the heats of sublimation of gaseous aluminum trifluoride monomer and dimer, and a study of the infrared spectrum of $AlF_3(g)$. The mass-spectrometric work was carried out on a 12-in. radius, 60°-sector, magnetic-deflection instrument built by Nuclide Associates. Matheson Coleman and Bell anhydrous aluminum fluoride was used in these experiments. Samples were contained in a platinum-lined two-piece nickel crucible, especially designed[2] for the accurate measurement of second-law heats of vaporization. A typical mass spectrum is shown in Table I. Data for two runs are given in Table II. From an inspection of these data, it is clear that the ions AlF_2^+ and AlF_3^+ must be assigned to the monomer AlF_3, and the ion $Al_2F_5^+$ to the dimer Al_2F_6. This assignment agrees with that of Porter and Zeller.[3] It also implies that the vaporization of $AlF_3(c)$ is congruent, with the vapor mainly monomeric and the dimer contributing at most a few per cent to the total pressure. The difference in the AlF_2^+ and AlF_3^+ slopes is probably not significant, although some temperature dependence of the fragmentation pattern cannot be excluded. We thus take the mean values of runs 1 and 2 to obtain the heats of sublimation at 1000°K.

Table I: Mass Spectrum of Aluminum Trifluoride Vapor at 1025°K[a]

	Species		
	AlF_2^+	AlF_3^+	$Al_2F_5^+$
Ion current	100	4.2	0.57

[a] 60-V ionizing electrons; ion current in arbitrary values.

Table II: Slopes of $2.303R \log (I^+T)$ *vs.* $10^3/T$[a]

Species	Run 1 951–1057°K	Run 2 970–1077°K
AlF_2^+	68.4 ± 0.8	67.6 ± 1.3
AlF_3^+	66.8 ± 0.8	66.3 ± 1.8
$Al_2F_5^+$	95.1 ± 2.8	86.5 ± 2.8

[a] I^+ is the ion current; T is the temperature, °K.

$$AlF_3(c) \longrightarrow AlF_3(g)$$
$$\Delta H_{s,1000} = 67.3 \pm 3 \text{ kcal mole}^{-1}$$
$$2AlF_3(c) \longrightarrow Al_2F_6(g)$$
$$\Delta H_{s,1000} = 85.8 \pm 3 \text{ kcal mole}^{-1}$$

The uncertainty of ±3 kcal reflects our estimate of the accuracy of second-law heat determinations with the experimental arrangement used. The value of $\Delta H_{s,1000}$ for $AlF_3(g)$ is in very good agreement with the value of 67.46 kcal mole^{-1} at 1000°K given by JANAF Thermochemical Tables,[4] on the basis of an extensive survey of the literature. The present data give a value of -48.8 ± 3 kcal mole^{-1} for the heat of dimerization of $AlF_3(g)$, in good agreement with the mass-spectrometric third-law value of -48 ± 4.0 kcal mole^{-1} reported by Porter and Zeller.[3]

The infrared spectrum of gaseous aluminum fluoride was obtained using a modified Perkin-Elmer Model 12C infrared spectrometer described earlier.[5] Sodium chloride, cesium bromide, and cesium iodide optics were used to scan the spectrum between 2500 and 200 cm^{-1}. The temperature of the experiments ranged from 1000 to 1200°. The observed absorption bands and their assignments are shown in Table III. The 935-cm^{-1} band clearly represents the asymmetric stretching vibration ν_3. The value obtained is in satisfactory agreement with the value of 945 cm^{-1} reported by McCory, Paule, and Margrave.[6] The assignment of the other

(1) This work was supported by the U. S. Army Research Office with funds provided by the Advanced Research Projects Agency.

(2) A. Büchler and J. B. Berkowitz-Mattuck, *J. Chem. Phys.*, **39**, 286 (1963).

(3) R. F. Porter and E. E. Zeller, *ibid.*, **33**, 858 (1960).

(4) "JANAF Thermochemical Tables," 1st addendum, The Thermal Research Laboratory, Dow Chemical Company, Midland, Mich., 1966. The vibrational frequencies used in the $AlF_3(g)$ table are based on the present work.

(5) A. Büchler and E. P. Marram, *J. Chem. Phys.*, **39**, 292 (1963).

Table III: Infrared Spectrum of $AlF_3(g)$

Assignment	Frequency, cm^{-1}
$\nu_2(A_2)$	297
$\nu_3(E)$	935
$\nu_4(E)$	263

two bands was made by analogy with the spectra of the boron trihalides.[7,8] The higher of the two, at 297 cm^{-1}, was thus assigned to the out-of-plane bending vibration, ν_2, while the lower, at 263 cm^{-1}, was assigned to the in-plane bending vibration, ν_4. Thus three of the four fundamental vibrations of $AlF_3(g)$ are accounted for. These three bands have also been observed in matrix isolation by Linevsky.[9] The frequencies obtained in a solid argon matrix are $\nu_2 \sim 266$ cm^{-1}, $\nu_3 \sim 940$ cm^{-1}, and $\nu_4 \sim 251$ cm^{-1}. Thus, there are only small shifts for the in-plane vibration frequencies, ν_3 and ν_4, while there is a shift of about 30 cm^{-1} for the out-of-plane vibration, ν_2. The Raman-active symmetric stretching frequency remains to be determined. Applying a valence force field[7] to ν_3 and ν_4, we derive a value of 642 cm^{-1} for ν_1. If the same analysis is applied to $^{11}BF_3$, one finds that the experimental value of ν_1, 888 cm^{-1}, is 25% higher than the value of 710 cm^{-1} calculated from ν_3 and ν_4. We are thus led similarly to increase the valence force field value of 642 cm^{-1} by 25%, obtaining

$$\nu_1(A_1) = 800 \text{ cm}^{-1} \text{ (estimated)}$$

for $AlF_3(g)$.

(6) L. D. McCory, R. C. Paule, and J. L. Margrave, *J. Phys. Chem.*, **67**, 1086 (1963).

(7) G. Herzberg, "Infrared and Raman Spectra of Polyatomic Molecules," D. Van Nostrand, Inc., Princeton, N. J., 1945, p 178.

(8) T. Wentinck, Jr., and V. H. Tiensuu, *J. Chem. Phys.*, **28**, 826 (1958).

(9) M. J. Linevsky, Working Group on Thermochemistry, Proceedings of the Second Meeting, Vol. 1, Applied Physics Laboratory, Johns Hopkins University, Silver Spring, Md., Chemical Propulsion Information Agency, June 1964, p 87.

Conductances of Some Uni-univalent Electrolytes in N-Methyl-2-pyrrolidone at 25°

by Michael D. Dyke, Paul G. Sears, and Alexander I. Popov

Department of Chemistry, Michigan State University, East Lansing, Michigan 48823 *(Received June 21, 1967)*

Previous studies on N-methyl-2-pyrrolidone, C_5H_9NO, a cyclic amide which is also known as N-methyl-γ-butyrolactam, have shown that this liquid has excellent solvent characteristics which appear to closely parallel those of dimethyl sulfoxide and of N,N-dimethylacetamide.[1] It has also been shown that N-methyl-2-pyrrolidone can act as a ligand in the formation of inorganic complex compounds.[2] The present

Table I: Conductances of Salts in N-Methyl-2-pyrrolidone at 25°[a]

10^4C	Λ	10^4C	Λ	10^4C	Λ
NaI		KI		$NaClO_4$	
2.581	40.14[a]	3.190	39.74[a]	3.929	39.95[a]
4.890	39.55	6.102	39.17	6.295	39.51
8.625	38.91	11.67	38.42	10.49	38.90
12.82	38.24	25.35	37.09	18.54	38.07
20.74	37.52	34.57	36.47	27.45	37.37
29.06	36.80	39.61	36.16	39.27	36.66
3.282	39.95[b]	3.319	39.73[b]	4.723	39.76[b]
5.936	39.37	7.055	39.06	7.243	39.32
11.73	38.54	13.27	38.22	13.11	38.57
19.34	37.71	20.06	37.56	19.95	37.91
28.13	36.91	31.48	36.66	26.87	37.39
		48.17	35.72	38.75	36.69
$NaBPh_4$**		$KClO_4$		$(i\text{-Am})_3BuNI$	
2.141	25.68[a]	3.750	40.13[a]	5.509	36.87[a]
3.703	25.36	6.975	39.52	9.182	36.19
6.316	25.01	11.63	38.88	13.93	35.53
10.24	24.57	18.24	38.16	21.18	34.70
15.34	24.15	26.90	37.48	29.55	33.95
21.61	23.75	39.41	36.66	43.41	32.97
1.233	25.97[b]	2.527	40.46[b]	4.548	37.09
3.281	25.50	4.802	39.97	8.296	36.33
5.378	25.18	8.799	39.24	13.97	35.53
8.601	24.78	14.61	38.55	20.27	34.84
12.26	24.44	22.55	37.80	27.66	34.15
17.29	24.06	33.00	37.09	36.06	33.51
$(i\text{-Am})_3BuNBPh_4$					
4.366	22.55[a]				
9.008	22.01				
15.52	21.49				
21.51	21.13				
29.75	20.71				
36.63	20.43				
3.734	22.66[b]				
8.829	22.00				
15.43	21.48				
21.06	21.13				
28.80	20.74				
35.63	20.45				

[a] Superscripts a and b designate series of determinations; ** Ph = phenyl; *i*-Am = isoamyl; Bu = *n*-butyl.

(1) P. G. Sears, W. H. Fortune, and R. L. Blumenshine, *J. Chem. Eng. Data*, **11**, 406 (1966).

(2) J. H. Bright, R. S. Drago, D. M. Hart, and S. K. Madan, *Inorg. Chem.*, **4**, 18 (1965).

Table II: Calculated Parameters of the Fuoss–Onsager Equation for Salts in N-Methyl-2-pyrrolidone

Salt	Series	Λ_0	$\sigma\Lambda^a$	$\mathring{a}$	K_A	S	E	J^b
NaI	a	41.58 ± 0.05	0.019	3.8 ± 0.2	0	87.30	259	632.1
	b	41.65 ± 0.03	0.014	3.9 ± 0.1	0	87.36	259	640.9
KI	a	41.52 ± 0.03	0.013	4.0 ± 0.1	0	87.25	258	653.4
	b	41.46 ± 0.04	0.012	4.1 ± 0.1	0	87.20	258	669.6
$NaClO_4$	a	41.80 ± 0.02	0.010	4.5 ± 0.1	0	87.50	260	716.7
	b	41.76 ± 0.02	0.006	4.6 ± 0.1	0	87.46	260	725.5
$NaBPh_4$	a	26.79 ± 0.01	0.006	5.8 ± 0.1	0	74.28	143	576.9
	b	26.83 ± 0.01	0.005	5.8 ± 0.1	0	74.32	143	583.1
$KClO_4$	a	41.94 ± 0.01	0.006	4.4 ± 0.1	0	87.62	261	703.5
	b	41.96 ± 0.03	0.012	4.2 ± 0.1	0	87.64	261	683.3
$(i\text{-Am})_3BuNI$	a	39.00 ± 0.02	0.007	2.8 ± 0.1	0	85.03	238	462.7
	b	39.01 ± 0.01	0.005	2.8 ± 0.1	0	85.04	238	472.6
$(i\text{-Am})_3BuNBPh_4$	a	24.08 ± 0.03	0.010	5.3 ± 0.1	0	71.89	122	492.6
	b	24.06 ± 0.02	0.008	5.3 ± 0.1	0	71.88	122	493.4

[a] Standard deviation of Λ. [b] No viscosity correction applied.

exploratory investigation focuses upon the conductances of seven selected uni-univalent electrolytes in NM2PY to elucidate further the potential of this medium as an electrolytic solvent. Values for several physical properties of NM2PY at 25° are as follows: dipole moment, 4.09 D.;[3] dielectric constant, 32.0;[1] viscosity, 0.01666 poise;[1] density, 1.0279 g/ml;[1] refractive index, 1.4680.[1] Most quaternary ammonium salts and metallic perchlorates, thiocyanates, bromides, and iodides readily dissolve in NM2PY whereas alkali metal chlorides and fluorides and symmetrical multivalent salts are practically insoluble.

Experimental Section

The solvent (Eastman practical grade) was refluxed over barium oxide and then fractionally distilled through a 24-in. Vigreux column at 1 mm and 48°. Each retained middle fraction had a specific conductance of 1–2 × 10^{-8} ohm^{-1} cm^{-1}. Triisoamylbutylammonium iodide and triisoamylbutylammonium tetraphenylborate were synthesized and recrystallized using the method of Coplan and Fuoss.[4] Reagent grade potassium and sodium salts were used without further purification. All salts were dried *in vacuo* at 50° to constant weight prior to their use in the preparation of stock solutions. The apparatus and procedures have been described previously.[5]

Results and Discussion

Values of the measured equivalent conductances and the corresponding concentrations are summarized in Table I. These data were analyzed by the Fuoss–Onsager equation[6,7] which may be expressed as

$$\Lambda = \Lambda_0 - SC^{1/2} + EC \log C + JC \qquad (1)$$

for unassociated electrolytes. All symbols in this equation have their usual meanings.[7]

The conductance parameters obtained from least-squares analyses[8] of the data in Table I using a CDC-3600 computer are summarized in Table II. The normally small viscosity corrections associated with J were omitted inasmuch as these are usually omitted for potassium and sodium salts having small anions and because viscosity data for solutions of the other salts were lacking. The viscosity correction in each case has no effect on the value of Λ_0 and, if applied, leads only to slightly higher values for J and $\mathring{a}$. Calculations based on Λ data weighted by C yielded a considerably improved fit to eq 1, as evidence by smaller values of $\sigma\Lambda$; hence, the final results are reported on this basis.

The constants α, β, E_1, and E_2 for NM2PY at 25° have values of 0.8802, 5.0696, 7.800, and 65.786, respectively. S and E in eq 1 are defined as

$$S = \alpha\Lambda_0 + \beta; \quad E = E_1\Lambda_0 - E_2$$

Calculated differences in the limiting equivalent conductances between corresponding iodides and perchlo-

(3) E. Fischer, *J. Chem. Soc.*, 1382 (1955).

(4) M. A. Coplan and R. M. Fuoss, *J. Phys. Chem.*, **68**, 1177 (1964).

(5) P. G. Sears, J. A. Caruso, and A. I. Popov, *ibid.*, **71**, 905 (1967).

(6) R. M. Fuoss and L. Onsager, *ibid.*, **61**, 668 (1957).

(7) R. M. Fuoss and F. Accascina, "Electrolytic Conductance," Interscience Publishers, Inc., New York, N. Y., 1959.

(8) Dr. R. L. Kay of the Mellon Institute, Pittsburgh, Pa., kindly provided the FORTRAN program which was used in the treatment of our data.

rates and between corresponding iodides and tetraphenylborates indicate a maximum uncertainty in the Λ_0 values of 0.20 unit or about 0.5%. Thus, the apparent level of accuracy and the general consistency of the over-all results are relatively good for this exploratory conductance study.

Single-ion limiting equivalent conductances were obtained by the method of Coplan and Fuoss,[4] which is based upon the assumption that the limiting conductances of the triisoamylbutylammonium and the tetraphenylborate ions are equal in any solvent. Limiting ionic equivalent conductances (ohm^{-1} cm^2 $equiv^{-1}$) in NM2PY are as follows: Na^+, 14.7; K^+, 14.7; I^-, 26.9; ClO_4^-, 27.2; $(i\text{-Am})_3BuN^+$, 12.0; BPh_4^-, 12.0. Within experimental error, the potassium and sodium ions are iso-conducting in NM2PY. Comparing the behavior of these ions in noncyclic amides, it is interesting to note that the potassium ion is very slightly more conducting than the sodium ion in N,N-dimethylformamide,[9] whereas their roles are reversed in N,N-dimethylacetamide.[10]

It is concluded from the above results that NM2PY is an excellent dissociating solvent since all of the salts are completely dissociated within the experimental concentration range. It is also worthwhile to point out that NM2PY, adiponitrile, and methanol have almost identical values for dielectric constants (32.0, 32.45, and 32.62, respectively); the dissociating powers of MN2PY and adiponitrile[5] toward electrolytes are comparable to, and possibly greater than, that of methanol.[11]

(9) D. P. Ames and P. G. Sears, *J. Phys. Chem.*, **59**, 16 (1955).

(10) G. R. Lester, T. A. Gover, and P. G. Sears, *ibid.*, **60**, 1076 (1956).

(11) R. L. Kay, C. Zawoyski, and D. F. Evans, *ibid.*, **69**, 4209 (1965).

A Pressure-Jump Study of the Kinetics of Uranyl Ion Hydrolysis and Dimerization[1]

by P. A. Hurwitz

Department of Chemistry, University of Massachusetts, Boston, Massachusetts

and G. Atkinson

Department of Chemistry, University of Maryland, College Park, Maryland (*Received June 5, 1967*)

During the past few years, there have been several studies of the kinetic and equilibrium reactions of uranyl ion in acidic, aqueous solutions. Baes and Meyer[2] studied the hydrolysis mechanism and equilibrium constants of uranyl ion in acidic, aqueous nitrate media. From the Baes and Meyer study, we have been able to evaluate rate constants for the various equilibria using the pressure-jump method while Eyring and co-workers[3] have evaluated the same system using the temperature-jump method.

Experimental Section

For our experiments, analytical reagent grade uranyl nitrate hexahydrate was purchased from Fisher Scientific Co. As a precaution the reagent was dried over concentrated sulfuric acid. Before using, the purity of the material was qualitatively examined by comparing experimental and literature absorption coefficients. We found that the material was uranyl nitrate hexahydrate within a few per cent of our determination.

Each solution was prepared by weighing out appropriate amounts of uranyl nitrate and then diluting to a known volume with distilled, demineralized water. An inert electrolyte such as potassium nitrate was not required to adjust the ionic strength, since the sensitivity of the method would have been seriously reduced by traces of nonreacting ions. For various initial concentrations of uranyl nitrate the ionic strength was not uniform. The effect of this inconsistency on the final conclusions did not appear to be significant. Each solution was brought to the desired pH by dropwise addition of dilute NaOH and/or dilute HNO_3.

The pressure-jump apparatus was constructed from a diagram given by Yeager[4] and co-workers. The solution cell was constructed from Lucite with the added advantage that the platinum electrodes were threaded to the Lucite. Such a means of attachment allowed for possible electrode adjustment. The cell was connected in turn to a Wheatstone bridge. Since we are only interested in measuring relative changes of the cell resistance, our bridge requirements are different from the usual conductance bridges. The bridge was constructed from available commercial components and mounted in an aluminum chassis. Special precautions were taken to insulate the components, and coaxial connections were made wherever feasible. Both the input and output connections to the bridge were isolated from the oscillator and detector, respectively,

(1) The experimental work reported here was done at the University of Maryland under Grant 14-01-001-405 from the Office of Saline Water of the U. S. Department of the Interior.

(2) C. F. Baes, Jr., and N. J. Meyer, *Inorg. Chem.*, **1**, 780 (1962).

(3) M. P. Whittaker, E. M. Eyring, and E. Dibble, *J. Phys. Chem.*, **69**, 2319 (1965).

(4) H. Hoffman, J. Stuehr, and E. Yeager, ONR, Contract Nonr 1439(04), Project NR 384-305, Technical Report 27, 1964, p 12.

Table I:[a] Relaxation Spectrum of Uranyl Dimerization at 25°

$[UO_2^{2+}]_0$	$[UO_2^{2+}]$	$[UO_2OH^+]$	$[D]^b$	$[T]^c$	pH	τ_{obsd}, msec	k_{-1}, M^{-1} sec^{-1}	k_2, M^{-1} sec^{-1}	Approximate ionic strength M
0.0208	0.0201	3.4×10^{-5}	3.5×10^{-7}	2.2×10^{-7}	2.93	0.25	$>3.3 \times 10^6$	...	0.06
						5.0	...	76	
0.0304	0.0280	5.7×10^{-5}	9.8×10^{-4}	1.4×10^{-4}	3.01	0.25	$>3.9 \times 10^6$	...	0.09
						4.7	...	50	
0.0208	0.0207	1.0×10^{-5}	3.2×10^{-5}	5.2×10^{-10}	2.40	0.25	$>1.0 \times 10^6$	...	0.06
						...	...	...	
						Av	$>2.7 \times 10^6$	63	

[a] All concentrations in moles per liter. [b] $D \equiv (UO_2)_2(OH)_2^{2+}$. [c] $T \equiv (UO_2)_3(OH)_5^+$.

by General Radio shielded transformers, Model 578-C. With a 50-kc signal, good results were obtained using a General Radio tuned amplifier and null detector, Type 1232-A. The signal was rectified using a very simple diode detector circuit. This rectified signal was fed directly into a Tektronix Model 502 oscilloscope fitted with a Polaroid camera attachment. The oscilloscope was triggered internally. Several experiments were carried out where the oscilloscope was triggered externally using a piezoelectric crystal with a charge amplifier. Similar results were obtained for both triggering modes.

The rate constants were given for a temperature of 25 ± 2°. Each relaxation time represents an average of at least three photographic determinations. The individual oscillograms could be evaluated to yield relaxation times with a relative error of ±20%.

The pressure above the reaction and comparison solutions was released spontaneously. For 0.0075 in. thick Mylar disks, the change in pressure was generally 30 atm. The rupture time for these disks was on the order of 250 μsec. In order to determine the rupture time, more commonly referred to as the apparatus response time, we employed a solution of 0.1 M $MgSO_4$. The relaxation time for the reaction $Mg^{2+} + SO_4^{2-} \rightleftarrows MgSO_4$ is less than 1 μsec.[5] The unassociated electrolyte barium benzenedisulfonate was used as the comparison with the $MgSO_4$ experiment.

For the uranyl experiments the nonreacting solution was $MgSO_4$ having a concentration such that both cells would have very nearly the same resistance. In this manner, we could then sort out the disturbing effects of the change of resistance due to physical effects from those due to the chemical relaxations.

Unlike Eyring[3] and co-workers, our experiments indicated that there were two relaxation effects occurring. We observed a fairly rapid relaxation time that coincided with our instrument rise time and a slower one having a value of about 5 msec. Although we are dealing with a coupled system, the relaxation times were separable and we could therefore evaluate the rate constants associated with two of the three equilibria involved in this study.

Results and Treatment of Data

The separate relaxation times were evaluated from a plot of the logarithm of the signal amplitude *vs.* time; the straight line obtained indicated a single relaxation process is being observed for that particular time range. The values of the relaxation times, the concentrations of the various uranyl ion species, and the rate constants are summarized in Table I.

The derivation of the relaxation times in terms of rate constants and equilibrium concentrations which follows is based on the equilibrium constants proposed by Baes and Meyer.[2] Accordingly, the uranyl equilibria with their corresponding equilibrium constants at 25° are

$$UO_2^{2+} + H_2O \underset{k_{-1}}{\overset{k_1}{\rightleftharpoons}} UO_2OH^+ + H^+$$

$$K_1 = 2 \times 10^{-6} \quad (1)$$

$$2UO_2^{2+} + 2H_2O \underset{k_{-2}}{\overset{k_2}{\rightleftharpoons}} (UO_2)_2(OH)_2^{2+} + 2H^+$$

$$K_2 = 1.2 \times 10^{-6} \quad (2)$$

$$3UO_2^{2+} + 5H_2O \underset{k_{-3}}{\overset{k_3}{\rightleftharpoons}} (UO_2)_3(OH)_5^+ + 5H^+$$

$$K_3 = 6 \times 10^{-17} \quad (3)$$

(5) M. Eigen, G. Kurtze, and K. Tamm, *Z. Elektrochem.*, **57**, 103 (1953); M. Eigen, *Z. Physik. Chem.* (Frankfurt), **1**, 134 (1954).

The observed relaxation times τ can be expressed as a function of the desired rate constants and known equilibrium concentrations by simple analysis of eq 1 and 2, respectively. This treatment is possible because two separable relaxation times are observed. To obtain the particular relaxation expressions, it is only necessary to linearize in the usual manner the rate law expressions for eq 1 and 2.[6]

For the system described by eq 1, the reciprocal of the relaxation time is given by

$$\frac{1}{\tau} = k_{-1}(\overline{UO_2OH} + \bar{H}) + k_1 \qquad (4)$$

where k_{-1} and k_1 are the bimolecular and unimolecular rate constants having the units of M^{-1} sec^{-1} and sec^{-1}, respectively. The bars above the species signify equilibrium concentrations, but the charges of the ions have been neglected here in order to simplify the notation.

For the system described by eq 2, in which the dimer species results, the reciprocal of the relaxation time is given by

$$\frac{1}{\tau} = 4k_2\frac{(\overline{UO_2})}{1+\alpha} + k_{-2}\left[\frac{4(\overline{(UO_2)_2(OH)_2})(\bar{H})}{1+\alpha} + \bar{H}^2\right] \qquad (5)$$

where k_2 is the bimolecular rate constant for the dimerization. The factor α, in this case, accounts for the rapid equilibrium step occurring in eq 1. This factor is explicitly

$$\alpha = \frac{\delta[\text{dimer}]}{\delta[UO_2]} = \frac{k_1 - \overline{UO_2OH}}{\bar{H}} \qquad (6)$$

In the absence of appreciable monomer (UO_2OH), α should be zero. Examination of eq 6 shows that

$$\lim_{k_1(UO_2OH)\to 0} \frac{\delta[\text{dimer}]}{\delta[UO_2]} = 0$$

A third relaxation time was not actually resolved at higher pH or higher concentrations of uranyl nitrate. It was only possible to determine the rate constant for the monomer–dimer equilibrium and to establish a lower limit for the protolytic reaction (k_{-1}) of eq 1. It might indeed be possible to observe the trimer formation even though the concentration of trimer is sometimes as low as 10^{-7} M for the present experimental conditions. Alternately, the magnitude of the trimer relaxation process may have been negligible for our conditions.

Discussion

The lower limit for k_{-1} of $\sim 3 \times 10^6$ M^{-1} sec^{-1} is consistent with the value of 1.5×10^{10} M^{-1} sec^{-1} directly determined by the dispersion of the dissociation field effect.[7] Alternately, an *a priori* calculation of k_{-1} can be made using the Smoluchowski–Debye–Eigen theory of diffusion-controlled reactions which agrees with the directly determined value.[8]

As Eyring[3] indicated, the possibility of uranyl nitrate complexation kinetics should be considered. Therefore, another experiment involving the same initial concentration of UO_2^{2+} was carried out at a pH of 2.4. At this pH the concentration of dimer is reduced. We no longer observed the slower relaxational process. The more rapid relaxation was still present and attributable to reaction 1. This experiment does not conclusively prove the observation. However, the temperature-jump work[3] included a series of similar experiments in which the NO_3^- concentration was varied. For these latter experiments, the relaxation time was observed to remain essentially constant. The independence of the relaxation time on NO_3^- precludes the occurrence of any uranyl nitrate complexation. In our case when the pH was lowered the slower process disappeared; this result can be most easily reconciled with dimerization as opposed to complexation.

The value determined for k_2 is 63 M^{-1} sec^{-1} at 25° at an ionic strength of 0.06 M. The value determined by Eyring and co-workers[3] is 116 M^{-1} sec^{-1} at 25° at an ionic strength of 0.5 M. Since reactions between species of the same charge are observed to increase in rate with increasing ionic strength, the rate constants determined in this work agree very well with that of Eyring.

There remains then the question of other possible uranylhydroxy species. There is at least another mechanism[3] for reaction 2, specifically the consideration of

$$2UO_2^{2+} + H_2O \underset{}{\overset{k_2}{\rightleftharpoons}} (UO_2)_2(OH)^{3+} + H^+$$

Inclusion of this latter possibility, however, does not alter the interpretation presented here.

(6) M. Eigen and L. DeMaeyer in "Techniques of Organic Chemistry," Vol. VIII, A. Weissberger, Ed., John Wiley and Sons, Inc., New York, N. Y., 1963, Part 2.

(7) D. L. Cole, E. M. Eyring, D. T. Rampton, A. Silzars, and R. P. Jensen, 153rd National Meeting of the American Chemical Society, Miami, Fla., April 9–14, 1967.

(8) *Cf.* ref 6, p 1032.

Calculation of the Conformation Change Controlled Ionization of Polyamino Acids from Titration Curves[1]

by Eugene Hamori

Department of Chemistry, University of Delaware, Newark, Delaware 19711

and Harold A. Scheraga

Department of Chemistry, Cornell University, Ithaca, New York 14850
(Received May 24, 1967)

If a polyamino acid in solution at the helix–coil transition region is subjected to a pH or temperature change, the degree of ionization α of the side chains will change. This total change is $\Delta\alpha_t = \Delta\alpha_i + \Delta\alpha_c$, where $\Delta\alpha_i$ is the change in ionization due to the pH or temperature change (without an accompanying conformation change) and $\Delta\alpha_c$ is the ionization change due to a conformation change (without a pH or temperature change). The latter term arises from the fact that the electrostatic interaction differs in the two conformations, *e.g.*, in the helix and coil forms. Since the time rate of $\Delta\alpha_i$ is normally very fast compared to the rate of $\Delta\alpha_c$, relaxation kinetic techniques may be used to measure the rate of $\Delta\alpha_c$ by observing the rate of $\Delta\alpha_t$; thus, information can be obtained about the kinetics of fast biopolymer conformation changes. Obviously, this method requires that $\Delta\alpha_c$ be a significant portion of $\Delta\alpha_t$. The necessity of establishing this fact becomes particularly important for those relaxation kinetic experiments in which the slow relaxation time assignable to $\Delta\alpha_c$ is not easily detected in the oscillograph record of the kinetic experiment. In these cases, in order to prove that $\Delta\alpha_c$ is part of the observed fast change (*i.e.*, as fast as $\Delta\alpha_i$), it has to be shown that $\Delta\alpha_c/\Delta\alpha_t$ is not negligibly small. In this note, we demonstrate how to calculate the ratio $\Delta\alpha_c/\Delta\alpha_t$ for pH-jump or temperature-jump experiments from titration data, and in the accompanying note,[2] we apply these considerations to the rate of the helix–coil transition in poly-L-tyrosine.

Figure 1 shows the titration curve of a polyamino acid (such as poly-L-glutamic acid[3–6]) on a y *vs.* α plot where $y = \text{pH} - \log [\alpha/(1 - \alpha)]$. If the conformation of the polymer did not change, the titration curve would be linear on this plot, according to the equation[7,8]

$$y = pK^\circ + W\alpha \qquad (1)$$

where pK° is the intrinsic pK value of the ionizing groups and W is a constant determined primarily by the conformation of the macromolecule. Such constant-conformation lines, including the limits for the perfect helix and pure coil, are also shown in Figure 1.

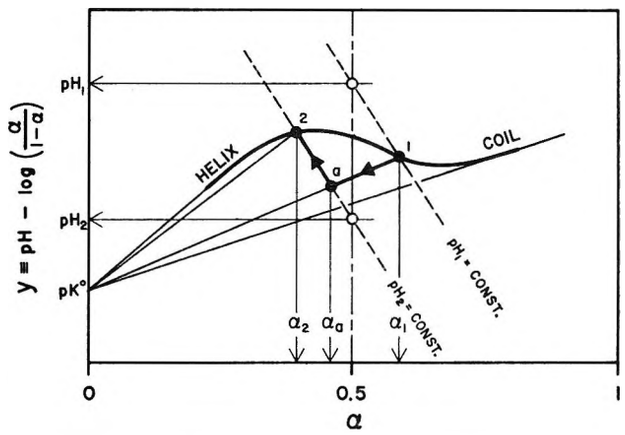

Figure 1. Determination of α_1, α_a, and α_2 for a pH jump. The heavily drawn curve is the experimental titration curve and the lines originating from pK° are constant-conformation lines (see text for other symbols).

Calculations for the pH-Jump Method

In this kinetic technique, the observed $\Delta\alpha_t$ is brought about by a perturbation of the equilibrium of the system by a sudden pH change.[2] In an ideal pH-jump experiment, the effect of any temperature change which may occur simultaneously with the pH change can be neglected. Consider, therefore, an isothermal pH change ($pH_1 \rightarrow pH_2$) such that the net change in the ionization of the polymer is from α_1 to α_2 (see Figure 1). This ionization change can be envisaged as occurring in two steps.

(1) α_1 to α_a. This is a rapid change in the ionization of the polymer *without an accompanying conformation change;* hence eq 1 is applicable and, on the plot of Figure 1, the system moves from state 1 to (an as yet undefined) state a on a straight (constant-conformation) line. The corresponding change in ionization is $\Delta\alpha_i = \alpha_a - \alpha_1$.

(1) The part of the work carried out at Cornell University was supported by a research grant (GB-4766) from the National Science Foundation, and by a research grant (GM-14312) from The National Institute of General Medical Sciences of the National Institutes of Health, U. S. Public Health Service.

(2) E. Hamori and H. A. Scheraga, *J. Phys. Chem.*, **71**, 4147 (1967).

(3) A. Wada, *J. Mol. Phys.*, **3**, 409 (1960).

(4) M. Nagasawa and A. Holtzer, *J. Am. Chem. Soc.*, **86**, 538 (1964).

(5) P. Appel and J. T. Yang, *Biochemistry*, **4**, 1244 (1965).

(6) J. Hermans, Jr., *J. Phys. Chem.*, **70**, 510 (1966).

(7) K. Linderstrom-Lang, *Compt. Rend. Trav. Lab. Carlsberg (Ser. Chim.)*, **15**, No. 7 (1924).

(8) R. K. Cannon, A. H. Palmer, and A. C. Kibrick, *J. Biol. Chem.*, **142**, 803 (1942).

(*2*) α_a *to* α_2. Subsequently, at constant pH (it being assumed that the solution is buffered), the polymer conformation changes spontaneously leading to a change in W, so that the system moves from its intermediate state a to its final state 2 on the plot of Figure 1. The ionization change for this process is $\Delta\alpha_c = \alpha_2 - \alpha_a$, and its rate will be controlled by the rate of conformation change of the macromolecule. We will show below that the curve from a to 2 is approximately a straight line at $\alpha \sim 0.5$.

According to eq 1, if pH, pK° (and temperature) are constant, the functional dependence of α on W is represented on the y *vs.* α plot by a family of curves for which pH = constant (iso-pH lines). A convenient equation can be obtained for these curves by expanding the expression, pH $-$ log $[\alpha/(1-\alpha)]$, in a power series in terms of $(\alpha - {}^1/_2)$

$$y \equiv \text{pH} - \log[\alpha/(1-\alpha)] = \text{pH} - (2/2.303)\sum_{n=0}^{n=\infty}[2(\alpha - {}^1/_2)]^{2n+1}/2n + 1 = \text{pH} - \frac{2}{2.303}\left[2(\alpha - {}^1/_2) + \frac{2^3(\alpha - {}^1/_2)^3}{3} + \frac{2^5(\alpha - {}^1/_2)^5}{5} + \ldots\right] \quad (2)$$

This equation indicates that the iso-pH lines are sigmoid curves such that $y = +\infty$ at $\alpha = 0$ and $y = -\infty$ at $\alpha = 1$. At $\alpha = {}^1/_2$ there is an inflection point and the value of y at this point is the pH of the system. In the neighborhood of $\alpha = 0.5$, higher terms in $(\alpha - {}^1/_2)$ can be neglected and eq 2 can be approximated by

$$y = \text{pH} - (2/2.303)[2 - (\alpha - {}^1/_2)] = \text{pH} + 0.8685 - 1.737\alpha \quad (3)$$

which represents a straight line of slope -1.737 on the y *vs.* α plot at constant pH. The difference between eq 2 and the approximation represented by eq 3 is rather small in comparison with the inaccuracies involved in the determination of pH and α. For example, at $\alpha = 0.6$ the accurate value of y is only 0.002 pH unit smaller (at $\alpha = 0.4$ it is 0.002 unit greater) than the value derived from eq 3. The accurate slope of the iso-pH lines at $\alpha = 0.4$ and 0.6 is -1.806, and that of the approximation is -1.737. If the approximation represented by eq 3 is accepted, straight lines of slope -1.737 can be substituted for the iso-pH lines in the region of $\alpha \sim {}^1/_2$. (Incidentally, this is the only α region of interest in most helix–coil relaxation-kinetic studies.) It should be noted that, on the y *vs.* α plot, these iso-pH lines cross the vertical $\alpha = {}^1/_2$ line at values of y identical with their respective pH values.

Based on these considerations, the desired ratio, $\Delta\alpha_c/\Delta\alpha_t$, can be determined by a graphical procedure as follows. On the y *vs.* α graph, which contains the experimental titration curve of a particular polyamino acid, two straight lines of slopes -1.737 are drawn; one of these must cross the vertical $\alpha = {}^1/_2$ line at $y = \text{pH}_1$, the other at $y = \text{pH}_2$. These pH values designate the initial and final pH, respectively, of the system in the pH-jump experiment (open circles of Figure 1). The intersections of these iso-pH lines with the experimental titration curve yield the initial and final states (1, 2) and the initial and final degree of dissociation (α_1, α_2) of the polyamino acid. From the point designated as 1, a straight line is drawn toward the pK° intercept on the y axis. The intersection of this line (W = constant) with the iso-pH line of the second pH value (pH_2 = constant) determines the position of the intermediate state a. The ratio $\Delta\alpha_c/\Delta\alpha_t$ then can be calculated by dividing $\alpha_2 - \alpha_a$ by $\alpha_2 - \alpha_1$. If this graphical construction is carried out on a sufficiently enlarged y *vs.* α plot, the accuracy of this technique appears to be limited only by the error of the experimental titration curve itself. The application of this method to the titration curve of poly-L-glutamic acid[6] yielded 0.35 for $\Delta\alpha_c/\Delta\alpha_t$ for a pH jump from 5.37 to 5.03 at 25° and at 0.1 M KCl ionic strength (in this case $\alpha_1 = 0.60$, $\alpha_a = 0.47$, and $\alpha_2 = 0.40$). For the smaller pH jumps of 5.25 to either 5.15 or 5.20, a value of 0.38 was derived for this ratio from the same titration curve. The graphical evaluation of this value for several hypothetical pH jumps indicated that the limiting value of 0.38 is about the maximum obtainable for the polyglutamic acid system under the conditions used.

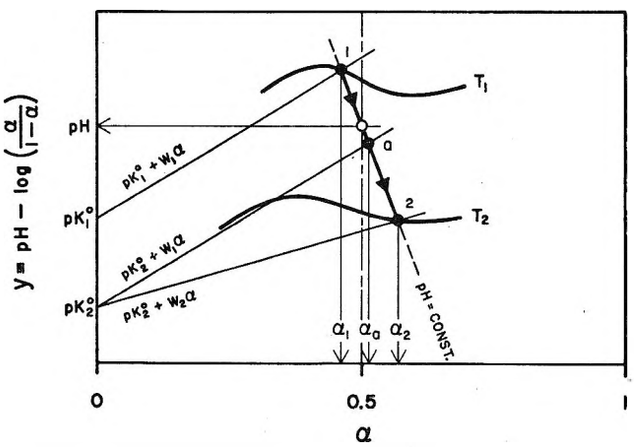

Figure 2. Determination of α_1, α_a, α_2 for a temperature jump from T_1 to T_2 (see Figure 1 and the text for definitions of the symbols). The curves are drawn relative to each other for a hypothetical group with a nonzero value of the heat of ionization. Actually, for poly-L-glutamic acid, the heat of ionization is small.

Calculations for the Temperature-Jump Method

In this method, the observed change in α is caused by the perturbation of the equilibrium of the system by a sudden change in temperature. Assuming that the change in pH is negligible during and after the temperature jump, the transition of the system from state 1 to state 2 can be described as follows (see Figure 2).

(1) α_1 to α_a. The intersection of the iso-pH line with the titration curve obtained at T_1 will determine the initial state of the system (1). In this condition, $\alpha = \alpha_1$ and $y = pK^\circ_1 + W_1\alpha_1$. The temperature jump changes pK°_1 to pK°_2 and W_1 to W_2. The former change is very fast in comparison with the latter which is controlled, for the most part, by the relatively slow conformation change of the macromolecule. If it is assumed that W_1 remains constant during the change in pK° (see below for further discussion of the validity of this assumption), the system can be considered as changing very rapidly from state 1 to an intermediate state a ($\alpha_1 \rightarrow \alpha_a$) while moving along the iso-pH line. The end position of this rapid change can be constructed on the y *vs.* α plot by drawing a line parallel to the $y = pK^\circ_1 + W_1\alpha$ line through the point pK°_2. The intersection of this line ($y = pK^\circ_2 + W_1\alpha$) with the iso-pH line will determine a.

(2) α_a to α_2. Subsequent to the rapid change in α from α_1 to α_a, W_1 changes to W_2 at a rate controlled by the conformation change. On the y *vs.* α plot, the point characterizing the state of the system moves from a to 2. It can be seen from Figure 2 that the latter point is defined by the intersection of the titration curve obtained at T_2 with the iso-pH line. The desired ratio $\Delta\alpha_c/\Delta\alpha_t$ in this case is calculated from the values as $(\alpha_2 - \alpha_a)/(\alpha_2 - \alpha_1)$. An application of this method to the poly-L-glutamic acid titration data,[6] assuming a temperature jump of 4° → 14° at pH 5.35, yielded a value of 0.68 for this ratio.

It appears that the assumed constancy of W during the fast step from α_1 to α_a is a reasonably good approximation since this quantity depends directly only on the absolute temperature of the system[7,9] which changes relatively little during a typical temperature jump (~10°), and the conformation has not yet changed as the system moves from 1 to a. However, if the need for high accuracy justifies this, the slope (W_1) used to determine α_a can be corrected for this temperature effect by taking into account the variation of W with T and by evaluating the temperature dependence of the various other parameters[9] (dielectric constant, Debye–Hückel parameter, etc.) determining W.

These calculations appear to indicate that the conformation-controlled part of the ionization change of a partially helical polyamino acid is a significant fraction of the total ionization change in a pH- or temperature-jump experiment.

(9) C. Tanford, *J. Am. Chem. Soc.*, 72, 441 (1950).

pH-Jump Measurements on the Helix–Coil Transition of Poly-L-Tyrosine[1]

by Eugene Hamori[2a] and Harold A. Scheraga[2b]

Department of Chemistry, Cornell University, Ithaca, New York 14850 *(Received September 2, 1966)*

It is known from the studies of Eigen, Hammes, and others[3-6] that the chemical relaxation which follows the perturbation of the helix–coil equilibrium in poly-L-glutamic acid is too fast for temperature-jump measurements. Since it has been proposed that the side chains of the helical form of poly-L-tyrosine interact with each other,[7,8] the possibility existed that such side-chain interactions might slow down the helix–coil transition in this polyamino acid sufficiently to bring the relaxation time within the range that can be studied by the temperature-jump technique ($>10^{-5}$ sec). Therefore, a study of poly-L-tyrosine was carried out with the temperature-jump apparatus described previously.[9] Actually, in the pH range used here (~pH 11.4), a rise in temperature leads to a *lowering* of the pH of the solvent, thereby inducing a conversion from coil to helix in the polymer. Thus, for this system, the temperature-jump technique becomes primarily a pH-jump technique.

(1) This work was supported by a research grant (GB-4766) from the National Science Foundation, and by a research grant (GM-14312) from the National Institute of General Medical Sciences of the National Institutes of Health, U. S. Public Health Service.

(2) (a) National Institutes of Health Postdoctoral Fellow of the National Institute of General Medical Sciences, 1964–1966. (b) To whom requests for reprints should be addressed.

(3) M. Eigen and G. G. Hammes, private communication.

(4) J. J. Burke, G. G. Hammes, and T. B. Lewis, *J. Chem. Phys.*, 42, 3520 (1965).

(5) G. Schwarz, *J. Mol. Biol.*, 11, 64 (1965).

(6) R. Lumry, R. Legare, and W. G. Miller, *Biopolymers*, 2, 489 (1964).

(7) J. D. Coombes, E. Katchalski, and P. Doty, *Nature*, 185, 534 (1960).

(8) G. D. Fasman, E. Bodenheimer, and C. Lindblow, *Biochemistry*, 3, 1665 (1964).

(9) G. C. Kresheck, E. Hamori, G. Davenport, and H. A. Scheraga, *J. Am. Chem. Soc.*, 88, 246 (1966).

Experimental Section

Poly-L-tyrosine (M_n = 58,000) was purchased from Gallard-Schlesinger Corp. It was converted into a highly helical material by slowly dialyzing its sodium salt against 0.01 N HCl at 40° as recommended by Fasman, *et al.*[8] The high degree of helicity was confirmed by optical rotatory dispersion measurements at pH 11.20.

A Beckman Model G meter was used with a Type E-2 glass electrode and a fiber-junction calomel reference electrode to measure the pH. During measurements, the solution and the electrodes were kept at constant temperature (±0.1°). For the standardization of the meter, a phosphate buffer was prepared according to Britton and Welford.[10] Since the pH of this buffer is accurately known at various temperatures,[10] the same buffer ($pH_{25°}$ 11.45) was used both for the routine 25° measurements and for the pH *vs.* temperature study. In the latter experiments, the pH of the solution was determined at each temperature only after the meter was standardized at the same temperature with the buffer. The solutions were kept under a purified nitrogen atmosphere during the pH measurements and also during the temperature jumps.

Optical density and optical rotation measurements were carried out with the Cary 14 and 60 instruments, respectively.

The temperature-jump apparatus used in this study has already been described.[9] An observation beam of 245-mμ wavelength was used. At this wavelength, one observes directly the protonation of the poly-L-tyrosine side chains.[11] Since this latter reaction is coupled to the helix–coil equilibrium a sufficiently slow conformation change of the polymer would also be observable at this wavelength.[12-14] To increase the sensitivity of the instrument in the ultraviolet region, two new high-gain photomultipliers (EMI, Type 9558 QB) were installed. The oscilloscope signal "blackout" which follows the high-voltage discharge was reduced to about 10^{-6} sec by placing the shielded photomultiplier tubes 20 in. away from the cell. The cell assembly unit was slightly modified to permit the use of a thermistor probe for measuring the temperature of the test solution in the cell directly. This instrument produces a 5.2 ± 0.2° temperature jump within a few microseconds.[9] The resistance of the cell filled with a 0.2 M NaCl solution was 80 ohms at 16°. From this value a time constant of 4.5 μsec can be calculated[9] for the exponential heating process. The polymer concentration used in all kinetic experiments was 0.002 g/100 g. The NaCl concentration was 0.2 M. All the relaxations were observed at the constant temperature of 21.2° (±0.5°), attained from an initial temperature of 16.0° (±0.2°) by the temperature jumps.

To extend the usable range of the apparatus to faster reaction rates ($\tau_r \sim 2$ μsec), an electronic relaxation process simulator (rps) was constructed.[15] This instrument, which is really a simple analog computer, is capable of producing curves on the oscilloscope screen which would be generated by a hypothetical reaction and a heating rate characterized by relaxation times τ_r and τ_h, respectively. The curves on the oscilloscope screen can be superimposed on the previously taken photographic record of the temperature-jump experiment to be analyzed. By varying the oscilloscope settings and the controls of the rps, the two images can be accurately matched. When this is accomplished, the settings of the calibrated controls of the rps yield τ_r and τ_h directly. In practice, due to the fact that τ_h can be calculated to a fair degree of accuracy,[12] the determination of τ_r is further facilitated by presetting the τ_h control on the instrument to the theoretical value and matching the unknown curve with only the τ_r control.

Results and Conclusions

It is well known that the hydrogen ion concentration of water in the presence of a sufficient concentration of strong base is strongly temperature dependent. For example, a 10° temperature increase lowers the pH of a 0.1 N NaOH solution by about 0.3 pH unit.[16] The helix–coil equilibrium of poly-L-tyrosine is very pH sensitive[7,8] near pH 11.4. Thus, rapid changes in temperature, which lead to changes in pH, can be conveniently utilized to perturb this equilibrium. The results of pH determinations carried out to demon-

(10) H. T. S. Britton, "Hydrogen Ions," Vol. 1, Chapman and Hall Ltd., London, 1955, p 359.

(11) J. Hermans, Jr., *Biochemistry*, 1, 193 (1962).

(12) M. Eigen and L. De Maeyer, "Technique of Organic Chemistry," Vol. 8, Part II, Interscience Publishers, Inc., New York, N. Y., 1963, p 895.

(13) Due to the lack of suitable experimental data on poly-L-tyrosine, the extent of this conformation change controlled optical density change cannot be quantitatively predicted. For poly-L-glutamic acid it was found[14] that this change is 38% of the total change for a pH change of 0.1 unit. Thus, on the assumption that, in this respect, poly-L-tyrosine behaves approximately in the same manner, a significant effect would be expected.

(14) E. Hamori and H. A. Scheraga, *J. Phys. Chem.*, 71, 4145 (1967).

(15) The circuit diagram and a discussion of the rps has been deposited as an appendix to this note with the American Documentation Institute, Auxiliary Publications Project, Photoduplication Service, Library of Congress, Washington 25, D. C., where it may be obtained by ordering Document 9623 and remitting $1.25 for microfilms or $1.25 for photoprints. Make checks payable to: Chief, Photoduplication Service, Library of Congress.

(16) R. G. Bates, "Electrometic pH Determinations," John Wiley and Sons, Inc., New York, N. Y., 1954, p 111.

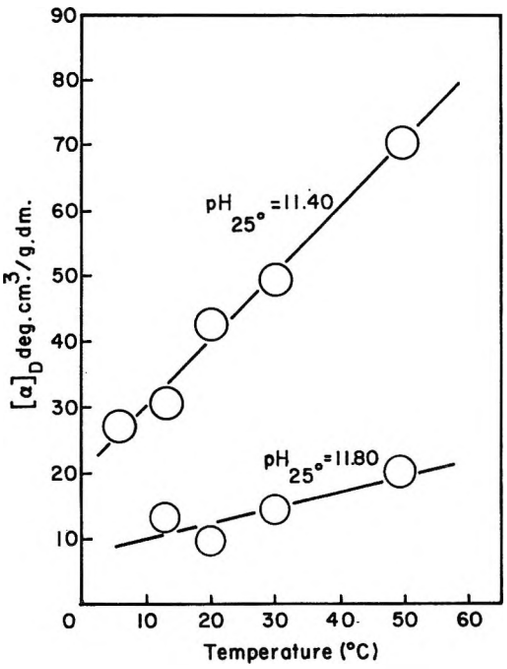

Figure 1. Variation of the specific optical rotation of poly-L-tyrosine solutions with temperature. Polymer concentration: 0.2 g/100 g, ionic strength: 0.2 *M* NaCl.

strate and measure the effect of temperature on the pH of the solutions are as follows: (poly-L-tyrosine concentration: 0.1 g/100 g, ionic strength: 0.2 *M* NaCl), at 12.5°, pH 11.72; at 25.0°, pH 11.46; and at 34.0°, pH 11.19. In spite of the higher polymer concentration used (to accentuate possible buffering), the decrease of pH with increasing temperature is clearly demonstrated by these data. It can be estimated from these values that a temperature increase from 16 to 21° would lower the pH of the solution used in the temperature-jump experiments from about 11.40 to about 11.30. As shown in the previous paper,[14] for poly-L-glutamic acid this small pH change would bring about a change in the ionization of the side chains, such that 38% of that ionization change would be kinetically controlled by the conformation change of the macromolecule. Under *isothermal* conditions, this change in pH would decrease the optical density of the same solution at 245 mμ by about 0.2 unit in a 1-cm cell.[8] To demonstrate the increase in helix content brought about by this temperature-induced pH change, optical rotation experiments were carried out. Figure 1 shows the results of these measurements at various temperatures under conditions described in the legend. A significant increase of the optical rotation, a commonly used qualitative measure of the helix content, is indicated for the solution at the transition pH of 11.4. These changes, however, are somewhat smaller

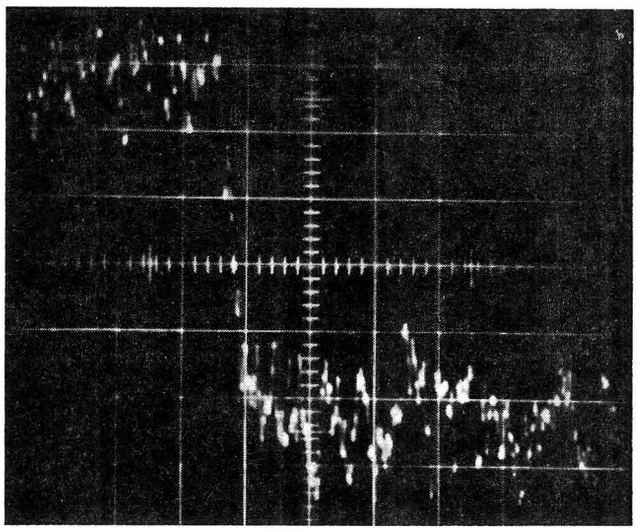

Figure 2. Oscillogram from a typical temperature jump. Ordinate: optical density of the solution at 245-mμ wavelength, arbitrary scale. Abscissa: time, 20 μsec/division. Poly-L-tyrosine concentration: 0.002 g/100 g, ionic strength: 0.2 *M* NaCl, pH_{25} 11.40.

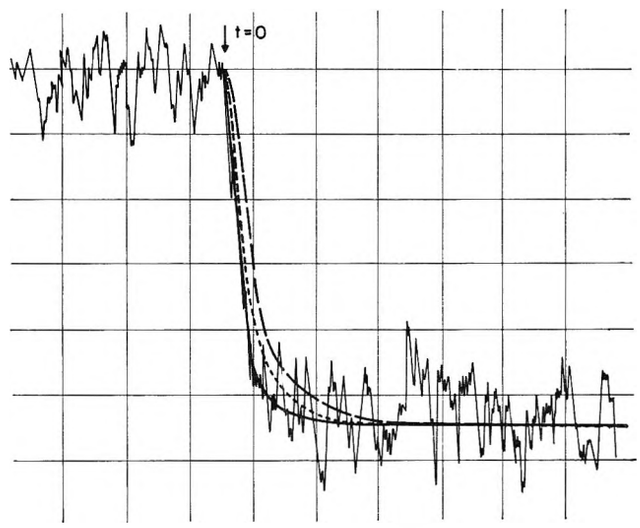

Figure 3. Illustration of the use of the relaxation process simulator. Thin jagged line: tracing of the oscillogram shown in Figure 2: ———, rps curve with τ_r = 0-μsec setting; – – – – – –, same with τ_r = 2-μsec setting; — — —, same with τ_r = 5-μsec setting; τ_h was set to 4.5 μsec for all three curves.

than expected from the published *isothermal* optical rotation *vs.* pH data.[7,8] These measurements indicate that the expected increase in helix content does take place when the temperature of the solutions is raised, as in the pH-jump experiments. The apparent difference between the literature values[7,8] and our data indicates that, in our experiments, the effect of decreas-

ing pH, which shifts the helix–coil equilibrium toward higher helix content, is *partially* compensated by the increasing temperature, which has the opposite effect.

Several experiments were carried out at pH 11.40 and 11.50. A typical oscillogram photograph is shown in Figure 2. It can be seen that the chemical relaxation is very fast and that the new equilibrium concentration is established in a few microseconds. To ascertain the slowest possible chemical relaxation which is hidden in the pH-jump records, the oscillograms were evaluated with the rps. Figure 3 demonstrates the use of this instrument in the evaluation of the pH-jump shown in Figure 2. The exponential lines of Figure 3 are the relaxation curves generated with a heating time-constant of 4.5 μsec and chemical relaxations characterized by $\tau_r = 0$, 2, and 5 μsec, respectively. The superposition of these on the actual oscillogram (jagged lines) shows that chemical relaxation times greater than 1 or 2 μsec are incompatible with the oscillogram obtained. (The seemingly small horizontal displacements are highly significant since the accuracy of the time coordinate is very high.) A similar evaluation of 20 oscillograms at pH 11.40 and at pH 11.50 indicated the same results. A limited study at ionic strengths different from 0.2 *M* (*i.e.*, 0.3–0.4 *M* NaCl) also indicated the same behavior.

Owing to the significant amount of stray light present in the ultraviolet observation beam of the temperature-jump apparatus, meaningful values for the absolute value of the change in optical density corresponding to the vertical oscilloscope beam deflections could not be obtained. Thus, the question arises as to whether the deflection seen on the oscilloscope in the first few microseconds is the entire reaction triggered by the pH jump or is only a part of the total optical density change which is followed by a slow reaction not noticeable at the fast sweep rate used. The possibility of a reaction slower than 2 μsec was eliminated by the following observations. (1) pH jumps recorded using a 500-μsec/cm oscilloscope sweep rate indicated no further deflections in the 0.1–4-msec time range. (2) The oscilloscope trace-position gauge[9] did not show voltage changes greater than those of the fast change up to a few seconds after the pH jump. (3) In the Cary 14 spectrophotometer the pH jump induced by a rapid stirring of the solution with a heated spatula did not give evidence of any further reaction in the 1 sec–1-min range.

Since no relaxation time was observed in the 2×10^{-6} sec–1 min range, it appears that the chemical relaxation arising from the changes in the helix content of a partially helical poly-L-tyrosine macromolecule is characterized by a time constant of less than 2 μsec. It is known from the studies of Hammes, Schwarz, Eigen, and Lumry that, in aqueous poly-L-glutamic acid solution, the relaxation time of the helix–coil transition is between 5×10^{-8} and 10^{-5} sec.[3-6] Considering the bulky side chains of poly-L-tyrosine, there appear to be no reasons to believe that the helix–coil relaxation time of this polymer would be *less* than that of poly-L-glutamic acid. With this assumption, the relaxation time characteristic of the helix–coil transition of poly-L-tyrosine can be given as 2×10^{-6} sec $> \tau > 5 \times 10^{-8}$ sec. Since neither the relaxation time of the poly-L-glutamic acid nor that of poly-L-tyrosine is known sufficiently accurately, the effects of side chains on helix–coil transition rates cannot be evaluated quantitatively. It appears, however, that the similarity of the range found in the present study with that for poly-L-glutamic acid renders unlikely the possibility that side-chain effects would have a *dominant* role in determining the rates involved in the helix–coil transformation changes of poly-L-tyrosine or poly-L-glutamic acid.

Acknowledgments. Thanks are due to Mr. Gary Davenport for the construction of the rps and to Mr. Terry Troxell for help with the experimental work.

A Filter Paper Diaphragm Technique for Diffusion Coefficients[1a]

by Maurice M. Kreevoy and Eugene M. Wewerka[1b]

School of Chemistry, University of Minnesota, Minneapolis, Minnesota 55455 (*Received July 6, 1967*)

The interpretation of kinetic data is often easier if certain diffusion coefficients are available. While a large number of these have been measured and collected,[2] the possible combinations of solute and solvent are almost infinite. In the present paper an apparatus and technique, generally applicable for the measurement of relative diffusion coefficients, is described. In many cases, a measurement can be completed in 1 hr, the reproducibility is of the order of $\pm 2\%$, and the technique used is familiar to kineticists. Its application to HgI_2 in water and in isooctane (2,2,4-trimethyl-

(1) (a) Supported, in part, by the Petroleum Research Foundation through Grant PRF 1912-A3,4. (b) Los Alamos Scientific Laboratory, Los Alamos, N. M.

(2) S. B. Tuwiner, "Diffusion and Membrane Technology," Reinhold Publishing Corp., New York. N. Y., 1962, pp 369–373.

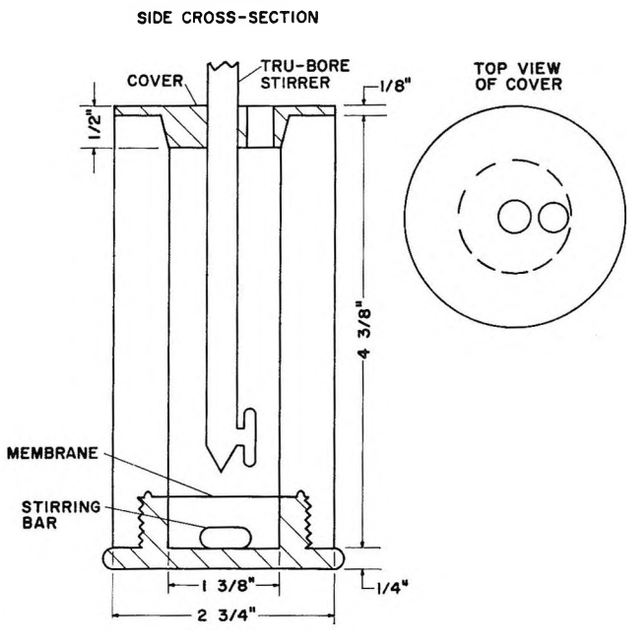

Figure 1. The apparatus.

pentane), to iodine in isooctane, and to toluene in *n*-hexane are described.

Experimental Section

The apparatus is depicted in Figure 1. It was entirely fabricated from Teflon. In operation, the lower, threaded cup was filled with a dilute solution containing both the unknown and the reference substance. The small lip permitted filling slightly above the flat surface so that the membrane, a piece of filter paper, could be wetted with the solution and placed in contact with the surface, leaving no air bubbles. Excess solution was then blotted up, the upper portion of the apparatus was screwed firmly in place, and an appropriate quantity of pure solvent was placed in the upper compartment. The lower part of the apparatus was enclosed in a thin polyethylene bag and was mounted in a constant-temperature bath. The magnetic stirring bar was driven by an air- or water-powered magnetic stirrer mounted in the bath directly beneath the apparatus. The stirrer in the upper compartment was driven mechanically at 300 rpm unless otherwise noted. Samples (3 ml) were withdrawn for spectrophotometric analysis from the upper compartment before stirring was begun and at appropriate intervals thereafter. Each sample was returned after the analysis and before the next was withdrawn so that the volume remained approximately constant.

The reference substance was chosen so that its concentration and that of the unknown could both be determined in the same sample by spectroscopic measurements at two wavelengths. The concentration of neither the unknown nor the reference exceeded 0.2 *M*, so that neither influenced the bulk properties of the medium (*i.e.*, viscosity, density) appreciably.

Commercial reagents, of at least reagent grade, were used throughout this work without further purification. Except where otherwise noted, Schleicher and Schuell No. 589 White Ribbon filter paper was used as the diaphragm.

Results

As expected,[3] each component, in each experiment, appeared in the upper compartment according to a first-order rate law, shown in eq 1.[4] The concentra-

$$\frac{2.303}{t - t_0} \log \left\{ \frac{C - C_0}{C - C_t} \right\} = k \qquad (1)$$

tion of a solute in the upper compartment at some time, t, is C_t.

Typical tests of eq 1 are shown in Figure 2. The best straight lines through the points were drawn by inspection, and were used to calculate values of k. The diffusion coefficient, D, is proportional to k, the proportionality constant depending on the physical characteristics of the apparatus and the diaphragm.[5] Thus, D_X, the diffusion coefficient of X, is given by

$$D_X = D_S k_X / k_S \qquad (2)$$

where quantities subscripted with S refer to a standard substance whose diffusion coefficient is known. The derived values of D_X should be independent of the volume of solvent in the upper compartment of the apparatus, the porosity of the filter paper, and the stirrer speeds.

Table I: Diffusion Coefficient of HgI_2 in Isooctane at 25°

Diaphragm paper	Volume, ml	$10^6 D_{HgI_2}$, $cm^2\ sec^{-1}$
a	30	2.61[d]
a	30	2.53[e]
b	60	2.48
c	60	2.57

[a] Schleicher and Schuell No. 589 White Ribbon filter paper. [b] Schleicher and Schuell No. 589 Blue Ribbon filter paper. [c] Eaton Dikeman Co. No. 615 qualitative filter paper. [d] Average of six determinations with average deviation from the mean of 0.05×10^{-6} $cm^2\ sec^{-1}$. [e] Mechanical stirrer slowed from 300 to 150.

(3) Reference 2, pp 39, 73.

(4) A. A. Frost and R. G. Pearson, "Kinetics and Mechanism," John Wiley and Sons, Inc., New York, N. Y., 1961, p 29.

(5) Reference 2, p 73.

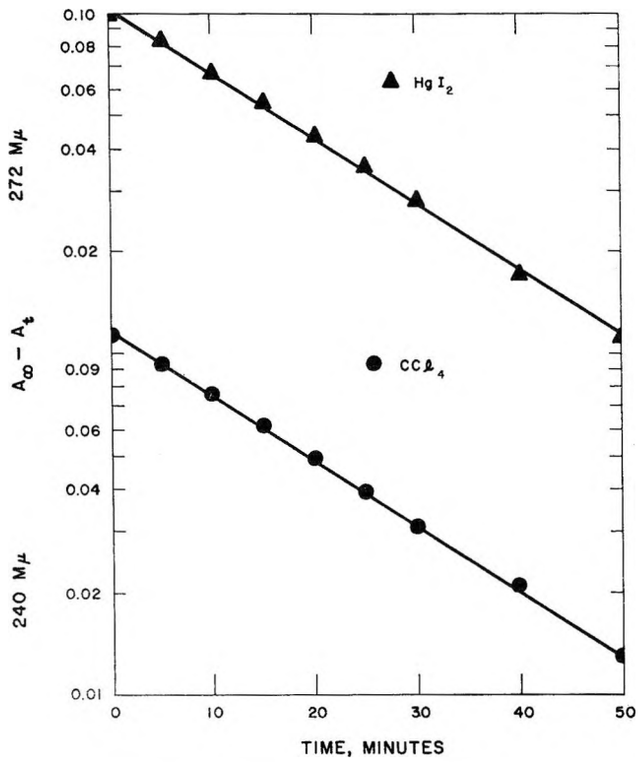

Figure 2. Optical densities, A, are proportional to concentration, so eq 1 was tested by plotting optical density differences, on a logarithmic scale, against t, as shown. A small correction, given by $A_t^{272}\ \epsilon_{HgI_2}^{240}/\epsilon_{HgI_2}^{272}$ has been substracted from each A_t^{240} before plotting, to remove the contribution of HgI_2 at that wavelength. The ϵ_{HgI_2}'s are extinction coefficients of mercuric iodide. The superscripts indicate wavelengths.

Table I shows that this is true for HgI_2 in isooctane (2,2,4-trimethylpentane) with CCl_4 as a standard. (In this solvent D_{CCl_4} is 2.57×10^{-5} cm^2 sec^{-1} at 25°.)[2]

The combined changes of variables shown in Table I resulted in changes in observed half-life of nearly an order of magnitude, from about 5 min to nearly 50 min, without appreciable change in D_{HgI_2}. The HgI_2 concentration used in these experiments was 10^{-4} M; the CCl_4 concentration was 0.2 M. Halving the latter, to 0.1 M, gave an inappreciably different D_{HgI_2}, 2.55×10^{-5} cm^2 sec^{-1}.

Table II summarizes the diffusion coefficients obtained, all at 25°.

Table II: Diffusion Coefficients at 25°

Substance	Solvent	Standard	$10^5 D_X$, cm^2 sec^{-1}
HgI_2	Isooctane	CCl_4	2.59
HgI_2	Water	CH_3COOH[a]	1.22
I_2	Isooctane	HgI_2	2.79
$C_6H_5CH_3$	*n*-Hexane	CCl_4[b]	4.11

[a] D_{CH_3COOH} in H_2O at 25° is 1.195×10^{-5} cm^2 sec^{-1} (V. Vitagliano and P. A. Lyons, *J. Am. Chem. Soc.*, **78**, 4538 (1956)). [b] D_{CCl_4} in *n*-hexane at 25° is 3.70×10^{-5} cm^2 sec^{-1} (ref 2).

The average deviation from the mean, among a total of 11 determinations of D_{HgI_2} in isooctane, was 2%. This is also the order of the difference between the present value of $D_{C_6H_5CH_3}$ and 4.21×10^{-5} cm^2 sec^{-1}, the value reported by Chang and Wilke.[6] Thus, D_X, measured by this procedure, seems to have an uncertainty of 1–2%, depending on the number of replications.

Discussion

None of the techniques described is new, but the present combination seems particularly suitable. The diaphragm cell was introduced by Northrup and Anson,[3,7] and the use of filter paper diaphragms was introduced by Gage.[8] The measurement of first-order rate constants is very well developed[4] and much more reliable than dependence on just two measurements of concentration.[3] It also does not depend on an accurate knowledge of proportionality constants if an instrumental method of analysis is used. The use of an internal standard is particularly desirable when filter paper diaphragms are used, as these may not be exactly reproducible. It also halves the time required for a determination.

(6) P. Chang and C. R. Wilke, *J. Phys. Chem.*, 59, 592 (1955).

(7) J. H. Northrup and M. L. Anson, *J. Gen. Physiol.*, 12, 543 (1929).

(8) J. C. Gage, *Trans. Faraday Soc.*, 44, 253 (1948).

COMMUNICATIONS TO THE EDITOR

Broadening of Carbonyl Stretching Vibration Bands Appearing for Acrylate Copolymers

Sir: Environmental effects upon infrared and nmr spectra have been discussed for the purpose of investigating the sequence distribution in copolymer chains.[1-4] However, reports available to date concerning this subject in infrared spectroscopy have been confined mainly to the shift of characteristic bands and the change in absorbing intensities.[1,2,4] The present communication deals with a preliminary result that the 1730-cm^{-1} band characteristic of the stretching vibration of C=O groups in methyl acrylate (MA)–styrene (ST) copolymers exhibited broadening with increase in the MA content. The half band width measurement in this study was made tentatively using the apparent band profile obtained directly on recording paper.

The samples were prepared by copolymerizing MA and ST monomers in benzene with azobisisobutyronitrile as the initiator at 75°. The whole polymers thus obtained were used for the infrared measurement. The infrared spectra were taken with a Perkin-Elmer Model 521 spectrometer with grating. The spectrometer was calibrated against the 1609.7- and 1603.0-cm^{-1} bands of indene and polystyrene, respectively. The spectra were recorded using films prepared from benzene solutions. The film thickness for each measurement was adjusted in such a way that the absorbance at 1730 cm^{-1} for each sample fell in a range of 0.7–0.8. The slit width of the spectrometer was set at 125 μ (80 cm^{-1}), and this affected the band height only by 1% according to the Ramsay estimation,[5,6] so that possible distortions of the true band shape in question should have been minimized.

The spectra in the proximity of the 1730-cm^{-1} band for copolymer samples and an MA homopolymer are shown in Figure 1, from which the peak position and the half band width (measured in cm^{-1}) were read. The reproducible accuracy of these readings was within ± 0.5 cm^{-1}. The result is given in Table I.

It can be seen from Table I that although no shift of peak position is observed practically with changes in the composition, the half band width, $\Delta\bar{\nu}_h$, decreases regularly with decreasing the MA content. Thus an attempt was made to interpret this trend in terms of the sequence length in copolymer chain, and values of $\Delta\bar{\nu}_h$ were plotted against P_2 and P_3, which are the probabilities for finding the connections MA–MA and MA–MA–MA in a chain, respectively. These probabilities were evaluated from the reactivity ratios for ST(1) and MA(2); $r_1 = 0.75$ and $r_2 = 0.20$ at 70°.[7] Figure 2 shows that $\Delta\bar{\nu}_h$ is linearly proportional to P_3, the triad sequence probability. This fact implies, at least, that the principal factor producing broadening of the 1730-cm^{-1} band is undoubtedly perturbation by neighboring carbonyl groups in an

Table I: Changes in Peak Position and Half Band Width of Carbonyl Absorption Band with Acrylate Content

Polymer code	MA content, mole %	Peak position, cm^{-1}	Band width, cm^{-1}
PMA 1	100	1733	36.1
SM 25	74.2	1733	31.2
SM 40	57.5	1733	22.4
SM 50	47.3	1734	19.2
SM 65	34.2	1733	19.2
SM 76-1	22.4	1733	17.5

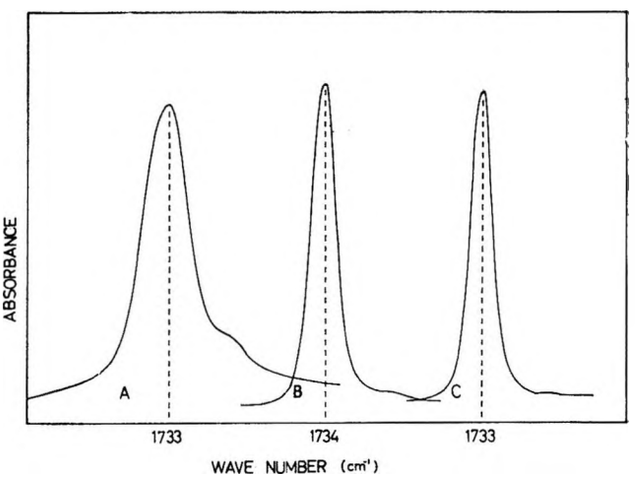

Figure 1. Absorption band profiles for carbonyl groups in the proximity of 1730 cm^{-1}. Curves A, B, and C are for PMA 1, SM 50 and SM 76-1, respectively.

(1) G. M. Kline, "Analytical Chemistry of Polymers," Part II, John Wiley and Sons, Inc., New York, N. Y., 1962.

(2) G. Schnell, *Ber. Bunsenges. Physik. Chem.*, **70**, 297 (1966).

(3) U. Johnsen, *ibid.*, **70**, 320 (1966).

(4) Y. Yamashita, *Kagaku* (Kyoto), **27**, 59 (1966).

(5) K. S. Seshadri and R. N. Jones, *Spectrochim. Acta*, **19**, 1013 (1963).

(6) D. A. Ramsay, *J. Am. Chem. Soc.*, **74**, 72 (1952).

(7) T. Alfrey, Jr., E. Merz, and H. Mark, *J. Polymer Sci.*, **1**, 37 (1946).

intramolecular sense. In addition, it is of interest to note that the plot passes, when extrapolated to $P_3 = 0$, through an intercept which corresponds to the $\Delta\bar{\nu}_h$ value obtained for MA homopolymer in benzene solution (17.7 cm^{-1}). Another finding is that the band width tends to increase with elevating temperature.

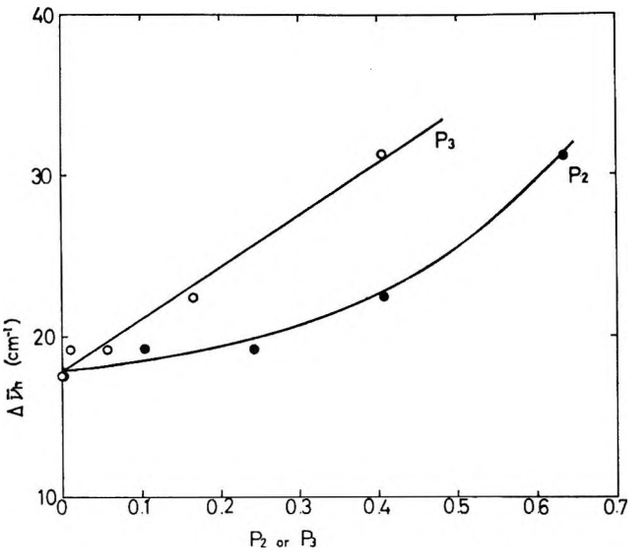

Figure 2. Plots of half band width against dyad and triad sequence probability, P_2 and P_3, respectively. For details, see text.

In connection with the above observations, it should be noted that the half band width of the C=O band found for dimethyl fumarate is clearly smaller than that for dimethyl maleate when they are determined in benzene solution. The difference in the steric configuration of carbonyl groups appears to be reflected in the band width. Further detailed observations and a pertinent interpretation of this phenomenon will be given in due course.

Acknowledgments. The authors thank Professor Toru Takenaka, Institute for Chemical Research, and Professor Hirotsugu Matsuda, Research Institute for Fundamental Physics, Kyoto University, for their helpful discussions during the course of this work.

RESEARCH LABORATORY
SEKISUI CHEMICAL COMPANY
MISHIMA-GUN, OSAKA-FU, JAPAN
FUMIO KAMIYAMA
HISAYUKI MATSUDA

INSTITUTE FOR CHEMICAL RESEARCH
KYOTO UNIVERSITY
TAKATSUKI, OSAKA-FU, JAPAN
HIROSHI INAGAKI

RECEIVED AUGUST 3, 1967

Proton Ejection Accompanying Light-Induced Electron Transfer in the Chlorophyll–Quinone System

Sir: Linschitz and Rennert[1] have shown that chlorophyll undergoes a reversible photobleaching in the presence of benzoquinone. Tollin and his co-workers[2,3] demonstrated by esr measurements that the benzosemiquinone ion radical is formed in these light-activated single electron transfer reactions. The present paper presents evidence to show that these reactions are accompanied by the ejection of a proton. Studies performed in the aprotic solvent, dimethylformamide, demonstrate that chlorophyll is the proton source.

The apparatus used to measure the proton ejection has recently been described.[4] A Corning S2-61 filter, which is opaque to all wavelengths below 600 mμ, was used. Chlorophylls a and b were prepared by the method of Zscheile and Comar.[5] *p*-Benzoquinone was purified by sublimation, *p*-chloranil was recrystallized from acetone, dimethylformamide was distilled under vacuum from calcium hydride, and the methanol used was the spectrophotometric grade (Fisher). Benzoquinone in alcohol slowly forms a species which absorbs at 355 mμ. Since this species is not formed in either dimethylformamide or with chloranil, it is assumed to have little or no effect on the final results presented.

Figure 1 shows the apparent proton ejection from both the chlorophyll a– and b–quinone systems in methanol. Solutions were deaerated by flushing with nitrogen pretreated with a chromous chloride solution. The dashed line illustrates results obtained after the air-free solutions were exposed to air for at least 0.5 hr. These are typical results obtained in a series of light and dark intervals. Irradiation of the chlorophylls alone in methanol in the presence of air gives irreversible alkaline reactions which are probably due to the basicity of the products from the photooxidation of the chlorophylls. Air-free systems of chlorophyll b give no pH response but a slight alkaline reaction is obtained with chlorophyll a. This may be due to residual oxygen present in the system. Studies of the chlorophyll b–*p*-chloranil system in methanol showed that more protons are ejected than observed with benzoquinone. The apparent proton ejection activity is in the range of

(1) H. Linschitz and J. Rennert, *Nature*, 169, 193 (1952).
(2) G. Tollin and G. Green, *Biochim. Biophys. Acta*, 60, 524 (1962).
(3) G. Tollin, K. K. Chatterjee, and G. Green, *Photochem. Photobiol.*, 4, 592 (1965).
(4) K. P. Quinlan and E. Fujimori, *ibid.*, 6, 665 (1967).
(5) F. P. Zscheile and C. L. Comar, *Botan. Gaz.*, 102, 463 (1941).

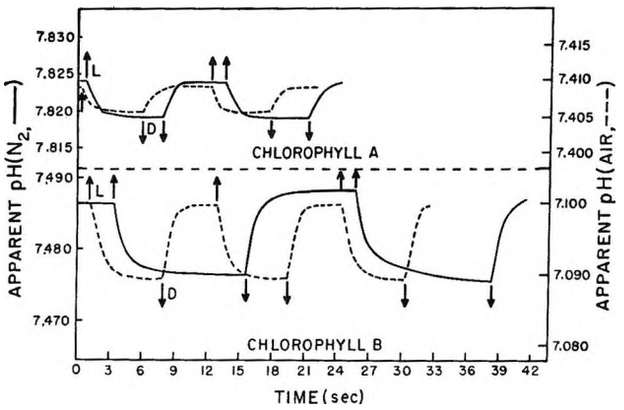

Figure 1. Ejection of protons from chlorophyll–quinone systems in methanol. Right ordinate represents results obtained in air. The upward arrows represent light on; downward, light off. Top figure: chlorophyll a, 3.7×10^{-5} *M*; with quinone, 0.03 *M*. Bottom figure: chlorophyll b, 2.3×10^{-5} *M*; with quinone, 0.03 *M*.

10^{-6} *M*. Proton ejection has also been observed in the present study with the quinone systems of pheophytin, bacteriochlorophyll, and hematoporphyrin. These studies will be reported later.

A possible explanation of the observations is presented in the following simplified scheme

$$\text{CHLH} \xrightarrow{h\nu} \text{CHLH}^* \quad (1)$$

$$\text{CHLH}^* \longrightarrow \text{CHLH}' \quad (2)$$

$$\text{CHLH}'(\text{CHLH}^*) + \text{Q} \longrightarrow \text{CHL}\cdot + \text{Q}\cdot^- + \text{H}^+ \quad (3)$$

where CHLH* and CHLH′ are the excited singlet and triplet states of chlorophyll. The interaction of quinone with either of the excited states of chlorophyll as in eq 3 is well documented.[6] Figure 1 also shows that the proton ejection activities are of the same order of magnitude whether air is present or not. This is surprising since both quinone and oxygen are known to compete for the excited states of chlorophyll.[6] The role of the chlorophyll–oxygen complex[7-9] in these light-activated reactions is uncertain. This aspect of the problem is currently under investigation.

The ejected proton in the present system can originate from two possible sources: (A) reaction 3 and (B) the solvent, where $\text{CHLH}\cdot^+$ is a cation of a weak base and $\text{Q}\cdot^-$ is an anion of a strong acid. Studies performed in the aprotic solvent, dimethylformamide, show that a proton is ejected as in reaction 3. In this study a calomel electrode, containing a saturated solution of KCl in dimethylformamide, was used. The theoretical behavior of this type of an electrode system has recently been shown by Ritchie and Megerle.[10]

The results presented in the present paper are not only important in gaining insight into the mechanism of the light-activated electron transfer of chlorophyll systems but also lend support to the current hypothesis[11] which relates the dissociation of some form of chlorophyll to the chemiosmotic[12] theory of photophosphorylation in photosynthesis.

(6) R. Livingston, *Quart. Rev.* (London), **14**, 174 (1960).

(7) E. Fujimori and M. Tavla, *Photochem. Photobiol.*, **5**, 877 (1966).

(8) R. Livingston and K. E. Owens, *J. Am. Chem. Soc.*, **78**, 3301 (1956).

(9) G. O. Schenck, *Naturwissenschaften*, **40**, 205 (1953).

(10) C. O. Ritchie and G. H. Megerle, *J. Am. Chem. Soc.*, **89**, 1447 (1967).

(11) H. T. Witt, G. Doring, B. Rumberg, P. Schmidt-Mende, U. Siggel, and H. H. Stiehl in "Energy Conversion by the Photosynthetic Apparatus," Publication No. 19, Biology Department, Brookhaven National Laboratory, Upton, N. Y., 1967, p 161.

(12) P. Mitchell, *Nature*, **191**, 144 (1961).

PHOTOCHEMISTRY SECTION
ENERGETICS BRANCH
SPACE PHYSICS LABORATORY
L. G. HANSCOM FIELD
BEDFORD, MASSACHUSETTS 01730

KENNETH P. QUINLAN
EIJI FUJIMORI

RECEIVED AUGUST 14, 1967

The Intracrystalline Rearrangement of Constitutive Water in Hydrogen Zeolite Y

Sir: The loss of constitutive or chemical water from hydrogen zeolite Y occurs at temperatures above 500° at 10^{-5} torr.[1,2] We have found that this reaction occurs in several minutes, using an inert purge gas at 650 to 750° and approximately 760 torr. The product has poor thermal stability.

Hydrogen zeolite Y heated 2–4 hr at 700–800° in an inert static atmosphere, where the chemical water remains in the environs of the hydrogen zeolite, yields a substance of unusually high thermal stability. This material remains crystalline on heating to 1000°, whereas sodium and hydrogen zeolite Y both lose their zeolite crystal structure at temperatures below 950°. McDaniel and Maher report the synthesis of a zeolite Y of similar high stability.[3] They do not define the critical requirements for its formation nor do they account for its composition.

(1) H. A. Szymanski, D. N. Stamires, and G. R. Lynch, *J. Opt. Soc. Am.*, **50**, 1323 (1960).

(2) J. B. Uytterhoeven, L. G. Christner, and W. K. Hall, *J. Phys. Chem.*, **69**, 2117 (1965).

(3) C. V. McDaniel and P. K. Maher, preprint of paper presented at Molecular Sieve Conference, London, April 1967.

Scheme I

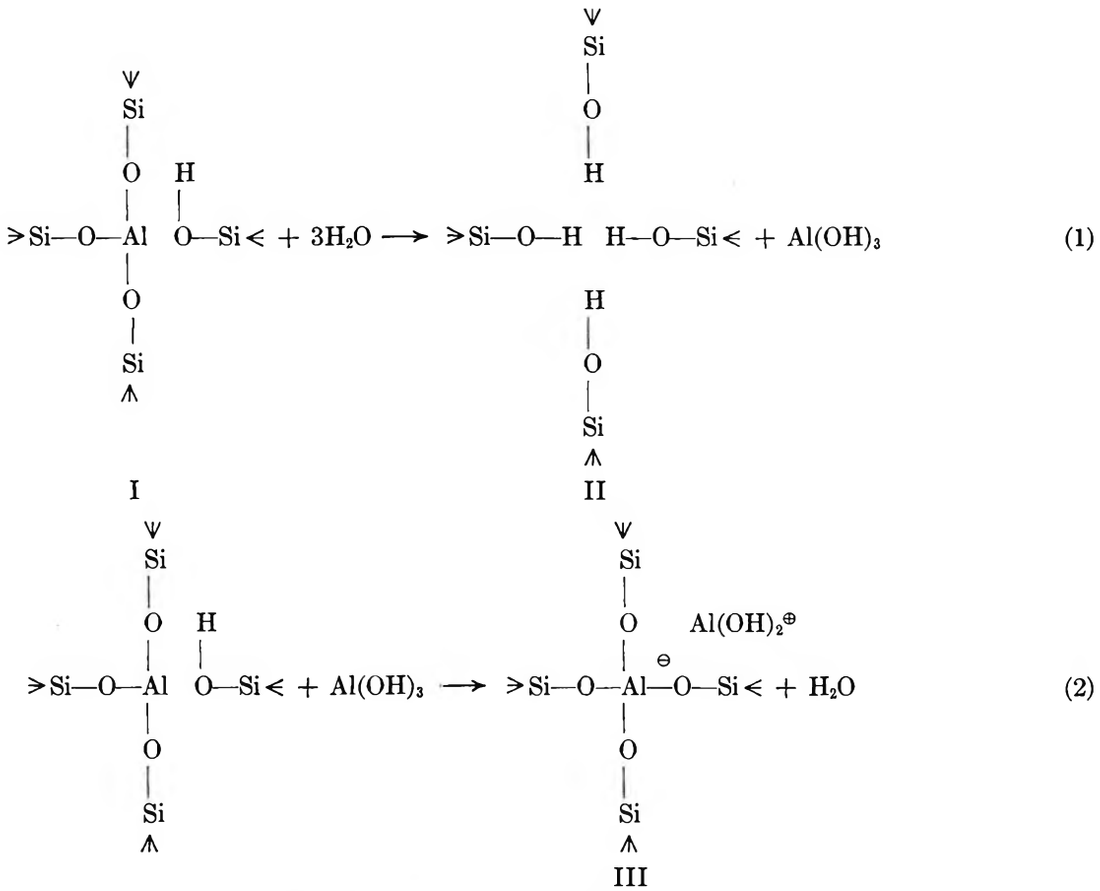

In this stable zeolite, approximately 25% of the aluminum is present in cationic form. Clearly this cationic aluminum is derived from tetrahedrally coordinated aluminum that was initially in the anionic zeolite framework. About 80–90% of this aluminum is exchanged by sodium ion on treatment with 0.10 *N* sodium hydroxide solution. The resulting sodium form of the aluminum-deficient zeolite is also markedly more thermally stable than the ordinary sodium zeolite Y. The cause of this increased stability is under study.

This zeolite contains 175 (Si + Al) tetrahedra per unit cell in the anionic framework compared with 192 universally recognized in faujasite. Obviously this stable material is chemically different from the usual faujasites.

We propose the mechanism shown in Scheme I to explain the role of chemical water and the formation of cationic aluminum. Reaction 1 is a hydrolysis involving chemically derived water. Any technique for keeping this water in the system during the heating process will result in a stable product. Reaction 2 is a neutralization involving the newly formed transient $Al(OH)_3$ and Brønsted acid sites that still contain chemical water. The cationic aluminum species in structure III may react with one or two additional protons to yield $Al(OH)^{2+}$ and Al^{3+}. Studies to be reported later show that cationic aluminum has an average charge of 1.5, indicating the presence of both $Al(OH)_2^+$ and $Al(OH)^{2+}$.

Thermogravimetric studies of the stable material suggest that it contains no chemical water in its final form. Therefore, the four hydroxyl groups in structure II are probably lost as water, resulting in some type of Si–O–Si bonding. The nature of these sites is not presently known, but the pronounced contraction of the unit-cell dimensions of this material, relative to sodium and hydrogen zeolite Y, is probably related to the formation of the aluminum-deficient sites. Water derived from these sites and from the proposed hydroxylated aluminum cations is available for hydrolysis of additional Brønsted acid sites. Details of our investigation will be reported later.

MOBIL RESEARCH AND DEVELOPMENT CORPORATION
CENTRAL RESEARCH DIVISION LABORATORY
PRINCETON, NEW JERSEY 08540

GEORGE T. KERR

RECEIVED JUNE 23, 1967

Double-Layer Effect on "External Transport Numbers" in Molten Lead Chloride[1]

Sir: The use of porous electrode-compartment separators as velocity reference in defining "external transport numbers" of the ions in molten salts has become commonplace in recent years.[2] The significance of such quantities has yet to be adequately elaborated,[3] but most workers have assumed them to be intrinsic properties of the molten salt. Although their measurement requires interaction of the salt with the porous separator, evidence has been presented in the case of $PbCl_2$ to indicate independence of experimental results on the nature of the separator.[4] In that study the transference number of Cl^- was found to be within 1% of 0.75 for each of three different separators: an "ultrafine" porosity Pyrex frit (max pore diam, 0.9 μ); a piece of unglazed porcelain; and a wad of asbestos fibers packed tightly between "coarse" porosity Pyrex frits. Subsequent conceptual analysis of these experiments has convinced us that they represent a form of electroosmosis in which the value of the "transference number" observed is determined inside the pores of the separator, within a few ionic diameters of the interface between salt and pore wall.[3]

Assuming the variations of separator material studied previously were insufficient for those transport number experiments to reflect corresponding differences in the properties of the interfacial region, we have been seeking a suitably porous material that is chemically inert to the melt but conducts electronically. Used as a separator of the electrode compartments, such a material could be charged to any potential between that at which lead deposits and that of chlorine evolution, a span of more than 1 v, without any electrochemical reaction occurring within its pores. If our hypothesis is correct, the corresponding effect on the structure of the electrical double layer might be expected to produce a noticeable dependence of the transference numbers on the potential.

As yet unable to produce a workable cell containing such a frit, we have nevertheless succeeded in demonstrating the proposed effect by means of a brute-force technique. Wrapping a platinum wire around the *outside* of the tube containing an ultrafine Pyrex frit, we applied potentials ranging from -10 to $+10$ v (relative to one of the lead electrodes) at this point, while carrying on normal transference runs by a method similar to that of Fischer and Klemm.[5] A pronounced effect of frit potential on the transference numbers is evident in the results summarized in Table I. It is seen that negative frit potentials enhance the transport numbers of the chloride ions passing through, while the effect of positive potentials is consistent with this trend at $+5$ v, but shows a change in direction upon reaching $+10$ v.

Table I: Effect of Externally Applied Potential on Transference Numbers of $PbCl_2$ in Ultrafine Pyrex Frits at 565°

Applied potential, v	Av t_- obsd	Std dev	No. of runs
0	0.762	±0.025	18
−5	0.802	±0.037	9
−10	0.858	±0.040	10
+5	0.716	±0.037	7
+10	0.760	±0.034	8

Although glass does not conduct electronically, it is reasonable to expect the high voltage on the external wire to have some effect on the double layer at the salt–glass interface. There is actually a detectable current flowing through this interface when the potential is applied to the wire, presumably carried by cations entering or leaving the glass. This current, initially greater than 1 ma, rapidly decays to a steady-state value less than 0.5 ma, which is negligible compared with the electrolysis current of around 50 ma. It was independently established that the "frit current" produces no detectable volume changes in the absence of electrolysis. We attribute the observed effect on t_- at negative potentials to an increase in the concentration of Pb^{2+} immobilized at the glass interface by increased electrostatic attraction. This results in enhancement of the concentration of mobile chloride ions in the salt immediately adjacent to this layer. It is the ions in this region that determine the motion of *all* the salt in the pore relative to its wall, so that we observe an apparent increase in the relative mobility of Cl^-.

The effect at $+10$ v is difficult to explain, but may be an indication that some Na^+ ions, rather than Pb^{2+}, are emerging from the glass in spite of our efforts to supply an excess of the latter during initial runs at negative potentials. It is known that Na^+ has a far

(1) This work is part of a program supported by the U. S. Atomic Energy Commission.

(2) For a summary of work prior to 1964, see the chapter by A. Klemm in "Molten Salt Chemistry," M. Blander, Ed., Academic Press, New York, N. Y., 1964.

(3) R. W. Laity in "Encyclopedia of Electrochemistry," by C. A. Hampel, Ed., Reinhold Publishing Co., New York, N. Y., 1964, p 653.

(4) F. R. Duke and R. W. Laity, *J. Phys. Chem.*, **59**, 549 (1955).

(5) W. Fischer and A. Klemm, *Z. Naturforsch.*, **16a**, 563 (1961).

greater mobility than any doubly charged ion in glass, and its presence on the salt side of the double layer could introduce complicating structural modifications.

SCHOOL OF CHEMISTRY
RUTGERS UNIVERSITY
NEW BRUNSWICK, NEW JERSEY 08903

RICHARD W. LAITY
CARL-AXEL SJÖBLOM

RECEIVED JULY 13, 1967

New Electron Spin Resonance Spectra in γ-Irradiated Alkyl Halides at 77°K[1]

Sir: The reported esr spectra of most alkyl halide glasses which have been γ irradiated at 77°K are attributable to the alkyl radical formed by rupture of the C–X bond,[2–4] indicating that other paramagnetic species (such as X, X_2^-, RX·X, RX^+, RX^-) postulated to account for portions of the optical spectra[5,6] are present at very low concentrations or are obscured by line-broadening effects. Relatively complex spectra observed from some polycrystalline alkyl iodides[4,7] and some alkyl bromides[8,9] have been attributed to spin–orbit coupling involving the halogen nucleus in halogen-containing radicals.

Using esr sensitivities ranging up to several hundred times that required to give full-scale deflection for alkyl radicals produced by radiolysis of glassy alkyl halides, we have found that all γ-irradiated glassy and polycrystalline alkyl iodides and bromides tested give esr spectra at much lower and higher magnetic fields than previously observed.

The low-field spectra fall into four types corresponding to spectra A, B, C, and D of Figure 1: (A) polycrystalline C_2H_5I, (B) polycrystalline *n*-C_4H_9I, (C) polycrystalline *n*-C_3H_7I, *n*-C_5H_9I, *n*-$C_6H_{13}I$, *n*-$C_7H_{15}I$, and (D) all glassy and polycrystalline *n*-alkyl bromides from C_2 through C_7. The low-field spectra of alkyl iodide glasses are similar to the type C spectra after some change in the relative peak heights of the latter during standing at 77°K. All of the alkyl iodides, in either the glassy or polycrystalline form, give high-field spectra similar to E. The high-field spectra of the bromides are all similar to F. γ-Irradiated polycrystalline *n*-alkyl chlorides from C_2 through C_6 give no esr spectra at fields more than 250 gauss below or above the free electron *g* value, although some structure above and below the alkyl radical signal is present in every case. Glassy chlorides, when obtainable, give similar results.

For all alkyl halides tested the central spectral features (in the region of 3260 gauss) decay at 77°K.

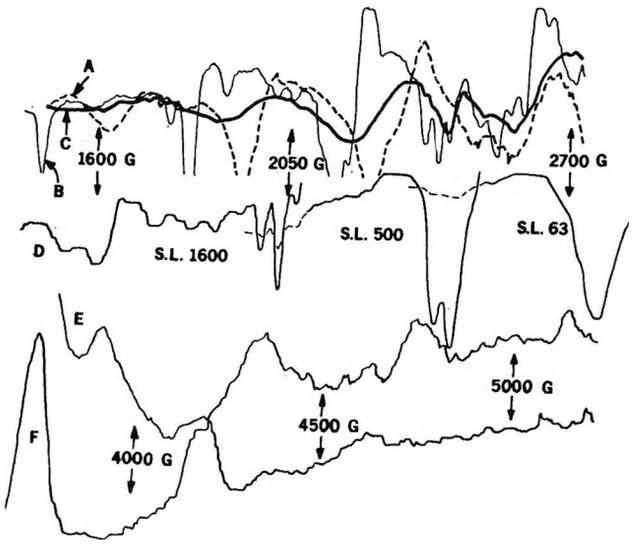

Figure 1. Low-field (A, B, C, D) and high-field (E, F) esr spectra of γ-irradiated polycrystalline alkyl iodides and bromides at 77°K: (A) C_2H_5I, signal level 400; (B) *n*-C_4H_9I, signal level 400; (C) *n*-$C_5H_{11}I$, signal level 400; (D) *n*-C_4H_9Br, the three sections of the spectrum being measured at different signal levels as indicated; (E) C_2H_5I, signal level 2500; (F) *n*-$C_5H_{11}Br$, signal level 1000. In all cases the modulation amplitude was about 12 gauss and the γ dose was 4×10^{19} ev g^{-1}. The magnetic field corresponding to the free-electron *g* value is *ca.* 3260 gauss.

However, some portions of the low- and high-field spectra grow while others decay, the growth in C_2H_5I glass being as much as fourfold in 2 days.

The low- and high-field spectra must be caused by halogen-containing species. Consistent with this conclusion are the differences between the spectra of iodides, bromides, and chlorides. The low- and high-field spectra of polycrystalline and glassy C_2D_5I are identical with those of C_2H_5I, indicating that the observed line widths and line splittings are not controlled by hydrogen.

(1) This work was supported in part by the United States Atomic Energy Commission under Contract AT(11-1)-1715 and by the W. F. Vilas Trust of the University of Wisconsin.

(2) B. Smaller and M. S. Matheson, *J. Chem. Phys.*, **28**, 1169 (1958).

(3) P. B. Ayscough and C. Thompson, *Trans. Faraday Soc.*, 1477 (1962).

(4) H. W. Fenrick, S. V. Filseth, A. L. Hanson, and J. E. Willard, *J. Am. Chem. Soc.*, **85**, 3731 (1963).

(5) (a) E. P. Bertin and W. H. Hamill, *ibid.*, **86**, 1301 (1964); (b) J. P. Mittal and W. H. Hamill, *ibid.*, **89**, 5749 (1967).

(6) R. F. C. Claridge and J. E. Willard, *ibid.*, **88**, 2404 (1966).

(7) H. W. Fenrick and J. E. Willard, *ibid.*, **88**, 412 (1966).

(8) F. W. Mitchell, B. C. Green, and J. W. T. Spinks, *J. Chem. Phys.*, **36**, 1095 (1962).

(9) R. M. A. Hahne and J. E. Willard, *J. Phys. Chem.*, **68**, 2582 (1964).

Among the species which may contribute to the spectra of Figure 1 are X, X_2^-, X_2^+, RX·X, RX^+, and RX^-. The esr spectrum of gaseous I atoms[10] extends from 3300 to 6223 gauss. We find a spectrum extending from 1500 to 5000 gauss from γ-irradiated polycrystals prepared by fusing KI with 0.1 mole % $AgNO_3$, a medium in which the optical spectrum has been attributed to I_2^-.[11] The esr spectrum of Br_2^- in X-irradiated KBr single crystals containing alkaline earth ions is observed[12] between 2000 and 4800 gauss.

Samples were irradiated to a dose of 4×10^{19} ev g^{-1} at a dose rate of 2×10^{18} ev g^{-1} min^{-1}. Magnetic field values were assigned with a Varian Fieldial accessory. The modulation amplitude of 4000 (about 12 gauss) used gave a maximum esr signal without distortion. The other experimental methods used have been described.[6]

(10) S. Aditya and J. E. Willard, *J. Chem. Phys.*, **44**, 833 (1966).

(11) C. J. Delbecq, W. Hayes, and P. H. Yuster, *Phys. Rev.*, **121**, 1043 (1961).

(12) W. Hayes and G. M. Nichols, *ibid.*, **117**, 993 (1960).

DEPARTMENT OF CHEMISTRY
UNIVERSITY OF WISCONSIN
MADISON, WISCONSIN 53706

RICHARD J. EGLAND
JOHN E. WILLARD

RECEIVED JULY 17, 1967

Computed Activation Energies for Bimolecular Reactions of O_2, N_2, NO, N_2O, NO_2, and CO_2

Sir: Although it had once been hoped that absolute rate theory would permit useful kinetic predictions for most reactions, the problem of predicting activation energies is still one of the major unsolved questions in chemistry since tractable accurate quantum-mechanical solutions do not exist for potential energy surfaces of reactions involving multielectron atoms. For hydrogen atom reactions in the gas phase, it has been shown, however, that transition-state computations[1,2] of activation energies and rate constants by a nonquantum method can exhibit good agreement with experiment when several tentative assumptions are used to provide interrelationships (such as Pauling's rule[3]) among bond energy, bond order, and bond length. In an effort to avoid this computing method's limitation to H-atom reactions, a reduced-variable treatment was devised[4] for other univalent atoms, such as the halogens.

The calculation of activation energies for the important class of bimolecular reactions involving multivalent bonds has been an even more difficult challenge because of the complexities introduced by the many modes of forming or breaking bonds accessible, in principle, to such compounds as N_2O, O_2, and CO_2. Nevertheless, certain trial postulates (outlined below) have been formulated which provide remarkably good agreement between computed and measured E_0, and, accordingly, show promise of adding to our understanding of the nature of bimolecular reactions. These E_0 computations do not use adjustable parameters, but rely on bond properties such as dissociation energy and vibrational frequency. For the multivalent bimolecular transfer reaction AX + B = A + BX, one of the trial postulates relating the bond order n_2 (in the transition state A···X···B) of X···B to the bond order n_1 of A···X can be written

$$n_2 = (n''_{BX}/n''_{AX})(n''_{AX} - n_1) \qquad (1)$$

where n''_{AX} is the bond order of the reactant AX, and n''_{BX} is the bond order of the product BX. Equation 1 meets the requirement that n_1 is n''_{AX} when n_2 is zero at the initiation of the reaction, and *vice versa*. For univalent reactions, eq 1 reduces to the previously used[1,2,4] trial postulate that $n_1 + n_2 = 1$. Correspondingly, eq 1 is equivalent to the simple postulate that the bond-order increase of the forming bond is linearly related to the decrease in bond order of the breaking bond, with the proportionality constant equal to the ratio of the bond order of BX to that of AX. As in univalent calculations, the potential energy of activation, V, in the transition state is taken as the energy lost by the bond AX as it dissociates to A···X of bond order n_1, less the energy supplied by the formation of B···X of bond order n_2, plus a repulsive energy V_r arising from parallel electron spins on A and B.

$$V = D_{e,AX} - D'_{AX}(n_1)^{\pi_{AX}} - D'_{XB}(n_2)^{\pi_{XB}} + V_r \text{ kcal/mole} \qquad (2)$$

where $D_{e,AX}$ is the dissociation potential energy of AX, D' is the dissociation potential energy of the single bond, and V_r is obtained from eq 10 of ref 4. The exponent π is log (D_e/D')/log n'', which is the slope of the log dissociation energy *vs.* log bond order line. When n_1 or n_2 in eq 2 is less than one, π is replaced by the slope p, calculated[1] for the bond-order region below one. As in previous investigations,[1,2,4] the computer program (modified for multivalent bonds) determines

(1) H. S. Johnston and C. Parr, *J. Am. Chem. Soc.*, **85**, 2544 (1963).

(2) S. W. Mayer, L. Schieler, and H. S. Johnston, *J. Chem. Phys.*, **45**, 385 (1966).

(3) L. Pauling, "The Nature of the Chemical Bond," 3rd ed, Cornell University Press, Ithaca, N. Y., 1960.

(4) S. W. Mayer, L. Schieler, and H. S. Johnston, "Proceedings of the Eleventh International Symposium on Combustion," The Combustion Institute, Pittsburgh, Pa., 1967, p 837.

the value of n_2 corresponding to the peak in the potential energy, V, of the transition state. The computed E_0 is equal to V plus a small zero-point energy correction.

Activation energies computed on the basis of eq 1 and 2 and data in the JANAF thermochemical tables are summarized in Table I and II, where the reactions are written in the exothermic direction. Although the thermal dissociation of N_2O probably involves singlet $O(^1D)$ crossing[5] to triplet $O(^3P)$ primarily, the computed E_0's of Table I indicate that bimolecular transition states for N_2O reactions are consistent with Wigner spin conservation since the trial postulate of spin conservation dissociation of $N_2O(^1\Sigma)$ in the transition state through $O(^1D)$ and $N_2(^1\Sigma g^+)$ leads to very good agreement between computed and measured E_0, whereas the calculation of E_0 for the reaction mechanism allowing crossing to ground state $O(^3P)$ produces very poor agreement with experiment. Furthermore, this spin conservation (and noncrossing) postulate for bimolecular transition states apparently also extends to the reactions involving $CO_2(^1\Sigma)$ and $OH(^2\Pi)$, since E_0 computed for the transfer of $O(^1D)$ generally agrees much better with experiment than does E_0 computed for crossing to $O(^3P)$. All of the reactions in Tables I and II exhibit conservation of orbital angular momentum[6] although momentum conservation is generally less restrictive than spin conservation.

Table I: Comparison of Computed with Measured Activation Energies

Reaction AX + B = A + BX	Measured E_0	Computed E_0, kcal/mole: Spin conservation	Computed E_0, kcal/mole: Ground state spin
$N_2O + NO = N_2 + NO_2$	50[a]	48	2
$N_2O + O = N_2 + O_2$	27[a]	29	0
$N_2O + H = N_2 + OH$	15[a]	15	0
$O_2 + CO = O + CO_2$	50[a]	49	37
$HO + CO = H + CO_2$	0[a]	1	0
$NO_2 + CO = NO + CO_2$	32[b]	28	1
$ONN + O = ON + NO$	27[c]	29	24
$O_2 + N = O + NO$	7[c]	...	8
$NO_2 + N = ON + NO$	0[a]	...	0

[a] Reviewed by K. Schofield, *Planet. Space Sci.*, **15**, 643 (1967). [b] H. S. Johnston, *et al.*, *J. Chem. Phys.*, **26**, 1002 (1957). [c] R. M. Fristrom and A. A. Westenberg, "Flame Structure," McGraw-Hill Book Co., Inc., New York, N. Y., 1965, p 371.

Table II: Transfers between Two Free Radicals, Negligible Activation Energy[a]

Reaction[b] AX + B = A + BX	Transition state formula	Computed activation energy, kcal/mole	Energy[c] of new bond, kcal/mole
$ONO + H = ON + OH$	HONO	1	78
$ONO + O = ON + O_2$	ONO_2	3	49
$ON + N = O + N_2$	N_2O	0	(61)
$HO + O = H + O_2$	HO_2	5	63
$ON + O = O + NO$	ONO	1	72
$O_2 + O = O + O_2$	O_3	4	26

[a] The experimental E_0 is ~0. (See J. T. Herron and F. S. Klein, *J. Chem. Phys.*, **40**, 2731 (1964) and source cited in footnote *a* of Table I.) [b] Spin conservation in the transition state can occur here *via* the ground state species. [c] JANAF thermochemical tables.

On the basis of the results summarized in Table II, another trial postulate can be suggested. Consider, for example, the transfer reaction between NO_2 and atomic hydrogen. Both of these reactants have an unpaired electron. When the H atom approaches the NO_2 radical, bond formation between the H atom and an oxygen atom on NO_2 can begin, therefore, without requiring corresponding breaking of the bond between N and O. If the structural formula of the transition state is similar to that of a stable molecule (*i.e.*, in which BX would have $D_e > 25$ kcal/mole), the energy released during this stage of forming the new bond can provide the activation potential energy required by eq 2. The experimental E_0 could be negligible in such cases, since the energy released during the early stage of bond formation between the free radicals would be subtracted from the computed E_0. The results in Table II support the postulate that experimental E_0 will be negligible for exothermic transfers in which the transition-state structure meets the aforementioned conditions. For each of these six reactions, the observed E_0 is less than 1.0 kcal/mole, and D_e for BX is sufficiently high so that the computed requirement for E_0 could readily be supplied by the initial bond formation between the reactant free radicals. No exceptions to this postulate have been found. The spin repulsion term, V_r, of eq 2 was generally small, less than 2 kcal/mole, for the reactions of Tables I and II.

A fuller examination of these bimolecular transition-state postulates of spin conservation and stable bond formation will be prepared, along with an evaluation

(5) E. K. Gill and K. J. Laidler, *Can. J. Chem.*, **36**, 1570 (1958).

(6) K. J. Laidler, "The Chemical Kinetics of Excited States," Oxford University Press, Oxford, England, 1955, p 22.

of the justification of the assumptions inherent in eq 1 and eq 2.

Acknowledgment. It is a pleasure to acknowledge the valuable correspondence with Professor H. S. Johnston of the University of California, Berkeley, Calif.

LABORATORIES DIVISION
AEROSPACE CORPORATION
EL SEGUNDO, CALIFORNIA 90245
S. W. MAYER

RECEIVED AUGUST 25, 1967

Radiolytic Products of Liquid Ammonia[1]

Sir: Radiolysis of liquid ammonia results in the formation of H_2, N_2, and N_2H_4.[2-6] A recent publication reports that HN_3 is also a radiolytic product.[7] In this communication, we present the results of experiments[8] showing that at least two other products, one of which is HN_3, are formed in the radiolysis of liquid ammonia.

Samples of liquid ammonia that had been purified by storage over sodium, followed by trap-to-trap distillation, were irradiated at 10° with Co^{60} γ-rays for total doses of 1×10^4 to 1.5×10^8 rads. The yields of H_2, N_2, and N_2H_4 were measured. The amount of excess hydrogen, calculated from the material balance equation

$$H_{2,\,excess} = H_{2,\,obsd} - N_2H_{4,\,obsd} - 3N_{2,\,obsd}$$

was plotted as a function of dose. Two distinct dose regions, (1) $\leq 30 \times 10^3$ rads, where $G(H_{2,excess}) = 0.51 \pm 0.03$, and (2) $>50 \times 10^3$ rads, where $G(H_{2,excess}) = 0.14 \pm 0.03$, were found where there was a lack of material balance. Thus either additional products with a $N_2:H_2$ ratio $> 1:2$ were present or impurities were an important influence in the radiolysis. No evidence for any impurity was found.

When alkaline aqueous solutions of ammonia, which had been irradiated to doses $\leq 30 \times 10^3$ rads, were examined spectroscopically, two broad absorption bands centered at 285 and 243 mμ were observed (Figure 1, curve III). On acidifying, these bands disappeared and a more intense band at 230 mμ was observed (Figure 1, curve IV). These absorption spectra were similar to that of a control solution of tetramethyl tetrazene (curves I and II) and to that previously observed for alkyl tetrazenes.[9,10] These results, together with the observation that on increasing the dose these bands disappear with the formation of nitrogen, suggest that the unknown species contains a N=N group. Possible compounds which may be present are diazene (N_2H_2), triazene (N_3H_3), or tetrazene (N_4H_4).

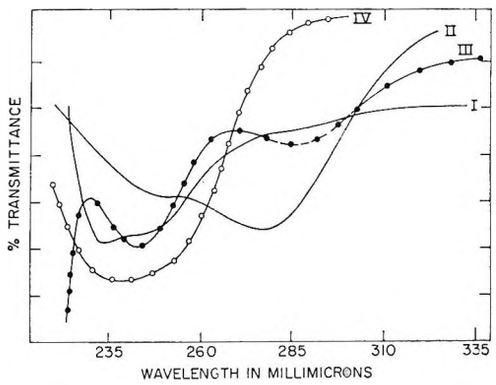

Figure 1. Typical ultraviolet spectra of aqueous solution of liquid ammonia irradiated to doses $\leq 30 \times 10^3$ rads: I, solution of tetramethyl tetrazene, pH 2.8; II, solution of tetramethyl tetrazene, pH 11.8; III, aqueous solution of irradiated ammonia, pH 11.8; and IV, aqueous solution of irradiated ammonia, pH 2.8.

Typical ultraviolet absorption spectra of aqueous solutions of ammonia, which had been irradiated to doses $>50 \times 10^3$ rads, are shown in Figure 2. In basic and neutral solution (curve III), absorption spectra show little structure, while in acid solution (curve IV), there is a broad absorption band at 260 mμ. This behavior is similar to that of control samples of NaN_3 (Figure 2, curves I and II). The presence of N_3^- was confirmed by measuring the infrared spectra of (1) an acidified aqueous solution of irradiated NH_3 and (2) of a KBr pellet prepared from this solution (Table I). Absorption bands characteristic of azide were observed. A further experiment was carried out in which helium was bubbled through an acidified aqueous solution of irradiated liquid ammonia and passed through a liquid nitrogen trap. The trap was allowed to warm up and the resulting vapor expanded

(1) This work was performed under the auspices of the U. S. Atomic Energy Commission.

(2) D. Cleaver, E. Collinson, and F. S. Dainton, *Trans. Faraday Soc.*, **56**, 1640 (1960).

(3) L. Kolditz and U. Prösch, *Z. Physik. Chem.*, **208**, 108 (1962).

(4) J. R. Puig and E. Schwarz, "Industrial Uses of Large Radiation Sources," Vol. I, International Atomic Energy Agency, Vienna, 1963.

(5) F. S. Dainton, T. Skarski, D. Smithies, and E. Wezramowski, *Trans. Faraday Soc.*, **60**, 1068 (1964).

(6) D. Schischkoff and D. Schulte-Frohlinde, *Z. Physik. Chem.*, **44**, 112 (1965).

(7) J. Belloni, *J. Chim. Phys.*, **9**, 1281 (1966).

(8) J. W. Sutherland and H. Kramer, Annual Reports, Nuclear Engineering Department, Brookhaven National Laboratory, Upton, Long Island, N. Y.: BNL 900 (S-67), p 83, 1964; BNL 954 (S-68), p 88, 1965; BNL 994 (AS-20), p 61, 1966.

(9) T. M. Bins and N. R. McBride, *Anal. Chem.*, **31**, 1382 (1959).

(10) N. R. McBride and H. W. Kruse, *J. Am. Chem. Soc.*, **79**, 572 (1957).

Table I: Infrared Data on Unknown "Species" Found at High Doses[a]

KBr pellet of sample, cm^{-1}	NaN_3 control, cm^{-1}	Lit. assignment[b,c]
3490	3490	3455
2107	2130	2128, 2189
1600	1600	1567
1267	1262	1267
730	740	718
655	658	644
637	641	628

Acidified aqueous solution, cm^{-1}	Control sample of HN_3, cm^{-1}	Lit. assignment,[b,c] cm^{-1}
3333	3333	3310[d]
2105	2105	2105
1600	1600	...

[a] Perkin-Elmer Model 221 spectrophotometer. [b] H. A. Papazian, *J. Chem. Phys.*, **34**, 1614 (1961). [c] P. Gray and T. C. Waddington, *Trans. Faraday Soc.*, **53**, 901 (1957). [d] A. M. Buswell, *et al.*, *J. Am. Chem. Soc.*, **61**, 2809 (1939).

into a 1-m infrared gas cell. Absorption bands characteristic of HN_3 were observed.

From these experiments, it is concluded that HN_3 is a product in the radiolysis of liquid ammonia at doses >40 × 10^3 rads, and at doses <30 × 10^3 rads, other hydronitrogen species, possibly N_2H_2, N_3H_3, or N_4H_4, are formed. From mass-balance considerations, $G(HN_3) = 0.035$ and $G(N_2H_2) = 0.26$ or $G(N_4H_4) = 0.13$ or $G(N_3H_3) = 0.17$.

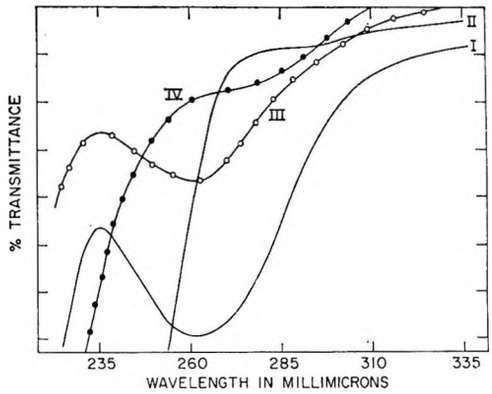

Figure 2. Typical ultraviolet spectra of aqueous solution of liquid ammonia irradiated to doses ≥50 × 10^3 rads: I, solution of KN_3, pH 2.8; II, solution of KN_3, pH 11.8; III, aqueous solution of irradiated ammonia, pH 2.8; IV, aqueous solution of irradiated ammonia, pH 11.8.

BROOKHAVEN NATIONAL LABORATORY
UPTON, NEW YORK 11973
J. W. SUTHERLAND
H. KRAMER

RECEIVED SEPTEMBER 5, 1967